Hydrology and Hydroclimatology

Principles and Applications

M. Karamouz · S. Nazif · M. Falahi

CRC Press
Taylor & Francis Group

Hydrology and Hydroclimatology

Principles and Applications

Hydrology and Hydroclimatology

Principles and Applications

M. Karamouz · S. Nazif · M. Falahi

CRC Press
Taylor & Francis Group
Boca Raton London New York

CRC Press is an imprint of the
Taylor & Francis Group, an **informa** business

CRC Press
Taylor & Francis Group
6000 Broken Sound Parkway NW, Suite 300
Boca Raton, FL 33487-2742

Version Date: 20121019

International Standard Book Number-13: 978-1-4665-1220-7 (eBook - PDF)

Dedication

To all who are in search of excellence, against all odds, including my wife, Setareh

Mohammad Karamouz

My husband, Hamed

Sara Nazif

My family

Mahdis Falahi

Contents

Preface

In this book, a system approach to understanding and applying the principles of hydrology and hydroclimatology considering interactions among different components of the water cycle is discussed. A fresh look at the fundamentals and new challenges in hydrologic and hydroclimatic systems and climate change is presented. The importance of the underlying concepts is magnified in the new millennium due to the emergence of nontraditional data sets and new investigation techniques applied to an expanding array of water-related problems. The understanding, definition, and formulation of the hydrologic system, time series analysis, long-lead forecasting and simulation, and risk and uncertainty in hydrologic design considering today's engineering issues are covered in this book.

Societies are becoming more independent, and their vulnerability to extreme events such as droughts and floods is emphasized in this book in order to help develop resilient and adaptive measures on the face of water-related natural disasters. Accelerated interest in accessing anthropogenic activities resulted in many concerns related to the urban water cycle, which are also addressed throughout the book.

Chapter 1 is as an introduction to the water cycle and its placement in the global system. The main topics covered in this book put emphasis on global water budget, spatial and temporal data analysis, modeling in hydrology, water security, and decision-making tools in hydrology. Chapter 2 introduces the interaction of different systems in the hydroclimate cycle. Chapter 3 includes the fundamentals of climate and hydrology relations and interactions as an important component of the water cycle. This chapter will provide some general information about the Earth's energy budget, modeling of the climate system, and internal climate variability such as El Niño–Southern Oscillation, The North Atlantic Oscillation, and the Southern Annular Mode. Cloud and precipitation formation processes are likewise discussed in this chapter. Chapter 4 presents an overview of the different components of the hydrology cycle. This chapter starts with precipitation and then deals with data gathering and analysis in time and space. Calculation of excess rainfall as the main source of runoff and water resources is then discussed in detail with regard to the different causes of precipitation loss such as evaporation, interception, depression storage, and infiltration. The snowmelt process as an effective parameter in the water cycle is also covered in this chapter. Chapter 5 discusses the watersheds' characteristic as a medium for runoff and other water cycle components. Also, the necessary data and sampling process in runoff analysis through a watershed are given. Chapter 6 covers the methods used practically for evaluation and analysis of surface water and flood. Different issues in hydrograph development and analysis are addressed in this chapter. The reservoir and river routing processes from a hydrologic aspect are included in this chapter as well to develop transitional hydrographs. Chapter 7 discusses the basic principles of groundwater hydrology as a component of the water cycle. This chapter does not aim to cover all the concepts in groundwater hydrology but only those needed to show the interactions with surface water. Chapter 8 introduces time series analysis and modeling. Parameter estimation techniques and evaluation of fitted models are discussed in this chapter. Different stochastic modeling processes such as AR, ARMA, ARIMA, and ARMAX are also covered in this chapter. Chapter 9 discusses the climate change and general circulation models used in climate change studies. In this chapter, the application of General Circulation Models in climate change studies and ways to downscale the model outputs are addressed, and then climate change impacts on components of the water cycle as well as hydrological processes are described. Chapter 10 introduces the basics for probability, risk, and uncertainty in different processes and components of hydrology. In this chapter, different schemes for risk analysis are addressed. Chapter 11 provides the basics for hydrologic simulation. In this

chapter, issues such as selection of appropriate predictors and development of different forecasting and simulation models, such as physical models, statistical models, and neural network models, through different real case studies are discussed. Chapters 12 and 13 deal with two important extreme hydrologic events—drought and flood. The issues related to prediction, monitoring, analysis, and mitigation of these phenomena are addressed in these chapters.

Mohammad Karamouz
Sara Nazif
Mahdis Falahi

Acknowledgments

Many individuals have contributed to the preparation of this book. The initial impetus for the book was provided by Professor Jacques W. Delleur of Purdue University, who has been a role model for Mohammad Karamouz, a PhD co-adviser to him, and an inspiring instructor, through his class notes in stochastic hydrology that later became a textbook, *Applied Modeling of Hydrological Time Series* (Water Resources Publication, 1988).

Many graduate students at the *Polytechnic Institute of New York University* (formerly known as Polytechnic University and University of Tehran), who attended the first author's graduate hydrology course, were a driving force for the completion of class notes that formed the basis for this book. The valuable contribution of Dr. Azadeh Ahmadi in preparation of Chapter 7, Dr. Shahab Arjhinejad in Chapters 2, 3, 5, 6, and 7, and Zahra Zahmatkesh (PhD Candidate) in Chapters 10 and 13 of this book is hereby acknowledged. Authors would also like to thank PhD students, H. Tavakolifar, and Y. Altayyar and MS students E. Goharian, E. Akbarian, B. C. Caraballo, N. Sharma, B. Ahmadi, A. Abolpour, M. Yousefi, and E. Ansari from the University of Tehran and the Polytechnic Institute of New York University. Special thanks to Mehrdad Karamouz, Mona Lotfi, Saba Karamouz and Mana Akhbari for preparing the front cover, figures, and artwork for this book.

Authors

Mohammad Karamouz is director of environmental engineering and science programs at the Polytechnic Institute of New York University and a professor (on leave) at the University of Tehran. He is an internationally known water resources engineer and consultant. He is the former dean of engineering at Pratt Institute in Brooklyn, New York. He is also a licensed professional engineer in the state of New York, a fellow of the American Society of Civil Engineers (ASCE), and a diplomat of the American Academy of Water Resources Engineers. Dr. Karamouz received his BS in civil engineering from Shiraz University, his MS in water resources and environmental engineering from George Washington University, and his PhD in hydraulics and systems engineering from Purdue University. He served as a member of the task committee on the urban water cycle in UNESCO-IHP VI and was a member of the planning committee for the development of a 5 year plan (2008–2013) for UNESCO's International Hydrology Program (IHP VII).

Among many professional positions and achievements, he also serves in a number of task committees for ASCE. In his academic career spanning 27 years, he has held positions as a tenured professor at Pratt Institute (Schools of Engineering and Architecture in Brooklyn) and at Tehran Polytechnic. He was a visiting professor in the Department of Hydrology and Water Resources at the University of Arizona, Tucson, 2000–2003. He was also the founder and former president of Arch Construction and Consulting Co. Inc. in New York City.

His teaching and research interests include integrated water resources planning and management, groundwater hydrology and pollution, drought analysis and management, water quality modeling and water pollution, decision support systems, climate forecasting, and conjunctive use of surface and groundwater. He has more than 300 research and scientific publications, books, and book chapters to his credit, including four books, *Groundwater Engineering and Management* (CRC Press 2011), *Urban Water Engineering and Management* (CRC Press 2010), *Water Resources System Analysis* (Lewis Publishers 2003), and a coauthored book, *Urban Water Cycle Processes and Interactions* (Taylor & Francis Group 2006). Professor Karamouz serves internationally as a consultant to both private and governmental agencies such as UNESCO and the World Bank.

Sara Nazif is an assistant professor in the School of Civil Engineering at the College of Engineering, University of Tehran. She received a BS in civil engineering and MS in water engineering from the University of Tehran. Her PhD is in Management of Urban Water Cycle considering Climate Change Impacts. She is an international expert and consultant in the application of systems engineering and computer modeling in Urban Water Engineering and Management. She has authored more than 70 research and scientific papers published in national and international journals and conferences, and has published the book *Urban Water Engineering and Management* (CRC Press 2010). Her research and training interests include water distribution systems, disaster management, urban water demand management, stochastic hydrology, climate change impacts on urban water engineering and management, drought and flood management, water and wastewater treatment plant operation, and systems analysis.

Mahdis Falahi is an international senior consultant and a Professional Engineer at Pishran Consulting Engineers. She received two BS degrees in civil engineering and applied mathematics and a MS degree in water resources engineering from Tehran Polytechnic (Amirkabir University of Technology). She is an associate member of the American Society of Civil Engineers (ASCE), the Iranian Water Resources Association, and the Iranian Society of Environmentalists. She has

also been involved with water and environmental R&D groups working on various universities' and industries' research collaborative projects. She has co-authored a number of journal and conference papers. Her teaching and research interests include integrated hydrology and hydroclimate modeling, climate change, geostatic analysis, systems analysis, analysis of risk and uncertainty, water resources management and planning, and remote sensing.

1 Introduction

1.1 INTRODUCTION

In hydrology and hydroclimatology, water science with engineering applications and the interaction of water with different mediums in the Earth–atmospheric system are studied. *Water* occurs on Earth in all its three states: liquid, solid, and gas, in various degrees of motion. Evaporation of water from water bodies such as oceans and lakes, formation and movement of clouds, rain and snowfall, streamflow and groundwater movement are the main topics studied in hydrology and hydroclimatology, which show the dynamic nature of water. The various aspects of water related to the Earth can be explained in terms of climatic variability in a cycle known as the *hydrologic cycle*.

Due to high interactions of water with other Earth–atmosphere components, it is necessary to manage water (in different phases) in a sustainable fashion through integrated water resources management (IWRM). Water more than ever, as an important element in the formation and conservation of the environment, is receiving global attention. The main challenge is to understand the principles and laws governing the formation and movement of water in nature.

Climate is usually described in terms of the variability and mean of relevant atmospheric variables such as precipitation, temperature, relative humidity, atmospheric pressure, and wind. Climate can thus be viewed as an aggregate or synthesis of weather. This implies that climate description in a particular region must contain an analysis of mean conditions of the seasonal cycle as well as the extreme events such as storms and severe frost occurrence and probabilities.

The climate is now defined in a wider sense. The statistical description of the climate system includes the analysis of the behavior of four major components of the Earth–atmosphere system and their interaction: the atmosphere, the lithosphere, the biosphere, and the hydrosphere (International Panel on Climate Change [IPCC] 2007). In the following sections, major elements of atmospheric processes that directly impact the hydroclimatic processes in general and the hydrologic cycle in particular are discussed.

1.2 SYSTEMS APPROACH

The study of any phenomenon, process, and/or structure such as climatic system or hydrologic cycle requires an integrated approach. The selected framework of study dictates the way an environment is dismantled for analysis. It also determines the integration of environmental components so that the results of analysis can be incorporated in a holistic fashion. For providing such a framework, understanding of system concepts is needed.

The Earth's environment is composed of several systems working together in harmony but with some complex relations and interactions. For a systems approach to hydroclimatology and hydrology, it is necessary to have a clear understanding of different components of the Earth's system and the positioning of each subsystem with respect to other subsystems. This will help to understand and provide a physical interpretation of different climatic events in global and regional scales.

The traditional knowledge of hydroclimatology and hydrology focuses on those variables that are more tangible and representative such as temperature and its variations, wind near the surface of the Earth, humidity, cloud characteristics, precipitation in its various forms, and seasonal variability of runoff. However, these variables could not completely define the hydroclimatic and hydrologic systems and their variations that depend on different parameters such as the vertical structure of the

atmosphere, the influence of the underlying land and sea, the anthropogenic activities, and many other factors that are not fully explored in many classical hydrology courses. The hydrologic cycle is a model of holistic nature and has been cited as a true system in the literature wherever examples of system integration have been brought up in art, science, and engineering.

1.3 HYDROLOGIC CYCLE

The hydrologic cycle is generally defined as a conceptual model describing the storage and circulation of water between the hydrosphere, atmosphere, lithosphere, and biosphere. In the hydrologic cycle, clouds, which are moist, send back the water to the oceans or land surfaces in different forms of precipitation such as rain, snow, and hail; however, only rain is considered in this discussion. During rainfall, water infiltrates into the ground after wetting vegetation and other surfaces. During infiltration, the soil is saturated and the excess water percolates slowly across the different soil layers and finally reaches the groundwater.

Whenever the rate of precipitation transcends the rate of infiltration, surface runoff occurs. *Surface runoff* is the excess water that flows over the land, when soil is infiltrated to full capacity. Surface runoff can be generated either by rainfall or by the melting of snow, ice, or glaciers. This is a major component of the hydrologic cycle and specific attention is given to it. The interaction between precipitation and surface runoff is highly dependent on meteorological factors and the physical geology and topography of the catchment (watershed).

The portion of the runoff that moves over the land surfaces to reach smaller channels is called *overland flow* and includes building up of and draining off the storages over the surface. The overland flow has a small length and depth and the flow is in the laminar (low velocity) regime. Flows of small channels join and form larger streams that finally reach the basin outlet. The rate of surface runoff is usually recorded at the basin outlet gauge for practical purposes. Finally, water reaches some streams, both by overland flow and from groundwater discharge, and moves to the sea, where it again evaporates to recontinue the cycle.

The urban setting could alter the natural movement of water and therefore the urban water cycle should be observed as a part of the overall water cycle. Drastic land use changes in urban areas as a subset of urban and industrial development affect natural landscapes and the hydrological response of watersheds. Although anthropogenic factors with respect to waterways, pipes, abstractions, and man-made infrastructures affect the elements of the natural environment, the main structure of the hydrological cycle remains the same in urban areas (McPherson and Schneider 1974). However, the characteristics of the hydrologic cycle are greatly altered by the impacts of the services to the urban population, such as water supply, drainage, and wastewater collection and management.

1.3.1 Watersheds and Aquifers

Watershed is the best hydrological unit used to carry out water studies and planning in a systematic fashion. Biosphere and anthropogenic activities and impacts are usually discussed in watershed scale. Therefore, determination of watershed characteristics is an important concept. The watershed can be well defined as an area that can be considered a bounded hydrologic system, within which all live components are linked to each other regarding their water supply resources. The main features of a watershed are outlet and boundary. Watershed boundary is also referred to as the water divide boundary and outlet is the point in which all the surface waters in the watershed are collected.

In addition to watershed characteristics that affect basin response to rainfall, there are some man-made structures such as reservoirs and channels that affect the outlet hydrograph. In small catchments or short channels, these effects are not very important, but by increasing the length of stream channels and the size of the contributing areas, the storage in the stream channels and reservoirs increases and the processes that occur in *rivers*, *channels*, and *reservoirs* become more

important. In urban areas, the major changes in land uses and watershed topography highly affect the surface flow regimes that should be incorporated in watershed-scale hydrologic studies.

The *infiltrated water* to the soil is pulled down by gravity through the pores until it reaches a depth where all of the pores are filled with water, called *groundwater.* Aquifer is the medium in which groundwater moves and stores. It is a combination of different layers of pervious or fractural strata. An aquifer provides similar characteristics as a watershed for water to move but is underground, is irregular, and is composed of tiny pathways between soil particles. When the soil or rock becomes saturated, the water level that results is called the water table. The water table is not always at the same depth below the land surface. During periods of high precipitation, the water table can rise. Conversely, during periods of low precipitation and *high evapotranspiration*, the water table falls. The water table is also affected by artificial charge and discharges made at different points by humans.

1.3.2 Rivers and Reservoirs

Streamflow is highly variable through time because of high dependency on precipitation in the watershed. Rainfall can result in rivers rising, even if it rains very far up in the watershed. The responses of rivers with different sizes are different to storms and rainfall. The rise-and-fall rate in large rivers is much slower than that in small rivers. The river response at different points through its length varies.

In many practices and engineering design problems, the primary design variable is the maximum volume flow rate passing the basin outlet during a storm event, called *peak discharge*. However, the peak discharge is inadequate for design problems where watershed or river storage is significant. In these cases, design work is usually based on hydrographs rather than on peak discharge rates. *Hydrograph* is a time record of the discharge of a stream, river, or watershed outlet and is a representation of how a watershed responds to rainfall. It is the result of integrated effects of a wide variety of catchment and rainfall parameters having complex interactions.

Reservoirs consist of natural or man-made means of retention or detention of water. They prolong water utilization in the local and regional scale. They expedite the rate of evaporation and are perceived by environmentalists as a way of generating balance between upstream and downstream water rights as well as environmental demand allocation specifically where massive dams are constructed. On a positive side, reservoirs help planned economic developments downstream. The process of computing the progressive time and shape of a surface flow at successive points along a river or successive times at the reservoir outflow is known as flow routing.

1.4 HYDROLOGIC VARIABILITY

Climate is defined in terms of statistical averages such as air temperature, hours of bright sunshine, and precipitation. There are periodic changes in the climate over diurnal and annual time scales, which are an integral part of the operation of the Earth–atmosphere system, and do not involve it in long-term structural changes.

It is also possible to identify longer-term changes in climate occurring over periods of decades and centuries. Some of these changes represent considerable modifications to the mode of operation of the Earth–atmosphere system. The Earth's surface reveals evidence of periods of extreme cold, when large areas were under thick sheets of ice. Areas that are deserts today contain landforms that are clearly fluvial in origin, suggesting periods of wetter climate conditions. These changes can be viewed alternatively as a result of the changing operation of factors external to the Earth–atmosphere system or as modifications of the disposition of internal energy and matter as explained in the next section.

Hydrologic processes such as rainfall, snowfall, floods, and drought are usually investigated by analyzing their records of observations. Many characteristics of these processes seem to vary

in time and space and are not amenable to *deterministic analysis*. In other words, deterministic relationships presented so far do not seem to be applicable for analysis of these characteristics. For the purpose of hydrologic analysis, the average or peak discharge is then considered to be a random variable. Other examples of *random variables* are maximum rainfall, maximum temperature, maximum wind speed, period of flooding, and minimum annual flow. *Probability and statistics* concepts and principles are used to analyze random variables and to deal with risk and uncertainty in hydrologic variability.

1.5 DISPOSITION OF ENERGY AND MATTER

If the Earth–atmosphere system is viewed as a black box, then the first alternative concerns explore the relationships between input and output. Changes within the system in response to energy inputs, the pathways along which energy and matter are transferred, the nature of storage, and the rate at which energy and matter are transferred and converted should be investigated. For example, changes in temperature of the lower part of the troposphere may be due to radiant energy exchange in the Earth–atmosphere system and its surrounding space. Alternatively, it may be the structural modification within the system such as building massive dams and hydraulic structures for interbasin transfer of water that has resulted in changing climatic patterns such as evaporation patterns and more or less energy being stored as sensible heat within the atmosphere of a region compared to the adjacent region.

The critical issues in this respect are the regulators, which are control points within the system, some with natural interaction between levels and layers with differences in temperature, pressure, and moisture content, and some under the influence of gravity, lift, and drag forces. Other control points are imposed by man-made intervention in atmospheric systems such as cloud seeding, abstracting, or slowing down or accelerating water movement in nature.

1.6 REPRESENTATIONS AND STATISTICAL AND SIMULATION MODELS

Simulation of hydrologic events is needed for the analysis and planning of watersheds. Hydrologic simulation models are used to provide not only a hydrologic prediction/projection but also a better understanding of processes within the hydrologic cycle. A variety of modeling approaches are used for this purpose. These models are a simplified *conceptual representation* of a part/component of the water cycle. Different classifications are considered for hydrologic simulation. Two groups of *hydrologic models* are often defined:

1. *Mathematical models:* These models are usually black box models developed through tools such as regression, transfer functions, neural networks, and fuzzy inferences. In these models, mathematical and statistical concepts are used to develop a relationship between model input(s) such as rainfall and temperature and model output such as runoff.
2. *Physical (process)-based models:* These models attempt to simulate the physical processes that happen in the real world through the hydrological cycle based on identified physical and empirical relationships. In other words, in this model, different components of the hydrologic cycle are quantified using the relationships that interpret the relations between hydrologic cycle components. Typically, these models include representations of surface/subsurface runoff formation, evapotranspiration, infiltration, and channel flow/streamflow.

The main concept that should be considered in models development is data availability and quality. Data limitation is an important issue that sometimes dictates what kind of model can or cannot be used. Furthermore, the type and characteristics of the output data needed for analysis and decision making should also be considered in model selection and development. Data are represented in different forms: lumped and distributed. The application of distributed data enforces the application of models that are linked with a geographical information system. To evaluate a model performance and

compare it with other models, some performance indices are defined. These indices should be selected with regard to the model, data characteristics, and behavior. For example, in drought studies, indices are used to represent the severity of different types of droughts as explained in Chapter 12.

There are some powerful software in both kinds of simulation approaches that can be used for hydrologic studies and analyses. A general, powerful, user-friendly software that is commonly used in recent years for developing mathematical models is MATLAB® developed by MathWorks. The wide range of functions and toolboxes provided in this software can be used to develop different applications based on data-driven methods/models such as artificial neural network (ANN), fuzzy inference system (FIS), and adaptive neuro fuzzy inference systems (ANFIS). There are a variety of physical models represented by different software, some of them explained in Chapter 11 for rainfall–runoff analysis in watershed scale. The performance of hydrologic models is highly dependent on data type and characteristics as well as on the watershed characteristics.

1.7 EXTREME VALUES, VULNERABILITY, RISK, AND UNCERTAINTY

Water can be utilized based on shorter- or longer-term assessment of its supply, retention and depletion and the nature of its use. Due to many social interdependencies and vulnerabilities associated with the need for water as urgent as water supply for domestic and industrial use, extreme low and high precipitations and extreme low and high temperatures are of major concern. Droughts and floods continuously devastate different regions in a variety of ways, targeting every essence of our ecosystem.

Drought is a natural hazard that originates from a deficiency of precipitation over an extended period of time. Drought should be considered relative to the long-term average condition of balance between precipitation and evapotranspiration in a particular area, a condition often perceived as "normal." It is also related to the timing (i.e., principal season of occurrence, delays in the start of the rainy season, occurrence of rain in relation to principal crop growth stages) and the effectiveness (i.e., rainfall intensity, number of rainfall events) of the rains. Other climatic factors such as high temperature, high wind, and low relative humidity are often associated with it in many regions of the world and can significantly aggravate its severity.

On the other hand, *floods* continue to be the most destructive natural hazard in terms of short-term damage and economic losses to a region. Flooding is caused primarily by hydrometeorological mechanisms, acting either as a single factor or as a combination of different factors. Measures can be taken, such as the repair of river embankments to make rivers capable of disposing rainfall of up to the conveyance capacity of the river and the improvement and expansion of reservoirs, diversion channels, and sewer systems to reduce/eliminate the danger of floods. Moreover, in order to promptly and correctly counter local changes in precipitation and the danger of high tides, an effective use of the information transmission system of a comprehensive flood prevention program is needed.

Therefore, vulnerability assessment and overlaying extreme hazards with vulnerability in risk management are in the forefront of today's hydrological and hydroclimatical challenges. Uncertainties range from

- Inherent natural uncertainties due to man's limited knowledge and complexity of comprehending principles and laws governing the formation of water and its migration through the Earth–atmosphere system
- Parameters and model uncertainty due to assumptions, lack of enough reliable data, oversimplification of models, and/or error accumulation from too many parameters

1.8 WATER AVAILABILITY

The primary input for estimating the volume of water naturally available to a given nation in the global scale is an information database (AQUASTAT) that has historically been developed and

maintained by the Food and Agriculture Organization of the United Nations (FAO). It is based on a water balance approach for each country and the quantity of available water resources (FAO 2003). This database has become a common reference tool used to estimate each nation's renewable water resources. FAO has compiled an index called Total Actual Renewable Water Resources (TARWR). This index is an indication of the water resources availability for development from all sources within a region. It is a calculated volume expressed in cubic kilometers per year, divided by the total population. The index estimates the total available water resources per person in each country, considering a number of individual components:

- Adding all internally generated surface water and groundwater from precipitation falling within a country's boundaries
- Adding flow entering from other countries, both surface water and groundwater
- Subtracting any potential shared resource from surface water and groundwater system interactions
- Subtracting the water that leaves a region/country, required by an existing treaty

TARWR gives the maximum amount of water that could actually be available for a country on a per capita basis. From 1989, this framework has been used to assess water scarcity and water stress. It is important to note that FAO considers what is shared in surface water and groundwater resources. However, as discussed by UNESCO (2006), these volumes do not consider the socioeconomic criteria that are applied to societies, nations, or regions that are developing and utilizing those resources. Water pricing and net costs can vary when developing surface water and groundwater sources. Therefore, the reported renewable volume of water will be less for a variety of economic and technical reasons.

- Roughly 27% of the surface water runoff is floods, and this share of water is not considered a usable resource, even though it contributes to the recharge of mainly overexploited aquifers. However, floods are counted in the nation's TARWR as part of the available, renewable annual water resource.
- Seasonal variations in precipitation, runoff, and recharge are not well reflected in annual figures. They are important for basin-scale decision making and setting regional strategy.
- Many sizable countries have different climatic zones as well as scattered population and the TARWR does not reflect the ranges of these factors that can occur within nations.
- TARWR has no data to identify the volume of water that sustains ecosystems, namely, the volume that provides water for forests and directs rain-fed agriculture, grazing, and grass areas.

It is also evident that not all of the internally renewable freshwater resources (IRWR) can be used and controlled by the population of a country. It is estimated that only about one-third of the IRWR can be potentially controlled even with the most possible technical, structural, nonstructural, social, environmental, and economic means. The global potentially usable water resources of the IRWR are estimated to be around 9000 to 14,000 km^3 (UN 1999; Seckler 1993). A part of the primary water supply (PWS) is evaporated, while other parts return to rivers, streams, and aquifers as return flows, and in many instances, this part is again withdrawn for different uses. This is known as the recycled portion of PWS. The PWS and the recycled water supply add up to 3300 km^3 worldwide, which constitute the water used in different sectors (agriculture, industry, public supply).

1.9 WATER SUSTAINABILITY

The term "sustainable development" was first globally introduced by the World Commission on Environment and Development in its 1987 report, "Our Common Future." The aim of the

Commission was to address the environmental and developmental problems in an integrated fashion. It has three general objectives:

1. Examine the critical environmental and developmental issues and how to deal with them
2. Formulate new forms of international cooperation that will influence policies in the direction of many changes needed
3. Raise the level of understanding and commitment to action of all adversaries including institutions and governments

Commissioners from 21 countries analyzed the report, with the final report accepted by the United Nations General Assembly in 1987 (UNESCO 2002). In various publications, the findings of the commission and the final resolution of the UN General Assembly were summarized as a single sentence describing sustainable development as "meeting the needs of the present generation without compromising the ability of future generations to meet their own needs." This definition was criticized for failing to address the natural environment.

Instances of poorly managed surface water and groundwater development and the inadvertent impact of inadequate land-use practices have produced adverse effects such as water-quality degradation, impairment of aquatic ecosystems, lowered groundwater levels, and, consequently, land subsidence and the drying of wetlands. As it is less costly and more effective to protect surface water and groundwater resources from degradation than to restore them, improved water management will diminish such problems and save money.

IPCC (2007) shows a broader perspective of sustainable development as shown in Figure 1.1. They have combined the socioeconomic development paths and economic growth with technology, population, and governance through adaptation with and by human and natural systems. The objective is to sustain food, water, ecosystems, biodiversity, and human health and prevent migration. At the same time, human systems are adapted and natural systems are adjusted to climate change including more frequent droughts and floods. The emission of greenhouse gases is the direct by-product of socioeconomic development that should be mitigated.

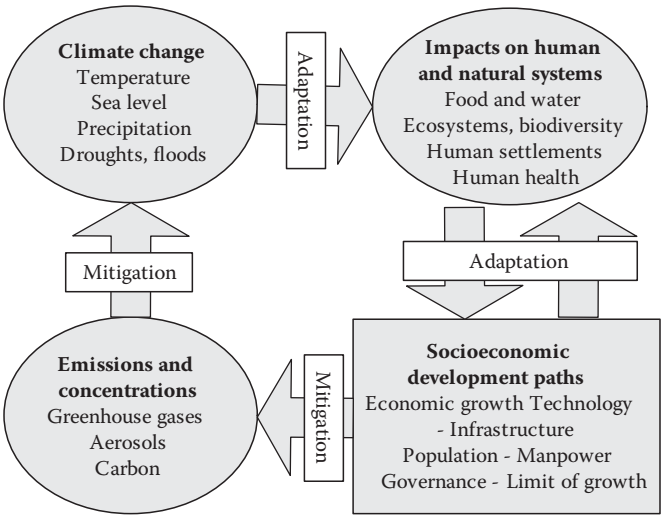

FIGURE 1.1 Sustainable development, adaptation, and mitigation interactions. (Adapted from IPCC, TAR, 2001.)

1.10 TOOLS AND TECHNIQUES

Identification, simulation, and projection models of hydrology and hydroclimatology cycle, in an integrated or component-by-component fashion, are representations of the water systems. The development and application of these models (the model-building process) consist of several interrelated stages. Hydrology is broad and complex, and due to the nature of its interactions in the Earth–atmosphere system with different elements including ecosystem, many tools are needed to analyze, assess, plan, and manage it. Figure 1.2 shows a framework for the combination of tools and methods needed for hydrology and hydroclimatic studies.

Guidelines are important tools used in the planning of the hydrologic cycle. They provide some guides in dealing with different components to minimize the trial-and-error efforts and to hasten the achievement of best results. *Algorithms* provide a step-by-step approach to achieve the desired goal in the planning of hydrologic components and are usually employed for hydrologic cycle planning and management purposes. Different modeling approaches through different software are highly developed in recent years for simulating hydrologic processes. *Heuristics* is a method of solving a problem for which no formula exists, based on informal methods or experience, and employing a form of trial-and-error iteration. They are often utilized for simulation purposes in hydrology when there is a high level of complexity, making it difficult to completely understand the nature and behavior of components and their interactions.

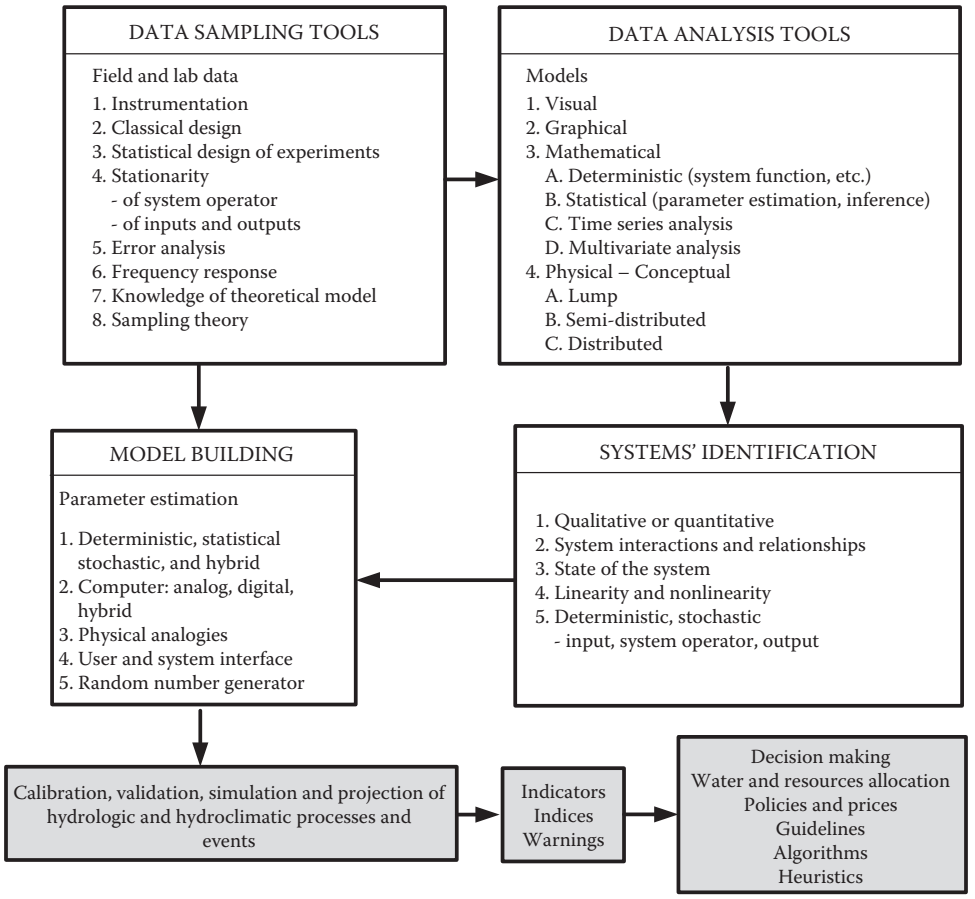

FIGURE 1.2 Framework of tools needed for hydrologic modeling.

Models are based on the available hydrologic and hydroclimatic information. In a first phase of the modeling process, data from different sources are gathered to describe the main components of the system or subsystem as well as other interrelated systems. On the basis of statistical reliability of this information, a choice has to be made regarding the most appropriate and realistic type of model. The model choice, as the second phase of the process, is characterized by a hierarchy of mathematical models. For example, in the case of limited or imprecise information regarding the underlying physical processes occurring in the watershed, a statistical or time series approach may be warranted. The analysis of trends, periodicities, and the correlation structure of the historical records may further define the mechanisms responsible for water movement and water quality variations.

An important phase of the model-building process is the calibration and validation of the model. Model calibration compares the model's response or predictions with the historical data. Different error criteria as a function of the differences between predicted and observed variables can be used, such as mean square error (MSE), sum squared error (SSE), root mean square error (RMSE), and Nash–Sutcliff, to judge the predictive capability of the model. See Chapter 11 for more details. If the predictions differ significantly from the historical conditions, then the model architecture, parameters, boundary, and initial conditions may be systematically varied to improve the model's performance. However, it is possible that although the model's performance may be acceptable, the parameter values may be physically unrealistic. In this event, the underlying assumptions of the model would have to be reexamined to determine their appropriateness in the context of the validation results. This is the feedback element of the model-building process. In model validation, the model's response and performance are tested based on the data that are not used to estimate the model parameters.

Following the calibration–validation process, the model can be used for the prediction (simulation) and/or projection of the hydrology and hydroclimatology systems. Simulation analysis provides only localized or limited information regarding the response properties of the system and the possible hydrologic and environmental trade-offs.

1.11 PEOPLE'S PERCEPTION—PUBLIC AWARENESS

It can be argued that, until recently, having clean water was a luxury as often cited by the delegates of developing countries at the United Nations. The developing countries should not make the mistakes made by developed countries and undermine pollution controls in their industrial and urban expansion as they rush toward economic development.

In most of the developed countries, legislation for pollution control was introduced in the 1960s and 1970s. The United States Environmental Protection Agency (USEPA) was created in 1970 to administer environmental programs. It was an encouraging effort, but many details were left out at that time. The United Nations Conference on the Human Environment in 1972 in Stockholm focused on starting a global effort to bring the governments together to work on a shared vision about water and environment. Many other United Nations conferences followed, dealing with population, food, women's rights, desertification, and human settlements, and continued to put emphasis on environmental issues.

Eckholm (1982) describes the enormous task faced by the developing countries, such as the provision of reasonable clean water and disposal facilities and the enforcement of sanitary standards. He estimated that, at that time, half of the people in the developing countries did not have reasonable access to safe water supplies and only one-fourth had access to adequate waste disposal facilities. Today, many people around the world still do not have access to clean water.

It will take extraordinary stewardship and wisdom at the national and international level to balance the economic development with the amount of sustainable water resources and the carrying capacity of rivers and aquifers to withstand quality degradation.

High priority for environmental improvement will be difficult to impose when the social costs of welfare and unemployment have caused huge financial deficits for governments of the developed world and have brought many developing and underdeveloped countries to the brink of financial disaster.

People's perception of water as a God-given resource with no intrinsic monetary value has been changed worldwide due to water scarcity, security, and frequent droughts. Now, people are willing to pay for clean, reliable water even in the form of bottled water. Water quality issues have frequently surfaced in the mass media due to accelerated incidences and increased concerns for water-related health issues. Public and professional awareness have been improved for certain water-related global changes such as climate change and local and regional problems such as polluted rivers and lakes, overpolluted aquifers, devastating floods, and vulnerabilities of surface waters and groundwaters to undetected pollutions. Still, there is much to be done in course offering and curriculum development to educate graduating college students as to what are their social and professional responsibilities to conserve and protect water resources.

1.12 INTEGRATED WATER CYCLE MANAGEMENT

The IWRM consists of schemes, politics, and the traditional fragmented and sectored approach to water that is made between resource management and the water service delivery functions. See Rogers and Hall (2003) for more details. It should be noted that integrated water cycle management (IWCM) is a political process, because it deals with reallocating water, the allocation of financial resources, and the implementation of environmental goals. For an effective water governance structure, much more work has to be done.

IWRM is also referred to as IWCM such as in Australia, where water supply and management in general are two top priorities for all levels of government, all water-related agencies, water utilities, and everybody else. This is understandable since Australia is the driest continent and in the midst of experiencing a continuous 1000-year drought.

In IWCM, there are two incompatibilities: the needs of ecosystems and the needs of the growing population. The shared dependence on water of both makes it natural that ecosystems must be given full attention within IWCM. At the same time, however, the Millennium Goals of 2000 set by the United Nations call for safe drinking water and sanitation for all populations suffering from poverty by year 2015 (Falkenmark 2003). Falkenmark suggested the following goals:

- Satisfy water consumption needs of the society while minimizing the pollution load
- Meet environmental flow requirements of river and aquifers with acceptable water quality
- Secure "hydro-solidarity" between upstream and downstream stakeholders and ecological needs

The fundamental objective is to sustain humans' and the planet's life support systems, and it should be done in a watershed scale. An important role for hydrogeologists is to educate both the public and the decision maker about the traditional role of rivers and lakes to receive treated (i.e., combined sewer overflow) or untreated waste in the watershed and in the hydrologic cycle as a whole.

1.13 ECONOMICS OF WATER

Water has an economic value and should be recognized as an economic good. Within this principle, it is vital to recognize first the basic right of all human beings to have access to clean water and sanitation at an affordable price. Past failure to recognize the economic value of water has led to wasteful and environmentally damaging uses of the resource (Karamouz et al. 2011). Managing water as an economic good is an important way of achieving efficient and equitable use and of encouraging conservation and protection of water resources.

Van der Zaag and Savenije (2006) explained the overall concerns over the true meaning of "water as an economic good" based on two schools of thought. The first is the pure market-driven price. Its economic value would arise spontaneously from the actions of willing buyers and willing sellers. This would ensure that water is allocated to uses based on its highest value. The second

school interprets the process of allocation of scarce resources in an integrated fashion, which may not involve financial transactions (McNeill 1998). Developing a water pricing framework based upon the cultural and social framework in a region, which could include subsidies for minimum consumption in low-income communities, is developed.

In a broader sense, a unique property of water is that it belongs to a system and it always affects many users. Any change in upstream water will affect the entire system downstream. Temporal and spatial variability of water resources is also constantly changing due to short- and long-term climate and land-use changes. Water could have negative economic value in case of floods. All of these make it difficult to establish the value of external impacts on water use.

The price of water could be defined as the price water users are willing to pay per unit volume of water delivered per unit of time (e.g., cubic meters). In most cases, neither water users nor self-providers pay the full price (value) of water, which should be equal to the real value of water and should include the following:

- Capital cost of water withdrawal and distribution system
- Cost of operating and maintaining the system
- Investments for augmenting the existing and/or finding new sources of water, and expanding the water transfer and distribution system
- Source protection cost reflecting its intrinsic value
- Environmental cost including the reduction of natural flows, water quality degradation, and loss of habitat
- Sustainability cost including the cost to bring the supply and demand to a level that could be managed over an extended amount of time

Kresic (2008) described the full price and value of water. Among different costs, it is difficult to assess the environmental and sustainable costs. For environmental cost, many intangible costs should be quantified. It has some common attributes with sustainable cost when considering environmental sustainability.

1.14 WATER SUPPLY VS. WATER DEMAND

The holistic or "ecological" paradigm has come to the forefront as a new alternative to solve man-made problems in the last three decades, replacing the mechanical way of thinking. See Karamouz et al. (2010) for more details. This new way of thinking began out of new discoveries and theories in science, such as Einstein's theory of relativity, Heisenberg's uncertainty principle, and chaos theory. Contrary to Newton's mechanistic universe, these new theories have taken away the foundation of the opposing paradigm, the Cartesian model. Because our way of thinking has been based so much on the Cartesian paradigm, this paradigm shift has changed the way we perceive and understand our world in general and water cycle, conservation, and sustainable use of that in particular.

Perhaps this dramatic shift of the paradigm has changed hydrology as a discipline for the study of multidisciplinary nature of water-related activities. Throughout history, water use has reflected some aspects of ecological thinking and has been shaping the water version of the new paradigm with much more historical relevance than any other resources.

For creating an opportunity for action, a paradigm shift in water management away from the entrenched supply-side focus toward a comprehensive demand-side management based on the soft path planning approach should be established. For instance, the recent National Round Table on the Environment and the Economy report, "Environmental Quality in Canadian Cities: The Federal Role," could easily be extended with explicitly less dependence on water supply. A schematic was proposed by Ashton and Haasbroek (2002) for the representation of the growth in water demand and the need to balance demand with a sustainable level of water supply in a region as presented in Figure 1.3. Two periods (demand I and demand II) are defined to bring the normal growth of

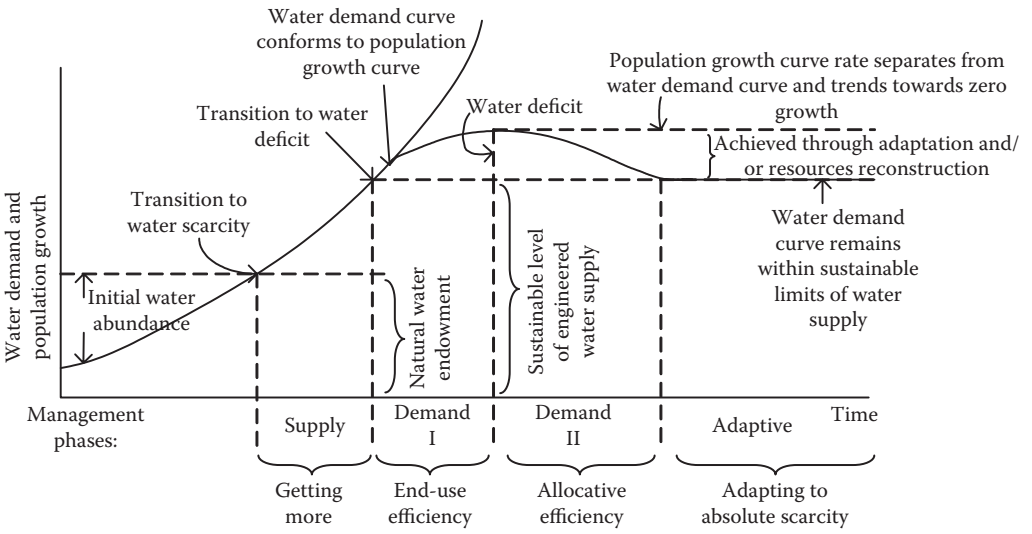

FIGURE 1.3 Schematic representation of historical phases of growth of water demand and supply. (From Ashton, P.J. and Haasbroek, B., *Hydropolitics in the Developing World: A Southern African Perspective,* 2002.)

demand, as a result of population growth, to the level of sustainable limits of water supply. The two periods are concentrated on end-user and allocation efficiencies.

As a result of this shift from supply to demand management, the limitation on the supply side is now much better understood and the urge to overexploit natural water resources has slowed significantly. The cost of water and supplying services and technologies have a major influence on the level of water demand in different nations, especially in developing countries.

Accessing the sustainability features in water supply, that is to say, the threefold goals of economic feasibility, social responsibility and environmental integrity, is linked to the purpose of water use. The sustainable water supply level can be determined in different ways but the most important point to consider is the total water balance of the study area within a region's system dynamics over a long term. For this purpose, usually the 5 to 10-year moving average is considered with in place adequate controlled structures (i.e., reservoirs, tunnels).

1.15 CLEAN WATER ACT

The enactment of the Federal Water Pollution Control Act Amendments of 1972 was the result of growing public awareness and concern for controlling surface water pollution. It was amended in 1977, and this law became commonly known as the Clean Water Act (CWA). Major amendments were also enacted in the Water Quality Act (WQA) of 1987. The Act established the basic structure for regulating discharges of pollutants into the surface waters of the United States. It gave the USEPA the authority to implement pollution control programs such as setting wastewater standards for industry. The CWA also continued requirements to set water quality standards (WQSs) for all contaminants in surface waters. The Act made it unlawful for any person to discharge any pollutant from a point source into navigable waters, unless a permit was obtained under its provisions. It also funded the construction of sewage treatment plants under the construction grants program and recognized the need for planning to address the critical problems posed by nonpoint source pollution. In the WQA of 1987, the stormwater problem was considered. It made it a requirement for industrial stormwater dischargers and municipal dischargers to separate their storm sewer system. The permit exemption for agricultural discharges continued, but Congress created a nonpoint source pollution

demonstration grant program at the USEPA to expand the research and development of nonpoint controls and management practices. The key elements of the CWA are establishment of WQSs, their monitoring, and, if WQSs are not met, developing strategies for meeting them. If all WQSs are met, then policies and programs against degradation are employed to keep to the National Primary Drinking Water Regulations which set enforceable maximum contaminant levels for particular contaminants otherwise the water should be treated to reach the standards. Each standard includes requirements for water systems to test for contaminants in the water to make sure standards are achieved. Maximum contaminant levels are legally enforceable, which means that both the USEPA and individual states can take enforcement actions against water systems not meeting safety standards. For more details, refer to Copeland (2010). The USEPA and states may issue administrative orders, take legal actions, or fine water utilities. In contrast, the National Secondary Drinking Water Standards are not enforceable. The Agency recommends them to water utilities and professional entities but does not require compliance systems to be in place. However, States of the union in the United States may choose to adopt them as enforceable standards or may relax them. In the next section, the bases of water law that governed and are enforced in the states are presented.

1.15.1 The Basis of State Water Laws in the United States

Technological changes and population growth have stressed legal regimes for water in general and for managing surface waters in particular. Water law must become a tool for accomplishing water environmental sustainability rather than serving to perpetuate water pollution and water right issues (Dellapenna 1999). Global climate disruption adds further complexities to the stresses facing water law regimes in the United States. Adaptation to climate change will necessarily center on water as one of the most essential resources for human survival and welfare. Global climate change adds stress to existing water law regimes as water management systems struggle to adapt. Dellapenna (1999) stated that technological changes in particular have not eased the problems. Globally, it inserted more strain on higher demand for water in domestic and industrial sectors and moderately have decreased the water demand in agricultural sectors through modern irrigation techniques.

The basis of applicable laws in the United States goes back to the time of settlement of English colonies. They have been called the "riparian rights" following the Latin term *ripa* (the bank of a stream). They have limited the right to use water to those who owned or leased land having a water source. A riparian owner for the most part was free to make any use wanted so long as no one complained about direct interference with his or her water use. See Dellapenna (2009) for more details.

As recently as 1950, riparian rights were applied in 32 states, and today, they still govern many states. The combination of increasing population, increasing demand (including environmental demand), and climate change has rendered both traditional riparian and traditional appropriative rights. For both rights, the difficulty arises from virtue of water being consumed over and over again by different users as it goes through the water cycle. According to Hardin (1968), lack of effective restraint on water use under riparian rights allows, and almost requires, users to exhaust the resource either by withdrawing and consuming the water or by polluting the water. This observation about water use still holds in many places in the United States and around the world.

As stated in detail by Dellapenna (2009), because of very different legal traditions, governments in the 32 riparian rights states and the 18 appropriative rights states have been faced with very different challenges. In riparian rights states, security of investment for water users as well as tightening protections for the public interest in the waters should be provided. In appropriative rights states, the needed flexibility into an increasingly sclerotic system of water rights is introduced while adequate protection to the public interest in waters should also be addressed. Devising proper responses in riparian rights states is easier than the other, because the water rights in riparian rights states are less firmly established than those in appropriative rights states.

State governments have already started to change the established systems of water rights. The 2009 list of current surface water law regime shows four classifications: 8 states such as Arizona,

Colorado, Montana, and Utah follow appropriate rights whereas 16 states such as Alabama, Indiana, Maine, Missouri, and West Virginia have riparian rights. The other 26 states have dual systems (10 states) or regulated riparian (16 states). More than half of the states within the riparian tradition have abandoned traditional riparian rights in favor of publicly managed regulated riparianism. That transition is likely to spread until traditional riparian rights have been entirely changed by regulated riparianism in the 32 states within the riparian tradition. In the 18 appropriative rights states, many claims are being made that markets will solve water management problems. See Anderson and Snyder (1997) for more details. However, it has been demonstrated that true markets for water have only operated at small scales and within a short domain. Indeed, such changes as experienced in the western part of the United States have been the result of state intervention to reallocate water and not for market transitions. Concerns about protecting ecosystems and property rights might also obstruct the construction of new reservoirs or other infrastructure that might be necessary to deal with changes in precipitation patterns and water storage needs. Careful attention to the true dimensions of legal rights might help alleviate these problems, but they are still more politically than legally motivated. See Dellapenna (2009) for more details.

1.16 OVERALL ORGANIZATION OF THIS BOOK

In the following chapters, attempt is made to develop a systems view of hydrologic and hydroclimatic cycle fundamentals and simulation techniques through science, engineering, planning, and management principles. In Chapter 2, the basic concepts from a systems view of the hydrologic cycle are presented. Chapter 3 and 4 introduce different components of the hydrologic and the hydroclimatic cycle, respectively, in the way of their simulation. Due to the importance of the watershed concept in hydrologic analyses, Chapter 5 is dedicated to watershed definition and related concepts regarding its interaction with different hydrologic components, especially runoff. Chapter 6 discusses issues related to runoff analysis as an important component of the water cycle in practical issues of water development as well as planning and management. Chapter 7 introduces the classical issues in groundwater hydrology and hydraulics. Chapter 8 is dedicated to the simulation of hydrologic variables' time series.

Chapter 9 discusses the climate change issue that has significantly altered the hydroclimatic system components and their interrelationships. Chapter 10 is related to the probability, risk, and uncertainty analysis that are commonly used in hydrologic studies. Chapter 11 is an introduction on different simulation techniques including data-driven and physical models. Chapters 12 and 13 discuss two extreme events—flood and drought—in the hydrologic cycle.

PROBLEMS

1. Make an assessment of surface water and groundwater resources around the world and compare them with the U.S. share of total surface water and groundwater resources. Hint: use UNESCO, World's water (www.worldwater.org), World Bank, and USGS sites, and publications.
2. Identify the federal and national agencies directly involved in the management of the hydroclimatic cycle, at least one in each part of the globe.
3. Name the main components of the hydrologic cycle and discuss their relationship.
4. Explain IWRM for the hydrologic cycle in the context of public awareness/participation and consideration of social impacts.
5. What is the estimated water cost for residential customers in the eastern (New York City) and western (Los Angeles) part of the United States? Compare it with the price of water in five other major cities around the world. Is the price of groundwater in selected areas different from surface water resources?

6. Briefly discuss a case of transboundary conflict over shared rivers and lakes.
7. Search and describe the current status of riparian rights and their transition to regulated water laws.
8. Identify and briefly explain factors affecting water supply schemes sustainability.
9. In demand side management, explain the two periods, demand I and demand II, in Figure 1.3.
10. Identify three local (city or county) agencies in the United States or in other countries with the charter of protection and enforcement issues related to surface water resources.

REFERENCES

Anderson, T.L. and Synder, P. (1997). *Water Markets: Priming the Invisible Pump*, Cato Institute, Washington, DC.

Ashton, P.J. and Haasbroek, B. (2002). Water demand management and social adaptive capacity: A South African case study. In *Hydropolitics in the Developing World: A Southern African Perspective*; Turton, A.R. and Henwood, R., eds. African Water Issues Research Unit (AWAIRU), Pretoria, South Africa.

Copeland, C. (2010). Clean Water Act: A Summary of the Law, Congressional Research Service.

Dellapenna, J.W. (1999). "Adapting the law of water management to global climate change and other hydro-political stresses," *Journal of the American Water Resources Association*, 35, 1301–1326.

Dellapenna, J.W. (2009). *Waters and Water Rights*, 3rd Ed., Vol. 1, Beck, R.E. and Kelley, A.K., eds., LexisNexis, Newark, NJ.

Eckholm, E. (1982). *Down to Earth: Environment and Human Needs*, Pluto Press, London.

Falkenmark, M. (2003). *Water Management and Ecosystems: Living with Change*. Global Water Partnership Technical Committee, Global Water Partnership, Stockholm.

FAO (Food and Agriculture Organization of the United Nations) (2003). Review of world water resources by country, Water Reports 23. FAO, Rome, http://www.fao.org//ag/agl/aglw/docs/wr23e.pdf.

Hardin, G. (1968). "The tragedy of the commons," *Science*, 162, 1243–1250.

IPCC (2007). *Fourth Assessment Report, Intergovernmental Panel on Climate Change (IPCC)*. http://www.ipcc.ch/.

IPCC TAR SYR. (2001). Watson, R.T.; and the Core Writing Team, ed., Climate Change 2001: Synthesis Report, Contribution of Working Groups I, II, and III to the Third Assessment Report of the Intergovernmental Panel on Climate Change, Cambridge University Press, ISBN 0-521-80770-0 (pb: 0-521-01507-3).

Karamouz, M., Ahmadi, A. and Akhabri, M. (2011). *Groundwater Hydrology: Engineering, Planning and Management*, CRC Press, Boca Raton, FL.

Karamouz, M., Moridi, A. and Nazif, S. (2010). *Urban Water Engineering and Management*, CRC Press, Boca Raton, FL.

Kresic, N. (2008). *Groundwater Resources: Sustainability, Management, and Restoration*, McGraw-Hill Professional, New York.

McNeill, D. (1998). "Water as an economic good," *Natural Resources Forum*, 22 (4), 253–261.

McPherson, M.B. and Schneider, W.J. (1974). "Problems in modeling urban watersheds," *Water Resources Research*, 10 (3), 434–440.

Rogers, P. and Hall, A.W. (2003). Effective water governance, TEC Background Papers No. 7, Global Water Partnership Technical Committee (TEC), Global Water Partnership, Stockholm.

Seckler, D. (1993). Designing water resources strategies for the twenty-first century. Discussion Paper 16. Water Resources and Irrigation Division, Winrock International, Arlington, VA.

UN (United Nations). (1999). World population prospect: 1998 revision. UN Department of Policy Coordination and Sustainable Development, New York.

UNESCO (2002). Manual of the General Conference, including texts and amendments adopted by the General Conference at its 31st session, Paris.

UNESCO (2006). *Non-Renewable Groundwater Resources*, United Nations Educational, Scientific and Cultural Organization, Paris.

Van der Zaag, P.V. and Savenije, H.H.G. (2006). "Water as an economic good: the value of pricing and the failure of the markets," *Value of Water Research Report Series*.

2 Hydroclimatic Systems

2.1 INTRODUCTION

The study of any phenomenon, process, and/or structure such as climatic systems or the hydrologic cycle requires an integrated approach. The selected framework of study dictates the way an environment is dismantled for analysis. It also determines how to integrate the environmental components so that the results of analysis can be incorporated in a holistic fashion. For providing such a framework, the understanding of system concepts is needed.

The Earth's environment is composed of several systems working together in harmony but with some complex relations and interactions. For a systems approach to hydroclimatology, it is necessary to have a clear understanding of different components of the Earth's system and the positioning of each hydroclimatic system with respect to other systems. This will help to understand and analyze the physical interpretation of different climatic events in global and regional scales.

The traditional knowledge of hydroclimatology focuses on those variables that are more tangible and representative such as temperature and its variations, wind near the surface of the Earth, humidity, cloud characteristics, precipitation in its various forms, and seasonal variability of runoff. However, these variables could not completely define the hydroclimatic systems. The variations in hydroclimatic systems depend on different parameters such as the vertical structure of the atmosphere, the influence of the underlying land and sea, anthropogenic activities, and many other factors that are not fully explained in hydrology books.

To understand the hydroclimatic system of the Earth, all of the elements and components that affect the hydroclimatic system and are affected by them should be considered. In order to do so, the components of the system including dynamics and composition of the atmosphere, the ocean, the ice and snow cover, and the land surface should be analyzed for a better understanding of the underlying behavior. Furthermore, the interactions and the variability in physical, chemical, and biological processes taking place in and among system components need to be addressed. This understanding and knowledge can also be used to develop prediction and early warning systems that are widely used in relation to the behavior of different components of the hydrologic cycle.

In this chapter, after introducing the system concept in general, a brief definition of the different components of the Earth's system as they relate to the hydrologic cycle is discussed to provide the basis for the study of hydrologic principles. Major spatial components of the cycle including watersheds and aquifers are also covered in this chapter.

2.2 GENERAL SYSTEMS' CHARACTERISTICS

Although the word "system" is referred to in different fields, which, at first, may seem to be completely different, there are some common characteristics between different types of systems. The main similarities of systems based on White et al. (1996) are as follows:

1. All systems have an organization with some structure components. In other words, a system is a collection of things that are organized in a specific way and there are connections and links among them. For example, in a hydrologic system, precipitation produces the runoff that flows in rivers and rivers recharge to different water bodies. The evaporated water from these bodies forms clouds, and again they form precipitation.

2. The systems are generalizations, abstractions, or idealizations of what happens in the real world.
3. A function is defined for every system and there are functional and structural relationships between the components of a system.
4. The function of a system determines the flow and transfer of material through the system. This material may be obvious, like the water in the hydrologic cycle, or it may be intangible, such as directives, decisions, ideas, and ideologies.
5. Certain driving forces or energy resources are needed for a system to function. In some systems, this motivation or stimuli is obvious, but in others, it is not clear what the impetus of the forces of supply and demand on people is. In the water cycle, heat is needed for evaporation and the Earth's gravity is one of the driving forces acting during precipitation.
6. Each system has a level of integration.

Different terms are used in relation to the system concepts. The main terms in describing systems are boundary, state, closed system, and open system. A system is separated from the surrounding environment by its boundary. Each system is identified with three kinds of property including elements, attributes, and relationships between elements and states or attributes in its boundary. For example, in a watershed system (as will be described in detail), the watershed boundary, the lower layer of the atmosphere, and the upper layer of the Earth can be considered as the system boundary. A watershed is composed of different elements such as precipitation, subbasins, drainage system, and groundwater where each of them has special attributes. These elements are related to each other in different ways that will be described in future sections. The state of the system is defined when each of its properties (variables), i.e., elements, attributes and relationships, has a definite value. Several distinct types of systems can be distinguished according to the behavior of the system boundary. The main types of systems are as follows:

1. Isolated system: In this kind of system, there is no interaction with the surroundings across the boundary and they could only exist in the laboratory and be used for development of some concepts.
2. Closed systems: These systems are closed with respect to matter, but energy may be transferred between the system and its surroundings. On the Earth, closed systems are rare but it is often useful to treat complicated environmental systems as closed systems.
3. Open systems: Both matter and energy are exchanged with the surroundings in the open system. All environmental systems are open systems and are characterized by the maintenance of structure in the face of continued throughputs of both matter and energy. For example, although there is a continuous throughput of water in a drainage system, it maintains the organization of the stream and river channel network and the contributing slopes.

Since the basis of environmental system function is the laws of thermodynamics, any change in the system state is important. Although, in theory, the initial and final states of a system are considered, in practice, the pathway of system state is often of interest. A process is the way in which a change in system state happens. When the system returns to its initial state after a process, it is called a cycle. Regarding this definition, the hydrologic cycle is the way water vapor in the atmosphere moves through the Earth's system and returns to the atmosphere.

Environmental systems must preserve a stable state regarding their elements, attributes, and relationships through time. This characteristic state is called stationary or steady (Figure 2.1a). When a system is steady, at the macroscopic scale, the system state appears to be stable but the steady state is completely dynamic, and only the average state is stable. For example, although there are considerable fluctuations in the rainfall pattern of a region even through several years and there are some very dry and very wet years, the mean rainfall of the region over the years is almost fixed in the long-term horizon.

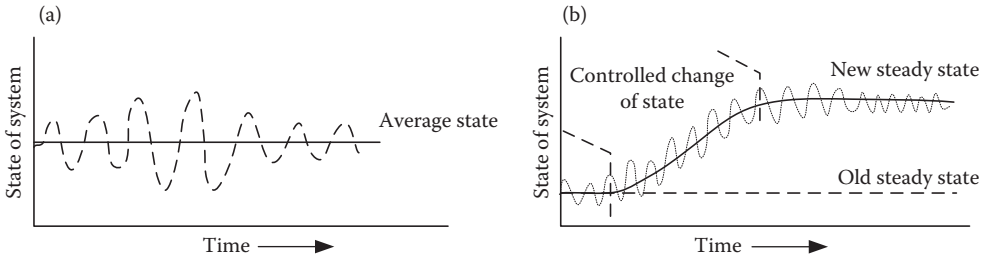

FIGURE 2.1 (a) System maintaining a steady (average) state through time. (b) Controlled change of state from an old to a new steady state effected by positive feedbacks. (From White, I.D. et al., *Environmental Systems*, Chapman and Hall, London, 1996. With permission.)

To maintain an open system in a steady state, it must have the capacity for self-regulation and be affected by some feedback from its surroundings. Negative-feedback mechanisms, which are control mechanisms, affect self-regulation in environmental systems. The result of the processes involved in negative feedback is returning the system to its initial state. For example, the detailed properties of a length of river channel may vary widely about the most effective state, but it will still transfer water and debris.

However, natural systems experience some changes, which are called positive-feedback mechanisms (homeorhetic). These mechanisms have a cumulative effect and cause particular directions of change. Positive feedback has a deviation-amplification character that highly changes the initial state of the system; however, the mechanism of this change may be closely regulated (Figure 2.1b). An example of positive feedback is the climate change impact that has increased mean temperature over time. A composition of positive- and negative-feedback mechanisms is involved in the regulation of natural systems' states.

Due to the cumulative effect of positive-feedback mechanisms, some thresholds are associated with them. Thresholds are state variables that result in sudden or dramatic changes of state when certain values are applied to them. For example, in a soil undergoing decalcification by leaching, when the calcium content reaches zero, the system will be transformed in state and the chemical characteristics of the soil will change rapidly. In other words, thresholds are extreme cases, and other certain state variables that play key roles in controlling the operation of the processes act as regulators.

2.2.1 System Properties

The main specifications of a system are as follows:

- Inputs
- Governing physical laws
- Initial and boundary conditions
- Outputs

Variables and parameters are used for definition of systems' inputs, outputs, and major characteristics. In system dynamics definitions, storage, converters, and connectors are perceived as physical laws and conditions. The system characteristics that vary through time are called variables. A parameter is also a system characteristic that normally does not change with time or can be considered fixed over a period of time. Different values of variables can be viewed as possible states of nature or as alternative futures. Regarding the spatial scale of variables/parameters, they are classified as follows:

- Lumped, which are considered constant in space
- Distributed, which vary in one or more space dimensions

When the source of a contamination in a watershed scale is considered, point and nonpoint sources are examples of lumped and distributed variables. Memory, as an important characteristic of a system, shows the length of time in the past in which variations during that time could have an impact on the output. Different levels of memory are defined as follows:

- Zero memory: Only the input in the present time affects the system state and output.
- Finite memory: The history of the system for a specific time span (memory) can affect the state, output, and behavior of the system.
- Infinite memory: The state and output of the system are dependent on the entire system history.

Strictly, a random number and lag one Markov process are examples of zero and finite/infinite memories, respectively. In another approach of system classification, systems are classified to be deterministic or stochastic. In deterministic systems, the system output for a specific input is always the same, whereas stochastic systems may result in different outputs for a given input because they contain one or more elements for which the relationship between input and output is probabilistic rather than deterministic.

The other detailed classifications of systems are as follows (Karamouz et al. 2003):

- Continuous systems: The system produces a continuous output.
- Discrete systems: The output changes after finite intervals of time.
- Quantized systems: The output values change only at certain discrete intervals of time and hold a constant value between these intervals.
- Natural systems: The system characteristics, including inputs, outputs, and other state variables, vary without any control on their behavior and only can be measured.
- Devised systems: The input of these systems may be both controllable and measurable.
- Simple systems: These systems do not include any feedback mechanism.
- Complex systems: There are complex loops and feedbacks in these systems' behavior.
- Adaptive systems: The performance of these systems is improved based on their history.
- Causal systems: An output cannot occur earlier than the corresponding input (cause and effect).
- Simulation systems: These systems are similar to causal systems providing a realization of environment.
- Stable systems: These systems have bounded output in case of bounded input, and vice versa.
- Damped systems: The output of the system dies out without ever crossing the timescale.

Most of the hydrologic systems are stable and causal systems. Figure 2.2 shows examples of outputs of continuous, discrete, and quantized systems. The outputs for any system depend on both the nature of the components and the structure of the system according to which they are connected. However, in the system approach, concentration is on the system operations that depend on the physical laws and the nature of the system that is represented by the vertical components in Figure 2.3.

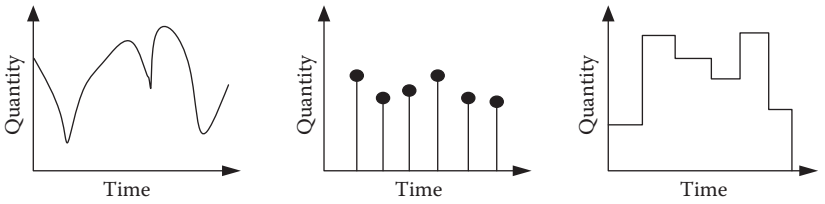

FIGURE 2.2 Outputs of continuous, discrete, and quantized systems. (From Karamouz, M. et al., *Water Resources Systems Analysis*, Lewis Publishers, New York, 2003. With permission.)

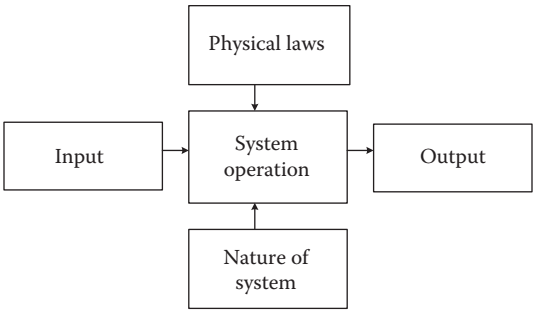

FIGURE 2.3 Specifications of a system. (From McCuen, R.H., *Hydrologic Analysis and Design*, 2nd edition, Prentice Hall, Upper Saddle River, New Jersey, 1997. With permission.)

Considering the three basic components of a system (inputs, system operation, and outputs, Figure 2.3), systems analysts could face several different types of problems (Table 2.1):

- Design problems: In these problems, the system output must be quantified for specified inputs and system structure.
- System identification problems: The system should be specified for given inputs and outputs.
- Detection problems: System and outputs are known and inputs must be identified.
- Synthetic problems (simulation): Inputs and outputs are known and the performance of models must be tested.

Hydrologists primarily deal with design and synthetic problems.

Example 2.1

Consider that temperature prediction is needed for reservoir design. Describe the system concept of this problem in analysis and synthesis stages.

Solution:

In this simplified problem, evaporation is needed for reservoir design; thus, evaporation serves as the output variable. Temperature serves as the input. In the analysis phase, the problem is identification of the model for predicting evaporation; therefore, the model represents all of the hydrologic processes involved in converting temperature (for example, heat energy) to evaporation. Obviously, temperature is only a single measurement of the processes that affect evaporation, but it is a surrogate variable for these processes in the conceptual representation of the system. The synthesis of the system output is used for the reservoir design problem. In summary, in the analysis phase, the temperature (input) and evaporation (output) are known, while in the synthesis phase, the temperature (input) and the model (transfer function) are known.
Note: The definition of system specifications is dependent on the purpose and applications.

TABLE 2.1
Classification for System Problems Based on What Is Given (G) and What Is Required (R)

Type of Problem		Input	System	Output
Analysis	Design	G	G	R
	Identification	G	R	G
	Detection	R	G	G
Synthesis	Simulation	G	G	R

2.3 SYSTEMS MODELING

Environmental systems are extremely complex. The identification of different systems involved in an environmental system helps to understand this complexity, but to analyze a system, it is necessary to simplify it, which is done through employing models. Environmental systems are simplified by construction of models or their replicas. Useful models idealize the system and clarify its structure and functions.

Models are developed to simplify the complex systems of the real world. A model of a system should incorporate the relationships in the system. The relationships in the system and hence in the model can be of several types: spatial distance, causation, conjunction, and succession of events. Some models are static, representing the structure of the system rather than the processes involved within and with its surroundings. However, to understand the functioning of systems, the dynamics of a system should be defined. The dynamic models could identify processes and model their effects on the system. This is particularly the case if the model is to be used to predict the behavior of the system; for example, a drainage basin model is used to predict flood hazard.

2.3.1 Model Resolution

The level of resolution of the models is dependent on the selected scale for study of the system. With fine resolution, reality is better resembled, and with coarse resolution, there is a gain in generality. The summarized model of the system cannot be truly the same as reality because it lumps together elements and relationships and valuable information inside each part is ignored.

Egler (1964) called this the "meat grinder" approach and compartment models. Each part of these models is treated as a black box, which can be defined as any unit whose function may be evaluated without specifying the contents. Models with very low resolution are composed of a few number of relatively large black box compartments and the entire system can be treated as a black box. By increasing the resolution level of the model, the size of the black box compartments decreases and their number increases. Models with an intermediate level of resolution are called gray box models and provide a partial view of the system. When most of the elements, states, relationships, and processes of the system are identified and incorporated in the model, the gray box becomes a white box. It should be noted that because a model could not be a complete representation of reality, even in a white box model, there are some black box components (Figure 2.4).

Example 2.2

Consider that simulation of produced runoff through a watershed is needed for a reservoir design. Discuss different modeling resolutions that could be applied for this purpose.

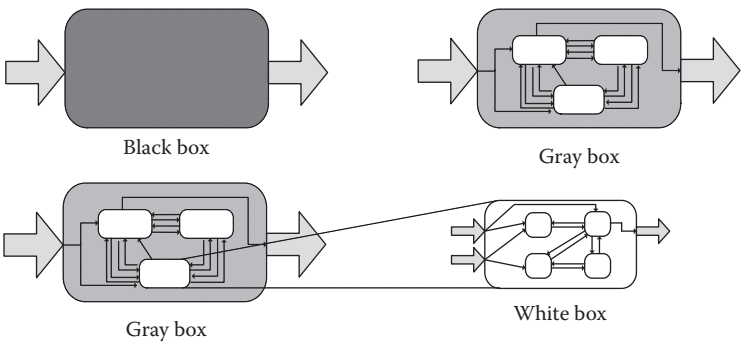

FIGURE 2.4 Levels of resolution in the modeling of systems. (From White, I.D. et al., *Environmental Systems*, Chapman and Hall, London, 1996. With permission.)

Solution:

Data availability and accessibility with different levels of resolution can be mentioned for this purpose. In cases with limited data and measurements of watershed properties, the black box models are preferred. For this purpose, different data-driven models such as artificial neural network, Fuzzy set theory, and statistical time series framework can be utilized. When some data on watershed characteristics and elements are available, some lumped rainfall–runoff models can be employed and the process of transformation of rainfall to runoff can be clarified. In this case, a gray box is developed. If there are enough detailed data about characteristics of watershed, complicated distributed models could be used to provide a level of white box models. However, it should be noted that it would not be a completely white box model. The details of the mentioned modeling approaches are given in the next sections.
Note: Data availability and accessibility as well as knowledge about the system function are the main factors in decision making about the level of resolution of the system model.

With this general description of systems, we are trying to follow a system approach in the rest of this chapter (as well as in the rest of this book). This can promote system thinking in hydrologic analysis, design, prediction, and simulation.

2.4 EARTH SYSTEM

One of the advantages of building system models is that they simplify the complexity of the real world. Using the concepts described in the previous sections, the Earth could be modeled as a closed system whose only interaction with its surrounding is the transfer of energy across its boundary. The boundary of this system is the outer surface of the atmosphere. This can be considered as a black box model.

The energy, at any point in time, is being transferred or stored within the Earth or its atmosphere. This is because with any closed system, the balance of energy exchange not only is a function of relative surface temperatures and absorbance and emittance characteristics of all parts of the system but also depends on modes of energy transfer other than radiation. These are conduction and convection as well as energy-dependent changes of state, such as the evaporation of water and linking latent heat exchange. Thus, although a long-term energy balance may exist for the whole system, there will still be energy imbalances, transfers, and changes in energy storage within the system.

Therefore, for better understanding of the energy balance of the Earth, the black box approach should be improved in order to follow the way energy is transferred or cascaded through the major subsystems of the Earth, each of which can be considered as an energy store. Figure 2.5 contains separate compartments of the atmosphere, for Earth surface systems, and for the Earth's interior. Each of these compartments can be considered as an open system, with transfers of matter as well as energy across its boundaries.

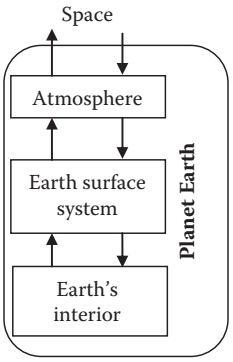

FIGURE 2.5 Schematic view of the Earth system.

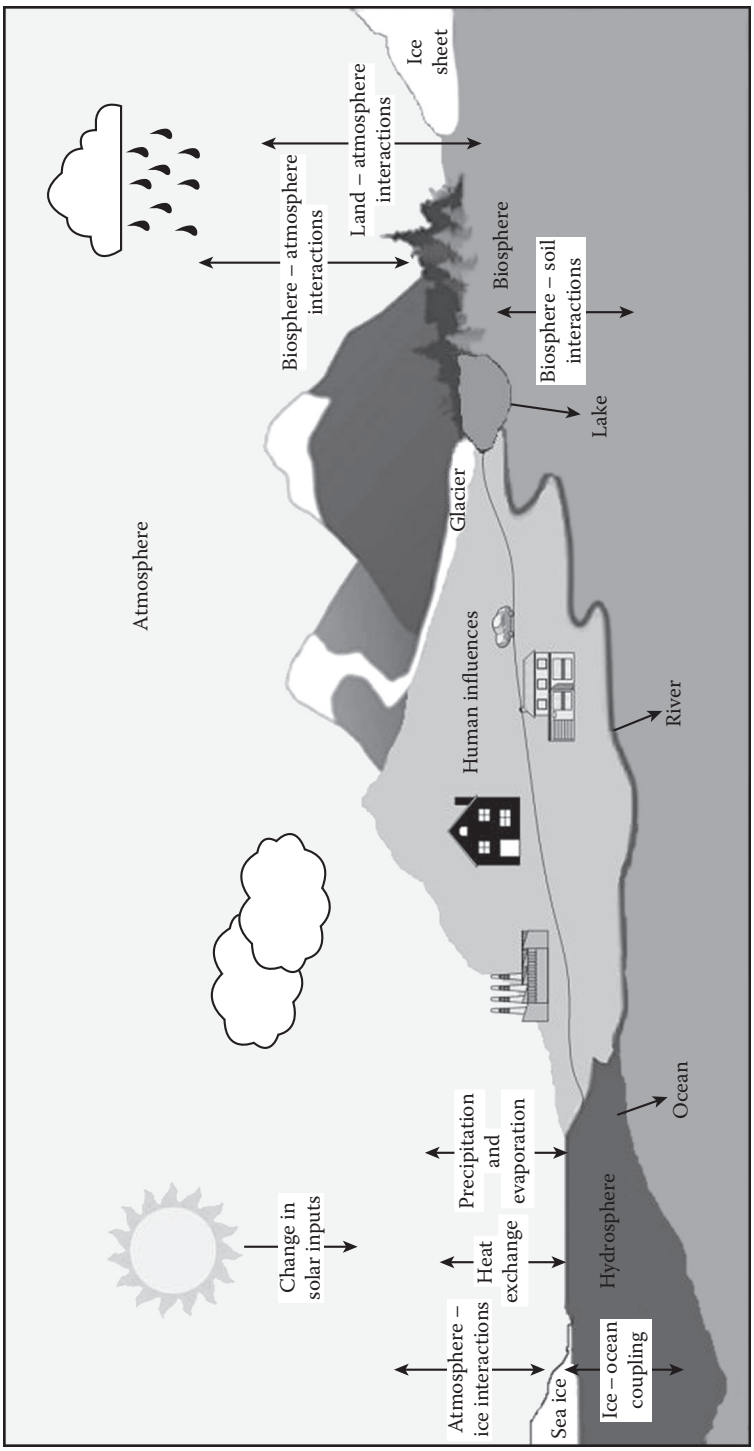

FIGURE 2.6 Schematic view of the hydroclimatic system. (From Intergovernmental Panel on Climate Change [IPCC], *Climate Change 2007: The Physical Science Basis*, Cambridge University Press, Cambridge and New York, 2007. With permission.)

The planet systems in the hydrologic cycle are atmosphere (the gaseous envelope encompassing the Earth) and Earth surface systems including hydrosphere (liquid water including ocean, lakes, underground water, etc.), lithosphere, and biosphere (all the living organisms) (Figure 2.6). The litosphere also includes some interior parts of the Earth system. Each of these systems is described in the next sections.

2.5 ATMOSPHERE

The Earth's atmosphere is a complex fluid system of suspended particles and gases. Chemical and biochemical reactions have derived the atmosphere from the Earth itself. The boundaries of the atmosphere are not easily specified, although in this fluid system, shapes of gases envelope the Earth. They can be arbitrarily delimited as the interface of Earth/atmosphere and atmosphere/space, but it should be mentioned that these are excessive simplifications. For example, although there is a zone of transition where the Earth and solar atmospheres merge, the atmosphere does not have any external edge. Also, at the Earth/atmosphere interface, the atmosphere penetrates into the pore spaces and voids between the soil particles and regolith and is continuous with the so-called soil atmosphere.

Gases such as nitrogen, oxygen, argon, carbon dioxide, and water vapor make up 99.9% of the total volume of the atmosphere. Other elements of this system are suspended particles such as dust and soot, water droplets, and the minor gases.

Through the atmosphere, the various gases' proportions change very slowly over time, but they show separate vertical divisions. Certainly, the preceding discussion has implied that the atmosphere is not uniform, and the distribution of the component elements indicates that it has a layered structure. This vertical constituent of the atmosphere structure can be related mainly to the distribution of absorption of radiant energy and can be described in terms of the temperature variable.

According to major changes in temperature, the atmosphere is divided into layers; these layers are shown in Figure 2.7. On the Earth's surface, gravity pushes down the air layers; this push is called air pressure. Ninety-nine percent of the atmosphere's total mass is below 32 km.

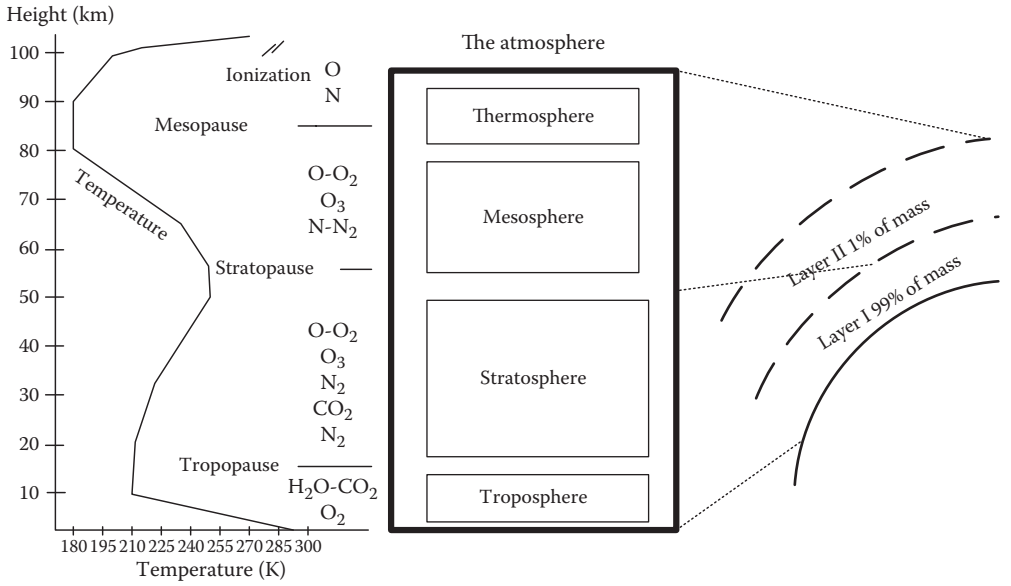

FIGURE 2.7 Model of the vertical structure of the atmosphere. (From White, I.D. et al., *Environmental Systems*, Chapman and Hall, London, 1996. With permission.)

The troposphere, which extends from 0 to 12 km, contains 75% of the gases in the atmosphere. This is where weather occurs; as height increases, temperature decreases. The temperature drops about 6.5°C for every kilometer above the Earth's surface.

At the top of the troposphere, the tropopause is located. In this zone, the temperature remains fairly constant. This layer divides the troposphere from the stratosphere. In this zone, jet streams, extremely strong winds that blow eastward, are observed.

The stratosphere is between 12 and 50 km in height. The temperature remains fairly constant about –60°C. This layer contains the ozone layer. Ozone acts as a shield in the Earth's surface. It absorbs ultraviolet radiation from the sun. This causes a temperature increase in the upper part of the layer.

The mesosphere extends from 50 to 80 km in height. The temperature drops about –100°C in this layer. This is the coldest region of the atmosphere. This layer protects the Earth from meteoroids by burning them up.

The thermosphere begins at a height of 80 km. The air is very thin in this layer. "Heat sphere" is the meaning of thermosphere. In this layer, the temperature is very high because ultraviolet radiation is turned into heat (temperatures often reach 2000°C or more). This layer contains the following:

1. The ionosphere is the lower component of the thermosphere. It extends from about 80 to 550 km. Gas particles absorb X-ray and ultraviolet radiation from the sun. The gas particles become electrically charged (ions). Radio waves are bounced off the ions and reflect waves back to Earth. This generally helps radio communication. However, the number of ions is increased by solar flares. These ions can interfere with some radio wave transmissions.
2. The upper section of the thermosphere is the exosphere. It extends from about 550 km to thousands of kilometers and the air is very thin in this part. In this area, satellites orbit the Earth.

Atmospheric specific humidity also displays a characteristic vertical profile with maximum values in the lower levels and with a considerable decrease in height. The air above the tropopause is nearly dry as a consequence. This vertical division is primarily due to two processes. First, at the surface, evaporation is the main source of atmospheric water vapor. Secondly, a much larger quantity of water is in the warmer air close to the surface. Saturation also leads to the formation of water or ice droplets, clouds, and eventually precipitation. Because of the higher incoming radiations, the temperature reaches its maximum in equatorial regions at the surface of the Earth. In these regions, temperature is relatively constant throughout the year.

At mid- and high latitudes, the north–south gradients are much larger in winter than in summer, because of the much stronger seasonal cycle. The distribution of the surface temperature is also influenced by atmospheric and oceanic heat transport as well as by the thermal inertia of the ocean. Moreover, at higher altitudes associated with the positive lapse rate in the troposphere, the topography role is important.

The governing equations describing movement of air and conservation of energy and momentum, mass and water vapor in the atmosphere are as follows:

1. Conservation of mass equation:

$$\frac{\partial}{\partial t}\int_{cv}\rho d\forall + \int_{cs}\rho \mathbf{V}\bullet \hat{n}dA = 0 \tag{2.1}$$

2a. Linear momentum equation:

$$\frac{D}{Dt}\int_{sys}\left(\mathbf{V}\rho\delta\forall\right) = \delta\mathbf{F} \tag{2.2a}$$

2b. Moment of momentum equation (Newton's second law):

$$\frac{\partial}{\partial t}\int_{cv}(\mathbf{r}\times\mathbf{V})\rho d\forall + \int_{cs}(\mathbf{r}\times\mathbf{V})\rho\mathbf{V}\bullet\hat{n}\,dA = \sum_{\text{contents of the control volume}}(\mathbf{r}\times\mathbf{F}) \tag{2.2b}$$

3. Conservation of energy equation:

$$\frac{D}{Dt}\int_{sys}e\rho d\forall = \left(\dot{Q}_{\text{net in}} + \dot{W}_{\text{net in}}\right)_{sys} \tag{2.3}$$

4. Ideal gas law:

$$p = \rho RT \tag{2.4}$$

where ρ is the atmosphere density, $\forall$ is the volume, $\mathbf{V}\bullet\hat{n}dA$ is the volume flow rate through dA, $\mathbf{V}$ is the velocity, $\mathbf{F}$ is the resultant force, $\mathbf{r}$ is the position vector from the origin of the inertial coordinate system, e is the total stored energy per unit mass, $\dot{Q}_{\text{net in}}$ is the net rate of heat transfer into the system, $\dot{W}_{\text{net in}}$ is the net rate of work transfer into the system, t is time, p is pressure, R is gas constant, and T is temperature. For atmosphere modeling, vertical and horizontal grids are defined, which form different elements. These equations are solved with defined values of divergence terms at each grid point and defined input and output for upper and lower surfaces of the variable for each defined element of the atmosphere.

Some simplifications and approximations are made before using these equations in models. The first approximation is hydrostatic equilibrium, which provides a considerable simplification of the equation of motion along the vertical dimension. Secondly, the time variation of the density is neglected compared to the other terms of the continuity equation, filtering the sound waves. However, supplementary equations for the liquid water content of atmospheric parcels or other variables related to clouds are often added to this set of equations.

These equations do not form a closed system. First, the frictional force and the heating rate must be specified, which needs a detailed analysis of the radiative transfer in the atmosphere, accounting for both the long-wave (i.e., radiation from the Earth >3 μm) and the short-wave (solar radiation <3 μm) radiation as well as of the heat transfers associated with evaporation, condensation, and sublimation. The influence of clouds in these processes usually causes a considerable uncertainty in modeling results. Then, the models can only adequately resolve some of the processes that are included in the equations. Therefore, some important processes that occur at scales that could not be resolved by the model grid need to be parameterized. For equations that describe the interactions between the atmosphere and the other components of the climate system, the boundary conditions should be specified.

2.5.1 General Circulation of the Atmosphere

At the equator, the high temperatures make the air less dense. It thus tends to ascend before being transported poleward at high altitudes in the troposphere. This motion is compensated for at the surface by an equator-ward displacement of the air. On a motionless Earth, this big convection cell would reach the poles, impelling direct exchanges between the warmest and coldest places

on Earth. However, due to the Earth's rotation, such an atmospheric structure would be unstable. Consequently, the two cells driven by the ascendance at the equator, called the Hadley cells, close with a downward branch at a latitude of about 30° (Figure 2.8). The northern boundary of these cells is signaled by strong westerly winds in the upper troposphere called the tropospheric jets. The Earth's rotation is responsible for a deflection toward the right in the Northern Hemisphere at the surface and due to the Coriolis force toward the left in the Southern Hemisphere of the flow coming from the mid-latitudes to the equator. This results in easterly trade winds characteristic of the tropical regions (Figure 2.9).

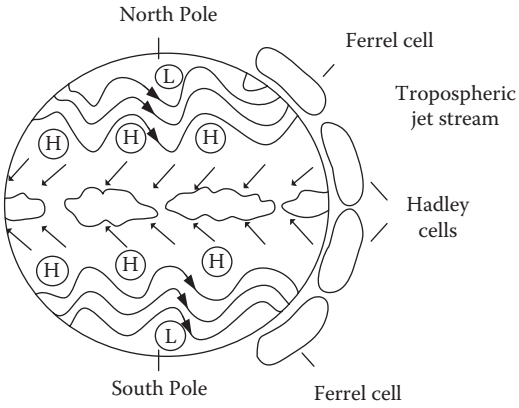

FIGURE 2.8 Schematic representation of the annual mean general atmospheric circulation. H (L) represents high (low)-pressure systems. (From Wallace, J.M. and Hobbs, P., *Atmospheric Science: An Introductory Survey*, Copyright 2006, with permission from Elsevier.)

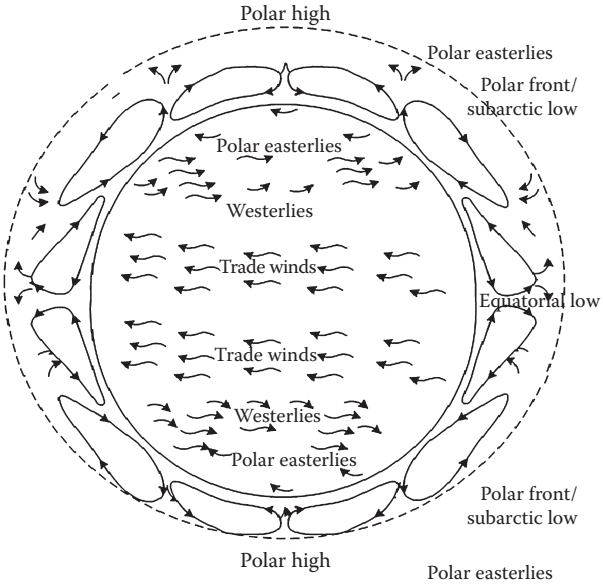

FIGURE 2.9 Idealized circulation of the atmosphere at the Earth's surface under effect of the Coriolis force. (From Marsh, W.M.: *Earthscape: A Physical Geography*. 1987. Copyright Wiley-VCH Verlag GmbH & Co. KGaA. Reproduced with permission.)

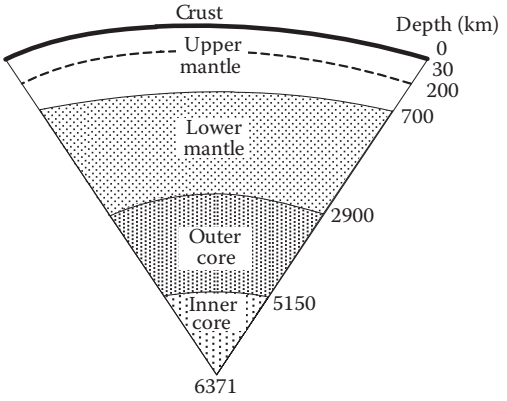

FIGURE 2.10 Schematic section through the crust, mantle, and core. (From White, I.D. et al., *Environmental Systems*, Chapman and Hall, London, 1996. With permission.)

The extra-tropical circulation is commanded at the surface by westerly winds whose zonal symmetry is disturbed by large wave-like patterns and the continuous succession of disturbances that governs the day-to-day variations in the weather of these regions. The dominant characteristic of the meridional circulation at those latitudes is the Ferrel cell (Figure 2.10), which is weaker than the Hadley cell. As it is described by rising motion in its poleward branch and downward motion in the equator branch, it is called an indirect cell by contrast with the Hadley cell, which is termed a direct cell.

2.6 LITHOSPHERE

The lithosphere includes the crust and the uppermost mantle, which constitute the hard and rigid external layer of the Earth. For very long geologic time periods, the lithosphere remains rigid in which it deforms elastically and through brittle failure. The lithosphere is broken into tectonic plates. Through the soil-forming process in the pedosphere, the uppermost part of the lithosphere reacts to the hydrosphere, biosphere, and atmosphere.

The lithosphere theory was based on the presence of significant gravity anomalies over the continental crust, from which there is a strong upper layer (the lithosphere) above a weaker layer that could flow (the asthenosphere). Daly (1940) expounded these concepts, and geologists and geophysicists have broadly accepted them. The lithosphere provides a conductive lid on the convecting mantle; as such, it affects heat transport through the Earth. There are two lithosphere types that are described:

1. Oceanic lithosphere, which is associated with and exists in the ocean basins and oceanic hard layer
2. Continental lithosphere, which is connected with continental crust

The thickness of the lithosphere is considered to be the depth to the isotherm associated with the transition between brittle and viscous behavior. The temperature at which olivine begins to deform viscously (~1000°C) is often used to set this isotherm because olivine is generally the weakest mineral in the upper mantle. The oceanic lithosphere is typically about 50–100 km thick, while the continental lithosphere has a range in thickness from about 40 km to perhaps 200 km; the upper ~30 to ~50 km of typical continental lithosphere is crust. In comparison with the other layers, it should be noted that the crust is very thin and constitutes only 1.55% of the Earth's total volume. This thin layer and its primarily surface characteristics have significant interactions with the hydrologic cycle.

This lithosphere structure differs in mineralogical and chemical composition, and physical properties evolved from the aggregation of originally uniform particles by the differentiation process under the influence of gravity. The least dense materials became segregated in the thin outer shell of the crust, while the denser iron and nickel settled towards the center of the Earth to form the core.

2.6.1 Crustal System

The lithosphere can be regarded as a system whose concentric boundaries are the external surface of the discontinuity and solid Earth within the mantle. The external boundary forms a complex boundary with the hydrosphere and atmosphere. Also, it is the environment in which life has evolved. The central boundary is adjacent to rock, which is near its melting point and is capable of motion relative to the lithosphere above. This system is called the crustal system (see Figure 2.10). The inner section of the Earth has three parts with different characteristics: crust, mantle, and core. The crust, on which we live, is the thinnest layer (with an average thickness of 30 km) and constitutes about 1.5% of the Earth's volume. The bulk mass of the Earth is composed of the mantle. What is called the crustal system includes the upper layer that mainly includes the crust. This is an open system and there are matter exchanges as well as energy across both its outer and inner boundaries. At its external boundary, the crustal system is responsible for the structure and division of the ocean basins and continents for the main relief units within them. As a prelude, therefore, to a closer examination of the systems operating at the Earth's surface, the transfer of matter and energy within the crustal system and across its boundaries is considered.

2.7 BIOSPHERE

At the top of the lithosphere, throughout the hydrosphere, and into the lower atmosphere lies a transition zone that contains and is created by an enigmatic arrangement of matter that we know as life. The existence of a global veneer of life (not forgetting the dead and decaying remains of that which once was alive) is undoubtedly the most profound feature of the surface of the planet.

Life far outweighs its small relative mass in the significance of its effect on the nature of the lithosphere, hydrosphere, and atmosphere. This living veneer is termed the biosphere, and the biosphere together with the transition zone that supports it and with which it interacts is called the ecosphere (Cole 1958; Hutchinson 1970). Hence, the ecosphere model includes the physical systems already discussed, namely, the upper part of the lithosphere, a major part of the atmosphere, and most of the hydrosphere, to the extent that they have functional links involving transfers of energy and matter with the living material of the biosphere.

The biosphere at the global level can be treated as one large living system containing all living material on the planet. Estimates of the number of different kinds of organisms constituting the biosphere range between 2 and 4 million, and the notion of "life" encompasses a vast spectrum of phenomena associated with all of these organisms. Fortunately, there are certain characteristics to be found in the simplest forms, which also prove essential for the most complex ones. The simplest organisms consist of a single cell and even the most complex consists of comparatively few cell types. The cell has therefore come to be regarded as the simplest independent structure that possesses all of the necessary properties of life. In attempting to answer these questions, therefore, it is appropriate to model the biosphere in terms of the structural and functional organization of the living cell. Therefore, the molecular basis is considered for cellular activity investigation. Fortunately, cells contain relatively few types of molecules and, although these include the most complex molecular structures known, many are universal in their occurrence in the biosphere.

2.8 THE HYDROSPHERE

"Water sphere" is another name for the hydrosphere. It includes all the Earth's water found in the lakes, soil, groundwater, streams, and air. Hydrosphere water is distributed among several different

stores found in the other spheres. Water is held in lakes, oceans, and streams at the Earth's surface. Water is found in vapor, solid, and liquid states in the atmosphere. By plant transpiration, the biosphere serves as an interface between the spheres, enabling water to move between the lithosphere, hydrosphere, and atmosphere as is accomplished. The hydrologic cycle traces the movement of energy and water between these spheres and stores.

The hydrosphere is always in motion like the atmosphere. The motion of streams and rivers can be seen, while the water motion within ponds and lakes is less obvious. These motions are in the current form that moves the warm waters in the tropics toward the poles and colder water from the Polar Regions toward the tropics. At great depths in the ocean (up to about 4 km), these currents exist on the ocean surface.

The ocean characteristics that affect its motion are its salinity and temperature. Warm water is lighter and therefore tends to move up toward the surface, while colder water is heavier or dense and therefore tends to sink toward the bottom. Salty water is also heavier or dense and thus tends to sink, while less or fresh salty water is lighter and thus tends to rise toward the surface. The combination of the water's temperature and salinity determines whether it rises to the surface, sinks to the bottom, or stays at some intermediate depth.

Also, the currents of oceans are affected by the atmosphere motion or winds above it. The energy in the wind gets transferred to the ocean at the ocean surface affecting the motion of the water there. At the ocean surface, the wind effect is the largest motion.

The ocean serves two major principles in the climate system:

1. It is a large chemical reservoir that can contribute to the greenhouse effect in the atmosphere and energy, absorbing 90% of the solar radiation that hits the surface. This reservoir changes so slowly, limiting how fast the climate can change.
2. It works with the atmosphere to redistribute the energy received from the sun like the heat in the topics, where it receives a lot of energy from the sun, transferring it toward the poles, where heat is generally lost to space.

2.8.1 Hydrologic Systems

Chow et al. (1988) defined a hydrologic system as a structure or volume in space with specified boundaries that have some inputs such as water on them internally and some outputs. The structure or volume in space is the totality of the flow paths through which the water may move from the entry point of the system to the end point. The boundary is a continuous surface defined in three dimensions enclosing the volume or structure. A working medium enters the system as input, interacts with the structure and other media, and leaves as output. Physical, chemical, and biological processes operate on the working media within the system. The most common working media considered in hydrologic analysis are water, air, and heat energy.

The global hydrologic cycle is composed of three subsystems: the atmospheric water system, the surface water system, and the subsurface water system, as shown in Figure 2.11. Another example is the storm–rainfall–runoff process on a watershed, which can be represented as a hydrologic system. The input is rainfall distributed in time and space over the watershed and the output is streamflow at the watershed outlet. The boundary is defined by the watershed divide and extends vertically upward and downward to horizontal planes.

2.8.2 Hydrologic System and Modeling Approaches

Complex systems are divided into subsystems, each having an input–output linkage as a component. The hydrologic systems are a subsystem of water resources that represents physical functioning of that system in a region. By analogy, a hydrologic system is defined as a structure or volume in space, surrounded by a boundary, that accepts water and other inputs, operates on them internally, and produces them as outputs (Chow et al. 1988).

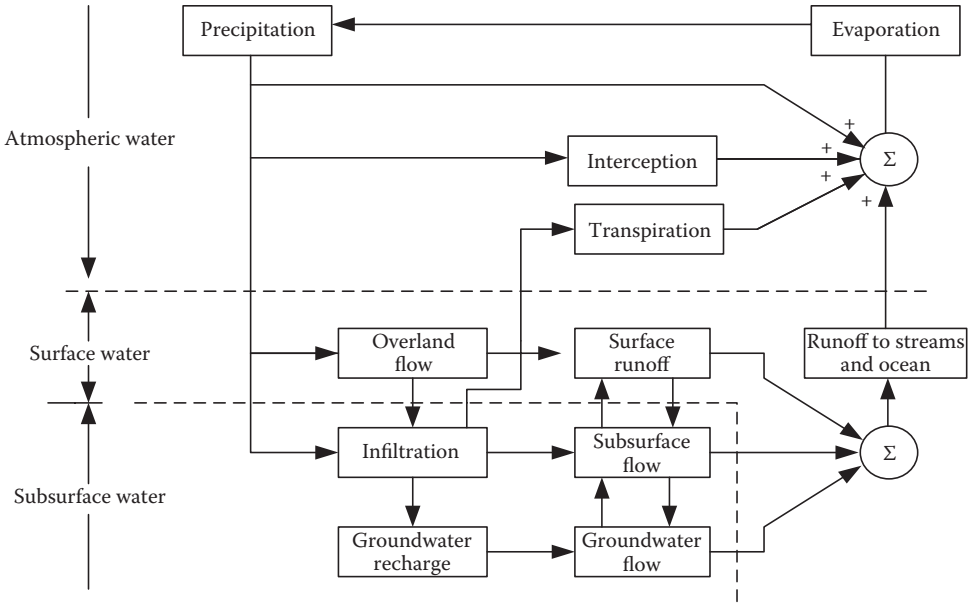

FIGURE 2.11 Block-diagram representation of the global hydrologic system. (From Chow, V.T. et al., *Applied Hydrology*, McGraw-Hill, New York, 1988. With permission.)

Two approaches are considered for modeling hydrologic systems:

1. Theoretical approach, which models the physical components of a system
2. Empirical approach, which uses historical observations of different components of the hydrologic cycle to model its behavior

More accurate models and outputs have resulted using the theoretical approach and it improves the knowledge about different hydrologic events. The difficulty in using theoretical approach is the lack of accurate information about inputs of the system and a wide range of natural complexities.

For developing models, the systems should be simplified. Loucks et al. (1981) refer to model development as an art in which model should provide an abstraction of the real world of the components that are important to the decision-making process. Mathematical models, as a kind of model developed using the empirical approach, can be classified into the following categories regarding the way they deal with relations between components and variables:

- Empirical versus theoretical
- Lumped versus distributed
- Deterministic versus stochastic
- Linear versus nonlinear

2.8.3 Hydrologic Variables and Parameters

All natural physical processes are subject to variability. For example, rainfall intensity, flood magnitude, or low flows in droughts have wide variations. To study these variations and incorporate them in the planning and operation of water resources, engineers gather and investigate data samples.

The hydrologic cycle is composed of various phenomena, such as precipitation, runoff, infiltration, evaporation, evapotranspiration, and abstraction. Different characteristic variables, which can

simply be called hydrologic variables, have been defined to describe each of these phenomena. Depth or intensity of rainfall in different time steps of a rainstorm, monthly inflow discharge to a reservoir, and daily evaporation are some examples of hydrologic variables (Shahin et al. 1993). A data set consists of a number of measurements of a phenomenon, and the quantities measured are variables.

A continuous variable can have any value on a continuous domain; examples include volume of water flowing in a river or the amount of daily evaporation measured in a climatic station. A discrete variable represents an interval or the number of occurrences within each interval of time and space; the number of rainy days in a certain period of time (e.g., a year) is an example of a discrete hydrologic variable.

Hydrologic variables can also be classified as qualitative or quantitative. A qualitative variable can be expressed as a real number in a sensible way; type of soil is an example of a qualitative hydrologic variable. The number of rainy days in a year and rainfall intensity in a day are examples of discrete and continuous quantitative hydrologic variables, respectively.

Hydrologic variables usually vary in time and space. A time series is a sequence of values arranged in order of their occurrence in time. Conflicts can arise upon analysis of the impact of various hydrologic variables on each other and modeling them during the decision-making process.

2.9 HYDROLOGIC CYCLE

The hydrologic cycle is defined as "the pathway of water as it moves in its various phases through the atmosphere, to the earth, over and through the land, to the ocean, and back to the atmosphere" (National Research Council 1991). The hydrologic cycle can be considered as a closed system because the total amount of water on Earth is constant. The hydrologic cycle generally includes six major components, as shown in Figure 2.12:

Precipitation
- Precipitation on the ocean
- Precipitation on ice
- Precipitation on land

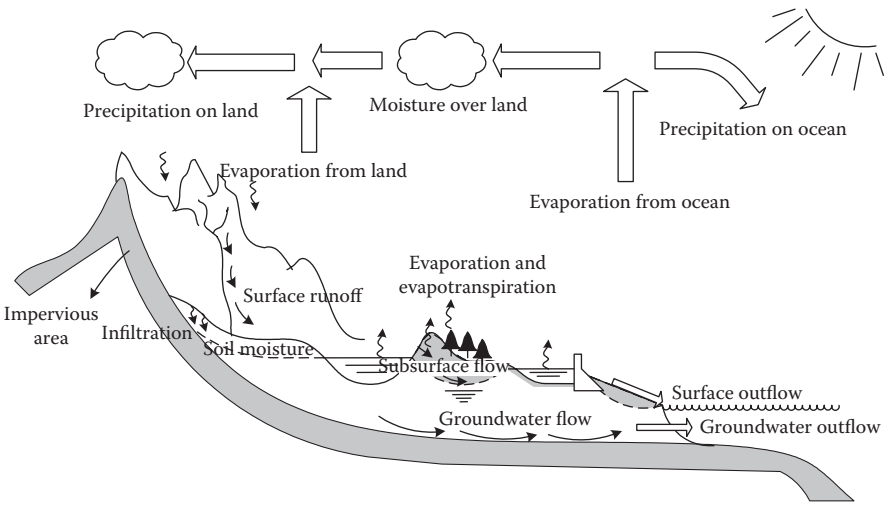

FIGURE 2.12 Hydrologic cycle at the global scale. (From U.S. National Research Council, *Opportunities in the Hydrologic Sciences*, National Academy Press, Washington, DC, 1991. With permission.)

Infiltration
Evaporation
    Evaporation from ocean
    Evaporation from ice
    Evapotranspiration from plants
    Evaporation from soil moisture
Surface runoff
Subsurface flow
Groundwater flow

The surface water budget (ΔS_s) and groundwater budget (ΔS_g) in a hydrologic cycle are estimated as follows:

$$\Delta S_s = P_1 + R_{in} - R_{out} + R_g - T_s - I \tag{2.5}$$

$$\Delta S_g = G_{in} - G_{out} - R_g - E_g + I \tag{2.6}$$

where R_{in} and G_{in}, and R_{out} and G_{out} represent the surface and groundwater inflows and outflows, respectively. Surface inflow in Figure 2.12 is an interbasin water transfer. R_g and E_g are groundwater appearing as surface runoff and evaporation from soil moisture. P_l, T_s, and I are precipitation, evapotranspiration from surface water resources, and infiltration, respectively.

Example 2.3

Describe the system concept of the hydrologic cycle.

Solution:

A schematic system view of the hydrologic cycle is shown in Figure 2.13a, which is a high degree of abstraction from the actual hydrological cycle. In this schematic, all the land surface and ocean surface have been taken as single elements and the complexities of local variation have been ignored. This abstraction is commonly used in classical hydrology to deal with the problems of hydrological analysis and synthesis.

The hydrological cycle as shown in Figure 2.13a is a system that operates as a result of the surplus of incoming radiation over back radiation. Therefore, if the cycle is seen as a system involving energy changes, the hydrological cycle is an open system. On the other hand, the hydrological cycle is a closed system if the hydrological cycle is only considered in terms of the movement of moisture. This closed system involves the transfer and transformation of water as the main concern of hydrologists.

The movement and storage of water are described conceptually by the hydrologic cycle. Snowfields, soils, glaciers, rivers, oceans, lakes, and the atmosphere are media for water storage in this cycle. Water flows from one medium to another through many processes. These processes include evaporation, condensation, precipitation, melting, infiltration, transpiration, runoff, and groundwater flow.

To describe how the hydrologic cycle is affected by external factors, it can be represented as a system in a watershed scale with different land uses (see Section 2.10 and Example 2.7). The interdependencies in such a watershed, as shown in Figure 2.13b, have changed the components and the processes affecting the hydrologic cycle. These interdependencies, mostly anthropogenic, have ripple effects on a subset of the hydrologic cycle, namely, the urban water cycle. Figure 2.13b is an overlay of four layers of components, links and correlations (processes), interdependencies, and externalities. Externalities are costs and benefits transmitted across the system as negative and positive implications of the system's component interaction and anthropogenic activities. Hence, to summarize, the hydrologic cycle as an open vapor/water/matter circulation system should be

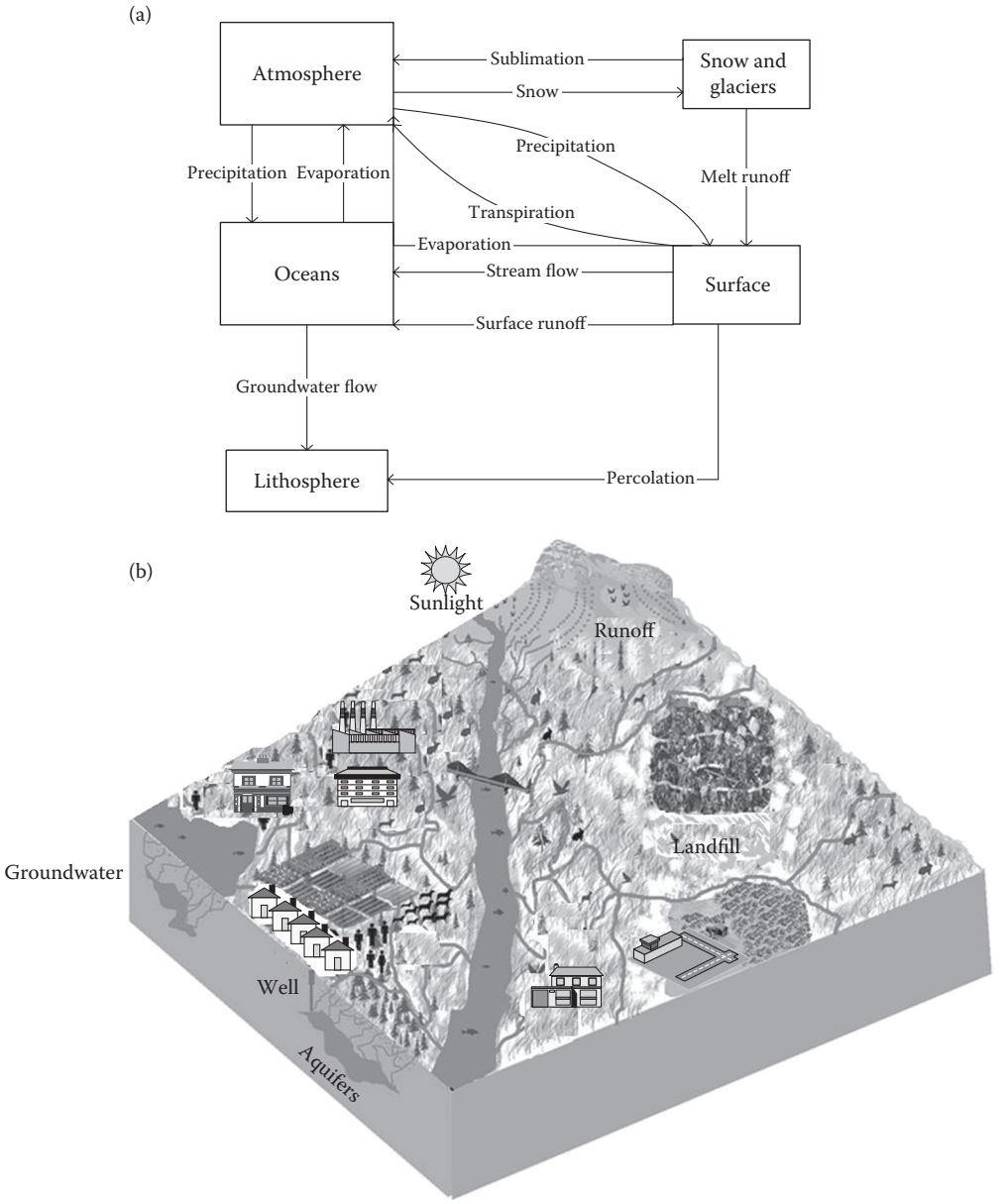

FIGURE 2.13 Hydrologic cycle. (a) Systems representation. (b) Interdependencies in watershed scale.

presented in a watershed scale and its subset of urban water cycle should be looked at as a hot spot (because of heat island forms in urban areas) as the temperature and pollution have intensified variations and impacts in these regions.

Example 2.4

The inflow and outflow rates to a river reach of 1500 m in length are 4 m^3/s and 3 m^3/s, respectively. Assume that precipitation and evaporation are zero and a flow of 0.5 m^3/s charges the groundwater. For a period of 10 min, calculate the water level change in the considered river reach with an average width of 16 m.

Solution:

The rate of change in storage based on Equation 2.5 equals 0.5 m^3/s or 300 m^3 during a 10 min period:

$$\Delta S_s = 0 + 4 - 3 - 0.5 - 0 - 0 = 0.5 \text{ m}^3/\text{s}$$

Since the river charges the groundwater, the groundwater flow is used as a negative value.

Since the inflow is greater than the outflow, the water surface elevation will rise. The increased storage would cause the water surface elevation to rise by $0.5 \times 10 \times 60$ $m^3/[16 \text{ m } (1500 \text{ m})] = 0.75$ m over the 10 min period.

According to the U.S. National Research Council (1991), on a global average, about 57% of the precipitation that falls on the land returns directly to the atmosphere, without reaching the ocean. The remainder is runoff, which flows toward the sea primarily by rivers as well as through subsurface (groundwater) movement and by the calving of icebergs from glaciers and ice shelves. In this gravitationally powered runoff process, the water may remain for a time period in one or more natural storage reservoirs such as snow, glaciers, ice sheets, lakes, streams, soils and sediments, vegetation, and rock. Evaporation from these reservoirs short-circuits the global hydrologic cycle into subcycles with a broad spectrum of scale. The runoff is perhaps the best-known element of the global hydrologic cycle, but even this is subject to significant uncertainty. The oceans hold about 97% of the world's water supply by volume held in. The other large reserves are groundwater (4%) and icecaps and glaciers, which provide about 4% and 2%, respectively, with all other water bodies together accounting for a fraction of 1%. Water residence times (the time of complete water replacement in a component) in these storage systems vary from several thousand years in the oceans to a few days in the atmosphere (Table 2.2).

The hydrologic variables are continuous or discrete depending on the nature of described phenomena. A continuous variable can have any value on a continuous domain, such as volume of water flowing in a river or the amount of daily rainfall measured in a climatic station. An interval or the number of occurrence within each interval of time and space is represented by a discrete vari-

TABLE 2.2
Estimate of World Water Balance

	Surface Area (million km^2)	Volume (million km^3)	Volume (%)	Equivalent Depth (m)	Residence Time
Oceans and seas	361	1370	94	2500	~4000 years
Lakes and reservoirs	1.55	0.13	<0.01	0.25	~10 years
Swamps	<0.1	<0.01	<0.01	0.007	1–10 years
River channels	<0.1	<0.01	<0.01	0.003	~2 weeks
Soil moisture	130	0.07	<0.01	0.13	2 weeks to 50 years
Groundwater	130	60	4	120	2 weeks to 100,000 years
Icecaps and glaciers	17.8	30	2	60	10 to 1000 years
Atmospheric water	504	0.01	<0.01	0.025	~10 days
Biospheric water	<0.1	<0.01	<0.01	0.001	~1 week

able. For example, the number of cloudy days in a certain period of time like a month is a discrete hydrologic variable.

The hydrologic variables could also be divided into qualitative and quantitative variables. If a realization of a variable cannot be expressed as a real number in a sensible way, it is called a qualitative variable. The type of soil is an example of a qualitative hydrologic variable. In contrast, quantitative variables could always be measured as a real number. The number of rainy days in a week and rainfall intensity in a day are examples of discrete and continuous quantitative hydrologic variables, respectively.

2.9.1 The Movement of Water in the Earth–Atmosphere System

Since water is not exchanged between space and atmosphere, its movement within the Earth–atmosphere system occurs as a closed system. The atmosphere alone is viewed as an open system, because the water movement across the Earth/atmosphere interface represents a transfer of both energy and matter across the system boundary. Across this boundary and within the system, water movement is maintained and initiated by an energy flow through the system. There are a number of locations at which water is stored within this hydrological system. The atmosphere, the oceans, the land, and the polar ice caps are the main stores. Figure 2.14 shows the water distribution between these stores. The atmosphere is the smallest store, which contains 0.001% of the total water in the Earth–atmosphere system, while the ocean store is the greatest, amounting to 97.6%. The processes of evaporation, condensation, precipitation, runoff, and freezing and melting happen by transfers between stores. In the greatest exchanges between the ocean and the atmosphere, 86% of evaporation occurs over oceans, while 78% of precipitation takes place over them (Baumgartner and Reichel 1975).

2.9.2 Evaporation and Transpiration

When liquid water changes into gaseous phase (water vapor), this process is called evaporation. Heat energy has the effect of weakening the bonding between water molecules and increasing their kinetic energy if it is supplied to a water surface. The faster-moving molecules thus have a greater capacity to break away from the water surface and enter the air above. This transfer is partly offset by water molecules returning to the surface, and the net loss represents the rate of evaporation from the water surface.

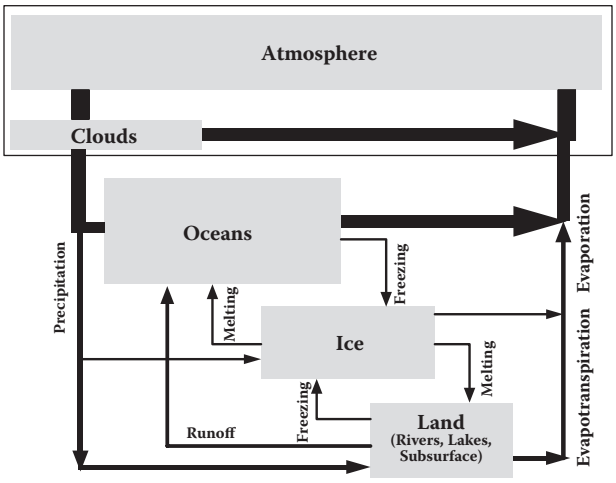

FIGURE 2.14 Hydrological system.

The change in phase from liquid to gas requires an input of heat energy, which is called the latent heat of vaporization. If an external source ceases supplying heat energy, the energy for evaporation will be drawn from the remaining water and will reduce its further evaporation and increasing temperature rate.

The most important factors that affect the rate of evaporation are the heat energy supply, the air humidity, the airflow characteristics across the nature of the evaporating surface, and the surface.

In the diffusion of water molecules into the lower layers of the atmosphere, the rate of evaporation is directly governed by the heat energy made available to them. Evaporation depends upon net radiation. Most of this net radiation is consumed in evaporation for wet soils and open water. The temporal and spatial variations of net radiation are thus imposed upon producing evaporation.

In the overlying air, the balance between molecules of water leaving the surface and those returning to it depends on their number. If the air is relatively dry, the numbers will be small in relation to those leaving the surface and thus the rate of evaporation will be high. If, however, the air approaches saturation, it has a higher population of water molecules, from which those returning to the surface will be only slightly fewer than those leaving, and consequently, the rate of evaporation will be low. At surface temperature and the vapor pressure of the air above (e_a), the evaporation rate is related to the difference between saturation vapor pressure (e_s). Molecules will continue to leave the surface while e_s is more than e_a. However, this effect increases e_a until it eventually reaches e_s; thus, the evaporation rate will be zero. There is a mechanism for mixing the air and thereby redistributing water molecules; evaporation will always exhibit a decrease with time.

By vertical and horizontal motion, the lower atmosphere mixing effectively results in the replacement of air before saturation is reached. Thus, evaporation is maintained at a higher rate than if there were no such replacement, as e_a no longer increases towards e_s. Increases in horizontal wind speed cause increases in the rate of evaporation, but only up to a point where further increases have little effect. The heat energy available for evaporation and the humidity of the air determine this maximum. Whether the surface is of an ocean or a glass of water, when a surface of water is exposed to the atmosphere, evaporation may occur. However, meteorologists determine the rate of evaporation by the rate at which molecules lost to the atmosphere can be replaced from the subsurface store. There is effectively an unlimited supply of water freely available for evaporation, in the case of an open water surface. However, there is usually a limited supply, thereby suppressing rates of loss in a soil. When the soil is saturated, for example, after a long period of rain, then evaporation may be considerably higher than from an equal area of open water, because of the water film hold on soil particles near to the surface. Also, the water quality affects the evaporation rate, in that it is reduced by the presence of impurities such as dissolved salts. The greatest reduction is from the saltwater of, for example, the oceans where there is, as a rough approximation, a 1% reduction in evaporation for a 1% increase in salinity.

If there is vegetation growing upon the surface, this provides an extra pathway for water molecules transferring from the ground surface into the atmosphere. Water vapor is transferred into the atmosphere on leaf surfaces and is diffused through pores (stomata). This is associated with a suction pressure inside the plant causing it to withdraw water from the soil through its root system. This water transfer into the atmosphere is referred to as transpiration and it accounts for a large proportion of moisture losses from vegetated surfaces.

Two groups of factors govern the rate of transpiration loss:

1. Those already discussed are the extrinsic factors that affect evaporation rates from water surfaces.
2. The factors intrinsic to the plant. For example, transpiration loss from most plants will be large when the atmosphere is relatively dry. In most plants, leaf stomata open under daylight conditions and close at night, thereby introducing a clear diurnal variation in transpiration losses. However, when the plant is unable to withdraw adequate water through its roots to match transpiration loss, internal stresses may be set up. In response to this, there may be a complete or partial closing of the stomata in order to limit transpiration.

With a dense plant cover, over vegetated surfaces, water losses to the atmosphere are largely accounted for by transpiration. For example, over 60% of water loss will be achieved through transpiration in a dense forest. If precipitation evaporation intercepted by the trees is included, over 80% of water transferred to the atmosphere may be due entirely to the presence of a vegetation cover. The transpiration will account for the entire surface-to-atmosphere water transfer in semiarid areas where there is virtually no surface water.

Most surfaces are neither absolutely bare nor completely vegetated but possess elements of both. Because of the complexity of these surfaces, separation of evaporation and transpiration is impracticable and the two are combined in the term *evapotranspiration*. A soil moisture shortage limits the rate at which evaporation and transpiration can take place. Actual evapotranspiration occurs under such limiting conditions. On the other hand, when no such limiting condition prevails, evapotranspiration can take place at its maximum rate within the constraints placed upon it by the availability of heat energy, atmospheric humidity, and wind speed. Potential evapotranspiration takes place under these no-limiting conditions. This idea is used extensively in studies of irrigation, for it represents the worst possible situation with regard to water loss from the ground surface. Over the Earth's surface, actual evapotranspiration is greater than that over land surfaces and over oceans.

2.9.3 Condensation

When the number of water molecules returning to a surface exceeds those leaving, there is a net deposition of water from the air, which is referred to as condensation. The implication of this statement is that a necessary condition for condensation is saturation, since a condition of non-saturation produces a net loss of water molecules from the underlying water surface. For simplicity, the two alternatives are considered:

1. Keeping its temperature constant by physically adding more vapor of water to the air.
2. In the atmosphere, the latter is responsible for the majority of condensation forms by cooling the air to its dew point.

If heat energy is withdrawn from the water molecules of vapor, the following decrease in their kinetic energy and strengthening of intermolecular bonding prevent them from remaining in the gaseous state. They return to liquid water and in so doing release the latent heat of vaporization they gained during evaporation.

With a water surface, if moist air is in contact, the cooling air molecules are readily absorbed into it. However, there are apparently no such surfaces over which condensation takes place in the free atmosphere. No condensation occurs if pure air without any suspended foreign matter is cooled to its dew point. It may continue to take up molecules of water to a state of supersaturation. Under laboratory conditions, it is possible to reach relative humidity of over 400% before condensation into water droplets takes place.

In reality, the Earth's atmosphere contains a number of impurities resulting from human activities or natural events. These provide surfaces upon which condensation may take place. The relative humidity at which this occurs is largely dependent upon the nature and number of the particles, which are referred to as condensation nuclei.

The presence of hygroscopic nuclei may initiate condensation in free air well before it reaches its saturation vapor pressure at relative humidity as low as 80%. Other less hygroscopic or nonhygroscopic materials, such as terrestrial dust, are less effective, but when present in large numbers, they encourage condensation in slightly supersaturated atmospheres.

Condensation occurs as a result of the atmosphere cooling in the presence of a receiving surface, whether this is a suspended condensation nucleus or a terrestrial surface. The condensation forms produced may be classified according to the nature of this cooling process, the most important of which are radiation cooling, advection cooling, dynamic cooling, and contact cooling.

2.9.4 Precipitation

In either solid or liquid form, water that falls from clouds to the ground is referred to as precipitation. Although this is derived from condensed water vapor, it is not true to say that condensation automatically leads to precipitation.

There are initially two forces operating on a cloud droplet, these being a gravitational attraction towards the Earth and the frictional force between the droplet and the air through which it is moving. When these two forces balance each other, in accordance with Newton's first law of motion, the droplet falls towards the Earth at a constant velocity—its terminal velocity—which is directly related to droplet size. The terminal velocities of cloud droplets are so small in relation to those of the updraughts that they are held within the cloud mass and are not precipitated.

A broad classification of precipitation can be developed from the nature of the condensation process from which precipitation is derived. The identified classification includes orographic, convectional, and cyclonic precipitation.

Over the Earth's surface, there is considerable variation in precipitation, which may be attributed to a number of factors operating over a spatial scales range. On a global scale, there are two areas associated with convergent airflow at the surface. The intertropical convergence and the middle latitudes are both areas of relatively higher precipitation, arising from the consequent uplift of air and its adiabatic cooling.

In contrast, the polar and subtropical regions have surface airflow of a divergent type and hence have much lower precipitation due to the subsidence of air. Especially, over ocean areas, this elementary zoning is apparent in the distribution of mean annual precipitation.

However, the mean atmospheric circulation is only one of a number of controls on the global distribution of precipitation. Precipitation also depends upon the type and number of condensation nuclei in the air and the presence of conditions conducive to the growth of cloud droplets.

The land masses, particularly those in the Northern Hemisphere, exert a marked control on the distribution of precipitation. As most atmospheric water vapor is derived from the oceans, the continental interiors may experience much drier atmospheric conditions than do locations near coasts. This is reflected in the interior of Eurasia, for example, which derives much of its moisture from the Atlantic Ocean, conveyed inland by the middle-latitude westerlies. As this air travels eastwards over the continent, it loses more water to the surface than it gains through evapotranspiration. There is thus an eastward decrease in precipitation, especially in winter when frozen surfaces give up little water to the atmosphere and the divergent airflow of the Siberian high pressure restricts the penetration of moist oceanic air.

2.9.5 The Surface Water Balance

A part of the precipitation is returned to the atmosphere by evaporation and transpiration, and the remainder is available for use in surface systems through storages on or within the surface. This surface water balance equation is used to represent this distribution:

$$P = E + T + \Delta S + \Delta G + R, \tag{2.7}$$

where P is precipitation, E is evaporation, T is transpiration, ΔS is the change in soil water storage, ΔG is the change in groundwater storage, and R represents overland flow across the surface. The components of this balance vary over time and space according to the prevailing moisture conditions in both the atmosphere and the surface. However, on a global scale, for simplicity, the two basic surface forms of open water and land are considered.

Example 2.5

A small catchment with an area of 150 ha received a rainfall of 10.5 cm in 90 min due to a storm. At the outlet of the catchment, the stream was dry before the storm and experienced a runoff lasting for 10 h with an average discharge value of 2 m^3/s. The stream was again dry after the runoff event.

a. What is the amount of water that was not available to runoff due to the combined effect of infiltration, evaporation, and transpiration?
b. What is the ratio of runoff to precipitation?

Solution:

a. The duration of runoff is 10 h, but the rainfall occurred in the first 90 min, and in the remaining 8.5 h, the precipitation was zero. Since the stream is dry after the rainfall, $\Delta S = 0$.

$\Delta G + T + E$ = water not available to runoff due to infiltration (causing addition to groundwater storage), evaporation, and transpiration = losses (L)

$$P - R = L$$

$P = 150 \times 10{,}000 \times 10.5/100 = 157{,}500\ m^3$
$R = 2.0 \times 10 \times 60 \times 60 = 72{,}000\ m^3$
$L = 157{,}500 - 72{,}000 = 85{,}500\ m^3$

b.

$R/P = 72{,}000/157{,}500 = 0.457$

Note: The rainfall abstractions, especially evapotranspiration, include a considerable part of it and it is very important to manage these abstractions in an appropriate way to protect the water resources.

The water balance given in Equation 2.7 may be rewritten for an open water surface, such as a large pan, in the simple form of

$$E = P + \Delta V. \tag{2.8}$$

In the case of the oceans, the R term can be ignored, but there is an extra inflow of water in the form of runoff from the surrounding land masses by way of rivers and of flow from one ocean area to another. By considering all the oceans as one surface, the inter-ocean flow of water and changes in storage over time are negligible. The surface water balance equation therefore becomes

$$P = E - \Delta F, \tag{2.9}$$

where ΔF is the flow of water from land to ocean.

The water balance equation for a land surface must remain as written, as all components are present. However, for practical purposes, evaporation and transpiration are considered together as evapotranspiration, E_t. The equation is therefore

$$P = E_t + \Delta S + \Delta G + R. \tag{2.10}$$

Example 2.6

In a reservoir dam, the average area of water surface is 35 km^2 for October, and at this time, average inflow and outflow to the reservoir are 15 and 20 m^3/s, respectively. If precipitation is 10 cm in October and the reservoir storage decreases 15 million cubic meters (MCM) due to other phenomena, calculate the evaporation during the month assuming that the groundwater state is constant.

Solution:

According to the water balance Equation 2.10:

$$E_t = P - (\Delta S + R)\ (\Delta G = 0).$$

The following are the values for the right-hand side of the equation:

$$P = (10/100) \times 35 \times 10^6 = 3.5 \times 10^6\ m^3$$

$$R\ (\text{inflow}) = 15 \times 86{,}400 \times 30 = 38.88 \times 10^6\ m^3$$

$$R\ (\text{outflow}) = 20 \times 86{,}400 \times 30 = 51.84 \times 10^6\ m^3$$

$$\Delta S = -15 \times 10^6\ m^3$$

Then,

$$E = 3.5 \times 10^6 - (51.84 \times 10^6 - 38.88 \times 10^6 - 15 \times 10^6) = 5.54 \times 10^6\ m^3.$$

Thus, the daily evaporation normally is equal to

$$E = (5.54 \times 10^6/35 \times 10^6 \times 30) \times 1000 = 5.28\ \text{mm/day}.$$

Indirect measurements of both potential and actual evapotranspiration using this equation may be made. If we assume that our surface is perfectly horizontal, then there is no gravitational acceleration of water drops along the surface, only into it. Thus, R is zero. If soil moisture levels are maintained such that evapotranspiration takes place at its potential maximum rate, then, effectively $\Delta S = 0$. In this case, the evapotranspirometer may be used to determine potential evapotranspiration. If irrigation of the soil tanks is not carried out, and a method of monitoring soil moisture changes (ΔS) is incorporated, actual evapotranspiration may be determined.

2.9.6 The Atmospheric Water Balance

Our discussion of water balance would be incomplete without a brief reconsideration of the atmosphere, which receives water from the surface beneath it and returns it through precipitation. The horizontal motion of the atmosphere transports water vapor so that the surfaces from which it is derived are not necessarily those to which it returns as precipitation.

The transport of water vapor is of significance in the distribution of heat energy in the atmospheric circulation. Water vapor transported in the atmosphere and subsequently condensed has, in releasing its latent heat of vaporization, acted as a vehicle for heat energy transfer. The meridional

transfer of latent heat is equatorward between latitudes 30°N and 30°S, where the trade winds blow across the ocean surfaces. In the middle latitudes, between 30° and 65°, there is a net poleward transport. This form of heat transfer is clearly greater in the Southern Hemisphere where there is a larger proportion of ocean surface acting as sources of water vapor.

2.9.7 Hydroclimatology

The climate is referred to mostly as the weather and other upper layers of the Earth phenomena. Even though the hydrologic cycle includes formation of clouds and precipitation, hydrological cycle processes mostly happen and appear on Earth. However, hydrogeologic processes are mostly considered in the subsurface of the Earth processes despite continuous interaction with the surface water. In the next section, the systems on which the hydrologic and hydrogeologic processes occur are discussed.

2.10 THE CATCHMENT BASIN SYSTEM

The drainage or catchment basin is the basic functional unit through which the denudation system operates. The boundaries of a catchment basin are well defined and there is a clear relationship between its component elements. The morphology of the catchment and the flow of matter and energy through the system show the structure and function of the relationships between system components. Figure 2.15a shows the inputs and outputs across the system boundary.

Channels, slopes, bedrock and regolith, and water are the major elements in the catchment system. The catchment system elements are related in an organization of slopes and converging channels. This organization facilitates the evacuation of runoff and debris from the catchment basin, which is the basic function of the system. A simple model of the catchment basin system is illustrated in Figure 2.15a. In this figure, the system elements are composed of several functional units or subsystems that are related to each other and all are an integral part of the function of the basin as a whole.

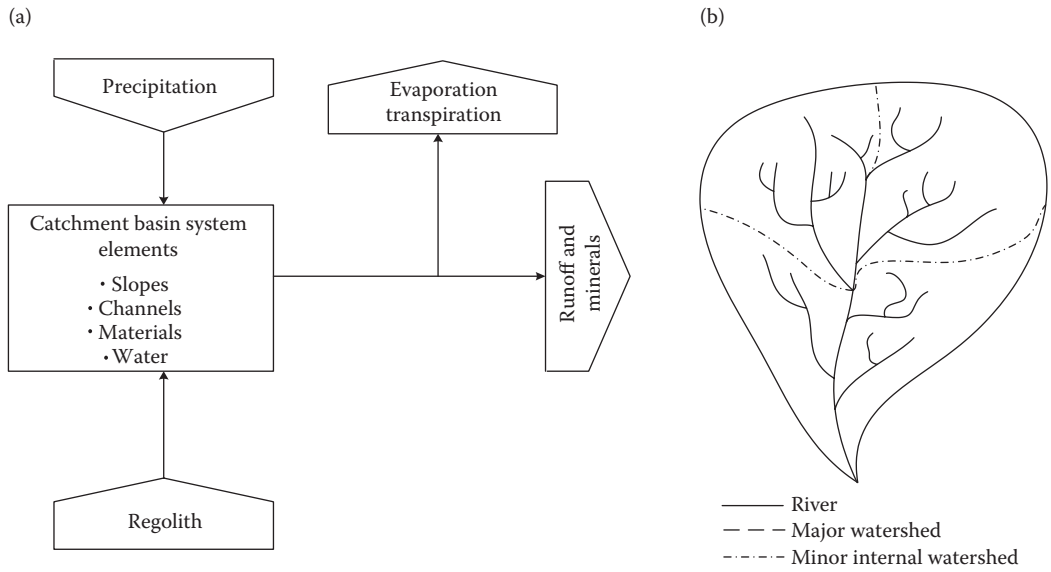

FIGURE 2.15 (a) Simplified schematic model of the catchment basin system. (b) Delimitation of catchment watersheds.

Example 2.7

Describe the system concept of a catchment.

Solution:

The catchment is a particular subsystem of the total hydrological cycle as shown in Figure 2.15b. In isolating this subsystem from the larger system represented by the whole system in Figure 2.16, it is necessary to cut across certain lines of transport of moisture from one part of the cycle to the other. The broken lines thus produced and shown in Figure 2.16 therefore represent either inputs (precipitation, *P*) or outputs from the subsystem representing the catchment area such as evaporation (*E*), transpiration (*T*), and outflow (*R.O.*). The catchment system, accordingly, is not a closed system and can only be treated as such if a record of all the inputs and outputs is available. A part of produced surface runoff penetrates to soil (*F*) that may flow in subsurface layer (*Q*) or recharge groundwater (*R*). The channel flow is composed of surface flow (Q_0), subsurface flow (*Q*), and groundwater flow (Q_s).

Though classical hydrology describes the hydrological cycle in terms of surface runoff, interflow, and groundwater flow, in practice, quantitative hydrology usually ignores this threefold division and considers the hydrograph (*Q*) to be made up of a direct storm response (Q_s) and a base flow (Q_b). Thus, in the analysis of the relationship between storm rainfall and flood runoff, the system analyzed by the practical hydrologist corresponds closely to that indicated by Figure 2.17.

The system shown in Figure 2.17 is composed of three subsystems: the subsystem involving direct storm response, the subsystem involving groundwater response, and the subsystem involving the soil phase, which has a feedback loop to the separation of precipitation (*P*) into precipitation excess (P_e) and infiltration (*F*), where the penetrated water will recharge the groundwater (*R*) or return to the atmosphere through evaporation (*E*) or transpiration (*T*). In the transition from classical hydrology to systems hydrology, the main emphasis has been on the subsystem involving direct storm response, which has been studied by unit hydrograph procedures.

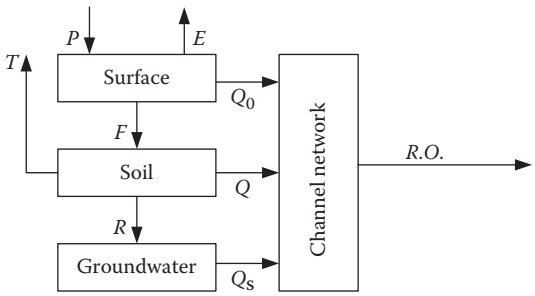

FIGURE 2.16 Catchment as a system.

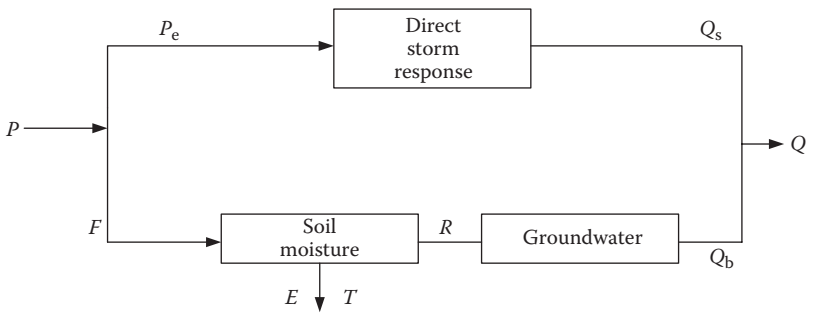

FIGURE 2.17 Simplified catchment model.

Figure 2.18 illustrates the slope system, channel system, and weathering system as well as the relationships among them in a more sophisticated model. The slope and weathering systems are functionally linked together by the transfer of materials. The weathering system produces materials from the regolith and through the soil and the ecosystem in the form of litter and decaying organic matter. The main linkage between the slope system and the atmospheric system is precipitation. The dissolved materials in that precipitation and the dry fallout from the atmosphere form other links between the slope and atmospheric systems. Furthermore, some atmospheric elements are fixed in the organisms of the ecosystem. These elements enter to the slope system after the death and decay of the organisms. Water output occurs in different forms and into different systems. Through evaporation and transpiration, water returns to the atmosphere, as surface runoff and infiltration water enters the soil and regolith, respectively, which will form soil water or groundwater. Materials such as solid sediment particles or solutes are removed by surface runoff.

The major link between the slope system and the channel system is formed by outputs from the slope system. The river channel is fed directly by overland flow of water down hillsides during storms, and the channel flow between rainstorms is sustained by the bulk of the percolating soil water and groundwater. Direct precipitation onto the river channel surface is the third and volumetrically the least important water input to the channel. A part of direct output of water from the channel is evaporation from the water surface, which is normally limited except under high temperatures and very broad channel sections (i.e., where the river passes through a lake). The main water output from the channel is via runoffs, which include sediments and solutes.

It can be concluded that the weathering, slope, and channel systems form a cascading system. In this way, the outputs of one are the inputs of another, and these systems together form the catchment basin system. The described model of the denotation system is applicable to different environmental systems such as deserts, landscapes experiencing active placation, and fluvial landscapes. These can be regarded as special cases, which differ only in the inputs to the system and in the pathways and rates of matter and energy flow through the system.

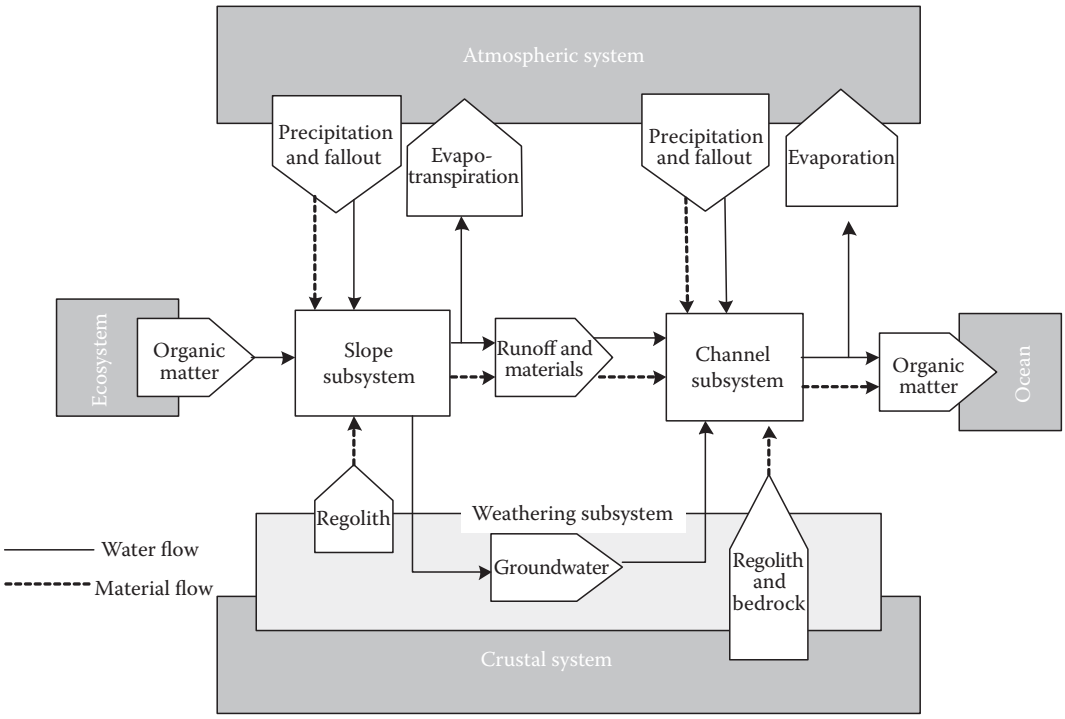

FIGURE 2.18 Schematic model of the function or organization of the catchment basin system.

2.10.1 Lake Catchment Systems

Some natural or artificial lakes are often available in catchment basin systems. Lakes act as sediment traps due to a very significant decrease in velocity of the rivers flowing into them. Lakes act as a sensor of environmental denotation because the accumulated sediment in them represents the output of the catchment draining to the lake.

The accumulated sediments in lakes usually have a stratified structure. The majority of accumulated sediments are mineral sediments that are delivered by rivers as suspended load and represent the mechanical erosion of the upstream catchment. The solute minerals that are incorporated in accumulated sediment of lakes are indicative of the chemical quality of the inflow. The vegetation throughout the catchment is represented by organic remains in the form of pollen, plant fossils, and the fossil remains of diatoms (diatoms are photosynthesizing algae that have a siliceous skeleton and are found in almost every aquatic environment including fresh and marine waters, soils, and, in fact, almost anywhere moist) and other lacustrine organisms representing the lake ecosystem. Particulate airfoil deposits and minerals that are washed out of the atmosphere during precipitation are also observed in the accumulated sediment. Therefore, the ecological erosions and chemical conditions within the catchment area upstream of the lake could be recognized by the range of materials in sediments.

The value of the historical information provided by lake sediments has been increasingly recognized in recent decades. A variety of stratigraphic (valve, pollen) and radiometric means are used to date the cores of lake sediments, as a consequence of which a chronology of events within the catchment can be built up. This can be used to link the observations of current conditions and monitoring of present processes with the history of the catchment. The history of catchment can be measured in decades to assess the human industrial development impact or in a millennia to evaluate climatic and land coverage changes through time.

Different events are recorded by lake sediment structure. The most important events recognized by sediments are as follows:

- The nature and volume of changes in environmental conditions can be recognized by the mineral sediment flux into the lake and the water quality indicated by individual elements present within sediment.
- Changes in vegetation as a result of climatic changes, human impact, and consequent implications for the water balance and denotation processes are identified by plant remains.
- The range of available diatoms is an indicator of acidification.
- Sewage and detergents used by humans for different purposes produce the influx of phosphates that cause eutrophication in diatoms.
- Industrialization processes are identified by pollution, input of magnetic minerals, and heavy metals.

Recently, a new type of river basin monitoring program called environmental niche modeling, which focuses on biological sampling and modeling, has received attention. The principle of this monitoring is embedded in the fate of sediments and the positions in natural resources such as lakes.

2.10.2 The Fluvial System

A wide variety of flow forms are observable along the river's path (Figure 2.19). The flow regimes range from small turbulent mountain streams flowing down irregular beds mantled with coarse boulders and plunging over more resistant outcrops of rock such as waterfalls, to the broad lowland river flowing in a tranquil manner in a channel cut into alluvium and often meandering in form. However, the flow of stream channels at all scales from fingertip tributaries to major trunk streams is governed by the laws of hydraulics governed by gravity, conveyance, resistance, kinematic wave,

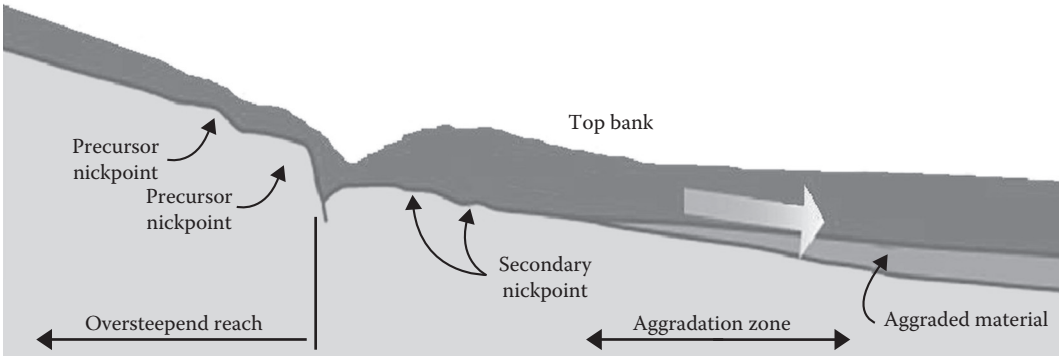

FIGURE 2.19 Variation of flow regimes along a river path.

jump, etc. The river systems are better understood in comparison with other environmental systems. This is due to their accessibility (it is possible to enter and observe channels especially small ones), clear definition of their boundaries, and operation of channel processes over short timescales (easy monitoring and measurement).

When the major water stores within the catchment such as canopy interception, surface depression, soil moisture, and groundwater are satisfied, or when a critical regulator such as infiltration capacity is exceeded, channel flow starts. Water arrives through a variety of routes at the channel. The velocities of flow in these routes are in completely different ranges (Table 2.3). The water in the channel is the sum of the outputs of two stores including direct precipitation on the channel surface and water falling on adjacent slopes. The runoff from adjacent slopes enters the channel through overland flow, soil throughflow, or seepage from subsurface and/or groundwater.

Due to the wide variety of channel input rates that come into play at different times, the magnitude of channel flow has high temporal variations. The temporal changes of channel flow are recorded graphically in the hydrograph (explained more in Chapter 5). To simplify, the hydrograph is separated into two components of direct runoff (water that rapidly enters into the channel) and indirect runoff (water that follows a slower and longer route) (Figure 2.20). Indirect runoff mostly includes the base flow, which is further described in Chapter 5.

TABLE 2.3
Estimated Velocities along Different Flow Routes in Catchment

Medium	Flow Routes	Velocities (m/h)
Surface flow	Channel flow	300–10,000
	Overland flow	50–500
Soil flow	Pipe flow	50–500
	Soil seepage	0.005–0.3
Groundwater	Flow through limestone (jointed)	10–500
	Flow through sandstone	0.001–10
	Flow through shale	10^{-8} to 1

Source: White, I.D. et al., *Environmental Systems*, Chapman and Hall, London, UK, 1996. With permission.

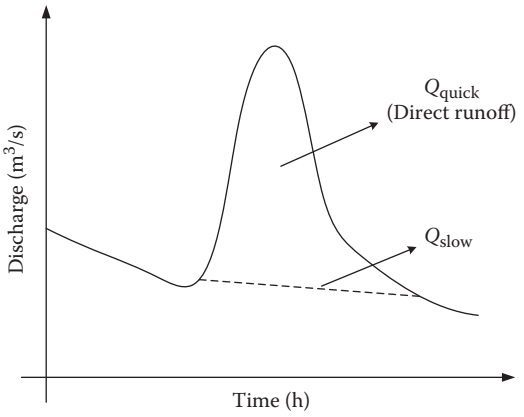

FIGURE 2.20 Separation hydrograph into quick and slow components.

2.10.3 Energy and Mass Transfer in Channel Systems

Energy is the fundamental dynamic force in the operation of all systems. The magnitude and expenses of this energy are an important factor in the stream channel processes. The sum of the potential gravitational and kinetic energies at each point along the stream channel is considered as the effective energy. Total energy in geomorphologic terms is related to the total mass of water flowing in the channel (discharge) at any one point. Therefore, the total mass of water is a major independent variable that controls the operation of stream channel processes. The major component of kinetic energy is the velocity, which is dependent on discharge.

The loss of energy through the channel is due to two factors. The majority of energy loss (more than 95%) is used to overcome the frictional drag of the channel margin on the flowing water. The amount of energy loss is dependent on channel size and shape and on the roughness of the channel. Energy lost to overcome the channel friction is hardly measurable because it is converted to heat and lost to the surroundings by radiation and conduction. The reamaining part of energy is converted to mechanical energy that transports mineral sediments as a part of the river load. Therefore, a small proportion of the energy of the river flow is used in erosion and transportation.

Figure 2.21 illustrates the inputs and outputs of water to the river channel system. The proportion of the rain that falls directly on the surface of the river channel contributes only a small volume of river discharge. When the river has a large effective surface area, the channel discharge will be larger. The part of rainfall that falls on slopes reaches the channel by overland flow or by way of throughflow. The overland flow and throughflow will carry different solutes and a considerable load of sediments. A proportion of water percolates to groundwater. Sometimes, seepage from the groundwater store returns this part of water to the channel as is the case in influent channels that are common in humid environments.

The direct evaporation from the channel surface is the first output of water from the channel system. In channels with a large surface area exposed to the atmosphere, the direct evaporation is more important. The second output of water from the channel system is the water that is lost from the channel to groundwater when the water table is below the level of the channel floor. This situation, which is called an effluent channel, is sometimes observed in arid environments where a permeable rock such as limestone is available. However, the most important part of output from the channel system is runoff. The runoff process transfers water along the channel system into the receiver water body.

The magnitude of runoff is highly variable in space and time. For example, within a catchment basin, the catchment area drained through a specific channel cross section determines the discharge amount. However, the temporal variations of discharge are important in the operation of channel

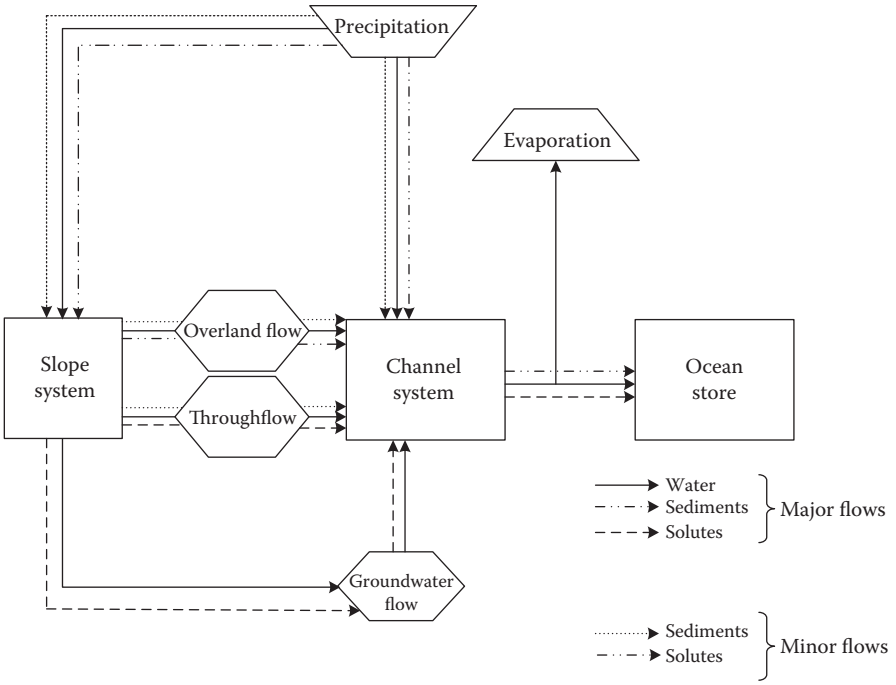

FIGURE 2.21 Pathways of water and mineral flow through the catchment basin system.

dynamics. This is due to different magnitudes of the four major inputs of water to the channel system that come into play at different times. The channel system inputs that result from precipitation (direct runoff) have the highest magnitude, and their temporal distribution is related to the seasonal distribution of rainfall events. The magnitude of inflow from groundwater is normally much less than direct runoff but is continuously distributed over time.

The temporal variations of rainfall input are illustrated with a storm hydrograph (Figure 2.22). At the start of rainfall, discharge rises sharply to reach its peak value, and when rainfall stops, the discharge descends gradually. There is a lag time between maximum rainfall intensity and peak discharge. The volume of direct runoff is measured by the area under the peak of storm hydrograph. Thus, the storm runoff is the result of processes associated with a rainfall event and the base flow is formed by groundwater seepage. It should be noted that storm hydrographs of different storms

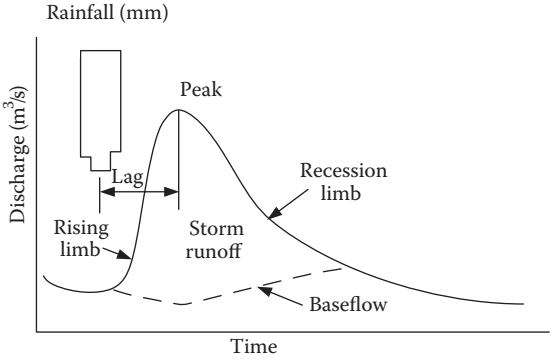

FIGURE 2.22 Characteristics of the flood hydrograph.

and in different catchments are not the same and the magnitude and shape of the hydrograph are dependent on many factors associated with the nature of the rainfall event and the characteristics of the catchment.

An idealized hydrograph of an individual storm flow is shown in Figure 2.22, but a real storm hydrograph includes a series of flood peaks distributed through time and superimposed upon base flow (Figure 2.23). The hydrographs depicted in Figure 2.23 can be the responses of two adjacent rivers with similar catchment area to the same rainfall inputs. The hydrograph with a series of sharp flood peaks is related to a river draining a catchment based mainly on clay. The base flow in winter is higher than that in summer, and this reflects the seasonal differences in groundwater storage level. Because of the impermeable base of the catchment, there are immediate and highly peaked responses to storm rainfall. The second hydrograph belongs to a chalk catchment. Because of high infiltration in the catchment, which precludes direct runoff, a much more stable regime is observed and the majority of discharge is due to groundwater flow.

The described flows of water in the previous paragraphs are associated with flows of materials in both solid and dissolved forms. A range of ions in solution as well as particulate matter are available in rainwater that is washed out of the atmosphere. Overland flow transports both sediment and solutes to the river channel, and the sediment load is more dominant. On the other hand, in this process, elements are washed out from adjacent slopes into the channel. Sometimes, a layer of deposits of elements transported by throughflow is observable in the channel banks. For example, the redeposition of formerly dissolved iron where the throughflow emerges can be detected by a reddish-brown stain. In the same way, some solutes are contributed to the channel through groundwater seepage. The erosion of the banks of the channel that fall into the stream when undermined is a considerable source of mineral sediment. Fresh erosion scars are often seen on the outside of bends in the channel. The behavior of sediments and solutes in stream is completely different. Solutes are continuously transported by the stream but sediments have an irregular movement. During floods, high concentrations of sediments are moved. After the floods, the sediments are again deposited on the channel bed until the next flood. Therefore, there is a two-way exchange of sediment between the channel bed and the stream.

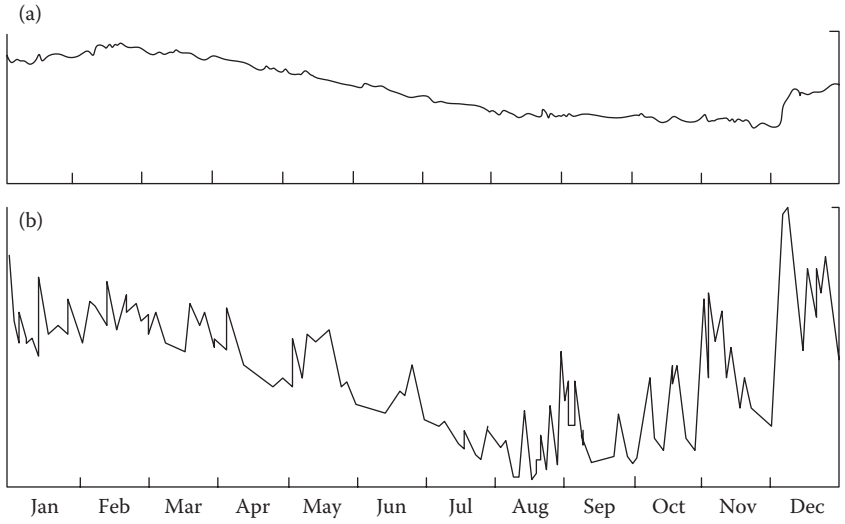

FIGURE 2.23 Comparison of the annual hydrograph for two adjacent catchments for the same rainfall events: (a) chalk-based catchment and (b) largely clay-based catchment.

2.11 GROUNDWATER SYSTEM

The groundwater system is a part of the hydrologic cycle and should be studied in a watershed scale. The combination of many elements and factors affecting groundwater, so related and connected, calls for a holistic view to groundwater challenges within a hydrologic cycle.

Groundwater constitutes about 30% of the world's available freshwater resources. Groundwater systems are traditionally developed as sources of water for different domestic, industrial, or agricultural purposes. The generally good quality of water and its accessibility in many regions of the world, where surface water is nonexistent or extremely costly to develop, have been important factors in stimulating the development of this relatively low-cost, reliable water resource.

Groundwater is formed in two zones: saturated zone and aeration zone. The soil part in which all the pores of the soil are filled with water is called the saturated zone, also known as groundwater zone. In such a case, the upper limit, which is a free surface of water table, is contiguous to atmospheric pressure. The soil part where the soil pores are only partially saturated with water is called the aeration zone, which includes three subzones:

1. Soil water zone: The uppermost zone, which is adjacent to the ground surface and water, is lost to atmosphere by evapotranspiration through the major root band of the vegetation.
2. Capillary fringe: Capillary action holds water in this zone, from the water table upwards to the limit of the capillary rise.
3. Intermediate zone: The middle zone between the soil water zone and the capillary fringe.

The saturated formations are classified based on the ease of extracting water from saturated materials. Based on this classification, four types of saturated zones are identified: aquifer, aquitard, aquiclude, and aquifuge. The characteristics of the above environments are as follows:

Aquifer: Saturated formation of earth material (a geologic unit) that is significantly good in storing and yielding water in good quantity. Because of high permeability, an aquifer transmits water relatively easily; such a property depends on the composition of the aquifer.
Aquitard: The term *aquitard* refers to a formation through which only seepage is possible (its hydraulic conductivity is too small to permit the development of wells or springs); thus, the yield is insignificant compared to an aquifer; it is considered as partly permeable. However, it may be sufficiently large to significantly influence the hydraulics of aquifers adjacent to it. In other words, it is possible that through an aquitard, appreciable quantities of water may leak to an aquifer below it.
Aquiclude: Geological formation that is essentially impermeable to the flow of water. It is worthwhile to notice that such a formation (such as clay) can hold large amounts of water due to its high porosity and still be closed to water movement.
Aquifuge: Aquifuge refers to a geological formation, such as massive compact rock, which is neither porous nor permeable, without any interconnected openings that cannot transmit water. They are important as boundaries of aquifers and sources of elastic material for aquifer formation.

2.11.1 Confined and Unconfined Aquifers

Aquifers can be both a transmission conduit and storage. Important factors of the availability of groundwater are rates of withdrawal and replenishment (recharge) of an aquifer. Based on the occurrence and field situation, aquifers are divided into two groups: confined and unconfined aquifers.

A confined aquifer, also known as artesian aquifer, is bounded by relatively impervious materials on the top and bottom, and water exists in such a confined aquifer at pressures greater than

atmospheric; in fact, it is only necessary for the water to rise above the top of the aquifer to be classified as a confined or artesian aquifer (Figure 2.24). Confined aquifers have very low storability values (much less than 0.01, and as little as 10^{-5}), which means that the aquifer is storing water using the mechanisms of aquifer matrix expansion and the compressibility of water, which typically are both quite small quantities.

Piezometric surface is an imaginary surface passing through all points to which water will rise in wells penetrating a confined aquifer. Besides, if the piezometric surface falls below the top of the aquifer, the aquifer becomes unconfined at that point and the piezometric surface and the water table coincide.

In an unconfined aquifer, free water surface is considered as the water table. Consider a well penetrating an unconfined aquifer; the static level of that is the water table at that point. In order to achieve a balance between the recharge and outflow from the subsurface storage, the water table is constantly in motion to adjust its surface. The pressure upon the surface of a water table is equal to atmospheric pressure (Figure 2.25).

Unconfined aquifers have storabilities (typically called specific yield) greater than 0.01 (1% of bulk volume); they release water from storage by the mechanism of actually draining the pores of the aquifer, releasing relatively large amounts of water (up to the drainable porosity of the aquifer material, or the minimum volumetric water content).

A perched water table is formed under a condition in which a lens or localized patch of impervious stratum exists inside an unconfined aquifer and locally the water table is retained above the general water table. In fact, a perched water table on a clay lens is the result of the collection of water that has percolated from the ground surface. For instance, some lakes are perched on low-permeability sediments and such ponds are especially vulnerable to widely fluctuating lake-stage levels with changes in the amount of rainfall.

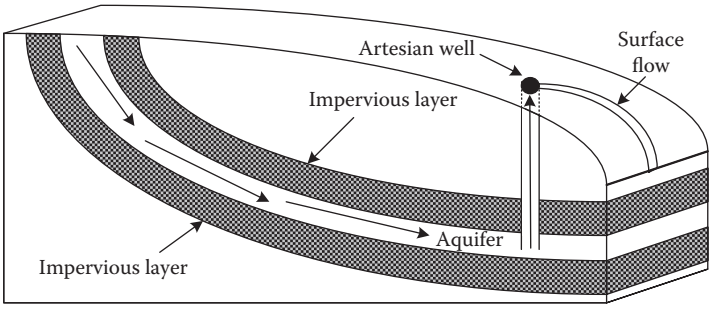

FIGURE 2.24 Confined groundwater and the development of an artesian well.

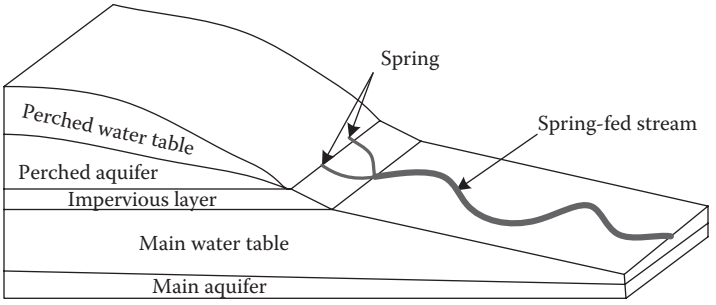

FIGURE 2.25 Unconfined groundwater, perched water tables, and the development of springs.

2.11.2 Stream–Aquifer Interaction

The relative position of the water level in a stream to the water table determines whether the water table contributes to the stream or the stream contributes to the water table. In times of low flows in stream, where the water surface of the stream is below the groundwater elevation, the groundwater contributes to the flow in the stream; such streams that receive groundwater flow are called effluent streams. The other case is called influent streams, where the water table is below the bed of the stream, the stream water percolates to the groundwater storage, and a hump is formed in the groundwater table.

General categories of interactions between the water table aquifer and the stream are as follows: (1) The water table aquifer contributes baseflow to the stream, i.e., streams that always flow on a relatively impervious bed or on the water table where the water table adjacent to the stream is at a higher elevation than the stream surface; (2) The stream contributes recharge to the water table aquifer; in fact, the stream bottom is always above the water table. This condition exists in ephemeral streams; and (3) The stream and aquifer alternately contribute to each other; examples of this category are those streams in which the stream channel and the water table are alternately higher and lower.

2.12 CONCLUDING REMARKS

In hydrology science, the movement of water through the hydrologic cycle is studied. Because of different components and factors affecting this movement, it is important to provide a system view for this study. In the system approach, the external factors that describe the interaction with the hydrologic cycle are recognized. Furthermore, the hydrologic system is decomposed to several internal components and the interactions and the process in each component are investigated.

Regarding the level of accuracy and resolution needed in hydrologic studies, different levels of modeling are used. By increasing the accuracy of modeling results and the accessibility of data, the modeling resolution would be increased.

The hydrologic cycle is used to model the storage and movement of water in Earth's system including the biosphere, atmosphere, lithosphere, and hydrosphere. Water is stored in the following reservoirs: atmosphere, oceans, lakes, rivers, glaciers, soils, snowfields, and groundwater. Through different processes such as evaporation, condensation, precipitation, deposition, runoff, infiltration, sublimation, transpiration, and groundwater flow, water moves from one reservoir to another.

The characteristics of different systems through which water moves and the relations and interactions between the systems are determinants of temporal and spatial distribution as well as the quality and quantity of water on Earth. For planning and management of water resources systems, it is necessary to study these systems and their interactions with internal and external factors, which may be natural or anthropogenic, and which may alter the path of water movement. The system approach should be followed in all hydrologic analysis and water resources assessment, planning, and management studies, and the modeling schemes should look at data availability and representation as well as sound assumptions to justify data scarcity to obtain desired outputs.

PROBLEMS

1. Explain the different levels of modeling resolution that are commonly used in rainfall prediction.
2. Provide examples of different closed and open systems in the hydrologic cycle.
3. Explain the urban water cycle in the context of the hydrologic cycle using a system approach.
4. Specify different components of groundwater system as black or white box. Explain how interactions with surface water can impact black and white box configuration.

5. Consider that river flow prediction is needed for reservoir design. Describe the system concept of this problem in design and synthesis stages.
6. Table 2.4 shows the measured rainfall and surface runoff from a 50 km^2 watershed. The given values are the averages over time intervals. Compute the accumulated storage (m^3) of the water within the watershed. Plot on the same graph the inflow, outflow, and cumulative storage as functions of time.
7. Identify the processes of the hydrologic cycle that affect flood runoff from a 1.5 km^2 forested lot. Discuss the relative importance of each of the processes. If the lot is cleared, what changes in the processes will occur? What will their importance be? If a single-family residence is constructed on the cleared lot, what processes will control flood runoff from the lot?
8. For a circular pipe flowing full, the head loss (h) can be computed using the Darcy–Weisbach equation:

$$h = f\left(\frac{L}{D}\right)\frac{V^2}{2g}$$

where f is the dimensionless friction factor that is a function of the Reynolds number and pipe roughness; L and D are the length and the diameter of the pipe, respectively; and V is the velocity of flow. A manufacturer intends to develop a pipe made of a new ceramic material for which f values are not available. Discuss the task in terms of analysis and synthesis.
9. Estimate the constant rate of withdrawal from a 1400 ha reservoir in a month of 30 days during which the reservoir level dropped by 0.7 m in spite of an average inflow into the reservoir of 0.5 MCM/day. During the month, the average seepage loss from the reservoir was 2.5 cm, the total precipitation on the reservoir was 18.5 cm, and the total evaporation was 9.5 cm.
10. A catchment has four subareas. The annual precipitation and evaporation from each of the subareas are given in Table 2.5. Assume that there is no change in groundwater storage on an annual basis and calculate for the whole catchment the values of annual average (a) precipitation and (b) evaporation.
11. A storm has an average rainfall depth of 9 cm over a 200 km^2 watershed. What size reservoir would be required to contain completely 20% of the rain?
12. A storm with a uniform depth of 3 cm falls on a 15 km^2 watershed. Determine the total volume of rainfall. If all of the water were collected in a storage basin having vertical walls and an area of 1000 m^2, how deep a basin would be needed?

TABLE 2.4
Measured Rainfall and Surface Runoff for Watershed in Problem 6

Time (min)	Rainfall (cm)	Runoff (m^3/s)
0	0	0
10	0.07	2.1
20	0.15	9.5
30	0.21	18.9
40	0.16	37.3
50	0.09	48.8
60	0.05	52.6

TABLE 2.5
Annual Precipitation and Evaporation of Catchment in Problem 10

Subarea	Area (m^2)	Annual Precipitation (mm)	Annual Evaporation (mm)
A	10.7	1030	535
B	3.0	830	458
C	8.3	900	469
D	17.9	1300	610

REFERENCES

Baumgartner, A. and Reichel, E. (1975). *The World Water Balance*, Elsevier, Amsterdam, 179 pp.

Chow, V.T., Maidment, D.R. and Mays, L.W. (1988). *Applied Hydrology*, McGraw-Hill, New York.

Cole, L.C. (1958). "The ecosphere," *Scientific American*, 198, 83–92.

Daly, R. (1940). *Strength and Structure of the Earth*, Prentice-Hall, New York.

Egler, F.E. (1964). "Pesticides in our ecosystem," *American Scientist*, 52, 110–136.

Hutchinson, G.E. (1970). "The biosphere," *Scientific American*, 233 (3), 45–53.

IPCC (2007). *Climate Change 2007: The Physical Science Basis*. Contribution of Working Group I to the Fourth Assessment Report of the Intergovernmental Panel on Climate Change. Solomon, S., Qin, D., Manning, M., Chen, Z., Marquis, M., Averyt, K.B., Tignor, M. and Miller, H.L., eds., Cambridge University Press, Cambridge and New York.

Karamouz, M., Szidarovszky, F. and Zahraie, B. (2003). *Water Resources Systems Analysis*, Lewis Publishers, Boca Raton, FL.

Loucks, D.P., Stedinger, J.R. and Haith, D.A. (1981). *Water Resources Systems Planning and Analysis*, Prentice-Hall, Englewood Cliffs, New Jersey, 559 pp.

McCuen, R.H. (1997). *Hydrologic Analysis and Design*, 2nd edition, Prentice Hall, Upper Saddle River, New Jersey.

Marsh, W.M. (1987). *Earthscape: A Physical Geography*, John Wiley & Sons, New York.

National Research Council (1991). *Opportunities in the Hydrologic Sciences*, National Academy Press, Washington, DC.

Shahin, M., Van Oorschot, H.J.L. and De Lange, S.J.D. (1993). *Statistical Analysis in Water Resources Engineering*, Applied Hydrology Monographs, Balkema, Rotterdam.

Wallace, J.M. and Hobbs, P. (2006). *Atmospheric Science: An Introductory Survey*, International Geophysics Series 92, Elsevier (Academic Press), London.

White, I.D., Mottershead, D.N. and Harrison, S.J. (1996). *Environmental Systems*, Chapman and Hall, London.

3 Hydroclimatic Processes

3.1 INTRODUCTION

Climate is usually described in terms of the variability and mean of relevant atmospheric variables such as precipitation, temperature, relative humidity, atmospheric pressure, and wind. Climate can thus be viewed as an aggregate or synthesis of weather. This implies that the climate description in a particular region must contain an analysis of mean conditions of the seasonal cycle and of the extreme event probabilities such as storms and severe floods.

As the statistical description of the climate system, climate is thus now more and more frequently defined in a wider sense. This includes the analysis of the behavior of its five major components: the atmosphere, the lithosphere, the biosphere, the hydrosphere, and the interactions between them (Intergovernmental Plane on Climate Change [IPCC] 2007). More details on climate systems are described in Chapter 2.

The formation of precipitation as the most important component of the hydrologic system, which is described in this chapter, is highly dependent on the climatic process that happens in the lower layer of the atmosphere. There is a strong relationship between hydrologic concepts and meteorological concepts in transforming the moisture provided through evapotranspiration to the precipitation. Therefore, to understand the hydrologic cycle and its performance well, it is necessary to have an idea about the climatic process affecting it. Furthermore, before making a conclusion based on the calculation and researches about the hydrologic cycle especially in the case of predictions, the designer and engineer should have some general information about the climate conditions that affect the hydrologic components' values and relationships.

This chapter introduces briefly the general state of the atmosphere and climate elements that affect the hydrologic components. It is focused on the main characteristics of the atmosphere in the lower layer (where the hydroclimatic processes happen), including radiation, temperature, pressure, and moisture content. Then, the hydroclimatic processes resulting in cloud and precipitation formation are discussed. In the second part of the chapter, the climatic variables and measures, such as sea surface pressure and temperature that highly affect the water cycle changes over time with emphasis on precipitation, are introduced. These measures are useful in precipitation prediction in different time periods.

3.2 ATMOSPHERE CHARACTERISTICS

When the Earth was formed, the atmosphere was made up of helium and hydrogen compounds such as molecular hydrogen, methane, and ammonia. That early atmosphere is thought to have escaped into space, after which our current atmosphere slowly began to form. Through volcanic activity, gases such as carbon dioxide, water vapor, and various compounds of nitrogen and sulfur were released over time. As atmospheric oxygen levels gradually increased, more and more ozone was formed in the atmosphere. Table 3.1 shows the composition of the Earth's atmosphere as it exists now, expressed in volumetric fractions. About 99% of the volume of the dry atmosphere is oxygen and nitrogen; they are the most important components of the atmosphere.

Nitrogen is the largest single constituent of the Earth's atmosphere. It is created by fusion processes in stars. At the Earth's surface, nitrogen is deposited when it is removed from the atmosphere. Another important gas in the Earth's lower atmosphere is carbon dioxide (see Table 3.1). Through

TABLE 3.1
Most Important Gases in Earth's Lower Atmosphere

Gas Name	Chemical Formulation	Volume (%)
Nitrogen	N_2	78.08
Oxygen	O_2	20.95
Water vapor	H_2O	0.40 over full atmosphere, typically 1–4 at surface
Argon	Ar	0.93
Carbon dioxide	CO_2	0.039
Neon	Ne	0.0018
Helium	He	0.00052
Methane	CH_2	0.00017
Nitrous oxide	N_2O	0.00003
Hydrogen	H_2	0.000055
Ozone	O_3	$0–7 \times 10^{-6}$

Source: NOAA Earth System Research Laboratory, 2010. With permission.

photosynthesis and respiration, carbon dioxide is exchanged between the atmosphere and life. In recent years, the increase of carbon dioxide in the atmosphere has contributed to global warming through the greenhouse effect. Water vapor is the next gas that has the highest concentration, especially near the oceans, the equator, and the tropical forests.

Methane is also one of the important gases shown in Table 3.1. Since 1750, the volume of this gas in the atmosphere has increased by more than 150%. Grazing animals, rice crop growing, landfills, termites, oil, coal mining, and gas extraction are the primary sources for the additional methane added to the atmosphere.

Every year, nitrous oxide gas increases, on average, by about 0.2–0.3% in the atmosphere; soil fertilization, land-use conversion, fossil fuel combustion, and biomass burning are the factors that contribute to the increase in nitrous oxide.

Ozone is another gas in the atmosphere. About 97% of the ozone is found in the stratosphere at about an altitude of 15 to 55 km above the surface of the Earth. In recent years, stratospheric ozone levels have become thinner due to the buildup of human-created chlorofluorocarbons. The ozone layer is important because it absorbs harmful ultraviolet radiation.

3.3 PHYSICAL BEHAVIOR OF THE ATMOSPHERE

The atmosphere is made up of a lot of different gases; the most important of these gases were described in the previous section. In the next sections, the important relationships between temperature, pressure, density, and volume that relate to the Earth's atmosphere are described.

3.3.1 Ideal Gas Law

The situation in which all collisions between atoms or molecules are perfectly elastic and in which no intermolecular attractive forces exist defines an ideal gas. It can be visualized by a collection of perfectly hard spheres that collide but do not interact with each other. All the internal energy of an ideal gas is in the form of kinetic energy and any change in internal energy is accompanied by a change in temperature as air is compressible.

3.3.1.1 Common Form

The state variables that characterize an ideal gas are as follows:

$$PV = nRT, \tag{3.1}$$

where P is absolute pressure (atm); V is volume (m^3); n is mass of gas (mole, a unit of measurement that expresses the amount of a chemical substance that contains 6.02×10^{23} elementary entities of the substance); R is ideal gas constant, which is equal to 0.082056 L atm K^{-1} mol^{-1}; and T is absolute temperature (K). The absolute temperature, which is measured in Kelvin (K), shows the distance from absolute zero temperature. Absolute zero is the theoretical temperature at which entropy reaches its minimum value. The relation between Kelvin and centigrade scales can be expressed as follows:

$$T_K = T_c + 273.15 \tag{3.2}$$

$$T_c = 5/9(T_f - 32). \tag{3.3}$$

Example 3.1

In a basin, the temperature is measured about 113°F. Estimate the air temperature in degrees centigrade and in Kelvin.

Solution:

If the temperature is measured in degrees Fahrenheit, then T_c in degrees centigrade is estimated from Equations 3.2 and 3.3 as follows:

$$T_c = 5/9(113 - 32) = 45°C,$$

$$T_K = 273.15 + T_c \rightarrow T_K = 318.15 \text{ K}.$$

There are a number of ways to express pressure in Equation 3.1. One atmosphere of pressure (atm) equals 101.325 kPa, 10.33 m H_2O, and 0.76 mm Hg. One atmosphere is also equal to 14.7 pounds per square inch (psi); thus, 1 psi = 6.89 kPa. Finally, 100 kPa is called a bar, and 100 Pa is a millibar (mb), which is the unit of pressure in meteorological studies.

Example 3.2

Find the volume that 1 mol of an ideal gas would occupy at a standard temperature and pressure (STP) condition of 1 atm pressure and 0°C temperature. Repeat the calculation for 1 atm and 30°C.

Solution:

Using Equation 3.1 at a temperature of 0°C (273.15 K), the volume of mentioned gas mass is obtained as

$$V = \frac{1\,\text{mol} \times 0.082056\,\text{L atm K}^{-1}\text{mol}^{-1} \times 273.15\,\text{K}}{1\,\text{atm}} = 22.414\,\text{L}$$

and at 30°C (= 303.15 K),

$$V = \frac{1\,\text{mol} \times 0.082056\ \text{L atm K}^{-1}\ \text{mol}^{-1} \times 303.15\ \text{K}}{1\,\text{atm}} = 24.875\ \text{L}.$$

As can be seen, with an increase in gas temperature of 30°C, its volume has been increased from 22.414 to 24.875, which is about a 10% increase.

3.3.1.2 Molar Form

As the amount of substance could be given in mass instead of moles, in this case, an alternative form of the ideal gas law is used. The number of moles, n, is equal to the mass (in, say, grams), m, divided by the molecular or atomic weight of mass (in gram), M:

$$n = \frac{m}{M}.$$

Hence, for example, 32 g of O_2 is 1 mol. Placing the above equation in the ideal gas law results in:

$$PV = \frac{m}{M} RT.$$

By replacing m with density $\rho = m/V$, the following relation is obtained:

$$P = \rho \frac{R}{M} T.$$

Defining the specific gas constant R_s as the ratio R/M,

$$P = \rho R_s T. \tag{3.4}$$

This form of the ideal gas law is useful because it links pressure, density, and temperature independent of the quantity of the considered gas. Alternatively, the law may be written in terms of the specific volume, v, the ratio of the gas volume to its mass, as follows:

$$Pv = R_s T. \tag{3.5}$$

It should be mentioned that air does not have all the characteristics of the theoretical ideal gas. However, it has been shown through different investigations at STP (1 atm pressure and 0°C temperature) that the behavior of air, like most other real gases, approaches that of an ideal gas. Many gases such as nitrogen, oxygen, and hydrogen can be treated as ideal gases. Therefore, air as a combination of these gases in normal condition could follow the same law.

Example 3.3

On the desert ground surface at an altitude of 3700 ft, the temperature and pressure of the air are measured as 113°F and 30 inches (in), respectively, and the relative humidity is 25%. Estimate the air pressure in millibars and in kilopascals.

Solution:

Because the atmosphere is equal to 1013.3 mb and 30.006 in Hg, then

$$P = (30 \times 1013.3)/30.006 \rightarrow P = 1000 \text{ mb}$$

$$P = 1000/10 = 100 \text{ kPa}.$$

3.3.1.3 Isothermal and Adiabatic Expansion

In the atmosphere, different mechanisms can affect the situation of air masses including temperature, volume, and pressure. These changes can result in the different behaviors of water cycle components. Regarding the mechanisms of air mass expansion, two major mechanisms—isothermal and adiabatic—are identified.

In isothermal expansion, the temperature of air mass is held constant ($\Delta T = 0$) by keeping the gas in thermal contact with a heat reservoir. Then, the gas is allowed to expand indefinitely without any change in temperature. In an isothermal condition, the ideal gas equation is as follows:

$$Pv = \text{constant}. \tag{3.6}$$

In adiabatic expansion, it is supposed that the gas is thermally isolated from its surroundings; thus, there is no heat exchange, $\Delta Q = 0$. In this case, when the gas is allowed to expand quasi-statically, it does work on its environment, and hence, its internal energy is reduced, and its temperature decreases. This case happens when an air mass goes upward beside a mountain. Hence, in the application of mass, heat, and energy conservation, the assumptions of isothermal and adiabatic processes could simplify the analysis if it could be justified.

3.3.2 Atmospheric Pressure

Atmospheric pressure is the force per unit area exerted into a surface by the weight of air above that surface. This defines pressure as the product of the density of the fluid, ρ, its depth or height above the surface, h, and the acceleration due to gravity, g:

$$P = \rho g h, \tag{3.7}$$

where the equation parameters are the same as those of previous equations. Atmospheric pressure varies smoothly from the Earth's surface to the top of the mesosphere in different layers of the atmosphere as shown in Figure 3.1. Based on this figure, air pressure at the Earth's surface is 1 kg/cm^2, 1013.25 mb, or 14.7 psi, and as the altitude increases, the atmospheric pressure decreases. It should be mentioned that the given data in Figure 3.1 show the changes in average atmospheric pressure. In different points of the Earth, in the same altitude, the pressure may be different due to different factors, weather condition being the most important one. The average altitude of the 500 hectopascal (hPa) pressure (which is equal to 500 mb pressure or 0.5 atm) level of the atmosphere is often used in meteorological studies. As can be shown in Figure 3.1, it is at about 4 km from the Earth's surface. At 10,000 km, the altitude at which airplanes fly, the atmospheric pressure is about 200 hPa or 0.2 atm.

3.3.3 Atmospheric Temperature

Atmospheric temperature is an important measure controlling different components of the hydroclimatic cycle and their relationships. Like pressure, temperature changes with altitude. As explained in the lapse rate section, in the troposphere, for every 100 m of increase in altitude, the temperature

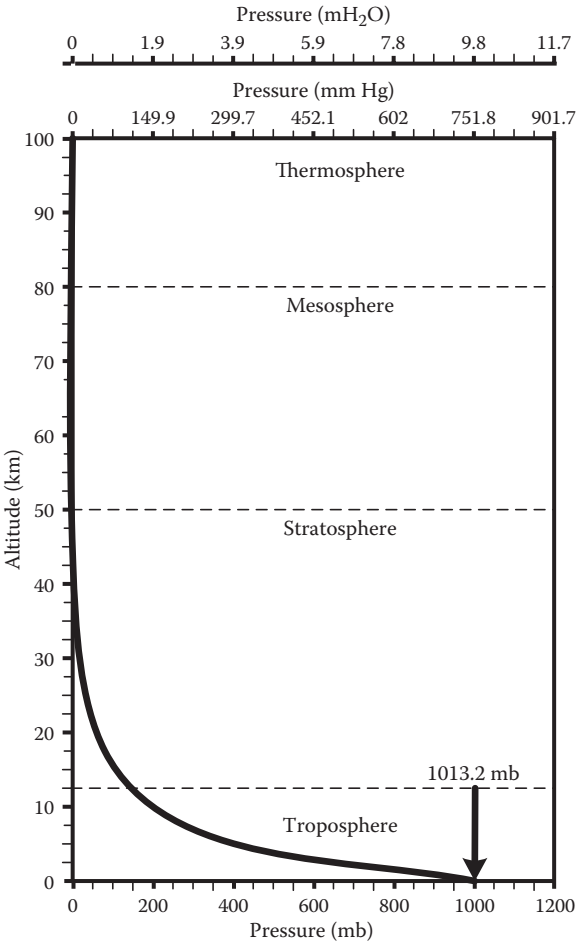

FIGURE 3.1 Change in average atmospheric pressure with altitude.

decreases by between 0.6°C and 1°C, but before discussing the temperature variation and how the water vapor in the atmosphere is affecting it, the presence of solar radiation and Earth reflection, which are the source of natural heat in the Earth's atmosphere, is discussed through a simple climate model.

This model focuses on simulating temperature. Other important factors such as precipitation patterns, ocean currents, winds and storms, sea ice, glacial cover, and soil moisture are neglected. Here, a single average global temperature is explained to demonstrate the significance of solar energy radiation and reflections from the Earth's surface that shows the magnificent energy balance that has been the major essence of life and motion forever. This balance has been violated lately due to excessive anthropogenic activities and the level of carbon dioxide and other greenhouse gases in the atmosphere.

This model considers the global Earth energy balance without considering any specific time and location. The global Earth energy balance is equal to the solar energy absorbed by the Earth with the energy that the Earth radiates back to space. The solar constant (S) is the radiation from the sun outside of the Earth's atmosphere. The annual intensity of solar constant at present is equal to 1370 W/m^2. All of the flux energy that strikes the Earth's surface passes through a circular area whose radius (R) is equal to the Earth's radius and is normal to the incoming radiation (Figure 3.2). Therefore, the rate at which solar energy strikes the Earth is $S\pi R^2(W)$.

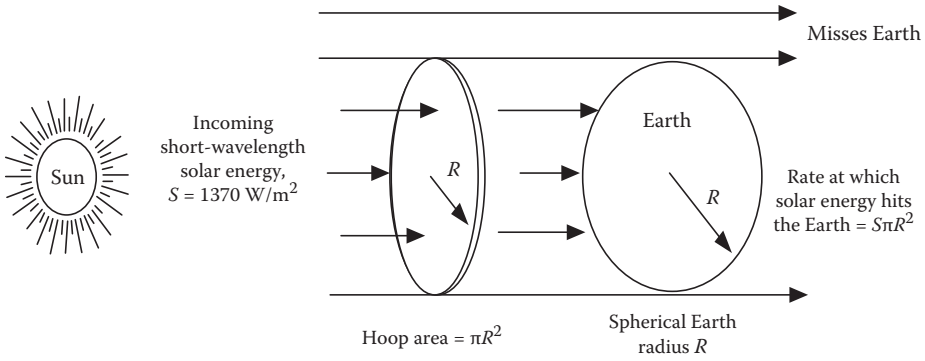

FIGURE 3.2 Simulation of solar energy gained by the Earth as a hoop.

Regarding Figure 3.3, some of the incoming solar energy to the Earth's surface is reflected back into space, which does not contribute to Earth surface or atmosphere heating. The fraction of incoming solar radiation that is reflected is named albedo, α. The global annual mean value of solar radiation received by the Earth is currently about 31%. Therefore, the absorbed energy would be $S\pi R^2(1 - \alpha)$.

The energy that is sent back to space by the Earth is also included in the global energy balance. The only way for the Earth to get rid of energy is by radiation because there cannot be heat transfer from the Earth to space by conduction or convection.

Considering the Earth as a blackbody, its radiation rate would be the same as an object with the same temperature and area. The resulting temperature by this assumption, which is called the Earth's effective blackbody temperature, T_e, is assumed to be the same everywhere on the planet. On the other hand, T_e can be interpreted as the temperature that would occur on the Earth's surface if it were a perfect blackbody, if there was no atmosphere, and if the temperature was the same at every point. Every object radiates energy at a rate that is proportional to its surface area times its absolute temperature raised to the fourth power. Since the area of the Earth, as a spherical object, is $4\pi R^2$, it can be written that

$$\text{Energy radiated back to space by Earth} = 4\sigma\pi R^2 T_e^4, \tag{3.8}$$

where σ is the Stefan–Boltzmann constant equal to 5.67×10^{-8} W/m^{-2} K^{-4} and T_e is the Earth's effective blackbody temperature (K).

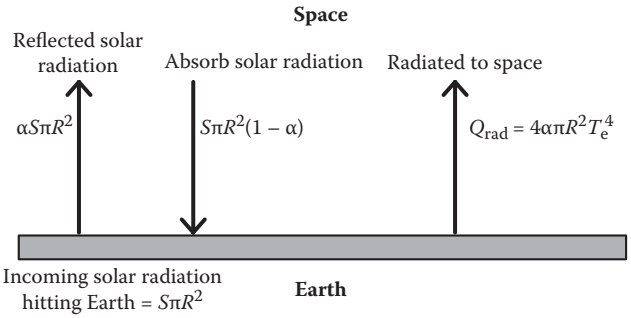

FIGURE 3.3 Simple global temperature model.

Under steady-state condition, the Earth's temperature remains constant over time. Therefore, the rate at which energy from the sun is absorbed and the rate at which energy is radiated from the Earth back to space are equal to each other. Also T_e is estimated as follows:

$$T_e = \left[\frac{S(1-\alpha)}{4\sigma}\right]^{\frac{1}{4}}. \tag{3.9}$$

By substituting the values of the constant terms in the above equation ($\alpha = 0.31$, $S = 1370$ and $\sigma = 5.67 \times 10^{-8}$ W/m^{-2} K^{-4}), T_e is estimated to be 254 K or –19°C:

$$T_e = \left[\frac{1370\,\frac{\mathrm{W}}{\mathrm{m}^2}(1-0.31)}{4\times 5.67\times 10^{-8}\,\frac{\mathrm{W}}{\mathrm{m}^2\,\mathrm{K}^4}}\right]^{\frac{1}{4}} = 254\ \mathrm{K} = -19°\mathrm{C}.$$

Earth's effective temperature cannot be defined in reality because there are different factors that affect not only the solar radiation in different points of the Earth but also the atmospheric condition. As it was mentioned in the previous chapter, the atmospheric temperature changes are completely different in the different layers of the atmosphere. The coldest temperatures lie near the mesopause, an area approximately 85 to 100 km above the surface. In contrast, some of the warmest temperatures can be found in the thermosphere, which receives strong ionizing radiation. In the troposphere where most of the hydroclimatic phenomena happen, the temperature decreases as the altitude increases in normal condition. In this layer, atmospheric temperature is governed by many factors, including incoming solar radiation, humidity, and altitude, as well as the presence (or absence) of water bodies. Due to the different positions of the Earth in relation to the sun in different seasons and parts of the world, the temperature is highly different in different parts of the Earth and in different times.

3.3.3.1 Global Energy Balance

The atmospheric temperature concepts can be used efficiently to describe the energy transfer in the Earth–atmosphere system as well as the greenhouse effect. Figure 3.4 shows a simple model of the greenhouse effect that considers the Earth's surface, the atmosphere, and outer space, as well as input solar radiation.

For simplicity, the energy flow between the considered spaces is expressed in terms of rates per unit of the surface area of the Earth. The total amount of solar radiation that the Earth surface receives is $S\pi R^2$. The average solar radiation is defined as the ratio of incoming solar radiation on the surface area of the Earth:

$$\frac{S\pi R^2}{4\pi R^2} = \frac{S}{4} = \frac{1370\ \mathrm{W/m^2}}{4} = 342\ \mathrm{W/m^2}, \tag{3.10}$$

where S is solar constant and R is Earth's radius.

Considering the albedo to be 31%, the amount of incoming radiation reflected back into space per square meter of the Earth's surface is the result of dividing the solar energy reflected on the surface area of the Earth.

$$\frac{S\pi R^2\alpha}{4\pi R^2} = \frac{S}{4}\alpha = 342\ \mathrm{W/m^2}\times 0.31 = 107\ \mathrm{W/m^2}. \tag{3.11}$$

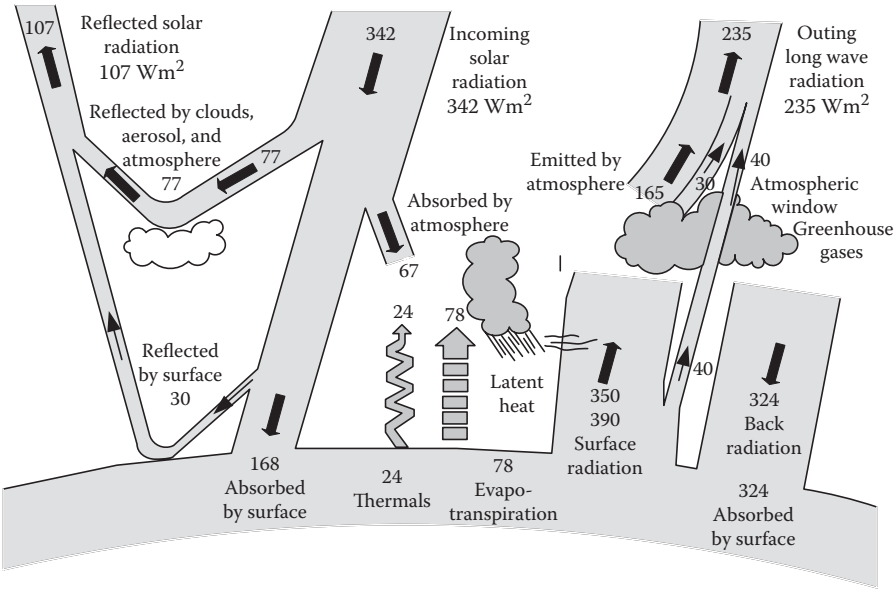

FIGURE 3.4 Global energy circulation model of the Earth–atmosphere system (W/m^2). (From IPCC, *Climate Change 1995*: *The Science of Climate Change*, Cambridge University Press, Cambridge, UK, 1996. With permission.)

Out of 107 W/m^2, it is estimated that 77 W/m^2 is reflected off the atmosphere itself, while the remaining 30 W/m^2 is reflected off the Earth's surface. The solar radiation that is not reflected is absorbed by the Earth and its atmosphere. The absorbed energy, Q_{abs} (with units of watts per square meter of surface), is the ratio of solar radiation absorbed by the surface area of the Earth:

$$Q_{abs} = \frac{S\pi R^2(1-\alpha)}{4\pi R^2} = \frac{S}{4}(1-\alpha) = 342 \text{ W/m}^2 \ \ (1-0.31) = 235 \text{ W/m}^2. \tag{3.12}$$

Of that 235 W/m^2, 67 W/m^2 is absorbed by the atmosphere, and the remaining 168 W/m^2 is absorbed by the surface of the Earth.

The Earth and its atmosphere absorb 235 W/m^2 of energy; thus, the same amount must be radiated back into space. If the Earth's surface were at 254 K, it would radiate 235 W/m^2, which is just enough to balance the incoming energy. However, the greenhouse gases absorb most of that outgoing 235 W/m^2; thus, the required energy balance cannot be satisfied. Therefore, the temperature of the Earth's surface must be higher than 254 K to force enough energy through the atmosphere to create the necessary balance.

Considering the actual temperature of the surface of the Earth, which is about 288 K, the radiated amount per unit of the Earth surface area would be the ratio of energy radiated by the surface area of the Earth:

$$\frac{\sigma 4\pi R^2 T_s^4}{4\pi R^2} = \sigma T_s^4 = 5.67\times10^{-8} \text{ W/m}^2 \text{ K}^4 \times (288 \text{ K})^4 = 390 \text{ W/m}^2. \tag{3.13}$$

Of this 390 W/m^2, 40 W/m^2 passes directly through the atmosphere; therefore, 350 W/m^2 of that is absorbed by greenhouse gases in the atmosphere. The atmosphere then radiates 324 W/m^2 back to the surface.

Heat is also transferred from the surface to the atmosphere by condensation of water and convective heating. Convection transfers 24 W/m^2 to the atmosphere, while condensation of water vapor provides 78 W/m^2 of latent heat. Furthermore, the rate of energy gain is equal to the rate of energy loss; hence, the model shows the necessary balances.

Since the early 20th century, Earth's average surface temperature has increased by about 0.8°C. The rising average temperature of the Earth's atmosphere and oceans is referred to as global warming. The energy balance described above has been interrupted by the existence of excessive greenhouse gases in the atmosphere that let the shorter wavelength solar radiation to pass through but intercept some of the longer wavelength (infrared radiation) reflecting from the Earth. In other words, the greenhouse effect is the process by which absorption and emission of infrared radiation by gases in the atmosphere take place, which is the most important cause of global warming. The properties of rising average temperature and global warming are described in depth in Chapter 9.

3.4 HEAT AND TEMPERATURE RELATIONSHIP

It is important to distinguish between heat and temperature in describing hydroclimatic phenomena. Heat is a source of energy that is directly related to the velocity of vibration of the molecules of each body, but temperature is a measure of the amount of heat energy that a body contains. Faster-vibrating molecules transmit some of their kinetic energy of motion to adjacent slower-moving molecules, a process that is referred to as conduction. In this way, heat energy is transmitted through parcels of air or any other controlled volume/body.

In order to measure the temperature of a body, heat energy is exchanged with an indicator, usually another substance that undergoes a known mode of (mechanical) deformation in response to such exchange. Most substances experience expansion or contraction in response to an input or output of heat energy, according to their coefficient of thermal expansion, which is the deformation produced per unit volume (or length) of material per unit change in temperature. If a thin-walled glass bulb full of fluid such as mercury is inserted into a medium such as water, air, or soil, kinetic energy will be exchanged between the molecules of the medium and those of the glass and mercury. If the mercury takes up energy from the medium, it will respond by expanding its volume. This will continue until a dynamic equilibrium is reached between the kinetic energy of the molecules of the substances on either side of the thin wall of the glass bulb.

In the next subsections, two important parameters—latent heat and lapse rate—that define temperature and heat relationships through the atmosphere are described. These factors highly affect the hydroclimatic processes that occur in the Earth–atmosphere system.

3.4.1 Latent Heat

When a substance phase changes such as when evaporation (distillation) occurs and water changes to vapor (vapor changes to water), energy is absorbed (released) without a change in temperature. The energy required to cause a phase change of a unit mass from solid to liquid (melting) at the same pressure is called the latent heat of fusion. Similarly, the energy required to change phase from liquid to vapor at constant pressure is called the latent heat of vaporization or the enthalpy of vaporization. For example, 333 kJ will melt 1 kg of ice, whereas 2257 kJ is required to convert 1 kg of water at 100°C to steam. When steam condenses or when water freezes, those same amounts of energy are released. When the temperature of a substance changes through heating, the process is referred to as sensible heating. When the addition of heat causes a phase change, as is the case when ice is melting or water is boiling, the addition is called latent heat. To account for latent heat stored in a substance, it can include the following equation:

$$Q = m \times L, \tag{3.14}$$

TABLE 3.2
Latent Heat of Water Fusion and Vaporization at Different Temperatures

Property	Unit
Heat of vaporization (100°C)	2257 kJ/kg
Heat of vaporization (15°C)	2465 kJ/kg
Heat of fusion	333 kJ/kg

where Q is energy released or absorbed in phase change, m is the mass, and L is the latent heat of fusion or vaporization. Values of heats of vaporization at different temperatures and fusion are given in Table 3.2.

Example 3.4

The volume of the stored water in the Caspian Sea, the world's largest lake, is 78,700 MCM (million cubic meters). Find the energy required to cause that much water to evaporate during a year if its temperature is considered to be 15°C. Compare this to the average energy consumption of 4.7×10^{17} kJ in the world and compare it to the average rate at which sunlight strikes the surface of the Earth, which is about 168 W/m^2. The Earth's surface is 5.10×10^{14} m^2.

Solution:

In Table 3.2, the energy required to vaporize 1 kg water at 15°C water is given as 2465 kJ/kg. The total energy required to vaporize all of that water is $78{,}700 \times 10^6$ m^3 $\times$ 10^3 kg/m^3 $\times$ 2465 kJ/kg = 1.94×10^{17} kJ.

This is roughly 40% of the 4.7×10^{17} kJ of energy that is used throughout the world in a year.

The energy that is obtained from the sun during a year is estimated as follows:

$$168 \times 365 \times 24 \times 3600 \times 5.10 \times 10^{14} = 2.70 \times 10^{21} \text{ kJ}$$

This is about 1400 times more than what is required for vaporizing the Caspian Sea water storage.

3.4.2 Lapse Rate

As mentioned before, the temperature changes significantly with latitude especially in the lower layer of the atmosphere. However, the rate of this change is highly dependent on the mechanism of expansion as well as on the mass moisture content. In general, the lapse rate is defined as the rate of atmospheric temperature decrease with height. In general, a lapse rate is the negative of the rate of change of temperature with altitude. Thus:

$$\gamma = -\frac{dT}{dz}, \tag{3.15}$$

where γ is the lapse rate given in units of temperature divided by units of altitude, T is temperature, and z is altitude. The rate of temperature change affects the climatic condition of the regions and the precipitation formation process as will be described.

There are two types of lapse rate: ambient lapse rate and the adiabatic lapse rates. Ambient (normal) lapse rate refers to the actual change of temperature with altitude in the stationary atmosphere at a given time and location. Although the actual atmospheric lapse rate varies, under normal atmospheric conditions, the average ambient atmospheric lapse rate results in a temperature decrease of about 10°C per 1000 m of altitude. The varying normal lapse rates throughout the atmosphere are very important in meteorological events within the troposphere. They are used to determine if the parcel of rising air will rise high enough for its water to condense to form clouds, and, having formed clouds, whether the air will continue to rise and form larger mass of clouds and whether these clouds will get even bigger and form thunderclouds. There are a number of factors (such as wind speed, sunlight, and geographical features) that cause the actual ambient lapse rate, Γ, in the real atmosphere to differ from the 10°C/1000 m lapse rate just calculated.

The adiabatic lapse rates refer to the change in temperature of a parcel of air as it moves upwards (or downwards) without exchanging heat with its surroundings. The temperature change that occurs within the air parcel reflects the adjusting balance between potential energy and kinetic energy of the molecules of gas that comprise the moving air mass. There are two adiabatic lapse rates—dry and moist (saturated)—that will be discussed in the next sections.

3.4.2.1 Dry Adiabatic Lapse Rate

The dry adiabatic lapse rate is the rate of temperature decrease with height for a parcel of dry or unsaturated air rising under adiabatic conditions. It is useful to imagine a parcel of air being made up of a number of air molecules with an imaginary boundary around them. If this parcel of air moves upward in the atmosphere, it will experience less pressure, causing it to expand and cool. On the other hand, if it moves downward, more pressure will compress the air, and its temperature will increase.

By applying both the ideal gas law and the first law of thermodynamics, the following expression is derived:

$$\mathrm{d}Q = C_\mathrm{p}\mathrm{d}T - V\mathrm{d}P, \tag{3.16}$$

where dQ is heat added to the parcel per unit mass (J/kg), C_p is specific heat of air at constant pressure, that is, the amount of heat required to raise the temperature of 1 kg of air by 1°C while holding its pressure constant at 1005 J/kg-K, dT is incremental temperature change (K), V is volume per unit mass (m^3/kg), and dP is incremental pressure change (Pa).

By making the accurate assumption that there is no heat transferred across its boundary as the parcel moves, this process is adiabatic. This means that dQ = 0, thus:

$$\frac{\mathrm{d}T}{\mathrm{d}P} = \frac{V}{C_\mathrm{p}}. \tag{3.17}$$

Equation 3.17 gives an indication of how atmospheric temperature would change with air pressure, but it is interesting how it changes with altitude to do that; it needs to know how pressure and altitude are related. Consider a static column of air with cross section A, as shown in Figure 3.5.

A horizontal slice of air in that column of thickness dz and air density ρ will have a mass of ρA dz. If the pressure at the top of the slice is $P(z)$, the pressure at the bottom of the slice will be $P(z + \mathrm{d}z)$ plus the added weight per unit area of the slice itself:

$$P(z) = P(z + \mathrm{d}z) + \frac{g\rho A\mathrm{d}z}{A} = P(z + \mathrm{d}z) + g\rho\mathrm{d}z, \tag{3.18}$$

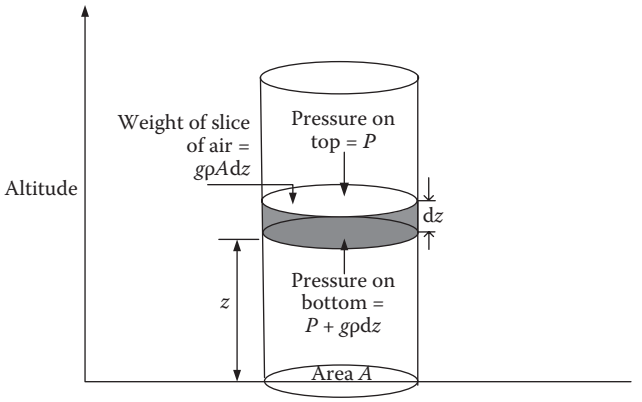

FIGURE 3.5 Column of air in static equilibrium used to determine the relationship between air pressure and altitude.

where g is the gravitational constant. Therefore, the incremental pressure, dP, for an incremental change in elevation, dz, is equal to

$$dP = P(z + dz) - P(z) = -g\rho dz. \tag{3.19}$$

The rate of temperature change with altitude can be obtained using Equations 3.16 and 3.19:

$$\frac{\mathrm{d}T}{\mathrm{d}z} = \frac{\mathrm{d}T}{\mathrm{d}P} \times \frac{\mathrm{d}p}{\mathrm{d}z} = \left(\frac{V}{C_\mathrm{p}}\right)(-g\rho). \tag{3.20}$$

Since V is volume per unit mass and ρ is mass per unit volume, their product results in $V\rho = 1$, and Equation 3.20 simplifies to

$$\frac{\mathrm{d}T}{\mathrm{d}z} = \frac{-g}{C_\mathrm{p}}. \tag{3.21}$$

The negative sign indicates that temperature decreases with increasing altitude. Substituting the constant $g = 9.806$ m/s^2 and the constant volume specific heat of dry air at room temperature $C_\mathrm{p} =$ 1005 J/kg-K in Equation 3.21 results in the dry adiabatic lapse rate, Γ_d:

$$\frac{\mathrm{d}T}{\mathrm{d}z} = \frac{-9.806}{1005} = -0.00976 \text{ K/m} = 9.76 \approx 9.8°\text{C/km}. \tag{3.22}$$

Therefore, for every kilometer of increase in altitude, the temperature decreases by about 9.8°C.

3.4.2.2 Saturated Adiabatic Lapse Rate

When the air is saturated with water vapor, the moist adiabatic lapse rate or saturated adiabatic lapse rate applies. This lapse rate varies with temperature. Equation 3.22 was derived assuming the parcel of air could be treated as an ideal gas that could be moved in the atmosphere without any heat transfer through and around it. If the air parcel contains some water vapor, C_p changes slightly from the values assumed. On the other hand, if enough water vapor is present when condensation occurs, the parcel is raised and cooled and the latent heat will be released. The added heat means a

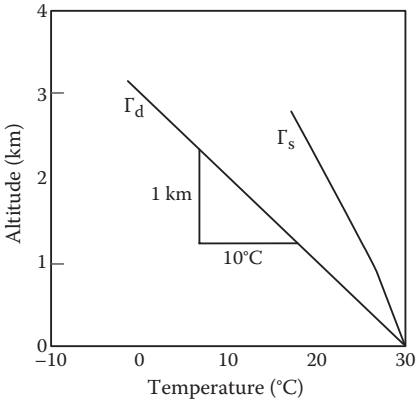

FIGURE 3.6 Dry, Γ_d, and saturated, Γ_s, adiabatic rates.

saturated air parcel will not cool the same as when it is dry. This heat release process is an important source of energy in the development of thunderstorms. Unlike the dry adiabatic rate, the saturated adiabatic lapse rate, Γ_s, is not a constant since the amount of moisture that air can hold before condensation is a function of temperature. A reasonable average value of the moist adiabatic lapse rate in the troposphere is 6°C/km. Figure 3.6 shows the changes of temperature with altitude in dry and saturated air parcels.

3.4.3 Atmospheric Stability

Stability is a fundamental underlying concept in the analysis of weather phenomena. A region of the atmosphere is stable if, on lifting a parcel of air, its immediate tendency is to sink back when released. This requires the displaced air to be colder (and thus denser) than its surroundings. The ascending dry air cools at the dry adiabatic lapse rate but the surrounding air cools with altitude in a normal lapse rate. Therefore, the difference between the ambient lapse rate and the adiabatic lapse rate determines the stability of the atmosphere.

The atmosphere becomes unstable if the temperature drops sufficiently rapidly with altitude or if the adiabatic lapse rate is more than the ambient lapse rate. The air is then unstable if it becomes saturated or, in more general form, when the ambient lapse rate is more than the adiabatic lapse rate. Conditional instability happens when the ambient lapse rate lies between the dry and moist rates.

In Figure 3.7, the stable and unstable conditions of weather are shown. Consider Figure 3.7a, which shows an ambient temperature profile for air that cools more rapidly with altitude than the dry adiabatic lapse rate. Imagine a 20°C parcel of air at 1 km to be just like the air surrounding it. If the parcel is raised to 2 km, it will cool adiabatically to 10°C. The 10°C parcel of air at 2 km is now warmer than the surrounding air (0°C in Figure 3.7); hence, it is less dense, is more buoyant, and will keep rising. Conversely, a parcel of air at 1 km that is nudged downward becomes colder than the surrounding air, and so it keeps sinking. It does not matter whether the parcel of air is nudged up or down; in either case, it keeps on going, and the atmosphere is said to be unstable. In Figure 3.7b, the ambient temperature profile is drawn for a case in which the ambient temperature cools less rapidly than the adiabatic lapse rate, which corresponds to atmosphere stability. In this situation, anything that starts a parcel of air moving up or down will cause the parcel to experience forces that will want it to return to its original altitude.

Figure 3.8 shows a summary of how lapse rates determine atmospheric stability. If the ambient lapse rate shows cooling at a faster rate than the dry adiabatic lapse rate, Γ_d, such as line A in Figure 3.8, the atmosphere is absolutely unstable in region A. The air will always have a tendency to move

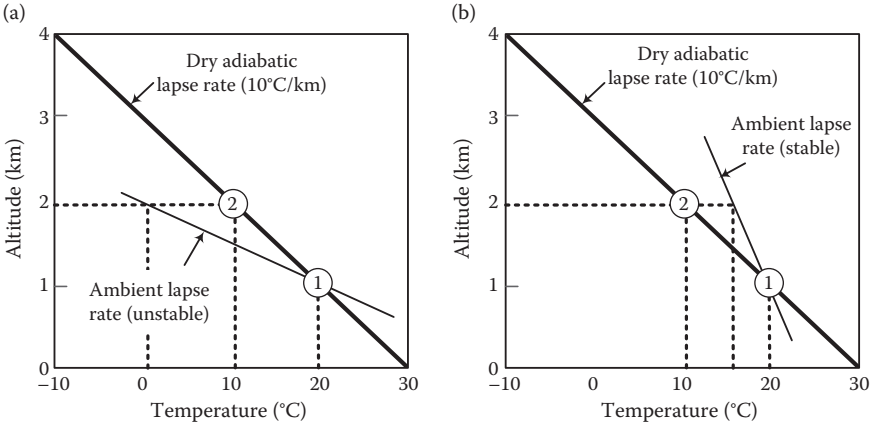

FIGURE 3.7 (a) Unstable and (b) stable atmosphere.

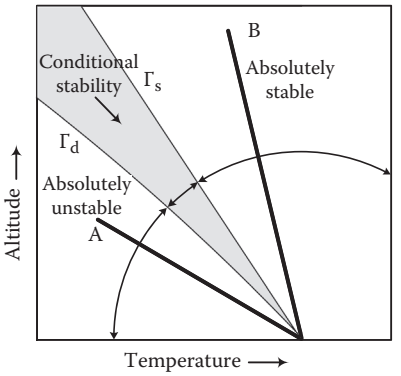

FIGURE 3.8 Absolute stable (region B), absolute unstable (region A), and conditional stability of atmosphere regarding the wet (Γ_s) and dry (Γ_d) lapse rates.

to some new altitude, enhancing the vertical dispersion of pollution. For ambient temperatures that cool less rapidly than the saturated adiabatic lapse rate, Γ_s, such as B in Figure 3.8, the atmosphere is absolutely stable in region B. For ambient lapse rate between the dry and wet adiabatic lapse rates, the atmosphere may be stable or it may be unstable. That region is labeled as having conditional stability.

The weather stability highly affects the climatic condition. Stable conditions can happen during a clear and calm night, trapping pollutants near the ground level. In moist stable weather, drizzle occurs. Over hot surfaces during warm days, unstable dry air can lead to significant refraction of the light within the air layer, which causes inferior mirages. When winds are light, dust devils can develop on dry days within a region of instability at ground level. Small-scale, tornado-like circulations can occur over or near any intense surface heat source, which would have significant instability in its vicinity. A steam devil is a rotating updraft that involves steam or smoke.

Atmospheric stability plays a major role in cloud formation. In general, an unstable or conditionally unstable atmosphere is more conducive to the development of clouds and precipitation. Sometimes, a parcel can be forced to rise in a stable environment, but the atmosphere strongly resists upward motion and any clouds that form are usually fairly thin and flat. An unstable atmosphere is necessary for the development of large convective clouds that are observed during thunderstorms.

Instability in the atmosphere makes the atmosphere conducive to cloud formation, but there still needs to be some mechanism that gives the initial upward thrust to start the process. The most common lifting methods are as follows: convection, convergence, lifting along fronts, and lifting caused by topography. Each lifting mechanism can result in clouds that have different physical characteristics. These are discussed further in Section 3.6.

3.4.3.1 Temperature Inversions

Temperature inversions represent the extreme case of atmospheric stability, creating a virtual lid on the upward movement of pollution. In this case, the temperature would increase by increasing the height. Inversions, such as radiation inversion and subsidence inversion, have several causes. Radiation inversions are caused by nocturnal cooling of the Earth's surface, especially on a clear winter night when the radiation from the surface of the Earth exceeds the amount of radiation received from the sun.

The second, subsidence inversion, is the result of the compressive heating of descending air masses in high-pressure zones. Warm air passing over a cold body of water, for example, creates an inversion. There are also inversions in valleys when cold air rolls down the canyons at night under warmer air that might exist aloft.

An important result of inversion is that pollutants are not allowed to rise and their concentration will increase near the surface, which may cause serious damage to human health. To illustrate how the atmospheric temperature profile affects the dispersion of pollutants, an example of pollutant distribution in air from a smokestack is illustrated in Figure 3.9. In a neutrally stable atmosphere, the plume of pollutants is expected to be relatively symmetrical, called coning (Figure 3.9a). In Figure 3.9b, the atmosphere is very unstable and because of the rapid vertical air movement upward and downward, a looping plume is formed. In Figure 3.9c, the stable atmosphere restricts the dispersion of the plume in the vertical direction, and a fanning plume results. In Figure 3.9d, the smokestack is under an inversion layer; therefore, emission moves downward. The resulting fumigation can

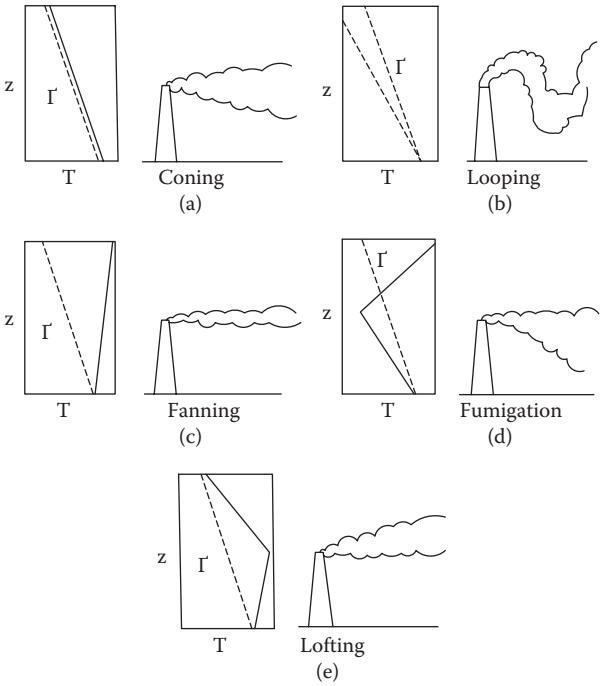

FIGURE 3.9 Effect of atmospheric lapse rates and stack height on plume behavior (the dashed line is ambient lapse rate, Γ). (a) Neutrally stable atmosphere; (b) very unstable atmosphere; (c) stable atmosphere; (d) inversion in upper layer of atmosphere; and (e) inversion in lower layer of atmosphere.

lead to greatly elevated downwind, ground-level concentrations. When the smokestack is above an inversion layer (Figure 3.9e), downward motion is limited because of the inversion's stable air and mixing in the upward direction is observed. This condition is called lofting. If the pollutant emission sources are placed in this position, it will help to keep the pollution high above the ground and reduce the exposure to people. In fact, a common result, however, has been that pollutants released from all stacks are able to travel great distances and may cause unexpected effects, such as acid deposition, hundreds of miles from the source.

Example 3.5

Consider a parcel of air at 25°C at the elevation of 1000 m above the mean sea level. While moving, this air encounters a mountain range 3000 m high. The air rises, moves over the mountains, and then descends to an elevation of 1500 m. If an ascent of 1500 m produces saturation and condensation, and if the average saturated lapse rate is about half of the dry adiabatic lapse rate, what will be the temperature of air? The dry adiabatic lapse rate is 7°C/km.

Solution:

The air reaches saturation at an elevation of 1000 + 1500 = 2500 m. Therefore, before 2500 m altitude, the air parcel cools at the dry adiabatic lapse rate (0.7°C/100 m), and after that and until the mountain top is reached because of saturation, it will cool at the wet adiabatic lapse rate.

The drop in the temperature during an initial climb of 1500 m is equal to 0.7 × (1500/100) = 10.5°C. The drop in the temperature during a final climb of 500 m to mountain top (from 2500 to 3000 m) is equal to (0.7/2) × (500/100) = 1.75°C. The air temperature (°C) at an elevation of 3000 m is equal to 25 – 10.5 – 1.75 = 12.75°C. The air descends to an elevation of 1500 m. The temperature rise is equal to 0.7 × (1500/100) = 10.5°C. The final temperature is 12.75 + 10.5 = 23.25°C.

3.5 MEASURES OF WATER VAPOR IN THE ATMOSPHERE

Water vapor is the gaseous phase of water and is derived from the diffusion of water molecules from their liquid state at the Earth's surface. Consequently, water vapor is concentrated in the lowest 10 km of the atmosphere, with approximately 90% of it occurring below 6 km. It is one of the most variable constituents of the atmosphere, contributing between 0.5% and 4% of the volume of moist air. The amount present may be expressed in terms of absolute humidity, specific humidity, or mixing ratio (Shuttleworth 2000).

1. Absolute humidity is the amount of water vapor present in a unit volume of air, usually expressed in kilograms per cubic meter.

$$\chi = \frac{m_v}{V}, \tag{3.23}$$

where χ is absolute humidity (kg/m^3), m_v is mass of vapor (kg), and V is volume of air it contains (m^3).

2. Specific humidity is the mass of water vapor in a unit mass of moist air, usually expressed as grams of vapor per kilogram of air.

$$q = \frac{m_v}{\left(m_v + m_a\right)}, \tag{3.24}$$

where m_v is mass of water air and m_a is mass of moist air.

3. Relative humidity is the amount of water vapor in the air at any given time and is usually less than that required to saturate the air. The relative humidity is the percentage of saturation humidity, generally calculated in relation to saturated vapor density.

$$\mathrm{RH} = \left(\frac{e_a}{e_s} \times 100 \right), \tag{3.25}$$

where e_a is actual vapor density and e_s is saturated vapor density.

RH in percentage can be expressed directly from air temperature T (°C) and dew point temperature T_d (°C) as

$$\mathrm{RH} = \left(\frac{112 - 0.1T + T_d}{112 + 0.9T} \right)^8. \tag{3.26}$$

Example 3.6

Compute the relative humidity if the air temperature and dew point are 30°C and 20°C, respectively.

Solution:

Equation 3.26 is used to compute RH:

$$\mathrm{RH} = \left(\frac{112 - 0.1 \times 30 + 20}{112 + 0.9 \times 30} \right)^8 = \left(\frac{129}{139} \right)^8 = (0.928)^8 = 0.5503 = 55.03\%.$$

Example 3.7

Compute the dew point temperature if the air temperature and relative humidity are 35°C and 80%, respectively.

Solution:

Equation 3.26 is used to compute T_d:

$$(0.8)^{0.125} = \left(\frac{112 - (0.1 \times 30) + T_d}{112 + (0.9 \times 35)} \right)^8$$

$$T_d = 31.13^\circ\mathrm{C}.$$

Water vapor exerts a partial pressure in the atmosphere, which is referred to as its vapor pressure (e). It normally varies between 5 and 30 mb. When the atmosphere lies above a liquid water surface,

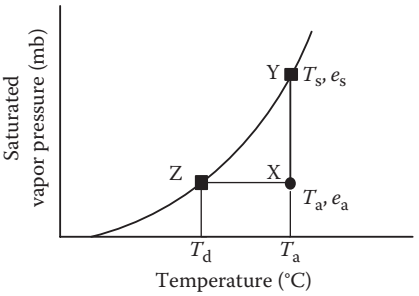

FIGURE 3.10 Saturation vapor pressure curves with respect to water.

water molecules are constantly being exchanged between them. When the atmosphere is dry, the rate of uptake of molecules is greater than the rate of return to the surface. When a point of equilibrium is reached where the number of molecules leaving the surface is equal to the number arriving, the vapor pressure of the air has reached saturation with respect to water. Subsequent addition of water molecules to the air is balanced by deposition on the surface.

The value of vapor pressure at which saturation occurs is dependent on air temperature, as indicated in the saturation vapor pressure curve of Figure 3.10. Its humidity can be measured using a parcel of dry air at point X with temperature T_a and vapor pressure e_a. If its temperature remains constant and more water molecules are added, the vapor pressure will increase until saturation is reached at Y where saturation vapor pressure is e_s. The difference between e_s and e_a is called pressure deficit. If vapor pressure remains constant, the saturation can be reached at point Z, by decreasing temperature to dew point temperature T_d. The difference between T_a and T_d may also be used as an indication of the humidity of the air.

To calculate the saturation vapor pressure (e_s) at air temperature (T) in degrees centigrade, use the following:

$$e_s = 0.6108 \exp\left(\frac{17.27T}{237.3+T}\right) \text{kPa}. \tag{3.27}$$

Example 3.8

Using Equation 3.27, derive the following expression for the air temperature with vapor pressure e.

$$T = \frac{\ln(e_s)+0.49299}{0.707-0.00421\times\ln(e_s)}.$$

Solution:

From Equation 3.27:

$$e_s = 0.6108 \exp(17.27T/(237.3 + T))$$

$$\ln(e_s) = \ln(0.6108) + 17.27T/(237.3 + T)$$

$$(237.3 + T)(\ln(e_s) - \ln(0.6108)) - 17.27T = 0$$

$$T = (-237.3\ln(0.6108) + 237.3\ln(e_s))/(17.27 - \ln(e_s))$$

$$T_{dew} = (\ln(e_s) + 0.49299)/(0.0707 - 0.00421\ln(e_s))$$

then

$$T = \frac{\ln(e_s) + 0.49299}{0.707 - 0.00421 \times \ln(e_s)}.$$

3.5.1 Density of Moist Air

The density of moist air ρ_a is defined as the mass of water vapor and the mass of dry air per unit volume of the moisture. If P_a is the pressure of the moist air and e is the vapor pressure, then $P_a - e$ is the partial pressure of dry air alone.

The ideal gas can be used for a mixture of gases such as air as well as each component of the mixture if the related variables to that component are used in the ideal gas law. Therefore, the ideal gas can be written for the water vapor as follows:

$$\rho_W = \frac{e}{R_{Sw}T}. \tag{3.28}$$

Since $R_S = \frac{R}{M}$ and due to different molar weights of water vapor (18 g) and air (28.97 g), R_{Sw} and R_{Sd} (dry air) would be different. Therefore, to make the constant number in density estimations the same, for water vapor density, R_{Sd} is employed, which is 1/0.622 of R_{Sw} (the molar weight of water vapor is 0.622 of dry air). Therefore, the density of water vapor ρ_w (g/cm^3) can be defined as

$$\rho_w = 0.622\frac{e}{R_{Sd}T}, \tag{3.29}$$

where T is the absolute temperature (°K), e is the vapor pressure (mb), and R_{Sd} is the dry air constant that is equal to 2.87×10^3. The density of dry air ρ_d in g/cm^3 can be expressed based on the ideal gas law as

$$\rho_d = \frac{p_d}{R_{Sd}T}, \tag{3.30}$$

where p_d is the pressure in millibars.

Because $\rho_a = \rho_w + \rho_d$, Equations 3.29 and 3.30 can be added to yield an expression for ρ_a as

$$\rho_a = 0.622\frac{e}{R_{Sd}T} + \frac{p_d}{R_{Sd}T} = \frac{1}{R_{Sd}T}(0.622e + p_d). \tag{3.31}$$

By replacing p_d by $p_a - e$ in Equation 3.31, then

$$\rho_a = \frac{1}{R_{Sd}T}(0.622e + p_a - e) = \frac{p_a}{R_{Sd}T}\left(1 - 0.378\frac{e}{p_a}\right). \tag{3.32}$$

In moist air, water vapor pressure is more than zero; therefore, the density of moist air would be less than that of wet air.

Example 3.9

Consider 1 m^3 of dry air. What will be the weight in kilograms if the air temperature and pressure are 5°C and 1000 mb, respectively?

Solution:

Equation 3.30 is used to compute the weight of dry air. $R = 2.87 \times 10^3$.

$$\rho_d = \frac{1000}{2.87 \times 10^3 \times (273+5)} = 0.001253 \text{ g/cm}^3.$$

Therefore, the weight of $1m^3$ of dry air would be $0.001253 \times 10^6/1000 = 1.253$ kg.

In this chapter, we have learned the following: the atmosphere is composed of a mixture of many different gases and the behavior of this mixture in many ways is like a single gas; the energy balance between sun and Earth can be expressed based on a simple model; there are important relationships between atmospheric temperature and pressure with the altitude as well as air density and volume; and water vapor and vapor pressure in the atmosphere are key elements in the transformation of water mass from the Earth to the atmosphere. In the next section, the transformation of different hydroclimatic processes explained so far in describing cloud and precipitation formation as the main attributes of the hydrologic cycle has been tried. This passage is an important step in relating hydrology and hydroclimatology. In a larger scale, the interconnection between long-range signals (change in temperature and pressure in a continental scale) is described, following similar principles but with many more complexities in order to project movement of wet air masses. This particular topic has the potential for long-lead (6 months ahead) prediction of precipitation and flood/drought.

3.6 CLOUDS AND PRECIPITATION FORMATION

A combination of specific hydroclimatic processes at the right time and place could transform the air moisture provided through evapotranspiration to form clouds and, after that, to trigger precipitation. This perhaps is the most critical step in the hydrologic cycle.

Precipitation is water released from clouds in the form of rain, freezing rain, sleet, snow, or hail. It is the primary connection in the water cycle that provides for the delivery of atmospheric water to the Earth. Air currents and reflected solar energy bring evaporated water from the ocean and the Earth's surface up into the sky. The evaporated liquid condenses in the cold air, forming moisture-filled rain clouds.

Clouds are important features of the climatic system that could affect different climatic variables such as temperature, pressure, and humidity. Cloud formation and development are also related to climatic variables. Even small changes in the abundance or location of clouds could change the climate more than the anticipated changes caused by greenhouse gases, human-produced aerosols, or other factors associated with global change. In order for scientists to create increasingly realistic computer simulations of Earth's current and future climate, they will have to include more accurate representations of the behavior of clouds.

Clouds are the key regulator of the Earth's average temperature. Some clouds contribute to cooling because they reflect some of the sun's energy or shortwave radiation back to space. Other clouds contribute to warming because they act like a blanket and trap some of the heat at the Earth's

surface and in the lower atmosphere. Cloud systems also help spread the sun's energy evenly over the Earth's surface. Storms move across the planet and transport energy from warm areas near the equator to cold areas near the poles.

The global prevalence of cloud cover is dependent on latitude. The maximum cloudiness is observed close to the equator and near 50° latitude in the Northern and Southern Hemispheres. These are zones of low pressure that encircle the Earth as part of a system of large latitudinal cells that influence atmospheric circulation.

Near the equator, increased cloudiness is due to the presence of the low-pressure Intertropical Convergence Zone or monsoon trough. The monsoon trough in the western Pacific reaches its latitudinal zenith in each hemisphere above and below the equator during the late summer when the wintertime surface high-pressure ridge in the opposite hemisphere is strongest.

3.6.1 Cloud Formation

Clouds are, in essence, massive collections of tiny water droplets and crystallized water molecules. The different shapes, textures, and other features of clouds depend largely on the conditions under which they form and later develop. For instance, temperature, humidity, and altitude are all factors that affect cloud formation. The main processes contributing in cloud formation are as follows:

1. Advection: Water vapor enters the atmosphere through evaporation from open water, the soil, or the leaves of plants. The wind transports water vapor from one region to another through a process called advection.
2. Convection: Convection is the process of ascending warm air and descending cold air due to their density difference. The main step in cloud formation is air mass rising, which is needed for air cooling and reaching the dew point. In general, an unstable or conditionally unstable atmosphere is more conducive to the development of clouds and precipitation. Sometimes, a parcel can be forced to rise in a stable environment, but the atmosphere strongly resists upward motion and any clouds that form are usually fairly thin and flat. The following mechanisms or processes can result in air mass rising (Figure 3.11):
   a. Orographic uplift occurs when air is forced to rise because of the physical presence of elevated land. As the air mass rises, it cools as a result of adiabatic expansion until saturation.
   b. Convectional lifting is associated with surface heating of the air at the ground surface. If enough heating occurs, the mass of air becomes warmer and lighter than the air in the surrounding environment, and it begins to rise, expand, and cool.

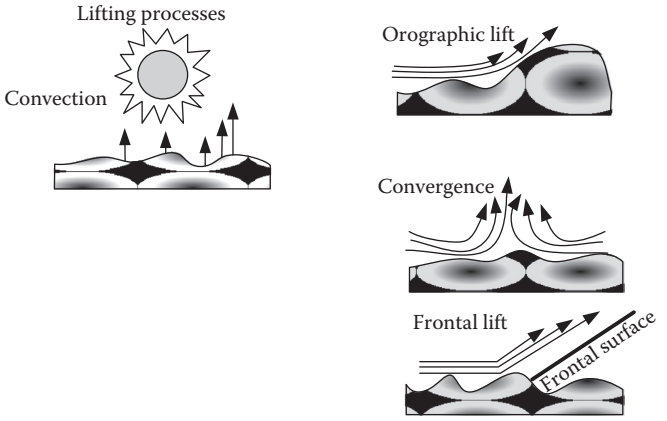

FIGURE 3.11 Different mechanisms and process of air mass rising.

   c. Convergence or frontal lifting takes place when two masses of air come together. In most cases, the two air masses have different temperature and moisture characteristics. One of the air masses is usually warm and moist, while the other is cold and dry. Of course, the lifting causes the warm moist air mass to cool due to expansion resulting in saturation.
3. Condensation: Cloud formation happens easily when water vapor has something to cling to, allowing the water vapor to change into its liquid or solid phase. A number of particles can act in this function, for example, the commonly called condensation nuclei or freezing nuclei (also known as aerosols or nucleators). Aerosols come from natural sources such as volcanoes or forest fires, as well as from human activities such as air pollution. Some aerosols are hygroscopic, meaning they readily absorb and retain water. When a parcel cools to its dew point, cloud droplets begin to form as the excess water vapor condenses on the largest aerosol particles. As the parcel keeps rising, more water condenses and the cloud droplets grow in size. If the droplets get large enough, they fall out of the cloud as precipitation.
4. Precipitation formation: After condensation, some additional process is necessary for droplets or crystals to grow to a size large enough to fall freely from the cloud and reach the ground as snow or rain. Because of their small size, consequent slight pull of gravity, and negligible rate of fall, and for all practical purposes, cloud droplets are suspended in the air. Even drizzle droplets seem to float in the air. Raindrops range in size from a diameter of about 1/50 to 1/5 in. Drops larger than 1/5 in tend to break up when they fall. It takes about 30 million cloud droplets of average size to make one raindrop with a diameter of about 1/8 in. There seem to be two processes that act together or separately to cause millions of cloud droplets to grow into a raindrop. One is the ice-crystal process and the other is the coalescence process (National Aeronautics and Space Administration 2005).

3.6.2 Hurricane Formation

A massive hurricane can start as a tropical thunderstorm that strengthens under certain conditions. When several thunderstorms start rotating around a central area of low pressure, a tropical depression is formed. When the wind speeds of a tropical depression increase to more than 74 mph, a hurricane or tropical cyclone is formed. Hurricanes can become stronger by taking energy from the warm ocean water that supplies warm, moist air for feeding. Therefore, while a hurricane is over warm water, it will become stronger and it dies when it moves away from the warm waters.

The rotation of the storm is due to the Coriolis effect, a product of the Earth's rotation. Hurricanes do not occur within 500 km of the equator because there is no Coriolis effect at the equator. This causes the air being drawn into the central low pressure to curve. The air rises as it rotates. This rising air, which is saturated with water, cools and condenses, forming clouds.

In recent years, long-lead forecasting of precipitation is important in water resources management and many models have been developed to forecast precipitation. Most of these models incorporate the effects of large-scale climate variables. For this purpose, initially, climate variables are defined, after which the relation and correlation between climate variables and precipitation are presented by two case studies.

3.7 CLIMATE VARIABILITY

When global heat balance was described, it was mentioned that the approximate average global temperature is constant, but there are high variations in atmosphere temperature at different times during the year and in different years. This is referred to as internal climate variability and has resulted in different seasons as well as having cold and hot years. Regarding the variations in temperature, other climatic variables, such as precipitation and humidity, are affected by these changes.

Furthermore, there are some climatic factors that intensify the internal climate variability. They can be a direct cause of variability, in the absence of any significant change in the external forcing factors, through interactions between various elements of the system. El Niño, La Niña, the Southern Oscillation, sea level pressure (SLP), and sea surface temperature (SST) are important examples of internal climate variability that affect the global climate system. There are also some systems that locally affect the climate such as monsoons. In the next sections, these variables are described. Due to the high correlation of these phenomena with the climatic condition in different parts of the world, these measures are used for climatic prediction purposes. In the last part of this chapter, two applications of these measures for rainfall prediction are discussed through two case studies.

3.7.1 El Niño, La Niña, and Southern Oscillation

El Niño is an abnormal warming of surface ocean waters in the eastern tropical Pacific and is one part of what is called the Southern Oscillation. The Southern Oscillation is the seesaw pattern of reversing surface air pressure between the eastern and western tropical Pacific; when the surface pressure is high in the eastern tropical Pacific, it is low in the western tropical Pacific, and vice versa. Because the ocean warming and pressure reversals are, for the most part, simultaneous, scientists call this phenomenon the El Niño/Southern Oscillation or ENSO for short. South American fishermen have given this phenomenon the name El Niño, which is Spanish for "the Christ Child," because it comes about the time of the celebration of the birth of the Christ Child—Christmas.

To really understand the effects of an El Niño event, compare the normal conditions of the Pacific region and then see what happens during El Niño below. Figures 3.12 and 3.13 show the

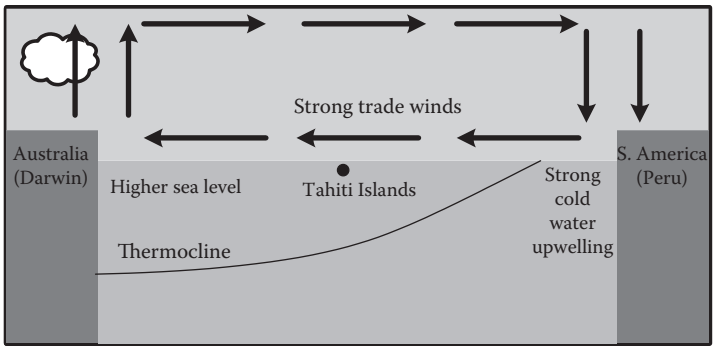

FIGURE 3.12 Normal condition between Tahiti and Darwin.

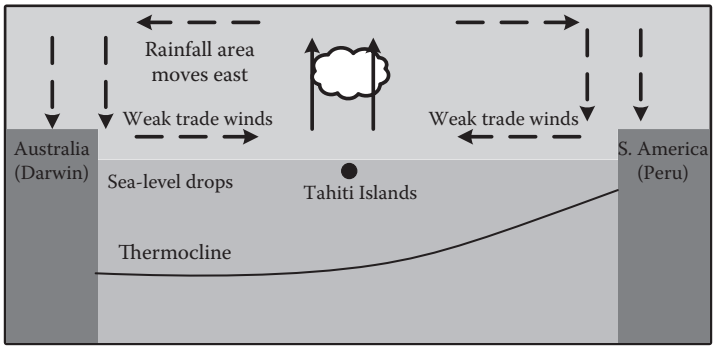

FIGURE 3.13 El Niño condition between Tahiti and Darwin.

pattern of atmospheric circulation typically found at the equatorial Pacific in a normal year and in an El Niño year in a cross section of the Pacific Ocean, along the equator. El Niño is defined based on the pressure difference between the Tahiti Islands and Darwin. The SLP at Darwin is always lower than that at the Tahiti Islands. Under the El Niño condition, the difference between the SLPs at these points decreases to less than average values. On the other hand, the SLP at the Tahiti Islands becomes less than its normal, and the SLP at Darwin increases to more than its average value.

There is no general agreement among scientists on how El Niño forms. It is believed that El Niño may have contributed to the extreme events in Mississippi (in 1993) and California (in 1995) as well as to floods and droughts in South America, Africa, and Australia.

Strong La Niña events have been responsible for opposite effects on climate such as El Niño. Figure 3.14 shows the schematic of El Niño and La Niña effects on the movement of air masses over North America. During El Niño, the trade winds are weaker than "normal," allowing stronger ocean currents to flow eastward, while during La Niña, the winds are stronger, pushing stronger westward currents. For example, a major La Niña event in 1988 caused significant drought across North America.

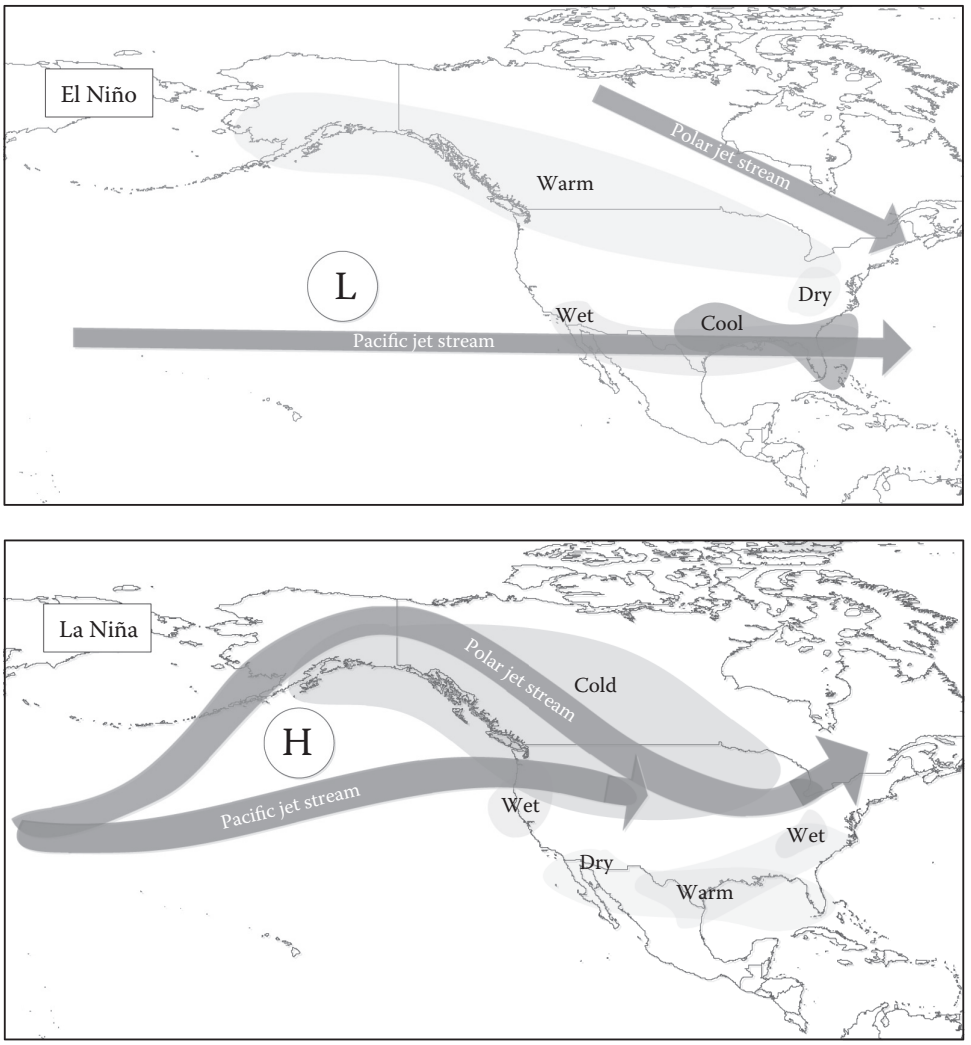

FIGURE 3.14 Typical weather changes in the United States during an El Niño (top) and during a La Niña (http://forces.si.edu/elnino/exhibition_3a1.html).

3.7.2 Sea Level Pressure

Atmospheric pressure at sea level is the result of the force of gravity on the matter above sea level (the atmospheric gases). The amount of matter is not constant due to the height and density of the atmosphere (mostly due to temperature and water content/humidity). It is common to develop a map of isobars (the points with the same SLP). These maps incorporate the effects of atmospheric processes at higher levels and show how the weather patterns are expected to develop. The wind speed is directly related to the distance between the isobars (the lines with the same pressure). The closer they are together, the pressure gradient and the wind will be stronger. As mentioned before, due to high correlation between pressure and cloud and storm formation, SLP can be used as a useful measure in rainfall prediction.

Most land surfaces are at some elevation above sea level. Just inland, near the coast, the elevation could be less than a meter above sea level, while the surface of mountainous regions may be thousands of meters above sea level. The relationship between the measured pressure in a specific point at the ground surface and the SLP at that point is as follows:

$$p = p_0 \exp\left(\frac{gZ_g}{R\mathrm{d}T_v}\right). \tag{3.33}$$

where p is SLP (kPa), p_0 is the actual measured air pressure at the ground surface (kPa), g is Earth's gravity, Z_g is ground surface elevation, and T_v is average virtual temperature (the virtual temperature is defined for a moist air parcel as the temperature at which a dry air parcel will have the same pressure and density).

3.7.3 Sea Surface Temperature

SST is the water temperature close to the ocean's surface. Air masses in the Earth's atmosphere are highly modified by SSTs within a short distance of the shore. Localized areas of heavy snow can form in bands downwind of warm water bodies within an otherwise cold air mass. Warm SSTs are known to be a cause of tropical cyclones over the Earth's oceans. SST changes diurnally, like the air above it, but to a lesser degree due to the water's higher specific heat. Furthermore, SSTs have a large influence on climate and weather. For example, every 3 to 7 years, a wide swath of the Pacific Ocean along the equator warms by 2–3°C. This warming is a hallmark of the El Niño climate pattern, which changes rainfall patterns around the globe, causing heavy rainfall in the southern United States and severe drought in Australia, Indonesia, and southern Asia. On a smaller scale, ocean temperatures influence the development of tropical cyclones (hurricanes and typhoons), which form and intensify by drawing energy from warmer ocean waters. The SST maps are based on observations from satellite.

3.7.4 Southern Oscillation Index

The Southern Oscillation Index, or SOI, gives an indication of the development and intensity of El Niño or La Niña events in the Pacific Ocean. The SOI is computed using monthly mean SLP anomalies at Tahiti and Darwin as follows:

$$\mathrm{SOI} = \frac{\mathrm{SLP}'_{\mathrm{Tahiti}} - \mathrm{SLP}'_{\mathrm{Darwin}}}{\sigma_{\Delta\mathrm{SLP}}}, \tag{3.34}$$

where $\mathrm{SLP}'_{\mathrm{Tahiti}}$ and $\mathrm{SLP}'_{\mathrm{Darwin}}$ are SLP anomalies (the difference between the current value and the long-term mean) at Tahiti and Darwin (Australia), respectively, and $\sigma_{\Delta\mathrm{SLP}}$ is the standard deviation of the difference between these two SLP anomalies.

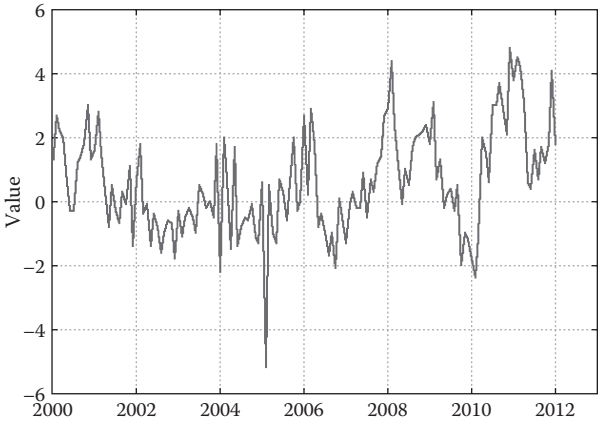

FIGURE 3.15 Monthly SOI (2000–2012).

The SOI is usually computed on a monthly basis, with values over longer periods such as yearly being sometimes used. Daily or weekly values of the SOI do not convey much useful information about the current state of the climate, and accordingly, the Bureau of Meteorology does not issue them. Daily values in particular can fluctuate markedly because of daily weather patterns and should not be used for climate purposes. Monthly standardized values of SOI from 2000 to 2012 are shown in Figure 3.15. The standardized SOI is calculated by subtracting the mean and dividing it by the standard deviation.

The long-term records of SOI can be used in long-lead precipitation prediction. For example, a strongly and consistently positive SOI pattern is related to a high probability of above the long-term average (median) rainfall for many areas of Australia, especially areas of eastern Australia. Conversely, a deep and consistently negative SOI pattern is related to a high probability of below-median rainfall for many areas of Australia at certain times of the year—El Niño.

However, it is important to remember that the pattern of relationship between SOI and rainfall (and temperature) can vary depending on the particular season and region. Additionally, the change in SOI over a period can be important in understanding the relationships between SOI and rainfall. In some studies, independent variables such as SOI and the previous season's rainfall are used to forecast the next season's rainfall.

3.7.5 The North Atlantic Oscillation

The North Atlantic Oscillation (NAO) is a climatic phenomenon in the North Atlantic Ocean resulting from the fluctuations in the atmospheric pressure at sea level between the Azores high and the Icelandic low. It controls the strength and direction of westerly winds and storm tracks across the North Atlantic. It is part of the Arctic oscillation and varies over time with no particular periodicity.

The intensity of this mode of variability is measured by the normalized SLP difference between meteorological stations in the Azores and in Iceland:

$$\mathrm{NAO}_{\mathrm{index}} = \frac{\mathrm{SLP}'_{\mathrm{Azores}}}{\sigma_{\mathrm{Azores}}} - \frac{\mathrm{SLP}'_{\mathrm{Iceland}}}{\sigma_{\mathrm{Iceland}}}, \tag{3.35}$$

where $\mathrm{SLP}'_{\mathrm{Azores}}$ and $\mathrm{SLP}'_{\mathrm{Iceland}}$ are the SLP anomalies (the difference from the long-term mean value) in the Azores and Iceland, respectively, and σ_{Azores} and $\sigma_{\mathrm{Iceland}}$ are the standard deviations of these anomalies.

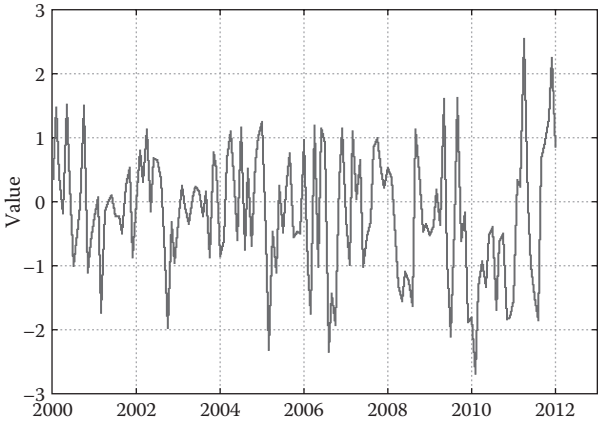

FIGURE 3.16 Monthly NAO index (2000–2012).

The NAO can be observed in all seasons, but its amplitude is greater in winter when the atmosphere is more dynamically active. When the winter NAO index is positive, the stronger westerly winds transport warm and moist oceanic air towards Europe. This leads to warming and increased precipitation at mid- and high latitudes in Europe as well as in large parts of northern Asia, the Greenland Sea, and the Barents Sea. By controlling the position of the Azores high, the NAO also influences the direction of general storm paths for major North Atlantic tropical cyclones: a position of the Azores high farther to the south tends to force storms into the Gulf of Mexico, whereas a northern position allows them to move toward the North American Atlantic Coast.

Meteorologists have shown the important impact of the NAO on the rainfall variability in Europe, in the Mediterranean Sea, extending into the Middle East. Time series of monthly standardized NAO index from 2000 to 2012 is shown in Figure 3.16.

3.7.6 Monsoon

Monsoons are some climatic systems that in special seasons affect the climate system of specific regions around the world. The most famous monsoons happen in summer on the southeastern parts of Asia. Traders plying the waters off the Indian and Arabian coasts noted for centuries that dry northeast winds in the winter suddenly turn to the southwest during the summer and bring beneficial yet torrential rains to the Asian subcontinent. These large-scale wind shifts, from dry desert areas to moist tropical areas, occur in other parts of the Earth, including the Oceanic subcontinent, Southeast Asia, Australia, North America, Africa, and South America.

Example 3.10

Find out the meaning of this sentence: "The hydroclimatological mechanism which most influences the food supply of half of the world's population is related to difference in the way surface radiation is shared for continents and ocean." Describe it using more examples.

Solution:

For example, the Asian–Australian Monsoon is the most influential hydroclimate phenomenon. It impacts the most populated area in the world. The mechanism of this hydroclimate phenomenon is the smaller heat capacity of the continents leading to higher seasonal temperature amplitude compared with ocean surface. These thermal differences drive monsoons' moist air, which flows

inward toward the thermal low pressure on the continent in the summer and outward from the continent in the winter. Abundance of rain is produced generally due to the convective rise of moist air over the heated ground surface.

3.8 CASE STUDIES

In this section, two case studies that use large-scale climatic signals for rainfall prediction are discussed.

3.8.1 Case Study 1

This case study features the Karoon drainage basin, which is located in southwestern Iran, carrying more than one-fifth of the surface water supply of the country. The total area of this basin is about 67,000 km^2. In general, the systems, which mainly affect the climate in the southwest of Iran, can be summarized into the following four groups:

1. Siberian high-pressure center
2. Azure high-pressure center
3. Mediterranean low-pressure center or Mediterranean cyclones
4. Sudanese low-pressure center

The results of this investigation have shown that another system located on the Red Sea also plays an important role in intensifying previous storms in the southwest of Iran. This system, which is called the "Red Sea Convergence Zone," is considered as the fifth system affecting the study area. Among the above-mentioned systems, most of the severe storms and heavy rainfalls that occur in the southwest and the south of the country are mostly affected by the Mediterranean and Sudanese systems.

The Mediterranean Sea is a dominating region in forming cyclones. All of the cyclones formed in this region do not reach the study area. Low-pressure centers or cyclones, after precipitation over the Anatolian Plateau, move towards Russia through Caucasus. The cyclones enter Iran and Iraq when the high-pressure centers are located at latitude 40–45° North. In that case, not only all of the low-pressure centers but also all of the low-pressure cyclones formed at the furthermost points of the east of the Mediterranean Sea will enter the west and northwest side of the country after passing through the Anatolian Plateau. The stronger the high-pressure center on the central part of Iran is, the more noticeable would be precipitation depth on the foothills of Zagros in the western parts of the country.

The Sudanese system is formed over Sudan when the air temperature is low. This system can absorb the water vapor due to the high temperature of its air mass. The humidity of this system is significantly increased after moving east over the Red Sea. Sometimes, this system becomes overhumid after movement over the Persian Gulf, and it can create heavy precipitation in the southern parts of the country. In some cases, both Mediterranean and Sudanese systems enter the country contemporaneously. Most of the severe floods in the southwestern part of the country are the result of this condition.

3.8.1.1 Data

The monthly SST data are estimated based on the weekly recorded data in the years 1981 to 2001. The spatial resolution in pixels per degree is approximately 5.689. The data range from 32°C in the summer months in the Persian Gulf to approximately –2°C in the Polar Regions. The SLP data are in the same period as SST.

Figure 3.17 shows the location of the selected points, which are considered in this study for quantifying the effects of climate signals on the precipitation of the Karoon drainage basin. The locations are mainly selected based on the high- and low-pressure zones affecting the precipitation and the moisture flux of the study area. Table 3.3 shows the basic statistics of the SLP in the selected

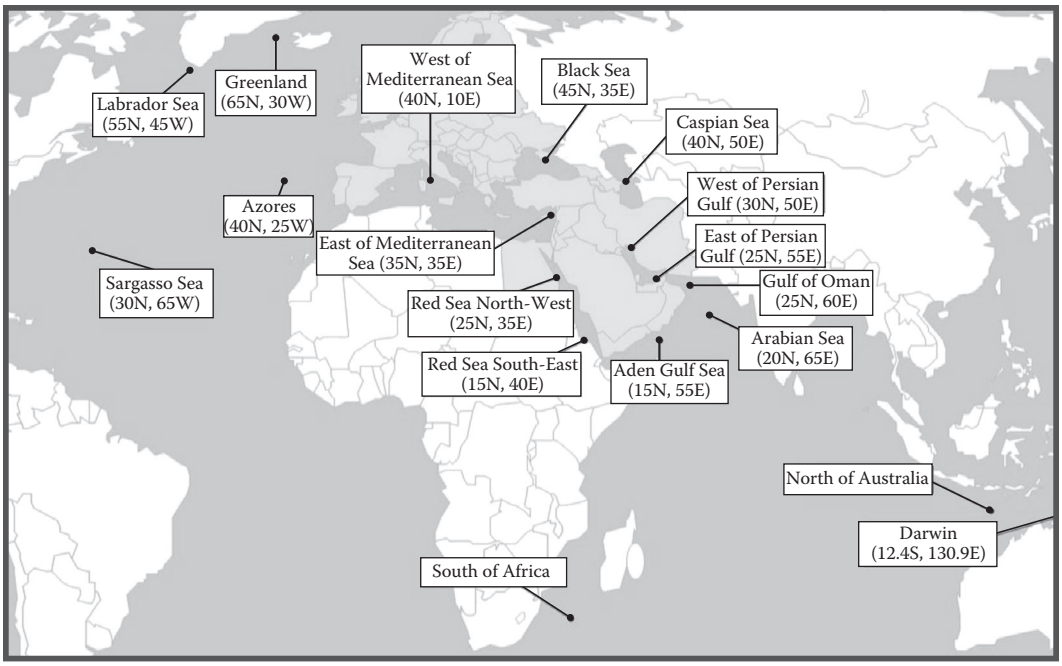

FIGURE 3.17 Selected locations for quantifying the effects of climate signals on the precipitation of the Karoon drainage basin.

locations. The mean precipitation for the Karoon River Basin is estimated based on the point measurements in the years 1968 to 2002 by the Iranian Water Resources Research Organization.

3.8.1.2 Results

In this study, the total average precipitation in the months of January until June (winter and spring) is estimated for the Karoon River Basin in the years 1968 to 2002. It should be noted that the

TABLE 3.3
Basic Statistics of SLP in Selected Locations

Selected Points	Latitude	Longitude	Average (mb)	STDEV	Max (mb)	Min (mb)
Black Sea	45.0N,	35.0E	1015.3	0.9	1018.1	1013.8
East of Mediterranean Sea	35.0N,	35.0E	1010.7	0.4	1011.2	1009.6
West of Mediterranean Sea	40.0N,	10.0E	1015.9	0.8	1017.8	1013.9
Caspian Sea	40.0N,	50.0E	1014.3	0.9	1016.7	1012.1
Arabian Sea	20.0N,	65.0E	1006.0	0.6	1007.5	1004.0
Aden Gulf Sea	15.0N,	55.0E	1007.2	0.5	1008.0	1006.1
Red Sea North-West	25.0N,	35.0E	1007.8	0.3	1008.4	1007.1
Azores	40.0N,	25.0W	1022.1	1.1	1023.9	1018.8
Greenland	65.0N,	30.0W	1007.7	1.8	1012.4	1005.3
Labrador Sea	55.0N,	45.0W	1009.7	1.1	1012.3	1007.4
Saragasso Sea	30.0N,	65.0W	1019.2	0.5	1020.6	1017.8
Gulf of Oman	25.0N,	60.0E	1004.1	0.6	1005.4	1002.6
East of Persian Gulf	25.0N,	55.0E	1004.0	0.6	1005.1	1002.7
West of Persian Gulf	30.0N,	50.0E	1005.0	0.8	1006.8	1003.6
Red Sea South-East	15.0N,	40.0E	1006.7	0.9	1007.8	1005.3

TABLE 3.4
High and Low Levels of Total Precipitation in Months of January through June Based on Gumbel Distribution

Precipitation Level	Name	Range of Precipitation (mm)	Probability (%)
Very high precipitation	VHP	$P > 670$	10
High precipitation	HP	$530 < P < 625$	18
Normal precipitation	NP	$400 < P < 530$	38
Low precipitation	LP	$345 < P < 400$	20
Very low precipitation	VLP	$P < 345$	13

precipitation in these months consists of more that 70% of the annual precipitation. In order to classify the low and high levels of precipitation, Gumbel distribution has been selected as the best fit among different types of probability distributions. Five precipitation level categories are selected as shown in Table 3.4.

The years 1969, 1976, 1993, and 1996 are in the very high precipitation years (VHP) category. The years 1973, 1978, 1985, 1990, 1994, 1995, 2000, and 2001 are in the very low precipitation years (VLP) category. Study of the SLP in the selected points in Figure 3.18 and the pressure gradient show that the following patterns can be identified as indicators for less- or higher-than-normal precipitation levels:

- The SLP gradient between south of Greenland and
  - Azores
  - West of the Mediterranean Sea
  - East of the Mediterranean Sea
  - The Black Sea
- The SLP gradient between Azores and East of Mediterranean Sea
- The SLP in the Caspian Sea and the Black Sea
- The SLP in the Persian Gulf and the Arabian Sea

In Figure 3.18, VL is very low, L is low, N is normal, H is high, and VH is very high.

The above first item, which is mainly affected by the NAO, can significantly increase (decrease) the transfer of moist air to the Mediterranean Sea and Middle East, when the SLP gradient decreases (increases). An increase in the SLP gradient between the Azores and East of Mediterranean Sea can intensify the moist air movement towards the East of the Mediterranean Sea and Iran. The higher-than-normal SLPs in the Caspian Sea, Black Sea, Persian Gulf, and Arabian Sea have been observed in the low-level precipitation years. As previous studies have shown, high SST in the Persian Gulf and Oman Sea has been observed in VLP years. Figure 3.18 shows the variations of SLP and ΔSLP in the selected points in two typical VHP and VLP years (Zahraie et al. 2004).

3.8.2 Case Study 2

The scattered signals initiated at the Bay of Bengal, Indian Ocean, Arabian Sea, and Oman Sea, which are partially responsible for heavy rainfalls that occur in the summer in the southeastern part of Iran, are mostly affected by the Bengal gulf.

In summer monsoons, winds circulate counterclockwise, crossing through India from the southwest, which brings in very moist air. These southwesterly winds bring a drop in temperature and heavy downpours of rain. As shown in Figure 3.19, the mountains located south of India split the summer winds into two arms. The western arm deflects northwards and passes through Western

FIGURE 3.18 Variations of SLP and ΔSLP in four typical very low, high, and very high precipitation years: (a) 1971 (high precipitation), (b) 1996 (very high precipitation), (c) 1990 (very low precipitation).

Ghats to Bombay and then Pakistan and Iran. The eastern arm passes through the bays of Bengal, Calcutta, and Assam, and is deflected northwestward toward the Himalayas. It is shown in Figure 3.19 that the Indian Ocean, Arabian Sea, northwestern India, Pakistan, and the southeastern part of Iran are the affected areas and that the SST and the SLP of Northern India could have a high potential as long-lead predictors for Iran's monsoon rainfall.

3.8.2.1 Study Area

The study area (South Baloochestan watershed) lies between latitude 60° and 62° North and longitude 25° and 27° East in the southeast of Iran near the Pakistan border in an area of about 25,000 km^2. The average annual precipitation in the South Baloochestan watershed is about 218 mm.

3.8.2.2 Results of Large-Scale Signal Analysis

The relation between long-term records of SLP and SLP difference in the months of March through May in selected locations is listed in Table 3.5, and the total average area precipitation in the summer has been used to define special predictors for forecasting Iran's southeastern summer monsoon rainfall.

The selected areas for the study of large-scale signals of Iran monsoon have been plotted at intervals of 2.5° by 2.5°. The correlation between climate signals with different lags (1–12 months) from each grid point and the total average precipitation of the study area has been computed. The

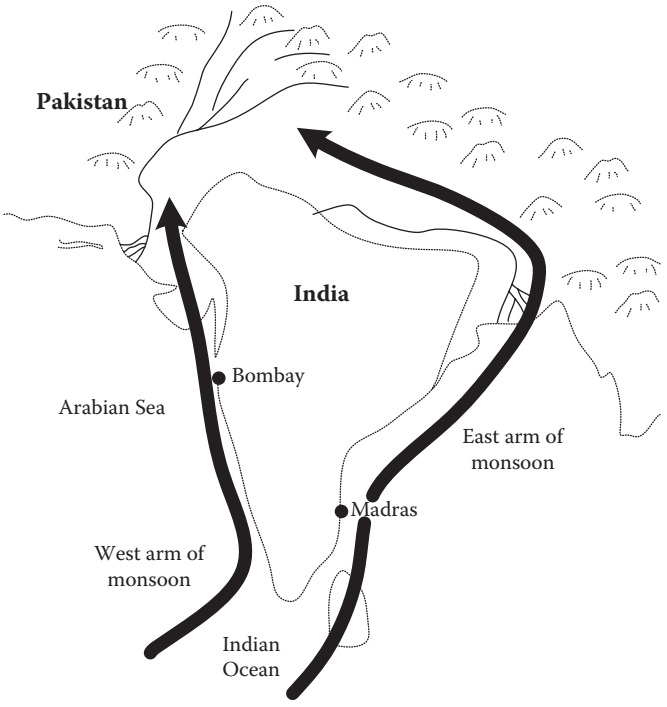

FIGURE 3.19 Deflection of summer monsoon winds by the mountains of southern India.

result of the best correlation obtained for each studied climate signal and considered water surfaces is presented in Table 3.5. Results show that the following indexes can be considered as indicators of summer precipitation in the study area and are shown in Figure 3.20 with P1 to P5, respectively:

P1: SLP of central Iran
P2: SLP of Pakistan and Northern India
P3: SLP of Northern India
P4: SLP difference between the Indian Ocean and the study area (ΔSLP_1)
P5: SLP difference between the Indian Ocean and Northern India (ΔSLP_2)

TABLE 3.5
Correlation of Each Climate Signal at Different Locations

		Monsoon Rainfall Predictor Characteristics			
		Location			
Signal	Name of Considered Area	Latitude	Longitude	Months of Effectiveness Signal	Coefficient Correlation
SLP	Central Iran (P1)	25°	55°	April–May	0.53
	Pakistan and Northern India (P2)	25°	67.5°	March–April–May	–0.50
	Northern India (P3)	20°	62.5°	March–April–May	–0.46
ΔSLP_1	Indian Ocean	0°	70°	April–May	0.47
	Study area	25°	61°		
ΔSLP_2	Indian Ocean	0°	70°	April–May	0.43
	Northern India	25°	80°		

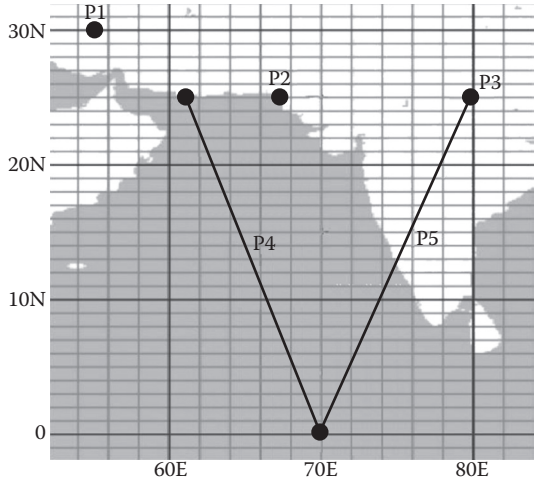

FIGURE 3.20 Selected points for Iran monsoon rainfall forecasting based on SLP and SST signals.

3.9 CONCLUSION

In this chapter, the main climatic processes that affect the hydrologic system were introduced. The chapter includes the discussion of climatic processes and large-scale climatic variables affecting the precipitation in different regions of the Earth. The most important concepts discussed in Sections 3.2 to 3.6 are the energy balance in the Earth–atmosphere system; the relationship between pressure, temperature, and humidity in the atmosphere; and finally cloud and precipitation formation. In Sections 3.7 and 3.8, the commonly used large-scale climatic signals including SLP, SST, NAO, and SOI are introduced. The variations in these signals result in dry and wet years around the world and are commonly used for rainfall prediction in different regions. Due to complicated interactions between different hydrologic and climatic systems, the knowledge about the principles of these processes will help to better understand the cause of some hydrologic processes and provide more accurate predictions of hydrologic events. Related concepts on rainfall analysis and other components of the hydrologic cycle are given in Chapters 4, 5, 6, and 7.

PROBLEMS

1. Assume that the global hydrological cycle can be approximated by just three subsystems:
   a. The circulation over the oceans:

      Ocean → (Oceanic evaporation) → Atmosphere → (Oceanic rainfall) → Ocean

   b. Circulation over continents:

      Ocean → (Oceanic evaporation) → Atmosphere → (Continental rainfall) →
      Rivers → (Runoff) → Ocean

   c. Circulation involving water evaporating from the oceans, precipitating over continents, and returning to the oceans in rivers:

      Land → (Continental evaporation) → Atmosphere → (Continental rainfall) → Land

Given:

- The area of the oceans is 361.3×10^6 km^2; they cover about 71% of the globe.
- The global average oceanic evaporation is 1176 mm/year, while the global average precipitation over the oceans is 1066 mm/year.
- The global average continental evaporation is 480 mm/year.
  a. Estimate how much water evaporating from oceans falls back to the oceans as precipitation (in km^3/year).
  b. Estimate how much water evaporating from oceans is moved in the atmosphere over land and ultimately returns as river runoff (in km^3/year).
  c. Estimate how much water falling as precipitation over the continents is recycled back to the atmosphere by continental evaporation (in km^3/year).

2. Estimate the density of dry air with a pressure and temperature of 900 mb and 30°C, respectively. Estimate the density for wet air with the same properties as the dry air when the air relative humidity is 80%.
3. Calculate the weight of a 1 m^3 dry air parcel when the temperature and pressure are 35°C and 950 mb (the constant of gasses is 2.87×10^3).
4. At an altitude of 3700 ft, the temperature and pressure of the (moist) air are measured to be 113°F and 29.612 in (of mercury) and the relative humidity is 25%. What are the following?
   a. The air temperature (in °C)
   b. The air temperature (in K)
   c. The air pressure (in mb)
   d. The air pressure (in kPa)
   e. Saturated vapor pressure at air temperature (in kPa)
   f. The vapor pressure (in kPa)
5. A meteorologist is making measurements at 8000 ft at the nearby Kitt Peak Observatory. Estimate what there will be measured for
   a. The air temperature
   b. Specific humidity
   c. Total air pressure

   Consider the lapse rate to be 0.0098°C per meter and the air temperature and pressure at the ground level to be 45°C and 100 kPa. The vapor pressure at 8000 ft is 5 kPa.
6. Compute the relative humidity if the air temperature and the dew point temperature are 25°C and 15°C, respectively.
7. Using Equation 3.27 for e_s, derive the following expression for the dew point temperature for the portion of air with vapor pressure e (kPa):

$$T_{\text{dew}}(e) = \frac{\ln(e) + 0.49299}{0.0707 - 0.00421 \times \ln(e)}$$

8. Compute the dew point temperature if the air temperature and relative humidity are 30°C and 75%, respectively.
9. Consider a parcel of air at 22°C at an elevation of 900 m above the mean sea level. While moving, this air encounters a mountain range 3500 m high. The air rises, moves over the mountains, and then descends to an elevation of 1400 m. If an ascent at 1400 m produces saturation and condensation and the rain occurs at the top of the mountain, and if the average pseudo-adiabatic lapse rate is about half of the dry adiabatic lapse rate, what will be the temperature of the air at an elevation of 1400 m at the opposite side of the mountain?

10. What will be the weight of 5 m^3 dry air if the air temperature and pressure are 10°C and 1000 mb, respectively?
11. What will be the density of dry air at 10°C and 1000 mb, and the density of moist air with a relative humidity of 50% at the same temperature and pressure?

REFERENCES

Intergovernmental Plane on Climate Change (IPCC) (1996). *Climate Change 1995*: *The Science of Climate Change*, Cambridge University Press, Cambridge.

Intergovernmental Plane on Climate Change (IPCC) (2007). *Climate Change 2007: The Physical Science Basis*, Cambridge University Press, Cambridge.

Karamouz, M., Yazdanpanah, A., Moridi, A. and Nazif, S. (2006). *Large Scale Climate Signals and Monsoon Rainfall*: *A Case Study*. Proceedings of ASCE Environmental and Water Resources Institute Conference, New Delhi.

National Aeronautics and Space Administration (2005). *The Importance of Understanding Clouds*. Available at http://www.nasa.gov.

NOAA Earth System Research Laboratory (2010). Available at http://www.esrl.noaa.gov.

Shuttleworth, W.J. (2000). Hydroclimatology Course, HWR524 class notes at the Department of Hydrology and Water Resources, University of Arizona, Tucson, AZ.

Zahraie, B., Karamouz M. and Eghdami, S. (2004). *Seasonal Precipitation Forecasting Using Large Scale Climate Signals: Application to the Karoon River Basin in Iran*, Proceedings of the 6th International Conference on Hydroinformatics, Liong Phoon and Babovic, eds, Singapore.

4 Hydrologic Cycle Analysis

4.1 INTRODUCTION

Water exists on Earth in all its three states, liquid, solid, and gas, in various degrees of motion. Evaporation of water from water bodies such as oceans and lakes, formation and movement of clouds, rain and snowfall, streamflow, and groundwater movement are some examples of the dynamic aspects of water. The various aspects of water related to the Earth can be explained in terms of a cycle known as the hydrologic cycle. A brief system description of hydrologic cycle was presented in Chapter 2 (see Figure 4.1). The hydrologic cycle generally includes the water interaction between the atmosphere and the Earth, namely, precipitation, infiltration, evaporation, and evapotranspiration, as well as water movement and storage on and under the surface of the Earth, namely, surface runoff, subsurface flow, groundwater flow, and reservoirs and lakes.

In this chapter, first, an estimation of precipitation, evaporation, evapotranspiration, and infiltration and excess rainfall calculation are discussed. Analysis of surface runoff and subsurface flows is addressed in detail in Chapter 6, and details of groundwater flow are described in Chapter 7. Furthermore, in this chapter, water balance in the hydrologic cycle is described. Finally, kriging as a method of regionalizing sample data is discussed.

4.2 PRECIPITATION

Precipitation is a major element of the hydrologic cycle. The measurement of precipitation is very important; there are essentially three different methods for precipitation measurements:

Measurement by standard gauges: This is the traditional and long-established method. Time series are developed using this method, and if the sampling location is moved, the time series should be adjusted. This method provides point measurements; thus, it may not be representative even for a small area. There are sampling error and poor spatial averaging as well as recording and instrument errors.

Measurement by weather radar: This method can provide spatially distributed measurements in real time. A weather radar is a type of radar used to locate precipitation, calculate its motion, estimate its type (rain, snow, hail, etc.), and forecast its future position and intensity.

Measurement by satellite: This is a speculative and unproven technology with the potential for global coverage. It has measurements for oceans and inaccessible land regions. A weather satellite is a type of satellite that is primarily used to monitor the weather and climate of the Earth and cloud systems. City lights, fires, effects of pollution, sand and dust storms, snow cover, ice mapping, boundaries of ocean currents, energy flows, etc., are other types of environmental information collected using weather satellites.

Many satellite services have two types of images: infrared and visible. Visible images are similar to those that a normal video camera (black and white) would see looking down at the Earth. The brightest clouds are usually the thicker ones low down in the atmosphere. Infrared images convert the temperature of the cloud, land, or sea (whichever the satellite can see at each point) to a shade of gray. The warmest points are shown as black at the ground surface and the coolest points are shown

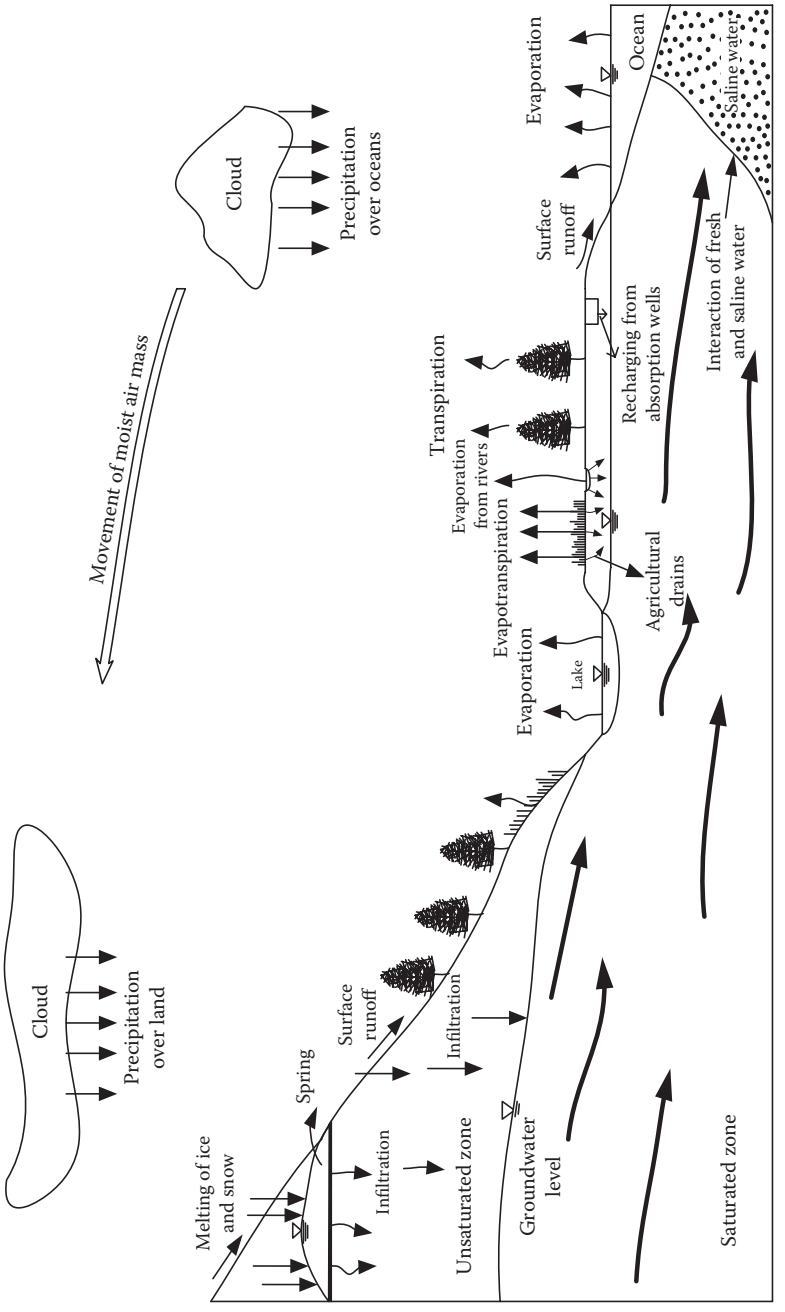

FIGURE 4.1 Hydrologic cycle and its components.

as white at a high level in the atmosphere. In between are shades of gray, which become brighter as clouds become colder (higher). Also, the differences in temperature of the ground can also be seen as different shades of gray. This type of information does not show actual rainfall; rather, it is inferred from the type of cloud cover.

The Tropical Rainfall Measuring Mission (TRMM) is a NASA satellite that provides more information both to test and to improve climate models. TRMM is particularly devoted to measuring precipitation in the tropics and subtropics of the Earth. Among the three primary instruments on TRMM, the most innovative is the Precipitation Radar. The Precipitation Radar, built by the National Space Development Agency of Japan, is the first space-borne instrument designed to provide three-dimensional maps of storm structure. The measurements should yield invaluable information on the intensity and distribution of the rain, the storm depth, and the height at which the snow melts into rain.

Also, in this method, other data such as sea level pressure are assimilated into General Circulation Models (GCMs) and interpreted and reanalyzed in terms of precipitation.

4.2.1 Estimation of Missing Rainfall Data

Before using the rainfall records of a station, it is necessary to first check the data for continuity and consistency. The continuity of a record may be broken with missing data due to many reasons such as damage or fault in a rain gauge during a period. The missing data can be estimated by using the data of the neighboring stations. There are some methods for estimating missing rainfall data. In this calculation, the normal rainfall (the long-term mean annual rainfall) is used as a mean for comparison. The normal ratio method is the conceptually simplest one, which is based on the following equation:

$$\frac{P_x}{A_x} = \frac{1}{n}\left(\frac{P_1}{A_1} + \frac{P_2}{A_2} + \frac{P_3}{A_3} + \ldots + \frac{P_n}{A_n}\right). \tag{4.1}$$

where $P_1, P_2, \ldots, P_n$ are precipitations at neighboring stations 1, 2… n and $A_1, A_2, \ldots, A_n$ are area at neighboring stations 1, 2… n. It should be noted that the missing annual rainfall, P_x, with area A_x at station x is not included in the above n stations.

Example 4.1

There are four rain gauges in a watershed named A, B, C, and D. A specific storm event for gauge A is missing. Data from other gauges for the storm event as well as the average annual rainfall of all gauges are given in Table 4.1. Estimate the missing data at gauge A.

TABLE 4.1
Data of Rainfall in Example 4.1

Gauge	Average Annual Rainfall (mm)	Total Storm Rainfall (cm)
A	1290	Missing data
B	1510	12.3
C	1680	14.8
D	1375	11.9

Solution:

From Equation 4.1:

$$P_x = \frac{A_x}{n}\left(\frac{P_1}{A_1} + \frac{P_2}{A_2} + ... + \frac{P_n}{A_n}\right) = \frac{1290}{3}\left\{\frac{123}{1510} + \frac{148}{1680} + \frac{119}{1375}\right\}$$

$$= 110.01\,\text{mm} = 11.0\ \text{cm}.$$

4.2.2 Average Areal Rainfall

For rainfall analyses in areas larger than a few square miles, it may be necessary to make estimates of average rainfall depths over sub-watershed areas. There are different methods used to provide an estimation of areal rainfall. These methods are selected based on the available data and the characteristics of the study region. Three methods of extending point estimates to areal average are presented in this chapter. Each of the three methods provides a weighted average of measured catches. The station average method assumes equal weights. The weights for the Thiessen method are proportional to the size of the area geographically closest to each gauge. The isohyetal method assigns weights on the basis of storm morphology, the spatial distribution of the rain gauge, and orographic effect. As a general model, the average rainfall of a watershed is defined as follows:

$$\bar{P} = \sum_{i=1}^{n} w_i P_i, \tag{4.2}$$

where $\bar{P}$ is the average rainfall, P_i is the rainfall measured in station i, n is the number of rain gauges, and w_i is the weight assigned to each station i. The mean $\bar{P}$ has the same units as P_i. Equation 4.2 is valid only when the following constraint holds:

$$\sum_{i=1}^{n} w_i = 1. \tag{4.3}$$

The general model of Equation 4.2 can be applied with all the methods discussed here. The difference in the application lies solely in the way that the weight is estimated.

4.2.2.1 Station Average Method

For this method, each gauge is given equal weight; thus, w_i equals $1/n$, and Equation 4.3 becomes

$$\bar{P} = 1/n \sum_{i=1}^{n} p_i. \tag{4.4}$$

The use of Equation 4.4 will provide a reasonably accurate estimate of $\bar{P}$ when there are no significant orographic effects, the gauges are uniformly spaced throughout the watershed, and the rainfall depth over the entire watershed is nearly constant.

4.2.2.2 Thiessen Method

For cases where there are large differences in the catches at the rain gauges, the Thiessen method is a good alternative to the station average method. In this method, at first, a network of polygons

is constructed by drawing a perpendicular bisector of lines joining each pair of gauges. Then, the area or portion of each polygon is calculated to give weights to different gauges. Finally, the mean rainfall of the basin is computed by weighting each gauge by area of within-basin polygon relevant to that gauge.

Example 4.2

For the illustrated catchment in Figure 4.2, estimate the mean areal rainfall using the Thiessen method.

Solution:

For calculating mean rainfall by using the Thiessen method, first, a network of polygons is constructed by drawing a perpendicular bisector of lines joining each pair of gauges (see Figure 4.2). The summary of calculations is shown in Table 4.2.

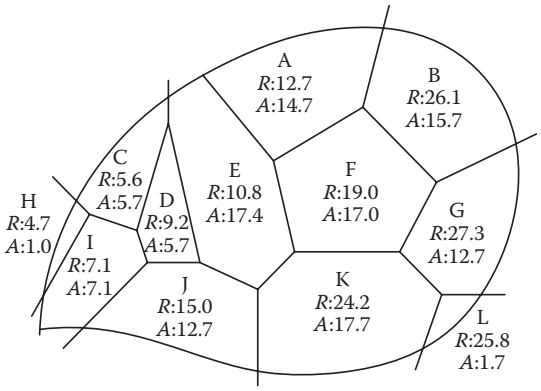

FIGURE 4.2 Application of the Thiessen method to the catchment of Example 4.2 (*R* is mean rainfall in millimeters and *A* is polygon area in square kilometers).

TABLE 4.2
Summary of Calculations for Example 4.2

Station	Mean Rainfall (mm)	Polygon Area (km²)	Weighted Rainfall
A	12.7	14.7	186.69
B	26.1	15.7	409.77
C	5.6	5.7	31.92
D	9.2	5.7	52.44
E	10.8	17.4	187.92
F	19.0	17.0	323.00
G	27.3	12.7	346.71
H	4.7	1.0	4.70
I	7.1	7.1	50.41
J	15.0	12.7	193.50
K	24.2	17.7	433.18
L	25.8	1.7	43.86
Sum		129.1	2264.1

Total area = 129 (km^2) and total weighted rainfall = 2264.1 (summation of the last column of Table 4.2); then,

$$\text{Thiessen mean rainfall} = \frac{2264.1}{129.1} = 17.5 \text{ mm}.$$

4.2.2.3 Isohyetal Method

The isohyetal method requires the hydrologist to delineate the boundaries of the region associated with the catch at each gauge by drawing isohyets (that is, lines of equal rainfall depths). The area within each pair of adjacent isohyets can then be used to weight the average rainfall associated with the adjacent isohyets. Mathematically, the estimated mean areal precipitation for a watershed of area A is estimated as follows:

$$\bar{P} = \sum_{i=1}^{n} \left(\frac{A_i}{A} \right) p_i, \tag{4.5}$$

where A_i is the watershed area between isohyets i and $i + 1$, p_i is the average precipitation for isohyets i and $i + 1$, and n is the number of isohyetal intervals. The ratio A_i/A is the weight applied to the particular precipitation range.

Example 4.3

If a watershed area is 24 km^2, estimate the mean areal rainfall by using Equation 4.5. Isohyetal mean area and mean rainfall are shown in Table 4.3.

Solution:

$$A = 24 \text{ km}^2, \quad n = 4$$

The mean areal rainfall is estimated by Equation 4.5 as

$$\bar{P} = \sum_{i=1}^{n} \left(\frac{A_i}{A} \right) \bar{p} \quad \text{then,} \quad \bar{p} = \frac{5.9}{24}(0.6) + \frac{13}{24}(1.7) + \frac{0.5}{24}(4.5) + \frac{4.6}{24}(5.5) = 2.22.$$

Because of the limitations of classic interpolation methods such as the station average, Thiessen, and isohyetal methods for estimating average areal rainfall and predicting missing hydrology data,

TABLE 4.3
Rainfall Data for Example 4.3

Isohyetal Mean Area	Mean Rainfall (in)	Area Range (mi^2)
0–1	0.6	5.9
1–2	1.7	13
2–3	4.5	0.5
3–4	5.5	4.6

different methods such as kriging have been developed. Kriging is an alternative to many other point interpolation techniques. Unlike straightforward classic methods, it is an advanced statistical method based on the theory of regionalized variables. Spatial analysis or regionalized variables and the kriging method will be discussed at the end of this chapter.

4.2.3 Snowmelt Estimation

Snowmelt and sequential streamflow form one of the most important phases of the hydrologic cycle. In hydrology, snowmelt is surface runoff produced from melting. In some cases, snowmelt is a high fraction of the annual runoff in a watershed. Because of the important role that the storage and melting of snow play in the hydrologic cycle of some areas, hydrologists must be able to reliably predict the contribution of snowmelt to overall runoff. Because snowmelt begins in the spring and the resulting runoff occurs before the peak water demand, control schemes such as building storage reservoirs should be a part of the planning and operation schemes for water supply. Under certain conditions, snowmelt can also contribute to flooding problems; snowmelt predictions are also valuable to power companies that generate hydroelectricity and to irrigation districts.

Snow mapping and monitoring are necessary for studies about snow melting. Furthermore, it is now widely recognized that satellite remote sensing has useful potential for snow mapping and monitoring. For repetitive ice and snow mapping over large areas, data from weather satellites, especially of the National Oceanic and Atmospheric Administration (NOAA) family, are more widely used. NOAA imagery is analyzed by the U.S. National Weather Satellite Service to provide its customers with a range of medium- to small-scale ice and snow reports. Additionally, fully objective (automatic) techniques based on NOAA-HRPT multispectral data are being developed for routine snow area and snow surface characteristics (surface temperature, melt accumulation statues, etc.), mapping, and monitoring. Evaluating snow depth is more difficult, as assessment from visible/infrared data is readily available only within a very few depth categories. Furthermore, cloud cover is still a nuisance, though much less so than in the case of the infrequently viewing Earth resources satellite systems. As with rainfall monitoring, new hope is emerging as passive microwave data will provide helpful supplementary information both spectrally and temporally (Figure 4.3).

Because of the range of uses for estimating the contribution of snowmelt to streamflow and the variation of condition applicable to each case, many methods have been developed for computing snowmelt as it affects streamflow. These methods have found that the timing and amount of runoff depend mainly on five factors: sensible heat condition from moist air to the snow surface, latent heat of condensation, solar radiation, heat transmitted by rainfall on the snowpack, and heat condition from underlying ground. Furthermore, it must be emphasized that snowmelt at a point involves

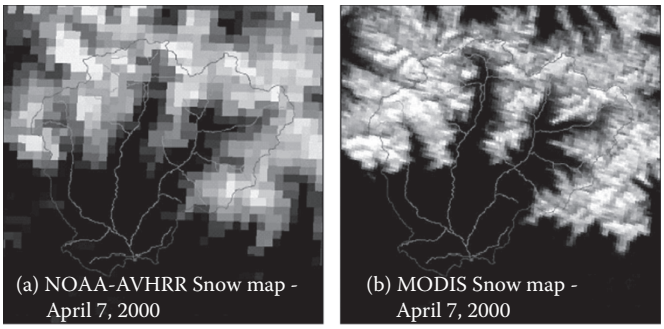

FIGURE 4.3 Computer snow maps for a basin in Spain: (a) NOAA-AVHRR satellite imagery; (b) MODIS satellite imagery.

a change of state requiring heat, whereas the production of snowmelt runoff from watershed is a much more complicated process. The simple method of snowmelt runoff estimation is presented as follows:

$$M = 4.57 \times C(T - T_B), \tag{4.6}$$

where M is the snowmelt runoff (cm/day), C is snowmelt coefficient (between 0.015 and 0.2), T is daily mean temperature or maximum temperature (°C), and T_B is base temperature (°C). The base temperature is considered to be 0°C when mean daily temperature is used and it would be 4.4°C when the maximum daily temperature is utilized. The suggested relations of snowmelt estimation by the U.S. Army Corps of Engineers are given in Table 4.4.

In Table 4.4, M is snowmelt rate (cm/day); F is average basin forest-canopy cover shading of the area from solar radiation (decimal fraction); W is wind speed at 15.2 m above the snow surface temperature; A is average snow surface albedo, which is equal to $0.75/D^{0.2}$, where D is the number of days from the last snow; K is basin convection–condensation melt factor expressing average exposure to wind, which is equal to 1 for open site and 0.3 for heavily forested site; K' is basin shortwave radiation melt factor between 0.9 and 1.1; T' is difference between the air temperature measured at 3 m and the snow surface temperature (°C); T'_D is the difference between the dew point temperature measured at 3 m and the snow surface temperature (°C); R is rainfall (cm/day); and S is solar radiation on a horizontal surface (langleys/day).

Example 4.4

The properties of a mountainous catchment are presented in Tables 4.5 and 4.6. Considering K = 0.6, K' = 1.0, and F = 0.5, estimate the snowmelt for each day. Assume the last snowfall occurred on January 31.

TABLE 4.4
U.S. Army Corps of Engineers' Suggested Snowmelt Equations

No.	Situation	Forest Cover Application	Equations
1	Rain in snow	Open site (0–60% cover)	$M = 2.54\ [0.09 + (0.029 + 0.005KW + 0.0027R)\ (1.8T)]$
2		Heavily forested (60–100% cover)	$M = 2.54\ [0.05 + (0.074 + 0.0027R)\ (1.8T)]$
3	Rain free	Open site (0–60% cover)	$M = 2.54\left[K'(1-F)(0.004S)(1-A) + K(0.005W)\left(0.396T' + 1.404T'_D + 32\right) + F\left(0.052T' + 0.928\right)\right]$
4		Heavily forested (60–100% cover)	$M = 2.54\left[0.074\left(0.953T' + 0.845T'_D + 32\right)\right]$

Source: U.S. Army Corps of Engineers, *Snow Hydrology*, North Pacific Division, Portland, Oregon, 1965. With permission.

TABLE 4.5
Catchment Properties for Example 4.4

Property	Area 1	Area 2
Height (m)	912–1216	1216–1520
Area (km^2)	815	1890
Snow height (cm)	45	33

TABLE 4.6
Weather Information for Example 4.4

	Temperature (°C)			Dew Point (°C)					
Date	912 m height	1216 m height	1520 m height	912 m height	1216 m height	1520 m height	Rainfall (cm)	Wind Speed (km/h)	Solar Radiation (langleys/day)
February 3	4.4	2.8	1.1	–0.5	–1.6	–3.3	0.127	16.9	400
February 4	8.9	7.2	5.5	–1.5	–3.2	0.1	0	17.7	567

Solution:

a. Area 1:
From Table 4.6, the temperature for a height of 912 m is 4.4 and that for 1216 m is 2.8 in area 1, then the mean temperature is (4.4 + 2.8)/2 = 3.6 and $K = 0.6$, $W = 16.9$, and $R = 0.127$. Equation 1 of Table 4.4 is used to estimate the snowmelt in this area because there is rain in snow and it is an open site.

$$M = 2.54\{0.09 + [0.029 + 0.005(0.6)(16.9) + 0.0027(0.127)](1.8 \times 3.6)\} = 1.54 \text{ cm/day}$$

Area 2:
From Table 4.6, the temperature for a height of 1216 m is 2.8 and that for 1520 m is 1.1 in area 2, then the mean temperature, T, is (2.8 + 1.1)/2 = 1.95, $K = 0.6$, $W = 16.9$, and $R = 0.127$. Equation 1 of Table 4.4 is used to estimate the snowmelt in this area because there is rain in snow and it is an open site.

$$M = 2.54\{0.09 + [0.029 + 0.005(0.6)(16.9) + 0.0027(0.127)](1.8 \times 1.95)\} = 0.94 \text{ cm/day}$$

b. Weighted average of snowmelt for February 3 is as follows:

$$M = \frac{1.54(815) + 0.94(1890)}{815 + 1890} = 1.120 \text{ cm/day}.$$

c. Snow storage at the end of February 3 is presented in Table 4.7.
d. There is no rainfall on February 4, and areas 1 and 2 are an open site. Equation 3 of Table 4.4 is then used to estimate the snowmelt in this area. In this equation, $F = 0.5$, $S = 576$, and $W = 17.7$.

TABLE 4.7
Estimation of Snow Storage at Day 1 of Example 4.4

	Area 1	Area 2
Snow Storage at Beginning of Day (cm)	45	33
Snowmelt in First Day (cm)	1.54	0.94
Snowfall During Day (cm)	0	0
Snow Storage at End of Day (cm)	43.46	32.06

Area 1:

$$D = 4 \quad A = \frac{0.75}{4^{0.2}} = 0.57$$

$$T' = \frac{(8.9 + 7.2)}{2} = 8.05$$

$$T'_D = \frac{(-1.5 + (-3.2))}{2} = -2.35$$

$$M = 2.54\Big[1(1 - 0.5)(0.004 \times 567)(1 - 0.57) + 0.6(0.005 \times 17.7)(0.396 \times 8.05 + 1.404 \times (-2.35 + 32))$$

$$+ 0.5(0.052 \times 8.05 + 0.928)\Big] = 7.24 \text{ cm/h}$$

Area 2:

$$T' = \frac{(7.2 + 5.5)}{2} = 6.35$$

$$T'_D = \frac{(-3.2 + 0.1)}{2} = -1.55$$

$$M = 2.54\Big[1(1 - 0.5)(0.004 \times 567)(1 - 0.57) + 0.6(0.005 \times 17.7)(0.396 \times 6.35 + 1.404 \times (-1.55 + 32))$$

$$+ 0.5(0.052 \times 6.35 + 0.928)\Big] = 3.5 \text{ cm/h}$$

Weighted average of snowmelt for catchment in day 2 is as follows:

$$M = \frac{7.24(815) + 3.5(1890)}{815 + 1890} = 4.62 \text{ cm/day.}$$

4.3 EVAPORATION AND EVAPOTRANSPIRATION

Evaporation and evapotranspiration are important links in the hydrologic cycle in which water is transferred to the atmosphere as water vapor. Evaporation is the process in which a liquid changes to a gaseous state at the free surface, below the boiling point through the transfer of heat energy. While transportation takes place, plants lose moisture by the evaporation of water from soil and water bodies in the land area. In hydrology and irrigation practice, it is found that evaporation and transportation can be considered under one process—evapotranspiration.

For the hydrologist, the loss of water by evaporation must be considered from two main aspects. Firstly, evaporation from an open water surface, E, is the direct transfer of water from lakes, rivers, and reservoirs to the atmosphere. This can be easily assessed if the water body has known capacity and does not leak by evaluating the changes in storage volume.

The second form of evaporation loss occurs in the form of the transpiration from vegetation, E_t. This is sometimes called evapotranspiration, since loss by direct evaporation of intercepted precipitation and transpired water on plant surfaces is also included. Thus, E_t is usually thought of as the total loss by both transpiration and evaporation from a land surface and its vegetation. The value of E_t varies according to the type of vegetation, its ability to transpire, and the availability of water in the soil. It is much more difficult to quantify E_t than E since transpiration rates can vary considerably over an area and the source of water from the ground for plants requires careful definition.

Both forms of evaporation, E and E_t, are influenced by the general climatic conditions. Although the instrumental measurements of evaporation are not as simple as rainfall, it is a compensating

factor that evaporation quantities are less variable from one season to another, and therefore can be more easily predicted than rainfall amounts. Evaporation is one of the most consistent elements with unlimited supplies of water in the hydrologic cycle.

4.3.1 Evaporation Evaluation

There are different major approaches adopted in calculating evaporation from open water, E. Four primary methods are used to estimate evaporation from a water surface, namely, the water budget method, the mass transfer method, pan evaporation, and the Penman equation.

4.3.1.1 Water Budget Method

The water budget method for lake evaporation is based on the hydrologic continuity equation. Assuming that change in storage ΔS, surface inflow I, surface outflow O, subsurface seepage to groundwater flow GW, and precipitation P can be measured, evaporation E can be computed as

$$E = -\Delta S + I + P - O - GW. \tag{4.7}$$

The approach is simple in theory, but evaluating seepage terms can make the method quite difficult to implement. The obvious problems with the method result from errors in measuring precipitation, inflow, outflow, change in storage, and subsurface seepage.

4.3.1.2 Mass Transfer Method

In the mass transfer method of computing evaporation, the mass transfer coefficients are determined using energy-budget evaporation as an independent measure of evaporation.

The simple equation used for measuring evaporation by mass transfer method is as follows:

$$E = f(u)(e_s - e_d), \tag{4.8}$$

where E is the evaporation rate, $f(u)$ is a function of wind speed u, e_s is saturated vapor pressure of air at water surface (mb), and e_d is the saturated vapor pressure of the air at T_d, the dew point (mb). From a study of numerous reservoirs of different sizes up to 12,000 ha, an additional factor, surface area, can be incorporated into the equation to determine evaporation loss from a reservoir; thus,

$$E = 0.291\, A^{-0.05} u_2 (e_s - e_d), \tag{4.9}$$

where E is evaporation (mm/day), A is area (m^2), u_2 is speed at 2 m (m/s), e_s is saturated vapor pressure of air at water surface (mb), and e_d is the saturated vapor pressure of the air at the dew point, T_d (mb).

Example 4.5

Calculate the annual water loss from a 5 km^2 reservoir, when u_2 is 10.3 km/h, e_s is 14.2, and e_d is 11.0 (mm Hg).

Solution:

$$A = 5\ \text{km}^2 = 5 \times 1000^2\ \text{m}^2$$

$$u_2 = 10.3\ \text{km/h} = \frac{10.3 \times 1000}{60 \times 60} = 2.86\ \text{m/s}$$

$$e_s = 14.2 \text{ mm Hg} = 14.2 \times 1.33 = 18.9 \text{ mb}$$

$$e_d = 11.0 \text{ mm Hg} = 11.0 \times 1.33 = 14.6 \text{ mb}$$

$$E = 0.291(5 \times 1000^2) - 0.05 \times 2.86(18.9 - 14.6) = \frac{0.291 \times 2.86 \times 4.3}{2.16} = 1.66 \text{ mm/day}$$
$$= 1.66 \times 365 = 0.605.9 \cong 606 \text{ mm/year}$$

Total annual water loss from reservoir = $0.606 \times 5 \times 1000^2 = 3.03 \times 10^6$ m^3.

4.3.1.3 Pan Evaporation

An evaporation pan is used to hold water during observations for the determination of the quantity of evaporation at a given location. Such pans are of varying sizes and shapes, the most commonly used being circular or square. The best known of the pans is the "Class A" evaporation pan. In Class A pan, an open galvanized iron tank 4 ft in diameter and 10 in depth is used mounted 12 in above the ground. To estimate evaporation, the pan is filled to a depth of 8 in and must be refilled when the depth has fallen to 7 in. The water surface level is measured daily, and evaporation is computed as the difference between observed levels, adjusted for any precipitation measured in a standard rain gauge. Alternatively, water is added each day to bring the level up to a fixed point. Pan evaporation rates are higher than actual lake evaporation and must be adjusted to account for radiation and heat exchange effects. The adjustment factor is called the pan coefficient, which ranges from 0.64 to 0.81 with an average of 0.70. However, the pan coefficient varies with exposure and climate conditions and should be used only for rough estimates of lake evaporation.

4.3.2 Measurement of Evapotranspiration

Evapotranspiration, E_t, can be measured by (a) tanks and lysimeters, (b) field plots, and (c) studies of groundwater fluctuations. A tank is a watertight container that is set into the ground with its rim nearly flush with the ground surface. The size should be sufficient to simulate natural growing conditions for the type of plants being studied. The tank is mounted on a scale to assist in necessary moisture measurements. Each plant requires certain moisture conditions for optimum growth and these conditions are maintained during consumptive-use measurements. E_t is determined by measuring the quantity of water necessary to maintain constant, optimum moisture conditions in the tank.

A lysimeter is essentially a tank with a pervious bottom. The bottom arrangement is such that excess soil moisture will drain through the soil, which can be collected and measured.

Specially designed field plots are used to determine E_t under field conditions. These plots are designed so that surface runoff water from the plot can be collected and measured. Deep percolation is captured by underground drain tiles. To determine E_t, water input in the form of precipitation or irrigation is measured.

Evapotranspiration equations have been developed to predict consumptive use for different conditions and different crops. These are empirical relations that have been useful to replace the difficult and expensive measurements.

4.3.2.1 Blaney–Criddle Method

An empirical relation between mean air temperature, evapotranspiration, and mean percentage of daytime hours was developed by Blaney and Criddle (1962). The underlying assumption of this procedure is that the heating of the air and evaporation share the heat budget in a fixed proportion.

As a result, E_t varies directly with the sum of the products of mean monthly air temperature and monthly percentage of daytime hours with an actively growing crop with sufficient soil moisture as

$$ET_o = p(0.46T_{mean} + 8), \tag{4.10}$$

where ET_o is reference crop evapotranspiration (mm/day) as an average for a period of 1 month, T_{mean} is mean daily temperature (°C), and p is mean daily percentage of annual daytime hours. The use of the Blaney–Criddle formula is as follows:

Step 1: Determination of the mean daily temperature (T_{mean})

$$T_{mean} = \frac{T_{max} + T_{min}}{2} \tag{4.11}$$

Step 2: Determination of the value of p for which Table 4.8 is used. To be able to determine the p value, it is essential to know the approximate latitude of the area and the number of degrees north or south of the equator. Suppose the p value for the month of March has to be determined for an area with latitude of 45° south. From Table 4.8, it can be seen that the p value during March is 0.28.
Step 3: Calculation of ET_o, using the formula $ET_o = p(0.46T_{mean} + 8)$. For example, in March, when $p = 0.28$ (from Table 4.8) and $T_{mean} = 21.5$°C, the ET_o is calculated as follows:

$$ET_o = 0.28(0.46 \times 21.5 + 8) = 0.28(9.89 + 8) = 0.29 \times 17.89 = 5.2 \text{ mm/day}$$

Example 4.6

Determine the mean ET_o (in mm/day) for the month of April using the Blaney–Criddle method with latitude 35° North, T_{max} in April = 29.5°C and T_{min} in April = 19.4°C.

TABLE 4.8
Mean Daily Percentage of Annual Daytime Hours (*p*) for Different Months

Latitude	North	Jan	Feb	Mar	Apr	May	June	July	Aug	Sept	Oct	Nov	Dec
Article I.	South	July	Aug	Sept	Oct	Nov	Dec	Jan	Feb	Mar	Apr	May	June
60°		0.15	0.20	0.26	0.32	0.38	0.41	0.40	0.34	0.28	0.22	0.17	0.13
55°		0.17	0.21	0.26	0.32	0.36	0.39	0.38	0.33	0.28	0.23	0.18	0.16
50°		0.19	0.23	0.27	0.31	0.34	0.36	0.35	0.32	0.28	0.24	0.20	0.18
45°		0.20	0.23	0.27	0.30	0.34	0.35	0.34	0.32	0.28	0.24	0.21	0.20
40°		0.22	0.24	0.27	0.30	0.32	0.34	0.33	0.31	0.28	0.25	0.22	0.21
35°		0.23	0.25	0.27	0.29	0.31	0.32	0.32	0.30	0.28	0.25	0.23	0.22
30°		0.24	0.25	0.27	0.29	0.31	0.32	0.31	0.30	0.28	0.26	0.24	0.23
25°		0.24	0.26	0.27	0.29	0.30	0.31	0.31	0.29	0.28	0.26	0.25	0.24
20°		0.25	0.26	0.27	0.28	0.29	0.30	0.30	0.29	0.28	0.26	0.25	0.25
15°		0.26	0.26	0.27	0.28	0.29	0.29	0.29	0.28	0.28	0.27	0.26	0.25
10°		0.26	0.27	0.27	0.28	0.28	0.29	0.29	0.28	0.28	0.27	0.26	0.26
5°		0.27	0.27	0.27	0.28	0.28	0.28	0.28	0.28	0.28	0.27	0.27	0.27
0°		0.27	0.27	0.27	0.27	0.27	0.27	0.27	0.27	0.27	0.27	0.27	0.27

Solution:

Formula: $ET_o = p(0.46T_{mean} + 8)$

Step 1: Determine T_{mean}: $T_{mean} = \frac{T_{max} + T_{min}}{2} = \frac{29.5 + 19.4}{2} = 24.5°C$.

Step 2: Determine p: Latitude: 35° North, month is April, from Table 4.8 → $p = 0.29$.

Step 3: Calculate ET_o: $ET_o = 0.29\ (0.46 \times 24.5 + 8) = 5.6$ mm/day.

Thus, the mean reference crop evapotranspiration $ET_o = 5.6$ mm/day during the whole month of April.

4.3.2.2 Thornthwaite Method

Thornthwaite (1948) derived an equation to be used for limited water conditions. This equation produces monthly estimates of E_t using assumptions similar to those of the Blaney–Criddle method and is written as follows:

$$E_t = 1.62\left(\frac{10T}{I}\right)^a, \tag{4.12}$$

where E_t is evapotranspiration (cm), T is the mean monthly temperature (°C), and a can be estimated as follows:

$$a = (6.75 \times 10^{-8})I^3 - (77.1 \times 10^{-6})I^2 + 0.0179I + 0.492, \tag{4.13}$$

where I is estimated as follows:

$$I = \sum_{j=1}^{12}\left(\frac{T_j}{5}\right)^{1.514}, \tag{4.14}$$

where T_j is the mean temperature of the jth month.

Example 4.7

Estimate the potential evapotranspiration for the data in Table 4.9.

Solution:

From Equation 4.14:

$$I = \sum_{j=1}^{12}\left(\frac{T_j}{5}\right)^{1.514}$$

$$I = \sum_{j=1}^{12}\left(\frac{T_j}{5}\right)^{1.51} = \left(\frac{3.3}{5}\right)^{1.51} + \left(\frac{5.6}{5}\right)^{1.51} + \left(\frac{10}{5}\right)^{1.51} + \left(\frac{15}{5}\right)^{1.51} + \left(\frac{20}{5}\right)^{1.51} + \left(\frac{23.9}{5}\right)^{1.51} + \left(\frac{26.1}{5}\right)^{1.51}$$

$$+ \left(\frac{25}{5}\right)^{1.51} + \left(\frac{21.1}{5}\right)^{1.51} + \left(\frac{15}{5}\right)^{1.51} + \left(\frac{8.9}{5}\right)^{1.51} + \left(\frac{5}{5}\right)^{1.51} = 69.84.$$

TABLE 4.9
Data of Example 4.7

Month	Precipitation (mm)	T (°C)
Jan	112.8	3.3
Feb	94	5.6
Mar	118.9	10
Apr	86.6	15
May	116.9	20
June	101.9	23.9
July	100.3	26.1
Aug	111.3	25
Sep	110.7	21.1
Oct	94.2	15
Nov	85.9	8.9
Dec	87.1	5

From Equation 4.13:

$$a = (6.75 \times 10^{-8})I^3 - (77.1 \times 10^{-6})I^2 + 0.0179I + 0.492 = 1.598.$$

From Equation 4.11 and $T_{mean} = 14.91$:

$$E_t = 1.62\left(\frac{10 \times 14.91}{69.84}\right)^{1.598} = 5.44 \text{ cm.}$$

Example 4.8

If the monthly mean temperature is 30°C, estimate the potential evapotranspiration using the Thornthwaite method.

Solution:

From Equations 4.12, 4.13, and 4.14:

$$I = \sum_{j=1}^{12}\left(\frac{T_j}{5}\right)^{1.514} = \sum_{j=1}^{12}\left(\frac{30}{5}\right)^{1.51} = 12 \times 6^{1.51} = 179.55$$

$$a = 67.5 \times 10^{-8}(179.55)^3 - (77.1 \times 10^{-6})(179.55)^2 + 0.0179 \times 179.55 + 0.492 = 10.1$$

$$E_t = 1.62\left(10 \times \frac{30}{179.55}\right)^{10.1} = 289.2 \text{ cm.}$$

4.3.2.3 Jensen–Haise Method

By analyzing 3000 observations of E_t determined by a soil-sampling procedure for a 35-year period, Jensen and Haise (1963) developed the following relation:

$$E_t = C_T(T - T_x)\, R_s, \tag{4.15}$$

where R_s, is the solar radiation, C_T is a temperature constant equal to 0.014, and T_x is the intercept of the temperature. These coefficients are constant for a particular area. Jensen (1966) defined C_T as

$$C_T = \frac{1}{C_1 + C_2 C_H}, \quad C_H = \frac{50}{e_2 - e_1}, \tag{4.16}$$

where e_1 and e_2 are the saturation vapor pressure at the mean maximum and mean minimum temperatures for the warmest month of the year, respectively, C_2 is equal to 7.6°C, and C_1 is defined as follows:

$$C_1 = 38 - \left(\frac{H}{152.5}\right), \tag{4.17}$$

where H is elevation (m) and

$$T_x = -2.5 - 0.14\left(e_2 - e_1\right) - \left(\frac{H}{550}\right). \tag{4.18}$$

Example 4.9

Compute the potential evapotranspiration using the Jensen–Haise method if the following data are available. The mean temperature is 30°C, the latitude is 33°N, R_s is 800 langleys/day, the mean maximum temperature of the warmest month is 35°C, the mean minimum temperature of the warmest month is 20°C, the elevation is 100 m, e_1 is 23.4 mb, and e_2 is 56.2 mb.

Solution:

From Equations 4.16 and 4.17:

$$C_T = \frac{1}{C_1 + C_2 C_H}, \quad C_H = \frac{50}{e_2 - e_1}$$

$$C_H = \frac{50}{56.2 - 23.4} = 1.542$$

$$C_1 = 38 - \left(\frac{100}{152.5}\right) = 37.34$$

$$C_T = \frac{1}{37.34 + 7.6 \times 1.524} = 0.0204.$$

From Equation 4.18:

$$T_x = -2.5 - 0.14(56.2 - 23.4) - \frac{100}{550} = -7.274.$$

From Equation 4.15:

$$E_t = 0.0204 \times [30 - (-7.274)] \times 800 = 608.31 \text{ langleys/day} = 10.45 \text{ mm/day}.$$

4.4 INTERCEPTION STORAGE AND DEPRESSION STORAGE

The process of interrupting the movement of water in the chain of transportation events leads to stream interception. By vegetation or cover depression storage in puddles and formations of land such as rills and furrows, the interception can take place. It is difficult to separate these sources of rainfall abstraction and they are usually dealt with using an overall figure.

When rain first begins, the water striking leaves and other organic materials spreads over the surfaces in a thin layer or it is collected at points or edges. When the maximum surface storage capability on the surface of the material is exceeded, the material stores additional water in growing drops along its edges. Eventually, the weight of the drops exceeds the surface tension and water falls to the ground. Wind and the impact of raindrops can also release the water from the organic material. The water layer on organic surfaces and the drops of water along the edges are also freely exposed to evaporation. Additionally, interception of water on the ground surface during freezing and subfreezing conditions can be substantial. The interception of falling snow and ice on vegetation also occurs. The highest level of interception occurs when it snows on forests and hardwood forests that have not yet lost their leaves.

Estimating the losses due to interception is done by empirical methods. Horton (1919) suggested the following expression:

$$L_i = a + bP_T^n, \tag{4.19}$$

where L_i is interception (in), P_T is total rainfall depth (in), and a, b, and n are constants.

Kibler et al. (1982) reanalyzed Horton's data (collected from summer storms) and developed the following expression for estimation of interception storage:

$$L_i = cP_T^m, \tag{4.20}$$

where c and m are parameters that are different for different types of crops. Values of a, b, n, c, and m for different types of crops are given in Table 4.10.

TABLE 4.10
Parameter Values for Interception Equations

	Equation 4.19			Equation 4.20	
Tree Type	***a***	***b***	***n***	***c***	***m***
Apple	0.04	0.18	1.0	0.25	0.73
Ash	0.015	0.23	1.0	0.26	0.88
Beech	0.02	0.23	1.0	0.21	0.65
Chestnut	0.04	0.20	1.0	0.30	0.77
Elm	0.0	0.23	0.5	0.15	0.48
Hemlock	0.0	0.20	0.5	0.32	0.74
Maple	0.03	0.23	1.0	0.29	0.77
Oak	0.03	0.22	1.0	0.24	0.66
Pine	0.0	0.20	0.5	0.30	0.70
Willow	0.02	0.40	1.0	0.43	0.85

Source: Kibler, D.F., 1982. With permission.

Viessman et al. (1989) suggested that while estimates of losses due to interception can be significant in annual or long-term models, accounting for interception could be negligible for heavy rainfalls during individual storm events.

4.5 INFILTRATION

The term *infiltration* refers to the process by which rainwater passes through the ground surface and fills the pores of the soil on both the surface and subsurface. This process is an important part of rainfall losses.

The infiltration capacity or infiltration rate is defined as the maximum rate at which water can infiltrate. The actual rate of infiltration will be equal to the rate of rainfall if the rainfall rate is less than the infiltration capacity. Otherwise, the actual rate of infiltration will be equivalent to the infiltration capacity, and the rainwater that does not infiltrate will flow over the ground surface after filling the surface depressions. In other words,

$$f = i \qquad \text{if } f_p > i \tag{4.21}$$

and

$$f = f_p \qquad \text{if } f_p < i, \tag{4.22}$$

where f_p is the infiltration capacity, f is actual rate of infiltration, and i is rate of rainfall.

If infiltration is the only (or the dominating) type of abstraction:

$$i_e = i - f, \tag{4.23}$$

where i_e is rate of excess rainfall. An accurate evaluation of the infiltration capacity is a difficult task. Here, some simple methods to calculate the infiltration capacity, which are extensively used in engineering practices, are covered. The infiltration capacity depends on the soil characteristics and the humidity of the soil. Therefore, a credible infiltration capacity model should take into account the initial moisture conditions of the soil and the amount of water that has already infiltrated into the soil after the start of rainfall.

4.5.1 Green–Ampt Model

The Green–Ampt model is the most physical-based algebraic infiltration model available. The earliest equation was proposed by Green and Ampt (1911). All the parameters involved in this model have a physical basis, which are determined based on soil characteristics. The typical profile of infiltration considered in this method is shown in Figure 4.4. In this figure, the vertical axis is the distance from the soil surface; the horizontal axis is the moisture content of the soil. In this method, the wetting front is considered to be a straight line separating the lower unsaturated layer of soil with the moisture content of θ_i, from the upper saturated soil with moisture content of η. The wetting front has reached the depth, L, in time t since the start of filtration. Water is ponded to a small depth, h_0, on the soil surface.

To formulate the Green–Ampt equations, a cylindrical control volume with unit cross section and depth of L is considered. Hence, the increase in the water stored within the control volume as a result of infiltration is $L(\eta - \theta_i)$, which is equal to the cumulative depth of water infiltrated into the soil, F.

$$F(t) = L(\eta - \theta_i) = L\Delta\theta. \tag{4.24}$$

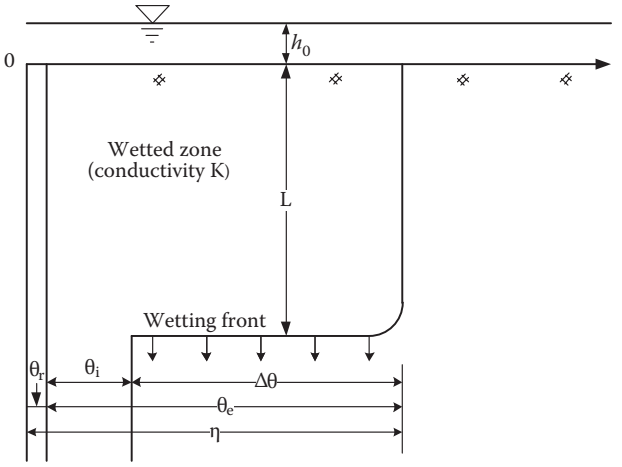

FIGURE 4.4 Typical profile during the infiltration process.

Darcy's law is applied to the saturated zone adjacent to the soil surface to determine the infiltration capacity as follows:

$$q = -K\frac{\delta h}{\delta z}. \tag{4.25}$$

In this case, the Darcy flux q is constant throughout the depth and is equal to $-f$, because q is positive upward while f is positive downward. If points 1 and 2 are located respectively at the ground surface and just on the dry side of the wetting front, the infiltration rate can be approximated by

$$f = K\left[\frac{h_1 - h_2}{z_1 - z_2}\right]. \tag{4.26}$$

The head h_1 at the surface is equal to the ponded depth h_0. The head h_2 in dry soil below the wetting front is equal to $-\Psi - L$. Darcy's law for this system is written as follows:

$$f = K\left[\frac{h_0 - (-\psi - L)}{L}\right] \approx K\left[\frac{\psi + L}{L}\right]. \tag{4.27}$$

The second part of Equation 4.27 is true when the ponded depth, h_0, is negligible compared to Ψ and L. This assumption is usually appropriate for surface water hydrology problems because it is assumed that ponded water becomes surface runoff.

From Equation 4.24, the wetting front depth is $L = F/\Delta\theta$; substitution into Equation 4.27 gives

$$f = K\left(\psi\frac{\Delta\theta}{F} + 1\right). \tag{4.28}$$

In the case when the ponded depth, h_0, is not negligible, the value of $-\Psi - h_0$ is substituted for Ψ in Equation 4.28.

Substituting $f = \frac{dF}{dt}$ in Equation 4.28 and integration of it will result in

$$F(t) = Kt + \psi\Delta\theta \ln\left(1 + \frac{F(t)}{\psi\Delta\theta}\right). \tag{4.29}$$

Given K, t, Ψ, and $\Delta\theta$, a trial value of F is substituted on the right-hand side (a good trial value is $F = Kt$), and a new value of F is calculated on the left-hand side, which is substituted as a trial value on the right-hand side, and so on, until the calculated values of F converge to a constant. The final value of cumulative infiltration F is substituted into Equation 4.28 to determine the corresponding potential infiltration rate f.

An important issue in application of the Green–Ampt model is estimation of soil characteristics including the hydraulic conductivity K, the porosity η, and the wetting front soil suction head (Ψ). Based on the laboratory tests of many soils, Ψ can be expressed as a logarithmic function of an effective saturation, S_e. If the residual moisture content of soil after it has been thoroughly drained is denoted by θ_r, the effective saturation is the ratio of the available moisture $\theta - \theta_r$ to the maximum possible available moisture content $\mu - \theta_r$:

$$S_e = \frac{\theta - \theta_r}{\mu - \theta_r}, \tag{4.30}$$

where $\mu - \theta_r$ is called the effective porosity, θ_e. The effective saturation has the range $0 \le S_e \le 1.0$, provided $\theta_r \le \theta \le \mu$.

For the initial condition, when $\theta = \theta_i$, cross multiplying from Equation 4.30 gives $\theta_i - \theta_r = S_e\theta_e$, and the change in the moisture content when the wetting front passes is $\Delta\theta = \mu - \theta_i = \mu - (S_e\theta_e + \theta_r)$; therefore,

$$\Delta\theta = (1 - S_e)\theta_e. \tag{4.31}$$

The average values of the Green–Ampt parameters μ, θ_e, Ψ, and K for different soil classes are given in Table 4.11.

TABLE 4.11
Soil Parameters for Green–Ampt Model

Soil Type	Porosity, η	Effective Porosity, θ_e	Wetting Front Soil Suction Head, Ψ	Hydraulic Conductivity, K (cm/h)
Sand	0.437 (0.374–0.500)	0.417 (0.354–0.480)	4.95 (0.97–25.36)	11.78
Loamy sand	0.437 (0.363–0.506)	0.401 (0.329–0.437)	6.13 (1.35–27.94)	2.99
Sandy loam	0.453 (0.351–0.555)	0.412 (0.283–0.541)	11.01 (2.67–45.47)	1.09
Loam	0.463 (0.375–0.551)	0.434 (0.334–0.534)	8.89 (1.33–59.38)	0.34
Silt loam	0.501 (0.420–0.572)	0.486 (0.394–0.578)	16.68 (2.92–95.39)	0.65
Sandy clay loam	0.398 (0.332–0.464)	0.330 (0.235–0.425)	21.85 (4.42–108.0)	0.15
Clay loam	0.464 (0.409–0.519)	0.309 (0.279–0.501)	20.88 (4.79–91.10)	0.10
Silty clay loam	0.471 (0.418–0.524)	0.432 (0.347–0.517)	27.30 (5.67–131.50)	0.10
Sandy clay	0.430 (0.370–0.490)	0.321 (0.207–0.435)	23.90 (4.08–140.2)	0.06
Silty clay	0.479 (0.425–0.533)	0.423 (0.334–0.512)	29.22 (6.13–139.4)	0.05
Clay	0.475 (0.427–0.523)	0.385 (0.269–0.501)	31.63 (6.39–156.5)	0.03

Source: Rawls, W.J. et al., *Journal of Hydraulic Engineering*, 109, 62–70, 1983. With permission.

4.5.1.1 Ponding Time

If rainfall intensity is constant and eventually exceeds infiltration rate, then at some moment the surface will become saturated and ponding starts when the infiltration rate is equal to the precipitation rate. The depth infiltrated at that moment, F_s is given by setting $f = i$ in Equation 4.28 and solving for F_s, then:

$$F_s = \frac{\left[\left(\theta_s - \theta_i\right)\psi\right]}{\left[\left(i/K - 1\right)\right]}, \tag{4.32}$$

in which i must be greater than K. Time of ponding, t_p, is defined as follows:

$$t_p = \frac{F_s}{i}. \tag{4.33}$$

Example 4.10

For the following soil properties, determine the amount of infiltrated water when ponding occurs and the time to ponding. K = 1.97 cm/h, θ_i = 0.318, θ_s = 0.518, i = 7.88 cm/h, and ψ_f = 9.37 cm.

Solution:

Using Equation 4.32, the infiltrated water until the ponding time is obtained as

$$F_s = \psi_f \frac{\theta_s - \theta_i}{\frac{f}{K} - 1} = 9.37 \frac{0.518 - 0.318}{\frac{7.88}{1.97} - 1} = 0.625 \text{ cm}.$$

From Equation 4.33:

$$t_p = (0.625/7.88) = 0.079 \text{ h} = 4.74 \text{ min} = 284 \text{ s}.$$

However, in the case of rainfall with variable intensity, determining the ponding time and infiltration depth is rather complicated. Here, a useful flow chart for estimating infiltration and ponding time by the Green–Ampt method proposed by Chow et al. (1988) is described.

Consider a time interval from t to $t + \Delta t$. The rainfall intensity during this interval is denoted i_t and is constant throughout the interval. The potential infiltration rate and cumulative infiltration at the beginning of the interval are f_t and F_t, respectively, and the corresponding values at the end of interval are $f_{t+\Delta t}$ and $F_{t+\Delta t}$. It is assumed that F_t is known from the given initial conditions or from previous computation.

The flow chart for determining ponding time is presented in Figure 4.5. There are two cases to be considered:

1. Ponding occurs throughout the interval.
2. There is no ponding throughout the interval.

The infiltration rate is always either decreasing or constant with time; thus, once ponding is established under a given rainfall intensity, it will continue. Hence, it is assumed that ponding

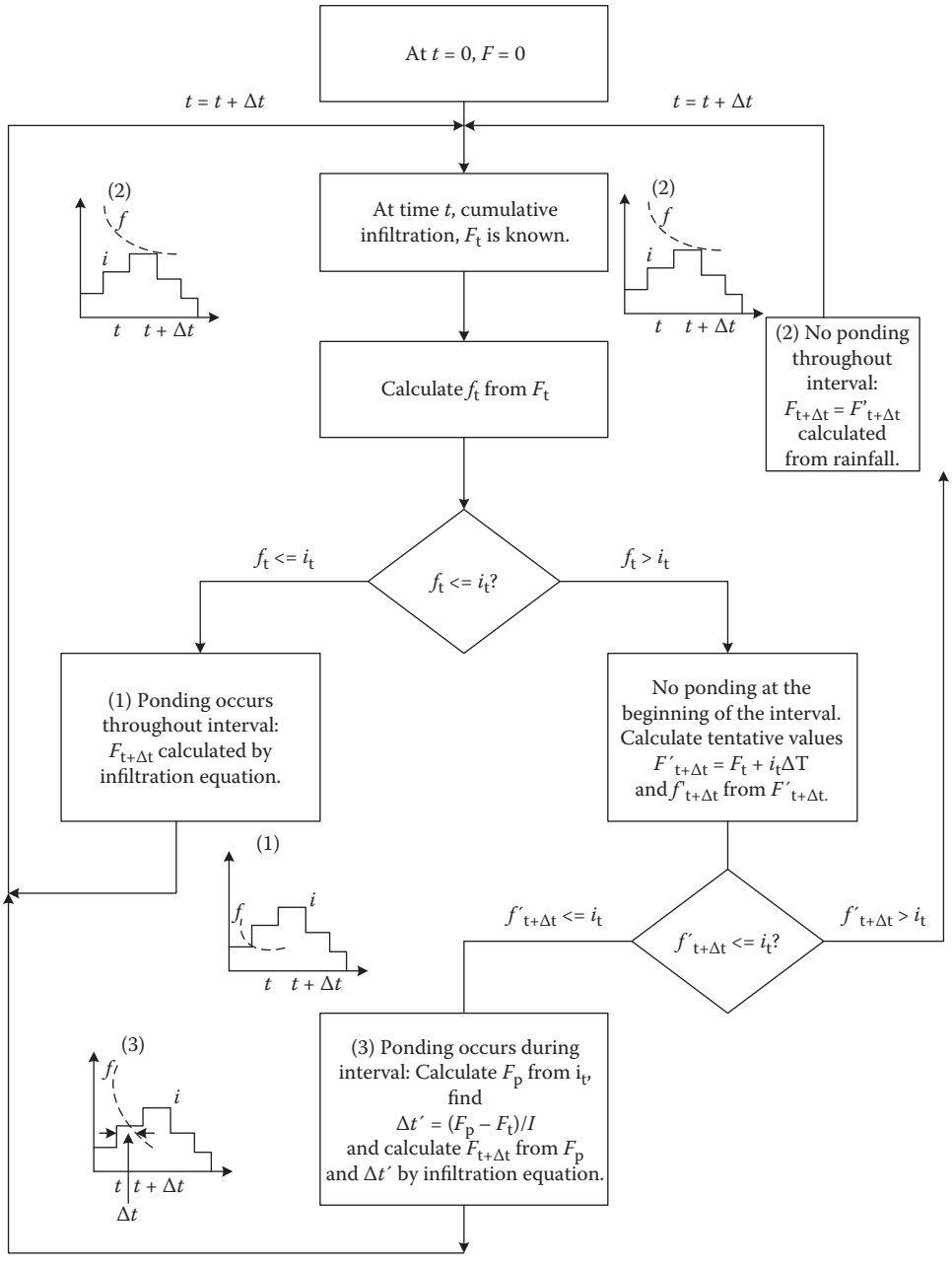

FIGURE 4.5 Flow chart for determining infiltration and ponding time under variable rainfall intensity. (From Chow, V.T. et al., *Applied Hydrology*, McGraw-Hill, New York, 1988. With permission.)

cannot occur in the middle of an interval, but at the end of it, when the value of the rainfall intensity changes.

Following the flow chart, the first step is to calculate the current potential infiltration rate f_t from the known value of cumulative infiltration F_t. For the Green–Ampt method, one uses

$$f_t = K\left(\psi \frac{\Delta\theta}{F_t} + 1\right), \tag{4.34}$$

where f_t is infiltration rate, $\Delta\theta$ is difference in dry versus wet soil moisture, K is soil conductivity (cm/h), F_t is cumulative infiltration (cm), and Ψ is suction head (cm). The Green–Ampt parameters can be estimated according to the soil texture and land-use practices (Table 4.11).

The resulting f_t is compared to the rainfall intensity i_t. If f_t is less than or equal to i_t, case (1) arises and there is ponding throughout the interval. In this case, the Green–Ampt equation, the cumulative infiltration at the end of the interval, $F_{t+\Delta t}$, is calculated from

$$F_{t+\Delta t} - F_t - \psi\Delta\theta \ln\left[\frac{F_{t+\Delta t} + \psi\Delta\theta}{F_t + \psi\Delta\theta}\right] = K\Delta t. \tag{4.35}$$

Both cases (2) and (3) have $f_t > i_t$ and no ponding at the beginning of the interval. Assume that this remains so throughout the interval; then, the infiltration rate is i_t and a tentative value for cumulative infiltration at the end of the time interval is

$$F'_{t+\Delta t} = F_t + i_t\Delta t. \tag{4.36}$$

Next, a corresponding infiltration rate $f'_{t+\Delta t}$ is calculated from $F'_{t+\Delta t}$. If $f'_{t+\Delta t}$ is greater than i_t, case (2) occurs and there is no ponding throughout the interval. The $F_{t+\Delta t} = F'_{t+\Delta t}$ and the problem is solved for this interval.

If $f'_{t+\Delta t}$ is less than or equal to i_t, ponding occurs during the interval [case (3)]. The cumulative infiltration F_p at ponding time is found by setting $f_t = i_t$ and $F_t = F_p$ in Equation 4.36 and solving for F_p to give, for the Green–Ampt equation,

$$F_p = \frac{K\psi\Delta\theta}{i_t - K}. \tag{4.37}$$

The ponding time is then $t + \Delta t$, where

$$\Delta t' = \frac{F_p - F_t}{i_t}, \tag{4.38}$$

and the cumulative infiltration $F_{t+\Delta t}$ is found by substituting $F_t = F_p$ and $\Delta t = \Delta t - \Delta t'$ in Equation 4.35. The excess rainfall values are calculated by subtracting cumulative infiltration from cumulative rainfall and then taking successive differences of the resulting values.

Example 4.11

A rainfall hyetograph is given in columns 1 and 2 of Table 4.12. If this rain falls on a sandy loam soil of initial effective saturation 40%, determine the excess rainfall hyetograph.

Solution:

From Table 4.11, for a sandy loam soil, K = 1.09 cm/h, Ψ = 11.01 cm, and

$$\Delta\theta = (1 - S_e)\theta_e = (1 - 0.4)\,(0.412) = 0.247$$

$$\psi\Delta\theta = 0.247 \times 11.01 = 2.72 \text{ cm}.$$

TABLE 4.12
Calculation of Excess Rainfall Hyetograph Using Green–Ampt Infiltration Equation (Example 4.11)

	Rainfall			Infiltration		Excess Rainfall	
Time (min)	Incremental (cm)	Cumulative (cm)	Intensity (cm/h)	Rate (cm/h)	Cumulative (cm)	Cumulative (cm)	Incremental (cm)
0		0	1.67		0		
5	0.14	0.14	2.02	22.27	0.14		
10	0.17	0.31	2.86	10.65	0.31		
15	0.24	0.55	3.93	6.48	0.55		
20	0.33	0.88	4.76	4.46	0.88	0	
25	0.4	1.28	5.71	3.54	1.21	0.07	
30	0.48	1.76	9.64	3.08	1.49	0.27	0.07
35	0.81	2.57	17.86	2.8	1.73	0.84	0.2
40	1.5	4.07	50.6	2.6	1.96	2.11	0.57
45	4.25	8.32	24.17	2.46	2.17	6.15	1.27
50	2.03	10.35	13.33	2.34	2.37	7.98	4.04
55	1.12	11.47	8.81	2.25	2.56	8.91	1.83
60	0.74	12.21	6.55	2.17	2.75	9.46	0.93
65	0.55	12.76	5.71	2.1	2.93	9.83	0.55
70	0.48	13.24	3.1	2.05	3.1	10.14	0.37
75	0.26	13.5	2.02	2	3.27	10.23	0.31
80	0.17	13.67	1.79	1.95	3.43	10.24	0.09
85	0.15	13.82	1.19	1.92	3.59		0.01
90	0.1	13.92		1.88	3.75		

The time interval in Table 4.12 is Δt = 5 min = 0.084 h. Column 3 of the table shows the cumulative rainfall depths by summing the incremental values in column 2. The rainfall hyetograph and the cumulative rainfall hyetograph are shown in Figure 4.6. The rainfall intensity in column 4 is found from column 2 by dividing by Δt. For example, during the first time interval, 0.14 cm of rainfall occurs; thus, i = 0.14/0.087 = 1.67 cm/h as shown. F = 0; thus, $f = \infty$ from Equation 4.35 and ponding does not occur at time 0. Hence, F at time 10 min is calculated by Equation 4.34,

$$f'_{t+\Delta t} = K\left(\frac{\psi\Delta\theta}{F'_{t+\Delta t}} + 1\right) = 1.09\left(\frac{2.72}{0.14} + 1\right) = 22.27 \text{ cm/h}$$

as shown in column 5 of Table 4.12. This value is greater than i; therefore, no ponding occurs during this interval and cumulative infiltration equals cumulative rainfall as shown in column 6. It is found that ponding does not occur up to 20 min of rainfall, but at 20 min,

$$f'_{t+\Delta t} = K\left(\frac{\psi\Delta\theta}{F'_{t+\Delta t}} + \right) = 1.09\left(\frac{2.72}{0.88} + 1\right) = 4.46 \text{ cm/h}$$

which is less than i_t = 4.76 cm/h for the interval from 20 to 25 min; thus, ponding begins at 20 min (see Figure 4.6).

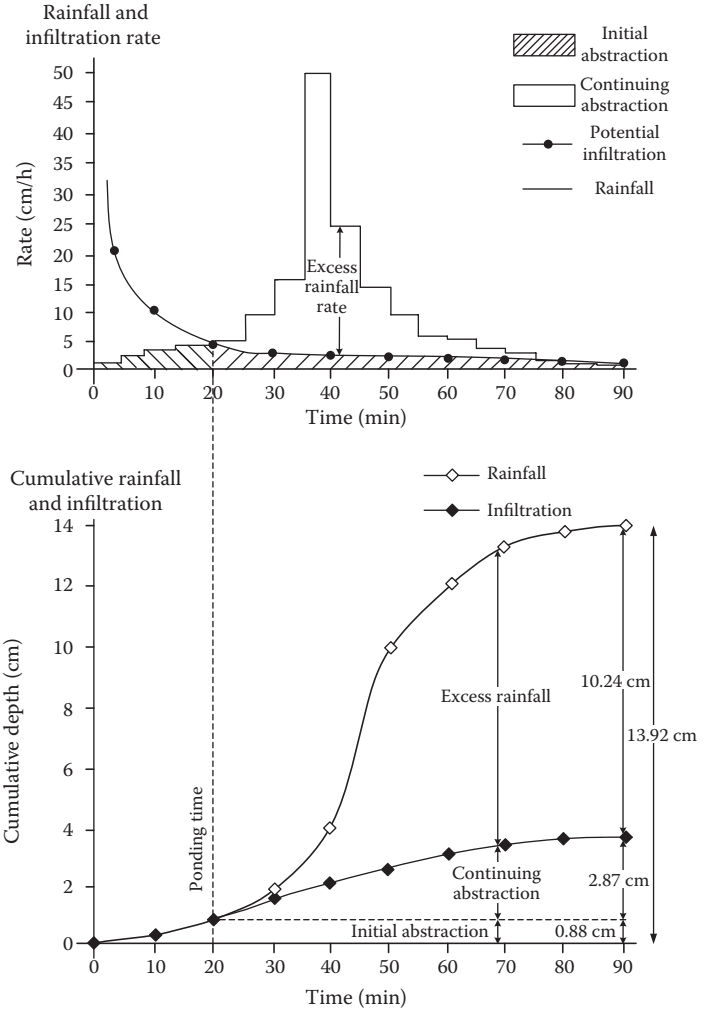

FIGURE 4.6 Infiltration and excess rainfall under variable rainfall intensity (Example 4.11).

During the ponded period, Equation 4.35 is used to calculate infiltration. The value of $F_{t+\Delta t}$ at 70 min is given by

$$F_{t+\Delta t} - F_t - \psi\Delta\theta \ln\left[\frac{F_{t+\Delta t} + \psi\Delta\theta}{F_t + \psi\Delta\theta}\right] = K\Delta t$$

$$F_{t+\Delta t} - 0.88 - 2.72\ln\left[\frac{F_{t+\Delta t} + 2.72}{0.88 + 2.72}\right] = 1.09 \times 0.084$$

which is solved by the method of successive approximation to give $F_{t+\Delta t} = 1.21$ cm as shown in column 6 of Table 4.12. The cumulative excess rainfall (column 7) is found by subtracting cumulative infiltration (column 6) from cumulative rainfall (column 3), and the excess rainfall values in column 8 are found by taking differences of successive cumulative rainfall values. Ponding ceases at 80 min when the rainfall intensity falls below the potential infiltration rate. After 80 min, cumulative infiltration is computed from the rate example at 85 min as shown in column 6.

As shown in Figure 4.6, the total rainfall of 13.92 cm is disposed of as an initial abstraction of 0.88 cm (cumulative infiltration at ponding time), a continuing abstraction of 2.87 cm (3.75 cm total infiltration – 0.88 cm initial abstraction), and an excess rainfall of 10.24 cm.

4.5.2 Horton Method

An exponential decay function (based on experimental data) to calculate the infiltration capacity, suggested by Horton (1919) is

$$f_p = f_f + (f_0 - f_f)e^{-kt}, \tag{4.39}$$

where f_p is infiltration capacity, f_f is final infiltration capacity, f_0 is initial infiltration capacity, k is exponential decay constant, and t is time from beginning of rainfall.

Equation 4.39 is dimensionally consistent. The unit of k should be the inverse of the unit used for t. Figure 4.7 is a graphical representation of Equation 4.39 and explains how the infiltration capacity varies with time. Equation 4.39 is empirical and despite its early years of development, it is still used in practice. The three parameters f_0, f_f, and k need to be determined by fitting Equation 4.39 to measured infiltration data. There is no generally accepted listing of these parameters for different types of soils.

Example 4.12

An area is subjected to the rainfall tabulated in column 3 of Table 4.13 and plotted in Figure 4.8. The Horton parameters are estimated as f_0 = 3.0 cm/h, f_f = 0.5 cm/h, and k = 1.0/h. We are to determine the losses due to infiltration in the pervious areas and the excess rainfall, assuming that losses occur due to infiltration only.

Solution:

The calculations are performed in tabular form, presented in Table 4.13. t_1 and t_2 values listed in columns 1 and 2 of Table 4.13 represent the beginning and end of a time interval. The average infiltration capacity, f_p, during a time interval is determined at the midpoint of each time interval; that is, $t = 0.5(t_1 + t_2)$. The values of t are entered in column 4. Equation 4.39 is utilized to calculate the values of f_p, listed in column 5. The infiltration rates f tabulated in column 6 are equal to the smaller value of f_p, and i. The rates of effective rainfall i_e in column 7 are achieved by using $i_e = i - f$. The results are plotted in Figure 4.8. The total depth of water lost due to infiltration is $F = \Delta t.\ \Sigma f$ = (0.05 h) (43.50 cm/h) = 2.18 cm. Similarly, the total excess rainfall is $\Delta t \Sigma i_e$ = (0.05 h)(9.0 cm/h) = 0.45 cm.

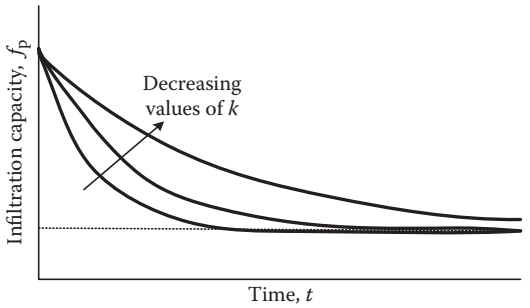

FIGURE 4.7 Horton infiltration capacity graph.

TABLE 4.13
Horton Infiltration Method, Example 4.12

(1)	(2)	(3)	(4)	(5)	(6)	(7)
t_1 (h)	t_2 (h)	i (cm/h)	t (h)	f_p (cm/h)	f (cm/h)	i_e (cm/h)
0.00	0.05	1.00	0.025	2.94	1.00	0.00
0.05	0.10	1.00	0.075	2.82	1.00	0.00
0.10	0.15	1.00	0.125	2.71	1.00	0.00
0.15	0.20	1.00	0.175	2.60	1.00	0.00
0.20	0.25	1.00	0.225	2.50	1.00	0.00
0.25	0.30	2.00	0.275	2.40	2.00	0.01
0.30	0.35	2.00	0.325	2.31	2.00	0.00
0.35	0.40	2.00	0.375	2.22	2.00	0.00
0.40	0.45	2.00	0.425	2.13	2.00	0.00
0.45	0.50	2.00	0.475	2.05	2.00	0.00
0.50	0.55	2.00	0.525	1.98	1.98	0.02
0.55	0.60	2.00	0.575	1.91	1.91	0.09
0.60	0.65	2.00	0.625	1.84	1.84	0.16
0.65	0.70	2.00	0.675	1.77	1.77	0.23
0.70	0.75	2.00	0.725	1.71	1.71	0.29
0.75	0.80	3.00	0.775	1.65	1.65	1.35
0.80	0.85	3.00	0.825	1.60	1.60	1.40
0.85	0.90	3.00	0.875	1.54	1.54	1.46
0.90	0.95	3.00	0.925	1.49	1.49	1.51
0.95	1.00	3.00	0.975	1.44	1.44	1.56
1.00	1.05	1.50	1.025	1.40	1.40	0.10
1.05	1.10	1.50	1.075	1.35	1.35	0.15
I.10	1.15	1.50	1.125	1.31	1.31	0.19
1.15	1.20	1.50	1.175	1.27	1.27	0.23
1.20	1.25	1.50	1.225	1.23	1.23	0.27
1.25	1.30	1.00	1.275	1.20	1.00	0.00
1.30	1.35	1.00	1.325	1.16	1.00	0.00
1.35	1.40	1.00	1.375	1.13	1.00	0.00
1.40	1.45	1.00	1.425	1 J 0	1.00	0.00
1.45	1.50	1.00	1.475	1.07	1.00	0.00
		Σ = 52.50			Σ = 43.50	Σ = 9.00

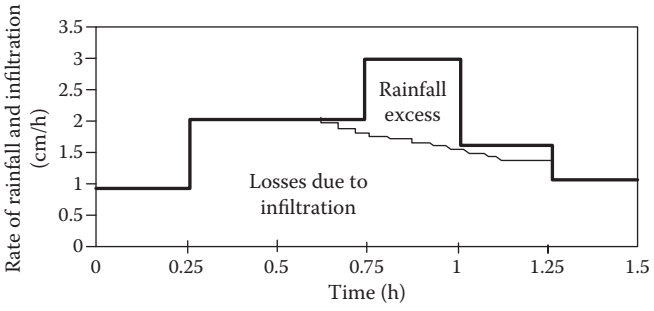

FIGURE 4.8 Rainfall and excess rainfall hyetographs of Example 4.12.

4.5.3 Holtan Method

The Holtan method is based on the concept that the infiltration capacity is proportional to the available storage to hold water in the surface layer of the soil. As water infiltrates to soil, this available storage is reduced, and consequently, the infiltration capacity decreases. The Holtan method is applicable for agricultural lands, calculating the rainfall losses in wooded parts of urban areas and the areas covered by grass and plants. The Holtan equation (Holtan and Lopez 1971) is written as

$$f_p = G \times a \times S_A^{1.4} + f_f, \tag{4.40}$$

where f_p is infiltration capacity (cm/h), G is the growth index of plants, a is vegetative factor, S_A is available storage to hold water in the surface layer of the soil (cm), and f_f is final infiltration capacity (cm/h). The growth index of plants, G, depends on the maturity of plants and varies between 0.1 and 1.0 during the growing season, which is equal to 1.0 for mature plants. The recommended values for the vegetative factor, a, are 0.80 for most wooded areas and 1.0 for permanent pasture.

The available storage S_A, as rainwater infiltrates into the soil during the rainfall–infiltration process, is reduced. Over a discrete time interval Δt, this reduction is calculated as

$$\Delta S_A = \Delta t(f - f_f). \tag{4.41}$$

Note that, as in the modified Horton method, part of the infiltrating water is supposed to percolate deeper underneath the surface layer at a rate of f_f. To start the calculations, the initial value of S_A is needed to be determined as the product of the depth of the surface soil layer, Φ, and initial moisture deficit, $\Phi(1 - S_i)$, where S_i is the initial degree of saturation.

Example 4.13

An area is subject to a 1.5 h rainfall with hourly intensity listed in column 4 of Table 4.14. Find the losses due to infiltration using the Holtan method. Assume that f_f = 0.2 cm/h, a = 0.9, and Φ = 1.0, and initially, S_A = 2.0 cm, which is the product of 10 cm of surface soil and an initial moisture deficit of $\Phi(1 - S_i)$ = 0.2 (this means that each centimeter of soil can absorb 0.2 cm of water before becoming saturated).

Solution:

The calculations are presented in Table 4.14. A time increment of Δt = 0.05 h is used. The times t_1 and t_2 listed in columns 2 and 3 represent the beginning and the end of each time interval. For the first time step, S_{A1} is the available storage at time t_1 = 0 and is equal to the initial value of 2.0 cm. The infiltration capacity f_p listed in column 6 is calculated using Equation 4.39 by substituting S_{A1} for S_A as an approximation. The infiltration rate, f, listed in column 7 is equal to the smaller value of i and f_p. Equation 4.39 is applied to estimate the reduction in available storage ΔS_A, which is presented in column 8. The S_{A2} in column 9 is equal to $S_{A1} - \Delta S_A$. The rate of effective rainfall i_e in column 10 is obtained as $i_e = i - f$. The same procedure is followed for all the time intervals.

$$F = \Delta t \cdot \Sigma f = (0.05 \text{ h})\ (33.68 \text{ cm/h}) = 1.68 \text{ cm}.$$

Likewise, the total excess rainfall is $\Delta t \cdot \Sigma i_e$ = (0.05 h)(13.82 cm/h) = 0.69 cm.

TABLE 4.14
Calculation Results of Example 4.13

(1)	(2)	(3)	(4)	(5)	(6)	(7)	(8)	(9)	(10)
Time Step	t_1 (h)	t_2 (h)	i (cm/h)	S_{A1} (cm)	f_p (cm/h)	f (cm/h)	ΔS_A (cm)	S_{A2} (cm)	i_e (cm/h)
1	0.00	0.05	1.00	2.00	2.58	1.00	0.04	1.96	0.00
2	0.05	0.10	1.00	1.96	2.51	1.00	0.04	1.92	0.00
3	0.1	0.15	1.00	1.92	2.44	1.00	0.04	1.88	0.00
4	0.15	0.20	1.00	1.88	2.38	1.00	0.04	1.84	0.00
5	0.20	0.25	1.00	1.84	2.31	1.00	0.04	1.80	0.00
6	0.25	0.30	2.00	1.80	2.25	2.00	0.09	1.71	0.00
7	0.30	0.35	2.00	1.71	2.11	2.00	0.09	1.62	0.00
8	0.35	0.40	2.00	1.62	1.97	1.97	0.09	1.53	0.03
9	0.40	0.45	2.00	1.53	1.83	1.83	0.08	1.45	0.17
10	0.45	0.50	2.00	1.45	1.71	1.71	0.08	1.37	0.29
11	0.50	0.55	3.00	1.37	1.60	1.60	0.07	1.30	1.40
12	0.55	0.60	3.00	1.30	1.50	1.50	0.07	1.24	1.50
13	0.60	0.65	3.00	1.24	1.41	1.41	0.06	1.18	1.59
14	0.65	0.70	3.00	1.18	1.33	1.33	0.06	1.12	1.67
15	0.70	0.75	3.00	1.12	1.26	1.26	0.05	1.07	1.74
16	0.75	0.80	2.00	1.07	1.19	1.19	0.05	1.02	0.81
17	0.80	0.85	2.00	1.02	1.12	1.12	0.05	0.97	0.88
18	0.85	0.90	2.00	0.97	1.07	1.07	0.04	0.93	0.93
19	0.90	0.95	2.00	0.93	1.01	1.01	0.04	0.89	0.99
20	0.95	1.00	2.00	0.89	0.96	0.96	0.04	0.85	1.04
21	1.00	1.05	1.00	0.85	0.92	0.92	0.04	0.81	0.08
22	1.05	1.10	1.00	0.81	0.88	0.88	0.03	0.78	0.12
23	1.10	1.15	1.00	0.78	0.84	0.84	0.03	0.75	0.16
24	1.15	1.20	1.00	0.75	0.80	0.80	0.03	0.72	0.20
25	1.20	1.25	1.00	0.72	0.77	0.77	0.03	0.69	0.23
26	1.25	1.30	0.50	0.69	0.74	0.50	0.02	0.68	0.00
27	1.30	1.35	0.50	0.68	0.72	0.50	0.02	0.66	0.00
28	1.35	1.40	0.50	0.66	0.70	0.50	0.02	0.65	0.00
29	1.40	1.45	0.50	0.65	0.69	0.50	0.02	0.63	0.00
30	1.45	1.50	0.50	0.63	0.67	0.50	0.02	0.62	0.00
			$\Sigma = 47.50$			$\Sigma = 33.68$			$\Sigma = 13.82$

4.6 CALCULATION OF EXCESS RAINFALL–RUNOFF

Runoff is an important component of the water cycle because of its role in supplying demand for different purposes. Therefore, a main concern in hydrologic analysis is the amount of excess rainfall (surface runoff) generated during a given rainfall event on a watershed. In calculation of excess rainfall or runoff, the system boundaries are adopted to the watershed boundaries, which are discussed in detail in Chapter 5. In general, runoff can be described as a product of rainfall's interaction with the land. This interaction is one of the several processes that the Earth's water may go through as it continually cycles between the land and the atmosphere.

Excess rainfall was calculated in the last section using the Green–Ampt method. Hydrologists calculate effective rainfall or excess rainfall as the total rainfall minus abstractions.

$$S = P - (D + M + U + \text{SEdt}), \tag{4.42}$$

where P is rainfall or precipitation received, S is excess rainfall (surface runoff), D is increase in surface detention, M is increase in soil water storage, U is increase in the groundwater storage, and SEdt is the total evaporation over a period of time.

The rate of effective rainfall or excess rainfall is defined as the depth of excess rainfall produced per unit time. When rainfall exceeds the infiltration rate at the surface, excess water begins to accumulate as surface storage in small depressions governed by surface topography. As depression storage begins to fill, overland flow may begin to occur in portions of a watershed, and the flow quickly concentrates into small channels, which can then flow into larger streams. Contributions to a stream can also come from the shallow subsurface via interflow or base flow and contribute to the overall discharge hydrograph from a rainfall event.

Different rainfall–runoff models and equations have been developed to investigate the potential runoff for a given rainfall. In general, all runoff computation methods are, to some degree, mathematical expressions of the hydrologic cycle. However, most of the models transform the cyclical character of the water cycle to a linear form, treating rainfall as an input and producing runoff as an output. During this transformation, each method uses mathematical approximations of the real rainfall–runoff processes to produce its estimates of runoff volume and rate.

Different factors are considered in selection of the appropriate model or equation for runoff simulation. Each method has its own complexity, data needs, accuracy, and range of results. Some methods, such as the rational method, estimate peak runoff rate but cannot predict total runoff volumes. Other methods, such as Soil Conservation Service (SCS), can only estimate the total runoff volume.

Simple methods, such as the rational method, require limited rainfall and drainage area data, while other, more sophisticated methods, have extensive data needs, including long-term rainfall and temperature data as well as drainage area soils, subsoil, and ground cover information. In general, the more data-intensive models can produce more comprehensive runoff predictions. The details of models and methods used for runoff evaluation and studying its variation over time through the watershed, channels, and reservoirs are given in Chapter 6.

One of the simplest rainfall–runoff relationships that is often used for estimation of peak flow used in drainage design purposes is the rational method. In this method, the peak flow, Q_p, is estimated from the following formula:

$$Q_p = C \times i \times A, \tag{4.43}$$

where C is runoff coefficient, which depends on watershed land use, and i is intensity of rainfall of chosen frequency for a duration equal to time of concentration (depending on watershed physiographic characteristics). Time of concentration is the equilibrium time for rainfall occurring at the most remote portion of the basin to contribute flow at the outlet. A is the area of the watershed. Watershed concepts and further details on the rational method are given in Chapters 5 and 6.

Hydrograph, which shows the flow rate variations versus time, is usually used for rainfall analysis and study. The rainfall depth (P) is obtained based on hydrograph orders:

$$P = \sum_{t=1}^{n-1} \frac{Q_{t+1} + Q_t}{2} \times \Delta t, \tag{4.44}$$

where Q_t is the hydrograph ordinate in time step, Δt is the time interval between hydrograph ordinates, and n is the number of hydrograph ordinates.

The details of actual physical processes that convert rainfall to runoff are very complicated and are not completely understood. Therefore, it is not possible to replicate these processes using mathematical models with a high level of certainty. Different simplifying assumptions and empirical data are made in developing mathematical models and equations for simulation of these processes and predicting resultant runoff volumes and rates with acceptable accuracy. In hydrograph analysis, it is assumed that the watershed response to rainfall variations is linear; therefore, concepts of superposition and multiplication are used for hydrograph analysis.

Hydrograph shape and volume of runoff depend on the physiographic characteristics of the watershed, the meteorological conditions, and human factors. Meteorological factors include the following:

- Rainfall intensity and pattern
- Areal distribution of rainfall over the basin
- Size and duration of the storm event

Physiographic or watershed factors of importance in hydrograph and runoff analysis are as follows:

- Size and shape of the drainage area
- Slope of the land surface and the main channel
- Channel morphology and drainage type
- Soil types and distribution
- Storage detention in the watershed

Human factors are considered in land use and land cover. The time of concentration, which is affected by a set of watershed parameters, is of high importance in determining the variations of flow at the basin outlet as well as the amount and time of peak discharge. The evaluation of watershed characteristics and how they affect the outflow and its variations over time are further discussed in Chapter 5. Some measuring methods, such as unit hydrograph theory, S-curved, Snyder, and SCS, are discussed in more detail in Chapter 6.

Due to the high variability of the rainfall hydrograph, as discussed, and the scarcity of flow data of different storm events, design storm events are developed using the unit hydrograph. The D hour unit hydrograph is the runoff caused by a unit rainfall depth during D hours over the watershed. For a case where M equal pulses of excess rainfall and N pulses of direct runoff are observed in a storm, $N - M + 1$ values will be needed to define the unit hydrograph. The discrete convolution equation (further described in Chapter 6) is used for the computation of direct runoff Q_n given excess rainfall P_m and the unit hydrograph U_{n-m+1}:

$$Q_n = \sum_{m=1}^{n \le M} P_m \times U_{n-m+1}. \tag{4.45}$$

A hydrograph is a function of discharge with time and describes the passage of a wave along the river. The shape of this wave will change as it moves down the river due to various factors such as channel storage, resistance, lateral addition or withdrawal, etc. The process of determination of these changes in any specific point of the river is known as routing. The principle of routing is the continuity equation that can be stated as follows:

$$I - Q = \mathrm{d}S/\mathrm{d}t, \tag{4.46}$$

where I is inflow, Q is outflow, and S is storage. Therefore after determining inflow and storage variations in each reach of river or reservoir, the outflow hydrograph can be determined. The detailed concepts in relation to runoff analysis over the watershed and runoff routing are given in Chapter 6.

4.7 GROUNDWATER

The water below the surface of the Earth primarily is groundwater, but it also includes soil water. Movement of water in the atmosphere and on the land surface is relatively easy to visualize, but the movement of groundwater is not.

Groundwater moves along flow paths of varying lengths from areas of recharge to areas of discharge. The generalized flow paths start at the water table, continue through the groundwater system, and terminate at the stream or at the pumped well. The source of water to the water table (groundwater recharge) is infiltration of precipitation through the unsaturated zone. In the uppermost, unconfined aquifer, flow paths near the stream can be tens to hundreds of meters in length and have corresponding travel times of days to a few years. The longest and deepest flow paths may be thousands of meters to tens of kilometers in length, and travel times may range from decades to millennia. In general, shallow groundwater is more susceptible to contamination from human sources and activities because of its close proximity to the land surface. Therefore, shallow, local patterns of groundwater flow near surface water are emphasized in this section.

The principal hydrologic properties of aquifers are permeability and specific yield. Permeability shows the material ability to transmit water while specific yield indicates the volume of water that the aquifer yields during drainage. The materials that form the crust of the Earth have a lot of voids called interstices. These voids hold the water that is found below the surface of the land and that is recoverable through springs and wells. The occurrence of water under the ground is related to the character, distribution, and structure of the voids in soil. If the interstices are connected, the water can move through the rocks by percolating from one interstice to another and therefore the groundwater flow forms.

The porosity is considered as the percentage of the total volume of the rock that is occupied by interstices. The porosity of soil depends on the shape and arrangement of its particles, the particles sorting, the degree of cementation and compacting, and the fracturing of the rock resulting in joints and other openings. It should be mentioned that there is not definitely a correlation between the porosity and permeability of a material; a rock may contain many large but disconnected interstices and thus have a high porosity yet a low permeability. Clay may have a very high porosity (higher than some gravel) but a very low permeability.

Just a part of stored water in the interstices is recovered through wells and the remainder will be retained by the rock formations. Specific yield corresponds to the part that will drain into wells, and the part that is retained by the rocks is called the specific retention. Both specific yield and specific retention are expressed as the percentages of the total volume of material and their summation is equal to the porosity.

The water table fluctuates in response to recharge and discharge from the aquifer. The shape and slope of the water table, which are determining factors in the movement of groundwater, are affected by many factors such as the differences in permeability of the aquifer materials, topography, and the configuration of the underlying layer, amount, and distribution of precipitation, as well as the method of discharge of the groundwater. However, as a general concept, the slope of the water table varies inversely with the permeability of the aquifer material. This is shown by Darcy's law governing the movement of groundwater:

$$Q = KiA, \tag{4.47}$$

where Q is the quantity of water moving through a given cross-sectional area, K is the permeability or hydraulic conductivity coefficient, i is the hydraulic gradient, and A is the total cross-sectional area through which the water is moving.

Streams, lakes, and reservoirs interact with groundwater in all types of landscapes. The interaction takes place in three basic ways: streams gain water from inflow of groundwater through the streambed (gaining stream), they lose water to groundwater by outflow through the streambed (losing stream), or they do both, gaining in some reaches and losing in other reaches. For groundwater to discharge into a stream channel, the altitude of the water table in the vicinity of the stream must be higher than the altitude of the stream water surface. Conversely, for surface water to seep to groundwater, the altitude of the water table in the vicinity of the stream must be lower than the altitude of the stream water surface. Contours of water table elevation indicate gaining streams by pointing in an upstream direction, and they indicate losing streams by pointing in a downstream direction in the immediate vicinity of the stream. These interactions play an important role in surface and groundwater resource volume changes over time that should be considered in water supply schemes. The concepts used in the study of groundwater resources and their interactions with the surface water resources are explained in detail in Chapter 7.

4.8 RESERVOIRS AND LAKES

Lakes and reservoirs are sites in a basin where surface water storage needs to be modeled. Thus, variables defining the water volumes at those sites must be defined. Let S_t^s be the initial storage volume of a lake or reservoir at site s in period t. Omitting the site index s for the moment, the final storage volume in period t, S_{t+1} (which is the same as the initial storage in the following period $t + 1$), will equal the initial volume, S_t, plus the net surface and groundwater inflows, Q_t, less the release or discharge, R_t, and evaporation and seepage losses, L_t. All models of lakes and reservoirs include this mass balance equation for each period t being modeled.

$$S_t + Q_t - R_t - L_t = S_{t+1}. \tag{4.48a}$$

The release from a natural lake is a function of its surrounding topography and its water surface elevation. It is determined by nature, and unless it is made into a reservoir, its discharge or release is not controlled or managed. The release from a reservoir is controllable and is usually a function of the reservoir storage volume and time of year. Reservoirs also have fixed storage capacities, K. In each period t, reservoir storage volumes, S_t, cannot exceed their storage capacities, K.

$$S_t \le K \text{ for each period } t. \tag{4.48b}$$

Equations 4.48a and 4.48b are the two fundamental equations required when modeling water supply reservoirs. They apply for each period t.

The primary purpose of all reservoirs is to provide a means of regulating downstream surface water flows over time and space. Other purposes may include storage volume management for recreation and flood control and storage and release management for hydropower production. Reservoirs are built to alter the natural spatial and temporal distribution of the streamflows. The capacity of a reservoir together with its release (or operating) policy determines the extent to which surface water flows can be stored for later release.

The use of reservoirs for temporarily storing streamflows often results in a net loss of total streamflow due to increased evaporation and seepage. Reservoirs also bring with them changes in the ecology of a watershed and river system. They may also displace communities and human settlements. When considering new reservoirs, any benefits derived from regulation of water supplies, from floodwater storage, from hydroelectric power, and from any navigational and recreational activities should be compared to any ecological and social losses and costs. The benefits of reservoirs can be substantial, but so may the costs. Such comparisons of benefits and costs are always challenging because of the difficulty of expressing all such benefits and costs in a common metric.

Reservoir storage capacity can be divided among three major uses: (1) the active storage used for downstream flow regulation and for water supply, recreational development, or hydropower production; (2) the dead storage required for sediment collection; and (3) the flood storage capacity reserved to reduce potential downstream flood damage during flood events. The distribution of active and flood control storage capacities may change over the year. For example, there is no need for flood control storage in seasons that are not going to experience floods. Often, these components of reservoir storage capacity can be modeled separately and then added together to determine total reservoir storage capacity.

4.9 WATER BALANCE

In the previous sections, the mathematical concepts representing hydrologic components including evapotranspiration, infiltration, runoff, and groundwater flow were presented. In water resources related fields of hydrologic studies, in addition to evaluation of hydrologic components, it is useful to evaluate the changes in water resources. For this purpose, the water balance concept is employed. The water balance can be used to show the flow of water in and out of a system. This system can be considered as a watershed, an aquifer, a lake, or a global hydrologic cycle, depending on the desired region of study and corresponding boundaries.

The general form of the hydrologic balance for a specific time period is represented as follows:

$$P - R - G - E - T = \Delta S, \tag{4.49}$$

where P is precipitation, R is surface runoff, G is groundwater flow, E is evaporation, T is transpiration, and ΔS is change in storage. Since the runoff is a portion of rainfall, it can be estimated using the runoff coefficient. The runoff coefficient is defined as the ratio R/P.

Due to difficulty in estimation of hydrologic components, some parametric water balance models are developed. In these models, coefficients are defined to investigate the relationship between different components. In the next section, a simple water balance model called the Thomas model is described.

Example 4.14

In a given year, a watershed with an area of 2500 km^2 received 130 cm of precipitation. The average rate of flow measured in a river draining the watershed was 30 m^3/s. Estimate the amount of water lost due to the combined effect of evaporation, transpiration, and infiltration to groundwater. How much runoff reached the river for the year (in cm)? What is the runoff coefficient?

Solution:

The water balance equation (Equation 4.49) can be arranged to produce

$$E + T + G = P - R - \Delta S.$$

Assuming that the water levels are the same for $t = 0$ and $t = 1$ year, then $\Delta S = 0$ and

$$E + T + G = 130 - \frac{30 \times 8600 \times 365 \times 100}{2500 \times 1000} = 130 - 37.9 = 91.1.$$

The runoff coefficient is divided by precipitation.

$$R/P = 37.8/130 = 0.29.$$

4.9.1 Thomas Model (*abcd* Model)

The Thomas model is a parametric water balance model that includes two main variables. The first variable is the available water, W_i at the beginning of time interval i, which is equal to the summation of the total precipitation in period i, P_i, and the soil moisture at the end of time interval $i - 1$, S_{i-1}. This variable is formulated as follows:

$$W_i = P_i + S_{i-1}. \tag{4.50}$$

The second variable is Y_i, which is calculated as follows:

$$Y_i = E_i + S_i, \tag{4.51}$$

where E_i is actual evapotranspiration.

Thomas developed a nonlinear equation for relating these two variables as follows:

$$Y_i = \frac{W_i + b}{2a} - \left[\left(\frac{W_i + b}{2a} \right)^2 - \frac{W_i b}{a} \right]^{0.5}, \tag{4.52}$$

where a and b are model parameters. The parameters show the produced runoff before soil saturation. In cases of $a < 1$, it will result in $W_i < b$. For determining the percentage of evapotranspiration and soil moisture at the end of interval i from Y_i, it is assumed that the moisture loss due to evapotranspiration is directly related to soil moisture content and potential evapotranspiration as follows:

$$S_i = Y_i e^{-ET_{pi}/b}, \tag{4.53}$$

The difference between W_i and Y_i is equal to the summation of the direct runoff, DR_i, and groundwater recharge, GR_i. A part of infiltrated water increases the soil moisture. The direct runoff and groundwater recharge are estimated as follows:

$$GR_i = c(W_i - Y_i) \tag{4.54}$$

$$DR_i = (1 - c)(W_i - Y_i), \tag{4.55}$$

where c is the mode parameter indicating the part of runoff that is supplied from groundwater resources. If G_i shows the groundwater storage at the end of time interval i, it can be calculated as follows:

$$G_i = \frac{GR_i + G_{i-1}}{d + 1}. \tag{4.56}$$

The provided runoff from groundwater resources is also estimated as follows:

$$(QG)_i = dG_i, \tag{4.57}$$

where d is the model parameter showing the part of groundwater that is transformed to the surface runoff. The surface runoff at the end of time interval i is equal to

$$DR_i + QG_i. \tag{4.58}$$

The model parameters a, b, c, and d are estimated during model calibration based on measured water balance components in a specified region and specified time period. The estimation of initial values of soil moisture content, S_0, and groundwater storage, G_0, is needed for model application. The potential evapotranspiration can be estimated using different available models such as the Thornthwaite model.

Example 4.15

The average monthly precipitation and potential evapotranspiration (ETP) are given in Table 4.15. The monthly precipitation and potential evapotranspiration data of Example 4.10 are used.

Estimate the average monthly soil moisture content, S_i, groundwater recharge, GR_i, and groundwater storage, G_i. Assume an initial moisture content of 8 cm, and an initial groundwater storage of 2 cm. a, b, c, and d are given as 0.98, 25, 0.1, and 0.35, respectively.

Solution:

For the first month, the following is obtained:

$$W_1 = P_1 + S_0 = 1.0 + 8.0 = 9.0 \text{ cm}.$$

The value of Y for the first month is calculated as follows:

$$Y_1 = \frac{W_1 + b}{2a} - \left[\left(\frac{W_1 + b}{2a}\right)^2 - \frac{W_1 b}{a}\right]^{0.5} = \frac{9 + 25}{2(0.98)} - \left[\left(\frac{9 + 25}{2(0.98)}\right)^2 - \frac{(9)(25)}{0.98}\right]^{0.5} = 8.9.$$

Soil moisture content is estimated as

$$S_1 = Y_1 e^{-ET_{P1}/b} = 8.9e^{-1.75/25} = 8.3.$$

Groundwater recharge is estimated as

$$GR_1 = c(W_1 - Y_1) = 0.1(9 - 8.9) = 0.01.$$

Direct runoff is equal to

$$DR_1 = (1 - c)(W_1 - Y_1) = (1 - 0.1)(9 - 8.9) = 0.09.$$

TABLE 4.15
Precipitation and Potential Evapotranspiration (ETP) of Example 4.15

Month	1	2	3	4	5	6	7	8	9	10	11	12
Precipitation (cm)	1.0	1.8	0	0.6	0	0.1	8.78	9.8	4.8	0.74	0.4	6.88
ETP (cm)	1.75	1.78	2.1	2.2	3.0	3.1	3.5	3.6	2.7	1.9	1.75	1.75

TABLE 4.16
Summary of Calculations of Example 4.15

Month No.	Precipitation (cm)	ETP (cm)	*W* (cm)	*Y* (cm)	*S* (cm)	*GR* (cm)	*DR* (cm)	*G* (cm)	*QG* (cm)	*TR* (cm)
1	1	1.75	9.00	8.90	8.30	0.01	0.09	1.49	0.52	0.61
2	1.8	1.78	10.10	9.97	9.28	0.01	0.12	1.11	0.39	0.51
3	0	2.1	9.28	9.18	8.44	0.01	0.10	0.83	0.29	0.39
4	0.6	2.2	9.04	8.94	8.18	0.01	0.09	0.62	0.22	0.31
5	0	3	8.18	8.11	7.19	0.01	0.07	0.47	0.16	0.23
6	0.1	3.1	7.29	7.23	6.39	0.01	0.05	0.35	0.12	0.18
7	8.78	3.5	15.17	14.74	12.82	0.04	0.38	0.29	0.10	0.48
8	9.8	3.6	22.62	20.65	17.88	0.20	1.77	0.36	0.13	1.89
9	4.8	2.7	22.68	20.69	18.58	0.20	1.79	0.41	0.15	1.94
10	0.74	1.9	19.32	18.31	16.97	0.10	0.90	0.38	0.13	1.04
11	0.4	1.75	17.37	16.70	15.57	0.07	0.60	0.33	0.12	0.72
12	6.88	1.75	22.45	20.55	19.16	0.19	1.71	0.39	0.14	1.84

Finally, groundwater storage is obtained as

$$G_1 = \frac{(GR)_1 + G_0}{d+1} = \frac{0.01+2}{1+0.35} = 1.49.$$

The runoff produced by groundwater will be

$$QG_1 = dG_1 = 0.35 \times 1.49 = 0.52.$$

The total runoff is estimated as

$$TR_1 = DR_1 + QG_1 = 0.09 + 0.52 = 0.61.$$

The calculations for the succeeding months are given in Table 4.16.

4.10 REGIONALIZING THE HYDROLOGIC DATA USING THE KRIGING METHOD

Many activities in applied and engineering hydrology involve measurements of one or more quantities at given spatial locations, with the goal of regionalizing the measured quantities at unsampled locations. Often, the unsampled locations are on a regular grid, and the regionalization is used to produce surface plots or contour maps.

A popular method of regionalization is kriging. This method requires the complete specification (the form and parameter's values) of the spatial dependence that characterizes the spatial process. For this purpose, models for the spatial dependence are expressed in terms of the distance between any two locations in the spatial domain of interest. These models take the form of a covariance or semivariance function. Spatial prediction, using the kriging method, involves two steps:

1. Model the semivariance or covariance of the spatial process. These measures are typically not known in advance. This step involves computing an empirical estimate, in addition to determining both the mathematical form and the values of any parameters for a theoretical form of the dependence model.

2. This dependence model is used to solve the kriging system at a specified set of spatial points, resulting in predicted values and associated standard errors.

4.10.1 Theoretical Semivariogram Models

Consider a stochastic spatial process represented by the stationary spatial random field $\{z(x), x \in R^2\}$. The variogram procedure computes the empirical (also known as sample or experimental) semivariance of $z(x)$. Regionalization $z(x)$ at unsampled locations by techniques such as kriging requires a theoretical semivariogram or covariance. A suitable theoretical semivariogram must be determined based on the sample semivariogram. In one of the simplest models for the definition of a semivariogram, the mean, m, is constant and the two-point covariance function depends only on the distance between two points as follows:

$$E\,[z(x)] = m \tag{4.59}$$

and

$$E[(z(x) - m)(z(x') - m)] = \gamma(h), \tag{4.60}$$

where

$$h = \|x - x'\| = \sqrt{\left(x_1 - x_1'\right)^2 + \left(x_2 - x_2'\right)^2}\,, \tag{4.61}$$

where h is the distance between sampling location x and x', $x = [x_1, x_2]$, and $x' = \left[x_1', x_2'\right]$. Equations 4.59 and 4.60 comprise the stationary model; a random function $z(x)$ satisfying these conditions is called stationary. This model is isotropic because it uses only the length and not the orientation of the linear segment that connects the two points. The values of the covariance at $h = 0$ is known as the variance or the sill of the stationary function. The semivariogram is defined as

$$\gamma(h) = \frac{1}{2} E\left[\left(z(x) - z\left(x'\right)\right)^2\right]. \tag{4.62}$$

Figure 4.9 displays a theoretical semivariogram of a spherical semivariance model and points out the semivariogram characteristics. In this figure, $\gamma(h)$ is semivariogram, a_0 is range, c_0 is sill, h is distance, c_n is nugget effect, and σ_0^2 is partial sill. Finally, for selecting the best variogram model, cross-validation is used and is defined in Subsection 4.10.4. Theoretical semivariogram models such as the Gaussian, exponential, spherical, sine hole effect, and power model are described in the following.

4.10.1.1 The Gaussian Semivariogram Model

The form of the Gaussian model is

$$\gamma(h) = c_0\left[1 - \exp\left(-\frac{h^2}{a_0^2}\right)\right], \tag{4.63}$$

where $\gamma(h)$ is semivariogram, a_0 is range, c_0 is sill, h is distance, and σ_0^2 is partial sill.

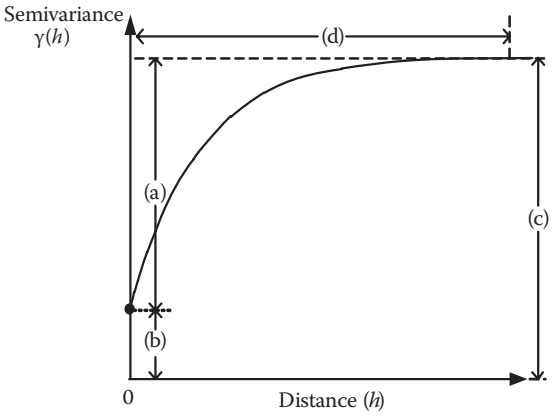

FIGURE 4.9 Theoretical semivariogram of spherical type and its characteristics [(a) partial sill $\left(\sigma_0^2\right)$, (b) nugget effect (c_n), (c) sill (c_0), (d) range (a_0)].

4.10.1.2 The Exponential Semivariogram Model

The form of the exponential model is

$$\gamma(h) = c_0 . \left[1 - \exp\left(-\frac{h}{a_0} \right) \right], \tag{4.64}$$

where $\gamma(h)$ is semivariogram, a_0 is range, c_0 is sill, and h is distance.

4.10.1.3 The Spherical Semivariogram Model

The form of the spherical model is

$$\gamma(h) = \begin{cases} \left(\frac{3}{2}\frac{h}{a_0} - \frac{1}{2}\frac{h^3}{a_0^3} \right) & \text{for} \quad \left(h \le a_0 \right) \\ c_0 \quad \text{for} \quad (h > a_0) \end{cases}, \tag{4.65}$$

where $\gamma(h)$ is semivariogram, a_0 is range, c_0 is sill, and h is distance.

4.10.1.4 The Sine Hole Effect Semivariogram Model

The form of the sine hole effect is

$$\gamma(h) = c_0 . \left[1 - \frac{\sin\left(\pi h / a_0 \right)}{\pi h / a_0} \right], \tag{4.66}$$

where $\gamma(h)$ is semivariogram, a_0 is range, c_0 is sill, and h is distance.

4.10.1.5 The Power Semivariogram Model

The form of the power model is

$$\gamma(h) = c_0 h^{a_0}, \tag{4.67}$$

where $\gamma(h)$ is semivariogram, a_0 is range, c_0 is sill, and h is distance.

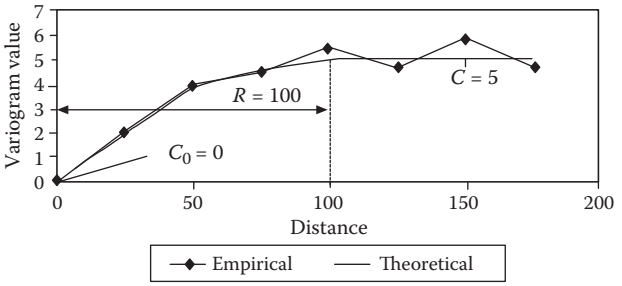

FIGURE 4.10 Pair of empirical and theoretical semivariogram.

An example of empirical and theoretical variograms and the definition of the above parameters are shown in Figure 4.10.

4.10.2 Kriging System

Kriging involves applying the general methodology known as best linear unbiased estimation to intrinsic functions. Given n measurements of z at location with spatial coordinate $x_1, x_2, x_3, \ldots x_n$, it estimates the value of z at point x_0. An estimator is simply a procedure or equation that uses data to find a representative value, or estimate, of the unknown quantity.

$$\hat{z}_0 = \sum_{i=1}^{n} \lambda_i z(x_i). \tag{4.68}$$

Thus, the problem is reduced to selecting a set of coefficients $\lambda_1, \lambda_2, \ldots \lambda_n$. The difference between the estimates $\hat{z}_0$ and the actual value $z(x_0)$ is the estimation error:

$$\hat{z}_0 - z(x_0) = \sum_{i=1}^{n} \lambda_i z(x_i) - z(x_0). \tag{4.69}$$

The coefficient is selected by considering the following specifications:

Unbiasedness: On the average, the estimation error must be zero. That is,

$$E\left[\hat{z}_0 - z(x_0)\right] = \sum_{i=1}^{n} \lambda_i m - m = \left(\sum_{i=1}^{n} \lambda_i - 1\right) m = 0. \tag{4.70}$$

However, the numerical value of the mean, m, is not specified. For the estimator to be unbiased for any value of the mean, it is required that

$$\sum_{j=1}^{n} \lambda_i = 1. \tag{4.71}$$

Imposing the unbiasedness constraint eliminates the unknown parameter m.

Minimum variance: The mean square estimation error must be minimized.

$$E\left[\hat{z}_0 - z\left(x_0\right)^2\right] = -\sum_{i=1}^{n}\sum_{j=1}^{n}\lambda_i\lambda_j\gamma\left(\left\|x_i - x_j\right\|\right) + 2\sum_{i=1}^{n}\lambda_i\gamma\left(\left\|x_i - x_0\right\|\right). \tag{4.72}$$

Thus, the problem of the best (minimum mean square error) unbiased estimation of the λ coefficients may be reduced to the constrained optimization problem:

Select the values of $\lambda_1, \lambda_2, \ldots \lambda_n$ that minimize Equation 4.72 while satisfying Equation 4.71. Equation 4.72 is called the objective function, because we try to minimize it; Equation 4.71 is called a constraint, because it poses a restriction on the values that might be assigned to the coefficients. A constrained optimization problem is formulated with a quadratic objective function and a linear constraint. This problem can be solved easily using Lagrange multipliers, a standard optimization method; the necessary conditions for the minimization are given by the linear kriging system of $n + 1$ equation with $n + 1$ unknowns as follows:

$$-\sum_{j=1}^{n}\lambda_i\gamma\left(\left\|x_i - x_j\right\|\right) + v = -\gamma\left(\left\|x_i - x_0\right\|\right), \quad i = 1,2,...,n \tag{4.73}$$

$$\sum_{j=1}^{n}\lambda_j = 1,$$

where ν is a Lagrange multiplier. It is common practice to write the kriging system in matrix notation. Let X be the vector of the unknowns as defined below:

$$X = \begin{bmatrix} \lambda_1 \\ \lambda_2 \\ \vdots \\ \lambda_n \\ v \end{bmatrix}. \tag{4.74}$$

b, the matrix of coefficients, and **A**, the right-hand-side vector, are defined as follows:

$$b = \begin{bmatrix} -\gamma\left(\left\|x_1 - x_0\right\|\right) \\ -\gamma\left(\left\|x_2 - x_0\right\|\right) \\ \vdots \\ -\gamma\left(\left\|x_n - x_0\right\|\right) \\ 1 \end{bmatrix} \tag{4.75}$$

$$\mathbf{A}=\begin{bmatrix} 0 & -\gamma\left(\|x_1-x_2\|\right) & \cdots & -\gamma\left(\|x_1-x_n\|\right) & 1 \\ -\gamma\left(\|x_2-x_1\|\right) & 0 & \cdots & -\gamma\left(\|x_2-x_n\|\right) & 1 \\ \vdots & \vdots & & \vdots & \vdots \\ -\gamma\left(\|x_n-x_1\|\right) & -\gamma\left(\|x_n-x_2\|\right) & \cdots & 0 & 1 \\ 1 & 1 & \cdots & 1 & 0 \end{bmatrix}. \tag{4.76}$$

Denote by A_{ij} the element of **A** at the ith row and the jth column, and denote by x_i and b_i the element at the ith row of x and b, respectively. Notice that **A** is symmetric, i.e., $A_{ij} = A_{ji}$.

The kriging system can be written as

$$\sum_{j=1}^{n+1} A_{ij}x_j = b_i \quad \text{for } i = 1,2,\ldots,n+1. \tag{4.77}$$

The matrix of kriging equations is defined as follows:

$$\mathbf{Ax} = \mathbf{b}. \tag{4.78}$$

Solving this system, we obtain $\lambda_1, \lambda_2, \ldots \lambda_n$, and υ. In this manner, the linear estimator of Equation 4.68 is fully specified. Furthermore, the accuracy of the estimate can be quantified through the mean square estimation error. The mean square estimation error may be obtained by substituting in Equation 4.72 the values of $\lambda_1, \lambda_2, \ldots \lambda_n$ obtained from the solution of the kriging system. Estimation of the variance in an unknown point at x_0 is defined as

$$\sigma_0^2 = E\left[\left(\hat{z}_0 - z\left(x_0\right)\right)^2\right] = -v + \sum_{i=1}^{n} \lambda_i \gamma\left(\|x_i - x_0\|\right). \tag{4.79}$$

4.10.3 Fitting Variogram

Variogram selection is an iterative process that usually starts with an examination of the experimental variogram. How the experimental variogram can be obtained from data has been discussed. Then, a variogram fits the model by selecting one of the equations from the list of basic models of the previous section and adjusting its parameters to reproduce the experimental variogram as closely as possible. For example, a linear variogram can be selected and then parameter θ can be obtained by approximating the experimental variogram, as illustrated in Figure 4.11.

Example 4.16

Consider 70 measurements that were synthetically generated from a one-dimensional random process (see Figure 4.12). Infer the variogram and test the intrinsic model.

Solution:

We always start by plotting and calculating basic statistics for the data (exploratory analysis). For one-dimensional data, the task of exploratory analysis is simplified because a plot of the observations versus location (see Figure 4.13) pretty much conveys a visual impression of the data. In this

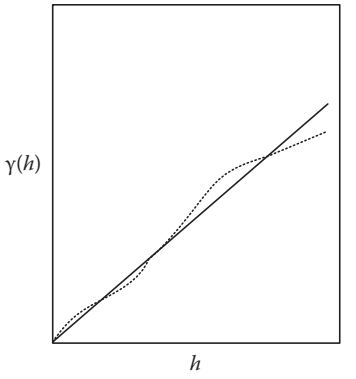

FIGURE 4.11 Variogram (continuous line) fitted to experimental variogram (dashed line).

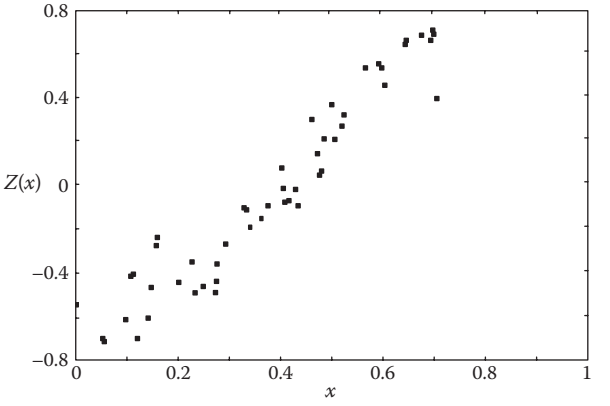

FIGURE 4.12 Plot of observations versus locations for Example 4.16.

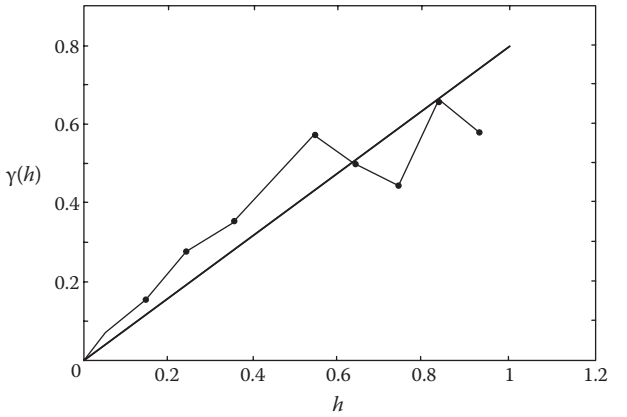

FIGURE 4.13 Experimental variogram and preliminary fit.

case, we infer that the data are reasonably continuous but without a well-defined slope. The data clearly indicate that much of the variability is at a scale comparable to the maximum separation distance, so that the function does not appear stationary. These observations are important in selecting the variogram.

Next, we plot the experimental variogram. For a preliminary estimate, we subdivide the separation distances into 10 equal intervals. One might proceed to draw a straight line from the origin through the experimental variogram, as shown in Figure 4.13. Our preliminary estimate is that the variogram is linear with slope 0.40.

4.10.4 Cross-Validation

A semivariogram model type must be chosen prior to the generation of the kriging model. Cross-validation can be used to assess the impact of many choices on the semivariogram models. It is used to compare estimated and true values using the information available in the sample data set. An error is calculated as the estimated value minus the true value. Considering kriging system equations and the cross-validation method, the error is estimated by the following equations:

1. The mean error (ME):

$$\mathrm{ME} = \frac{1}{N}\sum_{i=1}^{N}\left\{z(x_i) - \hat{z}(x_i)\right\}, \tag{4.80}$$

where $z(x_i)$ is sample data, $\hat{z}(x_i)$ is estimated data, and N is the number of data.

2. The mean square error (MSE):

$$\mathrm{MSE} = \frac{1}{N}\sum_{i=1}^{N}\left\{z(x_i) - \hat{z}(x_i)\right\}^2. \tag{4.81}$$

Example 4.17

Consider a one-dimensional function with variogram $\gamma(h) = 1 + h$, for $h > 0$, and three measurements, at location $x_1 = 0$, $x_2 = 1$, and $x_3 = 3$. Estimate the value of the function in the neighborhood of the measurement points, at location $x_0 = 2$.

Solution:

The kriging system of equations, with weights λ_1, λ_2, and λ_3, is

$$\begin{array}{ccccccc}
 & -2\lambda_2 & -4\lambda_3 & +\nu & = & -3 \\
-2\lambda_1 & & -3\lambda_3 & +\nu & = & -2 \\
-4\lambda_1 & -3\lambda_2 & & +\nu & = & -2 \\
\lambda_1 & +\lambda_2 & +\lambda_3 & & = & 1
\end{array}$$

or, in matrix notation,

$$\begin{bmatrix} 0 & -2 & -4 & 1 \\ -2 & 0 & -3 & 1 \\ -4 & -3 & 0 & 1 \\ 1 & 1 & 1 & 0 \end{bmatrix} \begin{bmatrix} \lambda_1 \\ \lambda_2 \\ \lambda_3 \\ v \end{bmatrix} = \begin{bmatrix} -3 \\ -2 \\ -2 \\ 1 \end{bmatrix}.$$

The mean square estimation error is

$$-\upsilon + 3\lambda_1 + 2\lambda_2 + 2\lambda_3.$$

Solving the system, we obtain $\lambda_1 = 0.1304$, $\lambda_2 = 0.3913$, $\lambda_3 = 0.4783$, and $\upsilon = -0.304$. The mean square estimation error (MSE) is 2.43.

For $x_0 = 0$, i.e., a position coinciding with an observation point, the kriging system is

$$\begin{bmatrix} 0 & -2 & -4 & 1 \\ -2 & 0 & -3 & 1 \\ -4 & -3 & 0 & 1 \\ 1 & 1 & 1 & 0 \end{bmatrix} \begin{bmatrix} \lambda_1 \\ \lambda_2 \\ \lambda_3 \\ v \end{bmatrix} = \begin{bmatrix} -1 \\ -2 \\ -4 \\ 1 \end{bmatrix}.$$

By inspection, one can verify that the only possible solution is $\lambda_1 = 0.7391$, $\lambda_2 = 0.2174$, $\lambda_3 = 0.0435$, and $\upsilon = -0.3913$. The MSE = 1.7391.

4.11 SUMMARY

Chapter 4 has covered the basic principles of hydrology, including precipitation, evaporation, evapotranspiration, and infiltration. Solar radiation and atmosphere water phase changes provide the main energy inputs and result in the generation of precipitation and evaporation. Once rain falls to the earth, it can infiltrate into the soil system, percolate to deeper groundwater, evaporate back to the atmosphere, or run off to the nearest stream system or river. Overall water balance is maintained through the various storage mechanisms within the hydrologic cycle.

Losses or abstractions in hydrology include evaporation, evapotranspiration, and filtration and are covered in detail in this chapter, including physics-based methods such as the Penman evaporation equation and Green–Ampt infiltration. The Horton method is presented in this chapter. Infiltration and evaporation are often computed as losses from the system and are not usually measured directly.

Finally, kriging as a main method of regionalizing sample data is discussed in this chapter. In this section, problem of fitting a variogram to the data and testing the efficacy of the model are presented. In all applications, data are insufficient for estimating accurately the whole variogram. Starting with the experimental variogram, a model is postulated, which is then improved using residuals. The recommended procedure for variogram fitting relies more on the residuals than on the experimental variogram.

PROBLEMS

1. The storage in a river reach at a specified time is 3 ha-m (hectare-meters). At the same time, the inflow to the reach is 15 m^3/s and the outflow is 20 m^3/s. One hour later, the inflow is 20 m^3/s and the outflow is 20.5 m^3/s. Determine the change in storage in the reach that occured during the hour. Is the storage at the hour greater or less than the initial value? What is the storage at the end of the hour?

2. For a given month, a 300-acre lake has 15 cfs (cubic feet per second) of inflow, 13 cfs of outflow, and a total storage reduction of 16 acre-ft. A station next to the lake recorded a total of 1.3 in of precipitation for the lake for the month. Assuming that infiltration is insignificant for the lake, determine the evaporation loss, in inches, over the lake.
3. Monthly precipitation in W, B, and A stations was observed to be 11.5, 9.0, and 12.4 cm, respectively. Precipitation for the same month could not be observed at X station. The normal annual precipitation values for X, W, B, and A are 102, 114, 95, and 122 cm, respectively. Estimate the storm precipitation for X station. All these cities are within a 50 km radius.
4. Rainfall values observed at different points on a watershed (12.5 km^2) are shown in Figure 4.14. Compute the mean rainfall using the Thiessen method.
5. Using the isohyetal method for the watershed shown in Figure 4.15, compute the mean storm rainfall (in).

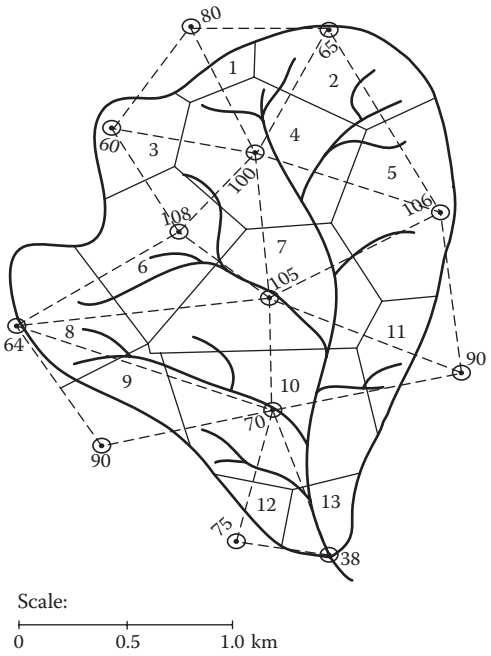

FIGURE 4.14 Thiessen polygon method for computing the mean areal rainfall for Problem 4.

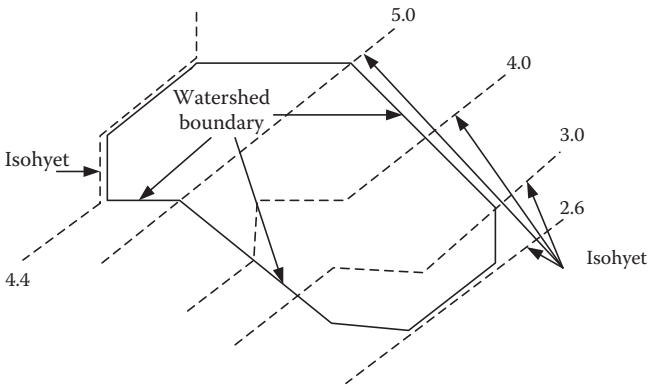

FIGURE 4.15 Watershed boundaries for Problem 5.

6. In a catchment area in northern England, the measurements of evaporation (mm) shown in the Table 4.17 were made for 1958–1962 and 1968–1972. For the years 1968–1972, measurements from the U.S. Class A pan only were available. Estimate the volume of water lost each year in the later period from a reservoir of surface area of 1.4 km^2.
7. The rainfall hyetograph is shown in Figure 4.16 and is listed in Table 4.18. It is subject to a depression storage loss of 0.15 cm and Horton infiltration with parameters f_0 = 0.45 cm/h, f_c = 0.05 cm/h, and k = 1 h. Calculate the hyetograph of excess rainfall.

TABLE 4.17
Measurements of Evaporation for 1958–1962 and 1968–1972 for Problem 6

Year	U.K. tank	U.S. Class A pan	Year	U.S. Class A pan
1958	351	491	1968	621
1959	536	713	1969	581
1960	502	653	1970	687
1961	437	586	1971	624
1962	486	612	1972	568

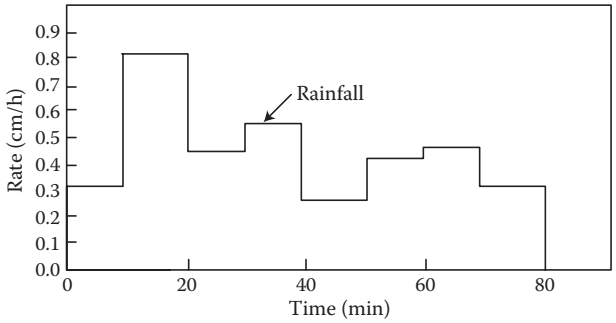

FIGURE 4.16 Rainfall hyetograph of Problem 7.

TABLE 4.18
Rainfall Hyetograph of Problem 7

Time Interval (min)	Rainfall (cm/hr)
0–10	0.30
10–20	0.80
20–30	0.45
30–40	0.55
40–50	0.25
50–60	0.40
60–70	0.45
70–80	0.30
80–90	0.00

8. Results to determine the Horton infiltration capacity in the exponential form are tabulated in Table 4.19. Determine the infiltration capacity exponential equation.
9. Compute the infiltration and cumulative infiltration after 1 h of infiltration into a silt loam soil that initially had an effective saturation of 30% (Note: $\Delta\theta = (1 - S_e)\theta_e$).
10. The data measured in 30 rain gauges and the corresponding coordinates are shown in Table 4.20.
    a. Draw the scattering of gauges.
    b. Estimate and draw the empirical variogram.

TABLE 4.19
Horton Infiltration Capacity Results of Problem 8

Time (h)	0.25	0.5	0.75	1.00	1.25	1.50	1.75	2.00
f_{ct} (cm/h)	5.60	3.20	2.10	1.50	1.20	1.10	1.00	1.00

TABLE 4.20
Data Measured in 30 Rain Gauges for Problem 10

Rainfall (mm)	*y*-Coordinate	*x*-Coordinate	Rain Gauge
1	1	1	230
2	1	3	260
3	1	4	310
4	1	7	420
5	2	11	350
6	2	13	290
7	2	20	260
8	3	3	230
9	3	6	250
10	3	20	280
11	5	5	380
12	5	6	450
13	5	15	480
14	5	19	490
15	6	2	510
16	6	4	520
17	6	9	640
18	6	10	510
19	6	13	450
20	6	18	380
21	6	20	450
22	7	3	510
23	7	14	530
24	8	2	650
25	8	15	630
26	8	20	680
27	9	6	690
28	9	18	540
29	10	5	555
30	10	19	520

c. Fit a theoretical variogram to an empirical variogram.
d. Specify and draw the spatial distribution of data at the network with one dimension.
e. Estimate rainfall at points with (3, 19), (5, 8), and (9, 9) coordinates using the developed kriging model.

REFERENCES

Blaney, H.F. and Criddle, W.D. (1962). Determining consumptive use and irrigation water requirements. U.S. Department of Agriculture. Agricultural Research Service Technical Bulletin 1275. 59 pp.

Chow, V.T., Maidment, D.R. and Mays, L.W. (1988). *Applied Hydrology*, McGraw-Hill, New York.

Green, W.H. and Ampt, G.A. (1911). "Studies on soil physics, 1: The flow of air and water through soils," *Journal of Agriculture Science*, 9, 1–24.

Holtan, H.N. and Lopez, N.C. (1971). USADHL-70, Model of Watershed Hydrology, Technical Bulletin No. 14, 15, U.S. Department of Agriculture, Washington, DC.

Horton, R.E. (1919). "An approach toward physical interpretation of infiltration capacity," *Soil Science Society Proceedings*, 5, 399–417.

Jensen, M.E. (1966). "Empirical Methods of Estimating or Predicting Evapotranspiration Using Radiation," Proc. Conf. on Evapotranspiration, ASAE, Chicago, pp. 57–61.

Jensen, M.E. and Haise, H.R. (1963). "Estimating evapotranspiration from solar radiation," *J. Irrig. Drainage Div. ASCE*, 89, 15–41.

Kibler, D.F. (1982). Urban Stormwater Hydrology. America Geophysical Union, Washington, D.C.

Rawls, W.J., Brakensick, D.I. and Miller, N. (1983). "Green–Ampt infiltration parameters from soils data," *Journal of Hydraulic Engineering, ASCE*, 109, 62–70.

Thornthwaite, C.W. (1948). "An approach toward a rational classification of climate," *Geographical Review*, 38 (1), 55–94.

U.S. Army Corps of Engineers (1965). *Snow Hydrology*, North Pacific Division, Portland, Oregon.

Viessman, W., Lewis, G.L. and Knapp, J.W. (1989). Introduction to Hydrology. Third Edition. Harper and Row, New York.

5 Watersheds

5.1 DEFINITION

Determination of watershed characteristics is an important concept in all hydrologic designs. The watershed is defined in terms of a point named "outlet." The designs in the watershed are being made with regard to the outlet. The watershed can be well defined as the area that can be considered a bounded hydrologic system, within which all live components are linked to each other regarding their water supply resources. Each watershed includes many smaller subwatersheds that transfer water to the outlet during a rainstorm. Watersheds come in all shapes and sizes. They cross county, state, and national boundaries; for example, the continental United States includes 2110 watersheds.

A typical watershed is shown in Figure 5.1. In this figure, point O represents the watershed outlet. In this case, if a structure for water resources management is designed at point B in Figure 5.1, the small area would be a desirable watershed. The two stream tributaries reflect the collecting areas for water resulting from rain on the smaller watershed for point B. As a real case, the Powell River watershed located in Virginia, USA, contains three small watersheds that eventually flow into the Powell River. The water in the Powell River ends up in the Gulf of Mexico; hence, the Powell River watershed is also in the Gulf of Mexico's watershed. Watershed boundary is defined in the highest areas around the outlet. In this regard, water falling as rain on one side of the mountain or hill runs down into one watershed while water falling on the other side of the mountain or hill runs down into another watershed.

5.2 WATERSHED GEOMORPHOLOGY

5.2.1 Drainage Area

Basin area (A) is hydrologically important because it directly affects the size of the storm hydrograph and the magnitude of mean and peak flows. The amount of sediment that eroded from the drainage basin is also related to the basin area. In fact, since almost every watershed characteristic is correlated with area, the area is the most important parameter in the description of form and processes of the drainage basin.

The first step in determining the drainage area of a watershed is specifying the watershed boundary, which is determined based on a watershed topography map. A commonly used tool in delineating watershed boundaries is Geographic Information Systems. There are also some software packages that can determine the watershed boundaries based on the introduced watershed outlet and given slope map. For manual computation of the watershed area, the planimeter can be used. The accuracy of the estimated value of the drainage area must be ensured because it is very important in hydrological design.

5.2.2 Basin Length

The basin length L_b is basically defined as the longest dimension of a basin parallel to its principal drainage channel, which is usually considered as the longest drainage channel in the watershed. This geomorphic definition should be distinguished from the definition used for the time of concentration and other hydrologic purposes, which will be discussed in the next sections. Hydrology

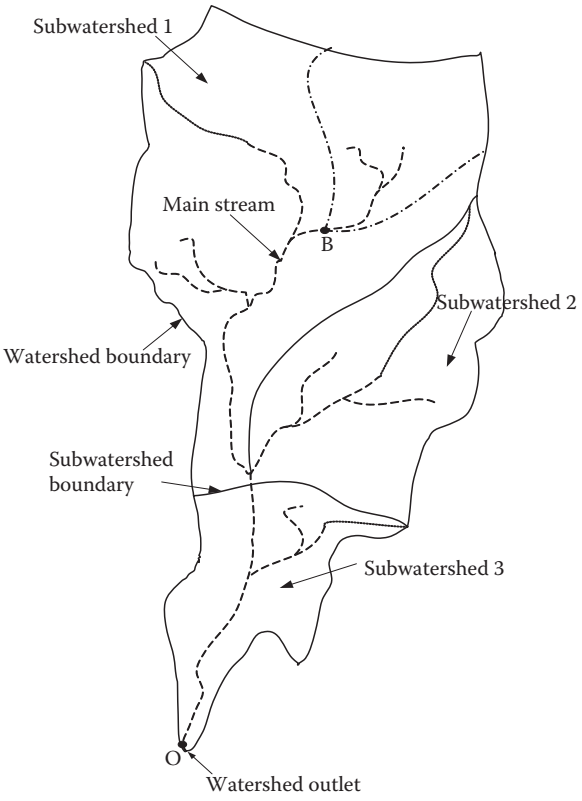

FIGURE 5.1 Illustration of a typical watershed.

is concerned with flow in the drainage channels and, therefore, specifically requires that such measurements are made along the drainage system to a given point. In a similar way, basin width can be measured in a direction approximately perpendicular to the length measurement. Basin length is defined in more than one way: (1) the greatest straight-line distance between any two points on the perimeter, (2) the greatest distance between the outlet and any point on the perimeter, or (3) the length of the main stream from its source (projected to the perimeter) to the outlet.

A relation between mainstream length and drainage-basin area is developed based on the gathered data from a number of small watersheds by Gray (1961):

$$L_b = 1.312A^{0.568}, \tag{5.1}$$

where L_b is basin length in kilometers and A is drainage-basin area in square kilometers. Equation 5.1 shows that larger watersheds tend to elongate.

5.2.3 Basin Slope

Basin slope highly affects the velocity of overland flow, watershed erosion potential, and local wind systems. When coupled with slope orientation, it influences the receipt of solar radiation and, in turn, microclimate, snowmelt, and distribution of precipitation. Basin slope, S, is defined as

$$S = h/L, \tag{5.2}$$

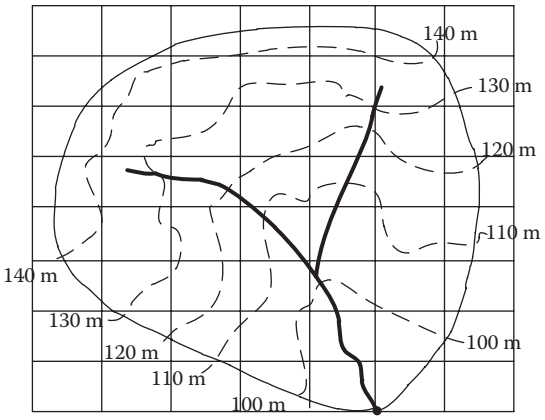

FIGURE 5.2 Grid system superimposed on the topographic map of a drainage area for slope determination.

where h is the fall and L is the horizontal distance (length) over which the fall occurs. Because ground slope varies greatly from point to point within the drainage basin, Equation 5.2 is not appropriate for estimation of the entire watershed slope. A better representative value of S can be obtained through representing the drainage area by a grid system on its topographic map, as shown in Figure 5.2.

The elevation contours are assumed to beat the same interval h. Each horizontal grid line is measured between its intersections with the watershed boundary, and the total length L of grid line segments is obtained; the same is done for vertical grid lines. Then, the number of intersections of each horizontal grid line with contour lines is obtained and the sum of these intersections, N, is obtained; the same is done for vertical grid lines. These data are used to get S as

$$S = \frac{S_{\mathrm{V}} + S_{\mathrm{H}}}{2}, \tag{5.3}$$

where

$$S_x = \frac{Nh}{L}, \quad x = \mathrm{V} \text{ or } \mathrm{H}, \tag{5.4}$$

where S_{V} is the average slope in vertical direction, S_{H} is the average slope in horizontal direction, and N and L correspond to vertical or horizontal slope.

5.2.4 Basin Shape

Basin shape reflects the influence of such factors as initial slope, inequalities in rock hardness, structural controls, and recent geomorphic and geologic history of the drainage basin. Basin shapes and their patterns are quite useful in the interpretation of geomorphic features, and their study represents one of the more practical approaches to the understanding of the structural and lithologic controls on landform evolution due to drainage patterns being influenced by many factors.

Numerous symmetrical and irregular forms of drainage areas are encountered in practice. A frequently occurring shape is a pear shape in plain view, as shown in Figure 5.3a. The watershed

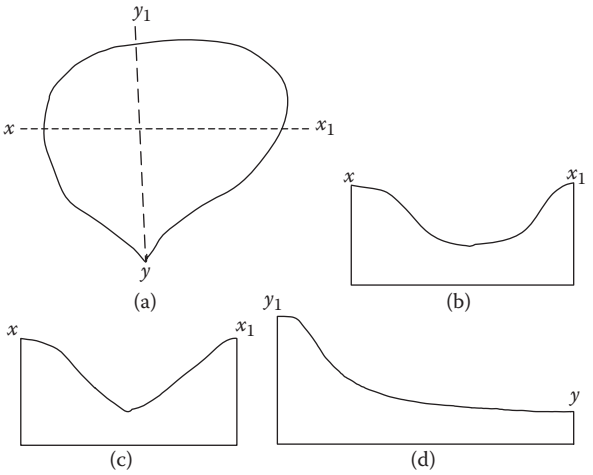

FIGURE 5.3 (a) Typical watershed shape. (b) Cross section along $x - x_1$ approximating a U-shaped valley. (c) Cross section along $x - x_1$ approximating a V-shaped valley. (d) Transverse section along $y - y_1$.

surface, however, is always a tilted concavity that determines the general direction of flow. Depending upon the interaction of climate and geologic processes, the lateral section, the cross section along $x - x_1$ of a watershed, may approximate a U-shaped valley (Figure 5.3b) or a V-shaped one (Figure 5.3c). Based on the transverse section, the cross section along $y - y_1$ (Figure 5.3d), the basin slope increases toward the upstream area of the watershed.

There are a variety of dimension parameters used for the quantitative definition of watershed shape (Morisawa 1958). Some of the commonly used parameters are formulated in Table 5.1. These

TABLE 5.1
List of Common Parameters Used to Quantitatively Define Watershed Shape

Parameter	Definition	Formula	Value	Description
Form factor	$FF = \dfrac{\text{Watershed area}}{(\text{Watershed length})^2}$	$\dfrac{A}{L^2}$	<1	The smaller values result in smaller peaks at outlet.
Basin shape factor	$B_s = \dfrac{(\text{Watershed length})^2}{\text{Watershed area}}$	$\dfrac{L^2}{A}$	>1	The smaller values result in bigger peaks at outlet.
Elongation ratio	$R_e = \dfrac{\text{Diameter or circle of watershed area}}{\text{Watershed length}}$	$\dfrac{1.128A^{0.5}}{L}$	≤1	The smaller values result in smaller peaks at outlet.
Circularity ratio	$R_c = \dfrac{\text{Watershed area}}{\text{Area of circle of watershed perimeter}}$	$\dfrac{12.57A}{P_r^2}$	≤1	The smaller values result in smaller peaks at outlet.
Compactness coefficient	$C_c = \dfrac{\text{Watershed perimeter}}{\text{Perimeter of circle of watershed area}}$	$\dfrac{0.2821P_r}{A^{0.5}}$	≥1	The smaller values result in bigger peaks at outlet.

Note: A = watershed area, L = watershed length, and P_r = perimeter.

factors involve watershed length (L), area (A), and/or perimeter (P_r). The possible values of these parameters is also given in Table 5.1. The elongation ratio, circularity ratio, and compactness coefficient approach 1 as the watershed shape is more similar to a circle.

A square drainage basin would have a shape factor $B_s = 1$, whereas the long narrow drainage basin would have a shape factor $B_s < 1$. The shape parameters can be used to quantify the degree of similarity of drainage-basin shapes.

The watershed shape may influence the hydrograph shape, especially for small watersheds. For example, if a watershed is long and narrow, then it will take longer for water to travel from watershed extremities to the outlet and the resulting runoff hydrograph will be flatter, as shown in Figure 5.4a. For more compact watersheds, the runoff hydrograph is expected to be sharper with a greater peak and shorter duration, as shown in Figure 5.4b. A compact watershed is more likely to be covered by the area of maximum rainfall intensity of local storms. For a watershed that is partly long and narrow, and partly compact, the runoff hydrograph is expected to be a complex composite of the aforementioned hydrographs, as shown in Figure 5.4c. However, other factors have a greater effect on the hydrograph shape than does the basin shape.

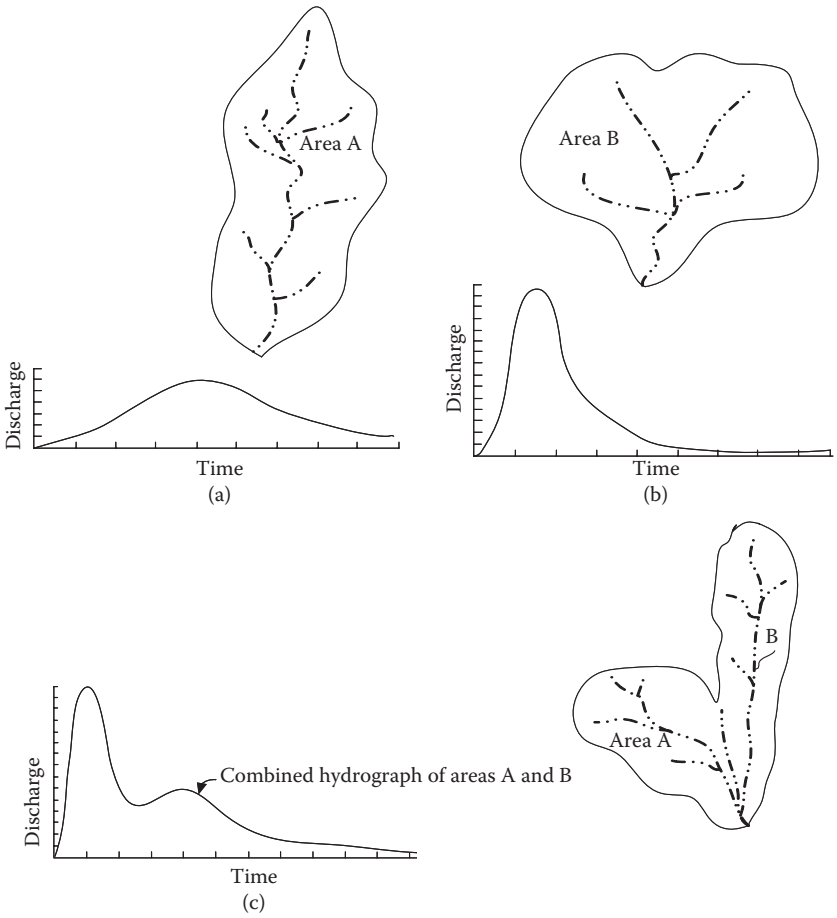

FIGURE 5.4 Effect of watershed shape on the runoff hydrograph. (a) Elliptical watershed. (b) Circular watershed. (c) Combination of a circular watershed and an elliptical watershed.

Example 5.1

Calculate the form factors of the schematic watersheds shown in Figure 5.5.

Solution:

$$FF = \frac{A}{L^2}$$

1. $\begin{cases} A = 86.6 \\ L = 17.32 \end{cases} \rightarrow FF = 0.288.$
2. $\begin{cases} A = 692.8 \\ L = 40 \end{cases} \rightarrow FF = 0.433.$
3. $\begin{cases} A = 692.82 \\ L = 34.64 \end{cases} \rightarrow FF = 0.577.$

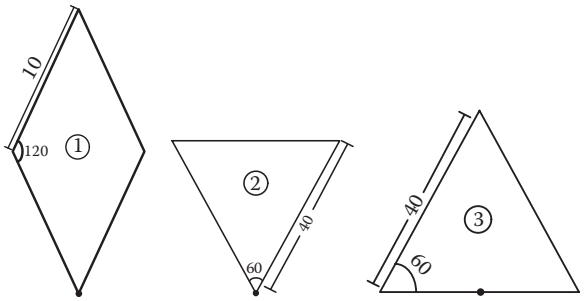

FIGURE 5.5 Schematic watersheds in Example 5.1.

Example 5.2

Calculate the compactness coefficient of the watersheds that are shown in Figure 5.6.

Solution:

$$\text{Compactness coefficient: } C_c = \frac{0.2821P}{\sqrt{A}}$$

1. $\begin{cases} A = 86.6 \\ L = 40 \end{cases} \rightarrow C = 1.21.$
2. $C = 1.$
3. $\begin{cases} A = 49.32 \\ L = 31.23 \end{cases} \rightarrow C = 1.254.$

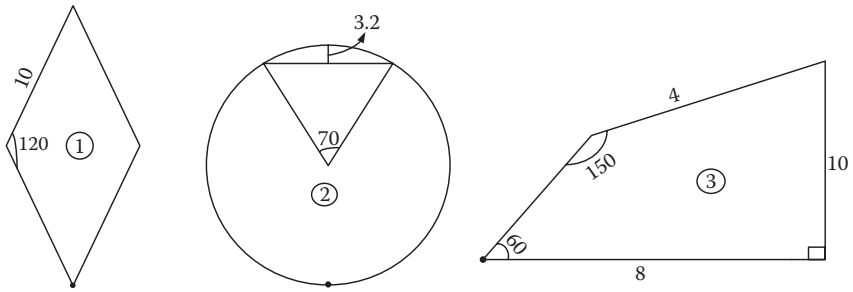

FIGURE 5.6 Watersheds in Example 5.2.

Example 5.3

Calculate the elongation ratio of the watersheds shown in Figure 5.7.

Solution:

$$\text{Elongation ratio: } R_e = \frac{1.128}{L} \times (A)^{0.5}$$

1. $\begin{cases} L = r \\ A = \dfrac{\Pi r^2}{2} \end{cases} \rightarrow R_e = 1.41.$

2. $\begin{cases} L = r \\ A = \dfrac{\Pi r^2}{6} \end{cases} \rightarrow R_e = 0.816.$

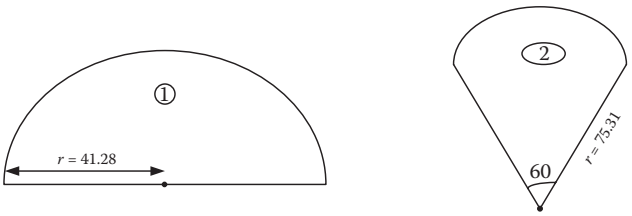

FIGURE 5.7 Watersheds in Example 5.3.

Example 5.4

Calculate the circularity ratio of a watershed with an area of 30 km^2 and a perimeter of 20 km.

Solution:

$$P = 2\pi r = 20 \rightarrow R = 3.18 \text{ km} \rightarrow A_o = \pi r^2 = 31.76 \text{ km}^2$$

$$\text{Circularity ratio: } R_c = \frac{A}{A_o} = \frac{30}{31.76} = 0.944$$

5.2.5 Length to the Center of Area (*LC*)

The measured distance along the main channel from the basin outlet to the nearest point on the main channel to the center of area is defined as *LC*. The location of the drainage area center can be determined using the "stone-age" method of suspending. A cardboard outline of the drainage area can be made by means of a straight pin inserted into the edge, drawing a vertical line, and then rotating the cardboard approximately 90° and drawing a second vertical line. The center of the watershed area is determined by the intersection of the two lines. In practice, for providing a slightly greater level of accuracy, three lines may be used, which are rotated approximately 60°. The length to the center of area is used in deriving Snyder's synthetic unit hydrograph (see Chapter 6).

Another factor, named the shape factor (L_1), is defined based on *LC* as follows:

$$L_1 = (L \cdot LC)^{0.3}, \tag{5.5}$$

where *L* is the length of the watershed. The hydrograph peak is inversely related with the shape factor.

5.2.6 Equivalent Rectangular

For comparison and definition of a watershed's shape, the equivalent rectangular concept is used. The equivalent rectangular has the same area, perimeter, and elongation coefficient as the considered watershed, and the other factors affecting the runoff are considered similar to the studied watershed. Considering the above criteria in equivalent rectangular definition, its length and width are calculated as follows:

$$L = \frac{C_c \times \sqrt{A} + \sqrt{\left(C_c^2 \times A - 1.2544 \times A\right)}}{1.12} \tag{5.6}$$

$$B = \frac{C_c \times \sqrt{A} - \sqrt{\left(C_c^2 \times A - 1.2544 \times A\right)}}{1.12}, \tag{5.7}$$

where *L* and *B* are the length and width of the equivalent rectangular of the study watershed, respectively, and C_c is the compactness coefficient and *A* is the watershed area.

Example 5.5

Determine the length and width of the equivalent rectangular for a basin with an area of 40 km^2 and a perimeter of 35 km.

Solution:

$$C_c = \frac{0.2821P}{\sqrt{A}} = \frac{0.2821 \times 35}{\sqrt{40}} = 1.56.$$

$$L = \frac{1.56 \times \sqrt{40} + \sqrt{1.56^2 \times 40 - 1.2554 \times 40}}{1.12} = 14.94 \text{ m}.$$

$$B = \frac{1.56 \times \sqrt{40} + \sqrt{1.56^2 \times 40 - 1.2554 \times 40}}{1.12} = 2.677 \text{ m.}$$

5.2.7 Drainage Density

The drainage density (D) is defined as the ratio of the total length of streams within a watershed to the watershed's total area.

$$D = \frac{L_T}{A} \tag{5.8}$$

Higher values of drainage density show higher density of streams and more rapid storm response of the watershed. The typical range of this measure is from 1.0 to 3.75 km/km^2. Due to difficulty in estimating D (because it is dependent on the map scale), drainage density is not commonly used.

Example 5.6

Calculate the drainage density for a typical watershed whose total area and the length of the main stream are 250 km^2 and 20.1 km, respectively.

Solution:

Based on Equation 5.8, the drainage density is

$$D = \frac{L_T}{A} = \frac{20.1 \text{ km}}{250 \text{ km}^2} = 0.08 \text{ km}/\text{km}^2$$

Due to the lack of channel network details, this value is lower than normal. This example shows the importance of accurate identification of the channel reaches.

5.2.7.1 Horton's Laws

A stream net or river net is the interrelated drainage pattern formed by a set of streams in a certain area. A junction is the point where two channels meet. A link is any unbroken stretch of the river between two junctions; this is then known as the interior link. If it is between the source and first junction, it is called the exterior link.

Quantitative analysis of the stream network really started with Horton (1945). This analysis has been developed to facilitate comparison between different drainage basins, to help obtain relations between various aspects of drainage patterns, and to define certain useful properties of drainage basins in significant terms.

According to Horton (1945), the main stream in the river net should be denoted by the same number order all the way from its mouth to its headwaters. Thus, at every junction where the order changes, one of the lower-order streams is renumbered to the higher order and the process is repeated. Thus, in Figure 5.8, the main stream is shown as the fourth-order stream right back to its source. The third-order streams, which are tributary to the fourth-order stream, are also extended back to their farthest source as the third-order streams and so on. The streams joining the third-order stream are

second-order streams, and they can be extended backward. It can be immediately realized that a certain amount of subjectivity is involved in the ordering of streams according to Horton's method. Figure 5.9 shows the stream ordering with a hypothetical watershed.

Other indicators of drainage character are computed using the concept of stream order. The ratio of the number of streams of any order to the number of streams of the next higher order defines the bifurcation ratio (R_b). Typical values of bifurcation ratio range from 2 to 4. Figure 5.9a through d display the same watershed, but the streams of each order have been specifically delineated. Figure 5.9a depicts that there are 17 first-order streams, with Figure 5.9b through d indicating 6, 2, and 1 stream of orders 2, 3, and 4, respectively. For stream orders 1 to 2, 2 to 3, and 3 to 4, bifurcation ratios are 2.83, 3.0, and 2.0, respectively, and the average value of the bifurcation ratio for this watershed is 2.6.

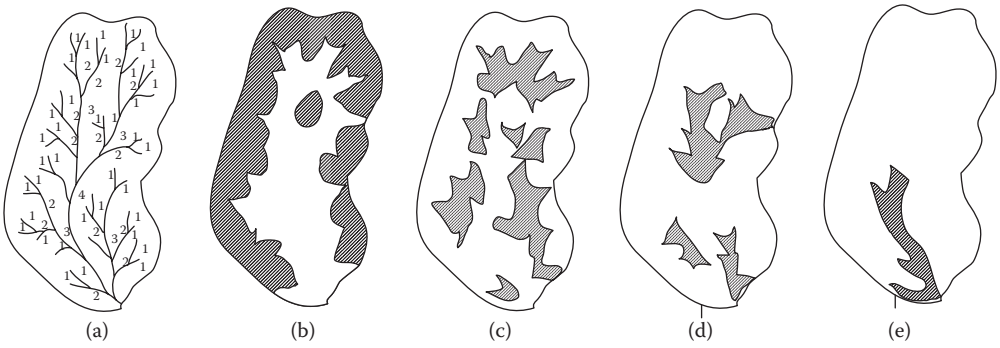

FIGURE 5.8 Identification of stream orders (a) and delineation of stream areas for first-order (b), second-order (c), third-order (d), and fourth-order (e) streams. (From McCuen, R., *Hydrologic Analysis and Design*, Prentice-Hall, London, 1998.)

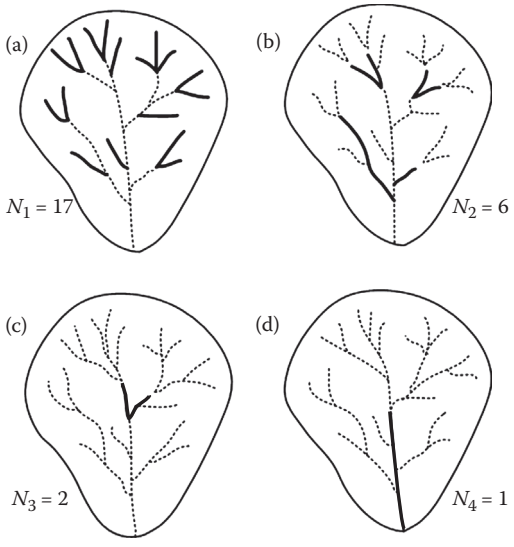

FIGURE 5.9 Stream-order separation for estimating the bifurcation ratio. (a) First-order streams, (b) second-order streams, (c) third-order streams, and (d) fourth-order streams. (From McCuen, R., *Hydrologic Analysis and Design*, Prentice-Hall, London, 1998.)

Example 5.7

The area of a watershed whose properties are shown in Table 5.2 is 25 km^2. Calculate the bifurcation rate and drainage density for each order and watershed.

Solution:

$$R_b = \left(\frac{1}{5-1}\right) \times \left(\frac{140}{41} + \frac{41}{15} + \frac{15}{6} + \frac{6}{1}\right) \rightarrow R_b = 3.66$$

$$D_1 = \frac{L_1}{A} = \frac{30}{25} = 1.2$$

$$D_2 = \frac{L_2}{A} = \frac{18}{25} = 0.72$$

$$D_3 = \frac{L_3}{A} = \frac{7}{25} = 0.28$$

$$D_4 = \frac{L_4}{A} = \frac{3}{25} = 0.12$$

$$D_5 = \frac{L_5}{A} = \frac{1}{25} = 0.04$$

$$D_m = \frac{\sum L_i}{A} = \frac{30+18+7+3+1}{25} = 2.36 \frac{\text{km}}{\text{km}^2}.$$

5.2.7.1.1 Law of Stream Numbers

The law of stream numbers, developed by Horton, relates the number of streams of order $i(N_i)$ to the bifurcation ratio and the principal order (k) as follows:

$$N_i = R_b^{k-i} \tag{5.9}$$

Example 5.8

In a river, the bifurcation rate for each order that is calculated is represented below. If we have only a main river in this basin, calculate the bifurcation rate for the whole watershed and estimate the number of bifurcations for each order and compare them with real ones.

$$R_b = 2.923,\ 3.25,\ 4.$$

TABLE 5.2
Characteristics of Given Watershed in Example 5.7

Order	1	2	3	4	5
Number of streams	140	41	15	6	1
River length (km)	30	18	7	3	1

Solution:

The bifurcation rate for the whole watershed is $R_b = \frac{1}{3} \times (2.923 + 3.25 + 4) \rightarrow R_b = 3.391$

$$N_4 = 1 \rightarrow \frac{N_3}{N_4} = 4 \rightarrow N_3 = 4$$

$$N_3 = 4 \rightarrow \frac{N_2}{N_3} = 3.25 \rightarrow N_2 = 13$$

$$N_2 = 13 \rightarrow \frac{N_1}{N_2} = 2.923 \rightarrow N_1 = 38$$

$$N_i = (3.391)^{4-i}$$

$$N_1 = (3.391)^{4-1} = 38.99$$

$$N_2 = (3.391)^{4-2} = 11.49$$

$$N_3 = (3.391)^{4-3} = 3.391$$

As can be seen, the obtained values from the law of stream numbers approximately match the observed values.

5.2.7.1.2 Law of Stream Lengths

The average length of streams of orders $i(L_i)$ is related to the stream length ratio (r_i) and the average length of first-order streams ($\overline{L}_1$) as the law of stream indicates:

$$L_i = \overline{L}_1 \cdot r_L^{i-1}, \tag{5.10}$$

and in this equation the stream length ratio is obtained by the ratio of the average length of streams of any order to the average length of streams of the next lower order.

5.2.7.1.3 Law of Stream Areas

The law of stream areas is similar to the law of stream lengths. Specifically, the mean tributary area of streams of orders $i(A_i)$ is related to the mean drainage area of first-order basins ($\overline{A}_1$) and the stream area ratio (r_a) by the law of stream areas:

$$A_i = \overline{A}_1 \cdot r_a^{i-1}. \tag{5.11}$$

Similarly to the previous law, stream area ratio is the average basin area of streams of one order to the average area of basins of the next lower order. Equations 5.12 and 5.13 are very similar and this is due to the high correlation that exists between watershed length and area.

5.2.7.1.4 Law of Stream Slopes

The average slope of streams of order $i(S_i)$ is related to the average slope of first-order streams $\left(\overline{S}_1\right)$ and the stream slope ratio (r_s) by the law of stream slopes:

$$S_i = \overline{S}_1 \cdot r_s^{1-i}, \tag{5.12}$$

and in this equation, the average slope of streams of order j to the average slope of streams of the next higher order, $j + 1$, defines the stream slope ratio.

Example 5.9

Estimate the three geomorphic parameters of R_b, r_L, and r_a for a watershed with an area of 250 km^2. The principal stream is of the fourth order. The numbers of streams of orders 1, 2, 3, and 4 are 35, 20, 7, and 1, respectively. The length of streams of orders 1, 2, 3, and 4 was measured and was equal to 1.32, 3.54, and 7.91, and 13 km, respectively. The average area for streams of orders 1, 2, 3, and 4 was computed as 3.8, 4.9, 5.3, and 15.5 km^2, respectively.

Solution:

These values can be substituted using Equation 5.10 to get the following:

$$35 = R_b^3$$
$$20 = R_b^2$$
$$7 = R_b$$

Using the principle of least squares, the above equations can be solved for R_b. Taking the natural logarithms of both sides of Equation 5.10 yields

$$\ln_e N_i = (k - i) \ln_e R_b.$$

Using the principle of least squares, it is easily demonstrated that the squares estimate of $\ln_e R_b$ is given by

$$\ln_e R_b = \frac{\sum\left[\left(\ln_e N_i\right)(K-i)\right]}{\sum\left[\left(K-i\right)^2\right]},$$

in which the range of each summation is from $i = 1$ to $i = K - i$, where K is the principal stream order. Hence, applying the least-squares algorithm, R_b is estimated as 3.77.

Application of Equation 5.11 yields

$$\ln_e r_L = \frac{\sum\left[\left(\ln_e \bar{L} - \ln_e \bar{L}_1\right)(i-1)\right]}{\sum\left[(i-1)^2\right]},$$

where each of the summations is over all values of i from 2 to the principal order for the watershed; 2.26 is the resulting stream length ratio.

The following equation computes the least-squares estimate of the stream area ratio (r_a) of Equation 5.12:

$$\ln_e r_a = \frac{\sum\left[\left(\ln_e \overline{A_i} - \ln_e \overline{A_j}\right)(i-1)\right]}{\sum\left[(i-1)^2\right]},$$

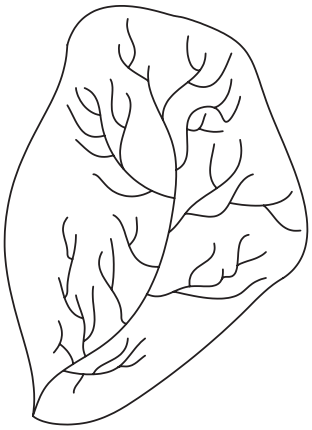

FIGURE 5.10 Watershed in Example 5.10.

where each of the summations is over all values of *i* from 2 to the principal order of the watershed. The stream area ratio of this watershed is 1.44.

This example demonstrates a case analysis where if a watershed is not fully defined, regional estimates of the three parameters (R_b, r_L, and r_a) can be obtained using regional averages. For the case analysis, it might be necessary to apply similar analyses on many watersheds in the region and determine the average values of the parameters. As a result, the regional averages could be used for hydrologic synthesis.

Example 5.10

Calculate the bifurcation rate of the watershed shown in Figure 5.10.

Solution:

$$n_1 = 42$$

$$n_2 = 14$$

$$n_3 = 3$$

$$n_4 = 1$$

$$R_b = \left(\frac{1}{t-1}\right) \times \left(\frac{n_1}{n_2} + \frac{n_2}{n_3} + \ldots + \frac{n_{i-1}}{n_i}\right) = \left(\frac{1}{4-1}\right) \times \left(\frac{42}{14} + \frac{14}{4} + \frac{4}{4}\right) = 3.5$$

or

$$R_b = \text{antilog}\left[\frac{\log n_1 - \log n_i}{i-1}\right] = \text{antilog}\left[\frac{\log 42 - \log 1}{4-1}\right] = 3.47.$$

5.3 HYPSOMETRIC CURVE

The hypsometric curve is a demonstration of the cumulative relationship between elevation and the area within elevation intervals. The hypsographical curve has practical utility in the comparison of watersheds or of different sections of a watershed. It is most often used to compare valley networks. Because runoff has more kinetic energy, the ground is cut away faster; thus, the curve of elevation vs. area falls off more quickly. Sapping is a lower-energy process, and hence, its curve appears rather flat at first and then falls off. The hypsographical curve can also be used in establishing the average amount of precipitation over the watershed. This will provide useful information about the hydrologic and hydraulic behavior of the watershed and about its hydrographical network.

The ordinate of the hypsometric curve is the elevation and its abscissa is the area within the watershed above the elevation. It can also be plotted by the cumulative fractions rather than the actual values in standardized form. The hypsometric curve for the given hypothetical watershed in Figure 5.11a is shown in Figure 5.11b.

Plotting the hypsometric curve in the standardized form is useful for comparing the area-elevation characteristics of watersheds. This would probably be useful when developing a regional hypsometric curve from the analysis of hypsometric curves of watersheds in the region in a way that an "average" curve for the region could be built from the standardized hypsometric curves for each watershed. If the necessary data are not available at some watersheds in the region, the regional average hypsometric curve could be used to represent the area-elevation characteristics of those watersheds.

Several indices have been developed to convert the hypsometric curve into a single-valued index of the area-elevation characteristics of a watershed. The hypsometric area ratio (H_a) index is the ratio of the area under the hypsometric curve to the area of the square formed by the points (0, 0), (0, l), (1, 1), and (1, 0) on the hypsometric curve developed based on the cumulative fractions, which can be changed between 0 and 1 (Figure 5.12). The changes in the amount of H_a give useful information about variations of slope over the study region. When H_a is approximately 0.5, there is approximately a uniform slope over the watershed. H_a values that are greater than 0.5 can be an indicator of large areas with very low slope whenever the low values of H_a show availability of large areas with steep slopes.

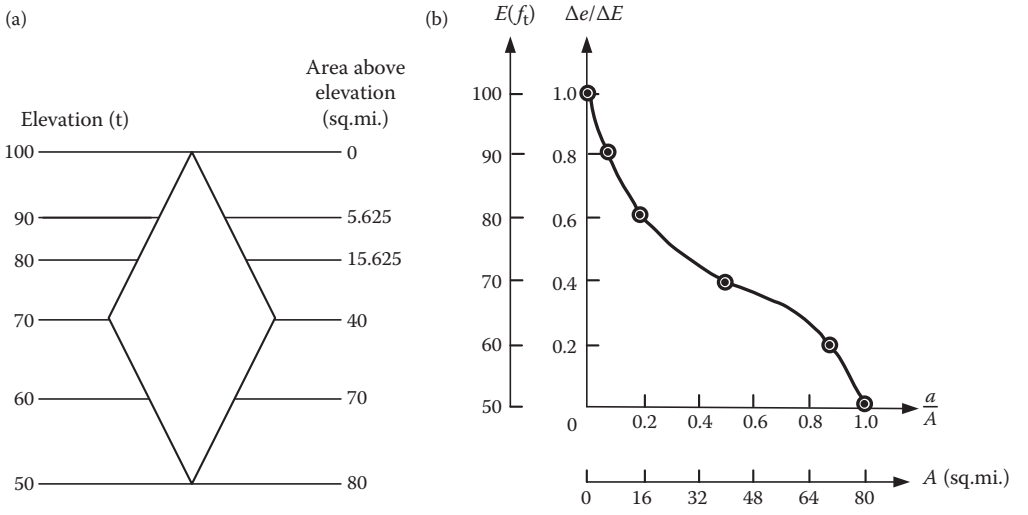

FIGURE 5.11 (a) Construction of a hypsometric curve for a hypothetical watershed. (b) Watershed hypsometric curve.

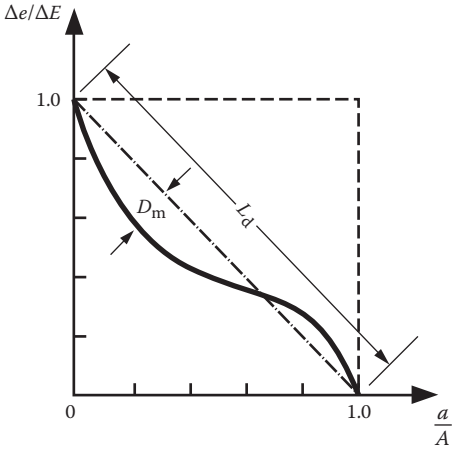

FIGURE 5.12 Estimation of the profile factor for the hypsometric curve.

By dividing the standard hypsometric curve into the linear parts, the hypsometric area ratio index is calculated using the trapezoidal rule:

$$H_a = \sum_{i=1}^{n} \frac{1}{2} \cdot \left[\left(\frac{\Delta e}{\Delta E} \right)_i + \left(\frac{\Delta e}{\Delta E} \right)_{i+1} \right] \cdot \left[\left(\frac{a}{A} \right)_i - \left(\frac{a}{A} \right)_{i+1} \right], \tag{5.13}$$

where A is the watershed area, a is the area between two elevation contours i and $i + 1$, ΔE is the elevation difference between the highest and the lowest points of the watershed, Δe is the elevation difference between two elevation contours of i and $i + 1$, and n is the number of considered elevation contours.

Example 5.11

Figure 5.13 shows the hypsometric curve of a watershed with an area of 80 km^2, which is developed using a 200 m elevation grid. Compute the hypsometric ratio for this watershed.

Solution:

Figure 5.13 shows the calculated values of a/A and $\Delta e/\Delta E$ with the hypsometric curve linear divisions. Using the trapezoidal rule (Equation 5.13), the hypsometric area ratio is estimated as follows:

$$\begin{aligned} H_a = {} & 0.5(0.002-0.0)(1+0.984)+0.5(0.068-0.002)(0.984+0.824) \\ & +0.5(0.249-0.068)(0.824+0.665)+0.5(0.563-0.249)(0.665+0.505) \\ & +0.5(0.766-0.563)(0.505+0.345)+0.5(0.945-0.766)(0.345+0.185) \\ & +0.5(0.998-0.945)(0.185+0.026)+0.5(1.0-0.998)(0.026+0.0)=0.519. \end{aligned}$$

Example 5.12

The hypsometric curve of a basin is shown in Figure 5.14. Considering the gradient of perception in this basin as $P = 200 + 0.07 \times H$ and the annual average temperature as 15°C, estimate the real

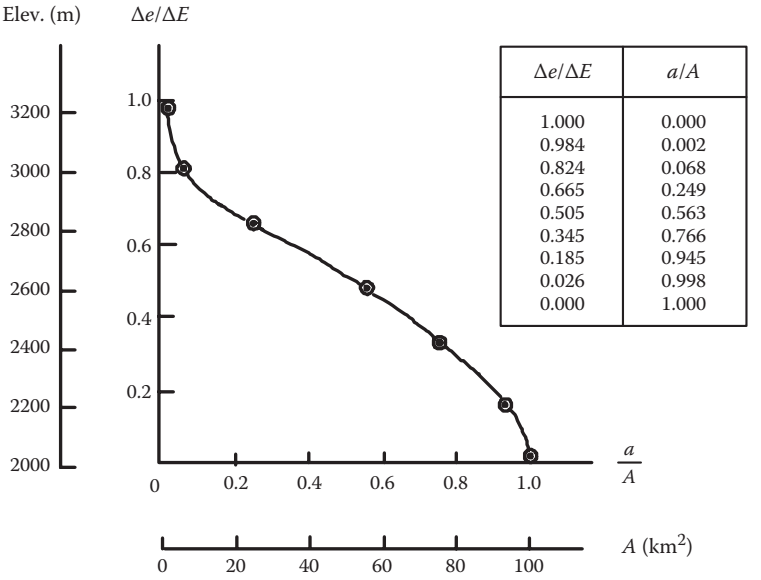

Δe/ΔE	a/A
1.000	0.000
0.984	0.002
0.824	0.068
0.665	0.249
0.505	0.563
0.345	0.766
0.185	0.945
0.026	0.998
0.000	1.000

FIGURE 5.13 Hypsometric curve for the watershed in Example 5.11.

rate of evaporation at this basin. Based on investigations in this basin, the evaporation rate can be estimated as follows:

$$E = \frac{P}{\left(0.90 + \left(\frac{p}{l}\right)^2\right)^{0.5}},$$

where l is estimated based on annual average temperature as $l = 300 + 25 \times T + 0.05 \times T^3$.

Solution:

Based on the hypsometric curve, the average watershed altitude is determined to be 1400 m. Then, the precipitation and evaporation rate are estimated using the given equations for the watershed.

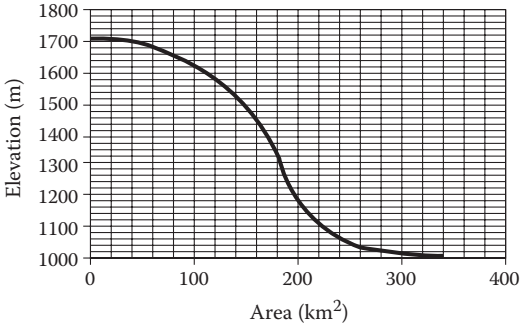

FIGURE 5.14 Hypsometric curve of a basin in Example 5.12.

$$P = 200 + 0.07H = 200 + 0.07 \times 1400 = 298 \text{ mm}$$
$$I = 300 + 25 \times T + 0.05 \times T^3 = 300 + 25 \times 15 + 0.05 \times 15^3 = 843.75$$
$$E = \frac{P}{\left(0.90 + \left(\frac{p}{I}\right)^2\right)^{0.5}} = \frac{298}{\left(0.90 + \left(\frac{298}{843.75}\right)^2\right)^{0.5}} = 294.38 \text{ mm}$$

The profile factor (F_p) is derived from a hypsometric curve as follows:

$$F_p = \frac{D_m}{L_d}, \tag{5.14}$$

where D_m is the maximum deviation of the hypsometric curve developed based on the cumulative fractions from a line connecting the points (0, 1) and (1, 0) and L_d is the length of the line connecting the points (0, 1) and (1, 0) (Figure 5.12). The typical values of the profile factor ranges from 0.01 to 0.15.

Example 5.13

For the hypsometric curve shown in Figure 5.15, estimate the profile factor.

Solution:

According to Figure 5.16, $L_d = 1.414$, and from Equation 5.14,

$$\begin{cases} L_d = 1.414 \\ D_m = 1 - 1 \times \sin(45°) = 0.293 \end{cases} \rightarrow F_p = \frac{0.293}{1.414} = 0.21.$$

Example 5.14

In Example 5.13, estimate the hypsometric area ratio.

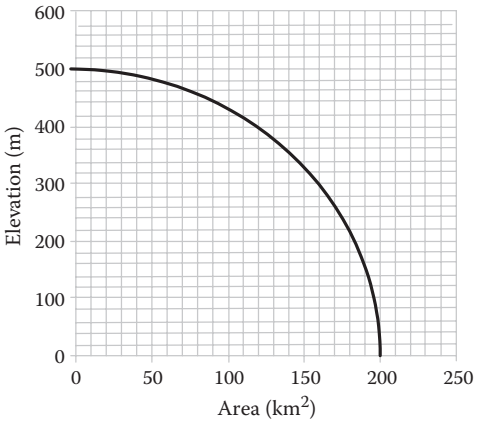

FIGURE 5.15 Hypsometric curve in Example 5.13.

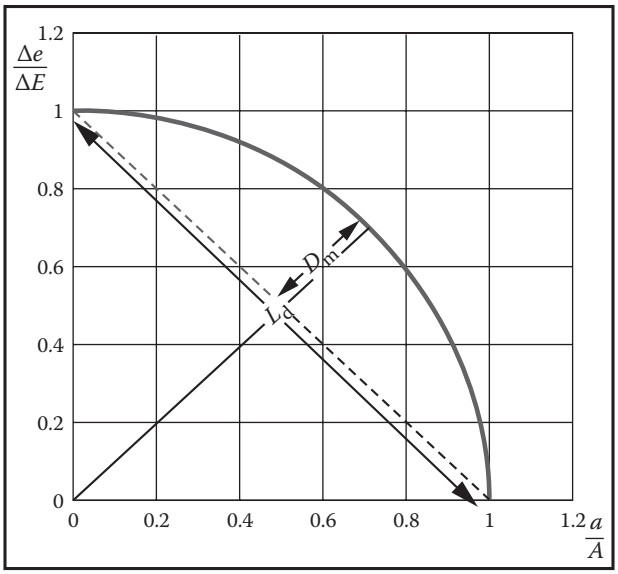

FIGURE 5.16 Estimation of the profile factor for the hypsometric curve in Example 5.13.

Solution:

From Example 5.13, the radius of the circle is 1 cm. Thus, the hypsometric area ratio is

$$H_a = \frac{\pi r^2}{4} = \frac{3.14}{4} = 0.785.$$

For determining the average elevation of the watershed, the following equation is employed:

$$\overline{H} = \frac{\sum a \cdot H}{A}, \tag{5.15}$$

where $\overline{H}$ is the average elevation of the watershed, A is watershed area, and a is the area between two elevation contours with an average elevation of H.

Example 5.15

In a basin shown in Figure 5.17, the gradient of perception is $P = 150 + 0.05 \times H$, where H is the height from sea level (m) and P is the annual perception (mm). Estimate the average annual perception of this basin.

Solution:

According to Equation 5.15 and Figure 5.17:

$$\overline{H} = \frac{\sum (a \cdot H)}{A} = \frac{75 \times 1725 + 77 \times 1675 + 62 \times 1625 + 50 \times 1575 + 41 \times 1525 + 20 \times 1490}{75 + 77 + 62 + 50 + 41 + 20} = 1631.3 \text{ m}$$

$$P = 150 + 0.05 \times H = 150 + 0.05 \times 1631.3 = 231.6 \text{ mm}$$

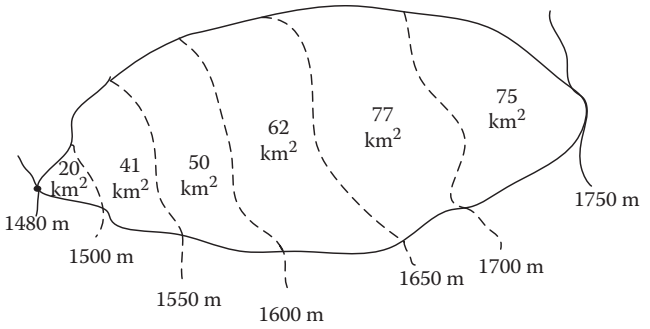

FIGURE 5.17 Delineation of the watershed in Example 5.15.

5.4 CHARACTERISTICS OF SOIL

The three phases of the soil system are solid, liquid, and gas. The liquid and gas phases are represented by the soil water and air, respectively, which occupy the pores and voids. However solid, liquid, and gas phases do not form a random mosaic in different dimensions but are more or less organized to impart a definite vertical and lateral structure to the system. Therefore, the properties of the soil solid as well as soil water and soil air vary vertically and laterally. The vertical component of the soil assembly is referred to as the *soil profile* and the soil layers are its *horizon*. The different soil horizons are as follows (McCuen 1998):

O horizon—Surface litter consisting primarily of organic matter
A horizon—Topsoil consisting of humus and inorganic minerals
E horizon—Leaching zone where percolating water dissolves water-soluble matter
B horizon—Subsoil below the A or E horizon that contains minerals and humic compounds
C horizon—A zone consisting primarily of undercomposed mineral particles and rock fragments
R horizon—An impermeable layer of bedrock

5.4.1 Texture of Soil

Soil texture refers to the size of mineral particles in different size categories. According to the mean diameter (d), particles of soil can be separated into four classes:

1. Gravel, $d \leq 2$ mm
2. Sand, $0.02 \leq d \leq 2$ mm
3. Silt, $0.002 \leq d \leq 0.02$ mm
4. Clay, $d \leq 0.002$ mm

Water-holding characteristics and the infiltration capacity of the soil can be determined by the soil texture. The soil capacity to pass and store infiltrating water increases with the size of the soil particles due to the increase in pore space.

5.4.2 Soil Structure

The kind, size, and distribution of soil aggregates and soil voids and pores determine the structure or fabric of the soil. The tendency of the soil particles to aggregate into lump is referred to as soil structure. The hydrologic response of the watershed, soil moisture, and water movement through the column of soil can be affected by the structure of the soil.

5.4.3 Soil Moisture

The water in the unsaturated zone of the soil is referred to as *soil moisture* and is acted upon by gravitation, surface tension, and molecular forces. Soil moisture is held as *capillary water* in the smaller pore spaces of the soil or as hygroscopic water absorbed on the surface of soil particles. Capillary water can be removed from soil by applying forces sufficient to overcome the capillary forces.

The moisture content of the soil after drainage is called *field capacity*. Drainage of water will continue for some time after a soil is saturated; hence, field capacity must be defined in terms of a specific drainage period. The *permanent wilting point* is a moisture content at which plants can no longer extract sufficient water from soil for growth. *Unavailable water* refers to the soil moisture below the water level of permanent wilting point, and the only moisture presented in the soil is the thin film or layer of moisture attached to the soil particles, which is referred to as *hygroscopic moisture*. The term *available water* refers to the moisture content of the soil that exists between field capacity and the permanent wilting point. An efficient irrigation procedure is to apply water when the moisture content of the soil approaches the wilting point in an amount sufficient to raise the soil moisture to the field capacity within the root zone.

5.5 CHANNEL GEOMORPHOLOGY

5.5.1 Length of a Channel

Besides drainage area and watershed length, channel length is used frequently in hydrologic computations. The channel length is computed in the following two computational schemes:

1. The distance is measured from the watershed outlet to the end of the channel, along the main channel as indicated on a map, which is denoted as L_e.
2. It is measured as the distance between two points located at the 10% and 85% of the distance along the main channel from the outlet, which is denoted as L_{10-85}.

Figure 5.18 illustrates these definitions along with the watershed length. An extension of a line on the map from the end of the main channel to the divide, L, is required to obtain the length of the watershed, which requires some subjective assessment and is often a source of inaccuracy.

A measure of subjectivity is also involved in the definitions for channel length because the endpoint of the channel is dependent on the way that map was drawn; the location of the channel end depends on the level of flow at the time the map was compiled. The final design bears an unknown

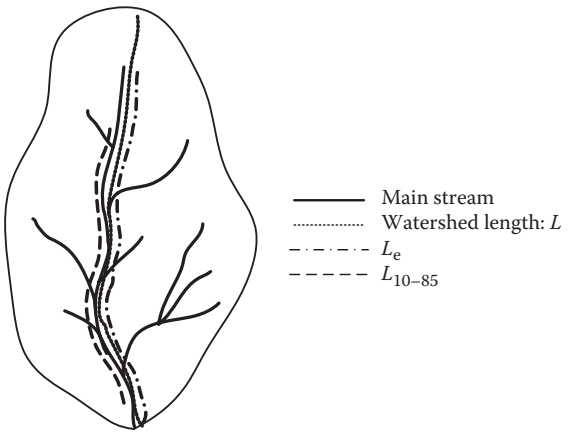

FIGURE 5.18 Delineation of watershed length and main stream length.

degree of inaccuracy due to these subjective assessments. Knowing exactly which definition was used in the development of a design aid is very important. For example, a bias may be introduced into the design if one of the definitions was used in developing the design method and the other is used in computing the channel length.

A stream channel may not be included in very small watersheds such as a section of overland flow or a section where the flow is in a swale or gully. As the size of the watershed increases, channel flow is in control and the watershed and channel lengths are essentially the same. Depending on the type of design problem, the appropriate measure of length can be chosen.

Example 5.16

The channel system shown in Figure 5.19 can be viewed as consisting of three reaches. Subareas 1, 2, and 3 have reaches of lengths 4940, 2440, and 3670 m, respectively. As it is shown in Figure 5.19, the watershed lengths are defined as subwatershed lengths, and the length measurements for subareas 1 and 2 must be extended to the basin divide. For subwatersheds 1 and 2, the lengths are 6810 and 4875 m, respectively. The length of subwatershed 3 is defined as the flow path from the most distant point on the watershed divide to the outlet, and this point is the northernmost point, which is on the boundary separating subareas 2 and 3. This flow path is made up of 2550 m of channel and 2450 m of overland and gully flow for a total watershed length of 5000 m. Determine the total basin length.

Solution:

Discussing time parameters reveals the importance of distinguishing between the channel length and the length of the subwatersheds. In the case of the demand for the subwatershed being indistinguishable from the need to estimate the total watershed length, the length would be the sum of the channel length for the reach through subarea 3 (e.g., 3670 m) and the watershed length of subarea 1 (i.e., 6810 m), or 10,480 m. This value provides the maximum length from the watershed boundary to its outlet.

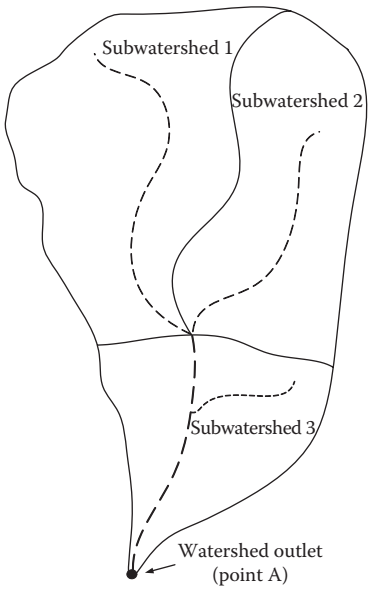

FIGURE 5.19 Watershed in Example 5.16.

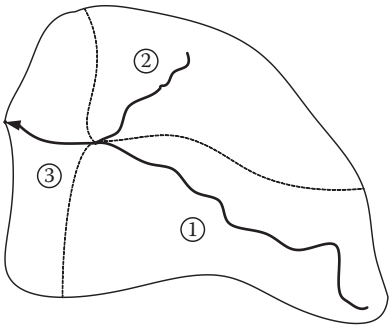

FIGURE 5.20 Watershed in Example 5.17.

Example 5.17

The total area of a watershed, divided into three subwatersheds as shown in Figure 5.20, is 26 km^2. The length of sub-basins 1, 2, and 3 are 1304, 342, and 252 m, respectively. If the lengths of the main rivers in these sub-basins are 1200, 311, and 220 m, respectively, calculate the elongation ratio for this basin.

Solution:

The length of sub-basin 1 is 1304 m and it is used because the main river in sub-basin 1 is less than the real length of the sub-basin; moreover, the length of the main river in sub-basin 3 along the length of the basin is 220 m. Hence, the sum of the length of sub-basins 1 and 3 (1524 m) is greater than the sum of the length of sub-basins 2 and 3, which is 562 m. Consequently, L_m is calculated as follows:

$$R_e = \frac{2}{L_m} \times \left(\frac{A}{\Pi}\right)^{0.5} = \frac{2}{1304 + 220} \times \left(\frac{26}{\Pi}\right)^{0.5} \rightarrow R_e = 3.78.$$

5.5.2 Slope of a Channel

Most of the computational schemes need to determine the channel slope. There are different definitions of the channel slope, the most common of which is

$$S_c = \frac{\Delta E_c}{L_c}, \tag{5.16}$$

where S_c is the channel slope, ΔE_c is the difference in elevation between the points that define the upper and lower ends of the channel, and L_c is the length of the channel between the same two points. In addition, the 10–85 slope, S_{10-85}, might be used, which is calculated as follows:

$$S_{10-85} = \frac{\Delta E_{10-85}}{L_{10-85}}, \tag{5.17}$$

where ΔE_{10-85} is the difference in elevation between the points defining the channel length L_{10-85}.

In cases where the channel slope is not uniform, the weighted slope index is used to better reflect the effect of slope on the hydrologic response of the watershed. A channel slope index, S_i, is defined as

$$S_i = \left(\frac{n}{k}\right)^2, \tag{5.18}$$

where n is the number of segments into which the channel is divided and k is given by

$$k = \sum_{i=1}^{n} \frac{1}{\left(\Delta e_i / l_i\right)^{0.5}}, \tag{5.19}$$

where Δe_i is the difference in elevation between the endpoints of channel segment i, and l_i is the length of segment i. The slope is considered relatively constant over the segmented channel.

Example 5.18

For the given watershed in Figure 5.19, calculate the channel and watershed slope based on the altitude data given in Table 5.3.

Solution:

For computing the channel slope of the watershed in Figure 5.19, the channel reach in each subwatershed is used. Channel and watershed slopes are given in Table 5.3 for both the subdivided watershed and the watershed as a whole. Generally, as a rule, the watershed slopes are greater than the channel slopes, because the side slopes of the watershed are almost always steeper than the channel.

Channel slope has a profound effect on the velocity of flow in a channel and, consequently, on the flow characteristics of runoff from a drainage basin. The importance of channel slope lies in two areas: (1) it helps in the determination of discharge and velocity using the Manning or Chezy equation and (2) it can be used as a variable in multivariate analysis to determine the amount of influence accounted for by the channel slope. Because the slope varies longitudinally, an average value of slope must be determined.

5.5.2.1 Method 1

For use in either the Manning or Chezy equation, the channel slope is a local measurement to approximate the energy slope, assuming uniform flow. For this purpose, the channel slope S is

TABLE 5.3
Length and Slope of Watershed in Figure 5.19

	Length (m)		Channel Elevation (m)			Watershed Elevation (m)			Slope	
Area	**Channel**	**Watershed**	**Upper**	**Lower**	**Difference**	**Upper**	**Lower**	**Difference**	**Channel**	**Watershed**
Sub 1	4940	6810	450	340	110	608	340	268	0.022	0.039
Sub 2	2440	4875	400	340	60	545	340	205	0.025	0.042
Sub 3	3670	5000	340	295	45	545	295	250	0.012	0.050
Total	8610	10480	450	295	155	608	295	313	0.018	0.030

computed from Equation 5.2. The fall over the channel reach of interest is measured. However, this measurement is a local measurement and cannot hold for other channel reaches in the drainage basin. Cross-sectional area, channel roughness, and cross-sectional shape also affect flow velocity. Therefore, there is not as much difference in the flow velocity between various reaches of the drainage basin as one might think.

5.5.2.2 Method 2

When used in multivariate analysis, the arithmetic slope in Equation 5.2 might be determined in many ways. One common method is to compute the fall from the head of the uppermost first-order channel to the basin outlet and divide this fall by its horizontal length.

5.5.2.3 Method 3

A geometric slope is sometimes used. This slope is determined by locating the median channel-profile elevation on the main channel and computing the fall from this point to the outlet. The length is the horizontal distance between the point of median elevation to the outlet. The slope is then computed using Equation 5.2.

5.5.2.4 Method 4

Benson (1962) found that the "85–10" slope factor was the most satisfactory in his study of floods in New England. This factor is the slope between 85% (excluding the upper 15%) and 10% (excluding the lower 10%) of the distance along the stream channel from the basin outlet to the divide. It should be noted that the distance is measured from the outlet to the divide and not to the end of the defined stream channel. The fall and horizontal length between these two points are computed using Equation 5.2.

5.5.2.5 Method 5

This method is from Johnstone and Cross (1949). The channel can be divided into N number of reaches, each having a uniform slope S_i. Then, the equivalent uniform slope S_m is

$$S_m = \left(\frac{\sum_{i=1}^{N} L_i S_i^{0.5}}{\sum_{i=1}^{N} L_i} \right)^2. \tag{5.20}$$

This is designed to estimate the slope that would result in the same total time of travel as the actual stream if length, roughness, channel cross section, and any other pertinent factors other than slope were unchanged.

5.5.2.6 Method 6

This method was initially introduced by Laurenson (1962). Again, the stream is divided into N reaches, each of uniform slope. Furthermore, it is assumed that the effects of roughness and hydraulic radius on velocity are the same for all reaches. This assumption is questionable but has been used previously (Taylor and Schwarz 1952). This assumption is also implied in the first method. The velocity U of flow through any reach i can be written as

$$U_i = BS_i^{0.5}, \tag{5.21}$$

where B is a constant. Then, the time of flow t_i is

$$t_i = \frac{L_i}{U_i}. \tag{5.22}$$

Therefore, the total time of travel T_c down the main channel is

$$T_c = \frac{1}{B}\sum_{i=1}^{N}\frac{L_i}{S_i^{0.5}}. \tag{5.23}$$

The mean velocity of flow U_m can be written as

$$U_m = \sum_{i=1}^{N}\frac{L_i}{T_c} = \frac{\sum_{i=1}^{N} L_i}{\sum_{i=1}^{N} L_i/S_i^{0.5}}. \tag{5.24}$$

Furthermore,

$$U_B = BS_m^{0.5}. \tag{5.25}$$

Hence,

$$S_m = \left(\frac{\sum_{i=1}^{N} L_i}{\sum_{i=1}^{N} L_i/S_i^{0.5}}\right)^2. \tag{5.26}$$

5.5.2.7 Method 7

This method is from Gray (1961) and Lane (1975). Gray defined S as the slope of a line drawn along the measured profile that has the same area as is under the observed profile. By referring to Figure 5.21, the slope is the slope of the hypotenuse of a right-angle triangle with the same A and length L as the observed profile. If A is the area under the observed profile, then

$$A = hL_c/2, \tag{5.27}$$

where h is the ordinate of the right-angle triangle. Therefore,

$$S_c = h/L_c \tag{5.28}$$

or

$$S_c = 2A/L_c^2. \tag{5.29}$$

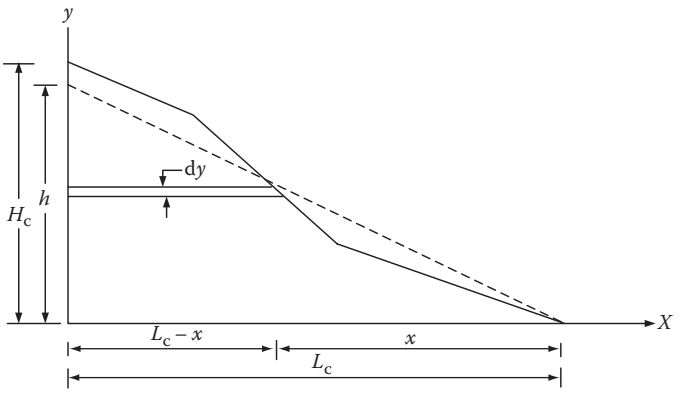

FIGURE 5.21 Observed channel profile shown by solid line and dash.

However, a more accurate measure of S_c can be obtained as follows:

$$A = \int_0^{H_c} \left(L_c - x\right) \mathrm{d}y. \tag{5.30}$$

Since the slope S is continuously changing with x,

$$\mathrm{d}y = S(x)\mathrm{d}x. \tag{5.31}$$

Therefore,

$$A = \int_0^{L_c} \left(L_c - x\right) S(x)\, \mathrm{d}x. \tag{5.32}$$

Then, the above equation yields

$$S_c = 2\int_0^{L_c} \frac{L_c - x}{L_c^2} S(x)\, \mathrm{d}x, \tag{5.33}$$

where $(L_c - x)/L_c^2$ can be considered as a weighting factor. Based on this relation, the slope is 0 at $x = L_c$ and reaches its maximum at $x = 0$ (at the outlet). Thus, Gray's method produces a channel slope that is weighted by distance from the head to the outlet.

The quantity h/H_c can be used as an index of concavity. Values less than 1, which is normally the case, show that the stream profile is concave and values greater than 1 correspond to a convex profile. Furthermore, this quantity can be used as an index of how well the natural channel slope is represented by a straight line. It can be seen from the foregoing methods of determining channel slope that the main channel is used to determine a slope that is presumed to be representative of all other channels in the drainage basin.

Example 5.19

Estimate the average slope of the watershed shown in Figure 5.22 regarding Table 5.4 if the watershed is divided into five intervals.

Solution:

$$K = \sum_{i=1}^{n} \frac{1}{\left(\frac{\Delta e_i}{L_i}\right)^{0.5}} = \left(\frac{1}{0.091^{0.5}} + \frac{1}{0.035^{0.5}} + \frac{1}{0.015^{0.5}} + \frac{1}{0.110^{0.5}} + \frac{1}{0.042^{0.5}} \right) = 24.72$$

$$S_i = \left(\frac{n}{K}\right)^2 = \left(\frac{5}{24.72}\right)^2 = 0.041.$$

Example 5.20

Estimate the average slope of Figure 5.22 without any interval.

Solution:

$$\Delta E = 3758 - 2994 = 764$$

$$S_e = \frac{\Delta E}{L_e} = \frac{764}{3200 + 1700 + 2000 + 2300 + 3000} = 0.062.$$

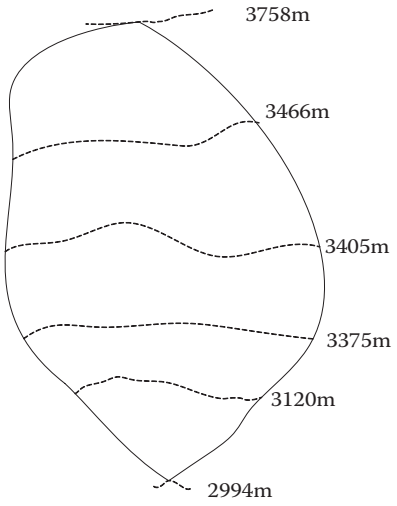

FIGURE 5.22 Watershed in Example 5.19.

TABLE 5.4
Characteristics of Watershed in Example 5.19

Interval Length (m)	Interval Number
3200	1
1700	2
2000	3
2300	4
3000	5

TABLE 5.5
Calculated Slopes for Watershed in Example 5.19

Interval Number	Δe_i	Interval Slope
1	292	0.091
2	61	0.035
3	30	0.015
4	255	0.110
5	126	0.042

The method that is used in Example 5.19 is more accurate because it is divided into some intervals and so the slope of the basin for each interval is calculated independently. On the other hand, in Example 5.20, the difference in elevation in the entire basin is calculated. As it is shown in Table 5.5, the slope in some intervals is sharper than the others. Hence, the result of the first method is more reliable than the second one.

5.5.3 Law of Stream Slopes

A composite stream profile in a drainage basin can be prepared in the following way. For each first-order stream, the horizontal length and the vertical drop of the segment are determined. Then, mean horizontal length and mean drop are determined. Streams of all orders follow this procedure. The triangles for each order are connected in sequence to produce a composite profile. Since each segment slope is governed by the average discharge and average sediment load, a segmented profile looks logical even though a continuous curve is drawn through these points.

Horton (1945) introduced the law of stream slopes, which states that the average slope of streams of each order tends to approximate an inverse geometric series.

$$\overline{S}_w = \overline{S}_1 R_s^{W-w}, \tag{5.34}$$

where $\overline{S}_w$ is the average slope of streams of order w; $\overline{S}_1$ is the average slope of first-order streams; R_s is the slope ratio, defined as $R_s = \overline{S}_w/\overline{S}_{w-1}$; and W is the order of the basin. The value of R_s is approximately 0.55.

5.5.4 Channel Cross Section

There are a number of reasons why the channel cross sections are a very important part of hydrologic analysis and design. Design problems usually require cross-section information, including the cross-sectional area. Other important characteristics are the wetted perimeter, slope, roughness, and average velocity. Stream cross sections can take on a wide variety of shapes and sizes, which is very apparent if one walks along a river or stream, even for short distances.

V-shaped cross sections are often in upland areas for small streams. As the stream drains larger areas, past floods have sculptured out larger, often rectangular or trapezoidal sections. Relatively small V- or U-shaped channels are frequent in many rivers that carry the runoff from small storms and the runoff during periods between storm events. This small channel area is often part of a much larger flat area on one side or on both sides of the channel; this flat area is called the floodplain, which is the area that is covered with water during times of higher discharges.

The low-flow cross section is approximately trapezoidal; however, it represents a small portion of the total cross section that is used to pass large flood events. The floodplain could easily be represented as a rectangular section due to its low side slopes. Cross sections can change shape during flood events on account of channel instability and erosional processes, and where such changes take place, they should be accounted for in developing a discharge rating table. Development within the floodplain may also change the channel cross sections.

The width of the section was decreased due to the abutments on each side and the four twin piers that support the bridge; in the meantime, the low-flow section remains unchanged. From the continuity equation, we know that for a given discharge, either the average velocity will have to increase because of the reduced cross-sectional area created by the bridge or the flood surface elevation will increase.

In practice, it is required to calculate the flood surface elevations along the entire section of the channel affected by the structure in design problems. For example, at the bridge, the cross section changes and it affects the flood profile both above and below the bridge, which should be considered in flood management practices.

5.5.5 Channel Roughness

The characteristics of runoff are affected by the roughness of a surface, whether the water is on the surface of the watershed or in the channel. The surface roughness retards the flow with respect to the hydrologic cycle. In case of overland flow, increasing roughness delays the runoff and should increase the potential for infiltration. The erosion amount decreases due to reduced velocity caused by an increase in roughness. The general effects of roughness on a channel flow are similar to those for overland flow.

A number of hydraulic computations require Manning's roughness coefficient (n), and it is a necessary input in floodplain delineation and a number of runoff time estimation methods. Moreover, it is used in the design of stable channel systems. Hence, it is an important input.

There are a number of methods in estimating the roughness coefficient. First, a series of pictures of stream channels are provided in books with a recommended n value for each picture; therefore, by comparing the roughness characteristics of the channel with the pictures that appear most similar, a value of n can be obtained for any natural channel. Second, typical or average values of n for various channel conditions are available in tables similar to Table 5.6. However, the degree of homogeneity of channel conditions and the degree of specificity of the table determine the accuracy of n values from such tables. Due to their simplicity and not being highly inaccurate, the picture comparison and tabular look-up methods are frequently used.

TABLE 5.6
Recommended Design Values of Manning's Roughness Coefficient, *n*, Used for Channel Flow Analysis

a. Unlined Open Channels	Manning *n* Range
A. Earth. Uniform section	
1. Clean recently completed	0.016–0.018
2. After weathering	0.018–0.020
3. With short grass, few weeds	0.022–0.027
4. In graveled soil, uniform section, clean	0.022–0.025
B. Earth. Fairly uniform section	
1. No vegetation	0.022–0.025
2. Grass. Some weeds	0.025–0.030
3. Dense weeds or aquatic plants in deep channels	0.030–0.035
4. Sides clean gravel bottom	0.025–0.030
5. Sides clean cobble bottom	0.030–0.040
C. Dragline excavated or dredged	
1. No vegetation	0.028–0.033
2. Light brush on banks	0.035–0.050
D. Rock	
1. Based on design section	0.035
2. Based on actual mean section	
a. Smooth and uniform	0.035–0.040
b. Jagged and irregular	0.040–0.045
E. Channels not maintained, weeds and brush uncut	
1. Dense weeds, high as flow depth	0.08–0.12
2. Clean bottom, brush on sides	0.05–0.08
3. Clean bottom brush on sides, highest stage of flow	0.07–0.11
4. Dense brush, high stage	0.10–014
b. Roadside Channels and Swales with Maintained Vegetation (Values Shown Are for Velocities of 0.6 and 1.8 m/s)	
A. Depth of flow, up to 0.2 m	
1. Bermuda grass, Kentucky bluegrass, buffalo grass	
a. Mowed to 5 cm	0.07–0.045
b. Length 10 to 15 cm	0.09–0.05
2. Good stand, any grass	
a. Length about 30 cm	0.18–0.09
b. Length about 60 cm	0.30–0.15
3. Fair stand, any grass	
a. Length about 30 cm	0.14–0.08
b. Length about 30 cm	0.25–0.13
B. Depth of flow, 0.2–0.45 m	
1. Bermuda grass, Kentucky bluegrass, buffalo grass	
a. Mowed to 5 cm	0.05–0.035
b. Length 10 to 15 cm	0.06–0.04
2. Good stand, any grass	
a. Length about 30 cm	0.12–0.07
b. Length about 60 cm	0.20–0.10

(*continued*)

TABLE 5.6 (Continued)
Recommended Design Values of Manning's Roughness Coefficient, *n*, Used for Channel Flow Analysis

	Manning *n* Range
3. Fair stand, any grass	
a. Length about 30 cm	0.10–0.06
b. Length about 60 cm	0.17–0.09
c. Natural Stream Channels	
A. Minor streams (surface width at flood stage less than 35 m)	
1. Fairly regular section	
a. Some grass and weeds, little or no brush	0.030–0.035
b. Dense growth of weeds, depth of flow materially greater than weed height	0.035–0.05
c. Some weeds. Light brush on bank	0.04–0.05
d. Some weeds. Heavy brush on bank	0.05–0.07
e. Some weeds. Dense willows on bank	0.06–0.08
f. For trees within channel, with branches submerged at high stage, increase all above values by	0.01–0.10
2. Irregular sections, with pools, slight channel meander, increase value in la–c by	0.01–0.02
3. Mountain streams, no vegetation in channel, bank usually steep, trees and brush along banks submerged at high stage	
a. Bottom of gravel, cobbles, and few boulders	0.04–0.05
b. Bottom of cobbles, with large boulders	0.05–0.07
B. Floodplains (adjacent to natural streams)	
1. Pasture, no brush	
a. Short grass	0.030–0.035
b. High grass	0.035–0.05
2. Cultivated areas	
a. No crop	0.03–0.04
b. Mature row crops	0.032–0.045
c. Mature field crops	0.04–0.05
3. Heavy weeds, scattered brush	0.05–0.07
4. Light brush and trees	
a. Winter	0.05–0.06
b. Summer	0.06–0.08
5. Medium to dense brush	
a. Winter	0.07–0.11
b. Summer	0.10–0.16
6. Dense willows, summer, not bent over by current	0.15–0.20
7. Cleared land with tree stumps, 0.4–0.6 per km^2	
a. No sprouts	0.04–0.05
b. With heavy growth of sprouts	0.06–0.08
8. Heavy stand of timber, a few down trees, little undergrowth	
a. Flood depth below branches	0.10–0.12
b. Flood depth reaches branches	0.12–0.16
C. Major stream (surface width at flood stage more than 35 m: Roughness coefficient is usually less than that for minor streams of similar description on account of less effective resistance offered by irregular banks or vegetation on banks; values of *n* may be somewhat reduced. The value of *n* for larger streams of most regular sections, with no boulders or brush, may be in the range shown.	0.028–0.033

Source: Adapted from McCuen, R., *Hydrologic Analysis and Design*, Prentice-Hall, London, 1998.

5.6 TRAVEL TIME

Most hydrologic designs involve some measure of flood discharge. The volume of flood runoff can be reflected by various watershed and hydrometeorological characteristics; for example, the product of the drainage area and the depth of rainfall give a volume of water that is potentially available for runoff, but volume alone is not adequate for many design problems. As the dimensions of discharge indicate (L^3/T), time is an important element in hydrologic design. However, a given volume of water may or may not present a flood hazard; in fact, the hazard will depend on the time distribution of the flood runoff. Flood damage occurs if a significant portion of the total volume passes a given location at about the same time.

Conversely, flood damage will be minimal in case of distribution of the total volume over a relatively long period of time. Instantaneous inundation causes major damage such as when an automobile is submerged, but an agricultural crop field does not usually experience major damage in short-duration inundation. Therefore, duration of flooding is an important factor.

Most hydrologic models require a watershed characteristic that reflects the timing of runoff due to the importance of the timing of runoff. A number of time parameters have been developed. As the runoff timing is a watershed characteristic, time parameters are formulated as a function of other watershed characteristics and, in some cases, rainfall intensity. Hydrologic and hydraulic models commonly use several time parameters such as the time of concentration, the time lag, and reach travel time.

The importance of time in hydrologic design is dependent on the type of hydrologic design problem. On small watershed designs, such as for the design of either rooftop drains or street-drainage inlets, the time parameter may be an indicator of three parameters: the intensity and volume of rainfall and the degree to which the rainfall will be attenuated. In these cases, since the storages of the hydrologic processes have minimal effects, a short time period would suggest little attenuation of rainfall intensity. On larger watershed designs, time parameters may be representative of watershed storage and the effect of storage on the time distribution of runoff. The shape and the time distribution of the runoff hydrograph are directly affected by the watershed storage. For designs where the time variation of flood runoff is routed through channel reaches, the effect of channel storage on the attenuation of the flood discharge is reflected by the reach travel time.

Errors in a time parameter will cause errors in designs. Errors in the estimated value of the time parameter is responsible for 75% of the total error in an estimate of the peak discharge. Numerous methods for estimating the various time parameters have developed due to the importance of time parameters in hydrologic design and evaluation. Unfortunately, most of the empirical formulas have been based on very limited data; therefore, lack of diversity in the data constrains their applicability. Considerable caution must be taken in the usage of an empirical estimation method either for watersheds having characteristics different from those of the watersheds used to calibrate the method or for watersheds in other geographic regions. Data extrapolation is represented in both uses. Therefore, a design engineer faced with a design problem requires an estimation of a time parameter and must choose from among many of the alternatives and often apply the time parameter with little or no knowledge of its accuracy.

The time of concentration, the lag time, the time to peak, the time to equilibrium, and the time–area curve are the most frequently used time parameters. They are usually defined in terms of either the physical characteristics of a watershed or the distribution of rainfall excess and direct runoff. The most widely used time parameter is the time of concentration; hence, at this point, the discussion will be limited to the time of concentration; others will be discussed in other chapters.

5.6.1 Definitions of Time of Concentration

The time of concentration has two commonly accepted definitions. First, required time for a water particle to flow hydraulically from the most distant point in the watershed to the outlet or design point defines t_c; on this definition, watershed characteristics and sometimes a precipitation index

such as the 2-year, 2-hour rainfall intensity are used in methods of estimation. Several empirical equations based on this definition will be discussed herein.

Some of the required terms have not been previously introduced; therefore, the second definition is introduced here only for completeness. In the second definition, t is based on a rainfall hyetograph (defined in Chapter 4) and the resulting runoff hydrograph (defined in Chapter 6). The rainfall excess and direct runoff are computed from the actual hyetograph and hydrograph. The time between the center of mass of rainfall excess and the inflection point on the recession of the direct runoff hydrograph defines the time of concentration. As an alternative, the time difference between the end of rainfall excess and the inflection point is sometimes accepted as t_c.

Both methods of estimating t_c do not provide either the true value or reproducible values of t_c. That is because the methods based on watershed characteristics may consider, for example, that Manning's equation is always valid and that the roughness coefficient applies throughout the flow regime. Even though one may ignore both the difficulties in selecting a single value of the roughness coefficient for a seemingly homogeneous flow regime and the assumption that the hydraulic radius remains constant, the design engineer must still contend with the problem of the input reproducibility; that is, different values of the input variables are selected by different users of a method even if on the same drainage area. In summary, in hydrologic design, an important input is the time of concentration; however, it is neither a highly accurate input nor highly reproducible.

There are some difficulties in estimation of t_c from rainfall and runoff data. There are no universally accepted methods of separating either base flow from direct runoff or losses from rainfall excess. Significant variation in estimated t values may be introduced by both of these separation requirements. In estimation of t_c using rainfall and runoff data, some factors must also be identified, such as antecedent soil moisture, intermittent rainfall patterns, nonlinearities in the convolution process, and variation in the recurrence intervals of the storm, and these require t_c to be adjusted. In summary, it is not possible to have a single correct method for estimating t_c, and therefore, the true value can never be determined.

5.6.2 Classifying Time Parameters

Numerous empirical formulas have been developed for time parameters evaluation, therefore it would be useful to provide a system for their classification. The role of four types of inputs, including slope, watershed size, flow resistance, and water input, is common in all methods. The pipe system or the channel system characteristics are used for the overland flow portion of the watershed. Sheet flow and concentrated flow methods are two classes for overland flow.

Input requirements and dominant flow regime can be used for classifying time parameters. The system could be further classified on the basis of the other time parameters such as time lag, time of concentration, and time to peak; however, in this chapter the time of concentration is considered.

The runoff coefficient of the rational method, C, Manning's roughness coefficient, n, the percentage of imperviousness, I, the Soil Conservation Service (SCS) runoff curve number, CN, and a qualitative descriptor of the land cover type are involved in measures of the overland flow resistance. The length and slope of overland flow can be represented by one of a number of size or slope parameters. A rainfall parameter is sometimes used as input to show the impact of the surface runoff availability on the time of travel.

Methods for estimating t_c, which include channel characteristics as input variables, should be used when channel flow makes an indicative contribution to the total travel time of runoff (see Table 5.7). The most widely used index of channel flow resistance is Manning's roughness coefficient, n. Espey and Winslow developed a coefficient that could also be an indicator of flow resistance to show the degree of channelization. Several slope and size parameters are used as variables. The precipitation intensity, the volume of surface runoff, and the hydraulic radius for bank full flow could be used as input factors for a channel.

TABLE 5.7
Criteria for Classifying Time Parameters and Variables Commonly Used

Flow Regime	Flow Resistance	Watershed Size	Slope	Inflow
Sheet flow	n	L	S	I
Concentrated flow	n, C, CN	L, A	S	I
Channel	n	L_{10-85}, L	S, S_{10-85}	R_h, i, Q
Pipe	n	L	S	R_h

n = Manning's roughness coefficient
L = watershed length
S = average slope
i = rainfall intensity
C = runoff coefficient
CN = runoff curve number
A = drainage area
L_{10-85} = length of channel within 10% and 85% points
S_{10-85} = channel slope between 10% and 85% points
R_h = hydraulic radius
Q = channel discharge rate

The timing characteristics of the runoff are controlled by a pipe system for most small urban watersheds (see Table 5.7). One or more input variables are needed for methods in order to predict the time parameters on such watersheds that reflect the physical characteristics of the pipe system. Manning's roughness coefficient for the pipe could be used to reflect flow resistance. The maximum flow rate, q, the largest or smallest pipe diameter, or the mean hydraulic radius of the pipe system could be the inputs of methods. Any one of a number of size variables could be included in these equations to represent size.

The classification system in Table 5.7 can be used for separating time parameter prediction methods. A significant number of others will have to be identified as a "mixed" method when some prediction methods will fall into one of the four classes based on flow regime (i.e., one that includes variables reflecting different flow regimes). For example, both a significant pipe system and an overland flow may require a time parameter model that needs designs for urbanized watersheds involving variables that reflect all four flow regimes: concentrated flow, sheet flow, pipe flow, and channel flow. It is worthwhile to clarify some common terms associated with the time of concentration so that the terminology is always applied consistently. Although the term *overland flow* could be applied to a number of flow regimes, it is worthwhile to classify this into sheet flow and concentrated flow. Sheet flow occurs usually over very short flow paths in the upper reaches of a basin. Typically, this is evident on steeply sloped paved surfaces often with small waves, where it appears as shallow layers. A kinematic wave equation is used in order to compute travel times for sheet flow most of the time. After some distance, the flow concentrates in rills, swales, or gutters and gullies because of topography. This is referred to as concentrated flow. The common method that is used to estimate travel times of concentrated flow is Manning's equation or the velocity.

Manning's equation is used to estimate velocities of overland flow, both sheet flow and concentrated flow. It can be represented that the kinematic wave equation for estimating sheet flow travel time is based on Manning's equation. Manning's equation must have an assumption that the hydraulic radius equals the product of the travel time and the rainfall intensity. The velocity method for concentrated flow uses Manning's equation with an assumed Manning's n and depth. Frequently used curves of velocity versus slope are valid only as long as the assumed depth and n are accurate.

5.6.3 Velocity Method

The travel time is the basic concept of the velocity method. Travel time (T_t) for a particular flow path is a function of the length of flow (L) and the velocity (V):

$$T_t = \frac{L}{V}. \tag{5.35}$$

The travel time is computed for the principal flow path. Where the principal flow path consists of segments that have different slopes or land cover, the principal flow path should be divided into segments and Equation 5.35 should be used for each flow segment. The time of concentration is then the sum of the travel times:

$$t_c = \sum_{i=1}^{k} T_{ti} = \sum_{i=1}^{k} \left(\frac{L_i}{V_i} \right), \tag{5.36}$$

where k is the number of segments and the subscript i refers to the flow segment.

The velocity of Equation 5.35 is a function of the type of flow (sheet, concentrated flow, gully flow, channel flow, pipe flow), the roughness of the flow path, and the slope of the flow path. Velocity

TABLE 5.8
Parameters Used in Velocity–Slope Relationship

Land Use/Flow Regime	n	R_h	$K = \frac{R_h^{2/3}}{n}$
	Forest		
Dense underbrush	0.8	0.83	1.11
Light underbrush	0.4	0.73	2.03
Heavy ground litter	0.20	0.67	3.82
	Grass		
Bermuda grass	0.41	0.50	1.54
Dense	0.24	0.40	2.26
Short	0.15	0.33	3.20
Short grass pasture	0.025	0.13	10.44
	Conventional Tillage		
With residue	0.19	0.20	1.80
No residue	0.09	0.17	3.37
	Agricultural		
Cultivated straight row	0.04	0.40	13.57
Contour or strip cropped	0.05	0.20	6.84
Trash fallow	0.045	0.17	6.73
Rangeland	0.13	0.13	2.01
Alluvial fans	0.017	0.13	15.35
Grassed Waterway	0.095	3.33	23.49
Small upland gullies	0.04	1.67	35.14
Paved area (sheet flow)	0.011	0.20	31.09
Paved gutter	0.11	0.07	14.95

can be estimated by various methods. Flow velocities in pipes and open channels can be computed using Manning's equation:

$$V = \frac{1}{n} R_h^{2/3} \cdot S^{1/2}, \tag{5.37}$$

where V is the velocity (m/s), n is the roughness coefficient, R_h is the hydraulic radius (m), and S is the slope. Equation 5.37 can be simplified so that V is only a function of the slope by assuming values for n and R_h. This gives a relationship between the velocity and the average slope of the surface as follows:

$$V = k \cdot S^{0.5} \text{ and } k = \frac{R_h^{2/3}}{n}, \tag{5.38}$$

where V is the velocity (m/s) and S is the slope. For Equation 5.38, the value of k is a function of the land cover with the effect measured by the value of n and R_h. Values for selected types of land cover are given in Table 5.8. After short distances, runoff tends to concentrate in rills and then gullies of increasing proportions. Manning's equation can be used where roughness coefficients exist for such flow. Alternatively, where values are given for grassed waterways, unpaved gullies, and paved areas, the average velocity can be obtained using Equation 5.38.

Flow in gullies empties into channels or pipes. Open channels are assumed to begin where either the blue stream shows on U.S. Geological Survey quadrangle sheets or the channel is visible on aerial photographs. For all channel reaches in the watershed, cross-section information (for example, depth, area, and roughness) should be obtained. Average flow velocities are estimated with the use of Manning's equation or water surface profile information. The velocity should be computed for normal depth, which varies with the magnitude of the storm. Flows with return periods from 1.5 to 3 years often show bank full conditions, with inundation of the floodplain caused by flows greater than bank full.

5.6.4 Sheet Flow Travel Time

Runoff does not concentrate into well-defined flow paths such as gullies or swales at the upper reaches of a watershed. Instead, it flows over the surface at reasonably uniform, shallow depths. It is evident on long, sloping streets during rainstorms. The flow begins to converge into concentrated flow paths after some distance that have depths noticeably greater than that of the shallow flow. The distance from the upper end of the watershed or flow surface to the point where significant concentrated flow begins is termed the sheet flow length. For impervious surfaces, the sheet flow length can be several hundred feet for steep slopes. For shallow slopes or for pervious surfaces, concentrated flow will begin after relatively short sheet flow lengths.

In the upper reaches of a watershed, sheet flow runoff during the intense part of the storm will flow as a shallow layer with a reasonably constant depth. An equation, referred to as the kinematic wave equation for the equilibrium time, can be developed using Manning's equation with the assumption that the hydraulic radius equals the product of the rainfall intensity and the travel time, for example, $R_h = iT_t$. Using the velocity equation of Equation 5.37 with the travel time equal to the time of concentration, Manning's equation becomes

$$V = \frac{L}{60T_t} = \frac{1}{n} R_h^{2/3} \cdot S^{1/2} = \frac{1}{n}\left(\frac{iT_t}{60(1000)}\right)^{2/3} \cdot S^{1/2}, \tag{5.39}$$

where i is in millimeters per hour, T is in minutes, and L is in meters. Solving for the travel time yields

$$T_t = \frac{7.0}{i^{0.4}}\left(\frac{nL}{\sqrt{S}}\right)^{0.6}. \tag{5.40}$$

Equation 5.40 requires the rainfall intensity i for the time of concentration. Since T_t is not initially known, it is necessary to assume a value of T_t to obtain i from a rainfall IDF curve and then compute T_t. A new estimate of i is obtained from the IDF curve using the computed value of T_t. If the initial assumption for T_t was incorrect, the iterative process should be repeated until the value of T_t does not change.

To bypass the need to solve Equation 5.40 iteratively, Welle and Woodward (1986) assumed a power–model relationship between rainfall intensity and rainfall duration. Using a return period of 2 years, they substituted the 2-year, 24-hour rainfall depth for the rainfall intensity i and derived the following alternative model for Equation 5.40:

$$T_t = \frac{5.48}{P_2^{0.5}} \left(\frac{nL}{S^{0.5}} \right)^{0.8}, \tag{5.41}$$

in which L is the flow length (m), S is the average slope, P_2 is the 2-year, 24-hour rainfall depth (mm), and T_t is in min. Equation 5.41 has the important advantage that an iterative solution is not necessary.

The n values used in Equations 5.40 and 5.41 are given in Table 5.9 and are for very shallow flow depths, 0.1 ft or so; these values reflect the effects of raindrop impact; drag over plane surfaces; obstacles such as litter, crop ridges, and rocks; and erosion and transportation of sediment. The rainfall depth P_2 in Equation 5.41 can be obtained from an IDF curve such as in Figure 5.23.

Furthermore, these kinematic equations make the following assumptions: (1) no local inflow; (2) no backwater effects; (3) no storage effects; (4) the discharge is only a function of depth, for example, $q = ay^b$; and (5) planar, nonconverging flow. These assumptions became less realistic for any of the following conditions: the surface roughness increases, the slope decreases, or the length of the flow path increases. Recognizing that Equations 5.40 and 5.41 can yield unusually long times of concentration, limits are often, somewhat arbitrarily, placed on flow lengths. Common length limits are from 30 to 90 m. TR-55 (SCS 1986) places a limit of 90 m on Equation 5.41; however, many feel that this is too long and a shorter length of 30 m should be used. This limit would not necessarily apply to Equation 5.40. However, it should be recognized that the five assumptions given above can be violated for the other inputs, n and S.

TABLE 5.9
Manning's Roughness Coefficient (n) for Overland Flow Surfaces

Surface	n	Surface	n
Plastic, glass	0.009	Cast iron	0.015
Fallow	0.010	Smooth earth	0.018
Bare sand	0.010	Corrugated metal pipes	0.023
Graveled surface	0.012	Cement rubble surface	0.024
Smooth concrete	0.011	Conventional tillage	
Asphalt	0.012	No residue	0.09
Bare clay	0.012	With residue	0.19
Ordinary concrete lining	0.013	Grass	
Good wood	0.014	Short	0.15
Brick with cement mortar	0.014	Dense	0.24
Unplanned timber	0.014	Bermuda grass	0.41
Vitrified clay	0.015	Woods	
Light underbrush	0.40	No underbrush	0.20
Dense underbrush	0.80	Rangeland	0.13

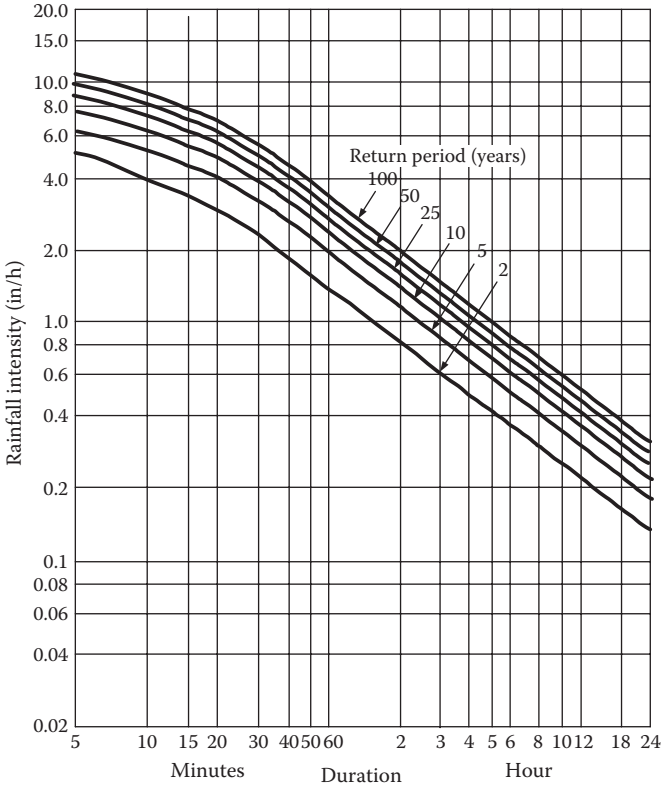

FIGURE 5.23 Typical rainfall intensity–frequency diagram developed by the National Weather Service.

Example 5.21

Consider a short-grass surface of 120 m in length and a slope of 0.2%. Assume that the local drainage policy requires use of a 10-year return period for design. Manning's n for short grass is 0.15 (see Table 5.9). When using IDF of Figure 5.23, estimate T_t.

Solution:

When using Equation 5.40, an estimate of T_t is used to obtain i from Figure 5.23. In this example, a T_t of 5 min is assumed; thus, the initial estimate of the intensity is 8 in/h (203.2 mm/h), which gives the following estimate of the sheet flow travel time:

$$T_t = \frac{7.0}{i^{0.4}}\left[\frac{0.15(120)}{(0.002)^{0.5}}\right]^{0.6} = \frac{255.8}{i^{0.4}} = \frac{255.8}{(203.2)^{0.4}} = 30.5\,\text{min.}$$

Since this is substantially greater than the initial estimate of 5 min, the revised travel time of 30.5 min is entered into Figure 5.23 to obtain a new estimate of the intensity, which is 4.0 in/h (101.6 mm/h). This produces a new estimate of T_t:

$$T_t = \frac{255.8}{(106.1)^{0.4}} = 40.3\,\text{min.}$$

A final iteration yields i = 3 in/h (76.2 mm/h) and T_t = 45 min.

As an alternative, the SCS kinematic wave equation could be used. From Figure 5.23, the 2-year, 24-hour intensity is 0.13 in/h (3.3 mm/h), which yields a P_2 of 79.2 mm. Thus, Equation 5.41 yields

$$T_t = \frac{5.48}{(79.2)^{0.5}}\left[\frac{0.15(120)}{(0.002)^{0.5}}\right]^{0.8} = 75\,\text{min}.$$

This is substantially greater than the 45 min obtained with Equation 5.40. The difference between the two estimates is due in part to the return period used and the structural coefficients of the two equations.

Example 5.22

Figure 5.24 shows the principal flow path for the existing and developed conditions of a small watershed. The characteristics of each section are given in Table 5.10, including the land use/cover, slope, and length. Estimate the time of concentration in each condition.

Solution:

Equation 5.38 is used to compute the velocity of flow for section A to B. k is obtained from Table 5.8 and is equal to 1.11.

$$V = kS^{0.5} = 1.11(0.07)^{0.5} = 0.294 \text{ m/s}.$$

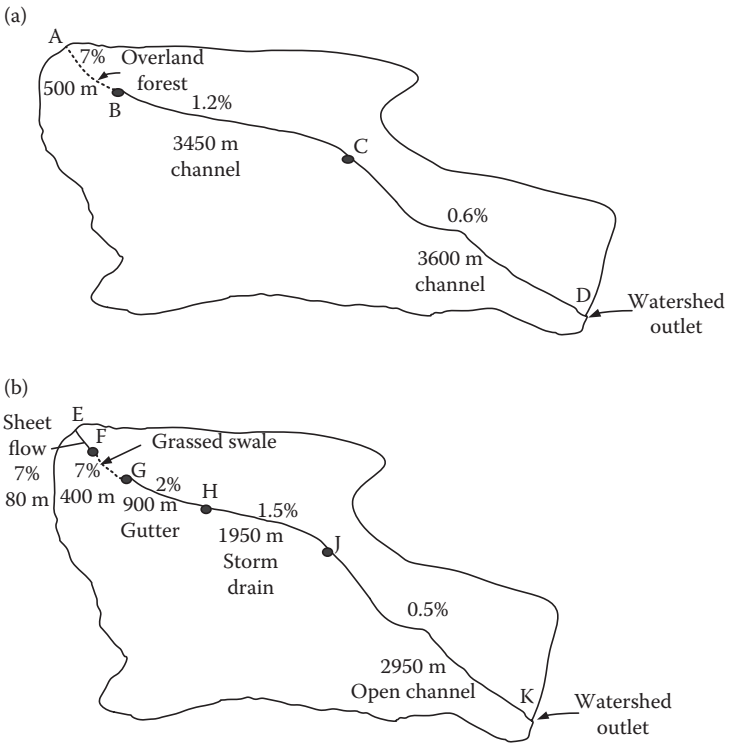

FIGURE 5.24 (a) Existing and (b) developed condition of the watershed in Example 5.22.

TABLE 5.10
Characteristics of Principal Flow Path: Example 5.22

Watershed Condition	Reach	Length (m)	Slope (%)	*n*	Land Use/Cover
Existing	A to B	500	7.0	–	Overland (forest)
	B to C	3450	1.2	0.040	Natural channel (trapezoidal): $w = 0.7$ m, $d = 0.3$ m, $z = 2{:}1$
	C to D	3600	0.6	0.030	Natural channel (trapezoidal): $w = 1.2$ m, $d = 0.7$ m, $z = 2{:}1$
Developed	E to F	80	7.0	0.013	Sheet flow: $i = 4.7/(0.285 + D)$; where i is expressed in mm/h, D is expressed in h
	F to G	400	7.0	–	Grassed swale
	G to H	900	2.0	–	Gutter flow
	H to J	1950	1.5	0.015	Storm drain ($D = 450$ mm)
	J to K	2950	0.5	0.019	Open channel (trapezoidal): $w = 1.5$ m, $d = 1.0$ m, $z = 1{:}1$

Thus, the travel time, which is computed using Equation 5.35, is

$$T_t = \frac{500 \text{ m}}{0.294 \text{ m/s}} = 1700 \text{ s} = 28.3 \text{ min}.$$

For the section from B to C, Manning's equation is used. For a trapezoidal channel, the hydraulic radius is

$$R_h = \frac{A}{WP} = \frac{dw + zd^2}{w + 2d\sqrt{1+z^2}} = \frac{0.3(0.7) + 2(0.3)^2}{0.7 + 2(0.3)\sqrt{1+(2)^2}} = 0.19 \text{ m}.$$

Thus, Manning's equation yields a velocity of

$$V = \frac{1}{0.040}(0.19)^{0.67}(0.012)^{0.5} = 0.9 \text{ m/s},$$

and the travel time is

$$T_t = \frac{3450 \text{ m}}{0.9 \text{ m/s}(60)} = 63.9 \text{ min}.$$

For the section from C to D, Manning's equation is used. The hydraulic radius is

$$R_h = \frac{0.7(1.2) + 2(0.7)^2}{1.2 + 2(0.7)\sqrt{1+(2)^2}} = 0.42 \text{ m}.$$

Thus, the velocity is

$$V = \frac{1}{0.03}(0.42)^{0.67}(0.006)^{0.5} = 1.44 \text{ m/s},$$

and the travel time is

$$T_t = \frac{3600\text{ m}}{1.44\text{ m/s}(60)} = 41.7\text{ min.}$$

Thus, the total travel time is the sum of the travel times for the individual segment:

$$t_c = 28.3 + 63.9 + 41.7 = 133.9\text{ min.}$$

For the developed conditions, the principal flow path is segmented into five parts (see Figure 5.24b). For the first part of sheet flow portion, Equation 5.40 is used. An initial time of concentration of 5 min is assumed and used with the 2-year IDF curve to estimate the intensity:

$$i = \frac{4.7}{0.285 + D} = \frac{4.7}{0.285 + 5/60} = 12.7\text{ mm/h.}$$

Thus, Equation 5.40 yields a revised estimate of the travel time:

$$T_t = \frac{7.0}{12.7^{0.4}}\left(\frac{0.013(80)}{\sqrt{0.07}}\right)^{0.6} = 5.75\text{ min.}$$

Since this differs from the initial estimate of 5 min, the intensity is recomputed from IDF relationship and a value of 12.3 mm/h results, which then yields the revised travel time of 5.83 min.

For the section from F to G, the flow path consists of grass-line swales. Equation 5.38 and Table 5.8 can be used to compute the velocity:

$$V = 23.49(0.07)^{0.05} = 6.21\text{ m/s.}$$

Thus, the travel time is

$$T_t = \frac{L}{V} = \frac{400\text{ m}}{6.21\text{ m/s}(60\text{ s/min})} = 1.1\text{min.}$$

For the segment G to H, the principal flow path consists of paved surface and gutters. Thus, Equation 5.38 and Table 5.8 is used:

$$V = 14.95S^{0.5} = 14.95(0.02)^{0.5} = 2.11\text{ m/s,}$$

and the travel time is

$$T_t = \frac{900\text{ m}}{2.11\text{ m/s}(60\text{ s/min})} = 7.1\text{min.}$$

The segment from H to J is a 450 mm pipe; thus, Manning's equation is used. The full flow hydraulic radius is one-fourth of the diameter ($D/4$); hence, the velocity for the full flow is

$$V = \frac{1}{0.015}\left(\frac{0.45}{4}\right)^{0.67}(0.015)^{0.5} = 1.89\text{ m/s,}$$

and the travel time is

$$T_t = \frac{L}{V} = \frac{1950 \text{ m}}{1.89 \text{ m/s}(60 \text{ s/min})} = 17.2 \text{ min.}$$

The final section J to K is an improved trapezoidal channel. The hydraulic radius is

$$R_h = \frac{wd + zd^2}{w + 2d\sqrt{1+z^2}} = \frac{1.5(1.0) + (1.0)^2}{1.5 + 2(1.0)\sqrt{1+1.0^2}} = 0.58 \text{ m.}$$

Manning's equation is used to compute the velocity:

$$V = \frac{1}{0.019}(0.58)^{0.67}(0.005)^{0.5} = 2.58 \text{ m/s,}$$

and the travel time is

$$T_t = \frac{L}{V} = \frac{2950 \text{ m}}{2.58 \text{ m/s}(60)} = 19.1 \text{ min.}$$

The total travel time through the watershed after development would be

$$t_c = \sum T_t = 5.8 + 1.1 + 7.1 + 17.2 + 19.1 = 50.3 \text{ min.}$$

The time of concentration for developed condition is reduced to 38% of the t_c for the existing condition.

The overland flow processes are less important than the channel processes when estimating time of concentration. The contribution of the upland area overland flow to the overall time of concentration can usually be neglected. Therefore, the principal flow path is usually taken as channel segments that are homogeneous in roughness, slope, and flow depth. Manning's equation is used to compute the velocities in the segment of the principal flow path. After determining the roughness and slope in each segment, the hydraulic radius is estimated to be used in time of concentration determination.

Example 5.23

Consider the data in Table 5.11 for a 52 km^2 watershed.

The given drainage area in this table is the total area upstream of the station. The channel length L is the length between stations. The depth (d), which is used as the hydraulic radius, is estimated based on empirical relations available for the study region. Determine the time of concentration for this watershed.

Solution:

Manning's equation is used to compute velocity, and Equation 5.35 is used to compute reach travel time (T_t) (see Table 5.12).

Therefore, the time of concentration of the watershed, which is equal to the sum of the travel time of different subwatersheds, is 41.31 min.

TABLE 5.11
Characteristics of Watershed in Example 5.23

Station	A (km²)	n	S	L (m)	d (m)
1	10	0.052	0.007	2840	2.1
2	24	0.047	0.006	1960	2.7
3	37	0.044	0.005	1420	3.1
4	52	0.043	0.005	1410	3.4

TABLE 5.12
Computed Travel Time in Example 5.23

Station	V (m/s)	T_t (min)
1	2.64	17.93
2	3.21	10.18
3	3.43	6.90
4	3.73	6.30

5.6.5 Empirical Formulas

There are a variety of empirical methods for estimation of time of concentration; nine methods will be reviewed here. Not all the methods were originally presented as equations for computing the time of concentration; therefore, it was necessary to adjust the empirical equations so that they would compute t in hours. For those methods designed to predict the lag time, the computed lag values were multiplied by a constant; the value of the constant depended on the definition of the lag. A value of 1.417 was used for the lag defined as the time difference between the centers of mass of rainfall excess and direct runoff, determined on the basis of the relationship between the time lag and the time of concentration for an SCS triangular hydrograph. This assumption is probably unimportant; that is, the results of comparisons are insensitive to this assumption. A conversion factor of 1.67 was used for methods in which the lag was defined as the time difference between the center of mass rainfall excess and the peak discharge; this constant was also based on analysis of a triangular hydrograph. Again, the use of this conversion factor would not be expected to affect the accuracy of the methods.

5.6.5.1 The Carter Lag Equation for Partially Sewered Watersheds

Using data from the Washington, DC, area, Carter (1961) calibrated an equation for predicting the watershed lag for watersheds that have natural channels and partially sewered land uses. The length (L_m in km) and slope (in m/m) variables in the equation should be measured from the longest channel:

$$t_c = 58.1 \cdot L_m^{0.6} \cdot S_m^{-0.03}, \tag{5.42}$$

where t_c is the time of concentration (min). The data used to calibrate the equation included watersheds less than 20 km² in area, with channel lengths less than 11.5 km and slopes less than 2%. Manning's coefficients for the channels varied between 0.013 and 0.025. While the input variables reflect the channel characteristics, one must assume that the coefficients reflect a significant amount of pipe flow because the watersheds were in urbanized areas and Manning's n suggests a concrete surface.

5.6.5.2 The Eagleson Lag Model

Eagleson (1962) presented an equation for predicting the time between the center of gravity of the rainfall excess and the peak of direct runoff; Equation 5.43 includes a factor for converting the time lag to a time of concentration:

$$t_c = 0.0165 \cdot L_f \cdot n \cdot R_h^{-2/3} \cdot S_f^{-1/2}, \tag{5.43}$$

where L_f is the hydraulic length (m), R_h is the hydraulic radius (m), S_f is the slope of the principal flow path (m/m), and t_c is the time of concentration (min). The original equation was calibrated from data for watersheds less than 20 km^2. The variables used in calibrating the model were computed using the characteristics of the sewer system. The length, slope, and n value are for the main sewer, while R_h is for the main channel when flowing at full capacity. This is a "mixed" method.

5.6.5.3 The Espey–Winslow Equation

Espey and Winslow, as reported by Schultz and Lopez (1974) and Espey et al. (1966), calibrated an equation for predicting the time to peak using data measured in Houston from 1964 to 1967. Of the 17 watersheds, 6 were predominately rural; the remaining ones were urbanized. The watersheds ranged in size from 2.5 to 90 km^2. The length and slope variables were measured from the channel. The channelization factor ϕ was designed to measure subjectively the hydraulic efficiency of the drainage network. The value of ϕ is the sum of two parts, one indicating the amount of channel vegetation and the other indicating the degree of channel improvement. The impervious area factor represents the resistance of the overland flow portion of the travel time. Equation 5.44 includes a coefficient to convert the model from a time to peak to a time of concentration equation:

$$t_c = 43.75 \cdot \phi \cdot L_c^{0.29} \cdot S_c^{-0.145} \cdot I^{-0.6}, \tag{5.44}$$

where L_c is the channel length (m), S_c is the channel slope (m/m), I is the percent imperviousness, and t_c is the time of concentration (min). Because it includes variables for both overland and channel flow, it is considered to be a "mixed" method.

5.6.5.4 Federal Aviation Agency (FAA) Equation

Equation 5.45 was developed from airfield drainage data (FAA 1970):

$$t_c = 3.26(1.1 - C) \cdot L^{0.5} \cdot S^{-0.0333}, \tag{5.45}$$

where C is the rational formula runoff coefficient, L is the flow length (m), S is the slope (m/m), and t_c is the time of concentration (min). Thus, it is probably most valid for small watersheds where sheet flow and overland flow dominate. The length, slope, and resistance variables are for the principal flow path.

5.6.5.5 Kerby–Hathaway Formula

Kerby (1959) calibrated Equation 5.46 for computing the time of concentration on very small watersheds in which surface flow dominated:

$$t_c = 1.45 \cdot \left(\frac{nL}{S^{0.5}} \right)^{0.47}, \tag{5.46}$$

where L is the flow length (m), S_c is the slope (m/m), and t_c is the time of concentration (min). The length used in the equation is the straight-line distance from the most distant point of the

watershed to the outlet and is measured parallel to the slope until a well-defined channel is reached. Watersheds of less than 10 acres were used to calibrate the model; the slopes were less than 1%, and Manning's n values were 0.8 and less.

5.6.5.6 Kirpich's Methods

Kirpich (1940) calibrated two equations for computing the time of concentration (min) for small watersheds in Pennsylvania

$$t_c = 0.0032 \cdot L_c^{0.77} \cdot S_c^{-0.05} \tag{5.47}$$

and Tennessee

$$t_c = 0.0195 \cdot L_c^{0.77} \cdot S_c^{-0.385}. \tag{5.48}$$

The length (m) and slope (m/m) parameters in the equations are for the channel. The Tennessee watersheds range in size from 0.004 to 0.5 km^2, with slopes from 3% to 10%. The computed times of concentration should be multiplied by 0.4 and 0.2 for watersheds where the overland flow path is either concrete or asphalt and the channel is concrete lined, respectively.

5.6.5.7 The SCS Lag Formula

The SCS provided an equation for estimating the watershed lag, which was defined as the time in hours from the center of mass of the excess rainfall to the peak discharge.

$$t_c = 0.0134 L^{0.8} \left(\frac{1000}{CN} - 10 \right)^{0.7} S^{-0.05}, \tag{5.49}$$

where L is the watershed length (m) and S is the watershed slope (m/m). The CN is the curve number index, which will be defined further in Chapter 6. Equation 5.49 is intended for use on watersheds where overland flow dominates and was developed for nonurban watersheds. The SCS had recommended that the lag equation be used for homogeneous watersheds 8 km^2 and less.

5.6.5.8 The Van Sickle Equation

Van Sickle provided a time-to-peak equation calibrated from data collected in Houston, with drainage areas less than 36 mi. The equation is based on two length variables; the first, L_t (km), is the total length of all drainage ways and storm sewers greater than 36 in. in diameter, while the second, L_m (km), is the total basin length. The prediction equation reflects both channel and pipe flow; thus, it is a "mixed" method. Equation 5.50 includes a factor for converting the time-to-peak equation to predict the time of concentration:

$$t_c = 0.49 \left(\frac{L_t \cdot L_m}{\sqrt{S_f}} \right)^{0.13}, \tag{5.50}$$

in which S_f is the slope (m/m) and t_c is the time of concentration (min).

Example 5.24

Calculate the time of concentration of the watershed with the length of the main river being 2600 ft and the average slope being 2.5%. If the curve number has estimated 70, use the SCS equation for calculation.

Solution:

$$t_c = 0.0134L^{0.8}\left(\frac{1000}{CN}-10\right)^{0.7} S^{-0.05} = 0.0134(2600)^{0.8}\left(\frac{1000}{70}-10\right)^{0.7} (0.025)^{-0.05} = 127 \text{ min.}$$

5.7 LAND USE AND COVER IMPACTS

When raining begins, people use trees as a temporary shield to protect themselves from the rain during the initial part of the storm. As the trees act like a barrier, it indicates that a forested watershed decreases the intensity of the flood runoff in comparison to a watershed without tree cover.

Another example of the impacts of land cover on runoff volume and rates is rooftop. You can see that the flow from the downspouts on houses starts very shortly and then increases gradually. This remarkable situation is enhanced due to impervious rooftops, planar surfaces, and steep slopes; therefore, there is delay in the flow. On the other hand, on the grassy hill that has the same size as the rooftop, after similar flow over a rooftop, flow down will begin. The sum of the water infiltrates into the topsoil and the grass, causing delay, which is hydraulically rougher than the shingles on the roof. These examples illustrate that flow from surfaces that are impervious would have smaller travel times and greater volumes than flow over surfaces that are pervious under conditions having similar shape, size, and slope.

Land cover could affect the runoff characteristics of a watershed. These two conceptual examples explain these effects even if all characteristics of watersheds stay the same except for land cover; the runoff characteristics such as the volume and timing of runoff and maximum flood flow rate would change significantly. Consequently, cover and use of land are among the primary problems in the hydrologic analysis and design phase.

Many descriptors of land cover/use are used in hydrologic design. A frequently used quantitative description is the index of runoff potential. As presented in Chapter 5, C is used in the rational method to reflect the runoff potential of a watershed. When a runoff coefficient C takes a high value, it reflects an increase in the runoff potential. For instance, the runoff potential values for commercial properties is $C = 0.75$; this value for residential areas is $C = 0.3$ and that for forested areas is $C = 0.15$. A transformed land cover/use index is used by the SCS, which is similar to that used in the rational method in their models. SCS also uses the runoff curve number (CN) in order to combine land use with the hydrologic effects of soil type and antecedent moisture. The runoff curve number will be discussed in Chapter 6.

In hydrology, how one considers urban land covers (impervious surfaces) is significant. Urban development can be considered as a source of many hydrologic design problems. The percentage of imperviousness is commonly used. Percentage of imperviousness ranges characteristic of "high-density residential areas" and "commercial and industrial areas" are from 40% to 70% and from 70% to 90%, respectively. Impervious covers in urban areas are not bounded to the watershed surface; for example, channels and pipes are used. Channels may be lined with concrete to increase the flow capacity of the channel cross section and also to shed the flood water rapidly. However, this is often criticized because of the fact that it can move the flooding problem from an upstream reach to a downstream reach.

5.7.1 Forest Areas

Plant cover is a very important factor in the hydrologic cycle due to the unique effects of its canopy and root systems on precipitation interception, infiltration, percolation, surface detention and roughness, transpiration, snow accumulation, and snowmelt. Forest cutting usually redounds to an increase in water yield. If the cutting is conducted in watersheds with conifer species, followed by hardwoods, chaparrals, and grasses, the increase becomes most significant. A forested watershed is expected to produce a hydrograph with lower peak flow, smaller volume of runoff, and broader time base than if the watershed had been cleared, cultivated, and pastured.

For example, changes in hydrographs due to forests can be illustrated by the comparative hydrographs from two adjacent watersheds (elevations, 2880 to 3536 m) in the Fraser Experimental Forest, Colorado (Figure 5.25). One of the watersheds, Lexen (124 ha), was used as the control to evaluate the effects of forest cutting on streamflow in the treatment watershed, North Fork, Deadhorse Creek (41 ha). The subalpine forest in the treatment watershed was reduced by 36% through patch cut in 1977–1978. Prior to the harvest, the annual streamflow for the treatment watershed was 37% of the control watershed (15.0 vs. 40.4 cm). After the treatment, the streamflow increased to 55% of the control watershed (23.1 vs. 41.9 cm). The increase in flows due to forest removal appears on the rising limb of the hydrograph, mainly in May (Troendle 1983).

In southern pine-dominated east Texas, a regional analysis showed that a reduction of watershed forest area by 10%, other things being equal, would increase annual streamflow about 20 mm (Chang and Waters 1984). Differences between full forest cover watersheds and watersheds devoid of vegetation could be as much as 200 mm. This difference was much less than that reported in western Oregon (Harr 1983), greater than that in Arizona (Hibbert 1983), and about the same as that in West Virginia (Kochenderfer and Aubertin 1975). The inverse effect of forest on flood flows can be expressed by the general equation

$$Q_{dt} = a(A^b)/(F^c), \tag{5.51}$$

where Q_{dt} is the maximum flood discharge (m^3/s) for a period of d days with a return period of t years; A is watershed area (m^2); F is percent forested area; and a, b, and c are coefficients, varying with d, t, and region. This equation shows that an increase in percent forest area brings a decrease in the maximum peak discharge. This effect is more considerable for large watersheds than for small watersheds and for watersheds of lower forest coverage (Figure 5.26).

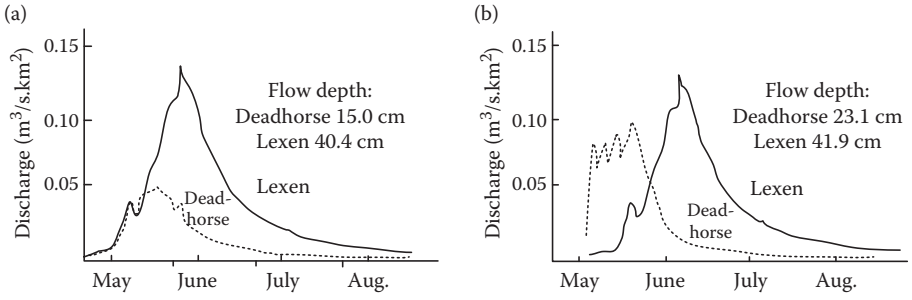

FIGURE 5.25 Comparative hydrograph for North Fork Deadhorse Creek (treatment) and Lexen Creek watersheds in the Fraser Experimental Forests, Colorado. (a) Before treatment, (b) after 36% of the subalpine forest in the North Fork Creek was cleared in patches of 1.2 ha each.

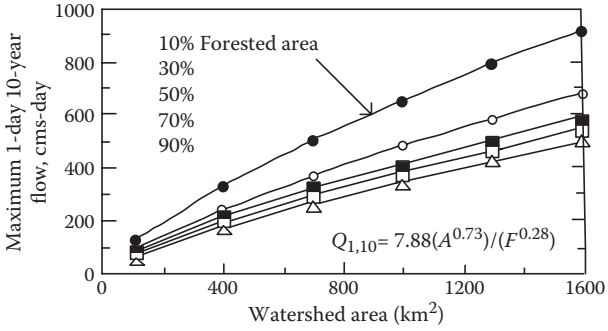

FIGURE 5.26 Maximum 1-day 10-year flow as a function of watershed area and percentage of forest cover.

5.7.2 Urban Areas

Land development has influences on how water naturally travels through the watershed. As mentioned above, about 50% of rainfall infiltrates into the ground with a natural ground cover, evaporation or plant transpiration make up 40% of rainfall (these together are called evapotranspiration), and only about 10% actually runs off the surface. Roads, houses, parking lots, sidewalks, and driveways are structures added onto the surface, as we develop the land, all of which are impervious surfaces. Water cannot pass through them as it can through soil; thus, instead of infiltrating, it is forced to either evaporate or run off.

Much of the evapotranspiration is due to plants, and because non-plant-friendly impervious surfaces are highly developed, evapotranspiration amount decreases and runoff increases. The rate of change in runoff is determined by the amount of impervious surface within a watershed. At 10–20% impervious (that is, medium-density residential areas), runoff is doubled but the amount of water infiltrating is reduced. At 30–50% impervious (similar to high-density residential developments), runoff is tripled, and at 75–100% impervious (such as commercial areas), the majority of rainfall becomes runoff, and infiltration is less than one-third of what it was prior to development (Figure 5.27).

The results of increased runoff and reduced groundwater are twofold. First of all, much higher flows than naturally would occur in streams due to the large amount of excess runoff, besides the flow rate increases much more rapidly and drops off more rapidly after the storm. Second, as infiltration volumes are reduced, less water is available to be released slowly into the stream over time, which results in lower water levels between rainfall events. In summary, under natural conditions, a certain amount of water

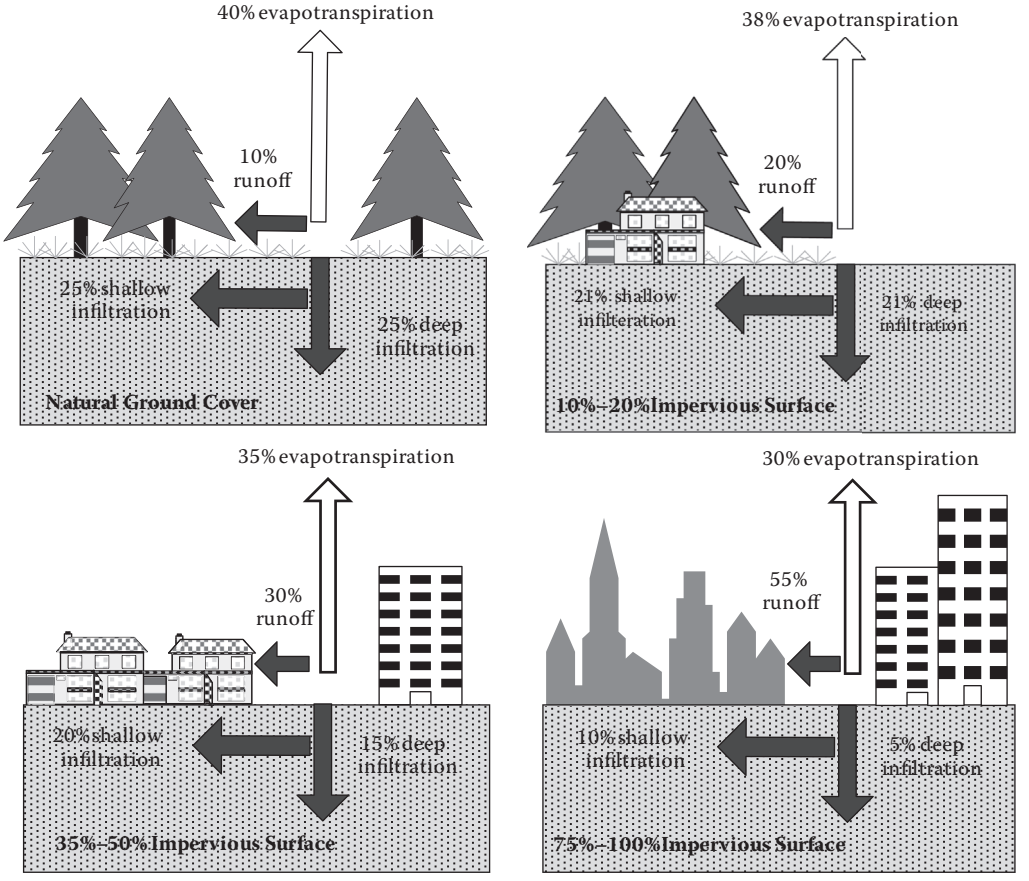

FIGURE 5.27 Effect of land use on runoff volume.

would infiltrate into the ground and would slowly make its way into nearby creeks; however, under urbanized conditions, that amount of water would run off and enter the stream all at once.

5.7.3 Wetland Areas

A distinctive hydrologic property of a landscape is wetland areas; this is mainly because of their position as a transition zone, that is, between aquatic and terrestrial ecosystems. Aspects of both aquatic and terrestrial environments are found in wetlands due to their position. Most of the available freshwater and marine aquatic environments, such as lakes, rivers, estuaries, and oceans, are characterized as having permanent water. However, terrestrial environments are generally characterized as having drier conditions, with an unsaturated (vadose) zone present for most of the annual cycle. As a result, the transition zone between predominantly wet and dry environments is occupied by wetlands.

One feature of wetlands that is very diagnostic is the proximity of the water surface (or water table below the surface) relative to the ground surface. In freshwater and marine aquatic habitats, the water surface lies well above the land surface; however, in terrestrial environments, it lies some distance below the root zone as a water table or zone of saturation. Unique biogeochemical conditions are created by the shallow hydrologic environment of wetlands that distinguish it from aquatic and terrestrial environments.

The water level, hydro pattern, and residence time are three hydrologic variables that are useful in characterizing wetland hydrologic behavior. A brief introduction of these concepts follows next. The general elevation of wetland water levels relative to the soil surface is considered as a hydrologic descriptor. Open water usually occurs in deeper areas where few, if any, emergent macrophytes exist. Any vegetation in these areas is not usually bonded to the wetland bottom, but vegetation may be floating on the surface of the water. An emergent zone may also be present in areas that are shallower than the open water zone, having substantial quantities of emergent macrophytic vegetation, either living or dead. However, it is possible for other wetlands to have large areas of exposed, saturated soil that is generally covered with macrophytic vegetation. Therefore, the water level can be used as an indicator of the vegetation types that probably occur in each of these zones.

In wetland hydrology, the second descriptor is the temporal variability of water levels. Wetland hydro pattern incorporates the timing, duration, and distribution of water levels into the duration and frequency of water level perturbations. Some systems' hydro pattern, such as tidal marshes, experience dramatic fluctuation over short periods of time, whereas in other systems, such as seasonally flooded bottomland hardwood communities, fluctuation is much slower over time. However, there are other more static wetland systems that may not display substantial short- or long-term variability. A function of the net difference between inflows and outflows from the atmosphere, groundwater, and surface water constitutes the wetland hydro pattern.

A third descriptor of wetland hydrology is the residence, or travel time, of water movement through the wetland. Water may be exchanged quickly in some wetland systems, with water remaining within the wetland for only a short duration of time, while water may travel very slowly through other wetland systems. The ratio of the volume of water within the wetland to the rate of flow through the wetland defines the residence time. When the flow through the wetland is large compared to its volume, the residence time is short and when the flow is small compared to its volume, residence time will be long. The residence time is often related to the hydro pattern of that wetland; a wetland with large water level fluctuations may have shorter residence times, such as in tidal marshes. On the other hand, fluctuations of some wetlands might be rapid due to large changes in inflow, yet they have very long residence times due to slow loss rates.

5.8 CONCLUDING REMARKS

Most of the hydrologic processes, especially those related to the surface water, are studied in the watershed scale. This makes it possible to consider the process in a closed system and therefore

simplifies the modeling. Furthermore, the characteristics of the watershed highly affect the behavior of the surface water, which is highly important in design and engineering processes. One of the most important characteristics is time of concentration, which is important in flood management practices, which will be further discussed in Chapter 12.

In this chapter, the methods of delineating the watershed and characterizing its shape, topology, and drainage system were discussed. The different approaches and methods used in estimating the time of concentration were discussed and examined through different examples. Due to the importance of land use on the runoff production, the main types of land uses were introduced and their effects on the runoff were discussed.

PROBLEMS

1. Two adjacent subwatersheds have characteristics as follows: Subarea 1: length = 2500 m; elevation drop = 52 m. Subarea 2: length = 1200 m; elevation drop = 65 m. Compute the slope of each subarea. Can you legitimately conclude that the average watershed slope for the entire area is the average of the two subarea slopes? Explain.
2. For the hypothetical watershed in Figure 5.28, compute the hypsometric curve and compute D_m, L_d, F_p, and H_a.
3. Construct two hypothetical, rectangular watersheds, A and B. The tops and bottoms of the watersheds have elevations of 150 m and 100 m, respectively. On watershed A, 50%, 75%, and 90% of the watershed area lies above elevations of 145, 130, and 115 m, respectively. On watershed B, 10%, 25%, and 50% of the watershed area lies above elevations of 145, 130, and 115 m, respectively. Construct the hypsometric curves and relate the curves to the flood potential of the two watersheds.
4. Derive expressions for computing the shape parameters (LC, L, L_i, R_e) of an elliptical watershed with lengths for the major and minor axes $2a$ and $2b$, respectively. Assume the watershed outlet is located at one end of the major axis.
5. Compute the channel slope between sections 1 and 6 and for each of the five reaches of the given data in Table 5.13. Compute the average of the computed slopes for the five reaches and compare it to the estimate for the entire reach. Discuss the results.
6. Compute the average channel slope using the station data from Problem 5.
7. Find the drainage density for the given watershed in Figure 5.29. The reach lengths, in miles, are shown in the figure (area = 80 km^2).

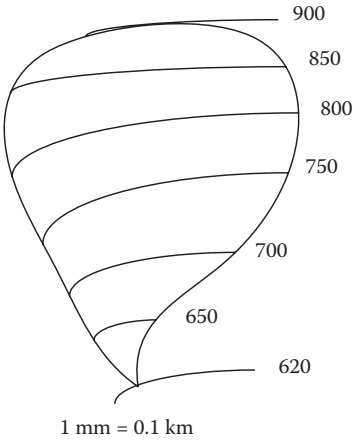

FIGURE 5.28 Watershed in Problem 2.

TABLE 5.13
Characteristics of River Reach in Problem 5

Section	Elevation (m)	Distance from Outlet (m)
1	150	0
2	168	4100
3	170	5020
4	190	8100
5	220	11,500
6	234	12,340

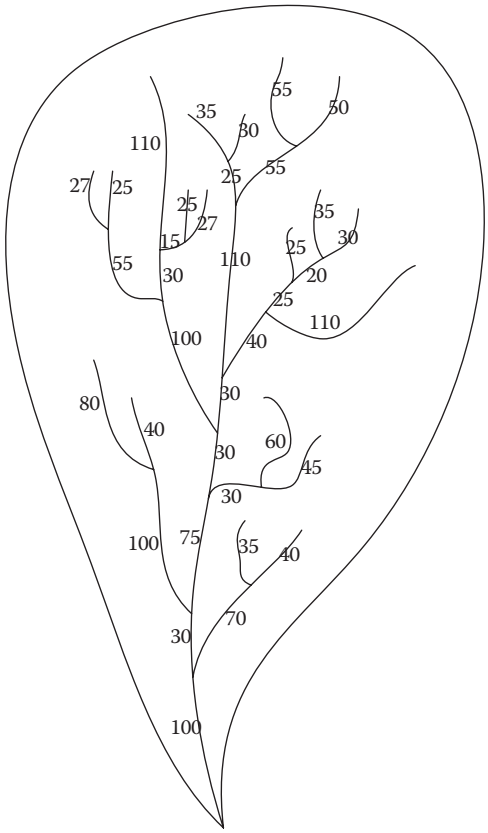

FIGURE 5.29 Watershed in Problem 7.

TABLE 5.14
Stream Data of Watershed in Problem 9

Stream Orders	Stream Number	Stream Length (km)	Stream Area (km²)
1	44	2.12	17.5
2	15	3.02	8.6
3	4	7.15	5
4	1	13.4	1.6

8. In a watershed, the number of streams of orders 1 to 6 is 42, 56, 19, 9, 3, and 1, respectively. Compute the bifurcation ratio.
9. The number, length, and area of each stream order are shown in Table 5.14. Compute the bifurcation ratio and the relations for estimation of stream number, total length, and area of different orders in this watershed.
10. Calculate the time of concentration of the watershed where the length of the main river is 3000 m and the average slope is 0.02. If the curve number is estimated at 80, use the SCS equation for calculation.
11. Using the velocity method, find the concentration time of a 1.6 ha drainage area which is primarily forested, with a natural channel having a good stand of high grass. The data of Table 5.8 can be used to estimate the time of concentration. The length and slope of the forested area are 100 km and 0.2% and the channel length is 20 km with a slope of 0.5%.
12. Consider a smooth concert surface of 30 m in length at a slope of 0.15%. If the rain intensity is 125 mm/h, calculate the estimated travel time.
13. Calculate the time of concentration of the dense grass watershed where the length of the main river is 2000 m, the length of drainage is 1200 m, and the average slope is 2%. If the curve number is estimated at 70, use the equations below for calculation.
    a. Kerby–Hathaway formula
    b. Kirpich's methods
    c. Van Sickle equation
14. Which one of the following characteristics is not a measure of basin shape? (a) The length to the center of area, (b) the elongation ratio, (c) the drainage density, (d) the circularity ratio.
15. Horton's stream order is a measure of (a) the drainage density, (b) the relative stream lengths, (c) the ratio of stream areas, (d) stream branching within a watershed.
16. The hypsometric curve is a description of (a) the relation between stream order and the proportion of the drainage area associated with that stream order, (b) the cumulative relation between elevation and area within (time of travel) isochrones, (c) the cumulative relation between elevation and area within elevation intervals, (d) the relation between elevation and rainfall intensity within elevation intervals.
17. Which one of the following is not a factor in controlling times of concentration of watershed runoff? (a) The drainage density, (b) the roughness of the flow surface, (c) the rainfall intensity, (d) the flow lengths, (e) all of the above are factors.

REFERENCES

Benson, M.A. (1962). *Factors Influencing the Occurrence of Floods in a Humid Region of Diverse Terrain: U.S. Geological Survey Water-Supply*, Paper 1580-B, 64p.

Carter, R.W. (1961). Magnitude and Frequency of Floods in Suburban Areas, U.S. Geological Survey Prof. Paper 424-B, B9-B11.

Chang, M. and Waters, S.P. (1984). "Forests and other factors associated with streamflows in east Texas," *Water Resource Bulletin*, 20, 713–719.

Eagleson, P.S. (1962). "Unit hydrograph characteristics for sewered areas," *Journal of the Hydraulics Division*, ASCE, 88 (HY2), 1–25.

Espey, W.H., Morgan, C.W., and Masch, F.D. (1966). *A Study of Some Effects of Urbanization on Storm Runoff from a Small Watershed*. Texas water development board, Austin, Texas. 3p.

Federal Aviation Agency. (1970). Dept. of Trans. Advisory Circular on Airport Drainage, Rep. AIC 150-5320-5B, Washington, DC.

Gray, D.M. (1961). "Interrelationships of watershed characteristics," *Journal of Geophysics Research*, 66, 1215–1223.

Harr, R.D. (1983). "Potential for augmenting water yield through forest practices in western Washington and western Oregon," *Water Resource Bulletin*, 19, 383–394.

Hibbert, A.R. (1983). "Water yield improvement potential by vegetation management on western rangelands," *Water Resource Bulletin*, 19, 375–381.

Horton, R.E. (1945). "Erosional development of streams and their drainage basins, hydrophysical approach to quantitative morphology," *Geological Society America Bull*, 56, 275–370.
Johnstone, D. and Cross W.P. (1949). *Elements of Applied Hydrology*, Ronald Press, New York.
Kerby, W.S. (1959). "Time of concentration for overland flow," *Civil Engineering*, 29 (3), 174.
Kirpich, Z.P. (1940). "Time of concentration of small agricultural watersheds," *Civil Engineering*, 10 (6), 362.
Kochenderfer, J.M. and Aubertin, G.M. (1975). Effects of management practices on water quality and quantity: Fernow Experimental Forest, West Virginia. In *Municipal Watershed Management, Sym. Proc.*, U.S. Forest Service Gen. Tech. Rep. NE-13, pp. 14–24.
Lane, L.J. (1975). *Influence of Simplifications of Watershed Geometry in Simulation of Surface Runoff*, Ph.D. Dissertation, Colorado University, Fort Collins, Colo., 198 pp.
Laurenson, E.M. (1962). *Hydrograph Synthesis by Runoff Routing*, Report No. 66, Water Research Lab., University of South Wales, UK.
McCuen, R. (1998). *Hydrologic Analysis and Design*, Prentice-Hall, London.
Morisawa, M.E. (1958). "Measurement of drainage basin outline form," *Journal of Geology*, 66, 587–591.
Schulz, E.F. and Lopez, O.G. (1974). *Determination of Urban Watershed Response Time*, Colorado State University, Fort Collins, Colorado.
Soil Conservation Service (SCS). (1986). *Urban Hydrology for Small Watersheds,* Tech. Release 55, Washington, DC.
Taylor, A.B. and Schwrz, H.E. (1952). "Unit-hydrograph lag and peak flow related to basin characteristics," *Transactions, American Geophysical Union*, 33(2), 235–246.
Troendle, C.A. (1983). "The potential for water yield augmentation from forest management in the Rocky Mountain region," *Water Resource Bulletin*, 19, 359–373.
Welle, P.I. and Woodward, D. (1986). *Time of Concentration*, Hydrology technology Note No. N4, USDA, Soil Conservation Service, NETC.

6 Surface Water Hydrology

6.1 INTRODUCTION

Surface runoff is the excess water that flows over the land when soil is infiltrated to full capacity. This is a major component of the hydrologic cycle. Surface runoff can be generated either by rainfall or by the melting of snow, ice, or glaciers. The interaction between precipitation and surface runoff is highly dependent on meteorological factors and the physical geology and topography of the catchment.

The portion of the runoff that moves over the land surfaces to reach smaller channels is called overland flow and includes building up and draining off the storages over the surface. The overland flow has a small length and depth and the flow is in the laminar regime. Flows of small channels join and form larger streams, which finally reach the basin outlet. The rate of surface runoff is usually recorded at the basin outlet gauge for practical purposes.

Streamflow is highly variable through time. The main result of streamflow fluctuations is that it is highly dependent to the resulting runoff from precipitation in the watershed. Rainfall can result in rivers rising, even if the rains are very far up in the watershed. The responses of rivers of different sizes varies with storms and rainfall. The rise and fall rate in large rivers is much slower than in small rivers.

In many practices and engineering design problems, the maximum volume flow rate passing the basin outlet during a storm event—peak discharge—is needed. It is a primary design variable for the design of stormwater runoff facilities. However, peak discharge is inadequate for design problems where watershed or river storage is significant. Where storage is significant, design work is usually based on hydrographs rather than on peak discharge rates. A hydrograph is a time record of the discharge of a stream, river, or watershed outlet. It consists of flow in all the three phases of runoff, which are surface runoff, interflow, and baseflow.

A hydrograph is a representation of how a watershed responds to rainfall. It is the result of integrated effects of a wide variety of catchment and rainfall parameters having complex interactions. Thus, the same storms in two different catchments produce different hydrographs, and in a given catchment, the hydrographs of two storms would be different. The storm and catchment characteristics and their complex interactions result in complex hydrographs. These complicated hydrographs are theoretically disaggregated into a set of simple hydrographs for analytical purposes.

In addition to watershed characteristics that affect basin response to rainfall, there are some manmade structures such as reservoirs and channels that affect the outlet hydrograph. In small catchments or short channels, these effects are not very important, but by increasing the length of stream channels and the size of the contributing areas, the storage in the stream channels and reservoirs increases and the processes occurring through channels and reservoirs become more important. The process of computing the progressive time and shape of a surface flow wave at successive points along a river or successive times at the reservoir outflow is known as flow routing.

This chapter starts with methods of estimation of runoff volume and peak discharge and then discusses and analyzes the development of the hydrograph, which is the main focus of this chapter. Different concepts related to hydrographs such as unit hydrograph, synthetic hydrographs, and adjustment of hydrographs are discussed in this chapter through different examples. Flow routing in reservoirs and channels is covered in the last part of this chapter.

6.2 ESTIMATION OF RUNOFF VOLUME

Total runoff volume and peak discharge are primary design variables in hydrology. Total runoff volume is used in the design of reservoirs and any other storage facilities. Peak discharge corresponds to the maximum volume flow rate passing a particular location during a storm event. Peak discharge is needed for the design of surface water drainage facilities such as pipe systems, storm inlets and culverts, and small open channels. Also, in some hydrologic planning, such as design and sizing of detention facilities in urban areas, peak discharge is used. It is an acceptable design variable for designs where the time variation of storage is not a primary factor in the runoff process. In this section, Soil Conservation Service (SCS) and rational methods used for estimating runoff volume and/or peak discharge are discussed.

6.2.1 SCS Method

This empirical procedure, which is also called the runoff curve number (CN) method, is presented by the SCS (1986) to calculate excess rainfall (runoff). The rainfall excess in this method is quantified using a CN. This is a basin parameter that varies from 0 to 100, and its value is dependent on the hydrologic soil group, the soil cover type and condition, the percentage of impervious areas in the considered area, and the initial moisture condition of the soil. If the considered area is composed of several subareas with different CNs, a weighted average (based on area) or composite CN should be estimated for the entire area. The recommended CN values for various land-use types are given in Table 6.1. CNs for four soil groups (A to D) are given in this table. These groups are defined by SCS (1986) according to their minimum infiltration rate. The soil of group A has the maximum infiltration capacity, whereas the soil of group D has the lowest infiltration capacity. The soil textures of these groups are as follows:

- Group A includes sand, loamy sand, and sandy loam.
- Group B includes silt loam and loam.
- Group C includes sandy clay loam
- Group D includes clay loam, silty clay loam, sandy clay, silty clay, and clay.

The given CNs in Table 6.1 are for average moisture conditions before a rainfall. The urban CNs given in Table 6.1 for commercial, industrial, and residential districts are composite estimated based on the average percent imperviousness displayed in the second column. Antecedent soil moisture is a determining factor in the volume and rate of runoff. Regarding this important factor, SCS has considered three classes of antecedent soil moisture conditions labeled as AMC I, AMC II, and AMC III. The soil conditions of each class are defined as follows:

> AMC I: Dry soils, but before reaching the wilting point, satisfactory cultivation has taken place.
> AMC II: Average conditions.
> AMC III: The soil is saturated due to a heavy rainfall, or light rainfall and low temperatures in the last few days. Table 6.2 gives seasonal rainfall limits for the three antecedent soil moisture conditions.

In cases where the soil moisture is under condition AMC I or AMC III, the CN values are modified based on Table 6.3. The given CN values for AMC I and AMC III correspond to the envelope curves for real measurements of rainfall (P) and runoff (Q). This is because for a given watershed, similar storm events with almost equal values of P may result in different values of Q.

The CN values of Table 6.3 result from this variation in Q, and the variation was assumed to result from variations in antecedent soil moisture conditions. The given CN values for AMC I and

TABLE 6.1
Runoff CNs for Different Types of Land Uses

Land Use		CNs for Hydrologic Soil Group			
Land Cover Type and Condition	Average Percent of Impervious Area	A	B	C	D
Rural Areas					
Fallow					
Straight row with poor condition		77	86	91	94
Row Crops					
Straight row with poor condition		72	81	88	91
Straight row with good condition		67	78	85	89
Contoured with poor condition		70	79	84	88
Contoured with good condition		65	75	82	86
Contoured and terraced with poor condition		66	74	80	82
Contoured and terraced with good condition		62	71	78	81
Small Grain					
Straight row with poor condition		65	76	84	88
Straight row with good condition		63	75	83	87
Contoured with poor condition		63	74	82	85
Contoured with good condition		61	73	81	84
Contoured and terraced with poor condition		61	72	79	82
Contoured and terrace with good condition		59	70	78	81
Closed-Seeded Legumes or Rotation Meadow					
Straight row with poor condition		66	77	85	89
Straight row with good condition		58	72	81	85
Contoured with poor condition		64	75	83	85
Contoured with good condition		55	69	78	83
Contoured and terraced with poor condition		63	73	80	83
Contoured and terraced with good condition		51	67	76	80
Pasture or Range					
Poor condition		68	79	86	89
Fair condition		49	69	79	84
Good condition		39	61	74	80
Contoured with poor condition		47	67	81	88
Contoured with fair condition		25	59	75	83
Contoured with good condition		6	35	70	79
Meadow					
Good condition		30	58	71	78
Woods					
Poor condition		45	66	77	83
Fair condition		36	60	73	79
Good condition		25	55	70	77
Farmsteads		59	74	82	86

(*continued*)

TABLE 6.1 (Continued)
Runoff CNs for Different Types of Land Uses

Land Use			CNs for Hydrologic Soil Group			
Land Cover Type and Condition		Average Percent of Impervious Area	A	B	C	D
Fully Developed Urban Areas (Vegetation Established)						
Open Space (Lawns, Parks, Golf Courses, Cemeteries, etc.)						
Poor condition (grass cover < 50%)			68	79	86	89
Fair condition (grass cover 50% to 75%)			49	69	79	84
Good condition (grass cover > 75%)			39	61	74	80
Impervious Areas						
Paved parking lots, roofs, driveways, etc. (excluding right-of-way)			98	98	98	98
Streets and Roads						
Paved; curbs and storm sewers (excluding right-of-way)			98	98	98	98
Paved; open ditches (including right-of-way)			83	89	92	93
Gravel (including right-of-way)			76	85	89	91
Dirt (including right-of-way)			72	82	87	89
Urban Districts						
Commercial and business		85	89	92	94	95
Industrial		72	81	88	91	93
Residential areas by average lot size	Less than 500 m^2	65	77	85	90	92
	1000 m^2	38	61	75	83	87
	2800 m^2	30	57	72	81	86
	2000 m^2	25	54	70	80	85
	4000 m^2	20	51	68	79	84
	8000 m^2	12	45	65	77	82
Developing Urban Areas						
Newly graded areas (pervious areas only, no vegetation)			77	86	91	94

Source: SCS, *Urban Hydrology for Small Watersheds*, 1986. With permission.

TABLE 6.2
Total 5-Day Antecedent Rainfall (mm)

AMC	Dormant Season	Growing Season
I	Less than 1.2	Less than 3.6
II	1.2–2.75	3.6–5.25
III	More than 2.75	More than 5.25

TABLE 6.3
Modification of CN for Different Soil Moisture Conditions

AMC I (Dry)	AMC II (Normal)	AMC III (Wet)
100	100	100
87	95	98
78	90	96
70	85	94
63	80	91
57	75	88
51	70	85
45	65	82
40	60	76
35	55	74
31	50	70
26	45	65
22	40	60
18	35	55
15	30	50
12	25	43
9	20	37
6	15	30
4	10	22
2	5	13

AMC III show likely CN values, but what is needed for design purposes is the "most likely" value rather than an extreme value that is much less probable. The resulting uncertainty because of CN estimation should be incorporated in risk analysis.

Table 6.1 provides CN values for a number of urban land uses with a specific percent of imperviousness. For example, consider an urban area with a composition of commercial and pasture in good condition land uses. The CN values for commercial land use are based on an imperviousness of 85% and CN values of 89, 92, 94, and 95 are used for hydrologic soil groups A, B, C, and D, respectively. The CN values of pasture in good condition are also obtained from Table 6.1 and the weighted CN (CN_w) for this region is computed as follows:

$$CN_w = CN_p\,(1 - f) + fCN_{im}, \tag{6.1}$$

where f is the proportion (not percentage) of impervious areas, CN_{im} is the CN for the impervious area, and CN_p is the CN for the pervious area (39, 61, 74, or 80). To show the use of Equation 6.1, the weighted CN value for this region considering soil group A is estimated as follows: 39(0.15) + (0.85)89 = 81.5.

Many local drainage policies collect runoff from certain types of impervious land uses such as rooftops, driveways, and patios and direct it to pervious surfaces without any connection to storm drain systems. The decision makers who use these policies believe that disconnecting such impervious areas results in smaller and less costly drainage systems and, furthermore, increases groundwater recharge and improves water quality. However, before applying these policies, how much this disconnecting will affect the peak rates and volumes in the design of the drainage system should be evaluated.

Three variables are needed for estimating CNs for regions with some unconnected imperviousness including the CN of the pervious area, the percentage of the impervious area, and the percentage of the impervious area that is disconnected. The adjusted CN (CN_c) is estimated as follows:

$$CN_c = CN_p + f(CN_{im} - CN_p)(1 - 0.5r_{ut}), \tag{6.2}$$

where f is the fraction of impervious cover, CN_p is CN of the pervious area, CN_{im} is the CN for the impervious area, and r_{ut} is the ratio of the unconnected impervious area to the total impervious area.

Example 6.1

Consider the case of a drainage area having 25% imperviousness, a pervious area with a CN of 61, and 50% of unconnected imperviousness. Compute the adjusted CN for this basin for the current soil condition.

Solution:

The CN of impervious area is determined as 98 for the impervious areas in Table 6.1 for all soil conditions. Using Equation 6.2, the adjusted CN (CN_c) is calculated as follows:

$$CN_c = 61 + 0.25\ (98 - 61)(1 - 0.5(0.5)) = 68.$$

If the unconnected impervious area were not important for this region, the composite CN would be 70. This means that in this region, by disconnecting 50% of the impervious cover, the CN value will be reduced by 2. This reduction can result in peak discharge and runoff volume reduction.
Note: The proportion of impervious areas over the basin is a determining factor of runoff volume and should be well managed to avoid flash floods over the urban areas.

After estimating the basin CN, the runoff is calculated as follows:

$$R = \frac{\left(P - I_a\right)^2}{\left(P - I_a\right) + S_r}, \tag{6.3}$$

where R is runoff (excess rainfall) in millimeters, P is rainfall in millimeters, I_a is initial abstraction in millimeters, and S_r is potential maximum soil moisture retention in millimeters at the time runoff (as opposed to rainfall) begins.

The initial abstraction is composed of different parts including the intercepted water by vegetation, the surface depressions, evaporation, and infiltration before runoff formation. It is often assumed that $I_a = 0.2S_r$. Substituting this into Equation 6.3 results in

$$R = \frac{\left(P - 0.2S_r\right)^2}{P + 0.8S_r}. \tag{6.4}$$

This equation is valid if $P > 0.2S_r$. In other cases, R is considered to be equal to 0.1 I_a. The empirical relationship presented in Equation 6.5 is used for estimating S_r.

$$S_r = \frac{25,400 - 254CN}{CN}. \tag{6.5}$$

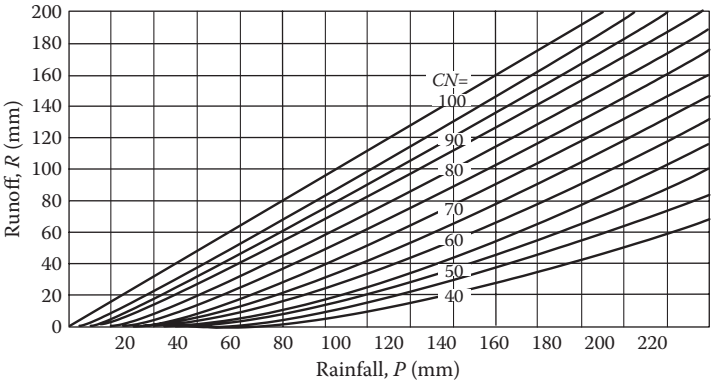

FIGURE 6.1 Graphical solution of Equations 6.5 and 6.4. (From SCS, *Urban Hydrology for Small* Watersheds, 1986. With permission.)

For given *CN* and *P* values, at first, S_r (mm) is calculated from Equation 6.5. Then *R* is determined from Equation 6.4. The family of curves given in Figure 6.1 represents a graphical solution to Equation 6.5. The CN method can be used to determine the total excess rainfall given the total rainfall. If the hyetograph of a rainfall is given, it can also be used to determine the rates of excess rainfall.

Example 6.2

A 400 km^2 watershed includes 350 km^2 of open area with 80% grass cover and 50 km^2 of an industrial district that is 72% impervious. The watershed is subjected to a 24 h rainfall with a total depth of 6.8 cm. Determine the total amount of excess rainfall. Assume that the soil of the watershed belongs to the hydrologic soil group B.

Solution:

From Table 6.1, *CN* = 61 for the open area and *CN* = 88 for the industrial district are used. The area-weighted composite CN representing the whole watershed is estimated as follows:

$$CN = \frac{(350\ \text{km}^2)(61) + (50\ \text{km}^2)(88)}{400\ \text{km}^2} = 65.$$

Substituting *P* = 6.8 cm and *CN* = 65 in Equations 6.4 and 6.5 (or Figure 6.1), *R* = 9.3 mm is obtained.

6.2.2 Rational Method

The rational method is an empirical relation between rainfall intensity and peak flow that is widely accepted by hydraulic engineers. It is used to predict the peak runoff from a storm event. Despite being one of the oldest methods, it is still commonly used especially in the design of storm sewers, because of its simplicity and popularity, although it contains some limitations that are not often treated. The peak runoff is calculated according to the following formula:

$$Q_p = k \cdot C \cdot i \cdot A, \tag{6.6}$$

where Q_p is peak flow [cms (cubic meters per second)], C is runoff coefficient, i is rainfall intensity (mm/h), A is drainage area (ha), and k is a conversion factor equal to 0.00278 for conversion of ha·mm/h to cms.

The rational method makes the following assumptions:

- Precipitation is uniform over the entire basin.
- Precipitation does not vary with time or space.
- Precipitation duration is equal to the time of concentration.
- A design storm of a specified frequency produces a design flood of the same frequency.
- The basin area increases roughly in proportion to increases in length.
- The time of concentration is relatively short and independent of storm intensity.
- The runoff coefficient does not vary with storm intensity or antecedent soil moisture.
- Runoff is dominated by overland flow.
- Basin storage effects are negligible.

It is important to note that all of these criteria are seldom met under natural conditions. In particular, the assumption of constant, uniform rainfall intensity is the least accurate. Hence, in watersheds with an area larger than about 2.5 km^2, the rational method should not be applied to the whole of the watershed. In these cases, the watershed is divided into some subdrainage areas considering the influence of routing through drainage channels. The rational method results become more conservative (i.e., the peak flows are overestimated) as the area becomes larger, because actual rainfall is not homogeneous in space and time.

The runoff coefficient, C, which is usually given as a function of land use, considers all drainage area losses. The runoff coefficient is affected by basin slope and soil type as well as the return period (T_r) of the considered storm. In Tables 6.4 and 6.5, the approximate C values considering different characteristics of the basin are given for rural and urban areas, respectively.

When the watershed is composed of multiple land uses, an area-weighted runoff coefficient is usually used in Equation 6.6. A better estimate of the rainfall coefficient is obtained from site measurements. There is often a considerable variation in C values in the analysis of actual storm data, but since a rational method gives a coarse estimate of rainfall losses, it could be useful. One of the major problems in applying the rational method is that it considers a constant rate of loss during the rainfall regardless of the total rainfall volume or initial conditions of the watershed. By increasing the imperviousness of the drainage area, this assumption becomes less important and the estimated runoff becomes closer to the observed value; in other words, Equation 6.6 gives almost exact values of runoff for a completely impervious area such as a rooftop.

The rainfall intensity (i) is determined using an intensity–duration–frequency (IDF) curve attributed to the studied watershed for a specified return period and duration equal to the time of concentration of the watershed (t_c). The effect of channels in large drainage areas should also be considered in t_c estimation. For this purpose, the wave travel times in channels and conduits, t_r (based on the wave speed, using an estimate of the channel size, depth, and velocity), along the flow pathways should be added to overland flow inlet times to yield an overall time of concentration.

For times less than watershed time of concentration, the total drainage area, A, should not be used in estimating watershed outflow, but after reaching the watershed equilibrium, an earlier and a higher intensity should be used. Because of the relation between t_c and the unknown intensity of the rainfall, an iterative solution that combines Equation 6.6 with the IDF curves is utilized. This iterative procedure could be easily followed as described in Example 6.3. The usage of IDF curves is further discussed in the next subsection.

6.2.2.1 IDF Curves

The total storm rainfall depth at a point, for a given rainfall duration and average return period, is a function of the local climate. Rainfall depths can be further processed and converted into rainfall intensities (intensity = depth/duration), which are then presented in IDF curves. The three variables,

TABLE 6.4
Runoff Coefficients for Rational Formula versus Hydrologic Soil Group (A, B, C, and D) and Slope Range—Rural Area

Soil Group		A			B			C			D		
Slope Range		0–2%	2–6%	6%+	0–2%	2–6%	6%+	0–2%	2–6%	6%+	0–2%	2–6%	6%+
Cultivated land	$T < 25$ years	0.08	0.13	0.16	0.11	0.15	0.21	0.14	0.19	0.26	0.18	0.23	0.31
	$T \geq 25$ years	0.14	0.18	0.22	0.16	0.21	0.28	0.2	0.25	0.34	0.24	0.29	0.41
Pasture	$T < 25$ years	0.12	0.2	0.3	0.18	0.28	0.37	0.24	0.34	0.44	0.3	0.4	0.5
	$T \geq 25$ years	0.15	0.25	0.37	0.23	0.34	0.45	0.3	0.42	0.52	0.37	0.5	0.62
Meadow	$T < 25$ years	0.1	0.16	0.25	0.14	0.22	0.3	0.2	0.28	0.36	0.24	0.3	0.4
	$T \geq 25$ years	0.14	0.22	0.3	0.2	0.28	0.37	0.26	0.35	0.44	0.3	0.4	0.5
Forest	$T < 25$ years	0.05	0.08	0.11	0.08	0.11	0.14	0.1	0.13	0.16	0.12	0.16	0.2
	$T \geq 25$ years	0.08	0.11	0.14	0.1	0.14	0.18	0.12	0.16	0.2	0.15	0.2	0.25

Source: McCuen, R., *Hydrologic Analysis and Design*, Third Edition, Pearson Prentice Hall, New Jersey, 2005. With permission.

TABLE 6.5
Runoff Coefficients for Rational Formula versus Hydrologic Soil Group (A, B, C, and D) and Slope Range—Urban Area

Soil Group		A			B			C			D		
Slope Range		0–2%	2–6%	6%+	0–2%	2–6%	6%+	0–2%	2–6%	6%+	0–2%	2–6%	6%+
Residential lot size 500 m^2	$T < 25$ years	0.25	0.28	0.31	0.27	0.3	0.35	0.3	0.33	0.38	0.33	0.36	0.42
	$T \geq 25$ years	0.33	0.37	0.4	0.35	0.39	0.44	0.38	0.42	0.49	0.41	0.45	0.54
Residential lot size 1000 m^2	$T < 25$ years	0.22	0.26	0.29	0.24	0.29	0.33	0.27	0.31	0.36	0.3	0.34	0.4
	$T \geq 25$ years	0.3	0.34	0.37	0.33	0.37	0.42	0.36	0.4	0.47	0.38	0.42	0.52
Residential lot size 1300 m^2	$T < 25$ years	0.19	0.23	0.26	0.22	0.26	0.3	0.25	0.29	0.34	0.28	0.32	0.39
	$T \geq 25$ years	0.28	0.32	0.35	0.3	0.35	0.39	0.33	0.38	0.45	0.36	0.4	0.5
Residential lot size 2000 m^2	$T < 25$ years	0.16	0.2	0.24	0.19	0.23	0.28	0.22	0.27	0.32	0.26	0.3	0.37
	$T \geq 25$ years	0.25	0.29	0.32	0.28	0.32	0.36	0.31	0.35	0.42	0.34	0.38	0.48
Residential lot size 4000 m^2	$T < 25$ years	0.14	0.19	0.22	0.17	0.21	0.26	0.2	0.25	0.31	0.24	0.29	0.35
	$T \geq 25$ years	0.22	0.26	0.29	0.24	0.28	0.34	0.28	0.32	0.4	0.31	0.35	0.46
Industrial	$T < 25$ years	0.67	0.68	0.68	0.68	0.68	0.69	0.68	0.69	0.69	0.69	0.69	0.7
	$T \geq 25$ years	0.85	0.85	0.86	0.85	0.86	0.86	0.86	0.86	0.87	0.86	0.86	0.88
Commercial	$T < 25$ years	0.71	0.71	0.72	0.71	0.72	0.72	0.72	0.72	0.72	0.72	0.72	0.72
	$T \geq 25$ years	0.88	0.88	0.89	0.89	0.89	0.89	0.89	0.89	0.9	0.89	0.89	0.9
Streets	$T < 25$ years	0.7	0.71	0.72	0.71	0.72	0.74	0.72	0.73	0.76	0.73	0.75	0.78
	$T \geq 25$ years	0.76	0.77	0.79	0.8	0.82	0.84	0.84	0.85	0.89	0.89	0.91	0.95
Open space	$T < 25$ years	0.05	0.1	0.14	0.08	0.13	0.19	0.12	0.17	0.24	0.16	0.21	0.28
	$T \geq 25$ years	0.11	0.16	0.2	0.14	0.19	0.26	0.18	0.23	0.32	0.22	0.27	0.39
Parking	$T < 25$ years	0.85	0.86	0.87	0.85	0.86	0.87	0.85	0.86	0.87	0.85	0.86	0.87
	$T \geq 25$ years	0.95	0.96	0.97	0.95	0.96	0.97	0.95	0.96	0.97	0.95	0.96	0.97

Source: McCuen, R., *Hydrologic Analysis and Design*, Third Edition, Pearson Prentice Hall, New Jersey, 2005. With permission.

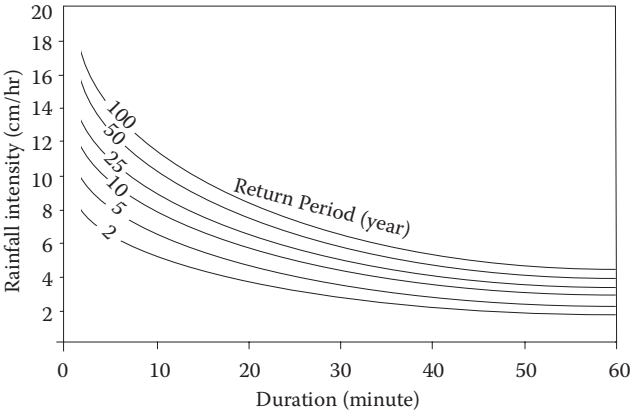

FIGURE 6.2 Typical IDF curve.

frequency, intensity, and duration, are all related to each other. The data are normally presented as curves displaying two of the variables, such as intensity and duration, for a range of frequencies.

IDF curves, the graphical symbols of the probability, summarize conditional possibilities (frequencies) of rainfall depths or average intensities. An important point that should be considered in applying IDF curves is that the intensities are averaged over the specified duration and do not represent actual time histories of rainfall. The contour for a given return period is the smoothed results of several different storms. Furthermore, the duration is not the actual length of a storm; rather, it is only a 20 min period, say, within a longer storm of any duration, during which the average intensity occurred to be the specified value. Since the IDF curves are really smoothed contours, unless a data point falls on a contour, they are completely hypothetical. A detailed description of the method of constructing IDF curves and the risks of inappropriate interpretations is given by McPherson (1978). An IDF curve for an urban area is presented in Figure 6.2.

The most common problem in applying IDF curves is that they are often misused to assign a return period to a storm with a specific depth or average intensity, or vice versa. Many combinations of average intensity and duration could result in a given depth, and as the duration decreases, the return period for a given depth increases. Since the durations on IDF curves are not the actual representatives of the storm durations, the curves can only be used to make an approximation of, say, the 20-year rainfall event on the basis of total depth. Instead, this should be done by a frequency analysis of storm depths on the time series of independent storm events.

The application of the IDF curves is almost limited to the rational method. As will be seen, the IDF data are properly applied in this case but it should be reiterated that

1. IDF curves do not represent time histories of real storms because the intensities are averaged over the indicated duration.
2. Data from several different storms are represented by a single curve.
3. The duration is not the duration of an actual storm and most likely represents a shorter period of a longer storm.
4. It is wrong to use IDF curves to obtain a storm event volume because the duration must be arbitrarily assigned.

Example 6.3

Determine the 25-year peak flow at the outlet of a 100 ha urban watershed. The corresponding IDF curve is given in Figure 6.3. Assume the time of concentration is 30 min, the watershed soil belongs to group B, and the land use pattern and slope are given in Table 6.6.

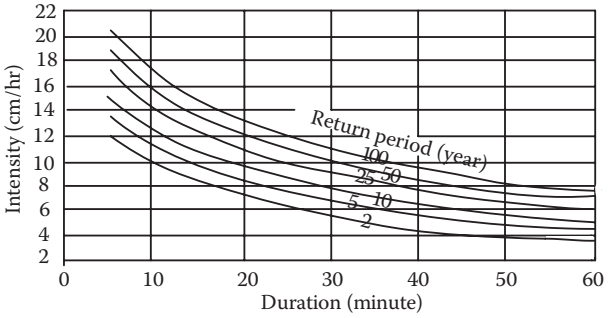

FIGURE 6.3 IDF curve in Example 6.3.

TABLE 6.6
Characteristics of the Watershed Considered in Example 6.3

Land Use	Area (ha)	Slope (%)
Open space	12	1.5
Streets and sideways	28	1
Residential lot size 1000 m^2	47	2.1
Pasture	13	3

Solution:

At first, the runoff coefficients of different land uses are determined using Tables 6.5 and 6.4 as shown below:

Open space: 0.14
Streets and driveways: 0.8
Residential lot size 1000 m^2: 0.37
Pasture: 0.34

The area-weighted runoff coefficient of the whole watershed is estimated as follows:

$$\overline{C} = \frac{\sum A_i C_i}{\sum A_i} = \frac{12\times 0.14 + 28\times 0.8 + 47\times 0.37 + 13\times 0.34}{100} = 0.46.$$

From Figure 6.3, for a 30 min storm with a 20-year return period, the average intensity is estimated to be equal to 90 mm/h. The peak flow of this storm is calculated from Equation 6.6 as follows:

$$Q_p = 0.00278 \times 0.46 \times 90 \times 100 = 11.51 \text{ m}^3/\text{s}.$$

Note: The spatial distribution of different land uses over the catchment does not affect the runoff peak; however, the proportion of them highly affects the volume of runoff and its peak value. The peak value of a stream is highly dependent on the intensity of the rainfall as well as its duration.

6.2.3 Coefficient and Regression Methods

The application of regression techniques for estimation of peak flows is usually limited to large non-urban drainage areas. This technique has also been used by the U.S. Geological Survey (USGS) for relating the frequency analysis results to drainage area characteristics. In the simplest application of these models, the measured values of desired independent variables such as rainfall and dependent variables such as runoff are related to each other through a simple regression. The usually fitted linear equation to the observed rainfall runoff values has the following form:

$$R = C_m(P - S), \tag{6.7}$$

where R is the runoff depth, P is the rainfall depth, C_m is the slope of the fitted line (approximate runoff coefficient), and S is the depression storage (depth).

It should be noted that in the above equation, depths are forecasted, not flows. Depth and volume are often used interchangeably because they are equivalent (runoff volume is equal to runoff depth multiplied by the drainage area). In this model, it is assumed that until the depression storage is filled by rainfall, the runoff depth will be zero. When S is negative, the equation can be rewritten to specify a positive interception on the runoff axis through adding a constant positive value to the right side of the equation. This situation may happen when there is a baseflow that contributes to runoff even if the rainfall depth is zero. Slope C_m is approximately equivalent to the runoff coefficient, except that losses due to depression storage are not considered. Equation 6.7 becomes more accurate as the duration of analysis increases to month and year from individual storm events. It is suggested that this equation not be used in situations with considerable carryover in the drainage area storage (Diskin 1970).

6.3 HYDROGRAPH THEORY

Although numerous engineering design problems require peak discharge estimates, they are inadequate in design cases when storage or the duration of flooding is important. This is also true when the watershed or channel storage is significant. In these cases, design work is usually based on hydrographs rather than on peak discharge rates. Hydrographs are used to estimate the variations of flow based on the recorded/given hyetograph of a specific rainfall after subtracting the rainfall losses (Figure 6.4). Hydrographs are commonly used for design of structures at nonhomogeneous watersheds, such as where significant variation in land use, soil types, or topography exists within the watershed such as urbanization or deforestation.

The conceptual frameworks used for hydrograph analysis involves the following items (Figure 6.4):

1. The rainfall hyetograph is separated into three time-dependent functions of the initial abstraction, the loss function, and the rainfall excess. A part of the rainfall that occurs prior to the start of direct runoff is considered as initial abstraction. The rainfall excess is equal to the direct runoff volume. The water loss occurs when direct runoff begins mostly due to infiltration. In some literature, two components are considered for rainfall hydrograph, and it is considered that the initial abstraction is a part of the loss function. To emphasize the differences between the important processes of the hydrologic cycle and for more clarity, the three-component process is used in this chapter.
2. The separation of the runoff hydrograph into two parts of direct runoff and baseflow. The direct runoff results from rainfall excess. The accumulated water in the watershed from past storm events that will appear as streamflow regardless of the current storm event happening usually forms baseflow.
3. The identification of the unit hydrograph as the transfer function or unit hydrograph, which is the function that transforms the rainfall excess into the direct runoff.

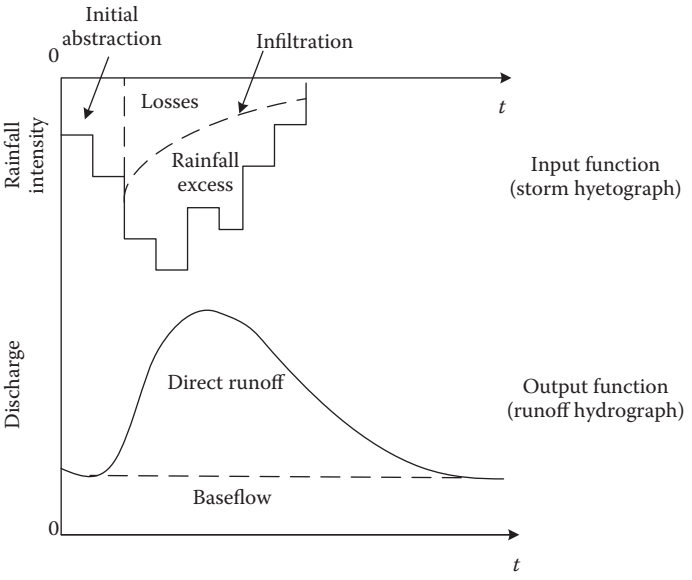

FIGURE 6.4 Concept of rainfall–runoff process.

The process of hydrograph analysis begins by separating the baseflow from the total runoff hydrograph to develop the direct runoff hydrograph (DRH). Baseflow is usually a smooth function and can be estimated more accurately in comparison with other hydrograph components; therefore, baseflow separation is considered as the first step in hydrograph analysis. After estimation of the baseflow and DRHs, the volume of direct runoff is computed.

6.4 BASEFLOW ESTIMATION

As mentioned before, the total runoff hydrograph consists of two parts, direct runoff and baseflow. The process of separating the time distribution of baseflow from the total runoff hydrograph is referred to as hydrograph separation. Different methods have been proposed for hydrograph separation. Each method reflects a different view on the hydrologic process. The selection of the appropriate method for watershed analysis highly depends on the type and amount of available measured data, the required accuracy for the design problem, and the computational effort. In this section, four popular methods of baseflow separation are introduced. It should be noted that all the variables used in this section are defined in Figure 6.5.

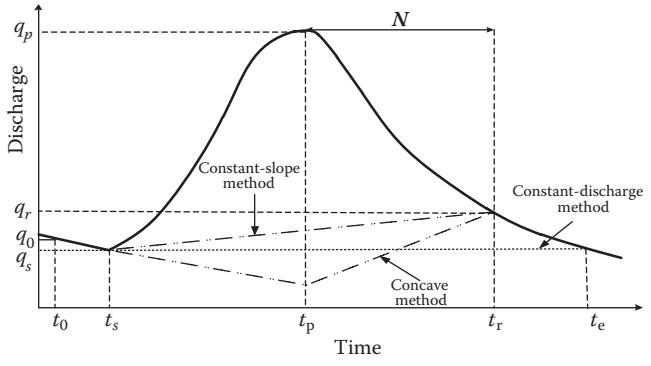

FIGURE 6.5 Baseflow separation methods illustration.

6.4.1 Constant-Discharge Baseflow

The constant-discharge method is the easiest method used to estimate baseflow. In this method, baseflow and direct runoff are separated by a straight line beginning at the point of the lowest discharge rate at the start of the flood runoff and extending at a constant discharge rate until it intersects the recession limb of the hydrograph (Figure 6.5). The baseflow is set by the lowest discharge rate, q_s, just prior to the start of the rising limb of the hydrograph. In some cases, instead of considering a constant value for baseflow, a straight line beginning from the lowest discharge value in the rising limb and extending with a constant slope until it intersects the recession limb of the hydrograph is considered for separating the total flow from baseflow.

Although this method is easily applicable, there are some weaknesses in the conceptual basis of the method. For example, the baseflow will continue to decrease beyond the start of the flood runoff, possibly to the time when the flood runoff is the maximum. Furthermore, it could also be argued that flow from groundwater storage begins before the time when the total runoff equals the baseflow rate prior to the start of flood runoff.

Example 6.4

The daily streamflow data for a river at a site having a drainage area of 7000 km^2 are given in Table 6.7. Separate the baseflow from the DRH by the constant-discharge baseflow method and estimate the depth of the direct runoff.

Solution:

The baseflow has been considered to have a constant value of 1550 cms. The direct runoff is obtained by subtracting 1550 cms from the given runoff values. In each time interval, the runoff volume is estimated and the total runoff volume is divided by the basin area to obtain the runoff depth. The results are given in Figure 6.6 and Table 6.8.

$$\text{Runoff} = 33{,}150\left(\text{m}^3 \cdot \text{day/s}\right) \times \frac{24 \times 60 \times 60 \text{ s}}{1 \text{ day}} = 2864.16 \times 10^6 \text{m}^3.$$

$$\text{Depth} = \frac{2864.16 \times 10^6 \text{m}^3}{7000 \times 1 \times 10^6 \text{m}^2} = 0.41 \text{ m}.$$

TABLE 6.7
Daily Streamflow Data for the River in Example 6.4

Time (day)	Flow (m^3/s)	Time (day)	Flow (m^3/s)
1	1600	9	2800
2	1550	10	2200
3	5000	11	1850
4	11,300	12	1600
5	8600	13	1330
6	6500	14	1300
7	5000	15	1280
8	3800		

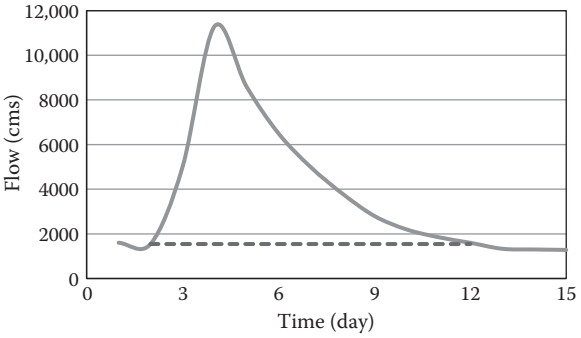

FIGURE 6.6 Separation of baseflow from direct runoff.

TABLE 6.8
Direct Runoff Estimation

Time (day)	Direct Runoff (m^3/s)	Average Runoff (m^3/s)	Duration (day)	Runoff × Time ($m^3 \cdot day/s$)
1	0	0	1	0
2	0	1725	1	1725
3	3450	6600	1	6600
4	9750	8400	1	8400
5	7050	6000	1	6000
6	4950	4200	1	4200
7	3450	2850	1	2850
8	2250	1750	1	1750
9	1250	950	1	950
10	650	475	1	475
11	300	175	1	175
12	50	25	1	25
13	0			
Total				33,150

Note: A considerable part of river flow is baseflow, which is usually related to recharge of river by groundwater. Therefore, analysis of river–groundwater interaction is an important issue in river flow management.

6.4.2 Constant-Slope Baseflow

In this method, it is just necessary to select the point on the recession limb where direct runoff ends. This is due to the runoff process conceptualization that considers that flow from groundwater aquifers begins on the hydrograph recession prior to the point used for the constant-discharge method. Different methods are used for identifying this point. In the most common method, the inflection point on the hydrograph recession is considered. At the inflection point, the hydrograph changes from being concave to convex (i.e., the slope of the hydrograph changes from greater than 1 to less than 1). An empirical formula can also be used for estimation of the needed point in this method. A typical relation proposed for very large watersheds is as follows:

$$N = 1.21A^{0.2}, \tag{6.8}$$

where N is the number of days between peak time of the measured runoff hydrograph and the end of direct runoff and A is the drainage area (km^2). After identification of the point at which direct runoff ends, direct runoff and baseflow are separated by connecting a straight line extending from the point of the lowest discharge rate at the start of the flood runoff to the identified point on the recession limb (Figure 6.5). The baseflow depends on the time and discharge at the low point of the discharge function and the time and discharge at the identified point on the recession limb.

6.4.3 Concave Baseflow

The starting and ending points for the line separating baseflow and direct runoff in the concave method are the same as those for the constant-slope method. In the concave method, baseflow decreases with a constant slope until the time of the peak discharge of the hydrograph. This slope of baseflow decrease is the same as the slope at the start of the hydrograph. After that, a straight separation line is considered between time of the peak discharge and the inflection point on the recession (Figure 6.5). Although the application of the concave method needs a little more computational effort than the two other methods, it is probably a more realistic representation of the actual baseflow variations during a storm as determined by the physical processes that control flow during storm events.

Example 6.5

A hydrograph of a particular rain in a particular basin is shown in Figure 6.7. Separate the direct runoff using constant-discharge and concave separation methods and find the direct runoff. Assume the drainage area is 2590 km^2.

Solution:

In the constant-discharge method, shown in Figure 6.7, the baseflow is estimated to be 30 cms. Then, the direct runoff volume after subtracting the baseflow from total flow (Table 6.9) is calculated as follows:

$$\text{Volume (constant discharge)} = \{(1/2)\,[(0 + 15) + (15 + 40) + (40 + 54) + (54 + 44) + (44 + 20) + (20 + 0)\}\,(2 \text{ days} \times 86{,}400 \text{ s/day}) = 2.989 \times 10^7 \text{ m}^3.$$

$$\text{Amount of direct runoff} = 2.989 \times 10^7 \text{ m}^3/2590 \text{ km}^2 = 0.0115 \text{ m}.$$

Applying the concave method, the ending point of the hydrograph is first estimated; Equation 6.8 can be used for this purpose:

$$N = 1.21\,(2590)^{0.2} = 3.98 \text{ days}.$$

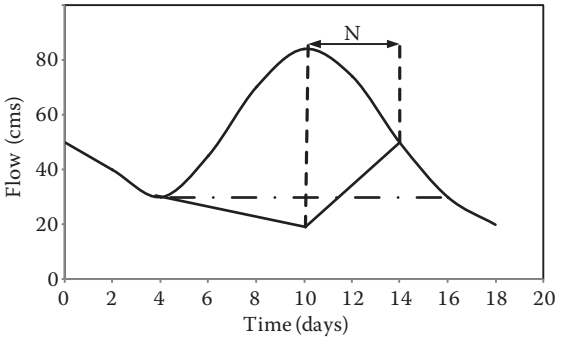

FIGURE 6.7 Hydrograph in Example 6.5.

TABLE 6.9
Results of Example 6.5

	Time (days)	4	6	8	10	12	14	16
	Q (cms)	30	45	70	84	74	50	30
Constant	Baseflow (cms)	30	30	30	30	30	30	30
discharge	Direct runoff (cms)	0	15	40	54	44	20	0
Concave	Baseflow (cms)	30	25	23	20	35	50	–
	Direct runoff (cms)	0	20	47	64	39	0	–

Then, the baseflow is determined as shown in Figure 6.7 and Table 6.9. Finally, the direct runoff volume is estimated as follows:

$$\text{Volume (concave)} = \{(1/2)\,[(0 + 20) + (20 + 47) + (47 + 64) + (64 + 39) + (39 + 0)\} \times (2 \text{ days} \times 86{,}400) = 2.9376 \times 10^7 \text{ m}^3.$$

$$\text{Amount of direct runoff} = 0.01134 \text{ m}.$$

Note. Amount of baseflow estimated using different methods of flow separation can be completely different. To use the most appropriate method for baseflow determination, it is important to take into account the river–aquifer interaction mechanism.

6.4.4 Master Depletion Curve Method

The master depletion curve method provides a model for estimation of baseflow provided from groundwater storage. This method helps to find the point on the recession where direct runoff ends and baseflow begins. Also, this method can be used to provide a model of the hydrograph recession limb. To employ this method, it is necessary to have a number of measured storm hydrographs for a variety of storm events in different seasons with different volumes. The procedure is as follows:

1. The recession limbs for each storm event are plotted in the form of log q versus time on separate pieces of semi-log papers (tracing paper).
2. The recession for the storm event having the smallest values of log q is plotted on a master sheet having a log q versus time-axis system (semi-log paper).
3. The tracing paper of the recession curve with the next smallest values of log q values is positioned such that the curve appears to extend along a line coincident with the recession of the first event plotted.
4. This process is continued using successively larger magnitude log q recessions until all storm events are plotted.
5. A master depletion curve that extends through the recessions of the observed storm events is constructed. Then, a mathematical model is fitted to the master depletion curve. The results of different practices show that the following functional form often provides a reasonable fit to the data:

$$q_t = q_0 e^{-k_f t}, \tag{6.9}$$

where q_t is the discharge at time t, q_0 is the discharge at time $t = 0$, and k_f is a fitting

coefficient. Any two points of the master depletion curve can be used to determine the value of k_f. Using q_0 as one point and solving Equation 6.9 for k_f yields

$$k_f = \frac{\ln q_0 - \ln q_t}{t}, \tag{6.10}$$

where t is the time at which discharge q_t is recorded. When there is a considerable scatter in the recession line, then the least-squares method could be used for estimation of k_f as follows:

$$k_f = \frac{\sum_{i=1}^{n} t_i \left(\ln q_0 - \ln q_i\right)}{\sum_{i=1}^{n} t_i^2}, \tag{6.11}$$

where n is the number of pairs of (q_i, t_i) points on the recession.

6.5 UNIT HYDROGRAPH

A flood hydrograph for a basin can be simulated using a unit hydrograph, defined as the direct runoff from a storm that produces unit of rainfall excess. Using the unit hydrograph method, the DRH at the watershed outlet for given excess rainfall resulting from a particular storm event is calculated. As the spatial variations of physical characteristics of the watershed are not directly entered in the runoff calculations of a unit hydrograph, it is classified as a lumped method. In other words, it is considered that the rainfall is time and space invariant even though in reality there are variations in rainfall intensity through time and space. This is a simplification assumption in unit hydrograph development. The accuracy of a unit hydrograph can be increased by division of basins into several smaller sub-basins. The watershed characteristics, through a mathematical procedure called a unit hydrograph, are combined. Although the unit hydrograph (UH) theory cannot be mathematically proven to be accurate, the unit hydrograph method is a useful tool for practical purposes due to its simplicity and usefulness due to its linear assumption.

The principal concept underlying the application of a unit hydrograph is that each basin has one unit hydrograph for a particular duration of the rainfall that does not change (in terms of its shape) unless the basin characteristics change. Because the physical characteristics (drainage area, slope, etc.) of a basin typically remain unchanged, changes in the unit hydrograph usually reflect changes in land-use patterns or urbanization. Given that the unit hydrograph does not change in shape and represents streamflow response to 1 unit of runoff (excess rainfall) within a basin, flood hydrographs for actual storms can be simulated by multiplying the discharge ordinates from a unit hydrograph by the excess rainfall computed from the observed rainfall record.

6.5.1 Definitions

There are five parameters that should be given special notice in the definition of unit hydrograph (UH) (McCuen 1998):

1. Unit rainfall excess: After developing a unit hydrograph, one should check that the sum of the ordinates become equivalent to 1 area depth of direct runoff.

2. Uniform spatial distribution of rainfall over the watershed (space invariant of rainfall): If the spatial distribution of rainfall over the watershed cannot be assumed to be uniform, the resulting unit hydrograph would not reflect the temporal characteristics of runoff.
3. A constant rainfall excess rate with time (time invariant of rainfall): This part of the definition is usually satisfied by acceptance of some departure from the constant rate because it is difficult to find storm events of significant volume where the excess rate is constant. Variation of the rainfall contributes to the size of the watershed. A hydrograph has a single peak value for a small watershed even if the rainfall period is short (5-minutes) but for large watershed the rainfall period should be several hours to get a single peak value.
4. Specific duration of rainfall excess: Since the peak and time to peak of a total rainfall hydrograph are sensitive to the duration of the rainfall excess, it must be specified when developing, and considered when using, a UH for design.
5. The uniform spatial distribution of watershed characteristics: As mentioned before, the unit hydrograph cannot include the spatial variations of watershed characteristics. Thus, the UH theory has no desirable results in watersheds with more than 5000 km^2 area (70 × 70 km). If the watershed's area is greater than this amount, the watershed must be divided into smaller subwatersheds in order to implement the UH theory. For example, if the rainfall intensity in the outlet point of the watershed is more than that upstream, the hydrograph will have a rapid rise, a sharp peak, and a rapid recession, and if the rainfall has a greater intensity upstream, the hydrograph will have a slow rise and recession and will have a wide and low peak.

A *T*-hour unit hydrograph is the hydrograph that results from a storm with a constant rate of rainfall excess of unit depth over duration of *T* hours. A special form of UH is developed when the duration of rainfall excess for a given UH becomes infinitesimally small. The resulting hydrograph is called instantaneous unit hydrograph (IUH). The intensity of the instantaneous rainfall excess is obviously not finite. Different types of IUH and the use of the concept of an IUH will be discussed later in this chapter. The dimensionless unit hydrograph is another form of unit hydrograph. In dimensionless unit hydrograph, the ordinates are given as ratios of the peak discharge and time axis is defined as the ratio of the time to the time to peak. In other words, a dimensionless UH has an axis system of y/q_p, versus t/t_p, where q_p is the discharge rate at the time to peak t_p. Before using a dimensionless UH, it is transformed to a *T*-hour UH. This form of UH is also further discussed in this chapter.

6.5.2 Limitations of Unit Hydrograph

The unit hydrograph has several assumptions that at first appearance would seem to make it inapplicable in many situations. The assumptions can be summarized as follows:

- The runoff that makes up stormflow is derived from rainfall excess overland flow. This is not a reasonable assumption to make in many areas of the world.
- The surface runoff occurs uniformly over the catchment because the rainfall is uniform over the catchment.
- The relationship between effective rainfall and surface runoff does not vary with time (i.e., the hydrograph shape remains the same between the data period of derivation and prediction). This would assume no land-use change within the catchment, as this could well affect the storm hydrograph shape.

Given the assumptions listed above, it would seem extremely irrational to use the unit hydrograph as a predictive tool. However, the unit hydrograph has been used successfully for many years in numerous different hydrological situations. It is a very simple method of deriving a storm hydrograph from a relatively small amount of data. The fact that it does work (i.e., produces meaningful

predictions of storm hydrographs), despite being theoretically flawed, would seem to raise questions about our understanding of hydrological processes. The answer to why it works may well lie in the way that it is applied, especially the use of effective rainfall. This is a nebulous concept that is difficult to describe from field measurements. Of course, in moving from actual to effective rainfall, there are different processes that are not completely understood and discount some of the assumptions listed above. Therefore, the unit hydrograph is a black box model of stormflow and as such hides many different processes within. The hydrograph shape is a reflection of the static characteristics and all the dynamic processes going on through runoff production in a catchment. Even though this makes hydrographs highly applicable, they cannot be explained in terms of hydrological theory because they are results of different complicated processes affecting the runoff production and some of them are not yet completely understood.

Example 6.6

The effective rainfall of 3 h duration has produced a flood hydrograph peak of 250 m^3/s. This flood hydrograph has a baseflow of 40 m^3/s. The average of watershed rainfall is 2 cm, and average loss rate is 0.2 cm/h. Compute the peak of a 3 h UH for this watershed.

Solution:

Regarding the effective rainfall duration and the given loss rate, the total loss is estimated as

$$\text{Amount of loss} = 0.2 \times 3 = 0.6 \text{ cm}.$$

Therefore, the amount of effective rainfall is equal to $2 - 0.6 = 1.4$ cm.

The peak of DRH is estimated by subtracting the peak minus the baseflow, equal to 210 m^3/s.

$$\text{Peak of 3 h UH} = 210/1.4 = 150 \ m^3/s.$$

The obtained peak corresponds to the 3 h rainfall producing 1 cm runoff over the watershed. Note: To generate the peak flow and hydrograph of direct runoff with depth other than one for a rainfall event with the same duration as the given unit hydrograph, it is just necessary to calculate the product of unit peak flow/hydrograph and depth of direct runoff.

Example 6.7

Considering the data given in Table 6.10, compute the 8 h UH for a 5400 km^2 basin.

TABLE 6.10
Data of 8-h Rainfall

Time (h)	Flow (m^3/s)	Baseflow (m^3/s)
1	132	132
2	250	130
3	400	125
4	740	125
5	530	118
6	420	115
7	350	100
8	220	98

TABLE 6.11
Calculations of Example 6.7

Time (h)	Total Flow (m^3/s)	Baseflow (m^3/s)	Direct Runoff (m^3/s)	Unit Hydrograph (m^3/s)
1	132	132	0	0.00
2	250	130	120	92.31
3	400	125	275	211.54
4	740	125	615	473.08
5	530	118	412	316.92
6	420	115	305	234.62
7	350	100	250	192.31
8	220	98	122	93.85

Solution:

Total flow is estimated by summation of recorded flows at different time steps and is equal to 3042 m^3/s. Total baseflow is calculated in the same way and is equal to 943 m^3/s. Therefore, the total direct runoff would be 2099 m^3/s. The rainfall depth is obtained by dividing the direct flow by the basin area as follows:

$$\text{Rainfall depth: } \frac{2099\,(\text{m}^3/\text{s}) \times 3600\,(\text{s})}{5400 \times 10^6\,(\text{m}^2)} = 0.0013\ \text{m}.$$

The ordinates of unit hydrograph with unit depth of 1 mm are obtained by dividing the DRH ordinates by 1.3, the depth of produced runoff over the basin. The results of different steps are given in Table 6.11.
Note: For construction of a unit hydrograph, one needs to determine the baseflow and subtract it from the measure flow to obtain the direct runoff.

6.5.3 Convolution

In the previous sections, different issues in unit hydrograph analysis were treated separately. Except for having the depths (or volumes) of rainfall excess and direct runoff equal, the separation of baseflow from direct runoff was independent of the separation of losses from rainfall excess. The transfer function for developing the unit hydrograph is identified after hydrograph separation analysis. The resulting unit hydrograph is used with a given storm to compute the design runoff hydrograph. The process by which the DRH is produced by the combination of the storm and the unit hydrograph is called convolution.

Conceptually different processes of multiplication, translation with time, and addition are included in convolution. The depth of rainfall excess at the first time step of duration D is multiplied by the ordinates of the D-hour UH. This is called the principal of proportionality. The UH is then translated for a time length of D and is multiplied by the depth of the next burst of rainfall excess. Then the produced hydrographs for each burst of rainfall excess of duration D are summed for each time interval. This is based on the principle of superposition. For a rainfall event with different intensities in different time steps, first, the rainfall hyetograph is decomposed to some pulses with constant intensity. The corresponding hydrographs are calculated for each of the pulses and then they are superpositioned considering the translation in time to result in the overall direct hydrograph. These principles are based on the linear behavior of the watershed, which is not true for real watersheds.

Usually, the processes of multiplication, translation, and addition are employed to derive a design runoff hydrograph from the rainfall excess and the basin UH. To further clarify the convolution process, some very simple examples are discussed to illustrate the multiplication–translation–addition operation. First, a part of rainfall excess of 2 cm that occurs over 2 h is considered. It is assumed that the UH consists of two ordinates, 0.3 and 0.7. First, the UH ordinates are multiplied by the rainfall excess depth to produce the direct runoff (Figure 6.8a). Regarding the definition of the direct runoff and rainfall excess, the depth of direct runoff equals the depth of rainfall excess, which here is considered to be 2 cm. If 4 cm of rainfall excess occurs over a period of 2 h, the depth of direct runoff would be 4 cm. The produced runoff hydrograph, using the UH of the previous example, is illustrated in Figure 6.8b. In both of these examples, the runoff hydrograph is computed solely by multiplication. In this example, the rainfall excess is just available at a single time interval of 2 h; therefore, some parts of the convolution process such as translation are not necessary.

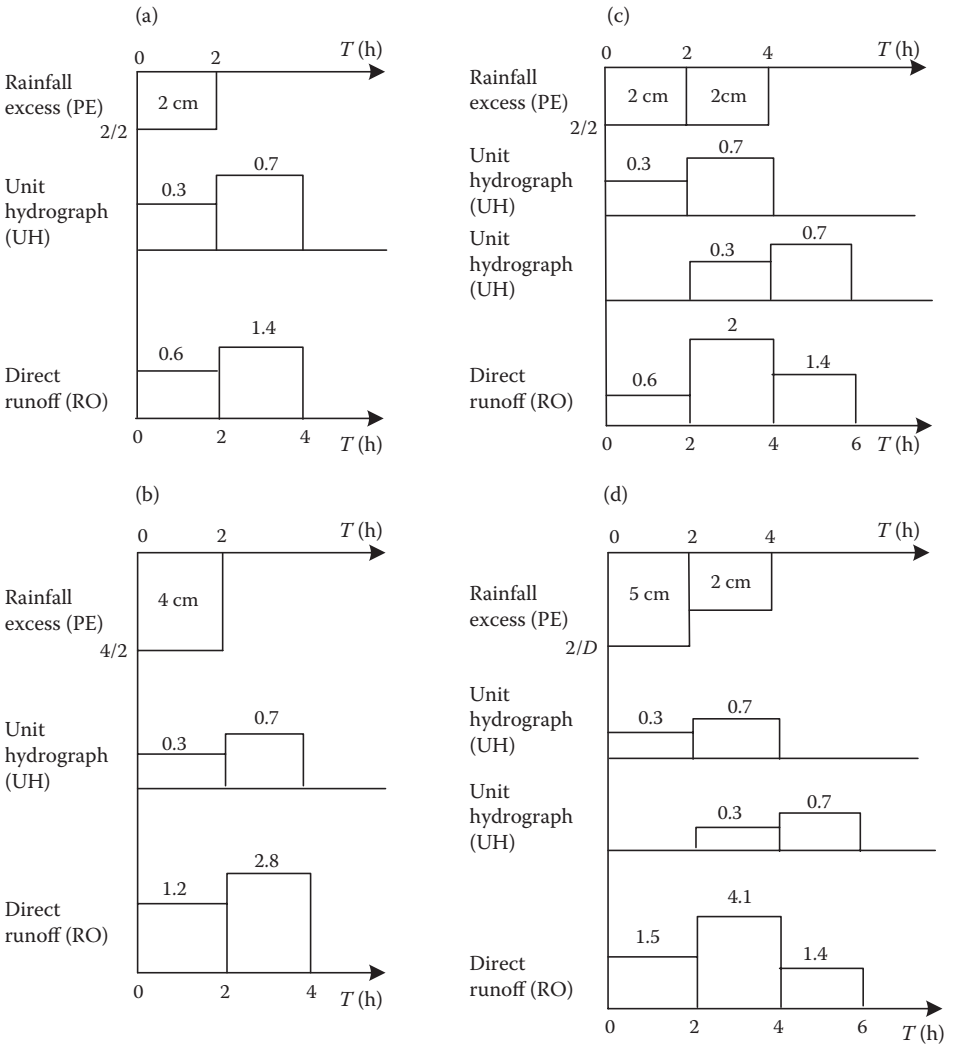

FIGURE 6.8 Illustration of different concepts of convolution: (a) runoff of excess rainfall of 2 cm in 2 h, (b) runoff of excess rainfall of 4 cm in 2 h, (c) runoff of excess rainfall of 4 cm in 4 h, (d) runoff of excess rainfall of 2 and 3 cm in the first 2 h and the succeeding 2 h, respectively.

In the next example, the entire convolution process of multiplication–translation–addition is illustrated. For this purpose, a 4 cm of rainfall excess that occurs uniformly over a period of 4 h is considered. This gives an intensity of 1 cm/h. In this example, similar to the previous example, the depth of direct runoff is 4 cm but the temporal distribution of direct runoff is completely different from that of the previous example due to the different time distribution of rainfall excess. Figure 6.8c shows the different parts of the convolution process (multiplication, translation, and summation) followed in this example. The time base of the runoff hydrograph is 6 h. Generally, the time base of the runoff (t_{bR}) is estimated as follows:

$$t_{bR} = t_{bD} + t_{bU} - D, \tag{6.12}$$

where t_{bD} and t_{bU} are the time bases of the rainfall excess and unit hydrograph, respectively, and D is the considered time interval. For this example, both t_{bD} and t_{bU} equal 2 h, and therefore, according to Equation 6.12, t_{bR} is equal to 6 h.

Here, another example is given to illustrate the convolution process. As illustrated in Figure 6.8d, the depth of rainfall excess equals 5 cm with 2 cm occurring in the first time unit and 3 cm in the next time unit. Therefore, the second ordinate of the runoff hydrograph is obtained by summation of 2 times of the second ordinate of the UH and 3 times of the first ordinate of the translated UH, which results in 2.7.

In summary, the governing convolution equation for the storm hydrograph in discrete form is called the convolution equation formulated as follows:

$$Q_n = \sum_{i=1}^{n} P_i U_{n-i+1} = P_n U_1 + P_{n-1} U_2 + \cdots + P_1 U_n, \tag{6.13}$$

where Q_n is the storm hydrograph ordinate, P_i is the rainfall excess, and U_j ($j = n - i + 1$) is the unit hydrograph ordinate.

Convolution Integral

The same convolution process described earlier is also used for continuous processes. For a continuous process, all of the issues included in the convolution process including multiplication, translation, and addition are done using convolution integral:

$$Q(t) = \int_0^t x(\tau) U(t - \tau)\, d\tau, \tag{6.14}$$

where $U(t)$ is the continuous function of UH often called IUH and $Q(t)$ is the continuous function of direct runoff. $x(\tau)$ is the computed time distribution of rainfall excess, and τ is the time lag between the beginning times of rainfall excess and the IUH of direct runoff (Figure 6.9).

In practice, the convolution integral of Equation 6.14 is treated in discrete form, which relates the time distributions of direct runoff $Q(t)$ with time distribution of rainfall excess $x(\tau)$ and the unit hydrograph $U(t - \tau)$:

$$Q(t) = \sum_{\tau=0}^{t} x(\tau) U(t - \tau). \tag{6.15}$$

This representation of the convolution process clearly indicates the multiplication, translation, and addition operations. The number of ordinates in the direct runoff distribution, the time base of

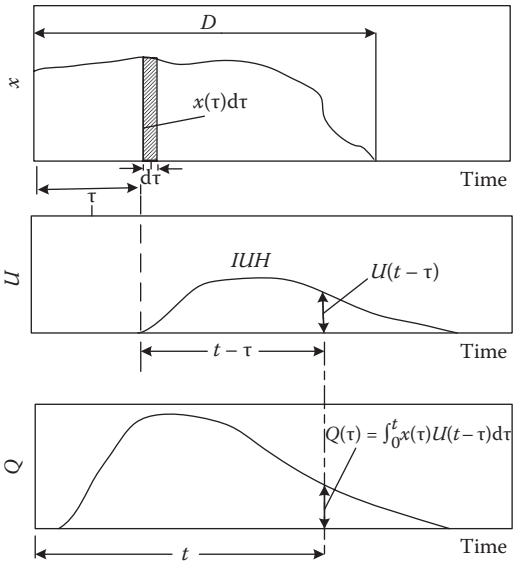

FIGURE 6.9 Schematic diagram of the convolution integral.

the runoff, is computed with Equation 6.12. The application of convolution integral in development of IUHs is discussed in Section 6.8.

Example 6.8

For the given rainfall excess hyetograph and 1 h unit hydrograph, compute the storm hydrograph for the corresponding watershed. Assume no losses, no infiltration, and no evaporation.

$$P_n = \{0.3, 0.5, 1.5, 0.2, 1\}\ \text{cm}$$

$$U_n = \{0, 200, 350, 270, 200, 125, 0\}\ \text{m}^3/\text{s}.$$

Solution:

Regarding Equation 6.13, the ordinates of direct hydrograph are computed as follows:

$$Q_n = P_n U_1 + P_{n-1} U_2 + P_{n-2} U_3 + \cdots + P_1 U_n.$$

Therefore,

$$Q_1 = (0.3)(0) = 0\ \text{m}^3/\text{s},$$

$$Q_2 = (0.5)(0) + (0.3)(200) = 60\ \text{m}^3/\text{s},$$

$$Q_3 = (1.5)(0) + (0.5)(200) + (0.3)(350) = 205\ \text{m}^3/\text{s}, \ldots$$

TABLE 6.12
Results for Example 6.8

Time (h)	P_1U_n	P_2U_n	P_3U_n	P_4U_n	P_5U_n	Q_n
0	0					0
1	60	0				60
2	105	100	0			205
3	81	175	300	0		556
4	60	135	525	40	0	760
5	37.5	100	405	70	200	812.5
6	0	62.5	300	54	350	766.5
7		0	187.5	40	270	497.5
8			0	25	200	225
9				0	125	125
10					0	0

The derived values from these calculations are tabulated in Table 6.12.

The DRH is given in Figure 6.10.

Note: To develop the hydrograph of some successive rainfall events, at first, the corresponding hydrographs of individual rainfall events are produced by multiplying the unit hydrograph in depth of direct runoff. The developed hydrographs are summed with the appropriate lag times to generate the final rainfall hydrograph. The important point is the duration of individual rainfall events that should be considered in the selection of unit hydrograph as well as delaying hydrographs before their summation.

Example 6.9

Construct a unit hydrograph from the hydrograph depicted in Figure 6.11 and given in Table 6.13 for a 2 h rainfall. The catchment area is 4.5 km^2. Use the constant value separation and construct a hydrograph representing the following complex rain pattern. The given values represent the excess rainfall depth (cm) in 2 h.

$$P = \{1.1,\ 2.1,\ 1.8\}$$

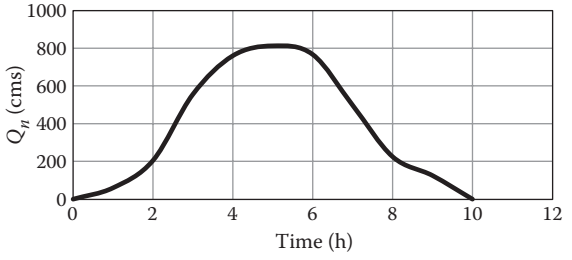

FIGURE 6.10 Derived storm hydrograph in Example 6.8.

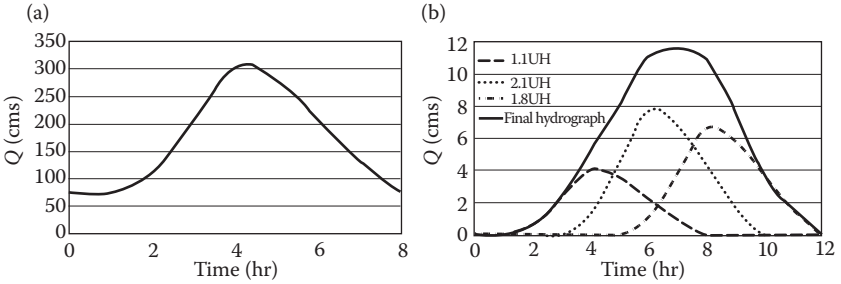

FIGURE 6.11 (a) Hydrograph in Example 6.9. (b) Development of hydrograph for a complex rainfall pattern.

TABLE 6.13
Calculation of Direct Runoff

t (h)	*Q* (m³/s)	Baseflow (m³/s)	Direct Runoff (m³/s)
1	75	75	0
2	110	75	35
3	205	75	130
4	305	75	230
5	280	75	205
6	205	75	130
7	130	75	55
8	75	75	0

Solution:

Volume of direct runoff is obtained as follows:

$$0.5\left[(0+35)+(35+130)+(130+230)+(230+205)\right.$$
$$\left.+(205+130)+(130+55)+(55+0)\right]\times(3600\,\text{s/h})=2.826\times10^{6}\,\text{m}^3$$

$$\text{Effective runoff}=\left(2.826\times10^{6}\,\text{m}^3\right)/\left(4.5\times10^{6}\,\text{m}^2\right)=0.628\ \text{m}.$$

The ordinates of UH are calculated by dividing the ordinates of the hydrograph by 62.8 cm (Table 6.14). The hydrograph of the complex rain is found by multiplying the ordinates of UH by the effective rain (rainfall minus the losses) and shifting the resulting hydrographs by 2 h and adding ordinates (Table 6.15).

TABLE 6.14
Ordinates of UH in Example 6.9

t (h)	Direct Runoff (m³/s)	UH (Direct Runoff/62.8) (m³/s)
1	0	0
2	35	0.56
3	130	2.07
4	230	3.66
5	205	3.26
6	130	2.07
7	55	0.88
8	0	0

TABLE 6.15
Ordinates of Complex Rainfall in Example 6.9

t (h)	UH	UH × 1.1	UH × 2.1	UH × 1.8	Hydrograph Ordinates
1	0.00	0	0	0	0
2	0.56	0.61	0	0	0.61
3	2.07	2.28	0	0	2.28
4	3.66	4.03	1.17	0	5.20
5	3.26	3.59	4.35	0	7.94
6	2.07	2.28	7.69	1.00	10.97
7	0.88	0.96	6.86	3.73	11.54
8	0.00	0	4.35	6.59	10.94
9		0	1.84	5.88	7.71
10		0	0	3.73	3.73
11		0	0	1.58	1.58

Baseflow (75 m^3/s) should be added to ordinates to obtain full hydrograph.
Note: In the development of a runoff hydrograph from a unit hydrograph, the baseflow should be extracted at first and in case of usage of unit hydrographs for streamflow generation, the baseflow should be added to the hydrograph to have an estimation of river flow.

6.5.4 Least-Squares Analysis of Unit Hydrographs

Least-squares regression is a convenient method for deriving unit hydrograph ordinates from rainfall excess and direct runoff ordinates. In this method, the rainfall excess is an independent variable and direct runoff is the dependent variable. For more clarity, the least-squares method is introduced using an example. In this example, it is assumed that the distribution of rainfall excess has two ordinates, P_1 and P_2, and the unit hydrograph has three ordinates, U_1, U_2, and U_3. The relationship between rainfall excess, the unit hydrograph, and the ordinates of the DRH (R_i, $i = 1, 2, \ldots, n$) is represented using the discrete form of the convolution integral as follows:

$$\begin{aligned} P_1U_1 &= R_1 \\ P_1U_2 + P_2U_1 &= R_2 \\ P_1U_3 + P_2U_2 &= R_3 \\ P_2U_3 &= R_4. \end{aligned} \tag{6.16}$$

There are four equations and three unknowns, which are the ordinates of the unit hydrograph in the above formulation. Equation 6.16 can be presented in matrix form as follows:

$$\begin{bmatrix} P_1 & 0 & 0 & 0 \\ P_2 & P_1 & 0 & 0 \\ 0 & P_2 & P_1 & 0 \\ 0 & 0 & P_2 & 0 \end{bmatrix} \begin{bmatrix} U_1 \\ U_2 \\ U_3 \\ 0 \end{bmatrix} = \begin{bmatrix} R_1 \\ R_2 \\ R_3 \\ R_4 \end{bmatrix}. \tag{6.17}$$

Equation 6.17 can be transformed in the form that the knowns are placed on one side of the equation and the unknowns are placed on the other side. The mathematical process is expressed as follows:

$$\begin{aligned} PU &= R \\ \left(P^{\mathrm{T}}P\right)U &= P^{\mathrm{T}}R \\ \left(P^{\mathrm{T}}P\right)^{-1}\left(P^{\mathrm{T}}P\right)U &= \left(P^{\mathrm{T}}P\right)^{-1}P^{\mathrm{T}}R \\ U &= \left(P^{\mathrm{T}}P\right)^{-1}P^{\mathrm{T}}R \end{aligned} \tag{6.18}$$

where P^{T} is the transpose of P, P^{-1} is the inverse matrix of P, and I is the identity matrix. Because of the irregularities in the shape of the unit hydrograph obtained from Equation 6.18, it should be adjusted. The probable irregularities are negative ordinates or undulations in the ordinates of the unit hydrograph recession. Manual smoothing or fitting a synthetic functional form to the resulting moments is used to eliminate these irregularities, which are a by-product of the regression method. It is also important to ensure that the ordinates produce unit depth of runoff over the watershed.

6.6 DIFFERENT TYPES OF UNIT HYDROGRAPHS

6.6.1 SCS Unit Hydrograph

The SCS curvilinear dimensionless unit hydrograph procedure is one of the best known methods for deriving synthetic unit hydrographs in use today. The dimensionless unit hydrograph used by the SCS is derived based on a large number of unit hydrographs from basins that varied in characteristics such as size and geographic location. The unit hydrographs are averaged and the final product is made dimensionless by considering the ratios of q/q_{p} (flow/peak flow) on the ordinate axis and t/t_{p} (time/time to peak) on the abscissa. This final dimensionless unit hydrograph, which is the result of averaging a large number of individual dimensionless unit hydrographs, has a time to peak located at approximately 20% of its time base and an inflection point at 1.7 times the time to peak. The dimensionless unit hydrograph is illustrated in Figure 6.12. Figure 6.12 also illustrates the cumulative mass curve (S-curve) for the dimensionless unit hydrograph. The ratios of dimensionless unit hydrograph and the corresponding mass curve are given in Table 6.16.

The curvilinear unit hydrograph may also be represented by an equivalent triangular unit hydrograph. Figure 6.13 shows the equivalent triangular unit hydrograph. Recall that the unit hydrograph

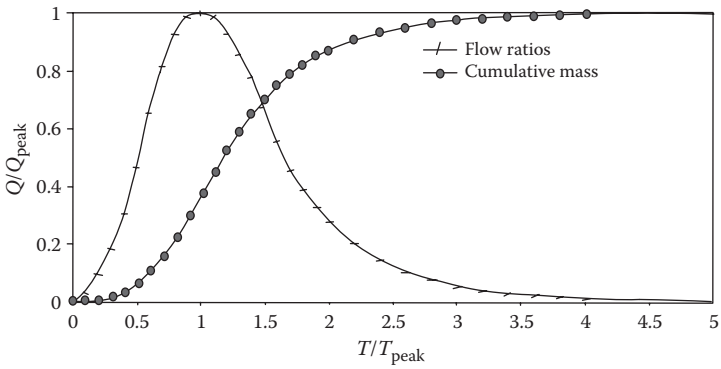

FIGURE 6.12 SCS dimensionless unit hydrograph and mass curve (S-hydrograph).

TABLE 6.16
Ratios for Dimensionless Unit Hydrograph and Mass Curve

Time Ratios (t/t_p)	Discharge Ratios (q/q_p)	Mass Curve Ratios (Q_a/Q)	Time Ratios (t/t_p)	Discharge Ratios (q/q_p)	Mass Curve Ratios (Q_a/Q)
0.0	0.000	0.000	1.6	0.560	0.751
0.1	0.030	0.001	1.7	0.460	0.790
0.2	0.100	0.006	1.8	0.390	0.822
0.3	0.190	0.012	1.9	0.330	0.849
0.4	0.310	0.035	2.0	0.280	0.871
0.5	0.470	0.065	2.2	0.207	0.908
0.6	0.660	0.107	2.4	0.147	0.934
0.7	0.820	0.163	2.6	0.107	0.953
0.8	0.930	0.228	2.8	0.077	0.967
0.9	0.990	0.300	3.0	0.055	0.977
1.0	1.000	0.375	3.2	0.040	0.984
1.1	0.990	0.450	3.4	0.029	0.989
1.2	0.930	0.522	3.6	0.021	0.993
1.3	0.860	0.589	3.8	0.015	0.995
1.4	0.780	0.650	4.0	0.011	0.997
1.5	0.680	0.700	4.5	0.005	0.999
			5.0	0.000	1.000

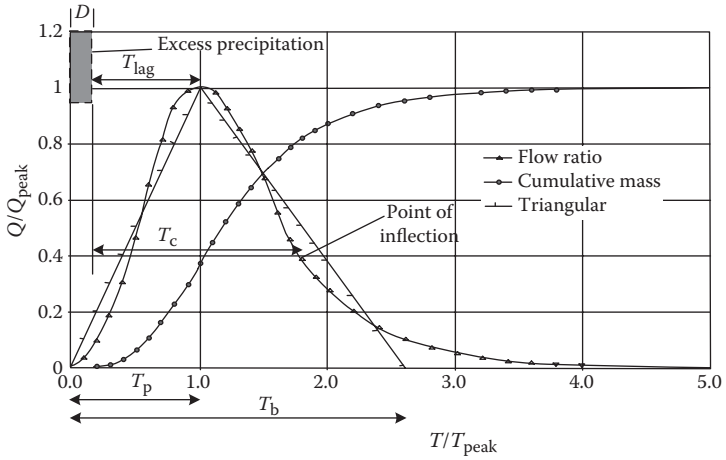

FIGURE 6.13 Dimensionless curvilinear unit hydrograph and equivalent triangular hydrograph.

is the result of unit excess rainfall (of duration D) spread uniformly over the basin. Using the geometry of the triangle, the unit hydrograph has 37.5% (or 3/8) of its volume on the rising side and the remaining 62.5% (or 5/8) of the volume on the recession side.

The following relationships are used in further developing the peak rate relationships. Note that the time base, T_b, of the triangular unit hydrograph extends from 0 to 2.67 and that the time to peak, T_p, is at 1.0; thus, the time base is 2.67 times the time to peak or

$$T_b = 2.67T_p \tag{6.19}$$

and that the recession limb time, T_r, is then 1.67 times the time to peak.

$$T_r = T_b - T_p = 1.67T_p. \tag{6.20}$$

Using the geometric relationships of the triangular unit hydrograph of Figure 6.13, the total volume under the hydrograph is found by (area under two triangles)

$$Q = \frac{q_p T_p}{2} + \frac{q_p T_r}{2} = \frac{q_p}{2}\left(T_p + T_r\right). \tag{6.21}$$

The volume, Q, is in centimeters (1 cm for a unit hydrograph) and the time, T, is in hours. The peak rate, q_p, in centimeters per hour, is

$$q_p = \frac{2Q}{T_p + T_r}. \tag{6.22}$$

To have the peak flow of the unit hydrograph in terms of cms per cm per km^2, the drainage area, A (km^2), is added to the equation, as follows:

$$q_p = \frac{2 \times 10^4 \times A \times Q}{T_p + T_r}. \tag{6.23}$$

Substituting Equation 6.20 in Equation 6.23 results in

$$q_p = \frac{7491AQ}{T_p}. \tag{6.24}$$

Because the above relationships were developed based on the volumetric constraints of the triangular unit hydrograph, the equations and conversions are also valid for the curvilinear unit hydrograph, which, proportionally, has the same volumes as the triangular representation. Note that the conversion constant (herein called the peaking factor) is the result of assuming that the recession limb is 1.67 times the rising limb (time to peak). This may not be applicable to all watersheds.

Steep terrain and urban areas may tend to produce higher early peaks and thus values of the peaking factor may increase. Likewise, flat swampy regions tend to retain and store the water, causing a delayed, lower peak. In these circumstances, values may tend towards 4500 or lower (USDA-SCS 1972; Wanielista et al. 1997). It would be very important to document any reasons for changing the constant from 7491 because it will considerably change the shape of the unit hydrograph.

The peak rate may also be expressed in terms of other timing parameters such as rainfall duration and basin lag time besides the time to peak. From Figure 6.13:

$$T_p = \frac{D}{2} + L_t, \tag{6.25}$$

where D is the duration of the unit excess rainfall and L_t is the basin lag time, which is defined as the time between the center of mass of excess rainfall and the time to peak of the unit hydrograph. The peak flow is now written as

$$q_p = \frac{7491AQ}{\frac{D}{2} + L_t}. \tag{6.26}$$

The USDA-SCS (1972) relates the basin lag time, L_t, to the time of concentration, T_c, by

$$L_t = 0.6T_c. \tag{6.27}$$

Combining this with other relationships, as illustrated in the triangular unit hydrograph, the following relationships are developed:

$$T_c + D = 1.7T_p \quad \text{and} \quad \frac{D}{2} + 0.6T_c = T_p. \tag{6.28}$$

From this, duration D can be expressed as

$$D = 0.133T_c. \tag{6.29}$$

Equations 6.19 through 6.29 provide the basis for the SCS dimensionless unit hydrograph method. Equation 6.29 provides a desirable relationship between duration and the time of concentration, which should provide enough points to accurately represent the unit hydrograph, particularly the rising limb.

Example 6.10

Develop a 30 min unit hydrograph for a 3.43 km^2 watershed.

Solution:

First, using Equation 6.29, the time of concentration of basin is determined as 0.5/0.133 = 3.76 h. Then, the basin lag time is calculated as (Equation 6.27) 0.6 × 3.76 = 2.26 h. Finally, the time to peak flow and peak flow are estimated as follows:

$$T_p = \frac{D}{2} + L_t = \frac{0.5}{2} + 2.26 = 2.51\,\text{h}$$

$$q_p = \frac{7491AQ}{T_p} = \frac{7491 \times 3.43 \times 1}{2.51 \times 3600} = 2.84\ \text{m}^3/\text{s/cm}.$$

Therefore, the peak discharge of the 30 min unit hydrograph, which is 2.84 m^3/s/cm of excess rainfall, occurs 2.51 h after the start of excess rainfall. For developing the 30 min unit hydrograph, the values of t/t_p and q/q_p in Table 6.16 are multiplied by 2.51 × 60 and 2.84, respectively. The developed hydrograph is presented in Table 6.17.

TABLE 6.17
SCS Unit Hydrograph in Example 6.10

t/T_p	q/q_p	t (min)	q (m³/s/cm)	t/T_p	q/q_p	t (min)	q (m³/s/cm)
0.00	0.000	0.00	0.00	1.70	0.460	256.02	1.31
0.10	0.300	15.06	0.85	1.80	0.390	271.08	1.11
0.20	0.100	30.12	0.28	1.90	0.330	286.14	0.94
0.30	0.190	45.18	0.54	2.00	0.280	301.20	0.80
0.40	0.310	60.24	0.88	2.20	0.207	331.32	0.59
0.50	0.470	75.30	1.33	2.40	0.147	361.44	0.42
0.60	0.660	90.36	1.87	2.60	0.107	391.56	0.30
0.70	0.820	105.42	2.33	2.80	0.077	421.68	0.22
0.80	0.930	120.48	2.64	3.00	0.055	451.80	0.16
0.90	0.990	135.54	2.81	3.20	0.400	481.92	1.14
1.00	1.000	150.60	2.84	3.40	0.029	512.04	0.08
1.10	0.990	165.66	2.81	3.60	0.021	542.16	0.06
1.20	0.930	180.72	2.64	3.80	0.015	572.28	0.04
1.30	0.860	195.78	2.44	4.00	0.011	602.40	0.03
1.40	0.780	210.84	2.22	4.50	0.005	677.70	0.01
1.50	0.680	225.90	1.93	5.00	0.000	753.00	0.00
1.60	0.560	240.96	1.59				

6.6.2 Espey 10 min Unit Hydrograph

This empirical method is proposed by Espey et al. (1978) to obtain a synthetic 10 min hydrograph for urban watersheds. This hydrograph can be used to develop corresponding hydrograph of any rainfall that can be usually disaggregated to several 10 min rainfalls based on recording time. This model is based on the analysis of the runoff data gathered from 41 urban watersheds located in eight different states in the United States. As illustrated in Figure 6.14, nine parameters should be

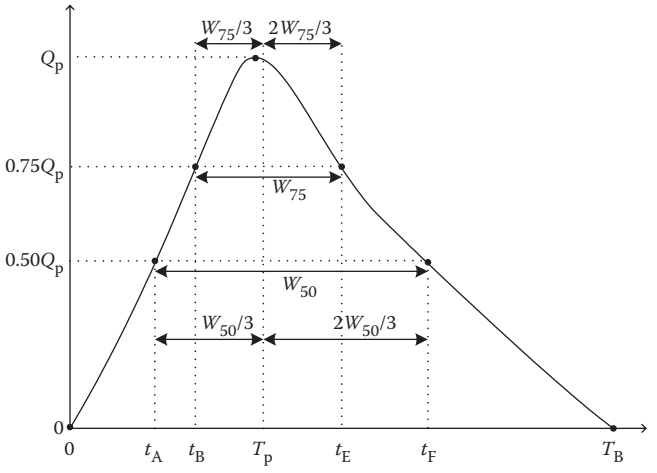

FIGURE 6.14 Elements of the Espey unit hydrograph. (From Espey, W.H. et al., 1977. With permission.)

estimated for describing the Espey 10 min unit hydrograph. The considered parameters are defined as follows:

Q_p: peak discharge of the unit hydrograph (m^3/s)
T_p: time of occurrence of the peak discharge
T_B: time base of the unit hydrograph
W_{50}: width of the unit hydrograph at $0.50Q_p$
W_{75}: width for the unit hydrograph at $0.75Q_p$
t_A: time of discharge of $0.50Q_p$ on the rising limb
t_B: time of discharge of $0.75Q_p$ on the rising limb
t_E: time of discharge of $0.75Q_p$ on the falling limb
t_F: time of discharge of $0.50Q_p$ on the falling limb

The time parameters are in minutes. These parameters are estimated using the physical basin characteristics. The useful basin features in developing unit hydrograph are listed below:

L: length of main water path through watershed from the upstream of the watershed to the watershed outlet (m).
S_a: average slope of the main water path.
H: difference between main water path altitude at outlet and 0.8 L upstream (m).
A: watershed drainage area (km^2).
I: percentage of imperviousness in the watershed (%).
n: Manning roughness coefficient of the main water path (Table 6.18).
ϕ: Dimensionless conveyance coefficient determined by using Figure 6.15.

The parameters of the Espey 10 min unit hydrograph are calculated as follows:

$$S_a = \frac{H}{0.8L} \tag{6.30}$$

TABLE 6.18
Manning Roughness Coefficient for Various Pipes and Open Channels

Conduit Material		Lining Condition/Type	Manning Coefficient
Closed conduits	Cast iron pipe		0.13
	Concrete pipe		0.13
	Corrugated metal pipe:	Plain	0.024
		Paved invert	0.020
		Fully paved	0.015
	Plastic		0.013
	Vitrified clay		0.013
Open channels	Lined channels	Asphalt	0.015
		Concrete	0.015
		Rubble or rip rap	0.030
		Vegetal	0.040
	Excavated or dredged	Earth, straight and uniform	0.030
		Earth, winding, fairly uniform	0.040
		Unmaintained	0.100
Natural channels (minor streams)	Fairly regular section		0.050
	Irregular section with pools		0.100

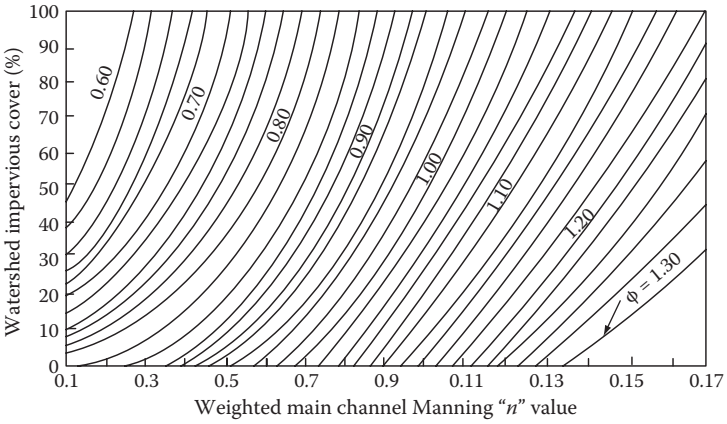

FIGURE 6.15 Values of ϕ for the Espey unit hydrograph. (From Espey, W.H. et al., 1977. With permission.)

$$T_p = \frac{4.1L^{0.23}\phi^{1.57}}{S_a^{0.25}I^{0.18}} \tag{6.31}$$

$$Q_p = \frac{138.7A^{0.96}}{T_p^{1.07}} \tag{6.32}$$

$$T_B = \frac{666.7A}{Q_p^{0.95}} \tag{6.33}$$

$$W_{50} = \frac{105.1A^{0.93}}{Q_p^{0.92}} \tag{6.34}$$

$$W_{75} = \frac{45.1A^{0.79}}{Q_p^{0.78}} \tag{6.35}$$

$$t_A = T_p - \frac{W_{50}}{3} \tag{6.36}$$

$$t_B = T_p - \frac{W_{75}}{3} \tag{6.37}$$

$$t_E = T_p + \frac{2W_{75}}{3} \tag{6.38}$$

$$t_F = T_p + \frac{2W_{50}}{3} \tag{6.39}$$

By estimation of these parameters, seven points of the unit hydrograph are determined and a graph is constructed passing through these points. Finally, it should be checked that the area under the hydrograph is equal to 1 cm of direct runoff.

Example 6.11

Calculate the Espey 10 min unit hydrograph for an urban watershed with the following characteristics:

A = 1.13 km^2, H = 50 m, L = 3250 m, I = 51.2% and n = 0.014.

Solution:

At first, conveyance coefficient (ϕ) is determined from Figure 6.15 using n = 0.014 and I = 51.2%, equal to 0.6. Then Equations 6.30 through 6.39 are employed to obtain the seven points of the hydrograph as follows:

$$S_a = \frac{50}{(0.8)(3250)} = 0.019$$

$$T_p = \frac{4.1(3250)^{0.23}(0.60)^{1.57}}{(0.019)^{0.25}(51.2)^{0.18}} = 11.34 \text{ min}$$

$$Q_p = \frac{138.7(1.13)^{0.96}}{(11.34)^{1.07}} = 11.56 \text{ m}^3/\text{s}$$

$$T_B = \frac{666.7(1.13)}{(11.56)^{0.95}} = 73.64 \text{ min}$$

$$W_{50} = \frac{105.1(1.13)^{0.93}}{(11.56)^{0.92}} = 12.39 \text{ min}$$

$$W_{75} = \frac{45.1(1.13)^{0.79}}{(11.56)^{0.78}} = 7.35 \text{ min}$$

$$t_A = 11.34 - \frac{12.39}{3} = 7.21 \text{min}$$

$$t_B = 11.34 - \frac{7.35}{3} = 8.89 \text{ min}$$

$$t_E = 11.34 + 2\left(\frac{7.35}{3}\right) = 16.24 \text{ min}$$

$$t_F = 11.34 + 2\left(\frac{12.39}{3}\right) = 19.6 \text{ min}$$

The discharge at t_A and t_F is $0.50Q_p$ = 5.78 m^3/s/cm, and at t_B and t_E, the discharge is $0.75Q_p$ = 8.67 m^3/s/cm. The developed 10 min unit hydrograph of the watershed is depicted in Figure 6.16. Now, the area under the hydrograph is checked to be equal to 1 cm depth of direct runoff. For this purpose, the discharges are read from the unit hydrograph presented in Figure 6.16 at equal time increments and tabulated in Table 6.19.

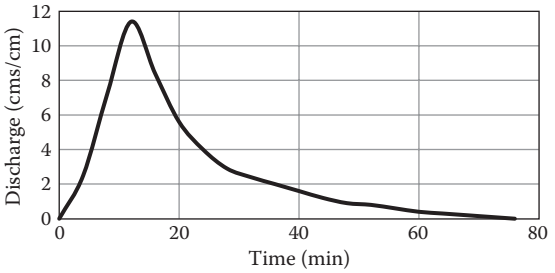

FIGURE 6.16 Developed Espey unit hydrograph for watershed in Example 6.11.

TABLE 6.19
Espey 10 min Unit Hydrograph (Example 6.11)

Time (min)	Q ($m^3/s/cm$)	Time (min)	Q ($m^3/s/cm$)
0	0	40	1.6
4	2.5	44	1.2
8	7.2	48	0.9
12	11.4	52	0.8
16	8.4	56	0.6
20	5.6	60	0.4
24	4	64	0.3
28	2.9	68	0.2
32	2.4	72	0.1
36	2	76	0

The runoff volume is calculated as follows:

$$\text{Runoff volume} = (52.5\ m^3/s)(4\ \text{min})(60\ s/\text{min}) = 12{,}600\ m^3.$$

The runoff depth is obtained by dividing the runoff volume by the basin area (1,130,000 m^2), as follows:

$$\text{Depth} = 12{,}600\ m^3/91{,}000\ m^2 = 0.0011\ m \cong 1\ cm.$$

As the depth of excess runoff is equal to 1, the hydrograph modification is not needed.
Note: The hydrograph ordinates should be adjusted if the estimated runoff depth turned out to be different from 1 cm because in the Epsey method a unit hydrograph is developed.

6.6.3 Snyder's Synthetic Unit Hydrograph

Snyder (1938) studied a large number of catchments in the Appalachian Highlands of eastern United States and developed a set of empirical equations to develop synthetic unit hydrographs in those areas. These equations can be used with some modifications in many countries other than the United States. This unit hydrograph shows that the most important characteristic of a basin affecting a hydrograph due to a given storm is basin time lag. The time lag, T_L, is considered as the time difference between the centroids of the rainfall excess hyetograph and the surface runoff hydrograph. The basin time lag is physically interpreted as the mean travel time of water particles from different points of the basin to the outlet during a given storm. The basin lag time is dependent on a variety of physical features of the catchment, such as size, length, stream density, and vegetation. However,

for determining the basin lag time, only a few important catchment characteristics are considered. Snyder has used a different definition of basin lag time (denoted by t_p) in his methodology for greater simplicity. This t_p is practically of the same order of magnitude as T_L, and in this section, the term basin lag refers to Snyder's t_p.

The first equation of Snyder's unit hydrograph relates the basin lag t_p, defined as the time interval from the midpoint of the unit rainfall excess to the peak of the unit hydrograph (Figure 6.17), to the basin characteristics as follows:

$$t_p = C_t (L \cdot L_{ca})^{0.3}, \tag{6.40}$$

where t_p is obtained in hours, L is basin length measured along the water course from the basin divide to the gauging station (km), L_{ca} is distance along the main water course from the gauging station to a point opposite the watershed centroid (km), and C_t is a regional constant representing watershed slope and storage.

The value of C_t in Snyder's study ranged from 1.35 to 1.65. However, the investigations in different regions have shown that C_t depends upon the region under study and a wide range of C_t variations from 0.3 to 6.0 has been reported.

Linsley et al. (1958) found that the basin lag t_p is better correlated with the catchment parameter $\left(\frac{L \cdot L_{ca}}{\sqrt{S}}\right)$, where S is basin slope. They suggested a modification to Equation 6.40 as follows:

$$t_p = C_{tL}\left(\frac{LL_{ca}}{\sqrt{S}}\right)^n, \tag{6.41}$$

where C_{tL} and n are basin constants. The value of n for the studied basins in the United States is equal to 0.38. The values of C_{tL} depend on the geography of the basin and are 1.715 for mountainous drainage areas, 1.03 for foothill drainage areas and 0.50 for valley drainage areas. Snyder adopted a standard duration t_R hours of effective rainfall given by

$$t_R = \frac{t_p}{5.5}. \tag{6.42}$$

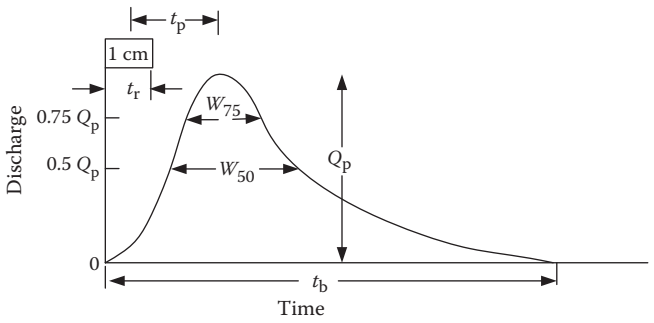

FIGURE 6.17 Elements of a synthetic hydrograph.

Snyder estimated the peak discharge Q_{ps} (m^3/s) of a unit hydrograph of standard duration t_R(h) as follows:

$$Q_{ps} = \frac{2.78 C_p A}{t_p}, \tag{6.43}$$

where A is catchment area (km^2) and C_p is a regional constant. This equation is based on the assumption that the peak discharge is proportional to the average discharge of $\left(\frac{\text{unit depth} \times \text{catchment area}}{\text{duration of rainfall excess}}\right)$. The values of the coefficient C_p range from 0.56 to 0.69 for Snyder's study area and is considered as an indication of the retention and storage capacity of the watershed. The values of C_p highly depend on the characteristics of the region, and different values of C_p in the range 0.31 to 0.93 are reported.

If a nonstandard rainfall duration t_r instead of the standard value is used to derive a unit hydrograph, the value of the basin lag will be affected. The modified basin lag is calculated as follows:

$$t_p' = t_p + \frac{t_r - t_R}{4}, \tag{6.44}$$

where t_p' is basin lag (h) for an effective duration of t_R and t_p is calculated using Equations 6.41 and 6.42. The value of t_p' must be used instead of t_p in Equation 6.43. The time base of a unit hydrograph (Figure 6.17) is given by Snyder as follows:

$$t_b = 3 + \frac{t_p'}{8}, \tag{6.45}$$

where t_b is time base in hours. While Equation 6.45 gives reasonable estimates of t_b for a large catchment, it may give excessively large values of the time base for a small catchment. The following formula is also recommended for estimation of t_b:

$$t_b = 5\left(t_p' + \frac{t_R}{2}\right), \tag{6.46}$$

where t_b is estimated in hours. t_b is taken as the next larger integer value divisible by t_R, i.e., t_b is about five times the time to peak.

To assist in the sketching of unit hydrographs, the widths of unit hydrographs at 50% and 75% of the peak (Figure 6.17) are needed. These widths (in time units) are correlated to the peak discharge intensity and are given by

$$W_{50} = \frac{5.87}{q^{1.08}} \tag{6.47}$$

$$W_{75} = W_{50}/1.75. \tag{6.48}$$

where W_{50} is the width of the unit hydrograph in hours at 50% peak discharge, W_{75} is the width of the unit hydrograph in hours at 75% peak discharge, and $q = Q_p/A$ is peak discharge per unit catchment area in $cm/s/km^2$.

Since the coefficients C_t and C_p vary from region to region, in practical applications, it is advisable that the value of these coefficients are determined from known unit hydrographs of a meteorologically homogeneous catchment and then used in the basin under study. On the other hand, Snyder's equations can be used for scaling the hydrograph information from one catchment to another similar catchment.

Example 6.12

Two catchments A and B are considered meteorologically similar. Their catchment characteristics are as follows:

Catchment A: L = 30 km, L_{Ca}= 15 km, A = 250 km^2

Catchment B: L = 45 km, L_{Ca}= 25 km, A = 400 km^2

For catchment A, a 2 h unit hydrograph was developed and was found to have a peak discharge of 50 m^3/s. The time to peak from the beginning of the rainfall excess in this unit hydrograph was 9.0 h. Using Snyder's method, develop a unit hydrograph for catchment B.

Solution:

The parameters of unit hydrograph are estimated for catchment A based on the available data and then are implemented to develop the unit hydrograph of catchment B.

For catchment A: t_r = 2 h.

$$\text{Time to pick from beginning of effective rainfall} = \frac{t_r}{2} + t_p' = 9\,\text{h}.$$

Therefore,

$$t_p' = 8.0\ \text{h}.$$

From Equations 6.44 and 6.42,

$$t_p' = t_p + \frac{t_r - t_R}{4} = t_p + \frac{\left(t_r - t_p/5.5\right)}{4} = \frac{21}{22}t_p + \frac{t_r}{4} = 8\,\text{h} \qquad t_p = \frac{(8 - 2/4)\times 22}{21} = 7.857\,\text{h}.$$

From Equation 6.40,

$$t_p = C_t\,(LL_{ca})^{0.3} \Rightarrow 7.857 = C_t(30 \times 15)^{0.3} \Rightarrow C_t = 1.257.$$

From Equation 6.43,

$$Q_p = \frac{2.78C_pA}{t_p'} \qquad 50 = \frac{2.78\times C_p \times 250}{8} \qquad C_p = 0.576.$$

For catchment B, using the value of C_t = 1.257 and C_p = 0.576 in catchment B, the parameters of the synthetic unit hydrograph for catchment B are determined. From Equation 6.40:

$$t_p = 1.257(45 \times 25)^{0.3} = 10.34\ \text{h}.$$

By using Equation 6.42,

$$t_R = \frac{t_p}{5.5} = \frac{10.34}{5.5} = 1.88 \text{ h}.$$

Using $t_r = 2$ h, that is, for a 2 h unit hydrograph, by Equation 6.44,

$$t'_p = \frac{21}{22}t_p + \frac{t_r}{4} = \frac{21}{22} \times 10.34 + \frac{2}{4} = 10.37 \text{ h}.$$

By Equation 6.43,

$$Q_p = \frac{2.78 \times 0.576 \times 400}{10.37} = 6.77 \text{ m}^3/\text{s, say } 62 \text{ m}^3/\text{s}.$$

From Equation 6.47,

$$W_{50} = \frac{5.87}{(62/40)^{1.08}} = 44 \text{ h}.$$

By Equation 6.48,

$$W_{75} = \frac{44}{1.75} = 25 \text{ h}.$$

Time base:
From Equation 6.43,

$$t_b = 72 + (3 \times 10.37) = 103 \text{ h}.$$

From Equation 6.44,

$$t_b = 5(10.37 + 10) = 58 \text{ h}.$$

Considering the value of W_{50} and W_{75} and noting the area of catchment B is rather small, $t_b \approx 58$ h is more appropriate in this case.
Note: In cases that there is no information about a catchment to provide an estimation of streamflow of the basin, the data of a watershed with the same geomorphologic and meteorological condition can be employed.

6.7 UNIT HYDROGRAPH ADJUSTMENTS

A unit hydrograph reflects the effects of watershed characteristics and conditions on rainfall excess. It is implicitly assumed that the characteristics and conditions of the watershed are constant for each storm. Additionally, it is assumed that rainfall characteristics do not affect the shape of the unit hydrograph. In practice, watershed conditions significantly change in different storm events and the effects of rainfall characteristics are not eliminated in the UH analysis procedure. Thus, there are considerable variations among produced unit hydrographs from different storm analysis on the same watershed. When a larger portion of the rainfall is dumped near the watershed outlet, the produced unit hydrographs have a peak earlier than average. When a unit storm occurs on a relatively dry watershed, the resulting hydrograph will have a delayed peak with a lower value than

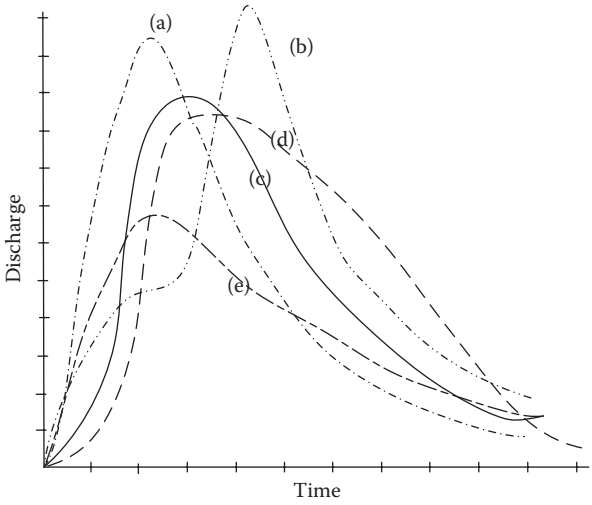

FIGURE 6.18 Fitted unit hydrographs from five storm events (a to e) on a given watershed.

the average discharge. The longer time to peak occurs due to a larger time period than is needed to fulfill initial abstractions and a lower than average soil moisture deficit. In summary, widely different unit hydrographs are produced because of differences in storm characteristics and watershed conditions.

This has been demonstrated in Figure 6.18, which shows the completely different unit hydrographs for four storm events in a given watershed. Four of these five hydrographs are similar to a typical unit hydrograph. A flat portion on the rising limb of the hydrograph b is observed. This probably shows a period of low rainfall. The hydrograph e has a low peak and a slower recession than the other events. Different factors such as rainfall characteristics, nonuniformity of rainfall over the storm duration, or unsaturated watershed conditions could have caused these special characteristics. All of these abnormalities demonstrate the necessity of adjusting the synthesized unit hydrograph.

The commonly needed adjustments in unit hydrograph analyses are categorized in four groups. First is the adjustment of the storm event UHs to a common duration of rainfall excess. The common method for changing the duration of a unit hydrograph is the S-hydrograph method. Second, the irregularities in shape of a computed hydrograph are smoothed using the gamma UH form. Third, when the unit hydrographs of different storm events for a watershed are available, the watershed-averaged UH is developed. Fourth, a regionalized UH can be computed when unit hydrographs from several watersheds in a region are available, by developing dimensionless hydrographs. In the next subsections, these adjustments are discussed.

Example 6.13

Table 6.20 shows the discharge rates resulting from the 2 h unit hydrograph:

TABLE 6.20
Data for Example 6.13

Time (h)	0	2	4	6	8	10	12
Q (m^3/s)	0	100	250	200	100	50	0

TABLE 6.21
Calculation for Example 6.13

Time h (1)	2 h UH m^3/s (2)	UH-Lagged m^3/s (3)	Σ(2) + (3) m^3/s (4)	4 h UH (4)/2 m^3/s (5)	4 h UH × 0.5 m^3/s (6)	4 h UH × 1.5 m^3/s (7)	Σ m^3/s (8)
0	0		0	0	0		0
2	100	0	100	50	25	0	25
4	250	100	350	175	87.5	75	162
6	200	250	450	225	12.5	262.5	375
8	100	200	300	10	75	37.5	412.5
10	5	100	150		37.5	225	262.5
12	0	50	50	25	2.5	112.5	125
14		0	0	0	0	37.5	37.5

1. Develop the 4 h unit hydrograph.
2. Find the total runoff resulting from the following rain:

Time Increment:	Rain Intensity (m/h)
First 4 h	0.5
Second 4 h	1.5

Solution:

Based on the descriptions given in this chapter, the solution is summarized in Table 6.21.
Total runoff:

$$(1/2)[(0 + 25) + (25 + 162.5) + (162.5 + 375) + (375 + 412.5) + (412.5 + 262.5) + (262.5 + 125) + (125 + 37.5) + (37.5 + 0)](2h)(60 \times 60) = (25 + 162.5 + 375 + 412.5 + 262.5 + 125 + 37.5)(7200) = 10{,}080{,}000\ m^3$$

Note: The duration of unit hydrographs can be modified to the desired values to generate every rainfall events' hydrograph.

6.7.1 S-Hydrograph Method

The characteristics of the obtained unit hydrograph from the measured storm data depend on the effective duration of the rainfall excess. This is a result of coordination of rainfall excess duration with the watershed time of concentration. The S-hydrograph method is used to change the excess rainfall duration of the unit hydrograph to represent a different effective duration of the rainfall excess. The basic idea of the S-hydrograph method is that though an infinite number of effective durations are possible, as opposed to the unit hydrograph, only one S-hydrograph exists for a watershed. The S-hydrograph is also referred to as the S-graph or summation hydrograph.

For a given unit hydrograph with effective duration of T hours, the S-curve is computed by adding an infinite series of T-hour unit hydrographs, each of them lagged by T hours (Figure 6.19), which is unique for each watershed. In Figure 6.19, a series of triangular unit hydrographs are lagged by their effective duration of the rainfall excess, T hours. At the top of Figure 6.19, the rainfall excess is shown with each burst of rainfall excess having a depth of 1 cm in a period of T hours. The shown S-graph is a result of the summation of the triangular unit hydrographs. It can be stated

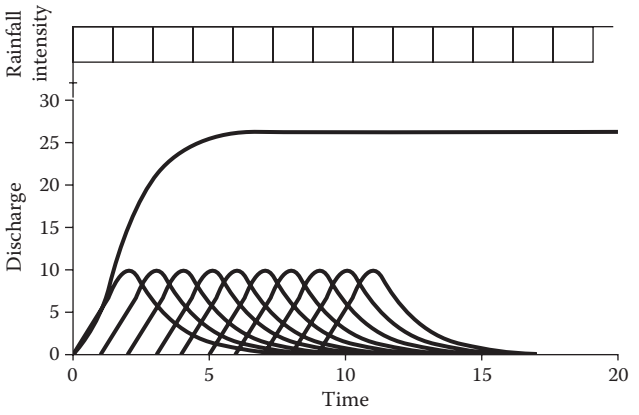

FIGURE 6.19 Derivation of an S-hydrograph.

that the *i*th ordinate of the S-graph, S_i, is the sum of all unit hydrograph ordinates, U_j, from the first ordinate to the *i*th ordinate as follows:

$$S_i = \sum_{j=1}^{i} U_j \tag{6.49}$$

$$S(t) = \int_0^t U(\tau)\,\mathrm{d}\tau. \tag{6.50}$$

This computation applies when the time interval of the unit hydrograph is equal to the unit duration of the unit hydrograph.

When an S-curve is used to derive a unit hydrograph with durations different from the duration of the unit hydrograph used to develop the S-curve, the ordinates should be recorded on the time interval of the shorter of the two durations. For example, if the given S-curve corresponds to effective duration of 30 min and a 50 min unit hydrograph is needed, the ordinates must be recorded on a 30 min interval, but when a 10 min unit hydrograph is needed, the ordinates must be recorded on a 10 min interval. The intermediate points are derived by interpolation of the S-curve. After interpolation, it should be checked that the sum of the ordinates is equivalent to one area depth. This is true if linear interpolation between points on the S-graph is used. However, linear interpolation from the S-graph is not recommended because it always results in a peak discharge for the shorter duration unit hydrograph that is smaller than the peak of the longer-duration unit hydrograph. Since the peak discharge of the unit hydrograph has an inverse relation with the duration of the rainfall excess (the peak discharge increases when the duration of rainfall excess decreases), this is not rational. Therefore, the nonlinear nature of the S-graph should be taken into account in selecting intermediate points from the S-graph, and a volume of 1.0 area depth of direct runoff should result after the interpolation.

Example 6.14

A 1 h unit hydrograph is given as a triangle whose base is 3 h, peak is $\frac{2}{3}\frac{\text{cm}}{\text{h}}$, and the time of rise and recession are 1 h and 2 h, respectively. Compute a 2 h unit hydrograph using the S-hydrograph method.

TABLE 6.22
Calculations for Example 6.14

Time	1 h UH (1/h)	S-Hydrograph (SH) (cm/h)	2 h Offset SH (cm/h)	2 h Hydrograph (cm/h)	2 h UH (1/h)
0	0	0	0	0	0
1	2/3	2/3	0	2/3	1/3
2	1/3	1	0	1	2/3
3	0	1	2/3	1/3	1/6
4	0	1	1	0	0
5	0	1	1	0	0
6	0	1	1	0	0
7	0	1	1	0	0

Solution:

The results are summarized in Table 6.22.

Example 6.15

Table 6.23 shows the data for a 4 h unit hydrograph for a basin of 27 km^2. Construct the S-hydrograph and derive a 2 h unit hydrograph.

Solution:

For deriving the S-curve, the 4 h unit hydrographs are lagged by 4 h and summed. The process of developing the S-hydrograph is tabulated in Table 6.24.

For deriving the 2 h unit hydrograph, the S-curve is lagged by 2 h and subtracted from the first S-curve. The resulting curve is multiplied by 4 (the duration of given hydrograph)/2 (the duration of desired hydrograph). The process is tabulated in Table 6.25.

TABLE 6.23
Data for Example 6.15

Time (h)	Flow (m^3/s/cm)	Time (h)	Flow (m^3/s/cm)
0	0	11	66
1	11.5	12	54
2	61.5	13	45
3	107	14	35
4	145	15	28
5	169	16	21
6	147	17	16
7	126	18	12
8	109	19	7
9	92	20	4.5
10	78	21	0

TABLE 6.24
Deriving S-Hydrograph for Example 6.15

Time (h)	UH ($m^3/s/cm$)	Lagged UHs ($m^3/s/cm$)				S-Curve
0	0					0
1	11.5					11.5
2	61.5					61.5
3	107					107
4	145	0				145
5	169	11.5				180.5
6	147	61.5				208.5
7	126	107				233
8	109	145	0			254
9	92	169	11.5			272.5
10	78	147	61.5			286.5
11	66	126	107			299
12	54	109	145	0		308
13	45	92	169	11.5		317.5
14	35	78	147	61.5		321.5
15	28	66	126	107		327
16	21	54	109	145	0	329
17	16	45	92	169	11.5	333.5
18	12	35	78	147	61.5	333.5
19	7	28	66	126	107	
20	4.5	21	54	109	145	
21	0	16	45	92	169	
22		12	35	78	147	
23		7	28	66	126	
24		4.5	21	54	109	
25		0	16	45	92	
26			12	35	78	
27			7	28	66	
28			4.5	21	54	
29			0	16	45	
30				12	35	

Example 6.16

Draw an 8 h unit hydrograph using the data from Example 6.15.

Solution:

The number of hydrographs needed for development of an S-hydrograph is

$$n = \frac{8}{4} = 2.$$

The process of the derived 8 h unit hydrograph, which is similar to the previous example, is given in Table 6.26. The derived 8 h unit hydrograph is illustrated in Figure 6.20.

TABLE 6.25
Development of 2 h UH for Example 6.15

Time (h)	S-Curve	2 h Lagged S-Curve		2 h UH ($m^3/s/cm$)
0	0		0	0
1	11.5		11.5	23
2	61.5	0	61.5	123
3	107	11.5	95.5	191
4	145	61.5	83.5	167
5	180.5	107	73.5	147
6	208.5	145	63.5	127
7	233	180.5	52.5	105
8	254	208.5	45.5	91
9	272.5	233	39.5	79
10	286.5	254	32.5	65
11	299	272.5	26.5	53
12	308	286.5	21.5	43
13	317.5	299	18.5	37
14	321.5	308	13.5	27
15	327	317.5	9.5	19
16	329	321.5	7.5	15
17	333.5	327	6.5	13
18	333.5	329	4.5	9
19	333.5	333.5	0	0
20	333.5			
21	333.5			
22	333.5			
23	333.5			
24	333.5			
25	333.5			
26	333.5			
27	333.5			

Example 6.17

Derive 2 h unit hydrograph from the 4 h unit hydrograph in Table 6.27.

Solution:

At first, the S-hydrograph is developed and then converted to a 2 h unit hydrograph. The results are given in Table 6.28.

Example 6.18

Given the 2 h unit hydrograph in Table 6.29, use the S-curve to develop the ordinates of a 3 h unit hydrograph.

Solution:

At first, the S-hydrograph is developed and then converted to a 3 h unit hydrograph. The results are given in Table 6.30.

TABLE 6.26
Results for Example 6.16

Time (h)	UH ($m^3/s/cm$)	4 Hydrograph with 4 h Lagged				Sum	8 h UH
0	0	0				0	0
1	11.5	11.5				23	5.75
2	61.5	61.5				123	30.75
3	107	107				214	53.5
4	145	145	0			290	72.5
5	169	169	11.5			349.5	87.375
6	147	147	61.5			355.5	88.875
7	126	126	107			359	89.75
8	109	109	145	0		363	90.75
9	92	92	169	11.5		364.5	91.125
10	78	78	147	61.5		364.5	91.125
11	66	66	126	107		365	91.25
12	54	54	109	145	0	362	90.5
13	45	45	92	169	11.5	362.5	90.625
14	35	35	78	147	61.5	356.5	89.125
15	28	28	66	126	107	355	88.75
16	21	21	54	109	145	350	87.5
17	16	16	45	92	169	338	84.5
18	12	12	35	78	147	284	71
19	7	7	28	66	126	234	58.5
20	4.5	4.5	21	54	109	193	48.25
21	0	0	16	45	92	153	38.25
22			12	35	78	125	31.25
23			7	28	66	101	25.25
24			4.5	21	54	79.5	19.875
25			0	16	45	61	15.25
26				12	35	47	11.75
27				7	28	35	8.75
28				4.5	21	25.5	6.375
29				0	16	16	4
30					12	12	3
31					7	7	1.75
32					4.5	4.5	1.125
33					0	0	0

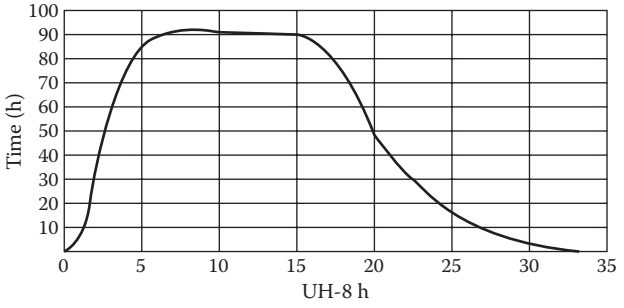

FIGURE 6.20 Eight-hour UH in Example 6.16.

TABLE 6.27
Ordinates of 4 h UH

Time (h)	0	2	4	6	8	10	12
Q (cfs)	0	100	250	200	100	50	0

TABLE 6.28
Calculations for Example 6.17

Time (h)	4 h UH	Shifted UH	4 h S-Curve	Lagged S-Curve for 2 h	ΔS-Curve	2 h UH
1	2	3	4	5	6	7
			2 + 3		4–5	(4/2) × 6
0	0	–	0	–	0	0
2	100	–	100	0	100	200
4	250	0	250	100	150	300
6	200	100	300	250	50	100
8	100	250	350	300	50	100
10	0	300	350	350	0	0
12	0	350	350	350	–	–

TABLE 6.29
Two-Hour Unit Hydrograph in Example 6.18

Time (h)	0	1	2	3	4	5	6
Q (m^3/s)	0	200	500	400	200	100	0

TABLE 6.30
Results for Example 6.18

Time (h) (1)	Q (m^3/s) (2)	S-Curve Additions (3)	S-Curve (4)	Lagged S-Curve (5)	Difference (6)	3 h UH (6) × 2/3 (7)
0	0	–	0		0	0
1	200	–	200		200	133.3
2	500	–	500		500	333.3
3	400	200	600	0	600	400
4	200	500	700	200	500	333.3
5	100	400 + 200	700	500	200	133.3
6	0	200 + 500	700	600	100	66.7
7		100 + 400 + 200	700	700	0	0
				700		

6.7.2 Gamma Function Unit Hydrograph

The gamma function unit hydrograph is a more general form of the SCS unit hydrograph, and the resulting unit hydrographs are very similar in shape and virtually identical. The SCS unit hydrograph is in tabular form, or in graphical form, and the gamma unit hydrograph is in a functional form, and is much easier to use than the SCS method. In a more general form, Equation 6.24 can be written as

$$q_p = \frac{P_r AQ}{T_p}, \tag{6.51}$$

where P_r is the peak rate factor, which is dependent on topographic characteristics of the watershed (Q = 1 cm) (Meadows 1991). The following equation is used to determine the ordinates of the gamma function unit hydrograph.

$$q_u = q_p \left[\frac{t}{T_p} \exp\left(1 - \frac{t}{T_p}\right) \right]^{n-1}, \tag{6.52}$$

where n is a shape factor. The parameters n and P_r are related to each other as given in Table 6.31. Considering these relations in developing the unit hydrograph, using Equations 6.30 and 6.31 ensures that the developed hydrograph will result in a unit depth excess rainfall. T_p and L_t (lag time) are estimated in a similar way as the SCS unit hydrograph using Equations 6.25 and 6.27, respectively.

Example 6.19

Develop a 25 min unit hydrograph for a 1.8 km^2 watershed using the gamma function unit hydrograph method. Assume that the time of concentration is 65 min and the peak rate factor P_r is equal to 1.28 cms · h/km^2 · cm.

Solution:

To determine the time of peak discharge, first the watershed lag time is determined by using Equation 6.27:

TABLE 6.31
Relationship of Gamma Function Unit Hydrograph Parameters

n	P_r (cms · h/km^2 · cm)
1.5	0.67
2	1.02
2.5	1.28
3	1.50
3.5	1.69
4	1.86
4.5	2.02
5	2.17

Note: cms/cm: cubic meter per second per centimeter.

TABLE 6.32
Calculation Steps in Example 6.19

(1) t (min)	(2) t/T_p	(3) $1 - (t/T_p)$	(4) Exp $(1 - (t/T_p))$	(5) q_u (cms/cm)
0	0.00	1.00	2.72	0.00
10	0.19	0.81	2.24	0.76
20	0.38	0.62	1.85	1.61
30	0.58	0.42	1.53	2.22
40	0.77	0.23	1.26	2.56
50	0.96	0.04	1.04	2.68
60	1.15	–0.15	0.86	2.64
70	1.35	–0.35	0.71	2.49
80	1.54	–0.54	0.58	2.28
90	1.73	–0.73	0.48	2.04
100	1.92	–0.92	0.40	1.79
110	2.12	–1.12	0.33	1.55
120	2.31	–1.31	0.27	1.32
130	2.50	–1.50	0.22	1.12
140	2.69	–1.69	0.18	0.94
150	2.88	–1.88	0.15	0.78
175	3.37	–2.37	0.09	0.48
200	3.85	–2.85	0.06	0.28
250	4.81	–3.81	0.02	0.09
375	7.21	–6.21	0.00	0.00

$$L_t = 0.6\left(\frac{65}{60}\right) = 0.65 \text{ h.}$$

Then, with D = 25 min = 0.42 h, the time of peak discharge is calculated using Equation 6.25 as follows:

$$T_p = \frac{0.42}{2} + 0.65 = 0.86 \text{ h} = 52 \text{ min.}$$

Then, the peak discharge is calculated by using Equation 6.51:

$$q_p = \frac{(1.28)(1.8)}{0.86} = 2.68 \text{ cms/cm.}$$

According to Table 6.31 for P_r = 1.28 cms·h/km²·cm, n = 2.5. Finally, Equation 6.52 is used to determine the ordinates of the unit hydrograph. The summary of calculations is given in Table 6.32.

6.7.3 Averaging Storm Event Unit Hydrographs

Due to high uncertainty in the rainfall–runoff process, different storm events with the same duration of rainfall excess on the same watershed will produce completely different hydrographs (Figure 6.18). The main factors affecting response of a watershed to a storm event are storm pattern, storm volume, storm cell movement, and antecedent watershed conditions.

Since a single representative unit hydrograph is used in design practices, the unit hydrographs from the individual storm events are averaged to produce the representative hydrograph of the

watershed where several unit hydrographs are available. The following steps should be taken for averaging multiple unit hydrographs computed from different storm events on the same watershed.

1. Estimation of the average peak discharge of hydrographs.
2. Computation of the average time to peak for available hydrographs.
3. Plotting the storm event UHs on a single graph.
4. Plotting a unit hydrograph in a way that passes through the points defined in steps 1 and 2 and represents the average of the shapes of the plotted UHs.
5. Deriving the ordinates of the average unit hydrograph developed in step 4 and computing the volume of the average UH.
6. Adjusting the ordinates of the UH to have a volume of one area depth; it should be noted that the adjustments are usually made in the recession of the UH.

A basic assumption in the averaging method is that all of the available UHs have approximately the same unit duration. In cases where this assumption is not true, it is necessary to adjust the considered UHs using the S-hydrograph method prior to averaging. It should be noted that it is incorrect to compute an average of the ordinates for each time because the watershed-averaged UH in this way would have a low peak discharge and the shape would not be representative of the true unit hydrograph.

6.7.4 Dimensionless Unit Hydrographs

Due to the different characteristics of watersheds even in a relatively homogeneous region, UHs developed from different watersheds cannot directly be used to develop a regionalized UH using the averaging procedure described in the previous section. To overcome this difficulty and develop a region-wide UH, the individual watershed UHs are converted to a dimensionless form by dividing the runoff and time ordinates by the peak discharge and the time to peak, respectively. The resulting dimensionless UHs are then plotted and an average of the individual dimensionless UHs is drawn. This average dimensionless UH can be used for watersheds in the same region when the peak discharge and time to peak are computed using the available relationships.

6.8 INSTANTANEOUS UNIT HYDROGRAPHS

When the duration of rainfall excess approaches zero with a constant quantity (unit depth) of rainfall, a new form of unit hydrograph is developed. The runoff produced by this instantaneous rainfall is called the IUH. In other words, IUH is a response function for a particular watershed to a unit impulse of rainfall excess. Each watershed has a unique function for the IUH, which is independent of time or antecedent conditions. The output function or total storm discharge, $y(t)$, is produced by the summation of the outputs due to all instantaneous input $x(t)$.

For a continuous process, all of the issues included in the convolution process including multiplication, translation, and addition are done using the convolution integral:

$$Q(t) = \int_0^t x(\tau)U(t-\tau)\,\mathrm{d}\tau, \tag{6.14}$$

where $U(t)$ is the continuous function of UH and $Q(t)$ is the continuous function of direct runoff. $x(\tau)$ is the computed time distribution of rainfall excess, and τ is the time lag between the beginning times of rainfall excess and the unit hydrograph of direct runoff. A practical application of convolution integral (Equation 6.14), which was described in Section 6.5.3, is in the development of IUH. Rainfall contributes in the calculation of direct runoff as an input of the system, in instant time with

a depth of $I(\tau)d\tau$. $U(t-\tau)$ in Equation 6.14 is considered as a weighting function of rainfall intensities. Hence, multiplying $I(\tau)d\tau$ by $U(t-\tau)$, the runoff depth will be calculated as an output of the system. As a result, if the IUH of the watershed is determined, the direct runoff of the watershed would be evaluated using Equation 6.14.

The IUH can be derived from the S-curve hydrograph. It can be assumed that an S-curve is formed by a continuous rainfall. This rainfall is an infinite series of time units each separated by D. Given the summation of all unit hydrographs of duration D, the corresponding S-curve ordinates is derived as follows:

$$S(t) = [U(t) + U(t-D) + U(t-2D) + \cdots]. \tag{6.53}$$

The ordinate of a unit hydrograph corresponding to a rainfall event with Δt duration, $U(t,\Delta t)$, is obtained as follows:

$$U(t,\Delta t) = \frac{D}{\Delta t}\left[S(t) - S(t-\Delta t)\right] = D\frac{\Delta S(t)}{\Delta t}. \tag{6.54}$$

Regarding the IUH definition, when Δt approaches zero, $U(t)$ will be equal to IUH(t):

$$\mathrm{IUH}(t) = \lim_{\Delta t\to 0} U(t,\Delta t) = D\frac{\mathrm{d}S(t)}{\mathrm{d}t}. \tag{6.55}$$

Therefore, the IUH in any time t can be calculated by multiplying the slope of the S-curve by D (the duration of the unit hydrograph used for developing the S-curve).

In the same way, the S-curve can be derived from the IUH. The direct runoff depth is calculated from the convolution integral. If the input rainfall of system continues for the infinite period of time with the uniform intensity of $\left(\frac{1}{D}\right)$, the resulting hydrograph would be the S-curve.

$$S(t) = \frac{1}{D}\int_0^t U(t-\tau)\,\mathrm{d}\tau. \tag{6.56}$$

If $z = (t-\tau)$ is substituted in Equation 6.56 and considering $d\tau = -dz$, it will result in

$$S(t) = -\frac{1}{D}\int_0^t U(z)\,\mathrm{d}z. \tag{6.57}$$

If $U(t,D)$ is considered as the ordinate of a D-hour direct unit hydrograph (DUH) at time t, and $S(t)$ is the resulting S-curve from that DUH in time t, it will result in

$$u(t,\Delta t) = S(t) - S(t-\Delta t) = \frac{1}{D}\int_0^t U(z)\,\mathrm{d}z - \frac{1}{D}\int_0^{t-D} U(z)\,\mathrm{d}z$$

$$u(t,\Delta t) = \frac{1}{D}\int_{t-D}^{t} U(z)\,\mathrm{d}z. \tag{6.58}$$

Suppose that IUH is linear between t and $(t - D)$, then

$$u(t, \Delta t) = U(t) = U\left(t - \frac{D}{2}\right). \tag{6.59}$$

If D is relatively small and the peak runoff has not occurred between the time t and $(t - D)$, then Equation 6.59 would be a good approximation.

Even though the IUH concept has some disadvantages and limitations especially when rainfall–runoff responses are nonlinear or are dependent on antecedent moisture conditions, it is widely used in practice.

Example 6.20

From the 1 cm/h S-curve in Table 6.33, determine the IUH and then use it to estimate a 2 h unit hydrograph.

Solution:

Here,

$$U(t) = D\frac{dS}{dt},$$

where D = 2 h based on the data given in the example (1 cm/h S-curve is given) and dS/dt is approximated as $(S_{t+1} - S_{t-1})/\Delta t$, where Δt = 1 h (Table 6.34).

TABLE 6.33
S-Curve in Example 6.20

Time (h)	0	1	2	3	4	5	6	7	8	9
S-Curve (cms)	0	50	200	450	500	650	700	750	800	800

TABLE 6.34
IUH in Example 6.20

Time	S-Curve	IUH	
0	0	0	
1	50	50	
2	200	150	
3	450	250	This value is found as (450 – 200) × 1/1 = 250
4	500	50	
5	650	150	
6	700	50	
7	750	50	
8	800	50	This value is found as (800 – 750) × 1/1 = 50
9	800	0	

TABLE 6.35
2 h UH in Example 6.20

Time	IUH	IUH_{t-1}	IUH_{t-2}	2 h UH = ½[0.5IUH_t + IUH_{t-1} + 0.5IUH_{t-2}]	
0	0	0	0	0	
1	50	0	0	12.5	This value is found as (0.5 × 50 + 0 + 0)/2 = 12.5
2	150	50	0	62.5	
3	250	150	50	150	
4	50	250	150	175	
5	150	50	250	125	
6	50	150	50	100	This value is found as (50 × 0.5 + 150 + 50 × 0.5)/2 = 100
7	50	50	150	75	
8	50	50	50	50	
9	0	50	50	37.5	
10	0	0	50	12.5	

From Equation 6.58, since the unit hydrograph duration is 2 h and Δt = 1 h, the 2 h unit hydrograph is obtained from the equation $Q = \frac{1}{2}[0.5IUH_t + IUH_{t-1} + 0.5IUH_{t-2}]$, and it is assumed that IUH is linear in each Δt (Table 6.35).

Note: IUHs are a more general form of the unit hydrograph that can be used to generate unit hydrographs of rainfalls with different duration.

6.8.1 Nash Model

The Nash model is a method for deriving the IUH. In the theoretical model of Nash (1958), a watershed is modeled as a cascade of n reservoirs in series. It has been assumed that the storage–discharge relation for each of the hypothetical reservoirs is linear, $S = KQ$, where K is the average delay time for each reservoir. Then, the continuity equation is combined with the storage relation as follows:

$$I - Q = \frac{dS}{dt} = K\frac{dQ}{dt}, \tag{6.60}$$

or

$$Q + K\frac{dQ}{dt} = I. \tag{6.61}$$

Multiplying it by $e^{t/k}$, the above differential equation is solved as follows:

$$\frac{d}{dt}\left(Qe^{t/k}\right) = \frac{I}{K}e^{t/k}, \tag{6.62}$$

or

$$Qe^{t/k} = \frac{1}{K}\int\left(Ie^{t/k}\right)dt + C_1. \tag{6.63}$$

Considering an instantaneous inflow of unit volume to the reservoir, the reservoir discharge will be equal to the IUH dimension and Equation 6.63 can be written as

$$Q = e^{-t/k}\left[\frac{1}{K}\int e^{t/k}\delta(0)\,\mathrm{d}t + C_1\right] = \frac{1}{K}\left(e^{-t/k}\right). \tag{6.64}$$

The above integral is a Laplace transform of the δ-function (Dirac delta function) that simply picks out the value of the function at $t = 0$:

$$L(\delta(0)) = \int \delta(0)e^{-pt}\mathrm{d}t = e^{po} = 1. \tag{6.65}$$

Equations 6.63 and 6.64 show that the response of a linear reservoir to the pulse input is a sudden jump at the moment of inflow followed by an exponential decline. Since it is assumed that there are n serial reservoirs in the basin, the outflow of the first reservoir flows into a second reservoir, where Q_1 is inflow and Q_2 is outflow, then

$$Q_1 - Q_2 = K\frac{\mathrm{d}Q_2}{\mathrm{d}t}, \tag{6.66}$$

and its solution is

$$Q_2 = \frac{1}{K}\left(\frac{t}{K}\right)e^{t/K}. \tag{6.67}$$

By continuing this process, the outflow of the nth reservoir (basin outflow) is estimated as follows:

$$Q_n = \frac{1}{K(n-1)!}\left(\frac{t}{K}\right)^{n-1}e^{-t/K}. \tag{6.68}$$

This equation is true for positive integer values of n, and for other real values of n, $(n - 1)!$ is substituted by the gamma function ($\Gamma(n)$) as follows:

$$Q_n = \frac{1}{K\Gamma(n)}\left(\frac{t}{K}\right)^{n-1}e^{-t/K}. \tag{6.69}$$

Equation 6.68 is the probability density function of the gamma distribution. The general integral form of the gamma distribution is as follows:

$$\Gamma_n = \int_0^\infty e^{-x}\cdot x^{n-1}\mathrm{d}x. \tag{6.70}$$

Although Nash (1958) suggests that the model of Equation 6.69 represents the general equation form of the IUH, Gray (1962) has developed a unit hydrograph model using the two-parameter

gamma distribution. Equation 6.68 can be used to derive the S-curve from the Nash model as follows:

$$S(t) = \int_0^t \mathrm{IUH}(t)\mathrm{d}t = \frac{1}{K}\int_0^t \left(\frac{t}{K}\right)^{n-1} \cdot \frac{e^{t/k}}{\Gamma(n)}\mathrm{d}t. \tag{6.71}$$

For a given instantaneous unit rainfall that spreads uniformly over the basin, the IUH can be interpreted as the frequency distribution of arrival times of water particles at the basin outlet. The time lag between centriods of the IUH and $x(\tau)$, the input rainfall hyetograph, is the expected value or average time. $E(t)$ also represents the first moment of the IUH about $t = 0$.

$$E(t) = \int_0^\infty u(t)t\,\mathrm{d}t = nK\int_0^\infty \left(\frac{t}{K}\right)^n \frac{e^{-t/K}}{n!}\mathrm{d}\left(t/K\right),$$

or

$$E(t) = nK. \tag{6.72}$$

The variance, Var(t), can also be derived as follows:

$$\mathrm{Var}(t) = E\left(t^2\right) - [E(t)]^2 = \int_0^\infty u(t)t^2\,\mathrm{d}t - (nk)^2 = K^2 n(n+1) - n^2K^2 = K^2 n. \tag{6.73}$$

The mth moment of area is defined as follows:

$$M_m = \frac{\int_A f(x)\cdot \mathrm{d}x \cdot x^m}{\int_A f(x)\cdot \mathrm{d}x}. \tag{6.74}$$

With regard to this definition, the mth moment of IUH is defined as follows:

$$M_m = \frac{\int_0^\infty u(t)\cdot \mathrm{d}t \cdot t^m}{\int_0^\infty u(t)\cdot \mathrm{d}t}. \tag{6.75}$$

Due to the area under the IUH curve being always equal to 1,

$$M_m = \frac{1}{K\Gamma_n}\int_0^\infty e^{\left(\frac{-t}{k}\right)}\left(\frac{t}{k}\right)^{n-1} t^m \mathrm{d}t = \frac{K^m}{\Gamma_n}\int_0^\infty e^{\left(\frac{-t}{k}\right)}\left(\frac{t}{k}\right)^{n-1}\left(\frac{t}{k}\right)^m \mathrm{d}\left(\frac{t}{k}\right). \tag{6.76}$$

Regarding Equation 6.70,

$$M_m = \frac{K_m \Gamma_{m+n}}{\Gamma_n}. \tag{6.77}$$

The two parameters n and k should be estimated in the Nash model; the first and second moments are necessary for the estimation.

If $m = 1$, the first moment of IUH is $M_1 = n \cdot K$.

If $m = 2$, the second moment of IUH is $M_2 = n(n + 1)K^2$.

Every time the center point of an element moves nK to the right side, the area of the outflow moves nK to the right too; thus, regarding Equations 6.72 and 6.73, the values of n and K in the Nash model can be estimated by the method of moments:

$$M_{Q1} - M_{I1} = nK \tag{6.78}$$

and

$$M_{Q2} - M_{I2} = n(n + 1)K^2 + 2nKM_{I1}, \tag{6.79}$$

where M_{I1} and M_{I2} are the first and second moments of rainfall hyetograph about the time origin divided by the total excess rainfall volume, respectively, and M_{Q1} and M_{Q2} are the first and second moments of the runoff hydrograph about the time origin divided by the total direct runoff volume, respectively.

Example 6.21

For a catchment, the effective rainfall hyetograph of an isolated storm and the corresponding DRH are given in Tables 6.36 and 6.37, respectively. Determine the coefficients n and k of Nash model IUH.

Solution:

As the first step, the M_{I1} and M_{I2} of rainfall hyetograph are estimated about the time origin as follows:

$$M_{I1} = \frac{4.3\times1\times0.5 + 3.2\times1\times1.5 + 2.4\times1.0\times2.5 + 1.8\times1.0\times3.5}{4.3\times1.0 + 3.2\times1.0 + 2.4\times1.0 + 1.8\times1.0} = 1.23 \text{ h}$$

TABLE 6.36
Effective Rainfall Hyetograph

Time from Start of Storm (h)	Effective Rainfall Intensity (cm/s)
0–1.0	4.3
1.0–2.0	3.2
2.0–3.0	2.4
3.0–4.0	1.8

TABLE 6.37
Coordinates of DRH

Time from Start of Storm (h)	Direct Runoff (m^3/s)	Time from Start of Storm (h)	Direct Runoff (m^3/s)
0	0	9	32.7
1	6.5	10	23.8
2	15.4	11	16.4
3	43.1	12	9.6
4	58.1	13	6.8
5	68.2	14	3.2
6	63.1	15	1.5
7	52.7	16	0
8	41.9		

(for first-moment estimation, the numerator of the above relation, the area of each part of the hyetograph is multiplied by its center distance from the time origin)

$$M_{I2} = \frac{4.3\times1\times0.5^2 + 3.2\times1\times1.5^2 + 2.4\times1.0\times2.5^2 + 1.8\times1.0\times3.5^2}{4.3\times1.0 + 3.2\times1.0 + 2.4\times1.0 + 1.8\times1.0} = 2.89\ \text{h}^2$$

(for second-moment estimation, the numerator of the above relation, the area of each part of the hyetograph is multiplied by the square of its center distance from the time origin).

The same procedure is followed to estimate M_{Q1} and M_{Q2} based on the given runoff hydrograph. The calculations are summarized in Table 6.38.

TABLE 6.38
First and Second Moments of Outflow Hydrograph

Time from Start of Storm (h)	Direct Runoff (m^3/s)	ΔQ	Distance of Time Interval Center from Time Origin, t	t^2	$\Delta Q \times t$	$\Delta Q \times t^2$
0	0	–	–	–	–	–
1	6.5	3.25	0.5	0.25	1.625	0.8125
2	15.4	7.7	1.5	2.25	11.55	17.325
3	43.1	21.55	2.5	6.25	53.875	134.6875
4	58.1	29.5	3.5	12.25	101.675	355.8625
5	68.2	34.1	4.5	20.25	153.45	690.525
6	63.1	31.55	5.5	30.25	173.525	954.3875
7	52.7	26.35	6.5	42.25	171.275	1113.288
8	41.9	20.95	7.5	56.25	157.125	1178.438
9	32.7	16.35	8.5	72.25	138.975	1181.288
10	23.8	11.9	9.5	90.25	113.05	1073.975
11	16.4	8.2	10.5	110.25	86.1	904.05
12	9.6	4.8	11.5	132.25	55.2	634.8
13	6.8	3.4	12.5	156.25	42.5	531.25
14	3.2	1.6	13.5	182.25	21.6	291.6
15	1.5	0.75	14.5	210.25	10.875	157.6875
16	0	0	15.5	240.25	0	0
Sum	–	221.5	–	–	1292.4	9220

$$M_{Q1} = \frac{\sum \Delta Q \cdot t}{\sum \Delta Q} = \frac{1292.4}{221.5} = 5.83 \text{ h}.$$

$$M_{Q2} = \frac{\sum \Delta Q \cdot t^2}{\sum \Delta Q} = \frac{9220}{221.5} = 41.63 \text{ h}^2.$$

Equations 6.78 and 6.79 are employed to determine the Nash IUH parameters based on calculated values of M_{I1}, M_{I2}, M_{Q1}, and M_{Q2} as follows:

$$nK = M_{Q1} - M_{I1} = 5.83 - 1.23 = 4.6 \text{ h}.$$

$$M_{Q2} - M_{I2} = n(n+1)K^2 + 2nKM_{I1} \qquad 41.63 - 2.89 = n(n+1)K^2 + 2 \times 4.6 \times 1.23.$$

By solving the above equations, n is determined to be 3.377 and K is determined to be 1.362 h.

Example 6.22

Develop an IUH and a 2 h unit hydrograph in the catchment with an area of 200 km^2 with Nash model parameters of $n = 3$ and $K = 5$ h.

Solution:

$$Q_n = \frac{1}{K\Gamma(n)}\left(\frac{t}{K}\right)^{n-1} e^{-t/K},$$

$$K = 5 \text{ h}, \; n = 3, \; \Gamma n = (n-1)!;$$

$$\Gamma_3 = 2! = 2, \; K\,\Gamma n = 10, \; n - 1 = 2.$$

The calculation of the IUH and 2 h UH is shown in Table 6.39. For example, the calculation for time = 2 h is as follows:

$$t = 2\text{h} \rightarrow \frac{t}{K} = 0.4 \rightarrow e^{-t/k} = 0.67 \rightarrow \left(\frac{t}{K}\right)^{n-1} = 0.16$$

$$Q_n = \frac{1}{5 \times 2}\left(\frac{t}{K}\right)^{n-1} e^{-t/K} = 0.01 \text{ (cm/h)}$$

$$\text{IUH}(2) = 2.778 \times A \times \text{U}(0,2) = 5.96 \text{ (m}^3\text{/s)}$$

$$\text{UH}(t) = (\text{IUH}(t) + \text{IUH}(t-1))/2 = 2.98 \text{ m}^3\text{/s}.$$

TABLE 6.39
IUH and 2 h UH Calculation Using NASH Model

Time (h) (1)	t/K (2)	$e^{-t/K}$ (3)	$(t/K)^{n-1}$ (4)	$U(0,t)$ (5)	IUH (6)	2 h UH (7)
0	0	1.00	0	0	0	0
2	0.4	0.670	0.16	0.010	5.96	2.98
4	0.8	0.449	0.64	0.028	16	10.98
6	1.2	0.301	1.44	0.043	24	20
8	1.6	0.201	2.56	0.051	28.4	26.2
10	2	0.135	4	0.054	30.1	29.3
12	2.4	0.090	5.76	0.052	29.1	29.6
14	2.8	0.060	7.84	0.047	26.7	27.9
16	3.2	0.040	10.24	0.041	23.4	25.1
18	3.6	0.027	12.96	0.035	19.4	21.4
20	4	0.018	16	0.029	16.3	17.8
22	4.4	0.012	19.36	0.023	13.1	14.7
24	4.8	0.008	23.04	0.018	10.5	11.8
26	5.2	0.005	27.04	0.014	8.3	9.4
28	5.6	0.003	31.36	0.011	6.45	7.38
30	6	0.002	36	0.008	5	5.73
32	6.4	0.001	40.96	0.006	3.83	4.42
34	6.8	0.002	46.24	0.005	2.82	3.32

6.8.2 Laplace Transformation Model

Laplace transformation can also be used for deriving the unit hydrograph. Two approaches are considered in this method's application. In the first approach, the basin is simulated as a linear reservoir, and in the second, the basin is simulated as a channel. Each of these cases is described in the next subsections.

6.8.2.1 Basin as a Linear Reservoir

The continuity equation for a linear reservoir is as follows:

$$I - Q = K\frac{\mathrm{d}Q}{\mathrm{d}t}, \tag{6.80}$$

where I is the basin input (rainfall), Q is the basin output (discharge), and K is the basin lag time. If the differential operator $D = \mathrm{d}/\mathrm{d}t$ is used, Equation 6.80 changes to

$$Q = \frac{1}{1+KD}I(t). \tag{6.81}$$

This mathematically equals

$$Q = \frac{1}{k}e^{-t/k}\int e^{t/k}I\,\mathrm{d}t. \tag{6.82}$$

If the input of Equation 6.82 is equal to 1, the resulting hydrograph would be an S-hydrograph as follows:

$$U(t) = 1 - e^{-t/k}. \tag{6.83}$$

As mentioned before, the slope of the S-curve is proportional to the ordinates of instantaneous hydrograph,

$$h(t) = \frac{e^{-t/k}}{K}. \tag{6.84}$$

If $1/K$ is replaced with a, then the Laplace transformation function of Equation 6.84 would be as follows:

$$h(s) = a\left(\frac{1}{s+a}\right). \tag{6.85}$$

Using the above equation, the IUH of the basin in the form of the Laplace function and based on its lag time is obtained. The runoff–rainfall analysis is done using the following equation:

$$Q(s) = h(s)I(s), \tag{6.86}$$

where $I(s)$, $h(s)$, and $Q(s)$ are rainfall in the form of the Laplace function, unit hydrograph, and runoff, respectively. The actual runoff values are determined by applying an inverse Laplace function on $Q(s)$.

For calculating $I(s)$, rainfall values should be defined in the form of a continuous function. Therefore, unit cascade function ($u_1(t)$) is used for definition of rainfall components.

$$I(t) = \sum_{j=0}^{m} w_j u_1(t - jD). \tag{6.87}$$

The unit cascade function is defined as follows:

$$u_1(t) = \begin{cases} 0, & t < 0 \\ 1, & t \geq 0 \end{cases}. \tag{6.88}$$

D is rainfall measurement interval and w values are determined as follows:

$$w_0 = I_0,\ w_j = I_j - I_{j-1} \quad j = 1,2,3,\ldots,m. \tag{6.89}$$

Example 6.23

Consider a basin as a linear reservoir with 6 h lag time. Determine the resulting runoff from the rainfall given in Table 6.40.

TABLE 6.40
Hyetograph in Example 6.23

Time (h)	0	0.5	1	1.5	2
i (cm/h)	5	2	1	2	0

Solution:

The weights and rainfall components are determined as follows:

$$w_j = I_j - I_{j-1}$$
$$w_0 = 5 - 0 = 5$$
$$w_1 = 2 - 5 = -3$$
$$w_2 = 1 - 2 = -1$$
$$w_3 = 2 - 1 = 1$$
$$w_4 = 0 - 2 = -2$$

and

$$I(t) = 5u_1(t) - 3u_1(t - 0.5) - u_1(t - 1) + u_1(t - 1.5) - 2u_1(t - 2).$$

Using the Laplace transformation function, the above equation is changed as follows:

$$I(s) = \frac{1}{s}\left[5 - 3\exp(-0.5s) - \exp(-s) + \exp(-1.5s) - 2\exp(-2s)\right],$$

which can be used in Equation 6.78.

According to Equation 6.85, the IUH Laplace function for this basin is

$$h(s) = \frac{1}{6}\left(\frac{1}{s + \frac{1}{6}}\right),$$

and using Equation 6.86, runoff is calculated as follows:

$$Q(s) = \frac{1}{6}\left(\frac{1}{s + \frac{1}{6}}\right)\left[5 - 3\exp(-0.5s) - \exp(-s) + \exp(-1.5s) - 2\exp(-2s)\right]\frac{1}{s}$$

$$= \frac{1}{6s\left(s + \frac{1}{6}\right)}\left[5 - 3\exp(-0.5s) - \exp(-s) + \exp(-1.5s) - 2\exp(-2s)\right].$$

Using the equation of $\frac{1}{s(s+a)}=\frac{1}{sa}-\frac{1}{a(s+a)}$, it is simplified as follows:

$$Q(s)=5\left(\frac{1}{s}-\frac{1}{1+\frac{1}{6}}\right)-3\exp(-0.5s)\left(\frac{1}{s}-\frac{1}{s+\frac{1}{6}}\right)-\exp(-s)\left(\frac{1}{s}-\frac{1}{s+\frac{1}{6}}\right)$$
$$+\exp(-1.5s)\left(\frac{1}{s}-\frac{1}{s+\frac{1}{6}}\right)-2\exp(-2s)\left(\frac{1}{s}-\frac{1}{s+\frac{1}{6}}\right).$$

Using the inverse Laplace transformation, runoff is determined as follows:

$$Q(t)=5\times u_1(t)\left[1-\exp(-t/6)\right]-3u_1(t-0.5)\left[1-\exp\left(-(t-0.5)/6\right)\right]$$
$$-u_1(t-1)\left[1-\exp\left(-(t-1)/6\right)\right]+u_1(t-1.5)\left[1-\exp\left(-(t-1.5)/6\right)\right]$$
$$-2u_1(t-2)\left[1-\exp\left(-(t-2)/6\right)\right].$$

The calculated runoff in different time steps is given in Table 6.41. For example, the calculation for the time = 0.5 h and 1 h are as follows:

$$Q(0.5) = 5 \times u_1(0.5)[1 - \exp(-0.5/6)] = 0.4$$

$$Q(0.5) = 5 \times u_1(1)[1 - \exp(-1/6)] - 2 \times u_1(0.5)[1 - \exp(-1/6)] = 0.53.$$

TABLE 6.41
Runoff in Example 6.23

Time (h)	Q (cm/h)	Time (h)	Q (cm/h)
0	0	5.5	0.38
0.5	0.4	6	0.35
1	0.53	6.5	0.32
1.5	0.57	7	0.30
2.0	0.68	7.5	0.27
2.5	0.63	8	0.25
3	0.58	9	0.21
3.5	0.53	12	0.13
4.0	0.49	16	0.07
4.5	0.45	20	0.03
5.0	0.41		

6.8.2.2 Basin as a Channel

In this case, by assuming the basin as a linear channel, the unit hydrograph is defined using the cascade function as follows:

$$h(t) = \frac{1}{T}\left[u_1(t) - u_1(1-T)\right], \tag{6.90}$$

where T is channel travel time. Considering the above equation and knowing the rainfall amount, the runoff is calculated using Equation 6.86. The Laplace transfers of commonly used functions are given in the Appendix.

Example 6.24

Consider a linear channel with 6 h travel time. Using the effective rainfall hyetograph of Example 6.23, develop the DRH.

Solution:

The IUH of the given example is calculated from Equation 6.90, when T = 6 h:

$$h(t) = \frac{1}{6}\left[u_1(t) - u_1(t-6)\right].$$

The Laplace form of this equation is

$$h(s) = \frac{1}{6s}\left[1 - \exp(-6s)\right].$$

Using the effective rainfall hydrograph given in the previous example, the direct runoff is estimated as follows:

$$\begin{aligned} Q(s) &= \frac{1}{6s}\left[1-\exp(-6s)\right]\left[5-3\exp(-0.5s)-\exp(-s)+\exp(-1.5s)-2\exp(-2s)\right]\frac{1}{s} \\ &= \frac{1}{6s^2}\left[5-3\exp(-0.5s)-\exp(-s)+\exp(-1.5s)-2\exp(-2s)-5\exp(-6s)+3\exp(-6.5s)\right. \\ &\left.+\exp(-7s)-\exp(-7.5s)+2\exp(-8s)\right]. \end{aligned}$$

Applying the inverse Laplace results in

$$\begin{aligned} Q(t) = \frac{1}{6}\big[&5t - 3u_1(t-0.5) - u_1(t-1)(t-1) + u_1(t-1.5)(t-1.5) - 2u_1(t-2)(t-2) \\ &- 5u_1(t-6)(t-6) + 3u_1(t-6.5)(t-6.5) + u_1(t-7)(t-7) \\ &- u_1(t-7.5)(t-7.5) + 2u_1(t-8)(t-8)\big]. \end{aligned}$$

TABLE 6.42
DRH in Example 6.24

Time (h)	*Q* (cm/h)	Time (h)	Q (cm/h)
0	0	4.5	0.833
0.5	0.417	5	0.833
1	0.583	5.5	0.833
1.5	0.667	6	0.833
2	0.833	6.5	0.415
2.5	0.833	7	0.250
3	0.833	7.5	0.167
3.5	0.833	8	0.0
4	0.833		

The results are tabulated in Table 6.42. For example, the calculations for time = 0.5 h and 1 h are as follows:

$$Q(0.5) = \frac{1}{6}\left[5 \times 0.5 - 3u_1(0)\right] = 0.417$$

$$Q(1) = \frac{1}{6}\left[5 - 3u_1(0.5) - u_1(0)(1-1)\right] = 0.583.$$

6.8.3 Time–Area Unit Hydrographs

The unit hydrographs are derived directly from gauged data, and therefore, their duration is equal to the duration of excess rainfall from which they were derived. However, the duration of developed synthetic unit hydrograph is generally dependent on the specific parameters employed in UH development method. The time–area synthetic unit hydrographs, which are also called Clark unit hydrographs, are IUHs with no duration, and in this respect, they are slightly different from other synthetic unit hydrographs. However the Clark unit hydrograph follows the fundamental properties of a unit hydrograph in that the runoff is the result of unit depth of uniformly generated excess precipitation over the basin. The excess precipitation at an infinitely small duration is applied uniformly over a watershed, which is broken into time–area increments.

The advantages of this method are as follows:

1. The procedure is repeatable with the same data because the parameters are estimated mathematically based on observed hydrographs. The only exception is in deriving the time–area curve, which is somehow related to individual judgment.
2. The method is not dependent on spatial distribution of runoff.
3. The method is able to incorporate the shape of the drainage area and to produce large peak flows from concentrated runoff, but its accuracy is dependent on the accuracy of the developed time–area relationship.
4. The duration of the rainfall is infinitely short. The time of concentration is defined as the time between the end of rainfall and the inflection point on the hygrograph's falling limb.

However, this method has some limitations as well:

1. Hydrographs usually underestimate the recession side, especially the part between the point of maximum recession rate and the point where baseflow becomes dominating.

2. There are some limitations on method applications in very large drainage areas. The method may result in too slow a rise and too rapid a recession of hydrograph because of the use of the same storage factor for points with different distances from the outlet. A specific value of the maximum size of the drainage basin is not recommended; however, the basin can be divided into several sub-basins to overcome this disadvantage.
3. Finally, Clark admits that while the method appears to account for the drainage basin shape and the capacity to produce high peak flows, it is possible that these influences are exaggerated by the method.

In this method, a translation hydrograph at the basin outlet is developed by translating (lagging) the excess hydrograph based on travel time to the outlet. The resulting outflow from routing the translation hydrograph through a single linear reservoir (a reservoir in which the storage, S, is a linear function of outflow, O, as $S = KO$) is the IUH for the basin. Figure 6.21 shows the components of the Clark method.

The translation hydrograph is derived from a time–area relation where the area is the accumulated area from the basin outlet and the time is the travel time as defined by isochrones (contours of constant travel time). The time–area relationship can also be presented in dimensionless form that area and time are presented as the percentage of total basin area and the percentage of time of concentration (t_c), respectively. The translation hydrograph can be estimated by determining the portion of the basin that contributes to the runoff at the outlet during each time interval after the occurrence of the instantaneous burst of unit excess rainfall. The ordinate of the translation hydrograph for an interval is the average discharge from the contributing area associated with that interval.

Isochrones, which are used in the definition of the translation hydrograph, are developed by estimating the overland flow and river travel times to the basin outlet for a number of points in the basin. In a simpler approach, a constant travel velocity is assumed and the position of isochrones is determined based on travel distance from the basin outlet. In this case, only the basin shape is reflected by the translation hydrograph.

In a simpler approach, a standard basin shape, such as an ellipse, is considered for the development of the translation hydrograph. In most basins, the storage effect, which is represented by the linear reservoir, results in a considerable decrease in the translation hydrograph, and therefore, the obtained IUH is not very sensitive to the shape of the translation hydrograph. However, in basins

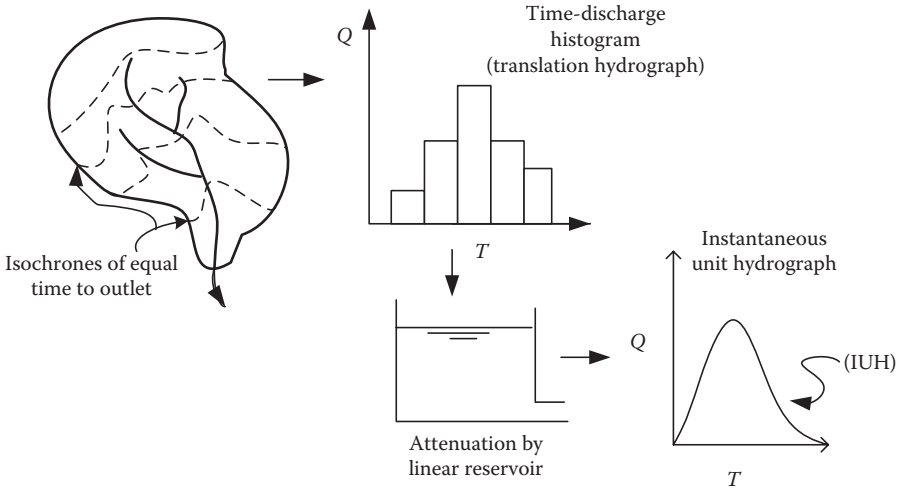

FIGURE 6.21 Components of the Clark model.

without considerable amounts of natural storage such as a steep urban basin, the IUHs are sensitive to the shape of the translation hydrograph and the usage of a standard shape is not recommended.

The translation hydrograph is routed through a linear reservoir using the simple storage routing method, which is based on the continuity equation, as follows:

$$O(t) = C_a I + C_b O(t-1), \tag{6.91}$$

where $O(t)$ is the ordinate of IUH at time t, t is the time interval with which IUH is defined, and I is the ordinate of the translation hydrograph for interval $t-1$ to t. If the calculations are in cubic meters per second, I is calculated as follows:

$$I = \frac{2.78}{\Delta t} \cdot a_t, \tag{6.92}$$

where a_t is the ordinate of time-discharge histogram at the end of time t in square kilometers and Δt is the time interval in the time-discharge histogram in hours. This equation is true for a unit hydrograph of 1 cm effective rainfall depth. This equation is based on the assumption that the produced runoff in each part of the time-discharge histogram will reach the outflow in a constant rate during the time interval of Δt. The runoff volume in each time step is equal to the corresponding area of the watershed (determined based on the time-discharge histogram) multiplied by excess rainfall depth, which in IUH is set as a unit.

The coefficients C_a and C_b are also defined as follows:

$$C_a = \frac{\Delta t}{R_s + 0.5\Delta t} \tag{6.93}$$

and

$$C_b = 1 - C_a, \tag{6.94}$$

where R_s is the storage coefficient for a linear reservoir. The difference between the time–area translation hydrograph and the basin outflow hydrograph is caused by basin storage and the resulting attenuation of the hydrograph. The Clark IUH relies on the Muskingum storage coefficient, K (now termed R_s in most references to the Clark method), to represent the attenuation imposed by basin storage properties. R_s is calculated as follows:

$$R_s = -\frac{O}{\left(\frac{dO}{dt}\right)}. \tag{6.95}$$

Clark defines the time of concentration, t_c, as the time between the cessation of runoff-producing precipitation and the time at which the minimum value of R_s occurs. This time of concentration is used to produce the translation histogram. The time of concentration is then the maximum value used in the time–area relationship and the time–area curve is broken into smaller time intervals representing percentages of the time of concentration. Clark notes that this time–area curve delineation is indeed a trial-and-error procedure in many cases.

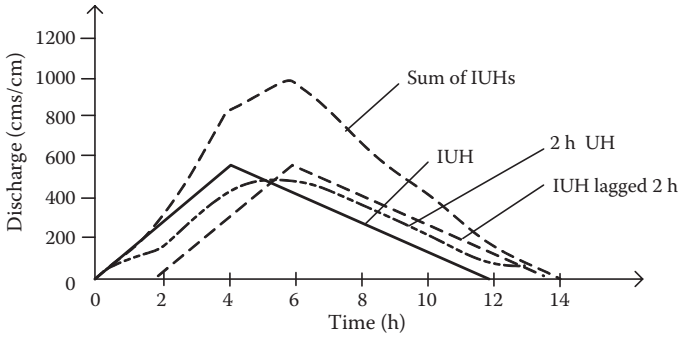

FIGURE 6.22 Conversion of IUH into UH with specific duration.

TABLE 6.43
Example of Developing a 2 h Unit Hydrograph from 2 h IUH

Time (h) (1)	IUH Coordinate ($m^3/s/cm$) (2)	IUH Lagged 2 h (3)	Sum of (2) and (3) (4)	2 h UH ($m^3/s/cm$) (5)
0	0	0	0	0
2	300	0	300	150
4	600	300	900	450
6	450	600	1050	525
8	300	450	750	375
10	150	300	450	225
12	0	150	150	75
14	0	0	0	0

The two parameters—t_c, the time of concentration (and time base for the translation hydrograph), and R_s, the storage coefficient for the linear reservoir—along with a time–area relation are used in the Clark method to derive a unit hydrograph.

For calculation of direct runoff, the IUH is converted into a unit hydrograph (UH) of finite duration. Techniques similar to those employed to change the duration of a UH are used to derive a UH of specified duration from the IUH. For example, for deriving a 2 h UH, the ordinates of two IUHs, one of which is lagged 2 h, are summed. The resulting hydrograph is the result of 2 cm of excess precipitation, and to obtain the required UH, the ordinates are divided by 2. This procedure is shown in Figure 6.22 and Table 6.43.

Example 6.25

Using the Clark method, develop a 15 min unit hydrograph for an urban watershed with an area of 43 ha and a time of concentration of 45 min. The time–area curve for this watershed is given in columns 1 and 2 of Table 6.44. Assume that the storage coefficient is equal to 10 min.

Solution:

For D = 15 min, the rainfall intensity is i_e = 1 cm/15 min = 0.0011 cm/s = 0.000011 m/s. The translation hydrograph presented in column 3 of Table 6.44 is calculated by multiplying the rainfall

TABLE 6.44
Summary of Time–Area Unit Hydrograph Analysis in Example 6.25

(1)	(2)	(3)	(4)	(5)	(6)	(7)
t (min)	A_c (ha)	I (m³/s)	IUH (m³/s)	15 min Lagged IUH (m³/s)	Sum of (4) and (5) (m³/s)	15 min UH (m³/s)
0	0	0.000	0.000	0.000	0	0
5	3.14	0.349	0.140	0.000	0.140	0.070
10	8.62	0.958	0.467	0.000	0.467	0.233
15	15.68	1.742	0.977	0.002	0.979	0.490
20	22.74	2.527	1.597	0.008	1.605	0.802
25	28.22	3.136	2.212	0.016	2.229	1.114
30	31.36	3.484	2.721	0.027	2.748	1.374
35	36.72	4.080	3.265	0.037	3.302	1.651
40	40.03	4.448	3.738	0.045	3.783	1.892
45	43	4.778	4.154	0.054	4.208	2.104
50		0.000	2.492	0.062	2.555	1.277
55		0.000	1.495	0.069	1.565	0.782
60		0.000	0.897	0.042	0.939	0.469
65		0.000	0.538	0.025	0.563	0.282
70		0.000	0.323	0.015	0.338	0.169
75		0.000	0.194	0.009	0.203	0.101
80		0.000	0.116	0.005	0.122	0.061
85		0.000	0.070	0.003	0.073	0.036
90		0.000	0.042	0.002	0.044	0.022
95		0.000	0.025	0.001	0.026	0.013
100		0.000	0.015	0.001	0.016	0.008
105		0.000	0.009	0.000	0.000	0.000

intensity by the corresponding area in the outlet flow at time t. Then, C_a and C_b are calculated as follows (using Equation 6.86):

$$C_a = \frac{5}{10 + 0.5 \times 5} = 0.4 \text{ and } C_b = 1 - C_a = 1 - 0.4 = 0.6.$$

The ordinates of IUH are calculated using Equation 6.93 (column 4). The outflow at time zero is equal to zero.

For calculation of the 15 min unit hydrograph, first, the ordinates of two IUHs, one of which is lagged 15 min, are summed. The resulting hydrograph results in 2 cm excess rainfall; therefore, the results are divided by 2 to develop the 15 min unit hydrograph of the watershed (column 7).

Also, the area under the unit hydrograph can be checked to correspond to 1 cm of excess rainfall. The volume of runoff represented by the unit hydrograph is equal to $\Delta t(\Sigma Q_u)$ = (5 min)(60 s/min)(12.95 m³/s) = 3885.37 m³. The basin area is (43 ha)(10,000 m²/ha) = 430,000 m². Dividing the runoff volume by the basin area, the rainfall depth is obtained as (3885.37)/(430,000) = 0.009 m = 0.9 cm < 1.0 cm.

Hence, there is about 10% error in this computation.

Example 6.26

A watershed is shown in Figure 6.23 and the isochrones are marked. A hydrograph observed due to a storm of 2 h duration is also shown in Figure 6.24. Determine the IUH and the 2 h duration unit hydrograph.

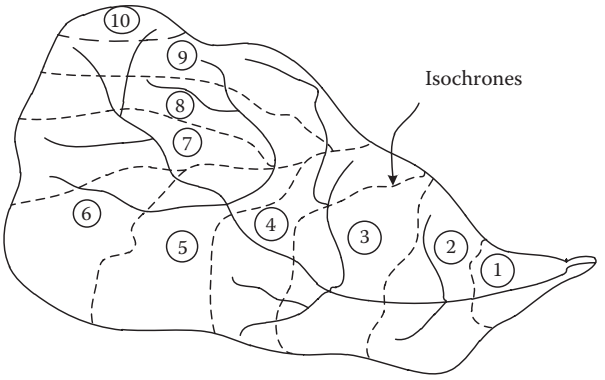

FIGURE 6.23 Watershed in Example 6.26.

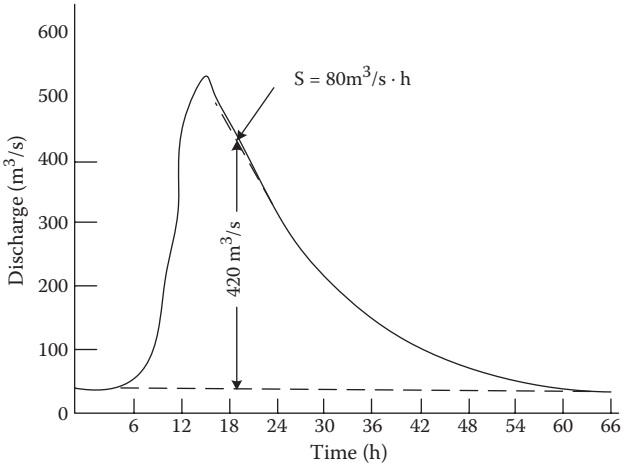

FIGURE 6.24 Hydrograph observed due to a storm of 2 h duration in the watershed in Example 6.26.

Solution:

Time of concentration is 10 h based on the largest travel time in Figure 6.24.

Based on Equation 6.95, R_s is calculated as follows:

$$R_s = \frac{420}{80} = 5.25 \text{ h}.$$

Based on Figure 6.23, the corresponding area in outflow at each time step is calculated as given in Table 6.45. Figure 6.25 shows the time–area graph of the given watershed using columns 3 and 5 of Table 6.45.

Table 6.46 is then completed using the following equations:

$$I_i = \frac{0.278}{2} a_i = 0.139 a_i$$

$$C_a = \frac{2\Delta t}{2K + \Delta t} = \frac{2(2)}{2(5.25) + 2} = 0.32$$

$$O_i = C_a I_i + (1 - C_a) O_{i-1} = 0.32 I_i + 0.68 O_i$$

TABLE 6.45
Travel Time Calculation for Example 6.26

Map Area Number	Area (km²)	Cumulated Area (km²)	Travel Time (h)	Travel Time (%)
1	10	10	1	10
2	25	35	2	20
3	50	85	3	30
4	55	140	4	40
5	70	210	5	50
6	65	275	6	60
7	80	355	7	70
8	100	455	8	80
9	110	565	9	90
10	30	595	10	100

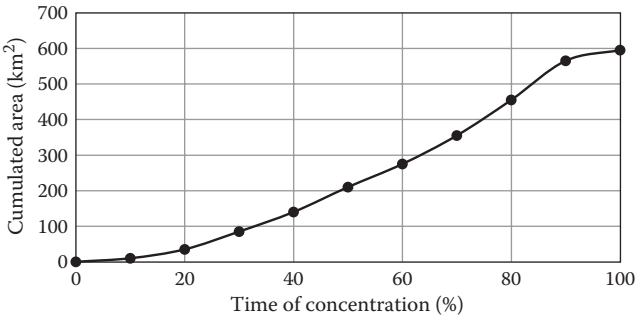

FIGURE 6.25 Time–area graph in Example 6.26.

TABLE 6.46
Developed 2 h Unit Hydrograph in Example 6.26

No.	Time (h)	Cumulated Area (km²)	Incremental Area a_i	I (m³/s)	IUH (m³/s)	2 h UH
1	0	0	0	0	0	0
2	2	35	35	4.9	1.57	0.39
3	4	140	105	14.6	5.74	2.22
4	6	275	135	18.8	9.92	5.74
5	8	460	185	25.7	15	10.15
6	10	595	135	18.8	16.22	14.04
7	12		0	0	11.03	14.62
8	14				7.5	11.45
9	16				5.1	7.78
10	18				3.47	5.29
11	20				2.36	3.60
12	22				1.6	2.45
13	24				1.09	1.66
14	26				0.74	1.13
15	28				0.5	0.77
16	30				0.34	0.52
17	32				0.23	0.35
18	34				0.16	0.24

The 2 h unit hydrograph ordinates are calculated based on Equation 6.58 as follows:

$$Q_i = 0.5(0.5O_{i-2} + O_{i-1} + 0.5O_i).$$

The above relationship is developed based on the assumption of linear behavior of the IUH within each time interval.

6.9 ROUTING METHODS

6.9.1 Hydrologic Methods of River Routing

The St. Venant equations are used to simulate the flow condition in unsteady and nonuniform rivers. Since the dynamic nature of the system is explained by these models, they are referred to as "dynamic models." However, there is no analytical solution for the St. Venant equations and complicated computer programs are needed to find the numerical solutions. Therefore, some methods with some simplifications are developed for river routing. The simplified methods are classified into two groups: hydraulic and hydrologic models. The St. Venant equations are used in hydraulic models; however, in developing hydrologic models, the momentum and continuity equations are replaced by some assumed relationships. These simpler models have some disadvantages, the most important of which is that some phenomena that affect the flow, such as downstream backwater, are not considered.

When a flood wave passes through a river reach, the peak of the outflow hydrograph is usually attenuated and delayed due to channel resistance and storage capacity. The shaded areas in Figure 6.26a show the difference between the ordinates of the inflow and outflow hydrographs, in a lumped storage approach for the river reach. Regarding the quantity equation, the difference between input and output hydrographs is equal to the rate of storage change in the considered river reach. This is formulated as follows:

$$\frac{\Delta S}{\Delta t} = I - Q. \tag{6.96}$$

The sign of $\Delta S/\Delta t$ is positive when storage is increasing and negative when storage is decreasing. The variation of S with time is also plotted in Figure 6.26b. Equation 6.86 can also be written in finite-difference form as given in Equation 6.97.

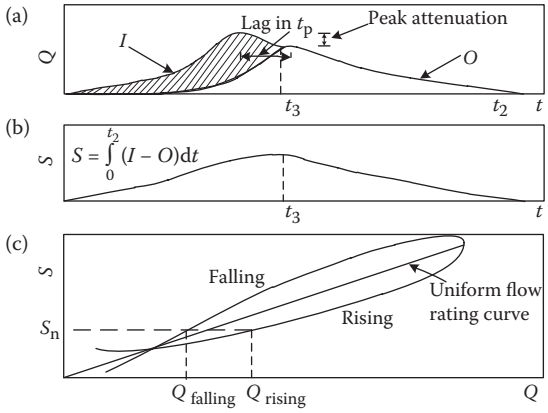

FIGURE 6.26 River routing. (a) Inflow and outflow hydrographs of a river reach. (b) Variation of storage in the river reach. (c) Variation of storage against outflow of the river reach.

$$\frac{S_2 - S_1}{\Delta t} = \frac{I_1 + I_2}{2} - \frac{Q_1 + Q_2}{2}, \tag{6.97}$$

where Δt is the routing time period and subscripts 1 and 2 denote the beginning and end of the time period, respectively.

By plotting storage variations against outflow for a river reach, it will result in a loop-form curve (Figure 6.26c). Therefore, the storage volumes during falling and rising stages are different and are bigger in the falling stage. The concept of prism and wedge storage can be used to evaluate water surface profile variations at various times during the passage of the flood wave from a river reach (Figure 6.27). During rising stages, before increasing the outflows, a large volume of wedge storage exists. During falling stages, the inflow decreases more rapidly than outflow, and the wedge storage becomes negative. Therefore, for hydrologic routing in rivers and channels, a storage relationship that allows for wedge storage is required. This is provided in the Muskingum method of flood routing by considering storage as a function of both inflow and outflow (McCarthy 1938). The main disadvantage of this method is the use of the uniform flow rating curve instead of the loop curve.

6.9.1.1 Muskingum Method

In this method, the outflow hydrograph at the downstream of a river reach is calculated for a given inflow hydrograph at the upstream. The uniform short branches of the river are modeled as a single reach, but the long branches with various characteristics in length are often divided into several reaches and each is modeled separately. When more than one reach is considered, the calculations start from the most upstream reach and then proceed in the direction of the downstream. The outflow from the upstream reach is used as the inflow for the next downstream reach.

As there are two unknown variables in the continuity equation including S and Q in Equation 6.86, a second relationship should be developed to solve the flood routing problem. In the Muskingum method, a linear relationship is assumed between S, I, and Q as follows:

$$S = K[XI + (1 - X)Q], \tag{6.98}$$

where K is the travel time constant and X is the weighting factor, which varies between 0 and 1. The parameters K and X are constant for a river and do not have physical meaning. These parameters

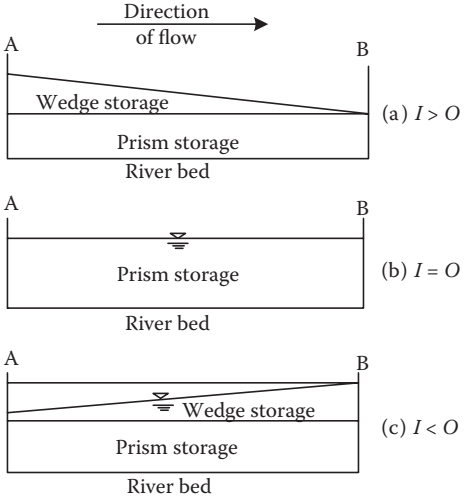

FIGURE 6.27 Prism and wedge storage concepts comparing inflow with outflow: (a) rising stage ($I > O$), (b) $I = O$, and (c) falling stage ($I < O$).

are determined during model calibration. For the case of linear reservoir routing where S depends only on outflow, $X = 0$ in Equation 6.88. In smooth uniform channels, $X = 0.5$ yields equal weight to inflow and outflow, which theoretically results in pure translation of the wave. A typical value for most natural streams is $X = 0.2$.

By substituting the obtained relation in Equation 6.101 into Equation 6.97, the following equation is obtained:

$$Q_2 = C_0 I_2 + C_1 I_1 + C_2 Q_1, \tag{6.99}$$

where

$$C_0 = \frac{(\Delta t/K) - 2X}{2(1-X) + (\Delta t/K)} \tag{6.100}$$

$$C_1 = \frac{(\Delta t/K) + 2X}{2(1-X) + (\Delta t/K)} \tag{6.101}$$

$$C_2 = \frac{2(1-X) - (\Delta t/K)}{2(1-X) + (\Delta t/K)}. \tag{6.102}$$

Note that $C_0 + C_1 + C_2 = 1.0$ and K and Δt must have the same units.

Q_2 is the only unknown variable in routing Equation 6.99. The I_2 and I_1 are obtained from the given inflow hydrograph and Q_1 is obtained from the initial condition of the river reach or from the previous time-step computation.

Example 6.27

The inflow hydrograph for a river reach with an initial steady flow equal to 45 m^3/s is given in Figure 6.28. Calculate the outflow hydrograph in 1 h time increments. The Muskingum parameters are determined as $K = 3$ h and $X = 0.15$.

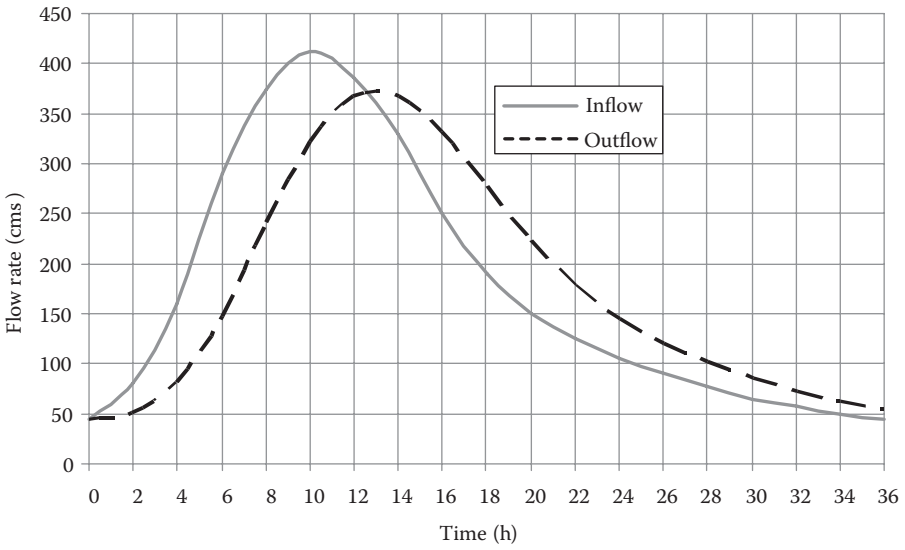

FIGURE 6.28 Inflow and outflow hydrographs in Example 6.27.

Solution:

Using Equations 6.100 through 6.102, the weighting factors are estimated as follows: $C_0 = 0.016$, $C_1 = 0.311$, and $C_2 = 0.672$. The routing calculations are given in Table 6.47. The I_1 and I_2 values for each time are calculated using the inflow hydrograph presented in Figure 6.28. The beginning and end time of each 1 h time increment are tabulated in columns 2 and 3 of Table 6.47. Because the initial flow in the river is equal to 45 m^3/s, Q_1 of the first time period has been set as 45 m^3/s. The routed outflow hydrograph is also presented in Figure 6.28.

TABLE 6.47
Summary of Example 6.27 Calculations

(1)	(2)	(3)	(4)	(5)	(6)	(7)
Time step	**t_1 (hr)**	**t_2 (hr)**	**I_1 (cms)**	**I_2 (cms)**	**Q_1 (cms)**	**Q_2 (cms)**
1	0	1	45	62	45	45
2	1	2	62	80	45	51
3	2	3	80	120	51	61
4	3	4	120	160	61	81
5	4	5	160	225	81	108
6	5	6	225	290	108	147
7	6	7	290	333	147	195
8	7	8	333	375	195	241
9	8	9	375	394	241	285
10	9	10	394	412	285	321
11	10	11	412	399	321	351
12	11	12	399	385	351	367
13	12	13	385	358	367	372
14	13	14	358	330	372	367
15	14	15	330	290	367	354
16	15	16	290	250	354	332
17	16	17	250	220	332	305
18	17	18	220	190	305	277
19	18	19	190	170	277	248
20	19	20	170	150	248	222
21	20	21	150	138	222	198
22	21	22	138	125	198	178
23	22	23	125	115	178	160
24	23	24	115	105	160	145
25	24	25	105	98	145	132
26	25	26	98	90	132	121
27	26	27	90	84	121	111
28	27	28	84	77	111	102
29	28	29	77	71	102	94
30	29	30	71	65	94	86
31	30	31	65	61	86	79
32	31	32	61	57	79	73
33	32	33	57	53	73	68
34	33	34	53	49	68	63
35	34	35	49	47	63	58
36	35	36	47	45	58	54

6.9.1.2 Determination of Storage Constants

For a natural stream, an average of 0.2 is considered for the Muskingum X and the travel time for a flood wave through the reach is used to estimate K. When both inflow and outflow hydrograph records are available, the graphical methods are preferred to better estimate K and X. In the graphical method considering different values of X, storage, S, is plotted against weighted discharge, $XI + (1 - X)O$. The best value for X corresponds to the plot that yields the most linear single-valued curve. In the Muskingum method, it is assumed that this curve is a straight line with reciprocal slope K. Thus, in the Muskingum method, storage is considered as a single-valued function of weighted inflow and outflow. Figure 6.29 shows the procedure of selecting appropriate values of X and K. The concept is further clarified in Example 6.27.

To achieve more accurate results from the Muskingum routing method, a river is divided into several reaches with slow flow changes over time. Thus, this method works quite well in ordinary streams with small slopes where the storage–discharge curve is approximately linear. In rivers with very steep or even mild slopes, different phenomena such as backwater effects, abrupt waves, or dynamic effects of flow affect the flow condition, and hydraulic routing methods are preferred. As another option in these cases, the Muskingum–Cunge method may be used.

Example 6.28

The values listed in Table 6.48 for inflow, outflow, and storage were measured for a particular reach of a river. Determine the coefficients K and X for use in the Muskingum routing equations for this reach.

Solution:

To determine Muskingum coefficients, a value of X is assumed and then $[XI + (1 - X)O]$ vs. S is plotted. The plot that comes closest to being a straight line is chosen to determine the coefficient values. Plots of $[XI + (1 - X)O]$ vs. S are made for $X = 0.1$, $X = 0.3$, and $X = 0.5$ using the values shown in Figure 6.30 and Table 6.49.

It can easily be seen that the plot for $X = 0.1$ is the straightest line. K is calculated as the inverse slope of the line:

$$1/K = \frac{17 - 9}{30{,}000 - 20{,}000} \cdot \frac{3600\ \text{s}}{1\ \text{h}}$$

$$K = 0.35\ \text{h}.$$

For most streams, there will be a larger looping effect for all values of X. The most linear relationship is chosen to determine K and X.

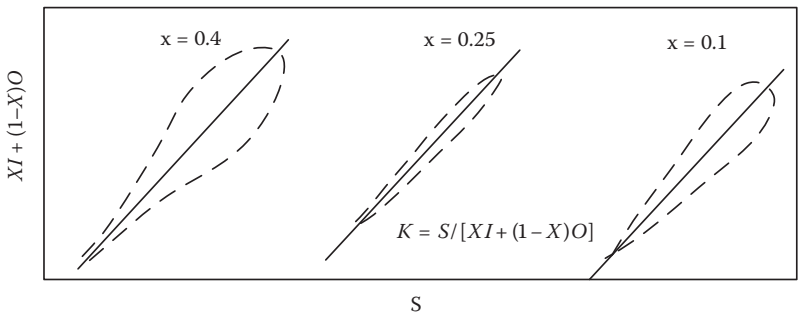

FIGURE 6.29 Selection of Muskingum routing method coefficients.

TABLE 6.48
Measured Inflow, Outflow, and Storage for a Particular Reach of a River

Time (h)	Inflow (m^3/s)	Outflow (m^3/s)	Storage (m^3)
1	4.00	4.00	0
2	7.00	4.14	10,285
3	11.00	5.69	11,170
4	17.00	8.51	16,870
5	22.00	12.79	24,180
6	27.00	17.41	31,950
7	30.00	22.12	39,170
8	28.00	25.78	43,340
9	25.00	26.69	43,560
10	23.00	25.79	41,710
11	20.00	24.32	38,780
12	17.00	22.12	34,870
13	14.00	19.54	30,460
14	11.00	16.76	25,800
15	8.00	13.87	20,990
16	5.00	10.93	16,110
17	4.00	8.06	11,980
18	4.00	6.13	9420
19	4.00	5.11	8080
20	4.00	4.58	7380

6.9.1.3 Muskingum–Cunge Method

The major disadvantage of the Muskingum method is that parameters K and X do not have a physical basis and are difficult to estimate. Cunge (1969) has suggested a new method called the Muskingum–Cunge method for solving this problem. In the Muskingum–Cunge method, K and X are defined based on the physical characteristics of the river as follows:

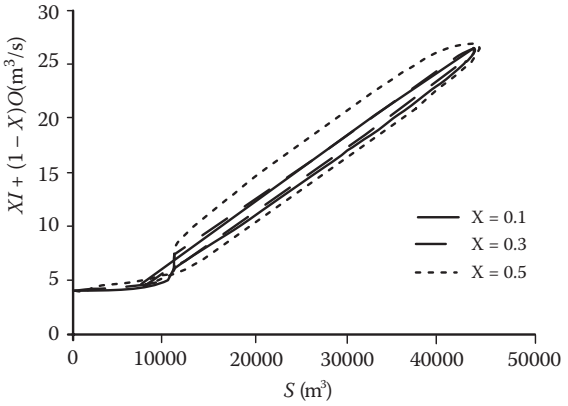

FIGURE 6.30 Determining X and K for river reach in Example 6.28.

TABLE 6.49
Resulting $[XI + (1 - X)O]$ for Different Values of X

	$[XI + (1 - X)O]$		
Storage (acre-ft)	$X = 0.1$	$X = 0.3$	$X = 0.5$
0	4	4	4
10,285	4.4287	4	5.5715
11,170	6.2246	4.998	8.347
16,870	9.3554	7.283	12.753
24,180	13.7101	11.057	17.3945
31,950	18.3717	15.553	22.2065
39,170	22.9089	20.287	26.0605
43,340	26.0002	24.484	26.889
43,560	26.5237	26.446	25.8465
41,710	25.5128	26.183	24.396
38,780	23.8871	24.953	22.1595
34,870	21.608	23.024	19.56
30,460	18.9851	20.584	16.7695
25,800	16.1822	17.878	13.879
20,990	13.2857	15.032	10.9365
16,110	10.3406	12.109	7.967
11,980	7.6549	9.151	6.0305
9420	5.9143	6.842	5.0635
8080	5.0026	5.491	4.557
7380	4.5247	4.777	4.2915

$$K = \frac{L}{mV_0} \tag{6.103}$$

$$X = 0.5\left(1 - \frac{Q_0/T_0}{S_0 m V_0 L}\right), \tag{6.104}$$

where Q_0 is a reference discharge, T_0 is the top width corresponding to the reference discharge, V_0 is the cross-sectional average velocity corresponding to the reference discharge, S is the slope of the river bottom, L is the length of the river reach, and m is a constant determined using the following equation that describes the relation between the flow area A and the discharge Q at a given river section.

$$Q = eA^{\mathrm{m}}, \tag{6.105}$$

where e is a constant determined analytically. Equation 6.105 is determined empirically based on measurements on a river section.

Different values can be considered for reference discharge such as dry-weather discharge in the river, the peak of the inflow hydrograph, or the average inflow rate. After determination of K and X from Equations 6.103 and 6.104, the weighting coefficients C_0, C_1, and C_2 are calculated from Equations 6.98 through 6.100, and then Equation 6.99 is used to calculate the outflow hydrograph. In the Muskingum–Cunge method, X can also take negative values. It should be noted that the Muskingum–Cunge and Muskingum methods are basically different; the Muskingum method is a

hydrologic routing method but the Muskingum–Cunge method is a hydraulic method that uses an approximation of the St. Venant equations.

For obtaining more accurate results, it is suggested that Δt be selected as less than one-fifth of the time between the beginning and the peak of the inflow hydrograph (Ponce and Theurer 1982), and also the length of the river reach for Muskingum–Cunge computations should satisfy the following inequality:

$$L \le 0.5\left(mV_0\Delta t + \frac{Q_0/T_0}{mV_0S_0} \right) \tag{6.106}$$

The selected reference discharge for calculating K and X parameters highly affects the results of the Muskingum–Cunge method. Ponce and Yevjevich (1978) have suggested Equation 6.107 for updating the reference discharge at every time step to eliminate the effect of the reference discharge on the model parameters.

$$Q_0 = \frac{I_1 + I_2 + Q_1}{3} \tag{6.107}$$

and T_0, V_0, X, K, C_0, C_1, and C_2 are recalculated using the updated reference discharge at each time step.

Example 6.29

A channel reach has a length L = 2420 m, slope S_o = 0.001 m/m, and a Manning roughness coefficient of n = 0.05. The channel is rectangular in shape with a side slope of 5:1 (H/V). The channel geometry is shown in Figure 6.31. An inflow hydrograph for a small watershed is tabulated in Table 6.50. Route this hydrograph through the given channel.

Solution:

Based on the given figure, the flow area, A, wetted perimeter, P, and the hydraulic radius, R, are calculated as follows:

$$A = (y)\,(10y)/2 = 5y^2$$

$$P = 2y\,(1 + 25)^{0.5} = 10.2y$$

$$R = A/P = 0.49y$$

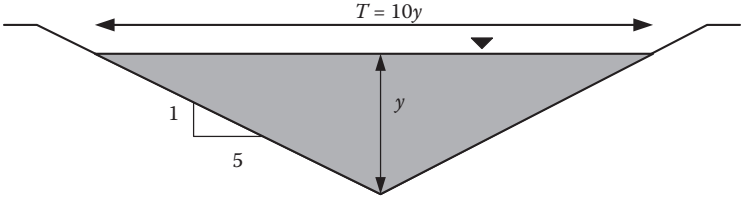

FIGURE 6.31 Characteristics of the channel in Example 6.29.

TABLE 6.50
Calculation of Example 6.29

1	2	3	4	5	6	7
Time Step	**t_1 (h)**	**t_2 (h)**	**I_1 (cms)**	**I_2 (cms)**	**Q_1 (cms)**	**Q_2 (cms)**
1	0	0.5	10	15	10	10.09
2	0.5	1.0	15	20	10.09	13.99
3	1.0	1.5	20	25	13.99	18.75
4	1.5	2.0	25	30	18.75	23.70
5	2.0	2.5	30	25	23.70	28.50
6	2.5	3.0	25	20	28.50	25.69
7	3.0	3.5	20	15	25.69	21.18
8	3.5	4.0	15	10	21.18	16.29
9	4.0	4.5	10	10	16.29	11.40
10	4.5	5.0	10	10	11.40	10.31
11	5.0	5.5	10	10	10.31	10.07
12	5.5	6.0	10	10	10.07	10.02

The estimated parameters are used in the Manning formula:

$$Q = 1.49/n\ [AR^{2/3}S_o^{0.5}]$$

$$Q = (1.49/0.05)(5y^2)(0.49y)^{2/3}\ (0.001)^{1/2}$$

$$Q = 2.928y^{8/3}$$

and since $A = 5y^2$:

$$Q = 0.343A^{4/3}.$$

Therefore, based on Equation 6.105, the following are obtained: $e = 0.343$ m$^{1/3}$/s and $m = 4/3$.

A time increment of $\Delta t = 0.5$ h and a reference discharge of 10 cms (baseflow) is considered. Using the reference discharge of $Q = 10$ cms, T_0 and V_0 are calculated as follows:

$$A_0 = (10/0.343)^{3/4} = 12.55 \text{ m}^2$$

$$y_0 = ((12.55 \text{ m}^2)/5)^{0.5} = 1.58 \text{ m}$$

$$T_0 = (10)(1.58) = 15.8 \text{ m}$$

$$V_0 = (10 \text{ cms})/(12.55 \text{ m}^2) = 0.797 \text{ mps}$$

$$K = (2420 \text{ m})/[(4/3)(0.797 \text{ mps})] = 2277 \text{ s} = 0.632 \text{ h}$$

$$X = 0.5\{1 - [(10 \text{ cms})/(15.8 \text{ m})/(0.001)(4/3)(0.797 \text{ mps})(2420 \text{ m})]\} = 0.377.$$

Then, C_0, C_1, and C_2 are calculated:

$$C_0 = 0.0182;\ C_1 = 0.7585;\ C_2 = 0.2233.$$

The calculations are summarized in Table 6.50. The 2 h unit hydrograph in column 7 is computed with $Q(t)$ linear variation in column 6. The given values in column 6 are calculated by multiplication of the values in column 5 to 566 = 2.788 × A for unit conversion of centimeters per hour (cm/h) to cubic meters per hour (m^3/h) based on the catchment with an area of 200 km^2.

6.10 HYDROLOGIC RESERVOIR ROUTING

6.10.1 Storage Indication Method

Reservoir or detention basin routing is easier to perform than river routing because storage–discharge relations for pipes, weirs, and spillways are single-valued functions independent of inflow. Pulse method as a simple storage indication method uses the finite-difference form of the continuity equation combined with a storage indication curve ($2S/\Delta t + O$ vs. O). In this case, Equation 6.86 is generalized to the following finite-difference equation considering two points in time:

$$\left(I_n + I_{n+1}\right) + \left(\frac{2S_n}{\Delta t} - O_n\right) = \left(\frac{2S_{n+1}}{\Delta t} + O_{n+1}\right), \tag{6.108}$$

where S_{n+1} and O_{n+1} are the only unknown variables in this equation. Since S_n and O_n are known for the initial time step and I is known for all n, the right-hand side of Equation 6.104 is calculated. Then, using the storage indication curve, outflow and after that storage at time step $n + 1$ are calculated. In the second time interval, by using the values of S_{n+1} and O_{n+1} as input on the left-hand side, the calculation is continued until the outflow reaches zero.

The elevation–discharge relationship of reservoir spillway as given in Equation 6.109 is utilized to determine the outflow given the depth of water over the spillway.

$$O = CLh^{3/2}, \tag{6.109}$$

where h is the water head over the spillway, L is the spillway length, and C is a constant coefficient related to the spillway shape. From topographic information, $y = 2S/\Delta t + O$ corresponding to h can be obtained. Then, the curve for either y versus O or h versus O can be constructed.

To construct the elevation–storage curve, the topographic map is utilized. The depth of water over spillway h multiplied by the reservoir surface area can yield the storage of the reservoir. The reservoir surface area is known from the topographic map. Therefore, the temporary storage S for any h is approximately:

$$S = \frac{h}{2}\left(A_1 + A_2\right), \tag{6.110}$$

where A_1 denotes the surface area of the reservoir when $h = 0$ and A_2 is the surface area of the reservoir when the depth of flow is h. The curves for either y versus S or h versus S can be constructed. The elevation–discharge and elevation–storage curves can be easily combined to form a storage discharge curve.

Subtracting $2O$ from $2S/\Delta t + O$ yields $2S/\Delta t - O$, which appears on the left-hand side of Equation 6.108. Before routing is performed, the curves of $2S/\Delta t \pm O$ versus O are thus constructed. The usage of this method is clarified in the next example.

Example 6.30

A small reservoir has an area of 50 km^2 at the spillway level, and the banks are essentially vertical for several meters above the spillway level. The spillway is 20 m long and has a coefficient of 3.75. Considering the inflow hydrograph given in Table 6.51, compute the maximum pool level and the maximum discharge to be expected if the reservoir is initially at the spillway level.

Solution:

First, the storage for different values of elevation using Equation 6.110 is calculated in Table 6.52.

Then, the discharge corresponding to the various values of elevation is determined in Table 6.53.

The quantity $(2S/\Delta t) + Q$ is obtained for different values of Q, as given in Table 6.54. Δt in this example is considered to be 12 h. A plot of $(2S/\Delta t) + Q$ versus Q is shown in Figure 6.32.

TABLE 6.51
Inflow Hydrograph in Example 6.30

Time (h)	Inflow (m^3/s)	Time (h)	Inflow (m^3/s)
0	0.40	22	2.45
2	0.35	24	1.92
4	0.37	26	1.44
6	1.25	28	1.18
8	3.40	30	0.95
10	5.75	32	0.80
12	7.22	34	0.67
14	7.40	36	0.56
16	6.73	38	0.50
18	4.56	40	0.42
20	3.20	42	0.30

TABLE 6.52
Corresponding Storage to Different Water Levels

h (m)	0	1	2	3	4	5
$S \times 10^6$ (m^3)	0	50	100	150	200	250

TABLE 6.53
Corresponding Discharge to Different Water Levels

h (m)	0	1	2	3	4	5
Q (m^3/s)	0	75	119.06	156.01	188.99	219.30

TABLE 6.54
Computation of $(2S/\Delta t) + Q$ versus Q for Example 6.30

h (m)	S (m³)	Q (cms)	$(2S/\Delta t) + Q$ (cms)
0.1	50	16.15826	16.16057
0.2	100	25.64964	25.65427
0.3	150	33.61054	33.6522
0.4	200	40.71626	40.77182
0.5	250	47.24704	47.31648
0.6	300	53.3534	53.43673
0.7	350	59.12801	59.22524
0.8	400	64.63304	64.74415
0.9	450	69.91273	70.03773
1	500	75	75.13889
1.1	550	79.92017	80.07295
1.2	600	84.69324	84.85991
1.3	650	89.33538	89.51594
1.4	700	93.85987	94.05432
1.5	750	98.2778	98.48614

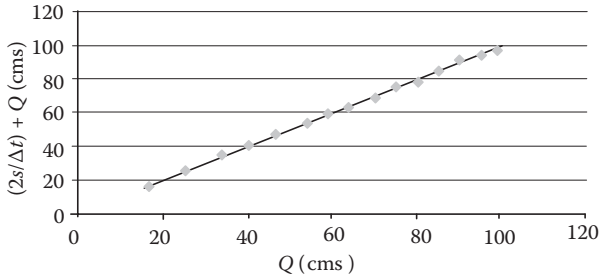

FIGURE 6.32 $(2S/\Delta t) + Q$ versus discharge.

The results of calculations for flow routing are shown in Table 6.55. These yield:

Maximum pool level: 0.035 m above spill level.
Maximum discharge: 8.07 cms.

6.10.2 Detention Basin Routing

Flood routing is necessary for detention basin design. It determines the variations of outflow from a detention basin and the storage in the basin with time for a given inflow hydrograph. An accurate numerical routing scheme for solving the continuity and storage equations is the Runge–Kutta (R–K) technique. The R–K method for solving ordinary differential equations can be developed to solve the routing equations with desired order of accuracy (first, second, third, fourth). The continuity equation can be presented as follows:

$$\frac{dV}{dt} = Q_{in}(t) - Q_{out}(H). \tag{6.111}$$

TABLE 6.55
Flow Routing for Example 6.30

Time (h)	Inflow (cms)	$I_i + I_{i+1}$ (cms)	$(2S_i/\Delta t) - Q_i$ (cms)	$(2S_{i+1}/\Delta t) + Q_{i+1}$ (cms)	Q_{i+1} (cms)
0	4	7.5	0		0
2	3.5	7.2	6.82	7.5	0.34
4	3.7	16.2	12.96	14.02	0.53
6	12.5	46.5	27.44	29.16	0.86
8	34	91.5	70.72	73.94	1.61
10	57.5	129.7	156.78	162.22	2.72
12	72.2	146.2	278.54	286.48	3.97
14	74	141.3	414.4	424.74	5.17
16	67.3	112.9	543.32	555.7	6.19
18	45.6	77.6	642.36	656.22	6.93
20	32	56.5	705.26	719.96	7.35
22	24.5	43.7	746.46	761.76	7.65
24	19.2	33.6	774.48	790.16	7.84
26	14.4	26.2	792.16	808.08	7.96
28	11.8	21.3	802.32	818.36	8.02
30	9.5	17.5	807.5	823.62	8.06
32	8	14.7	808.86	825	8.07
34	6.7	12.3	807.44	823.56	8.06
36	5.6	10.6	803.66	819.74	8.04
38	5	9.2	798.26	814.26	8
40	4.2	7.2	791.56	807.46	7.95
42	3		782.96	798.76	7.9

where V is volume of water storage in the basin, $Q_{\text{in}}(t)$ is inflow into the detention basin as a function of time, and $Q_{\text{out}}(H)$ is outflow from the detention basin as a function of head (H) in the basin.

Furthermore, the storage volume variation, dV, due to changes in depth, dH, is expressed as follows:

$$\mathrm{d}V = A_{\text{r}}(H)\mathrm{d}H, \tag{6.112}$$

where $A_{\text{r}}(H)$ is the corresponding surface area to H. Equation 6.112, using Equation 6.111, can be rewritten as follows:

$$\frac{\mathrm{d}H}{\mathrm{d}t} = \frac{Q_{\text{in}}(t) - Q_{\text{out}}(H)}{A_{\text{r}}(H)}. \tag{6.113}$$

The R–K technique can be employed for solving Equation 6.113. Figure 6.33a illustrates the first-order R–K technique application. For this purpose, Equation 6.113 is represented by

$$\frac{\mathrm{d}H}{\mathrm{d}t} = f\left(H_n, t_n\right), \tag{6.114}$$

where H is the dependent variable and t is the independent variable. In first-order R–K solutions, a finite time increment Δt is chosen. Then,

$$\Delta H = f(H_n, t_n)\Delta t,\ H_{n+1} = H_n + \Delta H. \tag{6.115}$$

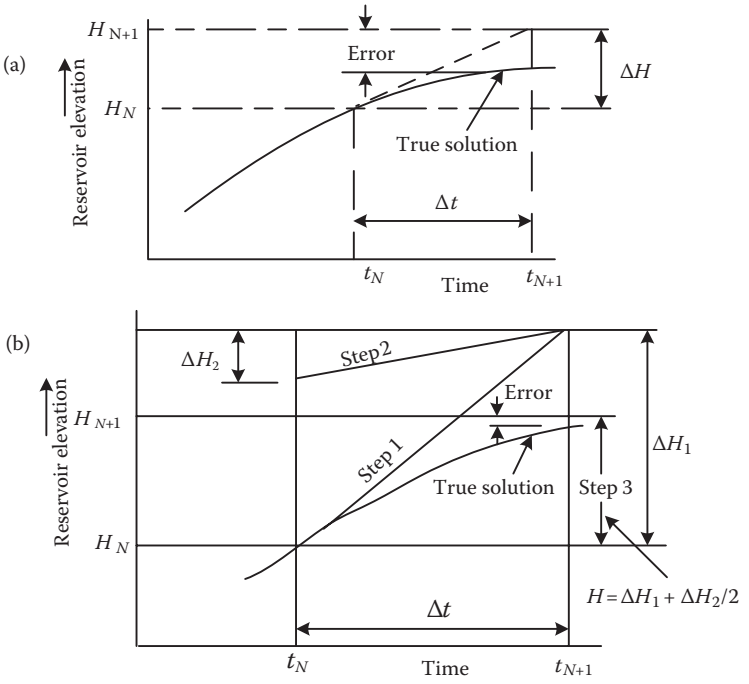

FIGURE 6.33 (a) First-order R–K technique. (b) Second-order R–K technique.

It is assumed that the initial head H_0 is known. However, an error is introduced due to continuous changes of ΔH with time (Figure 6.33a), which limits the application of first-order R–K solutions to cases with very small time increments.

Although, in this method, ΔH at the beginning and end of the chosen time increment is calculated, the averaged ΔH is used. Considering that the line for step 1 is tangent to $f(H_n, t_n)$ at t_n, ΔH_1 is estimated as follows:

$$\Delta H_1 = f(H_n, t_n)\Delta t.$$

ΔH_2 cannot be estimated at that point since H_{n+1} has not yet been calculated. ΔH_2 is estimated by evaluating Equation 6.115 at $H_n + \Delta H_1$ and $t_n + \Delta t$ as follows:

$$\Delta H_2 = f(H_n + \Delta H_1, t_n + \Delta t).$$

Then,

$$\begin{aligned} \Delta H &= \frac{H_1 + \Delta H_2}{2} \\ H_{n+1} &= H_n + \Delta H \end{aligned} \quad . \tag{6.116}$$

Some of this error is alleviated by the second-order R–K technique, as shown in Figure 6.33b.

Applying this technique to Equation 6.113 will result in the second-order R–K as follows:

$$\Delta H_1 = \frac{Q_{\text{in}}\left(t_n\right) - Q_{\text{out}}\left(H_n\right)}{A_{\text{r}}\left(H_n\right)}\Delta t$$

$$\Delta H_2 = \frac{Q_{\text{in}}\left(t_{\text{n}} + \Delta t\right) - Q_{\text{out}}\left(H_n + \Delta H_1\right)}{A_{\text{r}}\left(H_n \Delta H_1\right)}\Delta t.$$

The second-order R–K solution of Equation 6.113 is further illustrated by Figure 6.33b and the flow chart of Figure 6.34. The third- and fourth-order R–K solutions attempt to improve the accuracy of the estimate of ΔH by reasoning similar to what is used in developing the second-order R–K solution. The third-order technique estimates H_{n+1}, by

$$H_{n+1} = H_n + \frac{1}{6}\left[K_1 + 4K_2 + K_3\right]\Delta t. \tag{6.117}$$

where

$$K_1 = f\left(t_n, H_n\right)$$

$$K_2 = f\left(t_n + \Delta t/2, H_n + 1/2K_1\Delta t\right)$$

$$K_3 = f\left(t_n + \Delta t, H_n - K_1\Delta t + 2K_2\Delta t\right)$$

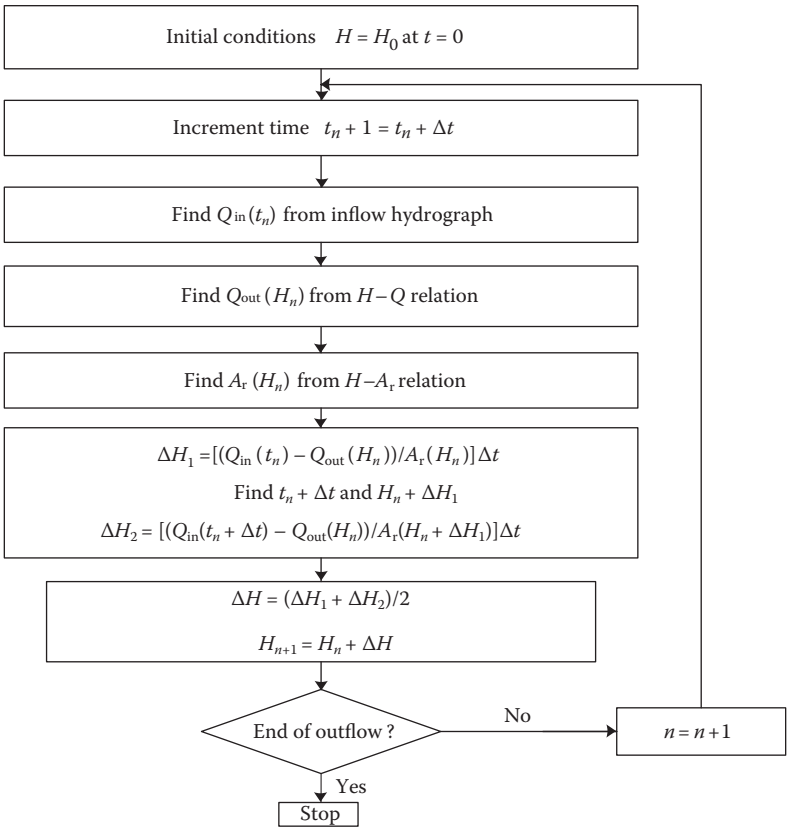

FIGURE 6.34 Flow chart for second-order R–K solutions.

In the classical fourth-order R–K technique,

$$H_{n+1} = H_n + \frac{1}{6}\left[K_1 + 2K_2 + 2K_3 + K_4\right]\Delta t, \tag{6.118}$$

where

$$K_1 = f\left(t_n, H_n\right)$$
$$K_2 = f\left(t_n + \Delta t/2, H_n + 1/2K_1\Delta t\right)$$
$$K_3 = f\left(t_n + \Delta t/2, \boldsymbol{H}_n + 1/2K_2\Delta t\right)$$
$$K_4 = f\left(t_n + \Delta t, H_n + K_3\Delta t\right).$$

The fourth-order R–K scheme is more accurate than the first-, second-, and third-order methods.

6.11 ESTUARIES

One of the important components in surface water hydrology is estuary. Estuaries are bodies of water and their surrounding coastal habitats are typically found where rivers meet the sea. In other words, estuary is a partly enclosed coastal body of water with one or more rivers or streams flowing into it, and with a free connection to the open sea. Estuaries form a transition zone between river environments and ocean environments and are subject to both marine influences, such as tides, waves, and the influx of saline water, and riverine effects, such as flows of freshwater and sediment. The inflow of both seawater and freshwater provides high levels of nutrients in both the water column and sediment, making estuaries among the most productive natural habitats in the world. Estuaries harbor unique plant and animal communities because their waters are brackish—a mixture of freshwater draining from the land and salty seawater. Many animal species rely on estuaries for food and as places to nest and breed.

Human communities also rely on estuaries for food, recreation, and jobs. Estuaries are among the most heavily populated areas throughout the world, with about 60% of the world's population living along estuaries and the coast. Of the 32 largest cities in the world, 22 are located on estuaries (Ross 1995). For example, New York City is located at the mouth of the Hudson River estuary.

Unlike freshwater rivers and lakes, estuaries can produce a wide range in the values of physical and chemical parameters that will be recorded, and frequent changes occur in these values both with tidal cycles and meteorological events. In streams, rivers, and lakes, water quality parameters are more likely to fluctuate within a well-defined range largely determined by rainfall and season, and these values are often homogeneous throughout the water body. In an estuary, in contrast, these parameters can change abruptly in time and space, are dependent on the measurement location, and may or may not reflect general environmental conditions throughout the estuary.

Two key phenomena that control physical and chemical parameters in estuaries are tidal flushing and stratification (vertical or horizontal). Tidal flushing is the net transport for water (as well as sediments and contaminants) out of an estuary with tidal flow and river flow. Stratification is layering of the estuary generally associated with the inflow of the denser saltwater at depth and the outflow of more buoyant freshwater at the surface. Layering can also occur when seasonal heating causes a sharp differential or thermocline (interface where temperature changes rapidly with depth) so that the warm surface layer is isolated from the colder bottom layer.

Superimposed on these naturally occurring variations are changes caused by human intervention, including modification of flow and bathymetry (for example, through construction of barriers to flow or dredging) and the input of pollutants, including excess nutrients and toxins. They are also threatened by sewage, coastal settlement, land clearance, and much more. Estuaries are affected by events far upstream and concentrate materials such as pollutants and sediments. Land runoff and industrial, agricultural, and domestic waste enter rivers and are discharged into estuaries. Contaminants such as plastics, pesticides, furans, dioxins, phenols, and heavy metals, which do not disintegrate rapidly in the marine environment, can be introduced.

Estuaries tend to be naturally eutrophic because land runoff discharges nutrients into estuaries. With human activities, land runoff also now includes the many chemicals used as fertilizers in agriculture as well as waste from livestock and humans. Excess oxygen-depleting chemicals in the water can lead to hypoxia and the creation of dead zones. It can result in reductions in water quality, fish, and other animal populations.

Estuaries are typically classified by their geomorphological features or by water circulation patterns and can be referred to by many different names, such as bays, harbors, lagoons, inlets, or sounds, although sometimes these water bodies do not necessarily meet the above criteria of an estuary and may be fully saline. Regarding the water circulation scheme, the following classes of estuaries are considered:

1. Salt wedge: In this type of estuary, river output greatly exceeds marine input and tidal effects have a minor importance. Freshwater floats on top of the seawater in a layer that gradually thins as it moves seaward. The denser seawater moves landward along the bottom of the estuary, forming a wedge-shaped layer that is thinner as it approaches land. As a velocity difference develops between the two layers, shear forces generate internal waves at the interface, mixing the seawater upward with the freshwater. An example of a salt wedge estuary is the Mississippi River.
2. Partially mixed: As tidal forcing increases, river output becomes less than the marine input. Here, current induced turbulence causes mixing of the whole water column such that salinity varies more longitudinally rather than vertically, leading to a moderately stratified condition. Examples include the Chesapeake Bay and Narragansett Bay.
3. Vertically homogeneous: Tidal mixing forces exceed river output, resulting in a well-mixed water column and the disappearance of the vertical salinity gradient. The freshwater–seawater boundary is eliminated due to the intense turbulent mixing and eddy effects. The lower reaches of the Delaware Bay and the Raritan River in New Jersey are examples of vertically homogeneous estuaries.
4. Inverse: Inverse estuaries occur in dry climates where evaporation greatly exceeds the inflow of freshwater. A salinity maximum zone is formed, and both riverine and oceanic water flow close to the surface towards this zone. This water is pushed downward and spreads along the bottom in both the seaward and landward direction. An example of an inverse estuary is Spencer Gulf in South Australia.
5. Intermittent: Estuary type varies dramatically depending on freshwater input and is capable of changing from a wholly marine embayment to any of the other estuary types.

6.12 WATER QUALITY ISSUES IN SURFACE WATER

The quality of surface water resources can significantly affect water use in many regions, especially in those that are arid and semiarid. In regions where water pollutants from human activities have seriously degraded water quality, the main issue is to control pollution sources. When the discharge

of wastes disturbs the natural ecological balance of a water body, water pollution occurs. The mass balance equation for pollutants is the basis for surface water quality modeling. From Reynolds' transport theorem in fluid mechanics, the pollutant material mass balance equation is derived as follows:

$$\frac{\mathrm{D}c}{\mathrm{D}t} = \frac{\partial c}{\partial t} + u\frac{\partial c}{\partial x} + v\frac{\partial c}{\partial y} + w\frac{\partial c}{\partial z}, \tag{6.119}$$

where c is the pollutant concentration; x, y, and z are the Cartesian coordinates; and u, v, and w are the respective components of velocity vector in the x, y, and z directions.

Many different parameters contribute to overall water quality, including the amount of oxygen in the water, the concentration of nutrients available to marine life, and turbidity (the number of particles in the water blocking sunlight). Water temperature, salinity, and current speed and direction are parameters that affect the distribution and impact of pollutants and the resulting health of a body of water. How all these parameters vary down through the water column is also important. The current state of technology allows scientists to measure these parameters continuously at different depths. Continuous monitoring lets us see whether or not the management initiatives used by many towns in the state are working to improve water quality.

Monitoring can be conducted at regular sites on a continuous basis ("fixed station" monitoring), at selected sites on an as-needed basis or to answer specific questions (intensive surveys), on a temporary or seasonal basis (for example, during the summer at bathing beaches), or on an emergency basis (such as after a spill). Increasingly, monitoring efforts are aimed at determining the condition of entire watersheds—the area drained by rivers, lakes, and estuaries. This is because scientists have come to realize the impact of land-based activities on the waters that drain the land and the interconnectedness of all types of water bodies, including those beneath the ground.

6.12.1 Physical Parameters

6.12.1.1 Temperature

Is a commonly measured water quality parameter and is a critical factor influencing chemical and biological processes in water bodies. For instance, increased temperature decreases the level of oxygen that can be dissolved in the water column. Water temperature influences the rate of plant photosynthesis, the metabolic rates of aquatic organisms, and the sensitivity of organisms to quality stresses.

6.12.1.2 Salinity

Is the amount of salts dissolved in water expressed in parts per thousand. It controls the type of species and influences physical and chemical processes such as flocculation and the amount of dissolved oxygen (DO) in the water column.

6.12.1.3 Suspended Material Concentration and Turbidity

Suspended material concentration is the amount of material that is suspended in the water column and is measured as the amount of material retained in a filter. Smaller particles are considered dissolved solids. The sum of suspended and dissolved solids is referred to as total solids. All three measures are recorded in terms of milligrams per liter. Turbidity is a measure of water clarity, that is, the ability of water to transmit light, and is influenced by the level of suspended material in the water column. Turbidity is often measured visually using a Secchi disk. Elevated levels of

suspended material and turbidity occur naturally through erosion, storm runoff, and the input of plant material on a seasonal basis. However, these parameters can also indicate degraded water quality if the elevated levels are caused by excessive erosion due to upland development, organic material due to nutrient enrichment, or uncontrolled discharges from sewage treatment plants and industrial facilities.

6.12.1.4 Current Speed and Direction

Understanding the current velocity in an estuary, and how it changes spatially and with depth, can provide valuable insight in interpreting changes in other physical and chemical parameters. For instance, high current velocities near the bottom can entrain sediment and increase turbidity. Flow into an estuary from the sea on an incoming tide can raise salinity and lower temperature. Current velocity is specified by direction (0–360°) and speed (m/s).

6.12.1.5 Meteorological Parameters (Weather)

The meteorological parameters typically measured are wind speed and direction, air temperature, and rainfall. Information on meteorological conditions can be very valuable in interpreting water quality data and explaining changes in water quality parameters. For instance, elevated temperatures and light winds can cause thermal stratification in an estuary, which may lead to decreased mixing and DO, particularly at depth. High winds associated with passage of a storm or cold front can promote vertical mixing, which will increase DO and possibly suspended material concentration, particularly in shallow water. Increased rainfall will decrease salinity in surface layers and perhaps lead to density stratification.

6.12.2 Chemical Parameters

6.12.2.1 Oxygen

Is a key parameter of interest in water quality monitoring, because nearly all aquatic life needs oxygen to survive. The two oxygen parameters monitored are DO and biological oxygen demand (BOD). DO is the level of oxygen in the water column in molecular form that is available to support life and is reported in milligrams per liter. The DO level is controlled by mixing at the air/water interface, temperature and salinity, the level of photosynthesis (which produces oxygen), and decomposition of organic material (which depletes oxygen). Generally, DO levels of greater than 4 mg/L indicate an adequate supply of DO to support marine species growth and activity, while levels from 1 to 3 mg/L indicate hypoxic conditions, which are detrimental to marine life. DO below 1 mg/L indicates anoxia, a condition in which no life that requires oxygen can be supported. BOD measures the amount of oxygen that organisms would require in decomposing the organic material in the water column and in chemical oxidation of inorganic matter and is indicative of pollution levels. For instance, unpolluted water has a BOD of less than 5 mg/L, while raw sewage has a BOD of 150 to 300 mg/L. Wastewater effluent might have a BOD from 8 to 150 mg/L.

6.12.2.2 Nutrients

Especially nitrogen and phosphorus, are key water quality parameters in estuaries, because they have significant direct or indirect impacts on plant growth, oxygen concentrations, water clarity, and sedimentation rates. They influence both the overall biological productivity of the estuary and the decline of the estuary through eutrophication. Nitrogen is essential in protein and DNA synthesis in organisms and photosynthesis in plants. Phosphorus is critical to metabolic processes. Primary nitrogen species of interest in the estuarine environment include nitrate (NO_3), nitrite (NO_2), and ammonia and ammonium (NH_3 and NH_4). Nutrient concentrations are reported in milligrams per liter. Unlike DO, there are no set criteria for nutrient levels because nutrients

themselves are not a threat to marine life, although they can contribute to problems such as excessive plant growth, low DO, and accelerated eutrophication. Excessive nutrients can also trigger toxic algae blooms. However, these adverse effects are dependent on other factors besides nutrient levels.

6.12.2.3 pH and Alkalinity

These are two additional parameters that provide insight into changing water quality conditions in an estuary. Both can be determined by simple tests. Although these parameters are generally not as critical as DO and nutrients, they are important to ecosystem health because most aquatic plants and animals are adapted to a specific range of pH and alkalinity. Sharp variations outside of this range can be detrimental. In addition, pH and alkalinity influence the estuarine carbon cycle, which involves the movement of carbon from the atmosphere into plant and animal tissue and into water bodies. The pH of water is the measure of how acidic or basic it is. A pH level of 1 to 7 indicates degrees of an acidic solution, while a level of 7 to 14 indicates degrees of a basic solution. Alkalinity is a measure of water's capacity to neutralize acids and is influenced by the presence of alkaline compounds in the water such as bicarbonates, carbonates, and hydroxides. Alkalinity is reported in milligrams per liter of calcium carbonate ($CaCO_3$).

6.12.2.4 Chlorophyll a

Is a green pigment found in phytoplankton, which represents the first trophic level in the primary production cycle. The amount of chlorophyll a in the water column is indicative of the biomass of phytoplankton, which in turn can indicate nutrient levels in the water column (or excess nutrients if the chlorophyll a values are elevated). Excessive nutrients and plant growth can in turn decrease DO levels and increase turbidity.

6.12.2.5 Toxic Contaminants

With the industrialization of many estuaries, the amount of toxic contaminants entering estuaries has greatly increased. These contaminants include heavy metals (such as mercury, lead, cadmium, zinc, chromium, and copper), petroleum hydrocarbons, and synthetic organic compounds such as polycyclic aromatic hydrocarbons, polychlorinated biphenyls, and pesticides (e.g., dichlorodiphenyl, trichloroethane). Many of these toxic contaminants are persistent, can be incorporated into sediments, and can be concentrated in the food chain; hence, they pose a magnified threat to animals at higher trophic levels and to humans. They are generally measured through laboratory analysis (which can often be complex and time-consuming), although field test kits are available for some heavy metals and other contaminants. The contaminant concentrations are usually reported in milligrams per liter.

6.12.3 Biological Parameters

6.12.3.1 Pathogens (Indicator Bacteria)

A key parameter of interest, particularly for estuaries in urban areas, is the presence of pathogens. Pathogens are viruses, bacteria, and protozoans that can cause disease. They are a critical concern in areas where waters are used for swimming, boating, fishing, shellfishing, or other pursuits that lead to human contact or food consumption. Direct testing for pathogens is very expensive and impractical. Instead, the potential levels of pathogens in estuaries are tracked by monitoring "indicator bacteria"—so called because their presence indicates that fecal contamination has occurred. The four indicators commonly monitored include total coliform, fecal coliform, *Escherichia coli*, and enterococci, all of which are bacteria normally prevalent in the intestines and feces of warm-blooded animals, including wildlife, farm animals, pets, and humans. The indicator bacteria themselves are not pathogenic. Values are recorded as the number of bacteria per milliliter of water.

Environmental managers establish numerical standards for limits to these values for swimming, shellfishing, and other activities.

6.12.4 Oxygen Sag Model

An oxygen-consuming pollutant, either organic or inorganic, discharged into a stream causes depletion of the dissolved oxygen. In this case, DO is initially consumed faster near the discharge point, which poses a danger for aquatic life if the concentration of oxygen falls below a critical level. Determining the amount of discharged waste and how much oxygen will be required to degrade the waste is necessary for predicting the extent of oxygen depletion. Oxygen is continuously being replenished from the atmosphere and consumed by organisms; thus, the oxygen concentration in a river is determined using the relative rates of these competing processes. Downstream of the discharge point, the river recovers and the DO concentration goes back up again. This profile of DO concentration along the river is referred to as DO sag. Figure 6.35 shows a plot of DO sag.

The one-dimensional mass balance equation for DO is as follows:

$$\frac{\mathrm{D}c}{\mathrm{D}t} = \frac{\partial}{\partial x}\left(E_{xx} \cdot \frac{\partial c}{\partial x}\right) + k_2\left(O_s - c\right) + P - R - k_c \cdot L_c - k_n \cdot L_n + G_o, \tag{6.120}$$

where G_o is the distributed dissolved oxygen source, c is the dissolved oxygen concentration, k_2 is the reaeration coefficient, O_s is the dissolved oxygen saturation, P is the rate of photosynthesis, R is the rate of respiration, k_c is the carbonaceous biochemical oxygen demand (CBOD) deoxygenation coefficient, L_c is the concentration of CBOD, k_n is the nitrogenous deoxygenation coefficient, L_n is the nitrogenous biochemical oxygen demand (NBOD) concentration, and E_{xx} is dispersion coefficient in the x direction.

If the effects of dispersion, P, R, NBOD, and G_o are neglected, then Equation 6.120 could be simplified as

$$\frac{\mathrm{D}c}{\mathrm{D}t} = k_2\left(O_s - c\right) - k_c \cdot L_c \tag{6.121}$$

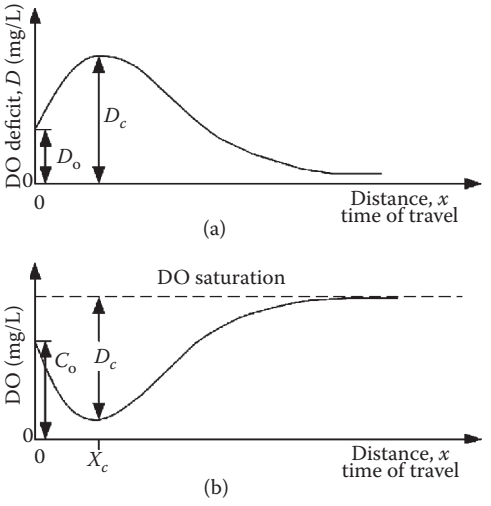

FIGURE 6.35 Dissolved oxygen sag. (a) DO deficit variation; (b) DO concentration.

$$L_c = L_{c0} e^{-k_c' \cdot t}, \tag{6.122}$$

where k_c is the rate of settling of CBOD, and L_{c0} is L_o at $t = 0$. Using Equation 6.121 and 6.122 and defining the DO deficit as $D = O_s - c$, $D = D_0$ at $t = 0$, $D = 0$ at $t = \infty$, and $k_c' = k_c$, the Streeter–Phelps equation is derived as

$$D = \frac{k_c \cdot L_{c0}}{k_2 - k_c}\left(e^{-k_c \cdot t} - e^{-k_2 \cdot t}\right) + D_0 \cdot e^{-k_2 \cdot t}. \tag{6.123}$$

If the deficit calculated from the above equation is greater than the saturation DO, all the dissolved oxygen has been depleted and the DO is zero. The lowest point on the DO sag curve indicates the worst water quality condition and is of major interest. The time to this minimum DO point, the critical time (t_c), can be found by differentiating Equation 6.123, setting it equal to 0, and solving for t:

$$t_c = \frac{1}{k_2 - k_c} \ln\left[\frac{k_2}{k_c}\left(1 - D_0 \times \frac{k_2 - k_c}{k_c - L_{c0}}\right)\right]. \tag{6.124}$$

The critical deficit (D_c) is then found by using t_c in Equation 6.124. The bio-oxidation rate (k_c) is dependent on the waste characteristics, the ability of organisms to oxidize the waste, and the water temperature. Temperature increases the speed of most of the biological processes. Laboratory testing is usually done at a standard temperature of 20°C, and the BOD rate constant at any temperature T (°C) is

$$k_{c,T} = k_{c,20}(\theta)^{T-20}, \tag{6.125}$$

where $k_{c,T}$ is the BOD rate constant (expressed in 1/day) at temperature T (°C), $k_{c,20}$ is the BOD rate constant determined under laboratory conditions at 20°C (1/day), and θ is the temperature coefficient. The value of θ is considered to be 1.135 for $4 < T < 20$°C and 1.056 for $20 < T < 30$°C.

The deoxygenation rate constant (k_c) in a river differs from the BOD rate constant (k) due to physical and biological differences between a bottle and a river. In river systems, the BOD is exerted more rapidly because of turbulent mixing and BOD removal by suspended and sediment organisms. k_c can be estimated from the BOD rate constant (k) by the following equation:

$$k_c = k + \frac{v}{h}\eta, \tag{6.126}$$

where k_c is the deoxygenation rate constant at 20°C (1/day), v is the average velocity of streamflow (m/s), k is the BOD rate constant determined in laboratory conditions at 20°C (1/day), η is the bed activity coefficient (0.1 for deep water; 0.6 or greater for a rapidly flowing stream), and h is the average depth (m).

When the stream temperature is not 20°C, the calculated k_c from the above equation should be adjusted using Equation 6.125. The value of the reaeration rate constant (k_2) depends on the degree of turbulent mixing, which is related to river flow velocity and the surface and depth of the water body (surface area exposed to the atmosphere per unit volume of water). The reaeration rate constant is also related to temperature and should be adjusted to river temperature using Equation 6.125 but with a temperature coefficient θ, which is equal to 1.024.

Example 6.31

A new industrial area of 100 km^2 has a 10-year discharge of 200 cms. The initial BOD concentration is 7 mg/L. Assume that the storm occurs in the summer (T = 25°C) and that the DO concentration in the runoff is 8 mg/L. The runoff discharges into a small stream where the flow rate is 8 cms at a temperature of 21°C, with a BOD of 3 mg/L and a dissolved oxygen concentration of 7.4 mg/L. Tests show that k_1 is 0.2/day at 20°C and that k_2 is 0.8/day at 25°C. Complete mixing of the storm discharge and the flow from upstream areas is assumed to occur at the outfall. The stream flows 5000 m at a velocity of about 1.2 mps before combining with another larger stream. The saturation concentration is 8.28 mg/L. Compute the time that the critical conditions will occur.

Solution:

$$T_c = \frac{8(21)+200(25)}{8+200} = 24.85°\text{C}$$

$$L_c = \frac{8(3)+200(7)}{8+200} = 6.85 \text{ mg/L}$$

$$C_c = \frac{8(7.4)+200(8)}{8+200} = 7.96 \text{ mg/L}.$$

The saturation concentration is 8.28 mg/L; therefore, the initial deficit is

$$D_o = C_s - C_0 = 8.28 - 7.96 = 0.32 \text{ mg/L}.$$

The value of k_1 needs to be adjusted for the temperature difference;

$$k_1 = 0.2(1.047)^{(24.85-20)} = 0.249/\text{day}.$$

Hence, the deficit at any time t is

$$D_t = \frac{0.249(6.85)}{(0.8-0.249)}\left[e^{0.249t} - e^{-0.8t}\right] + 0.32e^{-0.8t}.$$

The time of the critical deficit is computed from

$$t_c = \frac{1}{(0.8-0.249)}\ln\left[\frac{0.8}{0.249}\left(1-0.32\left(\frac{0.8-0.249}{0.249\times 6.85}\right)\right)\right] = 1.92 \text{ days} = 46.05 \text{ h}.$$

For a downstream reach of 3300 m, the travel time is

$$t = \frac{L}{V} = \frac{5000}{1.2} = 4166 \text{ s} = 1.16 \text{ h}.$$

Since the critical time is considerably longer than the time at which the flow enters the larger stream, the deficit will not fall to the critical value.

PROBLEMS

1. Rainfall of magnitude 3.1 and 1.9 cm occurring on two consecutive 6 h durations on catchments of area 42 km^2 produced the given hydrograph in Table 6.56 at the outlet of the catchments. Estimate the rainfall excess and phi (Φ) index.
2. Find the maximum discharge for a 25-year 24 h storm. Consider the following characteristics:
   - The basin area is around 8.3 km^2.
   - The entire basin has Type B soil and is thin-stand forest with light underbrush.
   - The 25-year 24 h precipitation for the area is 8.6 cm.
3. A 30 min hydrograph is given in Table 6.57. The watershed has a drainage area of 30 ha. Compute the volume of direct runoff using the concave method to separate baseflow from total discharge.
4. Table 6.58 contains several parts of storm hydrographs that are measured in 6 h intervals. Use the master depletion curve method to determine baseflow for this watershed. Unit of discharge is given in cubic meters per second.
5. The ordinates of the 6 h unit hydrograph of a catchment are given in Table 6.59. Calculate the ordinate of the DRH due to a rainfall excess of 2.5 cm occurring in 6 h.
6. The peak of flood hydrograph due to a 3 h duration isolated storm in a catchment is 300 m^3/s. The total depth of rainfall is 6.3 cm. Assuming an average infiltration loss of 0.3 cm/h and a constant baseflow of 18 m^3/s, estimate the peak of the 3 h unit hydrograph (UH) of this catchment. If the area of catchments is 420 km^2, determine the base width of the 3 h unit hydrograph by assuming it to be triangular in shape.
7. The data given in Table 6.60 are measured at stream. Compute the direct runoff and baseflow distribution and the volume of direct runoff (a) using the constant-discharge method and (b) using the constant slope method assuming direct runoff begins at 0404 and ends at 1604.
8. Is the given hydrograph in Table 6.61 a legitimate unit hydrograph for a 297-acre watershed?
9. If the rainfall excess consists of two bursts of 3.3 in/h and 1.8 in/h, each for 20 min, and the 20 min unit hydrograph has ordinates of 15, 40, 25, and 10 ft^3/s (in 20 min intervals), determine the distribution of direct runoff.
10. The storm event data for a 1012.5 ha watershed are given in Table 6.62. Assuming that baseflow equals 0 and that rainfall prior to the start of runoff is initial abstraction, find the unit hydrograph and the distribution of rainfall excess. Use the phi method to separate losses.

TABLE 6.56
Hydrograph in Problem 1

Time from Start of Rainfall (h)	–6	0	6	12	18	24	30	36	42	48	54	60	66
Observed Flow (m^3/s)	4	5	15	26	20	14	10	7	4	5	6	3	2

TABLE 6.57
Hydrograph in Problem 3

Time	9:30	10	10:30	11	11:30	12	12:30	13
Flow (cms)	3.5	2.7	2.3	3	6.4	9	8.4	6.8
Time	13:30	14	14:30	15	15:30	16	16:30	17
Flow (cms)	5.2	4	3.2	2.6	2	1.5	1.1	0.7

TABLE 6.58
Storm Events in Problem 4

	Storm Event				
Time Lag	**1st**	**2nd**	**3rd**	**4th**	**5th**
1	1.25	0.91	2.38	0.54	0.27
2	0.93	0.76	0.65	0.26	0.16
3	0.79	0.59	0.34	0.19	0.12
4	0.68	0.51	0.28	0.16	0.12
5	0.59	0.45	0.23	0.14	0.10
6	0.51	0.40	0.18	0.13	0.08
7	0.48	0.34	0.17	0.12	0.07
8	0.42	0.31	0.17	0.10	0.07
9	0.40	0.27	0.16	0.09	0.07
10	0.37	0.23	0.16	0.08	0.06
11	0.34	0.22	0.16	0.08	0.06
12	0.34	0.21			
13	0.31	0.20			

TABLE 6.59
Unit Hydrograph in Problem 5

Time (h)	0	3	6	9	12	15	18	24	30	36	42	48	54	60	66
UH Ordinate (m^3/s)	0	25	60	85	120	150	170	160	100	55	35	20	15	10	0

TABLE 6.60
Hydrograph in Problem 7

Time	***Q*** **(m^3/s)**	**Time**	***Q*** **(m^3/s)**	**Time**	***Q*** **(m^3/s)**
0204	142	0704	1018	1204	2940
0304	196	0804	1546	1304	1148
0404	200	0904	3987	1404	1380
0504	598	1004	1300	1504	815
0604	1308	1104	1200	1604	755

TABLE 6.61
Hydrograph in Problem 8

Time (h)	0	0.4	1	1.3	1.7	2.5	5	8
Q **(m^3/s)**	0	35	105	135	90	50	15	0

TABLE 6.62
Hydrograph in Problem 10

t **(min)**	0	10	20	30	40	50	60	70	80	90
i **(cm/h)**	0	0.2	5	5.2	0	0	0	0	0	0
Q **(m^3/s)**	0	0	10	20	50	40	30	15	5	0

11. The rainfall hyetograph P and runoff hydrograph R were measured on a 0.5 h time interval. A phi index of 0.5 cm/h is appropriate for the watershed. Use the least-squares method to derive the unit hydrograph.

$$P = \{0.5,1.8,1.5,0.0,1.0,1.6\} \text{ cm/h}$$

$$R = \{10,20,80,400,350,400,450,300,200,125,60,40,15\} \text{ m}^3/\text{s}$$

12. Using the least-squares UH developed from Problem 11, fit a gamma UH to the least-squares UH. Area = 630 ha. Time increment = 30 min. Compare the least-squares and gamma synthetic UHs.
13. A watershed has the following characteristics:
    - A = 2500 ha, L = 4 km, S = 5%, I = 40%.
    - The channel is lined with concrete.

    Using the Espey equations, determine the 10 min unit hydrograph (T_R, T_B, Q_P, W_{50}, W_{75}). Sketch the hydrograph.
14. The watershed in Problem 10 is a residential area with 1/4 ha lots. The soil is categorized as soil group B. Determine the unit hydrograph for this area for storm duration of 1 h using the SCS method. Assume that the average watershed slope is the same as the channel slope.
15. The characteristics of a given watershed are as follows:
    - Area: 800 km^2
    - Length of main channel: 35 km
    - Length of basin center to outlet point: 15 km
    - C_t = 1.6 and C_p = 0.16

    Derive a 4 h unit hydrograph using the Snyder method.
16. The effective rainfall and DRH for an event are given by a rectangular pulse and a symmetric triangle:

Effective rainfall	= 1 cm/h	$0 < t < 3$h
	= 0 cm/h	$t > 3$h
Direct runoff	= 0 cm/h	$t = 0$
	= 2/3 cm/h	$t = 2$h
	= 0 cm/h	$t = 4$h

    Compute the unit hydrograph for this event. What period unit hydrograph is this?
17. A 6 h unit hydrograph of a catchment is triangular in shape with a base width of 53 h and a peak ordinate of 25 m^3/s. Calculate the equilibrium discharge of an S-curve obtained by this 6 h unit hydrograph.
18. A 2 h unit hydrograph is given by a rectangle whose base is 4 h and height is 0.32 cm/h. Derive a 4 h unit hydrograph using the given 2 h unit hydrograph.
19. Construct and draw an S-hydrograph using the 2 h unit hydrograph of the above exercise.
20. The IUH of a catchment is given in Table 6.63. Extract the DRH for this catchment due to storm of duration 4 h and having a rainfall excess of 6 cm.
21. Consider a basin as a linear reservoir with 4 h lag time. Determine the resulting runoff from the rainfall given in Table 6.64.
22. Using the Muskingum method, route the inflow hydrograph given in Table 6.65, assuming (a) K = 4 h and X = 0.12 and (b) K = 4 h and X = 0.0. Plot the inflow and outflow hydrographs for each case, assuming that initial outflow equals inflow.
23. Determine the flow hydrograph at the downstream end of the channel. The channel has a length of L = 1000 m and a bottom slope of S_0 = 0.001. For a reference discharge of Q_0 = 60 cms, the flow area is A_0 = 48.10 m^2 and the top width is T_0 = 31.0 m. The upstream

inflow hydrograph is tabulated below at a constant time interval of Δt = 0.25 h = 900 s (e = 0.343 $m^{1/3}$/s and m = 4/3).

24. The elevation, discharge, and storage relationship of a reservoir is given in Table 6.66. When the reservoir level was at 100.50 m, the given flood hydrograph in Table 6.67 enters the reservoir. Route the flood and obtain the reservoir elevation vs. time curve during the passage of the flood wave.
25. In a particular residential area of 300 km^2, measurements of the concentration of toxic contaminants in storm runoff show the average value of 0.35 mg/L. Assume the average

TABLE 6.63
IUH in Problem 20

Time (h)	0	1	2	3	4	5	6	7	8	9	10	11	12
IUH Ordinates $u(t)$ (cms)	0	9	40	55	45	38	30	21	16	9	5	3	0

TABLE 6.64
Rainfall Hyetograph in Problem 21

Time (h)	0	1	2	3	4
i (cm/h)	4	3	2	1	0

TABLE 6.65
Hydrograph in Problem 22

Time (h)	0	2	4	6	8	10	12	14	16	18
Inflow (L/s)	0	135	675	1350	945	567	351	203	68	0

TABLE 6.66
Elevation, Discharge, and Storage Relationships of Reservoir in Problem 24

Elevation (m)	Storage (MCM)	Outflow Discharge (cms)
100.00	3.350	0
100.50	3.472	10
101.00	3.880	26
101.500	4.383	46
102.00	4.882	72
102.50	5.370	100
102.75	5.527	116
103.00	5.856	130

TABLE 6.67
Inflow Hydrograph in Problem 24

Time (h)	0	6	12	18	24	30	36	42	48	54	60	66	72
Inflow (cms)	10	20	55	80	73	58	46	36	55	20	15	13	11

discharge of 150 cms during the storm. The surface runoff is discharged into a stream with a normal flow of 35 cms and toxic concentrations of 0.003 mg/L. Compute the concentration of the toxic contaminants in the mixed flow.

APPENDIX

In mathematics, the Laplace transform is a widely used integral transform. Denoted $L\{f(t)\}$, it is a linear operator of a function $f(t)$ with a real argument $t(t \geq 0)$ that transforms it to a function $F(s)$ with a complex argument s. This transformation is essentially biobjective for the majority of practical uses; the respective pairs of $f(t)$ and $F(s)$ are matched in tables.

The Laplace transform of a function $f(t)$, defined for all real numbers $t \geq 0$, is the function $F(s)$, defined by

$$F(s) = L\left\{f(t)\right\} = \int_{\circ}^{\infty} e^{-st} \cdot f(t)\,\mathrm{d}t.$$

The parameter s is a complex number:

$$s = \sigma + i\omega,$$

where σ and ω are real numbers.

The meaning of the integral depends on types of functions of interest. A necessary condition for the existence of the integral is that f must be locally integrable on $[0,\infty)$. For locally integrable functions that decay at infinity or are of exponential type, the integral can be understood as a (proper) Lebesgue integral. However, for many applications, it is necessary to regard it as a conditionally convergent improper integral at ∞.

The Laplace transform has the useful property that many relationships and operations over the originals $f(t)$ correspond to simpler relationships and operations over the images $F(s)$. The Laplace transform has many important applications throughout the sciences. It is named after Pierre-Simon Laplace who introduced the transform in his work on probability theory.

The Laplace transform is related to the Fourier transform, but whereas the Fourier transform resolves a function or signal into its modes of vibration, the Laplace transform resolves a function into its moments. Like the Fourier transform, the Laplace transform is used for solving differential and integral equations. In physics and engineering, it is used for analysis of linear time-invariant systems such as electrical circuits, harmonic oscillators, optical devices, and mechanical systems. In this analysis, the Laplace transform is often interpreted as a transformation from the time domain, in which inputs and outputs are functions of time, to the frequency domain, where the same inputs and outputs are functions of complex angular frequency, in radians per unit time. Given a simple mathematical or functional description of an input or output to a system, the Laplace transform provides an alternative functional description that often simplifies the process of analyzing the behavior of the system or synthesizing a new system based on a set of specifications.

The inverse Laplace transform is given by the following complex integral:

$$F(t) = L^{-1}\left\{f(s)\right\} = \frac{1}{2\pi i T \to \infty} \lim \int_{\gamma i+t}^{\gamma i+t} e^{ts} \cdot F(s)\,\mathrm{d}t,$$

where γ is a real number so that the contour path of integration is in the region of convergence of $F(s)$. An alternative formula for the inverse Laplace transform is given by Post's inversion formula.

The following table provides Laplace transforms for many common functions of a single variable. For definitions and explanations.

Because the Laplace transform is a linear operator:

The Laplace transform of a sum is the sum of Laplace transforms of each term.

$$L\{f(t) + g(t)\} = L\{f(t)\} + L\{g(t)\}$$

The Laplace transform of a multiple of a function is that multiple times the Laplace transformation of that function.

$$L\{af(t)\} = aL\{f(t)\}$$

The unilateral Laplace transform takes as input a function whose time domain is the non-negative reals, which is why all of the time domain functions in the table below are multiples of the Heaviside step function, $u(t)$. The entries in the table that involve a time delay τ are required to be causal (meaning $\tau > 0$). A causal system is a system where the impulse response $h(t)$ is zero for all time t prior to $t = 0$. In general, the region of convergence for causal systems is not the same as that of anticausal systems.

Function	Time Domain $F(t) = L^{-1}\{f(s)\}$	Laplace s Domain $F(s) = L\{f(t)\}$	Region of Convergence
Unit impulse	$\delta(t)$	1	All s
Delayed impulse	$\delta(t-\tau)$	$e^{-\tau s}$	
Unit step	$u(t)$	$\frac{1}{s}$	$\mathrm{Re}\{s\} > 0$
Delayed unit step	$u(t-\tau)$	$\frac{e^{-\tau s}}{s}$	$\mathrm{Re}\{s\} > 0$
Ramp	$t \cdot u(t)$	$\frac{1}{s^2}$	$\mathrm{Re}\{s\} > 0$
Delayed nth power with frequency shift	$\frac{(t-\tau)^n}{n!} e^{-a(t-\tau)} \cdot u(t-\tau)$	$\frac{e^{-\tau s}}{(s+\alpha)^{n+1}}$	$\mathrm{Re}\{s\} > -\alpha$
nth power (for integer n)	$\frac{t^n}{n!} \cdot u(t)$	$\frac{1}{s^{n+1}}$	$\mathrm{Re}\{s\} > 0$ $(n > -1)$
qth power (for complex q)	$\frac{t^q}{\Gamma(q+1)} \cdot u(t)$	$\frac{1}{s^{q+1}}$	$\mathrm{Re}\{s\} > 0$; $\mathrm{Re}\{q\} > -1$
nth power with frequency shift	$\frac{t^n}{n!} e^{-\alpha t} \cdot u(t)$	$\frac{1}{(s+\alpha)^{n+1}}$	$\mathrm{Re}\{s\} > -\alpha$
Exponential decay	$e^{-\alpha t} \cdot u(t)$	$\frac{1}{(s+\alpha)}$	$\mathrm{Re}\{s\} > -\alpha$
Exponential approach	$(1 - e^{-\alpha t}) \cdot u(t)$	$\frac{a}{s(s+a)}$	$\mathrm{Re}\{s\} > 0$
Sine	$\sin(\omega t) \cdot u(t)$	$\frac{\omega}{s^2 + \omega^2}$	$\mathrm{Re}\{s\} > 0$

Cosine	$\cos(\omega t) \cdot u(t)$	$\frac{s}{s^2+\omega^2}$	$\mathrm{Re}\{s\} > 0$
Hyperbolic sine	$\sinh(at) \cdot u(t)$	$\frac{a}{s^2+a^2}$	$\mathrm{Re}\{s\} > \lvert a\rvert$
Hyperbolic cosine	$\cosh(at) \cdot u(t)$	$\frac{s}{s^2-a^2}$	$\mathrm{Re}\{s\} > \lvert a\rvert$
Exponentially decaying sine wave	$e^{-\alpha t}\sin(\omega t) \cdot u(t)$	$\frac{\omega}{(s+a)^2+\omega^2}$	$\mathrm{Re}\{s\} > -a$
Exponentially decaying cosine wave	$e^{-\alpha t}\cos(\omega t) \cdot u(t)$	$\frac{s+a}{(s+a)^2+\omega^2}$	$\mathrm{Re}\{s\} > -a$
nth root	$\sqrt[n]{t} \cdot u(t)$	$s^{-(n+1)/n} \cdot \Gamma\left(1+\frac{1}{n}\right)$	$\mathrm{Re}\{s\} > 0$

The Laplace transform has a number of properties that make it useful for analyzing linear dynamical systems. The most significant advantage is that differentiation and integration become multiplication and division, respectively, by s (similarly to logarithms changing multiplication of numbers to addition of their logarithms). Because of this property, the Laplace variable s is also known as an operator variable in the L domain: either a derivative operator or (for s^{-1}) an integration operator. The transform turns integral equations and differential equations to polynomial equations, which are much easier to solve. Once solved, use of the inverse Laplace transform reverts back to the time domain.

Given the functions $f(t)$ and $g(t)$ and their respective Laplace transforms $F(s)$ and $G(s)$:

$$f(t) = L^{-1}\{F(s)\}$$

$$g(t) = L^{-1}\{G(s)\}$$

The following table is a list of properties of the unilateral Laplace transform:

Properties of the Unilateral Laplace Transform

	Time Domain	s Domain	Comment
Linearity	$af(t) + bg(t)$	$aF(t) + bG(s)$	Can be proven using basic rules of integration
Frequency differentiation	$tf(t)$	$-f'(t)$	F' is the first derivative of F
Frequency differentiation	$t^n f(t)$	$(-1)^n F^{(n)}(s)$	More general form, nth derivative of $F(s)$
Differentiation	$f'(t)$	$sF(s) - f(0)$	f is assumed to be a differentiable function, and its derivative is assumed to be of exponential type. This can then be obtained by integration by parts

Second differentiation	$f''(t)$	$s^2F(s) - sf(0) - f'(0)$	f is assumed twice differentiable and the second derivative is assumed to be of exponential type. Follow by applying the differentiation property to $f'(t)$
General differentiation	$f^{(n)}(t)$	$-s^{n-1}f(0) - \ldots - f^{(n-1)}(0)$	f is assumed to be n-times differentiable, with nth derivative of exponential type. Follow by mathematical induction
Frequency integration	$\frac{f(t)}{t}$	$\int_s^\infty F(\sigma)\,d\sigma$	
Integration	$\int_0^t f(\tau)\,d\tau = (u * f)(t)$	$\frac{1}{s}F(s)$	$u(t)$ is the Heaviside step function. Note $(u * f)(t)$ is the convolution of $u(t)$ and $f(t)$
Time scaling	$f(at)$	$\frac{1}{\lvert a\rvert}F\left(\frac{s}{a}\right)$	
Frequency shifting	$e^{at}f(t)$	$F(s-a)$	
Time shifting	$f(t-a)u(t-a)$	$e^{-as}F(s)$	$u(t)$ is the Heaviside step function
Multiplication	$f(t)g(t)$	$\frac{1}{2\pi i}\lim_{T\to\infty}\int_{c-iT}^{c+iT} F(\sigma)G(s-\sigma)\,d\sigma$	The integration is done along the vertical line $Re(\sigma) = c$ that lies entirely within the region of convergence of F.[12]
Convolution	$(f * g)(t) = \int_0^t f(\tau)g(t-\tau)\,d\tau$	$F(s) \cdot G(s)$	$f(t)$ and $g(t)$ are extended by zero for $t < 0$ in the definition of the convolution
Complex conjugation	$f^*(t)$	$F^*(s^*)$	
Periodic function	$f(t)$	$\frac{1}{1-e^{-Ts}}\int_0^T e^{-st}f(t)\,dt$	$f(t)$ is a periodic function of period T so that $f(t) = f(t+T)$, $\forall t \geq 0$. This is the result of the time shifting property and the geometric series

REFERENCES

Cunge, J.A. (1969). "On the subject of flood propagation computational method (Muskingum method)." *J. Hydrol. Res*. 7 (2), 205–230.

Diskin, M.H. (1970). "Definition and uses of the linear regression model." *Water Resources Research*, 6 (6), 1668–1673.

Espey, W.H., Jr., Altman, D.G. and Graves, C.B., Jr. (1977). Nomographs for Ten-Minute Unit Hydrographs for Small Urban Watersheds. Technical Memorandum No. 32 (NTIS PB-282158). ASCE Urban Water Resources Research Program. ASCE, New York (also Addendum 3 in Urban Runoff Control Planning. EPA-600/9-78-035. EPA, Washington, DC). December.

Gray, O.M. (1962). Derivation of hydrographs for small watersheds from measurable physical characteristics. Res. Bull., 506, Agr. and Home Econ. Expt. Sta., Iowa State Univ., Ames, Iowa.

Karamouz, M., Moridi, A. and Nazif, S. (2010). *Urban Water Engineering and Management*, CRC Press, Taylor and Francis Group, 649 pp.

Linsley, R.K., Kohler, M.A., Paulhus, J.L.H. and Wallace, J.S. (1958), Hydrology for engineers. McGraw Hill, New York, 340 pp.

McCarthy, G.T. (1938). The unit hydrograph and flood routing. Unpublished Paper. Conference of North Atlantic Division, US Army Corps of Engineers, New London, CT. US Engineering Office, Providence RI.

McCuen, R.H. (1998). *Hydrologic Analysis and Design*, 2nd edition. Pearson Prentice-Hall, Englewood Cliffs, NJ.

McCuen, R.H., Rawls, W.J. and Wong, S.L. (1984). "SCS urban peak flow method," *J. Hydraulic Eng.*, 110 (3), 290–299.

McPherson, M.B. (1978). Urban Runoff Control Planning, EPA-600/9-78-035, Environmental Protection Agency, Washington D.C.

Meadows, M.E. (1991). Extension of SCS TR-55 and development of single outlet detention pond performance charts for various unit hydrograph peak rate factors: U.S. Geological Survey Project Completion Report, v. 3, 136 p.

Nash, J.E. (1958). Determining Runoff from Rainfall. Proceedings of the Institution of Civil Engineers, 10, 163–184.

Ponce, V.M. and Theurer, F.D. (1982). "Accuracy criteria in diffusion routing," *Journal of the Hydraulic Division, ASCE*, 108, 747–757.

Ponce, V.M. and Yevjevich, V. (1978). "Muskingum–Cunge method with variable parameters," *Journal of the Hydraulic Division, ASCE*, 104, 1663–1667.

Ross, D.A. (1995). Introduction to Oceanography. New York: Harper Collins College Publishers. ISBN 978-0673469380.

Soil Conservation Service (1986). Urban Hydrology for Small Watersheds. Technical Release 55, 2nd edition. U.S. Dept. of Agriculture. NTIS PB87-101580 (microcomputer version 1.11. NTIS PB87-101598), Springfield, VA.

Snyder, F.F. (1938). "Synthetic unit hydrographs." Transactions of the American Geophysical Union, vol. 19, part 1, 447–454.

USDA (1986). Natural Resources Conservation Service (NRCS). *Technical Release 55: Urban Hydrology for Small Watersheds, 2nd edition*. Washington, DC.

USDA-SCS (1972). National Engineering Handbook. *Hydrology Section 4*. Chapter 4–10. United States Department of Agriculture, Soil Conservation Service, Washington, DC.

Wanielista, M.P., Kersten, R. and Eaglin, R. (1997). Hydrology, J. Wiley and Sons, New York, 567 pp.

7 Groundwater Hydrology

7.1 INTRODUCTION

The infiltrated water to the Earth is pulled down by gravity through the pores until it reaches a depth in the ground where all of the pores are filled with water, which is called groundwater. At this point, the soil or rock becomes saturated, and the water level that results is called the water table. The water table is not always at the same depth below the land surface. During periods of high precipitation, the water table can rise. Conversely, during periods of low precipitation and high evapotranspiration, the water table falls. The water table is also affected by artificial charge and discharges made in different points by humans. Underground water consists of two different zones. The one that contains both water and air, and occurs immediately below the land surface in most areas, is referred to as the unsaturated zone. The other zone that is almost underlain by a zone in which all interconnected openings are full of water is considered as the saturated zone.

The only underground water that is readily available to supply wells and springs and also the only water to which the name groundwater is correctly applied is water in the saturated zone. Percolation of water from the land surface through the unsaturated zone forms the recharge of the saturated zone. This feature makes the unsaturated zone greatly important to groundwater hydrology. The unsaturated zone can be practically divided into three parts (Figure 7.1):

1. The soil zone: This zone extends from the land surface to a maximum depth of a meter or two and is the zone that supports plant growth. It is crisscrossed by living roots, by voids left by decayed roots of earlier vegetation, and by animal and worm burrows. Higher porosity and permeability of this zone rather than those of the underlying material are the specifications of the soil zone.
2. The intermediate zone: Underneath the soil zone is the intermediate zone, which differs in thickness from place to place based on the thickness of the soil zone and the depth of the capillary fringe.
3. The upper part of the capillary fringe: The lowest part of the unsaturated zone is occupied by the capillary fringe, the subzone between the unsaturated and saturated zones. Attraction between water and rocks causes the capillary fringe to form. Consequently, water clings as a film on the surface of rock particles and rises in small-diameter pores against the pull of gravity. A negative hydraulic pressure—a pressure less than the atmospheric (barometric) pressure is considered as a negative pressure—usually exists in the capillary fringe and in the overlying part of the unsaturated zone.

At the water table, the hydraulic pressure is equal to the atmospheric pressure and is also represented by the water level in unused wells. It should be noted that, below the water table, the hydraulic pressure increases with increasing depth.

In the hydrologic cycle, clouds are seeded and precipitate on the oceans or land surfaces in different forms such as rain, snow, and hail; however, only rain is considered in this discussion. During rainfall, water infiltrates into the ground after wetting vegetation and other surfaces. Whenever the rate of precipitation transcends the rate of infiltration, overland flow occurs. During infiltration, replacement of soil moisture would take place and the excess water would percolate slowly across the intermediate zone to the zone of saturation. Water in the zone of saturation moves downward and laterally and reaches the

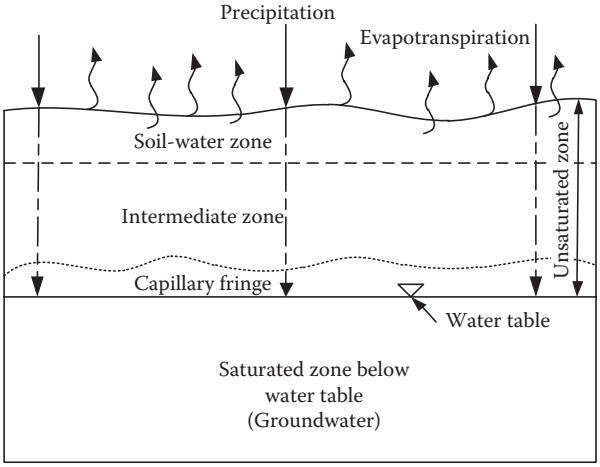

FIGURE 7.1 Groundwater system.

sites of groundwater discharge such as springs on hillsides or seeps in the bottoms of streams and lakes or beneath the ocean. Finally, water reaches some streams, both by overland flow and from groundwater discharge; hence, it moves to the sea, where it again evaporates to recontinue the cycle.

7.2 GROUNDWATER SYSTEMS

Similar to the surface runoff, the groundwater system should be studied in a watershed scale even though the surface watersheds and groundwater aquifers do not match each other. A holistic view is necessary for groundwater challenges within a hydrological cycle because of the combination of many elements and factors that are highly interconnected in the groundwater system.

One of the most traditionally developed sources of water is the groundwater system, which is used for domestic, industrial, or agricultural purposes. Some of the important factors of this system that have intensified the development of this relatively low-cost, reliable water resource can be mentioned, such as good quality of the water obtained from this resource and its accessibility in many regions of the world, even in those areas where surface water is nonexistent or extremely costly to develop. Figure 7.2 illustrates an example of system representation of groundwater; see Karamouz et al. (2011) for more details.

For computations of groundwater balance and pollution characteristics, a groundwater system can be isolated from upstream and downstream aquifers. Five groups of variables and parameters should be identified for system simulation:

1. Partially or completely controlled set of inputs to the system including precipitation, subsurface inflows, natural and artificial recharge, irrigation return flows, and interactions with streams.
2. The system outputs such as subsurface outflows to adjacent aquifers, discharges to surface waters, naturally occurring springs, and evapotranspiration losses.
3. The groundwater parameters that define the flow, quality, and thermal properties of the aquifer system, such as the hydrologic conductivity, transmissivity storability, storage coefficient, and dispersion/advection parameters.
4. The control or decision variables are policies in system planning and management such as details of the pumping, injection, and artificial recharge variables of the groundwater and surface water system. Restrictions over the decision variables are exerted in system simulation by legal, physical, and operational constraints.

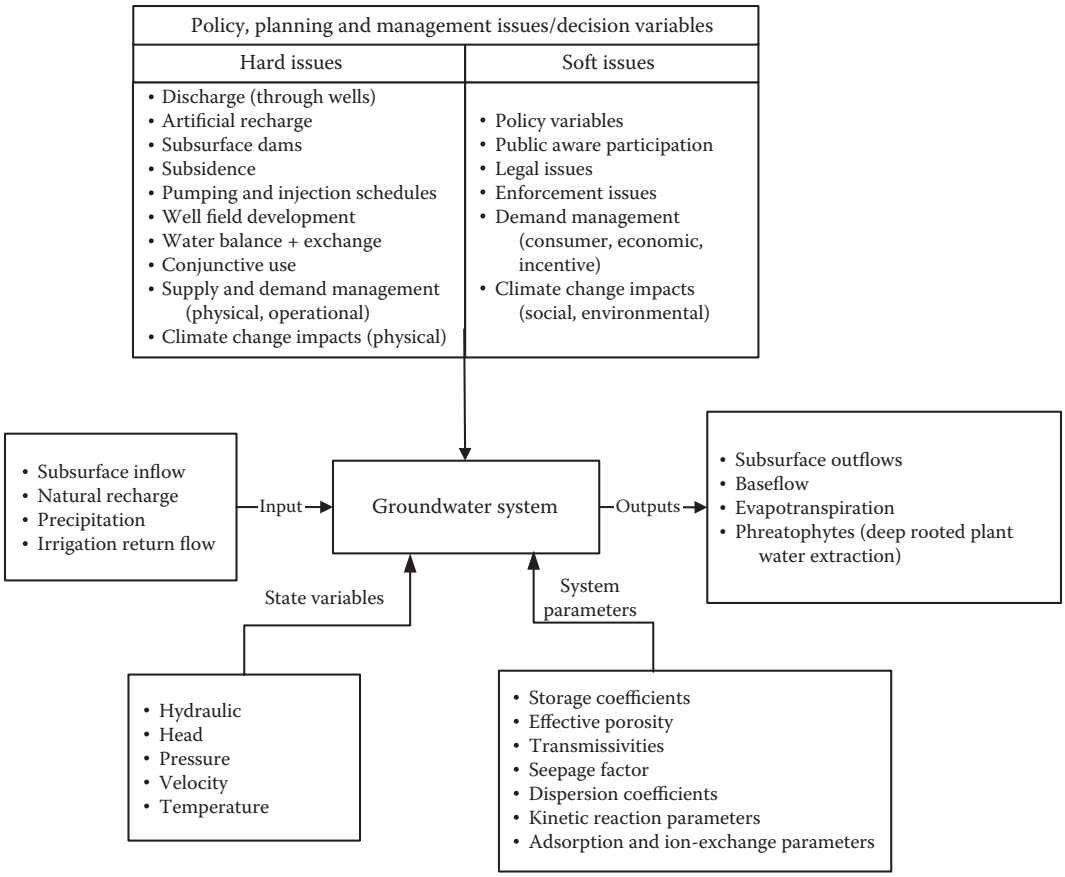

FIGURE 7.2 Groundwater system. (From Karamouz, M. et al., *Groundwater Hydrology: Engineering, Planning, and Management*, CRC Press Inc., 2011. With permission.)

5. The state variables that specify the condition of the system, such as the hydraulic head, pressure, velocity or temperature distribution, or the concentrations of pollutants in the groundwater system.

A lump system is often chosen to deal with groundwater systems even though in reality the systems contain distributed parameters. This is due to limited data availability about the spatial variation of system parameters. The lump system can be justified to consider the temporal variations of the system parameters, but most of the aquifers have major spatial variation in their parameters that cannot be ignored. These specifications are often referred to as nonhomogeneous properties that need to be tested and determined in many locations across aquifers. In engineering measures, the system can be simplified with constant dispersion and diffusion characteristics in any time and space element. While simplification of groundwater systems should be made, the overall characteristic of the system must be preserved.

7.3 GROUNDWATER AVAILABILITY

Groundwater is the most commonplace source of freshwater on continents outside the Polar Regions, followed by ice caps, lakes, wetlands, reservoirs, and rivers. About 1.5 billion people over the world rely on groundwater for their drinking water supply (World Resources Institute 1998). It

is estimated that groundwater withdrawal makes up about 20% of global water withdrawals (World Meteorological Organization 1998).

Based on the United Nations Environment Program report, annual global freshwater withdrawal has grown from 3790 to about 4430 km^3 during the years 1995–2000. If the rate of annual global water withdrawal increases by 10–20% over a decade, it is expected to reach approximately 5240 km^3 in 2025. However, the share of groundwater will increase at a slower rate due to the existence of already overdrafted aquifers in many parts of the world especially those with limited surface water resources.

These investigations show the importance of rehabilitation of aquifers and their optimal management as secure water resources in emergency cases. The main advantages in storage of groundwater compared to the surface storage are as follows:

1. The least evaporation losses, which are bounded to
   a. Groundwater near the surface by capillarity fringes.
   b. Phreatophytes, plants that feed on the capillary fringe.
2. Quality advantage that is gained from soil filtering action (however, in some cases, the dissolved solids concentration is too high in groundwater). There is general improvement of water quality because of the porous media filtration of airborne and surface runoff contaminants and pathogens.
3. Progressive and gradual outflow (good regulation in underground reservoir).
4. Low-cost development—no dam or other massive structures needed (however, it may involve high pumping costs when the groundwater is very deep).
5. Continuity of land use above the groundwater resources without any changes (there is no submergence of houses, abstraction to infrastructure, property, and agricultural development).

Continuous threats ambush groundwater quality. If groundwater is not protected effectively, quality deteriorates from saline intrusion, pollution from agricultural and urban activities, uncontrolled wastewater, and solid and hazardous waste disposal. The following strides should be considered:

- Improvement of the understanding of groundwater contribution to the hydrologic cycle and evaluation of the changes in groundwater storage and water table/piezometric surface fluctuation.
- Increasing the awareness of decision makers, water users, and public about the importance of groundwater and the necessity of its protection and sustainable use.
- Evaluation of the impacts of economic development on groundwater resources and corroborating international collaboration for these resources' protection.
- Measuring the impacts of climate change on groundwater resources such as sea level rise and intrusion of saltwater.

7.4 GROUNDWATER DEVELOPMENT

Groundwater is broadly spread under the ground and is a restorable resource unlike other resources of the Earth. Zones of occurrence and recharge are the main problems in groundwater investigation. The modern trends are bound to create more opportunity for recharge of groundwater from natural sources like rain, percolation dams, etc. Groundwater can be used for supplemental irrigation during periods of deficient surface supply, for the year-round irrigation practice.

An "aquifer" is a water-bearing geologic formation or stratum that is capable of transmitting water through its pores at a rate sufficient for economic extraction by wells. Dingman (1994) defined an *aquifer* as "a geologic unit that can store enough water and transmit it at a rate fast enough to be hydrologically significant." In general, it can be said that an aquifer is permeable enough to be economically exploited, while it is not economical to withdraw water from aquicludes (which were introduced in Chapter 2).

The good aquifers are usually developed in formations of

- Unconsolidated gravels, sands, alluvium
- Lake sediments, glacial deposits
- Sandstones
- Limestones with cavities (caverns) formed by the action of acid waters (solution openings in limestones and dolomites)
- Granites and marble with fissures and cracks, weathered gneisses, and schists
- Heavily shattered quartzites
- Vesicular basalts
- Slates (better than shales owing to their jointed conditions)

An "aquiclude" is a geologic formation that can absorb water, but water cannot be transmitted under ordinary hydraulic gradients in a saturated geologic formation. Some examples of aquiclude are clays and shales.

An "aquitard" is a geologic formation of rather impervious nature, which transmits water at a slow rate compared to an aquifer (just insufficient for pumping from wells). Although significant quantities of water might be transmitted through these media, their permeability is not sufficient to exploit water through wells within them. Very few geological formations such as clay, shale, and dense crystalline rocks have the characteristics of an aquiclude, and most of the geologic strata are considered as either aquifers or aquitards. However, it is really difficult to specify whether a formation with given constituents is an aquifer or an aquitard. In other words, there is vagueness in the definition of aquifers and aquitards. For example, in an interlayered sand–silt formation, the silt layer may be considered an aquitard, while if the formation is a silt–clay system, the silt may be considered an aquifer. In general, an aquifer has different meanings for different people, and it might even have various meanings to the same person at different times.

An "aquifuge" is a geologic formation with no interconnected pores and hence can neither absorb nor transmit water. Instances of aquifuge are basalts and granites (Todd 1980).

7.5 TYPES OF AQUIFERS

Most aquifers are underground storage reservoirs made up of water-bearing permeable rock or unconsolidated materials. Water is forced by gravity to penetrate downward through the pores until it reaches the saturated area. The water level, termed as "water table," is not always at the same depth below the land surface. Due to the presence or absence of a water table, classifications of aquifers are made as unconfined or confined, while a leaky aquifer is considered as a semiconfined aquifer, which has the characteristics of both types of aquifers.

7.5.1 Unconfined Aquifer

In an unconfined aquifer, the water table, which varies in fluctuation form and in slope, defines the top of the aquifer. The water table fluctuation totally relies on changes in volume of water storage prepared by areas of recharge and discharge, pump from wells, and permeability. In Figure 7.3, the upper aquifer is an unconfined aquifer. The contour maps and profiles of the water table are prepared by the water elevations in wells. Typically, the shallowest aquifer at a given location does not have a confining layer between it and the surface, and it is considered as an unconfined aquifer.

The perched water body refers to the groundwater accumulating above an impermeable stratum such as a clay layer. This term is a special case of an unconfined aquifer, which is indicated by a small local area and by an elevation higher than a regionally extensive aquifer. Clay lenses in sedimentary deposits often have shallow perched water bodies overlying them.

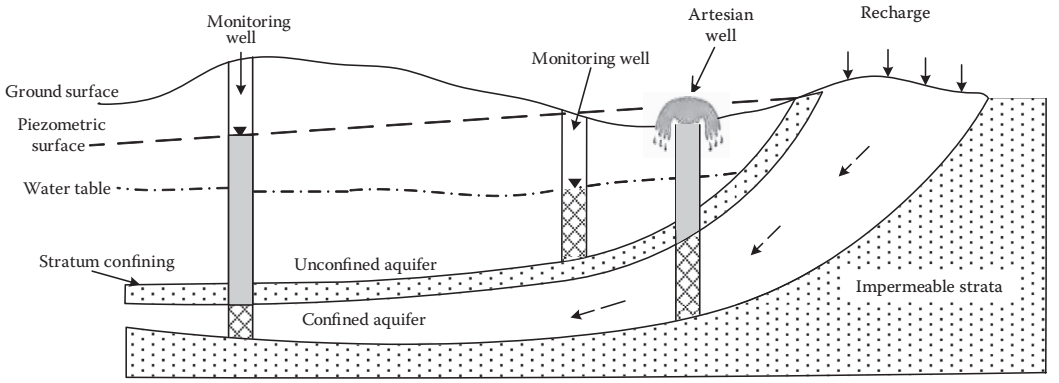

FIGURE 7.3 Schematic cross section illustrating unconfined and confined aquifers.

7.5.2 Confined Aquifers

Confined aquifers are restricted on the top by impermeable material. Water pressure in a confined aquifer is normally higher than atmospheric pressure. This pressure in a well permeating can cause the water level to rise above the ground surface, which is classified as a flowing artesian well as shown in Figure 7.3. A recharge area is an area where water flows into the earth to resupply a water body or an aquifer. Variation in pressure is much more related to water fluctuations in wells discharging water from confined aquifers than changes in water storage volume in the aquifer. Therefore, small change in storage will occur in confined aquifers and convey water from recharge areas to locations of natural or artificial discharge.

Figure 7.3 shows the potentiometric surface, which is known as the potential level or piezometric surface. The piezometric surface indicates the static head of groundwater and is defined by the level to which water will rise. An overflow well (artesian well) will occur when the potential level of the piezometric surface is higher than the land surface. Furthermore, when the piezometric surface is lower than the bottom of the upper confining bed, a confined aquifer becomes an unconfined aquifer.

7.5.3 Aquitard (Leaky) Aquifer

Aquitards are attributed to the zones within the Earth that limit the groundwater flow from one aquifer to another. Beds of these aquifers include characteristics of low permeability along the aquifer. Generally, the existence of leaky or semiconfined aquifers is more expected than that of confined or unconfined aquifers. This is because it is really hard to find an aquifer that is completely confined or unconfined. These characteristics are common in alluvial valleys, plains, or former lake basins.

7.6 AQUIFER CHARACTERISTICS

Some important characteristics of aquifers can be mentioned, such as porosity and void ratio, specific retention, specific yield, storage coefficient, specific storage coefficient, and safe yield. Specific yield and specific storage are usually used in unconfined and confined aquifers, respectively. Some explanations of these parameters are as follows.

7.6.1 Porosity and Void Ratio

The total volume of a porous medium such as soil, V_T, includes the volume of the solid portion, V_s, and the volume of the voids, V_V. The porosity of the medium, n, is defined as the ratio of volume of voids over the total volume:

$$n = V_V/V_T, \tag{7.1}$$

where porosity is in the form of a decimal fraction or a percentage.

Figure 7.4 illustrates the porosity of the medium in different rock and soil textures. The first part (Figure 7.4a) depicts a well-graded sedimentary deposit with porous pebbles that has high porosity. The second part (Figure 7.4b) shows poorly graded sedimentary deposit, and Figure 7.4c is about a well-graded sedimentary deposit containing mineral filling that has a very low porosity. Rock rendered porous by solution and fracturing with high porosity is depicted in Figure 7.4d.

Imagine a cylinder full of gravel and its cross section at the elevation z. The porosity at elevation z, $n(z)$, in this cylinder can be obtained as

$$n(z) = \frac{A_P}{A}, \tag{7.2}$$

where A_P is the cross section of the porous medium (the area of the pores), and A is the area of the cylinder. Thus, the porosity in the whole cylinder can be calculated as

$$n = \frac{1}{h}\int_0^h n(z)\,dz = \frac{1}{Ah}\int_0^h An(z)\,dz = \frac{1}{V_T}\int_0^h A_P(z)\,dz = \frac{V_V}{V_T} \tag{7.3}$$

and then,

$$n = 100\frac{V_V}{V_T} = 100\left(\frac{V_T - V_s}{V_T}\right) = 100\left(1 - \frac{V_s}{V_T}\right) \tag{7.4}$$

$$n = 100\left[1 - \frac{\rho_b}{\rho_d}\right], \tag{7.5}$$

where V_V is the volume of pores, V_T is the volume of cylinder, V_s is the volume of solids, ρ_b is the bulk density (about 1400–1900 kg/m^3), and ρ_d is the particle density (about 2650 kg/m^3). The common porosity ranges for various geologic materials are presented in Table 7.1.

As can be concluded from this table, gravels and sands, which are formed by angular and rounded particles, have lower porosities than soils made up of silt and clay minerals.

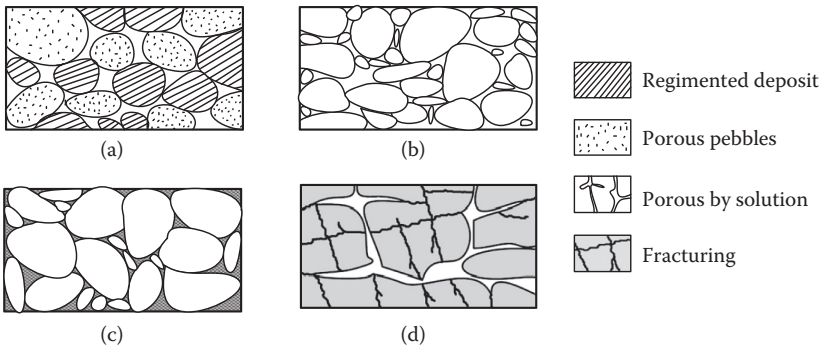

FIGURE 7.4 (a) Well-graded sedimentary deposit, with porous pebbles. (b) Poorly graded sedimentary deposit. (c) Well-graded sedimentary deposit with mineral filling. (d) Rock rendered porous by solution and fracturing. (From Karamouz, M. et al., *Groundwater Hydrology: Engineering, Planning, and Management*, CRC Press Inc., 2011. With permission.)

TABLE 7.1
Porosity of Different Geologic Materials (%)

Unconsolidated Deposits	Porosity	Effective Porosity
Clay	40–70	10–18
Silt	35–50	10–39
Sand	25–40	10–46
Gravel	25–40	13–44
Sandstone	5–30	2–41
Limestone, dolomite	0–20	10–24
Fractured basalt	5–50	–
Karst limestone	5–50	–
Shale	0–10	–
Fractured crystalline rock	0–10	–
Dense crystalline rock	0–5	–

Example 7.1

Calculate particle density if porosity of the matter is 0.25 and the dry bulk density is 1.85 g/cm^3.

Solution:

By rearranging Equation 7.5, the particle density can be calculated as follows:

$$\rho_d = \frac{\rho_b}{(1-n)} = \frac{1.85}{1-0.25} = 2.47 \text{ g/cm}^3.$$

Example 7.2

The wet bulk density, ρ_{bw}, and dry bulk density, ρ_d, of a saturated soil sample are determined as 2.32 and 1.97 g/cm^3, respectively. Determine the porosity of the sample.

Solution:

Let us consider the following notations:

m_s = mass of soil

m_w = mass of water

V = total volume

Then, it can be written as $\rho_{bw} = \frac{m_s + m_w}{V} = \frac{m_s}{V} + \frac{m_w}{V} = \rho_d + \frac{m_w}{V}$

$$m_w = \rho_w \cdot V_w.$$

The voids volume can be considered equal to water volume because the sample is saturated.

$$V_v = V_w \qquad \frac{m_w}{V} = \frac{\rho_w \cdot V_v}{V} = \rho_w \cdot n.$$

Therefore, $\rho_{bw} = \rho_d + n \cdot \rho_w \Rightarrow$

$$n = \frac{\rho_{bw} - \rho_d}{\rho_w} = \frac{2.32 - 1.97}{0.998} = 0.35 \ (\rho_w = 0.998 \text{ g/cm}^3 \text{ at } 20°\text{C}).$$

Another term encountered in studying the porosity of a medium and that is widely used in soil mechanics is void ratio, *e*, which is closely related to porosity. The void ratio can be defined as

$$e = V_v/V_s. \tag{7.6}$$

The void ratio usually ranges from 0 to 3. The relation between *e* and *n* can be expressed as

$$e = \frac{n}{1-n} \text{ or } n = \frac{e}{1+e}. \tag{7.7}$$

Another concept of porosity is effective porosity $(\hat{n})$, which can be defined as the volume of the continuously connected path for water movement through the soil. In other words, it is the ratio of the continuous fractures over total volume of the medium:

$$\hat{n} = \frac{V_{wm}}{V_T}, \tag{7.8}$$

where V_{wm} is the volume of the path of water movement.

7.6.2 Specific Yield in Unconfined Aquifers

Specific yield is another name for effective porosity and is defined as the volume of water that is released from storage in an unconfined aquifer per unit surface area of the aquifer per unit decline in the water table. In order to determine this coefficient, a given volume of the aquifer is extracted and put on a mesh surface. The ratio of the discharged water volume of the sample, considering the gravity, over total volume of the sample is its specific yield.

$$S_y = \frac{dV}{Adh}, \tag{7.9}$$

where S_y is the specific yield, *V* is the volume of withdrawn water, *h* is the level of water in the aquifer, and *A* is the aquifer area.

7.6.3 Specific Retention

Specific retention is expressed as follows:

$$S_r = n - \hat{n}, \tag{7.10}$$

where S_r is the specific retention, n is the porosity, and $\hat{n}$ is the effective porosity, which is the same as the specific yield for all practical purposes. Different soil particles have different yield and retention. For instance, clay has good retention and low yield.

Thus, porosity of an aquifer can be obtained from the summation of specific yield and specific retention of that aquifer:

$$n = S_y + S_r. \tag{7.11}$$

Example 7.3

Assume the specific yield of an aquifer is 2.7×10^{-3}. A head drop of 0.73 m is experienced after 7 years of pumping. If the area of the aquifer is 7.5 km^2, determine the pumping rate during this period.

Solution:

$$S_y = \frac{\Delta V}{A \cdot \Delta h} = \frac{Q \cdot \Delta t}{A \cdot \Delta h} \qquad Q = A \cdot \Delta h \cdot S_y / \Delta t$$

$$Q = \frac{7.5(\text{km}^2) \times 10^6 (\text{m}^2/\text{km}^2) \times 0.73(\text{m}) \times 2.7 \times 10^{-3}}{7(\text{years}) \times 365(\text{days/year})} = \frac{14{,}782.5}{2555} = 5.79 \text{ m}^3/\text{day}.$$

Example 7.4

An aquifer is exposed to the pumping rate of 6.0 m^3/day for a period of 4 years resulting a head drop of 1 m. A 190 cm^3 soil sample taken from this aquifer is tested, and the volume of voids is estimated to be equal to 76 cm^3, out of which water can move through only 54 cm^3. Calculate the porosity, effective porosity, specific retention, and specific yield of the soil and the area of the aquifer.

Solution:

$$n = \frac{V_v}{V_T} = \frac{76}{190} = 0.40$$

$$\hat{n} = \frac{V_{wm}}{V_T} = \frac{54}{190} = 0.28$$

$$S_r = n - \hat{n} = 0.40 - 0.28 = 0.12$$

$$S_y = n - S_r = 0.40 - 0.12 = 0.28$$

$$A = \frac{V_w}{S_y \cdot \Delta h} = \frac{Q \cdot \Delta t}{S_y \cdot \Delta h} = \frac{6.0(\text{m}^3/\text{day}) \times 4(\text{years}) \times 365(\text{days/year})}{0.28 \times 1.00(\text{m})} = \frac{8760 \text{ m}^3}{0.28 \text{ m}} = 31{,}285.7 \text{ m}^3.$$

7.6.4 Storage Coefficient and Specific Storage

The storage volume within an aquifer changes by discharging water from or recharging water to the aquifer. For unconfined aquifers, storage volume can be determined as the product of the volume of aquifer, between the beginning and the end of a certain period of time, and the average specific yield of the aquifer. Nonetheless, changes in pressure produce only small changes in storage volume in confined aquifers. Operating a well and pumping out water from an aquifer will reduce the hydrostatic pressure; subsequently, there would be an increase in the aquifer load, which causes compression of the aquifer. Besides, lowering of the pressure results in a small expansion and, in consequence, release of water. The storage coefficient can be used in order to express the water-yielding capacity of an aquifer.

A storage coefficient is calculated as the volume of water released from, or taken into storage of, an aquifer per unit surface area of aquifer over the unit change in the head normal to that surface. Specific storage can be calculated by dividing a given value of the storage coefficient by unit thickness of the aquifer. A vertical column of unit area extending through a confined aquifer is shown in Figure 7.5a. The storage coefficient, S, in this aquifer is equal to the volume of water released from the aquifer if the piezometric surface drops a unit distance. This coefficient expresses the volume of water per volume of aquifer, which is dimensionless. While the water is under pressure in a confined aquifer, the storage coefficient of an artesian aquifer is attributable to the compressibility of the aquifer skeleton and expansibility of the pore water (as it comes out of the aquifer to atmospheric pressure when the well is pumped). In an unconfined aquifer, the storage coefficient corresponds to the aquifer's specific yield (Figure 7.5b).

Jacob (1940) expressed the storage coefficient as follows:

$$S = \gamma_w b(\alpha + n\beta), \tag{7.12}$$

where S is the storage coefficient, γ_w is the specific weight of water (the specific weight of water in different temperatures is presented in Table 7.2), b is the thickness of the layer, α is the compressibility of the bed particles (acquired by the inverse of the soil particles' modulus of elasticity, $\alpha = 1/E_s$), β is the compressibility of water (inverse of water modulus of elasticity, $\beta = 1/E_w$), and n is the porosity of the medium. The modulus of elasticity of some kinds of soils are given in Table 7.3.

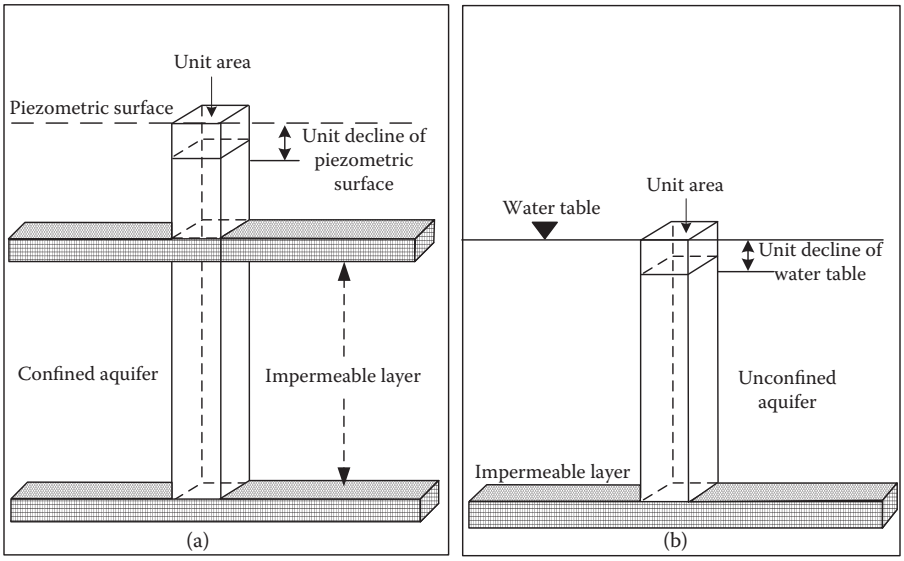

FIGURE 7.5 Schematic for defining storage coefficients of (a) confined and (b) unconfined aquifers.

TABLE 7.2
Density and Specific Weight of Water at Different Temperatures

Temperature (°C)	Density, ρ (kg/m³)	Specific Weight, γ_w (kN/m³)
0	999.9	9.806
5	1000	9.807
10	999.7	9.804
20	998.2	9.789
30	995.7	9.765
40	992.2	9.731
50	988.1	9.690
60	983.2	9.642
70	977.8	9.589
80	971.8	9.530
90	965.3	9.467
100	958.4	9.399

TABLE 7.3
Modulus of Elasticity of Some Soils

Soil Type	E_s(N/m²) × 10⁴
Clay	50–1470
Sand	980–7850
Gravel	9806–19,620
Rock	14,710–294,200

Because of very low compressibility of the water, expansibility of water adds a very small contribution to the value of the storage coefficient. The storage coefficient of an artesian aquifer ranges from 0.00005 to 0.005, while for a water table aquifer, $S = S_y = 0.05–0.30$. Because of this wide range, it can be concluded that there must be large pressure changes over extensive areas to create substantial water yields. Pumping tests of wells are usually applied in order to determine storage coefficients.

Example 7.5

Assume the modulus of elasticity of a clay soil is 4.788×10^7 and the porosity measured is equal to 0.30. Determine the corresponding storage coefficient of the layer if the thickness of the unsaturated layer is 7.6 m (assume the temperature is 20°C).

Solution:

First, the compressibility of water and the soil layer is calculated as

$$\beta = \frac{1}{E_w} = \frac{1}{2.1\times10^9} = 4.76\times10^{-10}\ \text{m}^2/\text{N}$$

$$\alpha = \frac{1}{E_s} = \frac{1}{4.788\times10^7} = 2.09\times10^{-8}\ \text{m}^2/\text{N}$$

$S = \gamma_w b\,(\alpha + n\beta) = 9789\ (\text{N/m}^3) \times 7.6\ \text{m} \times [2.09 \times 10^{-8}\ (\text{m}^2/\text{N}) + 0.30 \times 4.76 \times 10^{-10}\ (\text{m}^2/\text{N})] \Rightarrow S = 1.57 \times 10^{-3}$.

Example 7.6

An artesian aquifer with 30 m thickness has a porosity of 25% and bulk modulus of elasticity of 2×10^7 kg/cm^2. Estimate the storage coefficient of the aquifer. What fraction of this is attributable to the expansibility of water? Consider the bulk modulus of elasticity of water as 2.14×10^4 kg/cm^2.

Solution:

$$S = \gamma_w nb\left(\frac{1}{K_w} + \frac{1}{nK_s}\right) = 1000 \times 0.25 \times 30\left(\frac{1}{2.14 \times 10^8} + \frac{1}{0.25 \times 2 \times 10^7}\right)$$

$$= 7500(0.467 \times 10^{-8} + 20 \times 10^{-8}) = 1.54 \times 10^{-3}.$$

Storage coefficient due to the expansibility of water as a percentage of S above is equal to

$$\frac{7500 \times 0.467 \times 10^{-8}}{7500 \times 20.467 \times 10^{-8}} \times 100 = 2.28\%,$$

which is negligible.
Note: In less compressible formations like limestones for which $E_s \approx 2 \times 10^5$ kg/cm^2, $S = 5 \times 10^{-5}$, and the fractions of this attributable to water and aquifer skeleton are 70% and 30%, respectively, which makes water compressibility important to the aquifer storage coefficient.

It is notable that there is a difference between storage coefficient and specific storage, S_s. S is the storage coefficient per unit thickness of confined aquifer, while the specific storage of a saturated aquifer, S_s, is the volume of water that a unit volume of aquifer releases from storage due to a unit drop in hydraulic head.

De Wiest (1966) presented the specific storage coefficient as

$$S_s = \gamma_w [(1 - n)\,\alpha + n\beta)]. \tag{7.13}$$

Given the value of S_s, the storage coefficient for confined aquifers can be calculated as

$$S = b \cdot S_s. \tag{7.14}$$

In the case of unconfined aquifers, the concept of specific yield could be described as the difference between storage coefficient and specific storage times the aquifer thickness. Besides, for unconfined aquifers, the storage will be reduced by $\Delta b \cdot S$ or S_y; therefore, S and $S_s b$ are not the same:

$$S = S_y + b \cdot S_s. \tag{7.15}$$

Comparing Equation 7.14 with Equation 7.15, it can be concluded that specific yield is so small in confined aquifers that it can be considered negligible.

The specific yield (unconfined aquifers) and storage coefficient (confined aquifers) values of the aquifer have to be determined to estimate the changes in the groundwater storage due to fluctuation in the groundwater table (*GWT*) or piezometric surface (p_s). The following relationship can be used for estimation of groundwater storage (*GWS*) change:

$$\Delta GWS = A_{aq} \times \Delta GWT \text{ or } p_s \times S \text{ or } S_y, \tag{7.16}$$

where ΔGWS is change in groundwater storage, A_{aq} is involved area of the aquifer, ΔGWT or p_s is fluctuation in GWT or p_s, and S or S_y is storage coefficient (confined aquifer) or specific yield (unconfined aquifer).

Example 7.7

In a certain alluvial basin of 100 km^2, 90 Mm^3 of groundwater was pumped in a year and the groundwater table dropped by about 5 m during the year. Assuming no replenishment, estimate the specific yield of the aquifer. If the specific retention is 12%, what is the porosity of the soil?

Solution:

Change in groundwater storage is estimated using Equation 7.2.

$$\Delta GWS = A_{aq} \times GWT \times S_y$$

$$90 \times 10^6 = (100 \times 10^6) \times 5 \times S_y$$

$$S_y = 0.18.$$

Porosity $n = S_y + S_r = 0.18 + 0.12 = 0.30$, or 30%.

Example 7.8

The thickness of a confined aquifer is 78 m. The compressibility of granular medium and water are 3.65×10^{-9} and 4.76×10^{-10}. The porosity of this aquifer is measured to be equal to 25%. If there is a total head drop of 100 m and the area is 1200 km^2, calculate the storage coefficient and the volume of water that is released from the aquifer.

Solution:

First of all, specific storage must be calculated:

$$S_s = \rho g(\alpha + n\beta) = (998.2 \text{ kg/m}^3) \times (9.81 \text{ m/s}^2) \times [(4.76 \times 10^{-10} \text{ m}^2/\text{N}) + 0.25 \times (3.65 \times 10^{-9} \text{ m}^2/\text{N})]$$

$$S_s = 1.36 \times 10^{-5} \text{ (1/m)}.$$

Storage coefficient would be

$$S = b \cdot S_s = 78 \text{ (m)} \times 1.36 \times 10^{-5} \text{ (1/m)} = 1.06 \times 10^{-3}.$$

The volume of water withdrawn from the area due to the head drop in hydraulic head is

$$V = S \cdot \Delta h \cdot A = 1.36 \times 10^{-5} \times 100 \text{ (m)} \times 1200 \text{ (km}^2\text{)} \times 10^6 \text{ (m}^2/\text{km}^2\text{)} = 1.632 \times 10^6 \text{ m}^3.$$

7.6.5 Safe Yield of Aquifers

The yield of an aquifer, which is applied to the entire aquifer, is defined as the rate at which water can be withdrawn without depleting the supply to such an extreme where withdrawal of a rate higher than the safe yield is no longer economically practical. In other words, the limit to the quantity of water that can be regulatory withdrawn without depletion of aquifer storage reserve is considered as the safe yield.

7.7 GROUNDWATER BALANCE

For a specific area, the groundwater balance analysis is needed for the following purposes:

- To control whether all flow components in the system are quantitatively accounted for, and what elements have the greatest bearing
- To estimate one unknown component of the groundwater balance equation, providing the values of all other components are known with an acceptable accuracy
- To model the hydrological processes in the study area

Quantifying all individual inflows to or outflows from a groundwater system as well as changes in groundwater storage over a given time period is required in order to be able to estimate the groundwater balance of a region. The general form of water balance over a period of time is

$$I(t) - O(t) = \Delta S(t), \tag{7.17}$$

where $I(t)$ is the input to the system, $O(t)$ is the outflow from the system, and $\Delta S(t)$ is the change in storage of the system.

Before computing the groundwater balance of a system, the significant components must be identified. Then, the quantifying individual components are evaluated. Now, these quantified components can be expressed in the form of a water balance equation.

Considering the various inflow and outflow components in a given study area, the groundwater balance equation can be presented as

$$\Delta S = R_r + R_s + R_i + R_t + S_i + I_g - E_t + T_p - B_f - O_g, \tag{7.18}$$

where ΔS is change in groundwater storage, R_r is recharge from rainfall, R_s is recharge from canal seepage, R_i is recharge from field irrigation, R_t is recharge from tanks, S_i is influent seepage from rivers, I_g is inflow from other basins, E_t is evapotranspiration from groundwater, T_p is draft from groundwater, B_f is baseflow, the part of the groundwater that inflows to rivers, and O_g is outflow to other basins.

Different types of data are needed for developing the groundwater balance model. The main data needed are as follows:

- Rainfall data
- Land-use and cropping patterns data
- River stage and discharge data
- River cross sections
- Canals discharge and distributaries data and the possible seepage from canals
- Tank depths, capacity, area, and seepage data
- Water table data
- Groundwater draft (the number of each type of well operating in the area, their corresponding running hours each month, and their discharge)
- Aquifer parameters

Example 7.9

Consider an area whose recharge rate from irrigation is 220 mm/year while the rate of discharge through evapotranspiration is about 460 mm/year. There is 1000 mm rainfall annually over the region with a runoff coefficient of 0.43. The rate of outflow to the rivers is 160 mm/year and that to the other basins is 190 mm/year. Calculate the influent from seepage. Assume the groundwater

inflow and outflow remain unchanged; if the minimum baseflow is granted to be 260 mm/year, calculate the maximum rate of withdrawal that is allowed.

Solution:

a. When it rains, a portion of the precipitation, P, is evaporated, E_t, a portion flows over the land surface, O_f, and the rest recharges the groundwater, R_r. Therefore:

$$O_f = 0.43 \times P = 0.43 \times 1000 = 430 \text{ mm/year}$$

$$P + R_i = E_t + O_f + R_r \Rightarrow 1000 + 220 = 460 + 430 + R_r$$

$$R_r = 330 \text{ mm/year}$$

$$I_g + R_r = O_g + B_f \Rightarrow I_g = 190 + 160 - 330 = 20 \text{ mm/year.}$$

b. In this case, the outflow from the groundwater, baseflow, and the discharge from pumping are the outflows from the system and the inflow to groundwater, recharge from rainfall, and recharge from irrigation are the inflows:

$$I_g + R_i + R_r = O_g + B_f + Q_p \Rightarrow 20 + 220 + 330 = 190 + 260 + Q_p \Rightarrow Q_p = 120 \text{ mm/year.}$$

7.7.1 Water Balance in Confined Aquifers

In a short period (i.e., a day) in the water balance for the confined aquifer, the recharge and evaporation can be neglected. Thus, the daily water balance can be written as

$$w_{sc,i} = w_{sc,i-1} + w_{per} - w_{pc}, \tag{7.19a}$$

where $w_{sc,i}$ is the amount of water stored in the confined aquifer on day i, $w_{sc,i-1}$ is the amount of water stored in the confined aquifer on day $i - 1$, w_{per} is the amount of water percolating from the unconfined aquifer into the confined aquifer on day i, and w_{pc} is the amount of water removed from the confined aquifer by pumping on day i.

7.7.2 Water Balance in Unconfined Aquifers

Because of short-term input of recharge in unconfined aquifers and the interaction between surface and groundwater flow (baseflow), the water balance for unconfined aquifers can be expressed as

$$w_{su,i} = w_{su,i-1} + R_r - B_f - w_{sd} - w_{per} - w_{pu}, \tag{7.19b}$$

where $w_{su,i}$ is the amount of water stored in the unconfined aquifer on day i, $w_{su,i-1}$ is the amount of water stored in the unconfined aquifer on day $i - 1$, R_r is the amount of recharge entering the aquifer on day i, B_f is the baseflow to the main channel on day i, w_{sd} is the amount of water moving into the soil zone in response to water deficiencies on day i, w_{per} is the amount of water percolating from the unconfined aquifer into the confined aquifer on day i, and w_{pu} is the amount of water removed from the unconfined aquifer by pumping on day i.

7.7.3 Water Balance in Unsaturated Zone

Other terms of the unsaturated zone that must be taken into consideration are infiltration, capillary rise from the saturated zone, and lateral inflow. The outgoing terms consist of evapotranspiration, baseflow, and percolation to the saturated zone. The water balance set up for a given time interval is

$$\Delta S_{\text{unsat}} = w_{\text{inf}} + w_{\text{cap}} + I_{\text{g}} - w_{\text{per}} - E_{\text{t}} - B_{\text{f}}, \tag{7.19c}$$

where ΔS_{unsat} is storage change in unsaturated zone for the reflected time interval, w_{inf} is the amount of recharge entering the zone by infiltration, w_{cap} is the amount of recharge entering the zone by capillary rise, and the other terms are as described before.

7.8 GROUNDWATER MOVEMENT

The movement of groundwater, which is quite complex, will be discussed in this chapter in its simplest forms to present the principles involved. More complex groundwater models will be discussed in the next chapters.

7.8.1 Darcy's Law

A basic empirical relationship governing the movement of groundwater through a porous medium is Darcy's law (Bouwer 1978; De Wiest 1965; Freeze and Cherry 1979; Todd 1980). Suppose water flowing at a rate Q through a cylinder of cross-sectional area A, which is packed with sand and having piezometers at a distance L apart, as shown in Figure 7.6.

Darcy (1856) determined the velocity of water flowing through this cylinder as

$$v = -K \cdot \frac{h_1 - h_2}{\Delta l} = K \cdot i, \tag{7.20}$$

where v is superficial flow velocity (m/s), K is hydraulic conductivity (m/s), i is hydraulic gradient, $-\frac{dh}{dl}$ (m/m), h_1 is height of water in the upper piezometer (m), h_2 is height of water in the lower piezometer (m), and Δl is the distance between piezometers (m).

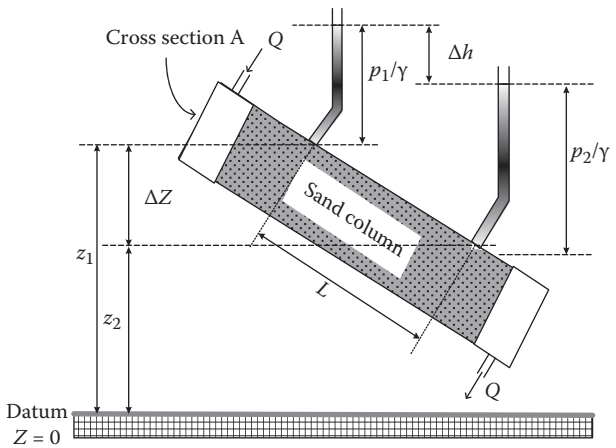

FIGURE 7.6 Pressure distribution and head loss in flow through a sand column.

The fact that the head loss is negative results in the minus sign in Darcy's law. The discharge through a cross-sectional area of an aquifer is calculated as

$$\frac{Q}{A} = K \cdot i \qquad Q = K \cdot i \cdot A \tag{7.21a}$$

or

$$q = K \cdot i \cdot b, \tag{7.21b}$$

where Q is hydraulic discharge, A is cross-sectional area, q is discharge in unit width of the aquifer, and b is thickness of the aquifer. It is worthwhile to mention that the application of Equation 7.26 is based on the assumption that the porous medium is homogeneous and is saturated with water. The application of Equation 7.21 is presented in Example 7.10.

Hydraulic conductivity, K, is affected by the porosity, n. In well-sorted sand or fractured rock formations, samples with a higher n generally also have a higher K. For instance, clay-rich soils usually have higher porosities than sandy or gravelly soils but lower hydraulic conductivities.

By the porosity of the medium and Darcy's law ($Q = A \cdot v$), the real velocity of water in a porous medium can be calculated. Considering the fact that the water moves through the pores in this medium, the value of average velocity (v) in the mentioned relation is not true and the equation should be modified to $Q = A_p \cdot v_{real}$, where A_p is the area of pores and v_{real} is the average velocity of water through the pores. Thus, there is a direct relation between the average velocity of water through the soil and the average velocity of water through the pores:

$$Q = A_p \cdot v_{real} \qquad v = \frac{A_p}{A} \cdot v_{real} \qquad v = n \cdot v_{real}. \tag{7.22}$$

The above relation indicates that the velocity in Darcy's law has a lower value than the real velocity of water through the soil. The pure velocity of groundwater is acquired from dividing the superficial flow velocity by the porosity of the porous medium.

Example 7.10

Suppose a field sample area of an unconfined aquifer is packed in a test cylinder, while the length and the diameter of the cylinder are 100 cm and 8 cm, respectively. The period of the test is about 5 min with a constant head difference of 22.4 cm. As a result, 65.2 cm^3 of water is collected at the outlet. Determine the hydraulic conductivity of the aquifer sample.

Solution:

Cross section:

$A = \pi D^2/4 = \pi(0.08\ m)^2/4 = 0.00502\ m^2$.

Hydraulic gradient:

$$\frac{dh}{dl} = (-22.4\ cm)/(100\ cm) = -0.224.$$

Average flow rate:

$$Q = (65.2\ \text{cm}^3/5\ \text{min}) = 13.04\ \text{cm}^3/\text{min} = 0.0188\ \text{m}^2/\text{day}.$$

Hydraulic conductivity:

$$K = -Q/\left(A \cdot \mathrm{d}h/\mathrm{d}l\right) = \frac{-\left(0.0188\ \text{m}^3/\text{day}\right)}{\left(0.00502\ \text{m}^2\right)(-0.224)} = 16.72\ \text{m/day}.$$

Example 7.11

Taking the same sample as in Example 7.10, the sample has a median grain size of 0.037 cm and a porosity of 0.32, determine the Darcy velocity and average interstitial velocity, if pure water at 20°C is to be used.

Solution:

Darcy velocity:

$$v = -k(\mathrm{d}h/\mathrm{d}l) = -(16.72\ \text{m/day}) \times (-0.224) = 3.75\ \text{m/day}.$$

Average linear velocity:

$$v_a = Q/(\eta A) = v/A = 12.5\ \text{m/day}$$

7.8.2 Hydraulic Head

In a groundwater system in the saturated zone, the hydraulic head at a point (Figure 7.7) can be presented as

$$h = z + p/\rho g, \tag{7.23}$$

where z is the elevation head above a datum plane, p is the fluid pressure at the point applied by the column of water above point, ρ is the water density, and g is the gravity constant. ρg expresses the specific weight of water, γ.

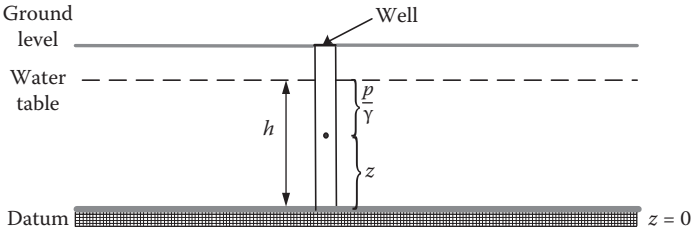

FIGURE 7.7 Illustration of hydraulic head.

In a groundwater context, the hydraulic head and fluid potential are equivalent; however, the hydraulic head is most commonly used. Water can flow from a region of lower pressure to a region of higher pressure if the total head at the starting point is greater than that at the ending point. In the field of petroleum and natural gas engineering, pressure is generally used instead of head because pressures at great depths are normally so great and elevation heads are often insignificant.

7.8.3 Hydraulic Conductivity

The hydraulic conductivity is expressed in two different parts considering the saturation or unsaturation status of the media.

7.8.3.1 Hydraulic Conductivity in Saturated Media

Hydraulic conductivity, K, involves the properties for both medium and fluid. It can be used for estimating water transmissivity in a porous medium. Hydraulic conductivity of a saturated medium is calculated as

$$K_s = k\frac{\gamma}{\mu}, \tag{7.24}$$

where K_s is saturated hydraulic conductivity (cm/s), $k = Cd^2$ is specific or intrinsic permeability, C is constant of proportionality, d is grain size of porous medium (m), γ is specific weight of water (kN/m^3), and μ is dynamic viscosity of water (Ns/m^2).

The physical meaning of hydraulic conductivity is expressed as "The volume of liquid flowing perpendicular to a unit area of porous medium per unit time under the influence of a hydraulic gradient of unity." In earlier literature, this phenomenon was described as field coefficient of permeability with units of gallons per day per square feet. However, this name and definition are now rarely used. Hydraulic conductivities of several lithologies are listed in Table 7.4. They can also be acquired from Table 7.5.

TABLE 7.4
Important Physical Properties of Soil and Rock

Unconsolidated Deposits	Hydraulic Conductivity (cm/s)	Compressibility, α (m^2/N or Pa^{-1})
Clay	10^{-10} to 10^{-7}	10^{-6} to 10^{-8}
Silt	10^{-7} to 10^{-3}	No data
Sand	10^{-4} to 1.0	10^{-7} to 10^{-9}
Gravel	10^{-2} to 10^{2}	10^{-8} to 10^{-10}
Sandstone	10^{-8} to 10^{-4}	10^{-11} to 10^{-10}
Limestone, dolomite	10^{-7} to 10^{-4}	$<10^{-10}$
Fractured basalt	10^{-5} to 1.0	10^{-8} to 10^{-10}
Karst limestone	10^{-4} to 10.0	Not applicable
Shale	10^{-11} to 10^{-7}	10^{-7} to 10^{-8}
Fractured crystalline rock	10^{-7} to 10^{-2}	10.0^{-10}
Dense crystalline rock	10^{-12} to 10^{-8}	10^{-9} to 10^{-11}

TABLE 7.5
Range of Values of Hydraulic Conductivity and Permeability

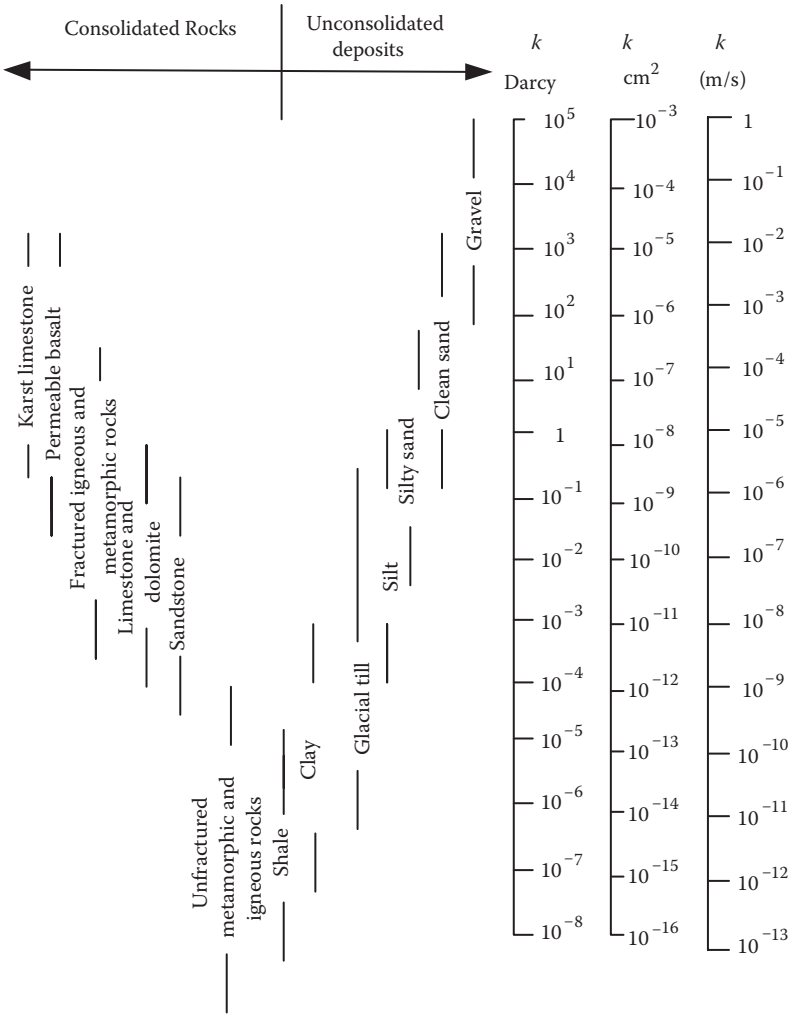

Example 7.12

Calculate the intrinsic permeability of the sample soil in the previous example (K = 16.72 m/day, water temperature = 20°C).

Solution:

Pure water at 20°C:

$$\mu = 1.005 \times 10^{-3}\ \text{Ns/m}^2 \text{ and } \rho = 998.2\ \text{kg/m}^3$$

$$k = \frac{K\mu}{\rho g} = \frac{(16.72\ \text{m/day})\left(1.005\times10^{-3}\ \text{Ns/m}^2\right)}{\left(998.2\ \text{kg/m}^3\right)\left(9.81\ \text{m/s}^2\right)}$$
$$= \frac{\left(16.72\dfrac{\text{m}}{86{,}400\ \text{s}}\right)\left(1.005\times10^{-3}\ \dfrac{\text{kg}\cdot\text{m/s}}{\text{m}^2}\right)}{\left(998.2\ \text{kg/m}^3\right)\left(9.81\ \text{m/s}^2\right)} = 1.9854\times10^{-3}\ \text{m}^2 = 19.854\ (\mu\text{m})^2.$$

7.9 HOMOGENEOUS AND ISOTROPIC SYSTEMS

A formation with uniform hydraulic conductivity at all points in the aquifer is considered as a homogeneous formation. In contrast, if the hydraulic conductivity varies with location, the formation is called heterogeneous. There are different ways that hydraulic conductivity changes in heterogeneous formations, and these are shown in Figure 7.8.

A geologic formation is considered as an isotropic formation, if at a given point the hydraulic conductivity is not changed in all directions. In anisotropic formations, the hydraulic conductivity varies with direction. The system illustrated in Figure 7.9a has the same consolidation in different directions and depicts an isotropic formation. In Figure 7.9b, the system has further consolidation in the vertical direction. This system shows an anisotropic formation.

It is considered as an isotropic flow medium if the coefficient of permeability of the soil is independent of the direction of the velocity. Moreover, the soil is said to be homogeneous and isotropic if the soil has the same coefficient of permeability at all points within the region of flow. On the other hand, the soil is considered homogeneous and anisotropic if the coefficient of permeability is dependent on the direction of the velocity and if this directional dependence is the same at all points of the flow region. The coefficient of permeability of a homogeneous and anisotropic soil is dependent on the direction of the velocity but independent of the space coordinates.

Most soils are anisotropic to some extent. Often, thin alternating layers are found in sedimentary soils. Generally, in homogeneous natural deposits, the horizontal coefficient of permeability is greater than the vertical one (Snow 1969).

Although homogeneous and isotropic aquifers do not exist, for mathematical calculations of the storage and flow of groundwater, the idealized aquifers are assumed to be homogeneous and isotropic. It should be mentioned that these assumptions give acceptable quantitative approximations, especially in large-scale studies.

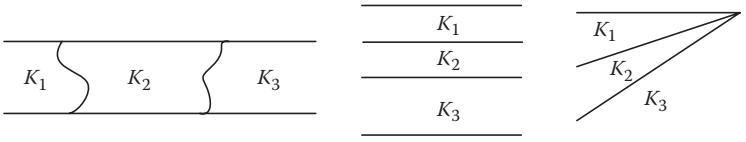

FIGURE 7.8 Hydraulic conductivity formations in three types of heterogeneous systems.

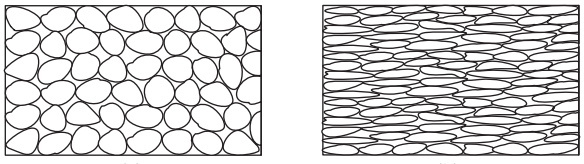

FIGURE 7.9 (a) Isotropic and (b) anisotropic sediment deposits.

7.9.1 Hydraulic Conductivity in Multilayer Structures

In geology, a structure is called a *multilayer structure* if it has various characteristics (soil type, permeability, compressibility, etc.) in different depths. This type of structure has different hydraulic conductivity values in vertical and horizontal directions; these values can be obtained as follows.

a. Average horizontal hydraulic conductivity: In this case, all layers have the same hydraulic gradient and total discharge is the summation of the discharge of all the layers.

$$i = i_1 = i_2 = ... = i_n$$

$$Q = Q_1 + Q_2 + ... + Q_n$$

$$K_H iA = K_1 i_1 A_1 + K_2 i_2 A_2 + ... + K_n i_n A_n$$

$$K_H ib = K_1 i_1 b_1 + K_2 i_2 b_2 + ... + K_n i_n b_n$$

$$K_H = \frac{\sum_{i=1}^{n} K_i b_i}{b}, \tag{7.25}$$

where K_H is the horizontal hydraulic conductivity, i_i is the hydraulic gradient of the layer, Q_i is the discharge of the layer, A_i is the area of the layer, and b_i is the thickness of the layer.

b. Average vertical hydraulic conductivity: The rate of discharge in all layers is equal in this case, but the summation of the head losses of all layers will result in the total head:

$$dh = dh_1 + dh_2 + ... + dh_n$$

$$Q = Q_1 = Q_2 = ... = Q_n$$

$$\frac{b}{K} Q = \frac{b_1}{K_1} Q_1 + \frac{b_2}{K_2} Q_2 + ... + \frac{b_n}{K_n} Q_n$$

$$K_V = \frac{b}{\sum_{i=1}^{n} \frac{b_i}{K_i}}. \tag{7.26}$$

The horizontal hydraulic conductivity in alluvium is usually greater than that in the vertical direction:

$$K_H > K_V. \tag{7.27}$$

The equivalent hydraulic conductivity, K, which can be used with Darcy's law, is

$$K = \sqrt{K_H \times K_V}\ . \tag{7.28}$$

Example 7.13

Three horizontal formations with thickness of 10, 20, and 15 m, respectively, exist in a hydrogeological system. Suppose the hydraulic conductivities of the formations are 20, 10, and 30 cm/day, respectively. Determine the equivalent horizontal and vertical hydraulic conductivities. Also, if the flow in the uppermost layer is at an angle of 40° away from the horizontal direction relative to the boundary, calculate flow directions in other formations.

Solution:

$$d_1 = 10 \text{ m}, \; d_2 = 20 \text{ m}, \; d_3 = 15 \text{ m}$$

$$K_1 = 20 \text{ cm/day}, \; K_2 = 10 \text{ cm/day}, \; K_3 = 30 \text{ cm/day}$$

$$K_{\text{H}} = \frac{\sum_{i=1}^{3} K_i \cdot d_i}{\sum_{i=1}^{3} d_i} = \frac{10\times 20 + 20\times 10 + 15\times 30}{10+20+15} = \frac{850}{45} = 18.9 \text{ (cm/day)}.$$

$$K_{\text{H}} = \frac{\sum_{i=1}^{3} d_i}{\sum_{i=1}^{3} \frac{d_i}{K_i}} = \frac{10+20+15}{10/20+20/10+15/30} = \frac{45}{3} = 15 \text{ (cm/day)}.$$

Angle of incidence: α_1. Angle of refraction: α_2.

$$\frac{k_i}{k_{\text{r}}} = \frac{\tan\alpha_i}{\tan\alpha_{\text{r}}} \qquad \alpha_{\text{i}} = \tan^{-1}\left(\frac{K_i}{K_{\text{r}}} \cdot \tan\alpha_{\text{r}}\right).$$

The angle of refraction in one layer constitutes the angle of incidence to the next one:

$$\frac{10}{20} = \frac{\tan\alpha_i}{\tan(40)} \qquad \alpha_i = \tan^{-1}\left(\frac{10}{20}\cdot\tan(40)\right) = 22.8°,$$

and considering the above relationship, the direction of all formations are

$$\alpha_1 = 40°, \quad \alpha_2 = 22.8°, \quad \alpha_3 = 51.5°.$$

7.10 TRANSMISSIVITY

The amount of water that moves horizontally through a unit width of a saturated aquifer due to a unit change in gradient is called the transmissivity.

$$T = K \cdot b, \tag{7.29}$$

where K is the hydraulic conductivity and b is the depth of the saturated aquifer.

The dimensionality of this term is the result of the definition of transmissivity as the flow rate of water passing through a unit width of aquifer perpendicular to flow direction over the entire thickness of the aquifer (Figure 7.10).

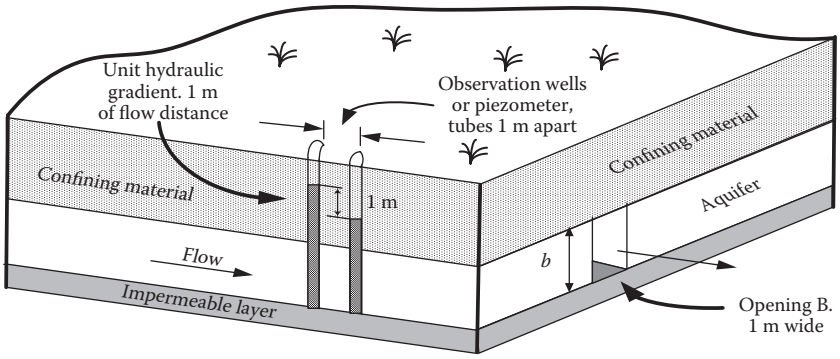

FIGURE 7.10 Schematic for defining transmissivity. (Adapted from Ferris, J.G. et al., Theory of Aquifer Tests. Water Supply Paper 1536-E. U.S. Geological Survey, 1962.)

Transmissivity is usually reported in units of square meters per day or square feet per day. The total rate of flow (Q) through any area (A) of the aquifer perpendicular to the flow direction under the gradient (i) is then calculated as

$$Q = W \cdot T \cdot i, \tag{7.30}$$

where W is the width of the aquifer, i is the hydraulic gradient, T is transmissivity (m^2/s), and Q is the discharge rate (m^3/s).

In multilayer aquifer cases, the transmissivity for j layers is estimated as follows:

$$T = \sum_{j=1}^{n} T_j. \tag{7.31}$$

Transmissivities greater than 0.015 m^2/s represent good aquifers for water well exploitation. The transmissivity in an unconfined aquifer is not as well defined as in a confined aquifer, but still Equation 7.31 is practical for an unconfined aquifer. However, in such a case, b is considered as the saturated thickness of the aquifer or the height of the water table above the top of the underlying aquitard that bounds the aquifer.

7.11 DUPUIT–FORCHHEIMER THEORY OF FREE-SURFACE FLOW

In unconfined systems that are bounded by a free surface, the movement of groundwater is usually treated as a steady-state flow problem, and a simple Dupuit–Forchheimer analysis is often used. The basic assumption of the Dupuit–Forchheimer analysis is that the streamlines are virtually horizontal (potential lines are vertical) and the slope of the hydraulic grade line is the same as the free-surface slope (Bouwer 1978; De Wiest 1965; Hansch and Leo 1979; Todd 1980). Although it is a model for unconfined aquifers, with suitable assumptions, it can be extended to confined aquifers.

Example 7.14

Suggest a relationship for calculating the highest level of the water table, if the irrigation water is being infiltrated with uniform intensity of f into the ground in x direction (Figure 7.11).

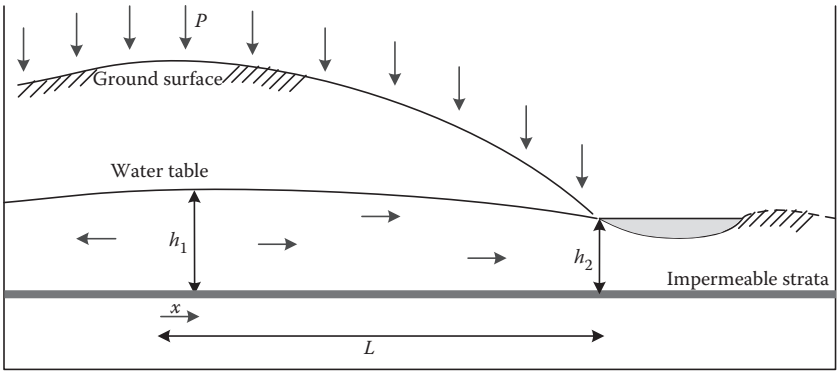

FIGURE 7.11 Definition sketch for Example 7.14.

Solution:

According to the Dupuit–Forchheimer assumptions and Darcy's law, the velocity of water in x direction at the highest point of the water table is

$$v_x = -K\frac{dh}{dx}.$$

$\frac{dh}{dx}$ shows the slope of the water table.

The rate of discharge in unit width at distance x is

$$q_x = -K \cdot h \cdot \frac{dh}{dx}.$$

On the other hand, the rate of discharge due to the infiltration, f, is

$$f = -K \cdot h \cdot \frac{dh}{dx} \qquad -f \cdot dx = K \cdot h \cdot dh.$$

Integrating the above equation from the point of peak (P) to the stream flow,

$$K \cdot \left(h_1^2 - h_2^2\right) = PL^2.$$

Thus,

$$h_1 = \sqrt{h_2^2 + \frac{PL^2}{K}}.$$

Example 7.15

During dry-weather (baseflow) periods, when all water in the stream is derived from groundwater discharge, the following are the results of some observations:

Average daily flow at station A (upstream): 2.183 m^3/s
Average daily flow at station B (downstream): 2.363 m^3/s

Distance (x) between stations A and B: 6500 m
Average thickness of aquifer (b): 65 m
Average slope of the water table (dh/dl) determined from measurements in the observation wells: 1/1500 (m/m)
Calculate the transmissivity and the hydraulic conductivity of this aquifer.

Solution:

Increase in flow due to groundwater discharge:

$$\Delta q = q_u - q_d = 2.363 - 2.183 = 0.180 \text{ m}^3/\text{s}.$$

Total daily groundwater discharge to stream:

$$\Delta q = 0.180 \text{ m}^3/\text{s} = 15{,}552 \text{ m}^3/\text{day}.$$

Discharge from half of aquifer (one side of the stream):

$$Q = 7776 \text{ m}^3/\text{day}.$$

Therefore:

$$Q = TW \cdot \frac{dh}{dl}$$

$$T = \frac{Q}{W} \times \frac{dl}{dh} = \frac{7776 \text{ m}^3/\text{day}}{6500 \text{ m}} \times \frac{1500 \text{ m}}{1 \text{ m}} = 1794.5 \text{ m}^2/\text{day}$$

$$T = 1794.5 \text{ m}^2/\text{day} = 0.0021 \text{ m}^2/\text{s}$$

$$K = \frac{T}{b} = \frac{0.032 \text{ m}^2/\text{s}}{65 \text{ m}} = 0.052 \text{ cm/s}.$$

7.12 FLOWNETS

The simplest procedure for solving flow equations is a graphical approach. In this approach, flow within a domain is described using a unique set of streamlines and equipotential lines. The streamlines (or flow lines) indicate the path through which water moves in the aquifer. The equipotential lines represent the contours of equal head in the aquifer intersecting the streamlines. In this section, development of flownets in isotropic and homogeneous media as well as heterogeneous and anisotropic media is discussed.

7.12.1 Isotropic and Homogeneous Media

For steady-state conditions, the two-dimensional groundwater flow equation for isotropic and homogeneous media is described as follows:

$$\frac{\partial^2 h}{\partial x^2} + \frac{\partial^2 h}{\partial y^2} = 0. \tag{7.32}$$

A flownet that depicts a selected number of flow lines and equipotential lines in the flow system is a graphical solution to the above equation. A flownet can provide useful information about distribution of heads, discharges, areas of high (or low) velocities, and the general flow pattern. The flow channel between adjacent streamlines is called a streamtube. Equipotential lines express the hydraulic head in the domain. The equipotential lines are perpendicular to the streamtubes (Figure 7.12). The discharge in the streamtube per unit width perpendicular to the plane of the grid shown in Figure 7.12 is

$$\Delta Q = \alpha_2 - \alpha_1 = \Delta\alpha \tag{7.33}$$

$$q = \Delta Q/\Delta W = \Delta\alpha/\Delta W. \tag{7.34}$$

Application of Darcy's law results in

$$q = -\frac{K\Delta h}{\Delta L} = \frac{\beta_2 - \beta_1}{\Delta L} = \frac{\Delta\beta}{\Delta L}. \tag{7.35}$$

Considering the continuity also results in

$$q = \frac{\Delta\alpha}{\Delta W} = \frac{\Delta\beta}{\Delta L}. \tag{7.36}$$

In the development of flownets, the first step is to draw the two-dimensional flow domain considering all boundary conditions, wells, etc. It may be necessary to employ a trial-and-error procedure to sketch a flownet.

If there is no inflow to/outflow from an isotropic and homogeneous region in the internal part of the net, the groundwater flows between adjacent pairs of flow lines would be the same. In addition, the hydraulic-head drop between two adjacent equipotential lines is the same. Figure 7.13 shows a

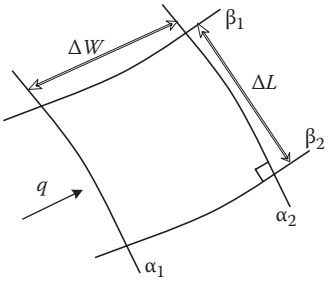

FIGURE 7.12 Flownet element of two-dimensional flow.

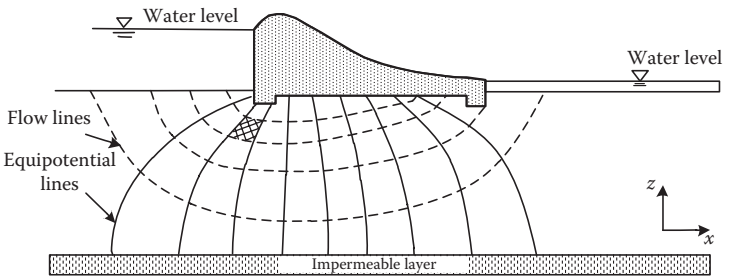

FIGURE 7.13 Flownet showing seepage under a dam.

flownet depicting seepage under a dam in an x–z plane. In Figure 7.13, the streamlines are shown by solid lines and the equipotential lines are presented by dashed lines. Due to the difference of the hydraulic head in different sides of the dam, the flow occurs between upstream and downstream pools. The flownet is a theoretical representation of flow beneath the dam. The bottom surface of the reservoir is considered as an equipotential line, which has a constant-head boundary across which the flow is directed downward.

The base of the dam corresponds to a flow line as a boundary condition. Due to constant head of downstream pool, it has been considered as a constant-head boundary or another equipotential line. Because the system is isotropic and homogeneous, flow lines and equipotential lines intersect to form curvilinear squares.

Some strategies for sketching a flownet suggested by Bennett (1962) are as follows:

1. Use limited, maximum of five, flow channels in a first attempt at sketching.
2. Consider the generality of the flownet and adjust details only when the entire net is approximately correct.
3. Develop the flownet considering that most of the parts of a flownet include straight and parallel lines resulting in uniformly sized true squares.
4. In symmetrical flow systems, construction of a section of the net is necessary and the other parts are images of developed section.
5. Change the size of the rectangles gradually; all transitions are smooth, and where the paths are curved they are of elliptical or parabolic shape.

There are some useful rules that can be used in the development of complex flow systems. Some of these rules are as follows:

1. A no-flow boundary is a streamline.
2. If there is no recharge or evapotranspiration, the water table is a streamline. When there is recharge, the water table is neither a flow line nor an equipotential line.
3. Streamlines end at extraction wells, drains, and gaining streams and they start from injection wells and losing streams.
4. Streamlines divide a flow system into two symmetric parts.
5. Streamlines begin and end at the water table in areas of groundwater recharge and discharge, respectively.

Using Darcy's equation for a flow channel in the two-dimensional space,

$$\Delta Q = T\Delta h \frac{\Delta W}{\Delta L}, \tag{7.37}$$

where ΔQ is the flow through a streamtube, T is the transmissivity of the aquifer, Δh is the hydraulic-head drop between two equipotential lines, ΔW is the distance between two streamlines, and ΔL is the distance between two equipotential lines (Figure 7.12). In sketching a flownet, we always try to provide a mesh of squares. Therefore, ΔW is equal to ΔL and $\Delta W/\Delta L$ is equal to 1. If there are a total number of n_f flow channels and n_d hydraulic-head drops (i.e., equipotential lines), Darcy's equation is written as

$$Q = \frac{n_f}{n_d} T\Delta H \tag{7.38}$$

or

$$q = \frac{n_f}{n_d} K \Delta H, \tag{7.39}$$

where Q is the total flow rate and is equal to $n_f \Delta Q$ and ΔH is the total hydraulic head drop and is equal to $n_d \Delta h$.

Example 7.16

The groundwater is withdrawn from an aquifer at a rate of 15,000 m^3/day. Due to this withdrawal, the hydraulic head drops at five equipotential lines. After sketching the flownet for this formation, it is determined that the groundwater is flowing through 10 tubes. Assuming the transmissivity is 650 m^2/day, determine the total hydraulic head drop.

Solution:

$$\Delta H = \frac{n_d \cdot Q}{T \cdot n_f} = \frac{(5)\left(15{,}000\ \text{m}^3/\text{day}\right)}{\left(650\ \text{m}^2/\text{day}\right)(10)} = 11.53\ \text{m}.$$

Example 7.17

Estimate the discharge under the dam shown in Figure 7.14 using the flownet method. $K = 3 \times 10^{-2}$ cm/s.

Solution:

The flownet construction is started with a vertical equipotential line, directly below the dam. The upper streamline is located right in the vicinity of the dam. Since it is assumed that the Darcy velocity will decrease with depth, the spacing between the streamlines is increased with depth. The equipotential line immediately adjacent to the vertical one is sketched next. In drawing these equipotential lines, the condition of orthogonality as well as the condition that each element forms a square must be taken into account. The process of drawing streamlines and equipotential lines is continued until we get to the vicinity of the terminal point. Since sketching a flownet is based on trial and error, some readjustments of both the streamlines and the equipotential lines are usually required.

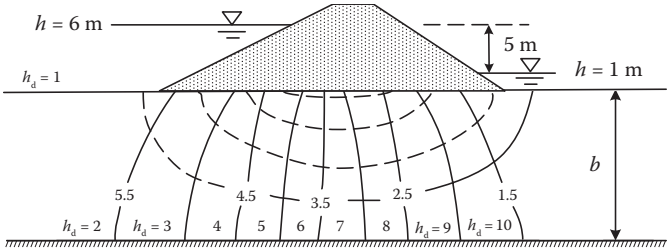

FIGURE 7.14 Flownet of seepage under a dam.

From Figure 7.14, the number of streamtubes is 5 and the number of equipotential drops is 10. Thus, the discharge per meter of sheet pile length is

$$Q = K\frac{n_f}{n_d}\Delta H = \frac{5}{10}\times 3\times 10^{-4}\ (\text{m/day})\times 5\ (\text{m}) = 7.5\times 10^{-4}\ \text{m}^2/\text{s}.$$

7.12.2 Heterogeneous Media

In heterogeneous media, the equipotential lines and the flow lines do not necessarily intersect to form squares. A constant discharge in a streamtube for two adjacent media with differing hydraulic conductivity is estimated as

$$\Delta Q = T_1\Delta h_1\frac{\Delta W_1}{\Delta L_1} = T_2\Delta h_2\frac{\Delta W_2}{\Delta L_2}. \tag{7.40}$$

If $\Delta h_1 = \Delta h_2$:

$$\frac{T_1}{T_2} = \frac{\Delta L_1\Delta W_2}{\Delta L_2\Delta W_1}. \tag{7.41}$$

Example 7.18

Calculate the flow rate and the length ΔL_2 for the heterogeneous aquifer shown in Figure 7.15.

Assume that $\Delta W_1 = \Delta W_2 = 8$ m and $\Delta L_1 = 10$ m and that the thickness of the aquifer is 150 m.

Solution:

$$\Delta Q = T_1\Delta h_1\frac{\Delta W_1}{\Delta L_1} = (85\ \text{m/day})(150\ \text{m})(1\ \text{m})\frac{(8\ \text{m})}{(10\ \text{m})} = 10{,}200\ \text{m}^3/\text{day}.$$

The segment length ΔL_2 is

$$\Delta L_2 = \frac{T_2}{T_1}\Delta L_1 = \frac{(100\ \text{m/day})(150\ \text{m})}{(85\ \text{m})(150\ \text{m})}(10\ \text{m}) = (11.76\ \text{m}).$$

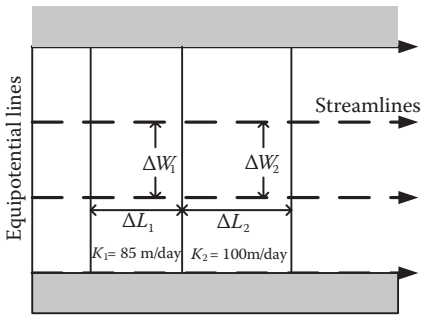

FIGURE 7.15 Definition sketch for Example 7.18.

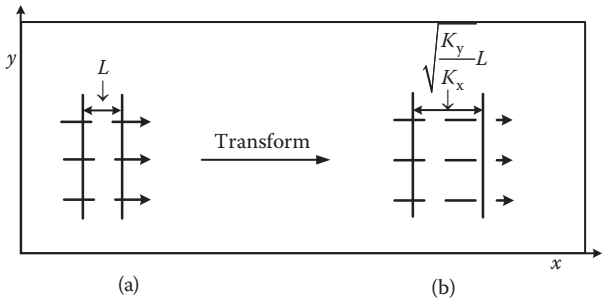

FIGURE 7.16 Flownet in anisotropic media. (a) Original cross section. (b) Transformed cross section.

7.12.3 Anisotropic Media

In anisotropic media, there are no right angles at the interception of streamlines and equipotential lines except when flow is aligned with one of the principal directions of hydraulic conductivity or transitivity. Therefore, in an anisotropy medium, the flownet may be sketched by transforming the flow field. This procedure can be summarized as follows (Schwartz and Zhang 2003):

1. Determine the direction of maximum transmissivity in the *x* direction and the direction of minimum transmissivity in the *y* direction.

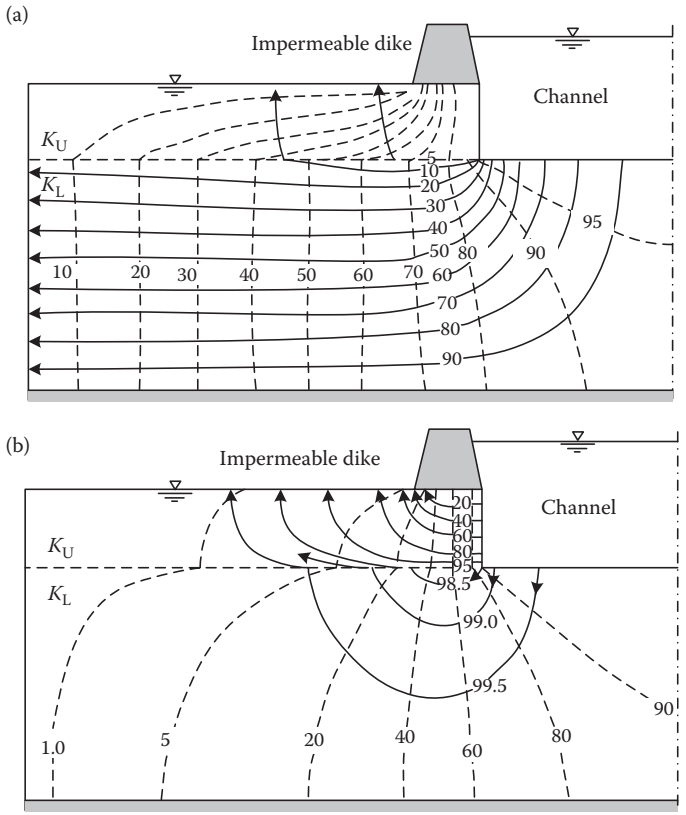

FIGURE 7.17 Flownets for seepage through two different anisotropic two-layer systems. (a) K_U/K_L = 1/50, (b) K_U/K_L = 1/50. (From Todd and Mays, *Ground Hydrology*, Hoboken, Wiley, 2005. With permission.)

2. Multiply the dimension in the x direction by a factor of $(K_y/K_x)^{1/2}$. Sketch the flownet in the transformed flow domain.
3. Project the flownet back to the original dimension by dividing the x coordinates of the flownet by a factor of $(K_y/K_x)^{1/2}$.

Figure 7.16 shows the flownets in original and transformed coordinate systems. As depicted in this figure, in the transformed system, the flownet consists of squares, while in the original system, it consists of rectangles. Flownets for seepage from one side of a channel through two different anisotropic two-layer systems are depicted in Figure 7.17.

7.13 WELLS

The objective of well drilling in helping groundwater exploration is to discover aquifers in different hydrogeological conditions and to determine hydraulic parameters. It leads to decline in the water level that limits the yield of the basin. During water pumping, water is removed from the aquifer surrounding the well and the piezometric surface decreases. The groundwater within the influence of the pump flows toward the well from every direction, instead of moving toward the natural discharge area. Drawdown is defined as the distance by which the piezometric surface is lowered. Thus, one of the goals of groundwater resource study is to predict hydraulic-head drawdowns in aquifers under proposed pumping schemes.

The pumping well creates an artificial discharge area by drawing down (lowering) the water table around the well. The cone of depression is attributed to a conical-shaped depression of the water table around a pumping well caused by the withdrawal of water, a valley in the water table. The initial discharge derived from casing storage and aquifer storage immediately surrounding the well when water is pumped from a well is given in Figure 7.18.

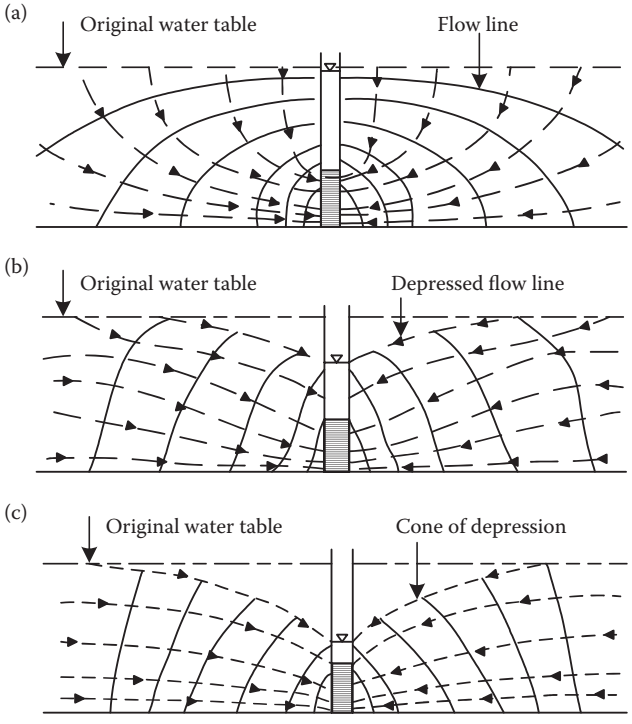

FIGURE 7.18 Development of flow distribution about a discharging well in an unconfined aquifer: (a) initial stage, (b) intermediate stage, and (c) steady-state stage. (From U.S. Bureau of Reclamation, *Groundwater Manual*, U.S. Gov. Printing Office, Denver, CO, 1981. With permission.)

Figure 7.18a shows the initial stage in pumping an unconfined aquifer: water begins to flow toward the well screen. Figure 7.18b depicts the intermediate stage in pumping an unconfined aquifer: although dewatering of the aquifer materials near the well bore continues, the radial component of flow becomes more pronounced. The profile of the cone of depression is established in the almost steady-state stage in pumping an unconfined aquifer. Figure 7.18c illustrates the established radial flow pattern, which originated near the outer edge of the area of influence.

By continuous pumping, more water is derived from the aquifer storage at greater distances from the bore of the well, resulting in the following:

1. The cone of depression is developed.
2. The influential radius of the well increases because of the expansion of the cone of depression.
3. The increased drawdown at any point is predictable due to the increase in the depth of the cone in order to supply the additional head required to move the water from greater distance.
4. The expansion of the cone will be slower with time, due to availability of an increasing volume of stored water with horizontal expansion of the cone.

Figure 7.19 shows the expansion of the cone of depression during equal intervals of time. It is determined by the calculations of the volume of each cone, that cone 2 has more volume than cone 1. It is because of a constant pumping rate, the same volume of water is discharged from the well. Thus, for a homogeneous aquifer exploited by a well at a constant pumping rate, the increase in the volume of the cone of depression will be constant over time. The conical water table is steepest where it meets the well. Farther away from the well, the surface is flatter and beyond a certain distance, also known as the radius of influence, the surface of the cone is almost as flat as the original water table.

After cone stabilization (when the cone deepened or expanded enough), the changes in cone shape during short intervals of pumping are barely visible and rate of the water table or piezometric surface slump highly decreases. Observers are often misled to conclude that the cone will not expand or deepen as pumping continues. In fact, the cone of depression continues to expand, until the flow in the aquifer with source of surface water, vertical recharge from precipitation is intercepted to equal the pumping rate while the leakage occurs through overlying or underlying formations. While pumping continues, when the cone stops expanding and there is no further drawdown, the equilibrium condition in groundwater is satisfied. It may occur within a few hours after pumping begins, or it never occurs even though the pumping period is prolonged for years. A radial flow equation, which will be discussed, relates the well discharges and the drawdown in an aquifer to each other.

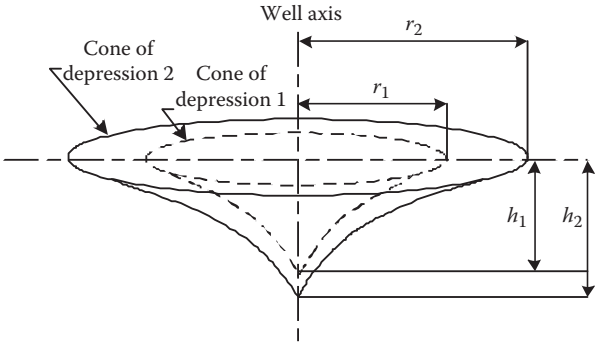

FIGURE 7.19 Changes in radius from r_1 to r_2 and depth of cone of depression from h_1 to h_2, respectively.

7.13.1 Steady Flow into a Well

Steady-state groundwater problems are easy to deal with. The steady-state radial flow into a well under both confined and unconfined aquifer conditions are discussed in this chapter.

7.13.1.1 Confined Flow

As was mentioned before, drawdown of the potentiometric surface occurs due to water discharge from a completely confined aquifer by water pumping. Water is released from storage, and fluid pressure decreases by expulsion of water due to aquifer compaction under increased effective stress. Figure 7.20 shows a confined aquifer with steady-state radial flow to the fully penetrating well being pumped. The aquifer discharge at any radial distance r from the pumped well in any direction is equal. In addition, by increasing the radial distance from the well, the area of discharging increases. Thus, by increasing the distance of the given point from the well, the flow velocity decreases, and the groundwater surface is flatter and becomes closer to the static piezometric surface.

Based on Figure 7.20, for a homogeneous, isotropic aquifer, the well discharge at any radial distance r from the pumped well is estimated as follows:

$$\sum_{CS} \rho V \cdot dA = Q = 2\pi K r b \frac{dh}{dr}. \tag{7.42}$$

Considering the boundary conditions of $h = h_1$, at $r = r_1$, and $h = h_2$, at $r = r_2$, Equation 7.42 can be rewritten as follows:

$$\int_{h_1}^{h_2} dh = \frac{Q}{2\pi K b} \int_{r_1}^{r_2} \frac{dr}{r} \tag{7.43}$$

$$h_2 - h_1 = \frac{Q}{2\pi K b} \ln \frac{r_2}{r_1}. \tag{7.44}$$

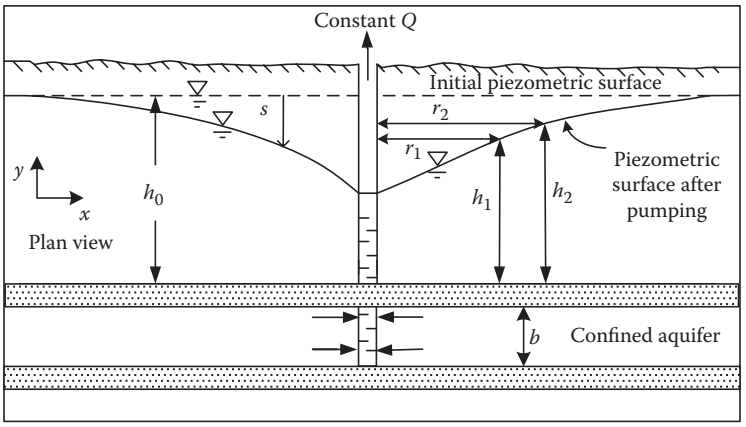

FIGURE 7.20 Characteristics of well hydraulics for a confined aquifer.

Solving Equation 7.44 for Q gives

$$Q = 2\pi Kb\left[\frac{h_2 - h_1}{\ln\left(r_2/r_1\right)}\right]. \tag{7.45}$$

Generally, Equation 7.45 at any radial distance r from the pumped well with a head of h can be written as

$$Q = 2\pi Kb\left[\frac{h - h_1}{\ln\left(r/r_1\right)}\right]. \tag{7.46}$$

Equation 7.46 is called the equilibrium or Thiem equation (Thiem 1906).

7.13.1.2 Unconfined Flow

In the case of an unconfined groundwater system, water of the saturated zone is in open contact with atmospheric pressures. As the aquifer response to pumping, groundwater released from storage occurs along permeable zones under the force of gravity. The streamline would be curved at the free surface of the aquifer; however, at the bottom of the aquifer, it becomes a horizontal line, converging to the well (Figure 7.21).

Based on Darcy's equation, the discharge rate would be equal to

$$Q = K2\pi rh\frac{\mathrm{d}h}{\mathrm{d}r}. \tag{7.47}$$

By reorganizing Equation 7.47,

$$h\cdot \mathrm{d}h = \frac{Q}{2\pi K}\frac{r}{\mathrm{d}r}. \tag{7.48}$$

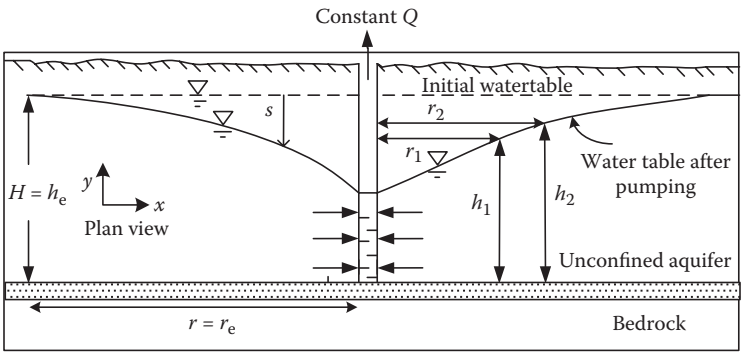

FIGURE 7.21 Radial flow in an unconfined aquifer.

By integrating between lines r_1 and r_2 where the water table depths are h_1 and h_2, respectively, the well discharge would be

$$Q = \frac{\pi K(h_2^2 - h_1^2)}{\ln\left(\frac{r_2}{r_1}\right)}. \tag{7.49}$$

This equation fails to describe accurately the drawdown curve near the well due to the large vertical flow components near the well, but it can be used for any two distances, away from the pumped well. At the edge of the zone of influence of radius r_e, H_e = saturated thickness of the aquifer, and Equation 7.49 can be modified as

$$Q = \frac{\pi K(H_e^2 - h_w^2)}{\ln\left(\frac{r_e}{r_w}\right)}. \tag{7.50}$$

Example 7.19

A fully penetrating well pumps water from an infinite horizontal unconfined aquifer at a constant rate of 0.7 m^3/s for a long period. Before pumping, the water table is in 25 m. The drawdowns at distances of 50 m from the well were observed 3 m. If $K = 6.32 \times 10^{-2}$ m/s, find the drawdowns at distances of 100, 150, and 200 m from the well.

Solution:

$$h_2^2 - h_1^2 = \frac{Q}{k\pi}\ln\left(\frac{r_2}{r}\right)$$

$$r = 100 \quad (25-s)^2 - (25-3)^2 = \frac{0.7\ln(100/50)}{\pi \times 6.32 \times 10^{-2}} = 2.44 \text{ m} \quad s = 2.945 \text{ m}$$

$$r = 150 \quad (25-s)^2 - (25-3)^2 = \frac{0.7\ln(150/50)}{\pi \times 6.32 \times 10^{-2}} = 3.88 \text{ m} \quad s = 2.912 \text{ m}$$

$$r = 200 \quad (25-s)^2 - (25-3)^2 = \frac{0.7\ln(200/50)}{\pi \times 6.32 \times 10^{-2}} = 4.89 \text{ m} \quad s = 2.889 \text{ m}.$$

7.13.2 Unsteady State in a Confined Aquifer

When a fully penetrated well in a confined aquifer is pumped at a constant rate Q, water is released from storage by the expansion of the water as pressure in the aquifer is reduced and by expulsion as the pore space is reduced as the aquifer compacts. By pumping out the water from such a well, the cone of depression continues to progress outward from the well and pumping affects a relatively large area of the aquifer. Further, if no recharge occurs, the area of drawdown of the potentiometric

surface will develop indefinitely and the rate of decline of the head continuously decreases as the cone of depression spreads.

The confined flow equation in radial coordinates can be presented as

$$\frac{\partial^2 s}{\partial r^2} + \frac{1}{r}\frac{\partial s}{\partial r} = \frac{S}{T}\frac{\partial s}{\partial t}, \tag{7.51}$$

where s is the drawdown ($s = h_0 - h$) and h_0 is the initial piezometric head. The initial and boundary conditions should be considered in solving this differential equation. These conditions are considered based on the basic assumptions about the groundwater flow. The initial condition of a horizontal potentiometric surface is

$$s(r, 0) = 0 \quad \forall r. \tag{7.52}$$

The boundary condition indicating an infinite horizontal extent with no drawdown at any time would be

$$s(\infty, t) = 0 \quad \forall r \tag{7.53}$$

$$\lim_{r \to 0} r\frac{\partial s}{\partial r} = -\frac{Q}{2\pi T}. \tag{7.54}$$

In a method known as the Theis or nonequilibrium equation (Theis 1935), the Boltzmann transformation is used to find the solution of Equation 7.51 based on the considered initial and boundary conditions. The considered variable in Boltzmann transformation, u, is defined as follows:

$$u = \frac{r^2 S}{4Tt}. \tag{7.55}$$

Substituting this variable into Equation 7.51, the flow equation in radial coordinates can be exhibited as

$$\frac{\mathrm{d}^2 s}{\mathrm{d}u^2} + (1 + 1/u)\frac{\mathrm{d}s}{\mathrm{d}u} = 0. \tag{7.56}$$

Then, the initial and boundary conditions in the transformed format are taken into consideration:

$$s(\infty) = 0 \tag{7.57a}$$

$$\lim_{u \to 0} u\frac{\mathrm{d}s}{\mathrm{d}u} = -\frac{Q}{4\pi T}. \tag{7.57b}$$

Using the substitution $\frac{\mathrm{d}s}{\mathrm{d}u}$, a first integration of the equation results in

$$u\frac{\mathrm{d}s}{\mathrm{d}u} = C_1 e^{-u}, \tag{7.58}$$

where C_1 is a constant of integration. For the second boundary condition, the equation simplifies to

$$\frac{ds}{du} = \frac{Q}{4\pi T} \times \frac{e^{-u}}{u}. \tag{7.59}$$

Considering the first boundary condition in the final integration, the drawdown equation is obtained as

$$s = \frac{Q}{4\pi T} \int_u^{\infty} \frac{e^{-a}}{a} da. \tag{7.60}$$

Equation 7.60 is a well-known integral in mathematics, which is called the exponential integral. An infinite series can approximately present the Theis equation:

$$s = \frac{Q}{4\pi T}\left[-0.5772 - \ln u + u - \frac{u^2}{2\times 2!} + \frac{u^3}{3\times 3!} - \frac{u^4}{4\times 4!} + \ldots\right] = s = \frac{Q}{4\pi T} W(u), \tag{7.61}$$

where $W(u)$ is called the dimensionless well function for non-leaky, isotropic, artesian aquifers fully penetrated by wells having constant discharge conditions. The values of well function against different values of u are provided in tables similar to that shown in Table 7.6.

Figure 7.22 shows a type curve of the well function. In this figure, both u and $W(u)$ are dimensionless.

A main utility of this model is its ability in dealing with variable groundwater pumping schedule. Suppose the aquifer is pumped at a variable extraction rate for n planning periods. For any period, the drawdown can be obtained from superposition of the well responses, due to the linearity of the

TABLE 7.6
Values of $W(u)$ for Various Values of u

U	1.0	2.0	3.0	4.0	5.0	6.0	7.0	8.0	9.0
×1	0.219	0.049	0.013	0.0038	0.0011	0.00036	0.00012	0.000038	0.000012
1×10^{-1}	1.82	1.22	0.91	0.70	0.56	0.45	0.37	0.31	0.26
1×10^{-2}	4.04	3.35	2.96	2.68	2.47	2.30	2.15	2.03	1.92
1×10^{-3}	6.33	5.64	5.23	4.95	4.73	4.54	4.39	4.26	4.14
1×10^{-4}	8.63	7.94	7.53	7.25	7.02	6.84	6.69	6.55	6.44
1×10^{-5}	10.94	10.24	9.84	9.55	9.33	9.14	8.99	8.86	8.74
1×10^{-6}	13.24	12.55	12.14	11.85	11.63	11.45	11.29	11.16	11.04
1×10^{-7}	15.54	14.85	14.44	14.15	13.93	13.75	13.60	13.46	13.34
1×10^{-8}	17.84	17.15	16.74	16.46	16.23	16.05	15.90	15.76	15.65
1×10^{-9}	20.15	19.45	19.05	18.76	18.54	18.35	18.20	18.07	17.95
1×10^{-10}	22.45	21.76	21.35	21.06	20.84	20.66	20.50	20.37	20.25
1×10^{-11}	24.75	24.06	23.65	23.36	23.14	22.96	22.81	22.67	22.55
1×10^{-12}	27.05	26.36	25.96	25.67	25.44	25.26	25.11	24.97	24.86
1×10^{-13}	29.36	28.66	28.26	27.97	27.75	27.56	27.41	27.28	27.16
1×10^{-14}	31.66	30.97	30.56	30.27	30.05	29.87	29.71	29.58	29.46
1×10^{-15}	33.96	33.27	32.86	32.58	32.35	32.17	32.02	31.88	31.76

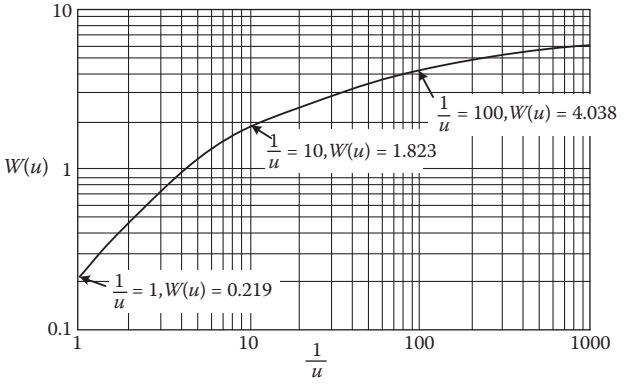

FIGURE 7.22 Values of $W(u)$ (well function of u) corresponding to values of $1/u$.

response functions of the extraction rates. The mathematical form of the equation for any period can be expressed as follows:

$$s = \frac{Q_1}{4\pi T} W\left(\frac{r^2 S}{4Tt}\right), \quad 0 \le t \le t_1 \tag{7.62a}$$

$$s = \frac{Q_1}{4\pi T} W\left(\frac{r^2 S}{4Tt}\right) + \left(\frac{Q_2 - Q_1}{4\pi T}\right) W\left(\frac{r^2 S}{4T\left(t - t_1\right)}\right), \quad t_1 \le t \le t_2 \tag{7.62b}$$

$$\begin{aligned} s = {} & \frac{Q_1}{4\pi T} W\left(\frac{r^2 S}{4Tt}\right) + \left(\frac{Q_2 - Q_1}{4\pi T}\right) W\left(\frac{r^2 S}{4T\left(t - t_1\right)}\right) + ... \\ & + \left(\frac{Q_n - Q_{n-1}}{4\pi T}\right) W\left(\frac{r^2 S}{4T\left(t - t_{n-1}\right)}\right), \quad t \ge t_{n-1} \end{aligned} \tag{7.62c}$$

where Q_k is the extraction rate for planning period k.

Example 7.20

You are asked to design a pump test for an aquifer in which the transmissivity is expected to be about 1.6×10^{-2} m²/s and the storage coefficient is about 1.2×10^{-4}. What pumping rate would you recommend for the test if it is desired that there be an easily measured drawdown of at least 0.5 m during the first 4 h of the test in an observation well 120 m from the pumping well?

Solution:

$$u = \frac{r^2 S}{4Tt} = \frac{120^2 \times 1.2 \times 10^{-4}}{4 \times 1.6 \times 10^{-4} \times (4 \times 3600)} = 1.875 \times 10^{-3}$$

$$W(u) = -0.5772 - \ln(u) + \frac{u^2}{2\times 2!} - \frac{u^3}{3\times 3!} + \ldots$$

$$W(u) = -0.5772 - \ln\left(1.875\times 10^{-3}\right) + \frac{\left(1.875\times 10^{-3}\right)^2}{2\times 2!} - \frac{\left(1.875\times 10^{-3}\right)^3}{3\times 3!} + \ldots = 6.856$$

$$Q = \frac{T\times 4\pi(h_0 - h)}{W(u)} = \frac{1.6\times 10^2 \times 4\pi \times 0.5}{6.856} = 1.465\times 10^{-2}\ \text{m}^3/\text{s} = 1266.2\ \text{m}^3/\text{day}.$$

7.13.2.1 Aquifer Test Application

The main objective of an aquifer test (or a pumping test) is to evaluate an aquifer by observing the aquifer's drawdown in observation wells. One or more monitoring wells or piezometers are used for aquifer testing as the observation/monitoring wells. It is important to notice that water is not being pumped from the observation well; these are just utilized to monitor the water drawdown. While water is being pumped from one well at a steady rate, the water tables are monitored in the observation wells. Typically, monitoring and pumping wells are screened across the same aquifers. Data processing, which is the basis of aquifer testing, yields valuable qualitative and quantitative features about the subsurface geological composition of the aquifer domain. The test data processing is achieved by matching the data with a suitable type curve. An analytical or numerical model of aquifer flow is used to match the data observed in the real world assuming the parameters from the idealized model applied to the real-world aquifer.

The common aquifer characteristics that are evaluated through aquifer tests are as follows:

- Hydraulic conductivity or transmissivity, which shows the permeability of the aquifer and the ability of an aquifer to transmit water.
- Specific storage/specific yield or storage coefficient is the measure of the amount of water an aquifer will give up for a certain change in head.
- Boundary determination, the type of boundaries that give up water to the aquifer, providing additional water to reduce drawdown or no-flow boundaries.

Design, field observations, and data analysis are the three major components for the aquifer tests with the ultimate objectives of quantifying the hydraulic properties, boundary determination, indication of the general type of aquifer, and hypothesis testing. In aquifer tests, in addition to knowing the geology of the site and characteristics of the wells (width, depth, materials used, and development), measuring devices such as time, discharge, and water level should be calibrated and verified. Hence, the observed data during the test are plotted and the best curve is fitted on data. Finally, based on the fitted curve, the aquifer characteristics are determined.

The method of analysis of aquifer test data utilizes graphical or computer estimation of parameter values using observed drawdown and well-produced rate records. Two graphical methods of the log–log plot of drawdown versus time for the Theis method and the semilog plot for the Cooper–Jacob method are used for confined aquifers.

7.13.2.2 Theis Method of Solution

Theis (1935) adopted the following equation and determined T and S by expressing Equations 7.55 and 7.62 as

$$\log s = \log\left(\frac{Q}{4\pi T}\right) + \log W(u) \tag{7.63}$$

$$\log\frac{t}{r^2} = \log\left(\frac{S}{4T}\right) + \log\frac{1}{u}. \tag{7.64}$$

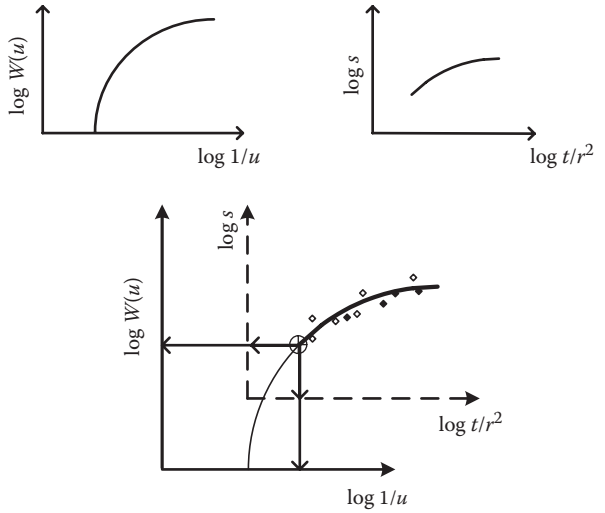

FIGURE 7.23 Graphical overlay of the type curve with drawdown data to determine T and S from pump test data.

As $Q/4\pi T$ and $S/4T$ are constants, the relation between $\log(s)$ and $\log(t/r^2)$ must be similar to the relation between $\log W(u)$ and $\log 1/u$. Therefore, drawdown measurements derived from pumping tests are plotted against t/r^2 on log-log paper and also $W(u)$ against $1/u$ is plotted on the same log-log paper. The two plotted curves have the same shape, but there is a shift in the center of coordinates equal to $(Q/4\pi T)$ and $(S/4T)$, vertically and horizontally, respectively, keeping the coordinate axes parallel. Therefore, each curve must be plotted on a separate sheet, and then they must be matched by placing one graph on top of the other and moving it horizontally and vertically until the curves are matched. By superimposing the type curve values of $W(u)$ and $1/u$ with the graph of t/r^2 and s on the log–log papers, desirable point (matching point) coordinates are substituted in the Theis equation to find T and S. Figure 7.23 shows the process.

Example 7.21

The thickness of a horizontal, confined, homogeneous, isotropic aquifer of infinite areal extent is 50 m. A fully penetrating well was continuously pumped at a constant rate of 0.15 m^3/s for a period of 1 day. The drawdowns given in Table 7.7 were observed in a penetrating well 75 m from the pumping well. Compute the transmissivity and the storage coefficient by using the Theis method.

TABLE 7.7
Drawdown Time Data Recorded at a Distance of 75 m

t (min)	$h_0 - h$ (m)	t	$h_0 - h$	t	$h_0 - h$	t	$h_0 - h$
1	0.126	7	0.351	40	0.594	100	0.729
2	0.198	8	0.36	50	0.63	200	0.81
3	0.252	9	0.378	60	0.639	400	0.891
4	0.288	10	0.396	70	0.657	800	0.963
5	0.306	20	0.495	80	0.684	1000	0.99
6	0.333	30	0.558	90	0.711		

Solution:

First, the function $W(u)$ versus $1/u$ and the measured time-drawdown values $h_0 - h$ versus t/r^2 are plotted on log–log paper, separately. Then, the field curve is superimposed on the type curve with keeping the axes parallel; it must be done by adjusting the curves until most of the observed data points fall on the type curve (Figure 7.24).

By selecting an arbitrary match point, the paired values of $W(u)$ and $1/u$, $h_0 - h$ and t/r^2 are easily read off. Having these values, accompanied by the pumping rate Q and the radial distance r from the well, T is calculated as follows:

$$T = \frac{QW(u)}{4\pi(h_0 - h)} = \frac{0.15 \times 1.0}{4\pi \times 0.122} = 9.79 \times 10^{-2}\ \mathrm{m^3/s}$$

S is obtained by

$$S = \frac{4uTt}{r^2} = 4 \times 1.0 \times 9.79 \times 10^{-2} \times 0.0032 = 1.267 \times 10^{-3}$$

7.13.2.3 Cooper–Jacob Method-Modified Theis

Cooper and Jacob (1946) noticed that for small values of r and large values of t, the parameter $u = r^2S/4T$ becomes very small and the following equation can approximate the infinite series:

$$W(u) = -0.5772 - \ln u. \tag{7.65}$$

Thus,

$$s' = \frac{Q}{4\pi T}\left(-0.5772 - \ln\left(\frac{r^2 S}{4Tt}\right)\right). \tag{7.66}$$

Rearranging and converting to decimal logs yields

$$s' = \frac{2.3Q}{4\pi T}\log\left(\frac{2.25Tt}{r^2 S}\right). \tag{7.67}$$

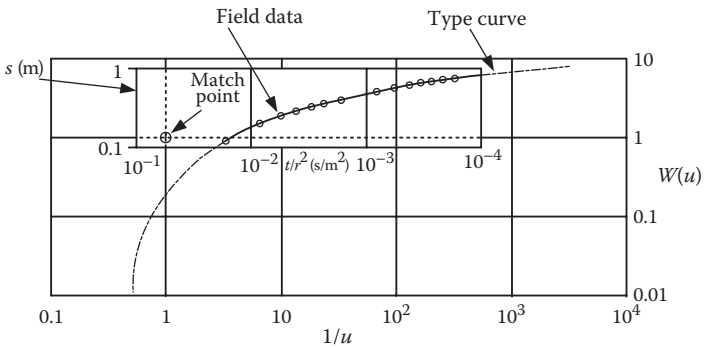

FIGURE 7.24 Matching the type curve with drawdown data.

A straight line is the result of the plot of drawdown s via log of t. A projection of the line back to $s = 0$, where $t = t_0$ yields the following relation:

$$S = \left(\frac{2.25Tt_0}{r^2} \right) \tag{7.68}$$

$$T = \left(\frac{2.3Q}{4\pi s'} \right), \tag{7.69}$$

where s' is the drawdown for a log cycle and t_0 is the time at which the drawdown line intercepts the zero drawdown axis. The Cooper–Jacob method first solves T and then S and is practical only for small values of $u < 0.01$.

Example 7.22

Compute the transmissivity and the storage coefficient of the aquifer in the previous example by using the Cooper–Jacob semilog plotting method.

Solution:

First, the measured time-drawdown value, $h_0 - h$ versus t is plotted on semilog paper. Points on semilog charts conclude a linear curve, a line is drawn to cover the points, and s' for one log cycle and t_0 are calculated (Figure 7.25). Having Q (the pumping rate) and r (the radial distance), T and S are calculated as follows:

$$T = \frac{2.3Q}{4\pi s'} = \frac{2.3 \times 0.15}{4\pi \times 0.32} = 8.584 \times 10^{-2}\ \text{m}^2/\text{s}$$

$$S = \frac{2.25Tt_0}{r^2} = \frac{2.25 \times 8.854 \times 10^{-2} \times 33}{75^2} = 1.113 \times 10^{-3}.$$

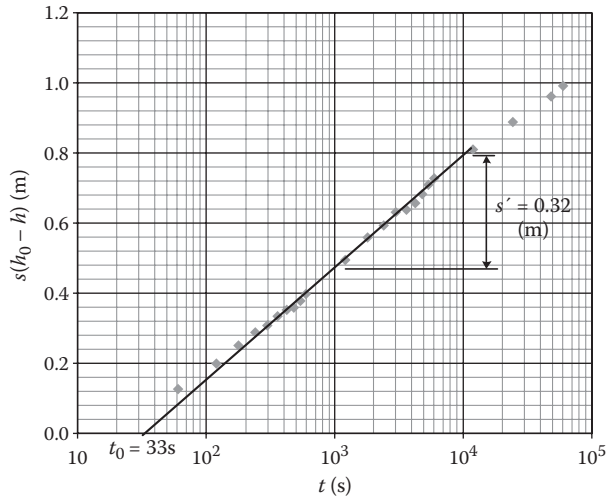

FIGURE 7.25 Time-drawdown plot for Example 7.22.

7.13.3 Unsteady State for Unconfined Aquifer

In an unconfined aquifer, the water that is pumped from the well is derived from storage by gravity drainage of tile interstices above the cone of depression. In the nonequilibrium solution, the effects of gravity drainage are not considered. Gravity drainage is not immediate and, for unsteady flow of water towards a well for unconfined conditions, is characterized by the slow drainage of interstices. Neuman (1975) developed a graphical method for analysis of an aquifer test in an unconfined aquifer.

The basic assumption of this method is shown in Figure 7.26. In this method, three distinct segments of the time-drawdown curve for water table condition are considered and therefore it does not require the definition of any empirical constants.

The first part corresponds to the early drawdown when immediate release of water from storage is occurring in the same manner as an artesian aquifer. The coefficient of transmissibility might be determined under certain conditions by applying the nonequilibrium solution to the time-drawdown data. As the gravity drainage is not immediate, the water is released instantaneously from storage. As time elapses, deviation from nonequilibrium type curves occurs due to the effects of gravity drainage and vertical flow. The coefficient of storage is calculated using the early time drawdown and it is in the artesian range and cannot be used to predict long-term drawdown.

The second segment is used for the intermediate stage of the decline of water level due to the slow expansion of the cone of depression and it is resupplied by the gravity drainage. Recharge is reflected as the slope of the time-drawdown curve. During the second segment, pump test data deviate significantly from the nonequilibrium theory.

The third segment represents the late drawdown data, when effects of gravity drainage are becoming smaller. This segment takes place at later times. As the delayed gravity drainage ceases to influence the drawdown in observation wells, the time-drawdown field data conform closely to the nonequilibrium. The coefficient of transmissibility of an aquifer can be determined by applying the nonequilibrium solution to the third segment of the time-drawdown data. The coefficient of storage can be used to predict long-term effects because it is in the unconfined range.

Three segments of the time-drawdown curve are reproduced in the Neuman (1975) solution and the solution does not require the definition of any empirical constants. The proposed equation for drawdown in an unconfined aquifer with fully penetrating wells and a constant discharge rate of Q is as follows:

$$s = h_0 - h = \frac{Q}{4\pi T} W\left(u_a, u_y, \eta\right), \tag{7.70}$$

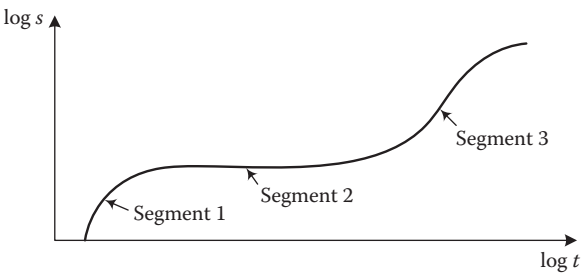

FIGURE 7.26 Three segments of time-drawdown curve for water table conditions.

where $W(u_a, u_y, \eta)$ is the well function for unconfined aquifer and

$$u_a = \frac{r^2 S}{4Tt} \quad \text{(for small values of } t\text{)} \tag{7.71}$$

$$u_y = \frac{r^2 S_y}{4Tt} \quad \text{(for large values of } t\text{)} \tag{7.72}$$

$$\eta = \frac{r^2 K_v}{b^2 K_h}, \tag{7.73}$$

where $s = h_0 - h$ is the drawdown, T is transmissivity, r is the radial distance from the pumping well, S is storage coefficient, S_y is the specific yield, t is time, K_v is the vertical hydraulic conductivity, K_h is the horizontal hydraulic conductivity, and b is initial saturated thickness of the aquifer. Figure 7.27 is a plot of well function for unconfined aquifers for various values of η with two sets of type curve. Type A curves that grow out of the left-hand Theis curve of Figure 7.27 are good for early drawdown data. Type B curves that are asymptotic to the right-hand Theis curve of Figure 7.27 are followed at a later time. The Type B curves end on a Theis curve, and then the distance-drawdown data can be analyzed using the nonequilibrium solution technique.

Example 7.23

A well in a water table aquifer was pumped at a rate of 873 m³/day. Drawdown was measured in a fully penetrating observation well located 90 m away as shown in Figure 7.28. Find the transmissivity, storage coefficient, and specific yield of the aquifer.

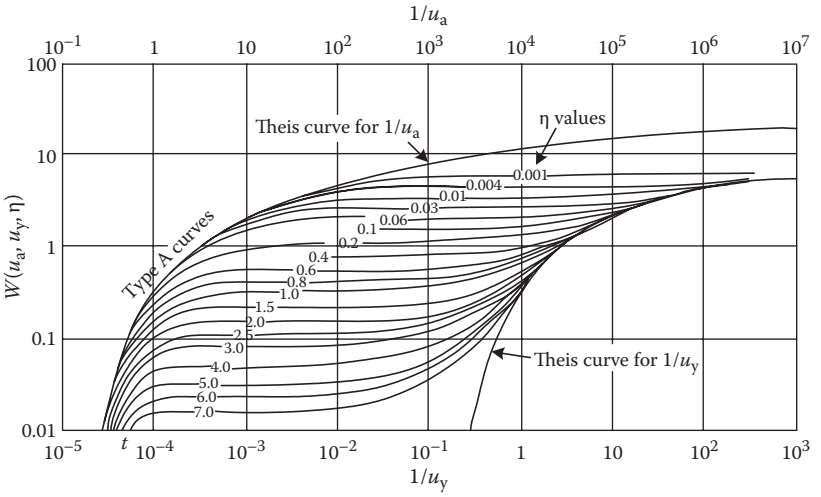

FIGURE 7.27 Theoretical curves of $W(u)$ versus $1/u$, for an unconfined aquifer. (From Neuman, S.P., *Water Resources Research*, 10(2), 303–312, 1975. With permission.)

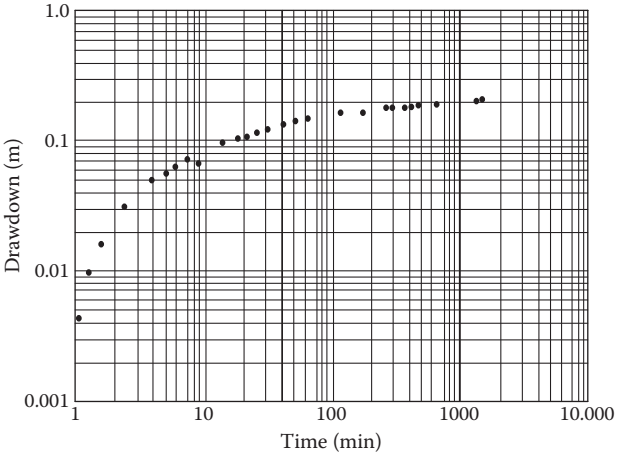

FIGURE 7.28 Drawdown in an unconfined aquifer as a function of time.

Solution:

The best match for Type A curve and the early drawdown data is with the $\eta = 0.01$ curve. At the match point, $1/u_A = 10$, $W(u_a, u_y, \eta) = 1$, $h_0 - h = 4.8 \times 10^{-2}$ m, and $t = 10.5$ min (7.3×10^{-3} days). Substituting these values into Equations 7.70 and 7.71,

$$T = \frac{Q}{4\pi(h_0 - h)} W\left(u_a, u_y, \eta\right),$$

given $Q = 873$ m^3/day.

$$T = \frac{873 \text{ m}^3/\text{day} \times 1.0}{4\pi \times 4.8 \times 10^{-2}} = 1400 \text{ m}^2/\text{day}$$

$S = \dfrac{4Tut}{r^2}$, given $r = 90$ m

$$1/u_A = 10,\ u_A = 0.1$$

$$S = \frac{4 \times 1400 \text{ m}^2/\text{day} \times 7.3 \times 10^{-3} \text{ day}}{90 \text{ m} \times 90 \text{ m}} \times 0.1 = 0.0005.$$

The Type B curve for $\eta = 0.01$ is matched to the late drawdown data. The match point values are $1/u_y = 10^2$, $W(u_a, u_y, \eta) = 1$, and $t = 880$ min (61×10^{-1} day).

$$T = \frac{873 \text{ m}^2/\text{day} \times 1.0}{4\pi \times 4.3 \times 10^{-2} \text{ m}} = 1600 \text{ m}^2/\text{day}$$

$$S_y = \frac{4 \times 1600 \text{ m}^2/\text{day} \times 6.1 \times 10^{-1} \text{ day} \times 0.01}{90 \text{ m} \times 90 \text{ m}} = 0.005.$$

7.14 MULTIPLE-WELL SYSTEMS

The drawdown in hydraulic head at any point of the aquifer with more than one well is considered as equal to the summation of the drawdown occurring from each of the wells independently. In fact, the total drawdown of n wells pumping at rates Q_1, Q_2, …Q_n can be calculated from superposition of well response individually. Wherever pumping is from a confined aquifer:

$$H_e - h = \sum_{i=1}^{n} \frac{Q_i}{2\pi Kb} \ln\left(\frac{r_{ei}}{r_i}\right), \tag{7.74}$$

where $H_e - h$ is the drawdown at any given point in the area of influence, r_{ei} is the distance from the ith well to a point at which the drawdown becomes negligible and r_i is the distance from the ith well to the given point. The total drawdown for an unconfined aquifer is presented as

$$H_e^2 - h^2 = \sum_{i=1}^{n} \frac{Q}{\pi K} \ln\left(\frac{r_{ei}}{r_i}\right). \tag{7.75}$$

For example, for an unconfined aquifer with unsteady state pumping, the arithmetic summation of the Theis solutions is the answer of the drawdown at a point whose radial distance from each well is given by r_1, r_2, …r_n, that is:

$$h_0 - h = \frac{Q_1}{4\pi T} W\left(u_1\right) + \frac{Q_2}{4\pi T} W\left(u_2\right) + \ldots + \frac{Q_n}{4\pi T} W\left(u_n\right), \tag{7.76}$$

where

$$u_i = \frac{r_i^2 S}{4Tt_i} \quad i = 1, 2, 3, \ldots, n.$$

t_i is the time since pumping started at the well whose discharge is Q_i.

This model might also be used to incorporate a variable groundwater pumping schedule. If an aquifer were pumped at a variable extraction rate for n planning periods, the drawdown for any period can be found from superposition of the well responses because the response equations are linear functions of the extraction rates.

Example 7.24

A specific building is supposed to be built where the water table is 60 m. Allowable depth is considered to be 30 m, the drawdown effect is predicted to be 600 m (point A), and $K = 10^{-3}$ m/s. If the building is located at the center of a square with a length of 70 m and four identical wells are at the corners of the square, calculate the rate of pumping of the wells (Figure 7.29).

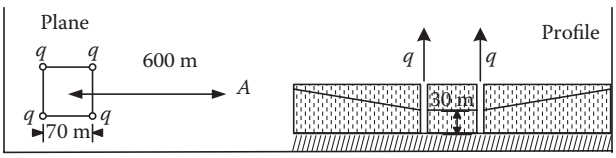

FIGURE 7.29 Plane and profile views of Example 7.24.

Solution:

r_{ei} is considered to be the distance between the well i and the negligible drawdown point, and r_i is the distance between the well i and the central point. The drawdown in the building center is equal to the sum of the drawdown that would arise from each of the wells independently.

$$H_e^2 - h^2 = \sum_{i=1}^{n} \frac{Q}{\pi K} \ln\left(\frac{r_{ei}}{r_i}\right)$$

$$60^2 - 30^2 = \frac{Q}{\pi \times 10^{-3}} \left[2\ln\left(\frac{\sqrt{635^2 + 35^2}}{\sqrt{35^2 + 35^2}}\right) + 2\ln\left(\frac{\sqrt{565^2 + 35^2}}{\sqrt{35^2 + 35^2}}\right) \right]$$

$$Q = 0.85 \text{ m}^3/\text{s}.$$

7.15 EFFECTIVE CONDITIONS ON TIME-DRAWDOWN DATA

Applying the Theis equation needs the basic assumptions made in developing the equations for groundwater flow, but geologic or hydrologic conditions do not conform fully in real aquifers. An infinite areal extent of an aquifer is one of these assumptions and clearly it is necessary in order to solve many groundwater problems, but it is obvious that this type of aquifer cannot exist in reality and the aquifers have some boundaries. Instances of hydrologic boundaries could be the edge of the aquifer, a region of the recharge to a fully confined artesian aquifer, or a source of recharge such as a stream or lake (Fetter 2001). In other words, the boundary conditions can be divided into two categories: recharge boundaries and impermeable boundaries. A fully penetrated well that leads to a change in the flow pattern is another assumption for applying the developed formula.

7.15.1 Recharge Boundary

Several general situations might help the equilibrium conditions stabilize the cone of depression around a pumping well. Recharging from a river or lake is one of these conditions. A recharge boundary is a region in which the aquifer is replenished. A recharge boundary of river, after reaching equilibrium, is shown in Figure 7.30.

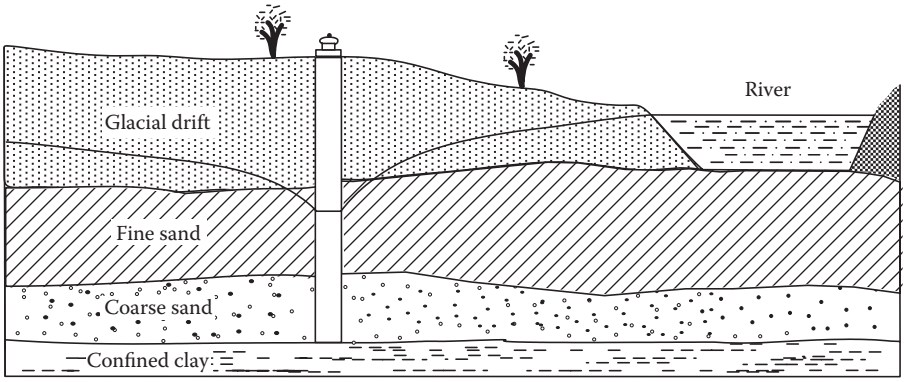

FIGURE 7.30 Cone of depression between the aquifer and river. (From Driscoll, F., *Groundwater and Wells*, Johnson Division, St. Paul, 1986. With permission.)

The drawdown data due to water pumping show that the cone of depression does not extend to the river and no recharge is evident. Water table in the well decreases as pumping goes on. When the cone of depression intersects a river channel, a hydraulic gradient develops between the groundwater in the aquifer and the water in the river. Provided the streambed is hydraulically connected to the aquifer, the river water will percolate downward through the pervious streambed under the influence of the hydraulic gradient. Hence, the aquifer is recharged by the river at an increasing rate as the cone of depression enlarges. The situation that the cone of depression and the pumping level become stable happens when the rate of recharge to the aquifer equals the rate of discharge from the well (Driscoll 1986).

In predicting aquifer behavior in the presence of boundaries, imaginary wells are introduced such that the response at the boundary is made true. The image well method is commonly used in heat-flow theory and has been modified for application in the groundwater milieu.

Predicting the decreased drawdown that occurs in a confined aquifer in the vicinity of a constant-head boundary would be possible by producing the slightly unrealistic case of a fully penetrating stream (Figure 7.31a). For such a case, the imaginary infinite stream (Figure 7.31b) is fabricated in order to set up a hydraulic flow system, which will be equivalent to the effects of a known physical boundary. A recharging image well duplicated in an equal and opposite side from the real well can simulate the recharge boundary (Figure 7.31c).

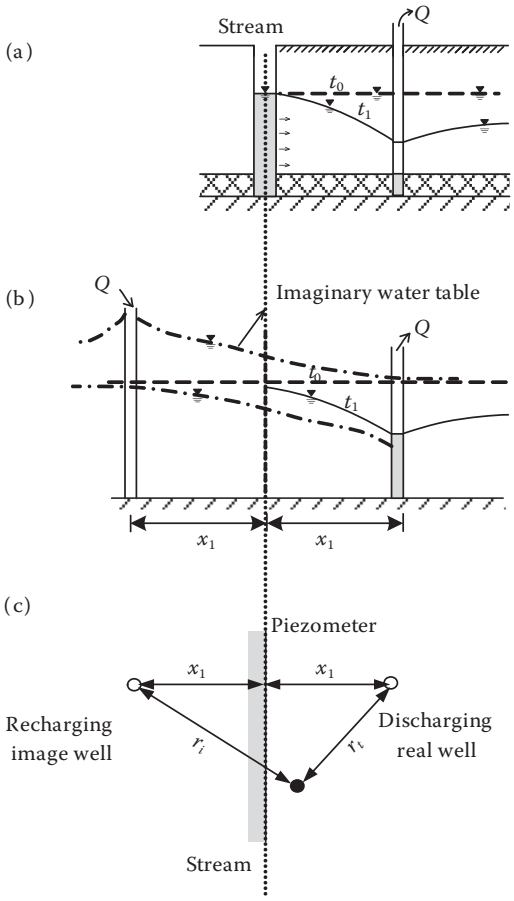

FIGURE 7.31 Drawdown in an aquifer bounded on one side by a stream, (a) The actual condition, (b) adding an imaginary well, (c) the schematic of real and image wells to determine the drawdown in a desired point. (From Karamouz, M. et al., *Groundwater Hydrology: Engineering, Planning, and Management*, CRC Press Inc., 2011. With permission.)

An expression for the drawdown in an aquifer bounded by a constant-head boundary is the result of summation of the cone of depression from the pumping well and the cone of impression from the recharge well:

$$h_0 - h = \frac{Q}{4\pi T}\left[W\left(u_r\right) - W\left(u_i\right)\right] \tag{7.77}$$

$$u_r = \frac{r_r^2 S}{4Tt} \quad \text{and} \quad u_i = \frac{r_i^2 S}{4Tt}. \tag{7.78}$$

7.15.2 Impermeable Boundary

Definite geologic and hydraulic boundaries in many localities limit aquifers to areas. An edge of the aquifer, where it terminates by thinning or abutting a low permeability formation or has been eroded away, is called an impermeable boundary (Fetter 2001). Suppose that there is no groundwater flow across this layer, it is called a zero-flux boundary. The effects of an impermeable boundary on the

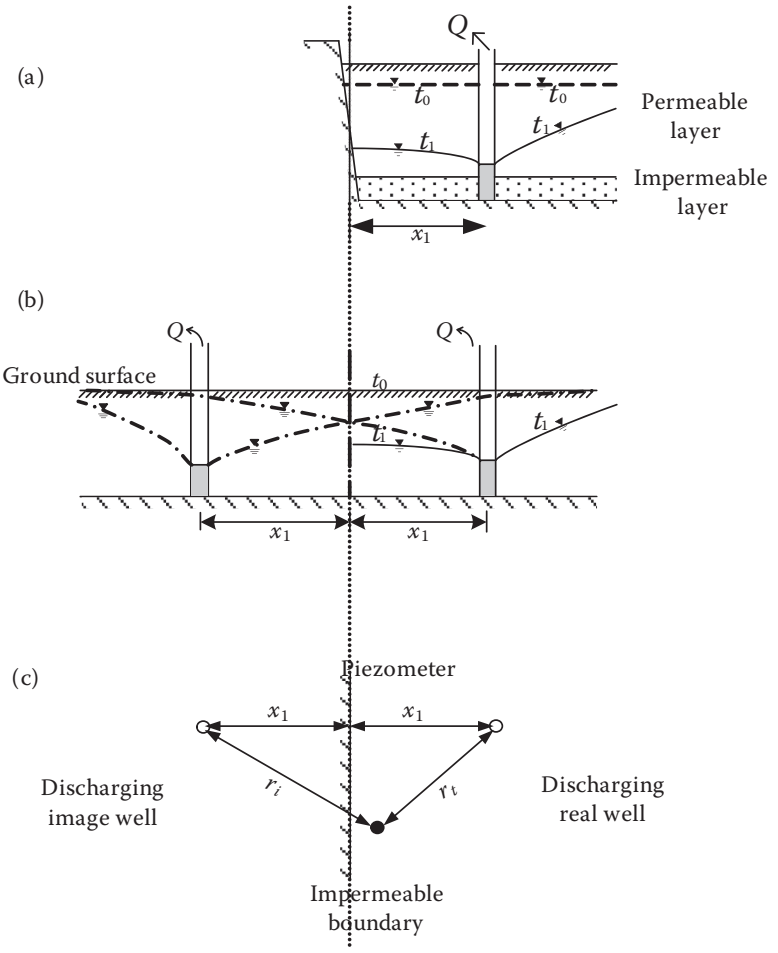

FIGURE 7.32 Drawdown in an aquifer bounded on one side by an impermeable boundary. (a) The actual condition, (b) adding an imaginary well, and (c) the schematic of real and image wells to determine the drawdown in a desired point. (From Karamouz, M. et al., *Groundwater Hydrology: Engineering, Planning, and Management*, CRC Press Inc., 2011. With permission.)

time-drawdown data are opposite to that of the recharge boundary. When a straight-line impermeable boundary bounds one side of an aquifer, drawdown due to pumping will be greater near the boundary (Figure 7.32a). Acceleration of the drawdown is the effect of the impermeable boundary to flow in some region of the aquifer (Figure 7.32b). In order to simulate an impermeable boundary, it is assumed that a imaginary well is located in an equal and opposite side from the real well (Figure 7.32c).

An expression for the drawdown in an aquifer bounded by a constant-head boundary is the result of the summation of the cone of depression from the pumping well and the cone of impression from the discharge well:

$$h_0 - h = \frac{Q}{4\pi T}\left[W\left(u_r\right) + W\left(u_i\right)\right], \tag{7.79}$$

where u_r and u_i are as defined in Equation 7.78. Using the image well approach to provide predictions of drawdown in systems with more than one boundary is possible.

7.15.3 Partially Penetrating Wells

In practice in well construction, partially penetrating wells are attributed to the wells where the bore length is less than the thickness of the aquifer. The flow pattern will differ from the radial flow that is thought to exist around wells that fully penetrate. Flow toward a partially penetrating well experiences convergence that is in addition to the convergence in flow toward a fully penetrating well. The presented equations cannot be used to estimate the drawdowns due to the changes in the flow pattern, which is not strictly radial anymore. Figure 7.33 shows that the flow has a vertical component in the vicinity of the well in partially penetrating wells.

Some typical flow lines or paths of water particles are presented by the arrows as they move through the formation to the intake portion of the well. Water in the lower part of the aquifer moves upward along the curved lines in order to reach the well screen. Thus, the water path is longer than radial flow lines. Also, the flow must converge through a smaller cross-sectional area while approaching the short screen. An increase in head loss is the result of the longer flow paths and smaller cross-sectional area. For a given yield, therefore, there would be greater drawdown in a pumping well if the aquifer thickness is only partially screened. From another point of view, for a given drawdown, the yield from a well partially penetrating the aquifer is less than the yield from one completely penetrating the aquifer (Driscoll 1986).

For distances from the well that exceed about $1.5b\sqrt{K_h/K_v}$ (K_h and K_v are the horizontal and vertical conductivity, respectively, in an anisotropic aquifer), the vertical components of flow are

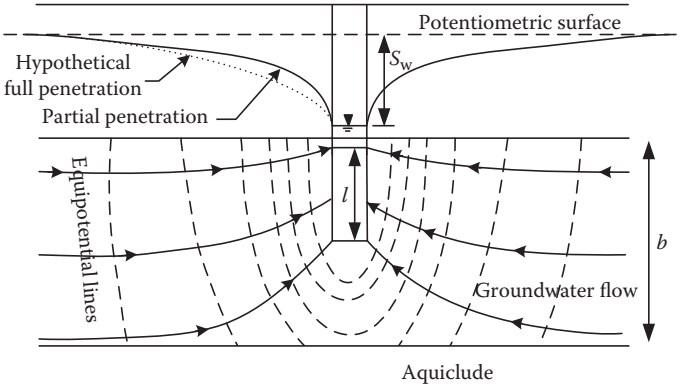

FIGURE 7.33 Flow lines toward a partially penetrating well.

assumed negligible and developed equations can be used for the partially penetrating case, provided that $r > 1.5b\sqrt{K_h/K_v}$. In the case of $r < 1.5b\sqrt{K_h/K_v}$, the discharge per unit of drawdown is smaller than that of a fully penetrating well. One of the basic equations that is developed for partially penetrating wells utilizes a continuous superposition of sinks to derive an approximate relationship between the discharge of a partially penetrating well and that of a fully penetrating well. Specific capacity is the discharge per unit drawdown and is widely used to characterize the discharge capacity of pumped wells.

$$\left(\frac{Q}{s_w}\right)_p = \left(\frac{Q}{s_w}\right)\left[\frac{l}{b}\left\{1+7\left(\frac{r_w}{2l}\right)^{1/2}\cos\frac{\pi l}{2b}\right\}\right], \tag{7.80}$$

where l is the length of well bore over which water enters the well and the subscript p denotes the partially penetrating case.

Example 7.25

In a 30 m thick aquifer with a specific capacity of 0.04 $m^3/s{\cdot}m$, a partially penetrating well with an effective radius of 0.20 m is located and the length of screened well bore is 15 m. Calculate the increase in specific capacity if the length of well screen is increased to 20 m.

Solution:

By applying Equation 7.80 for a partially penetrating case, the specific capacity for full penetration is

$$\left(\frac{Q}{s_w}\right) = \frac{\left(\frac{Q}{s_w}\right)_p}{\left[\frac{l}{b}\left\{1+7\left(\frac{r_w}{2l}\right)^{1/2}\cos\frac{\pi l}{2b}\right\}\right]}$$

$$\left(\frac{Q}{s_w}\right) = \frac{0.04}{\left[\frac{12}{30}\left\{1+7\left(\frac{0.20}{24}\right)^{1/2}\cos\frac{12\pi}{60}\right\}\right]} = 0.066\ m^2/s.$$

The specific capacity with l = 20 m is

$$\left(\frac{Q}{S_w}\right)_p = 0.066\left[\frac{20}{35}\left\{1+7\left(\frac{0.20}{40}\right)^{1/2}\cos\frac{20\pi}{60}\right\}\right] = 0.047\ m^2/s.$$

Increasing the length of well screen to 20 m will change the specific capacity from 0.04 to 0.047 m^2/s, an increase of 17.5%.

7.16 INTERACTION BETWEEN SURFACE AND GROUNDWATER

Surface water is the water that flows directly on top of the ground such as streams, lakes, springs, and reservoirs. When the rate of rainfall exceeds the infiltration capacity of the soil, overland flow can be generated.

Subsurface water includes infiltrated water, baseflow, and groundwater. Streams under the ground surface that contains leakages from the stream into the subsurface is called baseflow. Most of this water returns to the stream in sharp steps and it sustains flows during extended dry periods. The infiltration process is discussed in the following subsection.

7.16.1 Infiltration

Infiltration of precipitation through the unsaturated zone is the source of surface water for groundwater recharge. Effective elements in soil infiltration are rainwater chemistry, soil chemistry, vegetated land, soil moisture, and hydraulic conductivity. The unsaturated zone includes soil, air, and water that control the infiltration rates. Quantifying groundwater flow in this zone is more complicated than in the saturated zone. Water seepage from the surface into the subsurface depends on the gravity and moisture potential, which are called hydraulic and pressure heads, respectively. The moisture content and pore size of the medium are the key elements in moisture potential. In unsaturated flow, the total potential h is the summation of moisture potential $\psi(\theta)$ and gravity potential Z.

Any change in the infiltration rate demands a change in moisture content θ. In the unsaturated zone, regarding the infiltration that is controlled by moisture potential $\psi(\theta)$ and hydraulic conductivity $K(\theta_v)$, one-dimensional flow in the unsaturated zone is described as

$$\frac{\partial}{\partial z}\left[K\left(\theta_v\right)\left(\frac{\partial h}{\partial z}\right)\right]=\frac{\partial \theta}{\partial t} \tag{7.81}$$

$$\frac{\partial}{\partial z}\left[K\left(\theta_v\right)\left(\frac{\partial \psi}{\partial z}+\frac{\partial z}{\partial z}\right)\right]=\frac{\partial \theta}{\partial t}\,. \tag{7.82}$$

Cumulative infiltration decreases as a result of a decrease in moisture potential. The infiltration rate decreases to a rate equivalent to saturated vertical hydraulic conductivity, K_v, when the moisture potential approaches zero. Figure 7.34 shows the infiltration rate.

The initial infiltration capacity, f_o, is controlled by the moisture content of the soil, and the saturated vertical hydraulic conductivity of the soil, K_v, controls the final infiltration capacity.

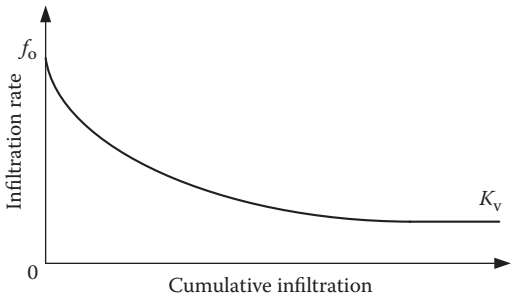

FIGURE 7.34 Infiltration capacity curve.

7.16.2 Concepts of Interaction between Surface Water and Groundwater

Seasonal conditions control the interaction between streams and groundwater and the direction of flow. When the hydraulic gradient of the aquifer is towards the stream, groundwater discharges to the stream, and the stream is a gaining or effluent stream. The gaining stream receives water from the groundwater system in Figure 7.35.

When the hydraulic gradient of the aquifer is away from the stream, the stream loses water to groundwater (as shown in Figure 7.36) by outflow through the streambed, and the stream is losing. The effective factors on the interaction flow are the depth of water and the hydraulic gradient. The losing streams lose water to the groundwater system (Figure 7.36).

In some situations, flow direction can vary in two sides of a stream; for example, one side receives groundwater, while the other side loses water to groundwater. The flow direction can vary along a stream. In some environments, some reaches receive groundwater, lose water to groundwater, or lose or gain water at different times of the year.

Losing streams as illustrated in Figure 7.37 can be directly connected to the groundwater by a continuous saturated zone or may be disconnected from the groundwater system by an unsaturated zone, where, in this case, the water seeps through a streambed of streams to a deep water table as shown in Figure 7.37.

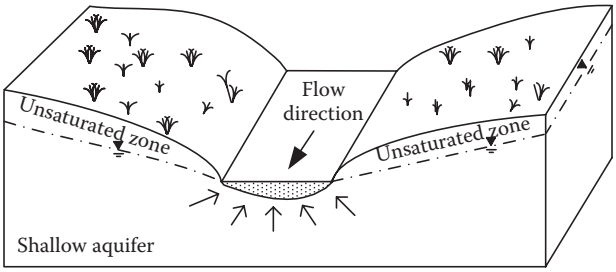

FIGURE 7.35 Groundwater discharges to the stream.

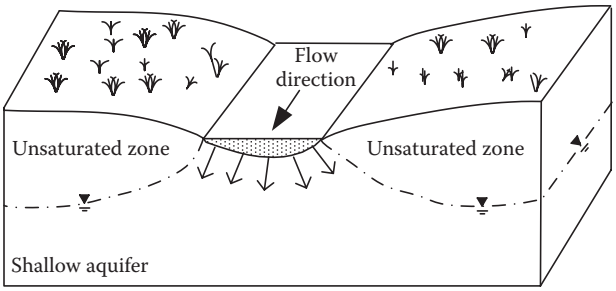

FIGURE 7.36 Stream loses water to groundwater.

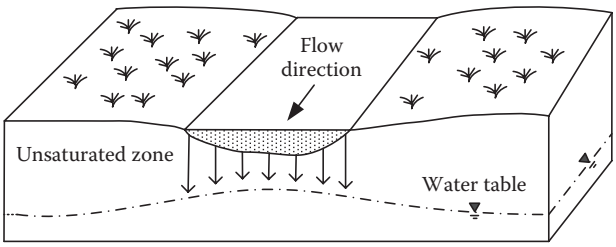

FIGURE 7.37 Disconnected streams.

In order to evaluate the interaction between a stream and the groundwater, it is assumed that water moves vertically through the streambed. Darcy's equation can be used to calculate the rate of flow between the stream and the aquifer:

$$q = -KLWi, \tag{7.83}$$

where K is the vertical hydraulic conductivity of the streambed, L is the length of the stream reach over which seepage is assessed, W is the average width of the stream over the reach, and i is the hydraulic gradient between the stream and the groundwater, which is equal to

$$i = \frac{h_{\text{aquifer}} - h_{\text{stream}}}{M}, \tag{7.84}$$

where h_{aquifer} is the elevation of the groundwater, h_{stream} is the elevation of the stream water surface, and M is the thickness of the streambed.

7.16.3 Bank Storage and Baseflow Recession

Another type of interaction between groundwater and streams is generated when a rapid rise in stream stage happens. Tremendous amounts of water flow from the stream into the stream banks during a period of high flows, such as floods, release from a dam, storm precipitation, or a rapid snowmelt. This flow will contribute seepage through the streambed to the underlying water table, thus saturating the depleted stream-side milieu. It takes a few days or weeks of high flow to replenish the groundwater reservoirs and stream banks return to the stream.

In a rapid rise in the stream, the rising and recession limbs of a hydrograph are generated. Discharge during this decay period is due to the groundwater contributions as the stream drains water from the declining groundwater reservoir. The lower part of the falling limb is called the baseflow recession. The baseflow recession curves represent withdrawal from groundwater storage and it is dependent on the overall topography, drainage patterns, soils, and geology of the watershed.

The process of separating the time distribution of baseflow from the total runoff hydrograph is referred to as "hydrograph separation." The baseflow recession equation is

$$Q = Q_0 e^{-at}, \tag{7.85}$$

where Q is the flow at time t in recession limbs of a hydrograph, Q_0 is the flow at the start of the recession (m^3/s), a is the recession constant for the watershed, and t is the time from the start of the recession.

Because of the steep water level gradient, the initial rate of bank storage discharge is high, but as the gradient decreases, so does groundwater runoff. The recession segment of the stream hydrograph gradually tapers off into what is called a depletion curve. For hydrograph separation, some methods are proposed, such as the master-depletion curve method, constant-discharge baseflow separation, constant-slope baseflow separation, and concave baseflow separation. Some hydrographs for different events in the watershed are needed.

7.16.4 Groundwater and Lakes

Groundwater interaction with lakes is similar to the interactions with streams. A much larger surface water and bed area is involved in lake interaction with the groundwater than with streams. Because of sediments in the lake floor, the permeability of the lake bed is lower than that of streams. It is obvious that lakes can receive groundwater inflow throughout their entire bed, have seepage

loss throughout the entire lake bed, or may receive groundwater inflow in some parts of the bed and lose groundwater inflow in other parts. The same approach of the stream interaction can be applied in order to estimate effects on lakes, wetlands, or any surface water feature on groundwater.

7.17 CONCLUDING REMARKS

In this chapter, the main concepts in dealing with groundwater and its analysis using a systems approach were discussed. Due to the importance of groundwater in securing water supply for society, especially in cases of water shortage, understanding its hydrology and incorporating it in practical situations are important issues. Due to the high number of parameters affecting the groundwater hydrology system's as well as low data availability, developing groundwater models is always challenging task with a high level of uncertainty. These uncertainties should be incorporated in planning and management in real cases.

PROBLEMS

1. Determine the specific yield of the aquifer and change in groundwater storage in an area of 800 km^2; the water table dropped by 0.45 m. The porosity is 32.0% and specific retention is 8.5%.
2. Suppose a 35 cm well penetrates 35 m below static water level (GWT). The pumping rate is 3.5 m^3/day for a long period of time; the drawdowns in the observation wells at 10 m and 30 m from the pumped well are 1.4 and 0.75 m, respectively. Determine (i) the transmissibility of the aquifer, (ii) the drawdown in the pumped well assuming influence radius equal to 250 m, and (iii) the specific capacity of the well.
3. The hydraulic conductivity of a pipe filled with sand is 1.3×10^6 m/s with an effective porosity of 0.15. The hydraulic gradient is 0.05 and the cross-sectional area of the pipe is 250 cm^2. Calculate the discharge and seepage velocities for water flowing through the pipe.
4. A well of size 8 × 4.5 m and depth 6 m in lateritic soil has its normal water level 5 m below ground level. By pumping for 3 h, the water level was depressed to 6 m below ground level and the pumping was stopped. The recuperation rates of the well during 5 h after the pumping stopped are given in Table 7.8. The total volume of water pumped during 3 h of pumping was 60 m^3.

TABLE 7.8
Data for Problem 4

Time Since Pumping Stopped (min)	Water Level Below Ground Level (m)
0	6
15	5.9
30	5.85
45	5.83
60	5.80
90	5.78
120	5.75
180	5.69
240	5.65

Determine (i) the rate of seepage into the well during pumping, (ii) the transmissivity coeficient.

5. Find yield of a well developed in an artesian aquifer for a drawdown of 5 m when the diameter of the well is 30 cm and the thickness of the aquifer is 20 m. The coefficient of permeability is assumed to be 25 m/day. Find the percentage increase in the yield if the diameter of the well is doubled, with the other conditions remaining constant. Assume the radius of influence as 200 m in both cases.
6. Compute the values of S_c and T using the Theis method for a well that is penetrating a confined aquifer that is pumped at a uniform rate of 2700 m^3/day. An observation well is located 75 m away. Drawdowns measured in the observation well during the period of pumping are given in Table 7.9.
7. Determine the porosity of a sample that has a wet bulk density of 2.8 g/cm^3 and a dry bulk density of 1.6 g/cm^3.
8. The specific yield of an aquifer is 2.5×10^{-3}. Determine the pumping rate during this period if the head drop is equal to 0.68 m after 5 years of pumping. The area of the aquifer is 5.3 km^2.
9. Calculate the porosity, effective porosity, specific retention, and specific yield of the soil and the area of the aquifer if the pumping rate of an aquifer is 4.0 m^3/day for a period of 5 years resulting in 1 m head drop. The volume of voids of a 100 cm^3 sample is estimated to be equal to 65 cm^3, out of which water can move through only 50 cm^3.
10. Estimate the storage coefficient of the aquifer where the artesian aquifer thickness is 20 m, the porosity is 26%, and the bulk modulus of compression is 1990 kg/cm^2. What fraction of this is attributable to the expansibility of water? Consider the bulk modulus of elasticity of water as 2.4×10^4 kg/cm^2.
11. Calculate the storage coefficient and the volume of water that is released from a proposed aquifer. The thickness of a confined aquifer is 70 m. The compressibility of the granular medium and water is 3.5×10^{-9} and 4.8×10^{-10}, respectively. The porosity of this aquifer is measured to be equal to 18%. The total head drop is 100 m and the area is 1000 km^2.

TABLE 7.9
Data for Problem 6

Time from Start of Pumping (min)	Observed Drawdown (m)	Time from Start of Pumping (min)	Observed Drawdown (m)
1	0.2	24	0.72
1.5	0.27	30	0.76
2	0.3	40	0.81
2.5	0.34	50	0.85
3	0.37	60	0.88
4	0.41	80	0.93
5	0.45	100	0.96
6	0.48	120	1
8	0.53	150	1.04
10	0.57	180	1.07
12	0.6	210	1.1
14	0.63	240	1.12
18	0.67		

12. Consider an area with an annual rainfall of 870 mm and with a runoff coefficient of 0.38. Its recharge rate from irrigation and the rate of discharge through evapotranspiration are 200 mm/year and 443 mm/year, respectively. The rate of outflow to the rivers is 125 mm/year and the rate of outflow to the other basins is 143 mm/year. Calculate the influent from seepage. Assume the groundwater inflow and outflow remain unchanged. If the minimum baseflow is granted to be 2450 mm/year, calculate the maximum rate of withdrawal that is allowed.
13. Suppose a field sample area of an unconfined aquifer is packed in a test cylinder, the length and the diameter of which are 100 cm and 8 cm, respectively. The period of the test is about 4 min with a constant head difference of 20.3 cm. As a result, 75.6 cm^3 of water is collected at the outlet. Determine the hydraulic conductivity of the aquifer sample.
14. Estimate the discharge under the sheet pile shown in Figure 7.38 using the flownet method. $K = 2.8 \times 10^{-2}$ cm/s.
15. Flow takes place through an 80 mm diameter and 300 mm long soil sample, from top to bottom, as shown in Figure 7.39. The manometers are 120 mm apart, and the water level difference within the two manometers is 100 mm at steady state. If the permeability of the soil is 4.5×10^{-4} cm/s, what is the flow rate?
16. A fully penetrating well pumps water from an infinite horizontal unconfined at a constant rate of 0.64 m^3/s for a long period. Before pumping, the water table is in 20 m. The drawdowns at distances of 65 m from the well were observed 2.5 m. If $K = 4.5 \times 10^{-2}$ m/s, find the drawdowns at distances of 100, 150, and 200 m from the well.
17. In a 25 m thick aquifer with a specific capacity of 0.06 m^3/s m, a partially penetrating well with an effective radius of 0.25 m is located and the length of the screened well bore is 20 m. Calculate the increase in specific capacity if the length of the well screen is increased to 30 and 50 m.
18. A stiff clay layer underlies a 12 m thick silty sand deposit (Figure 7.40). A sheet pile is driven into the sand to a depth of 7 m, and the upstream and downstream water levels are as shown in Figure 7.40. Permeability of the silty sand is 8.6×10^{-4} cm/s. The stiff clay can be assumed to be impervious. The void ratio of the silty sand is 0.72 and the specific gravity of the grains is 2.65.
    a. Draw a flownet and estimate the seepage beneath the sheet pile in m^3/(day·m).
    b. What is the head at the tip of the sheet pile?

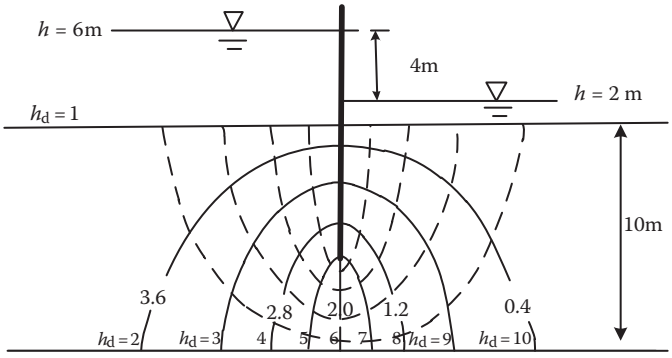

FIGURE 7.38 Seepage beneath a sheet pile.

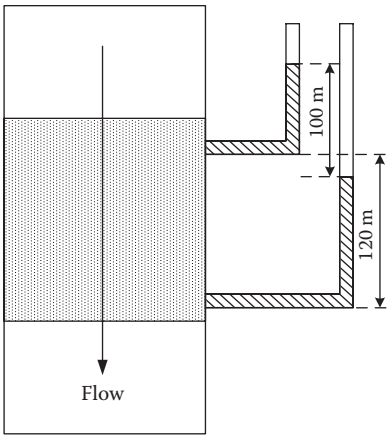

FIGURE 7.39 Proposed manometers of Problem 15.

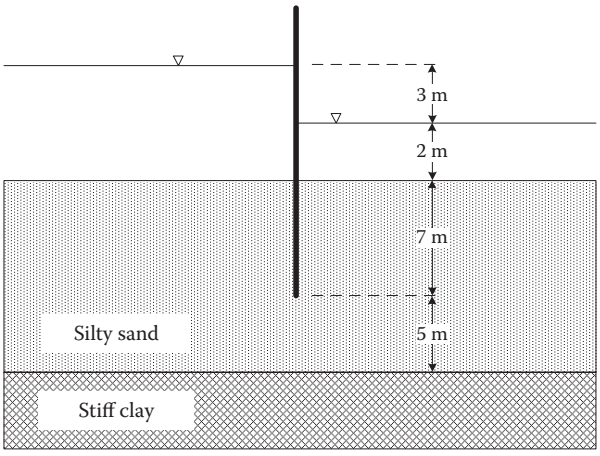

FIGURE 7.40 Seepage beneath a sheet pile in Problem 18.

REFERENCES

Bouwer, H. (1978). *Ground Water Hydrology*, McGraw-Hill, New York.

Bennett, R.R. (1962). Flow net analysis. *U.S. Geol. Surv. Water Supply Paper*. 1536-E, 139–144.

Cooper, H.H. and Jacob, C.E. (1946). "A generalized graphical method for evaluating formation constants and summarizing well field history," *Am. Geophys. Union Trans*., 27, 526–534.

Darcy, H. (1856). Determination des lois d'ecoulement de l'eau a travers le sable. In *Les ontaines Publiques de la Ville de Dijon*, pp. 590–594. Victor Dalmont, Paris.

De Wiest, R.J.M. (1965). *Geohydrology*, John Wiley & Sons, New York.

De Weist, R.J.M. (1966). "On the storage coefficient and the quations of groundwater flow," *J. Geophys. Res*., 71 (4), 1117–1122.

Dingman, S.L. (1994). *Physical Hydrology*, Prentice-Hall, Englewood Cliffs, NJ.

Driscoll, F. (1986). *Groundwater and Wells*, Johnson Division, St. Paul, MN.

Ferris, J.G., Knowles, D.B., Brown, R.H. and Stallman, R.W. (1962). Theory of Aquifer Tests. Water Supply Paper 1536-E. U.S. Geological Survey.

Fetter, C.W. (2001). *Applied Hydrogeology*, 4th edition. Prentice Hall, Upper Saddle River, NJ. ISBN 0-13-088239-9.

Freeze, R.A. and Cherry, J.A. (1979). *Groundwater*, Prentice-Hall International, Hemel Hempstead.

Jacob, C.E. (1940). "Flow of water in an elastic artesian aquifer," *Trans. Am. Geophys. Union*, 21, 574–586.
Hansch, C. and Leo, A. (1979). *Substituent Constants for Correlation Analysis in Chemistry and Biology*, John Wiley and Sons, New York.
Karamouz, M., Ahmadi, A. and Akhbari, M. (2011). *Groundwater Hydrology: Engineering, Planning, and Management*, CRC Press, Boca Raton, FL.
Neuman, S.P. (1975). "Analysis of pumping well data from anisotropic unconfined aquifers considering delayed gravity response," *Water Resour. Res.*, 10 (2), 303–312.
Schwartz, F.W. and Zhang, H. (2003). *Fundamentals of Ground Water*, Wiley, NY.
Snow, D.T. (1969). "Anisotropic permeability of fractured media," *Water Resour. Res.*, 5 (6), 1273–1289.
Theis, C.V. (1935). "The relation between the lowering of the piezometric surface and the rate and duration of discharge of a well using groundwater storage," *Trans. Am. Geophys. Union*, 16, 519–524.
Thiem, G. (1906). *Hydrologische Methoden*, Gebhardt, Leipzig, Germany.
Todd, D.K. (1980). *Ground-Water Hydrology*, 2nd edition, John Wiley and Sons, New York.
Todd, D.K. and Mays, L.W. (2005). *Groundwater Hydrology*, Wiley, Hoboken.
U.S. Bureau of Reclamation (1981). *Groundwater Manual*, U.S. Gov. Printing Office, Denver, CO.
World Meteorological Organization (1998). WMO Statement on the Status of the Global Climate in 1997, Geneva, Switzerland.
WRI (World Resources Institute) (1998). *World Resources, 1998–1999. A Guide to the Global Environment*, Oxford University Press, New York.

8 Time Series Analysis

8.1 INTRODUCTION

The concept of random variables has been widely used for over a century in the field of hydrology and water resources analysis and modeling. Great improvements have been made in recent years in the following fields:

- Understanding the stochastic nature of hydrologic variables such as streamflows and rainfall
- Modeling stochastic hydrological procedures
- Developing new statistical models
- Improving the parameter estimation techniques
- Proposing new model evaluation and fitness tests
- Quantifying uncertainty and imprecision

Forecasting the future state of the resources is necessary for application of operating policies of water resources systems in real-time decision making. For example, in a reservoir, which supplies water for different purposes, the amount of scheduled releases depends on the probable range of inflow to the reservoir. Due to lack of enough knowledge about physical processes in the hydrologic cycle, the application of statistical models in forecasting and generating synthetic data is highly expanded. Furthermore, generation of synthetic data helps to incorporate the uncertainties and probable extreme events in hydrological analyses.

The new advancements in this area have been mainly focused on coupling physical characteristics of the water resources systems and the effects of large-scale climate signals on water resources and early prediction of rainfall and streamflow. In this chapter, basic principles of hydrologic time series modeling and different types of statistical models as well as their application in water resources systems analysis are discussed. Details of statistical modeling are presented in many references such as Salas et al. (1988) and Brockwell and Davis (1987).

However, it is not reliable to suppose non-constant variance in many practical applications of time series modeling and forecasting. The variance of conditional heteroskedasticity or volatility models is not constant. Engle (1982) and Bollerslev (1986) proposed ARCH (the autoregressive conditional heteroskedasticity) and GARCH (the generalized ARCH) to deal with the problem of heteroskedasticity in the errors and also to model and forecast the conditional variance (or volatility).

An appropriate framework for studying volatility clustering (time-varying variance, for example, in which large changes tend to follow large changes, and small changes tend to follow small changes, which is known as conditional heteroskedasticity) is ARCH-type models, which have been well recognized in financial time series. Given that volatility clustering is noticeable in high-frequency financial returns, Franses et al. (2001) used a univariate model for weekly mean Dutch temperature data like GARCH models (Engle 1982; Bollerslev 1986). This modeling procedure has become widely used for modeling financial volatility. Tol (1996) used GARCH(1,1) and AR models for the volatility in daily mean Dutch temperature data. He addressed the seasonality issue by estimating separate models for the summer and winter. Also, Campbell and Diebold (2002) applied an AR-ARCH time series model for average daily US temperature data. Similarly, an AR-GARCH model was applied by Torró et al. (2001) for daily Spanish temperature data. Another application of

the AR-GARCH model is the daily time series of Australian maximum temperatures in the work of Hyndman and Wand (1997), in which the autocorrelation varies throughout the year, which also give an incentive for considering the possible inclusion of time-varying parameters.

This chapter covers the main concepts in hydrologic data analysis and modeling. It starts with an introduction on hydrologic data characteristics and then the issues in data preparation for modeling and analysis. After that, two approaches of data series modeling that are commonly used in hydrologic modeling including autoregressive models and GARCH models are introduced. The application of these models is described through various practical examples and it is demonstrated how the performance of these models can be quantified and examined to select the best one among the variety of models.

8.2 STOCHASTIC PROCESSES

All natural physical processes are subject to variability. For example, rainfall intensity, flood magnitude, or low flows in severe droughts have wide range variations. To study these variations and incorporate them in planning and operation of water resources, samples of data are collected. Because of the unpredictable nature of natural hydrological processes in the future, it is assumed that each data record is a representation of a random variable.

The hydrologic cycle is composed of different phenomena such as precipitation, runoff, infiltration, evaporation, evapotranspiration, abstraction, etc. Different characteristic variables that can be simply called hydrologic variables have been defined for describing each of these phenomena. Depth or intensity of rainfall in different time steps of a rainstorm, monthly inflow discharge to a reservoir, and daily evaporation are some examples of hydrologic variables (Shahin et al. 1993). A data set consists of a series of measurements of a phenomenon, and the quantities measured are termed variables. Hydrologic variables usually vary in time and space. A sequence of values arranged in their order of occurrence in time is called a time series.

The mathematical description of the behavior of a phenomenon in one or more dimensions in space and/or time is called a process. Due to variability of hydrologic phenomena in space or time, they are called hydrologic processes. The processes including a random component are called stochastic processes. A stochastic process is a family of random variables described in probability space.

The stochastic processes include two groups: stationary and nonstationary processes. In a stationary process, the expected values of statistical descriptors are fixed over time. For examination of a time series stationarity, the time series is divided into some non-overlapping subseries and the expected values of statistical description of each series are determined. For a stationary time series, statistical description of subseries should be the same.

The hydrologic variables are commonly nonstationary, because of variations resulting from natural and human activities. The main components of a hydrologic time series are as follows:

- Trend: This is a unidirectional and gradual change (increasing or decreasing) in the time series average value. The over-year trends are mainly a result of anthropogenic changes in nature. The trend is smooth and deterministic, and it can be modeled by a continuous and differentiable function of time such as the following:

$$\text{Linear form: } T_t = a + bt$$

$$\text{Polynomial form: } T_t = a + bt + ct^2 + \cdots + dt^m$$

$$\text{Power form: } T_t = a - br^t \quad (0 < r < 1) \quad \text{and} \quad T_t = 1/(a + br^t)(0 < r < 1)$$

- Jump: This is a sudden change in the time series in positive or negative direction caused commonly by human activities and natural disruptions.
- Periodicity: This refers to the cyclic variations in the hydrologic time series. These variations are repeated in fixed intervals.
- Randomness: These variations are the result of the uncertain nature of the stochastic process. This component of the hydrologic time series can be autoregressive or purely random.

In statistical modeling of time series, it is assumed that the time series is purely random. Therefore, different steps should be taken to remove trends, jumps, and periodicity from the data.

8.3 TIME SERIES

The measurements or numerical values of any variable that changes with time constitute a time series. In many instances, the pattern of changes can be ascribed to an obvious cause and is readily understood and explained, but if there are several causes for variation in the time series values, it becomes difficult to identify the several individual effects. In Figure 8.1, the top graph shows a series of observations changing with time along the abscissa; the ordinate axis represents the changing values of y with time t.

From visual inspection of the series, there are three discernible features in the pattern of the observations. Firstly, there is a regular gradual overall increase in the size of values; this trend, plotted as a separate component $y_1(t)$, indicates a linear increase in the average size of y with time. The second obvious regular pattern in the composite series is a cyclical variation, represented separately by $y_2(t)$, the periodic component. The third notable feature of the series may be considered the most outstanding, the single high peak halfway along the series. This typically results from a rare catastrophic event, which does not form part of a recognizable pattern. The definition of the function $y_3(t)$ needs very careful consideration and may not be possible. The remaining, hidden feature of the series is the partly random stochastic component, $y_4(t)$, which represents an irregular but continuing variation within the measured values and may have some persistence. It may be due to instrumental

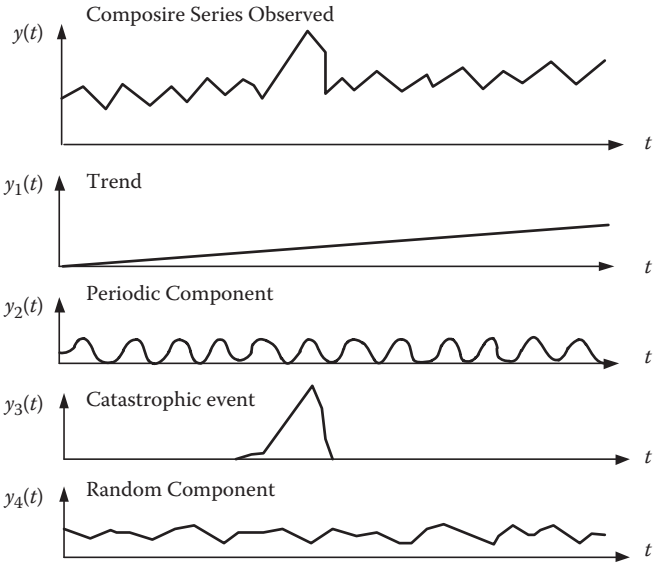

FIGURE 8.1 Time series components.

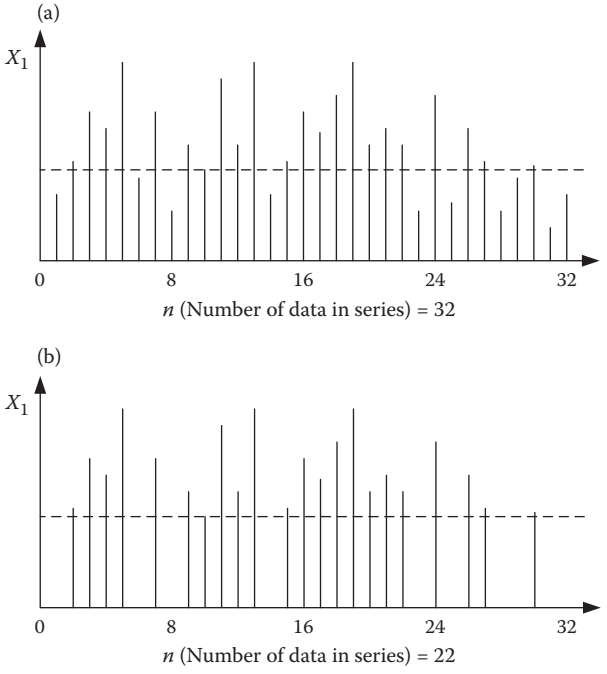

FIGURE 8.2 (a) Complete and (b) partial duration series.

or observational sampling errors or it may come from random unexplainable fluctuations in a natural physical process. The complete observed series, $y(t)$, can therefore be expressed by

$$y(t) = y_1(t) + y_2(t) + y_3(t) + y_4(t). \tag{8.1}$$

The first two terms are deterministic in form and can be identified and quantified fairly easily; the last two are stochastic with major random elements and some minor persistence effects and are less easily identified and quantified.

Various time series are developed using different methods of sampling hydrological time series data. Some of the main types of time series are as follows: complete duration series, partial duration series, and extreme values series. If given time series data cover all the available data from a start point to its end point, it is called a "complete duration series." "Partial duration series" is a series that contains only a number of data that fulfill a condition such as being larger than a certain value (like average value). Eliminating some data may happen in partial duration series in a way that several years (or time durations) fall in this situation. Figure 8.2 show complete duration series and partial duration series.

It is sometimes necessary to have data for each year; therefore, "extreme values series" is used, and it depends on circumstances whether to choose minimum or maximum values in a time series. Two of the most important extreme values time series are "annual maximum series" and "annual minimum series."

8.4 HYDROLOGICAL TIME SERIES

The composition of a hydrological time series depends on the nature of the variable and its mode of measurement. The variable may be continuous, like the discharge of a perennial stream, or intermittent, as with precipitation. There are differences according to climatic regime since river flow may

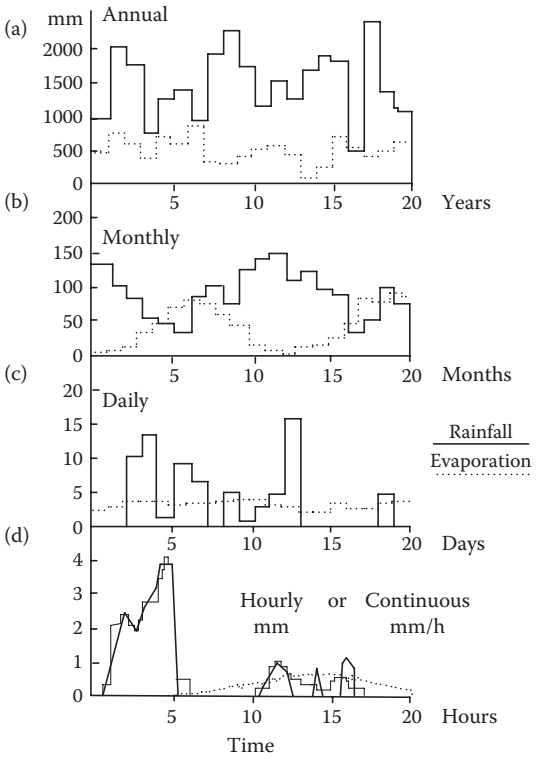

FIGURE 8.3 Samples of rainfall and evaporation data for a (a) 20-year, (b) 20-month, (c) 20-day, and (d) 20-h period.

not be continuous in semi-desert regions. For a more unusual example, the time series of water loss by evaporation and transpiration is fundamentally affected by vegetation type, and in those regions with scarce vegetation, daily evaporation losses become intermittent and depend on the infrequent rains.

The sampling of a continuous variable usually results in the data being recorded at discrete times or over discrete time intervals; most time series of hydrological variables are considered in the discrete form. The length of the time interval used in assembling the data series is quite fundamental to the resultant composition of the time series. The examples used in Figure 8.3 are for different locations and over unrelated time periods.

8.4.1 Rainfall

Typical patterns of rainfall data for different discrete time intervals of a typical range are shown in Figure 8.3. Four samples each of 20 time units in length are given for time units of a year, a month, a day, and an hour. The annual rainfall totals appear randomly scattered around some mean value, but no distinctive features of the series are immediately discernible. The monthly data, beginning in January, show clear signs of a periodic component, viz., an annual cycle, with minima in the summer months and maximum monthly totals in winter. Such a cycle is a regular feature of the rainfall patterns at the considered region, although individual monthly totals can be variable from year to year. The sequence of daily rainfall totals (Figure 8.3c) shows a very different pattern. There are many nil values. Such a different time series requires special treatment in any analysis. The discontinuity of short-period rainfalls is emphasized in the time series over 20 h. Discrete and continuous

representations have been drawn to demonstrate that even on a day with rain, the rainfall is not continuous throughout the day.

The annual values of evaporation are less variable than rainfall. The monthly evaporation totals have a more regular periodic component with the maxima in the warm summer months. Winter values are very low. On the whole, evaporation values are more conservative than rainfall, i.e., there is less variability from year to year. The summer month of July is selected to give a sample of likely daily totals; the occasional days with low evaporation would correspond to spells of dull, cool weather, which do occur in the summer, but the daily values provide a continuous discrete time series (Figure 8.3c). The continuous curve of the 20-h graph represents the actual rate of evaporation (mm/h), which is likely to occur on a sunny day in July (Figure 8.3d). Evaporation, negligible during the night, begins at dawn and reaches a maximum in the warmest part of the day in the afternoon. Certain irregularities in the curve would be caused by clouds inhibiting the incoming solar radiation. Thus, hourly evaporation sequences also form an interrupted time series with regular diurnal nil values.

8.4.2 Runoff

River flow records can be represented as time series of runoff expressed in millimeters of equivalent water depth over a catchment area, for ease of comparison with the other variables (Figure 8.4). The

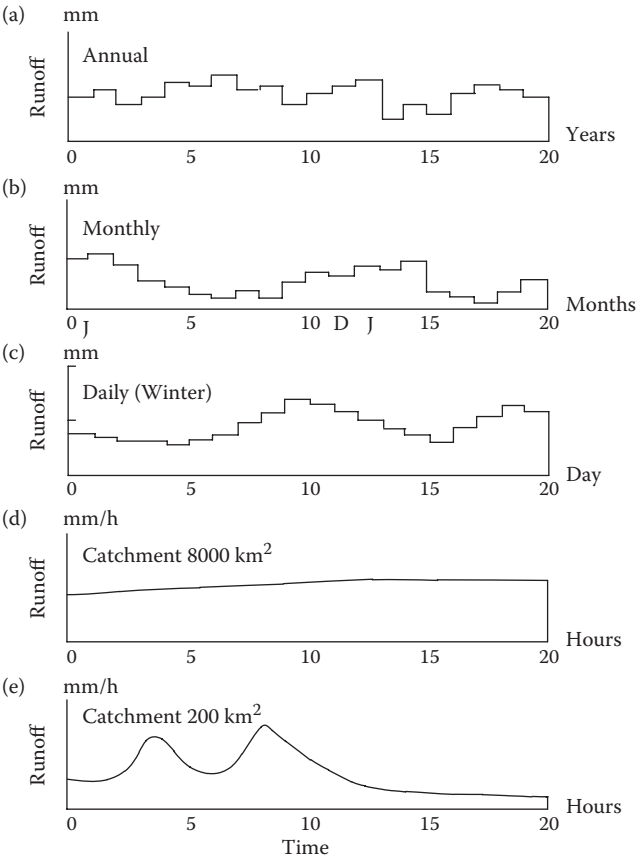

FIGURE 8.4 Runoff time series (a) in annual time scale, (b) in monthly time scale, (c) in daily time scale, (d) in hourly time scale for a typical catchment of 8000 km^2 area, and (e) in hourly time scale for a typical catchment with an area of 200 km^2.

annual values resemble those for rainfall or evaporation with no pronounced time series component; the individual values are less variable than the rainfall (Figure 8.4a). The monthly values of rainfall also show a periodic component, the annual cycle of runoff following the rainfall pattern, but the minima tend to be delayed to the late summer (Figure 8.4b). There is a lag effect from the low early summer rainfalls and peak evaporation months. The discrete values of the daily mean flows for a sequence of 20 days emphasize the continuing nature of river flows. There is no regular pattern in the time series over the 20 days shown in Figure 8.4c; the two increases in runoff would be directly related to the primary causes, two significant rainfall events (cross-correlation between two daily time series of rainfall and runoff could give a measure of catchment response to rainfall). In the last two runoff graphs (Figure 8.4d and e), both on an hourly basis, the distinction is drawn between the continuous records from a large and a small catchment. At a gauging station on a river draining 8000 km^2 (Figure 8.4d), a rainfall event can be expected to have a very slow and smoothed response, but from a small catchment of 200 km^2 area (Figure 8.4e), distinct hydrographs are quickly produced in response to distinct rainfall amounts. The presentation of the hourly runoff sequences in Figure 8.4 emphasizes the persistence between hourly discharge values. Daily discharges also exhibit this feature, but to a lesser extent. Hourly and daily discharges are not independent of each other. Even on a monthly basis, the mean discharge is generally dependent on that of the previous months to some extent. This correlation between data in a plotted time series, although possibly less obvious to the eye than trend and periodicity, has nevertheless to be identified and quantified in any time series analysis.

8.5 HYDROLOGIC TIME SERIES MODELING: BASIC STEPS

A systematic approach to hydrologic time series modeling could consist of the following main steps (Salas et al. 1988):

1. Data preparation: Removing trends, periodicity, outlying observations, and fitting the data to normal distribution by applying proper transformations.
2. Identification of model composition: In this step, it should be decided whether a univariate or a multivariate model, or a combination of each of these models with disaggregation models should be used. This decision can be taken based on the characteristics of the hydrologic system and available data.
3. Identification of model type: Different types of models such as autoregressive (AR), autoregressive moving average (ARMA), and autoregressive integrated moving average (ARIMA) as well as GARCH can be selected in this step. The details of these models are presented in the next sections of this chapter. Statistical characteristics of the time series and the modeler input and knowledge about different types of models are the key factors in identification of model type.
4. Identification of model form: Form of the selected model should be defined based on the statistical characteristics of the time series. The periodicity of the data and how it can be considered in the structure of the selected model is the main issue in this step.
5. Estimation of model parameters: Different methods such as method of moments and method of maximum likelihood can be used for estimating the model parameters.
6. Testing the goodness of fit of the model: In this step, different assumptions such as independence and normality of residuals should be checked. Different statistics are used for verifying these assumptions, which are briefly explained in the next sections.
7. Evaluation of uncertainties: In evaluating the uncertainties, model, parameter, and natural uncertainties in data should be analyzed separately. Model and parameter uncertainties should be evaluated in this step. Model uncertainty may be evaluated by testing whether significant differences in the statistics generated by alternative models exist. Parameter uncertainty may be determined by finding the distribution of parameter estimates, and by using the models with parameters sampled from such distributions.

8.6 DATA PREPARATION

The main issues in data preparation in summary are as follows:

- Removing trend
- Removing outlying observations
- Removing periodicity
- Fitting the data to normal or other well-known distributions by applying proper transformations

8.6.1 Removing Data Trend

The principal assumption in using statistical models for hydrologic time series is that the variable is considered as purely random. Therefore, if the series contains unnatural components such as regulated release from reservoirs or trend, they should be first removed. The time series plot can be used for trend and seasonality detection. The sample autocorrelation functions, which are slowly decaying and nearly periodic, also show the trend and seasonality.

For example, consider x_t, for a t time series with no seasonality, which contains trend component as follows:

$$x_t = T_t + z_t, \tag{8.2}$$

where T_t and z_t are the trend and random components, respectively. The trend components can be usually defined as a function of time as

$$T_t = f(\mathrm{t}, \cdots, tm, \beta_1, \cdots, \beta_m), \tag{8.3}$$

where $\beta_1, \cdots, \beta_m$ are trend function parameters. For example, the linear trend function can be defined as

$$T_t = \alpha t + \beta. \tag{8.4}$$

The parameters of the trend model can be estimated based on the least-squares method by minimizing the following sum:

$$\sum_t (x_t - T_t)^2. \tag{8.5}$$

For this purpose, the partial derivatives of the above sum with respect to each of the parameters, $\beta_1, \cdots, \beta_m$, are equal to zero.

Example 8.1

A series of annual runoff in a river for a period of 10 years is shown in Table 8.1. Estimate a linear trend function and generate the random series of runoff by removing the trend.

Solution:

The linear trend function was given in Equation 8.4. Using the least-squares method (which is described in Section 8.8.2) for estimation of model parameters, the following sum should be minimized:

TABLE 8.1
Annual Runoff in a River in Example 8.1

Year	Runoff (MCM)
1	61
2	66
3	71
4	73
5	80
6	94
7	96
8	107
9	128
10	137

$$\sum_{t=1}^{10}\left(x_t - T_t\right)^2 = \sum_{t=1}^{10}\left(x_t - \alpha t - \beta\right)^2$$

α and β can be calculated as

$$\alpha = \frac{10\sum_{t=1}^{10} t x_t - \sum_{t=1}^{10} t \sum_{t=1}^{10} x_t}{10\sum_{t=1}^{10} t^2 - \left(\sum_{t=1}^{10} t\right)^2} = 8.37$$

$$\beta = \bar{x} - \alpha \bar{t} = 45.3.$$

In Table 8.2, the estimated trend and random components (after subtracting the trend component) of runoff in each year are given.

TABLE 8.2
Random Components of Annual Runoff in Example 8.1

Year	Runoff (MCM)	Trend Component	Random Component
1	61	53.64	61 – 53.64 = 7.36
2	66	62.01	3.99
3	71	70.38	0.62
4	73	78.75	–5.75
5	80	87.12	–7.12
6	94	95.48	–1.48
7	96	103.85	–7.85
8	107	112.22	–5.22
9	128	120.59	7.41
10	137	128.96	8.04

Using the above method, series can be decomposed into trend, seasonality (if it is available), and random components. Another method for removing trend and seasonality is differencing, which is widely used in modeling of hydrologic time series. The first differencing operator, ∇, is formulated as follows:

$$\nabla(x_t) = x_t - x_{t-1} = (1 - B)x_t, \tag{8.6}$$

where B is the backward shift operator performing as follows:

$$B(x_t) = x_{t-1}. \tag{8.7}$$

The higher orders of the operators B and ∇ can be defined as follows:

$$\begin{cases} B^i\left(x_t\right) = x_{t-j} \\ {}^{j}\left(x_t\right) = \left({}^{j-1}(x_t)\right), \quad j \geq 1 \end{cases} \tag{8.8}$$

Application of the first-order difference operator to the linear trend function (Equation 8.4) results in the constant function of $\nabla(T_t) = \alpha$. Similarly, a polynomial trend of k order can be summarized in a constant through application of the operator ∇^k. Therefore, if a polynomial trend is detected in a hydrologic time series as

$$T_t = \sum_{i=0}^{m} a_i t^i, \tag{8.9}$$

it can be written using the differencing operator as follows:

$$\nabla^m (x_t) = m!\, a_m + \nabla^m z_t, \tag{8.10}$$

where z_t is the random variable.

Example 8.2

Remove the trend of the given time series in Example 8.1, using the differencing operator.

Solution:

In the previous example, it was shown that the given time series have a linear trend; therefore, it is sufficient to use the differencing operator once to remove the data trend. The differenced time series is given in Table 8.3.

The base time series and differenced time series are illustrated in Figure 8.5. As it can be seen in this figure, the trend of time series is successfully removed. Based on Equation 8.5, the average of the differenced time series would be equal to the slope of the trend line. This value has been determined to be 8.67, which is close to the result of the previous example.

TABLE 8.3
Times Series and Difference in Example 8.2

Year no.	Time Series	Difference
1	61	–
2	66	5
3	71	5
4	73	2
5	80	7
6	94	14
7	96	2
8	107	11
9	128	21
10	137	9

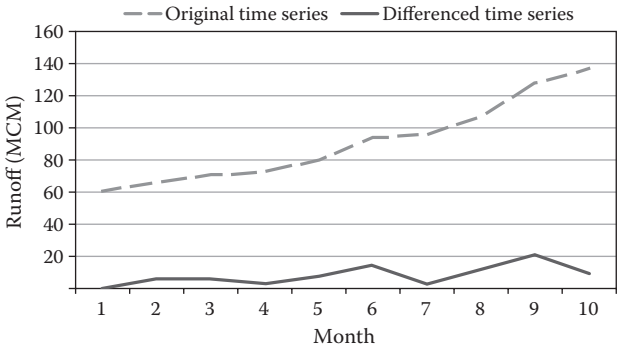

FIGURE 8.5 Comparison between the base and differenced time series in Example 8.2.

8.6.2 Jump

Jump or slippage in hydrological time series happens due to systematic error or inhomogeneity caused by humans and occurs gradually by natural phenomena or rapidly by building dams and water diversions. The values with considerable distance from the mean value should be checked for being a jump. For example, values with more than 3σ (standard deviation) from the mean can be a jump.

It is not expected that these variations be continued; therefore, they must be taken away from time series data. The removed data can be replaced with the long-term average, the average of two adjacent values or other logical values if the complete time series is needed.

8.6.3 Periodicity (Seasonality)

The repetition of a periodic component in time series data is mainly because of the periodicity of day and night, seasons, and years. Periodicity means that statistical specifications vary periodically by time. Two major approaches are available in order to determine the periodicity in time series, namely, parametric and spectral analysis approaches. The second one uses Fourier series in data preparation for modeling purposes.

8.6.4 Time Series Memory

The long-term memory of time series is defined based on the frequency of the extreme events during the time of study. In hydrological analysis used for design of water resources, the time series with a length of 500 to 1000 are produced to involve the expected number of extreme events in the time series. The long-term wet and dry periods that are observed in these long-term series highly affect the design and planning of water resources.

Analysis of frequency or long-term memory of time series is considered against the short-term memory. To analyze the adequacy of the considered length of time series, the Hurst coefficient can be employed, which is discussed in the next section.

8.6.4.1 Hurst Coefficient

The Hurst coefficient is a measure for checking the adequacy of the length of considered time series. In other words, it determines the long-term memory of a time series. Hurst et al. (1965) used this measure for the first time for evaluating the adequacy of the length of river flow time series in reservoir simulation. This measure determines if the considered length of data involves all of the expected extreme events or not. If the series involves the expected extreme events, it can be used in designs that are based on extreme events; otherwise, the appropriate methods should be used to expend the data length. The Hurst coefficient is estimated as follows:

$$K = \frac{\log(R/\sigma)}{\log(N/2)}, \tag{8.11}$$

where N is the number of data in the considered time series and σ is the standard deviation of the series. R is called range, and it shows the highest surplus and lowest deficit compared to a target release (i.e., average mean flow). R is estimated as follows:

$$R = S^{+} - S^{-}, \tag{8.12}$$

where S^{+} is the maximum positive cumulative distance from the mean value of the time series and S^{-} is the maximum negative cumulative distance from the mean value of the time series. The values of S are calculated in each time step, S_n, as follows:

$$S_n = \sum_{k=1}^{n} \left(X_k - \bar{X}\right), \tag{8.13}$$

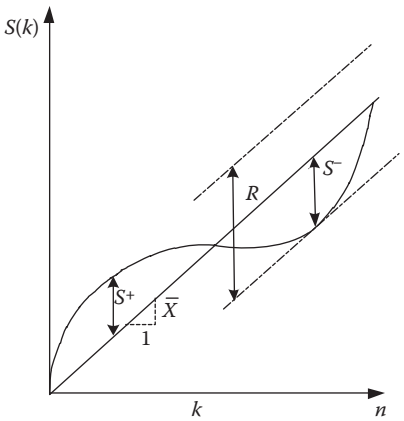

FIGURE 8.6 Estimation of Hurst coefficient parameters.

where X_k is the recorded value in time step k and $\bar{X}$ is the average of the time series. The process of the estimation parameter of R is shown in Figure 8.6.

Hurst analyzed different annual time series of flow, temperature, etc. with this method and concluded that the Hurst coefficients close to 0.5 are shown in independent series, while values greater than 0.5 show the longer memory of time series, which shows the necessity of extending the available time series of data.

8.6.5 Data Normalization

Most of the parameter estimation methods are based on the assumption that the time series follows the normal probability distribution. However, most of the hydrologic time series do not follow normal distribution; instead, they are asymmetrically distributed or can only get positive values. Therefore, it is often necessary to transform those variables to normal before statistical modeling. Different transformations have been used in hydrologic time series analysis. For example, many have found that the two-parameter log-normal distribution fits the annual series of precipitation and runoff in the United States (Salas et al. 1988). Therefore, if we show these series by X, the following transformation yields normal series, Y:

$$Y = \log(X). \tag{8.14}$$

If a two-parameter gamma probability distribution function is used for the annual series, X, then the following transformation yields a relatively normal distribution of Y:

$$Y = \sqrt{X}\,. \tag{8.15}$$

The following two-parameter transformation, which was first developed by Box and Cox (1964), has been used by many researchers:

$$z_t = \frac{\left(x_t + \lambda_2\right)^{\lambda_1} - 1}{\lambda_1 g^{(\lambda_1 - 1)}} \quad \lambda_1 > 0 \tag{8.16}$$

and

$$z_t = g \cdot \ln(x_t + \lambda_2) \quad \lambda_1 = 0, \tag{8.17}$$

where λ_1 and λ_2 are the model parameters, g is the geometric mean of $x_t + \lambda_2$, and x_t and z_t are the observed and transformed values, respectively. The first parameter λ_1 governs the strength of the transformation. $\lambda_1 = 1$ corresponds to the observed data and $\lambda_1 = 0$ corresponds to a logarithm. Values are scaled by the geometric mean to keep the variance constant, thus allowing for first comparison of mean squared errors between two different transformations.

Hashino and Delleur (1981) applied the following equation similar to the Box–Cox transformation:

$$z_t^{(\lambda)} = \frac{\left(x_t + c\right) - 1}{\lambda} \quad \lambda \neq 0 \tag{8.18}$$

and

$$z_t^{(\lambda)} = \ln\left(x_t + c\right) \quad \lambda = 0, \tag{8.19}$$

where λ and c correspond to λ_1 and λ_2 in the Box–Cox transformation. The values in the transformation are not scaled by the geometric mean and, therefore, do not allow for the direct comparison of mean squared errors between two different transformations. Delleur and Karamouz (1982) applied the following transformation on annual data for the Gunpowder and Patapsco rivers:

$$z_t = (x_t + a)^b \quad b \neq 0 \tag{8.20}$$

and

$$z_t = \log(x_t + a) \quad b = 0, \tag{8.21}$$

where a and b are the transformation parameters.

An informal approach to testing normality is comparing the histogram of the sample data with the normal probability curve. The histogram of the data should be bell shaped if it follows the normal distribution, but this is difficult to see especially when the sample size is small. The most commonly used method for testing the hypothesis that a given time series is normal is the graphical test. In this case, the data are regressed against the quantiles of a normal distribution with the same mean and variance as the sample. If data do not fit to the regression line, it can be concluded that there is a departure from normality.

A graphical tool for assessing normality is the normal probability plot, a quantile–quantile plot ($Q - Q$ plot) of the standardized data against the standard normal distribution. An example is shown in Figure 8.7. In this method, data are plotted against a theoretical normal distribution. If data follow the normal distribution, the points will form a straight line. Deviations from the straight line are indicators of deviations from normality. In the normal probability plot, the vertical axis is the ordered response values and the horizontal axis is normal order statistic medians or means. These values, z_i, are calculated as follows:

$$P\left(Z < z_i\right) = \begin{cases} 1 - 0.5^{1/n} & \text{for } i = 1 \\ 0.5^{1/n} & \text{for } i = n \\ \dfrac{i - 0.3175}{n + 0.365} & \text{otherwise} \end{cases} \tag{8.22}$$

In other words, in graphical normality test, the sample values are plotted against the expected values if they follow completely the normal distribution. If the sample values are taken from a normal distribution, the scatter of points will form a straight line. By increasing the distance of points from this line, the data are further from normality. The acceptable distance from the straight line to consider data as normal is dependent on the sample size. For large samples with more than

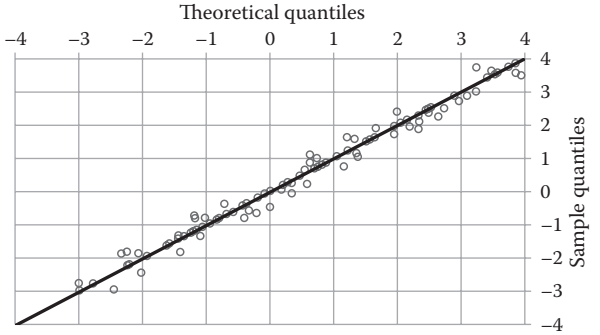

FIGURE 8.7 Example of graphical test of normality.

100 features, it is expected that the points be very close to the normal line. However, smaller samples, even with large departures from a straight line, can still be consistent with a normal sample.

The chi-square test has also been widely used for testing the normality of data. The test statistic and the procedure of testing the goodness-of-fit hypothesis are presented in Section 8.10.1. Another normality test, which is widely used in practice, is the skewness test. The skewness coefficient of a time series x_t is estimated as follows:

$$\hat{\gamma} = \frac{\frac{1}{N}\sum_{t=1}^{N}\left(x_t - \bar{x}\right)^3}{\left[\frac{1}{N}\sum_{t=1}^{N}\left(x_t - \bar{x}\right)^2\right]^{3/2}}, \tag{8.23}$$

where N is the number of sample data and $\bar{x}$ is the sample average. The skewness test is based on the fact that the skewness coefficient of a normal variable is zero. If the series is normally distributed, $\hat{\gamma}$ is asymptotically normally distributed with a mean of zero and a variance of $6/N$ (Snedecor and Cochran 1967) and $(1 - \alpha)$ probability limits on γ is defined as

$$\left[-u_{1-\alpha/2}\sqrt{6/N},\quad u_{1-\alpha/2}\sqrt{6/N}\right], \tag{8.24}$$

where $u_{1-\alpha/2}$ is the $1 - \alpha/2$ quantile of the standard normal distribution. Therefore, if $\hat{\gamma}$ falls within the limits of Equation 8.24, the hypothesis of normality is accepted. Otherwise, it is rejected. Snedecor and Cochran (1967) recommend the above procedure when the sample size is greater than 150. For smaller sample sizes, they suggest comparing the computed coefficient of skewness with the tabulated values ($\gamma_\alpha(N)$) presented in Table 8.4. If $|\hat{\gamma}| < \gamma_\alpha(N)$, the hypothesis of normality is accepted.

TABLE 8.4
Table of Skewness Test for Normality for Sample Size Less Than 150

N	$\alpha = 0.02$	$\alpha = 0.01$
25	1.061	0.711
30	0.986	0.662
35	0.923	0.621
40	0.870	0.587
45	0.825	0.558
50	0.787	0.534
60	0.723	0.492
70	0.673	0.459
80	0.631	0.432
90	0.596	0.409
100	0.567	0.389
125	0.508	0.350
150	0.464	0.321
175	0.430	0.298

Source: Snedecor, G. W., and Cochran, W. G., *Statistical Methods*, 6th ed., The Iowa State University Press, Ames, 1967. With permission.

Example 8.3

The logarithmic transformation is applied to bring the probability distribution of monthly streamflows closer to normal distribution, as follows:

$$y_t = \log_{10}(x_t),$$

where x_t and y_t are the observed and the transformed streamflow series in month t, respectively. Consider the data are available for 85 years. The skewness coefficient of the transformed series is estimated to be 0.8. Use the skewness test and comment on the normality of the transformed data.

Solution:

If the 5% significance level is selected, the 95% probability limits on the skewness coefficient can be estimated using Equation 8.24:

$$\left[-u_{0.975}\sqrt{6/N},\quad u_{0.975}\sqrt{6/N}\right]=\left[-1.96\sqrt{6/1020},\quad 1.96\times\sqrt{6/1020}\right]=[-0.15,\ 0.15].$$

Because 0.8 does not fall within the above limits, the series is not normally distributed.

8.6.6 Time Dependency

The modeling of a hydrologic time series usually assumes that the stochastic component, after removing periodic components and time dependence structure, is an independent and normally distributed series (Salas et al. 1988). The basic statistical representation of time dependence structure is the correlogram, which shows the fluctuations of the autocorrelation coefficient of the series with different lags. The autocorrelation coefficient, which is a dimensionless measure of linear dependence, can be estimated as follows:

$$r_k = \frac{\sum_{t=1}^{N-k}\left(x_t-\bar{x}\right)\left(x_{t+k}-\bar{x}\right)}{\sum_{t=1}^{N}\left(x_t-\bar{x}\right)^2}, \tag{8.25}$$

where r_k is the lag-k autocorrelation coefficient and $\bar{x}$ is the sample mean. For an independent series, the population correlogram is equal to zero for $k \neq 0$. Correlograms of samples of independent series show fluctuations around zero, but they are not necessarily equal to zero due to sampling variability. Anderson (1942) determined probability limits for the correlogram of independent series as follows:

- Anderson Test of Independence in Time
  Anderson (1942) gave the following limits with 95% and 99% probability levels:

$$r_k(95\%) = \frac{-1 \pm 1.645\sqrt{N-k-1}}{N-k} \tag{8.26}$$

$$r_k(99\%) = \frac{-1 \pm 2.326\sqrt{N-k-1}}{N-k}, \tag{8.27}$$

where N is the sample size. Based on this test, the autocorrelations, which fall outside of the probability limit, show significant time dependence. Otherwise, the series can be considered as an independent series.

- Turning Point Test of Randomness

  Consider the time series x_t are observations of a random sequence. The time t is considered as a turning point when $x_{t-1} < x_t$ and $x_t > x_{t+1}$ or $x_t < x_{t-1}$ and $x_t < x_{t+1}$. The expected number of turning points is (Brockwell and Davis 1987):

$$\mu_{T_p} = \frac{2(n-2)}{3}. \tag{8.28}$$

The variance of number of turning points can be determined as follows:

$$\sigma^2_{T_p} = \frac{(16n-29)}{90}. \tag{8.29}$$

It can be demonstrated that the number of turning points (T_p) for a random sequence has a $N\left(\mu_{T_p}, \sigma^2_{T_p}\right)$ distribution. Hence, the assumption that x_t is a random sequence is rejected if

$$\frac{\left|T_p - \mu_{T_p}\right|}{\sigma_{T_p}} > u_{1-\alpha/2}, \tag{8.30}$$

where $u_{1-\alpha/2}$ is the $(1 - \alpha/2)$ percentage point of a standard normal distribution.

Example 8.4

A series of residuals of a model fitted to precipitation data in a station in 20 time intervals is given in Table 8.5. Use the turning point test and comment on the randomness of the residuals.

TABLE 8.5
Series of Residuals in Example 8.4

Month	Residual	Month	Residual
1	0.85	11	0.29
2	0.43	12	0.42
3	0.29	13	0.38
4	0.43	14	0.18
5	0.22	15	0.49
6	0.20	16	0.62
7	0.32	17	0.05
8	0.19	18	0.77
9	0.86	19	0.29
10	0.91	20	0.25

Solution:

The turning points occurred in months 3, 4, 6, 7, 8, 10, 11, 12, 14, 16, 17, and 18. The expected value and variance of the number of turning points can be estimated using Equations 8.28 and 8.29:

$$\mu_{T_p} = \frac{2(20-2)}{3} = 12 \text{ and}$$

and

$$\sigma_{T_p} = \sqrt{\frac{(16\times 20-29)}{90}} = 1.80.$$

The statistic of testing the randomness is estimated using Equation 8.30 as follows:

$$\frac{|12-12|}{1.8} = 0$$

which is less than the critical value of $N(0,1)$ distribution with 5% significance level ($u_{1-0.05/2}$ = 1.96). Thus, the assumption of randomness is accepted.

8.7 TIME SERIES MODELING IN HYDROLOGY

It is impossible to know the exact mathematical models of hydrologic time series, and only approximations are made for the inferred population. Since the exact model parameters in hydrology must be estimated from limited data, they will never be known precisely. Theoretically, time series modeling or stochastic modeling of hydrologic series refers to the estimations of models and their parameters from available data.

Even though the improvement of time series modeling in hydrology has reached a level of complexity, unfortunately, simple methods are the basis of most time series modeling in practice. Here, there is an attempt to describe up-to-date advances in modeling in a systematic step-by-step approach, including various details and examples of modeling hydrologic time series.

Generally, an important step towards modeling a hydrologic time series is the identification of the model composition, which could be a univariate or multivariate model, or a combination of a univariate and a disaggregation model, or a combination of a multivariate and a disaggregation model, etc. After identifying the model composition, the type of the model(s) must be selected. Types of models could be AR (autoregressive), ARMA (autoregressive moving average), ARIMA (autoregressive integrated moving average), or any other model that is available in stochastic hydrology. An important deciding factor in the selection of the type of model is the statistical characteristics of the samples of hydrologic series. For example, ARMA models are required rather than AR models for a series with low decaying correlograms (long memory). Lastly, other factors such as time limitation to solve a particular problem, funds for computer time, and availability of readymade programs of alternative models also contribute in the decision of selecting the type of model. Furthermore, the identification of the form of model must be done. The statistical characteristics of the historic time series are important for such model identification. When the model identification is done, the estimation of the parameters of the model must be made. An appropriate method of estimation, such as the method of moments and the (approximate) method of maximum likelihood, should be selected. The estimated parameters must be checked in order to comply with certain conditions of the model. An alternative form of the model must be selected if these conditions are not met.

8.8 METHODS OF PARAMETER ESTIMATION

Method of moments, least squares, and maximum likelihood are three basic methods for estimating model parameters. These methods are explained in the following subsections:

8.8.1 Method of Moments

Consider a sample $x_1,\cdots, x_N$. The nth sample moment about a point c is defined as follows:

$$M_n = \left(\frac{1}{N}\right)\sum_{i=1}^{N}\left(x_i - c\right)^n, \tag{8.31}$$

where N is the number of data in the sample. In case of central moment, the c is replaced with the sample mean. Assume a model is fitted to the sample as follows:

$$\hat{x}_i = f\left(x_{i-1}, x_{i-2}, \cdots, \alpha_1, \alpha_2, \cdots, \alpha_m\right) + \varepsilon_i, \tag{8.32}$$

where ε_i is the model residual and $\alpha_1,\alpha_2,\cdots,\alpha_m$ are the model parameters. Then, the population moments of the series generated by this model are functions of model parameters. Therefore, the parameter estimates can be obtained by equating sample moments and population moments. In other words, the moments' method performs as follows:

$$M_n = \left(\frac{1}{N}\right)\sum_{i=1}^{N}\left(x_i - c\right)^n = \left(\frac{1}{N}\right)\sum_{i=1}^{N}\left(f\left(x_{i-1}, x_{i-2}, \cdots, \hat{\alpha}_1, \hat{\alpha}_2, \cdots, \hat{\alpha}_m\right) - c\right)^n \quad \forall n = 1, \cdots, m, \tag{8.33}$$

where m is the number of model parameters.

Example 8.5

Consider that the following model is used for the sample $x_1,\cdots,x_N$:

$$x_t = \alpha \cdot z_t + \beta,$$

where z_t is an independent random variable with a mean of zero and a variance of one. α and β are the model parameters. Estimate the model parameters with the method of moments.

Solution:

The first and second sample moments can be estimated as

$$M_1 = \left(\frac{1}{N}\right)\sum_{i=1}^{N} x_i$$

and

$$M_2 = \left(\frac{1}{N}\right)\sum_{i=1}^{N} x_i^2.$$

The first two population moments of the model are

$$M_1 = \left(\frac{1}{N}\right)\sum_{i=1}^{N} x_i = \frac{1}{N}\sum_{i=1}^{N}\left((\alpha z_i + \beta)\right) = \frac{\alpha}{N}\left(\sum_{i=1}^{N} z_i\right) + \frac{1}{N}\sum_{i=1}^{N}\beta = \alpha \times \mu_z (= 0) + \frac{N\beta}{N} = \beta$$

and

$$M_2 = \left(\frac{1}{N}\right)\sum_{i=1}^{N} x_i^2 = \frac{1}{N}\sum_{i=1}^{N}(\alpha z_i + \beta)^2 = \frac{1}{N}\left(\sum_{i=1}^{N}\alpha^2 z_i^2 + 2\alpha\beta z_i + \beta^2\right)$$

$$= \alpha^2 \times \sigma_z (= 1) + 2\alpha\beta\mu_z (= 0) + \beta^2 = \alpha^2 + \beta^2.$$

By equating the first population and sample moments, it can be written that

$$\hat{\beta} = \left(\frac{1}{N}\right)\sum_{i=1}^{N} x_i,$$

which is an estimate of the parameter β. By equating the second moments, an estimate of the second parameter can be obtained:

$$\hat{\alpha} = \sqrt{\frac{1}{N}\sum_{i=1}^{N} x_i^2 - \hat{\beta}^2}.$$

8.8.2 Method of Least Squares

Consider a sample $x_1,\cdots,x_N$. A model is fitted to the sample as follows:

$$\hat{x}_t = f\left(x_{t-1}, x_{t-2}, \cdots, \alpha_1, \alpha_2, \cdots, \alpha_m\right) + \varepsilon_t, \tag{8.34}$$

where ε_t is the model residual and $\alpha_1,\alpha_2,\cdots,\alpha_m$ are the model parameters. The objective of the least-squares method is to minimize the following:

$$\sum_{t=1}^{N}\left(x_t - \hat{x}_t\right)^2 = \sum_{t=1}^{N}\left(x_t - f\left(x_{t-1}, x_{t-2}, \cdots, \hat{\alpha}_1, \hat{\alpha}_2, \cdots, \hat{\alpha}_m\right)\right)^2. \tag{8.35}$$

To minimize the above sum, all partial derivatives with respect to estimated values of the parameters, $\hat{\alpha}_1, \hat{\alpha}_2, \cdots, \hat{\alpha}_m$, should be equal to zero. Therefore, they can be written as

$$\frac{\partial\sum_{t=1}^{N}\left(x_t - \hat{x}_t\right)^2}{\partial\hat{\alpha}_1} = 0, \quad \cdots, \quad \frac{\partial\sum_{t=1}^{N}\left(x_t - \hat{x}_t\right)^2}{\partial\hat{\alpha}_m} = 0. \tag{8.36}$$

The model parameters $\left(\hat{\alpha}_1, \hat{\alpha}_2, \cdots, \hat{\alpha}_m\right)$ can be estimated by simultaneous solving of these equations.

Example 8.6

Consider that the $x_t = \alpha x_{t-1} + \varepsilon_t$ model is used for the sample $x_1,\cdots,x_N$. Estimate the model parameter, α, using the least-squares method.

Solution:

The square of errors is estimated as

$$\sum \varepsilon_t^2 = \sum \left(x_t - \alpha x_{t-1}\right)^2.$$

The partial derivatives of the above equation with respect to α are written as

$$\frac{\partial \sum \left(x_t - \alpha x_{t-1}\right)^2}{\partial \alpha} = \sum \left(x_{t-1}\left(\alpha x_{t-1} - x_t\right)\right).$$

By equating the above relationship to zero, the parameter can be estimated as

$$\alpha = \frac{\sum x_t x_{t-1}}{\sum x_{t-1}^2}.$$

Example 8.7

Redo Example 8.5 using the least-squares method.

Solution:

The sum of square of errors of the simulation model is formulated as follows:

$$Q = \sum_{i=1}^{n} e_i^2 = \sum_{i=1}^{n} \left[x_i - \left(\hat{\alpha} + \hat{\beta} z_i\right)\right]^2.$$

The partial derivations of the above equation with respect to model parameters are governed as follows:

$$\frac{\partial Q}{\partial \hat{\alpha}} = \sum_{i=1}^{n} (-2)\left[x_i - \left((\hat{\alpha} + \hat{\beta} z_i)\right)\right] = 0$$

$$\frac{\partial Q}{\partial \hat{\beta}} = \sum_{i=1}^{n} (-2) x_i \left[x_i - \left(\hat{\alpha} + \hat{\beta} z_i\right)\right] = 0.$$

Solving the above equations results in

$$\sum_{i=1}^{n} x_i = \hat{\alpha} n + \hat{\beta} \cdot \sum_{i=1}^{n} z_i$$

$$\sum_{i=1}^{n} x_i z_i = \hat{\alpha} \cdot \sum_{i=1}^{n} z_i + \hat{\beta} \cdot \sum_{i=1}^{n} z_i^2,$$

and the model parameters are calculated as follows:

$$\hat{\beta} = \frac{n\left(\sum_{i=1}^{n} x_i z_i\right) - \left(\sum_{i=1}^{n} x_i\right)\left(\sum_{i=1}^{n} z_i\right)}{n\left(\sum_{i=1}^{n} z_i^2\right) - \left(\sum_{i=1}^{n} z_i\right)^2}$$

$$\hat{\alpha} = \frac{\sum_{i=1}^{n} x_i - \hat{\beta} \cdot \sum_{i=1}^{n} z_i}{n}.$$

8.8.3 Method of Maximum Likelihood

Consider a model including the parameters $\alpha_1,\cdots,\alpha_m$. The joint probability of $\varepsilon_1,\cdots,\varepsilon_N$ (error terms for different points in the sample) is called the likelihood function, which is estimated as follows:

$$L(\varepsilon) = \prod_{t=1}^{N} f\left(\varepsilon_t, \alpha_1, \cdots, \alpha_m\right), \tag{8.37}$$

where $f(\varepsilon_t,\alpha_1,\cdots,\alpha_m)$ is the probability distribution function of the sample. The maximum likelihood is obtained by maximizing the function $L(\varepsilon)$. Instead of the likelihood function, the log-likelihood function can also be maximized as follows:

$$\log(L(\varepsilon)) = \log \prod_{t=1}^{N} f\left(\varepsilon_t, \alpha_1, \cdots, \alpha_m\right) = \sum_{t=1}^{N} \log\left[f\left(\varepsilon_t, \alpha_1, \cdots, \alpha_m\right)\right]. \tag{8.38}$$

For maximizing the above sum, partial derivatives with respect to the parameters $\alpha_1,\cdots,\alpha_m$ should be equated to zero:

$$\frac{\partial \log\left(L(\varepsilon)\right)}{\partial \alpha_1} = 0, \cdots, \frac{\partial \log\left(\mathrm{L}(\varepsilon)\right)}{\partial \alpha_m} = 0. \tag{8.39}$$

The maximum likelihood estimate of the parameters can be obtained by simultaneously solving the above equations.

Example 8.8

Solve Example 8.5 using the maximum likelihood method.

Solution:

When using the maximum likelihood method, it is assumed that the *x* time series follows the normal probability distribution as follows (further details are given in Chapter 10):

$$f\left(x_i \middle| z_i\right) = \frac{1}{\sigma\sqrt{2\pi}} \cdot e^{-1/2\left[\frac{x_i-(\alpha+\beta z_i)}{\sigma}\right]},$$

where z_i is the independent variable. Therefore, the maximum likelihood function would be equal to

$$\log L = -n \cdot \log\sigma - {}^{n}\!/_{2} \cdot \log 2\pi - \frac{1}{2\sigma^2} \cdot \sum_{i=1}^{n}\left[x_i - \left(\alpha + \beta z_i\right)\right]^2.$$

The parameters α, β, and σ are obtained based on taking the partial derivatives of the above equation with respect to these parameters:

$$\frac{\partial \log L}{\partial \alpha} = \frac{1}{\sigma^2} \cdot \sum_{i=1}^{n}\left[x_i - \left(\alpha + \beta z_i\right)\right] = 0$$

$$\frac{\partial \log L}{\partial \beta} = \frac{1}{\sigma^2} \cdot \sum_{i=1}^{n} z_i\left[x_i - \left(\alpha + \beta z_i\right)\right] = 0$$

$$\frac{\partial \log L}{\partial \sigma} = -\frac{n}{\sigma} + \frac{1}{\sigma^3} \cdot \sum_{i=1}^{n}\left[x_i - \left(\alpha + \beta z_i\right)\right]^2 = 0,$$

which results in the following parameters:

$$\hat{\alpha} = \frac{\left(\sum_{i=1}^{n} z_i^2\right)\left(\sum_{i=1}^{n} x_i\right) - \left(\sum_{i=1}^{n} z_i\right)\left(\sum_{i=1}^{n} x_i z_i\right)}{n\left(\sum_{i=1}^{n} z_i^2\right) - \left(\sum_{i=1}^{n} z_i\right)^2}$$

$$\hat{\beta} = \frac{n\left(\sum_{i=1}^{n} x_i z_i\right) - \left(\sum_{i=1}^{n} x_i\right)\left(\sum_{i=1}^{n} z_i\right)}{n\left(\sum_{i=1}^{n} z_i^2\right) - \left(\sum_{i=1}^{n} z_i\right)^2}.$$

As can be seen, the model parameters are the same as the previous examples.

8.9 REGRESSION-BASED METHODS

The concepts and principles of development and application of regression-based models used for statistical simulation of hydrologic time series are introduced. The most general form of these models is called autoregressive integrated moving average modeling, ARIMA(p,d,q). These models are, in theory, the most general class of models for forecasting a time series by assumption of data stationarity and normality. In this section, first, ARMA(p,q) family is described with AR(p) and MA(q) series of models, then in Section 8.9.6, ARIMA(p,d,q) is discussed. It should be noted that trend removing and transformation should be performed before model development, if it is necessary.

8.9.1 ARMA(p,q) Model Identification

The first step in ARMA model development is to recognize the appropriate values of p and q. For this purpose, autocorrelation and partial autocorrelation functions are evaluated as follows:

8.9.1.1 Autocorrelation Function

The autocorrelations of a time series, $z_1, z_2, \cdots z_k$, are defined as follows:

$$\rho_j = \frac{\mathrm{cov}\left(z_t, z_{t-j}\right)}{\sigma^2\left(z_t\right)} = \frac{\gamma_j}{\gamma_0} \tag{8.40}$$

and

$$\gamma_j = \frac{1}{N}\sum_{t=j+1}^{N}\left(z_t - \overline{z}\right)\left(z_{t-j} - \overline{z}\right), \tag{8.41}$$

where N is sample size and $\overline{z}$ is sample mean value. The plot of ρ_j against j is called the autocorrelation function (ACF).

Autocorrelation plots can be used for checking the randomness of a time series. For random series, the autocorrelations with different lags are near zero, and for nonrandom series, one or more of the autocorrelations will be significantly more than zero. Also, these plots can be used for determining the order of ARMA(p,q) models as discussed later.

There are some suggestions for generating confidence bands (determining the significance of autocorrelations). If an ARMA(p,q) model is assumed for the data, the following confidence bands are considered:

$$\left\{-u_{1-\alpha/2}\sqrt{\frac{\left(1+2\sum_{i=1}^{k} z_i^2\right)}{N}};\ +u_{1-\alpha/2}\sqrt{\frac{\left(1+2\sum_{i=1}^{k} z_i^2\right)}{N}}\right\}, \tag{8.42}$$

where $u_{1-\alpha/2}$ is the $1 - \alpha/2$ quantile of the standard normal distribution, N is the sample size, α is the significance level, and k is the lag. In this case, the confidence bands increase as the lag increases.

8.9.1.2 Partial Autocorrelation Function (PACF)

PACF shows the time dependence structure of the series in a different way. The partial autocorrelation lag k can be considered as the correlation between z_1 and z_{k+1}, adjusted for the intervening

observations $z_2,\cdots,z_k$. The partial autocorrelation coefficient $\phi_p(p)$ in an ARMA(p,q) process of order p is a measure of the linear association between ρ_j and ρ_{j-p} for $j \le p$. $\phi_p(p)$ for $p = 1,2,...$ is the partial autocorrelation function. The pth autoregressive coefficient of the AR(p) model fitted to the autocorrelation coefficients is as follows:

$$\rho_j = \phi_1(p)\rho_{1-j} + \phi_2(p)\rho_{2-j} + \cdots + \phi_p(p)\rho_{p-j}; j = 1, \ldots, p, \tag{8.43}$$

where $\phi_j(p)$ is the jth autoregressive coefficient of the ARIMA(p,q) model. The partial autocorrelation is given by the last coefficient $\phi_p(p)$, $p = 1, 2,\ldots$. Equations 8.44 through 8.47 constitute the set of linear equations

$$\phi_1(p)\rho_0 + \phi_2(p)\rho_1 + \cdots + \phi_p(p)\rho_{p-1} = \rho_1 \tag{8.44}$$

$$\phi_1(p)\rho_1 + \phi_2(p)\rho_2 + \cdots + \phi_p(p)\rho_{p-2} = \rho_2 \tag{8.45}$$

$$\phi_1(p)\rho_2 + \phi_2(p)\rho_3 + \cdots + \phi_p(p)\rho_{p-3} = \rho_3 \tag{8.46}$$

$$\cdots$$

$$\phi_1(p)\rho_{p-1} + \phi_2(p)\rho_{p-2} + \cdots + \phi_p(p)\rho_0 = \rho_p, \tag{8.47}$$

which can be written as

$$\begin{bmatrix} 1 & \rho_1 & \rho_2 & \cdots & \rho_{p-1} \\ \rho_1 & 1 & \rho_1 & \cdots & \rho_{p-2} \\ \rho_2 & \rho_1 & 1 & \cdots & \rho_{p-3} \\ \vdots & \vdots & \vdots & & \vdots \\ \rho_{p-1} & \rho_{p-2} & \rho_{p-3} & \cdots & 1 \end{bmatrix} \begin{bmatrix} \phi_1(p) \\ \phi_2(p) \\ \phi_3(p) \\ \vdots \\ \phi_p(p) \end{bmatrix} = \begin{bmatrix} \rho_1 \\ \rho_2 \\ \rho_3 \\ \vdots \\ \rho_p \end{bmatrix} \tag{8.48}$$

or

$$\mathbf{P}_p\boldsymbol{\phi}_p = \boldsymbol{\psi}_p \rightarrow \boldsymbol{\phi}_p = \mathbf{P}_p^{-1}\boldsymbol{\psi}_p, p = 1,2,... \tag{8.49}$$

Thus, the partial autocorrelation function $\phi_p(p)$ is determined by successively applying Equations 8.43 through 8.48.

The partial autocorrelation function $\phi_p(p)$ may be also obtained recursively by means of Durbin's (1960) relations

$$\phi_1(1) = \rho_1, \quad \phi_1(2) = \frac{\rho_1\left(1-\rho_2\right)}{\left(1-\rho_2^2\right)}, \quad \phi_2(2) = \frac{\rho_2-\rho_1^2}{\left(1-\rho_1^2\right)} \tag{8.50}$$

$$\phi_p(p) = \frac{\rho_p - \sum_{j=1}^{p-1}\phi_j(p-1)\rho_{p-j}}{\left(1 - \sum_{j=1}^{p-1}\phi_j(p-1)\rho_j\right)} \tag{8.51}$$

$$\phi_j(p) = \phi_{j-1}(p) - \phi_p(p)\phi_{p-j}(p-1). \tag{8.52}$$

On the hypothesis that the process is AR(p), the estimated $\phi_p(p)$ for $k > p$ is asymptotically normal with a mean of zero and a variance $1/N$. Hence, the $1 - \alpha$ probability limits for zero partial autocorrelation may be determined by (Box and Jenkins 1970):

$$\left\{-u_{1-\alpha/2}/\sqrt{N}\,;\; +u_{1-\alpha/2}/\sqrt{N}\right\}, \tag{8.53}$$

where $u_{1-\alpha/2}$ is the $1 - \alpha/2$ quantile of the standard normal distribution, N is the sample size and α is the significance level. The limits of Equation 8.53 may be used to give some guide as to whether theoretical partial autocorrelations are practically zero beyond a particular lag.

8.9.2 Autoregressive (AR) Models

Autoregressive (AR) models have been widely used in hydrologic time series modeling. They incorporate the correlation between time sequences of variables. These models are the simplest models and their development goes back to the application of Thomas Fiering and Markov lag one models. They can be classified into the following subsets:

- AR models with constant parameters, which are typically used for modeling of annual series
- AR models with timely variable parameters, which are typically used for modeling of seasonal (periodic) series

The basic form of the AR model of order p(AR(p)) with constant parameters is

$$z_t = \sum_{i=1}^{p} \phi_i(p) z_{t-i} + \varepsilon_t, \tag{8.54}$$

where z_t is time-dependent normal and standardized series $N(0,1)$, $\phi_i(p)$ are autoregressive coefficients, ε_t is the time-independent variable (white noise), and p is the order of autoregressive model. In order to identify whether an AR(p) is an appropriate model for a specific time series, it is necessary to estimate and investigate the behavior of the PACF of the series. It can be shown that the partial correlogram of an autoregressive process of order p has peaks at lags 1 through p and then cuts off. Hence, the partial autocorrelation function can be used to identify the p of an AR(p) model.

The AR model with periodic parameters has the following form:

$$z_{\nu,\tau} = \sum_{i=1}^{P} \phi_{i,\tau}(p) z_{\nu,\tau-i} + \sigma_\tau(\varepsilon)\zeta_{\nu,\tau}, \tag{8.55}$$

where $z_{\upsilon,\tau}$ is the normal and standardized value in year ν and season τ, $\phi_{i,\tau}(p)$ are periodic autoregressive coefficients, and $\sigma_\tau(\varepsilon)$ is the periodic standard deviation of residuals. ζ_t is the standardized normal random variable. $z_{\upsilon,\tau}$ is estimated using seasonal mean and variances as follows:

$$z_{\nu,\tau} = \frac{x_{\nu,\tau} - \mu_\tau}{\sigma_\tau}, \tag{8.56}$$

where μ_τ and σ_τ are the mean and standard deviation of x in season τ. The parameter set of the model can be summarized as

$$\left\{\mu_\tau, \sigma_\tau, \phi_{1,\tau}(p), \cdots, \phi_{P,\tau}(p), \sigma_\tau^2(\varepsilon), \tau = 1, \cdots, \eta\right\}, \tag{8.57}$$

where η is the total number of seasons. Equation 8.55 can be similarly used for each season:

$$\rho_k = \sum_{i=1}^{P} \hat{\phi}_{i,\tau}(p)\rho_{|k-i|,\tau-\min(k,i)}, \quad k \geq 0, \tag{8.58}$$

where ρ_k is the sample correlation coefficients of lag k. ^ stands for estimated value. The residual variance can be estimated using the following relation:

$$\hat{\sigma}_\tau^2(\varepsilon) = 1 - \sum_{j=1}^{P} \hat{\phi}_{j,\tau}(p) \cdot \hat{\rho}_{j,\tau}. \tag{8.59}$$

For AR(2) model, Equation 8.58 can be written as

$$\begin{cases} \rho_1 = \phi_1(2) + \phi_2(2)\rho_1 \\ \rho_2 = \phi_2(2) + \phi_1(2)\rho_1 \end{cases}. \tag{8.60}$$

By solving the above equations,

$$\phi_1(2) = \frac{\rho_1\left(1-\rho_2\right)}{1-\rho_1^2} \tag{8.61}$$

and

$$\phi_2(2) = \frac{\rho_2 - \rho_1^2}{1-\rho_1^2}, \tag{8.62}$$

which is the same as what was obtained in Equation 8.50. As can be seen, the above formulation is based on the standardized series, which can be obtained as follows:

$$z_t = \frac{x_t - \mu}{\sigma}, \tag{8.63}$$

where μ and σ are the mean and standard deviation of the series x_t. The parameter set of the model is

$$\{\mu, \sigma, \phi_1(p), \cdots, \phi_p(p), \sigma^2(\varepsilon)\}, \tag{8.64}$$

where $\sigma^2(\varepsilon)$ is the variance of the time-independent series. The model parameters can be estimated by solving the following linear equations, which are called Yule–Walker equations, simultaneously as was mentioned before:

$$\rho_i = \hat{\phi}_1(p)\rho_{i-1} + \hat{\phi}_2(p)\rho_{i-2} + \cdots + \hat{\phi}_p(p)\rho_{i-p}, \quad i \geq 1, \tag{8.65}$$

where ρ_i are the sample correlation coefficients of lag i. The parameter $\sigma^2(\varepsilon)$ can also be estimated using the following relation:

$$\hat{\sigma}^2(\varepsilon) = \frac{N\hat{\sigma}^2}{(N-p)}\left(1 - \sum_{i=1}^{p} \hat{\phi}_i(p)\rho_i\right), \tag{8.66}$$

where N is the number of data and $\hat{\sigma}^2$ is the sample variance.

The stationary condition must be met by the model parameters. For this purpose, the roots of the following equation should lie inside the unit circle (Yevjevich 1972):

$$u^p - \hat{\phi}_1(p)u^{p-1} - \hat{\phi}_2(p)u^{p-2} - \cdots - \hat{\phi}_p(p) = 0. \tag{8.67}$$

In other words, we must have $|u_i| < 1$. In order to forecast or generate annual AR models, the following relation can be used:

$$\hat{z}_t = \hat{\phi}_1(p)\hat{z}_{t-1} + \cdots + \hat{\phi}_P(p)\hat{z}_{t-P} + \hat{\sigma}(\varepsilon)\zeta_t. \tag{8.68}$$

Example 8.9

For an AR(2) model, the parameters have been estimated as $\phi_1(1) = 0.3$ and $\phi_2(2) = 0.4$. Check the parameters' stationary condition.

Solution:

Using Equation 8.67, the following expressions can be written:

$$u^2 - 0.3u - 0.4 = 0 \qquad \begin{cases} u_1 = 0.8 \\ u_2 = -0.5 \end{cases}$$

The roots lie within the unit circle; therefore, the parameters pass the stationary condition.

Example 8.10

For a sample of 100-year normal and standardized annual inflows to a reservoir, an AR(2) model is selected. The first and second correlation coefficients are estimated as $\rho_1 = 0.65$ and $\rho_2 = 0.3$. Estimate the model parameters if the variance of normal and standardized inflow series is estimated as 1.8.

Solution:

Using Equations 8.61 and 8.62, it can be calculated that

$$\phi_1(2) = 0.79$$

and

$$\phi_2(2) = -0.21.$$

The variance of model residuals can also be estimated using Equation 8.66:

$$\hat{\sigma}^2(\varepsilon) = \frac{100 \times 1.8}{(100-2)}(1 - 0.65 \times 0.79 + 0.3 \times 0.21) = 0.96$$

Example 8.11

Estimate the parameters of AR(1) and AR(2) models for the given flow time series in Table 8.6. Assume that the flow data follow the normal probability distribution.

Solution:

The first step in developing AR models is estimation of autoregressive and partial autoregressive coefficients. For estimation of AR(1) and AR(2) model parameters, it is needed to solve the Yule–Walker equation considering $k = 2$. After estimation of the autoregressive coefficients, the model parameters are estimated as follows (Table 8.7):

TABLE 8.6
Flow Data Time Series in Example 8.11

Year	Flow (m^3/s) × 1000	Year	Flow (m^3/s) × 1000
1	59.8	18	14.6
2	63.3	19	44.2
3	57.7	20	131.0
4	64.0	21	73.3
5	63.5	22	46.6
6	38.0	23	39.4
7	74.6	24	41.2
8	13.1	25	41.3
9	37.6	26	62.0
10	67.5	27	90.0
11	21.7	28	50.6
12	37.0	29	41.9
13	93.5	30	35.0
14	58.5	31	16.5
15	63.3	32	35.3
16	74.4	33	30.0
17	34.2	34	52.6

TABLE 8.7
Estimated Autoregressive and Model Parameters for Example 8.11

Parameter	Estimated Value
ρ_1	0.15783
ρ_2	–0.3410
$\phi_1(1)$	0.15783
$\phi_1(2)$	0.16738
$\phi_2(2)$	0.29896

8.9.3 Moving Average Process

The autoregressive models can be used as an effective tool for modeling hydrologic time series such as streamflow in low-flow season, which is mainly supplied from groundwater and has low variations. However, previous studies have shown that the streamflows in high-flow season can be better formulated by adding a moving average component to the autoregressive component (Salas et al. 1980).

If the series, z_t, is dependent only on a finite number of previous values of a random variable, ε_t, then the process can be called a *moving average* (MA) process. The MA(q) process (the moving average model of order q) is formulated as follows:

$$z_t = \varepsilon_t - \theta_1\varepsilon_{t-1} - \theta_2\varepsilon_{t-2} - \theta_3\varepsilon_{t-3} - \cdots - \theta_q\varepsilon_{t-q}. \tag{8.69}$$

It can also be written as

$$z_t = -\sum_{j=0}^{q}\theta_j\varepsilon_{t-j}, \quad (\theta_0 = -1), \tag{8.70}$$

where $\theta_1,\cdots, \theta_q$ are q orders of MA(q) model parameters. The parameter set of the model can be summarized as

$$\{\mu, \theta_1,\cdots, \theta_q, \sigma^2(\varepsilon)\}. \tag{8.71}$$

The parameters of the model should satisfy the invertibility condition. For this purpose, the roots of the following polynomial should lie inside the unit circle:

$$u^q - \hat{\theta}_1 u^{q-1} - \hat{\theta}_2 u^{q-2} - \cdots - \hat{\theta}_q = 0. \tag{8.72}$$

Example 8.12

For an MA(2) model, the parameters have been estimated as $\theta_1 = 0.65$ and $\theta_2 = 0.3$. Check whether the parameters pass the invertibility condition.

Solution:

Using Equation 8.72, it can be written that

$$u^2 - 0.5u - 0.2 = 0 \qquad \begin{cases} u_1 = 0.76 \\ u_2 = -0.26. \end{cases}$$

The roots lie within the unit circle; therefore, the parameters pass the invertibility condition.

8.9.4 Autoregressive Moving Average Modeling

A combination of an autoregressive model of order p and a moving average model of order q forms an autoregressive moving average (ARMA) model of order (p,q). The ARMA(p,q) model is formulated as follows:

$$z_t - \phi_1(p)z_{t-1} - \cdots - \phi_p(p)z_{t-p} = \varepsilon_t + \theta_1\varepsilon_{t-1} + \cdots + \theta_q\varepsilon_{t-q}. \tag{8.73}$$

The ARMA(p,q) model can also be shown in the following compact form:

$$\phi(B)z_t = \theta(B)\varepsilon_t, \tag{8.74}$$

where $\phi(B)$ and θB are the pth and qth degree polynomials:

$$\phi(B) = 1 - \phi_1(p)B - \cdots - \phi_p(p)B^p \tag{8.75}$$

$$\theta(B) = 1 + \theta_1 B + \cdots + \theta_q B^q. \tag{8.76}$$

The parameter set of ARMA(p,q) model can be summarized as

$$\{\mu, \theta_1, \cdots, \theta_q, \phi_1(p), \cdots, \phi_p(p), \sigma^2(\varepsilon)\}. \tag{8.77}$$

The parameters of the ARMA(p,q) model should satisfy both the conditions of invertibility and stationarity. In Table 8.8, some relationships between parameters and correlations ρ_k of ARMA processes of low order are given. After estimation of correlation coefficients with different lags, regarding the order of the selected ARIMA model, these equations can be used to estimate model parameters.

Table 8.9 shows the characteristic behavior of the autocorrelation and of the partial autocorrelation for the AR, MA, and ARMA processes, which can be effectively incorporated in selecting the type and form of the statistical model.

Example 8.13

For a time series with given autoregressive and partial autoregressive coefficients in Example 8.11, estimate the parameters of model ARMA(1,1).

TABLE 8.8
Some Relationships between Parameters and Correlations ρ_k of ARMA Processes

ARMA(p,q)	Relationships
(1,0)	$\rho_k = (\phi_1(1))^k$
(2,0)	$\rho_1 = \dfrac{\phi_1(2)}{1-\phi_2(2)}$
	$\rho_2 = \phi_2(2) + \dfrac{\left(\phi_1(2)\right)^2}{1-\phi_2(2)}$
	$\rho_k = \phi_1(2)\rho_{k-1} + \phi_2(2)\rho_{k-2},\ k \geq 2$
(1,1)	$\rho_1 = \dfrac{\left(1-\theta_1\phi_1(1)\right)\left(\phi_1(1)-\theta_1\right)}{1+\theta_1^2-2\phi_1(1)\theta_1}$
	$\rho_k = \rho_1(\phi_1(1))^{k-1},\ k \geq 2$
(0,2)	$\rho_1 = \dfrac{-\theta_1(1-\theta_2)}{1+\theta_1^2+\theta_2^2}$
	$\rho_2 = \dfrac{-\theta_2}{1+\theta_1^2+\theta_2^2}$
	$\rho_k = 0,\ k \geq 3$
(0,1)	$\rho_1 = \dfrac{-\theta_1}{1+\theta_1^2}$
	$\rho_k = 0, \quad k \geq 2$

TABLE 8.9
Characteristic Behavior of AR, MA, and ARMA

Process	Autocorrelation	Partial Autocorrelation
AR(p)	Damped and infinite in extent exponentials and/or waves	Peaks at lags 1 through p and then cuts off
MA(q)	Peaks at lags 1 through q and then cuts off	Damped and infinite in extent exponentials and/or waves
ARMA(p,q)	Irregular in first q–p lags and then damped and infinite in extent exponentials and/or waves	Irregular in first p–q lags and then damped and infinite in extent exponentials and/or waves

Solution:

Regarding Table 8.8, for model ARMA(1,1), the following are obtained:

$$\rho_1 = \frac{\left(1-\theta_1\phi_1(1)\right)\left(\phi_1(1)-\theta_1\right)}{1+\theta_1^2-2\phi_1(1)\theta_1}$$

$$\rho_k = \rho_1(\phi_1(1))^{k-1}, \quad k \geq 2 \Rightarrow \rho_2 = \rho_1\phi_1(1)$$

Using the above, the following is obtained:

$$\phi_1(1) = \frac{\rho_2}{\rho_1} = \frac{0.034}{0.157} = -0.22.$$

It is checked that the roots of Equation 8.67 are placed in a circle with unit radius. Replacing these values in the first equation, the following second-order equation based on θ_1 is obtained:

$$\left(\rho_1 - \phi_1(1)\right)\theta_1^2 + \left(\phi_1(1)^2 - 2\rho_1\phi_1(1) + 1\right)\theta_1 + \rho_1 - \phi_1(1) = 0.$$

By solving this equation, two values (–0.3891 and –0.8282) are obtained, from which the value of $\theta_1 = -0.8282$ is finally selected. This value satisfies the invertibility condition (being between 1 and –1).

Example 8.14

What order of *p* and *q* in modeling the monthly runoff data of 3 years given in Table 8.10 is suggested?

Solution:

Step 1: The nonstationarity in the series is removed by taking annual (12-month) differencing because of the seasonality of the time series data of the runoff. Table 8.11 shows the

TABLE 8.10
Monthly Runoff Data (cms) in Example 8.14

Year/Month	1	2	3	4	5	6	7	8	9	10	11	12
1	7.21	2.69	4.05	0.68	0.00	0.01	1.34	1.07	2.97	3.92	2.91	2.55
2	7.15	1.15	3.94	0.26	0.00	0.02	0.47	0.01	1.84	2.2	3.61	2.8
3	6.75	1.04	3.12	0.36	0.00	0.03	1.92	1.78	2.96	2.68	3.31	3.51

TABLE 8.11
Twelve-Month Difference of Runoff in Example 8.14

Month	12-Month Difference of Runoff	Month	12-Month Difference of Runoff
1	–	19	0.13
2	–	20	0.94
3	–	21	–0.13
4	–	22	–0.02
5	–	23	–0.2
6	–	24	–0.05
7	–	25	–0.4
8	–	26	–0.11
9	–	27	–0.82
10	–	28	0.1
11	–	29	0
12	–	30	0.01
13	–0.06	31	1.45
14	–0.54	32	1.77
15	–0.11	33	1.12
16	–0.42	34	0.48
17	0	35	–0.3
18	0.01	36	0.71

12-month differencing values of runoff. For example, $u_{12} = 7.15 - 7.21 = -0.06$. Because of the 12-month differencing, the lengths of differenced series would be 12 months less than the original time series.

Step 2: The orders of p and q for the differenced series are determined through the next steps.

Step 2.1: The mean and standard deviation of the differenced series are estimated as mean = 0.15 and SD =0.63.

Step 2.2: The autocorrelation function of the difference of the runoff series is shown in Figure 8.8. The autocorrelation function has a dominant value at lag 1. Hence, regarding Table 8.9, the moving average order (q) is selected to be 1 for this model.

Step 2.3: The partial autocorrelation function is shown in Figure 8.9 and exhibits significant values at lag 1. Thus, the autoregressive value for this model based on Table 8.9 will be 1.

Step 2.4: The behavior of the ACF and PACF suggests an ARMA(1,1) model for the differenced series.

Step 2.5: The estimates of the autoregressive and moving average parameters based on the given equations in Table 8.8 are given in Table 8.12. The correlation coefficients used for parameters estimation are given in Figure 8.8.

Step 3: The normality of the model residuals is tested. Figure 8.10 illustrates the normal score against residual of monthly runoff simulation model based on the estimated parameters.

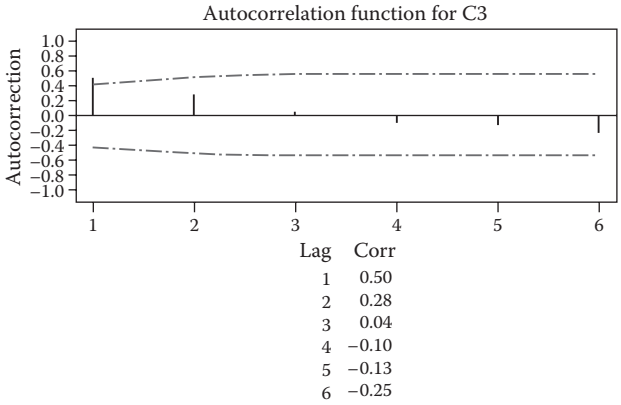

FIGURE 8.8 Autocorrelation function of data in Example 8.14.

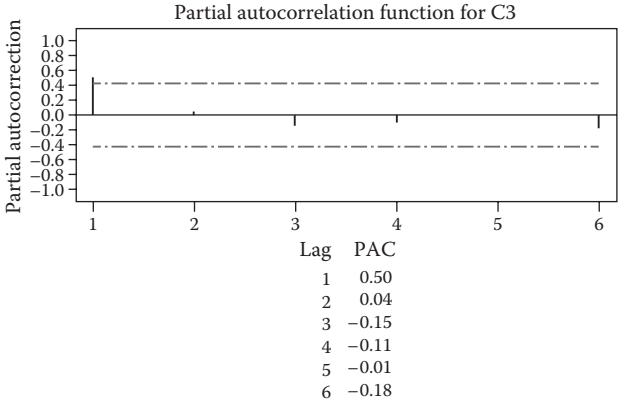

FIGURE 8.9 Partial autocorrelation function of data in Example 8.14.

TABLE 8.12
Twelve-Month Difference of Runoff in Example 8.14

Parameter	Value
$\varphi_1(1)$	0.5633
θ_1	0.4422

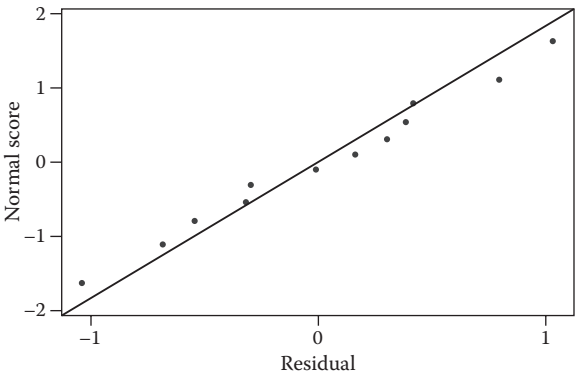

FIGURE 8.10 Normality plot of the modeling residuals in Example 8.14.

Since the results are close to the straight line, it can be concluded that they follow the normal distribution. That is to say, the model fits well to an ARMA(1,1) with 12 months' difference and is suitable for monthly runoff series simulation.

8.9.4.1 Generation and Forecasting Using ARMA Models

Once the ARMA model is fitted to a time series, the following procedures could be used for generating or forecasting the values of that time series. For generation using the ARMA(p,q) model (Equation 8.75), it is necessary to give p initial Z values to the model. Equations 8.78 and 8.79 may be used recursively to generate desired numbers of Z_t. By generating a sufficient long series and deleting 50 or 100 initial terms, the transient effect of the initial values is negligible (Salas et al. 1988). The synthetic generated values conserve the statistical properties of the historical data.

Also, ARMA(p,q) could be used to forecast Z values in a lead time L. If $Z_t(L)$ denotes the value of Z_t at lead time L, the following equations could be used for forecasting:

$$Z_t(L) = \phi_1(p)Z_{t+L-1} + \phi_2(p)Z_{t+L-2} + \cdots + \phi_p(p)Z_{t+L-p} - \theta_1\varepsilon_{t+L-1} - \cdots - \theta_q\varepsilon_{t+L-q} \quad \text{for} \quad L \le q \tag{8.78}$$

$$Z_t(L) = \phi_1(p)Z_{t+L-1} + \phi_2(p)Z_{t+L-2} + \cdots + \phi_p(p)Z_{t+L-p} \quad \text{for} \quad L > q. \tag{8.79}$$

8.9.5 Akaike's Information Criterion (AIC)

This criterion, which was first proposed by Akaike (1974), is usually used as the primary criterion for model selection. It considers the parsimony (using the least parameters in model development) in model building. He defined the Akaike Information Criterion (AIC) among competing ARMA(p,q) models as follows:

$$\text{AIC}(p,q) = N \cdot \ln\left(\hat{\sigma}^2(\varepsilon)\right) + 2(p+q) \tag{8.80}$$

where N is the sample size and $\hat{\sigma}^2(\varepsilon)$ is the maximum likelihood estimation of the residual variance. Based on this criterion, the model with minimum AIC is selected.

The goodness-of-fit tests should be applied to the model with minimum AIC to make sure the residuals are consistent with their expected behavior. If the model residuals do not pass the test, the models with higher values of AIC should be checked.

8.9.5.1 Generation and Forecasting

Two major uses of time series modeling are the generation of synthetic values and the forecasting of future events. The generation of synthetic time series often consists of the generation of the independent normal variables in a series, which is defined as a random process. The generated random component of a series will be added to its trend or deterministic component to produce real values of time series. In data generation using an ARMA(p,q) model, it is necessary to give p initial values. By generating a sufficiently long series, and neglecting the first 50 or 100 terms, the transient effect of the initial values is generally negligible. The synthetically generated series is expected to conserve some of the statistical properties of the historical data.

The second important application of time series models is forecasting future events. The forecasted values are often different from the real values; therefore, a confidence level is considered for the forecasted values as was mentioned before. The forecasting horizon cannot be extended to more than some time steps.

Example 8.15

The given models in Table 8.13 are fitted to a time series. The corresponding variances of the model residuals are also given in this table. What would be the selected model based on AIC criteria? The number of data in the time series is 51.

Solution:

The AIC criteria is estimated for each of the models based on the given data as follows:

AIC(1,0) = –18.96
AIC(2,0) = –20.22
AIC(1,1) = –19.73
AIC(2,1) = –17.97

Therefore, based on AIC, the model of ARMA(2,0) is selected as the best model.

Time series analysis and synthesis can be used to model most river flow records, but there are several models based on other statistical techniques that have been applied successfully in solving hydrological problems.

TABLE 8.13
Characteristics of Considered Models in Example 8.15

Variance of Model Residuals	Model Type
0.663	ARMA(1,0)
0.622	ARMA(2,0)
0.628	ARMA(1,1)
0.625	ARMA(2,1)

8.9.6 Autoregressive Integrated Moving Average Modeling

The ARMA models are suitable for data, which have the following two basic characteristics:

1. No apparent deviation from stationary
2. Rapidly decreasing autocorrelation function

If these conditions are not met by a time series, a proper transformation should be performed to generate the time series with the two above conditions. This has usually been achieved by differencing, which is the essence of autoregressive integrated moving average (ARIMA) models. The same principles of model identification for ARMA models can be applied to ARIMA models except the time series should be transformed by a simple d (for non-seasonal) or D (for seasonal) differencing between the data in time series. For example, if $d = 1$ and we have monthly time series, then each monthly data are subtracted from the previous month to form a new differing time series. For $D = 1$, then each monthly data are subtracted from the same month's data in the previous year. This class of models is effective for describing stationary and nonstationary time series. The nonseasonal form of ARIMA models of order (p,d,q) can be formulated as

$$\phi(B)(1 - B)^d z_t = \theta(B)\varepsilon_t, \tag{8.81}$$

where $\phi(B)$ and $\theta(B)$ are polynomials of degree p and q, respectively:

$$\phi(B) = 1 - \phi_1(p)B - \phi_2(p)B^2 - \ldots - \phi_p(p)B^p \tag{8.82}$$

$$\theta(B) = 1 - \theta_1 B - \theta_2 B^2 - \ldots - \theta_q B^q. \tag{8.83}$$

Therefore, there are $p + q + 1$ model parameters to be estimated. These parameters are

$$\{\phi_1(p),\cdots,\phi_p(p),\theta_1,\cdots,\theta_q,\sigma^2(\varepsilon)\}. \tag{8.84}$$

The model parameters are estimated in the same way as ARMA models using the differenced data correlation coefficients. In order to model the seasonal hydrologic time series, the seasonal form of ARIMA models of nonseasonal order (p,d,q) and of seasonal order $(P,D,Q)_w$ with seasonality w has also been developed. The general multiplicative ARIMA$(p,d,q)(P,D,Q)_w$ can be formulated as

$$\begin{aligned}&(1 - \Phi_1(p)B^w - \Phi_2(p)B^{2w} - .... - \Phi_p(p)B^{Pw})(1 - \phi_1(p)B - \phi_2(p)B^2 - .... - \phi_p(p)B^p)\\ &(1 - B^w)^D(1 - B)^d z_t = (1 - \Theta_1 B^w - \Theta_2 B^{2w} - ... - \Theta_Q B^{QW})(1 - \theta_1 B - \theta_2 B^2 - ... - \theta_q B^q)\varepsilon_t,\end{aligned} \tag{8.85}$$

where ε_t is an independently distributed random variable, B is backward operator as $B(z_t) = z_{t-1}$, $(1 - B^w)^D$ is Dth seasonal difference of season w, $(1 - B)^d$ is dth nonseasonal difference, p is order of nonseasonal autoregressive model, q is order of nonseasonal moving average model, P is order of seasonal autoregressive model, Q is order of seasonal moving average model, Φ is seasonal autoregressive parameter, Θ is seasonal moving average parameter, ϕ is nonseasonal autoregressive parameter, and θ is nonseasonal moving average parameter.

Equation 8.85 can also be shown in the following condensed form:

$$\Phi(B^w)\phi(B)(1 - B^w)^D(1 - B)^d z_t = \Theta(B^w)\theta(B)\varepsilon_t. \tag{8.86}$$

Example 8.16

Formulate the ARIMA(1,0,1)(1,0,1)$_{12}$.

Solution:

Using Equation 8.86, it can be written that

$$(1 - \Phi_1(1)B^w)(1 - \phi_1(1)B)z_t = (1 - \Theta_1 B^w)(1 - \theta_1 B)\varepsilon_t$$

or

$$z_t - \phi_1(1)z_{t-1} - \Phi_1(1)z_{t-12} + \phi_1(1)\Phi_1(1)z_{t-13} = \varepsilon_t - \theta_1\varepsilon_{t-1} - \Theta_1\varepsilon_{t-12} - \theta_1\Theta_1\varepsilon_{t-13}.$$

Since the model structure includes the product of its parameters including $\theta_1\Theta_1$ and $\phi_1(1)\Phi_1(1)$, the model has nonlinear parameters.

8.9.6.1 Time Series Forecasting Using ARIMA Models

The ARIMA models are nonstationary and cannot be used for synthetic generation of stationary time series but they will be useful for forecasting. The above equations of ARIMA models could be used for data forecasting. As an example, the forecasting equations for ARIMA(1,0,1)(1,0,1)$_{12}$, which is the same as periodic ARMA(1,1)(1,1)$_{12}$, could be represented as follows:

$$\begin{aligned} z_t(L) = {} & \phi_1(1)z_{t-1+L} + \Phi_1(1)z_{t-12+L} - \phi_1(1)\Phi_1(1)z_{t-13+L} - \theta_1\varepsilon_{t-1+L} \\ & - \Theta_1\varepsilon_{t-12+L} - \theta_1\Theta_1\varepsilon_{t-13+L} \quad \text{for} \quad L \le 12 \end{aligned} \tag{8.87}$$

$$z_t(L) = \phi_1(1)z_{t-1+L} + \Phi_1(1)z_{t-12+L} - \phi_1(1)\Phi_1(1)z_{t-13+L} \quad \text{for} \quad L > 12. \tag{8.88}$$

Since the ARIMA models are made stationary using the differencing operator, the regeneration of the based data needs integration (for continuous series) or summation (for discrete series) of the differencing series. Since the constant of integration is omitted in differencing or derivation, this constant value (or the average) cannot be considered in the integration process. Therefore, the ARIMA models are nonstationary and they cannot be used for data generation. However, they are very useful in forecasting the variability of a variable. The variance of forecasts with ARIMA models is estimated based on parameters called Ψ. For estimation of these parameters in a time series, it is assumed that the series is presented as infinite moving averages as follows:

$$X_t = \sum_{j=0}^{\infty} \Psi_j \varepsilon_{t-j} = \Psi(B)\varepsilon_t,\ \Psi_0 = 1. \tag{8.89}$$

Application of ARIMA(p,d,q)(P,D,Q)$_w$ to the time series of X_t results in

$$\phi(B)\phi(B^w)(1 - B)^d(1 - B^w)^D\Psi(B)\varepsilon_t = \theta(B)\theta(B^w)\varepsilon_t. \tag{8.90}$$

By omitting the residuals from both sides, the following is obtained:

$$\phi(B)\phi(B^w)(1 - B)^d(1 - B^w)^D\Psi(B = \theta(B)\theta(B^w). \tag{8.91}$$

The weights of Ψ are obtained by equating the coefficients of the B operator with the same power on both sides of the equation. Then, the standard deviation of forecasts for the period of L is estimated as follows:

$$s_y(L) = (1 + \Psi_1^2 + \cdots + \Psi_{L-1}^2)^{1/2}\sigma_\varepsilon. \tag{8.92}$$

Example 8.17

A model of ARIMA(2,0,0)(0,1,1)$_{12}$ is fitted to a normal series of y. Regarding the given values of the model, forecast the y_{17}. If y_{19} is equal to 5.7638, estimate the range of this forecast with 95% confidence interval.

$$\begin{matrix}\phi_1(2) = 0.555 \\ \phi_2(2) = 0.009\end{matrix}, \quad \Theta = -0.899 \text{ and } \varepsilon_5 = 0.626$$

$$y_3 = 5.37,\ y_4 = 3.98,\ y_5 = 4.69,\ y_{15} = 4.36,\ y_{16} = 3.98.$$

Solution:

The spread form of model ARIMA(2,0,0)(0,1,1)$_{12}$ is as follows:

$$y_t = \phi_1(2)y_{t-1} + \phi_2(2)y_{t-2} + y_{t-12} - \phi_1(2)y_{t-13} - \phi_2(2)y_{t-14} + \varepsilon_t - \Theta_1\varepsilon_{t-12}.$$

Regarding the above equation, the forecast form of the model would be as follows:

For $L < 13$,

$$y_{t+L} = \phi_1(2)y_{t+L-1} + \phi_2(2)y_{t-L-2} + y_{t+L-12} - \phi_1(2)y_{t+L-13} - \phi_2(2)y_{t+L-14} - \Theta_1\varepsilon_{t-12}.$$

For $L \geq 13$,

$$y_{t+L} = \phi_1(2)y_{t+L-1} + \phi_2(2)y_{t-L-2} + y_{t+L-12} - \phi_1(2)y_{t+L-13} - \phi_2(2)y_{t+L-14}.$$

As can be observed in the above relations, similar to ARMA models, when the forecast horizon is more than the effective time period of the moving average parameter on historical time series, the effect of the moving average is neglected in the forecast. Therefore, after a time horizon of 13, the moving average parameters are omitted in the above equation.

Therefore, for y_{17}, it can be written that

$$y_{17} = \phi_1(2)y_{16} + \phi_2(2)y_{15} + y_5 - \phi_1(2)y_4 - \phi_2(2)y_3 - \Theta_1\varepsilon_5.$$

Therefore, based on the given assumptions, y_{17} is obtained as 5.15343. For estimating the forecast errors, the weights of Ψ are estimated as follows:

$$(1 - \phi_1(2)B - \phi_2(2)B^2)(1 - B^{12})(\Psi_0 + \Psi_1 B + \Psi_2 B^2 + \cdots) = 1 - \Theta_1 B^{12}$$

or

$$(1 - \phi_1(2)B - \phi_2(2)B^2 - B^{12} + \phi_1(2)B^{13} + \phi_1(2)B^{14})(\Psi_0 + \Psi_1 B + \Psi_2 B^2 + \cdots) = 1 - \Theta_1 B^{12},$$

which results in

$$\Psi_0 = 1$$

$$\Psi_1 = \phi_1(2) = 0.555343$$

$$\Psi_2 = \phi_1(2)\Psi_1 + \phi_2(2) = 0.555343 \times 0.555343 + 0.0093856 = 0.31779$$

$$\Psi_3 = \phi_1(2)\Psi_2 + \phi_2(2)\Psi_1 = 0.555343 \times 0.31779 + 0.0093856 \times 0.555343 = 0.1817$$

$$\vdots$$

$$\Psi_{11} = \phi_1(2)\Psi_{10} + \phi_2(2)\Psi_9$$

$$\Psi_{12} = \phi_1(2)\Psi_{11} + \phi_2(2)\Psi_{10} + 1 - \Theta_1$$

$$\Psi_{13} = \phi_1(2)\Psi_{12} + \phi_2(2)\Psi_{11} + \Psi_1 + \phi_1(2)$$

$$\Psi_j = \phi_1(2)\Psi_{j-1} + \phi_2(2)\Psi_{j-2} + \Psi_{j-12} - \phi_1(2)\Psi_{j-13} - \phi_2(2)\Psi_{j-14} \quad j \geq 14.$$

For forecast of y_{19}, L is considered after y_{16}, which would be equal to 3. The standard deviation is estimated as 1.027 as follows:

$$S_y(3) = (1 + 0.555 + 0.318^2)^{0.5} \times 0.8652 = 1.0271.$$

Therefore, the confidence interval of 95% would be estimated as

$$y_{19} + S_y(3) \times z_{95} =$$

$$5.7638 + 1.0271 \times 1.96 = 7.77$$

$$5.7638 - 1.0271 \times 1.96 = 3.75.$$

Note: Based on normal distribution, $z_{95} = 1/96$.

It should be mentioned that the forecasted or generated time series by statistical models should be transformed to real values by the inverse processes of normalization, standardization, and addition of the removed trend.

When the average of the normalized series is close to zero but is not exactly equal to zero, the modification parameter θ_{00} is added to the right-hand side of Equation 8.93 or 8.94. The parameter θ_{00} is estimated as follows:

$$\theta_{00} = \bar{Z}\left(1 - \sum_{i=1}^{p} \phi_i(p)\right), \tag{8.93}$$

where $\bar{Z}$ is the average of standardized normal series.

The ARMA models perform well in analysis of stationary time series such as annual time series. For simulation of nonstationary series such as monthly, weekly, or daily time series, it is necessary to make the series stationary at first. This will result in better performance of models in the generation and forecast of data, even though in the case of application of ARMA models, the needed parameters for this modeling procedure will highly increase. An alternative model that is capable of making the series stationary in an annual time scale is the ARIMA model.

Example 8.18

The parameters $\phi_1(1)$ and θ_1 for the model ARMA(1,1) for a time series (Z) are estimated as 0.79 and 0.35, respectively. Considering $Z_t = 1.46$, $\sigma_\varepsilon^2 = 0.6277$, and $\varepsilon_t = 1.36$, forecast Z_{t+1}. Using the normal random numbers $\zeta_1 = 0.01$ and $\zeta_2 = 0.21$ with a standard deviation of 1, generate two numbers of this series. The normalized series have an average of 500 and a standard deviation of 50.

Solution:

The following relation can be used for data generation of series Z:

$$\text{ARMA}(1,1) \rightarrow Z_t = \phi_1(1)Z_{t-1} + \varepsilon_t - \theta\varepsilon_{t-1}.$$

The forecast relation for model ARMA(1,1) is obtained as follows:

$$\begin{aligned} &Z_{t+1} = \phi_1(1)Z_t - \theta_1\varepsilon_t \quad q \le 1 \\ &\left.\begin{aligned} Z_{t+2} &= \phi_1(1)Z_{t+1} \\ Z_{t+L} &= \phi_1(1)Z_{t+L-1} \end{aligned}\right\} \quad q > 1 \end{aligned}$$

The parameter θ_{00} is estimated as –0.000017, which is added to the right-hand side of the above equation. Therefore, the forecast for the next time step would be

$$Z_{t+1} = 0.79 \times 1.46 - 0.35 \times 1.36 - 0.000017 = 0.6774.$$

For determining the real value, the inverse of standardization is applied to the above number as follows:

$$y_{t+1} = 500 + 50 \times 0.6774 = 533.8.$$

Two numbers can be generated as follows:

$$\begin{aligned} Z_{t+1} &= \phi_1(1)Z_t + \varepsilon_{t+1} - \theta_1\varepsilon_t + \theta_{00} \\ Z_{t+2} &= \phi_1(1)Z_{t+1} + \varepsilon_{t+2} - \theta_1\varepsilon_{t+1} + \theta_{00}. \end{aligned} \tag{8.94}$$

Two values, ε_{t+1} and ε_{t+2}, are needed in the above equations, whose standard normal values are employed as follows:

$$\varepsilon_{t+1} = \sigma_\varepsilon\zeta_1 = 0.79 \times 0.01 = 0.08$$

$$\varepsilon_{t+2} = \sigma_\varepsilon\zeta_2 = 0.79 \times 0.21 = 0.17.$$

Therefore,

$$Z_{t+1} = 0.79 \times 1.46 - 0.35 \times 1.36 + 0.08 - 0.000017 = 0.757$$

$$Z_{t+2} = 0.79 \times 0.765 - 0.35 \times 0.08 + 0.17 - 0.000017 = 0.745,$$

which, by application of inverse normalization, will result in

$$y_{t+1} = 537.9$$

$$y_{t+2} = 537.2.$$

In practical cases, at first, 50 to 100 data are generated to neglect the effect of initial values.

8.9.7 Autoregressive–Moving Average Model with Exogenous Inputs (ARMAX) Model

Autoregressive–moving average models with exogenous inputs are denoted by ARMAX(p,q,b), which shows a model with p autoregressive terms (AR(p)), q moving average terms (MA(q)), and b exogenous input terms as a linear combination of the last b terms of a known and external time series d_t. The model formulation is as follows:

$$Z_t = \varepsilon_t + \sum_{i=1}^{p} {}_i(p) Z_{t-i} + \sum_{i=1}^{q} \theta_i \varepsilon_{t-i} + \sum_{i=1}^{b} \eta_i d_{t-i}, \tag{8.95}$$

where parameters $\eta_1,\cdots,\eta_b$ are related to the selected exogenous input. Some nonlinear types of models with exogenous variables are also available. These models can be successfully utilized in cases where the historical data cannot completely cover the variations and behavior of the studied variables. Due to the complicated process used for the estimation of these model parameters, they are not further discussed here. The MATLAB® software can be used efficiently to develop ARMAX models.

8.9.8 Multivariate and Disaggregation Modeling of Time Series

Planning, design, and operation of water resources systems often involve several hydrologic time series. In this case, the multivariate stochastic analysis and multivariate modeling are necessary to consider cross-correlations between different time series. Many investigators such as Fiering (1964), Matalas (1967), Mejia (1971), Valencia and Schaake (1973), and O'Connel (1974) have proposed multivariate models.

Disaggregation modeling is often within the multivariate model framework. Disaggregation models are used to decompose time series to several subseries that are temporal or spatial fractions of the key time series. Most applications of disaggregation have been in the temporal domain, although some investigators have applied the same principle in the spatial domain. Valencia and Schaake (1973) introduced the first well-known disaggregation model. Multivariate and disaggregation models may be used either for the generation of synthetic time series or for forecasting. For the disaggregation models, the key series must be available as an input to the model. AR(1) multivariate model may be represented as

$$Z_t = A_1 Z_{t-1} + B\varepsilon_t, \tag{8.96}$$

where Z is an ($n \times 1$) vector of elements z, which represent the values of n time series, A_1 and B are ($n \times n$) matrix of parameters, which are obtained by cross-correlation methods that are presented in the next section, and ε is an ($n \times 1$) vector of independent, normally distributed random variables with a mean of zero and a variance of one. Equation 8.96 may be written in matrix form as

$$\begin{bmatrix} Z_t^{(1)} \\ Z_t^{(2)} \\ \vdots \\ Z_t^{(n)} \end{bmatrix} = \begin{bmatrix} a^{11} & a^{12} & \cdots & a^{n1} \\ a^{21} & a^{22} & \cdots & a^{2n} \\ \vdots & \vdots & \vdots & \vdots \\ a^{n1} & a^{n2} & \cdots & a^{nn} \end{bmatrix} \begin{bmatrix} Z_{t-1}^{(1)} \\ Z_{t-1}^{(2)} \\ \vdots \\ Z_{t-1}^{(n)} \end{bmatrix} + \begin{bmatrix} b^{11} & b^{12} & \cdots & b^{n1} \\ b^{21} & b^{22} & \cdots & b^{2n} \\ \vdots & \vdots & \vdots & \vdots \\ b^{n1} & b^{n2} & \cdots & b^{nn} \end{bmatrix} \begin{bmatrix} \varepsilon_t^{(1)} \\ \varepsilon_t^{(2)} \\ \vdots \\ \varepsilon_t^{(n)} \end{bmatrix}. \tag{8.97}$$

The correlation structure of Z_t of the above equation indicates a lag-zero and lag-one cross-correlation in time. In the case of two time series ($n = 2$), the equations of the lag-one multivariate model are

$$\left.\begin{aligned} Z_t^{(1)} &= a_{11}Z_{t-1}^{(1)} + a_{12}Z_{t-1}^{(2)} + b_{11}\varepsilon_t^{(1)} + b_{12}\varepsilon_t^{(2)} \\ Z_t^{(2)} &= a_{21}Z_{t-1}^{(1)} + a_{22}Z_{t-1}^{(2)} + b_{21}\varepsilon_t^{(1)} + b_{22}\varepsilon_t^{(2)} \end{aligned}\right\} \tag{8.98}$$

The extended AR(2) multivariate model is

$$Z_t = A_1 Z_{t-1} + A_2 Z_{t-2} + B\varepsilon_t. \tag{8.99}$$

The parameters of Equation 8.99 are matrices A_1, A_2, and B. Salas et al. (1988) may be referred to for the details of the mathematical estimation of model parameters.

The main parameter for estimating the other parameters of multivariate models is covariance structure represented by a correlation matrix. The correlation matrix for n correlated time series can be obtained as

$$M_k = \begin{bmatrix} \rho_k^{11}, & \rho_k^{12}, & \ldots, & \rho_k^{1n} \\ \rho_k^{21}, & \rho_k^{22}, & \ldots, & \rho_k^{2n} \\ . & . & . & . \\ \rho_k^{n1}, & \rho_k^{n2}, & \ldots, & \rho_k^{nn} \end{bmatrix}, \tag{8.100}$$

where ρ_k^{ij} is the lag-k cross-correlation coefficient between time series Z_t^i and Z_t^j. For the multivariate AR(1) model, the multivariate correlation function is given by

$$M_k = A_1 M_{k-1}, k > 0$$

or

$$M_k = A_1^k M_0, k \geq 0 \tag{8.101}$$

For the multivariate AR(2) model, the multivariate correlation function is

$$M_k = A_1 M_{k-1} + A_2 M_{k-2},\ k > 0. \tag{8.102}$$

The moment estimates of the parameters A_1 and B for the multivariate AR(1) may be obtained from Equations 8.103 and 8.104:

$$\hat{A}_1 = \hat{M}_1 \hat{M}_0^{-1} \tag{8.103}$$

and

$$\hat{B}B^T = \hat{M}_0 - \hat{A}_1 \hat{M}_1^T. \tag{8.104}$$

Similarly, for the multivariate AR(2) model, the moment estimate of the parameters A_1, A_2, and B may be obtained from Equations 8.105 through 8.107 (Salas and Pegram 1977).

$$\hat{A}_1 = \left[\hat{M}_1 - \hat{M}_2 \hat{M}_0^{-1} \hat{M}_1^T\right] \times \left[\hat{M}_0 - \hat{M}_1 \hat{M}_0^{-1} \hat{M}_1^T\right]^{-1} \tag{8.105}$$

$$\hat{A}_2 = \left[\hat{M}_2 - \hat{M}_1\hat{M}_0^{-1}\hat{M}_1^T\right] \times \left[\hat{M}_0 - \hat{M}_1^T\hat{M}_0^{-1}\hat{M}_1\right]^{-1} \tag{8.106}$$

$$BB^T = \hat{M}_2 - \left[\hat{A}_1\hat{M}_1^T + \hat{A}_2\hat{M}_2^T\right]. \tag{8.107}$$

Example 8.19

Eighteen years of annual flows at two stations of a river basin are given in Table 8.14. Use multivariate modeling AR(1) to generate synthetic data for these two stations. Assume that the data are normal variables.

Solution:

The correlation coefficient matrix of lag 0 and lag 1 are computed by using Equation 8.101.

$$M_0 = \begin{bmatrix} 1 & 0.76 \\ 0.76 & 1 \end{bmatrix}$$

$$M_1 = \begin{bmatrix} 0.41 & 0.12 \\ 0.52 & 0.37 \end{bmatrix}$$

The parameters A_1 and BB^T are estimated using Equations 8.105 and 8.107, respectively.

TABLE 8.14
Annual Streamflows of Two Stations in Example 8.19

Years	Streamflows of Station 1	Streamflows of Station 2
1	150	250
2	200	450
3	330	502
4	401	720
5	550	550
6	662	600
7	445	465
8	551	650
9	302	390
10	203	300
11	405	520
12	470	740
13	502	780
14	608	705
15	402	600
16	501	590
17	460	480
18	230	320

$$A_1 = \begin{bmatrix} 0.78 & -0.47 \\ 0.56 & -0.05 \end{bmatrix}$$

$$BB^T = \begin{bmatrix} 0.74 & 0.54 \\ 0.54 & 0.73 \end{bmatrix}$$

Matrix B is determined by solving the above relation. See Salas et al. (1988) for the method of solving this equation.

Finally, B is estimated as follows:

$$B = \begin{bmatrix} 0.82 & 0 \\ 0.6 & -0.57 \end{bmatrix}$$

After estimating the multivariate AR(1) parameters, Equation 8.97 could be used to generate synthetic data of stations.

Disaggregation modeling is a process by which time series are generated dependent on a time series that is already available. Disaggregation models allow preserving statistics of time series at more than one level. The levels may be represented both in time and in space. Disaggregation models have two major benefits (Salas et al. 1988):

1. Reducing the number of parameters in comparison to the other data generation models
2. More flexibility in the methods used for data generation

The two basic forms of disaggregation are temporal and spatial models. A temporal example is the disaggregation of an annual time series into a seasonal time series. An example of spatial disaggregation is the disaggregation of total natural flow of a river basin into individual tributary flows. The general form of a disaggregation model is a linear dependence model, which can be formulated as follows:

$$Y = AX + B\varepsilon, \tag{8.108}$$

where Y is the subseries or dependent series, which is generated based on the key (independent) time series X, ε is a value from a completely random series and A and B are model parameters. In general, the above variables and parameters are represented in the form of vectors and matrices.

Two other disaggregation models are the extended and the condensed models. Mejia and Rousselle (1976) developed the extended model as an extension of the basic temporal model. In the extended model, an extra term is added to the model to incorporate the seasonal covariance between seasons of the consequent years. The model takes the following form:

$$Y = AX + B\varepsilon + CZ, \tag{8.109}$$

where Z is a column matrix containing as many seasonal values from the previous years and C is an additional parameter.

The condensed model is developed by Lane (1979) and is formulated as follows:

$$Y_\tau = A_\tau X + B_\tau \varepsilon + C_\tau Z_{\tau-1}. \tag{8.110}$$

The subscript τ denotes the current season being generated. Parameter estimation for the linear, extended, and condensed disaggregation models is obtained as follows (Salas et al. 1988):

For the linear model:

$$\hat{A} = S_{YX} S_{XX}^{-1} \tag{8.111}$$

$$\hat{B}\hat{B}^T = S_{YY} - \hat{A} \cdot S_{XY}, \tag{8.112}$$

where $\hat{A}$ and $\hat{B}$ are the estimated parameters. In a temporal disaggregation model, S_{YX} is the matrix of covariance between the seasonal and annual series, S_{XX} is the matrix of covariances among the annual series, and S_{YY} is the matrix of covariances among the seasonal series.

For the extended model, the parameters of the model are estimated as follows:

$$\hat{A} = \left(S_{YX} - S_{YZ} S_{ZZ}^{-1} S_{ZX}\right)\left(S_{XX} - S_{XZ} S_{ZZ}^{-1} S_{ZX}\right)^{-1} \tag{8.113}$$

$$\hat{C} = \left(S_{YZ} - \hat{A} S_{XZ}\right) S_{ZZ}^{-1} \tag{8.114}$$

$$\hat{B}\hat{B}^T = \left(S_{YY} - \hat{A} S_{XX} \hat{A}^T - \hat{A} S_{XZ} \hat{C}^T - \hat{C} S_{ZX} \hat{A}^T - \hat{C} S_{ZZ} \hat{C}^T\right) \tag{8.115}$$

or, equivalently,

$$\hat{B}\hat{B}^T = S_{YY} - \hat{A} S_{XY} - \hat{C} S_{ZY}. \tag{8.116}$$

The notation is the same as the basic linear model. Z consists of the lagged partial seasonal series, which are used in addition to those used in the linear basic model. The parameters of the condensed model are estimated as follows:

$$\begin{aligned} \hat{A}_\tau = &\left[S_{YX}(\tau,\tau) - S_{YY}(\tau-1,\tau) S_{YY}^{-1}(\tau-1,\tau-1) S_{YX}(\tau-1,\tau)\right] \\ &\times \left[S_{XX}(\tau,\tau) - S_{XY}(\tau,\tau-1) S_{YY}^{-1}(\tau-1,\tau-1) S_{YX}(\tau-1,\tau)\right]^{-1} \end{aligned} \tag{8.117}$$

$$\hat{C}_\tau = S_{YY}(\tau,\tau-1) - \hat{A}_\tau S_{XY}(\tau,\tau-1) S_{YY}^{-1}(\tau,\tau-1) \tag{8.118}$$

and

$$\hat{B}_\tau \hat{B}_\tau^T = S_{YY}(\tau,\tau) - \hat{A}_\tau S_{XX}(\tau,\tau) - \hat{C}_\tau S_{YY}(\tau-1,\tau). \tag{8.119}$$

In the condensed model, there is one equation for each season. The current season is denoted by τ. As an example, for covariance matrices, S_{YX} (τ, τ − 1) indicates the covariance matrix between the annual series associated with the current season and the seasonal values associated with the previous season.

If N is the number of data in the time series, X and Y are the main and lateral time series, respectively, and x_v^i is the vth variable in ith time series, the elements of the S_{XX} matrix, $S_{XX}(i, j)$, are estimated as follows:

$$S_{XX}(i,j) = \frac{1}{N-1}\sum_{v=1}^{N} x_v^{(i)} x_v^{(j)}, \tag{8.120}$$

where i and j show the row and column number of matrix S, respectively. The matrix S_{YY} (the correlation between lateral series) is also estimated in the same way. The elements of the matrix S for a main and a lateral series are estimated as follows:

$$S_{YX}(i,j) = \frac{1}{N-1}\sum_{v=1}^{N} y_v^{(i)} x_v^{(j)}. \tag{8.121}$$

Example 8.20

Using the annual data given in Table 8.15 and considering station E as the main station, develop a disaggregation model for generation of data in stations M, N, and O.

Solution:

For the development of the disaggregation model, the linear model (Equation 8.112) is employed. The time dimension is considered to be 1 year and there is one main series and three lateral series.

The simultaneous correlation between lateral time series is estimated as

$$S_{YY} = \begin{bmatrix} 3101 & 3002 & 2701 \\ 3002 & 2977 & 2762 \\ 2701 & 2762 & 2877 \end{bmatrix}.$$

The correlation of the lateral time series with last year's data of their own and other lateral series:

$$S_{YY}(1) = \begin{bmatrix} 1844 & 1609 & 861.5 \\ 1967 & 1760 & 1038 \\ 2168 & 2037 & 1416 \end{bmatrix}.$$

TABLE 8.15
Annual Time Series for Example 8.20

Station Name	1	2	3	4	5	6	7	8	9	10	11	12	13	14	15
E	467	639	712	423	427	437	706	914	902	705	634	518	599	567	450
M	183	234	251	156	160	177	278	345	322	249	220	201	216	214	186
N	158	220	234	135	135	152	240	204	304	233	207	174	192	183	513
O	126	182	227	132	132	108	188	265	276	223	207	142	190	170	111

The simultaneous correlation of the main series:

$$S_{XX} = [25, 880].$$

The correlation matrix of the lateral series with the main series:

$$S_{YX} = \begin{bmatrix} 8803 \\ 8741 \\ 8340 \end{bmatrix}.$$

The correlation of the main series with last year's data of the lateral series:

$$S_{XY}(1) = [5980\ 5407\ 3316].$$

Using the above correlation matrices, the model parameters are estimated based on Equations 8.113 through 8.115 as follows:

$$A = \begin{bmatrix} 0.3532 \\ 0.3372 \\ 0.3096 \end{bmatrix}$$

$$C = \begin{bmatrix} 0.5112 & -0.6510 & 0.03759 \\ 0.1707 & -0.1734 & -0.02162 \\ -0.6819 & 0.8244 & -0.01597 \end{bmatrix}$$

$$BB^T = \begin{bmatrix} 64.29 & 15.5 & -79.79 \\ 15.5 & 21.1 & -36.60 \\ -79.79 & -36.60 & 116.4 \end{bmatrix}$$

By solving the above equations, matrix B is estimated as follows:

$$B = \begin{bmatrix} 8.018 & 0 & 0 \\ 1.933 & 4.167 & 0 \\ -9.951 & -4.167 & 0 \end{bmatrix}$$

Finally, the disaggregation model with the structure of $Y_\tau = AX_\tau + B\varepsilon_\tau + CY_{\tau-1}$ is obtained. In this equation, matrices Y_τ, $Y_{\tau-1}$, and ε_τ have a 3 × 1 dimension and X has a 1 × 1 dimension. ε_τ is a matrix of random number with the same dimension as the input data. Using this equation and knowing the values of last year's main (station E) and lateral (stations M, N and O) series, the current values of lateral series can be estimated.

8.10 GOODNESS-OF-FIT TESTS

The goodness-of-fit tests presented in this section are used in making inferences regarding the nature of the unknown frequency distribution of the population. This procedure determines if a particular shape for the population frequency curve is consistent with the sample results obtained. Two of the most common test statistics for the goodness of fit are

1. The chi-square test for testing the hypothesis of goodness of fit of a given distribution
2. The Smirnov–Kolmogorov statistic for estimating maximum absolute difference between the cumulative frequency curve of sample data and the fitted distribution function

The following steps should be taken for hypothesis testing (Lapin 1990):

1. Developing the null hypothesis (H_0: The data represent a specific distribution).
2. Selecting the test procedure and test statistic (such as chi-square or Kolmogorov–Smirnov statistic).
3. Selecting the significance level and the acceptance and rejection regions for the decision rule.
4. Computing the test statistic for the sample data.
5. Making the decision.

8.10.1 Chi-Square Goodness-of-Fit Test

In this test, two sets of frequencies are compared. First, the data should be divided into a number of categories and then the actual frequencies (f_i) in each category (class) should be compared with the expected frequencies, $\left(\hat{f}_i\right)$, which are estimated based on the fitted distribution. The test statistic can be estimated as follows:

$$\chi^2 = \sum_{i=1}^{NC} \frac{\left(f_i - \hat{f}_i\right)^2}{\hat{f}_i}, \tag{8.122}$$

where i is the number of classes and NC is the total number of categories. This estimation is close enough for testing the goodness of fit whenever the expected frequency in any category is equal or greater than 5. χ^2 is chi-square distributed with $NC - NP - 1$ degree of freedom, where NP is the number of parameters to be estimated. The chi-square distribution is given in Table 8.A1 of the Appendix.

Example 8.21

The classified monthly precipitation data measured in a station are divided into nine categories (see Table 8.16). Previous studies have shown that the precipitation data in this station are

TABLE 8.16
Precipitation Data for Example 8.21

Interval (i)	Precipitation Depth Classes (mm)	Actual Frequency (f_i)
1	$0 \le P < 5$	38
2	$5 \le P < 10$	26
3	$10 \le P < 15$	12
4	$15 \le P < 20$	10
5	$20 \le P < 25$	8
6	$25 \le P < 30$	3
7	$30 \le P < 35$	2
8	$35 \le P < 40$	1
9	$40 \le P$	0

exponentially distributed. Therefore, the probability of the monthly rainfall depth, P, is equal to or below x and can be estimated as

$$\text{Prob}\,[P \le x] = 1 - e^{-\lambda x},$$

where λ is estimated to be equal to 0.105. Use the chi-square test with 5% significance level and comment on the selected distribution for the sample data.

Solution:

The expected frequencies are estimated using the selected exponential distribution as shown in the third column of Table 8.16. For example, for the first class of the data, the probability of having rain with depth less than 5 mm is

$$\text{Prob}\,[P < 5] = 1 - e^{-0.105\times 5} = 0.41.$$

The expected frequencies are then estimated based on the difference between cumulative probabilities (see Table 8.17). For example, for the second interval, it can be written that

$$\text{Expected frequency} = (0.65 - 0.41) \times 100 = 24.$$

As can be seen in Table 8.17, the actual frequency for intervals 6 to 9 is less than 5; therefore, these classes are grouped together. The chi-square statistic is then estimated as 2.73. The degree of freedom for the test is estimated as

$$\text{Degree of freedom} = 6 - 1 - 1 = 4.$$

TABLE 8.17
Random Components of Monthly Precipitation in Example 8.21

Interval (i)	Actual Frequency (f_i)	Exponential Cumulative Probability at Upper Limit	Expected Frequencies $\left(\hat{f}_i\right)$	$f_i - \hat{f}_i$	χ^2
1	38	0.41	41	–3	0.22
2	26	0.65	24	2	0.17
3	12	0.79	14	–2	0.29
4	10	0.88	9	1	0.11
5	8	0.93	5	3	1.8
6	3	0.96	3	–1	0.14
7	2	0.97	1		
8	1	0.99	2		
9	0	1	1		
Sum	100	–	100	–	2.73

Considering 5% significance level and 4 degrees of freedom and using Table 8.A1 of the Appendix, the critical value is $\chi^2_{0.05(4)} = 9.488$. Because the estimated value of test statistics is smaller than the critical value, the null hypothesis that the monthly precipitation is exponentially distributed is accepted.

8.10.2 Kolmogorov–Smirnov Goodness-of-Fit Test

The chi-square test performs better, where the sample size is large enough so there are at least five observations in each class interval. When the sample size is smaller, the Kolmogorov–Smirnov test performs better. This test is based on the maximum difference between actual and expected frequencies. The test statistic can be formulated as follows:

$$D = \max \left| F\left(x\right) - \hat{F}\left(x\right) \right|, \tag{8.123}$$

where F is actual cumulative relative frequency and $\hat{F}$ is expected cumulative relative frequency. The same steps should be taken for hypothesis testing as mentioned in Section 8.10. The estimated value for the test statistic should then be compared with the critical value (Table 8.A2 of the Appendix) selected based on the significance level and the number of data points.

Example 8.22

Solve Example 8.21 using the Kolmogorov–Smirnov goodness-of-fit test.

Solution:

Table 8.18 shows the actual and expected cumulative relative frequencies.

TABLE 8.18
Estimated Expected Frequencies and Kolmogorov–Smirnov Statistic for Data Presented in Example 8.22

Interval (i)	Actual Frequency (f_i)	Exponential Cumulative Relative Frequency ($F(x)$)	Expected Cumulative Relative Frequency $\left(\hat{F}(x)\right)$	D
1	38	0.38	0.41	0.03
2	26	0.64	0.65	0.01
3	12	0.76	0.79	0.03
4	10	0.86	0.88	0.02
5	8	0.94	0.93	0.01
6	3	0.97	0.96	0.01
7	2	0.99	0.97	0.02
8	1	1	0.99	0.01
9	0	1	1	0

8.10.3 The Portmanteau Test

The portmanteau lack-of-fit test was first initialized by Box and Pierce (1970) as an approximate test of model adequacy. Hipel and McLeod (1977) and others applied this test for verifying linear models of hydrologic time series. In this test, instead of checking to see if autocorrelations fall within the confidence bound, a single statistic, which depends on autocorrelation function, is used. Consider that the ARIMA(p,d,q) model (see Section 8.9.6) is selected for representing a time series, where p is the number of autoregressive terms, q is the number of moving average terms, and d is the number of differences. As was mentioned, this test determines the adequacy of the model by checking whether the residual series of the model is independent. The following statistics are used in this test:

$$Q = (N-d)\cdot\sum_{k=1}^{L} r_k^2(\varepsilon), \tag{8.124}$$

where L is maximum lag considered. The statistic Q is approximately chi-square distributed with L-p-q degrees of freedom. Therefore, if the estimated test statistic is smaller than the chi-square value, $\chi_\alpha^2(L-p-q)$, of a given significance level $(1-\alpha)$, ε_t is an independent series and thus the model is adequate. Ljung and Box (1978) argued that under the hypothesis of model adequacy, the cutoff value given by $\chi_\alpha^2(L-p-q)$ is closer to the $(1-\alpha)$ quantile of the distribution of the following statistic:

$$Q' = n(n+2)\sum_{k=1}^{L} r_k^2(\varepsilon)\Big/\big(n-j\big). \tag{8.125}$$

Tao and Delleur (1976) used the following statistic for testing the adequacy of the seasonal ARMA model:

$$Q_1 = N\cdot\sum_{k=1}^{L}\sum_{\tau=1}^{\omega} r_{k,\tau}^2\big(\varepsilon\big), \tag{8.126}$$

where ω is the number of time intervals per year (seasons). Granger and Andersen (1978) found examples where the residuals were uncorrelated while the squared residuals were correlated. The sample autocorrelation function of squared residuals can be estimated as (Brockwell and Davis 1987):

$$\hat{\rho}_{\varepsilon\varepsilon}(L) = \frac{\sum_{t=1}^{N-L}\left(\hat{\varepsilon}_t^2-\overline{\varepsilon^2}\right)\left(\hat{\varepsilon}_{t+L}^2-\overline{\varepsilon^2}\right)}{\sum_{t=1}^{N}\left(\hat{\varepsilon}_t^2-\overline{\varepsilon^2}\right)}, \quad L\geq 1, \tag{8.127}$$

where $\overline{\varepsilon^2} = N^{-1}\sum_{t=1}^{N}\hat{\varepsilon}_t^2$. McLeod and Li (1983) showed that

$$Q_{\varepsilon\varepsilon} = N(N+2)\sum_{k=1}^{L} \hat{\rho}_{\varepsilon\varepsilon}^2(k)/(N-k) \tag{8.128}$$

has an approximate $\chi^2(L)$ distribution under the assumption of model adequacy. Therefore, the adequacy of the model is rejected at level α if

$$Q_{\varepsilon\varepsilon} > \chi_{1-\alpha}^2(L). \tag{8.129}$$

Example 8.23

The ACF values for a white noise obtained from an ARMA(1,1) model fitting a sample of 40 data are given in Table 8.19. Is the considered model appropriate?

Solution:

The Q statistic is estimated using Equation 8.124 as follows:

$$Q = (40-0)\cdot\sum_{k=1}^{10} r_k^2(\varepsilon) = 40\left[(0.159)^2 + (-0.126)^2 + \cdots + (-0.0121)^2\right] = 5.66$$

($d = 0$ because of the ARMA model and L is considered to be 10).

The chi-square value, $\chi_\alpha^2(10-1-1=8)$, with a significance level of 5% is obtained as 15.5.

Since the Q statistic (5.66) is smaller than 15.5, it can be concluded that ε_t is an independent series and so the model is adequate.

TABLE 8.19
ACF of White Noise of ARMA(1,1) Model

Lag	ACF
1	0.159128
2	–0.12606
3	0.102384
4	–0.06662
5	–0.08255
6	0.176468
7	0.191626
8	0.05393
9	–0.08712
10	–0.01212
11	–0.05472
12	–0.22745
13	0.089477
14	0.017425
15	–0.20049

TABLE 8.20
Approximate Critical Values of Smirnov–Kolmogorov Statistic K_α

α	0.01	0.05	0.1	0.2	0.25
K_α	1.63	1.36	1.22	1.07	1.02

Source: Yevjevich, V., *Stochastic Process in Hydrology*, Water Resources Publications, Fort Collins, CO, 1972. With permission.

8.10.4 The Cumulative Periodogram Test

This test can be used for checking whether the periodicity is adequately removed from series. The periodogram of sample residual, $\hat{\varepsilon}_t$, can be estimated as follows (Salas et al. 1988):

$$\mathrm{MSD}\left(h_j\right) = \frac{2}{N^2}\left[\left(\sum_{t=1}^{N}\hat{\varepsilon}_t \cdot \cos\left(2\pi h_j t\right)\right)^2 + \left(\sum_{t=1}^{N}\hat{\varepsilon}_t \sin\left(2\pi h_j t\right)\right)^2\right], \tag{8.130}$$

where $h_j = j/N$ is the harmonic (frequency). The cumulative periodogram of $\hat{\varepsilon}_t$ can then be defined as

$$P_i = \frac{\sum_{j=1}^{i}\mathrm{MSD}\left(h_j\right)}{\sigma_\varepsilon^2}, \quad i = 1, \cdots, N/2 \tag{8.131}$$

where σ_ε^2 is the variance of $\hat{\varepsilon}_t$. For an independent series, the plot of P_i versus i will be scattered around a line joining (0,0) and (0.5N, 1). A periodicity with harmonic h_j in the residuals would produce a large value of MSD (h_j) and in turn would appear as a deviation from the straight line, which is valid for an independent series (Salas et al. 1980). Probability limit lines using the Smirnov–Kolmogorov statistic can be drawn to test the significance of such deviations (Box and Jenkins 1970). Considering the significance level of α, the limit lines for a real independent series are drawn approximately at distances $\pm K_\alpha / \sqrt{N'}$ around the theoretical straight line where $N' = (N - 2)/2$ or $N' = (N - 1)/2$ for even or odd N values, respectively. If more than αN of the plotted points fall outside the probability lines, the residual series still has some periodicity; otherwise, it can be concluded that residuals are independent. Approximate values of K_α are given in Table 8.20.

8.11 SPECTRAL-ANALYSIS-BASED METHODS

8.11.1 Spectral Analysis Primer

The spectral analysis of hydrological time series is a useful tool for examining data time series. Spectral analysis can be classified as an exploratory data analysis (EDA) method. EDA methods are usually characterized by revelation, re-expression, residuals, and resistance terms. These terms are described in the following:

- Revelation is a description of natural frequency of time series such as long memory, presence of high-frequency variation, and seasonal behavior.
- Re-expression is time series transformation for stabilizing purpose (removing nonstationarity features) through power transformation, differentiation, or other filtering methods.
- Residuals are the remaining components of time series after removing trends or fitting simple parametric models such as AR or ARMA.
- Resistance is insensitivity to very large outliers.

The spectral analysis includes the first three terms and partially the last one. Standard spectral methods do not exhibit resistance in the usual EDA sense. However, a degree of robustness is possessed in spectral analysis methods since it is needed to assume the normal distribution.

8.11.2 Periodogram

The periodogram is an estimator of the spectral density function of n given observations $z_1,..., z_n$ from a time series that is covariance stationary. The periodogram is used for detecting the periodicities in time series. The periodogram is estimated as follows:

$$I\left(f_j\right) = \frac{1}{n}\left|\sum_{t=1}^{n} z_t e^{-2\pi f_j (t-1)}\right|^2, \tag{8.132}$$

where $f_j = j/n$, $j = [-(n-1)/2],\ldots,0,\ldots, [n/2]$ ([] denotes the integer part function). Regarding Equation 8.132, $I(f_j) = I(-fj)$ and therefore the periodogram is symmetric about 0. That is why only the part of the periodogram or spectral density where $f_j > 0$ is plotted. When $f_j = 0$, $I(0) = n\overline{z}^2$, where $\overline{z} = \sum_{t=1}^{n} z_t/n$. Since $I(0)$ is usually very large, it is ignored in the periodogram and spectral plots. If the spectral density function exists, the expected value of $I(f_j)$ is approximated by $p(f_j)$, where $p(f)$ is the spectral density function. In large samples, $I(f_j)$ for $j = 1, \ldots, [(n-1)/2]$ are independent from each other and exponentially distributed with mean $p(f_j)$. $I(f_j)$ can be plotted against its period $1/f_j$. This approach is not that satisfactory when $I(f_j)$ is calculated at equal-spaced frequencies, because the low-frequency part would be too spread out.

8.11.3 Frequency Interpretation

Another important property of the periodogram is that $I(f_j)$ is related to the square of the multiple correlation between the observed data sequence $z_1, \ldots, z_n$ and a sinusoid having frequency f_j. For example, consider the following regression:

$$z_t = A_0 + A_j \cos(2\pi f_j) + B_j \sin(2\pi f_j) + e_t, \tag{8.133}$$

where e_t is the error term. The model parameters A_0, A_j, and B_j can be estimated using the least-squares method as follows:

$$A_0 = \frac{1}{n}\sum_{t=1}^{n} z_t \tag{8.134}$$

$$A_j = \frac{2}{n}\sum_{t=1}^{n} z_t \cos\left(2\pi f_j\right) \tag{8.135}$$

$$B_j = \frac{2}{n}\sum_{t=1}^{n} z_t \sin\left(2\pi f_j\right). \tag{8.136}$$

Then, the multiple correlation coefficient, R_j^2, is estimated as follows:

$$R_j^2 = A_j^2 + B_j^2. \tag{8.137}$$

The periodogram is estimated as follows:

$$I(f_j) = \frac{n}{2} R_j^2. \tag{8.138}$$

Thus, $p(f)$ is a measure of the strength of a random sinusoidal component having a period of $1/f$ in the data sequence. The spectral density function of time series with cycles or oscillatory behavior has a peak at the corresponding frequency to the cycle period. For example, in a time series with 1-year cyclical component, a peak is observed in the spectral density function at $f = 1$. The sharpness of the peak is dependent on the closeness of the appearance of period $1/f$ in the data sequence, and the relative size of the peak depends on the cycle amplitude in the time series. The units of f_j are cycles per unit time; therefore, the period corresponding to f_j is $T_j = 1/f_j$.

Example 8.24

Develop a mixture of the following three series for $t = 1$ to 100 and then draw the periodogram of this mixture.

$$x_{t1} = 2\cos(2\pi t6/100) + 3\sin(2\pi t6/100)$$
$$x_{t2} = 4\cos(2\pi t10/100) + 5\sin(2\pi t10/100)$$
$$x_{t3} = 6\cos(2\pi t40/100) + 7\sin(2\pi t40/100)$$

Solution:

For developing a mixture of these series, first for $t = 1, \ldots, 100$, three series are developed as illustrated in Figure 8.11. Then, the mixture series is defined as the summation of three series as follows:

$$X_t = x_{t1} + x_{t2} + x_{t3}.$$

The resulting time series is illustrated in Figure 8.12. As can be observed in Figure 8.12, X_t appears to behave as some of the periodic series. The systematic sorting out of the essential frequency components in a time series, including their relative contributions, constitutes one of the main objectives of spectral analysis.

The periodogram development is a way to discover the periodic components of a time series. The scaled periodogram is given by

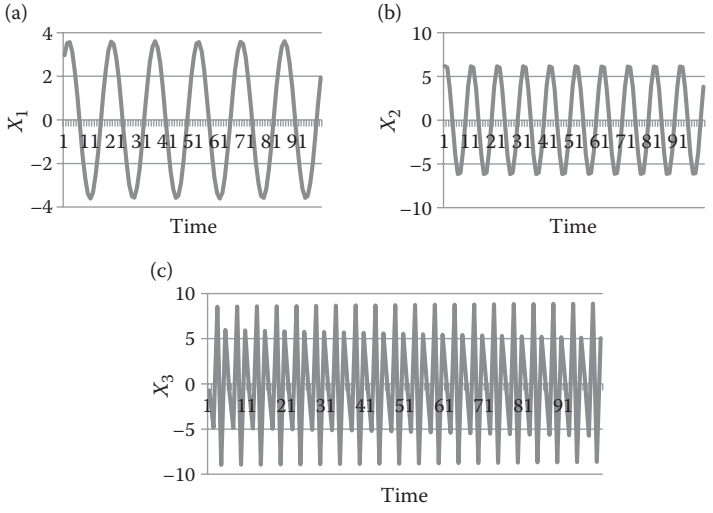

FIGURE 8.11 Generated time series (a) x_{1t}, (b) x_{2t}, and (c) x_{3t} for $t = 1, \ldots, 100$.

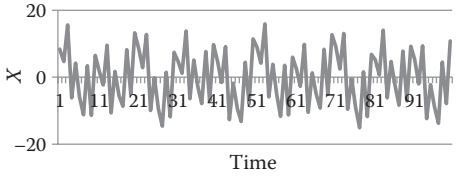

FIGURE 8.12 Generated mixture time series for $t = 1, \ldots, 100$.

$$I\left(f_j\right)=\left(\frac{2}{n}\sum_{t=1}^{n} z_t \cos\left(2\pi t f_j\right)\right)^2+\left(\frac{2}{n}\sum_{t=1}^{n} z_t \sin\left(2\pi t f_j\right)\right)^2,$$

where $f_j = j/n$ and z_t is the x_t series. The scaled periodogram of the data, X_t, simulated is shown in Figure 8.13, and it clearly identifies the three components x_{t1}, x_{t2}, and x_{t3} of X_t. Moreover, the heights of the scaled periodogram shown in the figure are

$$I(6/100) = 13, \quad I(10/100) = 41, \quad I(40/100) = 85$$

and $I(j/n) = 0$ otherwise. These are exactly the values of the squared amplitudes of the components generated.

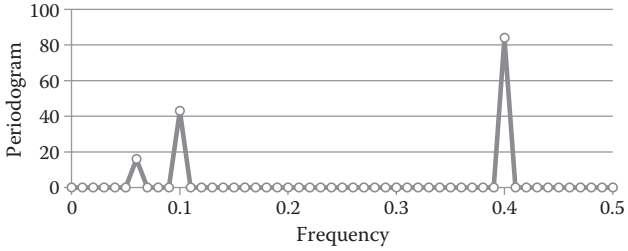

FIGURE 8.13 Periodogram in Example 8.24.

8.11.4 Spectral Density Function

Spectral analysis can be considered as a development of a Fourier analysis for stationary time series. The difference is that in classical Fourier analysis, a real function of $z(t)$ is represented by a Fourier series, but in spectral analysis, the autocovariance function of a stationary time series is represented in terms of a Fourier transform. This function was developed by Herglotz (1911). He stated that a positive-definite function, such as the autocovariance function, γ_k, of a stationary time series can be represented as follows:

$$\gamma_k = \int_{(-\pi,\pi]} e^{i\omega k}\, \mathrm{d}P(\omega), \tag{8.139}$$

where $P(\omega)$ is the spectral distribution function. If a spectral density function exists, it can be shown that $\mathrm{d}P(\omega) = p(\omega)\, \mathrm{d}\omega$ and Equation 8.139 can be written as

$$\gamma k = 2\int^{\pi} p(\omega)\cos(\omega k)\, \mathrm{d}\omega. \tag{8.140}$$

The function $p(\omega)$ $(-\pi \le \omega \le \pi)$ is called a spectral density function and has some properties of the probability density function. $p(\omega)$ is symmetric, $p(\omega) = p(-\omega)$. The unit of ω is radians per unit time, which is called angular or circular frequency. In practice, the units of cycles per unit time for ω is used by the equation $\omega = 2\pi f$, where f is cycles per unit time.

8.11.5 ANOVA Decomposition

Considering $k = 0$ in Equation 8.140, γ_0 is obtained, which is equal to $\mathrm{var}(z_t)$.

$$\mathrm{var}\left(z_t\right) = 2\int_0^{\pi} p(\omega)\, \mathrm{d}\omega. \tag{8.141}$$

The spectral analysis similar to analysis of variance (ANOVA) decomposes a time series into its frequency components as shown in Equation 8.141. The sample analog of Equation 8.141 is given in Equation 8.142.

$$\sum_{t=1}^{n}\left(z_t - \overline{z}\right)^2 = \sum_{j=1}^{[(n-1)/2]} I\left(f_j\right) + I\left(f_{[n/2]}\right), \tag{8.142}$$

where $I(f_{[n/2]})$ is omitted when n is an odd integer. The spectral density function is derived by taking the inverse Fourier transformation to Equation 8.142, resulting in

$$p(f) = \sum_{k=-\infty}^{\infty} \gamma_k e^{-2\pi f k}, \quad |f| \le 0.5. \tag{8.143}$$

The sample analog of this formula is as follows:

$$I(f) = \sum_{k=-(n-1)}^{n-1} c_k e^{-2\pi f k}, \tag{8.144}$$

where c_k denotes the sample autocovariance function estimated as follows:

$$c_k = \frac{1}{n}\sum_{l=k+1}^{n}(z_t - \overline{z})(z_{t-k} - \overline{z}) \qquad k \geq 0. \tag{8.145}$$

For $k < 0$, $c_k = c_{-k}$.

Example 8.25

For the polynomials of $z\,(t_1, t_2)$: $= a + bt_1 + ct_2 + dt_1t_2$ with parameters a, b, c, and $d \in R$, calculate the terms of the ANOVA decomposition.

Solution:

The terms of the ANOVA decomposition are given by

$$z_0 = a + \frac{b}{2} + \frac{c}{2} + \frac{d}{4}$$

$$z_1(t_1) = \left(a + \frac{d}{2}\right)\left(t_1 - \frac{1}{2}\right)$$

$$z_2(t_2) = \left(c + \frac{d}{2}\right)\left(t_2 - \frac{1}{2}\right)$$

$$z_{1,2}\left(t_1, t_2\right) = \frac{d}{4}\left(2t_1 - 1\right)\left(2t_2 - 1\right).$$

For the specific case $a = 0$, $b = 12$, $c = 6$, and $d = -6$, i.e., for the polynomial

$$z(t_1, t_2): = 12t_1 + 6t_2 - 6t_1t_2,$$

which gives

$$z_0 = \frac{15}{2}$$

$$z_1(t_1) = 9t_1 - \frac{9}{2}$$

$$z_2(t_2) = 3t_2 - \frac{3}{2}$$

$$z_{1,2}(t_1, t_2) = -6t_it_2 + 3t_1 + 3t_2 - \frac{3}{2}.$$

The variance of f is given by $\text{var}(z_t) = 31/4$ and we see that $\text{var}(z_1) = 27/4$, $\text{var}(z_2) = 3/4$, and $\text{var}(z_{1,2}) = 1/4$. Hence, the one-dimensional terms z_1 and z_2 explain about 87% and 10% of $\text{var}(z)$, respectively. The highest-order term $z_{1,2}$ contributes the remaining 3% of the total variance.

8.11.6 Spectral Density and ARMA Model

The ARMA(p,q) model can be shown as follows:

$$\phi(B)z_t = \phi(B)a_t, \tag{8.146}$$

where

$$\phi(B) = 1 - \phi_1 B - \ldots - \phi_p B^p,\ \theta B^q = 1 - \phi_1 B - \ldots - \phi_p B^p \tag{8.147}$$

and a_t is the white noise with variance σ_a^2 and B is the backshift operator on t. The theoretical spectral density function of generated time series by ARMA(p,q) model is given by

$$p(f) = \sigma_a^2 \mid \psi\left(e^{2\pi if}\right) \mid^2, \tag{8.148}$$

where

$$\psi(B) = \frac{\theta(B)}{\phi(B)}. \tag{8.149}$$

8.11.7 GARCH Model

Autoregressive conditionally heteroskedastic (ARCH) models were introduced by Engle (1982) and their GARCH (generalized ARCH) extension is due to Bollerslev (1986). In these models, the key concept is the conditional variance, that is, the variance conditional on the past. In the classical GARCH models, the conditional variance is expressed as a linear function of the squared past values of the series. This particular specification is able to capture the main stylized facts characterizing financial series, as described in Chapter 1. At the same time, it is simple enough to allow for a complete study of the solutions. The "linear" structure of these models can be displayed through several representations that will be studied in this chapter.

We first present definitions and representations of GARCH models. Then, we establish the strict and second-order stationary conditions. Starting with the first-order GARCH model, for which the proofs are easier and the results are more explicit, we extend the study to the general case. Then, we consider the existence of moments and the properties of the autocorrelation structure. We conclude this chapter by examining forecasting issues.

Definitions and Representations

For GARCH processes, first, two conditional moments are described. A process (ε_t) is called a GARCH(p,q) process if its first two conditional moments exist and satisfy

$$E(\varepsilon_t \mid \varepsilon_u\ u < t) = 0,\ t \in Z. \tag{8.150}$$

There exist constants ω, α_i, $i = 1, \ldots, q$ and β_j, $j = 1, \ldots, p$ such that

$$\sigma_t^2 = \mathrm{Var}\left(\varepsilon_t \mid \varepsilon_u, u < t\right) = \omega + \sum_{i=1}^{q} \alpha_i \varepsilon_{t-1}^2 + \sum_{j=1}^{q} \beta_i \sigma_{t-j}^2,\ t \in Z. \tag{8.151}$$

The process is called an ARCH(q) process (1); by definition, the innovation of the process $\left(\varepsilon_t^2\right)$ is the variable $v_t = \varepsilon_t^2 - \sigma_t^2$. Substituting in Equation 8.143 the variables σ_{t-j}^2 by $\varepsilon_{t-j}^2 - v_{t-j}$ results in

$$\varepsilon_t^2 = \omega + \sum_{i=1}^{r} (\alpha_i + \beta_i)\varepsilon_{t-i}^2 + v_t - \sum_{j=1}^{p} \beta_i v_{t-j},\ t \in Z, \tag{8.152}$$

where r is max(p,q), with the convention $\alpha_i = 0(\beta_j = 0)$ if $i > q$ ($j > p$). This equation has the linear structure of an ARMA model, allowing for simple computation of the linear predictions. Under additional assumptions (implying the second-order stationary of ε_t^2), we can state that if ε_t^2 is GARCH(p,q), then, ε_t^2 is an ARMA(r,p) process. In particular, the square of an ARCH(q) process admits, if it is stationary, an AR(q) representation. The ARMA representation will be useful for the estimation and identification of GARCH processes.

When η_t is a sequence with distribution η, the process ε_t^2 is called a strong GARCH(p,q) (with respect to the sequence, η_t) if

$$\begin{cases} \varepsilon_t = \sigma_t \eta_t \\ \sigma_t^2 = \omega + \sum_{i=1}^{q} \alpha_i \varepsilon_{t-i}^2 + \sum_{j=1}^{p} \beta_i \sigma_{t-i}^2, \end{cases} \tag{8.153}$$

where α_i and β_j are nonnegative constants and ω is a (strictly) positive constant.

GARCH processes are sometimes called semistrong, following the paper by Drost and Nijman (1993) on temporal aggregation. Substituting (ε_{t-1}) by $\sigma_{t-i}\eta_{t-i}$ in Equation 8.153, we get

$$\sigma_t^2 = \omega + \sum_{i=1}^{q} \alpha_i \sigma_{t-i}^2 \eta_{t-i}^2 + \sum_{j=1}^{p} \beta_i \sigma_{t-i}^2. \tag{8.154}$$

This can be written as

$$\sigma_t^2 = \omega + \sum_{i=1}^{r} a_i(\eta_{i-i})\sigma_{t-i}^2, \tag{8.155}$$

where $a_i(z) = \alpha_i Z^2 + \beta_i$, $i = 1,\ldots, r$. This representation shows that the volatility process of a strong GARCH is the solution of an autoregressive equation with random coefficients.

The GARCH(1,1) case:

When $p = q = 1$, Equation 8.155 has the form

$$\begin{cases} \varepsilon_t = \sigma_t \eta_t, \left(\eta_t\right) iid(0,1) \\ \sigma_t^2 = \omega + \alpha\varepsilon_{t-i}^2 + \beta\sigma_{t-i}^2 \end{cases}, \tag{8.156}$$

where $\omega \geq 0$, $\alpha \geq 0$, and $\beta \geq 0$. Let $a(z) = \alpha Z^2 + \beta$.

8.12 CONCLUDING REMARKS

In this chapter, the principles of the time series analysis and development of two well-known statistical models—ARMA and GARCH—are discussed. Due to the stochastic nature of hydrologic events and variables, these models are successfully employed for simulation of these models' behaviors. However, in these models' applications, great attention should be given to the compatibility of the selected model and the data behavior. For this purpose, different tests are used to ensure these models' performance. The calibrated models can then be used for simulation of hydrologic events and generation of synthetic data. ARIMA models as a special class of ARMA models can be used for forecasting behavior of hydrologic events.

PROBLEMS

1. Table 8.21 shows the annual rainfall at a rain gauge. Test the stationarity of the time series in its mean. Define a trend model and the residuals of the series.
2. Remove the trend of the given time series in Problem 1, using the differencing operator.
3. A series of residuals of a model fitted to precipitation data in a station in 20 time intervals is given in Table 8.22. Use the turning point test and comment on the randomness of the residuals.

TABLE 8.21
Rainfall Data for Problem 1

Time Sequences	Precipitation Data (mm)	Time Sequences	Precipitation Data (mm)
1	200	11	172
2	212	12	180
3	302	13	185
4	212	14	190
5	192	15	302
6	186	16	215
7	148	17	218
8	312	18	158
9	220	19	142
10	195	20	175

TABLE 8.22
Data for Problem 3

Month	Residual	Month	Residual
1	0.87	11	0.78
2	0.28	12	0.82
3	0.32	13	0.14
4	0.34	14	0.22
5	0.33	15	0.65
6	0.15	16	0.48
7	0.18	17	0.32
8	0.17	18	0.07
9	0.21	19	0.24
10	0.22	20	0.25

TABLE 8.23
Data for Problem 4

Interval (i)	Precipitation Depth Classes (mm)	Actual Frequency (f_i)
1	$0 \le P < 5$	27
2	$5 \le P < 10$	24
3	$10 \le P < 15$	9
4	$15 \le P < 20$	8
5	$20 \le P < 25$	5
6	$25 \le P < 30$	4
7	$30 \le P < 35$	2
8	$35 \le P$	1

4. The classified monthly precipitation data measured in a station is divided into eight categories as shown in Table 8.23. Previous studies have shown that the precipitation data in this station are normally distributed. Use the chi-square test with 5% significance level and comment on the selected distribution for the sample data.
5. Stream time series of a river could be shown in the form of the following equation. Categorize this model as a multiplicative ARIMA model.

$$(1 - B^{12})Z_t = (1 + 0.2B)(1 - 0.9B^{12})\,\varepsilon_t$$

6. For an AR(2) model, the parameters have been estimated as $\phi_1(2) = 0.35$ and $\phi_2(2) = 0.5$. Check the parameters' stationary condition. If it is used for 100-year normal and standardized annual inflows to a reservoir and the first and second correlation coefficients are estimated as $\rho_1 = 0.6$ and $\rho_2 = 0.35$, estimate the model parameters if the variance of normal and standardized inflow series is estimated as 1.6.
7. For an MA(2) model, the parameters have been estimated as $\theta_1 = 0.8$ and $\theta_2 = 0.45$. Check whether the parameters pass the invertibility condition.
8. What is the main property of the multivariate and disaggregation model? What is the benefit of these models in comparison to the univariate model?
9. Write the mathematical expression of order 1 and order 2 nonseasonal ARIMA. Why is the seasonal differencing done? Write the mathematical expression of the second-order seasonal differencing for monthly time series (assume 12 for the number of seasons).
10. The ARMA(1,1) model is fitted to the time series of streamflow at a station with parameters $\phi_1(1) = -0.6$ and $\theta_1 = -0.4$. Plot the autocorrelation functions of the time series from lag 1 to lag 5.
11. The given models in Table 8.24 are fitted to a time series. The corresponding variance of the model residuals is also given in this table. What would be the selected model based on AIC criteria? The number of data in the time series is 40.

TABLE 8.24
Data for Problem 11

Model Type	Variance of Model Residuals
ARMA(1,0)	0.572
ARMA(2,0)	0.534
ARMA(1,1)	0.546
ARMA(2,1)	0.523

12. Data in Table 8.25 are used in runoff modeling. The table shows the 30-year-duration data related to the summer rainfall of a given area. Investigate the adequacy of the length of data.
13. Develop an ARMA(1,1) for a time series data with these specifications:

Average inflow to reservoir = 653 m^3/s

Standard deviation = 186.6 m^3/s

Correlation parameters of $\rho_1 = 0.37$ and $\rho_2 = 0.24$.

Using the developed model and the given random numbers, generate the values of inflow to reservoir for the next 3 years. The current year inflow to reservoir is 653 m^3/s. $\varepsilon_0 = 0.638$, $\varepsilon_1 = 0.131$, $\varepsilon_2 = -0.859$, $\varepsilon_3 = -1.096$.

14. Develop ARIMA(1,1,1)(0,1,2)4. Consider that this model is used to predict the rainfall during a year, what would be the scale of the model outputs (daily, monthly, or seasonally)? At most, how many data are effectively used in order to predict the present rainfall values?
15. ARMA(2,0) is selected for a time series (Z). Predict $Z_t + 1$ to $Z_t + 3$. $\phi_1(2) = 0.79$, $\phi_2(2) = 0.13$, $Z_t = 0.75$, $Z_{t-1} = 0.53$, and the standard deviation is 0.45. Generate two values using the following normal random values:

$$\left.\begin{matrix}\mu = 100 \\ \sigma = 15\end{matrix}\right\} \zeta_1 = 0/02 \text{ and } \zeta_2 = 0/1$$

TABLE 8.25
Data for Problem 12

Year	0	1	2	3	4	5	6	7	8	9
1980	39.7	15.9	50.0	85.8	9.5	66.3	32.0	6.7	13.6	1.1
1990	57.8	15.0	0.5	18.1	9.8	40.3	20.2	7.4	0.5	20.1
2000	8.5	57.4	58.6	2.0	5.1	5.2	16.5	1.9	11.2	8.2

TABLE 8.26
Data for Problem 16

Number	1	2	3	4	5	6	7	8	9	10
SPI	0.10	0.55	0.57	0.78	0.00	–0.38	–0.57	–0.59	–0.63	0.52
Number	11	12	13	14	15	16	17	18	19	20
SPI	0.41	0.36	0.30	0.45	–0.91	–0.38	–0.38	–0.38	0.27	0.50

TABLE 8.27
Data for Problem 17

Model	Standard Deviation of the Model
AR(1)	0.41
MA(1)	0.23
ARMA(1,1)	0.29
ARMA(2,1)	0.18
ARMA(2,2)	0.29

16. State the short- or long-term memory of the given standard precipitation, SPI, data in Table 8.26.
17. The results of modeling for a 200-month time series of a river inflow are determined as given in Table 8.27. Select the best model(s).

APPENDIX

TABLE 8.A1
Chi-Square Distribution (the Following Table Provides the Values of χ^2_α That Correspond to a Given Upper-Tail Area α and a Specified Number of Degrees of Freedom)

Degrees of Freedom	Upper-Tail Area α						
	0.99	**0.98**	**0.95**	**0.90**	**0.80**	**0.70**	**0.50**
1	0.000157	0.000628	0.00393	0.0158	0.0642	0.148	0.455
2	0.0201	0.0404	0.103	0.211	0.446	0.713	1.386
3	0.115	0.185	0.352	0.584	1.005	1.424	2.366
4	0.297	0.429	0.711	1.064	1.649	2.195	3.357
5	0.554	0.752	1.145	1.610	2.343	3.000	4.351
6	0.872	1.134	1.635	2.204	3.070	3.828	5.348
7	1.239	1.564	2.167	2.833	3.822	4.671	6.346
8	1.646	2.032	2.733	3.490	4.594	5.527	7.344
9	2.088	2.532	3.325	4.168	5.380	6.393	8.343
10	2.558	3.059	3.940	4.865	6.179	7.267	9.342
11	3.053	3.609	4.575	5.578	6.989	8.148	10.341
12	3.571	4.178	5.226	6.304	7.807	9.034	11.340
13	4.107	4.765	5.892	7.042	8.634	9.926	12.340
14	4.660	5.368	6.571	7.790	9.467	10.821	13.339
15	5.229	5.985	7.261	8.547	10.307	11.721	14.339
16	5.812	6.614	7.962	9.312	11.152	12.624	15.338
17	6.408	7.255	8.672	10.085	12.002	13.531	16.338
18	7.015	7.906	9.390	10.865	12.857	14.440	17.338
19	7.633	8.567	10.117	11.651	13.716	15.352	18.338
20	8.260	9.237	10.851	12.443	14.578	16.266	19.337
21	8.897	9.915	11.591	13.240	15.445	17.182	20.337
22	9.542	10.600	12.338	14.041	16.314	18.101	21.337
23	10.196	11.293	13.091	14.848	17.187	19.021	22.337
24	10.856	11.992	13.848	15.659	18.062	19.943	23.337
25	11.524	12.697	14.611	16.473	18.940	20.867	24.337
26	12.189	13.409	15.379	17.292	19.820	21.792	25.336
27	12.879	14.125	16.151	18.114	20.703	22.719	26.336
28	13.565	14.847	16.928	18.939	21.588	23.647	27.336
29	14.256	15.574	17.708	19.768	22.475	24.577	28.336
30	14.953	16.306	18.493	20.599	23.364	25.508	26.336

Degrees of Freedom	Upper-Tail Area α						
	0.30	**0.20**	**0.10**	**0.05**	**0.02**	**0.01**	**0.001**
1	1.074	1.642	2.706	3.841	5.412	6.635	10.827
2	2.408	3.219	4.605	5.991	7.824	9.210	13.815
3	3.665	4.642	6.251	7.815	9.837	11.345	16.268
4	4.878	5.989	7.779	9.488	11.668	13.277	18.465

(*continued*)

TABLE 8.A1 (Continued)
Chi-Square Distribution (the Following Table Provides the Values of χ^2_α That Correspond to a Given Upper-Tail Area α and a Specified Number of Degrees of Freedom)

Degrees of Freedom	Upper-Tail Area α						
	0.99	**0.98**	**0.95**	**0.90**	**0.80**	**0.70**	**0.50**
5	6.064	7.289	9.236	11.070	13.388	15.086	20.517
6	7.231	8.558	10.645	12.592	15.033	16.812	22.457
7	8.383	9.803	12.017	14.067	16.622	18.475	24.322
8	9.524	11.030	13.362	15.507	18.168	20.090	26.125
9	10.656	12.242	14.684	16.919	19.679	21.666	27.877
10	11.781	13.442	15.987	18.307	21.161	23.209	29.588
11	12.899	14.631	17.275	19.675	22.618	24.725	31.264
12	14.011	15.812	18.549	21.026	24.054	26.217	32.909
13	15.119	16.985	19.812	22.362	25.472	27.688	34.528
14	16.222	18.151	21.064	23.685	26.873	29.141	36.123
15	17.322	19.311	22.307	24.996	28.259	30.578	37.697
16	18.418	20.465	23.542	26.296	29.633	32.000	39.252
17	19.511	21.615	24.769	27.587	30.995	33.409	40.790
18	20.601	22.760	25.989	28.869	32.346	34.805	42.312
19	21.689	23.900	27.204	30.144	33.687	36.191	43.820
20	22.775	25.038	28.412	31.410	35.020	37.566	45.315
21	23.858	26.171	29.615	32.671	36.343	38.932	46.797
22	24.939	27.301	30.813	33.924	37.659	40.289	48.268
23	26.018	28.429	32.007	35.172	38.968	41.638	49.728
24	27.096	29.553	33.196	36.415	40.270	42.980	51.179
25	28.172	30.675	34.382	37.652	41.566	44.314	52.620
26	29.246	31.795	35.563	38.885	42.856	45.642	54.052
27	30.319	32.912	36.741	40.113	44.140	46.963	55.476
28	31.391	34.027	37.916	41.337	45.419	48.278	56.893
29	32.461	35.139	39.087	42.557	46.693	49.588	58.302
30	33.530	36.250	40.256	43.773	47.962	50.892	59.703

TABLE 8.A2
Critical Values of *D* for Kolmogorov–Smirnov Maximum Deviation Test for Goodness of Fit (the Following Table Provides the Critical Values, D_α, Corresponding to an Upper-Tail Probability, α, of the Test Statistic *D*)

n	**α = 0.1**	**α = 0.05**	**α = 0.025**	**α = 0.01**	**α = 0.005**
1	0.90000	0.95000	0.97500	0.99000	0.99500
2	0.68377	0.77639	0.84189	0.90000	0.92929
3	0.56481	0.63604	0.70760	0.78456	0.82900
4	0.49265	0.56522	0.62394	0.68887	0.73424
5	0.44698	0.50945	0.56328	0.62718	0.66853
6	0.41037	0.46799	0.51926	0.57741	0.61661
7	0.38148	0.43607	0.48342	0.53844	0.57581
8	0.35831	0.40962	0.45427	0.50654	0.54179
9	0.33910	0.38746	0.43001	0.47960	0.51332
10	0.32260	0.36866	0.40925	0.45662	0.48893

(*continued*)

TABLE 8.A2 (Continued)
Critical Values of *D* for Kolmogorov–Smirnov Maximum Deviation Test for Goodness of Fit (the Following Table Provides the Critical Values, D_α, Corresponding to an Upper-Tail Probability, α, of the Test Statistic *D*)

n	α = 0.1	α = 0.05	α = 0.025	α = 0.01	α = 0.005
11	0.30829	0.35242	0.39122	0.43670	0.46770
12	0.29577	0.33815	0.37543	0.41918	0.44905
13	0.28470	0.32549	0.36143	0.40362	0.43247
14	0.27481	0.31417	0.34890	0.38970	0.41762
15	0.26588	0.30397	0.33760	0.37713	0.40420
16	0.25778	0.29472	0.32733	0.36571	0.39201
17	0.25039	0.28627	0.31796	0.35528	0.38086
18	0.24360	0.27851	0.30936	0.34569	0.37062
19	0.23735	0.27136	0.30143	0.33685	0.36117
20	0.23156	0.26473	0.29408	0.32866	0.35241
21	0.22617	0.25858	0.28724	0.32104	0.34427
22	0.22115	0.25283	0.28087	0.31394	0.33666
23	0.21645	0.24746	0.27490	0.30728	0.32954
24	0.21205	0.24242	0.26931	0.30104	0.32286
25	0.20790	0.23768	0.26404	0.29516	0.31657
26	0.20399	0.23320	0.25907	0.28962	0.31064
27	0.20030	0.22898	0.25438	0.28438	0.30502
28	0.19680	0.22497	0.24993	0.27942	0.29971
29	0.19348	0.22117	0.24571	0.27471	0.29466
30	0.19032	0.21756	0.24170	0.27023	0.28987
31	0.18732	0.21412	0.23788	0.26596	0.28530
32	0.18445	0.21085	0.23424	0.26189	0.28094
33	0.18171	0.20771	0.23076	0.25801	0.27677
34	0.17909	0.20472	0.22743	0.25429	0.27279
35	0.17659	0.20185	0.22425	0.25073	0.26897
36	0.17418	0.19910	0.22119	0.24732	0.26532
37	0.17188	0.19646	0.21826	0.24404	0.26180
38	0.16966	0.19392	0.21544	0.24089	0.25843
39	0.16753	0.19148	0.21273	0.23786	0.25518
40	0.16547	0.18913	0.21012	0.23494	0.25205
41	0.16349	0.18687	0.20760	0.23213	0.24904
42	0.16158	0.18468	0.20517	0.22941	0.24613
43	0.15974	0.18257	0.20283	0.22679	0.24332
44	0.15796	0.18053	0.20056	0.22426	0.24060
45	0.15623	0.17856	0.19837	0.22181	0.23798
46	0.15457	0.17665	0.19625	0.21944	0.23544
47	0.15295	0.17481	0.19420	0.21715	0.23298
48	0.15139	0.17302	0.19221	0.21493	0.23059
49	0.14987	0.17128	0.19028	0.21277	0.22828
50	0.14840	0.16959	0.18841	0.21068	0.22604
51	0.14697	0.16796	0.18659	0.20864	0.22386
52	0.14558	0.16637	0.18482	0.20667	0.22174
53	0.14423	0.16483	0.18311	0.20475	0.21968
54	0.14292	0.16332	0.18144	0.20289	0.21768
55	0.14164	0.16186	0.17981	0.20107	0.21574

(*continued*)

TABLE 8.A2 (Continued)
Critical Values of *D* for Kolmogorov–Smirnov Maximum Deviation Test for Goodness of Fit (the Following Table Provides the Critical Values, D_α, Corresponding to an Upper-Tail Probability, α, of the Test Statistic *D*)

n	α = 0.1	α = 0.05	α = 0.025	α = 0.01	α = 0.005
56	0.14040	0.16044	0.17823	0.19930	0.21384
57	0.13919	0.15906	0.17669	0.19758	0.21199
58	0.13801	0.15771	0.17519	0.19590	0.21019
59	0.13686	0.15639	0.17373	0.19427	0.20844
60	0.13573	0.15511	0.17231	0.19267	0.20673
61	0.13464	0.15385	0.17091	0.19112	0.20506
62	0.13357	0.15263	0.16956	0.18960	0.20343
63	0.13253	0.15144	0.16823	0.18812	0.20184
64	0.13151	0.15027	0.16693	0.18667	0.20029
65	0.13052	0.14913	0.16567	0.18525	0.19877
66	0.12954	0.14802	0.16443	0.18387	0.19729
67	0.12859	0.14693	0.16322	0.18252	0.19584
68	0.12766	0.14587	0.16204	0.18119	0.19442
69	0.12675	0.14483	0.16088	0.17990	0.19303
70	0.12586	0.14381	0.15975	0.17863	0.19167
71	0.12499	0.14281	0.15864	0.17739	0.19034
72	0.12413	0.14183	0.15755	0.17618	0.18903
73	0.12329	0.14087	0.15649	0.17498	0.18776
74	0.12247	0.13993	0.15544	0.17382	0.18650
75	0.12167	0.13901	0.15442	0.17268	0.18528
76	0.12088	0.13811	0.15342	0.17155	0.18408
77	0.12011	0.13723	0.15244	0.17045	0.18290
78	0.11935	0.13636	0.15147	0.16938	0.18174
79	0.11860	0.13551	0.15052	0.16832	0.18060
80	0.11787	0.13467	0.14960	0.16728	0.17949
81	0.11716	0.13385	0.14868	0.16626	0.17840
82	0.11645	0.13305	0.14779	0.16526	0.17732
83	0.11576	0.13226	0.14691	0.16428	0.17627
84	0.11508	0.13148	0.14605	0.16331	0.17523
85	0.11442	0.13072	0.14520	0.16236	0.17421
86	0.11376	0.12997	0.14437	0.16143	0.17321
87	0.11311	0.12923	0.14355	0.16051	0.17223
88	0.11248	0.12850	0.14274	0.15961	0.17126
89	0.11186	0.12779	0.14195	0.15873	0.17031
90	0.11125	0.12709	0.14117	0.15786	0.16938
91	0.11064	0.12640	0.14040	0.15700	0.16846
92	0.11005	0.12572	0.13965	0.15616	0.16755
93	0.10947	0.12506	0.13891	0.15533	0.16666
94	0.10889	0.12440	0.13818	0.15451	0.16579
95	0.10833	0.12375	0.13746	0.15371	0.16493
96	0.10777	0.12312	0.13675	0.15291	0.16408
97	0.10722	0.12249	0.13606	0.15214	0.16324
98	0.10668	0.12187	0.13537	0.15137	0.16242
99	0.10615	0.12126	0.13469	0.15061	0.16161
100	0.10563	0.12067	0.13403	0.14987	0.16081

REFERENCES

Akaike, H. (1974). "A new look at the statistical model identification," *IEEE Transactions on Automatic Control*, 19 (6), 716–723.

Anderson, R.L. (1942). "Distribution of the serial correlation coefficient," *Annals of Mathematical Statistics*, 13, 1–13.

Bollerslev, T. (1986). "Generalized autoregressive conditional heteroskedasticity," *Journal of Econometrics*, 31 (3), 307–327.

Box, G.E.P. and Cox, D.R. (1964). "An analysis of transformation," *Journal of the Royal Statistical Society*, B26, 211–252.

Box, G.E.P. and Jenkins, G. (1970). *Time Series Analysis: Forecasting and Control*, Holden-Day, San Francisco.

Box, G.E.P. and Pierce, D.A. (1970). "Distribution of residual autocorrelations in autoregressive integrated moving average time series models," *Journal of the American Statistical Association*, 65, 1509–1526.

Brockwell, P.J. and Davis, R.A. (1987). *Time Series Theory and Methods*, Springer, New York.

Campbell, S. and Diebold, F.X. (2002). Weather forecasting for weather derivatives. Working Paper 02-046, Penn Institute for Economic Research, Department of Economics, University of Pennsylvania.

Delleur, J.W. and Karamouz, M. (1982). Uncertainty in reservoir operation. Optimal Allocation of Water Resources, IAHS Publication no. 135.

Drost, F.C. and Nijman, T.E. (1993). "Temporal aggregation of GARCH processes," *Econometrica*, 61, 909–927.

Durbin, J. (1960). "The fitting of time series models," *Review of the International Statistical Institute*, 28, 233–244.

Engle, R.F. (1982). "Autoregressive conditional heteroskedasticity with estimates of the variance of United Kingdom inflation," *Econometrica*, 50 (4), 987–1007.

Fiering, M.B. (1964). "A multivariate technique for synthetic hydrology," *Journal of Hydraulic Division, ASCE*, 89, 43.

Franses, P.H., Neele, J. and van Dijk, D. (2001). "Modeling asymmetric volatility in weekly Dutch temperature data," *Environmental Modelling and Software*, 16, 131–137.

Granger, C.W. and Andersen, A.P. (1978). "On the invertibility of time series models," *Stochastic Processes and Their Applications*, 8, 87–92.

Hashino, M. and Delleur, J.W. (1981). Investigation of the Hurst coefficient and optimization of ARMA models for annual river flow. Report CE-HSE-81-1, Civil Engineering, Purdue University, West Lafayette, IN.

Herglotz, G. (1911). "Über die Mechanik des deformierbaren Körpers vom Standpunkt der Reletivistätsteorie," *Annalen der Physik*, 36, 493–533.

Hipel, K.W. and McLeod, A.I. (1977). "Advances in Box–Jenkins modelling. Part 1, model construction," *Water Resources Research*, 13, 567–575.

Hurst, H.E., Black, R.P. and Simaika, Y.M. (1965). *Long-Term Storage: An Experimental Study*, Constable, London.

Hyndman, R.J. and Wand, M.P. (1997). "Nonparametric autocovariance function estimation," *Australian Journal of Statistics*, 39, 313–324.

Lane, W.L. (1979). Applied Stochastic Techniques (LAST Computer Package), User Manual. Division of Planning Technical Services, Bureau of Reclamation, Denver, CO, December.

Lapin L.L. (1990). *Probability and Statistics for Modern Engineering*, PWS-KENT Publishing Company, Boston, MA.

Ljung, G. and Box, G. (1978). "On a measure of lack of fit in time series models," *Biometrika*, 65, 297–303.

Matalas, N.C. (1967). "Mathematical assessment of synthetic hydrology," *Journal of Water Resources*, 3 (4), 937–945.

McLeod, A.I. and Li, W.K. (1983). "Diagnostic checking ARMA time series models using squared residual autocorrelations," *Journal of Time Series Analysis*, 4, 269–273.

Mejia, J.M. (1971). On the generation of multivariate sequences exhibiting the Hurst phenomenon and some flood frequency analysis. Colorado State University, Fort Collins, CO.

Mejia, J.M. and Rousselle, J. (1976). "Disaggregation models in hydrology revisited," *Journal of Water Resources Research*, 12 (2), 185–186.

O'Connel, M.J. (1974). "Search program for significant variables," *Computer Physics Communications*, 8, 49.

O'Connell, P.E. (1974). Stochastic Modeling of Long-term Persistence in Streamflow Sequences. PhD Thesis Imperial College, University of London.

Salas, J.D. and Pegram, G.G.S. (1977). "A seasonal multivariate multilag autoregressive model in hydrology." *Proceeding of the Third International Symposium of Theoretical and Applied Hydrology*, Colorado State University, Fort Collins, Colorado.

Salas, J.D. and Smith, R.A. (1980). Uncertainties in hydrologic time series analysis. ASCE Spring Meeting, Portland, OR, Preprint 80-158.

Salas, J.D., Delleur, J.W., Yevjevich, V. and Lane, W.L. (1988). *Applied Modeling of Hydrological Time Series*, Water Resources Publication, Littleton, Colorado.

Shahin, M., Van Oorschot, H.J.K. and De Lang, S.J. (1993). *Statistical Analysis in Water Resources Engineering*, AA Balkema, Rotterdam.

Snedecor, G.W. and Cochran, W.G. (1967). *Statistical Methods*, 6th edition, The Iowa State University Press, Ames, IA.

Tao, P.C. and Delleur, J.W. (1976). "Multistation, multiyear synthesis of hydrologic time series by disaggregation," *Water Resources Research*, 12(6), 1303–1312.

Thomas, H.A. and Fiering, M.B. (1962)."Mathematical synthesis of streamflow sequences for the analysis of river basins by simulation." In *Design of Water Resources Systems*, Maas, A. et al., eds, Chapter 12. Harvard University Press, Cambridge, MA.

Tol, R.S.J. (1996). "Autoregressive conditional heteroscedasticity in daily temperature measurements," *Environmetrics*, 7, 67–75.

Torró, H., Meneu, V. and Valor, E. (2001). Single Factor Stochastic Models with Seasonality Applied to Underlying Weather Derivatives Variables. Manuscript, University of Valencia.

Valencia, D. and Schaake, J.C. (1973). "Disaggregation process in stochastic hydrology," *Journal of Water Resources Research*, 9 (3), 580–585.

Yevjevich, V. (1972). *Stochastic Process in Hydrology*, Water Resources Publications, Fort Collins, CO.

9 Climate Change Impacts and Models

9.1 INTRODUCTION

Climate is defined in terms of statistical averages such as air temperature, hours of bright sunshine, and precipitation. There are periodic changes in climate over diurnal and annual time scales, which are an integral part of the operation of the Earth–atmosphere system and which do not involve long-term structural changes. However, it is possible to identify longer-term changes in climate occurring over periods of decades and centuries. Some of these changes represent considerable modifications to the mode of operation of the Earth's surface and the atmospheric system. The Earth's surface reveals evidence of periods of extreme cold, when large areas were under thick sheets of ice. Areas that are deserts today contain landforms that are clearly fluvial in origin, suggesting periods of wetter climate conditions. Measurements of climatic parameters (which have been available only since the early 18th century) reveal, for example, general increase in global mean air temperature over the period from the late 19th century. More recently, the greater frequency of failure of monsoon rains to reach northwest India and the extension of desert conditions along the south side of Sahara in the Sahel in Africa indicate that major changes in the Earth–atmosphere system are currently taking place. These changes can be viewed alternatively as a result of the changing operation of factors external to the Earth–atmosphere system or as modifications of the disposition of internal energy and matter. For example, changes in temperature of the lower troposphere may be due to changing radiant energy exchange between the Earth–atmosphere system and its surroundings (space). Alternatively, it may be that structural modifications within the system have resulted in more or less energy being stored as sensible heat within the atmosphere. If we view the Earth–atmosphere system as a black box, then our first alternative concerns a discussion of the relationships between input and output and we may make general statements regarding throughput. Changes within the system concern its response to energy inputs, in which case we must consider the pathways along which energy and matter are transferred, the nature of stores, and the rate at which energy and matter are transferred between them. In this respect, the regulators, which are control points within the system, are critical.

This chapter deals with the cause and effect of climate change phenomena; its impact on the different components of, and the relationships within, the hydrologic cycle; and climate change simulation and analysis. The chapter starts by describing the climate change phenomenon and the greenhouse effect. Then, carbon cycle, which highly affects the climatic condition, is introduced, after which, the impact of climate change on the hydrologic cycle and water availability is discussed. What follows is a description of the climate change simulation and analysis process including the description of climate change scenarios and the downscaling processes. Then, the climate change study process in five real cases is discussed.

9.2 THE GREENHOUSE EFFECT

Greenhouse gases act as a thermal blanket around the globe, raising the Earth's surface temperature beyond the equivalent temperature calculated earlier. The importance of water vapor as a

greenhouse gas is quite evident on clear nights, when the Earth cools much more rapidly than it does on cloudy nights. It is also interesting to note that the term *greenhouse effect* is based on the concept of a conventional greenhouse with glass acting much like the aforementioned gases. Glass, which easily transmits short-wavelength solar energy into the greenhouse, absorbs almost all of the longer wavelengths radiated by the greenhouse interior. This radiation entrapment is partly responsible for the elevated temperatures inside the greenhouse, although much of the effect is simply due to the reduction in convective cooling of the interior space caused by the enclosure.

9.2.1 The Principle of Greenhouse Gas Effects

The greenhouse effect has been described as a natural phenomenon that is responsible for Earth having an average surface temperature of 34°C, warmer than what it would be if it did not have active gases in the atmosphere. However, in recent decades, anthropogenic sources of a number of gases and aerosols enhance the natural greenhouse effect. The principal greenhouse gases are carbon dioxide, methane, nitrous oxide, and a category of carbon-based gases called halocarbons. In addition, emissions of black carbon or soot particles also add to atmospheric warming. Carbon dioxide, which will be discussed here, has been recognized for its importance as a greenhouse gas for over a century.

9.2.2 Atmospheric Concentration of CO_2

In 1979, the National Oceanic and Atmospheric Administration (NOAA) began assembling data from a network of sites to determine a global average value. The global average concentration of CO_2 in 1990 was 354 ppm and grew at 1.6 ppm per year. In 2006, it reached 380 ppm, and the rate of growth had increased to about 2 ppm/year. Figure 9.1 shows NOAA data for monthly global CO_2 for the recent past. The oscillations, in the rates of photosynthesis and respiration, are caused by seasonal variations. Atmospheric CO_2 levels go down during spring and summer when the plants are growing very fast. The lowest level of atmospheric CO_2 is observed in about October in the Northern Hemisphere.

$$\text{Photosynthesis: } 6CO_2 + 6H_2O \xrightarrow{\text{sunlight, chlorophyll}} C_6H_{12}O_6 + 6O_2 \tag{9.1}$$

By reversing the foregoing reaction, the equation describing respiration is obtained, which is the process used by living things to gain energy. During respiration, complex organic molecules are broken down, returning carbon to the atmosphere. At the time that the rate of respiration goes beyond the rate of photosynthesis, as tends to happen in the seasons of fall and winter, there is a net replacement of carbon into the atmosphere, that globally results in peak concentrations around May.

$$\text{Respiration: } C_6H_{12}O_6 + 6O_2 \rightarrow 6CO_2 + 6H_2O + \text{energy} \tag{9.2}$$

Therefore during photosynthesis, carbon moves continually from the atmosphere into the food chain and during respiration returns back to the atmosphere.

Measurements, are illustrated in Figure 9.2. Over most of that time, the concentration of carbon dioxide hovered at near 280 ppm which is the value commonly used as a reference point for comparison with present readings and future projections. Carbon dioxide concentrations are now more than one-third higher than they were just before the Industrial Revolution in the mid-18th century.

Thus, the increase in concentration of CO_2 and the continuation of that will be one of the primary causes of global warning as was explained in Chapter 3. In the next section, the carbon cycle is discussed to expand the understanding of the major factors in CO_2 emission.

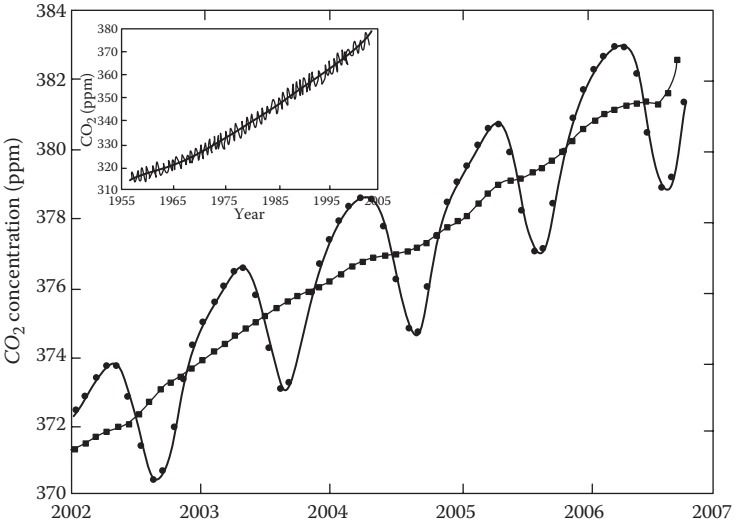

FIGURE 9.1 Recent global CO_2 concentrations. The oscillations are month-by-month mean values; the smoothed line is a moving average over 10 adjacent months. (From NOAA, http://www.cmdl.noaa.gov/ccgg/trends/index,php#mlo, 2006. With permission.)

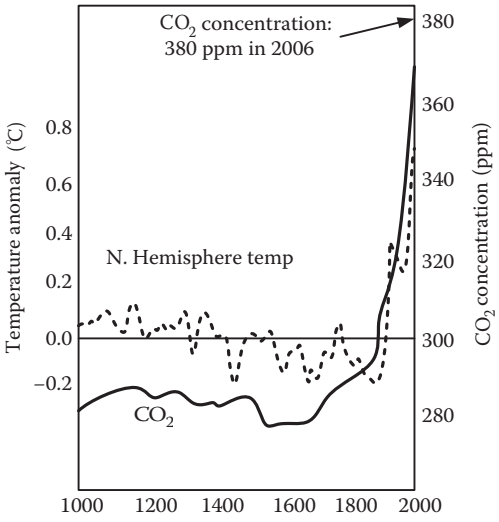

FIGURE 9.2 Carbon dioxide concentration and Northern Hemisphere temperature over the past 1000 years. (From Gilbert, M.M. and Ela, W.P. 2008. With permission.)

9.3 CARBON CYCLE

The atmosphere contains about 800 gigatons (giga = 10^9) of carbon (GtC), more than 99% of which is in the form of CO_2 and 610 GtC is locked up in vegetation. However, the oceans' carbon storage is much more than these values and is about 39,000 GtC. Nature continuously transports enormous amounts of carbon back and forth among the atmosphere, biosphere, and the oceans. The oceans absorb around 90 GtC/year and store almost all of it in the form of bicarbonate ions, HCO_3^-; however, some become part of the marine food chain and a similar quantity is returned to the atmosphere. A very small portion of nonliving organic matter each year ends up in sediments, which will

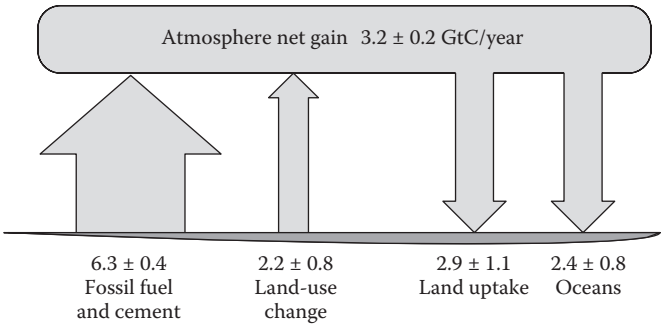

FIGURE 9.3 Human perturbations to the global carbon cycle during the 1990s. (From Houghton, J., *Global Warming: The Complete Briefing*, Cambridge University Press, 1997. With permission.)

be the source of our fossil fuels—oil, natural gas, and coal. When these are burned, ancient carbon is returned to the atmosphere.

Human development has highly affected the carbon cycle due to high usage of fossil fuels and land-use change. The United States emits 22% of global-energy-related CO_2, and the second largest emitter is China. Figure 9.3 summarizes the impact of human perturbations on the carbon fluxes into and out of the atmosphere during the 1990s. The accumulated emission from developed countries is the main cause of the rising CO_2 concentrations in the atmosphere. The amount of carbon released per unit of energy delivered is called the carbon intensity. Some fuels have high carbon intensity, such as coal, and some conversion systems release no direct carbon at all, such as wind turbines or nuclear power.

A number of manufacturing processes result in carbon emissions on sites that are not included in the usual accounting for fossil fuel combustion. These industrial emissions result from the production of cement, iron and steel, and glass, as well as the production and use of soda ash (Na_2CO_3), the manufacture of carbon dioxide, and the production of aluminum. The largest single industrial CO_2 source results from cement production. The average intensity of carbon emissions from cement production is about 2.2 GtC/year. This is about 5% of all anthropogenic carbon emissions. This results in leaving about 3.2 GtC/year in the atmosphere. The ratio of the amount of anthropogenic carbon emitted to the amount that remains in the atmosphere is known as the airborne fraction. The airborne fraction based on the values given in Figure 9.3 is obtained as 0.38 (38%). However, the airborne fraction is not necessarily a fixed quantity. For example, if large areas of land are deforested, the ability of the biosphere to absorb carbon would be reduced, and the atmospheric fraction would increase. The airborne fraction also depends on how fast carbon is being added to the atmosphere. For scenarios with little or no growth in emissions or even declining emissions, the oceans and plants have more time to absorb carbon; hence, the atmospheric fraction could be lower.

Example 9.1

Determine the carbon mass of the atmosphere if the total mass of the atmosphere is equal to 5.12×10^{21} g. Consider the standard temperature and pressure (0°C and 1 atm). The concentration of different gases in the atmosphere is given in Table 9.1.

Solution:

At standard condition, 1 mol of each gas occupies 22.414×10^{-3} m^3, which is 44.61 mol/m^3. Therefore, the mass of different gases in each cubic meter of atmosphere is determined as given in Table 9.1.

TABLE 9.1
Concentration of Each Gas in Air

Gas	$\frac{\text{gas}}{\text{air}}$ ratio	$\frac{\text{g}}{\text{mol}}$	$\frac{\text{mol}}{\text{m}^3\ \text{gas}}$	$\frac{\text{g}}{\text{m}^3\ \text{air}}$
N_2	0.71808	28	44.61	975.3
O_2	0.2095	32	44.61	299.1
Ar	0.0093	40	44.61	16.6
CO_2	0.00038	44	44.61	0.75
Total				1291.8 g/m^3

Based on the above table, the density of air is determined as 1291.8 g/m^3. Therefore, the carbon mass in 10^6 m^3 of air (1 ppm) is obtained as follows:

$$1\text{ppm} = \frac{1\text{m}^3\ \text{CO}_2}{10^6\ \text{m}^3\ \text{air}} \cdot 44.61 \frac{\text{mol}}{\text{m}^3\ \text{CO}_2} \cdot 12 \frac{\text{gC}}{\text{mol}} \cdot \frac{5.12 \times 10^{21} \text{g air}}{1291.8 \frac{\text{g air}}{\text{m}^3\ \text{air}}} \cdot 10^{-15}\ \frac{\text{GtC}}{\text{gC}} = 2.12\,\text{GtC}$$

Example 9.2

Estimate the rate of change in atmospheric CO_2 concentration and the amount of carbon in gigatons if the global fossil fuel consumption and cement production emit 6.8 GtC/year and 0.8 GtC/year to the atmosphere, respectively. Consider the airborne fraction as 0.38 and fixed emission from land use as 2.2 GtC/year.

Solution:

Based on the given data, the total emission rate is obtained as 2.2 + 6.8 + 0.8 = 9.8 GtC/year. Using the 0.38 airborne fraction along with the 2.12 GtC/ppm ratio (the result of previous example) gives

$$\Delta\text{CO}_2 = \frac{9.8\,\text{GtC/year} \times 0.38}{2.12\,\text{GtC/ppm CO}_2} = 1.76\,\text{ppm CO}_2\text{/year}$$

Total carbon = 1.76 × 2.12 GtC.

9.3.1 Estimating Carbon Emission: The Kaya Identity

Predicting future concentrations of carbon dioxide depends on numerous assumptions about population growth, economic factors, energy technology, and the carbon cycle itself. The usual approach involves developing a range of emission scenarios that depend on those factors and then using them to derive mathematical models on how the atmosphere and climate system will react to those inputs. This approach is called IPAT (Impact = Population × Affluence × Technology).

The application of the IPAT approach to carbon emissions from energy sources is referred to as the Kaya identity (Kaya 1990), which is formulated as follows:

$$C_{\text{rate}} = \text{Population} \times \frac{\text{GDP}}{\text{P}} \times \frac{\text{PE}}{\text{GDP}} \times \frac{\text{C}}{\text{PE}}, \tag{9.3}$$

where C_{rate} is the carbon emission rate (GtC/year), P is person, GDP is the gross domestic product, PE is the primary energy intensity, and C is carbon. Equation 9.3 expresses the carbon emission

rate as the product of four terms: population, GDP, carbon intensity, and energy intensity, which are measured per GDP. Assuming each of the factors in Equation 9.3 is growing exponentially, the overall growth rate of carbon emissions r is given by

$$r = r_p + r_{GDP/P} + r_{PE/GDP} + r_{C/PE}, \tag{9.4}$$

where r_p is population rate, $r_{GDP/P}$ is GDP rate per person, and $r_{C/PE}$ is the carbon rate per primary energy. Then, the carbon concentration after t years is obtained as

$$C = C_0 e^{rt}, \tag{9.5}$$

where C is carbon emission rate after t years (GtC/year), C_0 is initial emission rate (GtC/year), and r is overall exponential rate of growth (1/year). Therefore, the cumulative emissions, C_{tot}, of carbon with exponentially growing rate of r, over a period of time T, is given by

$$C_{tot} = \int_0^T C_0 e^{rt} dt = \frac{C_0}{r}(e^{rT} - 1). \tag{9.6}$$

Example 9.3

The emissions from fossil fuel burning and atmospheric CO_2 concentration in a year are estimated to be 8.1 GtC/year and 376 ppm, respectively. The average annual growth rate (%) of world population, $\frac{GDP}{P}$, $\frac{PE}{GDP}$, and $\frac{C}{PE}$ are considered to be 1.42, 1.56, –0.93, and –0.28, respectively. Considering the fixed atmospheric fraction of 0.38, estimate the following terms in the next 40 years:

a. The energy-related carbon-emission rate.
b. The cumulative energy-related carbon added to the atmosphere.
c. If the carbon emission from industrial processes is 0.6 GtC/year in the base year with an annual growth rate of 1.2% and the carbon emission from land-use changes is constant and is equal to 0.85 GtC/year, estimate the CO_2 concentration in the last year regarding the results obtained from the previous section.

Solution:

a. The overall growth rate in energy-related carbon emissions is the sum of the individual growth rates:

$$r = r_p + r_{GDP/P} + r_{PE/GDP} + r_{C/PE} = 1.42 + 1.56 - 0.93 - 0.28 = 0.0177/\text{year} = 1.77\%.$$

With 40 years of growth at 1.77% per year, the emission rate in the next 40 years would be

$$C_{40} = C_0 e^{rT} = 8.1 e^{0.0177 \times 40} = 16.44 \text{ GtC/year}.$$

b. Over the next 40 years, the cumulative energy emissions would be

$$C_{tot} = \frac{C_0}{r}(e^{rT} - 1) = \frac{8.1}{0.0177}(e^{0.0177 \times 40} - 1) = 471.3 \text{ GtC}.$$

c. The cumulative carbon emissions from industrial processes would be

$$\text{Industrial } C_{\text{tot}} = \frac{C_0}{r}(e^{rT} - 1) = \frac{0.6}{0.012}(e^{0.012\times 40} - 1) = 30.8 \text{ GtC}$$

Land use C_{tot}= 0.85 GtC/year×40 years = 34 GtC.

The amount of initial atmospheric CO_2 concentration in the base year is 376 ppm. Using the 2.12 GtC/ppm CO_2 conversion factor and a 0.38 atmospheric fraction, CO_2 in the next 40 years is estimated as follows:

$$CO_2 = 376 + \frac{(471.3(\text{Energy related}) + 30.8(\text{Industrial}) + 34(\text{Land use}))\text{ GtC} \times 0.38}{2.12 \text{ GtC/ppm } CO_2} = 472 \text{ ppm}.$$

By increasing the CO_2 concentration in the atmosphere, the marginal impact of each additional ton decreases as it approaches the saturation concentration. This relation is formulated as follows:

$$\Delta T_e = \frac{\Delta T_{2\times}}{\ln 2} \ln\left[\frac{(CO_2)}{(CO_2)_0}\right], \tag{9.7}$$

where ΔT_e is the equilibrium global mean surface temperature change, $\Delta T_{2\times}$ is the equilibrium temperature change for a doubling of atmospheric CO_2, $(CO_2)_0$ is the initial concentration of CO_2, and (CO_2) is the concentration of CO_2 at another given time. The climate sensitivity $\Delta T_{2\times}$ has long been estimated to be between 1.5°C and 4.5°C. The logarithmic function suggests that for every doubling of CO_2, the surface temperature goes up. For example, if $\Delta T_{2\times}$ is 3°C, then the first doubling raises the surface temperature by 3°C, doubling it again to four times its initial value raises the temperature by another 3°C, and so on. The temperature increase as a result of excessive CO_2 and greenhouse gases is considered a primary reason for climate change and has a significant impact on the hydrologic cycle.

9.4 CLIMATE CHANGE IMPACT ON HYDROLOGIC CYCLE

The hydrologic cycle is a natural machine supplied with heat energy by the sun, which, together with the force of gravity, keeps the water moving. Water flows from the Earth to the atmosphere as evaporation and transpiration, from the atmosphere to the Earth as condensation and precipitation, and on the Earth as streamflow and groundwater movement, and then to the ocean.

Altered precipitation, evapotranspiration, and soil moisture patterns defined as climate change impacts have extreme effects on the hydrologic cycle. Since the Industrial Revolution, carbon dioxide concentration in the atmosphere has increased. The continuation of this event may meaningfully change global and local temperature and precipitation. Because of unequal distribution of external precipitation around the globe, decline in the amount of precipitation in some regions may occur, or the timing of wet and dry seasons may alter significantly. Therefore, information on the local or regional impacts of climate change on hydrological processes and coastal water resources is becoming more important.

The key changes brought about by the effects of greenhouse gases on the hydrological cycle include changes in temperature, precipitation, evapotranspiration, soil moisture, vegetation cover, melting glacial ice, sea level, and groundwater recharge. In most situations, precipitation, evaporation, and sea level increase and soil moisture decreases under climate change impact.

In Figure 9.4, different aspects of climate change impacts on hydrology system are presented. The details of Figure 9.5 are described in the following section.

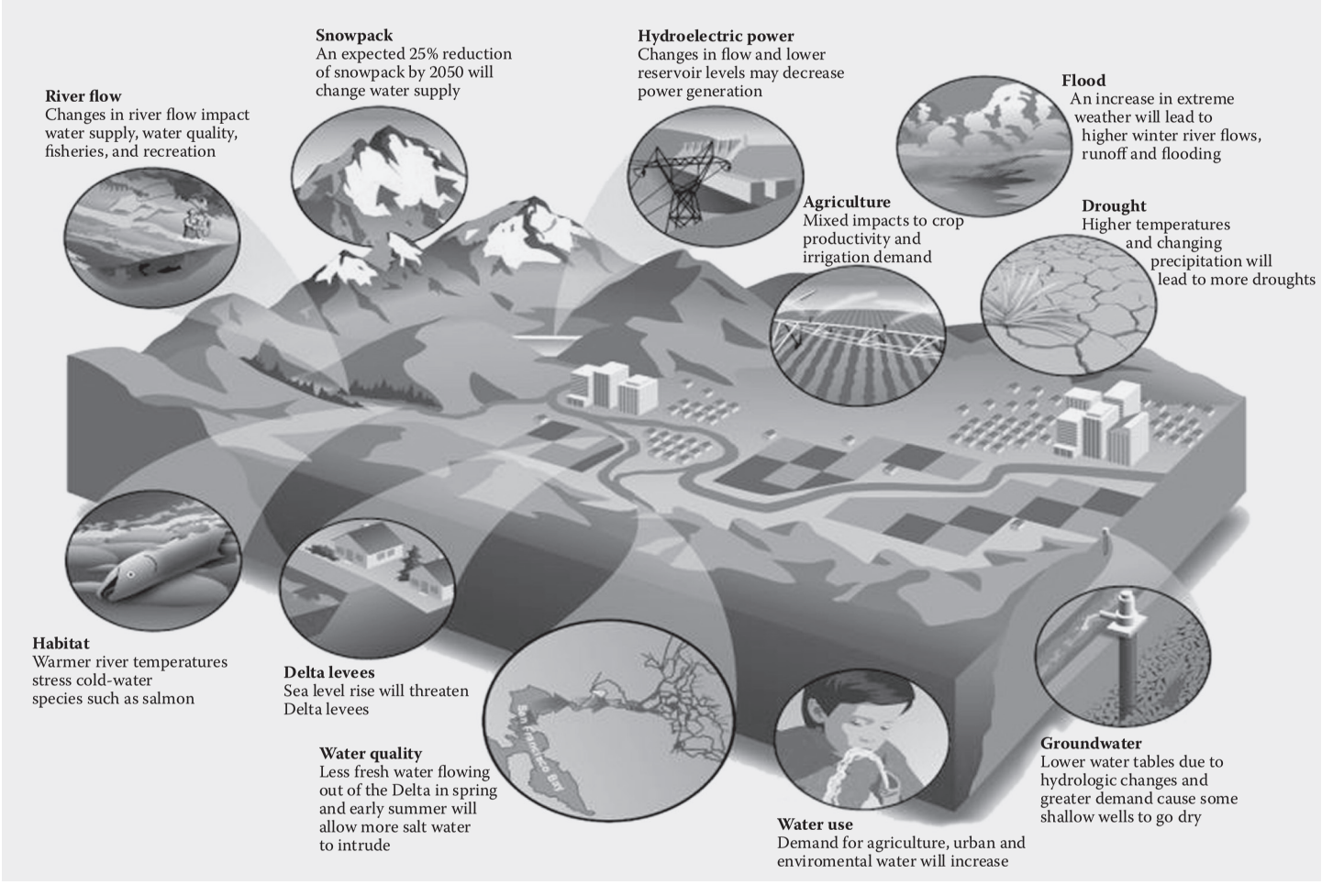

FIGURE 9.4 Different impacts of climate change on hydrological cycle components. (From California Department of Water Resource, Climate Change in California, State of California, http://www.water.ca.gov/, 2007. With permission.)

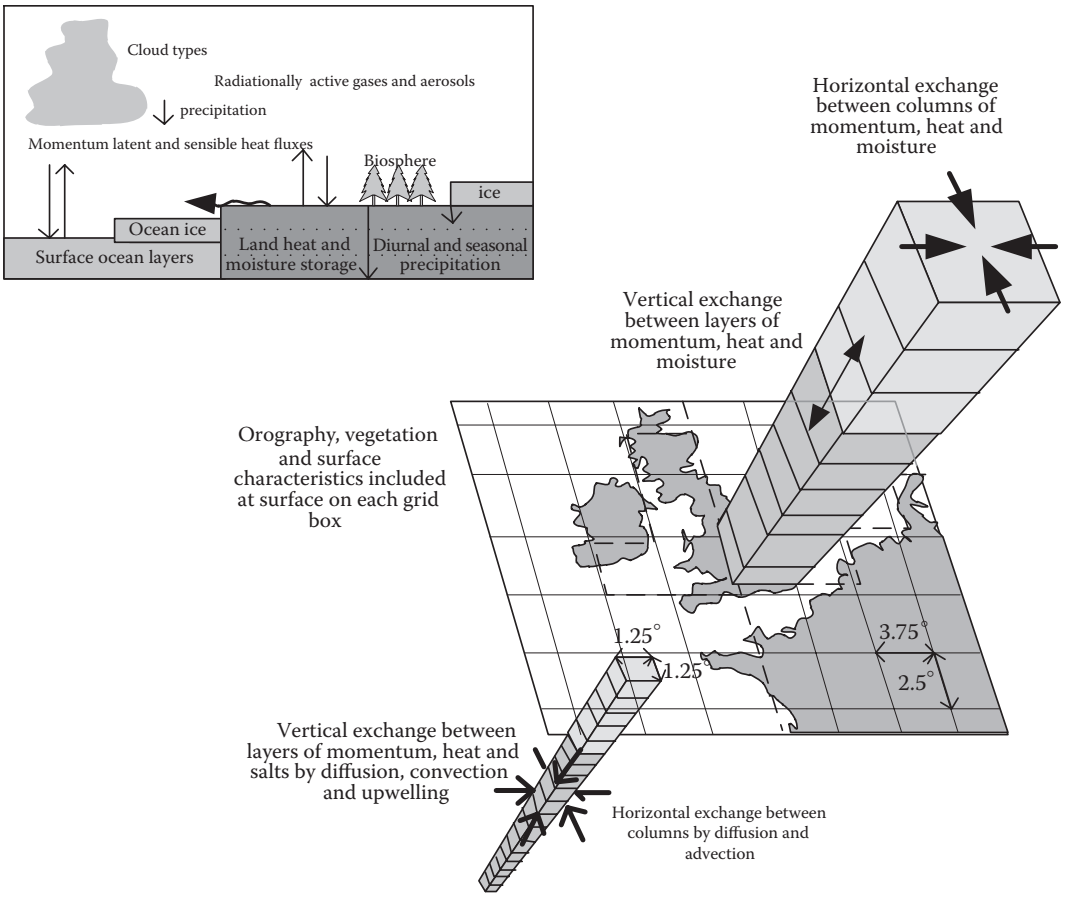

FIGURE 9.5 Schematic discrete of atmosphere for utilizing GCMs and the way of consideration of the system characteristics. (From Viner, D. and Hulme, M., *Climate Change Scenarios for Impact Studies in the UK*. Climatic Research Unit, University of East Anglia, Norwich, UK, 1992. With permission.)

9.5 WATER RESOURCE SYSTEM EFFECTS

Lattenmaier et al. (1996) evaluated the sensitivity of the six major water systems in the United States through analysis of system performance indices including reliability, resiliency, and vulnerability, the definitions of which are discussed in Chapters 10 and 13. They finally concluded that the most important factors in system performance sensitivity to climate changes are changes in runoff and water demands. They also mentioned that the system sensitivities depend on the water usage purposes and their priorities. For example, in the urban water supply system, because of the large demand for high-quality water with considerable temporal changes, and limited water resources, any little change in quantity of water resources or their temporal variations will highly impact the system's performance. In this case, flexible water supply schemes are needed to provide enough resiliencies in the system and decrease possible damages.

9.5.1 Floods and Droughts

In response to global warming, the average volume of runoff will intensify considerably. Indeed, a rise in temperature due to the greenhouse effect leads to an increase in evaporation and in the intensity of water cycling, and consequently causes a high amount of moisture in the air. Sea levels rise because snowy regions become rainy and oceans get warmer by increasing global temperatures.

Rising sea levels also make coastal areas more vulnerable to storm surges and, in turn, to flooding. The Intergovernmental Panel on Climate Change (IPCC) predicts that warming tropical seas—hurricanes feed off of warm water—will likely make these storms and floods more powerful especially in coastal areas. Also, in some regions, the amount of precipitation is expected to decrease as part of climatic changes in the twenty-first century, and therefore, droughts in these regions will be longer in duration. This could imperil species and also could put harvests at risk and decrease global food production.

9.5.2 Agricultural Droughts

One aspect of drought impact is crop damage, which depends upon climatic changes, and agriculture is the first economic subdivision affected by drought. The relationship between harvest and water shortage is considered in the assessment of agricultural droughts. The lack of moisture to support average crop yield on the farm results in agricultural drought. It can also be a result of a long period of low precipitation and/or the type of water usage. Other climatic factors such as high temperature, high wind, and low relative humidity are related to droughts in many regions of the world, and as mentioned before, global climate change causes these variations that can influence local agriculture.

9.5.3 Water Use

Potential changes in climate factors such as temperature and precipitation could affect water use and water resource availability. Under these impacts, demand management, resource expansion, and changes in resource management play significant roles to satisfy demand. Use of water is expressed by industrial, commercial, and agricultural generation and is managed by a number of measures that are applicable under conditions with and without climate change. Some aspects of climate change, such as changes in the frequency and severity of extreme events such as flood and drought, as well as higher temperatures due to global warming, increase evaporation and therefore reduce water availability for humans and ecosystems.

9.5.4 Water Quality

Climate change is expected to have significant impacts on water quality. As mentioned in Section 9.5.1, severe floods due to climatic change transport pollutants into water bodies, overload storm and sewage systems and wastewater treatment devices, and, therefore, increase the risks of water pollution. In addition, water quality is influenced by temperature and water amount. Warmer air temperature will result in warm water. Higher temperatures decrease dissolved oxygen levels, which can endanger aquatic ecosystems. For instance, more frequent intensive precipitation events will release more contaminants and sediments into lakes and rivers and result in declining water resource quality including surface water and groundwater. Also, global warming increases the melting of snow and contributes to sea level rise, which affects groundwater quality. It will cause saltwater intrusion particularly in coastal aquifers, with the amount of intrusion depending upon local groundwater gradients.

9.5.5 Habitat

Global warming threatens people and habitats today, and it is difficult for plants and animals to keep up with the rapid change of climate. Some species such as polar bears, and even trout and salmon, are being adversely affected by global warming. It is likely that through direct energy transfer from the atmosphere, climate change will affect lake, reservoir, and stream temperature. Indeed, high temperatures decrease the dissolved oxygen, increase metabolic rates, and result in the decline of the salmon's resistance to pests. In addition, warmer temperatures can increase the infection rate or vulnerability of fish to illness. Changes in temperature regimes also affect ice cover and result in

sea level rise, which leads to the flooding of low-lying areas. This event is likely to imperil riparian habitats and to inundate some agricultural lands of residents located on the bank of the river.

9.5.6 Hydroelectric Power

The impacts of climate change on river flows are uncertain, but any considerable changes would influence hydroelectric generation. The amount of electricity produced by hydroelectric power and the timing of power production depend on the climate change. Hydroelectric generation is more sensitive to changes in river flows than other types of water systems. As a consequence, the amount of reduction in hydroelectric generation may be significantly more than the reduction in river flow. Changes in the magnitude and timing of river runoff, together with high evaporation from reservoirs, will have adverse effects on producing hydroelectric power.

In addition, climate change will affect both electricity demand and supply. In fact, at high temperatures, winter heating demand will decrease and, on the contrary, summer cooling demand will increase. In addition, hydroelectric generation is one form of water use for energy production, and changes in the production of hydroelectric power will contribute to water use.

9.5.7 Snowpack

Hydroclimatic change results in the general change in snowpack and snow cover. Temperature affects winter snowfall and, consequently, accumulated snowpack in complex ways. Increasing temperature contributes to higher moisture availability and total precipitation, and then to greater snow accumulation, but if temperatures increase intensely, snowmelt will increase, and consequently, snowpack will reduce.

As a result, reduced snowpack and earlier spring snowmelt influence other hydrologic variables such as the amount and timing of runoff, evapotranspiration, and soil moisture. Also, surface water supplies depending upon snowmelt are influenced by changes in the intensity of precipitation occurring due to climate change. Indeed, warmer temperature leads to a shift from falling snow to rain, changes in snow accumulation, and earlier melting. All these events affect the amount and timing of water supply. Moreover, groundwater recharge from snowmelt is influenced by snowmelt mechanisms and local recharge conditions. During snowmelt, soils are frozen, and then upland infiltration is reduced and sinking of snowmelt water is increased. The characteristics of the groundwater basin and the soil moisture condition affect the interaction between infiltrating meltwater and streamflow.

9.5.8 Riverflow

Climate change affects streamflow timing through the temperature increase and change in the amount of precipitation. Changes in the onset or duration of rainy seasons can affect river flow. A lot of hydrological studies have been made to assess the impacts of climate change on streamflow and runoff. Global warming increases the amount of evaporation and precipitation. Changes in these hydrological factors will alter the severity of some hydrological events such as increase in streamflow variability. As a result of streamflow intensification and the change in soil moisture, the infiltration rate is affected.

9.6 CLIMATE CHANGE SIMULATION

Quantifying atmospheric systems results in setting up processes that occur on a wide range of time and space scales. Some numerical models of these processes are applied for various purposes, such as predictions of global weather and global climate change. The climate system has dealt with large changes in a geological time scale due to changes in atmospheric composition, location of continents, and Earth's orbital parameters. The current focuses are on climate change studies on time scales of seasons to centuries. Projecting the climate system in the spatial scales is difficult, both in the atmosphere and in the terrestrial surface.

The high complexities of the Earth's climate result in uncertainty about changes that will arise from the increase in carbon dioxide concentrations. To increase the reliability of predicted climate and to decrease the errors in predictions, more research and refinement of the global circulation models (GCMs) are needed. GCMs describe the atmosphere by using a rectangular grid, covering the Earth with cubes of air, which are 2–5° grids in latitude and longitude, with 6–15 vertical levels above the earth surface that are assumed to be representative of volume elements in the atmosphere as presented in Figure 9.5.

In the Earth's climate simulation by GCMs, a high number of variables describing the physical and chemical properties of the atmosphere, oceans, and continents are considered. By developing the technology over the past decade, the quality of GCMs has improved markedly. However, some weaknesses should be corrected to improve the GCMs' precision. Much work on these weaknesses needs to be done to simulate the behavior of the Earth's oceans in the GCMs more accurately. Moreover, there are some ambiguities such as the physics of clouds, which are poorly understood and add another measure of uncertainty to the GCMs. In the following sections, the procedure of developing climate change scenarios, GCM model structure, and the downscaling procedure are introduced.

9.6.1 Climate Change Scenarios

The choice of climate change scenarios is important because it can determine the outcome of a climate change impact analysis, from which water resources planning and management strategies will be developed. Extreme scenarios can produce extreme results, and moderate scenarios can produce moderate results. The selection of scenarios is controversial because scenarios are often criticized for being too extreme, too moderate, too unreliable, and too dependent on important factors such as changes in variability. All of these inaccuracies in developing climate change scenarios will cause huge socioeconomic damage to the water system.

Therefore, more than one scenario should be used to show that there is uncertainty about regional climate change. Using one scenario can be misinterpreted as a prediction. Using multiple scenarios, particularly if they reflect a wide range of conditions (e.g., wet and dry), indicates some of the uncertainty about regional climate change. Climate change scenarios have been typically developed for a particular point in the future. Many climate change scenarios examine the climate associated with a doubling of carbon dioxide levels in the atmosphere over pre-industrial levels ($2\times CO_2$). This will most likely happen in the last half of the 21st century. These could be considered static scenarios because they are based on a false presumption that a stable climate will be reached in the future. This assumption is made to simplify analysis, not because it is widely believed that climate will reach a static condition. In contrast, transient scenarios examine how climate may change over time. They typically start in the present day and cover a number of decades into the future.

There are three generic types of climate change scenarios: scenarios based on outputs from GCMs, synthetic scenarios, and analogue scenarios. Since a majority of impact studies have used scenarios based on GCMs, this method is described in the following section. Figure 9.6 shows the Special Report on Emissions Scenarios. The A storylines focus more on economic growth, while the B storylines have more of an environmental emphasis. The A1 and B1 lines are based on a more homogeneous, globalized future, while the A2 and B2 lines imagine a more fractured world with different regional properties and growth rate. The A1 line is further designed to be fossil fuel intensive (A1-F); nonfossil, with emphasis on technology (A1-T); or a more balanced combination of the two (A1-B).

9.6.1.1 Spatial Variability

A sufficient number of climate variables on the spatial scales are estimated by a number of scenarios to assess climate changes. Some scenarios result in a uniform change in climate over an area. Indeed, the diversity of some factors such as land uses, which have completely different responses to climate change impacts, are not considered. The regional changes in climate are defined by GCM grid boxes, between 250 and 600 km depending on a specific GCM model resolution listed in Table 9.2. Due to the lack of accuracy about regional climates in a GCM model, Von Storch et al. (1993)

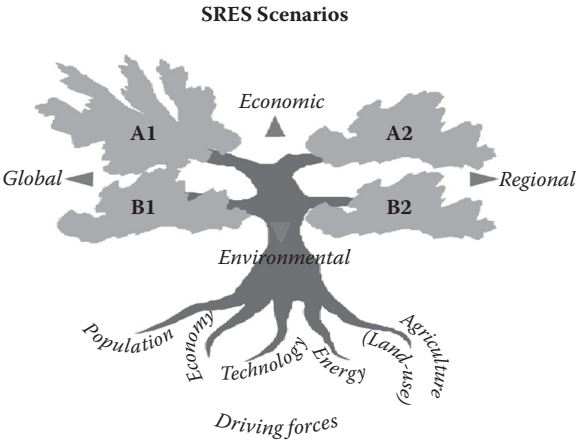

FIGURE 9.6 Special Report on Emissions Scenarios. (From IPCC, Third Assessment Report, http://www.ipcc.ch/, 2001. With permission.)

TABLE 9.2
Characteristics of Available GCM Models for Globe

Model Number	Model Name	Description				
		Scenario	Country	Organization	Resolution	
1	CSIRO-Mk3.0	A2,A1B,B1	Australia	CSIRO Atmospheric Research	192 × 96	L18
2	ECHOG-G	A2,A1B	Germany	University of Bonn	96 × 48	L19
3	GFDL-CM2.0	A2,A1B,B1	USA	Geophysical Fluid Dynamics Laboratory	144 × 90	L24
4	GFDL-CM2.1	A2,A1B,B1	USA	Geophysical Fluid Dynamics Laboratory	144 × 90	L24
5	GISS-ER	A2,B1	USA	NASA/Goddard Institute for Space Shuttles	72 × 46	L20
6	UKMO-HadGEM1	A2,A1B	United Kingdom	Hadley Centre for Climate Prediction and Research	192 × 145	L38
7	INM-CM3.0	A2,A1B,B1	Russia	Institute of Numerical Mathematics	72 × 45	L21
8	IPSL-CM3.0	A2,A1B,B1	France	Institute Pierre Simon Laplace	96 × 72	L19
9	MIROC3.2(mr)	A2,A1B,B1	Japan	The University of Tokyo	128 × 64	L20
10	ECHAM5_MPI-OM	A2,A1B,B1	Germany	Max Planck Institute for Meteorology	192 × 96	L31
11	MRI-CGCM2.3.2.	A2,A1B,B1	Japan	Meteorological Research Institute	128 × 64	L30
12	CCSM3	A2,A1B,B1	USA	The National Center of Atmospheric Research	156 × 128	L26
13	PCM-NCAR	A2,A1B	USA	The National Center of Atmospheric Research	128 × 64	L26
14	UKMO-HadCM3	A2,A1B,B1	United Kingdom	Hadley Centre for Climate Prediction and Research	96 × 73	L19

support the opinion that generally the minimum effective spatial resolution should be defined by at least four GCM grid boxes. The precision of GCM simulations depends on the spatial autocorrelation of a particular weather variable for an individual grid box.

In the last few years, the hydrological schemes have also been considered in GCMs with higher complexity and integration. Nonlinearity in climate systems leads to difficulty in using deterministic estimation of precipitation from GCMs for hydrological modeling purposes. In this aspect, methods to transform output from GCM to local weather variables are needed. A weakness of numerical models of natural systems is their impossibility to validate the described nonclosed systems. However, it is a pivotal need to improve the quality of these models and the benefits in operational use. Although the spatial resolution of GCMs is increasing, they still simulate climate at a very coarse spatial scale—in the order of 250 × 250 km, which is not enough for evaluation of climate change effects in the regional scale. In the following sections, some methods of improving the spatial precision of the GCM outputs are described.

9.6.2 Downscaling

The GCMs are unreliable when simulating climate variable variations; however, application of a stochastic model in space and time could overcome this problem. Because of the low spatial resolution of GCMs, downscaling the results from such models is necessary. Downscaling methods are still under development and more work needs to be done to increase the accuracy of such models. It creates a connection between the large-scale circulation defined as predictors and local weather variables defined as predictands, but downscaling pertains more to the process of moving from the large-scale predictor to the local predictand. Figure 9.7 shows a schematic of moving from a large scale to a small scale.

The two main approaches to downscaling have used either significant relationships between large-area and site-specific climates (Wigley et al. 1990) or relationships between atmospheric

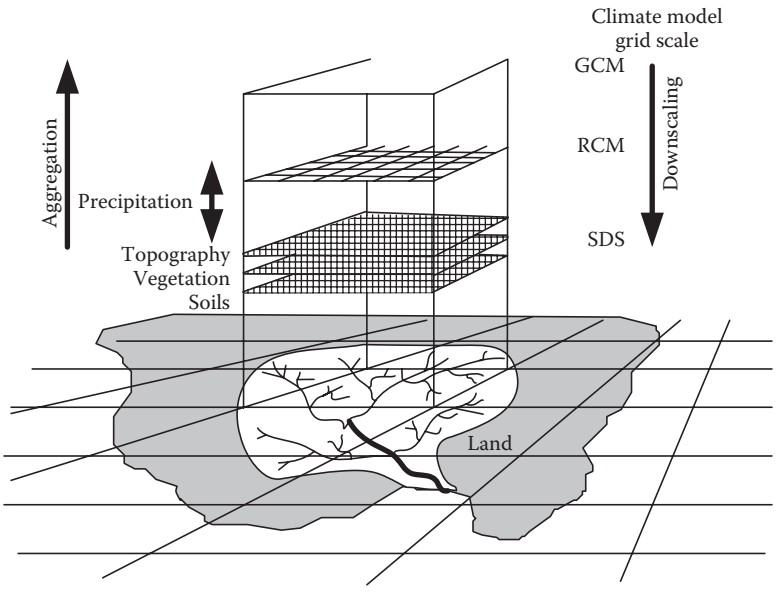

FIGURE 9.7 Schematic drawing of the basic principles of downscaling from GCM output. (From Wilby, R.L. and Dawson, C.W., *Using SDSM Version 3.1—A Decision Support Tool for the Assessment of Regional Climate Change Impacts*, 2004. With permission.)

circulation types and local weather (Von Storch et al. 1993). The disadvantage of the downscaling approach is the calibration of the statistical relationship. In doing so, it requires large amounts of observed data, which can be computationally very intensive. Also, as unique relationships need to be derived for each site or region, these methods are very time-consuming. There are a wide range of techniques used for downscaling:

1. Regional models: When using high-resolution regional climate models (RCMs), an alternative approach is involved. RCMs are typically assembled at a much finer resolution than GCMs (often 50 km) with the domain limited to continents or subcontinents. In such applications, detailed information at spatial scales down to 10–20 km may be established at temporal scales of hours or less. However, RCMs are still compelled at their boundaries by the coarse-scale output from GCMs. Therefore, in an area, RCMs can have a performance similar to that of the driving GCM; their performance in relation to downscaling techniques has not yet been assessed completely. Indeed, there are some difficulties in creating the interface between the GCM and the regional model. Moreover, the costs of setting up these models for a new region and running a climate change experiment are extremely high; therefore, they are not easily accessible. Nevertheless, in the long term, this technique could have useful results, and their development should be encouraged. Most of the regional models are employed on the Northern Hemisphere, whereas many of the areas that are most vulnerable to global change lie in the Southern Hemisphere. Therefore, its use in many regions for climate impact assessments remains premature.

   Dynamic downscaling has many advantages, particularly on factors such as temperature, precipitation, soil moisture, wind direction, and strength, which are available in both GCMs and the nested finer-scale grid. However, there is a problem with regard to the availability of supercomputer systems, which are required in dynamic downscaling and in performing these simulations globally to evaluate local and/or regional impacts and consequences of climate change. Increasing the availability of supercomputers will lead to a wider accessibility of dynamic downscaling. In the next section, statistical downscaling is described to simulate GCM output to downscale data in a regional watershed scale.
2. Statistical downscaling: Statistical downscaling is an empirical relationship that exists between atmospheric processes at different temporal and spatial scales (Wilby et al. 1998).

The major steps of downscaling are presented as follows:

1. Reduction or processing of the predictor
2. Spatial analysis and selection of predictor and predictand domain
3. Temporal analysis of the predictor and the predictand
4. Temporal manipulation of the predictor, e.g., time lagging
5. Calibration of transfer function between predictor and predictand
6. Evaluating the relationship between predictor and predictand
7. Application of the developed model to GCM data

Items 2 to 7 are repeated until an optimum result is reached for the target objective. The following are three statistical downscaling methods: analog methods, regression methods, and conditional probability approaches. The last one has two main subdivisions: weather patterns and weather states. These methods are largely used in anticipated hydrological impact studies under climate change scenarios.

The main advantages of the statistical downscaling approach are its easy implementation and cheap computation. The integrated feature of the downscaling procedure is that it is calibrated to the local level. Furthermore, with very few parameters, these methods will be attractive for many hydrological applications (Wilby et al. 2000).

In this part, statistical-versus-statistical downscaling models or regional-versus-regional models are compared. However, a growing number of studies have compared statistical-versus-regional models, and in Table 9.3, the relative strengths and weaknesses that have come out are summarized.

Downscaling methods must be valid in a troubled climate to be useful in future studies of climate change. The methods are assumed to estimate the difference between climate situations and must, therefore, work under a situation different from under which it was developed. Also, the climate should be stationary and no major shift in the physical processes governing the climate must occur or else it will result in a downscaling scheme outside the calibrated and validated range. To assess the ability of a model to deal with different climate situations, the model is calibrated on data from the driest seasons and then is validated on the wettest seasons in the calibration period and conversely. This is a simple test of the method's sensitivity to different climate situations. The stability of model performance in extreme years is evaluated. Long time series containing many different situations are used in the downscaling. These situations will be more frequent in a perturbed future climate. If the method can model those situations and if the range of variability of the large-scale variable in a future climate is of the same order as today, the problem will be minimized. There is some difficulty in dealing with stability and nonstationarity in downscaling and one should be careful when applying a model to the output of GCM simulations. If the climate is nonstationary, the underlying assumptions of the statistical link are unaffected by the climate change for model validity. The physical laws governing the climate are not likely to change, but the physical processes are parameterized for a specific climate. A multivariate approach is recommended to overcome

TABLE 9.3
Main Strengths and Weaknesses of Statistical Downscaling and Regional Model

	Statistical Downscaling	Regional Model
Strengths	• Information of climate station from GCM output • Inexpensive and easily transferable • Analyses of risk and uncertainty by producing ensembles of climate scenarios • Applicable to unusual predictands such as wave heights and air quality	• There are 10–50 km resolution information of climate from GCM-scale output • Respond in physically consistent ways to different external forces • Resolve atmospheric processes such as orographic precipitation • Consistency with GCM
Weaknesses	• Dependent on the GCM boundary • Choice of domain size and location affects results • Needs high-quality data for calibration of model • Relationships between predictand and predictor are often nonstationary • Choice of variables of predictor affects the results • Choice of empirical transfer scheme affects the results • Low-frequency climate variability is problematic • Always applied off-line; therefore, results do not feedback into the host GCM	• Dependent on the realism of GCM boundary forcing • Choice of location affects results and size of domain • Needs significant computing resources • Ensembles of climate scenarios seldom produced • Initial boundary conditions affects results • Choice of cloud/convection scheme affects (precipitation) results • Not readily transferred to new regions or domains • Typically applied off-line; therefore, results do not always feedback into the host GCM

Source: Wilby, R.L. and Dawson, C.W., *Using SDSM Version 3.1—A Decision Support Tool for the Assessment of Regional Climate Change Impacts*, 2004. With permission.

the problem with nonstationarity of climate. In this approach, sufficient data should be available to ensure statistical integrity of the results. When considering nonstationarity, a stochastic model must be conditioned on the observed inter-annual variability.

As mentioned before, statistical downscaling of climate variables is used to determine the impacts of climate change. Although the GCM is still the best tool to predict future climates, the assumption that the statistical relationships derived will remain fixed in the future is a weak point in this context. In this section, two downscaling models that are widely employed in climate change studies are introduced: Statistical Downscaling Model (SDSM) (Wilby and Dawson 2004) and Long Ashton Research Station Weather Generator (LARS-WG) (Semenov and Barrow 2002), as a stochastic weather generator.

9.6.2.1 Statistical Downscaling Model

SDSM is used to simulate the climate change scenarios at daily timescales, by using GCM output. Large-scale predictor variable information has been prepared for a large North American window. Some employed climate variables in the SDSM are listed, including mean temperature, mean sea level pressure, vorticity, and near-surface specific humidity.

The choice of predictors is the most difficult step in the development of any SDSM. The decision process is also complicated by the fact that the explanatory power of individual predictor variables varies both spatially and temporally.

The known large-scale predictor variables are used for determining multiple linear regression relationships between local station data and the climate variables to calibrate the model. It also regulates the average and variance of downscaled daily rainfall considering factors such as bias and variance to confirm the simulated values to the observed ones. The first step in the application of SDSM is to determine that rainfall should occur daily, as follows:

$$\omega_i = \alpha_0 + \sum_{j=1}^{n} \alpha_j \hat{u}_i^{(j)}, \tag{9.8}$$

where α_0 is the constant coefficient, ω_i is the candidate in a random process generator that indicates a state of rainfall occurring or not occuring on day i, $\hat{u}_i$ is the normalized predictor on day i, and α_j are the estimated regression coefficients. Precipitation in day i occurs if $\omega_i \le r_i$, where r_i is a stochastic output from a linear random-number generator.

In the second step, the value of rainfall in each rainy day is estimated using z-score as follows:

$$Z_i = \beta_0 + \sum_{j=1}^{n} \beta_j \hat{u}_i^{(j)} + \varepsilon, \tag{9.9}$$

where β_0 is the constant coefficient, Z_i is the z-score for day i, β_j are estimated regression coefficients for each month, ε is a normally distributed stochastic error term, and

$$Y_i = F^{-1}[\phi(Z_i)], \tag{9.10}$$

where ϕ is the normal cumulative distribution function and F is the empirical function of the Y_i daily precipitation amounts. The standardized predictors used in this method are provided by subtracting the mean and dividing them by the standard deviations over the calibration period.

In downscaling, a multiple linear regression model is developed between selected large-scale predictors and local-scale predictands such as temperature or precipitation. Based on the correlation analysis, partial correlation, and scattered plots, and considering the physical sensitivity between

predictors and predictands, the suitable large-scale predictors are chosen. Higher correlation values imply a high degree of association and lower P values indicate more chances for association between variables (Wilby and Dawson 2004). The P value is a statistical parameter that measures the probability of accidental high correlation between predictands and predictors numerically. If the P value is small, the correlation is more realistic. In other words, the P value is used for checking the null hypothesis of the correlation between the predictors and predictands.

Example 9.4

A rain gauge named Station A is located at 60°34′ East longitude and 26°12′ North latitude. The precipitation data for 6 years from 1994 to 1999 are available in this rain gauge. The monthly data are given in Table 9.4. Produce the precipitation data of Station A under the HadCM3 B2 scenario outputs from 2010 to 2014 using SDSM.

Solution:

The downscaling procedure at Station A is described step by step as follows:

Step 1: The input file is prepared, and the daily precipitation data are sorted based on time in two columns: first, the date, and second, the precipitation amount (the monthly data are interpolated to develop the daily data needed as input for SDSM).

Step 2: The process of quality control is run to test the format of the prepared input file.

Step 3: In this step, all of the available weather variables are screened to find the variables that could be used as precipitation predictand. For Station A, data start from 1/1/1994 and end at 12/31/1999. The analysis is done in an annual period under an unconditional process.

At the end of this analysis, the results of explained variance and correlation matrix between precipitation and selected weather variables are given (Figure 9.8). Two variables are selected for precipitation simulation:

1. Relative humidity at 850 hPa height
2. Near-surface specific humidity

The P value of these variables is low and partial correlations are high, which show the high correlation of selected predictands with rainfall (Figure 9.9).

Step 4: The model is calibrated using the observed data and the selected signals.

In this part, the model is required, whether the process is unconditional or conditional. In unconditional models, a direct link is assumed between the predictors and predictand (e.g., local wind speeds may be a function of regional airflow indices). In conditional models, there is an intermediate process between regional forcing and local weather (e.g., local precipitation amounts depend on the occurrence of wet days, which, in turn, depend on regional-scale predictors such as humidity and atmospheric pressure).

Furthermore, at the end of this step, the R^2 and standard error for conditional precipitation amount are reported (Figure 9.10).

TABLE 9.4
Monthly Observed Precipitation for Station A for Period 1994–1999

	Jan	Feb	Mar	April	May	June	July	Aug	Sep	Oct	Nov	Dec
1994	1.20	0.00	0.08	0.20	0.00	0.00	0.77	1.50	0.00	0.05	0.00	0.69
1995	0.00	0.24	0.00	0.61	0.00	0.24	2.51	0.20	0.27	0.36	0.05	3.01
1996	2.35	0.63	0.87	0.00	0.45	0.15	0.00	0.00	0.00	0.08	0.53	0.00
1997	0.86	0.00	3.26	0.10	0.00	1.42	0.00	0.00	0.00	3.52	0.64	2.45
1998	1.60	0.13	3.85	0.00	0.00	0.00	0.00	0.10	0.00	0.00	0.00	0.00
1999	0.00	0.75	1.30	0.00	0.00	0.00	1.32	0.00	0.00	0.00	0.00	0.00

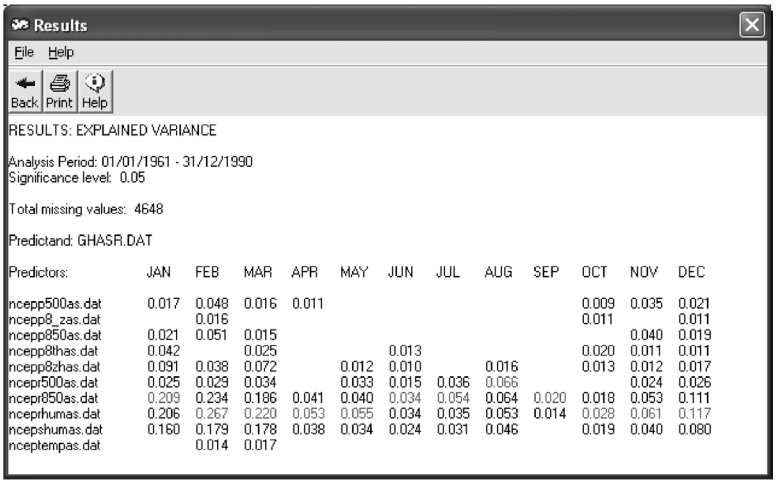

FIGURE 9.8 Results of correlation analysis between predictors and daily precipitation.

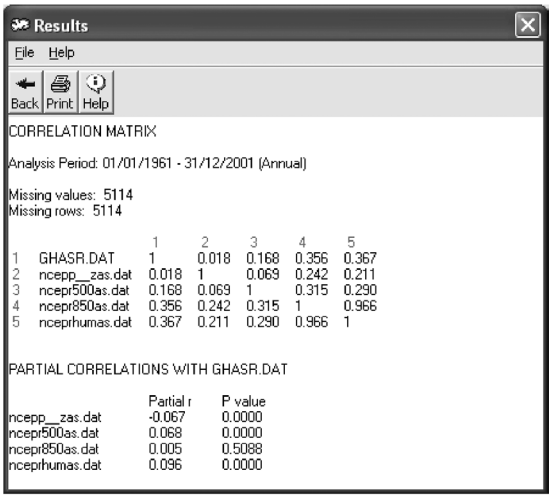

FIGURE 9.9 Matrix of correlation between predictors and predictands.

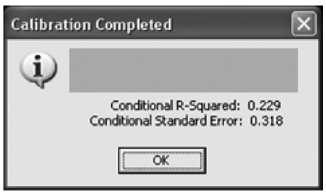

FIGURE 9.10 Model calibration results.

Step 5 (Weather generator): In this step, data for the considered period and selected climate change scenario (here, HadCM3 B2) are developed. The start date of data generation and the amount of data to generate (based on the duration of the simulation period) will be entered. In this step, one can choose production of one or more ensembles of data. In this example just one ensemble of data is generated.

Step 6: In this step, the statistical analysis of the observed and developed data through tables and graphs is given (Figure 9.11).

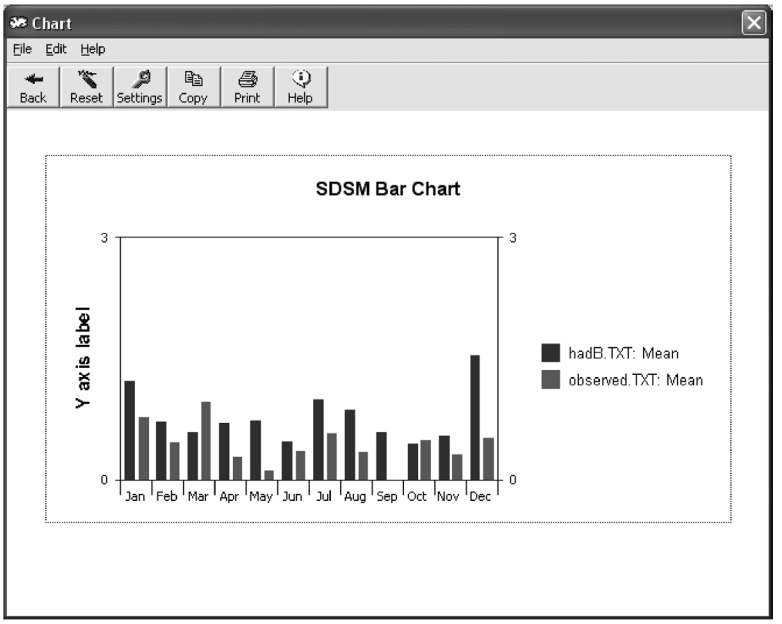

FIGURE 9.11 Comparison of the HadCM3 B2 scenario results and observed precipitation.

9.6.2.2 Stochastic Weather Generator Model (LARS-WG)

One of the most important downscaling models is LARS-WG. The model input data are daily time series of climate variables such as precipitation, solar radiation, and maximum and minimum temperature. This stochastic weather generator model simulates the data of weather at a single site under both future and current climate situations (Racsko et al. 1991; Semenov et al. 1998; Semenov and Brooks 1999).

The main purposes in developing a stochastic weather generator are as follows:

1. To make an assessment of the averages of simulated synthetic weather time series with statistical characteristics analogous to the observed statistics at a site. This can be used for estimation of risk and uncertainty in agricultural and hydrological applications.
2. To simulate weather time series to unobserved data, through the interpolation of the parameters from the weather generator obtained by running the models at neighboring sites.

A stochastic weather generator cannot be used in weather forecasting as a predictive tool, but it can generate an identical time series of synthetic weather to the observations.

The LARS-WG model is based on the series weather generator described in Racsko et al. (1991). The semi-empirical distributions are used for the dry and wet day series, daily solar radiation, and daily precipitation. The equations of the LARS-WG model are based as follows:

$$Emp = \{a_0, \ldots, a_i; h_i, i = 1,\ldots,10\},$$

where *Emp* is the semi-empirical distribution histogram with 10 intervals, i is interval, and h_i is the number of observed data events in the ith interval.

Random values of the semi-empirical distributions are chosen by first selecting one of the intervals and then selecting a value within that interval from the uniform distribution; such a distribution is flexible and can approximate a wide variety of shapes by adjusting the intervals $[a_i - 1, a_i)$. The intervals $[a_i - 1, a_i)$ are chosen based on the expected properties of the weather variables. For the

lengths of dry and wet series and for precipitation, the size of intervals $[a_i - 1, a_i)$ gradually increases with the increasing of i. This choice of interval structure prevents a very coarse resolution from being used for the small values.

The simulation of precipitation occurrence is modeled as alternate wet and dry series, where a wet day is defined to be a day with precipitation. The length of each series is chosen randomly from the wet or dry semi-empirical distribution for the month in which the series starts. In determining the distributions, observed series are also allocated to the month in which they start. For a wet day, the precipitation value is generated from the semi-empirical precipitation distribution for the particular month independent of the length of the wet series or the amount of precipitation on previous days. Therefore, in LARS-WG, rainfall modeling is a two-step process like the SDSM conditioned on wet and dry days. In LARS-WG downscaling, unlike SDSM, large-scale atmospheric variables are not directly used in the model; rather, based on the relative monthly changes in mean daily precipitation amount and daily wet and dry series duration between current and future periods predicted by a GCM, local station climate variables are adjusted proportionately to represent climate change.

The three main parts of the model consist of the following:

1. Analysis: First, the observed gauge data are analyzed to estimate the parameters of the weather generator. Precipitation, sunshine hours, and maximum and minimum temperature are observed inputs. In this model, Fourier series are used for maximum and minimum temperature estimation. Also, the output data are used in the process of generation.
2. Generator: In this step, the scenario file which includes the information of changes in dry and wet series duration, amount of precipitation, average of temperature, temperature variability and solar radiation is generated using the parameter files developed as a result of step 1. The scenario file contains the monthly changes if LARS-WG is used to generate data for a climate change scenario.
3. Qtest: Qtest is used to estimate the correctness of simulating observed data. The observed and synthetic generated data are compared in this step.

Example 9.5

Consider the rain gauge of Example 9.4. Produce the precipitation data of this station under the HadCM3 A2 scenario outputs from 2011 to 2030, from 2046 to 2065, and from 2080 to 2099 using the LARS model. Show the results from 2011 to 2020 in a table.

Solution:

Step 1: For applying the LARS model, two input files should be developed:

Station A.st file: This file includes site name, latitude, longitude, and altitude of the Station A rain gauge, the directory path location and name of the file containing the observed weather data for the Station A, and the format of the observed weather data in the file, which here is the year (YEAR), Julian day (JDAY, i.e., from 1 to 365), minimum temperature (MIN; °C), maximum temperature (MAX; °C), precipitation (RAIN; mm), and solar radiation (RAD; MJ m^{-2} day^{-1}) or sunshine hours (SUN). Note that if you have SUN as an input variable, LARS-WG automatically converts it to global radiation (Figure 9.12).

(Station A.sr) file: This contains the daily data of rainfall, maximum temperature, minimum temperature, and solar radiation at Station A in the order mentioned in Station A.st file.

Step 2: After preparing the mentioned files, and for calibrating the model, the SITE ANALYSIS option is selected and Station A.st is addressed to model. Two files called Station A.sta and Station A.wg are created. These files make up the statistical characteristics of the parameter and data that are used to synthesize simulated weather data in the generator process. In the Station A.sta file, the statistical characteristics of the observed weather data in daily, monthly, and seasonal time scales are presented.

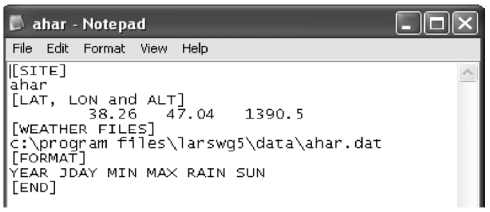

FIGURE 9.12 Layout of basic characteristics of Station A (Station A.st file).

File Station A.wg contains the monthly histogram intervals and frequency of events in these intervals for dry, wet, and rainfall series.

Step 3: For model validation, the Test option is selected from the Q Test module in the LARS model. The Q Test option carries out a statistical comparison of synthetic weather data generated using LARS with the parameters derived from observed weather data in the calibrated model. Selecting the Test option, first, the name of Station A would be selected, then simulation period (20 years) and random segment related to stochastic predicting model will be selected (Figure 9.13). The performance of the model in simulating the observed precipitation pattern in the calibration period is evaluated in Figure 9.13. The model output matches closely the observed values (Rain 1986–2007).

Step 4: The Generator option in the LARS model is used to simulate synthetic weather data. This option is used to generate synthetic data, which have the same statistical characteristics as the observed weather data, or to generate synthetic weather data corresponding to a scenario of climate change.

First, the scenario related to the considered area would be determined. Here, scenarios obtained according to the GCM, namely, ECHO-G A1 for grid 17–31, is used. Initial inputs at this stage are name and address of the GCM scenario.

There are three further options to be completed after selection of the site and setting up the appropriate scenario files. The scaling factor is determined by assuming that the changes in climate over time are linear. If a climate change scenario is implemented for a particular future time period, say, the year 2100, to obtain data for an earlier time period without having to create a scenario file for that, then this factor is used. In this example, the scaling factor is equal to one and the model is simulated in 20 years with random seed 877. The monthly data are simulated for the period 2011–2020. The final result is summarized in Table 9.5.

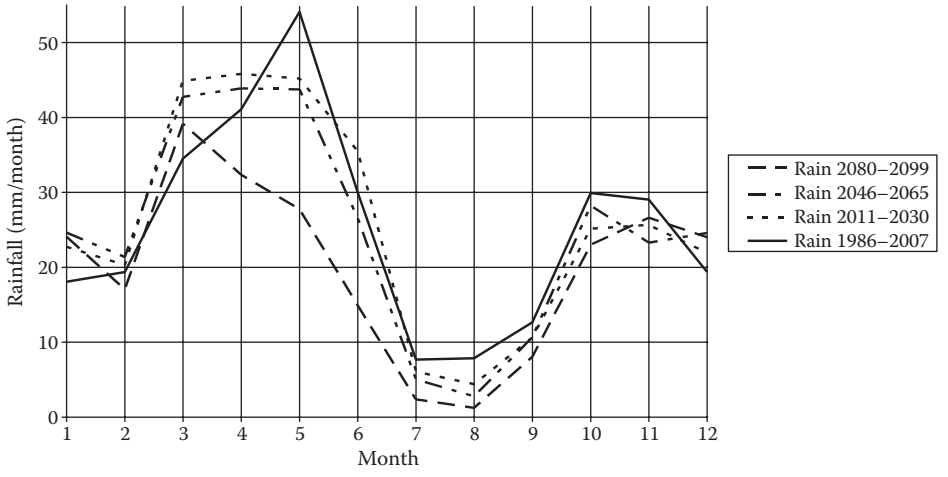

FIGURE 9.13 Generated and observed monthly total rainfall in different intervals.

TABLE 9.5
Generated Precipitation (Scenario A1B for the 2011–2020 Period) for 10 Years

	Monthly Total Precipitation (mm)											
Year	**Jan**	**Feb**	**Mar**	**Apr**	**May**	**Jun**	**Jul**	**Aug**	**Sep**	**Oct**	**Nov**	**Dec**
1	23.90	27.60	59.80	11.80	46.60	52.80	14.80	4.90	0.50	3.40	16.50	44.50
2	49.90	18.50	9.30	55.90	75.20	35.70	3.60	0.00	3.60	22.90	22.30	44.70
3	22.90	0.90	23.30	60.20	95.00	68.30	5.00	14.60	0.00	17.20	11.60	23.20
4	1.40	23.60	40.50	61.00	26.20	8.70	5.80	0.00	0.00	9.70	0.00	16.00
5	29.10	42.10	27.20	75.50	57.30	44.70	1.70	4.00	8.20	8.30	55.20	21.80
6	19.90	15.10	56.50	50.10	67.20	42.30	0.30	9.20	0.00	46.80	14.60	14.80
7	40.90	32.30	71.20	43.50	60.40	31.70	3.50	3.20	0.00	27.10	24.50	53.10
8	18.10	2.00	55.40	40.00	67.10	0.00	13.90	0.00	7.70	30.90	21.60	10.90
9	6.40	38.30	46.80	32.90	26.50	26.40	1.70	11.10	10.90	54.50	8.20	28.00
10	25.50	3.10	57.80	32.80	35.70	60.80	1.30	0.00	30.30	41.10	25.10	68.40

9.7 CASE STUDIES

In previous sections, the theoretic concepts of climate change evaluation were described. In this section, the practical approaches to evaluation of climate change impacts are described through four case studies.

9.7.1 Case Study 1: Assessment of Climate Change Impacts on Hydroclimatic Variables in the Aharchai River Basin

Karamouz et al. (2011) evaluated the climate change impacts on temperature, rainfall, and streamflow in the Aharchai River watershed upstream of the Satarkhan reservoir in the northwestern part of Iran.

9.7.1.1 Study Area

The Aharchai River basin is located between 47°20′ and 47°30′ East longitude and 38°20′ and 38°45′ North latitude. The location of the study area with an area of 950 km^2 is shown in Figure 9.14. The mean annual rainfall and temperature at this basin are about 320 mm and 10°C, respectively. The average inflow to the reservoir is about 51 MCM/year.

There are two meteorological stations, called "Kasanagh," a rain gauge upstream of the reservoir, and "Ahar," a synoptic station downstream of the reservoir, and a hydrometeorological station, which is called "Orang," just upstream of the Satarkhan reservoirs, which, in this study, are called KH, AR, and OG stations, respectively. Karamouz et al. (2011) demonstrated that these stations can be considered as representative of the meteorological and hydrological conditions of the study area. The GCM outputs that are necessary for evaluation of climate change effects are downloaded from http://www.cics.uvic.ca/scenarios. This site includes the HadCM3 GCM model outputs developed in the UK, for the location of the study region on the GCM model grid. The considered CO_2 emission scenarios are A2 and B2, which are both regional scenarios of climate change.

9.7.1.2 Methodology and Results

For simulation of future drought conditions, it is necessary to simulate the streamflow, and for this purpose, simulation of rainfall and temperature is necessary. Future precipitation and temperature are simulated using the effective climatic predictors selected among HadCM3 output data and through SDSM. To select the best set of rainfall predictors in the region, the relation between

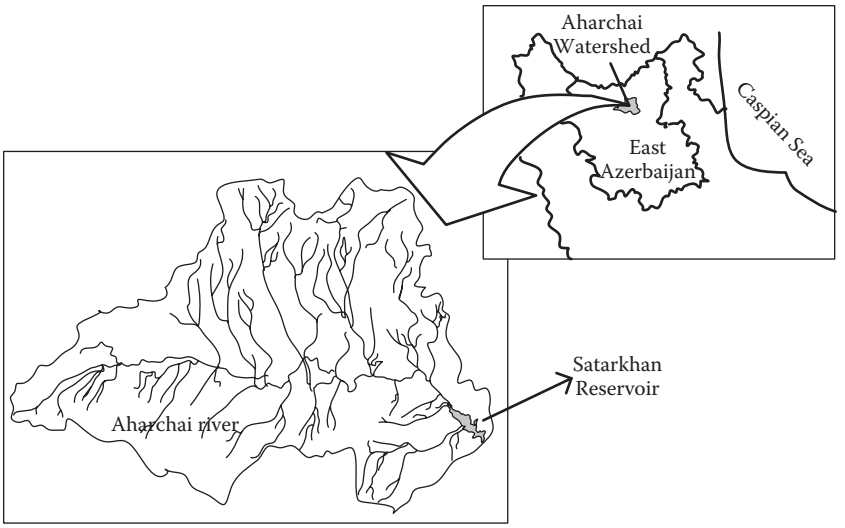

FIGURE 9.14 Aharchai River and Satarkhan reservoir watershed in East Azerbaijan–northwestern Iran.

different combinations of climatic predictors and regional rainfall has been examined through the evaluation of physical relationship and statistical tests.

The results showed that different combinations of predictors should be used for rainfall simulation in different months of a year. This is due to different climatic systems that affect rainfall variations during a year. In fact, the first group includes two predictors: relative 500 hPa (hectopascal) geopotential height and humidity at 500 hPa. These predictors are used for the rainfall projection of all months except April, May, and June (spring season). The predictors of the second group that are used to project spring rainfall include surface divergence, mean sea level pressure, and 500 hPa vorticity.

The downscaling model has been calibrated during 1971–1980, and the results have been validated for 10 years during 1981–1990. Global reanalysis by the National Centers for Environmental Prediction (NCEP) is used to find relationships between large-scale predictors and local predictands in model calibration. In Figure 9.15a, the monthly mean of observed and Had B2 scenario results are compared for the period 1971–2000. An investigation of climate change scenarios on the rainfall shows that the rate of rainfall fluctuates with a decreasing trend.

Two predictors—500 hPa geopotential height and mean sea level pressure—have been identified for temperature simulation. The model has been calibrated for the period 1986–1995 (because of the availability of the observed data in this period), where the correlation coefficient between effective predictors and temperature in the calibration period is 76%, which is significant in climate studies. The model is validated for the period 1996–2000.

A comparison between the monthly mean of the Had B2 scenario and the observed temperature is shown in Figure 9.15b. An investigation of climate change effects on temperature during 2004–2042 shows that there is an increasing trend in temperature as there is an almost 0.8°C increase every 20 years after 2004 (the final year of available data for this study).

The predicted rainfall is converted to runoff by IHACRES (Identification of unit Hydrographs and Components from Rainfall, Evaporation, and Streamflow) developed by the Integrated Catchment Assessment and Management Centre (ICAM) of the Australian National University to estimate inflow to the reservoir. This model performs well in simulation of streamflow and its variation scheme, but it is not capable of simulating the peak values. To overcome this shortcoming of IHACRES, a multi-layer artificial neural network (ANN) perceptron model has been used to modify the peak values.

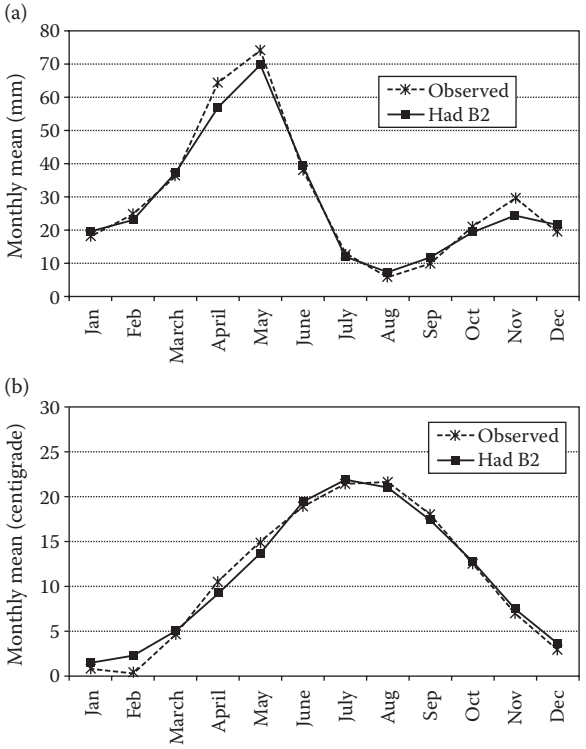

FIGURE 9.15 Comparison between the monthly mean of the Had B2 scenario and observed (a) rainfall (1971–2000) and (b) temperature (1986–2000).

The results of the streamflow simulation showed that the average streamflow during 2005–2023 in comparison with historical data (1986–2004) will decrease about 13%, but during 2024–2042, it will increase about 17% in the study area. In addition, the results show that in the future, the time of maximum streamflow occurrence at the OG station will be shifted from April to June, which should be considered in deriving reservoir operation policies.

The results of this study show that climate change highly affects the hydroclimatic characteristics of the region. This alters the water availability in the region. The reservoir operation is also affected, which may cause intensive losses and serious damages to regional contributions.

9.7.2 Case Study 2: Evaluation of Climate Change Impacts on Urban Floods

In urban areas, due to some special characteristics such as population concentration and limitations on natural water systems, the effects of climate change on hydrologic cycle components are intensified. One of the most important components of the water cycle is surface runoff, which is highly affected by climate change and urbanization. Karamouz et al. (2011) studied the urban rainfall and runoff variations under climate change impacts in the metropolitan area of Tehran in Iran.

9.7.2.1 Study Area

In recent years, Tehran, the capital of Iran, has been rapidly developing without consideration of the diverse impacts on the environment and especially the water cycle. This has resulted in a wide range of challenges and obstacles in water- and sanitation-related infrastructures in this area. The northeastern part of Tehran, between 51°22′ and 51°30′ East longitudes, and 35°42′ and 35°53′ North latitudes, has been considered as the case study. It is a mountainous area with a high population

density. Therefore, urban flooding can cause considerable damage and the evaluation and simulation of the flood effects in this area are very important. The altitude of the region varies between 3900 m upstream of the Darband sub-basin and 1290 m at the end point of the region. The total area of the study region is about 110 km^2. The percentage of the impervious area is about 85%, and the average slope of the region is about 20%. In recent years, some river training projects have been performed on these channels, which have changed the characteristics of the surface water collection system. Also, some structural plans are being studied to improve the drainage system of the study area. For evaluating the effects of these projects on the runoff collection system of Tehran, besides the climate change impacts, three scenarios have been considered:

- Scenario a: This was developed for evaluating the surface water collection system about 10 years ago. The model for this scenario is developed to evaluate the effectiveness of developmental projects done in recent years for improving the past situation.
- Scenario b: In this scenario, the present surface water collection system is modeled.
- Scenario c: The future plans for improving and developing a case study drainage system have been modeled in this scenario.

The general characteristics of these scenarios are presented in Table 9.6. The configured drainage systems in these scenarios are shown in Figure 9.16. The circled areas in Figure 9.16 show the main differences between scenarios, which are tabulated in detail in Table 9.7. The effects of climate change and land-use variations have been considered in runoff modeling in each of these scenarios.

9.7.2.2 Methodology

Different best management practices (BMPs) are employed to improve system performance in flood transitions. An algorithm is proposed to evaluate the urban drainage system performance in flood transmission using an optimal scheme of BMPs, as shown in Figure 9.17. The five main steps of the proposed algorithm are as follows:

Step 1: Data gathering, preparation, and analysis (box 2): In this step, the data needed for different parts of the study are collected and analyzed. These data are classified into three groups: hydrologic data (box 3) (runoff and sediment load), climatic data (box 4) (rainfall, temperature, and snow), and climatic signals (box 5) (GCM models' outputs under climate change scenarios A2 and B2). Due to the low resolution of GCM outputs, downscaling models are developed to explore the relation between large-scale climatic signals and regional rainfall. In this study, SDSM has been used for downscaling.

Step 2: Joint probability of rainfall and sediment using the Copula method (box 7): For providing a more realistic configuration of the urban drainage system performance, the effect of sediment load should be considered in the development of the flood hydrograph.

TABLE 9.6
Characteristics of Different Scenarios for Drainage System Structure

	Impervious Area (%)	Number of Detention Ponds	Total Capacity of Detention Ponds (m^3)	Length (m)		
				Natural Channel	Man-Made Closed Channel	Man-Made Open Channel
Scenario a	81.09	4	7500	17,720	16,940	45,690
Scenario b	85	5	9450	16,170	21,095	30,650
Scenario c	90.09	7	13,380	16,170	29,915	30,650

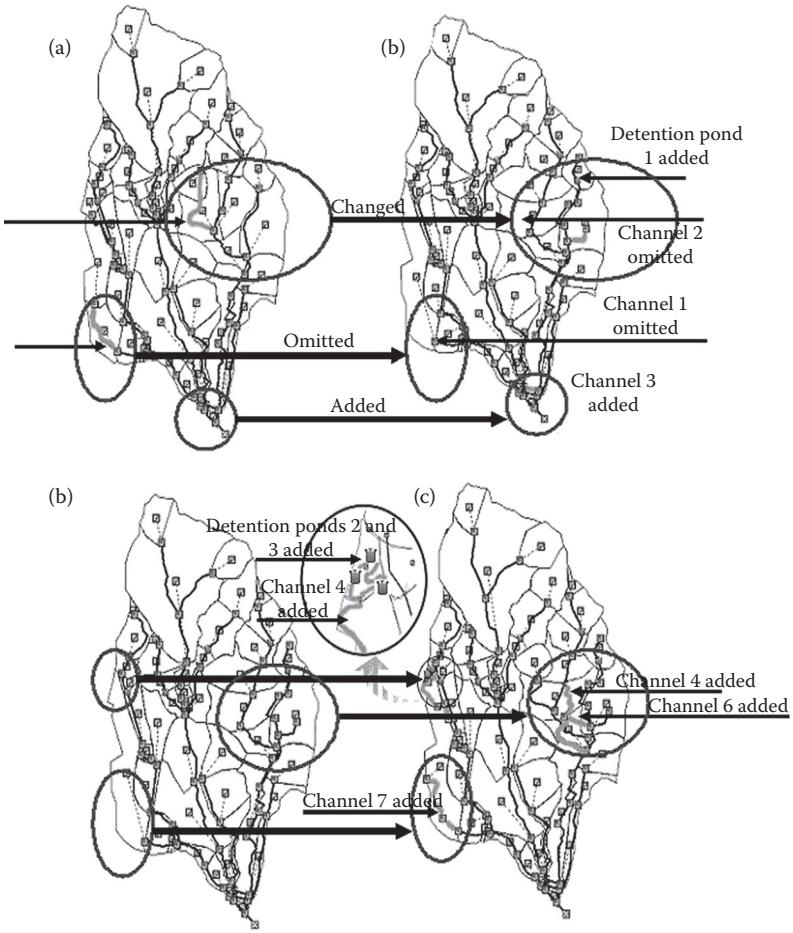

FIGURE 9.16 Drainage system layout (a) past, (b) present, (c) future. (From Karamouz, M. et al., *ASCE Journal of Hydrologic Engineering*, 2011. With permission.)

TABLE 9.7
Differences between Three Defined Scenarios

Added Detention Ponds	Added Channels			Omitted Channels			Article I
Volume (m^3)	Dimension (m)	Length (m)	Number	Section Area (m^2)	Length (m)	Number[a]	Scenario
12,500—Jamshidieh basin	8.4	700	3	5.4	2600	1	**a → b**
				5	4300	2	
10,000—upstream of Velenjak channel	0.8	2000	4	Article II	Article III	Article IV	**b →c**
	6	800	4				
	1.75	2200	5				
	5.7	1000	6				
	5	1500	6	Article V	Article VI	Article VII	

[a] The channel numbers are shown in Figure 9.16

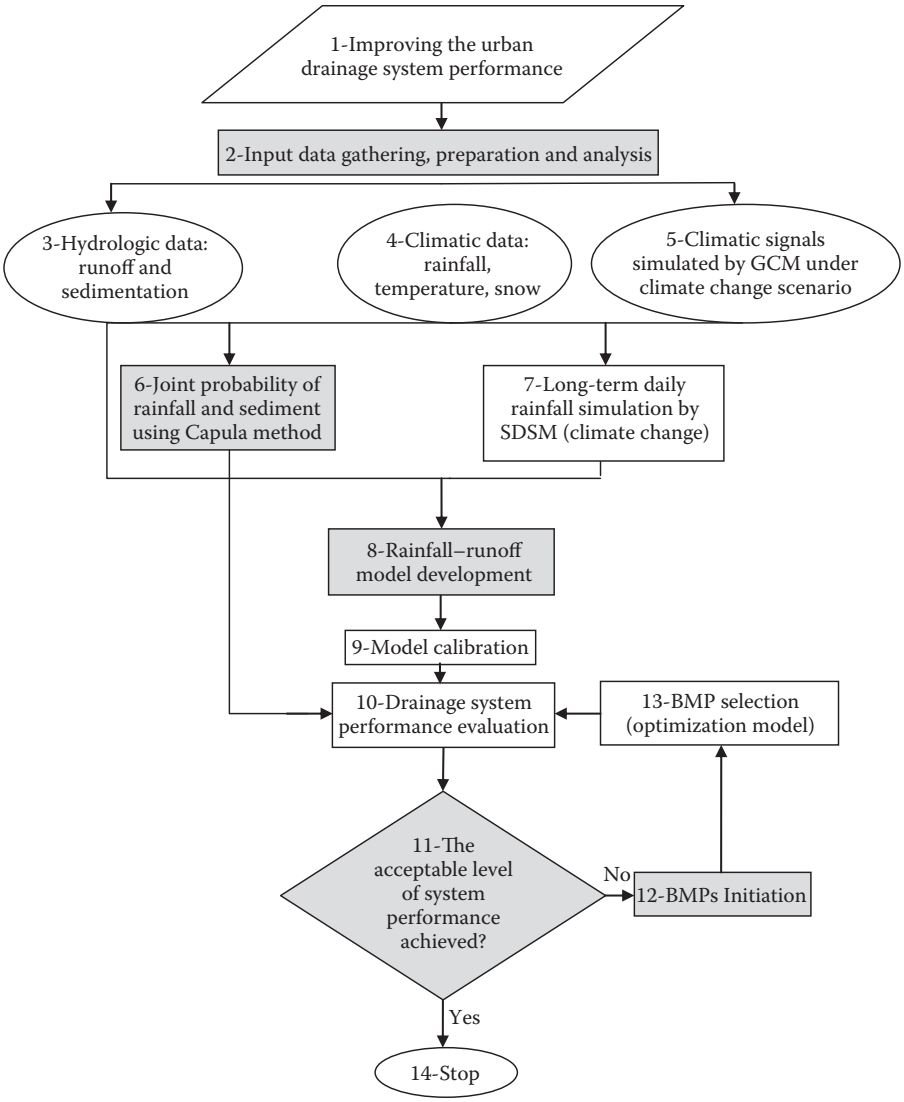

FIGURE 9.17 Proposed algorithm for the improvement of urban drainage system performance (the main steps are highlighted). (From Karamouz, M. et al., *ASCE Journal of Hydrologic Engineering*, 2011. With permission.)

Step 3: Rainfall–runoff model development (box 8): The StormNET model has been employed to simulate the performance of the flood and drainage system in the study area.

Step 4: System performance evaluation (box 11): In this step, the performance of the system is evaluated and compared with predefined criteria to decide on the application of the BMPs. If the system performance criteria are satisfied, the algorithm terminates (box 14); otherwise, the algorithm continues by selecting a new group of BMPs.

Step 5: BMP initiation (box 12): The appropriate and applicable BMPs are determined.

Step 6: BMP selection (box 13): An optimization model is proposed to select the best composition of different BMPs to improve system performance. In this model, minimizing the system costs, including BMPs, construction, and flood damage costs, are considered.

Here, the results of the first four steps are presented.

9.7.2.3 Results

Three signals are selected for rainfall simulation based on the maximum correlation of their combination and daily rainfall. These signals include the following: (1) divergence near surface (P-zh), (2) divergence at 500 hPa pressure, and (3) mean temperature (Temp). The model is structured in monthly time steps for rainfall downscaling, in which 12 regression equations are obtained for 12 months. HadCM3 (Second Hadley Centre Coupled Ocean–Atmosphere GCM) data are used as downscaling model input signal and then rainfall is simulated.

In order to choose the critical daily rainfall of each season that may result in a flood, the maximum value of each season's rainfall is selected among the rainfall data of each year as the most critical rainfall of that season of that year. These values are selected among every 10-year rainfall data from 2007 to 2097 of scenario A2(a). Then, the proper probability distribution based on statistical analysis is fitted to selected extreme events, and the rainfall with different return periods of 20, 50, 100, and 200 years is obtained for each season. Data regarding these rainfall events are shown in Figures 9.18 and 9.19. As is clear in these figures, the extreme events are numerically less in summer, but their intensity is the highest.

Here, the results of system performance without considering the sediment load under climate change impacts are given. The performance of three scenarios of the drainage system is assessed using the developed rainfall hyetographs with return periods of 20, 50, 100, and 200 years. For

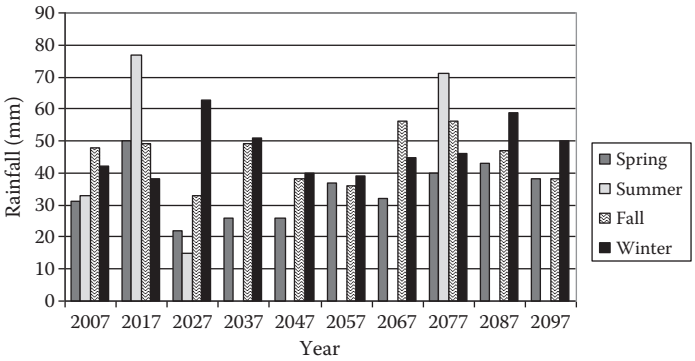

FIGURE 9.18 Critical values of projected future rainfall. (From Karamouz, M. et al., *ASCE Journal of Hydrologic Engineering*, 2011. With permission.)

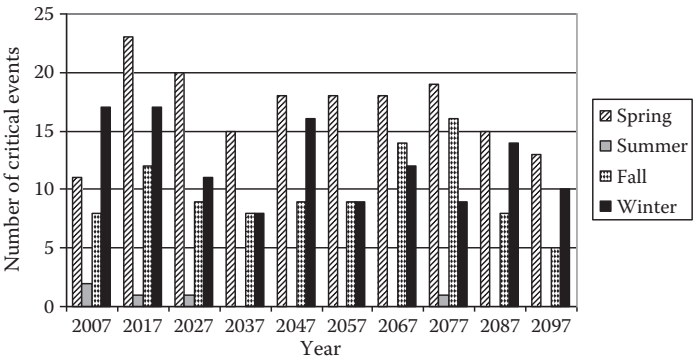

FIGURE 9.19 Number of critical projected rainfall. (From Karamouz, M. et al., *ASCE Journal of Hydrologic Engineering*, 2011. With permission.)

instance, the resulting flood volume with a return period of 20 years considering the changes due to climate impacts in the next 90 years at the basin outlet is illustrated in Figure 9.20. This figure shows that the flood volume of the basin outlet in scenario a is about 35% less than that in scenario b. The main reason for this phenomenon is the decrease of pervious area because of more urbanization in recent years. The flood volume at the basin outlet in scenario c has a slight difference with that in scenario b. Although the pervious area has been decreased considerably in the third scenario in comparison with the second scenario, it seems that the improvement of the drainage system in the third scenario, considering detention ponds, has resulted in more efficient performance of the system and decreased flood volume.

Also, the simulated hydrograph at the basin outlet for scenarios a and b considering the same rainfall hyetograph is shown in Figure 9.21. Blocked and semi-blocked channels of the drainage system, as well as an increase in the number and capacity of detention ponds, have declined the peak of discharge at the basin outlet in scenario b in comparison with scenario a. By blocking the channels in scenario b, overland flow increases, which results in higher time of concentration in comparison with scenario a. Therefore, the surface flood of the basin increases, and the peak runoff at the outlet happens later with less quantity. Also, less perviousness and added drainage channels in scenario c

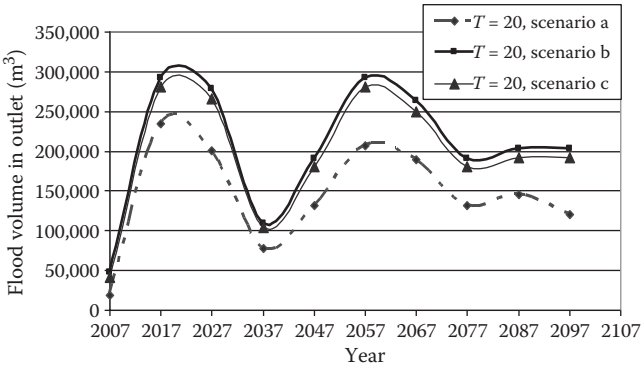

FIGURE 9.20 Variation of 20-year return period flood volume at the outlet of the study area in different scenarios in the next 90 years (ignoring the sediment load). (From Karamouz, M. et al., *ASCE Journal of Hydrologic Engineering*, 2011. With permission.)

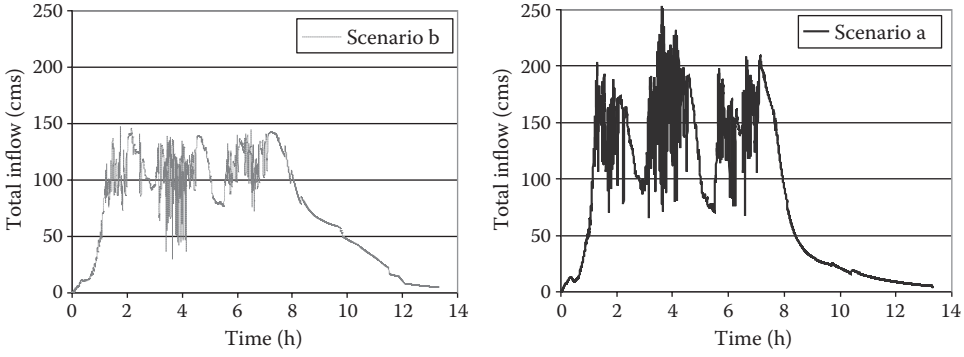

FIGURE 9.21 Comparison of outlet hydrograph in scenarios a and b in the same rainfall. (From Karamouz, M. et al., *ASCE Journal of Hydrologic Engineering*, 2011. With permission.)

cause higher discharge peaks in this scenario in comparison with scenario b. According to these results, the flood hydrograph at the second scenario is more moderate than the other scenarios.

9.7.3 Case Study 3: Impacts on Future Droughts

Karamouz et al. (2007) evaluated the climate change impacts on drought characteristics in the future. To consider different aspects of drought impacts, they used different indices including Standardized Precipitation Index (SPI), Surface Water Supply Index (SWSI), and Soil Moisture Deficit Index (SMDI), representing meteorological, hydrological, and agricultural droughts, respectively. These indices are developed based on changes in precipitation, water supply, and soil moisture during droughts. For integration of these indices, a hybrid index is developed based on drought damage using probabilistic neural network. The drought characteristics based on the proposed hybrid index are estimated over a 100-year time horizon (the time horizon in which GCM outputs are available).

Furthermore, to incorporate the uncertainties in the long-lead drought prediction, 100 ensembles of data are generated using SDSM. The uncertainty analysis is performed by fitting a probability distribution function to the estimated drought characteristics for each ensemble of data. The Aharchai River basin located in the northwestern part of Iran is used as the case study.

The characteristics of this region were given in the first case study. Since gardens form a large part of agricultural lands in this region, which may perish due to long periods of water shortages, the prediction of drought periods and their characteristics are very important in this region. The algorithm of the study is given in Figure 9.22.

The effective sets of predictors based on GCMs' outputs are selected to downscale and evaluate climate change impacts on the temperature, rainfall, and soil moisture. The streamflow is simulated using the IHACRES model based on the downscaled rainfall and temperature data. The drought indices SPI, SWSI, and SMDI are calculated based on the downscaled data for two climate change scenarios: A2 and B2. The probability distribution of the developed drought indices in the next 100 years is developed as given in Figure 9.23. The results of this study show that the uncertainty of prediction will be significantly high if the uncertainties involved in the input data are high and the predicted drought indices in the future show that climate changes alter considerably the drought behaviors. Implementing the changes in the basin's climate, one can predict the probable dry conditions and estimate the damage it may cause and therefore use appropriate preventive activities for the minimization of drought damage.

9.7.4 Case Study 4: Evaluation of Climate Change Impacts on Irrigation Water Demand

Karamouz et al. (2012) developed an agricultural planning optimization–simulation model to determine the optimal cultivated area, cropping pattern, and irrigation efficiency considering limited water supply resources in a region.

The Aharchai River basin in the northwestern part of Iran has been selected as the case study. Water supply in this part of Iran depends on seasonal rainfall, temperature, and runoff. Therefore, predicting the hydrological variables within an acceptable confidence interval is required for obtaining the optimal operation of the available resources and assessing the climate change impact on water availability in the future. The proposed methodology in this study is illustrated in Figure 9.24.

To study the potential regional-scale impacts of climate change on crop water requirements and water supply, future climate change scenarios A1B, A2, and B1 obtained from the GCM outputs are considered.

In order to downscale the climate regional data, the LARS-WG model is used. In the next step, downscaled data are used in CROPWAT to estimate agricultural water demand. The crop water

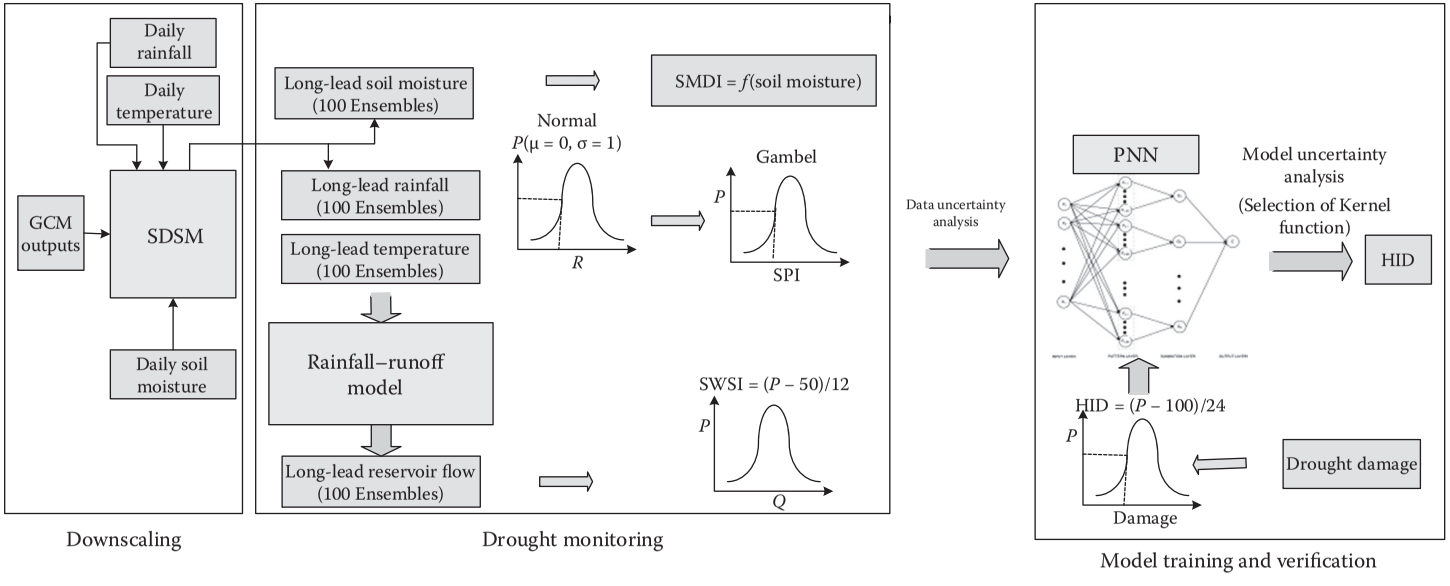

FIGURE 9.22 Proposed algorithm for uncertainty assessment in long-lead drought prediction. (From Karamouz, M. et al., 2007. "Evaluation of dry spans characteristics considering climate change effects" Second International Conference on Earth Systems Modeling (ICESM), Vol. 1, ICESM2007-A-0043. With permission.)

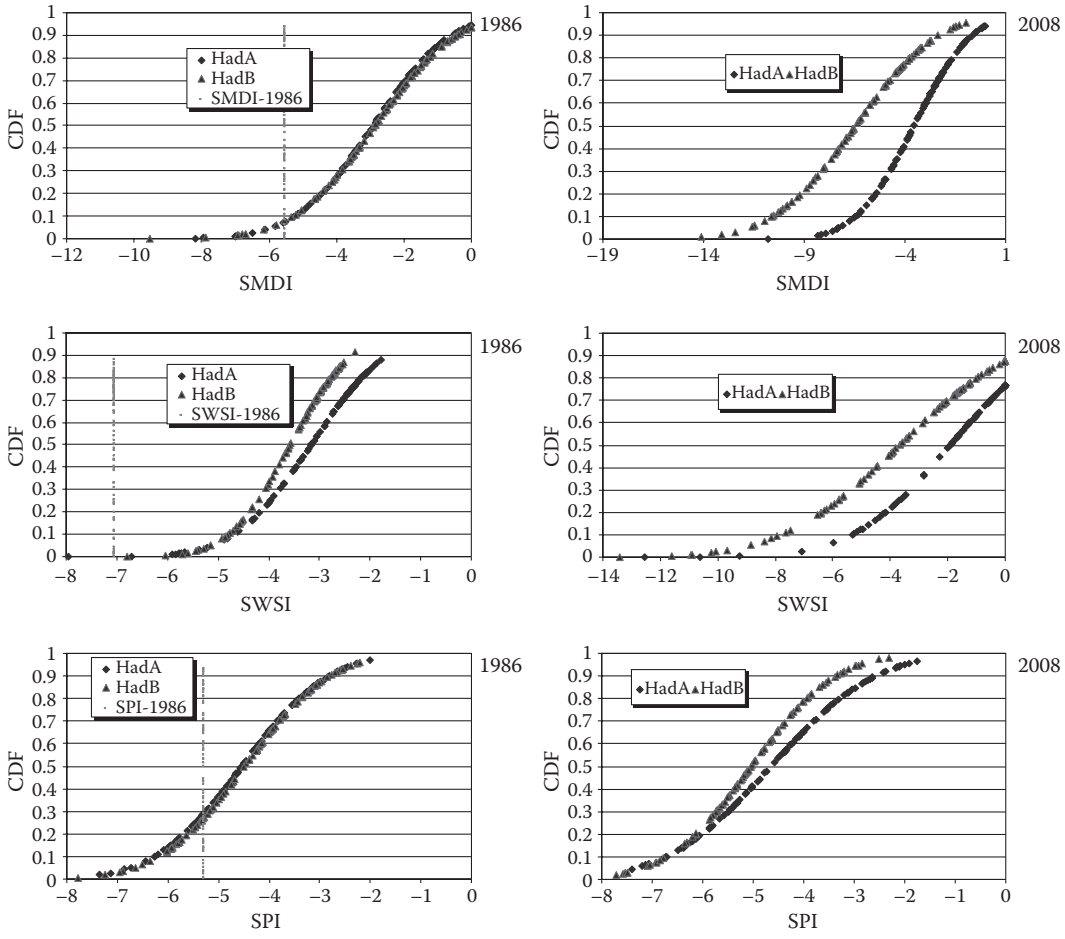

FIGURE 9.23 CDF of three different drought indices: indicators of meteorological, hydrological, and agricultural aspects of drought for two scenarios HadA and HadB. (From Karamouz, M. et al., 2007. "Evaluation of dry spans characteristics considering climate change effects" Second International Conference on Earth Systems Modeling (ICESM), Vol. 1, ICESM2007-A-0043. With permission.)

demand in the study region is calculated based on the crops' evapotranspiration by utilizing the FAO Penman method. Then, for simulating the watershed streamflow, the IHACRES model is run using the LARS-WG outputs.

The developed model in this study is composed of an optimization and a simulation model. In the next step, the results of the agricultural optimization model (crop pattern, cultivated area, and irrigation efficiency) are fed into the watershed simulation model to simulate future demands and water allocation in the study area. The developed model is run several times based on different scenarios.

Results of simulated evapotranspiration time series under climate change scenarios show that ET_o increases about 4%, 10%, and 12.1% in 2011–2030, 2046–2065, and 2080–2099, respectively (Figure 9.25). Consequently, agricultural water demand is increasing in different time periods. Also, simulated yearly streamflow under climate change impacts in all scenarios is decreasing. Taking into account these changes, the importance of considering climate effect in water resource and agricultural planning and management has been evaluated.

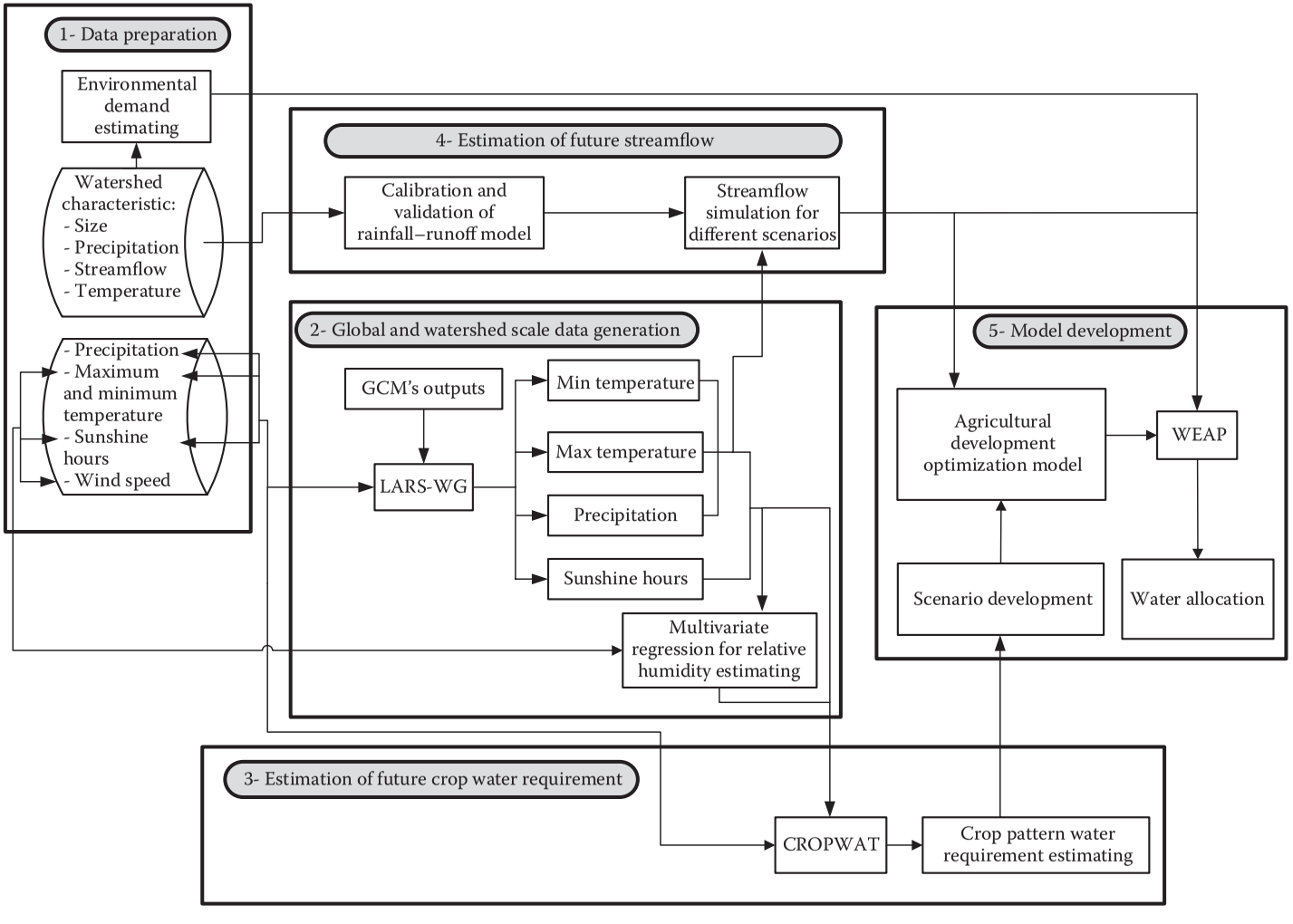

FIGURE 9.24 Flow chart for the proposed methodology in case study 4. (From Karamouz, M. et al., 2012, *Journal of Water Resources Planning and Management* (In press). With permission.).

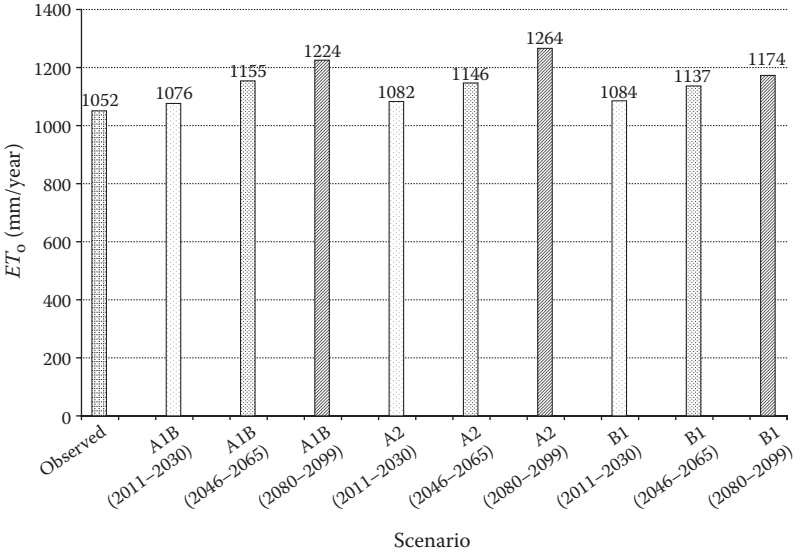

FIGURE 9.25 Yearly long-term mean observed and estimated ET_o under A1B, A2, and B1 climate scenarios in different time periods for case study 4. (From Karamouz, M. et al., 2012, *Journal of Water Resources Planning and Management* (In press). With permission.).

PROBLEMS

1. Annual anthropogenic emissions of CO_2, CH_4, and N_2O are estimated to be 27,000 Mt CO_2/year, 370 Mt CH_4/year and 6 Mt N_2O/year (where Mt is million metric tons). Compute the impacts of these three gases over a 100-year time horizon, and find the total equivalent CO_2 emissions.
2. Using the downloaded monthly mean relative humidity data developed by the HadCM3 GCM model for the period 1961–1999 based on climate change scenario B1, draw the diagram of monthly variations of relative humidity at point (20, 41).
3. A rain gauge of an urban area called Station A is located at 51°46′ East longitude and 31°38′ North latitude with 1200 m altitude. The precipitation data for 10 years from 1992 to 2001 are available in this rain gauge. The monthly data are given in Table 9.8. Produce the precipitation data of Station A under the HadCM3 A2 scenario outputs from 2002 to 2012 using the LARS-WG model.
4. Using the precipitation data of a station in a selected city, evaluate the changes in mean, maximum, and minimum monthly rainfall and wet and dry spells under HadCM3 B2 and A2 scenarios. Estimate the changes that occurred in each scenario and the intensity of the climate change effects.
5. Utilize the rainfall, minimum temperature, and maximum temperature data of a station in a city in the LARS model and downscale it. Define different scenarios and evaluate the effect of climate change on the statistics of the considered variables.
6. Use daily temperature data (for the period 1980–2000) of Station B located at 56°01′ East longitude and 30°24′ North latitude, with an elevation of 1469 m. Generate the data of Station B under the HadCM3 A2 and B1 scenario outputs from 2020 to 2025 using both SDSM and LARS models and compare the difference between the results. Judge which one will be more accurate.
7. Which parameters in the SCS, Horton, and Green and Ampt models are affected by climate change?

TABLE 9.8
Monthly Observed Precipitation for Station A under the HadCM3 A2 Scenario for Period 1992–2001 (in mm)

Year	January	February	March	April	May	June	July	August	September	October	November	December
1992	7.74	21.72	17.42	15.00	44.52	29.00	6.77	0.00	5.00	4.84	32.00	22.26
1993	–	–	–	–	–	–	–	–	–	–	–	–
1994	8.71	6.43	–	19.00	–	20.00	11.61	0.00	0.00	15.48	10.00	–
1995	11.61	17.41	3.87	38.00	33.87	26.00	5.81	0.00	2.00	22.26	10.00	2.90
1996	18.39	26.90	28.06	53.00	41.61	27.00	0.00	15.48	3.00	6.77	27.00	30.97
1997	15.48	23.57	36.77	29.00	15.58	63.00	70.65	9.68	0.00	12.58	14.00	7.74
1998	23.23	34.29	49.53	16.00	42.58	44.00	20.32	2.90	7.00	2.90	29.00	0.00
1999	16.45	10.71	–	–	–	–	–	–	–	–	–	–
2000	–	9.31	51.29	30.00	44.52	24.00	17.42	0.00	0.00	0.00	32.00	70.65
2001	33.87	7.50	45.48	58.00	21.29	13.00	4.48	2.90	16.00	12.58	73.00	7.74

REFERENCES

California Department of Water Resource (2007). Climate Change in California, State of California, http://www.water.ca.gov/.

Gilbert, M.M. and Ela, W.P. (2008). *Introduction to Environmental Engineering and Science*, 3rd edition, Prentice-Hall, Englewood Cliffs, NJ.

Houghton, J. (1997). *Global Warming: The Complete Briefing*, Cambridge University Press, Cambridge.

IPCC (2001). Third Assessment Report, Intergovernmental Panel on Climate Change (IPCC). http://www.ipcc.ch/.

Karamouz, M., Hosseinpour, A. and Nazif, S. (2011). "Improvement of urban drainage system performance under climate change impact: A case study," *ASCE Journal of Hydrologic Engineering*, 16 (5), 395–412.

Karamouz, M., Rasouli, K., Nazif, S., (2007), "Evaluation of dry spans characteristics considering climate change effects" Second International Conference on Earth Systems Modeling (ICESM), Vol. 1, ICESM2007-A-0043.

Karamouz, M., Ahmadi, B., Zahmatkehs, Z., (2012). Developing an Agricultural Planning Model in a Watershed Considering Climate Change Impacts Developing an Agricultural Planning Model in a Watershed Considering Climate Change Impacts, Journal of Water Resources Planning and Management (In press).

Kaya, Y. (1990). *Impact of Carbon Dioxide Emission Control on GNP Growth: Interpretation of Proposed Scenarios*, IPCC Energy and Industry Subgroup, Response Strategies Working Group, Paris, Cambridge University Press, Cambridge.

Lattenmaier, D.P., McCabe, G. and Stakhiv, E.Z. (1996). "Global climate change: Effect on hydrologic cycle." In *Water Resources Handbook*, McGraw-Hill, New York.

NOAA (2006). http://www.cmdl.noaa.gov/ccgg/trends.

Racsko, P., Szeidl, L. and Semenov, M. (1991). "A serial approach to local stochastic weather models," *Ecological Modeling*, 57, 27–41.

Semenov, M.A. and Brooks, R.J. (1999). "Spatial interpolation of the LARS-WG stochastic weather generator in Great Britain," *Climate Research*, 11, 137–148.

Semenov, M.A., Brooks, R.J., Barrow, E.M. and Richardson, C.W. (1998). "Comparison of the WGEN and LARS-WG stochastic weather generators in diverse climates," *Climate Research*, 10, 95–107.

Semenov, M.A. and Barrow, E.M. (2002). *LARS-WG, A Stochastic Weather Generator for Use in Climate Impact Studies. User Manual, Ver 3.0*, available at http://www.iacr.bbsrc.ac.uk/mas-models/larswg.html.

Viner, D. and Hulme, M. (1992). *Climate Change Scenarios for Impact Studies in the UK*, Climatic Research Unit, University of East Anglia, Norwich.

Von Storch, H., Zorita, E. and Cubasch, U. (1993). "Downscaling of global climate change estimates to regional scales: An application to Iberian rainfall in wintertime," *Journal of Climate*, 6, 1161–1171.

Wigley, T.M.L., Jones, P.D., Briffa, K.R. and Smith, G. (1990). "Obtaining sub-grid-scale information from coarse-resolution general circulation model output," *Journal of Geophysical Research*, 95, 1943–1954.

Wilby, R.L. and Dawson, C.W. (2004). *Using SDSM Version 3.1—A Decision Support Tool for the Assessment of Regional Climate Change Impacts*, Climate Change Unit, Environment Agency of England and Wales, Nottingham, and Department of Computer Science, Loughborough University, UK.

Wilby, R.L., Hassan, H. and Hanaki, K. (1998). "Statistical downscaling of hydrometeorological variables using general circulation model output," *Journal of Hydrology*, 205, 1–19.

Wilby, R.L., Hay, L.E., Gutowski, W.J., Arritt, R.W., Takle, E.S., Pan, Z., Leavesley, G.H. and Clark, M.P. (2002). "Hydrological responses to dynamically and statistically downscaled climate model output," *Geophysical Research Letters*, 27, 1199–1202.

10 Probability, Risk, and Uncertainty in Hydrologic Analysis

10.1 INTRODUCTION

Hydrologic variables and events such as rainfall, runoff, floods, drought, etc., are usually investigated by analyzing their records of observations. Many characteristics of these processes seem to vary in a way not amenable to deterministic analysis. In other words, deterministic relationships, presented so far, do not seem to be applicable for analysis of these characteristics. For the purpose of hydrologic analysis, the annual peak discharge is considered to be a random variable. Methods of probability and statistics are employed for analysis of random variables.

Also, in all fields of hydrologic analysis, we face uncertainty arising from hydrologic phenomena that cannot be predicted accurately. Any prediction is uncertain, and in the mathematical modeling of hydrological processes, this uncertainty has to be taken into account.

The methods discussed in this chapter are: (1) probability concepts; (2) statistical moments; (3) common probabilistic model; (4) return period; (5) risk, reliability, vulnerability, and resiliency; and (6) uncertainty.

10.2 PROBABILITY TREATMENT OF HYDROLOGIC DATA

A random variable X is a variable described by a probability distribution. The distribution specifies the chance that observation x of the variable will fall in a specified range of X. For example, if X is annual precipitation at a specified location, then the probability distribution of X specifies the chance that the observed annual precipitation in a given year will lie in a defined range, such as less than 40 in, and so on.

A set of observations $x_1, x_2, \ldots, x_n$ of the random variable is called a sample. It is assumed that samples are drawn from a hypothetical infinite population possessing constant statistical properties, while the properties of a sample may vary from one sample to another. The set of all possible samples that could be drawn from the population is called the sample space, and an event is a subset of the sample space.

The probability is defined as follows:

$$P(X_0) = \frac{n}{N}, \tag{10.1}$$

where n is the number of occurrences (frequency) of event X_i in N trials. Thus, $\frac{n}{N}$ is the relative frequency or probability of occurrence of X_i.

If one defines $P(X_i)$ as the probability of the random events X_i, the following condition holds on the discrete probabilities of these events when considered over the sample space of all possible outcomes:

$$0 \le P(X_i) \le 1 \tag{10.2}$$

$$\sum_{i=1}^{N} P(X_i) = 1. \tag{10.3}$$

The probability of the union (occurrence of either, symbolized by "∪") of two mutually exclusive events is the sum of probabilities of each:

$$P(X \cup Y) = P(X) + P(Y). \tag{10.4}$$

In other cases, the union probability is obtained as follows:

$$P(X \cup Y) = P(X) + P(Y) - P(X \cap Y). \tag{10.5}$$

Two events of X and Y are independent if the occurrence of one does not influence the occurrence of the other. The probability of the intersection of two independent events is the product of either of their individual probabilities:

$$P(X \cap Y) = P(X) \times P(Y). \tag{10.6}$$

The conditional probability of event X given that event Y has occurred is

$$P(X|Y) = P(X \cap Y)/P(Y). \tag{10.7}$$

If events X and Y are independent, the result of joining of Equations 10.6 and 10.7 is as follows:

$$P(X|Y) = P(X) \cdot P(Y)/P(Y) = P(X). \tag{10.8}$$

Example 10.1

Let event X be the condition that a rainstorm occurs on a given day and event Y be the condition that lightning is observed on a given day. Let probabilities of these events be

$$P(X) = 0.3$$

$$P(Y) = 0.1$$

$$P(Y|X) = 0.5$$

a. What is the probability that both rain and lightning occur?
b. What would be the answer to part (a) if both events were independent?

Solution:

a. From Equation 10.8, $P(X \cap Y) = P(Y|X) \cdot P(X) = 0.15$.
b. Such that $P(Y|X) = P(Y) = 0.1$, then $P(X \cap Y) = P(X) \cdot P(Y) = 0.03$.

The probability of the joint occurrence of independent events will always be less than or equal to the probability of their joint occurrence if they are dependent.

10.2.1 Discrete and Continuous Random Variables

The behavior of a random variable may be described by its probability distribution. Every possible outcome of an experiment is assigned a numerical value according to a discrete probability mass function or a continuous probability density function (PDF). In hydrology, discrete random variables are most commonly used to describe the number of occurrences that satisfy a certain criterion, such as the number of floods that exceed a specified value or the number of storms that occur at a given location. For discrete probabilities:

$$P(a \le x \le b) = \sum_{a \le x_i \le b} P(x_i). \tag{10.9}$$

The cumulative distribution function (CDF) is defined as

$$F(x) = P(X \le x) = \sum_{x_i \le x} P(x_i). \tag{10.10}$$

Continuous random variables are usually used to represent hydrologic phenomena such as flow, rainfall, volume, depth, and time. Values are not restricted to integers, although continuous variables might be commonly rounded to integers. For a continuous random variable, the area under PDF $f(x)$ represents probability.

$$P(x_1 \le x \le x_2) = \int_{x_1}^{x_2} f(x)\,\mathrm{d}x, \tag{10.11}$$

where the entire area under the PDF equals 1.0. The continuous CDF is defined similarly to its discrete counterpart:

$$P(x_1 < x \le x_2) = F(x_2) - F(x_1). \tag{10.12}$$

10.2.2 Moments of Distribution

A PDF is a functional from whose moments are related to its parameters. Thus, if moments can be found, then the parameters of the distribution can be estimated. The moments themselves are also indicative of the shape of the distribution. For a discrete distribution, the Nth moment about the origin can be defined as follows:

1. For a discrete distribution

$$\mu'_N = \sum_{i=-\infty}^{\infty} x_i^N P(x_i). \tag{10.13}$$

2. For a continuous distribution

$$\mu'_N = \int_{-\infty}^{\infty} x^N f(x)\,\mathrm{d}x. \tag{10.14}$$

The first moment, μ, is the mean value and is defined as follows:

1. For a discrete distribution

$$E(x) = \mu = \sum_{-\infty}^{\infty} x_i P(x_i). \tag{10.15}$$

2. For a continuous distribution

$$E(x) = \mu = \int_{-\infty}^{\infty} x f(x)\, dx. \tag{10.16}$$

Example 10.2

The probability mass function of floods is shown in Figure 10.1. Estimate the mean number of floods in a 10-year period where $f(x_0) = f(x_{10}) = 0.0010$.

Solution:

Equation 10.15 can be used to compute the mean for a discrete random variable of floods in a 10-year period:

$$E(x) = \mu = 0(0.0010) + 1(0.0097) + 2(0.0440) + 3(0.1172) + 4(0.2051) + 5(0.2460) + 6(0.2051) + 7(0.1172) + 8(0.0440) + 9(0.0097) + 10(0.0010) = 5.$$

Thus, the mean number of floods in a 10-year period is 5.

Central moment about the mean may be defined as follows:

1. For a discrete distribution

$$\mu_N = \sum_{-\infty}^{\infty} (x_i - \mu)^N \, P(x_i). \tag{10.17}$$

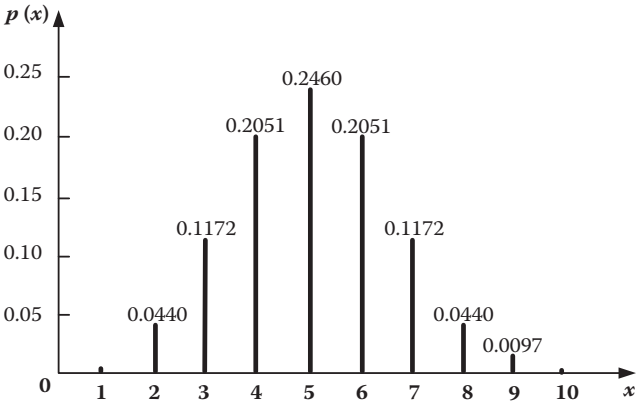

FIGURE 10.1 Probability mass function for a discrete random variable.

2. For a continuous distribution

$$\mu_N = \int_{-\infty}^{\infty} (x-\mu)^N f(x)\,dx. \tag{10.18}$$

Furthermore, the first central moment is zero. The second central moment is called the variance and is computed as follows:

1. For a discrete distribution

$$\text{Var}(x) = \sigma^2 = \mu_2 = E[(x-\mu)^2] = \sum_{-\infty}^{\infty} (x_i-\mu)^2\ P(x_i). \tag{10.19}$$

2. For a continuous distribution

$$\text{Var}(x) = \sigma^2 = \mu_2 = E[(x-\mu)^2] = \int_{-\infty}^{\infty} (x_i-\mu)^2 f(x)\,dx. \tag{10.20}$$

An equivalent measure is the standard deviation, which is simply the square root of the variance. Higher moments are subject to bias in their estimates. An unbiased estimate is one for which the expected value of the estimate equals the population value. For the variance, an unbiased estimate is

$$\sigma^2 = S^2 = \frac{1}{n-1}\sum_{i=1}^{n} (x_i-\mu)^2 \tag{10.21}$$

or

$$\sigma^2 = S^2 = \frac{1}{n-1}\left[\sum_{i=1}^{n} x_i^2 - \frac{1}{n}\left(\sum_{i=1}^{n} x_i\right)^2\right]. \tag{10.22}$$

Example 10.3

Estimate the variance of the mass function of Example 10.1.

Solution:

From Figure 10.1, the variance can be computed by Equation 10.19.

$$\begin{aligned}\sigma^2 = {} & (0-5)^2\,(0.0010) + (1-5)^2\,(0.0097) + (2-5)^2\,(0.00440) + (3-5)^2\,(0.1172) \\ & + (4-5)^2\,(0.2051) + (5-5)^2\,(0.2460) + (6-5)^2\,(0.2051) + (7-5)^2\,(0.1172) \\ & + (8-5)^2\,(0.0440) + (9-5)^2\,(0.0097) + (10-5)^2\,(0.0010) = 2.5.\end{aligned}$$

Example 10.4

Four rain gauges measure 1.7, 2.1, 1.8, and 2.4 cm of rainfall; estimate the variance of the data.

Solution:

The variance of a sample can be computed from Equation 10.22 as follows:

$$\bar{x} = \left(\frac{1.7 + 2.1 + 1.8 + 2.4}{4} \right) = 2 \text{ cm}.$$

$$\text{Var} = \sigma^2 = S^2 = 1/(4 - 1)[(1.7 - 2)^2 + (2.1 - 2)^2 + (1.8 - 2)^2 + (2.4 - 2)^2] = 0.10 \text{ cm}.$$

Example 10.5

The measurement of precipitation at five stations is 2.7, 2.9, 3.4, 3.1, and 2.9 cm. Calculate the mean, variance, and standard deviation of the precipitation data.

Solution:

In Table 10.1, the estimations of mean, variance, and standard deviation are summarized.

The mean is estimated as follows:

$$\bar{x} = \frac{1}{5}(15) = 3 \text{ cm}.$$

From Equation 10.21, the variance is calculated as follows:

$$\sigma^2 = \frac{1}{5-1}(0.28) = 0.07 \text{ cm}^2 .$$

The third central moment is called skew and is defined as follows:

1. For a discrete distribution

$$g = \int_{-\infty}^{+\infty} (x - \mu)^3 f(x)\, dx . \tag{10.23}$$

where the sample skew is g and $f(x)$ is the function of random variable x.

TABLE 10.1
Estimation of Statistics of Rain Measured at Five Rain Gauges in Example 10.5

Gauge Number	Rain Depth (x)	x^2	$(x - \bar{x})$	$(x - \bar{x})^2$
1	2.7	7.29	–0.3	0.09
2	2.9	8.41	–0.1	0.01
3	3.4	11.56	0.4	0.16
4	3.1	9.61	0.1	0.01
5	2.9	8.41	–0.1	0.01
Sum	15.0	45.28	0.0	0.28

2. For a continuous distribution

$$g = \sum_{i=1}^{n} (x - \mu)^3 f(x_i) \,. \tag{10.24}$$

An approximately unbiased estimate is as follows:

$$g = \frac{n\sum_{i=1}^{n} (x - \bar{x})^3}{(n-1)(n-2)S^3} \,. \tag{10.25}$$

The three conditions of the skew are shown in Figure 10.2. A skew is zero for the symmetric distribution and the skew is positive or negative when the distribution is nonsymmetrical. If the more extreme tail of the distribution is to the right, the skew is positive and it is negative when the more extreme tail is to the left of the mean.

Example 10.6

Estimate the mean, variance, standard deviation, and skew of 18-year precipitation data on a small basin that is given in Table 10.2.

Solution:

Values of $(x - \bar{x})$, $(x - \bar{x})^2$, $(x - \bar{x})^3$ are estimated for precipitation data in each year; the summation of the annual data are given in the last row. The mean, variance, standard deviation, and skew are estimated as follows:

$$\bar{x} = \frac{1}{n}\sum x_i = \frac{1}{18}(68.12) = 3.78 \text{ cm.}$$

The variance is computed using Equation 10.21.

$S^2 = \frac{1}{18-1}(73.639) = 4.322\,\text{cm}^2$, which gives a standard deviation of 2.081 cm. The skew is estimated using Equation 10.25 and the summation from Table 10.2, with $f(x_i)$ set equal to $1/n$:

$$g = \frac{1}{n}\sum (x - x_i)^3 = \frac{1}{18}(215.28) = 11.96\,\text{cm}^3.$$

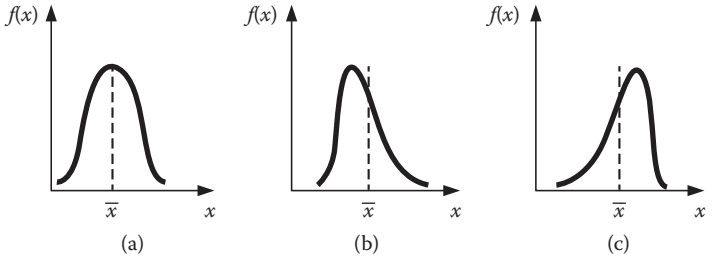

FIGURE 10.2 Comparison of the skew of distributions: (a) $g = 0$; (b) $g > 0$; (c) $g < 0$.

TABLE 10.2
Computations of Moments of June Precipitation

Year	Precipitation x (cm)	$(x - \bar{x})$	$(x - \bar{x})^2$	$(x - \bar{x})^3$
1954	4.27	0.486	0.236	0.1145
1955	2.92	–0.864	0.747	–0.6460
1956	2.00	–1.784	3.184	–5.6821
1957	3.34	–0.444	0.198	–0.0878
1958	2.32	–1.464	2.145	–3.1406
1959	2.89	–0.894	0.800	–0.7156
1960	2.79	–0.994	0.989	–0.9834
1961	5.52	1.736	3.012	5.2278
1962	4.09	0.306	0.093	0.0285
1963	9.86	6.076	36.912	224.2632
1964	3.90	0.116	0.013	0.0015
1965	6.85	3.066	9.398	28.8090
1966	2.33	–1.454	2.115	–3.0767
1967	4.16	0.376	0.141	0.0530
1968	2.10	–1.684	2.837	–4.7794
1969	0.85	–2.934	8.611	–25.2684
1970	5.00	1.216	1.478	1.7961
1971	2.93	–0.854	0.730	–0.6238
Sum	68.12	0.008	73.639	215.2898

The kurtosis expresses the peakedness of a distribution. It is obtained from the fourth central moment:

$$m_4 = \frac{1}{n}\sum_{i=1}^{N}(x_i - \mu)^4 \tag{10.26}$$

$$g_2 = \frac{m_4}{m_2^2} - 3 = \frac{m_4}{(S^2)^2} - 3. \tag{10.27}$$

Its significance relates mainly to the normal distribution, for which $g_2 = 0$. Distributions that are more peaked than normal have $g_2 > 0$; flatter ones have $g_2 < 0$.

10.3 COMMON PROBABILISTIC MODELS

Many discrete and continuous PDFs are used in hydrology, but this subsection focuses on only a few of the most common. For discrete analysis, there may be interest in both of the CDFs, but for continuous analysis, the value of the PDF itself is rarely of interest. Rather, only the CDF for the continuous random variable need be evaluated. These distributions will be seen as the various distributions are presented.

10.3.1 The Binomial Distribution

It is common to examine a sequence of independent events for which the outcome of each can be either a success or a failure; for example, either the T-year flood occurs or it does not. The number of possible ways of choosing x events out of n possible events is given by the binomial coefficient:

$$\binom{n}{x} = \frac{n!}{x!(n-x)!}, \tag{10.28}$$

where n is trials and x is occurrence. Thus, the desired probability is the product of the probability of any one sequence, and the number of ways in which such a sequence can accrue is as follows:

$$P(x) = \binom{n}{x} P^x (1-P)^{n-x}. \tag{10.29}$$

The CDF is defined as follows:

$$F(x) = \sum_{i=0}^{x} \binom{n}{i} p^i (1-p)^{n-i}. \tag{10.30}$$

10.3.2 Normal Distribution

The normal distribution is a well-known probability distribution. Two parameters are involved in a normal distribution: the mean and the variance. A normal random variable having a mean μ and variance σ^2 is herein denoted as $X \cong N(\mu, \sigma^2)$ with a PDF given as follows:

$$f(x) = \frac{1}{\sqrt{2\pi}} \exp\left[-\frac{1}{2}\left(\frac{x-\mu}{\sigma} \right)^2 \right]. \tag{10.31}$$

A normal distribution is bell-shaped and symmetric with respect to $x = \mu$. Therefore, the skew coefficient for a normal random variable is zero. A random variable Y that is a linear function of a normal random variable X is also normal. That is, if $X \cong N(\mu, \sigma^2)$ and $Y = aX + b$, then $Y \cong N(a\mu + b, a^2\sigma^2)$. An extension of this is that the sum of normal random variables (independent or dependent) is also a normal random variable.

Probability computations for normal random variables are made by first transforming to the standardized variant as follows:

$$Z = (X - \mu)/\sigma. \tag{10.32}$$

in which Z has a zero mean and unit variance. Since Z is a linear function of the random variable X, Z is also normally distributed. For cumulative probability of Normal distribution use Tables 10.A1(a) and (b) in the Appendix. The PDF of Z, ϕ, called the standard normal distribution, can be expressed as follows:

$$\phi(z) = \frac{1}{\sqrt{2\pi}} \exp\left(-\frac{z^2}{2} \right) \quad \text{for } -\infty < z < \infty. \tag{10.33}$$

Computations of probability for $X \approx N(\mu, \sigma^2)$ can be performed as follows:

$$p(X \le x) = p\left[\frac{X-\mu}{\sigma} \le \frac{x-\mu}{\sigma} \right] = p(Z \le z). \tag{10.34}$$

10.3.3 Lognormal Distribution

The lognormal distribution is a commonly used continuous distribution in hydrologic event analysis when random variables cannot be negative. The PDF of the lognormal random variable is as follows:

$$f(X) = \frac{1}{x\sigma\sqrt{2\pi}} \exp\left(-\frac{1}{2}\left(\frac{(\ln - \mu)^2}{2\sigma^2} \right) \right) \quad \text{for } x > 0. \tag{10.35}$$

It can be derived from the normal PDF. Statistical properties of a lognormal random variable of the original scale can be computed from those of the log-transformed variable. To compute the statistical moments of X from those of ln X, the following equations are used:

$$E(x) = e^{\left(\mu + \frac{\sigma^2}{2}\right)} \tag{10.36}$$

$$\text{Var}(x) = (e^{\sigma^2} - 1)e^{2\mu + \sigma^2}. \tag{10.37}$$

Example 10.7

The mean and standard deviation of flood data in a region are 14,776 and 5243 (m^3/s), respectively. With the following assumptions, calculate the 10- and 100-year flood discharge for this region.

a. If the data follow a normal distribution
b. If the data follow a lognormal distribution

Solution:

a. The frequency for a probability of 0.1 and 0.01 is 1.282 and 2.326. Hence,

$$Q_{10} = \bar{Q} + zS = 14{,}776 + 1.282 \times 5242 = 21{,}500$$

$$Q_{100} = \bar{Q} + zS = 14{,}776 + 2.326 \times 5242 = 27{,}000.$$

b. Taking a logarithm from the numbers in normal distribution:

$$\overline{\log Q} = 4.170$$

$$S_{\log Q} = 0.1511$$

$$\log Q_{10} = \overline{\log Q} + zS_{\log Q} = 4.419 + 1.282 \times 0.1511 = 4.363$$

$$Q_{10} = 10^{4.363} = 23{,}067.47$$

$$\log Q_{100} = \log \bar{Q} + zS_{\log Q} = 4.419 + 2.326 \times 0.1511 = 4.5005$$

$$Q_{100} = 10^{4.5005} = 31{,}700.$$

10.3.4 The Exponential Distribution

Consider a process of random arrivals such that the arrivals (events) are independent, the process is stationary, and it is not possible to have more than one arrival at an instant in time. If the random variable t represents the inter-arrival time (the time between events), it is found to be exponentially distributed with PDF

$$f(t) = \lambda e^{-\lambda t},\ t \geq 0 \tag{10.38}$$

The mean of the distribution is

$$E(t) = \frac{1}{\lambda}, \tag{10.39}$$

and the variance is

$$\mathrm{Var}(t) = \frac{1}{\lambda^2} \tag{10.40}$$

The CDF is evaluated as follows:

$$F(t) = \int_0^t \lambda e^{-\lambda t} = 1 - e^{-\lambda t} \tag{10.41}$$

10.3.5 The Gamma (Pearson Type 3) Distribution

This distribution receives extensive use in hydrology simply because of its shape and its well-known mathematical properties. The frequency factor K is a function of the skewness and return period (or CDF) and values are given in Table 10.A2 of the Appendix. Thus, to evaluate the T-year flood, the moments of the data are computed and

$$Q_T = \bar{Q} + K(C_s, T)S_Q \tag{10.42}$$

The two-parameter gamma distribution corresponds to setting the left boundary to zero.

Example 10.8

What is the magnitude of the 100-year flood for a river ($\bar{Q} = 4144$ cm, S_Q = 6089 cm) using the gamma-3 and gamma-2 distribution?

Solution:

For gamma-3, C_s = 1.981. Linear interpolation in the Appendix gives K = 2.884. Thus,

$$Q_{100} = 4144 + 3.595 \times 3311 = 16{,}050 \text{ cm}.$$

For gamma-2, g or $C_s = 2CV = 1.277$. Linear interpolation in the Appendix gives K = 3.197. Thus,

$$Q_{100} = 4144 + 3.197 \times 3311 = 14{,}730 \text{ cm}.$$

10.3.6 The Log Pearson Type 3 Distribution

The three-parameter gamma distribution is applied to the logs of the random variables and in hydrology because it has been recommended for application to flood flow. The shape of the LP3 is quite flexible due to its three parameters.

Its use is entirely analogous to the lognormal discussed earlier; however, the moments of the transformed and untransformed variables will not be related here. Instead, the data are transformed by taking logarithms, and the gamma-3 distribution is applied exactly as in the preceding section.

10.4 RETURN PERIOD OR RECURRENCE INTERVAL

Return period is defined as the average number of trials required to the first occurrence of an event $X \geq X_0$ or an event that is greater than or equal to a particular critical event or design event X_0 (Bras 1990). The foregoing definition assumes that an event $X \geq X_0$ occurred in the past, a finite time τ has elapsed since then, and the interest is in the residual or remaining waiting time N for the next occurrence of $X \geq X_0$ (see Figure 10.3). For example, such a critical event, X_0, may be flood (flood of a given return period T or T-year flood) or drought (a drought of a given return period). Definition of variables involved in estimation of return period and risk of failure is shown in Figure 10.3. In this figure, Y_t is a hydrological process, Y_0 is a threshold value, e is an event representing a continuous sequence in which $Y_t < Y_0$. Thus, the events e_1, e_2, …,e_n occur at t_1, t_2,…,t_n, respectively. In addition, the events e can be described by a certain characteristic of interest X and the resulting sequence X_1,

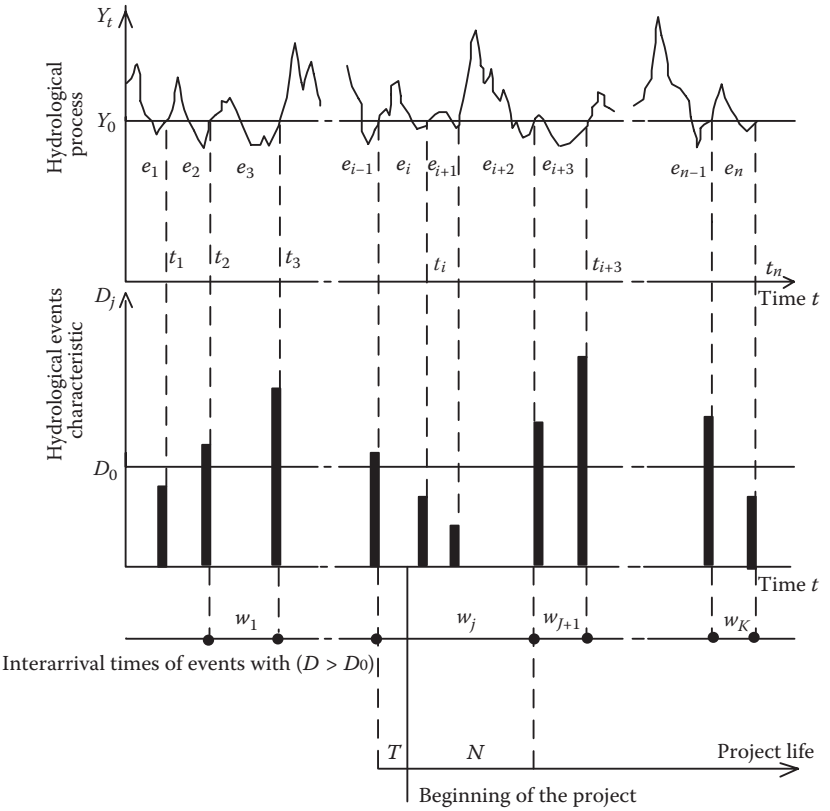

FIGURE 10.3 Definition of variables involved in estimation of return period and risk of failure.

$X_2, \ldots, X_n$ occurring at times $t_1, t_2, \ldots, t_n$ is shown in Figure 10.3. Furthermore, the sequence $X_1, X_2, \ldots, X_n$ may be censored using a critical value X_0. Figure 10.3 shows an example related to droughts, where the duration of a drought is considered to be the property of interest, and critical drought duration on censoring level X_0 is used to distinguish the common droughts from the critical drought. In the case of annual floods, the events $e_1, e_2, \ldots$ are simply the sequence $Y_1, Y_2, \ldots$ and $X_0 = Y_0$ is the design flood.

The return period is defined as follows:

$$T = \frac{1}{P}, \tag{10.43}$$

where T is return period and P is probability of event. An annual maximum event has a return period (or recurrence interval) of T years if its magnitude is equaled or exceeded once, on the average, every T years. The reciprocal of T is the exceedance probability of the event, that is, the probability that the event is equaled or exceeded in any one year. Thus, the 50-year flood has a probability of 0.02, or 2%, of being equaled or exceeded in any single year. The concept of a return period implies independent events and is usually found by analyzing the series of maximum annual data. The largest event in one year is assumed to be independent of the largest event in any other year, but it is also possible to apply such an analysis to the n largest independent events from an n-year period, regardless of the year in which they occur. In this case, if the second largest event in one year was greater than the largest event in another year, it could be included in the frequency analysis. This section of n largest (independent) values is called the series of annual exceedance, as opposed to an annual maximum series. Series of annual exceedances and annual maximum are used in hydrology, with little difference at high return periods. There are likely to be more problems of ensuring independence when using annual exceedances, but for low return periods, annual exceedances give a more realistic lower return period for the same magnitude than do annual maxima. The relationship between return period based on annual exceedances T_e and annual maxima T_m is (Chaw et al. 1988)

$$T_e = \frac{1}{\ln T_m - \ln(T_{m-1})}. \tag{10.44}$$

Finally, return periods need to be independent, and are not limited to units of years. As long as the events are independent, months or even weeks can be used. The 6-month rainfall thus has a probability of 1/6 of being equaled or exceeded in any one month.

10.5 RELIABILITY

The system output, X_t, as a random variable, is classified into two groups of failure and success outputs. The system reliability is the probability that X_t belongs to the success outputs group (Hashimoto et al. 1982), which can be formulated as follows:

$$\alpha = \text{Prob}[X_t \in S] \; \forall t, \tag{10.45}$$

where S is the set of all satisfactory outputs.

All systems, whether natural or man-made, may fail for a variety of reasons, including structural inadequacies, natural causes exceeding the design parameters of the system (e.g., droughts and floods), and human causes such as population growth that raises the system's demands above the supply capacity. Thus, reliability is conceptually related to the probability of system failure and to the rate and consequences of failure. It can be measured in several different but related ways, depending on the needs and relevance of a particular situation. For example, it may be useful to express and characterize the expected length of time between successive failures (i.e., time to

failure), similar to the notion of a 100-year flood event, an event that is expected to occur on average once in 100 years.

While reliability term is frequently used in water resources planning and management, but there some difficulties in its using in practical cases. The main difficulties are as follows:

- Reliability is not formally defined by agencies or institutions and there is no existing and widely accepted framework of reliability measurement that is applicable in all aspects of influence and pplications.
- Reliability is considered with different water management entities' operating and planning processes with substantial variation
- Reliability is often considered in qualitative rather than quantitative terms

Reliability at key points within the sphere of influence ultimately depends on the complexity of interactions of a web of rights, regulations, laws, and rules that affect all institutions that manage water in a municipality. It will be necessary to understand these interactions in order to develop meaningful definitions of reliability, and based on these definitions, related indicators could be defined. These interactions play out across numerous dimensions that, primarily, include:

- System scale and complexity
- The specific management function (i.e., operations, planning)
- The purpose of the service, i.e., the intended use of water

In reliability theory, the Weibull distribution is assumed to model lifetime (the time between two consecutive system failures) most appropriately. The cumulative probability function of the system failures could be formulated as follows:

$$F(t) = 1 - e^{-\alpha t^{\beta}} \quad (t > 0). \tag{10.46}$$

where $\alpha,\beta > 0$ are parameters to be estimated. A definition of reliability is the probability that no failure will occur within the planning horizon (Karamouz et al. 2003). Therefore, using Equation 10.46, reliability could be formulated as follows:

$$R(t) = 1 - F(t) = e^{-\alpha t^{\beta}}. \tag{10.47}$$

The density function of the time of failure occurrences is obtained by simple differentiation of Equation 10.46 as follows:

$$f(t) = \alpha\beta t^{\beta-1} e^{-\alpha t^{\beta}} \quad (t > 0). \tag{10.48}$$

In the special case of $\beta = 1$, $f(t) = \alpha e^{-\alpha t}$, which is the density function of the exponential distribution. The exponential distribution is only seldom used in reliability studies, since it has the so-called forgetfulness property. If X is an exponential variable indicating the time when the system fails, then for all t and $\tau > 0$:

$$P(X > t + \tau | X > \tau) = P(X > t). \tag{10.49}$$

This relation shows that the probability of the working condition in any time length t is independent of how long the system was working before. Equation 10.49 can be shown as

$$P\left(X > t+\tau \,\middle|\, X > \tau\right) = \frac{P\left(X > t+\tau\right)}{P\left(X > \tau\right)} = \frac{R\left(t+\tau\right)}{R\left(\tau\right)} = \frac{e^{-\alpha\left(t+\tau\right)}}{e^{-\alpha\tau}} = e^{-\alpha t} = R\left(t\right) = P\left(X > t\right). \quad (10.50)$$

In most practical cases, the breakdown probabilities are increasing in time as the system becomes older; thus, the exponential variable is inappropriate in such cases.

The hazard rate is given as follows:

$$\rho(t) = \lim_{\Delta t \to 0} \frac{P\left(t \le X \le t+\Delta t \,\middle|\, t \le X\right)}{\Delta t}. \quad (10.51)$$

It shows how often failures will occur after time period t as follows:

$$\rho(t) = \lim_{\Delta t \to 0} \frac{P(t \le X \le t+\Delta t)}{P(t \le X)\Delta t} = \lim_{\Delta t \to 0} \frac{F(t+\Delta t) - F(t)}{\Delta t} \cdot \frac{1}{R(t)} = \frac{f(t)}{R(t)}. \quad (10.52)$$

Therefore, the hazard rate can be computed as the ratio of the density function of time between failure occurrences and the reliability function (Karamouz et al. 2003).

Example 10.9

Assume the time between drought occurrences in a watershed follows the Weibull distribution. Formulate the reliability and hazard rate of this watershed in dealing with droughts.

Solution:

The watershed reliability is calculated as follows:

$$R(t) = 1 - F(t) = e^{-\alpha t^{\beta}},$$

and therefore, from Equation 10.52, the hazard rate is calculated as follows:

$$\rho(t) = \frac{\alpha\beta t^{\beta-1} e^{-\alpha t^{\beta}}}{e^{-\alpha t^{\beta}}} = \alpha\beta t^{\beta-1},$$

which is an increasing polynomial of t showing that failure will occur more frequently for larger values of t. In the special case of an exponential distribution, $\beta = 1$, so $\rho(t) = \alpha$ being a constant.

It is an important problem in reliability engineering to reconstruct $F(t)$ or the reliability function if the hazard rate is given (Karamouz et al. 2003). Notice first that

$$\rho(t) = \frac{f(t)}{1-F(t)} = \frac{(F(t))'}{1-F(t)} = -\frac{(1-F(t))'}{1-F(t)}.$$

By integration of both sides in the interval $[0,t]$ it will achieve

$$\int_0^t \rho(\tau)\, d\tau = [-\ln(1-F(\tau))]_{\tau=0}^{t} = -\ln(1-F(t)) + \ln(1-F(0)).$$

Since $F(0) = 0$, the second term equals zero; hence,

$$\ln(1 - F(t)) = -\int_0^t \rho(\tau)\, d\tau,$$

implying that

$$1 - F(t) = \exp\left(-\int_0^t \rho(\tau)\, d\tau \right)$$

and, finally,

$$F(t) = 1 - \exp\left(-\int_0^t \rho(\tau)\, d\tau \right). \tag{10.53}$$

Example 10.10

Construct the CDF of failure occurrences in two given situations: (1) The hazard rate is constant, $\rho(t) = \alpha$; and (2) $\rho(t) = \alpha\beta t^{\beta-1}$.

Solution:

Using Equation 10.53 for $\rho(t) = \alpha$, it is obtained that

$$F(t) = 1 - \exp\left(-\int_0^t \rho(\tau)\, d\tau \right) = 1 - \exp\left(-\int_0^t \alpha\, d\tau \right) = 1 - e^{-\alpha t}.$$

Similarly, when $\rho(t) = \alpha\beta t^{\beta-1}$, and then showing that the distribution is Weibull,

$$F(t) = 1 - \exp\left(-\int_0^t \alpha\beta\tau^{\beta-1}\, d\tau \right) = 1 - \exp\left(-[\alpha\tau^{\beta}]_0^t \right) = 1 - e^{-\alpha t^{\beta}}.$$

In contrast with $F(t)$, which is increasing, $F(0) = 0$ and $\lim_{t\to\infty} F(t) = 1$, $R(t)$ is decreasing, $R(0) = 1$, and $\lim_{t\to\infty} R(t) = 0$. In the case of $\beta > 2$ and Weibull distribution, $\rho(0) = 0$, $\lim_{t\to\infty} \rho(t) = \infty$, and $\rho(t)$ is a strictly increasing and strictly convex function. If $\beta = 2$, then $\rho(t)$ is linear, and if $1 < \beta < 2$, then $\rho(t)$ is strictly increasing and strictly concave. If $\beta = 1$, then $\rho(t)$ is a constant. In the case of $\beta < 1$, the hazard rate is decreasing in t, in which case defective systems tend to fail early. Thus, hazard rate decreases for a well-made system. Notice that

$$\rho'(t) = \frac{f'(t)(1 - F(t)) + f(t)^2}{(1 - F(t))^2},$$

which is positive if and only if the numerator is positive:

$$f'(t) > -\frac{f(t)^2}{1 - F(t)} = -f(t)\, \rho(t). \tag{10.54}$$

If inequity of Equation 10.54 is satisfied, $\rho(t)$ is locally increasing; otherwise, $\rho(t)$ decreases.

The above discussions about reliability are applicable to a component of a system. The reliability of a system with several components depends on what kind of configuration of the components is

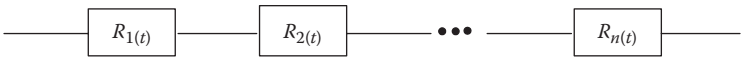

FIGURE 10.4 Series combination of components.

the entire system. Systems could be arranged in "series," "parallel," or in combinations. The failure of any component in a series system results in system failure, but in a parallel system, only when all components fail simultaneously does failure occur.

A typical series combination is shown in Figure 10.4. If $R_i(t)$ denotes the reliability function of component i ($i = 1, 2, \ldots, n$), then the reliability function of the system could be estimated as follows:

$$R(t) = P(X > t) = P((X_1 > t) \cap (X_2 > t) \cap \cdots \cap (X_n > t)), \tag{10.55}$$

where X is the time when the system fails, and $X_1, \cdots, X_n$ are the same for the components. It can be assumed that the failures of the different system components occur independently of each other, then

$$R(t) = P(X_1 > t)\, P(X_2 > t) \cdots P(X_n > t) = \prod_{i=1}^{n} R_i(t). \tag{10.56}$$

Note that the inclusion of a new component into the system results in a smaller reliability function, since it is multiplied by the new factor $R_{n+1}(t)$, which is below 1.

In a parallel system as shown in Figure 10.5, the system fails, if all components fail; hence, the system failure probability is calculated as follows:

$$P(X \le t) = P((X_1 \le t) \cap (X_2 \le t) \cap \cdots \cap (X_n \le t)) \tag{10.57}$$

If the components fail independently of each other, then

$$R(t) = 1 - F(t) = 1 - P(X \le t) = 1 - \prod_{i=1}^{n} P(X_i \le t) = 1 - \prod_{i=1}^{n} F_i(t) = 1 - \prod_{i=1}^{n} (1 - R_i(t)), \tag{10.58}$$

where F and F_i are the cumulative distribution until the first failure of the system and component i, respectively. In this case, including a new component in the system will increase the system reliability, since the second term is multiplied by $1 - R_{n+1}(t)$, which is less than 1. In practical cases, commonly a mixture of series and parallel connections between systems components is used. In these cases, Equations 10.57 and 10.58 should be combined appropriately as shown in the following example.

Example 10.11

The system illustrated in Figure 10.6 includes five components, where components 2, 3, and 5 are parallel. Calculate system reliability at $t = 0.1$ assuming that $R_1(t) = R_4(t) = e^{-2t}$ and $R_2^i(t) = R_3^j(t) = R_5^i(t) = e^{-t} \quad (1 \le i \le 2, 1 \le j \le 3)$.

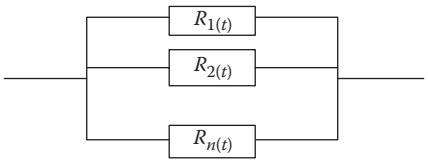

FIGURE 10.5 Parallel combination of system components.

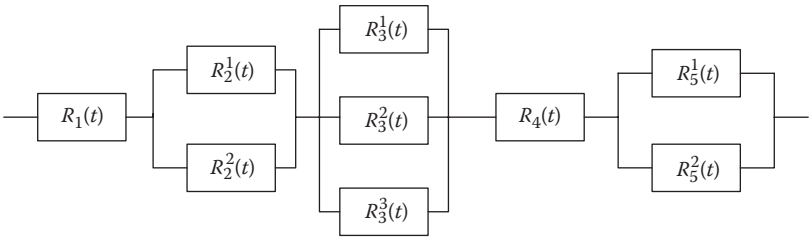

FIGURE 10.6 Combined connections in a system.

Solution:

At first, the reliability of parallel components is calculated using Equation 10.58.

$$R_2(t) = 1 - \left(1 - R_2^1(t)\right)\left(1 - R_2^2(t)\right)$$

$$R_3(t) = 1 - \prod_{i=1}^{3}\left(1 - R_3^i(t)\right)$$

$$R_5(t) = 1 - \left(1 - R_5^1(t)\right)\left(1 - R_5^2(t)\right).$$

The reliability function of the system using Equation 10.58 is estimated as follows:

$$R(t) = R_1(t)\left[1 - \prod_{i=1}^{2}\left(1 - R_2^i(t)\right)\right]\cdot\left[1 - \prod_{i=1}^{3}\left(1 - R_3^i(t)\right)\right]\cdot R_4(t)\cdot\left[1 - \prod_{i=1}^{2}\left(1 - R_5^i(t)\right)\right].$$

At $t = 0.1$,

$$R_1(0.1) = R_4(0.1) = e^{-0.2} = 0.8187$$

$$R_2^i(0.1) = R_3^j(0.1) = R_5^i(0.1) = e^{-0.1} = 0.9048.$$

Then,

$$R_2(0.1) = R_5(0.1) = 1 - (1 - 0.0952)^2 = 0.9909$$

$$R_3(0.1) = 1 - 0.0952^3 = 0.9991.$$

Hence,

$$R(0.1) = 0.8187^2(0.9909)^2(0.9991) = 06575 = 65.75\%.$$

10.5.1 Reliability Analysis Load-Resistance Concept

External loads in combination with uncertainties in analysis, design, build, and operation with lead to system failure. A system fails when the external loads, L (e.g., generated runoff over the

watershed), exceed the system resistance, R_e (e.g., carrying capacity of river). Reliability (R) of any component or the entire system is equal to its safety probability:

$$R = p[L \le R_e]. \tag{10.59}$$

In hydrology and hydraulics, load and resistance are functions of some random variables:

$$R_e = h\left(X_{R_e}\right) \tag{10.60}$$

$$L = g(X_L). \tag{10.61}$$

Thus, reliability is a function of random variables:

$$R = p\left[g(X_L) \le h(X_{R_e})\right]. \tag{10.62}$$

Reliability variations with time are not considered in the above equation. X_{R_e} and X_L are stationary random variables and the resulting model is called the static reliability model. The word "static," from the reliability computation point of view, represents the worst single stress, or load, applied. Actually, the loading applied to many hydrologic systems is a random variable. Also, the number of times a loading is imposed is random. The static reliability model is used for the evaluation of system performance in a special situation (the most critical loading).

For reliability analysis, a performance function is proposed by Mays (2001) as follows:

$$W(X) = W(X_L, X_{R_e}). \tag{10.63}$$

The system reliability is defined based on this function as follows:

$$R = p[W(X_L X_{R_e}) \ge 0] = p[W(X) \ge 0]. \tag{10.64}$$

$W(X) = 0$ is called the failure surface or limit. $W(X) \ge 0$ is the safety region and $W(X) < 0$ is the failure region. The performance function $W(X)$ can be defined in the following forms:

$$W_1(X) = R_e - L = h(X_{R_e}) - g(X_L) \tag{10.65}$$

$$W_2(X) = \left(\frac{R_e}{L}\right) - 1 = [h(X_{R_e})/g(X_L)] - 1 \tag{10.66}$$

$$W_3(X) = \ln\left(\frac{R_e}{L}\right) = \ln[h(X_{R_e})] - \ln[g(X_L)]. \tag{10.67}$$

Another reliability index is the β reliability index, which is equal to the inverse of the coefficient of variation of the performance function, $W(X)$, and is calculated as follows:

$$\beta = \frac{\mu_w}{\sigma_w}. \tag{10.68}$$

σ_w and μ_w are mean and standard deviations of the performance function, respectively. By assuming an appropriate PDF for random performance functions, $W(X)$, using Equation 10.58, the reliability is estimated as

$$R = 1 - F_W(0) = 1 - F_{W'}(-\beta), \tag{10.69}$$

where F_W is the CDF of variable W and W' is the standardized variable as follows:

$$W' = \frac{W - \mu_W}{\sigma_W}. \tag{10.70}$$

10.5.2 Direct Integration Method

Following the reliability definition, the reliability is expressed by Mays (2001) as follows:

$$R = \int_0^\infty f_{R_e}(r)\left[\int_0^r f_L(l)\,\mathrm{d}l\right]\mathrm{d}r = \int_0^\infty f_{R_e}(r)\,F_L(l)\mathrm{d}r, \tag{10.71}$$

where $f_{R_e}(\,)$ and $f_L(\,)$ are the PDFs of resistance and load functions, respectively. If load and resistance are independent, then reliability is formulated as

$$R = E_{R_e}[F_L(r)] = 1 - E_L[F_{R_e}(l)], \tag{10.72}$$

where $E_{R_e}[F_L(r)]$ is the expected value of CDF of load in the probable resistance limitation. The reliability computations require the knowledge of the probability distributions of loading and resistance. A schematic diagram of the reliability analysis by Equation 10.72 is shown in Figure 10.7.

To illustrate the computation procedure involved, the exponential distribution has been considered for loading L and the resistance R_e:

$$f_L(l) = \lambda_L e^{-\lambda_L l}, \quad l \geq 0 \tag{10.73}$$

$$f_{R_e}(r) = \lambda_{R_e} e^{-\lambda_{R_e} r}, \quad r \geq 0. \tag{10.74}$$

The static reliability can then be derived as

$$R = \int_0^\infty \lambda_{R_e} e^{-\lambda_{R_e} r}\left[\int_0^r \lambda_L e^{-\lambda_L l}\,\mathrm{d}l\right]\mathrm{d}r = \int_0^\infty \lambda_{R_e} e^{-\lambda_{R_e} r}[1 - e^{-\lambda_L r}]\,\mathrm{d}r = \frac{\lambda_L}{\lambda_{R_e} + \lambda_L}. \tag{10.75}$$

For some special combinations of load and resistance distributions, the static reliability can be derived analytically in the closed form. Kapur and Lamberson (1977) considered the loading L and resistance R_e lognormally distributed and computed reliability as

$$R = \int^\infty \phi(z)\,\mathrm{d}z = \Phi(z), \tag{10.76}$$

where $\phi(z)$ and $\Phi(z)$ are the PDF and the CDF, respectively, for the standard normal variant z:

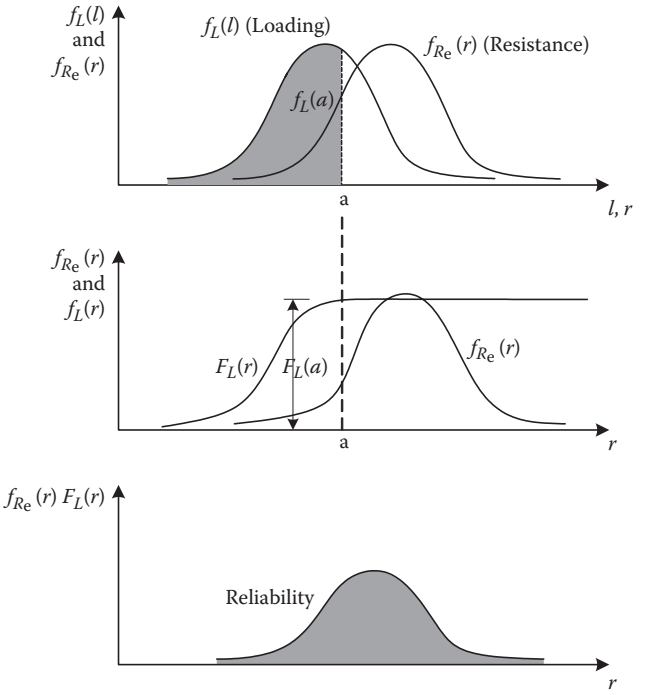

FIGURE 10.7 Graphical illustration of the steps involved in reliability computation (Mays 2001).

$$z = \frac{\mu_{\ln R_e} - \mu_{\ln L}}{\sqrt{\sigma^2_{\ln R_e} - \sigma^2_{\ln L}}}. \tag{10.77}$$

The values of the CDF $\Phi(z)$ for the standard normal variant are given in normal distribution tables.

By considering exponential distribution for the load and the normal distribution for the resistance, the reliability was expressed by Kapur and Lamberson (1977) as

$$R = 1 - \Phi\left(\frac{\mu_{R_e}}{\sigma_{R_e}}\right) - \exp\left[-\frac{1}{2}\left(2\mu_{R_e}\lambda_L - \lambda_L^2\sigma^2_{R_e}\right)\right] \times \left[1 - \Phi\left(-\frac{\mu_{R_e} - \lambda_L\sigma^2_{R_e}}{\sigma_{R_e}}\right)\right]. \tag{10.78}$$

10.5.3 Margin of Safety

The margin of safety (*MS*) is defined as the difference between the project capacity (resistance) and the value calculated for the design loading, $MS = R_e - L$. The reliability is equal to the probability that $R_e > L$, or equivalently,

$$R = p(R_e - L > 0) = p(MS > 0). \tag{10.79}$$

If R_e and L are independent random variables, then the mean value of *MS* is given by

$$\mu_{MS} = \mu_{R_e} - \mu_L \tag{10.80}$$

and its variance is given by

$$\sigma_{MS}^2 = \sigma_{R_e}^2 + \sigma_L^2. \tag{10.81}$$

If the margin of safety is normally distributed, then

$$z = \frac{MS - \mu_{MS}}{\sigma_{MS}}, \tag{10.82}$$

where z is a standard normal variant. By subtracting μ_{MS} from both sides of the inequality in Equation 10.78 and dividing both sides by σ_{MS}, it can be seen that

$$R = p\left(z \le \frac{\mu_{MS}}{\sigma_{MS}}\right) = \Phi\left(\frac{\mu_{MS}}{\sigma_{MS}}\right). \tag{10.83}$$

The key assumption of this analysis is that it considers that the margin of safety is normally distributed but does not specify the distributions of loading and capacity. Ang (1973) indicated that, provided $R > 0.001$, R is not greatly influenced by the choice of distribution for R_e and L and the assumption of a normal distribution for MS is satisfactory. For lower risk than this (e.g., $R = 0.00001$), the shape of the tails of the distributions for R_e and L becomes critical, in which case accurate assessment of the distribution of MS of direct integration procedure should be used to evaluate the risk or probability of failure.

10.5.4 Factor of Safety

The factor of safety (FS) is given by the ratio R_e/L and the reliability can be specified by $P(FS > 1)$. Several factors of safety measures and their usefulness in hydraulic engineering are discussed by Yen (1978) and Mays (2001). By taking the logarithm of both sides of this inequality, it yields to

$$R = p(FS > 1) = p(\ln(FS) > 0) = p\left(\ln\left(\frac{R_e}{L}\right) > 0\right)$$

$$R = p\left(z \le \frac{\mu_{\ln FS}}{\sigma_{\ln FS}}\right) = \Phi\left(\frac{\mu_{\ln FS}}{\sigma_{\ln FS}}\right), \tag{10.84}$$

where $z = \dfrac{\ln(FS) - \mu_{\ln FS}}{\sigma_{\ln FS}}$ and Φ is the standard cumulative normal probability distribution. It is assumed that the factor of safety is normally distributed.

10.5.5 Multivariate Reliability Analysis

In most of the systems, more than one variable affects the system performance and its reliability. Furthermore, there are some interactions between these variables, which may affect the probability of different statuses when variables are analyzed individually. Due to these interactions between systems' characteristics, it would be useful to incorporate the relationships between these variables in reliability analysis. In such cases, multivariate reliability analysis is necessary. In these cases, different variables (here, say, m variables) that affect the system reliability (or its satisfactory output) are determined, and the desired area of system performance is determined in an m-dimensional environment, the boundaries of which are determined based on acceptable values of the considered

variables. This is more common when water quality issues are also incorporated in analysis because as it was mentioned in Chapter 6, the quality of water is affected by its quantity.

For example, in evaluating the reliability of water supply from a river, both the flow rate and contamination load should be considered. Consider the river flow and the amount of pollutant that is drained into the river to be denoted by $Q(t)$ and $E(t)$, respectively, and both of them follow a continuous function. There are some limitations on pollutant load, PL, that is imposed along the river even at a level below a critical level. Often, TDS (Total Dissolved Solid) is used as an example to represent the pollution load.

The local environmental protection agency decides that emission of the pollutant is permissible if the concentration stays below a standard level, PL_{st}, more than 95% of the time during a year, which is formulated as follows:

$$P_F = P\{PL(t) < PL_{st}\} \le P_{st} = 0.05 \text{ per year.} \tag{10.85}$$

The condition of $PL(t) < PL_{st}$ is formulated in terms of the random functions of $E(t)$ and $Q(t)$ as follows:

$$\frac{E(t)}{Q(t)} \le PL_{st}. \tag{10.86}$$

However, the solution of this problem is not easy to obtain, as it involves the division of $E(t)$ by $Q(t)$ at all times. In this case, the P_F can be obtained by multiplying both sides of the inequality by $Q(t)$, and thus,

$$E(t) \le PL_{st} \times Q(t). \tag{10.87}$$

In this way, the condition of $PL(t) < PL_{st}$ can be defined as a curve, with slope PL_{st}, on the joint probability density distribution of both pollutant and river flow, $f(E,Q)$, as is shown in Figure 10.8.

The probability of failure is equal to the area under the joint PDF, which satisfies the criteria of $PL(t) < PL_{st}$, which is obtained as follows:

$$P_F(PL_{st}) = \int \left\{ \int_0^{\hat{Q}} f(Q,E)\,dQ \right\} dE, \tag{10.88}$$

where $\hat{Q}$ is equal to $\dfrac{E}{PL_{st}}$. To determine the above integration result, it is necessary to first develop the $f(Q,E)$ based on the simultaneous measurements of E and Q. If these variables are independent

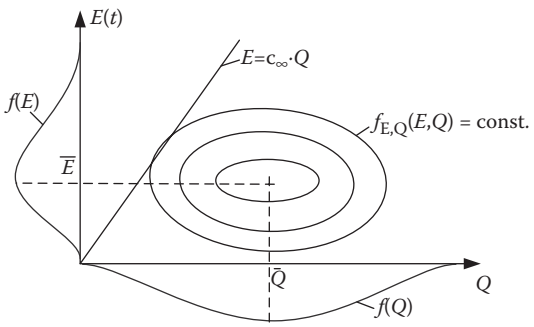

FIGURE 10.8 Failure probability for a pollution-loaded river.

from each other since $f(E,Q) = f_E(E) \times f_Q(Q)$, the task of determining the $f(E,Q)$ can be reduced to finding the marginal probability functions of $f_E(E)$ and $f_Q(Q)$ for the two random variables E and Q. In this case, Equation 10.88 can be rewritten as follows:

$$P_{\mathrm{F}}(PL_{\mathrm{st}}) = \int_0^{\infty} \left\{ \int_0^{\hat{Q}} f_E(E) f_Q(Q)\, \mathrm{d}Q \right\} \mathrm{d}E. \tag{10.89}$$

This can be rewritten as follows:

$$P_{\mathrm{F}}(PL_{\mathrm{st}}) = \int_0^{\infty} f_Q(\hat{Q})\, F_E(E)\, \mathrm{d}E, \tag{10.90}$$

where

$$F_Q(\hat{Q}) = \int_0^{\hat{Q}} f_Q(Q)\, \mathrm{d}Q \tag{10.91}$$

is the probability distribution of Q evaluated at $\hat{Q}$.

In cases where the considered variables for reliability analysis are not independent from each other, it is necessary to develop the joint PDF by analysis of simultaneous measurements of the considered variables. For this purpose, the methods for the development of multivariate probability distributions such as Copula can be successfully used.

10.5.5.1 Copula Theory

In order to provide an introduction to joint probability distribution using Copula theory, a more subject/case-specific example of urban drainage is presented here. In order to provide a more realistic configuration of the urban drainage system performance, simultaneous simulation of rainfall and sediment load during flood is needed. For this purpose, the Copula theory has been used to calculate the joint return period of rainfall and sediment.

Copula is a stochastic and probability-based model that has had rapid growth in recent decades. Sklar (1959) states that the joint distribution function of any randomly distributed pair (x, y) may be written as

$$F(x, y) = C[F_x(x), F_y(y)],\ x, y \in R, \tag{10.92}$$

where $F_x(x)$ and $F_y(y)$ are marginal probability distributions and C: *[0,1] → [0,1], is a "Copula." Therefore, Copula is a distribution function [0,1] to join n-variable functions to a one-variable function in the domain of [0,1]. The Copula equation is as follows:

$$\Phi[F(x, y)] = \Phi[C(F_X(x), F_Y(y))] = \Phi[F_X(x)] + \Phi[F_Y(y)], \tag{10.93}$$

where Φ is a continuous, strictly decreasing function from I [0,1] → [0,∞] and with $\Phi(1) = 0$, which is called a generating function. The joint probability function can then be written as

$$F(x, y) = C[F_X(x), F_Y(y)] = \Phi^{-1}\{\Phi[F_X(x)] + \Phi[F_Y(y)]\}. \tag{10.94}$$

There are different families of Copula functions. The family of Archimedean Copulas has been studied extensively by a number of authors. This family is the most useful model for purposes of moderate dimension because of the simple closed functional forms that arise. Well-known representatives of the Archimedean family are the Gumbel, Frank, and Clayton Copulas. The Clayton Copula is used in this book as an effective Copula in the field of hydrometeorology suggested by Chowdhary et al. (2008). The generating function of the Clayton Copula is as follows:

$$\Phi(t) = \frac{1}{\theta}(t^{-\theta} - 1), \theta \in [-1, \infty), \theta \neq 0. \tag{10.95}$$

The bivariate cumulative probability distribution and density functions in the Clayton Copula are obtained as

$$F(x, y) = \left\{[F_X(x)]^{-\theta} + [F_Y(y)]^{-\theta} - 1\right\}^{-\frac{1}{\theta}} \tag{10.96}$$

$$f(x, y) = (1 + \theta) f_X(x) f_Y(y) \left\{F_X(x) F_Y(y)\right\}^{-\theta-1} \left\{[F_X(x)]^{-\theta} + [F_Y(y)]^{-\theta} - 1\right\}^{-\frac{1}{\theta}-2}, \tag{10.97}$$

where $F_x(x)$ and $F_y(y)$ are the marginal densities and $f(x,y)$ and $F(x,y)$ are the joint bivariate density and probability functions, respectively (Chowdhary et al. 2008). The optimal value of θ is estimated using the maximum likelihood method.

10.6 RISK

An important concept in hydrology analysis is risk. Risk is the probability of an event occurring per year, P, during a specific time period, n. Risk can also be expressed as one minus reliability in probability terms. Also, the risk of failure in extreme events such as failure of flood-related structures (culverts and bridges) is related to the return period T or exceedance probability P of the design flood. The risk of failure is typically defined as the probability of at least one flood that is equal to or greater than the design flood in an n-year period. Thus, assuming that annual floods are independent, it may be shown that the risk of failure is given as follows:

$$R = 1 - (1 - P)^n = 1 - \left(1 - \frac{1}{T}\right)^n. \tag{10.98}$$

This simple equation of risk is valid for independent annual floods.

Example 10.12

Consider the 50-year flood (p = 0.02).

a. What is the probability that at least one 50-year flood will occur during the 30-year lifetime of a flood control project?
b. What is the probability that the 100-year flood will not occur in 10 years? In 100 years?
c. In general, what is the probability of having no floods greater than the T-year flood during a sequence of T_{year}?

Solution:

a. This is just the risk of failure discussed above, and the distribution of the number of failures is $B(30, 0.02)$. Thus, from Equation 10.98,

$$\begin{aligned}\text{Risk} &= 1-(1-0.02)^{30}\\ &= 1-0.98^{30}\\ &= 1-0.545\\ &= 0.455.\end{aligned}$$

b. For $n = 10$, $P(x = 0) = 1 - (1 - p)^{10} = 0.99^{10} = 0.92$.
For $n = 100$, $P(x = 0) = 1 - (1 - p)^{100} = 0.99^{100} = 0.37$.

c. $P(x=0)=1-\left(1-\dfrac{1}{T}\right)^{T}$.

Example 10.13

A cofferdam has been built to protect homes in a floodplain until a major channel project can be completed. The cofferdam was built for a 20-year flood event. The channel project will require 3 years to complete. Hence, the process is $B(3, 0.05)$. What are the probabilities that

a. The cofferdam will not be overtopped during the 3 years (the reliability)?
b. The cofferdam will be overtopped in any one year?
c. The cofferdam will be overtopped exactly once in 3 years?
d. The cofferdam will be overtopped at least once in 3 years (the risk)?
e. The cofferdam will be overtopped only in the third year?

Solution:

a. $\text{Reliability}=\left(1-\dfrac{1}{20}\right)^{3}=0.95^{3}=0.86$.

b. $\text{Prob}=\dfrac{1}{T}=0.05$.

c. $P(x=1)=\binom{3}{1}p^{1}(1-p)^{2}=3\times 0.05\times 0.95^{2}=0.135$.

d. Risk = 1 − Reliability = 0.14.

e. Prob = $(1 - p)(1 - p)p = 0.95^2 \times 0.05 = 0.045$.

Example 10.14

Determine the design return period for the culvert of the previous example, if the acceptable hydrologic risk is 0.15 (or 15%).

Solution:

Equation 10.98 is employed again for determination of the return period of the design rainfall event as follows:

$$0.15 = 1 - \left(1 - \frac{1}{T_r}\right)^{25}.$$

T_r hvas been calculated to be 154 years where, in practice, a return period of 150 years is considered for determination of culvert size.

Risk is defined differently in engineering applications as follows:

a. Risk versus Probability: Some descriptions of risk focus only on the event occurring probability but other explanations include both the probability and the consequences of the event. For example, the probability of a severe earthquake may be very small, but the effects are so disastrous that it would be classified as a high-risk event.
b. Risk versus Threat: In some disciplines, there is a difference between a threat and risk. A threat can be any event with low probability and very large negative consequences. However, a risk is defined to be a higher probability event, where there is enough information to make assessments of consequences.
c. All outcomes versus negative outcomes: Definitions of risk mostly focus on the downside scenarios, while all consequences are considered. Risk is defined as the product of the probability of an event occurring and the corresponding damage it causes.

10.6.1 Risk Components

In order to understand risk, it is important to be familiar with different components that create risk. Risk is the occurrence of an extreme event such as earthquake, flood, drought, hurricane, and storm, as a result of natural forces, with or without human influences. Although hazard events are a major condition, it is only one component in the realization of risk. The next components in risk characterization are that somebody or something has exposure and vulnerability to a hazard. The last component in risk is the system exposure to the hazard or the occurrence of hazard probability of a system. Hence, risk is the probability of a loss that depends on three aspects: hazard, vulnerability, and exposure. Furthermore, risk is defined as follows:

$$\text{risk} = \text{function (hazard, exposure, vulnerability)} \tag{10.99}$$

Figure 10.9 shows the risk as the overlay and intersection of these components. While exposure refers, for example, for floods, only to the question whether assets or people are physically in the floodwaters' path or not, vulnerability is defined as the conditions determined by social, economic, environmental, and physical factors, which increase the susceptibility of a community to the impact of hazards (Glossary of the UN International Strategy for Disaster Reduction 2004). The risk increases or decreases respectively when any of these three elements in risk decreases or increases (Crichton 1999).

By changing the system and its surrounding environmental characteristics, the risk components and risk as a consequence are changed. For example, through application of mitigation practices, system vulnerability and exposure would decrease (as shown by arrows in Figure 10.9), resulting in a decrease in system risk. Beside this, by decreasing the possible hazards, system risk would highly decrease. The hazards can be changed by changing the system's surrounding environment. For example, climate change may increase the flooding hazard in some places or application of best management practices (BMPs) in urban areas could decrease the flood hazard severity as will be discussed in Chapter 13.

Some other factors that could affect system risk are social and climate sensitivity, which should be considered in risk assessment. For example, Figure 10.10 shows how these factors can affect the

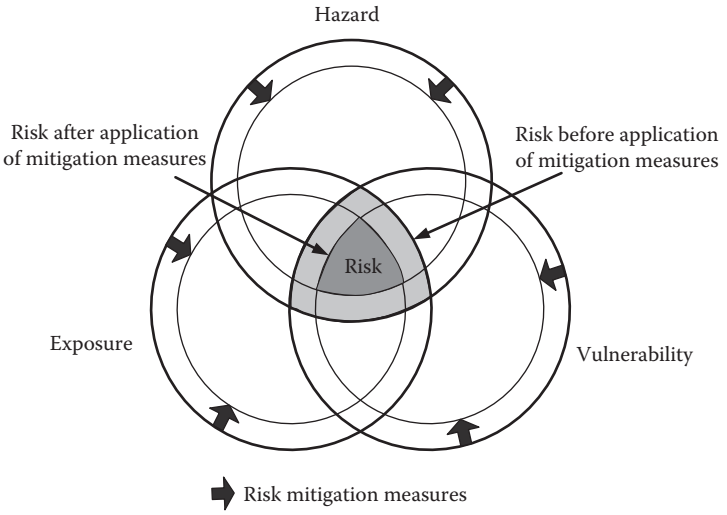

FIGURE 10.9 Risk components and lower risk with mitigation of hazard, exposure, and vulnerability space.

system's adaptive capacity, which is an important issue in assessing the system's vulnerability. The adaptive capacity of a system to face different threats and hazards is directly related to the measures that can be taken to reduce future vulnerabilities (Figure 10.10). Brooks (2003) describes adaptation as adjustments in a system's behavior and characteristics that enhance its ability to cope with external stress.

Climate change can highly affect system exposure to hazards (mostly natural hazards), which should be considered in future assessment of the system's situation. Aside from this, social changes

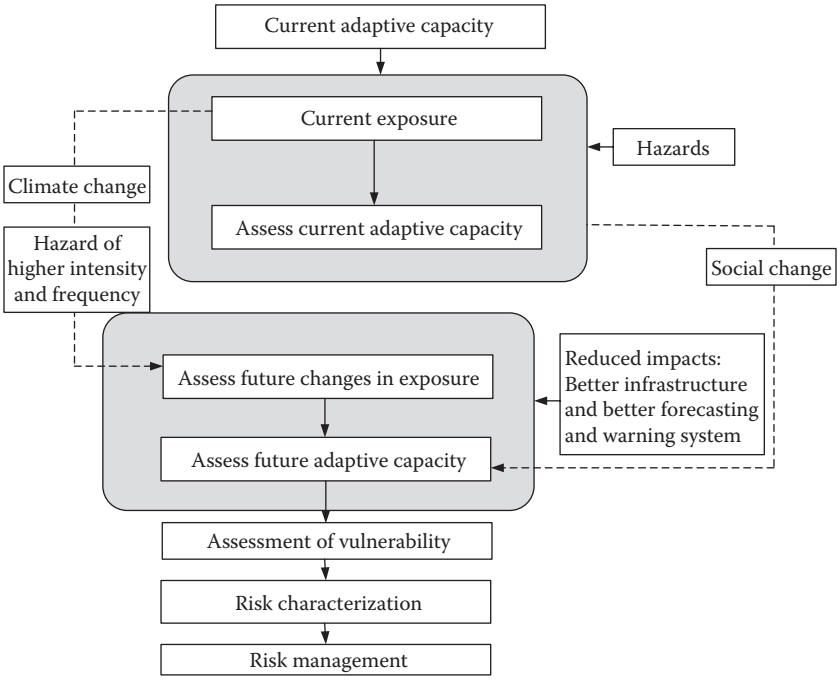

FIGURE 10.10 Main steps in assessment of adaptive capacity and vulnerability of system.

may result in changes in the system's adaptive capacity. These changes may be the result of better infrastructures and warning systems. These changes should be considered in an integrated fashion in risk components' evaluation and management.

10.6.2 Risk Analysis Methods and Tools

Risk is a characteristic of a situation in which a number of outcomes are possible; the particular one that will occur is uncertain and at least one of the possibilities is undesirable. Risk analysis is not only for extreme or low probability events (e.g., floods and hurricanes) but also for any situation in which there is a range of possibilities, such as natural events that have profound economic, environmental, and safety implications. Statistical measures can provide important insight into the variability associated with these processes and their consequences. The incorporation of factors describing uncertainty and variability into the decision-making process comes under the general term of risk analysis. Risk analysis provides an important decision-making tool.

An event tree (decision tree) is a tool that provides a structure for risk quantification. The basic steps in decision tree analysis include the following:

- Specification of the decision context
- Development of a decision model (decision tree) including
  - Management options
  - The consequences of each option
  - Likelihood and desirability of each outcome

The decision tree structure develops sequentially from base to terminal ends based on the components of nodes, branches, and outcomes. There are three types of nodes including decision (choice) nodes, chance (probability) nodes, and terminal nodes. For example, in cases of decision making on flood planning, decision nodes can be the application of a specific flood management practice, chance nodes are the corresponding probability of flooding and not flooding before and after the application of flood management practices. The terminal nodes will indicate corresponding flood damage in different situations.

The branches indicate different choices if they are extended from a decision node with different outcomes. Each of the branches emanating from a chance node has associated probabilities and each of the terminal ends had associated utilities or values. It is important that the branches representing choices are mutually exclusive, meaning that only one branch can be chosen at a time. In the case of chance nodes, the branches have to correspond to mutually exclusive and collectively exhaustive outcomes. This means only one of them can happen and the different branches include all possible outcomes. Chance events placed in front of decision nodes indicate the chance of that decision to happen.

When consequences are assigned to the ultimate nodes of the tree, the tree can be rolled back to determine, using the rules of probability and decision rules at decision nodes, the best choice (i.e., the decision that maximizes or minimizes the desired value) based on the various event probabilities. More sophisticated decision tree software allows for more complex specification of probability distributions and, through the use of Monte Carlo simulation techniques, can display probability distributions for desired decision variables.

Decision trees are the form of graphical display of problem structuring, particularly well suited for limited situations where the possible events can be well defined. Event trees provide a structured approach for risk quantification as shown in Figure 10.11. In this figure, the initiating event can be a natural hazardous event such as drought or flood with the probability of occurrence of θ_0. There are two systems dealing with this hazard. Each of these systems has a specified probability of not failure, which is θ_1 for system 1 and θ_2 for system 2. Therefore, in this example, four different situations with different consequences, shown by X_1 to X_4, can happen. The probability of occurrence

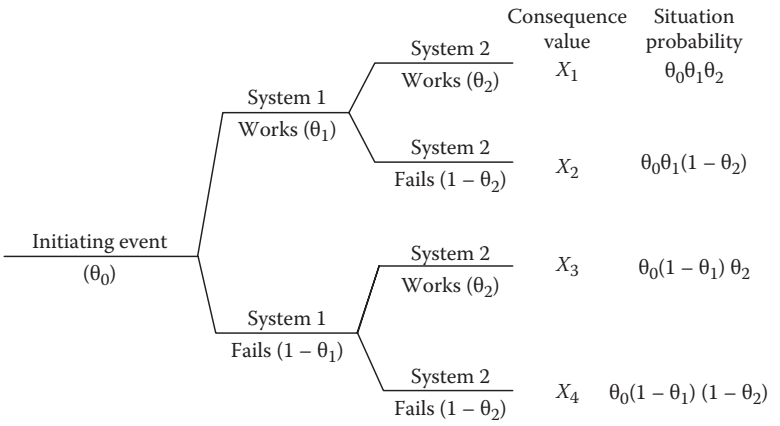

FIGURE 10.11 Risk quantification using an event tree for two subsystems. (From Lee, W.W. and Nair, K., Risk Quantification and Risk Evaluation, Proceedings of the National Conference on Hazardous Material Risk Assessment, Disposal and Management, Information Transfer, Inc., Silver Spring, Maryland, 1979. With permission.)

of each of these situations, considering the independency of the systems performance, is calculated as given in Figure 10.11.

The probability of each situation's occurrence is determined as the product of the probability of different branches from the first node to the terminal node (considering systems and events are independent from each other). Then, the expected consequence in each situation is obtained by multiplying the consequence value by the corresponding probability.

Example 10.15

Develop a decision tree for evaluating the effect of a flood warning system development at a cost of $20,000 on the flooding mitigation. The probability of flooding is 0.1, and the damage associated with flooding in the absence of the warning system is $50,000, but is reduced to $5000 with the flood warning system.

Solution:

The decision tree shown in Figure 10.12 represents a simple analysis of the advisability of installing a flood warning system. The initial decision, at the leftmost node, is whether or not to develop a flood warning system. Subsequent nodes at the next level to the right represent possible states and the associated probability of a flood.

If the flood warning system is developed, for the case of flood happening, the expected cost would be 20,000 (for flood warning development) plus 5000 × 0.1 (probability of this situation), which is equal to 20,500. If the flood warning system is not developed, the expected cost would be 50,000 × 0.1 = 5000. Since in the second case the maximum cost is less, the decision tree analysis suggests that the preferred choice is not to build the flood warning system. While this simple decision tree is based on expected value analysis, more complex decision tree technologies do provide more complete risk profiles.

10.6.2.1 Environmental Risk Analysis

In hydrological analysis, environmental issues are of high importance. Environmental risk deals with the probability of the occurrence of situations with potentially undesirable effects. Environmental agencies, such as the US Environmental Protection Agency, use risk assessment as an objective

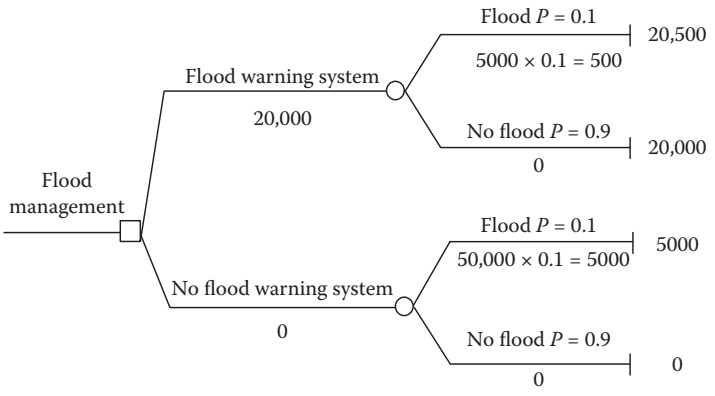

FIGURE 10.12 Event tree in Example 10.15.

tool for setting standards and defining priorities and as assistance in decision making. For example, it can be used for evaluating the risks to human health arising from hazardous chemicals in the environment.

When risk assessment is used to determine environmental priorities at different levels (national, state, regional, community, and tribal), it is called comparative risk assessment. In this method, the issues are ranked based on their probability of occurrence and the magnitude of the consequences.

There are four major approaches suggested by Conway (1982) for environmental risk analysis. These approaches are as follows:

1. The "deterministic" approach: A simple mathematical model is used in this approach to describe the rates of individual transformations and transports of the chemical in the environment. Figure 10.13 depicts a sample of this approach. Two models—fate and effect—are considered in this approach; the results of fate models are concentrations of a chemical in one or more environmental compartments. The effect model estimates the effect of a given concentration of a chemical on an organism, a population, a community, an ecosystem, a landscape (consisting of two or more ecosystems), or the entire ecosphere. The results of a fate model can be used to find the ratio between the computed concentration, the predicted environmental concentration, and the non-observed effect concentration, which is determined by the application of literature values or laboratory experiments (Jørgensen and Bendoricchio 2001).

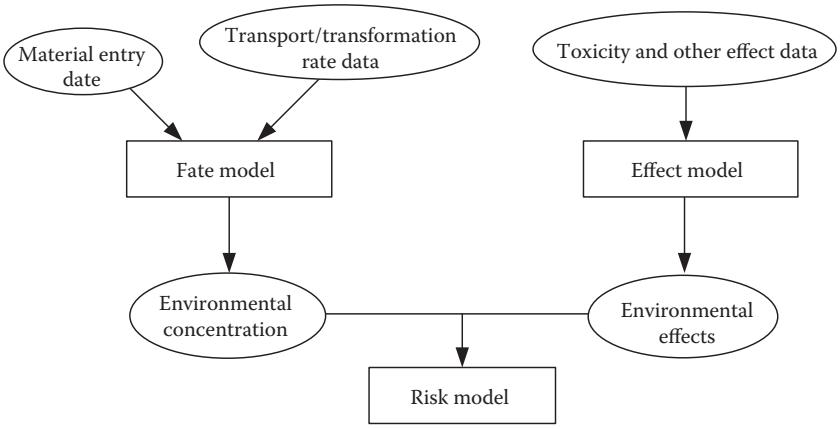

FIGURE 10.13 Sample of deterministic approach to environmental risk analysis.

In environmental risk evaluation, the joint probability of environmental effects and concentration can be used for risk evaluation. In other words, the joint probability of chemical concentration and effects is a measure of their overlap, which can be compared with the system standards used for risk definition.

2. The stochastic/statistical approach: In this approach, large amounts of data are obtained under a variety of conditions. Then, the correlations between the input of a certain material and its observed concentrations and its effects are determined in various environmental compartments.
3. The ecosystem model approach: In this approach, which is also called microcosm, a physical model of a given environmental situation is constructed. A chemical is then applied to the model. The fate and effects of the chemical are observed through the model.
4. The "baseline chemical" approach: In this approach, transformations, transports, and effects are measured as in the deterministic approach. Then, the results are compared with data on chemicals of known degrees of risk.

10.6.3 Risk Management

Risk management has to follow the stages of a risk cycle, through recovery, preparedness, and response (Figure 10.14).

Preparedness decreases potential risks of disasters at social and individual levels. This includes risks improvement to an acceptable and affordable level and the preparation of activities to manage residual risks.

Response and adoptive measures are needed during and after a hazard occurrence. Advance preparation/preparedness is necessary when responding to emergencies. The respective measures deal with the mitigation of emergency situations and the conditional recondition of basic services and infrastructure.

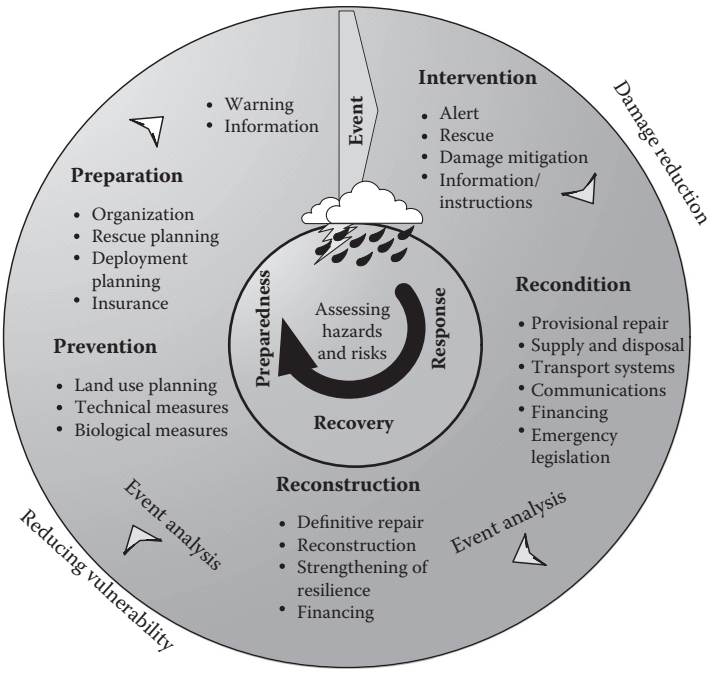

FIGURE 10.14 Risk management cycle.

In most cases, there is a tendency to overlook preparatory and preventive measures. Response is certainly the preferred method of risk management, especially in medium- and low-income countries. Furthermore, decision makers often are willing to invest more in preparedness only after key disasters. However, preparatory and preventive measures are generally more sustainable and cost-efficient than emergency response measures. Based on the information that suitable preparedness measures are still missing in many regions, the structural and nonstructural measures can be used to one or more of the three factors of risk, either as joint or decreased.

In order to make possible classification of aims and to decide the possible approaches towards risk reduction, it is necessary to distinguish between measures that address mitigation of exposure, hazard, and vulnerability. Hazard mitigation measures refer to what can be done to mitigate extreme negative events in both quality and quantity aspects. Exposure mitigation addresses primarily spatial planning, which aims to reconcile the spatial demands of water courses and development in order to minimize the location of infrastructure and vulnerable people in harm's way. Measures in the field of vulnerability plan to mitigate the tangible and intangible susceptibility of infrastructure and people.

It must be identified that certain measures apply to more than one of the three categories, e.g., measures of hazard transfer can also be understood as measures of exposure reduction. Therefore, the discussion has to be seen as an exercise in practice rather than making theoretical distinctions. By considering the selection of measures, experience shows that the most promising approach is to adopt a mixed strategy that addresses multiple risk components. Finally, it is important to know that all suggested measures are subject to local situations and their suitability and applicability will depend on socioeconomic and political conditions.

10.7 VULNERABILITY

The most important factor of risk is vulnerability, which determines whether or not exposure to a hazard constitutes a risk that may actually result in a disaster. There are three types of vulnerability: physical vulnerability of people and infrastructure, unfavorable economic and organizational conditions, and motivations and attitudes (Associated Programme on Flood Management [APFM] 2008).

10.7.1 Vulnerability Estimation

Vulnerability can be defined as the distance of failed character state from the desired condition in historical time series. There are three ways for vulnerability estimation. Some researchers consider the maximum distance from the desired situation, other groups consider the expected value of system failure cases, and the last group considers the probability of failure occurrence. Among these different ideas, the second idea is the most common.

Similarly, the techniques used to measure vulnerability have also varied according to the objective and the discipline trying to assess it. The Third Assessment Report of the Intergovernmental Panel on Climate Change (IPCC) defines vulnerability due to climate change as the extent to which a natural or social system is susceptible to sustaining damage from climate change. It is defined as a function of the sensitivity of the system to change in climate (hazard), its adaptive capacity, and the degree of exposure of the system to climatic hazards (McCarthy et al. 2001). Characterizing vulnerability in a quantitative manner will allow us to assess security risks.

According to Figure 10.9, vulnerability can also be considered as a function of hazard, exposure, and adaptive capacity.

$$\text{vulnerability} = \text{f(hazard, exposure, adaptive capacity)}. \tag{10.100}$$

For measuring vulnerability, a everity index, s_j, should be defined. For example, when the objective is satisfying water demands, the severity index can be defined as the volume of water shortage in

each time interval. Using the probability of failure occurrence, the vulnerability of a system can be calculated by the following formula:

$$v = \sum_{j \in F} s_j e_j, \tag{10.101}$$

where e_j is the probability of x_j corresponding to s_j, the most unsatisfactory and severe outcome that occurs among a set of unsatisfactory states.

Vulnerability analysis is a worthwhile tool in evaluating the entire event chain causing water disaster. Recovery analysis means a systematic investigation on how a system returns to a state of normal operation (Karamouz et al. 2003).

In order to provide a systematic examination of the vulnerability of a built environment to hazards, some models have been developed. For example, the Eastern Shore Regional GIS Cooperative (ESRGC) at Salisbury University undertook a vulnerability modeling effort to riverine and coastal flooding. Using the HAZUS-MH (Hazards US Multi-Hazard) hazard vulnerability analysis modeling software (which is described in the next section) of the Federal Emergency Management Agency (FEMA), the ESRGC sought to generate maps and tables of Maryland's potential for loss related to buildings from flooding on a county-by-county basis. This potential for loss, or the degree of vulnerability, was measured using four different factors: amount of county land area susceptible to a 100-year flood, the amount of square footage of buildings potentially damaged, the number of buildings potentially damaged, and the amount of direct economic losses related to buildings. These four measures of loss help give a more complete picture of the very complex issue of vulnerability to floods.

In order to perform a vulnerability assessment of hydrologic systems, it is important to review indices and indicators of vulnerability developed by previous authors. Some of these indices have been developed as indicators of general human welfare, economic well-being, or development status, while others specifically address vulnerability. A framework for vulnerability assessment should include indicators that could cover all components of a water supply system. The vulnerability process is divided into five main stages (Mohamed et al. 2009):

Stage 1: There are many approaches to indicator development. However, the cause–effect approach is the most widely used (Bossel 1999; Meadows 1998). The Driving force–Pressure–State–Impact–Response (DPSIR) approach developed by Karageorgis et al. (2005) can be used for indicator development and classification. DPSIR not only provides a cause–effect relationship but also can be used as an analytical framework for assessing water issues. This approach allows a comprehensive assessment of the issues through examination of the relevant driving forces and pressures on the system, their consequent state and impacts, and the responses undertaken as shown in Figure 10.15.

Stage 2: The indicators are categorized according to the system components that they correspond to.

Stage 3: A screening process for the prepared list of indicators is carried out regarding the predefined system objectives and the spatial and temporal scales of the system. Two general approaches are considered in the procedures for indicator selection. One approach is based on a theoretical understanding of relationships and the other one is based on statistical relationships. Conceptual understanding does, however, play a key role in both approaches (Adger et al. 2004). Avoiding an overlap between the indicators is of main importance at this stage. In the screening process, if two indicators measure similar or overlapping aspects of the water supply system, only one could be used in the vulnerability assessment.

Stage 4: Indicator evaluation is carried out based on data availability.

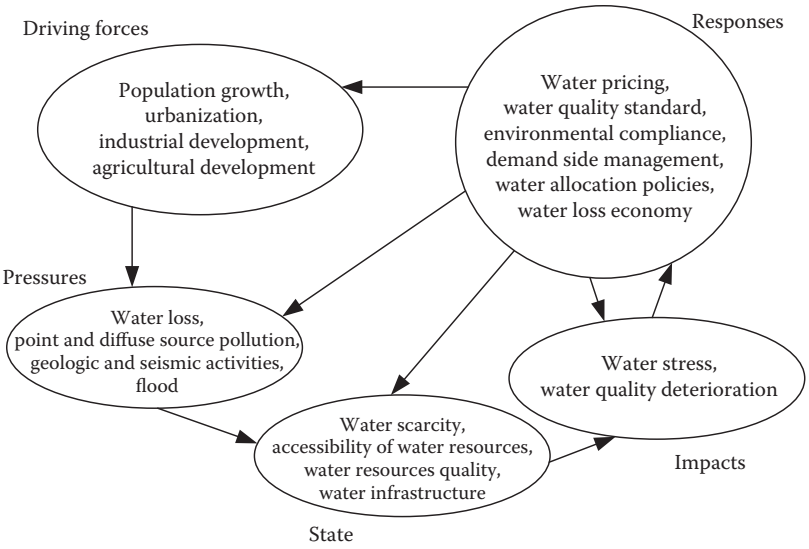

FIGURE 10.15 DPSIR framework to water vulnerability assessment.

Stage 5: The evaluated indicators are presented using a graphical display method for each cluster of indicators.

The presented indicators were used to analyze the status of water supply systems and outline possible vulnerability mitigation strategies.

Calculations are confined to simple mathematical operations needed to arrive to the required form of the indicator value. There are two major steps in developing indices: (1) calculation of values for vulnerability indicators and (2) the subsequent aggregation of these sub-indices into an overall index. An aggregation scheme is usually used to summarize all the indicators into a few indices of water system vulnerability. On the other hand, aggregation causes a loss of information.

Displaying indicators in diagrams requires certain consistency in the displayed value; it is impossible to display two indicators of different units or different range on the same diagram. Thus, before displaying and interpreting the results of indicators, it is important to make some alterations in the indicators' values. The details of data manipulation and alteration can be found in Hamouda (2006). These alterations are done to ease the interpretation of the graphical display; the main alterations include the following:

1. Some indicators are reversed such that the trend is that of an increase in the indicator value leading to greater vulnerability.
2. All indicators are standardized as the ratio of their respective thresholds.
3. After standardizing the values, a cutoff value (here 4) is used for values that are very high as they can cause graphical distortion.

Furthermore, for aggregation of the results of diagrams, in order for them to be better employed in the decision-making process, the readiness index (RI) is calculated as follows:

$$RI = \frac{W_i A_i}{\sum_{i=1}^{n} W_i}. \tag{10.102}$$

where A_i is the average vulnerability of the water supply system to cluster i and W_i is the weight of cluster i in total system vulnerability condition.

10.7.1.1 Vulnerability Software

Vulnerability software is an effective tool for different levels of decision making in relation to risk analysis. For example, FEMA developed a hazard vulnerability analysis software package named HAZUS-MH, which can be used to estimate the potential losses from earthquakes, wind, and floods. The model can be used for emergency preparedness, response and recovery, and loss reduction (mitigation). There are three levels of analysis that can be performed for floods. Level 1 is the most basic level of analysis. Supplied datasets can be used for this type of analysis. A Level 2 analysis is a slightly more detailed analysis that requires more accurate building information. Finally, Level 3 analysis is the most detailed level of analysis.

The methodology used in HAZUS-MH for flood damage analysis is illustrated in Figure 10.16. At first, the hazard and the study regions' characteristics are identified. These are used to estimate the direct and induced damage and then the direct and indirect losses. In losses estimation, different aspects—economic, social, system functionality, and system performance—are included.

To perform the flood analysis, FEMA developed software components to support HAZUS-MH. The Flood Information Tool (FIT) was designed to support the integration of local data. The Inventory Collection and Survey Tool (CAST) is a building inventory tool that allows the user to prepare building information for entry into HAZUS (Figure 10.17). The Building Information Tool (BIT)

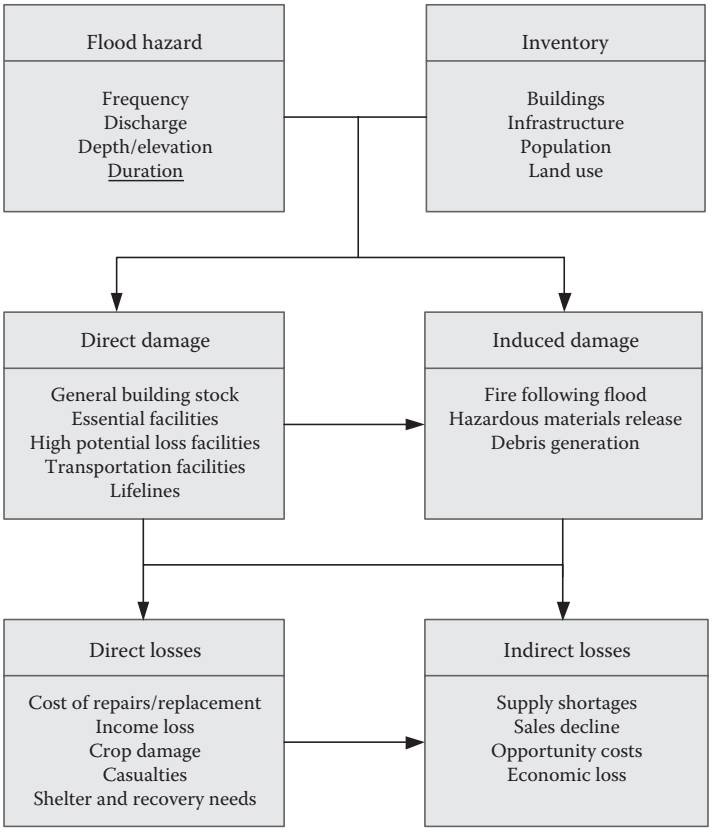

FIGURE 10.16 Flood vulnerability estimation methodology in HAZUS-MH.

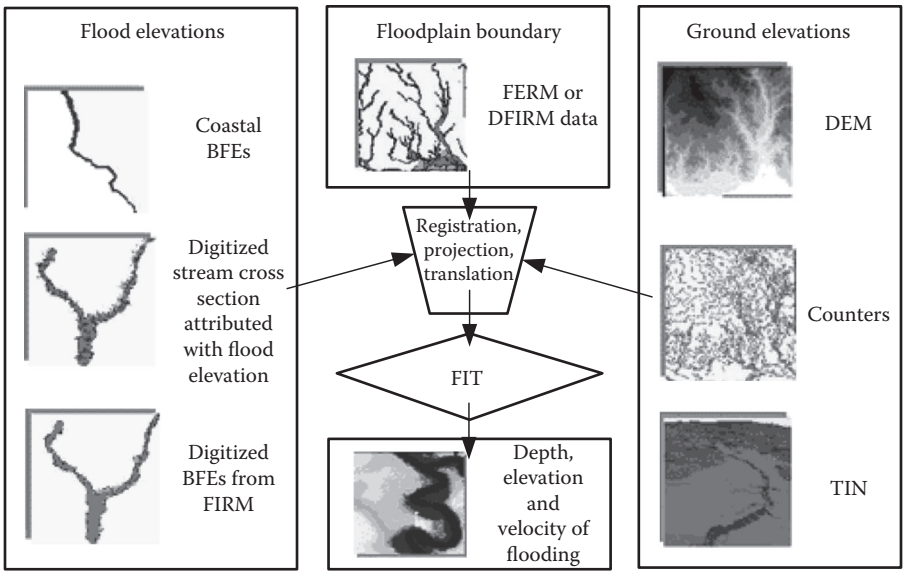

FIGURE 10.17 Key elements of the FIT tool in the HAZUS-MH vulnerability analysis model.

was developed to take large databases and extract information needed for HAZUS. In the following section, the application of the HAZUS-MH model in a hypothetical case adopted from http:// www .fema.gov/hazus/ is illustrated.

10.7.2 Risk Reduction through Reducing Vulnerability

Reducing the vulnerability of communities to hazards is a crucial aspect of risk management. Poverty and lack of resources increase vulnerability, weakens coping strategies, and delays the recovery process. Poor people everywhere, especially in urban areas, are the most at risk. Local authorities in developing countries are usually ill-equipped to provide sufficient infrastructure and services in urban areas. As a result, most of the world's poor live in densely populated squatter settlements, on the periphery of cities, which lack the basics of life, leaving many inhabitants caught in a spiral of increasing vulnerability.

Demand for commercial and residential land in cities has led to the use of unsuitable terrain prone to natural hazards. Many informal settlements are therefore located in dangerous or unsuitable areas, such as floodplains, unstable slopes, or reclaimed land. Moreover, these cities are often unable to manage rapid population growth; poorly planned urbanization and increasing numbers of inadequately constructed and badly maintained buildings further increase the level of vulnerabilities in cities. Ironically, most of today's largest cities are in areas where earthquakes, floods, landslides, and other disasters are likely to happen. Therefore, reducing the risk of societies to hazards through reduction of vulnerability is critical in risk management.

Risk reduction is an approach to identifying, assessing, and reducing the risks of disaster. This concept aims to reduce socioeconomic vulnerabilities to disaster and to deal with the environmental and other hazards that trigger them. Reducing disaster risks is essential if we are to consolidate progress made in development and poverty reduction. An important part of disaster risk reduction is becoming aware of risk itself and its components. The relation between vulnerability and risk is not commutative: reduced vulnerability always means reduced risk of a negative outcome, but not vice versa. This asymmetry ought to create a policy incentive to focus on vulnerability reduction, since it leverages more than risk reduction. Generally, vulnerabilities are not just the given circumstances, but rather unsafe conditions that have developed through human actions or inactions.

In spatial analysis of vulnerability, the areas that are exposed to the considered hazard are determined first. For example, the floodplain in flood vulnerability is first configured. Then, the study region is divided into some zones with different levels of vulnerability. Regarding the severity of vulnerability in different zones, the mitigation practices can be selected and prioritized for application. In flood planning, the floodplain is mixed with insurance zones to determine the evacuation zones with different priorities as will be discussed in Chapter 13.

10.8 RESILIENCY

Over the past decades, there has been a shift away from structural and large-scale defense against hazards towards integrated risk management. The modern risk management concept acknowledges that hazards such as floods cannot be stopped from occurring and emphasizes reducing vulnerability, exposure, and sensibility of risk-prone communities. The resilience concept provides a practical framework for this end.

Resiliency describes how quickly a system recovers from failure once failure has occurred. In other words, resiliency is basically a measure of the duration of an unsatisfactory condition. It is perhaps the most important indicator of crisis recovery and how successful the disaster has been managed. By this description, the inverse of average break time is considered as the resiliency index in time t (Res_t), which can be formulated as follows:

$$\text{Res}_t = \frac{k}{\sum_{t=1}^{k} T_t} \times 100 , \tag{10.103}$$

where k is the number of system breaks in the considered time period and T_t is the duration of break t.

Resilience is a dynamic quality within a community that is used to develop and strengthen over time. A community can take action to increase the capacity of its organizations, resources, processes, and people, to respond to influence change.

The impacts of disaster on the community are importantly influenced by community preparedness. Community resilience is the group's capacity to recover from, withstand, and respond positively to adversity or crisis. Community resilience is often defined as the following three properties:

1. Resistance is the disruption degree that can be accommodated without the community undergoing long-term change. Before undergoing long-term change, a highly resilient community can withstand considerable disruption.
2. Recovery is the ability of a community to pull through or bounce back to its pre-disaster state. A highly resilient community returns to its pre-disaster state, or moves beyond that, quicker than a less-resilient community.
3. Learning process is the ability of a community to build on learning of a crisis or disaster, to gain an improved functioning level and increase resilience levels. A highly resilient community will adapt to its new conditions and learn from the experience of disaster.

Resiliency could be considered as the most important indicator of system performance in disaster recovery and how successful the management of disaster strategies have been. Communities are vulnerable to natural disasters. In some areas, there is a high risk of floods in the plain and landslide in the hills, and the frequency of such disaster is increasing year by year. Low awareness level in terms of disaster preparedness and management and the lack of efficient mechanisms and capacity to deal with these natural disasters have had severe impacts on the lives of the people, property, and economy at large. Climate change has also added to these challenges, especially for the poor in rural areas.

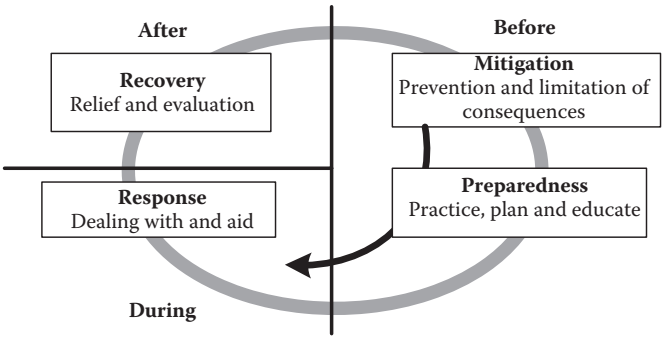

FIGURE 10.18 Resilient communities have an improved capacity in each phase of the disaster management cycle. (From Joosten-ten Brinke, D. et al., *Educational Research Review*, 3, 51–65, 2008. With permission.)

Resiliency therefore works to reduce the impacts by helping people meet their household food needs through home-based agriculture, cash crop production, and non-farm alternative livelihood strategies. It has also helped reduce loss of lives and assets—from landslide, floods and other forms of natural disaster—through the use of early warning systems, improved physical infrastructure and local preparedness planning, among other initiatives.

The defining and thus taken-for-granted characteristic of resilient communities is the ability to reduce, prevent, and cope with the risk. Resilient communities have improved their capacity in each phase of the management cycle as shown in Figure 10.18. There are four steps in disaster management including mitigation, preparedness, response, and recovery. Mitigation and preparedness are considered before disaster happens, response refers to the activities during the disaster, and recovery refers to the activities after disaster. Preparedness activities help to build community resilience to disasters. Preparation not only helps in preventing disasters but also can lessen the impact of disasters when they do occur. Strategies, tools, and training are provided to assist in preparation for disasters. In mitigation prevention and limitation of disaster, consequences are considered and preparedness includes practicing, planning, and education of the society to deal with disasters. They are knowledgeable and aware of the risk, are well prepared and respond better when a hazard occurs, and recover more quickly from disasters. Resilience is also promoted through programs that encourage, create, and develop resources and connections that can be drawn on in times of crisis.

It is arguable that the overall performance of the risk management system can be improved by adopting a resilient approach. While a resistant approach is directed to maintain the structure and functions of the system, the resilient approach enhances the capacity of the system to recover from nonstructural changes in dynamics. The resilience of a system relates to three aspects that determine the reaction of a system to hazard: (1) the amplitude of the reaction, (2) the gradual increase of reaction with increasing disturbances, and (3) the recovery rate. The resilience of a system is larger when the amplitudes (i.e., amount of damage) are smaller. Design strategies based on suitable indicators could provide larger magnitude of reactions. This will lead to a more gradual slope of the damage frequency curve and enhance system resiliency.

10.9 UNCERTAINTY

Hydrology is a science that is highly uncertain. The main reason for this uncertainty is that the intrinsic dynamics of many hydrological processes are still not known. Moreover, the geometry of hydrological control volumes (river beds, subsurface preferential flow paths, etc.), as well as most of the related initial and boundary conditions and biogeochemical processes, cannot be observed in detail and, consequently, cannot be mathematically represented. Finally, hydrologists are typically working under conditions of data scarcity, which limits the efficiency of an

inductive approach for tackling the above problems. Uncertainties are caused by lack of perfect understanding of hydrologic phenomena and processes involved. Uncertainties could arise from the following: (1) inherent randomness (e.g., weather), (2) model structural error that reflects the inability of a model to represent precisely the system's true behavior, (3) model parameter value error, and (4) data error.

It is pointed out that, in spite of this initial stimulus, stochastic hydrology is a discipline essentially independent of water management and that a hydrological uncertainty need not necessarily be important for a water management decision and may carry a different degree of importance in different contexts.

Hydrology design and analysis deal with the occurrence of water in various parts of a hydrosystem and its effects on environmental, ecological, and socioeconomic settings. Due to the extreme complex nature of the physical, chemical, biological, and socioeconomic processes involved, major efforts have been devoted by different investigations to have a better understanding of the processes.

In general, uncertainty due to inherent randomness of physical processes cannot be eliminated. On the other hand, uncertainties such as those associated with lack of complete knowledge about the parameters, data, process, and models could be reduced through research, data collection, and careful design and manufacturing. In hydrology engineering, uncertainties can be divided into four basic categories: hydraulic, structural, hydrologic, and economic. More specifically, in hydrology engineering analyses and designs, uncertainties could arise from different sources including intrinsic or natural uncertainties, parameter uncertainties, model uncertainties, operational uncertainties, and data uncertainties.

Natural uncertainty is associated with the inherent randomness of natural processes such as the occurrence of flood and precipitation events. The occurrence of hydrological events often shows variations in space and in time. A model is only an abstraction of the reality, which generally involves certain simplifications; model uncertainty reflects the inability of a model or design technique to represent precisely the system's true physical behavior. Parameter uncertainties result from the inability to accurately quantify model parameters and inputs. Parameter uncertainty could also be caused by change in operational conditions of hydraulic structures, inherent variability of inputs and parameters in time and in space, and lack of sufficient data.

Data uncertainties include (1) measurement errors, (2) nonhomogeneity and inconsistency of data, (3) transcription and data handling errors, and (4) inadequate representation of data sample due to space and time limitations. Operational uncertainties include those associated with deterioration, manufacturing, construction process, human factors, and maintenance impact. The magnitude of this type of uncertainty is largely dependent on the workmanship and quality control during manufacturing and construction.

Another measure of the uncertainty of a quantity is expressing it in terms of a reliability domain such as the confidence interval. A confidence interval is a numerical interval that would capture the quantity subject to uncertainty with a specified probabilistic confidence. Nevertheless, the use of confidence intervals has a few drawbacks: (1) the parameter population may not be normally distributed as assumed in the conventional procedures, and this problem is particularly important when the sample size is small; and (2) there are no means available to directly combine the confidence intervals of individual contributing random components to give the overall confidence interval of the system. A useful alternative to quantify the level of uncertainty is to use the statistical moments associated with a quantity subject to uncertainty. In particular, the variance and standard deviation, which measure the dispersion of a stochastic variable, are commonly used. It is shown in Figure 10.19, by increasing the standard deviation of data, that the corresponding uncertainty increases due to higher range of data variations.

Figure 10.20 shows the design procedure involving the above discussion of load and resistance and how reliability and uncertainty could be integrated into the design process. In urban water systems, there are two types of basic input: natural input, such as rainfall, temperature, sediment yield, etc., which are random variables describing the natural environment; and inputs coming

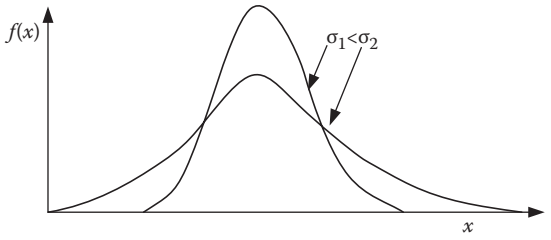

FIGURE 10.19 Relationship between standard deviation and uncertainty.

from human activities, such as water demand, sewage effluents, pollutants, etc., which are random numbers describing the interaction of people with the environment. The hydrologic, hydraulic, and structural uncertainties are identified and coupled with a loss function to determine the expected damage resulting from a disaster/failure.

Figure 10.21 shows the framework of the proposed algorithm in dealing with risk and uncertainty. Probability distribution functions are developed for hydraulic and/or structural behavior of the system as well as quality of supplied water considering different values for uncertain variables and parameters and simulation of system performance under these values. The identified uncertainties by these PDFs are incorporated in the base simulation model and then alternative models are developed to evaluate uncertainties that are affecting the system performance.

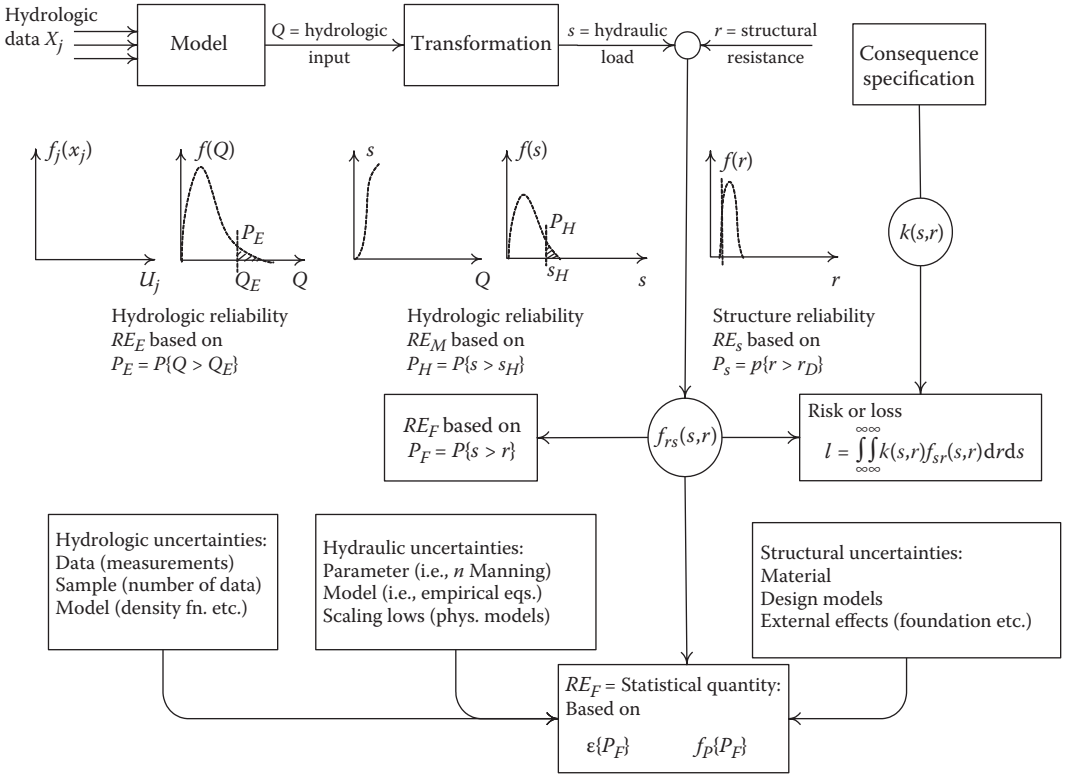

FIGURE 10.20 Generalized concept of risk and reliability analysis for structures. (From Plate, E.J. and Duckstein, L., *Water Resources Bulletin*, 24 (2), 1988. With permission.)

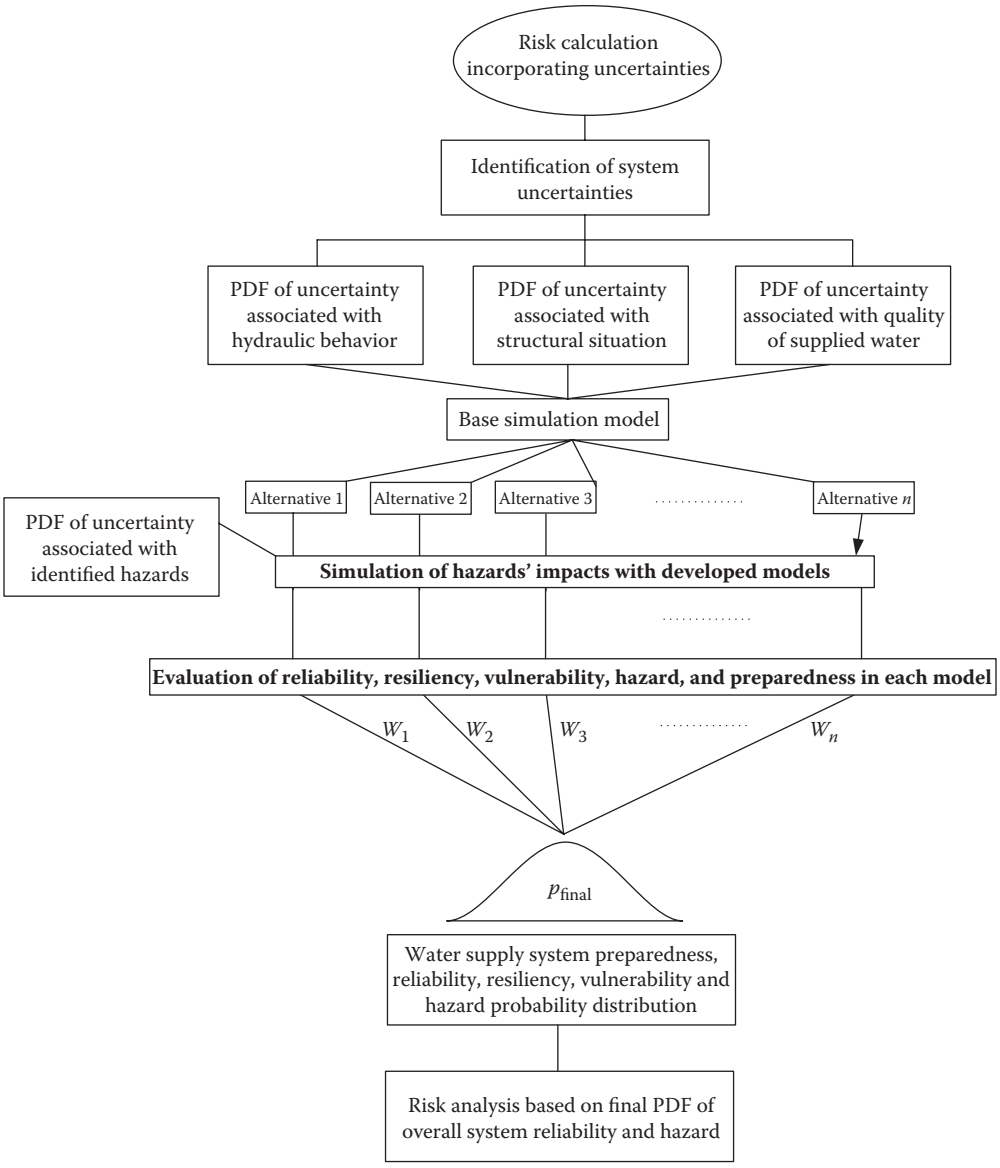

FIGURE 10.21 Generalized concept of risk and reliability analysis for water supply structure.

10.9.1 Implications of Uncertainty

In hydrologic design and modeling, the design quantity and system output are functions of several system parameters, not all of which can be quantified with absolute accuracy. The task of uncertainty analysis is to quantify the uncertainty features of the system outputs as a function of model characteristics and the stochastic variables involved. It provides a formal system framework to quantify the uncertainty associated with the system's output. Furthermore, it offers the designer useful insights regarding the contribution of each stochastic variable to the overall uncertainty of the system outputs. Such knowledge is essential to identify the "important" parameters to which more attention should be given to have a better assessment of their values and, accordingly, to reduce the overall uncertainty of the system outputs.

10.9.2 Uncertainty of Hydrological Forecasting

An important issue in modeling hydrological processes and forecasting is the results' confidence to be used for decision making in real-time applications. In other words, each model is an approximation to reality; therefore, a decision maker needs to know how reliable the results from a model are and how they affect the final decision. There are different levels of uncertainty in almost all circumstances and at all times, which is a common experience in everyday life.

All natural events in the hydrologic cycle are inherently uncertain in essence. The main source of uncertainty is related to data and information. As an example, there is an uncertainty of 20% or more in flow measurements, and therefore the results of the models that are developed using these data will have an uncertainty of 20%, at least. Uncertainty arises from system complexity, ignorance, imprecision, different classes of randomness, knowledge unclarity, and so forth.

There are many different factors affecting the final quality of hydrological forecasts. According to Krzysztofowicz (2001), these sources of uncertainty could be divided into three groups based on their origin:

1. Operational uncertainty is caused by an unpredictable event during the forecasting process such as dam breaks, ice jams, etc. Hydrologists operating the model have a very important impact on the final hydrological forecast (human impact also belongs to the group of operational uncertainty). Unfortunately, operational uncertainty could not be quantified in advance and therefore stays unexpressed not only in deterministic but also in probabilistic approaches.
2. Hydrological uncertainty is represented by uncertainty of hydrological tools and techniques. The uncertainty of model parameters' calibration and the uncertainty of rating curves and measurement could be mentioned, to name a few.
3. Input uncertainty is represented by other uncertainty of input data. The most important member of that group is the Quantitative Precipitation Forecast (QPF) uncertainty. Experience shows that QPF is the most sensitive factor affecting the result of hydrological forecast in headwater areas including the area of the Czech Republic.

In general, different sources of uncertainty in hydrological simulation can be classified: uncertainty of model, uncertainty of input, uncertainty of parameter, and operational and natural uncertainty, such as unforeseen causes, malfunctioning of system components, erroneous and missing data, human errors, and mistakes.

Although input uncertainties have been treated (through climate change studies) within water resources management models and although a full range of uncertainties have been included in hydrological models, studies that investigate and address end-to-end impacts of hydrological modeling uncertainties from a water supply point of view are lacking.

10.9.3 Measures of Uncertainty

In statistical analysis, the uncertainty measurement is based on measures of the distribution that describes the uncertainty. The most ordinary estimate of uncertainty is variance. The variance of a calculated parameter describes how the parameter calculation would be different in repeated sampling. Other procedures of uncertainty are based on distribution quantiles such as lower and upper quantiles. The likelihood method can also be used to estimate the uncertainty when parameters are measured. The likelihood is associated with the data and how likely the observed data are, given the estimated parameter(s) (Ramsey and Schafer 1997). The likelihood is usually used to evaluate uncertainty of models.

Several expressions have been used to describe the level of uncertainty of a parameter, a function, a model, or a system. In general, the uncertainty associated with the latter three is a result of

the combined effect of the uncertainties of the contributing parameters. The most complete and ideal description of uncertainty is the PDF of the quantity subject to uncertainty. However, in most practical problems such as probability function, it cannot be precisely derived or obtained.

The concept of the entropy theory is the central role of information theory, sometimes referred to as the measure of uncertainty. The entropy of a random variable is defined in terms of its probability distribution and can be shown to be a good measure of randomness or uncertainty. This part mainly deals with its characterizations and properties. Properties of discrete finite random variables are studied. The study is extended to random vectors with finite and infinite values. The idea of entropy series is explained. Finally, the continuous case generally referred to as differential entropy with different probability distributions and power inequality is studied.

10.9.3.1 Entropy Theory

The entropy (or information) theory, developed by Shannon (1948), recently has been applied in many different fields. The entropy theory has also been applied in hydrology and water resources for measuring the information content of random variables and models, evaluating information transfer between hydrological processes, evaluating data acquisition systems, and designing water quality monitoring networks.

There are four basic information measures based on entropy: marginal, joint, and conditional entropies and transinformation. Shannon and Weaver (1949) were the first to define the marginal entropy, $H(x)$, of a discrete random variable x as

$$H(x) = -\sum_{i=1}^{n} p(x_i) \log_b p(x_i), \tag{10.104}$$

where n represents the number of elementary events with probabilities $p(x_i)$ ($i = 1,...,N$) and b is the base of the logarithm.

Example 10.16

Let x_i be the uncertain variable of rainfall depth of event i with uncertain distribution of inundation probability as follows:

$$p(x_i) = \begin{cases} 10\% & i = 1 \\ 30\% & i = 2 \\ 50\% & i = 3 \\ 70\% & i = 4 \\ 100\% & i = 5 \end{cases}$$

Using the entropy definition for a discrete random variable, and assuming $b = 10$ as the base of the logarithm, calculate the entropy of x.

Solution:

It follows from the definition of entropy that

$$H(x) = -\sum_{i=1}^{n} p(x_i) \log_b p(x_i) = -\sum_{i=1}^{5} p(x_i) \log_b p(x_i) = -(0.1 \times -1 + 0.3 \times -0.52288$$

$$+ 0.5 \times -0.30103 + 0.7 \times -0.1549 + 1 \times 0) \qquad H(x) = 0.51581.$$

The total entropy of two independent random variables x and y is equal to the sum of their marginal entropies.

$$H(x,y) = H(x) + H(y), \tag{10.105}$$

where x and y are stochastically dependent, their joint entropy is less than the total entropy. Conditional entropy of x given y represents the uncertainty remaining in x when y is known, and vice versa.

$$H(x|y) = H(x, y) - H(y). \tag{10.106}$$

Transinformation is another entropy measure that measures the redundant or mutual information between x and y. It is described as the difference between the total entropy and the joint entropy of dependent x and y.

$$T(x,y) = H(x) + H(y) - H(x,y) \tag{10.107}$$

or

$$T(x, y) = H(x) - H(x|y) = H(y) - H(y|x). \tag{10.108}$$

The above expression can be extended to the multivariate case with M variables (Harmancioglu et al., 1999). The total entropy of independent variables X_m ($m = 1,..., M$) equals

$$H(X_1, X_2, ..., X_m) = \sum_{m=1}^{M} H(X_m). \tag{10.109}$$

If the variables are dependent, their joint entropy can be expressed as

$$H(X_1, X_2, ..., X_m) = H(X_1) + \sum_{m=2}^{M} H(X_m \,|\, X_1, X_2, ..., X_{m-1}). \tag{10.110}$$

It is sufficient to compute the joint entropy of the variables to estimate the conditional entropies of Equation 10.110 as the latter can be obtained as the difference between two joint entropies; for example,

$$H(X_m|X_1, X_2, \ldots, X_{m-1}) = H(X_1, X_2, \ldots, X_m) - H(X_1, X_2, \ldots, X_{m-1}). \tag{10.111}$$

Finally, when the multivariate normal distribution is assumed for $f(X_1, X_2,...,X_M)$, the joint entropy of X, with X being the vector of M variables, can be expressed as

$$H(x_1, x_1, \ldots, x_M) = (M/2)\ln 2\Pi + (1/2)\ln|C| + M/2 - M \ln(\Delta x), \tag{10.112}$$

where $|C|$ is the determinant of the covariance matrix C; and Δx is the class interval size assumed to be the same for all M variables.

The design of water quality monitoring networks is still a challenging issue, for there are difficulties in the selection of temporal and spatial sampling frequencies, the variables to be monitored, the sampling duration, and the objectives of sampling (Harmancioglu et al. 1999). The

entropy theory can be used in the optimal design of water quality monitoring systems. By adding new stations and gathering new information, the uncertainty (entropy) in the quality of the water is reduced. In other words, transinformation can show the redundant information obtained from a monitoring system, which is due to spatial and temporal correlation among the values of water quality variables. Therefore, this index can be effectively used for optimal location of the monitoring stations and for determining the sampling frequencies. Refer to Karamouz et al. (2009) for more information.

10.9.3.2 Probability Theory—Bayes' Theorem

The probability theory can be used in two ways for uncertainty evaluation: subjective or Bayesian view and frequents view. When using Bayes' theorem, a rule is provided for updating the probability of H based on additional information E and background information I:

$$P(H|E,I) = \frac{P(H|I)P(E|H,I)}{P(E|I)}, \tag{10.113}$$

where $P(H|E,I)$ indicates the posterior probability, which shows the probability of H after incorporating the effect of information E in the context I. $P(H|I)$ is the posterior probability of H just based on background information I. In other words, prior probability is the belief in H before considering the additional information of E. The term $P(E|H,I)$ is the likelihood indicating the probability of E when the hypothesis H and background information I are true. $P(E|I)$ is the prior probability of E, which is used as a normalizing or scaling constant.

In frequency analysis, the situation that an event can be repeated without any limitation in identical conditions is considered; however, the event consequence is random.

Example 10.17

In order to drill a well, the water depth needs to be known. In primary designs, water depth is divided into four categories: less than 5 m, between 5 and 10 m, between 10 and 15 m, and more than 15 m. The following assumptions are known based on the experiences of the hydrology of the area:

The probability of depth to be less than 5 m = $\Pr[B_1] = 0.6$.
The probability of depth to be between 5 and 10 m = $\Pr[B_2] = 0.2$.
The probability of depth to be between 10 and 15 m = $\Pr[B_3] = 0.15$.
The probability of depth to be more than 15 m = $\Pr[B_4] = 0.05$.

The depth h is measured and tabulated in Table 10.3 (the depth includes measurement error).
The h value is obtained 7 m from the measurements. Considering the error measurements and other assumptions, calculate the probability of h to be in each category.

TABLE 10.3
Probability of Correctness of Measurements

		$h \le 5$	$5 < h \le 10$	$10 < h \le 15$	$h > 15$
$i = 1$	$h \le 5$	0.9	0.05	0.03	0.02
$i = 2$	$5 < h \le 10$	0.07	0.88	0.06	0.06
$i = 3$	$10 < h \le 15$	0.03	0.05	0.85	0.12
$i = 4$	$h > 15$	0.0	0.02	0.06	0.8

Solution:

In this example, B probabilities are actually the prior probabilities of the water depth in the well. The aim of sampling is to update and correct the information, by knowing that the results of sampling include measurement error (sample likelihood). Using Bayes' theorem, posterior probability can be obtained from the following equation:

$$\Pr\left[B_i \middle| \text{Sampleno. } 2\right] = \frac{\Pr\left[\text{Sampleno. } 2 \middle| B_i\right]\Pr[B_i]}{\sum_{i=1}^{4}\Pr\left[\text{Sampleno. } 1 \middle| B_i\right]\Pr[B_i]}.$$

Therefore,

$$\sum_{i=1}^{4}\Pr\left[\{5 < h \le 10\} \middle| B_i\right]\Pr[B_i] = 0.07\times 0.6 + 0.88\times 0.20 + 0.10\times 0.15 + 0.06\times 0.05 = 0.236$$

$$\Pr\left[B_1 \middle| \text{Sampleno. } 2\right] = \frac{0.07\times 0.6}{0.236} = 0.178$$

$$\Pr\left[B_2 \middle| \text{Sampleno. } 2\right] = \frac{0.88\times 0.2}{0.236} = 0.746$$

$$\Pr\left[B_3 \middle| \text{Sampleno. } 2\right] = \frac{0.10\times 0.15}{0.236} = 0.063$$

$$\Pr\left[B_4 \middle| \text{Sampleno. } 2\right] = \frac{0.06\times 0.05}{0.236} = 0.13.$$

10.9.3.3 Fuzzy Set Theory

In classical or crisp set theory, a component x of the universal set X belongs to a subset A ($x \in A$) or its complement. In other words, an element in the universe is a member and nonmember of a given set and its membership is either 1 (which definitely belongs to the set) or 0 (which definitely does not belong to the set). For many practical purposes, it would be useful to define the boundaries of sets vaguely. In that situation, an element can be a member of a set with a degree of membership less than 1. This concept was first proposed by Zadeh (1965) by introduction of the fuzzy set theory. In the fuzzy set theory, there is a gradual transition between membership and nonmembership.

This gradual transition of membership in fuzzy set theory is because of the vague definition of the boundaries of fuzzy sets. This feature of a fuzzy set makes the fuzzy set theory appropriate for the representation of uncertainty other than the probabilistic form.

For example, in hydrological applications, we can refer to river stage and discharge records, which are essential for hydrological and hydraulic analyses. While river stage is measured directly, discharge value is calculated from measurements of flow velocity, depth, and channel cross-section dimensions. The measurements are affected by random and systematic measurement errors and other inaccuracies, such as approximation of velocity distribution and channel geometry with a finite number of measurements. Such errors lead to uncertainty in both the stage and the discharge values, which propagates into the rating curve established from the measurements. The relationship between stage and discharge is not strictly single valued but takes a looped form due to the unsteady flow in rivers. The fuzzy set theory can be used for consideration of different sources of uncertainty

in the stage and discharge measurements and their aggregation into a combined uncertainty. The uncertainty in individual measurements of stage and discharge can be represented using triangular fuzzy numbers, and their spread is determined. The details of fuzzy set theory are described in Chapter 11.

10.9.4 Analysis of Uncertainty

Uncertainty analysis investigates the uncertainty of variables that are used in decision-making problems in which observations and models represent the knowledge base. In other words, uncertainty analysis aims to make a technical contribution to decision making through the quantification of uncertainties in the relevant variables.

Through risk assessment, the system information is collected to make a decision based on the associated risk of a particular event. Due to vagueness of information and system performance, all of the decisions made in the risk assessment process have a level of uncertainty. Therefore, uncertainty analysis with focus on uncertainties in the assessment is a necessary issue in risk assessment. Uncertainty analysis includes three components: qualitative analysis, quantitative analysis, and communication of the uncertainty. Qualitative analysis identifies the uncertainties and quantitative analysis explores the effects of the uncertainties on the decision process. The uncertainty analysis process depends on the problem type. The process of uncertainty analysis in risk assessment of global warming would be quite different from the uncertainty analysis for hazardous agents in water. Furthermore, the results of analysis are highly dependent on the spatial and temporal scale, available data and information, models, and objectives.

The uncertainty analysis methods vary from simple descriptive procedures to sophisticated quantitative methods of uncertainty estimation, to more formal decision-based procedures. Depending on the required level of resolution and the available information, qualitative or quantitative analysis methods can be used. Uncertainty assessment should also incorporate the view of uncertainty from both a scientist and a risk manager approach.

In the design and analysis of hydrologic systems, many quantities of interest are functionally related to a number of variables, some of which are subject to uncertainty. For example, hydraulic engineers frequently apply weir flow equations such as $Q = CLH^{1.5}$ to estimate spillway capacity in which the coefficient C and head H are subject to uncertainty. As a result, discharge over the spillway is not certain. A rather straightforward and useful technique for the approximation of such uncertainties is the first-order analysis of uncertainties, sometimes called the delta method.

The use of the first-order analysis of uncertainties is quite popular in many fields of engineering because of its relative ease in application to a wide array of problems. First-order analysis is used to estimate the uncertainty in a deterministic model formulation involving parameters that are uncertain (not known with certainty). More specifically, first-order analysis enables one to estimate the mean and variance of a random variable that is functionally related to several other variables, some of which are random. By using first-order analysis, the combined effect of uncertainty in a model formulation, as well as the use of uncertain parameters, can be assessed.

Consider a random variable Y that is a function of k random variables (multivariate case):

$$y = g(x_1, x_2, \ldots, x_k). \tag{10.114}$$

This can be a deterministic equation such as the rational formula or Darcy–Weisbach's equation, or this function can be a complex model that must be solved on a computer. The objective is to treat a deterministic model that has uncertain inputs in order to determine the effect of the uncertain parameters $x_1, x_2, \ldots, x_k$ on the model output y.

Equation 10.114 can be expressed as $y = g(x)$, where $X = x_1, x_2, \ldots, x_k$. A Taylor series expansion about k random variables, ignoring the second- and higher-order terms, is as follows:

$$y \approx g(\bar{X}) + \sum_{i=1}^{k} \left[\frac{\partial g}{\partial x_i} \right]_{\bar{X}} \left(x_i - \bar{X} \right). \tag{10.115}$$

The derivation $\left[\partial g / \partial x_i \right]_{\bar{X}}$ are the sensitivity coefficients that represent the rate of change of the function value $g(\bar{X})$ at $x = \bar{X}$ where $\bar{X}$ is mean and σ^2 is variance.

Assuming that the k random variables are independent, the variance of y is approximated as

$$\sigma_y^2 = \mathrm{Var}[y] = \sum a_i^2 \sigma_{x_i}^2 \tag{10.116}$$

and the coefficient of variation, Ω_y, which is often used as the measure of uncertainty, is estimated as follows:

$$\Omega_y = \left[\sum_{t=1}^{k} a_i^2 \left(\frac{\bar{x}_i}{\mu_y} \right)^2 \Omega_{x_i}^2 \right]^{1/2}, \tag{10.117}$$

where $a_i = \left(\partial g / \partial x \right)_{\bar{x}}$.

10.9.4.1 Mean Value First-Order Second-Moment Method

The mean and standard deviation of the performance function $W(X)$ are estimated using the first-order variance method in uncertainty analysis. These values are used for β reliability index estimation as follows:

$$\beta = \frac{W(\mu)}{\sqrt{S^{\mathrm{T}} C(X) S}}, \tag{10.118}$$

where μ is the mean vector and $C(X)$ is the covariance matrix of random variable X and S is the N-dimensional matrix equal to the partial differential of W to X.

Studies have shown that in a confidence boundary of less than 0.99, the reliability value is not sensitive to the distribution function of W and assumption of a normal distribution for W would be sufficient, but for confidence levels that are more restricted than 0.99 such as 0.995, the extreme edges of distribution function of W will be critical.

The application of this model is easy; however, it must be noted that there are some weaknesses because of the nonlinearity and non-invariability of the performance function in critical situations. Therefore, the application of this method in the following situations is not recommended:

- Estimation of risk and reliability with high precision
- Highly nonlinear performance function
- Existence of random variables with high skewness in performance function

Example 10.18

Applying the first-order analysis, formulate σ_Q and Ω_Q in Manning's equation $\left(Q = \frac{0.311}{n} S^{1/2} D^{8/3} \right)$ when diameter D is a deterministic parameter and n and S are considered to be uncertain.

Solution:

Since n and S are uncertain, Manning's equation can be rewritten as

$$Q = K n^{-1} S^{1/2},$$

where $K = 0.311D^{8/3}$. The first-order approximation of Q is determined using the above equation, so that

$$Q \approx \bar{Q} + \left[\frac{\partial Q}{\partial n}\right]_{\bar{n},\bar{S}} (n - \bar{n}) + \left[\frac{\partial Q}{\partial S}\right]_{\bar{n},\bar{S}} (S - \bar{S})$$

$$= \bar{Q} + \left[-K \bar{n}^{-2} \bar{S}^{1/2}\right](n - \bar{n}) + \left[0.5K \bar{n}^{-1} \bar{S}^{-1/2}\right](S - \bar{S}),$$

where $\bar{Q} = K \bar{n}^{-1} \bar{S}^{1/2}$.

The variance of the pipe capacity can be computed as follows:

$$\sigma_Q^2 = \left[\frac{\partial Q}{\partial n}\right]_{\bar{n},\bar{S}}^2 \sigma_n^2 + \left[\frac{\partial Q}{\partial S}\right]_{\bar{n},\bar{S}}^2 \sigma_S^2$$

$$\sigma_Q = \left\{\left[\frac{\partial Q}{\partial n}\right]_{\bar{n},\bar{S}}^2 \sigma_n^2 + \left[\frac{\partial Q}{\partial S}\right]_{\bar{n},\bar{S}}^2 \sigma_S^2\right\}^{1/2}.$$

The coefficient of variation of Q is determined as follows:

$$\Omega_Q^2 = \sum_{i=1}^{2} \left[\frac{\partial Q}{\partial x_i}\right]^2 \left[\frac{\bar{x}_i}{\bar{Q}}\right]^2 \Omega_{x_i}^2$$

$$\Omega_Q^2 = \left[\frac{\partial Q}{\partial n}\right]_{\bar{n},\bar{S}}^2 \left[\frac{\bar{n}}{\bar{Q}}\right]^2 \Omega_n^2 + \left[\frac{\partial Q}{\partial S}\right]_{\bar{n},\bar{S}}^2 \left[\frac{\bar{S}}{\bar{Q}}\right]^2 \Omega_S^2$$

$$\Omega_Q^2 = \left[\frac{-K\bar{S}^{1/2}}{\bar{n}^2}\right]^2 \left[\frac{\bar{n}}{\bar{Q}}\right]^2 \Omega_n^2 + \left[\frac{0.5K}{\bar{n}\,\bar{S}^{1/2}}\right]^2 \left[\frac{\bar{S}}{\bar{Q}}\right]^2 \Omega_S^2$$

$$\Omega_Q^2 = \left[\frac{-K\bar{S}^{1/2}}{\bar{Q}}\right]^2 \left[\frac{1}{\bar{n}^2}\right] \Omega_n^2 + (0.5)^2 \left[\frac{K}{\bar{n}\,\bar{S}^{1/2}}\right]^2 \left[\frac{\bar{S}}{\bar{Q}}\right]^2 \Omega_S^2$$

$$\Omega_Q^2 = \left[\bar{n}^2\right]\left[\frac{1}{\bar{n}^2}\right] \Omega_n^2 + 0.25 \left[\frac{1}{\bar{S}}\right][\bar{S}] \Omega_S^2$$

$$\Omega_Q^2 = \Omega_n^2 + 0.25 \Omega_S^2$$

TABLE 10.4
Parameters of Storm Sewer Pipe in Example 10.19

Parameter	Mean	Coefficient of Variation
n	0.015	0.01
D	1.5 m	0
S	0.001	0.05

$$\Omega_Q = \left[\Omega_n^2 + 0.25\Omega_S^2\right]^{1/2}.$$

Example 10.19

Determine the mean capacity of a storm sewer pipe, the coefficient of variation of the pipe capacity, and the standard deviation of the pipe capacity using Manning's equation. The parameter values are as shown in Table 10.4.

Solution:

Manning's equation for full pipe flow is $Q = \frac{0.311}{n} S^{1/2} D^{8/3}$; thus, for first-order analysis, we have

$$\bar{Q} = \frac{0.311}{0.015}(0.001)^{1/2}(1.5)^{8/3} = 1.93\,\text{m}^3/\text{s}.$$

Using the results of Example 10.18, it is found that

$$\Omega_Q = [(0.01)^2 + 0.25(0.25)^2]^{1/2} = 0.027.$$

$$\sigma_Q = \bar{Q}\Omega_Q = 1.93(0.027) = 0.052\,\text{m}^3/\text{s}$$

PROBLEMS

1. Calculate the sample mean, sample standard deviation, and sample coefficient of skewness of the annual precipitation data given in Table 10.5.
2. Consider the 100-year flood ($P = 0.01$).
   a. What is the probability that at least one 100-year flood will occur during the 50-year lifetime of a flood control project?
   b. What is the probability that the 200-year flood will not occur in 50 years? In 100 years?
   c. In general, what is the probability of having no floods greater than the T-year flood during a sequence of T years?
3. A cofferdam has been built to protect homes in a floodplain until a major channel project can be completed. The cofferdam was built for the 40-year flood event. The channel project will require 5 years to complete. What are the probabilities that

TABLE 10.5
Annual Precipitation Data for Problem 1

Year	Precipitation (cm)
1970	44.9
1971	41.7
1972	41.6
1973	61.2
1974	49.7
1975	41.2
1976	36.3
1977	46.4
1978	52.1
1979	31

   a. The cofferdam will not be overtopped during the 5 years (the reliability)?
   b. The cofferdam will be overtopped in any one year?
   c. The cofferdam will be overtopped exactly one in 5 years?
   d. The cofferdam will be overtopped at least once in 5 years (the risk)?
   e. The cofferdam will be overtopped only in the third year?
4. During the course of a year, about 150 independent storm events occur in two cities and their average duration is 6.4 h. Ignoring seasonal variations, in a year of 8760 h,
   a. Estimate the average time interval between two storms.
   b. What is the probability that at least 5 days will elapse between storms?
   c. What is the probability that the separation between two storms will be exactly 15 h?
   d. What is the probability that the separation between two storms will be less than or equal to 15 h?
5. Determine the hydrologic risk of a roadway culvert with 25 years expected service life designed to carry a 50-year storm.
6. Construct the CDF of failure occurrences in two hazard rate situations: (1) $\rho(t) = t\alpha$; and (2) $\rho(t) = e^{t-1}$.
7. Calculate the reliability of the system shown in Figure 10.22 at $t = 0.5$ using reliability functions of system components.
8. Calculate the reliability of the system shown in Figure 10.23 at $t = 0.1$ assuming that $R_4(t) = R_5(t) = e^{-3t}$ and $R_1^i(t) = R_2^j(t) = R_3^i(t) = e^{-0.8t} \quad (1 \le i \le 3, 1 \le j \le 2)$.
9. Determine the hydrologic risk of a roadway culvert to be flooded with 50 years expected service life designed to carry a 100-year storm.

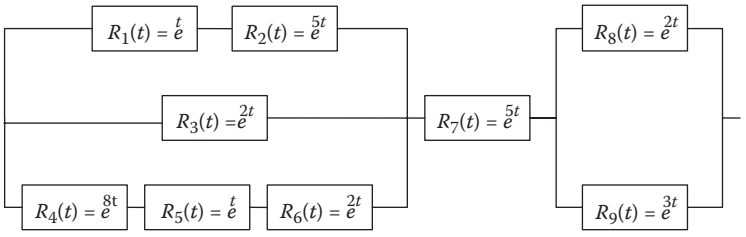

FIGURE 10.22 System in Problem 7.

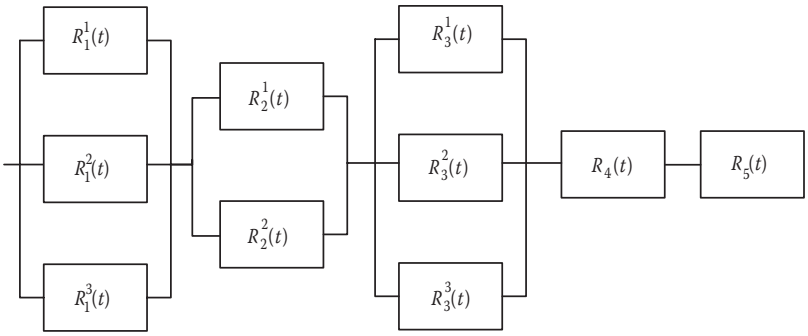

FIGURE 10.23 System in Problem 8.

APPENDIX

TABLE 10.A1(a)
Cumulative Probability of Normal Distribution Probability Content from $-\infty$ to Z

Z^*	0	0.01	0.02	0.03	0.04	0.05	0.06	0.07	0.08	0.09
0	0.5	0.504	0.508	0.512	0.516	0.5199	0.5239	0.5279	0.5319	0.5359
0.1	0.5398	0.5438	0.5478	0.5517	0.5557	0.5596	0.5636	0.5675	0.5714	0.5753
0.2	0.5793	0.5832	0.5871	0.591	0.5948	0.5987	0.6026	0.6064	0.6103	0.6141
0.3	0.6179	0.6217	0.6255	0.6293	0.6331	0.6368	0.6406	0.6443	0.648	0.6517
0.4	0.6554	0.6591	0.6628	0.6664	0.67	0.6736	0.6772	0.6808	0.6844	0.6879
0.5	0.6915	0.695	0.6985	0.7019	0.7054	0.7088	0.7123	0.7157	0.719	0.7224
0.6	0.7257	0.7291	0.7324	0.7357	0.7389	0.7422	0.7454	0.7486	0.7517	0.7549
0.7	0.758	0.7611	0.7642	0.7673	0.7704	0.7734	0.7764	0.7794	0.7823	0.7852
0.8	0.7881	0.791	0.7939	0.7967	0.7995	0.8023	0.8051	0.8078	0.8106	.8133
0.9	0.8159	0.8186	0.8212	0.8238	0.8264	0.8289	0.8315	0.834	0.8365	0.8389
1	0.8413	0.8438	0.8461	0.8485	0.8508	0.8531	0.8554	0.8577	0.8599	0.8621
1.1	0.8643	0.8665	0.8686	0.8708	0.8729	0.8749	0.877	0.879	0.881	0.883
1.2	0.8849	0.8869	0.8888	0.8907	0.8925	0.8944	0.8962	0.898	0.8997	0.9015
1.3	0.9032	0.9049	0.9066	0.9082	0.9099	0.9115	0.9131	0.9147	0.9162	0.9177
1.4	0.9192	0.9207	0.9222	0.9236	0.9251	0.9265	0.9279	0.9292	0.9306	0.9319
1.5	0.9332	0.9345	0.9357	0.937	0.9382	0.9394	0.9406	0.9418	0.9429	0.9441
1.6	0.9452	0.9463	0.9474	0.9484	0.9495	0.9505	0.9515	0.9525	0.9535	0.9545
1.7	0.9554	0.9564	0.9573	0.9582	0.9591	0.9599	0.9608	0.9616	0.9625	0.9633
1.8	0.9641	0.9649	0.9656	0.9664	0.9671	0.9678	0.9686	0.9693	0.9699	0.9706
1.9	0.9713	0.9719	0.9726	0.9732	0.9738	0.9744	0.975	0.9756	0.9761	0.9767
2	0.9772	0.9778	0.9783	0.9788	0.9793	0.9798	0.9803	0.9808	0.9812	0.9817
2.1	0.9821	0.9826	0.983	0.9834	0.9838	0.9842	0.9846	0.985	0.9854	0.9857
2.2	0.9861	0.9864	0.9868	0.9871	0.9875	0.9878	0.9881	0.9884	0.9887	0.989
2.3	0.9893	0.9896	0.9898	0.9901	0.9904	0.9906	0.9909	0.9911	0.9913	0.9916
2.4	0.9918	0.992	0.9922	0.9925	0.9927	0.9929	0.9931	0.9932	0.9934	0.9936
2.5	0.9938	0.994	0.9941	0.9943	0.9945	0.9946	0.9948	0.9949	0.9951	0.9952
2.6	0.9953	0.9955	0.9956	0.9957	0.9959	0.996	0.9961	0.9962	0.9963	0.9964
2.7	0.9965	0.9966	0.9967	0.9968	0.9969	0.997	0.9971	0.9972	0.9973	0.9974
2.8	0.9974	0.9975	0.9976	0.9977	0.9977	0.9978	0.9979	0.9979	0.998	0.9981
2.9	0.9981	0.9982	0.9982	0.9983	0.9984	0.9984	0.9985	0.9985	0.9986	0.9986
3	0.9987	0.9987	0.9987	0.9988	0.9988	0.9989	0.9989	0.9989	0.999	0.999

*Z in this table is considered as it is shown in Figure 10.A1.

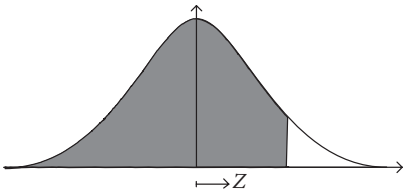

FIGURE 10.A1 The estimation of *Z* in Table 10.A1(a).

TABLE 10.A1(b)
Cumulative Probability of normal distribution Probability content from Z to +∞

Z*	Cumulative Probability	Z	Cumulative Probability	Z	Cumulative Probability	Z	Cumulative Probability
2	0.02275	3	0.00135	4	3.17E-05	5	2.867E-7
2.1	0.01786	3.1	0.000968	4.1	2.07E-05	5.5	1.899E-8
2.2	0.0139	3.2	0.000687	4.2	1.34E-05	6	9.866E-10
2.3	0.01072	3.3	0.000483	4.3	8.54E-06	6.5	4.016E-11
2.4	0.0082	3.4	0.000337	4.4	5.41E-06	7	1.28E-12
2.5	0.00621	3.5	0.000233	4.5	3.4E-06	7.5	3.191E-14
2.6	0.004661	3.6	0.000159	4.6	2.11E-06	8	6.221E-16
2.7	0.003467	3.7	0.000108	4.7	1.3E-06	8.5	9.48E-18
2.8	0.002555	3.8	7.24E-05	4.8	7.933E-7	9	1.129E-19
2.9	0.001866	3.9	4.81E-05	4.9	4.792E-7	9.5	1.049E-21

*Z in this table is considered as it is shown in Figure 10.A2.

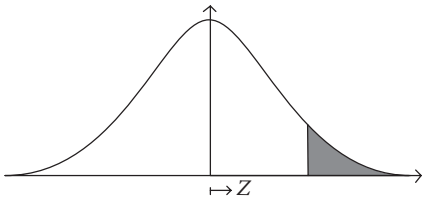

FIGURE 10.A2 The estimation of *Z* in Table 10.A1(b).

TABLE 10.A2
Frequency Factors *K* for Gamma and Log-Pearson Type III Distributions

	Recurrence Interval in Years							
Weighted	**1.0101**	**2**	**5**	**10**	**25**	**50**	**100**	**200**
Skew Coefficient,	**Percent Chance (≥) = 1–*F***							
C_w	**99**	**50**	**20**	**10**	**4**	**2**	**1**	**0.5**
3	–0.667	–0.396	0.42	1.18	2.278	3.152	4.051	4.97
2.9	–0.69	–0.39	0.44	1.195	2.277	3.134	4.013	4.904

(*continued*)

TABLE 10.A2 (Continued)
Frequency Factors *K* for Gamma and Log-Pearson Type III Distributions

	Recurrence Interval in Years							
Weighted	**1.0101**	**2**	**5**	**10**	**25**	**50**	**100**	**200**
Skew Coefficient,	**Percent Chance (≥) = 1–*F***							
C_w	**99**	**50**	**20**	**10**	**4**	**2**	**1**	**0.5**
2.8	–0.714	–0.384	0.46	1.21	2.275	3.114	3.973	4.847
2.7	–0.74	–0.376	0.479	1.224	2.272	3.093	3.932	4.783
2.6	–0.769	–0.368	0.499	1.238	2.267	3.071	3.889	4.718
2.5	–0.799	–0.36	0.518	1.25	2.262	3.048	3.845	4.652
2.4	–0.832	–0.351	0.537	1.262	2.256	3.023	3.8	4.584
2.3	–0.867	–0.341	0.555	1.274	2.248	2.997	3.753	4.515
2.2	–0.905	–0.33	0.574	1.284	2.24	2.97	3.705	4.444
2.1	–0.946	–0.319	0.592	1.294	2.23	2.942	3.656	4.372
2	–0.99	–0.307	0.609	1.302	2.219	2.912	3.605	4.298
1.9	–1.037	–0.294	0.627	1.31	2.207	2.881	3.553	4.223
1.8	–1.087	–0.282	0.643	1.318	2.193	2.848	3.499	4.147
1.7	–1.14	–0.268	0.66	1.324	2.179	2.815	3.444	4.069
1.6	–1.197	–0.254	0.675	1.329	2.163	2.78	3.388	3.99
1.5	–1.256	–0.24	0.69	1.333	2.146	2.743	3.33	3.91
1.4	–1.318	–0.225	0.705	1.337	2.128	2.706	3.271	3.828
1.3	–1.383	–0.21	0.719	1.339	2.108	2.666	3.211	3.745
1.2	–1.449	–0.195	0.732	1.34	2.087	2.626	3.149	3.661
1.1	–1.518	–0.18	0.745	1.341	2.066	2.585	3.087	3.575
1	–1.588	–0.164	0.758	1.34	2.043	2.542	3.022	3.489
0.9	–1.66	–0.148	0.769	1.339	2.018	2.498	2.957	3.401
0.8	–1.733	–0.132	0.78	1.336	1.993	2.453	2.891	3.312
0.7	–1.806	–0.116	0.79	1.333	1.967	2.407	2.824	3.223
0.6	–1.88	–0.099	0.8	1.328	1.939	2.359	2.755	3.132
0.5	–1.955	–0.083	0.808	1.323	1.91	2.311	2.686	3.041
0.4	–2.029	–0.066	0.816	1.317	1.88	2.261	2.615	2.949
0.3	–2.104	–0.05	0.824	1.309	1.849	2.211	2.544	2.856
0.2	–2.178	–0.033	0.83	1.301	1.818	2.159	2.472	2.763
0.1	–2.252	–0.017	0.836	1.292	1.785	2.107	2.4	2.67
0	–2.326	0	0.842	1.282	1.751	2.054	2.326	2.576
–0.1	–2.4	0.017	0.846	1.27	1.716	2	2.252	2.482
–0.2	–2.472	0.033	0.85	1.258	1.68	1.945	2.178	2.388
–0.3	–2.544	0.05	0.853	1.245	1.643	1.89	2.104	2.294
–0.4	–2.615	0.066	0.855	1.231	1.606	1.834	2.029	2.201
–0.5	–2.686	0.083	0.856	1.216	1.567	1.777	1.955	2.108
–0.6	–2.755	0.099	0.857	1.2	1.528	1.72	1.88	2.016
–0.7	–2.824	0.116	0.857	1.183	1.488	1.663	1.806	1.926
–0.8	–2.891	0.132	0.856	1.166	1.448	1.606	1.733	1.837
–0.9	–2.957	0.148	0.854	1.147	1.407	1.549	1.66	1.749
–1	–3.022	0.164	0.852	1.128	1.366	1.492	1.588	1.664
–1.1	–3.087	0.18	0.848	1.107	1.324	1.435	1.518	1.581
–1.2	–3.149	0.195	0.844	1.086	1.282	1.379	1.449	1.501
–1.3	–3.211	0.21	0.838	1.064	1.24	1.324	1.383	1.424
–1.4	–3.271	0.225	0.832	1.041	1.198	1.27	1.318	1.351

(*continued*)

TABLE 10.A2 (Continued)
Frequency Factors *K* for Gamma and Log-Pearson Type III Distributions

	Recurrence Interval in Years							
Weighted	**1.0101**	**2**	**5**	**10**	**25**	**50**	**100**	**200**
Skew Coefficient,	**Percent Chance (≥) = 1–*F***							
C_w	**99**	**50**	**20**	**10**	**4**	**2**	**1**	**0.5**
–1.5	–3.33	0.24	0.825	1.018	1.157	1.217	1.256	1.282
–1.6	–3.88	0.254	0.817	0.994	1.116	1.166	1.197	1.216
–1.7	–3.444	0.268	0.808	0.97	1.075	1.116	1.14	1.155
–1.8	–3.499	0.282	0.799	0.945	1.035	1.069	1.087	1.097
–1.9	–3.553	0.294	0.788	0.92	0.996	1.023	1.037	1.044
–2	–3.605	0.307	0.777	0.895	0.959	0.98	0.99	0.995
–2.1	–3.656	0.319	0.765	0.869	0.923	0.939	0.946	0.949
–2.2	–3.705	0.33	0.752	0.844	0.888	0.9	0.905	0.907
–2.3	–3.753	0.341	0.739	0.819	0.855	0.864	0.867	0.869
–2.4	–3.8	0.351	0.725	0.795	0.823	0.83	0.832	0.833
–2.5	–3.845	0.36	0.711	0.711	0.793	0.798	0.799	0.8
–2.6	–3.899	0.368	0.696	0.747	0.764	0.768	0.769	0.769
–2.7	–3.932	0.376	0.681	0.724	0.738	0.74	0.74	0.741
–2.8	–3.973	0.384	0.666	0.702	0.712	0.714	0.714	0.714
–2.9	–4.013	0.39	0.651	0.681	0.683	0.689	0.69	0.69
–3	–4.051	0.396	0.636	0.66	0.666	0.666	0.667	0.667

REFERENCES

Adger, W.N., Brooks, N., Bentham, G., Agnew, M., Eriksen, S. (2004). New indicators for vulnerability and adaptive capacity. In *Technical Report 7*, Centre, T., ed, Tyndall Centre, Norwich.

Ang, A.H.S. (1973). "Structural risk analysis and reliability based design," *Journal of the Structural Engineering Division. ASCE* 99 (ST9), 1891–1910.

APFM (2008). Urban flood risk management. A tool for integrated flood management version 1, http://www.apfm.info/pdf/ifm_tools/Tools_Urban_Flood_Risk_Management.pdf.

Bossel, H. (1999) Indicators for Sustainable Development: Theory, Method, Applications. A Report to the Balaton Group. International Institute for Sustainable Development, Winnipeg, Canada. http://www.iisd.org/pdf/balatonreport.pdf.

Bras, R.L. (1990). *Hydrology: An Introduction to Hydrologic Science*, Addison-Wesley, Reading, MA.

Brooks, N. (2003). Vulnerability, Risk and Adaptation: A Conceptual Framework. Working Paper 38, Tyndall Centre for Climate Change Research, University of East Anglia, Norwich.

Chow, V.T., Maidment, D.R. and Mays, L.W. (1988). *Applied Hydrology*, McGraw-Hill, New York.

Chowdhary, H., Deng, Z.Q. and Singh, V.P. (2008). Assessing the Effectiveness of Agricultural BMPs Using the Copula Approach. ASCE, World Environmental and Water Resources Congress, Ahupua'a.

Conway, R.A. (1982). "Introduction to environmental risk analysis." In *Environmental Risk Analysis for Chemicals*, Conway, R.A., ed, Van Nostrand Reinhold Company, New York, 1–30.

Crichton, D. (1999). "The risk triangle." In *Natural Disaster Management*, Ingleton, J., ed, Tudor Rose, London, 102–103.

Glossary of the UN International Strategy for Disaster Reduction (2004). http://www.unisdr.org/eng/library/lib-terminology-eng%20home.htm.

Hamouda, M.A.A. 2006. Vulnerability Assessment of Water Resources Systems in the Eastern Nile Basin to Environmental Facors. Master's thesis Cairo University, Institute of African Research and Studies, Department of Natural Resource.

Harmancioglu, N.B., Fistikoglu, O., Ozkul, S.D., Singh, V.P. and Alpaslan, M.N. (1999). *Water Quality Monitoring Network Design*, Kluwer, Boston, MA.

Hashimoto, T., Stedinger, J.R. and Loucks, D.P. (1982). "Reliability, resiliency, and vulnerability criteria for water resources performance evaluation," *Water Resources Research*, 18 (1), 14–20.

Joosten-ten Brinke, D., Sluijsmans, D.M.A., Brand-Gruwel, S. and Jochems, W.M.G. (2008). "The quality of procedures to assess and credit prior learning: Implications for design," *Educational Research Review*, 3, 51–65.

Jørgensen, S.E. and Bendoricchio, G. (2001). *Fundamentals of Ecological Modeling*, Gulf Professional Publishing, Netherlands.

Kapur, K.C. and Lamberson, L.R. (1977). *Reliability in Engineering Design*, Wiley, New York.

Karageorgis, A.P., Skourtos, M.S., Kapsimalis, V., Kontogianni, A.D., Skoulikidis, N.Th., Pagou, K., Nikolaidis, N.P., Drakopoulou, P., Zanou, B., Karamanos, H., Levkov, Z. and Anagnostou, Ch. (2005). An integrated approach to watershed management within the DPSIR framework: Axios River catchment and Thermaikos Gulf. *Regional Environmental Change*, 5, 138–160.

Karamouz, M., Szidarovszky, F. and Zahraie, B. (2003). *Water Resources System Analysis*, Lewis Publishers, CRC Press, Boca Raton, FL.

Karamouz, M., Nokhandan, A.K., Kerachian, R. and Maksimovic, C. (2009). "Design of on-line river water quality monitoring systems using the entropy theory: A case study," *Journal of Environmental Modeling and Assessment*, 155, 63–81.

Krzysztofowicz, R. (2001). "Integrator of uncertainties for probabilistic river stage forecasting: Precipitation dependent model," *Journal of Hydrology*, 249, 69–85.

Lee, W.W. and Nair, K. (1979). Risk Quantification and Risk Evaluation, Proceedings of the National Conference on Hazardous Material Risk Assessment, Disposal and Management, Information Transfer, Inc., Silver Spring, MD, 44–48.

Mays, L.W. (2001). *Water Resources Engineering*, John Wiley and Sons Inc., New York.

McCarthy, J.J., Canziani, O.F., Leary, N.A., Dokken, D.J. and White, K.S. (2001). *Climate Change 2001: Impacts, Adaptation and Vulnerability*, Cambridge University Press, Cambridge.

Meadows, D. (1998). Indicators and Information Systems for Sustainable Development. A Report to the Balaton Group. Hartland Four Corners, USA: The Sustainability Institute.

Mohamed, M.O.S., Neukermans, G., Kairo, J.F., Dahdouh-Guebas, F., and Koedam, N. (2009). Mangrove forests in a peri-urban setting: the case of Mombasa (Kenya). *Wetland Ecology and Management*, 17, 243–255.

Plate, E.J. and Duckstein, L. (1988). "Reliability-based design concepts in hydraulic engineering," *Water Resources Bulletin*, 24 (2), 235–245.

Ramsey, F.L. and Schafer, D.W. (1997). *The Statistical Sleuth: A Course in the Methods of Statistics*, Duxbury Press, Belmont, CA.

Shannon, C.E. (1948). "A mathematical theory of communication, part I," *Bell Systems Technical Journal*, 27, 379–423.

Shannon, C.E. and Weaver, W. (1949). *A Mathematical Model of Communication*, University of Illinois Press, Urbana, IL.

Sklar, A. (1959). "Fonctions de répartition à n dimensions et leurs marges", *Publications de l'Institut de Statistique de l'Université de Paris*, 8, 229–231.

Yen, B.C. (1978). Safety Factor in Hydrologic and Hydraulic Design, Proceedings of the International Symposium on Risk Reliability in Water Resources, University of Waterloo, Waterloo, Ontario, Canada.

Zadeh, L.A. (1965). "Fuzzy sets," *Information Control*, 8, 338–353.

11 Hydrologic Simulation

11.1 INTRODUCTION

For analysis and planning purposes of watersheds, simulation of hydrologic events is needed. Hydrologic simulation models are used to provide a hydrologic prediction/projection as well as better understanding of processes within the hydrologic cycle. A variety of modeling approaches are used for this purpose. These models are a simplified conceptual representation of a part/component of the global water cycle. Different classifications are considered for hydrologic simulation. Two groups of hydrologic models are often defined:

1. Data-driven mathematical models: In these models, mathematical and statistical concepts are used to develop a relationship between model input(s) such as rainfall and temperature and model output such as runoff. The common procedures used in these models are regression, transfer functions, neural networks, fuzzy inference, and system identification. These models can be deterministic or stochastic.
2. Physical (process)-based models: These models attempt to simulate the physical processes that happen in the real world through the hydrological cycle based on identified physical and empirical relationships. Typically, these models include representations of surface/subsurface runoff formation, evapotranspiration, and channel flows/streamflows.

The details considered in these models may become too sophisticated. If simulation models provide unique deterministic outputs for each set of model inputs, they are considered as deterministic models. Based on the above classification of hydrologic simulations, this chapter includes two sections dealing with these hydrologic simulation approaches. In the first part, data-driven mathematical models with emphasis on new data-based models such as artificial neural network (ANN) and fuzzy logic are discussed. In the second section, different types of physical-based hydrologic models of rainfall–runoff including lumped models, semi-distributed models, and distributed models with applications to HEC-HMS (Hydrologic Modeling System), IHACRES (acronym for Identification of unit Hydrographs And Component flows from Rainfall, Evaporation, and Streamflow data), StormNET, and HBV (Hydrologiska Byråns Vattenbalansavdelning) are introduced.

11.2 MATHEMATICAL SIMULATION TECHNIQUES

The basis of the simulation techniques is the mathematical representation of hydrologic systems. Due to the mathematical simplicity and versatility of these techniques, they can be easily employed for analyzing the water cycle systems. Mathematical models, which are also called data-driven models, are used for evaluation of a system performance under a given set of inputs and operating conditions. They can be used for simulating a large number of scenarios. By using the simulation models, very detailed and realistic representation of a complex process/component of the water cycle can be given in the form of mathematical formulations. The concepts inherent in the simulation approach are easier to comprehend and communicate than physical modeling concepts.

Furthermore, simulation methods are able to represent the highly nonlinear processes of the water cycle. The simulation models may deal with steady-state or transient conditions. For example, in order to study the water balance of an urban area over a relatively long period of time during

which no major alterations in the system occur, the steady-state analysis is used. The study of drainage systems that transit floods lies in the area of transient analysis. The simulation models are categorized into two groups, namely, deterministic and stochastic. If the system is subject to random input events, or generates them implicitly, the model is called stochastic. The model is deterministic if no random components are involved. In this chapter, stochastic simulation is discussed first and then deterministic simulation is discussed in the context of ANN, fuzzy set theory, fuzzy inference system, and adaptive neuro-fuzzy inference system (ANFIS) applications.

11.2.1 Stochastic Simulation

Most of the hydrologic systems follow stochastic processes, which results in stochastic variables such as rainfall and runoff. The behavior of stochastic systems is intrinsically nondeterministic and a system's subsequent state is composed of a predictable and a random element. In order to assess the effects of the random elements on the consequences of events, simulation models can be used. The basis for stochastic simulation of the hydrologic system is the generation of independent random numbers that are uniformly distributed. The generated random number cannot be used directly, because most random elements in nature have different distributions. Hence, a transformation method is necessary in order to obtain random values from other than uniform distributions. The common probability distributions are discussed in detail in Chapter 10. The most appropriate probability function for dealing with a specific hydrologic variable is determined by analyzing its historical behavior and using goodness-of-fit tests, some of which were discussed in Chapter 8. Here, some examples are given in this regard.

Example 11.1

The historical data show that the probability of water shortage in a river during a year is 0.01. What is the probability of occurrence of the following events within 50 years? (use the Poisson distribution)

a. Occurrence of two water shortage events
b. Maximum occurrence of two water shortage events

Solution:

In this example, the failure probability (P) is 0.01 and n is 50; thus, the average of the failures is $\lambda = 0.5$.

a. $f(x=2)=\dfrac{0.5^2 e^{-0.5}}{2!}=0.0758$
b. $f(x \le 2) = f(0) + f(1) + f(2) = 0.6065 + 0.3033 + 0.0758 = 0.9856$.

11.2.2 Stochastic Processes

Assume a certain event occurs at random time point $0 \le t_1 < t_2 < \ldots$. These events constitute a *stochastic process*. Most hydrologic events are stochastic processes, whose output cannot be predicted deterministically, and there is always a random component in their output. For instance, during floods, rainfalls, and so on, there is a stochastic process present. To deal with these processes, providing a measure on the range of their output variations is necessary.

The process can be mathematically defined if the distribution functions of t_1, $t_2 - t_1$, $t_3 - t_2$, … is known. A very important characteristic of the stochastic process is the number of events $N(t)$ that

occur in the time interval [0,*t*]. The *Poisson process*, which is defined as follows, is the most frequently used stochastic process as expressed by Karamouz et al. (2003):

1. The number of events are zero at $t = 0$. This illustrates that the process starts at $t = 0$.
2. The number of events occurring in mutually exclusive time intervals is independent, which is called "the independent increment assumption." For example, for time intervals of $0 \leq t_1 < t_2 < t_3 < t_4$, this condition states that the number of events in interval $[t_1,t_2]$ [which is $N(t_2) - N(t_1)$] is independent of the number of events in interval $[t_3,t_4]$, which is $N(t_4) - N(t_3)$.
3. The function of $N(t + s) - N(t)$ is independent of t and is only dependent on s. This means that the distribution of the number of events occurring in any given time interval depends on only the length of the interval and not on its location. This condition is known as the stationary increment assumption.
4. In a small interval of length Δt, the probability that one event occurs is a multiplier of Δt.
5. In a small interval of length Δt, the probability that at least two events take place is approximately zero.

Conditions (4) and (5) can be expressed in mathematical format as follows:

$$\lim_{\Delta t \to 0} \frac{P(N(\Delta t) = 1)}{\Delta t} = \lambda, \tag{11.1}$$

where $\lambda > 0$ is a constant.

$$\lim_{\Delta t \to 0} \frac{P(N(\Delta t) \geq 2)}{\Delta t} = 0. \tag{11.2}$$

Equation 11.3 denotes a Poisson distribution with parameter λt for $N(t)$ based on the above-mentioned assumptions.

$$P(N(t) = k) = \frac{(\lambda t)^k}{k!} e^{-\lambda t}. \tag{11.3}$$

The distribution functions of different time intervals ($X_1 = t_1$, $X_2 = t_2 - t_1$, $X_3 = t_3 - t_2$, …), which can be denoted by F_1, F_2, F_3, …, are as shown in Equation 11.4.

$$F_1(t) = P(t_1 < t) = 1 - P(t_1 \geq t) = 1 - P(N(t) = 0) = 1 - e^{-\lambda t}. \tag{11.4}$$

From Equation 11.4, therefore, X_1 is exponentially distributed with expectation $1/\lambda$.

For all $k \geq 2$ and $s,t \geq 0$, the distribution function of X_k is the same as that of X_1. All variables X_1, X_2, X_3, … are independent of each other and are exponential with the same parameter λ as illustrated in Equation 11.5.

$$\begin{aligned} P(X_k > t | X_{k-1} = s) &= P(0 \text{ event occurs in } (s, s + t) | X_{k-1} = s) = P(0 \text{ event occurs in} \\ &(s, s + t)) = P(0 \text{ event occurs in } (0, t)) = P(N(t) = 0) = e^{-\lambda t}. \end{aligned} \tag{11.5}$$

Different probability distributions were previously discussed in Chapter 10. Here, some examples of their application in hydrologic studies are given.

Example 11.2

A total of 110 storms occur in a region within a year that last 5.3 h on average. Determine the following, regardless of seasonal changes in a year:

a. The probability of a minimum of 4 days between two consequent storms
b. The probability of 12 h (exactly) between two consequent storms
c. The probability of a maximum of 12 h between two consequent storms

Solution:

The mean time of occurrence within a year is

$$\bar{t} = \frac{8760(\text{the hours in a year}) - 110 \times 5.3}{110} = 74.3\,\text{h}.$$

For an exponential test, we have $\lambda = \frac{1}{\bar{t}} = 0.0135\,\text{h}^{-1}$ (the average rate of storming in an hour)

a. Four days is 96 h, thus

$$P(t \geq 96) = 1 - F(96) = e^{-0.0135 \times 96} = 0.27.$$

b. The probability that a particular number is exactly equivalent to a continuous variable is small and almost equal to zero; therefore, $P(t = 12) = 0$.
c. $P(t \leq 12) = F(12) = 1 - e^{-0.0135 \times 12} = 1 - 0.85 = 0.15$.

11.2.3 Markov Processes and Markov Chains

Most of the stochastic hydrologic processes, $X(t)$, follow the Markov process. In this process, the dependency of future values of the process on past values is summarized by the current value. In other words, the future values are considered to be just dependent on current values as follows (for $k > 0$):

$$F_x[X(t+k)|X(t), X(t-1), X(t-2), \ldots] = F_X[X(t+k)|X(t)]. \tag{11.6}$$

Therefore, the current value, which shows the state of the process, is often referred to as the state. This also provides a physical sense when discussing the state or level of an aquifer or reservoir. The Markov chain is a special kind of Markov process, wherein the state $X(t)$ can take on only discrete values. However, in practical studies of the hydrologic cycle, the continuous stochastic processes can also be approximated by Markov chains. This facilitates the development of stochastic simulation models. Here, the basic notation and properties of Markov chains are presented.

Consider a stationary time series of a continuous random variable that would be simulated through Markov chains. This continuous random variable can be approximated by a discrete random variable Q_y, in year y, which takes on values q_i, with unconditional probabilities p_i where

$$\sum_{i=1}^{n} p_i = 1. \tag{11.7}$$

q_i is the representative of the ith state of the Q variable. In most hydrologic cases, the value of Q_{y+1} is dependent on Q_y, whose Markov chain process can be used for its simulation. Developing transition probabilities is the first necessity for applying the Markov chain process. A transition probability is the conditional probability that the next state is q_j, given that the current state is q_i. For a Markov chain, the transition matrix, P, contains all the information necessary to describe the behavior of the system. The matrix elements, p_{ij}, are estimated as follows:

$$p_{ij} = \Pr[Q_{y+1} = q_j | Q_y = q_i]. \tag{11.8}$$

The transition probabilities satisfy the following criteria:

$$\sum_{j=1}^{n} p_{ij} = 1 \quad \text{for all } i, \tag{11.9}$$

where n is the considered state for the simulating variable. If p_i^y show the probability that the system resides in state i in year y, then the probability that $Q_{y+1} = q_j$ is the sum of the probabilities p_i^y; that $Q = q_i$ times the probability p_{ij}:

$$p_j^{y+1} = p_1^y p_{1j} + p_2^y p_{2j} + \ldots + p_y^n p_{nj} = \sum_{i=1}^{n} p_i^y p_{ij}. \tag{11.10}$$

Considering P^y as the row vector of state resident probabilities $(p_1^y, \ldots, p_n^y)$, the above equation can be summarized as follows:

$$p^{(y+1)} = p^{(y)} P. \tag{11.11}$$

To estimate the probabilities of each streamflow state in year $y + 2$, the $p^{(y+1)}$ obtained from Equation 11.11 is used as follows:

$$p^{(y+2)} = p^{(y+1)} P \tag{11.12a}$$

or

$$p^{(y+2)} = p^{(y+1)} P^2. \tag{11.12b}$$

This process can be continued to estimate the probabilities of each possible streamflow state for k next years as follows:

$$p^{(y+k)} = p^{(y)} P^k. \tag{11.13}$$

Example 11.3

The transition matrix, P, for annual streamflow data considering four states (low, normal, high, and very high) is estimated as follows:

Streamflow state, q_j probability in year $y + 1$

Streamflow state, q_i probability in year y		(L)	(N)	(H)	(VH)
	Low (L)	0.4	0.3	0.2	0.1
	Normal (N)	0.2	0.4	0.3	0.1
	High (H)	0.1	0.3	0.4	0.2
	Very high (VH)	0.0	0.2	0.3	0.5

a. Find the probability vectors for nine future years if at the current year the streamflow state is normal.
b. What is the probability of having low flow in the next 2 years considering that the state of the current year is low?

Solution:

a. Since the current streamflow state is given to be normal, the unconditional streamflow probabilities p_i^0 are [0, 1, 0, 0]. Knowing each p_i^y, the probabilities p_j^{y+1} corresponding to each of the four streamflow states can be determined. From the transition matrix, the probabilities p_j^1 are determined as 0.2, 0.4, 0.3, and 0.1 for low, normal, high, and very high states, respectively. For the second year, the probabilities are estimated as

$$p^2 = p^1 P = \begin{bmatrix} 0.2 & 0.4 & 0.3 & 0.1 \end{bmatrix} \begin{bmatrix} 0.4 & 0.3 & 0.2 & 0.1 \\ 0.2 & 0.4 & 0.3 & 0.1 \\ 0.1 & 0.3 & 0.4 & 0.2 \\ 0.0 & 0.2 & 0.3 & 0.5 \end{bmatrix} = \begin{bmatrix} 0.19 & 0.33 & 0.31 & 0.17 \end{bmatrix}.$$

This can also be obtained as follows, with the same results:

$$p^2 = p^0 P^2 = \begin{bmatrix} 0 & 1 & 0 & 0 \end{bmatrix} \begin{bmatrix} 0.4 & 0.3 & 0.2 & 0.1 \\ 0.2 & 0.4 & 0.3 & 0.1 \\ 0.1 & 0.3 & 0.4 & 0.2 \\ 0.0 & 0.2 & 0.3 & 0.5 \end{bmatrix}^2 = \begin{bmatrix} 0.19 & 0.33 & 0.31 & 0.17 \end{bmatrix}.$$

The probability vectors for the next 9 years are tabulated in Table 11.1.

TABLE 11.1
Successive Streamflow Probability Vectors

	Streamflow State Probabilities			
Year	p_1^y	p_2^y	p_3^y	p_4^y
y	0.000	1.000	0.000	0.000
$y+1$	0.200	0.400	0.300	0.100
$y+2$	0.190	0.330	0.310	0.170
$y+3$	0.173	0.316	0.312	0.199
$y+4$	0.163	0.312	0.314	0.211
$y+5$	0.159	0.310	0.315	0.216
$y+6$	0.157	0.309	0.316	0.218
$y+7$	0.156	0.309	0.316	0.219
$y+8$	0.156	0.309	0.316	0.219
$y+9$	0.156	0.309	0.316	0.219

b. From the transition matrix, the probability of having low flow in the next year when the current year has low flow is obtained as 0.4. For the second year of low flow, the probability is estimated as $0.4 \times 0.4 = 0.16$.

As it is obvious from the results of the previous example as time progresses, the probabilities will reach limiting values (last three rows of Table 11.1). These are the unconditional or steady-state probabilities. The quantity p_i has been defined as the unconditional probability of q_i. These are the steady-state probabilities, which $p^{(y+k)}$ approaches for large k. As k becomes larger, Equation 11.10 becomes

$$p_j = \sum_{i=1}^{n} p_i p_{ij}, \tag{11.14}$$

or in vector notation, Equation 11.14 becomes

$$p = pP, \tag{11.15}$$

where p is the row vector of unconditional probabilities (p_1, …, p_n). The steady-state probabilities for any Markov chain can be found by solving Equation 11.14 simultaneously for all but one of the state's j together with the constraint

$$\sum_{i=1}^{n} p_i = 1. \tag{11.16}$$

11.2.4 Monte Carlo Technique

Some hydrologic analyses are based on different scenarios of possible hydroclimatic variables or, in general, random sample generation methods. For generating evaluation points in a more systematic way, adaptive random sampling (ARS) techniques have been developed. The main idea of ARS is that the new generated point around the actual one should improve the objective function; otherwise, it is rejected (Rubinstein 1981). Price (1965) proposed an advanced ARS strategy, which is the controlled random search technique that introduced the concept of an evolving population of feasible points. This concept is the basis of most modern global optimization methods. At each step, a simplex is formed from a sample of the population, which is reformed by reflecting one of its vertices through its centroid.

Monte Carlo simulation techniques are a group of ARS methods. A specific category of Monte Carlo techniques is the multi-start strategy, which consists of running several independent trials of a local search algorithm. In an ideal case, these methods aim at starting the local search once in every region of attraction of local optima that may be identified via clustering analysis (Solomatine 1999). A simple step-by-step procedure for using Monte Carlo simulation to calculate a desired quantity u_k in the e_kth quintile of variable a that has m quintiles is proposed by Fujiwara et al. (1988) as follows:

1. Select the random independent variables to produce a.
2. Generate random numbers and calculate m independent values for a.
3. Label the calculated values of a as $Y_1, Y_2, \ldots Y_m$ and sort them in ascending order $Y_1 \le Y_2 \le \ldots \le Y_m$.
4. Determine Y_i where i is the first $i > m \cdot e_k$. Y_i is the e_kth quintile of a_k.
5. Let $Z_1 = Y_i$ and replicate the above procedure to determine $Z_2, \ldots, Z_N$.

6. Calculate the mean and variance of sample Z_i as follows:

$$\bar{Z}_N = \frac{\sum_{j=1}^{N} Z_j}{N} \tag{11.17}$$

$$S_N^2 = \frac{\sum_{j=1}^{N} \left(Z_j - \bar{Z}_N\right)^2}{(N-1)}. \tag{11.18}$$

7. Calculate the relative precision (*RP*) using Equation 11.18.

$$RP = \frac{\delta(N,\alpha)}{\bar{Z}_N}. \tag{11.19}$$

$\delta(N,\alpha)$ is calculated using Equation 11.20.

$$\delta(N,\alpha) = t_{N-1,1-\frac{\alpha}{2}} \cdot \left(S_N^2 \Big/ N\right), \tag{11.20}$$

where $t_{N-1,1-\frac{\alpha}{2}}$ is the $(1 - \alpha/2)$ quintile of t distribution with $N - 1$ degree of freedom.

8. The Monte Carlo simulation terminates when the relative precision becomes less than a given value $\beta(0 < \beta < 1)$, and the desired quintile u_k is $\bar{Z}_N$; otherwise, N is increased until the desired precision is reached.

Example 11.4

Use the Monte Carlo technique for a flood control simulation. Use the random number of a uniform distribution. The value of *U* (random number from uniform distribution) is transformed into a value of *x* as follows:

$$\begin{cases} x = a + \sqrt{(b-a)(c-a)U} & \text{for } 0 \le U \le \dfrac{b-a}{c-a} \\ x = c - \sqrt{(c-b)(c-a)(1-U)} & \text{for } \dfrac{b-a}{c-a} \le U \le 1 \end{cases},$$

where *x* is the value of benefit and *a*($) = 10,000, *b*($) = 20,000, and *c*($) = 50,000. The value of cost for flood control is obtained by a similar procedure and *a*($) = 8000, *b*($) = 15,000, and *c*($) = 40,000. Similarly, a value of benefit and a value of cost are obtained for each of the proposed projects. Determine the expected value of *B*/*C* for the project.

TABLE 11.2
Loss and Benefit Calculations for Random Numbers Generated Using Monte Carlo Method

Series Number	1	2	3	4	5	6	7	8	9	10
U	0.505	0.322	0.143	0.95	0.234	0.751	0.589	0.339	0.521	0.295
B	25,628.5	21,478.3	17,571.9	42,260.3	19,679.6	32,703.2	27,797.5	21,835.8	26,023.2	20,919.9
C	380,100.8	376,712.7	13,666.3	393,680.6	375,249	385,877.2	381,871.7	377,004	380,423	376,256.2
B/C	0.067	0.057	1.286	0.0107	0.052	0.085	0.073	0.058	0.068	0.056
Series Number	**11**	**12**	**13**	**14**	**15**	**16**	**17**	**18**	**19**	**20**
U	0.126	0.244	0.531	0.353	0.119	0.994	0.169	0.755	0.3	0.366
B	17,105.2	19,875.4	26,272.5	22,133	16,907	47,417.4	18,226.8	32,857.4	21,020.9	22,416.5
C	13,317	375,404.2	380,626.6	377,246.7	13,168.7	397,891.4	14,156.4	386,003.1	376,338.6	377,478.1
B/C	1.284	0.053	0.069	0.059	1.284	0.119	1.288	0.085	0.056	0.059

Solution:

The value of U is drawn from a table of random numbers and gives a value of x as follows for example when U is equal to 0.20:

$$\begin{cases} x = 10{,}000 + \sqrt{(10{,}000)(40{,}000)U} & \text{for } 0 \le U \le 0.25 \\ x = 50{,}000 - \sqrt{(30{,}000)(40{,}000)(1-U)} & \text{for } 0.25 \le U \le 1 \end{cases} \rightarrow \text{ if } \quad U = 0.2, \text{ then } \quad x(\$) = 18{,}945.$$

The same procedure would be repeated for all benefit values, and these are summarized for total project benefits and the same for value of total project cost. By repeating the same process for 20 times, the outcomes from a probability distribution are obtained and a mean and standard deviation are calculated (Table 11.2).

Based on the obtained values in Table 11.2, the mean and standard deviation of the *B/C* values are calculated as 0.31 and 0.5, respectively. The coefficient of variation (the result of division of standard deviation to mean) is also equal to 0.25 for this example. This value reflects too much uncertainty or may be within the acceptable limit of the evaluating agency. A second interpretation is based on confidence limits. For example, for a 95% confidence interval based on a normal distribution of errors (where Z is determined to be equal to 1.96 from a normal probability table), *B/C* will be in the range of

$$B/C = 0.31 \pm 1.96 \times 0.5 = 0.31 \pm 0.98.$$

Thus, 0 (because *B/C* cannot be less than zero) ≤ *B/C* < 1.19. Therefore, with 95% confidence, *B/C* would fall within the range indicated.

11.2.5 Artificial Neural Networks

ANNs are a widely used type of data-driven models. ANNs provide a convenient means of either (1) simulating a system for which there is a large data set, but no known mathematical model exists, or (2) simplifying an excessively complex model. ANNs are global nonlinear function approximates and are powerful and easy to use (StatSoft 2002). ANNs have a high potential to be used as an alternative modeling tool in practical hydrology. The robustness of ANNs in modeling different complicated hydrologic processes has been proven in recent investigations. ANNs have been successfully employed in modeling precipitation, rainfall–runoff, surface flows, groundwater, and water quality in surface water and groundwater resources. To develop an efficient network, having a good physical understanding of the hydrologic process being modeled is necessary.

However, the performance and development of ANNs are very data dependent, and there is no established methodology for their successful design and implementation. To make ANN useful in practice, some important aspects should be further studied, such as providing a physical interpretation for ANN architecture, learning algorithm, optimal training set of ANN, and extrapolation capability.

ANN emulates the structure of biological neural networks by distributing the computation to small and simple processing units, called artificial neurons, or nodes. A simple neural network is shown in Figure 11.1. In ANNs, neurons receive a number of inputs from either the original data or other neurons. Each connection to a given neuron has a particular weight, which could get positive or negative values. A layer can be seen as a group of neurons with similar characteristics, which are connected to other layers or the external environment, which have no interconnections. There are basically three types of layers. The first layer connecting to the input variables is called the input layer. The network illustrated in Figure 11.1 includes R neurons (R inputs) in the input layer. The last layer connecting to the output variables is called the output layer. In an example of ANN

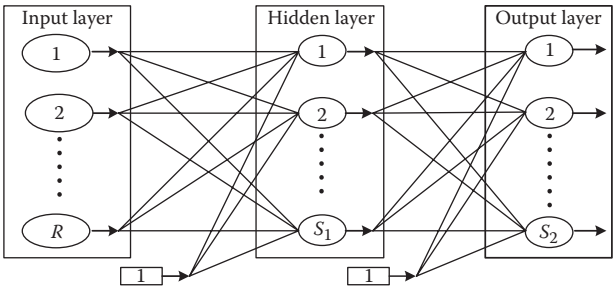

FIGURE 11.1 Simple neural network.

in Figure 11.1, the output layer includes S_2 neurons. Layers between the input and output layers are called hidden layers; there can be more than one hidden layer. For more flexibility in model formulation, the hidden layers are introduced in the middle and its nodes correspond to the hidden or artificial variables. The given ANN in Figure 11.1 has one hidden layer with S_1 neurons.

Let z_j denote the artificial variables corresponding to the jth neuron of a hidden layer. In the case of linear neural networks, this variable is calculated as follows:

$$z_j = \sum_{i=1}^{m} w_{ij} x_i, \tag{11.21}$$

where m is the number of input variables. The coefficients w_{ij} are constants, which are determined by the training procedure to be explained later. The relations between the output and hidden variables are also linear:

$$y_k = \sum_{j=1}^{l} \bar{w}_{jk} z_j, \tag{11.22}$$

where l is the number of hidden variables. The coefficients $\bar{w}_{jk}$ are also estimated by the training process. If more than one hidden layer is used, similar relations to Equations 11.21 and 11.22 are assumed between the variables of the consecutive hidden layers. In the case of nonlinear neural network relations (transfer functions), Equations 11.21 and 11.22 have certain nonlinear elements that are determined by the training process. Transfer functions are divided below into four categories including step-like functions, radial and sigmoidal functions, multivariate functions with independent parameters for each dimension, and finally the most flexible transfer functions such as universal transfer functions. Here, some common transfer functions are introduced.

The hard-limit transfer function shown in Figure 11.2 limits the output of the neuron (a) to either 0, if the input of neuron, n, is less than 0; or 1, if n is greater than or equal to 0. This function is used to create neurons that make classification decisions (Demuth and Beale 2002).

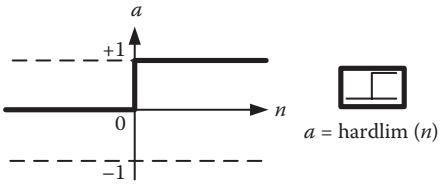

FIGURE 11.2 Hard-limit transfer function.

The linear transfer function is shown in Figure 11.3. Neurons of this type are used as a linear approximate and/or also employed in the output layer. The log-sigmoid transfer function depicted in Figure 11.4 takes the input, which may have any value between plus and minus infinity, and gives an output in the range of 0 to 1. This transfer function is commonly used in back-propagation networks, in part because it is differentiable (Demuth and Beale 2002). The tan-sigmoid transfer function is similar to the log-sigmoid transfer function but its output is in the range of –1 to 1.

ANNs can be trained using back-propagation algorithm (BPA) during supervised learning. The BPA provides a way to calculate the gradient of the error function efficiently using the chain rule of differentiation. In this algorithm, network weights are moved along the negative of the gradient of the performance function. The term *back propagation* refers to the manner in which the gradient is computed for nonlinear multilayer networks. There are several performance functions that may be selected to evaluate network performance, such as root-mean-square error (RMSE), mean absolute error (MAE), and sum square error (SSE), which are calculated as follows:

$$\text{RMSE} = \sqrt{\frac{\sum_{k=1}^{S_2} (a_k^2 - T_k)^2}{S_2}} \tag{11.23}$$

$$\text{MAE} = \frac{\sum_{k=1}^{S_2} | a_k^2 - T_k |}{S_2} \tag{11.24}$$

$$\text{SSE} = \sum_{k=1}^{S_2} (a_k^2 - T_k)^2, \tag{11.25}$$

where a_k^2 is the output of kth neuron of the output layer, T_k is its corresponding target, and S_2 is the number of neurons in the output layer.

There are varieties of ANNs that are developed with different characteristics for different applications. In one approach, ANNs are static or temporal. In static ANNs, the information is transmitted

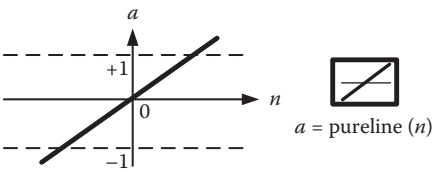

FIGURE 11.3 Linear transfer function.

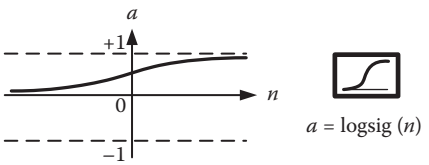

FIGURE 11.4 Log-sigmoid transfer function.

through the connections between its forward neurons only and the network has no feedback that covers its initial and past states.

Static networks only process input patterns that are spatial in nature, i.e., input patterns that can be arranged along one or more spatial axes such as a vector or an array. In many tasks, the input pattern comprises one or more temporal signals, as in speech recognition, time series prediction, and signal filtering (Bose and Liang 1996). Time delay operators, recurrent connections, and the hybrid method are different approaches that are used to design temporal neural networks.

In temporal neural networks, the feedback from past information can be provided through tapped delay lines (TDLs). TDLs help networks to process dynamically through the flexibility in considering a sequential input. TDLs are a combination of time delay operators in a sequential order. The architecture of the TDL is shown in Figure 11.5. It includes a buffer containing the N most recent inputs generated by a delay unit operator D. Given an input variable $p(t)$, D operating on $p(t)$ yields its past values $p(t-1)$, $p(t-2)$, ..., $p(t-N)$, where N is the TDL memory length. Thus, the output of the TDL is an $(N+1)$-dimensional vector including the input signal at the current time and the previous input signals.

11.2.5.1 Multilayer Perceptron Network (Static Network)

Multilayer perceptron (MLP), also called feed forward network, implements mappings from the input pattern space to the output space. Once the network weights are fixed, the states of the units are totally determined by inputs independent of initial and past states of the units. MLP is a static network. MLP can be trained with the standard BPA. Figure 11.1 shows a typical three-layer MLP, which, mathematically, can be expressed in the following formulations:

$$a_j^1(t) = F\left(\sum_{i=1}^{R} w_{j,i}^1 p_i(t) + b_j^1\right) \quad 1 \le j \le S_1 \tag{11.26}$$

$$a_k^2(t) = G\left(\sum_{j=1}^{S_1} w_{k,j}^2 a_j^1(t) + b_k^2\right) \quad 1 \le k \le S_2, \tag{11.27}$$

where t denotes a discrete time, R is the number of input signals, and S_1 and S_2 are the numbers of hidden and output neurons, respectively. w^1 and w^2 are the weight matrices of hidden and output layers. b^1 and b^2 are the bias vectors of hidden and output layers. p is the input matrix and a^1 and a^2 are the output vectors of the hidden and output layers. F and G are the activation functions of the hidden and output layers, respectively (Karamouz et al. 2007).

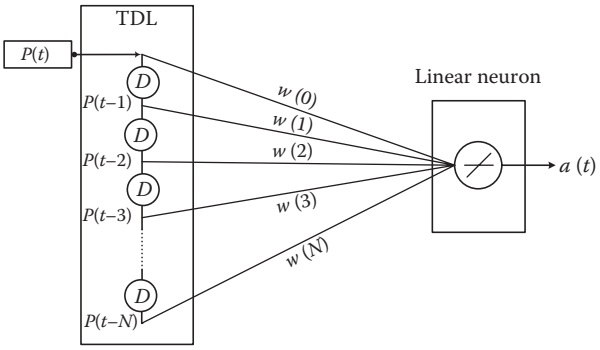

FIGURE 11.5 Architecture of the TDL.

Example 11.5

The studies in a reservoir have shown that the water inflow is a function of three climatic variables including precipitation, evaporation, and average temperature. The daily data of water inflow, daily rainfall, evaporation, and temperature of this dam are given in Table 11.3. Studies have also demonstrated that the relation of water inflow with these parameters is complicated and could not be formulated in regular form. Develop an MLP model to simulate the daily water inflow of this dam as a function of daily precipitation, evaporation, and temperature.

Solution:

The input data of the MLP model should be completely random. For simulating daily water inflow, a three-layer neural network with three neurons in the hidden layer and logsig transit functions in the hidden and output layers is employed, where the matrix *P* is the input data, *T* is the

TABLE 11.3
Data of Daily Inflow, Precipitation, Temperature, and Evaporation in Example 11.5

Day No.	Inflow (MCM)	Evaporation (mm)	Temperature (°C)	Rainfall (mm)	Day No.	Inflow (MCM)	Evaporation (mm)	Temperature (°C)	Rainfall (mm)
1	0.373	3.5	15.1	0	31	0.567	0	4.7	6
2	0.374	3.5	14.2	0	32	0.52	0	5	0
3	0.371	2.3	14.9	10	33	0.577	0	5.6	0
4	0.39	1.6	8.7	2.5	34	0.588	0	8.6	0
5	0.392	1.7	12.1	3.5	35	0.566	0	6.3	0
6	0.479	2.5	13.3	2.5	36	0.577	0	9.4	0
7	0.468	3.9	13.5	0	37	0.632	0	9.3	1.5
8	0.279	2.2	10.3	0	38	0.631	0	6.2	0
9	0.278	2.2	9.1	0	39	0.697	0	3.9	9.5
10	0.284	1.7	11.2	0	40	0.647	0	5	4.3
11	0.284	3.1	11.6	0	41	0.59	0	6.1	0
12	0.289	1.3	13.7	0	42	0.648	0	3.6	5
13	0.262	3.1	15.7	0	43	0.589	0	4.6	11
14	0.26	3.5	15.7	0	44	0.558	0	6.5	0
15	0.265	2.2	13.2	1.7	45	0.577	0	6.6	0
16	0.279	2.2	11	2.2	46	0.575	0	5.8	0.5
17	0.28	2.6	13.2	0	47	0.521	0	7.7	0
18	0.276	3.1	13.8	0	48	0.529	0	8.6	0
19	0.298	2.6	11.8	0	49	0.605	0	5.3	1
20	0.375	2.3	9.3	8	50	0.604	0	6	2.5
21	0.376	1.9	8.6	4.3	51	0.766	0	5.6	0
22	0.39	2.2	10.2	0	52	0.766	0	6.7	0
23	0.396	2.6	12.2	0	53	0.61	0	7.1	6.5
24	0.38	2.2	12.4	0	54	0.611	0	7.4	1
25	0.346	1.3	8.6	0	55	0.52	0	4.6	0
26	0.977	0.2	6.8	26	56	0.42	0	5.7	0
27	0.81	0	1	23	57	0.698	0	5.8	3
28	0.72	0	0.3	0	58	0.702	0	7.3	0.8
29	0.562	0	4	0	59	0.696	0	5.9	0
30	0.512	0	6.9	0					

observed inflow, and *Y* is the simulated matrix of inflow with MLP. The coding used in MATLAB® environment for developing MLP is as follows:

```
net = newff (P,T,[3 3]);

Y = sim (net,P);
```

The simulated and recorded daily inflow data are compared in Figure 11.6. As can be seen, the model has well simulated the inflow variations even though there are some periods of underestimation and overestimations. This makes model results unreliable.

11.2.5.2 Recurrent Neural Network

Recurrent neural network (RNN) is a nonlinear dynamic system. In RNN involving dynamic behavior, dependence of the initial and past states and serial processing on cyclic connections is described by directed loops in the network graph (Bose and Liang 1996). The main difference between RNN and MLP is that the outputs of RNN recur either from the output layer or the hidden layer back to its input layer. A common type of an RNN model is Elman RNN (Elman 1990), which has feedback connections from the hidden layer to the input layer as shown in Figure 11.7.

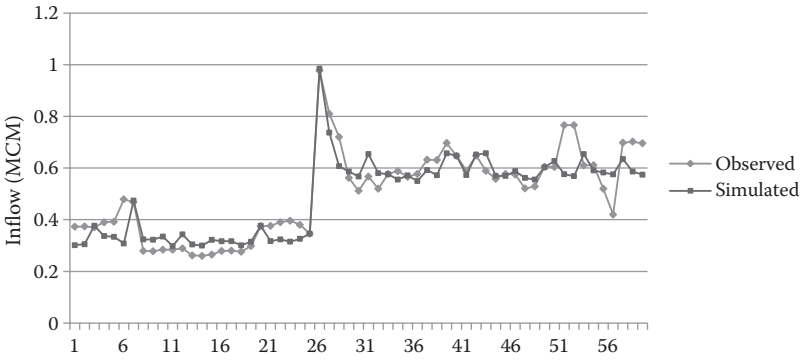

FIGURE 11.6 Comparison between the daily simulated inflow with MLP and the observed data.

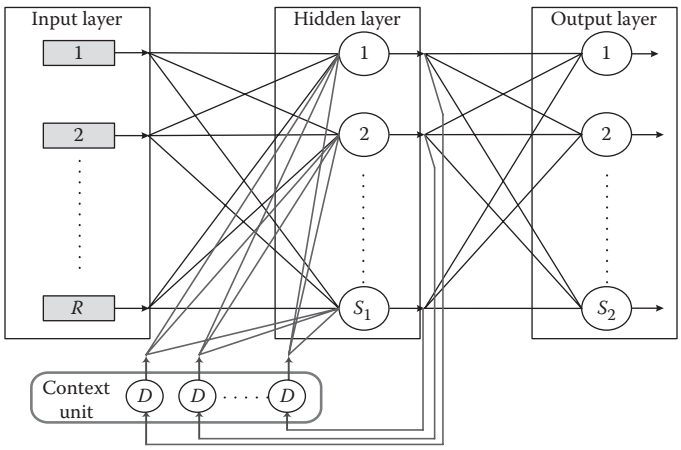

FIGURE 11.7 Elman RNN model structure (the context unit is a TDL memory of neurons in the hidden layer).

The network employs its output signals from the hidden layer to train the networks. The input layer is divided into two parts: the true input units and the context unit, which are a TDL memory of S_1 neurons from the hidden layer. Elman RNN formulation is as follows:

$$a_j^1(t) = F\left(\sum_{i=1}^{R} w_{j,i}^1 p_i(t) + \sum_{c=1}^{S_1} w_{j,c}^C a_c^1(t-1) + b_j^1\right) 1 \le j \le S_1 \tag{11.28}$$

$$a_k^2(t) = G\left(\sum_{j=1}^{S_1} w_{k,j}^2 a_j^1(t) + b_k^2\right) 1 \le k \le S_2, \tag{11.29}$$

where t denotes a discrete time, R is the number of input signals, and S_1 and S_2 are the numbers of hidden neurons and output neurons, respectively. w^1 and w^C are the weight matrices of the hidden layer for real inputs and context unit. w^2 is the output layer weight matrix. b^1 and b^2 are the bias vectors of the hidden and output layers. p is the input matrix and a^1 and a^2 are the output vectors of the hidden and output layers. F and G are the activation functions of the hidden and output layers, respectively.

11.2.5.3 Input-Delayed Neural Network

In many tasks, the input pattern comprises one or more temporal signals, as in hydrological time series prediction (Bose and Liang 1996). A simple, commonly used method converts the temporal signal at the input into a spatial pattern by using a TDL, which provides the signal values at different time instants. This model is called input-delayed neural network (IDNN). An IDNN is a dynamic network and its memory makes it capable of processing the temporal relationship of input sequences such as prediction of a temporal pattern. IDNN consists of a static network (in this case, an MLP), wherein some TDLs are attached to its input layer (Coulibaly et al. 2001). Figure 11.8 shows a generic IDNN in which each input variable is delayed several time steps and fully connected to the hidden layer. This model can combine RNN with IDNN to form the IDRNN model as shown in Figure 11.8. A major feature of this architecture is that the nonlinear hidden layer receives the contents of both the input time delays and the context unit.

The output of IDNN is given by

$$a_j^1(t) = F\left(\sum_{d=0}^{D}\sum_{i=1}^{R} w_{j,i,d}^1 p_{i,d+1}(t) + b_j^1\right) \quad 1 \le j \le S_1 \tag{11.30}$$

$$a_k^2(t) = G\left(\sum_{j=1}^{S_1} w_{k,j}^2 a_j^1(t) + b_k^2\right) \quad 1 \le k \le S_2 \tag{11.31}$$

where t denotes a discrete time, D is the time delay memory order, R is the number of input signals, and S_1 and S_2 are the numbers of hidden neurons and output neurons, respectively. w^1 and w^2 are the weight matrices of the hidden and output layers. b^1 and b^2 are the bias vectors of the hidden and output layers. p is the input matrix, and a^1 and a^2 are the output vectors of the hidden and output layers. F and G are the activation functions of the hidden and output layers, respectively.

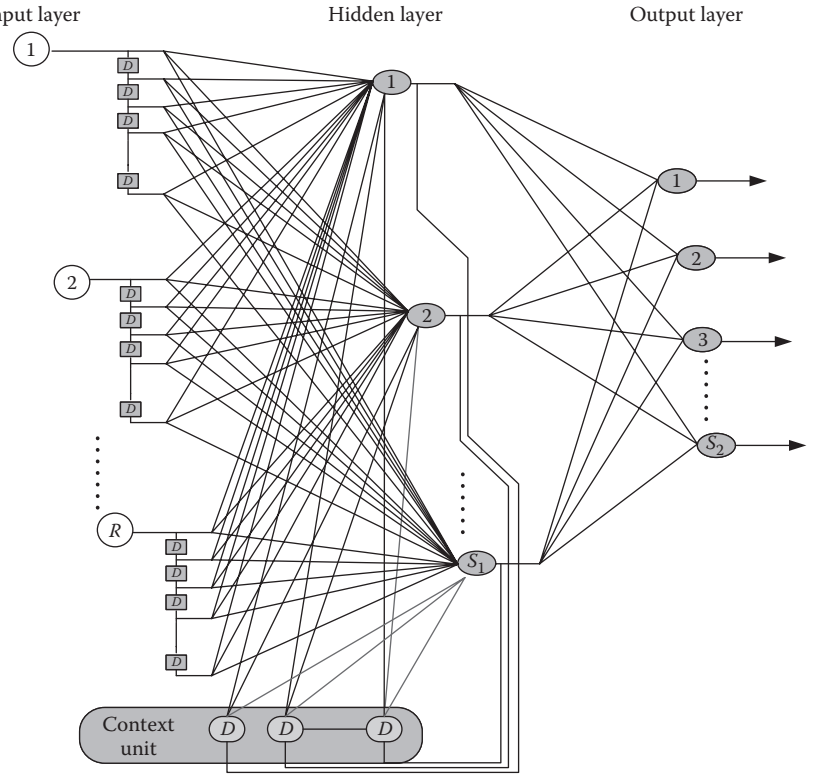

FIGURE 11.8 Generic IDNN (without recurrent connections) and typical IDRNN (with recurrent connections).

Example 11.6

For the reservoir of Example 11.5, simulate the water inflow using the IDNN model.

Solution:

The TDL memory of the developed model is 2, and there are 8 neurons in its hidden layer. The transit function of hidden and output layers are tansig and linear, respectively. The coding used in MATLAB environment for IDNN development is as follows:

net = newfftd (*P*,*T*,[0 1 2], [8 1], ("tansig");

Y = sim (net,*P*);

The simulated and recorded monthly consumption data are compared in Figure 11.9. As can be seen, the results are much better than the MLP model application, which was given in the previous example. The maximum error in estimation belongs to the periods of low flow, whose model overestimates the runoff volume.

11.2.5.4 Time Delay Neural Network

A more general form of IDNNs is obtained by replacing the internal connection weights in the network by TDL (Waibel et al. 1989; Atiya and Parlos 1992; Wan 1993). The resulting network is called time delay neural network (TDNN) or spatiotemporal network. A schematic representation

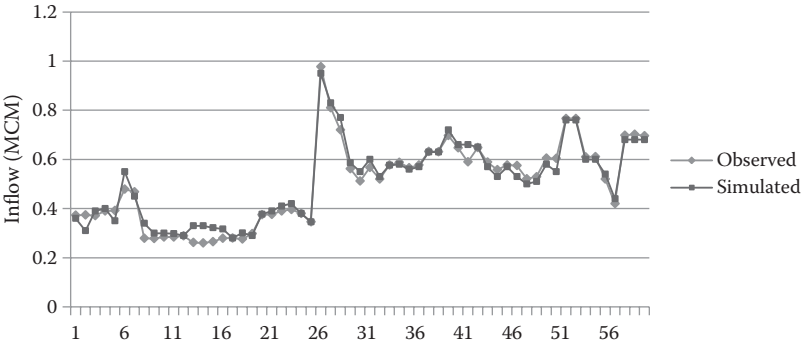

FIGURE 11.9 Comparison between the daily simulated inflow with IDNN and the observed data.

of the network is shown in Figure 11.10. To model this network, three-dimensional weight matrices should be considered for each layer, the third dimensions of which are provided to represent temporal patterns.

In TDNN, the input vectors of each layer turn to two-dimensional matrices, whose second dimension represents discrete time. During the system modeling process, after each time step, columns of the input matrix are shifted once and the instant input signals are substituted for the first column of the input matrix. Simultaneously, the instant outputs of each layer are substituted for the first column of the input matrix of the next layer. A three-layer TDNN can be described by the following equations:

$$a^1_{j,0}(t) = F\left(\sum_{d_1=0}^{D_1}\sum_{i=1}^{R} w^1_{j,i,d_1} p_{i,d_1+1}(t) + b^1_j\right) \quad 1 \le j \le S_1 \tag{11.32}$$

$$a^2_k(t) = G\left(\sum_{d_2=0}^{D_2}\sum_{j=1}^{S_1} w^2_{k,j,d_2} a^1_{j,d_2}(t) + b^2_k\right) \quad 1 \le k \le S_2, \tag{11.33}$$

where t denotes a discrete time, D_1 and D_2 are the time delay memory order of the input and hidden layers, R is the number of input signals, and S_1 and S_2 are the numbers of hidden neurons and output neurons, respectively. w^1 and w^2 are the weight matrices of the hidden and output layers. b^1 and b^2 are the bias vectors of the hidden and output layers. p is the input matrix, and a^1 and a^2 are the output vectors of the hidden and output layers. F and G are the activation functions of the hidden and output layers, respectively. The TDNN output layer can be trained with the standard BPA. However, the instant error signal is only back propagated through the current time route of each layer to train their previous layers (Clouse 1997).

For improving the performance of TDNN, they are coupled with RNN and a new model of TRNN is formed. Consequently, the TDRNN has both static and adaptive memory, which makes it suitable for complex sequential input learning (Coulibaly et al. 2001). The TDRNN output layer can be trained with the standard BPA. However, the instant error signal is only back propagated through the current time route of each layer to train their previous layers.

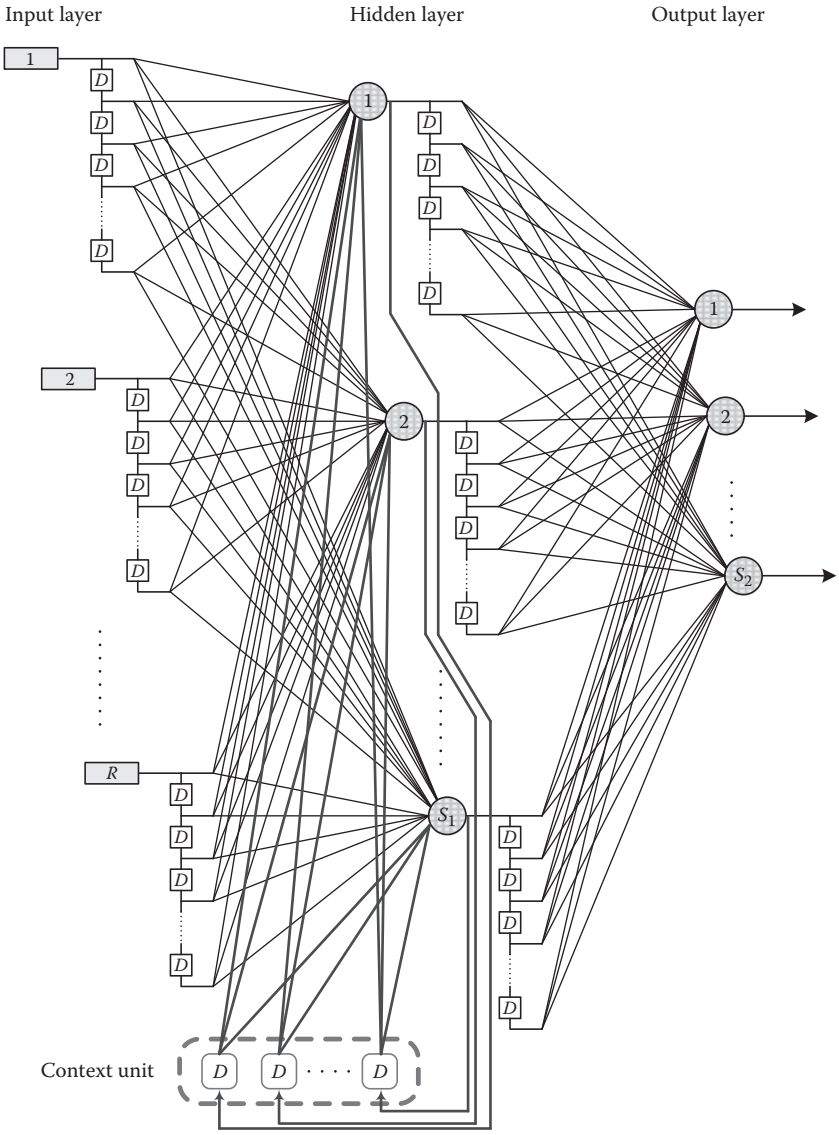

FIGURE 11.10 Generic TDNN (without recurrent connections) and typical TDRNN (with recurrent connections).

Example 11.7

For the reservoir in Example 11.5, simulate the water inflow using the TDNN model.

Solution:

The problem consists of input data *P* and target data *T*, solved here by a one-delay network. A network is created with one hidden layer of five neurons. Then, the network is simulated in matrix *Y* and the coding used in MATLAB environment for TDNN model development is as follows:

net = newdtdnn (*P*,*T*,5, ([0 1] [0 1]);

Y = sim (net,*P*);

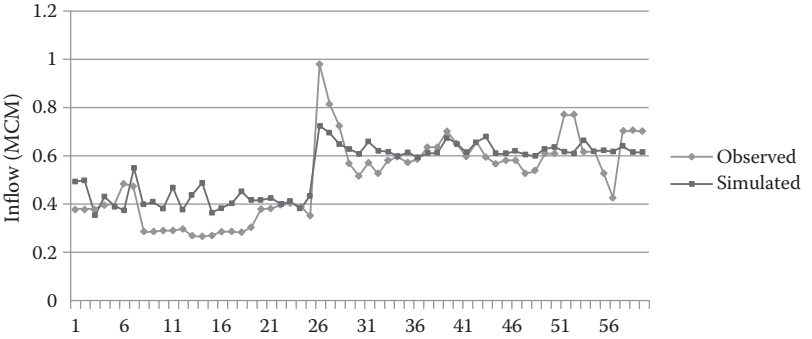

FIGURE 11.11 Comparison between the daily simulated inflow with TDNN and the observed data.

The simulated and recorded monthly consumption data are compared in Figure 11.11. The model performance is not acceptable either in inflow variation simulation or in the estimation of its value. The model outputs are smooth and do not follow the observed behavior of the inflow.

11.2.5.5 General Regression Neural Network

General regression neural network (GRNN), which was developed by Specht (1991), is a probabilistic neural network. The probabilistic neural networks need far fewer training samples in comparison with the back-propagation neural networks. Therefore, especially in cases where only few training samples are available to be used for model development, the use of a probabilistic neural network is advantageous due to its ability to converge to the underlying function of the data. The needed data for model training are relatively small; therefore, GRNN is a useful tool in engineering practices.

The probability density function used in GRNN is the normal distribution. Each training sample, X_i, is used as the mean of a normal distribution.

$$Y(X) = \frac{\sum_{i=1}^{n} Y_i \exp\left(-D_i^2 \Big/ 2\sigma^2\right)}{\sum_{i=1}^{n} \exp\left(-D_i^2 \Big/ 2\sigma^2\right)}, \tag{11.34}$$

where $D_i^2 = (X - X_i)^T \cdot (X - X_i)$, X is the predicted output, and σ is the smoothness parameter, which is arbitrarily chosen. The signals of the pattern neuron i, going into the denominator neuron, are weighted with the corresponding values of the training samples, Y_i. The distance, D_i, between the trained and predicted values, is considered as a measure of how well the model can represent the position of X. For small values of the distance, D_i, between the training sample and the point of prediction, $\exp\left(-D_i^2/2\sigma^2\right)$ becomes big. For $D_i = 0$, $\exp\left(-D_i^2/2\sigma^2\right)$ becomes 1 and the point of evaluation is represented best by this training sample. Therefore, the distance to all the other training samples would be more. A bigger distance, D_i, causes the term $\exp\left(-D_i^2/2\sigma^2\right)$ to become smaller and therefore the contribution of the other training samples to the prediction is relatively small. Using Equation 11.34, it is possible to

- Predict the behavior of systems based on few training data
- Predict smooth multi-dimensional curves
- Interpolate between training samples

Example 11.8

For the reservoir of Example 11.5, simulate the water inflow using the GRNN model. Moreover, discuss the results and simulation error of various ANNs developed in Examples 11.5 through 11.8.

Solution:

Bigger spreads will result in smoother function approximation. Therefore, for better data fit, a spread smaller than the typical distance between input vectors should be used. In this example, the spread of the model has been considered to be 1.0. The command line used for development of GRNN in MATLAB environment is as follows:

net = newgrnn (*P*,*T*);

Y = sim (net,*P*);

The simulated and recorded monthly consumption data are compared in Figure 11.12. The model has well simulated the inflow variations through time but there are some periods of underestimation and overestimation, which make it difficult to rely on model results.

The measure of RMSE is used to compare the results of the ANN models developed in this and the three previous examples. The results are shown in Table 11.4.

It is obvious from Table 11.4 that the IDNN model is the best model in predicting runoff in this example.

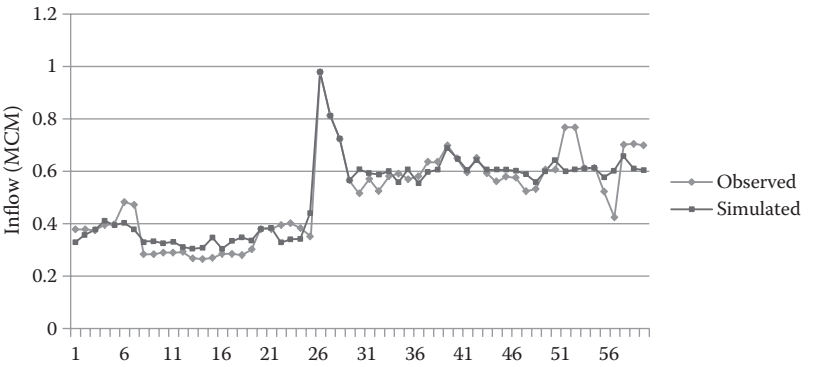

FIGURE 11.12 Comparison between the daily simulated inflow with GRNN and the observed data.

TABLE 11.4
Comparison of Different ANN Models' Performance in Inflow Prediction

ANN Model	MLP	IDNN	TDNN	GRNN
RMSE	0.0676	0.0203	0.112	0.0583

11.2.5.6 Probabilistic Neural Network

As an alternative, probabilistic neural network (PNN) models, due to their probabilistic nature and simplicity in their application, can be an efficient tool in the classification of common states of variables into specified groups such as classification of system preparedness situation. PNN is based on a Bayesian rule and has been used for functional approximation in time series modeling and in pattern classification. PNN models can generalize the results and can estimate anomalies. The architecture of a PNN model for classifying input pattern X into two categories is shown in Figure 11.13.

There are four units in a PNN structure, namely, input, pattern, summation, and output layers. An input vector $X = (x_1, \ldots, x_P)^T$ is applied to the n neurons in the input layer and is passed to the pattern layer. In this layer, the neurons are divided into k groups equal to the output classes. The output of the ith neuron in the kth group of pattern layer is calculated using a Gaussian kernel as follows:

$$F_{k,t}(X) = \frac{1}{(2\pi\sigma^2)^{n/2}} \exp\left(-\frac{\| X - X_{k,t} \|^2}{2\sigma^2} \right), \tag{11.35}$$

where $X_{k,t} \in R^P$ is the mean and σ is the spread of the kernel function. The summation layer of the network computes the approximation of the conditional class probability functions, $G_k(X)$, through a combination of the previously observed densities as follows:

$$G_k(X) = \sum_{t=1}^{M_k} \omega_{k,t} F_{k,t}(X), \quad k \in \{1, \ldots, K\}, \tag{11.36}$$

where M_k is the number of pattern neurons of class k and $\omega_{k,t}$ are positive weights satisfying $\sum_{t=1}^{M_k} \omega_{k,t} = 1$. The input vector X belongs to the class that has maximum output in the summation unit.

11.2.6 *k*-Nearest Neighbor Algorithm

The k-nearest neighbor (k-NN) is one of the simplest machine learning algorithms, used for classifying purposes based on closest feature in the training data set. Therefore, it can be said that k-NN is an instance-based learning because the output is approximated locally based on available data. Therefore, the k-NN algorithm is sensitive to the local structure of the data. It can be simply said

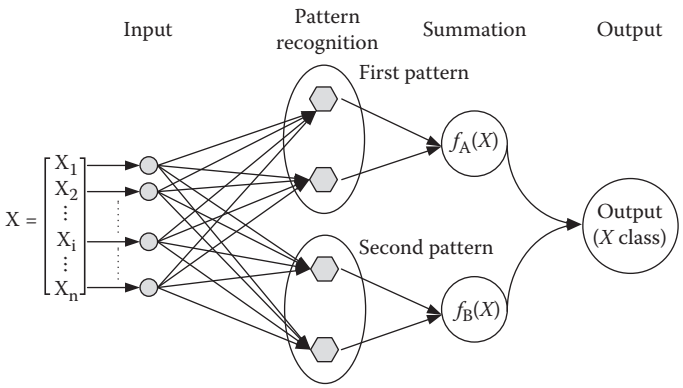

FIGURE 11.13 Typical PNN model layout.

that in *k*-NN, an object is assigned to the class where its *k*-NNs commonly belong. The number of considered neighbors, *k*, is a small positive integer value.

Since different neighbors may belong to different classes, it is needed to average their results. To consider the distance of different neighbors from the considered object, the contributions of the neighbors are weighted. In this way, bigger weights are considered for the nearer neighbors. For weighting, the measure of $1/d_i$ is commonly used. d_i is the distance of the considered object to the neighbor *i*.

Here, the general *k*-NN algorithm is explained. The training features are multidimensional vectors with a class label. There is no explicit training step in *k*-NN application and it consists only of storing the feature vectors and class labels of the training set based on their distance from the considered object.

The best value of *k* depends on the training data. The larger value of *k* reduces the effect of data noises on the classification but distinguishing between different classes becomes more difficult. The value of *k* is determined by the user based on trial and error to achieve the least model performance error. The distance of different features is usually determined based on Euclidean distance (the length of the line segment connecting two points) for continuous variables. For example, for two points $p = (p_1, p_2, \ldots, p_n)$ and $q = (q_1, q_2, \ldots, q_n)$, the distance is estimated as follows:

$$d(p,q) = \sqrt{(q_1 - p_1)^2 + (q_2 - p_2)^2 + \ldots + (q_n - p_n)^2}\,. \tag{11.37}$$

The performance and accuracy of the *k*-NN algorithm are decreased if noisy or irrelevant features are available in the training set or if the importance of the feature is not considered in their scaling. Therefore, selecting or scaling features is an important task in improving classification using the *k*-NN algorithm. In some cases, evolutionary algorithms are used to optimize feature scaling. In another approach, features are scaled by the mutual information of the training data with the training classes.

The *k*-NN algorithm can also be used in estimating continuous variables. In this case, the inverse distance weighted average of the *k*-NNs' values is used as output. The step-by-step definition of model performance is given in the following:

- Computation of the Euclidean distance from the subject point to the features in the training set. In general, the distance is calculated as follows:

$$Dis_{pq} = \sqrt{W_1(q_1 - p_1)^2 + W_2(q_2 - p_2)^2 + \cdots + W_i(q_i - p_i)^2 + \cdots + W_n(q_n - p_n)^2}\,, \tag{11.38}$$

  where q_i and p_i are the values of the *i*th component of the *n*-dimensional vectors of features *q* and *p*, respectively. In this case, due to the different importance of the components of the features, different weights, W_i, are considered in distance calculation. The optimal value of these weights should be determined to achieve the best model performance.
- Ranking the samples in ascending order based on the calculated distances.
- Determining the optimal value of *k* based on model performance indices such as RMSE estimated by cross-validation technique.
- Calculate the model output for feature *p*, D_p, as follows:

$$D_r = \sum_{q=1}^{k} \left(\frac{\dfrac{1}{Dis_{pq}}}{\displaystyle\sum_{q=1}^{k} \frac{1}{Dis_{pq}}} \right) \times D_q, \tag{11.39}$$

TABLE 11.5
Spring Runoff Information and Its Predictors

Year	Snow Depth in February (mm)	Runoff Volume in February (MCM)	Runoff Volume in Spring (MCM)
1	150.4	155	1274
2	313.7	396	1248
3	14.6	237	645
4	7.5	222	732
5	289.3	156	972
6	32.3	89	725
7	400.1	260	977
8	59.0	143	522
9	111.5	105	536
10	21.3	112	406

where k is the number of neighbors that are used for prediction and $\left(\frac{\frac{1}{Dis_t}}{\sum_1^m \frac{1}{Dis_t}} \right)$ is the kernel function, and evaluate the probability of occurrence of D_q.

Example 11.9

Taking into account Table 11.5, predict the runoff in spring using the *k*-NN method and the observed data of runoff and snow in February.

Solution:

To determine the optimum weight and the appropriate numbers of the neighbors, the prediction algorithm is combined with an optimization model. The goal of this model is to determine the optimum value of the weights and the number of neighbors with minimum prediction error.

The results of the prediction (Table 11.6 and Figure 11.14) show that the best prediction is when the variable weight of the runoff and the snow in February are 0 and 1, respectively [Prediction (1)]. The best prediction is gained with one variable. The other prediction mode is when the weight of the runoff and the snow in February are 0.1 and 0.9, respectively [Prediction (2)]. The results of both predictions are given in Table 11.6. As seen in this table, the error in Prediction (1) is less than that in Prediction (2).

TABLE 11.6
Prediction Error of *k*-NN for Both Conditions

Statistic	Information	Prediction (1)	Prediction (2)
RMSE (MCM)	Calibration	52.2	41
	Validation	67.1	103
Correlation coefficient	Calibration	0.44	0.7
	Validation	0.69	0.57

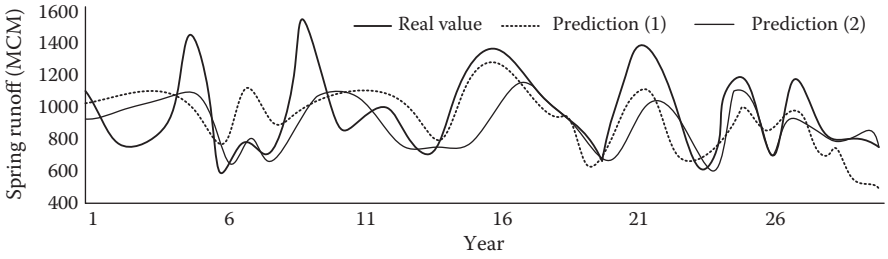

FIGURE 11.14 *k*-NN predictions of runoff volume in spring using two sets of *k*-NN parameters.

11.2.7 Fuzzy Sets and Parameter Imprecision

Two approaches, randomization and fuzzification, are used for evaluating the uncertainty of the parameters in hydrologic modeling. In the previous sections, the randomization concepts and probabilistic methods were discussed. In this section, the fundamentals of fuzzy sets and fuzzy decisions will be introduced.

Let X be the set of certain objects. A *fuzzy set* A in X, is a set of ordered pairs as follows:

$$A = \{(x, \mu_A(x))\}, x \in X, \tag{11.40}$$

where $\mu_A : X \mapsto [0,1]$ is called the membership function.

For normalizing a nonempty fuzzy set, the normalized membership function is computed as follows:

$$\bar{\mu}_A(x) = \frac{\mu_A(x)}{\sup_x \mu_A(x)}. \tag{11.41}$$

(i) The *support* of a fuzzy set A is defined as

$$S(A) = \{x | x \in X, \mu_A(x) > 0\}. \tag{11.42}$$

(ii) The fuzzy sets A and B are equal, if for all $x \in X$

$$\mu_A(x) = \mu_B(x). \tag{11.43}$$

(iii) A fuzzy set A is a *subset* of B ($A \subseteq B$), if for all $x \in X$,

$$\mu_A(x) \leq \mu_B(x). \tag{11.44}$$

(iv) A' is the *complement* of A, if for all $x \in X$,

$$\mu_{A'}(x) = 1 - \mu_A(x). \tag{11.45}$$

(v) The *intersection* of fuzzy sets A and B is defined as

$$\mu_{A \cap B}(x) = \min\{\mu_A(x); \mu_B(x)\} \text{ (for all } x \in X). \tag{11.46}$$

Notice that (v) and (vii) imply that $A \subseteq B$ if and only if $A \cap B = A$.

(vi) The *union* of fuzzy sets A and B is given as

$$\mu_{A\cup B}(x) = \max\{\mu_A(x); \mu_B(x)\} \text{ (for all } x \in X). \tag{11.47}$$

(vii) The *algebraic product* of fuzzy sets A and B is denoted by AB and is defined by the relation

$$\mu_{AB}(x) = \mu_A(x)\mu_B(x) \text{ (for all } x \in X). \tag{11.48}$$

(viii) The *algebraic sum* of fuzzy sets A and B is denoted by $A + B$ and has the membership function

$$\mu_{A+B}(x) = \mu_A(x) + \mu_B(x) - \mu_A(x)\mu_B(x) \text{ (for all } x \in X). \tag{11.49}$$

(ix) A fuzzy set A is *convex*, if for all $x,y \in X$ and $\lambda \in [0,1]$,

$$\mu_A(\lambda x + (1 - \lambda)y) \geq \min\{\mu_A(x); \mu_A(y)\}. \tag{11.50}$$

If A and B are convex, then it can be demonstrated that $A \cap B$ is also convex.

(x) A fuzzy set A is *concave*, if A' is convex. In the case that A and B are concave, $A \cup B$ will also be concave.

(xi) Consider $f:X\mapsto Y$ a mapping from set X to set Y and A, a fuzzy set in X. The fuzzy set B *induced* by mapping f is defined in Y with the following membership function:

$$\mu_B(y) = \sup_{x\in f^{-1}(y)} \mu_A(x) \tag{11.51}$$

where $f^{-1}(y) = \{x|x \in X, f(x) = y\}$.

Example 11.10

Fuzzy sets A and B are defined in $X = [-\infty, \infty]$, by the membership functions as follows:

$$\mu_A(x) = \begin{cases} x/3 & \text{if} \quad 0 \leq x \leq 3 \\ -x+4 & \text{if} \quad 3 < x \leq 4 \\ 0 & \text{otherwise.} \end{cases}$$

$$\mu_B(x) = \begin{cases} x & \text{if} \quad 0 \leq x \leq 1 \\ 1 & \text{if} \quad 1 \leq x \leq 2 \\ -x+3 & \text{if} \quad 2 \leq x \leq 3 \\ 0 & \text{otherwise.} \end{cases}$$

Determine the membership functions of $A \cap B$, $A \cup B$, and $A + B$ fuzzy sets.

Solution:

Considering Equation 11.46, $\mu_{A\cap B}(x) = \min\{\mu_A(x); \mu_B(x)\}$; therefore, $A \cap B$ is

$$\mu_{A\cap B}(x) = \begin{cases} x/3 & \text{if} \quad 0 \le x \le 2.25 \\ -x+3 & \text{if} \quad 2.25 < x \le 3 \\ 0 & \text{otherwise.} \end{cases}$$

From Equation 11.47, we have $\mu_{A\cup B}(x) = \max\{\mu_A(x); \mu_B(x)\}$; thus, $A \cup B$ is as follows:

$$\mu_{A\cup B}(x) = \begin{cases} x & \text{if} \quad 0 \le x \le 1 \\ 1 & \text{if} \quad 1 < x \le 2 \\ -x+3 & \text{if} \quad 2 < x \le 2.25 \\ x/3 & \text{if} \quad 2.25 < x \le 3 \\ -x+4 & \text{if} \quad 3 < x \le 4 \\ 0 & \text{otherwise.} \end{cases}$$

Finally, the summation of fuzzy sets is determined as follows:

$$\mu_{A+B}(x) = \begin{cases} \dfrac{4x-x^2}{3} & \text{if} \quad 0 \le x \le 1 \\ 1 & \text{if} \quad 1 < x \le 2 \\ \dfrac{x^2-5x}{3}+3 & \text{if} \quad 2 < x \le 3 \\ -x+4 & \text{if} \quad 3 < x \le 4 \\ 0 & \text{otherwise.} \end{cases}$$

The membership functions of $A \cap B$, $A \cup B$, and $A + B$ fuzzy sets are illustrated in Figure 11.15.

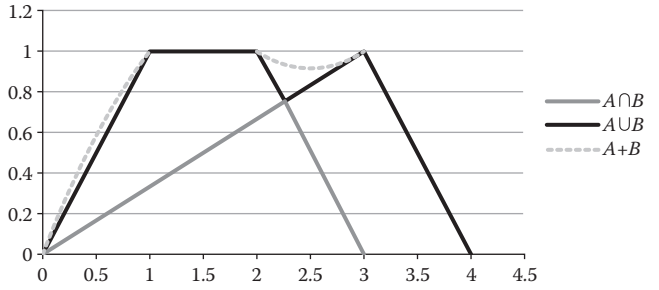

FIGURE 11.15 Membership functions of $A \cap B$, $A \cup B$, and $A + B$.

Example 11.11

Consider fuzzy set A defined in $X = [-4,4]$ as follows:

$$\mu_A(x) = \begin{cases} \dfrac{4+x}{2} & \text{if} \quad -4 \le x \le 0 \\ \dfrac{4-x}{2} & \text{if} \quad 0 < x \le 4 \\ 0 & \text{otherwise.} \end{cases}$$

Determine the membership function of the fuzzy set induced by the function $f(x) = x^2$.

Solution:

Since $f([-4,4]) = [0,16]$, $\mu_B(y) = 0$ if $y \notin [0,16]$. If $y \in [0,16]$, then $f^{-1}(y) = \left\{\sqrt{y}, -\sqrt{y}\right\}$, and since $\mu_A\left(\sqrt{y}\right) = \dfrac{4-\sqrt{y}}{2} = \mu_A\left(-\sqrt{y}\right)$,

$$\mu_B(y) = \sup_{x \in f^{-1}(y)} \mu_A(x) = \frac{4-\sqrt{y}}{2}.$$

Uncertain model parameters can be considered as fuzzy sets, and the result on any series of operations results in a fuzzy set. Uncertainty in constraints and in the objective functions can also be expressed by fuzzy sets. See Karamouz et al. (2003) for more details.

11.2.8 Fuzzy Inference System

Fuzzy logics are powerful tools for solving problems using very simple mathematical concepts. It can be stated that fuzzy logic does not solve new problems but it offers new methods for solving everyday problems. A fuzzy inference system (FIS) uses fuzzy logic for providing a relationship between the input and output spaces. This system follows the reasoning process of human language using the fuzzy logic for building fuzzy IF–THEN rules. FISs are used in decision-making problems. An example of these rules is indicated as follows:

If rainfall depth is high and the reservoir is full, the flood damages will be high.

The simplest form of a fuzzy "if–then" rule is as follows:

If x is A, then y is B,

where A and B are fuzzy values defined by fuzzy sets in the universes of discourse X and Y, respectively. x and y are the input and output variables, respectively. The *is* has different meanings in the antecedent and consequent parts of the rule. The antecedent is an interpretation that returns a value between 0 and 1, and the consequent assigns a fuzzy set B to the variable y.

FIS is built based on the knowledge of experts, or in other words, it relies on the know-how of the ones who understand the system. However, FIS is a very flexible system. A FIS can be easily modified by adding or deleting rules without the need for creating a new FIS. Furthermore, imprecise data can be used in FIS (but it does not work with uncertainty) because of the use of elements in a

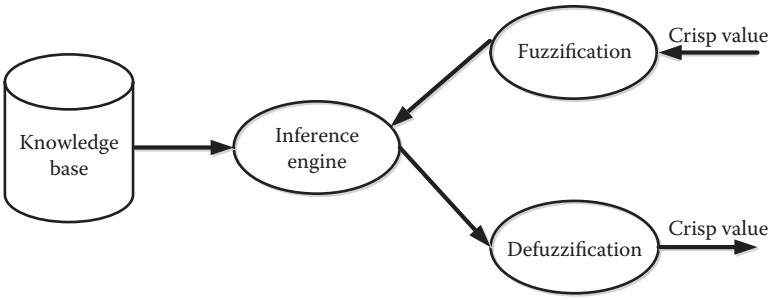

FIGURE 11.16 Four main modules of FIS.

fuzzy set (membership values). An important advantage of FIS is that it can be used together with other classic methods.

In general, as shown in Figure 11.16, a FIS includes four main modules:

- **Fuzzification module:** In this module, the crisp system inputs are transformed into fuzzy sets through applying a fuzzification function.
- **Knowledge base:** Based on the available data of inputs and outputs, some IF–THEN rules are developed by experts and stored in this module.
- **Inference engine:** The fuzzy output of the system is determined by making fuzzy inference on the inputs and IF–THEN rules.
- **Defuzzification module:** Finally, the fuzzy output of the system obtained by the inference engine is changed into a crisp value.

Fuzzy inference methods include two groups of direct and indirect methods. Direct methods, such as Mamdani's and Sugeno's, are the most commonly used (these two methods only differ in how they obtain the outputs), but indirect methods are more complex. Here, Mamdani's and Sugeno's methods are introduced.

11.2.8.1 Mamdani's Method

Mamdani's method is the most common FIS system used for practical purposes and uses the simple structure of "min–max" operations. This system includes the following steps, which will be discussed further in the next paragraphs:

Step 1: Evaluate the antecedent for each rule.
Step 2: Obtain each rule's conclusion.
Step 3: Aggregate conclusions.
Step 4: Defuzzification.

Step 1. Evaluate the antecedent for each rule

The first step is "input fuzzification," where the corresponding membership values of the given crisp input values are obtained. If the antecedent of the rule has more than one part, a fuzzy operator (or – and) is applied to obtain a single membership value. This process is described in the given example in Figure 11.17.

When fuzzifying the first part of the antecedent (the rainfall depth is high), the degree to which the rainfall is high should be obtained with regard to the rainfall depth, which here is 20 mm. As shown in Figure 11.17, a 20 mm rainfall stands for a low rainfall, which results in a membership value of 0. When fuzzifying the second part of the antecedent (reservoir is full), the degree to which the reservoir is full is obtained based on reservoir storage, which here is 350 MCM. Regarding Figure 11.17, this storage volume stands for

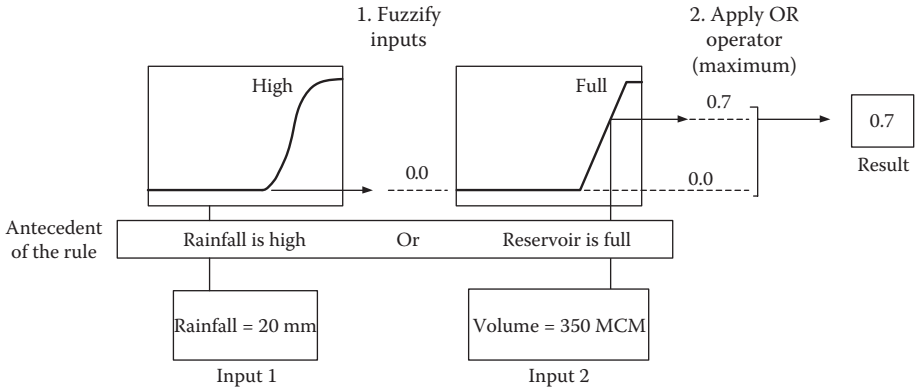

FIGURE 11.17 Input fuzzification process.

a quite full reservoir. Using the "or" fuzzy operator, the maximum membership function value of 0.7 is selected in this step.

If both parts of the antecedent were joined by a conjunction ("and"), an AND operation was employed and minimum value would be selected.

Step 2. Obtain each rule's conclusion

Based on the given consequent of each rule (a fuzzy set) and the antecedent value obtained in step 1, a fuzzy implication operator is applied to obtain a new fuzzy set. Two commonly used implication methods are the minimum, which truncates the consequent's membership function, and the product, which scales it. In the example discussed, the minimum operator is used as shown in Figure 11.18.

Step 3. Aggregate conclusions

In this step, the fuzzy aggregation operator is used to combine the obtained outputs (membership functions) for each rule in step 2 into a single fuzzy set. Some of the most commonly used aggregation operators are the maximum, sum, and probabilistic sum. In this example, the maximum aggregation operator is used as shown in Figure 11.19.

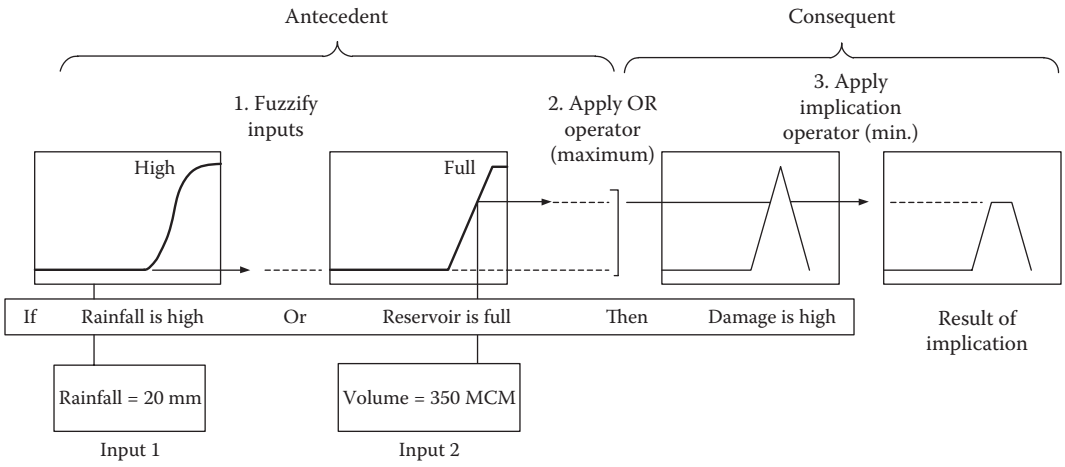

FIGURE 11.18 Obtaining the rule's conclusion.

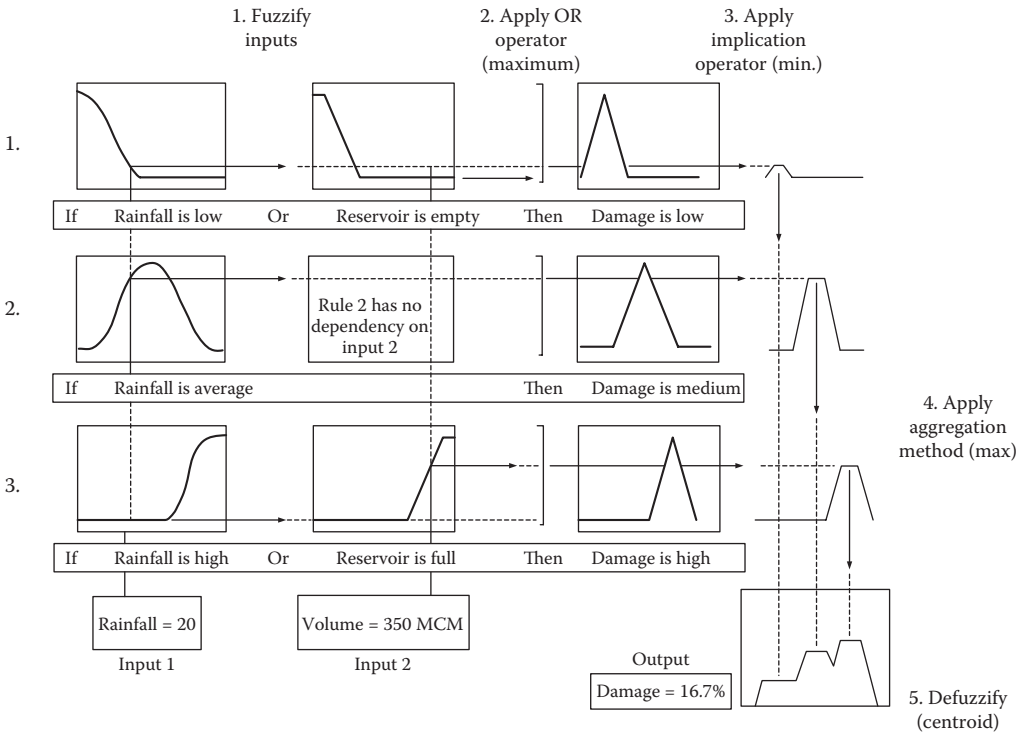

FIGURE 11.19 Aggregation of fuzzy conclusions.

Step 4. Defuzzification

In most cases of FIS application, it is more desired to give the output as a number (crisp value) instead of a fuzzy set. For the given example in this section about flooding damage for instance, it is preferred to state the amount of flood damage instead of just stating it is high. Hence, transforming the obtained fuzzy set in step 3 into a single numerical value is necessary. One of the most popular defuzzification methods is the centroid, which returns the center of the area under the fuzzy set obtained in step 3. The other defuzzification methods are described in detail in reference books. The calculation of this method is as follows (Figure 11.20):

$$g = \frac{\sum_{i=1}^{n+1} x_i . u(x_i)}{\sum_{i=1}^{n+1} u(x_i)}, \tag{11.52}$$

where g is the FIS output value, x_i is the value of the output, $u(x_i)$ is the membership value of x_i and n is the number of segments in the aggregated output membership function.

It should be mentioned that Mamdani's method is useful when there is a small number of variables. In the case of a considerable number of variables, the following difficulties happen:

1. When the number of variables increases, the number of rules increases exponentially.
2. It is difficult to determine the suitable rules for the problem.

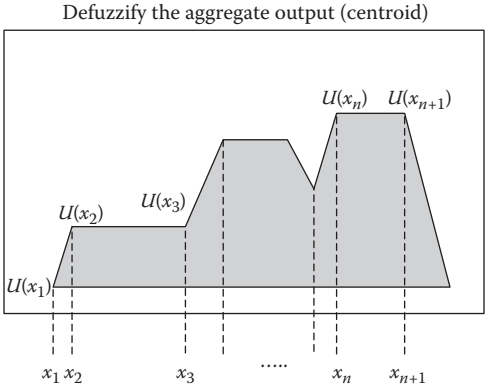

FIGURE 11.20 Defuzzification of the aggregated output using the centroid method.

3. By increasing the number of variables in the antecedent, it will be difficult to explore the relationship between the antecedents and the consequents. Therefore, rule development would be difficult.

In Sugeno's method, some of these difficulties are solved.

11.2.8.2 Sugeno's Method

Sugeno's method is similar to Mamdani's method in many respects, specifically in the first two parts of the fuzzy inference process, fuzzifying the inputs and applying the fuzzy operator (determining rules consequents). The main difference is that the output membership functions for Sugeno's method are only linear or constant. The form of a typical fuzzy rule in a Sugeno fuzzy model is as follows:

$$\textit{If } x \textit{ is } A \textit{ and } y \textit{ is } B, \textit{ then } z = k,$$

where A and B are fuzzy sets and k is a crisp constant. Therefore, all output membership functions are singleton spikes, and the implication and aggregation methods cannot be edited. Multiplication is used as the implication method, and the aggregation operator includes all of the singletons. The structure of Sugeno's method for the previously mentioned example is given in Figure 11.21.

11.2.9 Adaptive Neuro-Fuzzy Inference System

ANFIS is a hybrid neuro-fuzzy inference system that works based on Sugeno FIS. The structure of ANFIS is similar to an MLP neural network but the links in an ANFIS only indicate the flow direction of signals between nodes and there is no weight associated with the links. Generally, ANFIS includes five layers of nodes. The nodes of the first and fourth layers are adaptive nodes and the nodes in the other three layers are fixed nodes. The adaptive nodes have specific parameters that are estimated in several iterations. The fixed nodes do not have any parameters. The general structure of rules in ANFIS is as follows:

$$\textit{If } x \textit{ is } A \textit{ and } y \textit{ is } B, \textit{ then } f = px + qy + r,$$

where x and y are the inputs, A and B are the fuzzy sets, f is the outputs within the fuzzy region specified by the fuzzy rule, and p, q, and r are the design parameters that are determined during the training process. The ANFIS architecture with two rules is shown in Figure 11.22 where circles and squares show fixed and adaptive nodes, respectively.

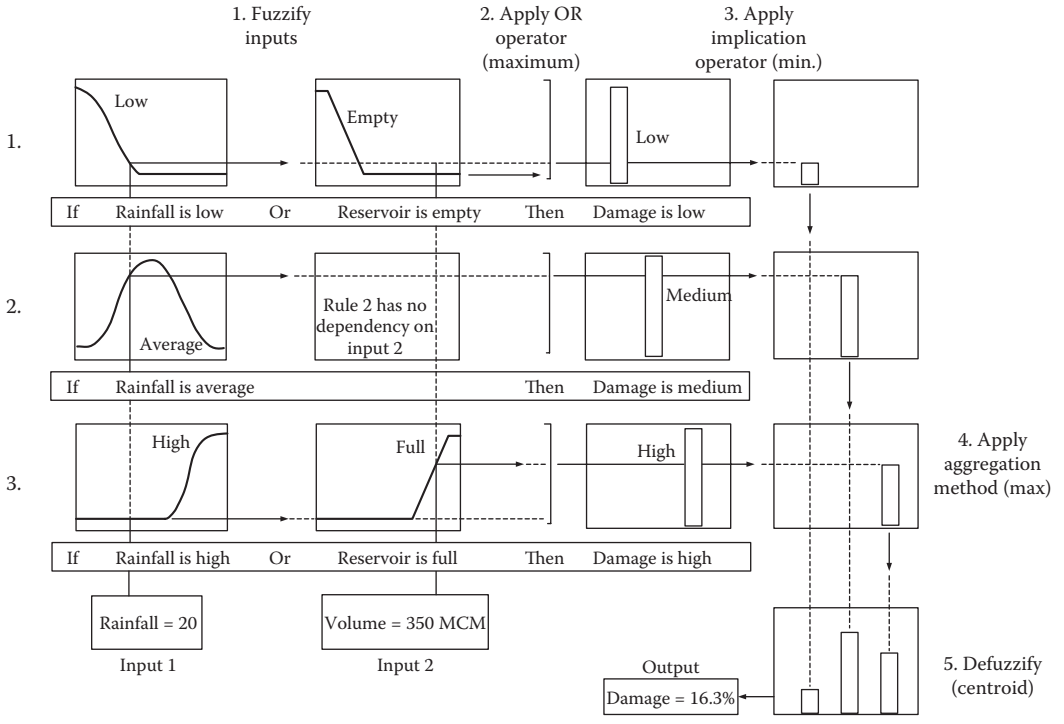

FIGURE 11.21 Structure of the developed Sugeno FIS for flood damage example.

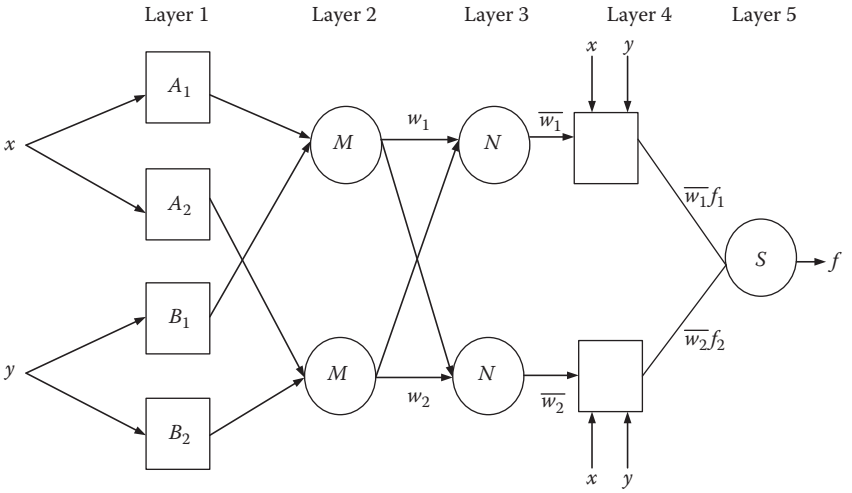

FIGURE 11.22 ANFIS architecture.

Model performance in different layers is described in the example model in Figure 11.22.

Layer 1, Fuzzification layer: The nodes of this layer are adaptive. The outputs of this layer are the fuzzy membership degree of the inputs, determined as follows:

$$\begin{aligned} O_i^1 &= \mu_{Ai}(x), \quad \text{For } i = 1,2 \\ O_i^1 &= \mu_{Bi-2}(y), \quad \text{For } i = 3,4 \end{aligned}, \tag{11.53}$$

where x and y are the inputs to the ith node, $\mu_{Ai}(x)$, $\mu_{Bi-2}(y)$ can get any fuzzy membership function, and O_i^1 is the output of layer 1. $\mu_{Ai}(x)$ is commonly developed in bell shape varying between 0 and 1, such as

$$\mu_{Ai}(x) = 1/1 + \left\{\left(x - c_i/a_i\right)^2\right\}^b, \tag{11.54}$$

where a_i, b_i, and c_i are the membership function parameters determined based on the model developer's opinion.

Layer 2, Rule layer: The output of the fixed nodes in this layer (labeled in Figure 11.21 by *M*) is the product of all the incoming signals, which is calculated as follows:

$$O_i^2 = w_i = \mu_{Ai}(x)\mu_{Bi}(y) \qquad i = 1, 2. \tag{11.55}$$

Layer 3, Normalization layer: This layer also includes fixed nodes (nodes labeled *N* in Figure 11.21) whose output is estimated as follows:

$$O_i^3 = w_i = w_i/(w_1 + w_2) \qquad i = 1, 2. \tag{11.56}$$

Layer 4, Defuzzification layer: The neurons of this layer are adaptive nodes and their outputs are the product of the normalized firing strength and a first-order polynomial.

$$O_i^4 = w_i f_i = w_i(p_i x + q_i y + r_i) \qquad i = 1, 2. \tag{11.57}$$

Layer 5, Summation neuron: This layer has a fixed node, giving the system output as the summation of all incoming signals:

$$O_i^5 = \sum_{i=1}^{2} w_i f_i = \sum_{i=1}^{2} w_i\, f_i/(w_1 + w_2). \tag{11.58}$$

Example 11.12

Considering the data given in Example 11.9, predict the runoff volume in spring based on the snow and runoff volume in February using FIS.

Solution:

By using the fuzzy logic toolbox of MATLAB, a Mamdani FIS is developed. The following functions are used in FIS development:

AND method → min Function
OR method → max Function
Implication → min Function
Aggregation → max Function
Defuzzification → centroid Function

Step 1: Definition of input and output variables.

The amounts of snow and discharge volume in February are input variables and spring discharge volume is the output variable as shown in Figure 11.23.

Step 2: Definition of membership function for each input and output variable.

In this example, three membership functions are defined for each variable as given in Table 11.7. The triangular functions are defined by three points while the trapezoidal functions are presented by four points. An example of developed membership functions for snow is illustrated in Figure 11.24.

Step 3: Definition of rules.

Three simple rules are inferred from the observed data:

If Snow is light and Runoff_Per is low, then Runoff is low.

If Snow is medium and Runoff_Per is medium, then Runoff is medium.

If Snow is heavy and Runoff_Per is high, then Runoff is high.

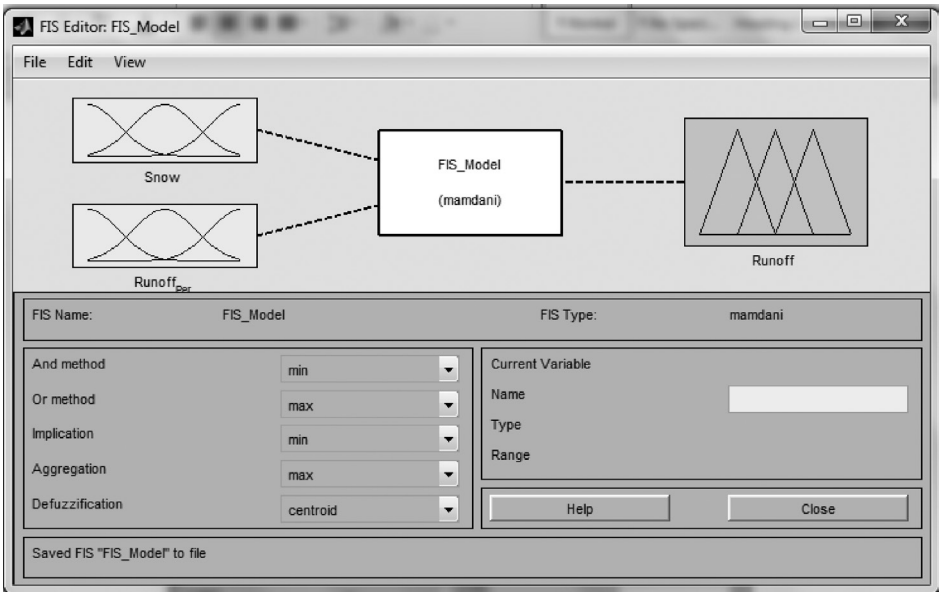

FIGURE 11.23 Development of model input–output structure.

TABLE 11.7
Membership Functions Developed for FIS Inputs and Outputs

Variable Name	Membership Function Name	Type of Membership Function	Parameters
Snow	Low	Triangular	[0 5 150]
	Average	Trapezoidal	[60 150 250 350]
	High	Triangular	[250 400 500]
Runoff_Per (Feb. runoff)	Low	Triangular	[0 80 230]
	Average	Trapezoidal	[120 190 280 350]
	High	Triangular	[250 400 528]
Runoff	Low	Triangular	[40 400 760]
	Average	Trapezoidal	[525 720 958 1170]
	High	Triangular	[940 1300 1660]

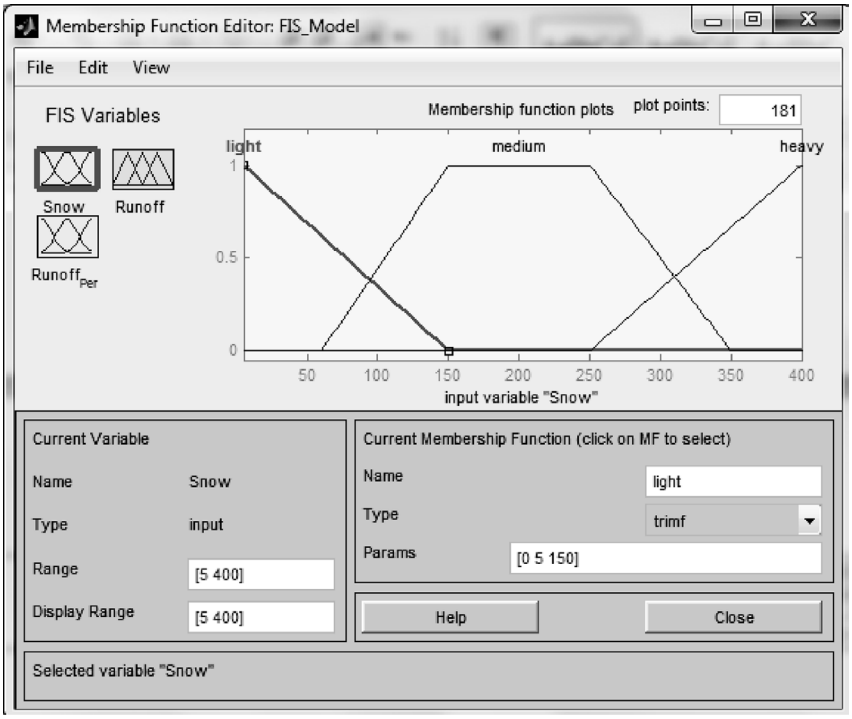

FIGURE 11.24 Developed membership function for snow depth.

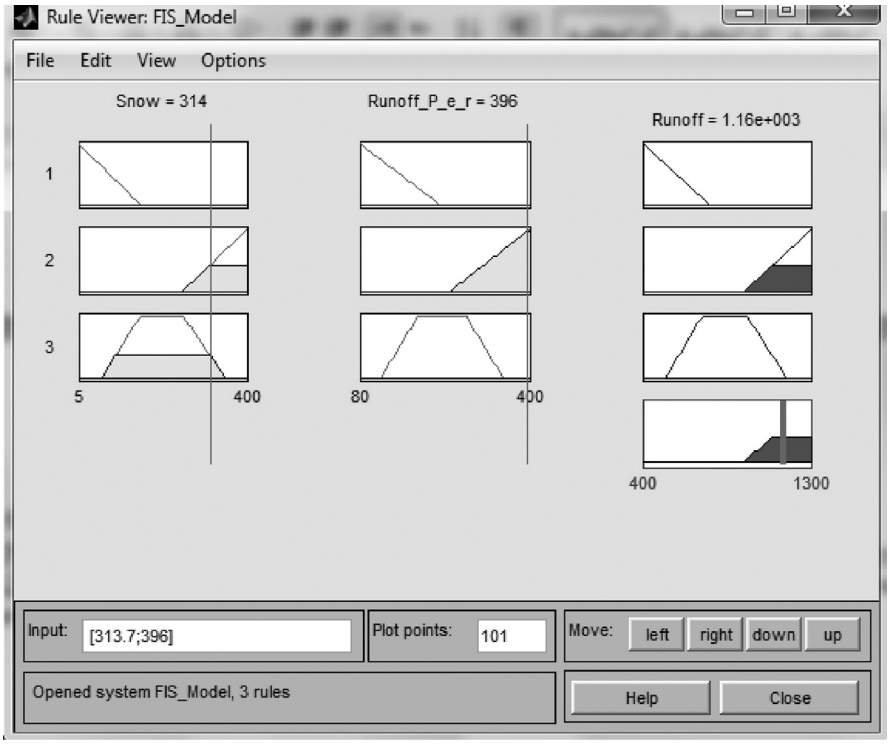

FIGURE 11.25 Application of developed FIS for a year with a snow volume of 313.7 MCM and a February discharge volume of 396 MCM.

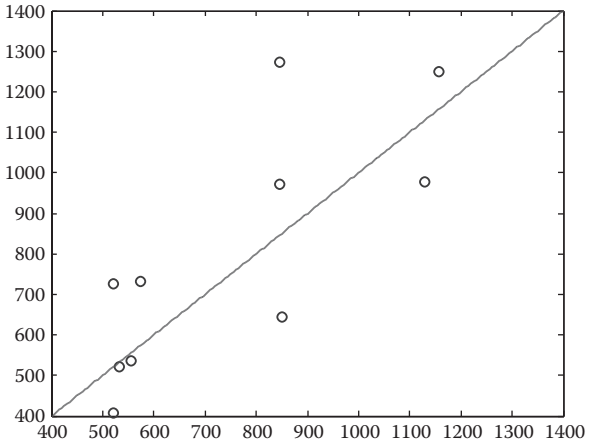

FIGURE 11.26 FIS outputs vs. the observed values.

Step 4: Rules application.

Performance of the developed FIS can be tested by different inputs. For example, in year 21 when the snow volume is 313.7 MCM and the February discharge volume is 396 MCM, the FIS output is 1157 MCM for spring discharge volume and the observed value is 1248 MCM. The application of FIS for this year is illustrated in Figure 11.25.

In Figure 11.26, the FIS outputs vs. the observed values are illustrated.

Example 11.13

Considering the data given in Example 11.9, predict the runoff volume in spring based on the snow and runoff volume in February using ANFIS.

Solution:

By using the fuzzy logic toolbox of MATLAB, an ANFIS model is developed. The type of FIS used in the ANFIS model is Sugeno FIS. The model development process is explained step by step.

Step 1: Inserting input and output variables to model.

Input and output variables are loaded to the ANFIS module in a single matrix (each column is allocated to a variable). The observed data are divided into two parts: the first part for training (7 cases) and the second part (3 cases) for testing.

Step 2: Specifying the FIS.

For each input variable, two triangular-type membership functions are used. In this case, the output variable will have four membership functions. The FIS structure is shown in Figure 11.27.

Step 3: Training the FIS.

By using the hybrid method for optimization, the developed FIS is trained within training data and in three epochs.

Step 4: Evaluation of model.

Performance of the developed FIS can be seen for training data in Figure 11.28 and for testing data in Figure 11.29. As can be seen in these figures, the developed model performed well in the calibration period but its performance in the validation period is poor. This could be caused by model over-fitting in the calibration or poor definition of input variables' membership functions. Further work on definition of membership functions may result in better model performance even in the validation period.

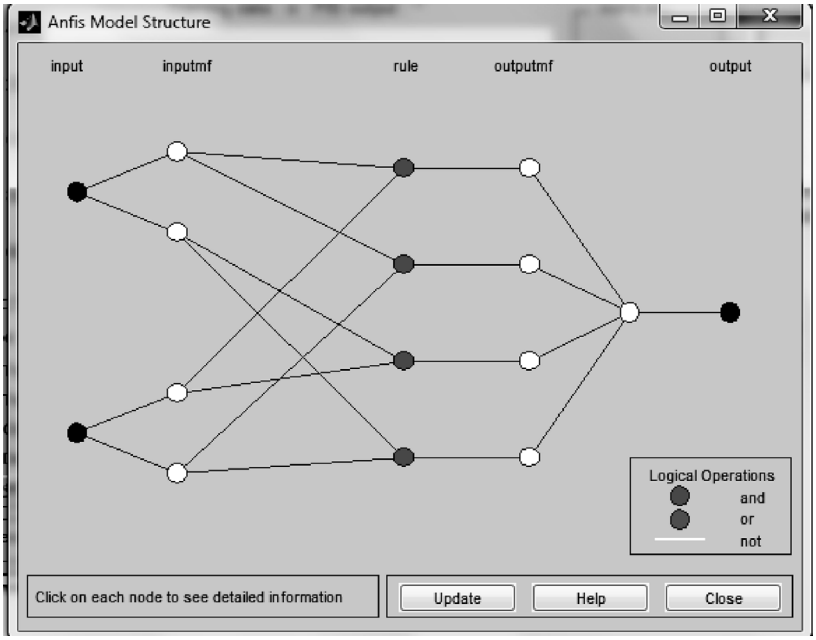

FIGURE 11.27 General structure of the ANFIS model developed in Example 11.13.

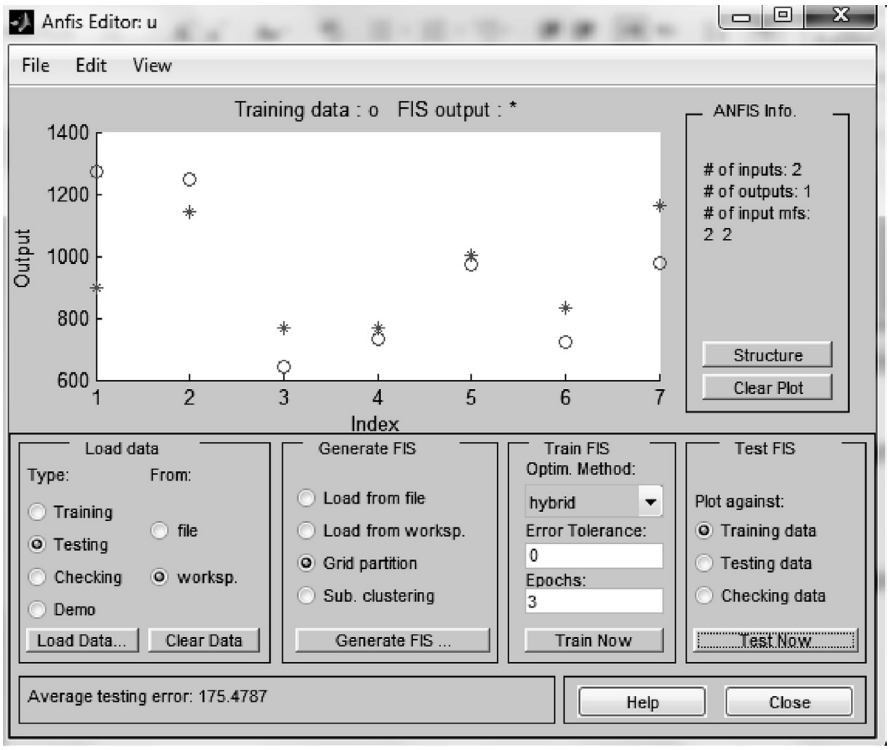

FIGURE 11.28 ANFIS model performance in calibration.

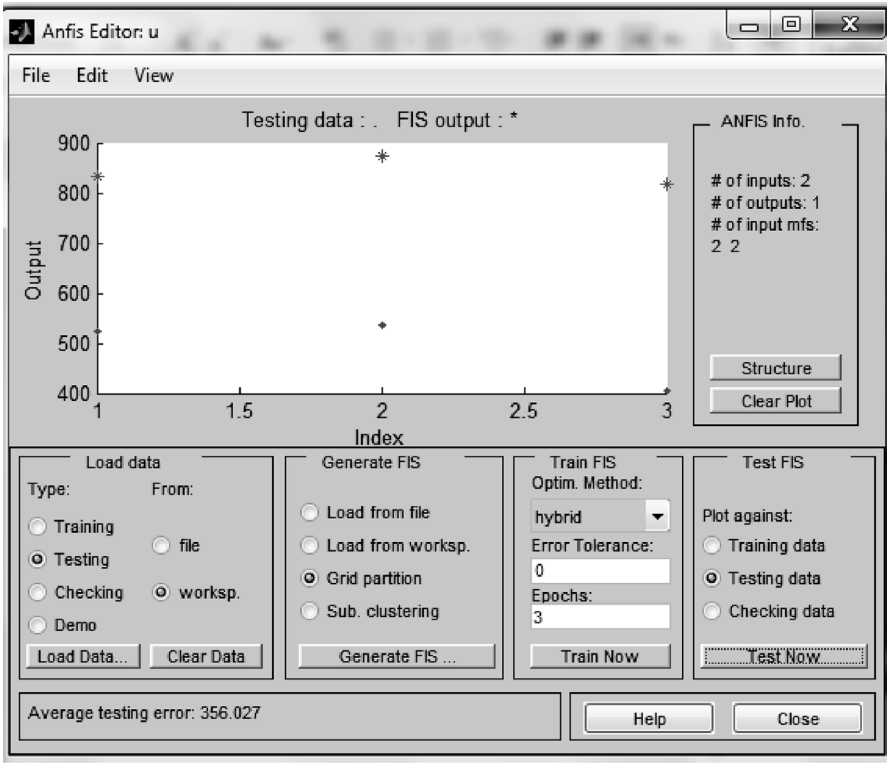

FIGURE 11.29 ANFIS model performance in validation.

11.3 PHYSICAL MODELS' SIMULATION

As described in Chapter 2, physical hydrological models are divided into three groups: lumped, semi-distributed, and distributed. Based on these different modeling approaches, different software is developed for the hydrologic analysis and development of the corresponding flood hydrograph for a given storm.

The choice of these models is highly dependent on the objectives of the study, and different considerations are taken into account. Some of these considerations are as follows:

1. Availability and the quality of hydrological data, especially rainfall and runoff data
2. Model structure and regionalization ability of the model
3. Catchment characteristics and flow homogeneity. For example, in arid and semiarid regions, due to flash floods and rapid variations of flow, only some models can be employed successfully for flow simulation.

Therefore, enough attention should be paid to the selection of the most appropriate model based on the characteristics of the study region. In this section, an example of a lumped model named IHACRES and three examples of semi-distributed models including HEC-HMS, StormNET, and HBV are described. In semi-distributed models, the study area can be divided into different sub-basins to consider different parameters for their modeling. There is no limitation on the number of sub-basins, but by increasing the division numbers, the computational time and effort will highly increase. The distributed models are commonly GIS based to empower them to include the spatial variation of model parameters and variables in high resolution.

11.3.1 Lumped Hydrological Models

The most common models in hydrological analysis are the lumped models. As an example, in rainfall–runoff process simulation, these models describe the watershed as a single entity with a single rainfall input. The discharge at the watershed outlet is described based on a global dynamic of the system. The lump hydrologic models are usually based on the concept of the unit hydrograph, which is valid in the case of watershed being considered as a linear causative and time-invariant system, where only part of the rainfall, the rainfall excess, produces runoff. In the following section, the IHACRES model, which uses the lump concept, is described.

11.3.2 IHACRES

IHACRES is the acronym for "Identification of unit Hydrographs And Component flows from Rainfall, Evaporation, and Streamflow data." It is a catchment-scale rainfall–runoff model that aims to characterize the dynamic relationship between rainfall and runoff. The first version of the model (Version 1.0) was developed in 1994 by the Institute of Hydrology, Wallingford, UK (Littlewood and Jakeman 1994).

Its purpose is to assist the hydrologist or water resources engineer in characterizing the dynamic relationship between basin rainfall and streamflow. The model can be used in the following applications:

- Identification of unit hydrographs
- Continuous time series streamflow modeling
- Environmental change–hydrological regime studies
- Runoff event modeling
- Hydrograph separation
- Derivation of a slow flow index (SFI)
- Derivation of dynamic response characteristics (DRCs)
- Investigation of relationships between DRSs and physical catchment descriptors
- Teaching unit hydrograph theory and its applications
- Hydrographic data quality assurance/control
- Infilling missing streamflow data

The only field data required is time series of rainfall and streamflow, and a third variable by which evapotranspiration effects can be approximated. The third variable can be air temperature but pan evaporation, or potential evaporation derived from hydrometeorological measurements, can also be used as alternatives if they are available. It is assumed that there is a linear relationship between effective rainfall and streamflow. This allows the application of the well-known unit hydrograph theory, which concentrates the catchment as a configuration of linear storages acting in series and/or parallel. All of the nonlinearity that is commonly observed between rainfall and streamflow is therefore accommodated in the module, which converts rainfall to effective rainfall.

The general structure of the IHACRES model is illustrated in Figure 11.30. It includes a nonlinear loss module to transform rainfall to effective rainfall (that portion which eventually reaches

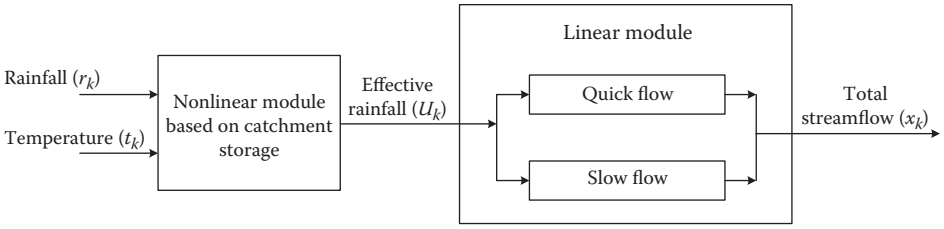

FIGURE 11.30 IHACRES model structure.

the stream prediction point) and a linear module to transfer effective rainfall to stream discharge. The flexibility of IHACRES can be increased by inclusion of different nonlinear loss modules to incorporate the effects of climate and land-use change. The effective rainfall is routed to stream in linear module through any configuration of stores in parallel and/or in series. The observed data are used for configuration of stores but usually there is one store, representing ephemeral streams, or two in parallel, to show baseflow (slow flow) besides the quick flow (Jakeman and Hornberger 1993).

The IHACRES model comprises essentially two parts: (i) a component that divides rainfall into effective rainfall and the remainder, which is assumed to be lost only by evapotranspiration; and (ii) a linear transfer function (or unit hydrograph, UH) component that transforms the effective rainfall to streamflow. Here, these two parts are called the "loss" module and the "transfer-function" (or "UH") module, respectively. The loss module accounts for all of the nonlinearity in the catchment-scale rainfall–streamflow process; the transfer function module is based on linear systems theory. Conceptually, the transfer function module can represent different configurations of linear stores, but the configuration used here is two linear stores in parallel, in which case the whole model has just six parameters (or catchment-scale DRCs), three in each of the loss and UH modules.

Equations 11.59 through 11.63 define the model: superscripts (q) and (s) denote quick and slow flow, respectively; r_k is rainfall (mm) over time step k; u_k is effective rainfall (mm); S_k is a dimensionless catchment wetness index ($0 < S_k < 1$); t_k is air temperature (°C); R is a reference temperature (°C); x_k is modeled streamflow ($m^3\ s^{-1}$); the a and b terms are transfer function parameters; and z^{-1} is the backward shift operator ($z^{-1}x_k = x_{k-1}$). In Equation 11.60, parameter τ_w is a catchment wetness drying time constant (days), and f ($°C^{-1}$) modulates $\tau_w(t_k)$ according to temperature. Parameter C (mm^{-1}) in Equation 11.60 is calculated to equate volumes of effective rainfall and observed streamflow over the model calibration period. The six DRCs are the three loss module parameters τ_w, f, and C in Equations 11.60 and 11.61.

$$\begin{aligned} u_k &= r_k \cdot S_k \\ S_0 &= 0 \end{aligned} \tag{11.59}$$

$$\begin{aligned} S_k &= Cr_k + \left(1 - \frac{1}{\tau_w(t_k)}\right) S_{k-1} \\ \tau_w(t_k) &> 1 \end{aligned} \tag{11.60}$$

$$\tau_w(t_k) = \tau_w e^{f(R-t_k)} \tag{11.61}$$

$$x_k = \left[\left(\frac{b_0^{(q)}}{1 + a_1^{(q)} \cdot z^{-1}}\right) + \left(\frac{b_0^{(s)}}{1 + a_1^{(s)} \cdot z^{-1}}\right)\right] \tag{11.62}$$

$$X_K = \left(\frac{b_0^{(q)} + b_1 \cdot z^{-1}}{1 + a_1 \cdot z^{-1} + a_1 \cdot z^{-1}}\right) \cdot u_{k-\delta} \tag{11.63}$$

The three UH DRCs, $\tau^{(q)}$, $\tau^{(s)}$, and $v^{(s)}$, are given by Equations 11.59, 11.60, and 11.61 (Equation 11.61 is given for completeness). By definition, $\tau^{(q)} + \tau^{(s)} = 1$; thus, the UH is completely defined by any three of the four attributes $\tau^{(q)}$, $\tau^{(s)}$, $v^{(q)}$, and $v^{(s)}$. $v^{(s)}$ is an SFI. The DRCs $\tau^{(q)}$ and $\tau^{(s)}$ are exponential decay time constants for separate quick and slow response UHs, respectively.

$$\tau^{(q)} = \frac{-\Delta}{\ln(-a_1^{(q)})} \tag{11.64}$$

$$\tau^{(s)} = \frac{-\Delta}{\ln(-a_1^{(s)})} \tag{11.65}$$

$$v^{(q)} = \left(\frac{b_0^{(q)}}{1 + a_1^{q}}\right) \cdot \left(\frac{1}{V}\right) \tag{11.66}$$

$$v^{(s)} = \left(\frac{b_0^{(s)}}{1 + a_1^{s}}\right) \cdot \left(\frac{1}{V}\right) \tag{11.67}$$

11.3.3 Semi-Distributed Hydrological Models

In these kinds of physical hydrological models, incorporating the spatial variability of watershed parameters over the analysis has been tried. This may be applicable for some important watershed parameters that highly affect the desired output. In this section, three kinds of software employing this hydrologic modeling approach are described.

11.3.3.1 HEC-HMS

The HMS is a popular model employed for rainfall–runoff analysis in dendrite watershed systems. This model is applicable in different geographic areas for different problems related to rainfall–runoff analysis. These problems vary from large basin water supply and flood hydrology to small urban or natural watershed runoff analysis. The model outputs in the form of runoff hydrographs can be used directly or indirectly for studies of water availability, urban drainage, flow forecasting, future urbanization impact, reservoir spillway design, flood damage reduction, floodplain regulation, and system operation. An integrated framework is provided in this model, including a database, data entry utilities, computation engine, and reporting modules.

Modeling Basin Components: In the basin model, watersheds and rivers are configured physically. A dendritic network is used to connect hydrological elements for simulation of the runoff process. The available elements in the model include sub-basin, reach, junction, reservoir, diversion, source, and sink (Figure 11.31). Computation from the upstream toward the downstream of the system is followed.

The loss rate methods include the following:

1. The deficit constant
2. The initial constant
3. SCS curve number (CN) and its gridded form
4. Green–Ampt
5. Soil moisture accounting (SMA) and its gridded form

The included transform methods are as follows:

1. Clark
2. SCS
3. Snyder
4. Kinematic wave
5. Modclark
6. User-specified graph or unit hydrograph

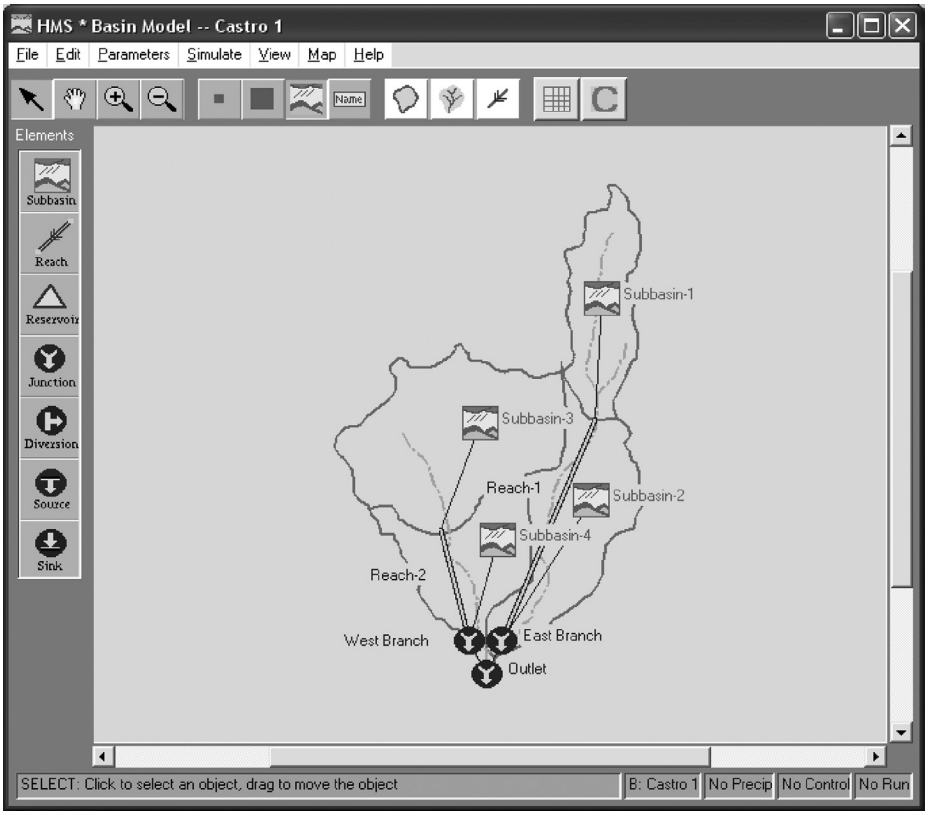

FIGURE 11.31 Basin model screen in the HEC-HMS model.

Analysis of Meteorological Data: The meteorological model is used for analysis of meteorological data including precipitation and evaporation. It includes six different historical and synthetic precipitation methods as well as one evaporation method.

Different precipitation methods considered in the model are as follows:

1. User hyetograph
2. User gauge weighting
3. Inverse-distance gauge weighting
4. Girded precipitation, frequency storm
5. Standard project storm—eastern United States
6. SCS hypothetical storm (SMA)

Rainfall–Runoff Simulation: In control specifications, starting date and time, ending date and time, and computation time step are determined (Figure 11.32).

Parameters Estimation: The optimization manager can be used to automatically estimate the parameters used in related methods to sub-basin and reach elements. For the application of this tool, the observed discharge for at least one element upstream of the observed flow should be available. Various objective functions can be used in available search methods to evaluate the goodness of fit between the computed results and the observed discharge. Different constraints are incorporated to restrict the parameter search space.

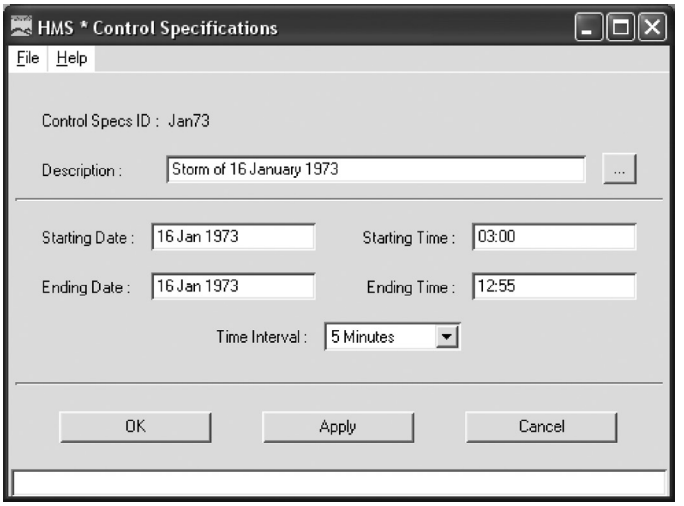

FIGURE 11.32 Control specification screen.

Starting the Program: The project definition screen (Figure 11.33) is used to create and manage projects. It also provides access to components, analysis tools, and other data sets such as precipitation and discharge gauges. This part includes the following:

1. The File menu which contains items for creating and managing projects.
2. The Components section which contains three lists: basin model, meteorologic models, and control specifications.
3. The Data menu which contains items for accessing time series and other data managers.
4. The View menu which contains items for accessing log files. The project log contains information messages generated since the project was opened.
5. The Tools menu which contains items for working with simulation and optimization runs.

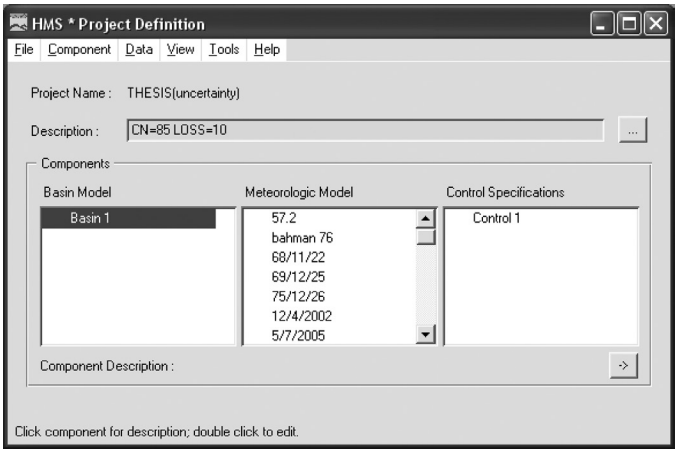

FIGURE 11.33 Project definition screen.

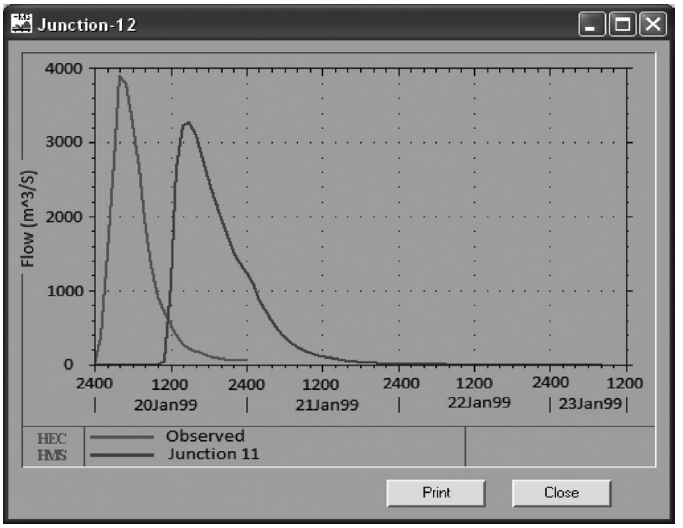

FIGURE 11.34 Comparing the observed hydrograph and the outflow hydrograph.

Based on the different methods that are used in the basin model for determination of loss rate, transform, baseflow, and other items, or in the meteorologic method, diverse inputs are needed. As an illustration, CN, initial abstraction, and imperviousness are the inputs of the SCS CN method for determining the loss rate. Also, storm depth is necessary in the SCS hypothetical storm model for the meteorologic model. Furthermore, the sub-basin area is needed.

The outflow discharge in the junctions and the output hydrograph from the last junction are the output data obtained from this model. Figure 11.34 compared the observed hydrograph and outflow hydrograph in the last junction in a simulated basin.

Example 11.14

Create a single sub-basin model with an area of 50 acres (0.078125 mi^2) in HEC-HMS software. Consider a CN of 87 and an SCS lag time of 15 min. There is a constant baseflow of 3 cfs. Determine the outlet hydrograph for the given precipitation hydrograph in Figure 11.35, which starts at 3:00 p.m. on 3/21/72 and is used as model input data. Begin the analysis at 1:00 p.m. on 3/21/72 and end at 1:00 p.m. on 3/22/72, with a time interval of 10 min.

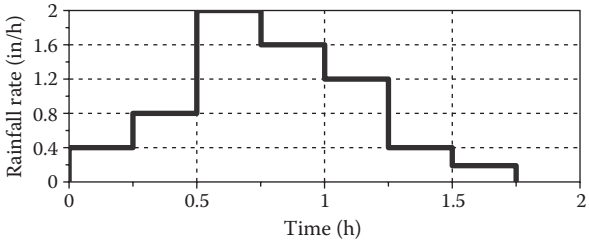

FIGURE 11.35 Proposed hyetograph for Example 11.14.

Solution:

To create a new project, select the *Create a New Project* from the File menu. A window will open where you can name, select the location on your computer or network computer to store the project, and describe the project. Click the Tools menu and select the Options command to access the *Options* window. The window allows you to change any of the optional settings for the project. You can select the default unit system.

A new basin model is created using the *Basin Model Manager*. To access the manager, click on the Components menu and select the Basin Model Manager command.

Several optional features are available at every hydrologic element regardless of the type of element. All optional features are contained in a *Component Editor* that is automatically displayed along with the main element editor. Select an element in the *Watershed Explorer* or the basin map to view its *Component Editor*.

While a sub-basin element conceptually represents infiltration, surface runoff, and subsurface processes interacting together, the actual infiltration calculations are performed by a loss method contained within the sub-basin. A total of 10 different loss methods are provided.

The gridded SCS CN loss method essentially implements the SCS CN method on a grid cell-by-grid cell basis. Each grid cell receives separate precipitation from the meteorologic model. All cells are initialized by scaling based on the CN at each cell and then allowed to evolve separately during the simulation based on individual precipitation inputs. There are also seven different precipitation methods or you can choose to have no precipitation. Select the precipitation method in the *Component Editor* for the meteorologic model. Only one precipitation method can be selected at a time. A new gauge is created using the time-series data manager. To access the manager, click on the Components menu and select the Time-Series Data Manager menu command.

The data for the current time window are shown in tabular form on the "Table" tab of the *Component Editor*. If you select a time-series gauge in the *Watershed Explorer*, only the tab for the "Time-Series Gauge" is shown in the *Component Editor*. If you select a time window under a time-series gauge in the *Watershed Explorer*, the "Table" tab will be added to the *Component Editor*. A new curve is created using the paired data manager. To access the manager, click on the Components menu and select the Paired Data Manager menu item. The data for the current paired data are shown in tabular form on the "Table" tab of the *Component Editor*. A new control specification is created using the *Control Specifications Manager*. To access the manager, click on the Components menu and select the Control Specifications Manager command. The manager will open and show all of the control specifications currently in the project.

Creating a New Run: A new simulation run is created using a wizard that helps you navigate the steps to creating a new run. There are two ways to access the wizard:

The first way to access the wizard is to click on the Compute menu and select the Create Simulation Run command. The wizard will open and begin the process of creating a new simulation run.

The second way to access the wizard is from the *Simulation Run Manager*. Click on the Compute menu and select the Run Manager command. The *Simulation Run Manager* will open and show any runs that already exist. Press the New… button to access the wizard and begin the process of creating a simulation run.

For viewing global summary results, one needs to use the button on the toolbar. Press the toolbar button with a picture of a table plus a globe. Each element in the basin model is shown in the *Watershed Explorer* under the simulation run node. The information included in the summary table varies by element type but always includes the peak flow, time of peak flow, and outflow volume. The element summary table of this example is shown in Figure 11.36.

All of the time-series data computed by an individual element are available for viewing. The time-series data are listed under each element node in the *Watershed Explorer*. Click on a time-series node to preview the data in the *Component Editor*. The outflow hydrograph of this example is shown in Figure 11.37.

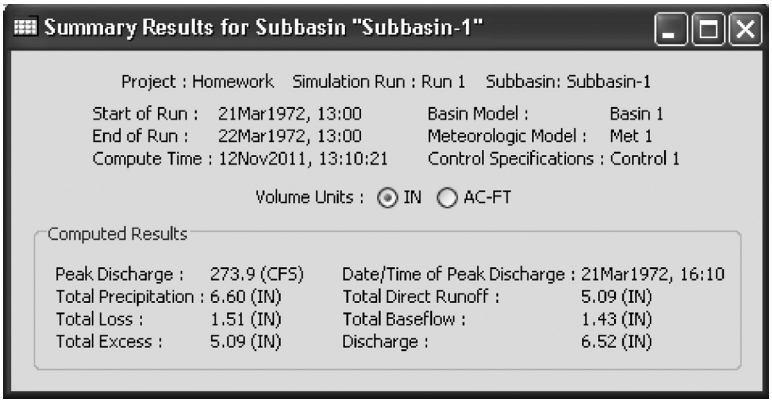

FIGURE 11.36 Result of the simulation.

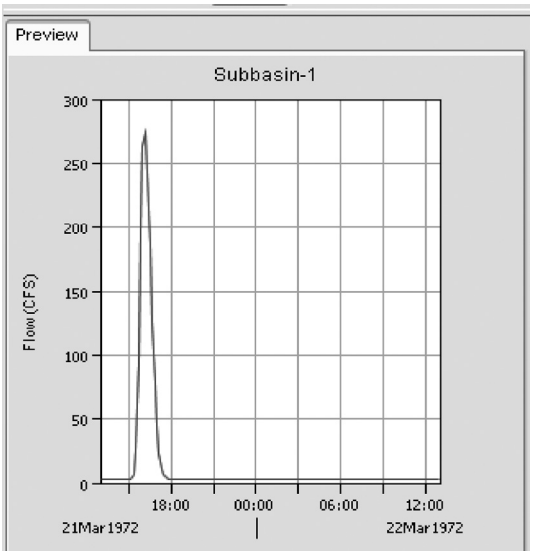

FIGURE 11.37 Discharge of sub-basin in simulation.

Example 11.15

Remodel the basin in Example 11.14 considering the following changes:

a. Add a 3500 ft long channel to the basin outlet. The bed slope of the channel is 0.0024 with trapezoidal cross section with a bottom width of 10 ft and side slopes of 3:1 (H:V). Manning's n is 0.034. Use the Muskingum–Cunge method for hydrograph routing through the channel.
b. Add a new sub-basin with an area of 250 acres (0.390625 mi^2) to the model. The new basin has a CN of 9 and a lag time of 28 min. Consider the baseflow to be zero in the basin.
c. Add the resulting hydrographs from the above parts at a junction point.
d. Place a reservoir with an elevation–storage–discharge relation (Table 11.8) after the junction.

TABLE 11.8
Elevation–Storage–Discharge

Elevation (ft)	Storage (acre-ft)	Discharge (cfs)	Elevation (ft)	Storage (acre-ft)	Discharge (cfs)
0	0	0	9.07	292.35	3.73
0.9	10	0.26	9.39	303.88	3.87
1.4	20	0.42	9.71	315.42	4.01
1.8	30	0.56	10.03	326.95	4.15
2.2	40	0.69	10.35	338.48	4.29
2.5	50	0.81	10.67	350.01	4.43
2.9	60	0.93	10.99	361.54	4.57
3.2	70	1.05	11.31	373.07	4.71
3.5	80	1.17	11.63	384.6	4.85
3.7	90	1.28	11.95	396.13	4.99
4	100	1.4	12.26	407.66	5.13
4.5	120	1.63	12.58	419.19	5.27
4.8	130	1.75	12.9	430.72	5.41
5	140	1.87	13.22	442.25	5.55
5.3	150	1.98	13.54	453.78	5.69
5.5	160	2.1	13.86	465.31	5.83
5.7	170	2.22	14.18	476.84	5.97
6	180	2.34	14.5	488.37	6.11
6.4	200	2.58	14.82	499.9	6.26
6.8	220	2.83	15.14	511.43	6.4
7	230	2.95	15.46	522.96	6.54
7.4	250	3.21	15.78	534.49	6.68
7.79	255.23	3.26	16.1	546.02	6.82
8.11	257.76	3.3	16.42	557.55	6.96
8.43	269.29	3.44	16.74	569.08	7.1
8.75	280.82	3.58			

Solution:

New hydrologic elements are created directly in the *Basin Model* map. Begin the process of creating a new element by opening the basin model into which you wish to add a new element. Select a basin model in the *Watershed Explorer* to open it. Separate tools are provided in the toolbar for each of the seven different kinds of element. Select the tool corresponding to the type of element you wish to create: sub-basin, reach, reservoir, junction, source, diversion, or sink. Hydrologic elements can be connected or disconnected from the network using two different methods. The first method uses the mouse in the *Basin Model* window. The second method is found on the *Component Editor* for the element. To connect an element in the *Basin Model* window, start by selecting the *Arrow Tool* from the toolbar. Next, move the mouse over the element you wish to connect to a downstream element, and then press the right mouse button. A context menu is displayed, which includes the Connect Downstream command. After adding the new elements to the model, the schematic scheme of the watershed should look like the one in Figure 11.38.

While a reach element conceptually represents a segment of stream or river, the actual calculations are performed by a routing method contained within the reach. A total of six different routing methods are provided. You must specify the storage characteristics for the reservoir. The exact form of the characteristics will depend on which routing method you select.

While a reservoir element conceptually represents a natural lake or a lake behind a dam, the actual storage simulation calculations are performed by a routing method contained within the

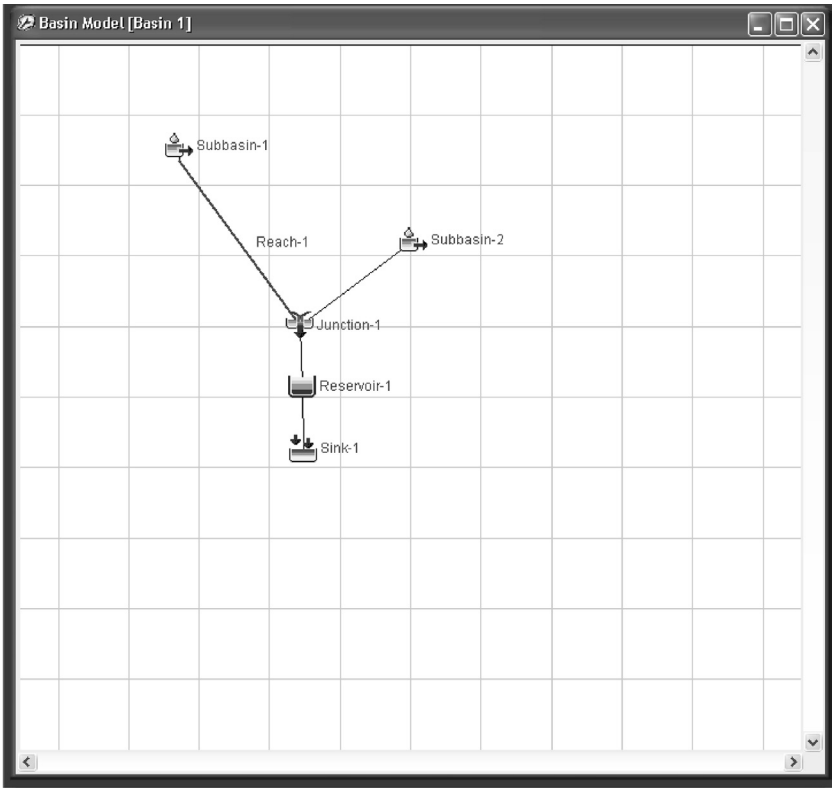

FIGURE 11.38 Scheme of the model.

reservoir. Three different routing methods are available. The routing method for a reservoir is selected on the *Component Editor* for the reservoir element. Access the *Component Editor* by clicking the reservoir element icon on the "Components" tab of the *Watershed Explorer*.

A junction is an element with one or more inflows and only one outflow. All inflow is added together to produce the outflow by assuming zero storage at the junction. It is usually used to represent a river or stream confluence.

The junction element does not have any special data or properties; it only has the standard *Component Editor* used by all elements. Access the *Component Editor* by clicking the junction element icon on the "Components" tab of the *Watershed Explorer*.

A sink is an element with one or more inflows but no outflow. Multiple inflows are added together to determine the total amount of water entering the element. Sinks can be used to represent the lowest point of an interior drainage area or the outlet of the basin model.

After running the models with new data, the results are as shown in Figure 11.39.

11.3.3.2 StormNET

StormNET is one of the most advanced, powerful, and comprehensive stormwater modeling packages available for analyzing and designing urban drainage systems, stormwater sewers, and sanitary sewers. It was developed by BOSS International in 2005. The StormNET model can combine hydrology, hydraulics, and water quality issues in a graphical, user-friendly interface. Different graphical symbols are used for representing network elements such as pipes, channels, and detention ponds. A variety of modeling elements are provided in StormNET.

StormNET is a link-node-based model that combines different aspects of hydrology, hydraulics, and water quality in analysis of stormwater drainage systems. Hydraulic elements such as a pipe, channel, or culvert are represented by links that transport flow and constituents. Nodes are used to

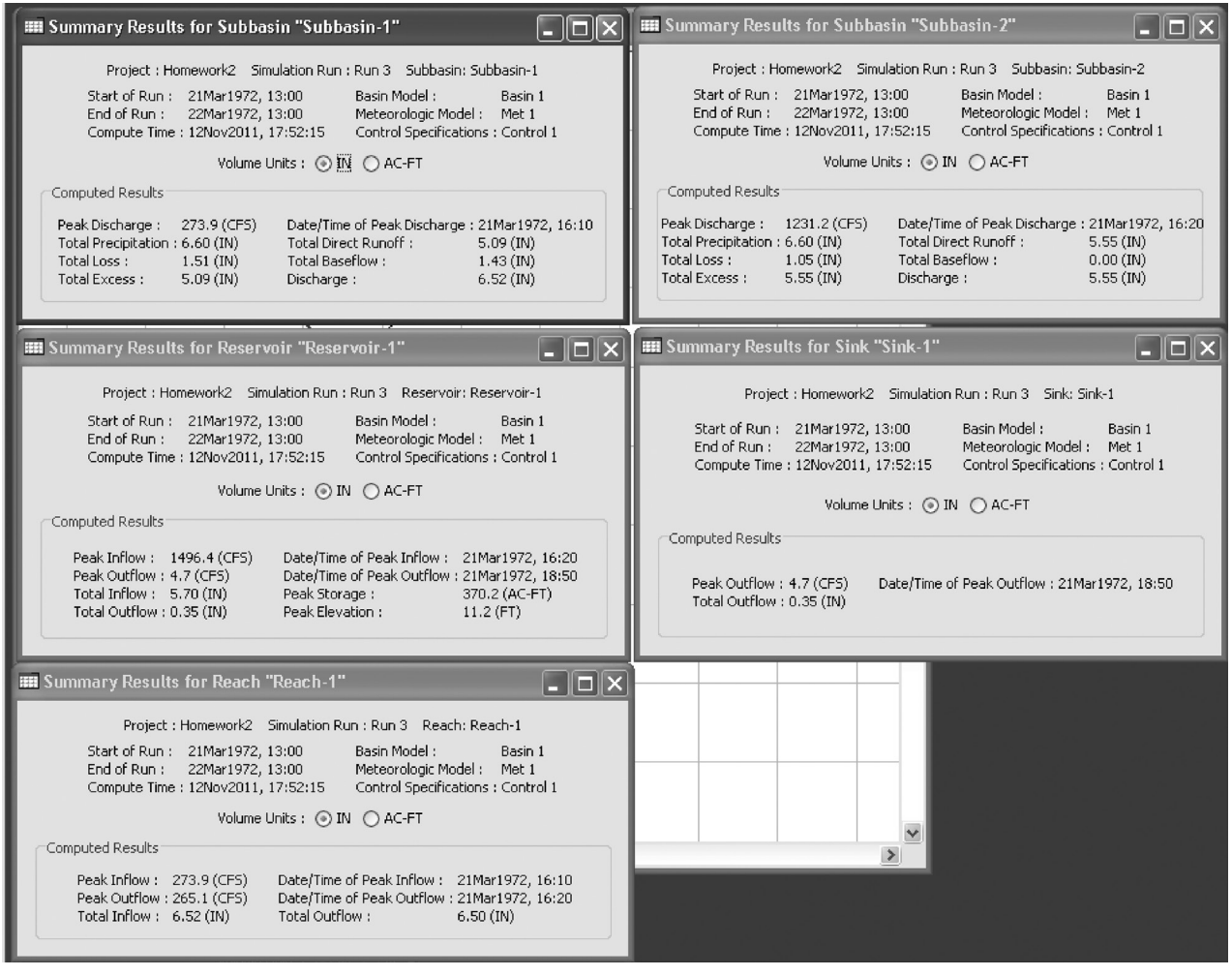

FIGURE 11.39 Results of the different elements of the simulation.

illustrate two or more link junctions, the location of lateral inflows into the system, or storage elements like detention pond, settling pond, or lake.

Capabilities of Hydrologic Simulation: StormNET incorporates different hydrologic processes in runoff production, including the following:

- Temporal variations of rainfall
- Evaporation from water bodies
- Snowpack and melting
- Depression storage
- Infiltration
- Percolation of water into groundwater layers
- Interflow between surface water bodies and groundwater
- Nonlinear reservoir routing

To consider the spatial variability of different parameters, the study area is divided into a number of smaller, homogeneous sub-basins. The overland flow is routed between sub-basins or between entry points of a drainage system.

Capabilities of Hydraulic Simulation: StormNET is empowered through incorporating different hydraulic modeling capabilities for routing runoff and external inflows through the drainage system network. Therefore, the model is able to

- Analyze networks with different sizes
- Configure various closed and open conduit shapes as well as natural channels
- Consider specific components of drainage system such as flow dividers, weirs, and orifices
- Apply external flows and water quality inputs from different sources
- Utilize different flow routing methods regarding the available data and the accuracy of the required results
- Model various flow regimes
- Incorporate pumps, orifice openings, and weir crest levels based on user-defined dynamic control rules

Capabilities in Detention Pond Simulation: StormNET is capable of routing in complex detention ponds. StormNET's interconnected pond routing enables the user to easily model the complex ponding situations caused by downstream conditions (which may result in backwater effects that influence the performance of a detention pond) with confidence.

Capabilities in Water Quality Simulation: StormNET is capable of runoff computation and routing of pollutants. Some of the water quality simulation capabilities are as follows:

- Pollutant buildup in dry weather over different land uses and effects of street cleaning on it
- Pollutant washoff during storms from different land uses and effects of best management practices (BMPs) on its reduction
- Direct contribution of rainfall on water quality
- Entry sanitary flows in dry weather and specific external inflows at different points of the system
- Routing of water quality constituents through the drainage system
- Reduction in constituent concentration because of treatment or natural processes in the system

Typical Applications of StormNET: StormNET has been used in a variety of studies around the world. The fields of applications of this model are as follows:

- Design of drainage systems for flood control purposes
- Design of detention structures for flood control and water quality protection

- Mapping floodplains of natural channel systems
- Minimizing combined sewer overflows through application of some strategies and evaluation of inflow and infiltration impact on sanitary sewer overflows
- Evaluating the nonpoint source pollutant loadings for waste load allocation studies and effects of BMP application on reducing wet weather pollutant loadings

Program Output: The following sections are included in the output summary report of StormNET:

1. List of errors that occurred during the simulation
2. Summary list of input data
3. Summary of rainfall data used during the simulation
4. Description of control rule actions used during the analysis
5. Reporting of mass continuity errors for runoff quantity and quality, groundwater flow, and transportation system water flow and quality
6. Summary of sub-basin runoff calculations including total rainfall, inflow from adjacent sub-basins, evaporation, infiltration, runoff, and runoff coefficient
7. Summary of node depths including average water depth, maximum water depth, maximum hydraulic head, time of maximum water depth occurrence, flooding volume, and flood duration
8. Summary of conduit flow including maximum flow rate and its timing, maximum flow velocity, conduit design flow (i.e., full normal flow), ratio of the maximum flow to the conduit's design flow, duration of conduit surcharging for each conduit
9. Flow classification summary (for dynamic wave routing only) including the following for each conduit:
   - Fraction of time that the conduit is in each of the following conditions:
     - Dry on both ends or each of the upstream or downstream ends
     - Subcritical and supercritical flow
     - Critical flow at different points of the conduit
   - Average Froude number of the flow
   - Average change in flow over time
10. Identities of the five nodes with the highest flow continuity errors
11. Identities of the five elements that most often determine the time step length used for the flow routing
12. Range of taken flow routing time steps and the percentage of steady-state time steps

Example 11.16

Consider a basin with an area of 81 ha. The basin can be divided into four sub-basins with different slopes (Figure 11.40). An earth-filled trapezoidal cross-section open channel is used for basin drainage. The bottom width of the channel is 4 m and its height is 2 m. The CN of the basin is determined to be 80. Determine the outlet discharge hydrograph of a channel for a 24 h storm with a 100-year return period, as given in Figure 11.41.

The specifications of the sub-basins, channels, and junctions are given in Tables 11.9 through 11.11, respectively. For other properties, use the default values given in StormNET.

Solution:

Step 1: The basins are developed in the StormNET environment based on the data given in Table 11.9. The properties of the sheet of basins and the values considered as default are illustrated in Figure 11.42.

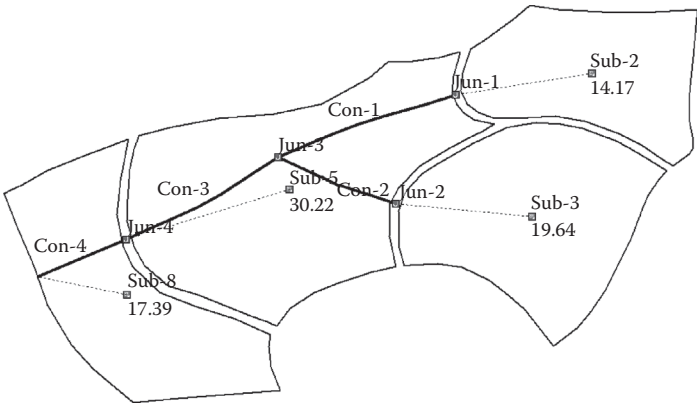

FIGURE 11.40 Schematic of the sub-basin in Example 11.16.

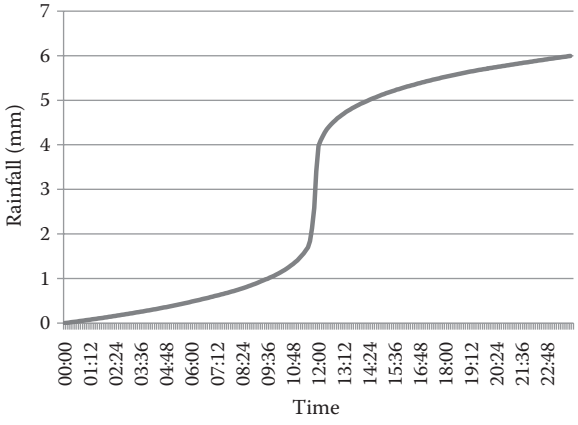

FIGURE 11.41 Cumulative distribution of a 24 h storm with a 100-year return period.

Step 2: In this step, the junctions and channels are defined based on the data given in Tables 11.10 and 11.11 (Figure 11.43).
Step 3: Define the rain gauge and time series of the storm in the related window as illustrated in Figure 11.44.
Step 4: Run the model and view the results (Figure 11.45).

TABLE 11.9
Example 11.16 Sub-Basin Specifications

Sub-Basin Name	Area (ha)	Slope (%)	CN	Outlet Junction
Sub-2	14.17	0.05	80	Jun-1
Sub-3	19.64	0.04	80	Jun-2
Sub-5	30.22	0.04	80	Jun-4
Sub-8	17.39	0.03	80	Out-1

TABLE 11.10
Channel Length

Link Name	Length (m)
Con-1	922
Con-2	618
Con-3	850
Con-4	468

TABLE 11.11
Junction Elevation

Outlet Junction	Elevation (m)
Jun-1	907.25
Jun-2	906.0
Jun-3	903.0
Jun-4	902.0
Out-1	898.5

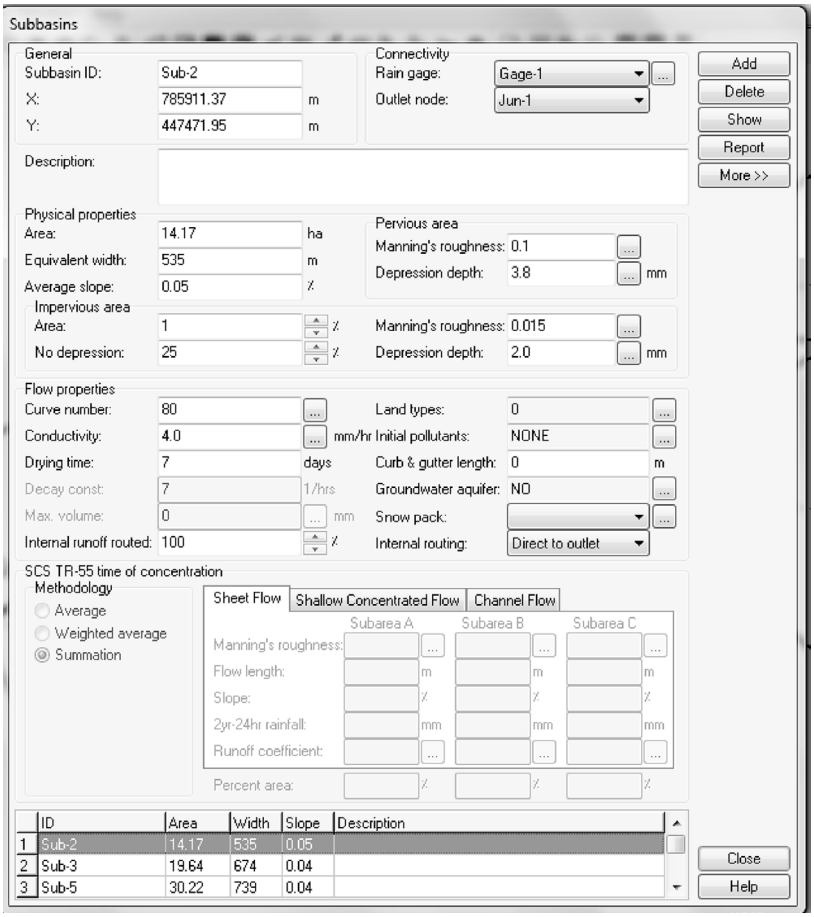

FIGURE 11.42 Defining the sub-basin properties.

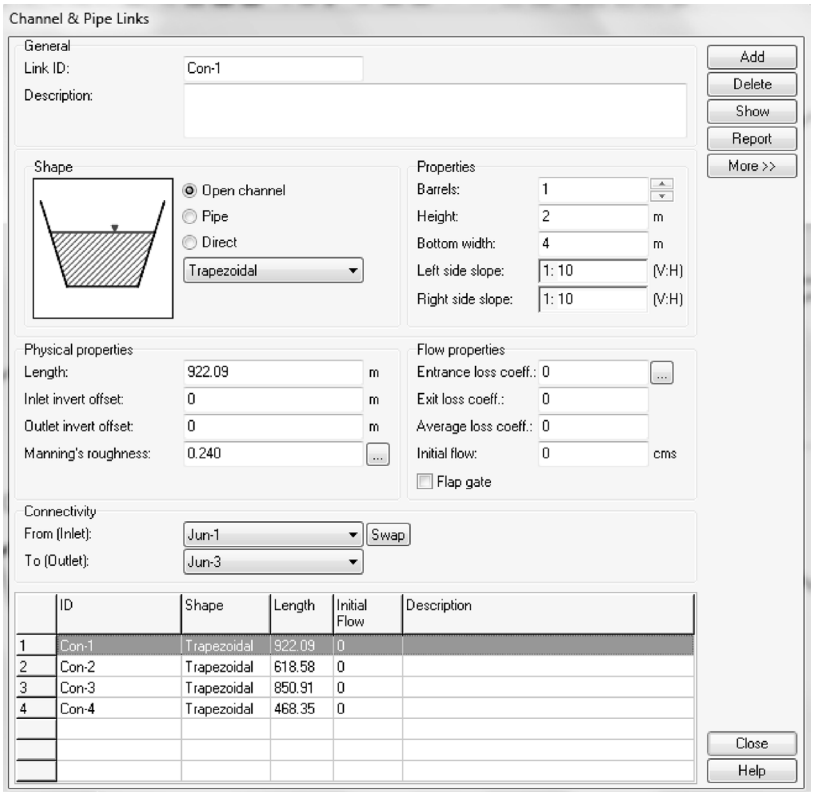

FIGURE 11.43 Defining the channel properties.

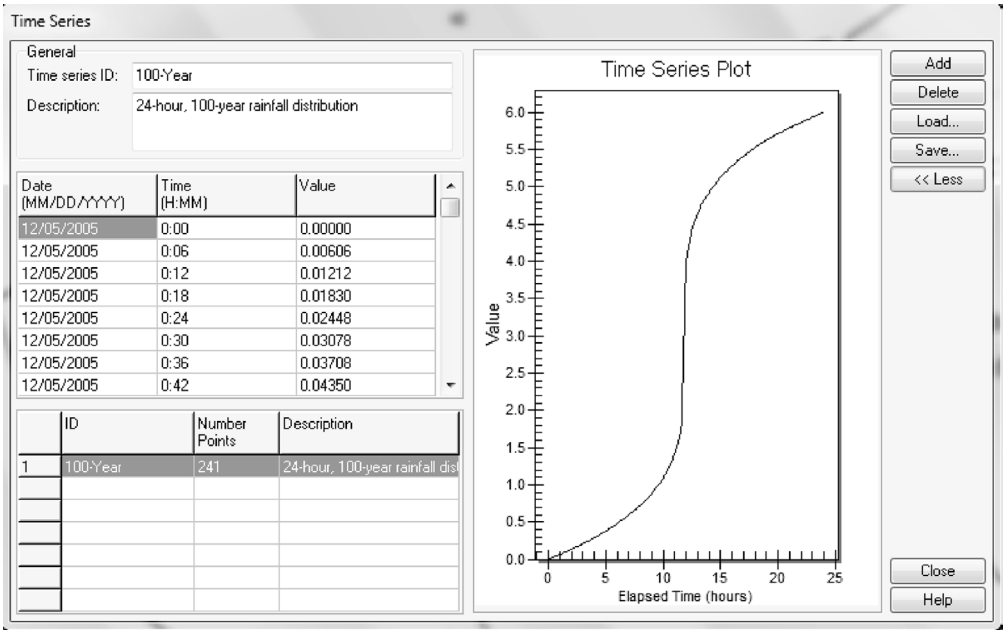

FIGURE 11.44 Defining the storm time series.

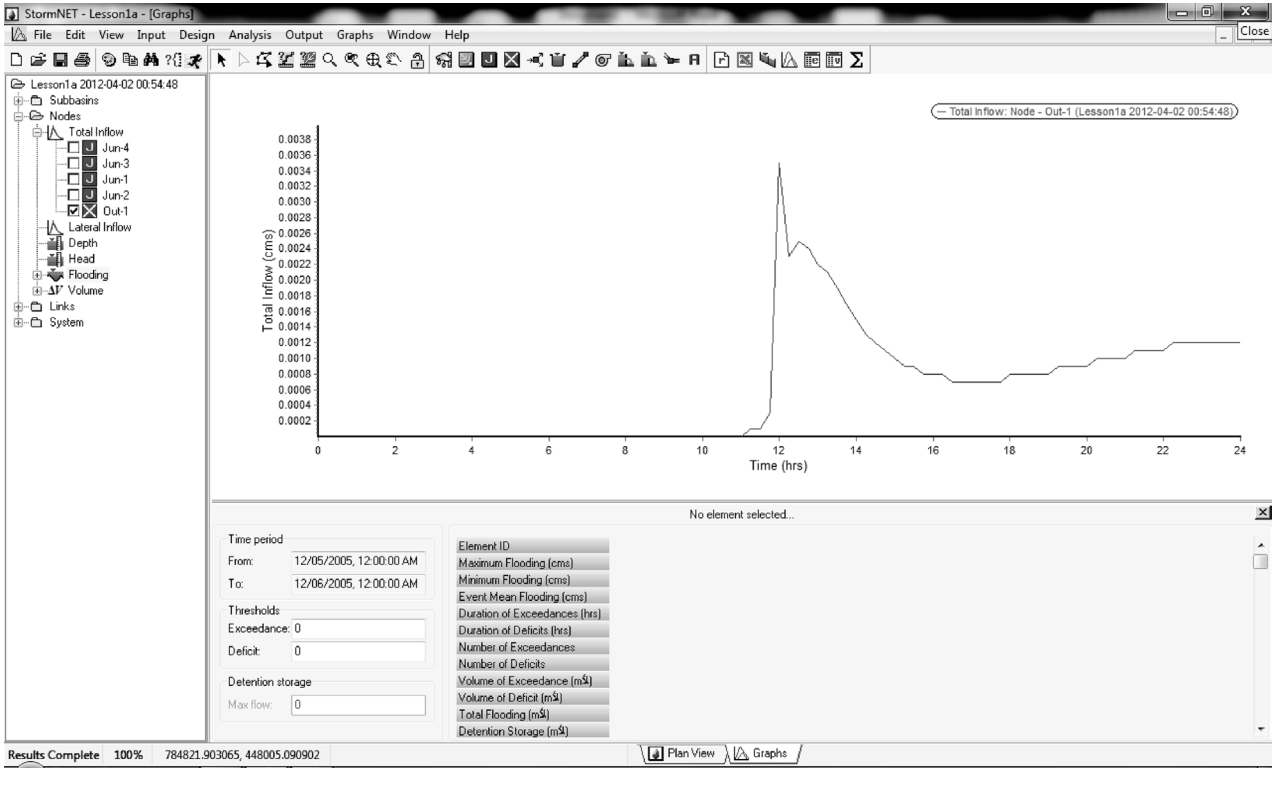

FIGURE 11.45 Outlet hydrograph.

11.3.3.3 HBV

The HBV rainfall–runoff model (Bergström 1992) considers both conceptual and numerical descriptions in the simulation of hydrological processes. The basis of this model is the general water balance, which is described as

$$P - E - Q = \frac{\mathrm{d}}{\mathrm{d}t}[SP + SM + UZ + LZ + lakes], \tag{11.68}$$

where P is precipitation, E is evapotranspiration, Q is runoff, SP is snowpack, SM is soil moisture, UZ and LZ are water storage in the upper and lower groundwater zone, respectively, and *lakes* is the water storage volume in a lake.

Different versions of HBV have been successfully utilized for rainfall–runoff modeling in more than 40 countries all over the world with completely different climatic conditions such as Sweden, Zimbabwe, India, Iran, and Colombia. The spatial variations of system parameters are incorporated in the modeling process by considering some sub-basins. The model inputs are daily values of rainfall and temperature as well as daily or monthly values of potential evapotranspiration. HBV is used for different purposes such as flood forecasting, simulation of spillways' design flood (Bergström 1992), water resources planning and management (Brandt et al. 1998), and nutrient load estimates (Arheimer and Brandt 1998).

11.3.4 Model Structure

The model inputs are recorded time series of precipitation and temperature as well as the estimated values of potential evapotranspiration in monthly or daily time steps. The usual model analysis time step is 1 day but shorter time steps can also be used. Temperature is used for snow accumulation and melt analysis. It is also used for adjusting potential evaporation for abnormal temperatures, or to calculate potential evaporation. Therefore, in snow-free areas, the temperature data are not needed if the last options are not used.

The model includes the following different subroutines (Seibert 2005):

- Meteorological interpolation
- Snow accumulation and melt
- Evapotranspiration estimation
- Soil moisture accounting
- Routines for runoff generation
- Flow routing between sub-basins and lakes

It is possible to run and calibrate the model separately for different sub-basins and then integrate the outputs of individual sub-basins. In areas with considerable elevation changes such as mountainous areas, some elevation zones are defined for the snow and soil moisture routines. It is also possible to consider some vegetation zones (e.g., forested and non-forested areas) for each elevation zone.

The daily rainfall, temperature, and potential evaporation data are used as model inputs for simulation of daily discharges. The type of precipitation, be it snow or rain, is determined based on the temperature. When the temperature is below threshold temperature, all precipitation is considered to be snow multiplied by a snowfall correction factor, SFCF. The snowmelt volume is estimated using the degree-day method (Equation 11.69). Melt water and rainfall are retained within the snowpack until they exceed the capacity of water holding (CWH). CWH is a certain fraction of the water equivalent of the snow. If the temperature goes below the threshold temperature, liquid water within the snowpack refreezes according to Equation 11.70.

$$melt = CFMAX(T(t) - TT) \tag{11.69}$$

$$refreezing = CFR\ CFMAX(TT - T(t)). \tag{11.70}$$

Rainfall and snowmelt (P) will fill the soil and/or recharge the groundwater depending on the proportion of the soil filling capacity (FC) that is currently filled with water or initial soil moisture (SM) (Equation 11.71). Actual evaporation, E_{act}, from the soil equals the potential evaporation, E_{pot}, if SM/FC is above LP (soil moisture value above which E_{act} reaches E_{pot}). Otherwise, the potential evaporation will decrease linearly with SM/FC (Equation 11.72). LP is groundwater recharge added to the upper groundwater box (SUZ).

$$\frac{\text{recharge}}{P(t)} = \left(\frac{\text{SM}(t)}{\text{FC}}\right)^{\text{BETA}} \tag{11.71}$$

$$E_{act} = E_{pot} \min\left(\frac{\text{SM}(t)}{\text{FC} \cdot \text{LP}}, 1\right). \tag{11.72}$$

PERC is the maximum percolation rate from the upper to the lower groundwater box (SLZ). Runoff from the groundwater storage is calculated based on two or three linear outflow equations depending on whether SUZ is above a threshold value, UZL, or not as expressed in Equation 11.73. The estimated runoff is transformed by a triangular weighting function based on the parameter MAXBAS (Equation 11.74) to result in simulated runoff. In cases with different elevation zones, the changes in precipitation and temperature with elevation are incorporated using parameters of PCALT and TCALT (Equations 11.74 and 11.75).

$$Q_{GW}(t) = K_2\text{SLZ} + K_1\text{SUZ} + K_0 \max(\text{SUZ} - \text{UZL}, 0) \tag{11.73}$$

$$Q_{sim}(t) = \sum_{i=1}^{\text{MAXBAS}} c(i)\, Q_{GW}(t - i + 1) \tag{11.74}$$

$$c(i) = \int_{i-1}^{i} \frac{2}{\text{MAXBAS}} - \left|u - \frac{\text{MAXBAS}}{2}\right| \frac{4}{\text{MAXBAS}^2}\, \mathrm{d}u. \tag{11.75}$$

The mean potential evaporation, $E_{pot,M}$ can be adjusted for a specific day of the year, $E_{pot}(t)$, based on the deviation of the temperature, $T(t)$, from its long-term mean, T_M, and a correction factor, C_{ET} (Equation 11.76).

$$\begin{aligned} &E_{pot}(t) = (1 + C_{ET}(T(t) - T_M))\, E_{pot,M} \\ &0 \le E_{pot}(t) \le 2E_{pot,M} \end{aligned} \tag{11.76}$$

Spatial analysis of precipitation and temperature: A simple weighting routine and lapse rates are used for computation of areal rainfall and temperature. In HBV, a geostatistical method similar to kriging is used. The utilized method works based on optimal interpolation of the recorded data at meteorological stations and the general pattern of the rainfall and temperature.

Snow routine: The degree-day approach described in Chapter 3 is used in the snowmelt routine of the HBV, considering a water holding capacity for snow for delaying runoff. Based on discussions in Chapter 3, different models are used for snowmelt modeling in forests and open areas and are distributed according to the temperature lapse rate. The glacier melt process is similar to snowmelt considering the different degree-day factor. Glacier melt begins when snow storage becomes zero. The snow distribution in each zone is considered by its division into a number of areas with different snow accumulation including snowdrift and snow that is trapped in creeks and other irregularities in rugged terrain.

Evapotranspiration: Long-term mean potential evapotranspiration is used as model input. These data can be adjusted based on temperature anomalies (Lindström et al. 1997). The daily values of evapotranspiration can also be calculated as a proportion of temperature in a monthly time scale. As long as water is available in interception storage form (even in snow form), evaporation will be equal to the potential evaporation. If the interception routine is employed, soil evaporation can be reduced to avoid large values of total evaporation. When the interception routine is not used, the potential evapotranspiration from forested areas is considered to be 15% higher than that from open areas. Therefore, the potential evapotranspiration is dependent on the time of the year, temperature, vegetation, elevation, and precipitation (optionally). Evaporation from lakes is zero until there is ice. A simple weighting subroutine on temperature is used for ice condition modeling. This results in a lag between air temperature and lake temperature. When the weighted temperature becomes negative, the lake is frozen.

Soil routine: The soil routine is an important issue in runoff production. The soil moisture analysis in the HBV model is based on the modified bucket theory. In this theory, a statistical distribution is considered for storage capacities in a basin.

Response function and routing: In this routine, excess water from the soil moisture zone is transformed to runoff and the changes of water storage in lakes, rivers, and other wet areas resulting from direct precipitation and evaporation are also considered. Two components—quick (superficial channels) and slow (baseflow) runoff—are considered for hydrograph. For lakes at the outlet of a sub-basin, level pool routing is performed. For better representation of dynamics of the runoff, it is important to define submodels, based on the outlets of major lakes. The Muskingum or simple time lag methods are used for the routing between sub-basins with different response functions.

Lakes: Precipitation on lakes is considered to be the same as that on non-forested zones at the same altitude. It is added to the lake water storage (regardless of ice condition) regardless of its type (rain or snow). Runoff is formed after water routing based on the rating curve.

Model calibration: For evaluation of model calibration efficiency, the Nash and Sutcliffe (1970) efficiency, R_{eff}, is used.

$$R_{\text{eff}} = 1 - \frac{\sum (Q_{\text{sim}}(t) - Q_{\text{obs}}(t))^2}{\sum \left(Q_{\text{sim}}(t) - \bar{Q}_{\text{obs}}\right)^2}, \tag{11.77}$$

where Q_{sim} and Q_{obs} are simulated runoff and observed runoff of the basin, respectively. R_{eff} compares the model prediction with the simplest possible prediction considered to be the mean observed value over the entire period. Larger values of R_{eff} show better model performance. R_{eff} values of more than zero are acceptable and when R_{eff} is equal to 1, the model is perfectly simulated and it means $Q_{\text{sim}(t)} = Q_{\text{obs}(t)}$. When $R_{\text{eff}} < 0$, the simulation of the model is very poor.

Example 11.17

Calibrate the HBV model for a catchment for the period 2006-01-01 to 1990-01-01. The data needed are shown in Tables 11.12 and 11.13.

TABLE 11.12
Monthly Evaporation

Month	1	2	3	4	5	6	7	8	9	10	11	12
Evaporation (mm)	1.445	0	3.336	93.255	195.336	272.927	288.745	280.9	212.027	137.882	55.968	16.227

TABLE 11.13
Daily Precipitation, Temperature, and Runoff

Date	Precipitation (mm)	Temperature (°C)	Q_{sim} (m^3/s)	Date	Precipitation (mm)	Temperature (°C)	Q_{sim} (m^3/s)
2006-01-01	0	0	0.41	2006-01-31	0	–1.4	0.682
2006-01-02	0	–0.8	0.409	2006-02-01	0	–0.4	0.559
2006-01-03	0	–0.3	0.389	2006-02-02	0	–0.3	0.54
2006-01-04	0	1.3	0.379	2006-02-03	10	4.9	0.592
2006-01-05	0	2.6	0.412	2006-02-04	9.5	5.1	1.109
2006-01-06	0	3.5	0.436	2006-02-05	0	3.4	1.093
2006-01-07	0	5.2	0.381	2006-02-06	0	3.3	0.949
2006-01-08	9.5	1.6	0.441	2006-02-07	0.7	2.7	0.942
2006-01-09	0	0.5	0.472	2006-02-08	6.7	6.1	1.538
2006-01-10	0	0.7	0.424	2006-02-09	35.9	8.5	5.824
2006-01-11	0	–0.6	0.448	2006-02-10	1.5	5.9	3.414
2006-01-12	0	–0.9	0.432	2006-02-11	0	7.9	2.163
2006-01-13	0	0.3	0.391	2006-02-12	0	5.5	1.868
2006-01-14	0	–1.8	0.41	2006-02-13	0	7.4	1.642
2006-01-15	0	–1	0.424	2006-02-14	5.8	6	1.493
2006-01-16	0	–2.5	0.445	2006-02-15	16.7	5.9	1.767
2006-01-17	0	–2.7	0.391	2006-02-16	10	4.4	1.909
2006-01-18	0	–3.5	0.395	2006-02-17	0.5	0.3	1.509
2006-01-19	0	–3	0.369	2006-02-18	0	–0.4	1.222
2006-01-20	0	–2.3	0.354	2006-02-19	0	3.4	1.116
2006-01-21	0	–0.9	0.457	2006-02-20	0	3.1	1.071
2006-01-22	0	–2.8	0.369	2006-02-21	0	4.4	1.015
2006-01-23	0	–2.9	0.401	2006-02-22	0	5.5	1.033
2006-01-24	1.3	4.6	0.402	2006-02-23	0	5.4	1.066
2006-01-25	1	3.9	0.468	2006-02-24	0	6.4	1.118
2006-01-26	23	2.8	0.572	2006-02-25	0	7.3	1.18
2006-01-27	1	3.9	0.731	2006-02-26	0	8.5	1.316
2006-01-28	0	2.1	0.738	2006-02-27	2.2	8.6	1.397
2006-01-29	0	–2.3	0.67	2006-02-28	0	10	1.291
2006-01-30	0	–3.4	0.626				

Solution:

This catchment behaves exactly as the HBV model sees the world; therefore, you might be able to achieve a perfect fit. It is a good idea to start with the snow routine, and then work on the soil routine parameters to get the water balance correct and finally fix the response function. You might have to do this in iterations. During calibration, search for different variables as well, i.e., soil moisture and storage in the upper groundwater box. Once you have reached a perfect fit,

TABLE 11.14
HBV-Light Model Parameter

	Parameter	Definition	Units	Best Value
Snow routine	TT	Threshold temperature	C	0.355
	CFMAX	Degree-day factor	mm C^{-1} day^{-1}	0.65
	SFCF			0.5
	CFR	Refreezing coefficient		0.05
	CWH			0.1
Soil moisture routine	FC	Maximum value of soil moisture storage	mm	550
	LP	Soil moisture value above which actual ET equals potential ET	mm	0.85
	BETA	Parameter that determines the relative contribution to runoff from rain or snowmelt	–	1
Response routine	PERC	Maximum rate of recharge between the upper and lower groundwater boxes	mm day^{-1}	3.73
	UZL	Threshold for Q_0 flow	mm	12.73
	K_0	Recession coefficient (upper box)	day^{-1}	0.48
	K_1	Recession coefficient (upper box)	day^{-1}	0.053
	K_2	Recession coefficient (lower box)	day^{-1}	0.018
Routing routine	MAXBAS	Length of triangular weighting function in routing routine	day	1.48

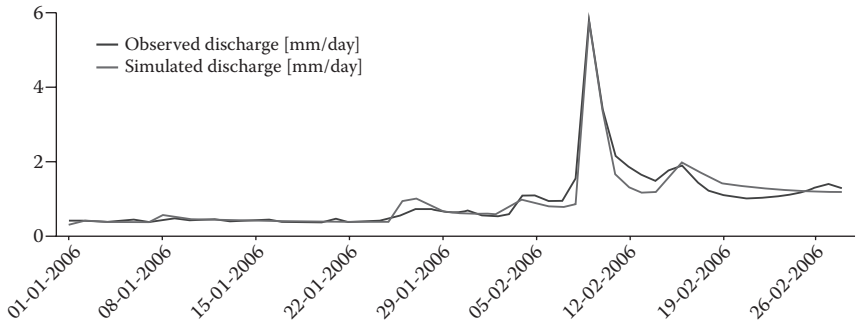

FIGURE 11.46 Difference between simulated and observed runoff.

you may again change parameter values and study the effects of different parameter values. The final model's parameters are shown in Table 11.14. Figure 11.46 shows the difference between the simulated and observed runoff. The value of R^2 for the calibration period is 0.94.

11.3.5 Distributed Hydrological Models

Today, it is possible to capture and manage a large amount of data of spatially distributed hydrological parameters and variables by application of developments of remote sensing technology and geographic information system (GIS). GISs provide the geo-referenced data that can be overlaid and merged and provide a visualization of the data (Figure 11.47). These are key tasks that simplify distributed hydrological modeling. In this section, as an example of distributed hydrological models, the watershed modeling system (WMS) is described.

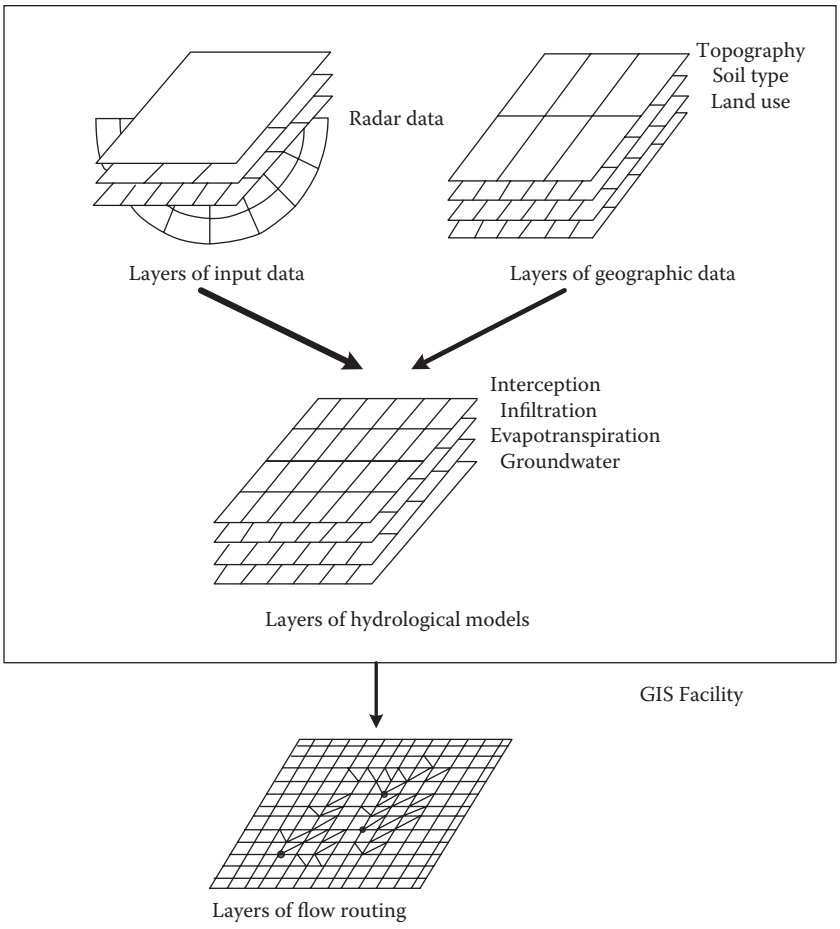

FIGURE 11.47 Schematic of the distributed hydrological modeling system.

11.3.5.1 Watershed Modeling System

WMS is a distributed graphical modeling environment for modeling watershed hydrology and hydraulics. WMS is empowered by different tools that facilitate the modeling procedures such as

- Automated basin delineation
- Geometric parameter calculations
- GIS overlay computations such as CN, rainfall depth, and roughness coefficients
- Cross-section extraction from terrain data.
- Automated watershed delineation

If digital elevation map (DEM) is used, WMS can automatically determine watershed boundaries (Figure 11.48). After determining the watershed boundary, different useful basin data such as area, slope, mean elevation, and maximum flow distance are calculated. WMS locates all flow paths on the whole terrain model, which make it possible to examine flow patterns in different parts of the basin. The longest flow path in each sub-basin, which is used for estimation of the time of concentration, is also calculated.

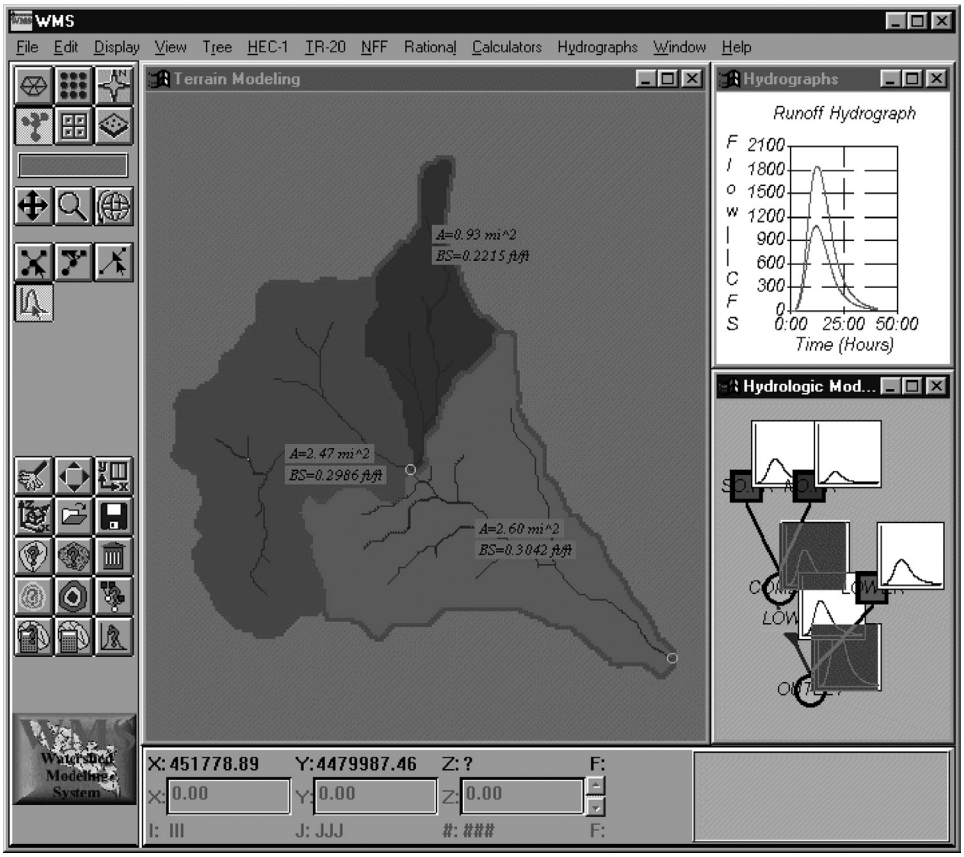

FIGURE 11.48 WMS screenshot.

- Floodplain modeling and mapping

  Using the interpolation algorithms of WMS, flood extents and flooding depth maps can be developed based on DEMs and water surface data can be obtained from hydraulic analysis. There are fast and easy channel hydraulics analysis tools in WMS to create approximate maps. There is an interface with HEC-RAS (Hydrologic Engineering Center River Analysis System) and flood mapping tools in WMS for detail analysis.
- Stochastic modeling

  The model parameters' uncertainty can be analyzed using the automated stochastic modeling tools in WMS. These tools automatically change the values of certain parameters (such as CN or roughness) in the model input file and the simulation can be run with different values.
- Storm drain network modeling

  WMS can simulate the storm drain system. A storm drain network with different components is created in integration with the surface runoff model or any other hydrologic model supported by WMS.
- 2D (Distributed) hydrology

  A 2D finite-difference grid analysis approach is used for surface runoff analysis. Also, 1D channel hydraulics and groundwater interaction are incorporated in a comprehensive

hydrologic cycle model. The single-event or long-term rainfall can be simulated by WMS. This model can be applied in

Flood forecasting (in 2D scheme)
Thunderstorm (localized rainfall) flood analysis
Surface ponding and infiltration analysis
Groundwater/surface water interaction modeling

PROBLEMS

1. Assume that you want to model the rainfall–runoff of a basin in order to forecast the runoff in the coming years. The historical data of temperature, evaporation, and precipitation in a 10-year time horizon are presented in Table 11.15. Formulate a multiple regression model for estimating the runoff data and comment on selecting the independent variables.
2. A 200 km^2 watershed has a lag time of 100 min. Baseflow is considered constant at 20 cms. The watershed has a CN of 72 and 30% of imperviousness. Use HEC-HMS to determine the direct runoff for a storm using the SCS Unit Hydrograph method. Precipitation data are presented in Table 11.16.
3. An 8 km^2 watershed has a time of concentration of 1.0 h. Use HEC-HMS to determine the direct runoff for a storm (rainfall hyetograph given in Table 11.17) using the SCS Unit Hydrograph method.

   Hint:

   a. You must create new basin, Meteorologic, and Control Specifications files either in the same project or in a new project.

TABLE 11.15
Historical Data of Temperature, Evaporation, and Precipitation in a 10-Year Time Horizon in Problem 1

Year	Temperature (°C)	Evaporation (mm)	Annual Precipitation (mm)
1991	6.56	745	812
1992	8.2	967	648
1993	7.42	833	670.4
1994	6.68	712	772
1995	7.3	850	670.4
1996	7.45	897	629.6
1997	7.9	915	576
1998	8.8	942	556
1999	8.64	888	656
2000	8.02	832	640

TABLE 11.16
Precipitation Data for Problem 2

Date	2000-01-01, 00:00	2000-01-01, 03:00	2000-01-01, 06:00	2000-01-01, 09:00	2000-01-01, 12:00
Incremental rainfall (cm)	0	0.5	1.25	1.25	0.5

TABLE 11.17
Precipitation Data for Problem 3

Time (min)	Excess Rainfall (cm)
0	0
10	0.6
20	1.5
30	1.2
40	0.1
50	0
60	0

b. You will need only one sub-basin element in the basin file with area and SCS hydrograph details. You will only need the transform method. Specify None for loss method (input provided is excess rainfall) and baseflow.
c. The input to the Meteorologic file involves using the Time Series Data Manager from the Components menu. This will add a time series data folder in the watershed explorer and you will expand this folder to specify the rainfall hyetograph. When you edit the Meteorologic model in the component editor, you will use the Specified hyetograph (default) method. You will then click on the specified hyetograph option in the watershed explorer and link the time series data to the Meteorologic model.
d. In the Control Specifications model, use 10 min time interval and 12 h simulation time (end time = 12 h past start time).

4. The parameters of a small undeveloped watershed are listed in Tables 11.18 and 11.19. A unit hydrograph and Muskingum routing coefficients are known for sub-basin 3, as shown in Figure 11.49. TC and R values for sub-basins 1 and 2 and associated SCS CNs are provided as shown. A 5 h rainfall hyetograph (in cm/h) is shown in Figure 11.50 for a storm event that occurred on June 19, 2010. Assume that the rain fell uniformly over the watershed. Use the information given to develop a HEC-HMS input data set to model this storm. Run the model to determine the predicted outflow at point B (Muskingum coefficient: X = 0.15, K = 3 h, area = 3.3 km^2).

TABLE 11.18
Properties of Sub-Basins in Problem 4

Sub-Basin Number	TC (h)	R (h)	SCS CN	% Impervious	Area (km^2)
1	2.5	5.5	66	0	2.5
2	2.8	7.5	58	0	2.7
3	–	–	58	00	3.3

TABLE 11.19
UH for Sub-Basin 3 in Problem 4

Time (h)	0	1	2	3	4	5	6	7
U (cms)	0	200	400	600	450	300	150	0

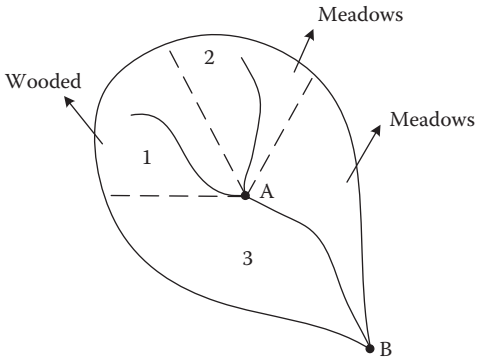

FIGURE 11.49 Watershed in Problem 4.

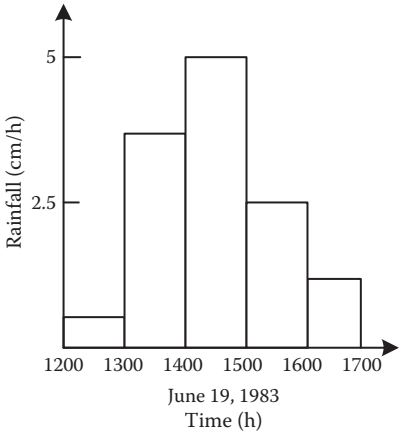

FIGURE 11.50 Rainfall hyetograph in Problem 4.

5. Develop an MLP model with two hidden layers and three perceptrons with logsig and linear function in each layer, respectively. The input of the MLP model is rainfall, evaporation, and temperature, and the inflow must be simulated. Use the given data in Table 11.20 for model development.
6. Develop a TDL, GRNN, and RNN model for the data of Problem 5 and then compare and discuss the results of different simulations with ANN's models.
7. Calibrate the HBV model for the catchment described in Tables 11.21 and 11.22 for the period 2002-03-01 to 2002-05-01. Discuss, before running the model, what effects you expect and then make a note of each change in parameter value and its effect on the simulation.
8. Simulate the rainfall–runoff model in Problem 5 with IHACRES and then compare the difference between the next 2 months' predictions with these two models.
9. Fuzzy sets A and B are defined in $X = [-\infty, \infty]$ by the membership functions as follows:

$$\mu_A(x) = \begin{cases} x & \text{if} \quad 0 \le x \le 1 \\ -x + 2 & \text{if} \quad 1 < x \le 2 \\ 0 & \text{otherwise.} \end{cases}$$

TABLE 11.20
Observed Rainfall, Evaporation, and Temperature, and Inflow Data for Problem 5

Inflow (m^3/s)	Temperature (°C)	Rainfall (mm)	Evaporation (mm)	Day	Inflow (m^3/s)	Temperature (°C)	Rainfall (mm)	Evaporation (mm)	Day
3.32	14.7	4.5	2.4	1	5.93	6.9	0	0	31
4.31	15.1	0	3.5	2	6.57	4.7	6	0	32
4.33	14.2	0	3.5	3	6.02	5	0	0	33
4.29	14.9	10	2.3	4	6.68	5.6	0	0	34
4.51	8.7	2.5	1.6	5	6.81	8.6	0	0	35
4.53	12.1	3.5	1.7	6	6.55	6.3	0	0	36
5.54	13.3	2.5	2.5	7	6.67	9.4	0	0	37
5.41	13.5	0	3.9	8	7.31	9.3	1.5	0	38
3.23	10.3	0	2.2	9	7.3	6.2	0	0	39
3.21	9.1	0	2.2	10	8.07	3.9	9.5	0	40
3.29	11.2	0	1.7	11	7.49	5	4.3	0	41
3.28	11.6	0	3.1	12	6.83	6.1	0	0	42
3.34	13.7	0	1.3	13	7.5	3.6	5	0	43
3.03	15.7	0	3.1	14	6.82	4.6	11	0	44
3.01	15.7	0	3.5	15	6.45	6.5	0	0	45
3.06	13.2	1.7	2.2	16	6.68	6.6	0	0	46
3.23	11	2.2	2.2	17	6.66	5.8	0.5	0	47
3.25	13.2	0	2.6	18	6.04	7.7	0	0	48
3.19	13.8	0	3.1	19	6.13	8.6	0	0	49
3.45	11.8	0	2.6	20	7	5.3	1	0	50
4.34	9.3	8	2.3	21	6.99	6	2.5	0	51
4.36	8.6	4.3	1.9	22	8.86	5.6	0	0	52
4.51	10.2	0	2.2	23	8.86	6.7	0	0	53
4.59	12.2	0	2.6	24	7.06	7.1	6.5	0	54
4.4	12.4	0	2.2	25	7.07	7.4	1	0	55
4.01	8.6	0	1.3	26	6.02	4.6	0	0	56
11.31	6.8	26	0.2	27	4.86	5.7	0	0	57
9.38	1	23	0	28	8.08	5.8	3	0	58
8.33	0.3	0	0	29	8.12	7.3	0.8	0	59
6.5	4	0	0	30	8.06	5.9	0	0	60

TABLE 11.21
Monthly Average of Evaporation in Problem 7

Month	1	2	3	4	5	6	7	8	9	10	11	12
Evaporation (mm)	1.445	0	3.336	93.255	195.336	272.927	288.745	280.9	212.027	137.882	55.968	16.227

TABLE 11.22
Observed Rainfall, Temperature, and Inflow in Problem 7

Date	Precipitation (mm)	Temperature (°C)	Q (m^3/s)	Date	Precipitation (mm)	Temperature (°C)	Q (m^3/s)
2002-03-01	0	6.6	0.68	2002-04-01	0	8.6	1.973
2002-03-02	0	8.3	0.778	2002-04-02	15.5	6.2	2.808
2002-03-03	0	9.3	0.865	2002-04-03	16.2	5.8	3.284
2002-03-04	0	12.1	0.823	2002-04-04	2.5	5.6	2.523
2002-03-05	0	13.1	0.943	2002-04-05	0.5	8.3	2.283
2002-03-06	0	8.8	1.03	2002-04-06	0	10.1	2.369
2002-03-07	0	6.1	1.03	2002-04-07	2	12.3	2.494
2002-03-08	0	7.2	1.038	2002-04-08	0	13.1	2.686
2002-03-09	0	9.6	0.823	2002-04-09	0	13.8	2.798
2002-03-10	0	7.2	0.804	2002-04-10	0	13.2	2.914
2002-03-11	0	6.7	0.827	2002-04-11	5.7	9.8	2.917
2002-03-12	0	8.7	0.815	2002-04-12	13.1	6.2	3.061
2002-03-13	0	11.2	0.889	2002-04-13	18.8	5	3.484
2002-03-14	0	13.7	0.898	2002-04-14	0	7.7	3.183
2002-03-15	0	14	0.88	2002-04-15	0	11.2	3.038
2002-03-16	1.7	11.5	0.91	2002-04-16	2.5	12.8	2.543
2002-03-17	1.5	10.1	1.059	2002-04-17	6	15.5	3.432
2002-03-18	1	8.3	1.63	2002-04-18	5	13.3	4.867
2002-03-19	13.5	9.5	2.816	2002-04-19	35.6	11.5	6.546
2002-03-20	3.5	13.3	1.832	2002-04-20	4	10.5	6.911
2002-03-21	7.5	8.6	1.901	2002-04-21	1	11	5.117
2002-03-22	1.7	6.2	1.985	2002-04-22	2	9.1	3.867
2002-03-23	6.7	6.2	2.283	2002-04-23	0	9.1	3.87
2002-03-24	0	9.7	1.834	2002-04-24	0	10.4	3.753
2002-03-25	0	12.3	1.849	2002-04-25	6	12.6	3.725
2002-03-26	0	15	1.729	2002-04-26	0	11.8	3.789
2002-03-27	0	14.8	2.065	2002-04-27	1.5	11.1	4.052
2002-03-28	5.7	12.7	2.184	2002-04-28	0	16.2	3.826
2002-03-29	7	6.5	2.237	2002-04-29	0.7	15.8	3.945
2002-03-30	0	6.4	1.237	2002-04-30	0	14.2	4.092
2002-03-31	3.5	6.2	1.973				

TABLE 11.23
Streamflow of Season 1 in Problem 11

	Streamflow Following Season 2		
Streamflow in Season 1	**0–3 m^3/s**	**3–6 m^3/s**	**>6 m^3/s**
0–10 m^3/s	0.25	0.50	0.25
>10 m^3/s	0.05	0.55	0.40

TABLE 11.24
Streamflow of Season 2 in Problem 11

	Streamflow Following Season 2	
Streamflow in Season 2	**0–10 m^3/s**	**>10 m^3/s**
0–3 m^3/s	0.70	0.30
3–6 m^3/s	0.50	0.50
>6 m^3/s	0.40	0.60

$$\mu_B(x) = \begin{cases} x/2 & \text{if} \quad 0 \le x \le 2 \\ 1 & \text{if} \quad 2 \le x \le 3 \\ -x+4 & \text{if} \quad 3 \le x \le 4 \\ 0 & \text{otherwise.} \end{cases}$$

Determine the membership functions of $A \cap B$, $A \cup B$, and $A + B$ fuzzy sets.

10. Consider fuzzy set A defined in $X = [-2,2]$ as follows:

$$\mu_A(x) = \begin{cases} \dfrac{2+x}{1} & \text{if} \quad -2 \le x \le 0 \\ \dfrac{2-x}{1} & \text{if} \quad 0 < x \le 2 \\ 0 & \text{otherwise.} \end{cases}$$

Determine the membership function of the fuzzy set induced by the function $f(x) = 2x$.

11. The transition probabilities of a Markov chain model for streamflow in two different seasons are given in Tables 11.23 and 11.24.

Calculate the steady-state probabilities of flows in each interval in each season.

REFERENCES

Arheimer, B. and Brandt, M. (1998). "Modelling nitrogen transport and retention in the catchments of southern Sweden," *Ambio*, 27 (6), 471–480.

Atiya, A. and Parlos, A. (1992). Nonlinear system identification using spatiotemporal neural networks, Proc. Intl. Joint Conf. on Neural Networks, Baltimore, MD, The IEEE, Inc., Piscataway, NJ, 2, pp. 504–509.

Bergström, S. (1992). The HBV model—its structure and applications. SMHI RH No 4, Norrköping.

Bose, N.K. and Liang, P. (1996). *Neural Network Fundamentals with Graphs, Algorithms, and Application*, McGraw-Hill, New York.

Brandt, M., Bergström, S. and Gardelin, M. (1988). "Modelling the effects of clearcutting on runoff—examples from Central Sweden," *Ambio*, 17 (5), 307–313.

Clouse, D.S., Giles, C.L., Horne, B.G. and Cottrell, G.W. (1997). "Time-delay neural networks: Representation and induction of finite state machines," *IEEE Trans. on Neural Networks*, 8 (5), 1065–1070.

Coulibaly, P., Anctil, F. and Bobe, E.B. (2001). "Multivariate reservoir inflow forecasting using temporal neural networks," *Journal of Hydrologic Engineering ASCE*, 6 (5), 367–376.

Demuth, H. and Beale, M. (2002). Neural Network Toolboox for MATLAB, User's Guide. http://www.mathworks.com/.

Elman, J.L. (1990). "Finding structure in time," *Cognitive Science*, 14, 179–211.

Fujiwara O., Puangmaha, W. and Hanaki, K. (1988). "River basin water quality management in stochastic environment" *Journal of Environmental Engineering, ASCE*, 114 (4), 864–877.

Jakeman, A.J. and Hornberger, G.M. (1993). "How much complexity is warranted in a rainfall–runoff model?" *Water Resour. Res.*, 29 (8), 2637–2649.

Karamouz, M., Szidarovszky, F. and Zahraie, B. (2003). *Water Resources Systems Analysis*, Lewis Publishers, CRC Press, Boca Raton, FL

Karamouz, M., Razavi, S. and Araghinejad, Sh. (2007). "Long-lead seasonal rainfall forecasting using time-delay recurrent neural networks: A case study," *Journal of Hydrological Processes*, 22 (2), 229–238.

Lindström, G., Johansson, B., Persson, M., Gardelin, M. and Bergström, S. (1997). "Development and test of the distributed HBV-96 hydrological model," *Journal of Hydrology*, 201, 272–288.

Littlewood, I.G. and Jakeman, A.J. (1994). "A new method of rainfall–runoff modelling and its applications in catchment hydrology." In *Environmental Modeling* (Volume II), Zannetti, P., ed, Computational Mechanics Publications, Southampton, UK, 143–171.

Nash, J.E. and Sutcliffe, J.V. (1970). "River flow forecasting through conceptual models, Part I—A discussion of principles," *Journal of Hydrology*, 10, 282–290.

Price, W.L. (1965). "A controlled random search procedure for global optimization," *Computer Journal*, 7, 347–370.

Rubinstein, R.Y. (1981). *Simulation and Monte Carlo Method*, Wiley, New York.

Seibert, J. (2005). *HBV Light Version 2, User's Manual*, Stockholm University.

Solomatine, D.P. (1999). "Two strategies of adaptive cluster covering with descent and their comparison to other algorithms," *Journal of Global Optimization*, 14 (1), 55–78.

Specht, D. (1991). "A general regression neural network, *IEEE Transactions on Neural Networks*," 2 (6), 568–576.

StatSoft, Inc. (2012). Electronic Statistics Textbook. Tulsa, OK: StatSoft. http://www.statsoft.com/textbook/.

Waibel, A., Hanazawa, T., Hintin, G., Shikano, K. and Lang, K.J. (1989). "Phoneme recognition using time delay neural networks," *IEEE Trans. on ASSP*, 37 (3), 328–339.

Wan, E.A. (1993). "Time series prediction using a connectionist network with internal delay lines." In *Time Series Prediction: Forecasting the Future and Understanding the Past*, Weigend, A.S. and Gershenfeld, N.A., eds, Addison-Wesley, Reading, MA, 195–217.

12 Drought Analysis and Management

12.1 INTRODUCTION

Drought is a normal, recurrent feature of climate, although many people think that it is a rare and random event. Drought happens in any climate condition even though its characteristics may be completely different in different regions. Drought is a temporary deviation from normal weather condition and it is different from aridity. Aridity refers to the low rainfall regions and is a permanent feature of climate.

Drought originates from a deficiency of precipitation over an extended period of time. Drought should be considered relative to some long-term average condition of balance between precipitation and evapotranspiration in a particular area, a condition often perceived as "normal." It is also related to the timing (i.e., principal season of occurrence, delays in the start of the rainy season, occurrence of rains in relation to principal crop growth stages) and the effectiveness (i.e., rainfall intensity, number of rainfall events) of the rains. Other climatic factors such as high temperature, high wind, and low relative humidity are often associated with it in many regions of the world and can significantly aggravate its severity.

Based on the hydrologic components that are affected by drought consequences, different types of drought are distinguished, including meteorological, hydrologic, and agricultural drought. Meteorological drought is related to deficiency in precipitation. Hydrologic and agricultural droughts are related to deficit in water resources and soil moisture, respectively. The analysis of drought severity and magnitude is highly dependent on its type and different indices are employed in each case.

Drought is beyond just a physical phenomenon or natural event. Its impacts on society result from the interplay between natural event water resources (less than least expected precipitation resulting from natural climatic variability) and the demand people place on water supply. Human beings often exacerbate the impact of drought. Recent droughts in both developing and developed countries and the resulting economic and environmental impacts and personal hardships have underscored the vulnerability of all societies to this "natural" hazard. Therefore, a type of drought named socio-economic drought is also identified.

In this chapter, different types of drought events including climate, hydrologic, and agricultural drought are defined. The major aspects of drought analysis and prediction as a tool for drought management studies are also covered. Also, some common drought indices as a measure of drought severity and duration are introduced. Finally, this chapter takes a look at drought planning, management, and preparedness. The drought management practices are discussed through case studies.

12.2 DROUGHT AS A HAZARD

Drought differs from other natural hazards in a variety of ways. Drought is a slow-onset natural hazard that is often referred to as a creeping phenomenon. It is an accumulated departure of precipitation from normal or expected (i.e., a long-term mean or average). This accumulated precipitation deficit may accumulate quickly over a period of time, or it may take months before the deficiency

begins to show up in reduced streamflows, reservoir levels, or increased depth to the groundwater table. Because of its creeping nature, the effects of drought are often slow to appear, lagging precipitation deficits by weeks or months. Because precipitation deficits usually first appear as deficits in soil water, agriculture is often the first sector to be affected.

It is often difficult to know when a drought begins. Likewise, it is also difficult to determine when a drought is over and on what criteria this determination should be made. Is an end to drought signaled by a return to normal precipitation and, if so, over what period of time does normal or above-normal precipitation need to be sustained for the drought to be declared officially over? Since drought represents an accumulated precipitation deficit over an extended period of time, does the precipitation deficit need to be erased for the event to end? Do reservoirs and groundwater levels need to return to normal or average conditions? Impacts linger for a considerable period of time following the return of normal precipitation, so is the end of drought signaled by meteorological or climatological factors, or by the diminishing negative impact on human activities and the environment?

Another factor that distinguishes drought from other natural hazards is the absence of a precise and universally accepted definition for it. There are hundreds of definitions, adding to the confusion about whether or not a drought exists and its degree of severity. Definitions of drought should be specific to a region, an application, or an impact. Droughts are regional in extent and, as previously stated, each region has specific climatic characteristics.

Temperature, wind, and relative humidity are also important factors to include in characterizing drought from one location to another. Definitions also need to be application specific because drought impacts will vary between sectors. Drought means something different to a water manager, an agricultural producer, a hydroelectric power plant operator, and a wildlife biologist. Even within sectors, there are many different perspectives on drought because impacts may differ markedly. For example, the impacts of drought on crop yield may differ greatly for maize, wheat, soybeans, and sorghum because they are planted at different times during the growing season and have different water requirements and different sensitivities at various growth stages to water and temperature stress.

In general, drought impacts are nonstructural and spread over a larger geographical area than the damages that result from other natural hazards such as floods, tropical storms, and earthquakes. This, combined with drought's creeping nature, makes it particularly challenging to quantify impacts and even more challenging to provide disaster relief for drought than for other natural hazards. These characteristics of drought have hindered development of accurate, reliable, and timely estimates of its severity and impacts (i.e., drought early warning systems) and, ultimately, the formulation of drought preparedness plans. Similarly, it is difficult for disaster officials that are tasked with the assignment of responding to drought to deal with the large spatial coverage usually associated with its occurrence.

12.3 DROUGHT DEFINITION

In general, droughts are classified into three groups: climatic, hydrological, and agricultural. When drought is just defined from rainfall deficit, it is called climatic drought. For industries and water consumers, drought happens when water supply declines. Therefore, hydrological drought is a result of deficit in effective rainfall over a period compared to the previous periods. For farmers, drought is a condition that causes less harvest (production). Agricultural drought most of the time is defined by the reduction of agricultural products and loss of plants. Continuing rainfall deficits may cause a permanent shortage in soil moisture in the growth season. Therefore, average shortage in soil moisture over a period of several months, manifested through plants that are sensitive to soil moisture and have high water demands, can be used as an indicator for drought severity measurements.

Drought indices are used to monitor the variations in drought condition over a region. A drought index value is typically a single number, far more useful than raw data for decision making. Drought

indices assimilate data from different hydroclimatological variables such as rainfall, snowpack, streamflow, and other water supply indicators into a comprehensible index. Several drought-severity indices for different types of drought have been developed for evaluation and forecasting purposes.

Karamouz and Araghinejad (2008) defined extreme drought as when the system is unable to supply any portion of agricultural water demands and noted that there will be no hydrological drought (normal condition) if the system can supply total agricultural water demands. Any case between these two conditions (no agricultural water supply and complete agricultural supply) could be defined as mild to severe drought according to the portion of allocated agricultural water demands. In their study, two well-known characteristics of drought events, duration and severity, were used to examine the performance of the water resources system. Drought duration gives an indication of how slow the recovery will be, once the system experiences a failure. Severity is a measure of the magnitude of failure in the water supply system.

Various investigations, which can be divided into two categories, have been carried out: studies on point (localized) drought and studies on regional drought. In the point drought analysis, drought in a station or a small area is investigated. Yevjevich (1967), Griffiths (1990), Beric et al. (1990), and Sen (1991a) have studied point drought. In point investigations, a time series of hydroclimatological factors or a drought indicator are evaluated in a specific point. A time sequence and then a truncation level are assigned to separate drought events from other events in order to perform the analytical evaluation.

According to Yevjevich (1967), application of run theory is a fundamental method of analyzing point drought. In this theory, one could detect a consecutive period of shortage or surplus after choosing a truncation level for existing data, by assuming that they are stationary. Then, from the detected consecutive shortage periods, the probability distribution of drought parameters like duration and the amount of shortage is evaluated (Guerrero-Salazer and Yevjevich 1975). Each of the above investigators chose a truncation level based on their specific goals. For example, Sen (1991b) used various probabilities of successful events (wet years) and failure events (shortage). Griffiths (1990) used average and Beric et al. (1990) used consecutive time intervals with no rain (15 days) in the growth season as truncation levels.

In regional drought, severe water shortage conditions in contiguous and extended regions are investigated. Tase (1982), Tase and Yevjevich (1978), Rossi (1979), Sen (1980a), and Santos (1983) worked on this topic. Santos (1983) suggested that besides defining truncation level, the critical area should also be defined. Based on this approach, regional drought is said to occur when the drought-affected area is larger than the critical area.

In regional studies, Tase (1982) and Tase and Yevjevich (1978) used standardized normal distribution values for drought events with different return periods as a truncation level, assuming that all the specified rain gauges in the study area follow the normal distribution. Santos (1983), who has done intensive studies on the analysis of regional droughts, used 0.1 or 0.2 of average areal precipitation as a truncation level.

The objective of analyzing a natural phenomenon is to quantify its behavior. This can usually be done by using the probability distribution function (PDF) of the data. For this purpose, the PDFs are obtained by frequency analysis of generated data after determining the duration and severity of droughts. It is common to use the concept of return period for frequency analysis by answering basic questions like

- What is the largest drought duration between probable droughts and what is its severity?
- What is the most severe drought between the probable drought events?

It requires a large number of statistical data series for which long-term generated data are not enough. Therefore, a planning horizon should be considered the same as the available historical data period. The number of samples that must be generated is also determined. Since each sample

represents only one value for each predefined objective (for example, there is only one drought with maximum intensity in each sample), the number of generated series should be large enough for frequency analysis.

12.4 CLIMATIC DROUGHT

Climatic or meteorological drought is defined usually on the basis of the degree of dryness in comparison to the normal condition and the duration of the dry period. Meteorological drought definitions are dependent on the specific characteristics of the region due to the high dependency of atmospheric conditions to regional characteristics. For example, some definitions of meteorological drought identify periods of drought on the basis of the number of days with precipitation less than some specified threshold. This measure is only appropriate for regions characterized by a year-round precipitation regime such as a tropical rainforest, humid subtropical climate, or humid mid-latitude climate. Other climatic regimes are characterized by a seasonal rainfall pattern, wherein extended periods without rainfall are common. In these regions, a definition based on the number of days with precipitation less than some specified threshold is unrealistic. There are also some other definitions that relate actual precipitation departures to average amounts on monthly, seasonal, or annual time scales. Furthermore, the desired spatial scale of drought analysis is an important concept that should be considered in the selection of the drought analysis method. Two approaches—point evaluation and regional evaluation—are considered and are further discussed in the next subsections.

12.4.1 Point Evaluation

In point evaluation of climatic drought to detect dry events, the behavior and variation of precipitation at each sub-basin represented by a rain gauge are evaluated. The following approaches could be taken in point evaluation of climatic drought:

- Fitting statistical distribution
- Analysis of moving averages
- Point evaluation of drought events in a monthly scale

12.4.1.1 Fitting Statistical Distribution

Assume that $\{X_i \,|i = 1, \ldots, N\}$ is a discrete point series vector of a drought characteristic in N existing rain gauges of the study area. In the analysis of climatic drought, the drought characteristic is precipitation and the time sequence is usually considered to be annual. To choose the best statistical distribution for the time series of each station, X_i, the following assumptions should be verified:

- Data are independent.
- Precipitation time series are stationary.
- X_i may have different probability distributions.

To choose the best statistical distribution, the classical approach can be used; however, it has many shortcomings. In this approach, first, all of the existing data in point (station) i, X_i, should be sorted in ascending order to form a new set, $x_{(1)}, x_{(2)}, \ldots x_{(n)}$, in such a way that $x_{(1)} = \min(X_i)$ and $x_{(n)} = \max(X_i)$. Then, if there are enough data, at least 30 values [recommended by Kottegoda and Rosso (1998) and Mendenhall et al. (1990)], the range between $x_{(1)}$ and $x_{(n)}$ will be divided into K intervals and a histogram for point i can be plotted. Considering the shape of the histogram and comparing it with the shape of different statistical distributions and by using the result of different goodness-of-fit tests such as the Kolmogorov–Smirnov test and the chi-square test, the best distribution can be chosen. As alternatives, to choose the best distribution, the observed data distribution plot will be

compared with the expected values from the statistical distribution plot. Quintile–quintile (Q–Q) and probability–probability (P–P) graphs can be used as methods for comparing observed values with values from a given distribution. By using these methods, the best distributions can be found, with more flexibility and accuracy compared with the classical method.

In general, it is possible to obtain $(n - 1)$ values in the observed sample, dividing the cumulative frequency of the sample equally into n values. Each of these values is called a quintile. The objective is to compare the observed value of events with their corresponding values from a statistical distribution function. To prepare a Q–Q graph, the observed values should be ordered ($x_1 \le x_2 \le \ldots \le x_n$) and then these values are plotted against the inversion of the cumulative PDF as

$$Q = F^{-1}\left(\frac{(i - r_{\text{adj}})}{(n + n_{\text{adj}})}\right) \quad i = 1, 2, \ldots n, \tag{12.1}$$

where n_{adj} and r_{adj} are constants and should be less than or equal to 0.5 and F^{-1} is the inverse of the cumulative distribution function (CDF) for a statistical distribution.

This yields a graph of observed values versus standardized expected values from a specific distribution. The best statistical distribution is the one that falls into a linear regression relationship of high correlation coefficient with the distribution of observed values. n_{adj} and r_{adj} are limiting the p value for the CDF to be between 0 and 1.

In preparing the P–P graphs, the CDF of the observed values is plotted versus the CDF of a statistical distribution. To plot P–P graphs, after sorting the observed values in ascending order, one axis will be the CDF of the observation i, versus a CDF of a statistical distribution for observed values (X_i). If the selected statistical distribution estimates the observed values closely, then in the P–P graph, all of the points should be on a 45° line.

To find a good fit for statistical distribution, parameters of a distribution should be calibrated. One of the most sensitive parameters is the "location" parameter, which is a measure of truncation level (threshold), on a given distribution. For example, in Weibull distribution, the location parameter has been used in the following density function:

$$f(x) = c/b \times [(x - \theta)/b]^{c-1} \times e^{-[(x-\theta]/b]^c}; \quad 0 \le x < \infty; b > 0; c > 0; \theta > 0, \tag{12.2}$$

where b is the scale parameter, c is the shape parameter, and θ is the location parameter (threshold). The extra parameter b, scale parameter, could also be considered. Variation of this parameter can change the size of the distribution. As can be seen in Equation 12.2, by increasing b, the size of the distribution (height of its peak) becomes smaller. In this case, to keep the area under the curve equal to 1, the distribution will have to be spread out more. By changing these parameters, a better fit of a Weibull distribution to the observed data can be obtained. The other types of distributions have similar parameters.

Beta distribution is another suitable distribution family to predict the behavior of precipitation data even though it has not been frequently used in previous drought studies. This distribution may change from a normal distribution to a much skewed distribution and provides the high level of flexibility needed in drought studies. The beta distribution has the following PDF:

$$f(x) = \Gamma(\upsilon + \omega)/[\Gamma(\upsilon) \times \Gamma(\omega)] \times [(x - \theta)^{\upsilon-1} \times (\sigma + \theta - x)^{\omega-1}]/\sigma^{\upsilon+\omega+1} \tag{12.3}$$

$$0 < x < 1; \upsilon > 0; \omega > 0,$$

where Γ is the gamma function, υ and ω are the distribution parameters that determine its appearance, θ is the threshold (location) parameter, and σ is the scale parameter.

The standardized beta distribution has a valid range from 0 to 1. A smaller threshold can be considered by standardizing the variable as $(x - \theta)/\sigma$. Note that the location parameter must be less than the smallest observed value, and the $(\sigma + \theta)$ must be greater than the largest observed value. In general, if the points in the Q–Q plot form a straight line, then the respective family of distributions provides a good fit to the data. In that case, the intercept and the slope of the fitted line can be interpreted as graphical estimates of the threshold (θ) and scale (σ) parameters, respectively.

12.4.1.2 Analysis of Moving Averages

In the moving average method, the cumulative impact of precipitation deficit and surplus in previous years is considered. By using this method, the drought investigation is diverted from climatic drought to hydrological (real) drought. The n year moving average, X_j' in jth year, can be calculated from the following expression:

$$X_j' = \frac{1}{n}\sum_{i=0}^{n-1} X_{j+i}. \tag{12.4}$$

Usually 3-, 5-, and 10-year moving averages are investigated for recognizing the drought spells.

Example 12.1

Use the 3-year moving averages and compare the two series of annual average precipitation for two different regions presented in Table 12.1. Which of these regions has been facing a more severe drought in the current year? If the long-term average precipitation in regions A and B is estimated to be 350 and 250 mm, respectively, discuss the drought periods and their durations.

Solution:

Table 12.2 shows the estimated 3-year moving averages for regions A and B using Equation 12.4.

Figures 12.1 and 12.2 show the 3-year moving average and long-term average of precipitation for the two regions. As can be seen in Figure 12.1, there has been one drought event with a 2-year duration in region A. The current year in that region is in a wet spell. Region B has been in the middle of a drought period during the first few years on record, and the current year seems to be the first year of a drought event.

TABLE 12.1
Average Precipitation Data in a 10-Year Period for Two Regions Presented in Example 12.1

Year	Average Precipitation of Region A (mm)	Average Precipitation of Region B (mm)
1	640	230
2	456	127
3	236	261
4	456	301
5	235	261
6	601	322
7	532	400
8	731	223
9	256	128
Current year	541	112

TABLE 12.2
Three-Year Moving Average for Two Regions Presented in Example 12.1

Year	3-Year Moving Average for Region A	3-Year Moving Average for Region B
1	–	–
2	–	–
3	444.00	206.00
4	382.67	229.67
5	309.00	274.33
6	430.67	294.67
7	456.00	327.67
8	621.33	315.00
9	506.33	250.33
Current year	509.33	154.33

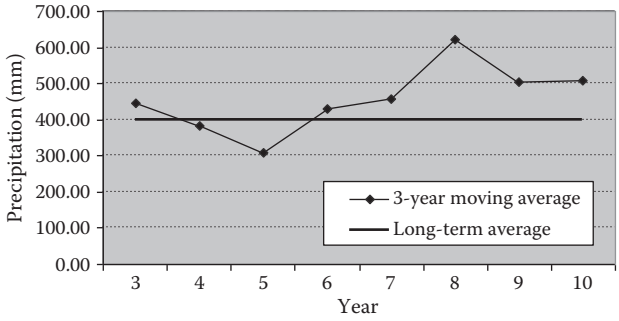

FIGURE 12.1 Long-term average and 3-year moving average of annual precipitation for region A in Example 12.1.

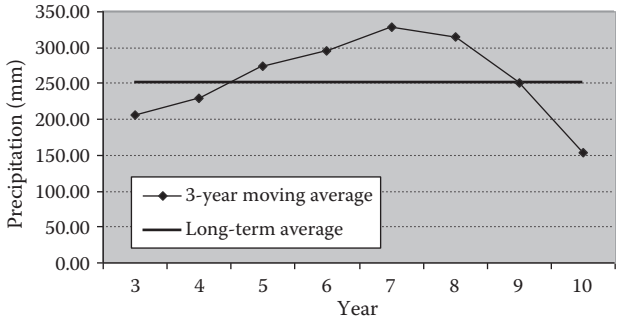

FIGURE 12.2 Long-term average and 3-year moving average of annual precipitation for region B in Example 12.1.

12.4.1.3 Point Evaluation of Drought Events in a Monthly Scale

In this method, it is assumed that farming in any region is adapted to the prevailing climatic pattern so that maximum advantage is taken during the months of high average rainfall. Due to variations in mean monthly rainfall, a seasonal drought of a certain severity and duration is often a normal feature of that particular climate and as such should not be included in the assessment of droughts of severe consequences. In the following sections, it is assumed that the benefit to vegetation continues for some time after excessive rain due to the storage of moisture in the soil, and conversely, that the recovery of vegetation after a drought is not immediate, since the impact persists for some time.

12.4.1.4 Effective Rainfall and Rainfall Difference Series

In drought studies, the definition of effective rainfall is different from that of the term *effective rainfall* or *excess rainfall* used in hydrological analysis, which is the portion of precipitation that is converted to runoff. The effective rainfall for drought analysis purposes is calculated as follows:

$$ER_{i,n} = M_{i,n} + W_i\left(ER_{i-1,n} - \bar{M}_{i-1}\right) \quad (n = 1,\ldots,NY),(i = 1,\ldots,12) \tag{12.5}$$

$$ER_{1,1} = \bar{M}_1$$

and

$$W_i = C\left(1 + \frac{\bar{M}_i}{\frac{1}{12} \times MAR}\right), \tag{12.6}$$

where MAR is the mean annual rainfall, $ER_{i,n}$ is effective rainfall in month i of year n, $M_{i,n}$ is rainfall in month i of year n, $\bar{M}_j$ is long-term monthly mean for month i (i = 1, …, 12), W_i is a weighting factor for month I, and NY is number of years on record. C is a constant that is determined by trial and error in order to better simulate the observed wet and dry periods. It is common to set C as 0.1. The weighting factors obtained from Equation 12.6 show the effect of rainfall at each month on the drought situation of the next months. An average deficit $\left(\overline{RD_i}\right)$ for month i is defined as

$$\overline{RD_i} = \frac{\sum_{n=1}^{N} DELTA_{i,n}}{N} \quad (i = 1,\ldots,12), \tag{12.7}$$

where

$$DELTA_{i,n} = \begin{cases} \bar{M}_i - ER_{i,n} & ER_{i,n} < \bar{M}_i \\ 0 & ER_{i,n} \geq \bar{M}_i \end{cases} \quad (n = 1,\ldots,NY). \tag{12.8}$$

Whenever the $RD_{i,n} < \overline{RD_i}$, it shows a normal trend of rainfall variations, and when $RD_{i,n} > \overline{RD_i}$, the excess deficit can be considered as a sign of drought.

The carryover from month to month is defined as the effect of rainfall deficit or surplus from the previous month in following three fashions:

$$ERS_{i,n} = \begin{cases} ER_{i,n} - \bar{M}_i & \text{if} \quad ER_{i,n} \geq \bar{M}_i \\ 0 & \text{otherwise} \end{cases} \tag{12.9}$$

$$ERD_{i,n} = \bar{M}_i - ER_{i,n} - \overline{RD_i} \tag{12.10}$$

$$RD_{i,n} = \text{Min}\left[(M_i - ER_{i,n}), \overline{RD_i}\right] \quad (n = 1, \ldots, NY), \tag{12.11}$$

where $ERS_{i,n}$ is excess rainfall surplus in month i of year n, $ERD_{i,n}$ is excess rainfall deficit in month i of year n, $RD_{i,n}$ is rainfall deficit in month i of year n, and $\overline{RD_i}$ is long-term monthly mean for rainfall deficit in month i. Therefore, $ERS_{i,n}$ is the deficit in excess of the average deficit experienced. It could be an indication of drought occurrence. It can be referred to as a "drought symptom."

As expressed, the carryover from month to month is determined by subtracting the mean rainfall for a particular month from the effective rainfall for the same month so that a deficit or surplus rainfall for that month is obtained. The deficit and surplus rainfall are multiplied by a weighting factor for the next month, and the product, whether negative or positive, is added algebraically to the rainfall figures of that month. This sum is called effective rainfall. The weighting factor is used to calculate the carryover effect of a particular month and shows the relative effect of the deviation from mean in a month as it contributes to the soil moisture of the following month.

From the above equations, for the first month on record, the carryover is assumed to be zero. The process is continued to obtain the effective monthly rainfall for the entire period on record. Excessive rainfall deficit (*ERD*) is of particular importance to drought studies. It shows how much deficit the system is tolerate beyond the normal amount of deficit the system naturally and over the course of historical data has experienced. This parameter is the main feature in detecting a drought occurrence if it persists in the following month and in calculating drought severity. In Figure 12.3, the results of effective rainfall calculations for 12 years of monthly data (1989–2001) for a region

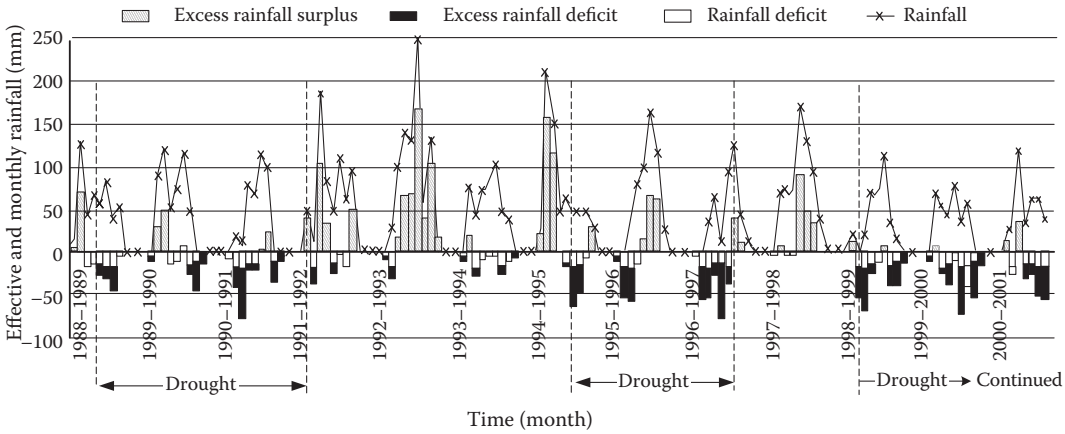

FIGURE 12.3 Wet and dry spells identification using effective rainfall investigation.

located in the central part of Iran are illustrated. The longest and most severe drought has occurred during the last 38 months and was still continuing at the end of the study period.

The dry spells, which are rainfall deficits and excess rainfall deficits, have been shown in Figure 12.3 with blank and solid black bars, respectively. Precipitation records are also shown in Figure 12.3 to show their variations compared to the variations in effective rainfall. The effective rainfall calculation is affected by the effective rainfall of the previous months; therefore, the cumulative impact of the consecutive deficits can be better seen than the rainfall data. For example, in Water Year 2001, the total rainfall is close to the average, but the effective rainfall shows a drought event for the region (Karamouz et al. 2002).

Example 12.2

The monthly rainfall data for a period of 24 months and the long-term monthly average rainfall are presented in Table 12.3. The mean annual rainfall (*MAR*) is also estimated as 535.2 mm from long-term data. Assume *C* (the constant in Equation 12.6) is 0.1. Calculate the effective rainfall, rainfall deficit, and excess rainfall deficit for the region.

TABLE 12.3
Rainfall Data for the Region Presented in Example 12.2

Month	Rainfall (mm)	Mean Monthly Rainfall (mm)
1	0.99	1.25
2	3.99	1.13
3	1.59	0.67
4	19.59	10.43
5	2.45	57.51
6	21.06	77.7
7	72.31	76.75
8	75.21	80.91
9	116.42	106.08
10	34.81	75.22
11	14.62	43.37
12	0.00	4.17
13	1.02	1.25
14	0.86	1.13
15	0	0.67
16	0.7	10.43
17	67.4	57.51
18	51.7	77.7
19	45.4	76.75
20	81.2	80.91
21	38.1	106.08
22	57.1	75.22
23	2.3	43.37
24	0.1	4.17

Solution:

Equations 12.5 and 12.6 are used for estimating the effective rainfall. Based on Equation 12.5, the effective rainfall in the first month is considered to be equal to the average rainfall in that month, which is 1.25 mm. For the second month, the weighting factor can be estimated as follows:

$$W_2 = 0.1 \times \left(1 + \frac{1.13}{\frac{1}{2} \times 535.2} \right) = 0.103.$$

Then, the effective rainfall for this month can be estimated using Equation 12.5:

$$ER_{2,1} = 3.99 + 0.103 \times (0.99 - 1.13) = 4.002 \text{ mm}.$$

For estimating the rainfall deficit, Equations 12.7 and 12.8 are used. For example, for the first month, it can be written that

$$ER_{1,1} = M_1 < \bar{M}_1 \qquad DELTA_{1,1} = 1.25 - 0.99 = 0.26 \text{ mm}.$$

$$ER_{1,2} < \bar{M}_1 \qquad DELTA_{1,2} = 1.25 - 1.007 = 0.243 \text{ mm}.$$

Therefore,

$$\overline{RD}_1 = \frac{\sum_{n=1}^{2} DELTA_{i,n}}{2} = \frac{0.26 + 0.243}{2} = 0.122 \text{ mm}.$$

Using Equation 12.11, it can be written that

$$RD_{1,1} = \text{Min}[(0.99 - 1.25), 0.122] = -0.26 \text{ mm}.$$

The excess rainfall deficit for the first month is estimated using Equation 12.10 as follows:

$$ERD_{1,1} = 1.25 - 1.25 - 0.122 = -0.122 \text{ mm}.$$

Table 12.4 shows the values of effective rainfall, rainfall deficit, and excess rainfall deficit estimated for the 24 months' data presented in Table 12.3.

12.4.1.5 Onset and Termination of Drought

In a test to signify the onset of a drought, it can be assumed that a single month could constitute a drought only if no rain occurred in the month of highest mean rainfall. The test is based on a comparison of the sum of the negative differences (deficits) from the point in time the test begins, with a sliding scale of 12 values calculated by linear interpolation between the maximum value of mean monthly rainfall (*MMMR*) and the mean annual deficit (*MAD*). A monthly sliding scale, *x*, is thus obtained from the following equation:

$$x = \frac{MAD - MMMR}{11}, \tag{12.12}$$

TABLE 12.4
Effective Rainfall, Rainfall Deficit, and Excess Rainfall Deficit (mm) Estimated for the Data in Example 12.2

Month	Effective Rainfall	Rainfall Deficit	Excess Rainfall Deficit	Effective Rainfall – Average Monthly Rainfall
1	1.250	–0.260	–0.122	0.000
2	4.002	–0.012	–3.014	2.872
3	1.928	–0.338	–1.584	1.258
4	18.541	1.049	–13.618	8.111
5	–6.472	8.922	30.286	–63.982
6	–2.021	23.081	23.625	–79.721
7	50.878	21.432	–7.027	–25.872
8	66.758	8.452	1.018	–14.152
9	103.135	13.285	–38.816	–2.945
10	42.310	–7.500	0.717	–32.910
11	14.411	0.209	–6.019	–28.959
12	1.120	–1.120	–0.608	–3.050
13	1.007	0.013	0.243	–0.243
14	0.847	0.013	0.283	–0.283
15	0.018	–0.018	0.652	–0.652
16	–0.585	1.285	11.015	–11.015
17	54.099	13.301	3.411	–3.411
18	45.228	6.472	32.472	–32.472
19	36.823	8.577	39.927	–39.927
20	68.793	12.407	12.117	–12.117
21	25.503	12.597	80.577	–80.577
22	43.743	13.357	31.477	–31.477
23	2.374	–0.074	40.996	–40.996
24	–0.096	0.196	4.266	–4.266
Sum	–	135.325	–	

where *MMMR is* Max $[\bar{M}_j]$ and *MAD* is calculated as follows:

$$MAD = \sum \text{Annual deficit/No. of years of deficit.} \tag{12.13}$$

The sliding scale is a line connecting the *MAD* to *MMMR*. The first value on the sliding scale is equal to the maximum deficit that can occur in a single month. The second value on the sliding scale is obtained by adding x to *MMMR*, the third by adding $2x$ and so on up to $MMMR + 11x$, which is equivalent to *MAD*. At the start of the test, it is assumed that no drought prevailed prior to the start of the available rainfall record. The first month of available data with negative difference (RD_i) is considered as the possible start of a drought, then a comparison is made between the absolute value of this deficit with the first value of the sliding scale. If it exceeds this, then a drought is deemed to have started. Likewise, if the difference of the next month was checked, and if it was negative, then it is added to the negative difference of the first month and compared with the second value on the sliding scale. If this criterion was exceeded by the absolute value of the two deficits combined, a drought was deemed to have started from the first month and the process continues until the sliding scale reaches *MAD*.

In the test of drought termination, in the first instance, the test was applied to the period following the first month with a positive difference (surplus) occurring after the start of a drought. The test

for termination of a drought consisted of either a continuous period of slightly above-average rainfall or a few successive months of abnormally high rainfall. This constitutes the drought termination. The *duration of the drought* is the period between the onset and the termination of the drought. Therefore, the successive surplus periods are considered and compared with the maximum of 3, 4, … 12 months' successive averages. If it has exceeded this, then termination of the drought period could be considered. After determining a drought period, its severity, S_d, is calculated as follows:

$$S_d = \frac{\sum_j (ERD_j) \times D}{\sum_d \overline{RD_d}}, \tag{12.14}$$

where d is index of drought, j is all months of excess rainfall deficit in drought d, D is drought duration (month), ERD_j is excess rainfall deficit observed in month j, and $\overline{RD_d}$ is average deficit in each month of period d.

Example 12.3

Determine the onset, duration, and severity of drought for the data presented in Example 12.2. Consider that the mean annual deficit is 150 mm and the maximum values of n-month average rainfall are as shown in Table 12.5.

Solution:

As shown in Table 12.3, the maximum value of mean monthly rainfall (*MMMR*) is 106.08 mm. The sliding scale is then estimated using Equation 12.12 as follows:

$$x = \frac{150 - 106.08}{11} = 3.99$$

Table 12.6 shows the values estimated for the sliding scale in different months. For testing the onset of droughts, the differences between measured rainfall and the long-term average of rainfall in that month are estimated and shown in Table 12.5.

TABLE 12.5
Maximum *n*-Month Average of Rainfall Series (mm)

2 months	175.0
3 months	243.1
4 months	265.3
5 months	275.3
6 months	283.9
7 months	298.4
8 months	310.5
9 months	345.6
10 months	366.3
11 months	380.5
12 months	410.1

TABLE 12.6
Estimated Values for Sliding Scale in Example 12.3

Month	Sliding Scales
1	106.08
2	110.07
3	114.06
4	118.05
5	122.04
6	126.03
7	130.02
8	134.01
9	138
10	141.98
11	145.97
12	150

As can be seen in Table 12.4, the first negative difference occurred in the fifth month; therefore, it could be considered as the onset of a drought event. The cumulative summations of the differences after the first negative value are compared with the sliding scales (x) (Table 12.7). As shown in this table, the absolute values of the difference series become greater than the sliding scale series after the seventh month. Now, it is said that a drought has started from month 5. If this test is not passed after considering 11 sliding scales, the test is started after observing another negative difference.

The test of termination of a drought starts after the first positive difference between effective rainfall and monthly mean rainfall observed during a drought (Table 12.8). In this example, the application of the test starting from the first positive value shows that the drought has not terminated yet. In the second iteration, the cumulative summation of differences (column 4) is compared with the maximum n-month averages (column 5). It is shown that the values in column 4 become greater than the values in column 5 after the 20th month. Therefore, it is said that the drought has been terminated and 20 months is considered as the duration of drought.

TABLE 12.7
Cumulative Differences and Sliding Scales for Data in Example 12.3

Month	Sliding Scales	Cumulative Difference
1	106.08	0
2	110.07	0
3	114.06	0
4	118.05	0
5	122.04	–52.9
6	126.03	–124.1
7	130.02	–147.9
8	134.01	–160.3
9	138	–160.3
10	141.98	–199.0
11	145.97	–235.4
12	150.00	–243.6

TABLE 12.8
Results of Drought Termination Analysis for Data in Example 12.3

Month	Rainfall	Difference = Effective Rainfall – Monthly Mean Rainfall	Cumulative Rainfall after the First Positive Difference	Maximum *n*-Month Averages
1	0.99	0.000		
2	3.99	2.860		
3	1.59	1.210		
4	19.59	9.309		
5	2.45	–52.929		
6	21.06	–71.154		
7	72.31	–23.800		
8	75.21	–12.398		
9	116.42	6.152	116.42	
10	34.81	–38.757	151.23	175.0
11	14.62	–36.395	165.85	243.1
12	0.00	–8.150	165.85	265.3
13	1.02	–1.068	166.87	275.3
14	0.86	–0.379	167.73	283.9
15	0	–0.709	167.73	298.4
16	0.7	–9.817	168.43	310.5
17	67.4	7.642	235.83	345.6
18	51.7	–23.904	287.53	366.3
19	45.4	–37.854	332.93	380.5
20	81.2	–10.363	414.13	410.1
21	38.1	–71.481		
22	57.1	–37.324		
23	2.3	–48.432		
24	0.1	–9.366		

After determining a drought period, its severity is obtained from the following:

$$S_d = \frac{\sum_j (ERD_j) \times D_d}{\sum_d \overline{RD_d}}$$

$$D_d = 20.0$$

$$\sum_j (ERD_j) = 64.84$$

$$\sum_d \overline{RD_d} = 363.34$$

$$S_d = \frac{64.84 \times 20}{363.34} = 3.57.$$

12.4.2 Regional Analysis of Climatic Drought

The main objective for regional analysis is to find a suitable criterion for defining the dry events in a regional scale. Three methods can be used for this analysis: weighting, median of ratios, and combined methods.

12.4.2.1 Weighting Method

In this method, the weight of each station is calculated by applying the Thiessen polygon network, and accordingly, the long-term average regional precipitation data set will be obtained for the entire region. Then, the best statistical distributions are chosen for the long-term average precipitation data set ($\bar{P}$), and based on this, the ratio of average regional precipitation to long-term average precipitation with different probabilities (different return periods) is calculated. These ratios are applied as a regional criterion to separate the precipitation data sets of each rain gauge of the region to wet and dry events.

Example 12.4

The historical annual precipitation in a basin is given in Table 12.9. Table 12.10 shows annual rainfall in drought events with different return periods. If a 10-year climatic drought occurs in the region, find which sub-basins face a drought with 10-year or more return periods.

Solution:

In order to find the annual rainfall associated with a 10-year drought event, the data given in Table 12.9 are sorted in ascending order (see column 3 of Table 12.9). Then, the probability for each data is estimated as $P = \frac{m}{n+1}$.

TABLE 12.9
Annual Average Precipitation (mm) in the Basin Presented in Example 12.4

No. of Years	Precipitation (mm)	Sorted Precipitation (mm)	Probability	Return Period (year)
1	618.23	101.47	0.05	19.00
2	563.54	284.2	0.11	9.50
3	546.6	307.44	0.16	6.33
4	501.51	345.81	0.21	4.75
5	480.41	350.1	0.26	3.80
6	451.88	368.51	0.32	3.17
7	418.34	369.99	0.37	2.71
8	403.34	403.34	0.42	2.38
9	369.99	418.34	0.47	2.11
10	368.51	451.88	0.53	1.90
11	350.1	480.41	0.58	1.73
12	345.81	501.51	0.63	1.58
13	307.44	546.6	0.68	1.46
14	284.2	563.54	0.74	1.36
15	776.02	617.04	0.79	1.27
16	1001.96	618.23	0.84	1.19
17	101.47	776.02	0.89	1.12
18	617.04	1001.96	0.95	1.06

TABLE 12.10
Regional Precipitation Data Estimated for Drought Events with Different Return Periods in Example 12.4

		Drought Event Precipitation in Different Droughts (mm)				
Sub-Basin	**Area (%)**	**2 years**	**5 years**	**10 years**	**25 years**	**50 years**
A	20	380	280	180	100	70
B	30	600	540	510	490	350
C	15	550	520	480	320	250
D	15	280	250	200	180	70
E	20	400	350	310	280	190

As can be seen in Table 12.9, 284 mm annual precipitation has a 10-year return period and sub-basins A and D are facing droughts with 10-year and more return periods.

Example 12.5

In a specific year, the data in Table 12.11 have been recorded in the region presented in Example 12.4. What is the appropriate return period of the regional drought?

Solution:

The average precipitation over the region can be estimated using the Thiessen polygon network as follows:

$$\text{Average rainfall} = \frac{(380\times 20)+(520\times 30)+(320\times 15)+(250\times 15)+(410\times 20)}{100} = 399.5\,\text{mm}.$$

Considering the data presented in Table 12.9, the regional drought is estimated to have a 2.4-year (between 2- and 3-year) return period.

12.4.2.2 Median of Ratios Method

The objective is to obtain a regional truncation level. Therefore, the median of calculated $\left(\frac{P}{P_{\text{mean}}}\right)$ ratios have been calculated for different return periods in point evaluation for different stations in the region:

$$\left(\frac{P}{P_{\text{mean}}}\right)_T = \text{Median}\left\{\left(\frac{P}{P_{\text{mean}}}\right)_i^T ; i = 1,...,N\right\}; \quad T = 2,5,10,..., \tag{12.15}$$

TABLE 12.11
Recorded Precipitation Data (mm) in Different Stations in Example 12.5

Station	**A**	**B**	**C**	**D**	**E**
Annual Precipitation (mm)	380	520	320	250	410

where $\left(\frac{P}{P_{\text{mean}}}\right)_T$ is the regional criteria of precipitation ratio to long-term average precipitation for return period T, $\left(\frac{P}{P_{\text{mean}}}\right)_i^T$ is the ratio of precipitation to long-term average precipitation in rain gauge i for return period T, and N is the number of total rain gauges in the study region.

12.4.2.3 Combined Method

This method is a combination of the above two methods. In this method, estimated values for $\left(\frac{P}{P_{\text{mean}}}\right)_T$ in point evaluation for each station will be weighted by using their relative area in the Thiessen network. Therefore, the third regional criterion can be calculated as follows:

$$\left(\frac{P}{P_{\text{mean}}}\right)_T = \sum_{i=1}^{N} \alpha_i \times \left(\frac{P}{P_{\text{mean}}}\right)_i^T; \quad T = 2,5,10,..., \tag{12.16}$$

where α_i is the weighting factor determined based on the Thiessen network.

In addition to truncation level, other important factors should be considered in the regional drought analysis. Santos (1983) suggested that besides defining critical and truncation levels, the critical area should also be defined. Regional drought is said to occur when the drought-affected area is larger than the critical area. The critical area can be considered to be equal to a percentage of the total area depending upon the severity of the decisions imposed by using this threshold. For example, if the threshold is selected as 50% of the area of the region, then the corresponding return period that yields a drought-affected area that is equal to or more than that value will be announced as the return period for that year.

The other factor that should be considered in drought regionalization is the range of variation for point averages in the entire region. For this purpose, the dimensionless precipitation has been used as a ratio of precipitation to average precipitation. Rossi et al. (1992) suggested the use of dimensionless precipitation. Doornkamp and Gregory (1980) also used this method in regional evaluation. Then, the drought-affected area in the current period will be defined and analyzed by applying the observed data, as follows:

- The total observed data for all of the rain gauges could be changed to be dimensionless.
- A regional isohyetal map can be plotted over the entire observed period.
- Based on regional criteria definitions, drought-affected areas are estimated by summation of all drought-affected subareas over different time periods as follows:

$$A_{\text{D}}^T(t) = \sum \beta_i \cdot a_i(t) \tag{12.17}$$

$$\beta_i = \begin{cases} 1 & \text{if} \quad P_i(t) \le P_{iT} \\ 0 & \text{otherwise,} \end{cases}$$

where $A_{\text{D}}^T(t)$ is the drought-affected area with return period T during time t, $a_i(t)$ is the subarea represented by station i during time t, $P_i(t)$ is the precipitation in station i in a given time period t, and P_{iT} is the precipitation at station i with a return period of T obtained from the best-fitted distribution for that station.

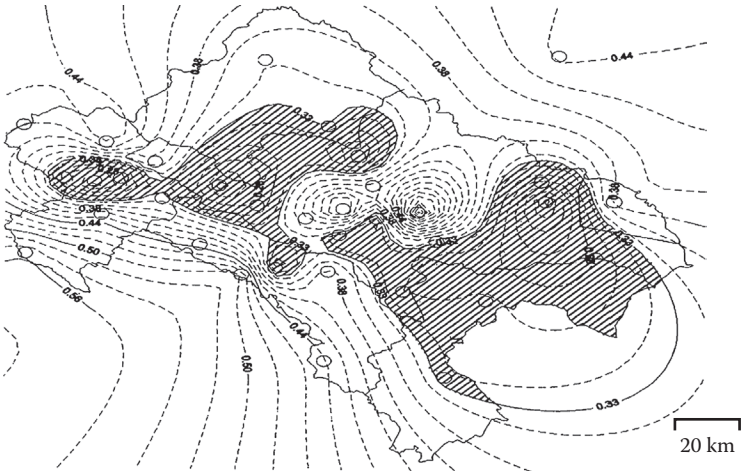

FIGURE 12.4 Isohyetal map for $\left(\frac{P}{P_{\text{mean}}}\right)$ ratios for a 50-year return period for a basin. (From Karamouz, M. et al., 2003. With permission.)

Figure 12.4 shows an isohyetal map for $\left(\frac{P}{P_{\text{mean}}}\right)$ ratios for a 50-year return period, which is drawn for a river basin in the central part of Iran (Karamouz et al. 2003). Such similar maps can be generated using spatial kriging with different return periods. According to these maps, if the region is affected by a drought with return period *T*, one can identify parts of the region that are in the most critical situation.

12.4.3 Climatic Drought Indicators

Deciles, effective rainfall, and Standard Precipitation Index (SPI) are used for assessing climatic drought. SPI is discussed in this part due to its popularity.

12.4.3.1 Standard Precipitation Index

McKee et al. (1993) invented SPI to monitor drought. It is proved empirically that the precipitation probability distribution of a station is a gamma distribution. The density function of this distribution is as follows:

$$f(x) = \frac{1}{\beta^{\alpha}\Gamma(\alpha)} x^{\alpha-1} e^{\frac{-x}{\beta}} \quad x > 0, \tag{12.18}$$

where x is a random variable, α is the shape parameter, β is a scale parameter, and $\Gamma(\alpha)$ is the gamma function whose relation is given as

$$\Gamma(\alpha) = \int_0^{\infty} y^{\alpha-1} e^{-y}\, dy. \tag{12.19}$$

α and β are calculated from the following equations:

$$\widehat{\alpha} = \frac{1}{4A}\left[1 + \sqrt{1 + \frac{4A}{3}}\right] \tag{12.20}$$

$$\widehat{\beta} = \frac{\overline{x}}{\widehat{\alpha}}, \tag{12.21}$$

where

$$A = \ln(\overline{x}) - \frac{\sum \ln(x)}{n}. \tag{12.22}$$

n is the number of precipitation observations.

A gamma distribution with computed parameter is fitted to the precipitation of each station for SPI calculation. For each series of precipitation, α and β are calculated separately. CDF is utilized in SPI calculation:

$$F(x) = \int_0^{\infty} f(x)\,\mathrm{d}x = \frac{1}{\widehat{\beta}\Gamma(\widehat{\alpha})} \int_0^{\infty} x^{\widehat{\alpha}-1} e^{-x/\widehat{\beta}}\,\mathrm{d}x. \tag{12.23}$$

The next step in SPI calculation is the transmission of the cumulative gamma distribution to a standard normal cumulative distribution. In fact, SPI is a standard normal distribution variable whose corresponding cumulative probability is equal to the value of cumulative probability calculated with a gamma distribution. Determination of SPI is presented in Figure 12.5. Table 12.12 is used for drought status description.

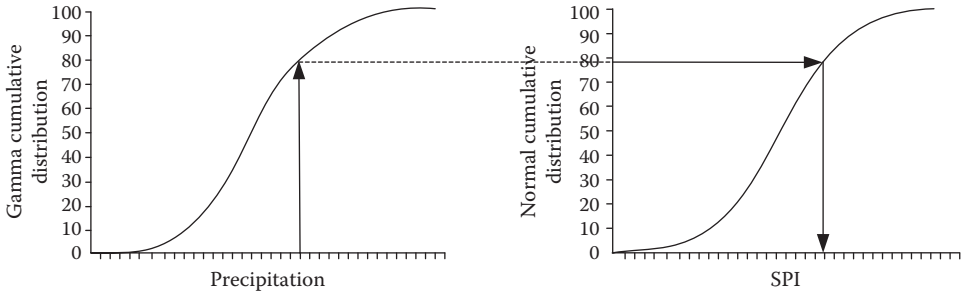

FIGURE 12.5 Determining the SPI.

TABLE 12.12
Drought Status due to SPI

SPI	Climatic Drought Status
–2.5 to –3	Extreme drought
–2 to –2.5	Severe drought
–1.5 to –2	Moderate drought
–1 to –1.5	Slightly dry
–0.5 to –1	Abnormally dry
–0.5 to 0.5	Normal
0.5 to 1	Abnormally wet
1 to 1.5	Slightly wet
1.5 to 2	Moderate wet
2 to 2.5	Severe wet
2.5 to 3	Extreme wet

12.5 HYDROLOGICAL DROUGHT

Hydrological drought is associated with the effects of periods of precipitation (including snowfall) shortfalls on surface or subsurface water supply (i.e., streamflow, reservoir and lake levels, groundwater). The frequency and severity of hydrological drought are often defined on a watershed or river basin scale. Although all droughts originate with precipitation deficiency, hydrologists are more concerned with how this deficiency plays out through the hydrologic system. Hydrological droughts are usually out of phase with or lag the occurrence of meteorological and agricultural droughts. It takes longer for precipitation deficiencies to show up in components of the hydrological system such as soil moisture, streamflow, and groundwater and reservoir levels. As a result, these impacts are out of phase with impacts in other economic sectors. For example, a precipitation deficiency may result in a rapid depletion of soil moisture that is almost immediately discernible to agriculturalists, but the impact of this deficiency on reservoir levels may not affect hydroelectric power production or recreational uses for many months. Also, water in hydrologic storage systems (e.g., reservoirs, rivers) is often used for multiple and competing purposes (e.g., flood control, irrigation, recreation, navigation, hydropower, wildlife habitat), further complicating the sequence and quantification of impacts. Competition for water in these storage systems escalates during drought and conflicts between water users increase significantly.

In hydrological drought, most of the literature is concentrated on analysis of historical and generated streamflow data including estimation of PDF of drought characteristics. These efforts can be classified into the following categories:

1. *Experimental investigation of data:* means description of drought characteristics based on observed series such as streamflows and demands. Based on this method, Chang (1990) defined the expected time between drought events using Poisson distribution, and then he investigated the variation in streamflow behavior during a drought, using daily streamflow data. Dracup et al. (1980) studied stationary and stochastic characteristics of data and the correlation between different drought characteristics in the historical data. They emphasized that the results based on observed data may be insufficient because of the short range of the recorded data. Ben-Zvi (1987) considered volume of streamflows as an indicator of drought. He defined average data as the truncation level of water shortages during small droughts and standard deviation as truncation for severe droughts and then studied droughts with different severity. Yevjevich (1967) introduced a series of the difference between water supply and demand as the indicator of hydrological drought. He defined sequential periods (runs) as drought spells in series and emphasized that run theory is the best method of studying hydrological droughts.
2. *Investigation of generated data:* means that the above methodology should be applied to the generated data. Different methods may be used to generate data. Zucchini and Adamson (1988) used the bootstrap method to evaluate risk of shortage of annual inflow to a reservoir. Yevjevich and Obeysekera (1985) studied the results of different drought characteristics and correlation between them, using generated data with different assumptions such as number of data generated and using different lag on correlation coefficients. Guerrero-Salazer and Yevjevich (1975) analyzed the PDF of duration and severity after identifying the wet and dry spells in a year.
3. *Estimation of PDF of drought characteristics:* is a common method in hydrological drought investigation. Different drought studies were done by Sen (1976; 1980b). He tried to use sequential periods (runs) as an analytical tool to solve different drought problems such as the PDF of drought characteristics. Yevjevich and Obeysekera (1985) and Yevjevich (1967; 1988) used generated data to determine the PDF of drought characteristics. Griffiths (1990) determined the PDF of each drought characteristic and their multivariate distributions.

12.5.1 Reservoir Operation and Demand Allocation

One of the most critical aspects in hydrological drought is consideration of water demand. Reservoirs are usually used as the water supply system in large basins. The operating policy of existing reservoirs is an important tool in facing hydrological droughts. Some researchers have focused on the effects of reservoir during drought. The optimal operating policy of a reservoir tends to allocate water to meet demand during droughts as much as possible.

12.5.2 Hydrological Drought Indices: SWSI

The Surface Water Supply Index (SWSI) was developed by Shafer and Dezman (1982) to be an indicator of surface water conditions and described the index as "mountain water dependent," in which mountain snowpack is a major component. SWSI is expressed as

$$SWSI = \frac{aP_{\text{snow}} + bP_{\text{prec}} + cP_{\text{strm}} + dP_{\text{resv}} - 50}{12}, \tag{12.24}$$

where a, b, c, and d are weight for snow, rain, streamflow, and reservoir, respectively ($a + b + c + d = 1$), and P_i is the probability (%) of non-exceedance for each of these four water balance components. Calculations are performed with a monthly time step. In winter months, SWSI is computed using snowpack, precipitation, and reservoir storage. In summer, streamflow, precipitation, and reservoir storage data are used. For each month, the values of each component measured at all stations (or reservoirs) across the region/basin are summed.

The objective of the SWSI was to incorporate both hydrological and climatological features into a single index value resembling the Palmer Index for each major river basin in the state of Colorado (Shafer and Dezman 1982). These values would be standardized to allow comparisons between basins. Four inputs are required within the SWSI: snowpack, streamflow, precipitation, and reservoir storage. Because it is dependent on the season, the SWSI is computed with only snowpack, precipitation, and reservoir storage in the winter. During the summer months, streamflow replaces snowpack as a component within the SWSI equation.

The procedure to determine the SWSI for a particular basin is as follows: monthly data are collected and summed for all the precipitation stations, reservoirs, and snowpack/streamflow measuring stations over the basin. Each summed component is normalized using a frequency analysis gathered from a long-term data set. The probability of non-exceedance—the probability that subsequent sums of that component will not be greater than the current sum—is determined for each component based on the frequency analysis. This allows comparisons of the probabilities to be made between the components. Each component has a weight assigned to it depending on its typical contribution to the surface water within that basin, and these weighted components are summed to determine an SWSI value representing the entire basin. Like the Palmer Index, the SWSI is centered on zero and has a range between –4.2 and +4.2.

The SWSI has been used, along with the Palmer Index, to trigger the activation and deactivation of the Colorado Drought Plan. One of its advantages is that it is simple to calculate and gives a representative measurement of surface water supplies across the state. It has been modified and applied in other western states as well. These states include Oregon, Montana, Idaho, and Utah. Monthly SWSI maps for Montana are available from the Montana Natural Resource Information System.

Several characteristics of the SWSI limit its application. Because SWSI calculation is unique to each basin or region, it is difficult to compare SWSI values between basins or between regions (Doesken et al. 1991). Within a particular basin or region, discontinuing any station means that new stations need to be added to the system and new frequency distributions need to be determined for that component. Additional changes in the water management within a basin, such as flow diversions or new reservoirs, mean that the entire SWSI algorithm for that basin needs to be redeveloped to account for changes in the weight of each component. Thus, it is difficult to maintain a homogeneous time series of the index (Heddinghaus and Sabol 1991). Extreme events also cause a problem

if the events are beyond the historical time series, and the index will need to be reevaluated to include these events within the frequency distribution of a basin component.

There are some limitations in estimation of SWSI based on this method:

- It is not easy to determine the weight of different components in this equation.
- It is difficult to determine the equal water depth of snow, and there is a high level of uncertainty.
- Even though a probability distribution is fitted to each component of this relation, the summation of these weighted probabilities does not follow a specific distribution.

To deal with these limitations, Garren (1993) in his studies on Felt river in Montana used the series of forecasted flow and reservoir storage in the above relation. Therefore, equal snow depth is implicitly considered and SWSI is calculated as follows:

$$SWSI = \frac{P - 50}{12} \tag{12.25}$$

where P is the corresponding probability of the summation of reservoir storage and forecasted flow. This method is called Modified SWSI.

12.6 AGRICULTURAL DROUGHT

In the study of *agricultural droughts*, many investigators believe that soil moisture shortage is the best and the most practical drought indicator. Soil moisture shortage is the result of moisture loss during dry periods in which evapotranspiration is more than precipitation. Such losses depend on the type of plants. The potential evapotranspiration happens only when the soil is completely wet. Once the soil moisture drops to a level lower than the plant roots, the actual evapotranspiration decreases to a very low rate, compared to the potential evapotranspiration. It is necessary to use water balance models to determine soil moisture shortage in different time periods, especially in regions with limited data availability.

Water balance models are based on theoretical methods to simulate runoff and soil moisture variations in a river basin. Water balance models were first developed by Thornthwaite (1948) and later modified by Thornthwaite and Mather (1955). These models include methods for estimating the water balance between the river basin inflow (from precipitation and snowmelt) and outflow (evapotranspiration and groundwater supply). Since the first water balance model development by Thornthwaite and its modifications, these models have been used widely for irrigation management, prediction of runoff, and reservoir and groundwater supply (Haan 1972; Mather 1981). Revelle and Waggoner (1983), Gleick (1987), and Schaake (1990) have also used water balance to estimate the effect of general climatic changes on hydrologic characteristics of specific regional models.

An application of water balance models is to obtain a drought indicator. Palmer (1965) designed a drought indicator known as the PDSI (Palmer Drought Severity Index) by using a water balance model between moisture supply and demand for a two-layer soil. The PDSI is a tool to determine spatial and temporal variation in soil moisture stresses. Its calculation includes determination of the Z index, the monthly soil moisture indicator, which reflects the deviation of actual precipitation, and soil moisture supply from the expected values for the normal condition known as climatically appropriate for the existing condition (CAFEC).

12.6.1 Agricultural Drought Indicators

For trend studies, climatic factors such as temperature and precipitation are considered in addition to the hydrological factors such as runoff (Thornthwaite 1948). The following steps have been taken to calculate the moisture anomaly index (Z), which is necessary for calculation of the PDSI.

12.6.1.1 Thornthwaite Water Balance Model

This model was initially developed by Thornthwaite (1948). Even though it is an old model and may be considered as outdated, it is still being used by many investigators such as Alley (1984). It is also true with PDSI. This model is not data intensive and works in regions with data deficiencies. Furthermore, it can be calibrated in different stages so that it is less susceptive to error accumulation. This model has been developed based on different factors such as existing soil moisture, soil moisture deficit, and total amount of rainfall. This model could provide a general view of the soil moisture variation resulting from variation in precipitation over the historical record. In other words, results of this model can be used for a general evaluation of current conditions caused by the impacts of regional climatic parameters on hydrologic and agricultural conditions. This water balance model is applicable to daily, monthly, or even annual time sequences.

The input data of the model are precipitation, monthly average temperature, and potential soil moisture. The model output consists of actual soil moisture, infiltration, excess rainfall, and actual and potential evapotranspiration. The Thornthwaite equation, which is discussed in Chapter 4, can be used to calculate the monthly potential evapotranspiration.

When precipitation for a specific month is more than the potential evapotranspiration, the actual evapotranspiration is equal to the potential evapotranspiration and the remaining rainfall is compared with both the soil moisture capacity and the initial soil moisture of the previous month. The remaining rainfall supplies the soil moisture until it reaches its potential value. There is no runoff until the soil approaches its moisture capacity. Obviously, if the summation of rainfall and soil moisture is less than the potential evapotranspiration, the actual evapotranspiration is less than the potential evapotranspiration.

12.6.1.2 Potential Evapotranspiration

As explained above, the Thornthwaite equation is applied to calculate potential evapotranspiration. An advantage of this method is that temperature is the only required input parameter, which is measured for most regions at acceptable intervals. Other methods such as the *T* model by Mather (1981), and the *ABCD* model by Thomas et al. (1983) require different climatic parameters, which are seldom measured for one region at the same intervals.

12.6.1.3 Soil Moisture Condition

The objective of this step is to identify the pattern of *soil moisture* variation as a function of temperature and precipitation. First, the precipitation at a specific month should be compared with the potential evapotranspiration for that month. If the precipitation is sufficient, then the actual and potential evapotranspiration are assumed to be equal. After subtracting the potential evapotranspiration, the remaining amount will supply the soil moisture until it reaches its capacity (Φ). If still any rain remains, the rest forms runoff and groundwater recharge. If the precipitation is less than potential evaporation, then the actual evapotranspiration could practically be provided by the soil moisture from the previous month. The following equations express these situations:

$$\text{If } P_i \geq PE_i, \text{ then: } \begin{cases} ET_i = PE_i \\ S_i = \text{Min}\{(P_i - PE_i) + S_{i-1}, \Phi\} \\ R_i = S_i - S_{i-1} \\ L_i = 0 \\ EP_i = (P_i - PE_i + S_{i-1}) - \Phi \end{cases} \tag{12.26}$$

$$\text{otherwise:}\begin{cases} ET_i = \text{Min}\{PE_i, (P_i + S_{i-1})\} \\ S_i = (P_i + S_{i-1}) - ET_{ri} \\ R_i = 0 \\ L_i = S_{i-1} - S_i \\ EP_i = 0, \end{cases} \tag{12.27}$$

where P_i is precipitation in month i, PE_i is potential evapotranspiration in month i, ET_i is actual evapotranspiration in month i, S_i is soil moisture in month i, R_i is the amount of water that soil gained in month i, L_i is soil moisture loss in month i, Φ is soil moisture capacity, and EP_i is excess rainfall in month i.

Then, the *soil moisture deficit*, D_i is calculated as follows:

$$D_i = \Phi - S_i. \tag{12.28}$$

In the first condition, the excess rainfall can be greater than zero, which means that the soil moisture deficit is equal to zero and there is excess water for runoff.

12.6.1.4 Runoff Calculation

When there is excess rainfall, then runoff is generated. The simplified water balance model is applied to calculate excess rainfall. Separation of runoff and groundwater recharge is difficult. Runoff can be calculated as follows:

$$RO_i = F * EP_i, \tag{12.29}$$

where RO_i is calculated runoff from excess rainfall in month i, F is lag factor, for converting excess rainfall to runoff, and EP_i is excess rainfall in month i.

As can be seen in this equation, a lag factor is necessary to calculate the runoff, which depends on the geophysical condition of the region. This factor is less than 1 and it is calibrated by using a long-term runoff data set, measured in gagging stations, and the long-term excess rainfall data set that has been calculated in the previous step. The method of least mean-square error is used to calibrate the model and select the best lag factor for the region.

Example 12.6

The monthly water balance parameters of a region are given in Table 12.13. Assume that the soil moisture content does not change before and after rainfall. What is the evapotranspiration in that month in millimeters?

TABLE 12.13
Parameters of Water Balance Model (Example 12.6)

Precipitation (mm)	Runoff Coefficient	Changes in Water Table (cm)	Storage Coefficient of the Aquifer
50	25	+10	8%

Solution:

Direct runoff and groundwater recharge can be estimated as

$$\text{Direct runoff} = 50 \times 0.25 = 12.5 \text{ mm.}$$

$$\text{Groundwater recharge} = 100 \times 0.08 = 8 \text{ mm.}$$

The evapotranspiration can then be estimated as the difference between rainfall depth and depth of direct runoff and groundwater recharge:

$$\text{Evapotranspiration} = 50 - 12.5 - 8 = 29.5 \text{ mm.}$$

12.6.1.5 Potential Climatic Values

Besides the potential evapotranspiration, other potential values should be calculated:

- Potential recharge (PR): the moisture needed by the soil to reach its moisture capacity. It is the difference between soil moisture capacity and the actual soil moisture, which is the same as soil moisture deficit, D_i.
- Potential moisture loss (PL): the amount of moisture loss from soil to supply the evapotranspiration demand ($PE_i - S_{i-1}$). The moisture loss approaches its potential when there is no precipitation.

$$PL_i = \text{Min}\{PE_i, S_{i-1}\} \tag{12.30}$$

- Potential runoff (PRO): the maximum runoff that can occur. It is a function of precipitation less the soil moisture gain. In the most critical conditions, often it could be assumed that when the amount of runoff is high, the amount of potential recharge (PR) is low, and when it is low, the potential recharge is high. When S reaches its maximum value, the potential runoff is maximized too. The nature of potential runoff is much more complicated than other potential values. Different investigators assumed values as high as three times the amount of precipitation and as ambiguous as the difference between soil moisture capacity and potential recharge. On the absence of solid grounds that could relate PRO to other hydrologic parameters, the value of PRO for each month is assumed to be the highest runoff experienced during the historical record for that month.

12.6.1.6 Coefficients of Water Balance Parameters

- Evapotranspiration coefficient (α): In dry climates, real evapotranspiration is less than potential evapotranspiration. The amount of precipitation needed for the near-normal condition is dependent on the average climate and on the prevailing meteorological conditions both during and preceding the month or period in question. α is used to estimate the expected evapotranspiration of CAFEC from the potential evapotranspiration. This terminology has been used frequently in drought studies. It simply implies the expected normal condition:

$$\alpha = \frac{\overline{ET_i}}{\overline{PE_i}}, \tag{12.31}$$

where $\overline{ET_i}$ and $\overline{PE_i}$ are the averages of historical ET and PE in month i. The expected ET after applying this coefficient could be compared with its actual amount in a specific month to obtain the deviation from normal condition for that month.

- Recharge coefficient (β): In many regions, soil moisture recharge is a seasonal property of the soil. The proportion of average recharge for month *i* to average potential recharge is called (β).

$$\beta = \frac{\overline{R_i}}{\overline{PR_i}} \tag{12.32}$$

This coefficient could be used to compare the expected recharge in a specific climatic condition with its actual amount.

- Runoff coefficient (γ): This is calculated as the ratio of average runoff for month *i* to potential runoff:

$$\gamma = \frac{\overline{RO_i}}{\overline{PRO_i}}. \tag{12.33}$$

By applying this coefficient, the expected runoff in a specific climatic condition is calculated.

- Moisture loss coefficient (δ): This is the ratio of average moisture losses in month *i* to potential loss:

$$\delta = \frac{\overline{L_i}}{\overline{PL_i}}. \tag{12.34}$$

The amount of soil moisture losses, which is calculated by this coefficient, could be subtracted from the sum of the other three factors to obtain the amount of precipitation for a region to be in normal condition.

12.6.1.7 Climatically Appropriate for Existing Condition ($\hat{P}$)

Using the above equations, the amounts of evapotranspiration, recharge, runoff, moisture loss, and expected precipitation in each month for the normal condition could be calculated as follows:

$$\hat{ET}_i = \alpha \cdot PE_i \tag{12.35}$$

$$\hat{R}_i = \beta \cdot PR_i \tag{12.36}$$

$$\hat{RO}_i = \gamma \cdot PRO_i \tag{12.37}$$

$$\hat{L}_i = \delta \cdot PL_i \tag{12.38}$$

$$\hat{P}_i = \hat{ET}_i + \hat{R}_i + \hat{RO}_i - \hat{L}_i. \tag{12.39}$$

Each component of CAFEC precipitation has an average equal to the average historical observations. For the expected evapotranspiration, $\hat{ET}$, it is equal to

$$\hat{ET}_i = \alpha \cdot PE_i = \frac{\sum_{i=1}^{n}(ET_i)}{\sum_{i=1}^{n}(PE_i)} PE_i, \tag{12.40}$$

By taking the summation of both sides,

$$\sum_{i=1}^{n}\left(\hat{ET}_i\right) = \frac{\sum_{i=1}^{n}(ET_i)}{\sum_{i=1}^{n}(PE_i)} \sum_{i=1}^{n}(PE_i). \tag{12.41}$$

Therefore,

$$\sum_{i=1}^{n}\left(\hat{ET}_i\right) = \sum_{i=1}^{n}(ET_i). \tag{12.42}$$

The average value of CAFEC evapotranspiration is equal to the average evapotranspiration from historical hydrologic accounting. The same reasoning holds for the average of the other components of CAFEC precipitation. Therefore, the estimated value of CAFEC precipitation is unbiased. Despite having the same average, the CAFEC values and the actual/observed values for each period are seldom in complete agreement, but in long-period studies and observation, they tend to converge.

12.6.1.8 Moisture Anomaly Index (*Z*)

After calculating CAFEC precipitation and comparing it with the observed precipitation, the difference, d, can be calculated as

$$d = P - \hat{P}. \tag{12.43}$$

These departures from normal series show the deviation of the weather from its normal condition. This new series provides a good description of the moisture or lack of moisture in the climate.

12.6.1.9 Climatic Character, *k*

Average moisture supply is not always dependent on the precipitation in a period. On some occasions, when there is insufficient precipitation, storage of moisture in the previous period is used. Using the average of moisture supplied, a climatic character, k_i, for each month i is calculated as follows (Palmer 1965):

$$k_i = 17.67\hat{K}_j / \sum_{i=1}^{12} \bar{D}_i \times \hat{K}_j \quad j = 1\ldots12, \tag{12.44}$$

where

$$\hat{k}_j = 1.5 \log_{10}\left(\frac{T_j + 2.8}{\bar{D}_j}\right) + 0.5 \tag{12.45}$$

and

$$T_j = \left(\overline{PE}_j + \overline{R}_j + \overline{RO}_j\right)/\left(\overline{P}_j + \overline{L}_j\right). \tag{12.46}$$

T_j is a measure of the ratio of moisture demand to moisture supply for a month. k_j is a regional climatic character. To estimate the Z index for a specific region, the coefficients of the above equations must be calculated based on the climatic character of the region. The monthly constants (k) are used as weighting factors of monthly deviations during dry spells. Then, a moisture anomaly index, Z, for month i is defined as follows:

$$Z_i = k_i \times d_i \quad (i = 1, 2, \ldots, N). \tag{12.47}$$

12.6.1.10 Palmer Drought Severity Index

PDSI is an index for evaluating the severity of a drought. After determining the Z index, the PDSI formulation is expressed as follows:

$$PDSI_i = 0.897 PDSI_{i-1} + (1/3)Z_i \quad i = 1, 2, \ldots, N \tag{12.48}$$

$$PDSI_i = (1/3)Z_i, \tag{12.49}$$

where N is the number of time periods.

Based on Palmer's definition, dry and wet spells are categorized by PDSI. Table 12.14 shows the drought classification based on the PDSI value.

TABLE 12.14
Drought Categories Based on PDSI

PDSI	Drought Category
≤ –4	Most severe drought
–4 to –3	Severe drought
–3 to –2	Medium drought
–2 to –1	Nearly drought
–1 to 1	Normal
1 to 2	Nearly wet
2 to 3	Medium wet
3 to 4	Severe wet
≥4	Most severe wet

Source: Palmer, W.C., 1965. With permission.

In order to obtain drought and wet spells using PDSI, one of the three different indices (X_i^k) must be used:

$$X_i^k = 0.897 * X_{i-1}^k + (1/3) \times Z_i \quad k = 1,2,3 \quad i = 1,2,3 \ldots n, \tag{12.50}$$

X_i^1 = Severity index for a wet spell in month i
X_i^2 = Severity index for a dry spell in month i
X_i^3 = Severity index for a spell that cannot be classified as either dry or wet in month i

To determine the drought severity index, the following steps should be taken:

If X_i^2 is less than or equal to –1, then month i is in a drought spell. If X_i^k is greater than or equal to 1, then month i is in a wet spell. During a period of drought, X_i^3 is equal to X_i^2, and during a wet period, X_i^3 is equal to X_i^1. In this situation, when the indicators (X_i^1 or X_i^2) are between –0.5 and 0.5, then X_i^3 is equal to zero and it is the termination time of a dry or wet spell, respectively. Often, there is only one indicator that is not equal to zero, and this non-zero indicator will be the PDSI. The advantage of this method is that once a dry or wet period is observed by either X_i^2 or X_i^1, then the other resets to zero. Therefore, the value of PDSI does not grow without any limits, which could be the case if only Equation 12.48 is used (Alley 1984).

The termination of an established drought is assumed to occur when $Z_i \geq Ze_i$, where Ze_i is the moisture required to reduce the severity of a drought to –0.5. Similarly, the termination of a wet spell is assumed to occur when $Z_i \leq Ze_i$. Ze_i can be derived by solving Equation 12.48 for Z_i and substituting –0.5 and 0.5 for X_i, respectively. The parameter introduced by Palmer (1965), Pe, is used to determine the correct value for PDSI in different conditions. Pe is a percentage probability that an established wet or drought spell has ended and is defined as

$$Pe_i = \frac{100 \sum_{j=0}^{j^*} U(i-j)}{Ze_i + \sum_{j=1}^{j^*} U(i-j)}, \tag{12.51}$$

where

$$U_i = Z_i + 0.15 \text{ for an established drought spell} \tag{12.52}$$

and

$$U_i = Z_i + 0.15 \text{ for and established wet spell.} \tag{12.53}$$

Based on the study of Palmer (1965), in the case of an established drought, a value of $Z = 0.15$ will maintain an index of –0.5 from month to month. Therefore, any value of Z greater than or equal to –0.15 will tend to end a drought. A similar assumption could be considered for the termination of a wet spell. Thus, Palmer proposed the U_i as defined before.

The parameter j^* corresponds to the number of successive values of U_i computed prior to the current month. When the PDSI series shows a drought or wetness period, Pe must meet its extreme values (0 or 100) to change the current condition. When $0 < Pe < 50$, then PDSI = X^3, and when $50 < Pe < 100$, then PDSI will be equal to X^2 or X^1, depending on which term has the opposite of X^3. Readers are referred to Palmer (1965) and Alley (1984) for more details.

TABLE 12.15
CMI Classification

–3.0 or less	Severely dry
–2 or –2.9	Excessively dry
–1 or –1.9	Abnormally dry
–0.9 or +0.9	Slightly dry/favorably moist
+1.0 or +1.9	Abnormally moist
+2 or +2.9	Wet
3.0 and above	Excessively wet

As previously mentioned in the methodology of calculating the PDSI, the coefficients of the PDSI are dependent on the regional climate and may change with the different climatic characteristics of different regions. Hence, it is necessary to derive new coefficients for the PDSI equation in different study areas.

12.6.1.11 Crop Moisture Index

Crop Moisture Index (CMI) reflects moisture supply in the short term across major crop-producing regions and is not intended to assess long-term droughts. The CMI uses a meteorological approach to monitor week-to-week crop conditions. It was developed by Palmer (1968) from procedures within the calculation of the PDSI. Whereas the PDSI monitors long-term meteorological wet and dry spells, the CMI was designed to evaluate short-term moisture conditions across major crop-producing regions. This index is calculated as follows:

$$CMI = ET_{obs} - ET_{exp}, \tag{12.54}$$

where ET_{obs} is the observed evapotranspiration and ET_{exp} is the expected evapotranspiration. If the potential moisture demand exceeds available moisture supplies, the CMI is negative. However, if moisture meets or exceeds the demand, the index is positive. It is necessary to use two separate legends because the resulting effects are different when the moisture supply is improving than when it is deteriorating. The CMI classification, which is similar to PDSI, is given in Table 12.15. The stage of crop development and soil type should be considered when using this index. The CMI responds rapidly to changing conditions, and it is weighted by location and time so that maps, which commonly display the weekly CMI, can be used to compare moisture conditions at different locations.

Because it is designed to monitor short-term moisture conditions affecting a developing crop, the CMI is not a good long-term drought monitoring tool. The CMI's rapid response to changing short-term conditions may provide misleading information about long-term conditions. For example, a beneficial rainfall during a drought may allow the CMI value to indicate adequate moisture conditions, while the long-term drought at that location persists. Another characteristic of the CMI that limits its use as a long-term drought monitoring tool is that the CMI typically begins and ends near zero each growing season. This limitation prevents the CMI from being used to monitor moisture conditions outside the general growing season, especially in droughts that extend over several years. The CMI also may not be applicable during seed germination at the beginning of a specific crop's growing season.

12.6.2 Sequence of Drought Impacts

The reduction in rainfall, soil moisture, and water in dams and rivers causes meteorological, agricultural, and hydrological drought, respectively. Figure 12.6 shows that the sequence of impacts associated with meteorological, agricultural, and hydrological drought further emphasizes their

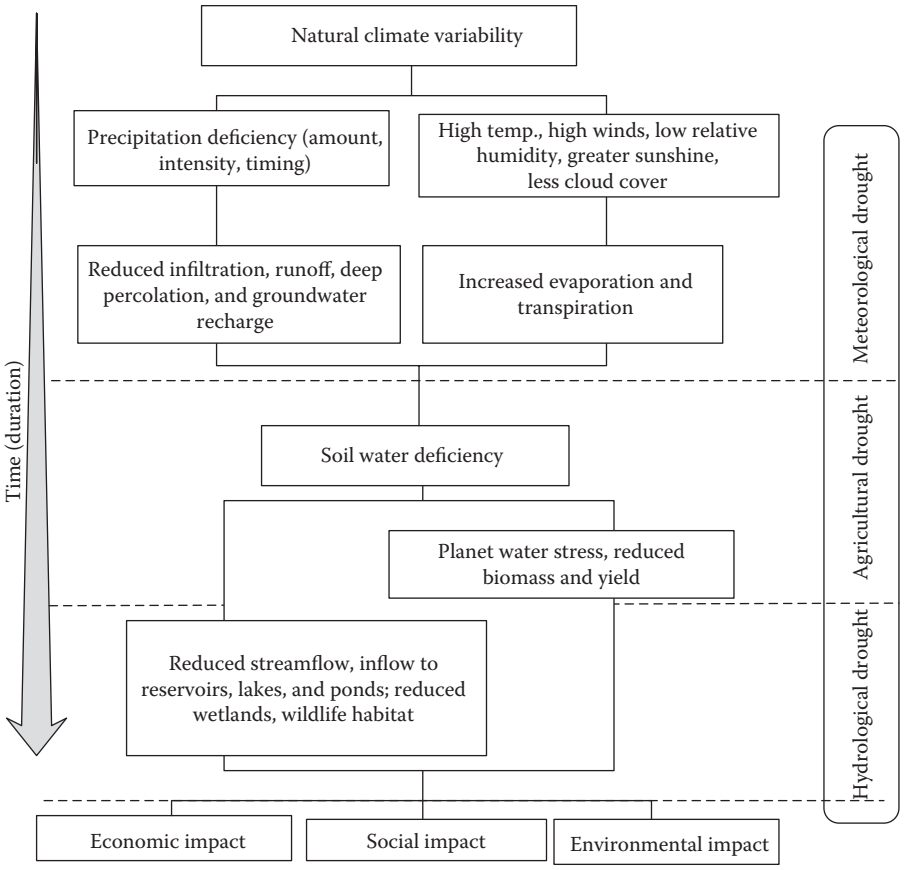

FIGURE 12.6 Schematic of droughts and sequences of impacts.

differences. When drought begins, the agricultural sector is usually the first to be affected because of its heavy dependence on stored soil water. Soil water can be rapidly depleted during extended dry periods. If precipitation deficiencies continue, then people and industries dependent on other sources of water will begin to feel the effects of the shortage. Those who rely on surface water (i.e., reservoirs and lakes) and subsurface water (i.e., groundwater) are usually the last to be affected. A short-term drought that persists for 3 to 6 months may have little impact on these sectors, depending on the characteristics of the hydrologic system and water use requirements.

When precipitation returns to normal and meteorological drought conditions have abated, the sequence is repeated for the recovery of surface and subsurface water supplies. Soil water reserves are replenished first, followed by streamflow, reservoirs, and lakes, and then groundwater. Drought impacts may diminish rapidly in the agricultural sector because of its reliance on soil water but linger for months or even years in other sectors dependent on stored surface or subsurface supplies. Groundwater users, often the last to be affected by drought during its onset, may be the last to experience a return to normal water levels. The length of the recovery period is a function of the intensity of the drought, its duration, and the quantity of precipitation received as the episode terminates.

12.6.3 Economic Aspects of Water Shortage

Socioeconomic definitions of drought are associated with consequences of deficiencies in supplying the demand. Some economic goods are being lost as a result of meteorological, hydrological,

and agricultural drought. It differs from the aforementioned types of drought because its occurrence depends on the time and space processes of supply and demand and how losses in production and income affect social interest. The supply of many economic goods, such as water, forage, food grains, fish, and hydroelectric power, depends on weather. Because of the natural variability of climate, water supply is ample in some years but unable to meet human and environmental needs in other years. Socioeconomic drought occurs when the demand for an economic good exceeds supply as a result of a weather-related shortfall in water supply. For example, in Uruguay in 1988–1989, drought resulted in significantly reduced hydroelectric power production because power plants were dependent on streamflow rather than on storage for power generation. Reducing hydroelectric power production required the government to rely on more expensive (imported) petroleum and stringent energy conservation measures to meet the nation's power needs.

In most instances, the demand for economic goods is increasing as a result of increasing population and per capita consumption. Supply may also increase because of improved production efficiency, technology, or the construction of reservoirs that increase surface water storage capacity. If both supply and demand are increasing, the critical factor is the relative rate of change. If demand is increasing more rapidly than supply, then vulnerability and the incidence of drought may increase in the future and demand needs to be adjusted proportional to the expected supply.

Figure 12.7 shows the general trend of the average water demand with the return period of drought severity. The demand enlarges with the return period of the drought severity. Different demand curves are demonstrated in Figure 12.8 for diverse cost levels. As revealed in this figure, the upper bound is the price and the lower bound is the demand for the given hydrologic conditions.

The demand is associated with the hydrologic index W, which is related to the return period. The available supply (flow) q is estimated for different return periods (Hudson and Hazen 1964).

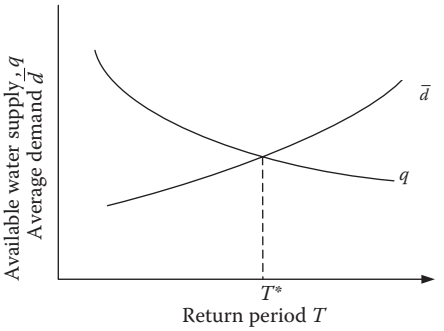

FIGURE 12.7 Water supply availability and average demand as a function of return period of drought (T).

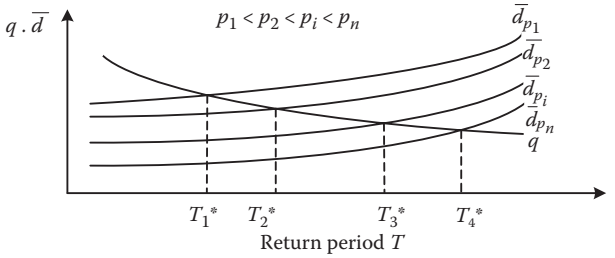

FIGURE 12.8 Water supply and average demand for different price values (p_i) as related.

Therefore, the wide-ranging relationships among return period and demand and return and supply period exposed in Figure 12.8 are based on these correlations.

Scarcity of water supply during drought periods results in diverse types of losses in the economy, as well as, but not limited to, commercial, agricultural, and industrial loss. In agriculture, shortage of water supply may result in crop failure; in commerce, it may translate into recession; and in industry, it may result in underproduction of merchandise. The loss in each manufacture or service sector depends on the point of the sector. For example, the economic impact of drought on agriculture depends on the crop type, etc. (Easterling 1993). There is no single ordinary way of evaluating the economic impact of drought on any one of the sectors. Assessing and evaluating what in point of fact happens during a drought period with what would have happened had there been no drought may be one way of assessing the effects of drought. Dixon et al. (1996) adopted the concept of willingness-to-pay to value changes in well-being. They define willingness-to-pay as the maximum individuals would have been willing to pay to keep away from the drought management strategies enforced by water agencies.

In contrast, as water is supplied through a drought period at a larger cost, it can be viewed as a revenue generator. Consequently, when the demand surpasses the available supply, the revenue collected by the water supply agency is less than what could have been collected had there been more supply than that actually accessible. In other words, if the demand surpasses the supply, the difficulty is not limited to the need for water; there will also be economic loss, since the clientele would pay for more supply. If there were sufficient water, it is possible to make a decision whether supply increase is essential or the greater demand could be borne by the available supply, depending on the risk level.

Some water borne release efforts can be assumed so that emergency water supplies may be made available to users. This can be done by well drilling, trucking in potable supplies, or transporting water all the way through small-diameter emergency water lines. In such cases, it may be necessary that the emergency supply building costs be paid by the users (Dziegielewski et al. 1991). The assessment of the expected economic loss can be used to determine and inform the users of its amount and advise them of the necessity, if any, of paying for the emergency supply building expenditure.

If the option for emergency supply construction is justified, the optimization needs to take into consideration the different possibilities for design of the water supply system. The design of the construction should be done in such a way that it result in optimized financial risk and cost of construction.

The economic loss (damage) from drought events can be calculated. The damage that would result from a certain drought event is one of the main decision factors. Since the time of occurrence of the drought event that causes the damage is hard to determine, only the predictable value is evaluated by relating its magnitude with its probability of occurrence. The expected annual damage cost D_T for the water shortage $x > x_T$ is given as follows:

$$D_T = \int_{X_T}^{\infty} D(x) f(x)\,\mathrm{d}x, \tag{12.55a}$$

where $f(x)\mathrm{d}x$ is the likelihood that a drought of magnitude (water deficient) x will occur in any given year and $D(x)$ is the damage cost that would result from that event. The event x in this case can be taken as the demand and x_T can be the available supply during a drought event of return period T.

Breaking down the expected damage cost into intervals, we get

$$\Delta D_i = \int_{x_{i-1}}^{x_i} D(x) f(x)\,\mathrm{d}x, \tag{12.55b}$$

from which the finite-difference approximation is obtained

$$\Delta D_i = \left[\frac{D(x_{i-1}) + D(x_i)}{2}\right] \int_{x_{i-1}}^{x_i} f(x)\,\mathrm{d}x$$
$$= \left[\frac{D(x_{i-1}) + D(x_i)}{2}\right] [P(x \geq x_{i-1}) - P(x \geq x_i)]. \tag{12.55c}$$

Thus, the annual damage cost for a return period T is given as

$$D_T = \sum_{i=1}^{\infty} \left[\frac{D(x_{i-1}) + D(x_i)}{2}\right] [P(x \geq x_{i-1}) - P(x \geq x_i)]. \tag{12.56}$$

To determine the annual estimated damage in the above equation, the damage that results from drought events of different severity levels must be quantified.

The magnitude of the drought (in monetary units) may be obtained by estimating the volume of water shortage that would result from that drought. In other words, the water shortage results in some economic loss to the water supply customer. The resulting economic loss to the customer from a confident drought event is accordingly well thought out as the damage from that drought occurrence.

As shown in Figure 12.9, after the critical return period T^*, the deviation between the demand and the supply increases with the return period. Expressing the demand and the supply as a function of return period T of drought events enables one to estimate the annual predictable water supply deficiency volume, as given by the following expression:

$$S_v = \int_T^T [d(T) - q(T)]\,\mathrm{d}t. \tag{12.57}$$

The deficiency volume S_v is shown by the shaded area in Figure 12.9. The deficiency volume for a drought occurrence of a higher return period above the critical one results in higher deficiency volume and higher related damage. The connection between the deficiency volume and the related damage in general depends on several factors, including water use category—residential,

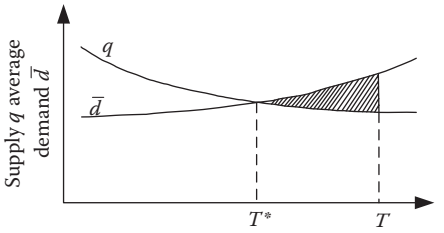

FIGURE 12.9 Demand and supply, showing water shortage volume when demand exceeds supply.

commercial, agricultural, industrial, and so on. To use the method presented here for evaluating the damage that results from certain water shortage volume, the damage given by Equation 12.57 must be developed for a specific user category.

Example 12.7

The supposed annual damage price that would happen if a drought of return period T were to take place is given, in \$1000, as

$$D(T) = T^2 - T = \frac{1}{P^2} - \frac{1}{P},$$

where $p = 1/T$, that is, annual exceedance probability. Determine

a. $D(T)$ for $T = 1, 2, 5, 10, 20, 50, 100, 200, 500$, and 1000
b. The damages between the return period intervals given in part (a)
c. The annual expected damage price for a drought mitigation plan for each of the return periods given in (a)

Solution:

The solutions to this problem are given in Table 12.16. Column 3 gives $D(T)$ for $T = 1, 2, 5, 10, 20, 50, 100, 200, 500$, and 1000. Column 6 gives the damage between the return periods indicated and column 7 gives the total expected damage.

12.7 HYBRID DROUGHT INDEX

Karamouz et al. (2009) developed an integrated drought index for evaluating drought impacts. It should be noted that drought indices have some shortcomings but it does not mean that they are not reliable tools for drought assessment; in fact, their shortcomings can be improved on by utilizing other indices in hybridized form such as the Hybrid Drought Index (HDI).

In many drought studies, the focus has been on agricultural droughts due to vulnerability of crops in severe droughts. PDSI, as the most important index of drought evaluation, has been considered in many studies, but there are some shortcomings in the way it is determined. This index is sensitive

TABLE 12.16
Cost Estimation of Damage in Example 12.7

(1)	(2)	(3)	(4)	(5)	(6)	(7)
1	1.000	0				0.000
2	0.500	2	0.500	1	0.5	0.500
5	0.200	20	0.300	11	3.3	3.800
10	0.100	90	0.100	55	5.5	9.300
20	0.050	380	0.050	235	11.75	21.050
40	0.025	1560	0.025	970	24.25	45.300
100	0.010	9900	0.015	5730	85.95	131.250
200	0.005	39,800	0.005	24,850	124.25	255.500
500	0.002	249,500	0.003	144,650	433.95	689.450
1000	0.001	999,000	0.001	624,250	624.25	1313.700

to the available water capacity of soil, but for simplifying index computations, soil properties are considered to be fixed in different depths. Furthermore, the lag time between precipitation and the resulting runoff is not considered, which leads to an inaccurate estimation of the index (Alley 1984). Therefore, hybridizing the indices could cover the combined impacts of different factors affecting drought severity. Here, PDSI, SWSI, and SPI have been combined through the analysis of drought damage as a new approach for quantifying drought impacts. Drought damage is selected because it is the result of all aspects of meteorological, hydrological, and agricultural droughts. Therefore, one may consider a relation to estimate the drought damage:

$$\text{Damage}_t = f(SPI_{t-1}, SWSI_{t-1}, PDSI_{t-1}). \tag{12.58}$$

Because of the difficulties in determining the form of function f in Equation 12.58, the damage is estimated based on SPI, SWSI, and PDSI. Based on the estimated damage, the HDI has been developed. The framework of the adjusted SWSI developed by Garren (1993) has been adapted in the definition of the HDI according to Equation 12.59.

$$HDI_t = f(\text{Damage}_t) = \frac{P_t(\text{Damage}) - 100}{24}, \tag{12.59}$$

where P_t is the cumulative probability of damage in month t. The characteristics of the damage for the three types of droughts are complex, with a significant degree of nonlinearity and uncertainties. The following steps are carried out for HDI determination and utilization for the drought severity prediction using artificial neural networks:

1. Calculation of time series of SPI, SWSI, and PDSI as indices for meteorological, hydrological, and agricultural aspects of droughts
2. Analysis and adjustment of historical drought damage data and estimating the monthly damage
3. Finding the most appropriate cumulative probability distribution that fits the historical monthly damage
4. Determination of HDI values from the cumulative probability of damage (Equation 12.59)
5. Classification of HDI values into subcategories wherein Class 1 and the last class denote the normal and extremely severe drought conditions, respectively
6. Estimation of HDI subcategories and consequently the range of drought damage through calculated indices of different drought types by training a system

It should be mentioned that two types of ANN (artificial neural network) models have been used, namely, MLP and PNN, for training. SPI, SWSI, and PDSI for the current time scale are the network inputs and the HDI subcategories specified in Step 5 for the next time scale are their outputs. The 1-month time delay between drought indices and HDI is considered because of the lag time between the occurrence of drought and its consequences. Once ANNs are trained, the values of HDI can be estimated simply by having field observations of rainfall, temperature, reservoir inflow, and soil moisture.

Obviously, the range of probable damage can be obtained using upper and lower bounds of the HDI subcategories and Equation 12.59. The flow chart of the proposed approach for determining the HDI is shown in Figure 12.10. In comparison to the SWSI, HDI is utilized only for the evaluation of dry spans (unlike SWSI, HDI has only negative values, so it can be used only for drought classification). According to the HDI, drought starts when the HDI goes below −2 and continues unless it comes back above −1. The reason for selecting −2 as a threshold of drought beginning is that at

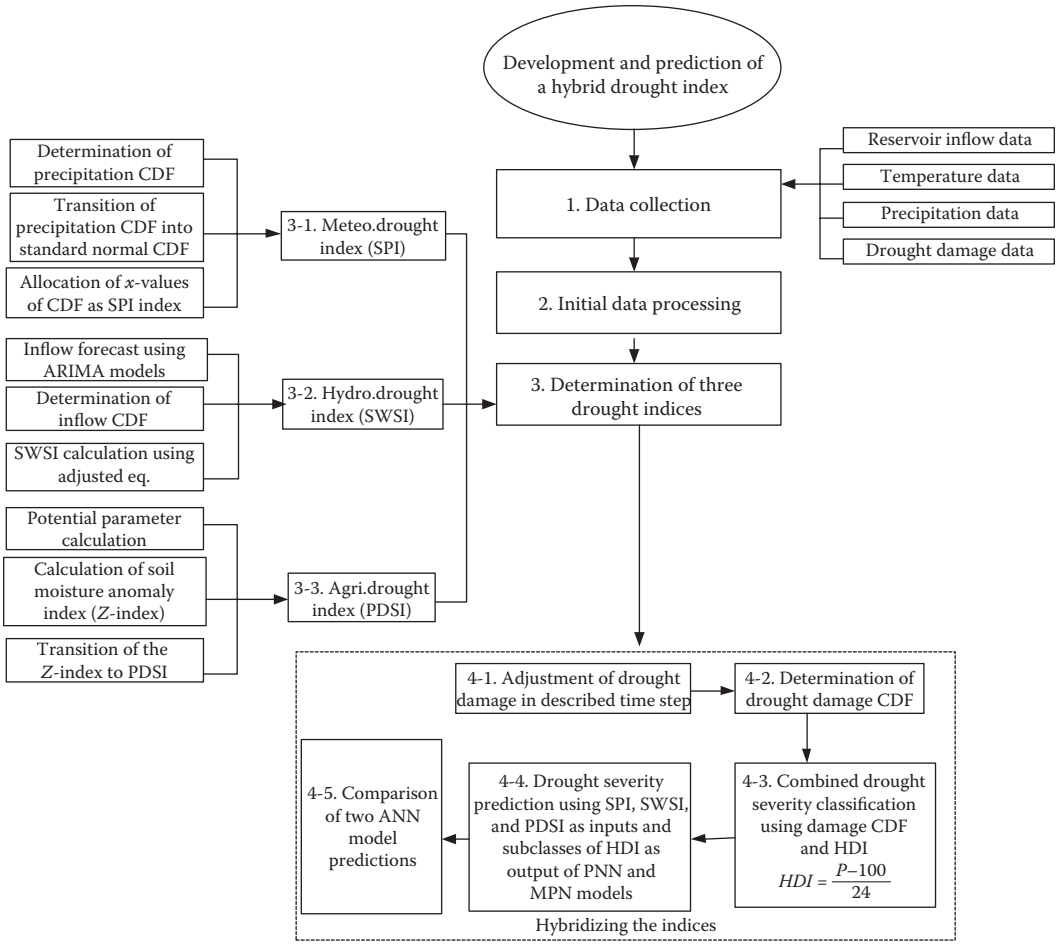

FIGURE 12.10 Algorithm for calculation of an HDI.

the beginning of drought spells, observed impacts are not very much due to gradual occurrence of droughts.

There are four main categories of drought severity according to the HDI: negligible, mild, moderate, and extreme. This classification of drought, which is shown in Table 12.17, is based on the cumulative probability of drought damage. For damage with the cumulative probability and the HDI value of less than 0.25 and −1, respectively, drought severity is considered to be negligible. This is because although there is damage, it is not significant enough to be attributed only to drought occurrence. When the value of HDI reaches −2, the damage caused by drought is moderate, and it can be assumed that drought span starts. Finally, when the value of HDI reaches −3, different water users, especially agriculture and animal husbandry sectors, suffer from water shortages, and it is considered the critical stage of drought. In regions where drought damage is generally high, small climate changes may cause extensive variations in damage. Therefore, in these regions, in order to evaluate the variations of drought impact, the classification of drought severity in smaller intervals can be helpful. For more accurate evaluation of drought, each of the four major categories of drought severity obtained through the HDI classification has been divided into four subcategories except the fourth category, which has four subcategories considering the fact that values less than −4 might be predicted by the neural networks (see Table 12.17). As a result, 16 subcategories have been defined according to the cumulative probability of drought damage.

TABLE 12.17
Classification of Drought Severity Based on HDI

Drought	Number Subclass	HDI Interval	Average of HDI
Negligible	1	−0.25 < HDI ≤ 0	−0.125
	2	−0.5 < HDI ≤ 0.25	−0.375
Mild	3	−0.75 < HDI ≤ 0.5	−0.625
	4	−1 < HDI ≤ 0.75	−0.875
	5	−1.25 < HDI ≤ 1	−1.125
	6	−1.5 < HDI ≤ 1.25	−1.375
Moderate	7	−1.75 < HDI ≤ 1.5	−1.625
	8	−2 < HDI ≤ 1.75	−1.875
	9	−2.25 < HDI ≤ 2	−2.125
	10	−2.5 < HDI ≤ 2.25	−2.375
	11	−2.75 < HDI ≤ 2.5	−2.625
Extreme	12	−3 < HDI ≤ 2.75	−2.875
	13	−3.25 < HDI ≤ 3	−3.125
	14	−3.5 < HDI ≤ 3.25	−3.375
	15	−3.75 < HDI ≤ 3.5	−3.625
	16	−4 < HDI ≤ 3.75	−3.875

12.7.1 Evaluation of Water Availability and Drought Damage

Damage caused by drought depends on water availability and demand and is significant in areas that have demand greater than the water supply. In order to assess the effect of water shortage on different water users, the annual damage (loss of property and life) data have been disaggregated to monthly time series. For disaggregation of the annual damage to a monthly time scale, the role of water demand and agricultural parameters (i.e., crop type and coverage area, as well as its sensitivity to soil water shortages) are considered. Moreover, reservoir storage and its releases have direct effects on the extent of damage. The effective variables in the assessment of damage have been considered in two terms. The first involves agriculture-related variables (Equation 12.60) and the second term addresses the water availability as expressed in Equation 12.61.

Variables such as crop coverage and type of crops, as well as crop sensitivity to water shortages $K_y^{i,j}$ in different stages of growth, have been considered in the assessment of drought damage. These variations are coupled into a coefficient of agricultural damage (AD) according to the following equations:

$$AD_i = \frac{B_i}{\sum_{i=1}^{12} B_i} \times 100 \tag{12.60}$$

$$B_i = \frac{\sum_{j=1}^{m} K_y^{i,j} A_{i,j}}{\sum_{j=11}^{m} A_{i,j}}, \tag{12.61}$$

where AD_i is the ratio of agricultural damage for month i to the annual damage (%); $A_{i,j}$ is crop j coverage area in month i; $K_y^{i,j}$ is crop j sensitivity to soil water shortages; B_i is the coefficient of the crop yield, which is the weighted mean of $K_y^{i,j}$ based on the crop coverage area; and m is the number of crops in the region. Calculating AD_i for every month of a year, one can find the critical months in the study area during which agricultural crops are vulnerable to drought. This is used to obtain the associated damage of each month out of the annual damage. According to the definition of $K_y^{i,j}$, when its value is 1 for a specified crop during one of its growth stages, for any one unit deficit in its water demand, the final crop yield will be decreased by one unit. The lower crop yield $K_y^{i,j}$ varies during different stages of its growth.

The other term—water availability (WA) of the reservoir—has been considered in the evaluation of drought damage. It controls the allocation of water to different sectors. For this purpose, the entire water demand of the agricultural, industrial, domestic, and environmental sectors (in streamflow) for every month of a normal year has been defined as WD, and it is combined with a factor, $Q_i^{'}$, that justifies the role of the reservoir in supplying the demands:

$$WA_i = \frac{WD_i \cdot Q_i^{'}}{\sum_{i=1}^{12} WD_i \cdot Q_i^{'}} \times 100 \tag{12.62}$$

$$Q_i^{'} = 1 - \frac{Q_i}{Q_{\max}}, \tag{12.63}$$

where $Q_i^{'}$ and $Q_{\max}$ are monthly and maximum reservoir outflows, respectively, and $Q_i^{'}$ is used as the water deficit penalty coefficient in computing the monthly damage, which varies between 0 and 1 for the highest and lowest reservoir outflows. WA_i shows that when the reservoir inflow in month i increases, the vulnerability of different sectors to water shortages and then the probable damage of drought will decrease. Also, it shows that when water demand (WD) during a month increases, water shortages cause more damage. Combining Equations 12.60 and 12.62, one may obtain an expression for determining the percentage of monthly damages (MD):

$$MD_i = \frac{WA_i \cdot AD_i}{\sum_{i=1}^{12} WA_i \cdot AD_i} \times 100. \tag{12.64}$$

Using Equation 12.64, the drought damage of each month is determined. Drought damage is a function of the physical conditions and also of social settings. It seems that social settings change over time, particularly as experience accumulates. For example, social response in an early drought is not likely to be the same compared with a later drought, and therefore, different drought damage for two sequential droughts having similar physical characteristics is possible and the reported damage is different than the actual values. In order to represent variability in social settings and estimate real damage, an adjusting coefficient, $\alpha_m(i)$, is introduced. This causes the damage to be reduced for later droughts in comparison to earlier droughts as the experience of dealing with droughts accumulates. Therefore, reported values of damage are adjusted by the coefficient $\alpha_m(i)$. Consider that there have been n dry months in a given drought in the basin preceded by another drought, a social setting factor $\alpha_m(i)$ for dry month i in the mth drought could be formulated as a parabola function as follows:

$$\alpha_m(i) = ai^2 + bi + c + d\alpha_{m-1}(n_{m-1})c = 1, \quad i = 1, 2, 3, \ldots, n_m, \tag{12.65}$$

where $\alpha_{m-1}(n_{m-1})$ is the social setting factor for the last month of the previous drought. This term shows that as the previous experience of drought accumulates, the social preparedness to cope with the incoming droughts improves and the associated damage decreases.

12.7.2 A Case Study

The HDI is evaluated for the Gavkhooni/Zayandeh-rud basin in central Iran (hereinafter, Case study basin). This basin has five sub-basins with a total area of 41,347 km^2. The dominant climate in this region is arid and semiarid. Precipitation varies throughout the basin between 2300 mm in the west (where most of the precipitation is in snow form) and 130 mm in the central part of Iran (near the desert). Annual average precipitation in this basin is about 1500 mm. The average precipitation in the Case study basin has been used for the calculation of drought indices. Acting as the main surface resource, there is a river that supplies the irrigation demands in this basin. As water and energy demands increase in this region, water withdrawals from the river increase, and it is important to incorporate climate variability in the decision-making process regarding water resources.

A reservoir controls the streamflow with a volume of 1470 MCM (million cubic meters). The location of this reservoir is shown in Figure 12.11. The average annual inflow to this reservoir is about 1600 MCM, of which an average flow of 600 MCM is transferred from the adjacent river basin. Drought trends in the basin have been studied between the years 1971 and 2004.

The Case study basin greatly affects the development and economy of the region through agricultural, industrial, and tourism activities. Statistics show that the amount of precipitation, especially in the high altitudes from October 1999 to April 2000, has decreased 35–45% compared to the long-term average and resulted in 250 MCM water shortages in the region in the year 2000.

As the first step in the HDI calculations, the monthly time series of SPI, modified SWSI, and PDSI are calculated from 1971 to 2004. The time series of damage is converted to year 2006 values for comparison purposes. The interest rate is considered as 17%. This time series of monthly damage is shown in Figure 12.12. As mentioned in the steps in calculating HDI, the cumulative probability function of damage occurrence is developed using the Weibull probability distribution (Figure 12.13) and used for determining the HDI values. Different thresholds of drought intensity according to the HDI, which are obtained from the probability–damage diagram, are shown in Figure 12.14.

The values of three indices (which indicate the climatic, hydrological, and agricultural aspects of drought) including SPI, SWSI, and PDSI, as well as the hybrid index, HDI, have been calculated for the Case study basin. The time series of these indices, their associated number of drought spans, and duration of dry periods are illustrated in Figure 12.14. This figure shows that during the drought periods determined by HDI, in most of the cases, three types of droughts have occurred: agricultural,

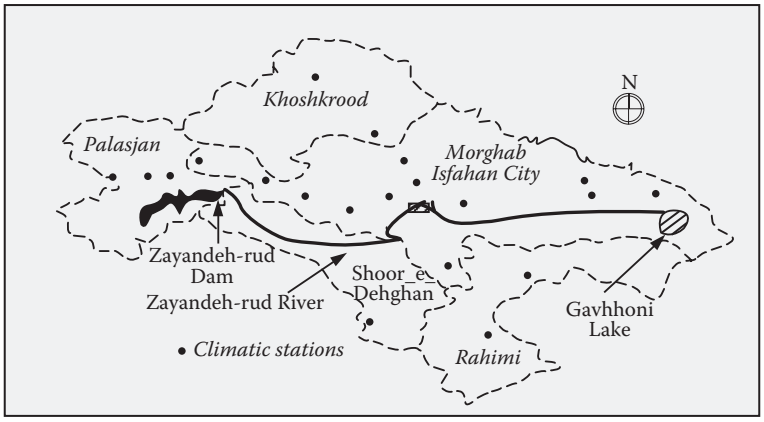

FIGURE 12.11 Gavkhooni/Zayandeh-rud basin with sub-basins and climatic stations.

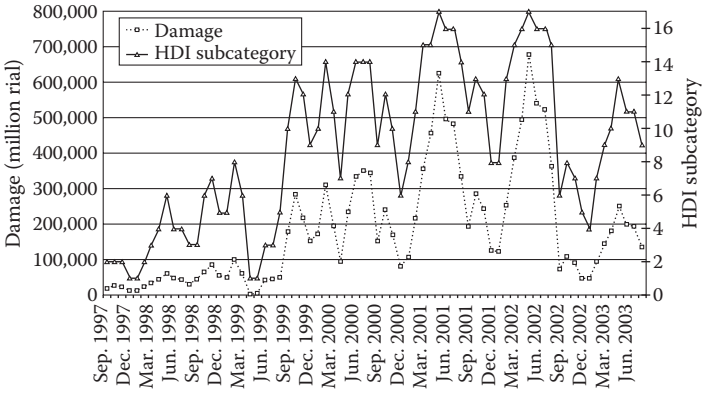

FIGURE 12.12 Monthly time series of damage (converted to values in the year 2006).

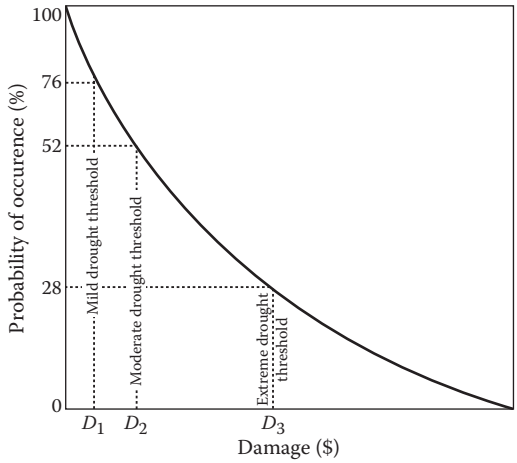

FIGURE 12.13 Diagram of cumulative probability of historical damages and thresholds of different drought severity.

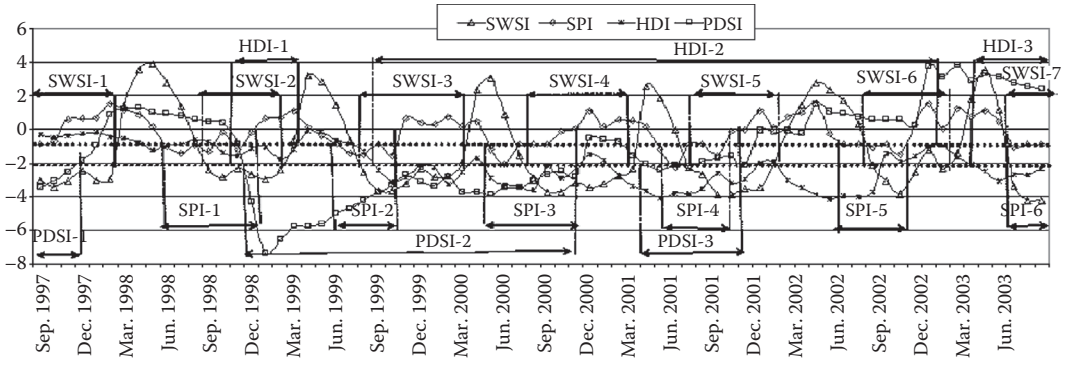

FIGURE 12.14 Time series of three indices of drought indicating the drought duration in comparison with HDI.

TABLE 12.18
Duration of Drought Spans (month)

Drought Span's Number	SPI	SWSI	PDSI	HDI
1	7	6	4	5
2		6	24	
3	5	8		40
4	7	8		
5	6	7	8	
6	5	6		
7	3	3		6
Overlapping with HDI	22	34	27	51

climatic, and hydrological. According to Figure 12.14, agricultural drought spans are wider because of their gradual progress and have lower frequencies but greater durations than hydrological and particularly meteorological droughts. Table 12.18 compares quantitatively the drought spans determined by the common drought indices and their overlapping periods with the HDI. Based on the results shown in Table 12.18, it can be concluded that HDI can cover different aspects of drought. It can also be said that hydrological and agricultural droughts have the main role in the magnitude of drought damage due to the higher overlapping of drought periods according to the SWSI and PDSI as hydrological and agricultural drought indices with those reported according to the HDI.

12.8 GEOSTATISTIC TOOLS IN DROUGHT STUDIES

Geostatistics refers to the study of a phenomenon that fluctuates in space and/or in time. Geostatistics offers a collection of deterministic and statistical tools for modeling spatial and/or temporal variability. The basic concept of geostatistics is to determine any unknown value z as a random variable Z, with a probability distribution, which models the uncertainty of z. The random variable is a variable that can take a variety of values according to a probability distribution. One of the most famous methods of geostatistics is kriging, which is used widely in the field of environment, mining, surveying, and water resources engineering studies. In regional drought analysis, geostatistics has been widely used in recent years. The ability of regionalizing spatial–temporal processes has made these methods efficient tools for drought studies especially in the field of climatic drought assessment. It is of importance to have an area-wide distribution of drought information before applying a drought-control measure to the entire basin. Kriging could be used in its spatial form to determine the drought-affected areas in a region or for future installation of new gauge stations in an ungauged area. In Chapter 4, kriging is thoroughly discussed. In this section, an application of this method to drought analysis is presented.

12.8.1 Spatial Kriging in Drought Studies

An important factor that should be considered in drought regionalization is the drought-affected area of the entire region. Kriging could be used in its spatial form to determine the drought-affected areas in a region. To determine the drought-affected areas in a region, these steps should be followed:

- A spatial network with specific grids is considered over the entire region.
- The observed data of all rain gauges are considered as known measured data at their nearest nodes of the network.
- The spatial variogram of precipitation is calculated and is fitted by a theoretical variogram.

- The unknown precipitation at each node of the network is obtained using the characteristics of the fitted variogram in a kriging method.
- Based on a regional criteria definition, drought-affected areas are estimated by summation of all drought-affected subareas that have experienced a precipitation less than the defined criteria.

12.8.2 Spatial–Temporal Kriging

The behavior of environmental variables such as seasonal rainfall patterns can usually be explained by time-dependent patterns and requires different water supply policies. These policies will be more important during drought events. A spatial–temporal study of precipitation over a region makes it possible to find out the space and time variation of precipitation in a region. Also, simulation methods in geostatistics could be used to simulate different realizations of precipitation time series at each location of the region. The realization will be useful for calculating the probable characteristics of a climatic drought (severity and/or duration) at each zone of a region at a given significance level.

The spatial–temporal time series could be studied through the assessment of a trend model and the residuals of precipitation time series at each station of a region.

The methods of regionalizing and simulation of data using different kriging and simulation methods could be applied both on the trends and on the residuals of time series modeling. Most of the methods in geostatistics need time series to be in a Gaussian distribution environment. Therefore, transformation of the data to normal values will be necessary in most cases.

The most straightforward algorithm for generating the realizations of a multivariate Gaussian field is provided by the sequential Gaussian simulation (Deutsch and Journel 1998). Simulation through LU (lower and upper triangular matrices) decomposition of the covariance matrix is another method in geostatistical simulation. The final real precipitation time series of each realization is obtained by the combination of the results of simulated trend and residual models of all points (nodes) of the region.

Example 12.8

Consider a region with 36 rain gauges (Figure 12.15), which have recorded 50 years of precipitation data. The rain gauges are shown as points in a 30 unit-by-30 unit network. Set up an algorithm for monthly space–time regionalization of precipitation time series.

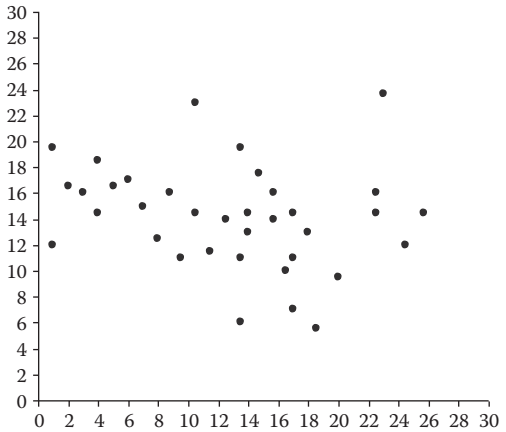

FIGURE 12.15 Location of rain gauges in the region.

Solution:

The step-by-step space–time regionalization of precipitation for this region is discussed as follows:

1. Transformation is done to convert the real values of precipitation to normal values.
2. The trend model for each station is obtained by fitting time series models such as spectral analysis-based models. If we use a model with n coefficient for all stations, the $36 \times n$ values will be the output of this step.
3. Using the coefficients from the trend model and sequential time steps, the precipitation trend series are obtained at each station, equal to 36 vectors (number of rain gauges) of 600 precipitation (the 50 years of monthly precipitation data) trend values.
4. The precipitation residual time series at each station is obtained by subtracting the trend model from the real values of precipitation. This will provide 36 vectors of 600 precipitation residual values.
5. The coefficients from the trend model are regionalized using methods of kriging. The results are presented as 900 (30 nodes long × 30 nodes wide) × n values.
6. Using the coefficients from the trend model and sequential time steps, the precipitation trend series are obtained at each grid of the considered network which are equal to 900m vectors of 600 values.
7. The precipitation residual time series at each grid are regionalized using geostatistical methods. This will provide 900 time series of 600 values.
8. Compose the trend values and residuals at 900 nodes of the network to provide 900m vectors of 600 values of the normalized precipitation time series.
9. Use back transformations to convert normalized data to real values.
10. Finally, the result consists of m realizations of 50-year (600-month) time series at each of the 900 nodes of the network.

This step-by-step algorithm can be coded in any computer language environment to calculate the time series of rainfall in different points of the region.

12.9 DROUGHT PREPAREDNESS/MANAGEMENT

The immediate result of a drought event is water shortage with impacts on the economy, the social life and the environment. Hence, it would be advisable that the relevant authority takes steps to remedy or improve the situation. Institutional and legal frameworks should be adequate to enable the collection, process, storage, and analysis of the data and information required for the preparation of rational water management plans and efficient and effective drought preparedness plans. The legal frameworks should give the right, the power, and the means to those responsible to implement the water management plans under drought conditions to act within legal and rational frameworks so that they are effective and efficient. It is also necessary to make sure that drought preparedness plans are made for water shortages caused by drought phenomena and not by human actions. All stakeholders should contribute to the formulation of rational water management plans, which, under normal conditions, do not create water shortages or water scarcity. Other deficiencies such as scientific know-how and methodologies of those responsible for the execution of these operations should be addressed by attendance to training and educational courses including the use of a common language. Finally, the most important issue is to create awareness of the water issues and the education of the users to consume water in an efficient and effective way. The drought preparedness plans are probably destined to fail if there is no cooperation and understanding from the water users.

12.9.1 Drought Monitoring as a Component of Drought Preparedness Planning

12.9.1.1 Principles of Drought Policy

The primary goal of an effective national drought strategy is to document the risk associated with severe drought events and therefore find ways to reduce impacts. This strategy has four key components:

1. The availability of timely and reliable information on which to base management and policy decisions
2. Policies and institutional arrangements that encourage assessment, communication, and application of that information
3. A set of appropriate risk management measures for decision makers
4. Actions by decision makers that are effective and consistent in support of a national drought strategy

A drought monitoring and early warning system is designed with the goal of providing timely and reliable information to decision makers. This information is provided through a delivery system that is appropriate for the region in question. The delivery system can be primarily Internet-based, or it can rely on a combination of print and electronic materials distributed via the Internet, television, radio, or fax to agricultural extension personnel or advisers. The drought policies should promote the development of decision-support tools to aid decision makers from agricultural producers to policy makers. Risk management measures or mitigation tools should be ready to implement with the onset of drought conditions and tailored to the most vulnerable sectors, regions, and population groups. These measures must be developed in support of a national drought strategy and with its principal goals as noted above. It will take some time for a full range of mitigation options to evolve for the most vulnerable sectors, regions, and population groups.

12.9.1.2 Drought Mitigation Planning

Mitigating the effects of drought requires the use of all components of the cycle of disaster management (Figure 12.16), rather than only the crisis management portion of this cycle. Typically, when a natural hazard event and resultant disaster has occurred, governments and appropriate agencies have followed with impact assessment, response, recovery, and reconstruction activities to return the region or locality to a pre-disaster state. Historically, little attention has been given to preparedness, mitigation, and prediction/early warning actions (i.e., risk management) that could reduce future impacts and lessen the need for government or donor intervention in the future. Because of this emphasis on crisis management, regions have generally moved from one disaster to another

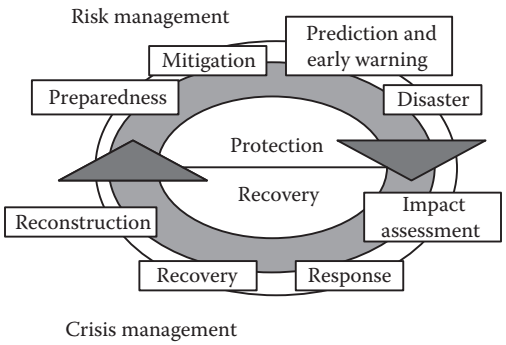

FIGURE 12.16 Cycle of disaster management. (From National Drought Mitigation Center (NDMC), 2007, University of Nebraska, Lincoln, Available at http://www.drought.unl.edu.)

with little, if any, reduction in risk. In addition, in most drought-prone regions, another drought event is likely to occur before the region fully recovers from the previous event.

Past experience with drought management in most regions has been reactive or oriented toward managing the crisis. Individuals, agencies, and others consider drought to be a rare and random event. As a result, little, if any, planning is completed in preparation for the next event. Since drought is a normal part of climate, strategies for reducing its impacts and responding to emergencies should be well defined in advance.

General drought mitigation planning objectives that are recommended for regions facing drought to consider include the following:

1. Collect and analyze drought-related information at the right time and in a systematic manner.
2. Establish criteria for declaring drought emergencies and triggering various mitigation and response activities.
3. Provide an organizational structure and delivery system that assures information flow between and within levels of government.
4. Define the duties and responsibilities of all ministries, departments, and non-governmental organizations with respect to drought.
5. Maintain an inventory of government programs previously used and available to respond to drought emergencies.
6. Identify the most drought-prone areas and vulnerable economic sectors, population groups, or environments.
7. Identify mitigation actions that can be taken to address vulnerabilities and reduce drought impacts.
8. Provide a mechanism to ensure on time and accurate assessment of drought's impacts on agriculture, industry, municipalities, wildlife, tourism and recreation, health, and other sectors.
9. Keep decision makers and the public informed of current conditions and mitigation and response actions by providing accurate information.
10. Establish and pursue a strategy to remove obstacles to the equitable allocation of water during shortages and establish requirements or provide incentives encouraging demand management.
11. Establish a set of procedures to continuously evaluate and exercise the drought mitigation plan, with periodic revising for the plan to stay responsive to the needs of a region.

These objectives are an integral part of a drought mitigation plan developed through the application of the 10-step drought planning process, which will not be discussed in detail in this chapter but only briefly as follows:

1. Appoint a drought task force.
2. State the purpose and objectives of the drought preparedness plan.
3. Seek stakeholder participation and resolve conflict.
4. Prepare inventory of resources and identity groups at risk.
5. Prepare/write the drought preparedness plan.
6. Identify research needs and fill institutional gaps.
7. Integrate science and policy.
8. Publicize the drought preparedness plan and build public awareness.
9. Develop education programs.
10. Evaluate and revise the drought preparedness plan.

In brief, Steps 1–4 of the planning process focus on making sure the right people/organizations are brought together, have a clear understanding of the process, know what the drought plan must accomplish,

and are supplied with adequate data to make fair and equitable decisions when formulating and writing the actual drought plan. Step 5 describes the process of developing an organizational structure or framework for completion of the tasks necessary to prepare the plan. The plan should be viewed as a process, rather than a discrete event that produces a static document. A risk assessment is undertaken in conjunction with this step in order to construct a vulnerability profile for key economic sectors, population groups, regions, and communities. Steps 6 and 7 detail the need for ongoing research and coordination between scientists and policy makers. Steps 8 and 9 stress the importance of promoting and testing the plan before drought occurs. Finally, Step 10 emphasizes revising the plan to keep it current and making an evaluation of the plan's effectiveness in the post-drought period.

Like other hazards, the impacts of drought span economic, environmental, and social sectors and can be reduced through mitigation and preparedness. Because droughts are a normal part of climate variability for virtually all regions, it is important to develop plans to deal with these extended periods of water shortage in a systematic manner. To be effective, these plans must evaluate a region's exposure and vulnerability to the hazard and incorporate these elements into a drought preparedness plan that is dynamic, evolving with societal changes. A comprehensive, integrated drought monitoring and early warning system is an integral part of drought preparedness planning.

PROBLEMS

1. Use the 3-year moving averages and compare the two series of annual average precipitation for two different regions presented in Table 12.19. (a) Which of these regions faced a more severe drought in the current year? (b) If the long-term average precipitation in regions A

TABLE 12.19
Data for Problem 1

No. of Years	Precipitation of Region A (mm)	Precipitation of Region B (mm)
1	50	71
2	3	40
3	8	118
4	59	99
5	58	48
6	141	134
7	30	107
8	22	92
9	41	28
10	47	32
11	103	45
12	23	53
13	64	66
14	46	142
15	129	153
16	82	59
17	128	46
18	89	121
19	17	11
20	15	191
21	28	101
Current year	15	45

and B is estimated to be 350 and 250 mm, respectively, discuss the drought periods and their durations. (c) Estimate the drought severity for each of the drought periods.

2. The monthly rainfall data for 22 years is presented in Table 12.20. Assume *C* (the constant in Equation 12.6) is 0.1. Calculate the following items for the region:
   a. Effective rainfall
   b. Rainfall deficit
   c. Excess rainfall deficit
3. Determine the onset, duration, and severity of drought for the first year of data presented in Problem 2.
4. The historical annual precipitation in a basin and the annual rainfall in drought events with different return periods are shown in Tables 12.21 and 12.22. If a 25-year climatic drought occurs in the region, find which sub-basins face drought with 10-year or more return periods.
5. Drought has been found in two regions. According to data from Table 12.23, which hydrological drought is worse? Both zones use tanks to supply water. The average inflow to the first and the second area is 1500 and 2000 MCM, respectively. Drought duration probability and intensities corresponding to these areas are given in Table 12.24 (use the average inflow for predicting the drought).
6. Drought in a river has a 30-year duration with $\lambda = 10$ in Poisson distribution. What is the probability of drought with a duration of less than 5 years?
7. In a specified year, the data presented in Table 12.25 have been recorded in the region presented in Problem 4. What is the appropriate return period of the regional drought?

TABLE 12.20
The Monthly Rainfall Data (mm) for Problem 2

No. of Years	Sep	Oct	Nov	Dec	Jan	Feb	Mar	Apr	May	Jun	Jul	Aug
1	0.2	49.6	71.0	40.9	77.1	109.2	153.3	40.9	9.8	0.7	1.6	0.4
2	0.4	2.9	40.3	106.8	73.7	90.8	83.5	5.0	0.0	15.9	0.8	0.0
3	10.4	8.3	117.7	88.4	67.2	88.7	59.8	12.8	0.0	1.4	0.0	0.0
4	0.0	59.2	98.6	205.1	179.7	76.5	37.4	73.1	13.6	0.0	0.6	0.0
5	8.8	57.9	47.5	124.3	28.1	77.7	124.5	27.8	1.4	1.4	6.7	0.2
6	38.0	140.7	133.9	54.5	55.6	128.8	82.4	45.5	14.2	0.3	2.0	0.0
7	2.5	29.5	106.6	48.1	43.3	31.7	15.4	31.5	0.3	0.3	0.0	0.0
8	4.7	22.0	91.8	61.2	164.8	159.9	83.7	97.4	8.7	0.3	1.3	1.4
9	1.9	40.5	27.5	122.9	74.9	73.2	93.9	23.1	0.0	0.4	0.0	0.0
10	15.3	46.8	31.7	62.6	80.1	121.3	125.4	27.5	0.1	0.4	0.0	0.0
11	50.2	102.7	44.6	93.1	58.3	107.0	65.1	28.0	9.6	0.0	0.0	0.0
12	0.0	22.6	53.2	63.0	40.8	117.3	39.2	55.3	2.8	0.0	0.4	0.1
13	17.4	64.4	66.2	59.5	64.3	55.5	92.3	49.9	0.2	0.0	0.0	0.0
14	0.5	46.4	142.0	24.2	67.2	90.2	41.8	29.5	0.9	0.0	0.1	1.1
15	0.5	128.8	153.2	73.5	69.6	175.7	73.3	95.6	2.9	0.0	0.6	0.5
16	33.4	82.2	58.5	151.7	99.0	145.9	57.1	38.1	0.2	10.6	14.9	0.0
17	16.3	127.5	45.7	67.7	56.6	82.2	24.9	34.5	0.3	0.9	0.2	0.2
18	0.0	88.7	120.8	49.2	74.0	115.2	41.4	51.6	0.2	0.0	0.0	0.0
19	2.1	17.2	10.7	77.8	65.4	116.4	47.0	4.8	0.0	0.9	0.0	0.0
20	47.7	14.8	190.6	82.5	48.0	110.6	97.8	1.9	0.4	1.0	0.0	0.3
21	2.3	28.2	101.3	139.0	131.2	252.9	59.4	96.9	5.5	0.7	0.0	0.5
22	0.7	77.2	45.3	74.7	78.2	102.9	59.1	135.8	0.0	0.0	0.3	1.1

TABLE 12.21
Regional Precipitation Data for Drought Events with Different Return Periods in Problem 4

		Precipitation in Different Droughts (mm)				
Sub-Basin	**Area (%)**	**2 years**	**5 years**	**10 years**	**25 years**	**50 years**
A	20	380	280	180	100	70
B	30	600	540	510	490	350
C	15	550	520	480	320	250
D	15	280	250	200	180	70
E	20	400	350	310	280	190

TABLE 12.22
Annual Average Precipitation in the Basin Presented in Problem 4

No. of Years	**Precipitation (mm)**	**Sorted Precipitation (mm)**	**Probability**	**Return Period (year)**
1	618.23	101.47	0.05	19.00
2	563.54	284.2	0.11	9.50
3	546.6	307.44	0.16	6.33
4	501.51	345.81	0.21	4.75
5	480.41	350.1	0.26	3.80
6	451.88	368.51	0.32	3.17
7	418.34	369.99	0.37	2.71
8	403.34	403.34	0.42	2.38
9	369.99	418.34	0.47	2.11
10	368.51	451.88	0.53	1.90
11	350.1	480.41	0.58	1.73
12	345.81	501.51	0.63	1.58
13	307.44	546.6	0.68	1.46
14	284.2	563.54	0.74	1.36
15	776.02	617.04	0.79	1.27
16	1001.96	618.23	0.84	1.19
17	101.47	776.02	0.89	1.12
18	617.04	1001.96	0.95	1.06

TABLE 12.23
Characteristics of Regions in Problem 5

	Annual Demand (MCM)	**Annual Inflow Prediction**	**Reservoir Volume**
Region 1	1200	1100	500
Region 2	1800	1400	700

TABLE 12.24
Probability of Occurrence of the Regions Considered in Problem 5

Region 1						Region 2					
Prob. 20%		Prob. 50%		Prob. 70%		Prob. 20%		Prob. 50%		Prob. 70%	
Dur. (years)	Int. (MCM)	Dur. (years)	Int. (MCM)	Dur. (years)	Int. (MCM)	Dur. (years)	Int. (MCM)	Dur. (years)	Int. (MCM)	Dur. (years)	Int. (MCM)
6	2500	4	1900	3	1200	5	3500	4	2500	2	1700

TABLE 12.25
Data for Problem 7

Station	A	B	C	D	E
Annual Precipitation (mm)	310	490	350	275	390

REFERENCES

Alley, W. (1984). "On the treatment of evapotranspiration, soil moisture accounting and aquifer recharge in monthly water balance models," *Water Resource Research*, 20(8), 1137–1149.

Ben-Zvi, A. (1987). "Indices of hydrological drought in Israel," *Journal of Hydrology*, 92, 179–191.

Chang, T.J. (1990). "Effects of drought on streadow characteristic," *Journal of Irrigation and Drainage Engineering*, 116(3), 332–339.

Deutsch, C. and Journel, A. (1998). *GSLIB: Geostatistical Software Library*. s.l. Oxford University Press.

Dixon, L., Moore, N. and Pint, E. (1996). *Drought Management Policies and Economic Effects in Urban Areas of California, 1987–1992*. RAND Corporation, Santa Monica, CA.

Doesken, N., McKee, T. and Kleist, J. (1991). Development of a surface water supply index for the western United States. Climatology Report Number 91-3. Colorado State University, Fort Collins, CO.

Doornkamp, J.C. and Gregory, S. (eds.) (1980). *Atlas of Drought in Britain*. London.

Dracup, J., Lee, K. and Paulson, E. (1980). "On the statistical characteristics of drought events," *Water Resource Research*, 16, 289–296.

Dziegielewski, B., Lynne, G., Wilhite, D. and Sheer, D. (1991). *National Study of Water Management During Drought: A Research Assessment*. U.S. Army Corps of Engineers Water Resources Support Center, Institute for Water Resources, Fort Belvoir, VA.

Easterling, W. (1993). Adapting United States agriculture to climate change. In: *Preparing for an Uncertain Climate*, vol. 1, pp. 303–305. Office of Technology Assessment, Washington, DC.

Garren, D.C. (1993). "Revised surface water supply index for Western United States," *Journal of Water Resources and Planning and Management*, 119(4), 437–454.

Gleick, P. (1987). "Developing and testing of a water balance model for climatic impact assessment: Modeling the Sacramento Basin," *Water Resource Research*, 23(6), 1049–1061.

Griffiths, G.A. (1990). "Rainfall deficits: Distribution of monthly runs," *Journal of Hydrology*, 115, 219–229.

Guerrero-Salazer, P.L.A. and Yevjevich, V. (1975). Analysis of drought characteristics by the theory of runs. Colorado State University, Fort Collins, Colorado, Hydrology Paper 80.

Haan, C. (1972). "A water yield model for small watersheds," *Water Resource Research*, 8(1), 28–69.

Heddinghaus, T. and Sabol, P. (1991). A review of the Palmer Drought Severity Index and where do we go from here?. In: *Proc. 7th Conf. on Applied Climatology*, pp. 242–246. American Meteorological Society, Boston.

Hudson, H. and Hazen, R. (1964). *Drought and Low Stram Flows. In: Hand Book of Applied Hydrology*, V.T. Chow, ed. McGraw Hill, New York.

Karamouz, M. and Araghinejad, S. (2008). "Drought mitigation through long-term operation of reservoirs: Case Study," *Journal of Irrigation and Drainage Engineering*, 134(4), 471–478.

Karamouz, M., Torabi, S., Araghinejad, Sh. and Asgharzadeh, D. (2002). Analysis of droughts: Application to Isfahan region in Iran, Proc. 2002 EWRI Conference on Water Resources Planning and Management, Roanoke, VA.

Karamouz, M., Zahraie, B. and Szidarovszky, F. (2003). *Water Resources System Analysis*, Lewis Publishers, Boca Raton, FL, 529–573.

Karamouz, M., Rasouli, K. and Nazif, S. (2009). "Development of a hybrid index for drought prediction: A case study," *ASCE Journal of Hydrologic Engineering*, 14(6), 617–627.

Kottegoda, N.T. and Rosso, R. (1997). *Statistics, Probability and Reliability for Civil and Environmental Engineers*. McGraw-Hill.

Mather, J. (1981). "Using computed stream flow in watershed analysis," *Water Resources Bulletin*, 17(3), 474–482.

McKee, T.B., Doesken, N.J. and Kleist, J. (1993). The Relationship of Drought Frequency and Duration to Time Scales, 8th Conf. Applied Climatology, Anaheim, California.

Mendenhall, W., Wackerly, D.D. and Scheaffer, R.L. (1990). *Mathematical statistics with Applications*. PWS-Kent Publishing Company, Boston.

National Drought Mitigation Center (NDMC) (2007). University of Nebraska, Lincoln, NE. Available at http://www.drought.unl.edu.

Palmer, W. C. (1965). *Meteorological Drought. Research Paper No. 45*. U.S. Department of Commerce Weather Bureau, Washington, DC.

Revelle, R. and Waggoner, P. (1983). *Effects of a Carbon Dioxide-Induced Climatic Change on Water Supplies in the Western United States*, pp. 419–432. National Academy Press, Washington, DC.

Rossi, G. (1979). Characteristics of Drought over a Region and Shortage Control Strategies, Proceedings of 18th IAHR Congress, Cagliari, Vol. 2.

Rossi, G., Benedini, M., Tsakiris, G. and Giakoumakis, S. (1992). "On regional drought estimation and analysis," *Water Resources Management*, 6, 249–277.

Santos, M.A. (1983). "Regional droughts: A stochastic characterization," *Journal of Hydrology*, 66, 183–211.

Schaake, J. C. (1990). From climate to flow. In: *Climate Change and U.S. Water Resources*, P.E. Waggoner, ed., pp. 177–206. John Wiley, New York.

Sen, Z. (1976). "Wet and dry periods of annual flow series," *Journal of Hydraulic*, 10, 1503–1514.

Sen, Z. (1980a). "Regional drought and flood frequency analysis: Theoretical consideration," *Journal of Hydrology*, 46, 265–279.

Sen, Z. (1980b). "Statistical analysis of hydrologic critical droughts," *Journal of Hydraulics Division*, 106, 99–115.

Sen, Z. (1991a). "On the probability of the longest run length in an independent series," *Journal of Hydrology*, 125, 37–46.

Sen, Z. (1991b). "Probabilistic modeling of crossing in small samples and application of runs to hydrology," *Journal of Hydrology*, 124, 345–362.

Shafer, B. and Dezman, L. (1982). Development of a Surface Water Supply Index (SWSI) to assess the severity of drought conditions in snowpack runoff areas. *Proceedings of the Western Snow Conference*, pp. 164–175.

Tase, N. (1982). Probability of Drought Coverage with Various Return Periods for Japan, Proceedings of International Symposium on Hydrometeorology Records.

Tase, N. and Yevjevich, V. (1978). "Effects of size and shape of a region on drought coverage," *Hydrological Science Bulletin*, 23, 203–212.

Thomas, H., Martin, C., Brown, M. and Fiering, M. (1983). *Methodology for Water Resource Assessment, Report to U.S. Geological Survey*, National Technical Information Service, Springfield, VA.

Thornthwaite, C. (1948). "An approach towards a rational classification of climate," *Geographical Review*, 38, 55–94.

Thornthwaite, C. and Mather, J. (1955). "The water balance," *Publications in Climatology*, 8(1).

Yevjevich, V. (1967). An objective approach to definition and investigations of continental hydrologic. In: *Hydrology Papers*. Colorado State University, Fort Collins, CO.

Yevjevich, V. and Obeysekera, J. (1985). "Correlation between sample first autocorrelation coefficient and extreme hydrologic runs," *Journal of Hydrology*, 79, 171–186.

Zucchini, W. and Adamson, P. (1988). "On the application of the bootstrap to assess the risk of deficient annual inflows to a reservoir," *Water Resource Management*, 2, 245–254.

13 Flood

13.1 INTRODUCTION

Flood is an overflow of an expanse of water that covers the land not normally covered by water. This water can come from the sea, lakes, rivers, canals, or sewers as well as rainwater. There are seasonal and intra-annual variations in river flow resulting in very high flow periods, but floods are considered to happen when the excess rainfall (runoff) escapes the boundaries of the flowing water body and damages the surrounding area used by humans like a village, city, or other inhabited area. Flooding is caused primarily by hydrometeorological mechanisms, acting either as a single factor or in combination with different factors. Whatever the type of flooding, the phenomenon can always be described as a volume of water that enters a certain area that cannot be discharged quickly enough. As a consequence, therefore, the water level rises and flooding occurs.

Floods in coastal areas, which are enhanced by sea level rise, especially in coastal regions of the United States, Japan, and southeastern parts of Asia, cause serious damage to human societies. Most urban areas are subject to some kinds of flooding after spring rains, heavy thunderstorms, or winter snow thaws because of high percentages of imperviousness. A variety of structures such as dams, levees, bunds, and weirs are employed in order to control the floods and decrease the damage. However, floods continue to be the most destructive natural hazards in terms of short-term damage and economic losses to a region. The large damage caused by floods are due to the short warning time before flooding occurs, which makes it difficult to move people and valuable moveable properties from the flooding area. According to the Federal Emergency Management Agency (FEMA) of the United States, floods are the second most common and widespread of all natural disasters (drought is first globally). Within the United States, an average of 225 people are killed and more than $3.5 billion in property damage is experienced through heavy rains and flooding each year (FEMA 2008).

The following are examples of severe floods: the storm surge flood of Bangladesh in 1991 (killed 140,000 people), the Midwest flood of 1993 in the United States, two floods (100-year flood size) on the Rhine in 1993 and 1995, the flood of summer 1995 in North Korea, the flood of 1996 in South Korea, floods in China in 1996 and 1998, the devastating flood of 1997 on the Oder in Poland and Germany, and the flood of August 2002 in the Elbe in Germany and Czech Republic. Determining the inundation zone could give early warning to some residents' activities, which will lead to a decrease in the damage due to flooding. Floods account for about 40% of all deaths caused by natural disasters, most of which are in the developing nations. For example, 3.7 million people were killed in a 1931 flood on China's Yangtze River. In 2000, four of the world's five largest natural disasters were floods.

However, despite the large amount of damage, floods also bring benefits to people in developing nations, especially those in arid and semiarid regions, as floods provide water resources for irrigation and development and fertilize the ground for agricultural purposes. These benefits can be utilized through logical management of flood and the flooding regions. Furthermore, flood-related property losses can be minimized by making flood insurance available on reasonable terms and encouraging its purchase by people who need flood insurance protection particularly those living in flood-prone areas.

For effective flood management, it is necessary to first determine the characteristics of the flood in the study region. This includes determining the severity of floods with different return periods as

well as the corresponding hydrographs. The most important information obtained from flood hydrographs are peak flow and its timing. Furthermore, the flood design and the appropriate practices for flood control and conveyance are determined for different facilities. In this regard, regional characteristics should be incorporated in design procedure, where the most important concept is quantifying the flooding risk based on its components. In this chapter, the procedure of flood management is explained in detail, and finally, some case studies are introduced as examples of integration of different methods and tools for flood planning and management.

13.2 FLOOD TYPES

With regard to the speed, geography, and cause of flooding, different types of floods are considered.

13.2.1 Flash Floods

Heavy rains in areas with steep slopes may result in a riverbed with little or no water to suddenly overflow with fast flowing water. A flash flood is a very direct response to rainfall with a very high intensity, sudden massive cloud bursts, landslides, and melting of snow. Flash flood has a sharp peak, which is followed by relatively rapid recession, resulting in high flow velocities. In urban areas, small streams can also rise quickly after heavy rain because of the high volume of runoff generated and the short time of concentration (Figure 13.1).

In these floods, two key factors are fast formation of runoff and short time of concentration. Due to high flow speed in flash floods, it has the strength to carry away heavy objects and cause serious damage. The timing and the speed of the flash floods are comparable with the resulting flood from a dike break. The flash floods stop as suddenly as they start and develop. The area affected by flash floods is relatively small compared to other types of floods; therefore, even though the amount of water is not usually very large, it can rise very high because of concentration in a small area.

13.2.2 Coastal Floods

In coastal floods, the coast is flooded by the sea due to a severe storm. In such cases, the storm wind pushes the water up and creates high waves. The resulting high tides and storm surges from tropical depressions and cyclones can produce coastal floods in estuaries, tidal flats, and low-lying land near the sea. There are different factors affecting the intensity of coastal floods; the most important ones are coastline configurations, offshore water depth, and estuary shape. Furthermore, high tides may lead to local or riverine floods through impeding the discharge of rivers and drainage systems. An

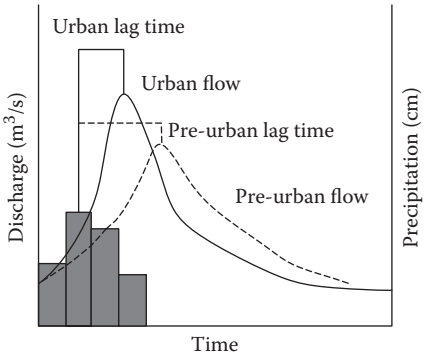

FIGURE 13.1 Discharge accentuation due to urbanization. (From Associated Programme on Flood Management [APFM], Urban flood risk management, *Flood Management Tools Series*, 2008. With permission.)

interesting fact is that beneath a low pressure area, the sea level is higher. This contributes to the high sea level, but the wind can have a larger effect. One important characteristic of a coastal flood is that the water level drops and rises with the tide.

13.2.3 Urban Floods

The specification of urban flooding is in its cause, which is lack of drainage in an urban area. Figure 13.2 shows the typical impacts of urbanization on decreasing the rate of infiltration and increasing surface runoff. Due to the very low percentage of pervious areas in urban regions, nearly all the precipitation is transformed into runoff and flows to the surface water or the sewage system. High-intensity rainfall can cause flooding when the city sewage system and draining canals do not have the necessary capacity to drain away the amount of rain that is falling. Urban floods result in great disturbance in the daily life of city residents. The economic damage is high, but the number of casualties is usually very limited because of the nature of the flood.

13.2.4 River Floods

River (fluvial) floods are the result of heavy rainfall (over an extended period and an extended area) or snowmelt upstream or tidal fluctuations downstream. In river floods, a major river overflows its banks (exceeding local flow capacities). In huge river floods, especially those occurring in flat regions, the water covers widespread areas and affects downstream areas. The amount of generated runoff is

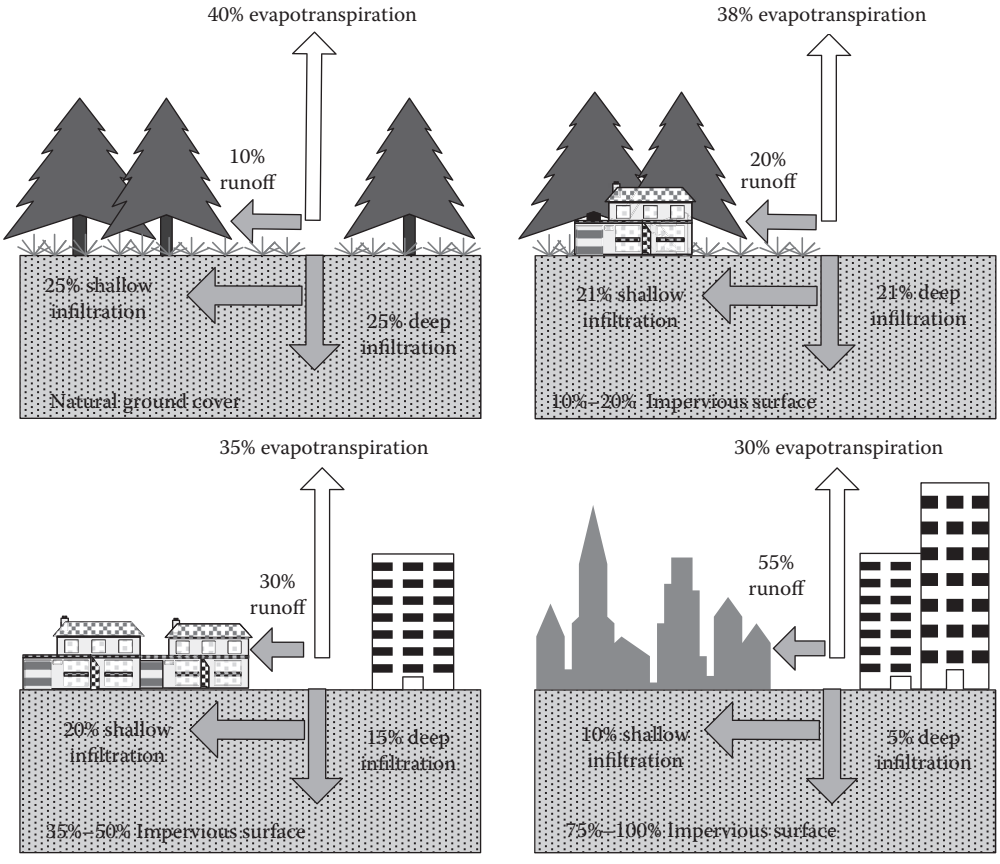

FIGURE 13.2 Influence of urbanization on decreasing rate of infiltration and increasing surface runoff.

influenced by ground conditions such as soil, vegetation cover, and land use. In this flood, the river level rises slowly and the rise and fall of water level happens over a long period of time, especially in areas with flat slopes and deltaic areas. Due to gradual water level rise, people can be evacuated before the river overflows. Sometimes, the whole community becomes isolated from the rest of the world because of flooding, as roads are blocked and communications are down. Sometimes, river floods are the result of failure or bad operation of drainage or flood control practices upstream.

13.2.5 Ponding or Pluvial Flooding

Ponding flood is common in relatively flat areas. The runoff produced in an area is normally stored in the ground and in canals or lakes, or is drained away, or pumped out. When the runoff produced exceeds the storage and conveyance capacity of a water system, flooding occurs. In this case, rain is the source of the flood: not water coming from a river, but water on its way to the river. That is why it is also called "pluvial flood." In this case, puddles and ponds are formed on land, canals overflow, and gradually a layer of water covers the land. It is like urban flooding, but it is more common in rural areas without sewage systems. Due to gradual flooding and the low height of flooding, people have time to go indoors or leave the area and there is no immediate threat to people's lives. The economic damage is dependent on the economic activity and size of the area that is covered by water.

13.2.6 Inland and Coastal Flooding

In another way, floods can be categorized into two main groups: inland and coastal. In coastal areas of the United States, land-induced floods are often combined with coastal flood storm surges with a higher probability of occurrence as could be quantified by classical flood frequency analysis. Coastal floods occur due to hurricanes or tropical storms. Hurricane Katrina smashed entire neighborhoods in New Orleans, Louisiana, in the United States in 2005 and killed at least 1300 people. An estimated 46 million people living in cities are at risk yearly from flooding from storm surges in the East Asia Region (World Bank 2007). In March 2011, the Tōhoku earthquake and tsunami happened on the east coast of Tōhoku in Japan. The earthquake triggered powerful tsunami waves that reached heights of up to 40.5 m in Miyako in Tōhoku's Iwate Prefecture and traveled up to 10 km inland in the area of Sendai. This tsunami resulted in 12,915 deaths, 4711 injured people, and 14,921 people missing across 18 prefectures, as well as over 125,000 damaged or destroyed buildings (http://www.tsunami.noaa.gov). Hurricane Irene in 2011 led to the deaths of at least 40 people in 11 states in the United States. It knocked out power to 1.8 million homes and businesses, disrupted oil refineries, and forced nuclear plants to reduce power (http://www.stormpulse.com/hurricane-irene-2011).

13.2.6.1 Inland Flooding

Inland flooding occurs when the surface runoff volume exceeds the drainage system capacity. The overflow will follow the basin surface slope direction to reach its outlet. The depth of overflow is dependent on its volume as well as on the topography of the basin. The changes in basin and the increasing percentage of impervious areas result in increasing surface runoff volume and, due to the limited capacity of the drainage system, increasing overflow. The inland flood damage is related to the flooding depth. At small depths, the damage will increase by a small increase in flood depth, but by increasing the flooding depth, the rate of damage will decrease. Therefore, reducing the flooding depth is an essential step in decreasing flood damage. Different BMPs (best management practices) can be employed for this purpose. Providing warnings for flood events as soon as possible will also help to mitigate casualties especially in extreme flood events due to people's preparedness to deal with flooding.

Providing prediction with adequate lead (1–6 months) will highly increase system preparedness in dealing with floods. To do long-lead extreme rainfall prediction, one should rely on the use of large-scale climate signals—such as NAO (North Atlantic Oscillation), SOI (Southern Oscillation

Index), SST (Sea Surface Temperature), SLP (Sea Level Pressure), and ΔSLP (SLP difference)—of key points in the Atlantic and/or Pacific Ocean as climate variability footsteps. The teleconnections between climate-sensitive high- and low-pressure key points, such as Azure and Greenland in the Atlantic Ocean and Tahiti and Darwin in the Pacific Ocean, are among long-lead weather footprints.

13.2.6.2 Coastal Flooding

Coastal flooding occurs due to the deadly storm surges of hurricanes, tropical storms, or tropical depressions, which greatly affect shore locations, causing landslides. The water carried by storm winds towards the coast is called a "storm surge." Hurricane storm tide is caused by the combination of this surge in movement with normal tides, and the water level may increase 15 ft or more after this point. Coastal floods are caused by long and short wave surges that take effect on an open ocean, bays, and rivers, streams, and inlets of tidal influence. With the help of official definitions from the National Hurricane Center, according to the Saffir–Simpson hurricane scale, five hurricane categories are defined as given in Table 13.1.

Table 13.2 lists some hurricanes in different categories that have impacted the North American continent between 1992 and 2011. The 2005 Atlantic hurricane season was the most active in recorded history, repeatedly breaking many meteorological records. The year 2005 saw the strongest hurricane in recorded history. This section will briefly highlight three of the storms including hurricanes Katrina and Irene and the Tōhoku tsunami.

13.2.6.2.1 Hurricane Katrina (August 2005, United States)

The most damaging storm ever hit the United States was Hurricane Katrina, which set records as the most costly US natural disaster and the third deadliest hurricane to strike this country. Lashing the southeast Louisiana coast with winds up to 140 mph and a 27 ft storm surge, the storm devastated costal Mississippi towns, breached the Lake Pontchartrain levees, and flooded 80% of New Orleans.

Katrina began as a tropical depression on August 13, 2005, located 175 mi northeast of Nassau, Bahamas. By the next day, Katrina was anticipated to hit the Florida coast near Miami as a category 1 hurricane. The hurricane made landfall on August 25 at 6:30 p.m. and traveled quickly across the state to exit into the Gulf of Mexico considerably weaker than before. However, by early morning of August 26, it became apparent that Katrina would intensify into a serious threat and affect much of the Gulf Coast. The above-average sea surface temperatures and reduced wind shear helped the storm grow from a tropical storm to a category 5 hurricane within 48 h. By 10 p.m. of August 27, the Katrina hurricane warning from the National Weather Service indicated a major and ominous storm approaching the City of New Orleans and warned of massive storm surges of 15 to 20 ft from Morgan City to the Alabama/Florida border. New Orleans was bracing itself for a devastating storm since the levees protecting the city were only built to withstand a category 3 hurricane and had never been fully tested. When Katrina made landfall near Buras, Louisiana, at 6:10 a.m. Central Time, August 29, the maximum wind speed had reached 125 mph and a central pressure of 920 mb officially made it a category 3 hurricane. Nonetheless, New Orleans suffered massive damage due to

TABLE 13.1
Hurricane Categories Based on the Saffir–Simpson Hurricane Scale

Hurricane Category	Maximum Sustained Wind Speed (mi/h)	Damage Category	Approximate Pressure (mb)	Approximate Storm Surge (ft)
One	74–95	Minimal	>980	3–5
Two	96–110	Moderate	979–965	6–8
Three	111–130	Extensive	964–945	9–12
Four	131–155	Extreme	944–920	13–18
Five	>155	Catastrophic	<920	>18

TABLE 13.2
Selected Hurricanes Affecting North America, 1992–2011

Name	Year	Category	Areas Affected	Damage	Deaths	Formed–Dissipated
Andrew	1992	5	Bahamas; South Florida, Louisiana	$26.5 billion	26 direct, 39 indirect	August 16–August 28
Alberto	1994	Tropical storm	Florida Panhandle, Alabama, Georgia	$1 billion	32 direct	June 30–July 10
Opal	1995	4	Guatemala, Yucatán Peninsula, Alabama, Florida Panhandle, Georgia	$3.9 billion	59 direct, 10 indirect	September 27–October 6
Floyd	1999	4	Bahamas, US East Coast from Florida to Maine, Atlantic Canada	$4.5 billion	57 direct, 20–30 indirect	September 7–September 19
Allison	2001	Tropical storm	Texas, Louisiana	$5.5 billion	41 direct, 14 indirect	June 4–June 18
Isabel	2003	5	Greater Antilles, Bahamas, most western and southern US states, Canada (Ontario)	$3.6 billion	16 direct, 35 indirect	September 6–September 20
Charley	2004	4	Jamaica, Cayman Islands, Cuba, Florida, South Carolina, North Carolina	$16.3 billion	15 direct, 20 indirect	August 9–August 15
Frances	2004	4	British Virgin Islands, Puerto Rico, US Virgin Islands, Bahamas, Florida, Georgia, North and South Carolina, Ohio	$12 billion	7 direct, 42 indirect	August 24–September 10
Ivan	2004	5	Venezuela, Jamaica, Grand Cayman, Cuba, Alabama, Florida, Louisiana, Texas	$18 billion	91 direct, 32 indirect	September 2–September 24
Jeanne	2004	3	US Virgin Islands, Puerto Rico, Dominican Republic, Haiti, Bahamas, Florida	$7 billion	3035 direct	September 13–September 28
Dennis	2005	4	Grenada, Haiti, Jamaica, Cuba, Florida, Alabama, Mississippi, Georgia, Tennessee, Ohio	$4 billion	42 direct, 47 indirect	July 4–July 13
Katrina	2005	5	Bahamas, South Florida, Cuba, Louisiana, Mississippi, Alabama, Florida Panhandle	$108 billion	1833	August 23–August 30
Rita	2005	5	Arkansas, South Florida, Cuba, Florida Panhandle, Louisiana, Mississippi, Texas	$12 billion	97–125	September 18–September 26
Ophelia	2005	1	Northeast Florida, North Carolina, Massachusetts, Atlantic Canada	$70 million	1 direct, 2 indirect	September 6–September 23
Wilma	2005	5	Jamaica, Haiti, Cuba, Honduras, Nicaragua, Belize, Florida, Bahamas	$29.1 billion	23 direct, 39 indirect	October 15–October 26
Humberto	2007	1	Southeast Texas, Louisiana	$50 million	1	September 12–September 14

(*continued*)

TABLE 13.2 (Continued)
Selected Hurricanes Affecting North America, 1992–2011

Name	Year	Category	Areas Affected	Damage	Deaths	Formed–Dissipated
Gustav	2008	4	Dominican Republic, Haiti, Jamaica, Cuba, Florida, Louisiana, Mississippi, Alabama, Arkansas	$6.61 billion	112 direct, 41 indirect	August 25–September 4
Dolly	2008	2	Guatemala, Yucatan Peninsula, western Cuba, Northern Mexico, South Texas, New Mexico	$1.35 billion	1 direct, 21 indirect	July 20–July 25
Ike	2008	4	Bahamas, Haiti, Dominican Republic, Cuba, Florida, Mississippi, Louisiana, Texas, Mississippi, Ohio, eastern Canada	$37.6 billion	103 direct, 92 indirect	September 1–September 14
Irene	2011	3	Bahamas, eastern United States (landfalls in North Carolina, Connecticut, New Jersey, and New York), eastern Canada	$10.1 billion	49 direct, 7 indirect	August 20–August 28

levee failure. Katrina then continued inland, weakening as it went, becoming a category 1 by 6 p.m. that day, a tropical storm around midnight as it passed through Northern Mississippi, and a tropical depression near Clarksville, Tennessee, on August 30.

13.2.6.2.2 Tōhoku Earthquake and Tsunami (March 2011, Japan)

The 2011 Tōhoku earthquake and tsunami was a 9-magnitude earthquake followed by tsunami waves. The earthquake happened 130 km off Sendai, Miyagi Prefecture, on the east coast of Tōhoku, Japan, on March 11, 2011. It was at a depth of 24.4 km. This makes it the largest earthquake to hit Japan and the seventh biggest earthquake in the world in recorded history. The earthquake triggered powerful tsunami waves that reached heights of up to 40.5 m in Miyako in Tōhoku's Iwate Prefecture and traveled up to 10 km inland in the Sendai area.

The earthquake started a tsunami warning for Japan's Pacific coast and other countries, including New Zealand, Australia, Russia, Guam, Philippines, Indonesia, Papua New Guinea, Nauru, Hawaii, Northern Marianas (United States), and Taiwan. It warned that the wave could be as much as 10 m high. A 0.5 m high wave hit Japan's northern coast. News reported that a 4 m high tsunami hit the Iwate Prefecture in Japan. The Miyagi Prefecture was flooded, with waves carrying buildings and cars along as they traveled inland. In some areas, the waves reached 10 km inland. A wave 2 m high reached California, after traveling across the Pacific Ocean at a speed of 500 km/h.

13.2.6.2.3 Hurricane Irene (August 2011, United States)

Hurricane Irene was a costly hurricane that occurred in the Northeastern United States. Irene originated from an Atlantic tropical wave, showing signs of organization east of the Lesser Antilles. The system was labeled as Tropical Storm Irene on August 20, 2011, because of the development of atmospheric convection and a closed center of circulation. After intensifying, while crossing through St. Croix, it made landfalls as a strong tropical storm. However, after a day, it strengthened into a category 1 hurricane. The storm continued along the offshore of Hispaniola and intensified gradually to become a category 3 hurricane. At that time, Irene peaked with wind speeds up to 120 mph (195 km/h).

After reaching the Bahamas, the storm slowly leveled off in intensity and then curved northward. Before reaching the Outer Banks of North Carolina on August 27, Irene weakened to a category 1 hurricane.

Irene caused huge destruction and at least 56 deaths. The monetary losses in the Caribbean alone have been estimated to be about $3.1 billion. There is no exact estimate of the total damage across the United States, but available estimations are about $7 billion.

13.3 FLOOD ANALYSIS

The first step in developing flood planning and management practices is to analyze the frequency of floods of different intensities. In this section, the data and steps needed for flood analysis are described.

13.3.1 Flood Time Series

The measured instantaneous flood peak discharges are one of the most valuable data sets for the hydrologist. The longer a record continues, homogeneous and with no missing peaks, the more is its value enhanced. Even so, it is very rare to have a satisfactory record long enough to match the expected life of many engineering works required to be designed. As many peak flows as possible are needed in assessing flood frequencies. The hydrologist defines two data series of peak flows: the annual maximum series and the partial duration series (as defined in Chapter 8).

13.3.1.1 Peaks over Threshold Series

The annual maximum series takes the single maximum peak discharge in each year of record so that the number of data values equals the record length in years. For statistical purposes, it is necessary to ensure that the selected annual peaks are independent of one another. This is sometimes difficult, e.g., when an annual maximum flow in January may be related to an annual maximum flow in the previous December. For this reason, it is sometimes advisable to use the water year rather than the calendar year. In hydrology, any 12-month period, usually selected to begin and end during a relatively dry season, used as a basis for processing streamflow and other hydrologic data, is called a water year. The definition of the water year depends on the seasonal climatic and flow regimes; for example, the period from October 1 to September 30 is most widely used in the United States. The partial duration series takes all the peaks over a selected level of discharge, a threshold. Hence, the series is often called the "Peaks over Threshold" (POT) series, which is shown in Figure 13.3. There are generally more data values for analysis in this series than in the annual series, but there is more chance of the peaks being related and the assumption of true independence is less valid.

In Figure 13.3, p_1, p_2, and p_3 form an annual series and p_1, ρ_1, p_2, p_3, and ρ_3 form a POT series. It will be noted that one of the peaks in the POT series, p_3, is higher than the maximum annual value in the

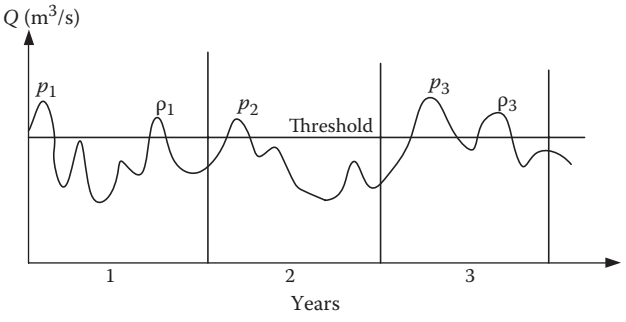

FIGURE 13.3 Peaks over threshold series.

second year, p_2. For sufficiently long records, it may be prudent to consider all the major peaks and then the threshold is chosen so that there are N peaks in the N years of record, but not necessarily one in each year. This is called the annual exceedance series, a special case of the POT series.

Flood frequency analysis entails the estimation of the peak discharge, which is likely to be equaled or exceeded on average once in a specified period, T years. This is called the T-year event, and the peak, Q_T, is said to have a return period or recurrence interval of T years. The thresholds for the return period could be 100 years, 50 years, 25 years, and so forth for a given storm. The return period, T years, is the long-term average of the intervals between successive exceedances of a flood magnitude, Q_T, but it should be emphasized that those intervals may vary considerably around the average value T. Thus, a given record may show 25-year events, Q_{25}, occurring at intervals both much greater and much less than 25 years, even in successive years. Alternatively, it may be required to estimate the return period of a specified flood peak.

The annual series and the partial duration series of peak flows form different probability distributions, but for return periods of 10 years and more, the differences are minimal and the annual maximum series is usually one of the most analyzed.

13.3.2 Flood Probability Analysis

When a series of annual maximum flows is divided by magnitude into discharge groups or classes of class interval ΔQ, the number of occurrences of the peak flows (f_i) in each class can be plotted against the discharge values to give a frequency diagram (Figure 13.4a). It is convenient to transform the ordinates of the diagram in two ways: with respect to both the size of the discharge classes (ΔQ) and the total number, N, of events in the series.

By plotting $\dfrac{f_i}{N \cdot \Delta Q}$ as ordinates, it is seen that the panel areas of the diagram will each be given by $\dfrac{f_i}{N}$, and hence the sum of those areas will be unity.

$$\sum_{i=1}^{n}\left(\frac{f_i}{N \cdot \Delta Q} \cdot \Delta Q\right) = \frac{N}{N} = 1, \tag{13.1}$$

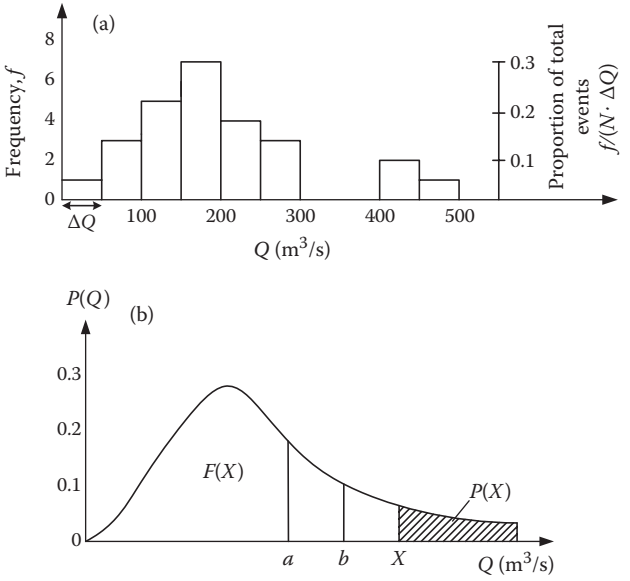

FIGURE 13.4 (a) Frequency diagram and (b) probability distribution of annual maximum peak flows.

where n is the number of discharge classes. If the data series is large in number and the class intervals are made infinitesimally small, then at the limit, a smooth curve of the probability density distribution is obtained (Figure 13.4b); the area under this curve is 1:

$$\int_0^\infty p(Q)\,\mathrm{d}Q = 1. \tag{13.2}$$

The probability that an annual maximum, Q, lies between two values, a and b, is defined as follows:

$$p = \int_a^b p(Q)\,\mathrm{d}Q. \tag{13.3}$$

For any given magnitude, X, the probability that an annual maximum equals or exceeds X, i.e., that $Q \geq X$, is as follows:

$$P(X) = \int_x^\infty p(Q)\,\mathrm{d}Q, \tag{13.4}$$

which is the area shaded under the probability curve (Figure 13.4b). $F(X)$ is the probability of $Q < X$ and is defined as

$$F(X) = \int_0^x p(Q)\,\mathrm{d}Q \tag{13.5}$$

and clearly

$$P(X) = 1 - F(X). \tag{13.6}$$

$P(X)$ is the probability of an annual maximum equaling or exceeding X in any given year, since it is the relative proportion of the total number of annual maxima that have equaled or exceeded X. If X is equaled or exceeded r times in N years (N is large), then $P(X) \rightarrow r/N$. The return period for X is, however, $T(X) = N/r$. Thus,

$$P(X) = \frac{1}{T(X)}. \tag{13.7}$$

It follows that

$$T(X) = \frac{1}{P(X)} = \frac{1}{1 - F(X)} \tag{13.8}$$

and

$$F(X) = \frac{T(X) - 1}{T(X)}. \tag{13.9}$$

Thus, if, for example, $T(X) = 100$ years, $P(X) = 0.01$ and $F(X) = 0.99$.

The procedure for analyzing annual maximum flows uses the annual maximum discharges from a continuous homogeneous gauged river record. The peak flows (m^3/s) should be arranged in decreasing order of magnitude with the rank position. The probability of exceedance, $F(X)$, is then calculated for each value, X, according to a plotting position equation devised to overcome the fact that when N is not large, r/N is not a good estimator. There are a variety of equations used for estimation of the probability of exceedance. Among these equations, the equation suggested by Gringorten (1963) has the best performance:

$$F(X) = \frac{r - 0.44}{N + 0.12}, \tag{13.10}$$

where r is the rank of X (when data are sorted in descending order) and N is the total number of data values. Another equation that is frequently used is the Weibull equation, which is easier than calculating the Gringorten equation:

$$F(X) = \frac{r}{N + 1}. \tag{13.11}$$

Other equations that are commonly used to estimate the probability of exceedance are listed as follows:

Hazan equation:

$$F(X) = \frac{2r - 1}{2N}. \tag{13.12}$$

Blom equation:

$$F(X) = \frac{r - 0.375}{N + 0.25}. \tag{13.13}$$

Chegodayev equation:

$$F(X) = \frac{r - 0.3}{N + 0.4}. \tag{13.14}$$

Tukey equation:

$$F(X) = \frac{3r - 1}{3N + 1}. \tag{13.15}$$

All the values of $F(X)$ should be plotted for their corresponding values of X to show the location of their main divergence from the Weibull points. The distribution of the plotted points on the graph would be linear if the annual maxima came from a Gumbel distribution and N was large, but with small samples, departures from a straight line are always to be expected. Outliers commonly occur and arise from the inclusion in a short record of an event with a long return period.

Although the Gumbel distribution is commonly used, many other probability distributions have been investigated for application to the extreme values produced by flood peak discharges. In the United States, after comparing six different distributions, the log-Pearson Type III was selected, although many factors, other than statistical, governed the final choice (Benson 1968). The log-normal distribution, in which the logarithms of the peak flows conform to the Gaussian or normal distribution, also takes the form of the probability curve with a positive skew shown in Figure 13.4 and is often applied successfully to peak flow series.

Example 13.1

Table 13.3 shows the 24 annual maximum discharges from a continuous homogeneous gauged river record. Estimate the probability of exceedance using the Gringorten and Weibull equations.

Solution:

The peak flows (m^3/s) are arranged in decreasing order of magnitude. The second column shows the rank position. The probability of exceedance, $F(X)$, is then calculated for each value, X. Equations 13.10 and 13.11 are used in order to estimate the probability of exceedance for the Gringorten and Weibull equations, respectively.

Both equations, which give very similar results, have been applied and the values of $F(X)$ are shown in Table 13.3.

All the Weibull values of $F(X)$ have been plotted for their corresponding values of X (Figure 13.5) but only the top 5 and bottom 4 Gringorten values have been plotted to show the location of their main divergence from the Weibull points. It is noted that the highest peak (594.7 m^3/s), which has the appearance of an outlier, falls into line better in the Gringorten plotting position.

TABLE 13.3
Flood Frequency Analysis (24 Years of an Annual Series)

X (m^3/s)	Rank (r)	$P(X)$ (Gringorten)	$P(X)$ (Weibull)
594.7	1	0.023	0.040
434.7	2	0.06	0.080
430.4	3	0.106	0.120
402.1	4	0.148	0.160
395.9	5	0.189	0.200
390.8	6	0.231	0.240
369.5	7	0.272	0.280
356.8	8	0.313	0.320
346.9	9	0.355	0.360
342.9	10	0.396	0.400
342.6	11	0.438	0.440
321.4	12	0.479	0.480
318.0	13	0.479	0.520
317.2	14	0.521	0.560
300.2	15	0.604	0.600
290.0	16	0.645	0.640
284.6	17	0.687	0.680
283.2	18	0.728	0.720
273.3	19	0.769	0.760
256.3	20	0.811	0.800
196.8	21	0.852	0.840
190.3	22	0.894	0.880
185.5	23	0.935	0.920
138.8	24	0.977	0.960

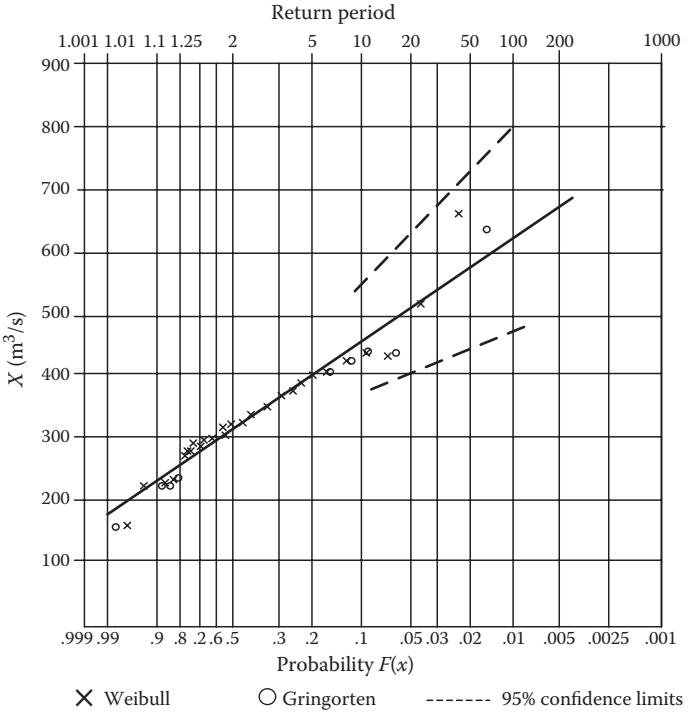

FIGURE 13.5 Flood frequency (Gumbel plot).

To facilitate flood frequency analysis for a data sample, special probability graph papers may be used. The probabilities, $F(X)$, are made the abscissa with X being the ordinate. For any given probability distribution, the values of $F(X)$ are transformed to a new scale such that the X versus $F(X)$ relationship is made linear for that distribution. An example of the Gumbel probability paper, designed for the Gumbel extreme value Type 1, is shown in Figure 13.5.

Example 13.2

The 24 annual maximum discharges are given in Table 13.4. Suppose that the normal distribution probability is fitted with the observed data. Use the normal probability function so that

a. The probability of the annual maximum discharge is less than 400
b. The probability of the annual maximum discharge is between 350 and 400
c. The probability of the annual maximum discharge is exactly 350

TABLE 13.4
Annual Maximum Discharges of Example 13.2

Year	1	2	3	4	5	6	7	8	9	10	11	12
Discharge (m^3/s)	212.7	193.2	103.2	295.4	546.9	378.9	469.3	203.6	183.6	474	398.9	184.7
Year	13	14	15	16	17	18	19	20	21	22	23	24
Discharge (m^3/s)	106.7	311.1	360.9	139.1	357	378.2	444.9	427.8	475.4	417.4	357	278.2

Solution:

a. From data in Table 13.4, the mean value and the standard deviation of 24 annual maximum discharges are 320.75 and 128.8, respectively.
For a discharge of 400, the standard normal variable is calculated as follows:

$$z = \frac{400 - 320.75}{128.8} = 0.615.$$

From Table 10.A1(a) for $z = 0.615$, the cumulative probability is 0.7626. Hence, the probability of the annual maximum discharge to be less than 400 is 76.26%.

b. The value of z for a discharge of 350 is

$$z = \frac{350 - 320.75}{128.8} = 0.227.$$

From Table 10.A1(a) for $z = 0.227$, the cumulative probability is 0.59. Thus, the probability of the annual maximum discharge to be less than 400 is 58.31%. The probability of the annual maximum discharge being between 350 and 400 is calculated from the difference of these values.

$$P(350 < x < 400) = 27.26\%.$$

c. In order to calculate the value of the probability when the discharge is exactly 350, the difference between the cumulative probabilities should be calculated as follows:

$$P(350 < x < 350) = 58.31\% - 58.31\% = 0.$$

Thus, in the normal probability distribution, like other probabilities with smooth curve, the probability of the exact variable is always equals to zero. Flood frequency analysis of the US Water Resources Council (USWRC 1981) proposed a method in order to analyze the flood frequency; the procedure that is described here is based on this method. The probability distribution of runoff is highly skewed because the extreme flood events in flow time series are very far from average flows. The sensitivity of the skewness coefficient is very high and it is related to the size of the sample; therefore, it is difficult to get a precise estimation from small samples. Hence, it is recommended that generalized estimation of the skewness coefficient is used when short records of the skew approximation are needed. Weighted averages between skewness coefficients give a generalized skew. Increasing record length usually leads to a more reliable skew. The weighted skew, G_w, is achieved as follows:

$$G_w = WG_s + (1 - W)G_m, \tag{13.16}$$

where W is weight, G_s is the skew coefficient computed using the sample data, and G_m is a map skewness coefficient, the values of which for the United States are found in Figure 13.6.

A weighting procedure is a function of the variance of the derived sample skew and the variance of the derived map skewness. In this procedure, the uncertainty of deriving skewness coefficients from both sample data and regional or map values are considered to find a generalized skew that reduces the uncertainty to the minimum based upon information known.

Assessment of the sample skew coefficient and the map skewness coefficient in Equation 13.16 is assumed to be independent with the same mean and respective variances. Assuming independency of G_s and G_m, the variance (mean square error) of weighted skew, $V(G_w)$, can be expressed as

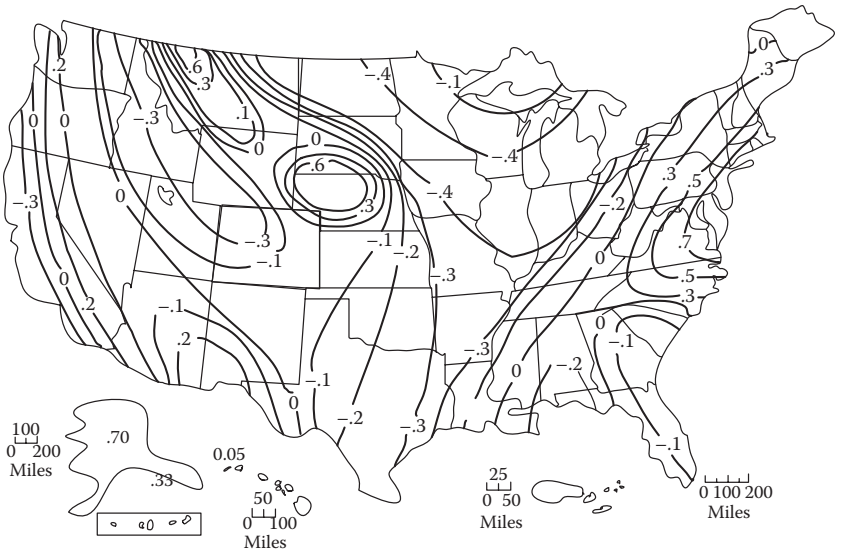

FIGURE 13.6 Generalized skew coefficients of annual maximum streamflow. (From USWRC, *Estimating Peak Flow Frequencies for Natural Ungauged Watersheds—A Proposed Nationwide Test*, Hydrology Subcommittee, US Water Resources Council, 1981. With permission.)

$$V(G_w) = W^2 \cdot V(G_s) + (1 - W)^2 \cdot V(G_m), \tag{13.17}$$

where $V(G_s)$ is the variance of the sample skew and $V(G_m)$ is the variance of the map skewness. The skew weight that minimizes the variance of the weighted skew can be determined by differentiating Equation 13.17 with respect to W and solving $d[V(G_w)]/dW = 0$ for W to obtain

$$W = \frac{V(G_m)}{V(G_s) + V(G_m)}. \tag{13.18}$$

Equation 13.18 is a convex function and the second derivative of Equation 13.17 is greater than 0, proving that Equation 13.18 gives the value of W that minimizes the weighted skew.

The values of $V(G_m)$ and $V(G_s) + V(G_m)$, which are estimated from the map skewness coefficient as the square of the standard deviation of station values of skew coefficients about the isolines of the skew map, are required in order to determine W using Equation 13.18. In the USWRC (1981) skew map, the value of $V(G_m)$ is 0.3025. Otherwise, $V(G_m)$ could be obtained from a regression study relating the skew to physiographical and meteorological characteristics of the basins and determining $V(G_m)$ as the square of the standard error of the regression equation (Tung and Mays 1981).

The weighted skew, G_w, can be determined by substituting Equation 13.18 into Equation 13.16, resulting in

$$G_w = \frac{V(G_m) \cdot G_s + V(G_s) \cdot G_m}{V(G_s) + V(G_m)}. \tag{13.19}$$

The results of Monte Carlo experiments by Wallis et al. (1974) give the variance (mean square error) of the station skews for log-Pearson Type III random variables. The results of the study showed that $V(G_m)$ of the logarithmic station skew is a function of population skew and record

length. For use in calculating G_w, this function, $V(G_s)$, can be approximated with enough accuracy using

$$V(G_s) = 10^{A-B\left[\log\left(\frac{n}{10}\right)\right]}, \tag{13.20}$$

where

$$A = -0.33 + 0.08|G_s| \text{ if } |G_s| \le 0.90 \tag{13.21a}$$

$$A = -0.52 + 0.30|G_s| \text{ if } |G_s| > 0.90 \tag{13.21b}$$

$$B = 0.94 - 0.26|G_s| \text{ if } |G_s| \le 1.50 \tag{13.22a}$$

$$B = 0.55 \text{ if } |G_s| > 1.50, \tag{13.22b}$$

in which $|G_s|$ is the absolute value of the station skew (used as an estimation of population skew) and n is the record length in years.

13.3.3 Testing for Quilters

The USWRC method suggests that outliers be identified and adjusted according to their recommended methods. Data points that depart significantly from the trend of the remaining data are called outliers. The preservation or removal of these outliers can have a considerable effect on the magnitude of statistical parameters computed from the data, particularly for small samples. Procedures for treating outliers need judgment involving both mathematical and hydrologic consideration. Tests for high outliers are considered first if the station skew is greater than +0.4 according to the USWRC (1981). Otherwise, tests for low outliers should be applied before removing any outliers from the data set.

The following frequency equation can be used to identify high outliers:

$$\overline{y}_H = y + K_N S_y, \tag{13.23}$$

where $\overline{y}_H$ is the high outlier threshold in log units, K_N is the K value from Table 13.5 for sample size N, and S_y is the standard deviation. High outliers are the peaks in the sample when they are greater than $\overline{y}_H$ in Equation 13.23. Then they should be compared with historic flood data and flood information in close sites. According to the USWRC (1981), if information is available indicating that a high outlier is the maximum over an extended period of time, the outlier is treated as historic flood data. If useful historic information is not available to adjust for high outliers, then the outliers should be retained as part of the record. The following frequency equation can be used to detect low outliers:

$$\overline{y}_L = y - K_N S_y \tag{13.24}$$

where $\overline{y}_L$ is the low outlier threshold in log units. Flood peaks considered low outliers are removed from the record and a conditional probability adjustment explained in USWRC (1981) is applied.

TABLE 13.5
Outlier Test *K* Values: 10% Significant Level *K* Values

Sample Size	*K* Value	Sample Size	*K* Value	Sample Size	*K* Value	Sample Size	*K* Value
10	2.036	45	2.727	80	2.940	115	3.064
11	2.088	46	2.736	81	2.945	116	3.067
12	2.134	47	2.744	82	2.949	117	3.070
13	2.175	48	2.753	83	2.953	118	3.073
14	2.213	49	2.76	84	2.957	119	3.075
15	2.247	50	2.768	85	2.961	120	3.078
16	2.279	51	2.775	86	2.966	121	3.081
17	2.309	52	2.783	87	2.970	122	3.083
18	2.335	53	2.79	88	2.973	123	3.086
19	2.361	54	2.798	89	2.977	124	3.089
20	2.385	55	2.804	90	2.981	125	3.092
21	2.408	56	2.811	91	2.984	126	3.095
22	2.429	57	2.818	92	2.989	127	3.097
23	2.448	58	2.824	93	2.993	128	3.100
24	2.467	59	2.831	94	2.996	129	3.102
25	2.486	60	2.837	95	3.000	130	3.104
26	2.502	61	2.842	96	3.003	131	3.107
27	2.519	62	2.849	97	3.006	132	3.109
28	2.534	63	2.854	98	3.011	133	3.112
29	2.549	64	2.86	99	3.014	134	3.114
30	2.563	65	2.866	100	3.017	135	3.116
31	2.577	66	2.871	101	3.021	136	3.119
32	2.591	67	2.877	102	3.024	137	3.122
33	2.604	68	2.883	103	3.027	138	3.124
34	2.616	69	2.888	104	3.030	139	3.126
35	2.628	70	2.893	105	3.033	140	3.129
36	2.639	71	2.897	106	3.037	141	3.131
37	2.650	72	2.903	107	3.040	142	3.133
38	2.661	73	2.908	108	3.043	143	3.135
39	2.671	74	2.912	109	30.460	144	3.138
40	2.682	75	2.917	110	3.049	145	3.140
41	2.692	76	2.922	111	3.052	146	3.142
42	2.700	77	2.927	112	3.055	147	3.144
43	2.710	78	2.931	113	3.058	148	1.146
44	2.719	79	2.953	114	3.061	149	3.148

Source: USWRC, *Estimating Peak Flow Frequencies for Natural Ungauged Watersheds—A Proposed Nationwide Test*, Hydrology Subcommittee, US Water Resources Council, 1981. With permission.

Use of the *K* values in Table 13.5 is equivalent to a one-sided test that detects outliers at the 10% level of significance. The *K* values are based on a normal distribution for detection of single outliers.

Example 13.3

The mean, standard deviation, and skewness coefficient for a gauge are 3.338, 0.653, and –0.3, respectively. Compute the 25-year and the 100-year peak discharges using the USWRC guideline. The map skewness coefficient for this location is –0.015.

Solution:

In this example, $\bar{y} = 3.338$, $S_y = 0.653$, and $G_s = -0.3$.

Step 1: Compute A, B, and $V(G_s)$ using Equations 13.21, 13.22, and 13.20.

$$A = -0.33 + 0.08|-0.3| = -0.306$$

$$B = 0.94 - 0.26|-0.3| = 0.86$$

$$V(G_s) = 10^{A-B\left[\log\left(\frac{n}{10}\right)\right]} = 10^{-0.306-0.864\log\left(\frac{47}{10}\right)} = 0.13.$$

Step 2: Use Equation 13.19 to compute the weighted skewness coefficient using $V(G_m) = 0.302$ [as estimated in USWRC (1981)]:

$$G_w = \frac{0.302(-0.3) + 0.130(-0.015)}{0.302 + 0.130} = -0.12.$$

Step 3: Use Table A.2 in the Appendix to Chapter 10 (K_T values for Pearson Type III distribution) to obtain the frequency factor equation to determine Q_{25} and Q_{100}:

$$\log Q_{25} = \bar{y} + K(25 - 0.125)S_y = 3.338 + 1.676(0.653) = 4.432 \qquad Q_{25} = 27{,}070 \text{ cfs}$$
$$\log Q_{100} = 3.338 + 2.171(0.653) = 4.432 \qquad Q_{100} = 56{,}975 \text{ cfs}$$

13.4 FLOOD PREDICTION

The concept of the return period states that the T-year event, Q_T, is the average chance of exceedance once every T years over a long record. However, it is often required to know the actual probability of exceedance of the T-year flood in a specific period of n years.

$F(X)$ is the probability of X not being equaled or exceeded in any one year. With the assumption that annual maxima are independent, the probability of no annual maxima exceeding X in the whole n years is given by $(F(X))^n$. The probability of exceedance of X at least once in n years is then $1 - (F(X))^n$, which may be signified by $P_n(X) = 1 - (1 - P(X))^n$. Substituting for $F(X)$ is as follows:

$$P(Q_T \geq X) \text{ in } n \text{ years} = P_n(X) = 1 - \left(\frac{T(X) - 1}{T(X)}\right)^n. \tag{13.25}$$

Thus, for $T(X) = 100$ years and $n = 100$ years, the following is obtained:

$$P_n(X) = P(Q_{100} \geq X) = 1 - \left(\frac{99}{100}\right)^{100} = 0.634. \tag{13.26}$$

This means that the chance of the 100-year flood being equaled or exceeded at least once in 100 years is 63.4%; i.e., there is roughly a 2 in 3 chance that a 100-year event in any given 100-year record will happen (and a 1 in 3 chance that it will not). Rearranging Equation 13.25 gives

$$n = \frac{\log[1 - P_n(X)]}{\log\left[\dfrac{T(X) - 1}{T(X)}\right]}. \tag{13.27}$$

Thus, for a required probability, $P_n(X)$, and return period, T, the length of record, n years, in which the T-year event of one or more equal or higher magnitude has the probability $P_n(X)$, which can be calculated. Such information is essential to engineers designing dams or flood protection structures.

13.5 FLOOD ROUTING

A flood hydrograph is modified in two ways as the storm water flows downstream. Firstly, and obviously, the time of the peak rate of flow occurs later at downstream points. This is known as translation. Secondly, the magnitude of the peak rate of flow is diminished at downstream points, the shape of the hydrograph flattens out, and the volume of floodwater takes longer to pass a lower section. This modification to the hydrograph is called attenuation (Figure 13.7).

The derivation of downstream hydrographs like B in Figure 13.7 from an upstream known flood pattern A is essential for river managers concerned with forecasting floods in the lower parts of a river basin. The design engineer also needs to be able to route flood hydrographs in assessing the capacity of reservoir spillways, in designing flood protection schemes, or in evaluating the span and height of bridges or other river structures. In any situation where it is planned to modify the channel of a river, it is necessary to know the likely effect on the shape of the flood hydrograph in addition to that on the peak stage, i.e., the whole hydrograph of water passing through a section, not just the peak instantaneous rate.

Flood routing methods may be divided into two main categories, differing in their fundamental approaches to the problem. One category of methods uses the principle of continuity and a relationship between discharge and the temporary storage of excess volumes of water during the flood period. The calculations are relatively simple and reasonably accurate and, from the hydrologist's point of view, generally give satisfactory results. The second category of methods, favored by hydraulic engineers, adopts the more rigorous equations of motion for unsteady flow in open channels, but complex calculations, assumptions, and approximations are often necessary, and some of the terms of the dynamic equation must be omitted in certain circumstances to obtain solutions. The choice of method depends very much on the nature of the problem and the data available. Flood routing computations are more easily carried out for a single reach of river that has no tributaries

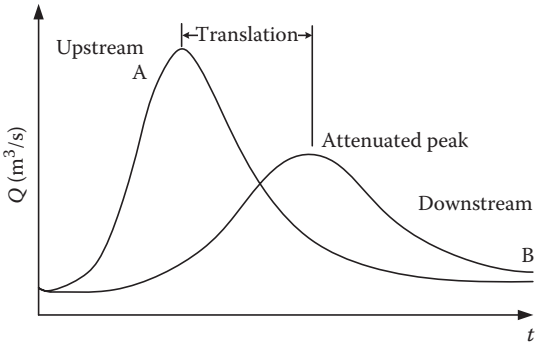

FIGURE 13.7 Flood peak translation and attenuation.

joining it between the two ends of the reach. According to the length of reach and the magnitude of the flood event being considered, it may be necessary to assess contributions to the river from lateral inflow, i.e., seepage or overland flow draining from, and distributed along, the banks. Furthermore, river networks can be very complex systems, and in routing a flood down a main channel, the calculations must be done for separate reaches with additional hydrographs being introduced for major tributaries. In order to develop an operational a flood routing procedure for a major river system, detailed knowledge of the main stream and the various feeder channels is necessary. In addition, the experience of several major flood events with discharge measurements made at strategic points on the drainage network is an essential requirement.

In floodplain hydrology, the movement of a flood wave down a channel or through a reservoir is an important topic. It is necessary to understand the theoretical and practical aspects of flood routing through a river reach or reservoir. Flood routing methods can also be used to predict the outflow hydrograph from a watershed subjected to a specific amount of precipitation. In this chapter, a selection of flood routing methods will be presented.

13.5.1 Simple Non-Storage Routing

It has been said that "engineering is the solution of practical problems with insufficient data." If there are no gauging stations on the problem river and therefore no measurements of discharge, the engineer may have to make do with stage measurements.

In such circumstances, it is usually the flood peaks that have been recorded, and indeed it is common to find that people living alongside a river have marked on a wall or bridge pier the heights reached by notable floods. Hence, the derivation of a relationship between peak stages at upstream and downstream points on a single river reach may be made (Figure 13.8) when it is known that the floods are caused by similar notable conditions.

This is a very approximate method, and there should be no major tributaries and very low lateral inflows between the points with the stage measurements. However, with enough stage records, it may be possible to fit a curve to the relationship to give satisfactory forecasts of the downstream peak stage from an upstream peak stage measurement.

For example, on the River Irrawaddy in Burma, a linear relationship exists between the peak stages of an upstream gauging station at Nyaung Oo and a station at Prome, 345 km downstream. A total of 35 comparable stages (m) for irregular flood events over 5 years (1965–1969) are shown in Figure 13.9. An equation, $H_D = 1.3H_U + 1.4$, relating H_D, the downstream stage, to H_U, the upstream stage, can then give forecast values of H_D from H_U (Shaw 1983).

The time of travel of the hydrograph crest (peak flow) also needs to be determined; curves of upstream stage plotted against time of travel to the required downstream point can be compiled from the experience of several flood events. (The time of travel of the flood peaks between Nyaung Oo and Prome on the Irrawaddy ranged from 1 to 4 days.)

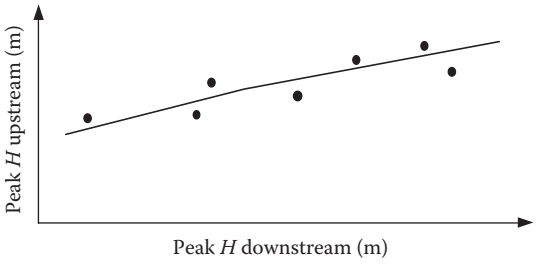

FIGURE 13.8 Peak stage relationship.

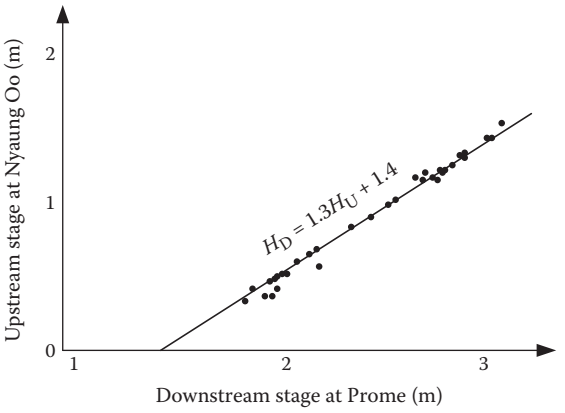

FIGURE 13.9 Comparable peak stages on the River Irrawaddy.

A typical stage time of travel plot is shown in Figure 13.10. This figure shows that the minimum time of travel at the stage range occurs when the bankfull capacity of the river channel is reached.

After reaching a minimum at this bankfull stage, the time of travel tends to increase again as the flood peak spreads over the floodplain and its downstream progress is retarded owing to storage effects on the floodplain.

The complexities of rainfall–runoff relationships are such that these simple methods allow only for average conditions. Flood events can have very many different causes that produce flood hydrographs of different shapes. Flood hydrographs at an upstream point, with peaks of the same magnitude but containing different flood volumes, traveling downstream will produce different peaks at a downstream point. Modifications to the flow by the channel conditions will differ between steep, peaky flood hydrographs and gentle fat hydrographs with the same peak discharges.

The principal advantages of these simple methods are that they can be developed for stations with only stage measurements and no rating curve, and they are quick and easy to apply, especially for warning of impending flood inundations when the required answers are immediately given in stage heights. The advantages of speed and simplicity are less important now that fast computers are available and more accurate and comprehensive real-time techniques can be used.

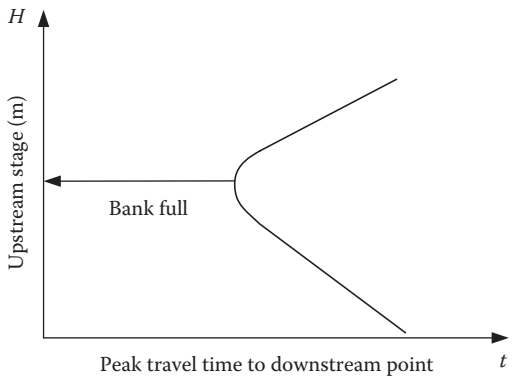

FIGURE 13.10 Flood peak travel times.

13.5.2 Storage-Based Routing

Routing techniques can be classified into two major categories: simple hydrologic routing and more complex hydraulic routing. Hydraulic routing is more complex and accurate than hydrologic routing. It is based on the solution of the continuity equation and the momentum equation for unsteady flow in open channels. Usually solved by explicit or implicit numerical methods on a computer, these differential equations are known as the Saint Venant equations, first derived in 1871.

Hydrologic routing involves the balancing of inflow, outflow, and volume of storage through use of the continuity equation. A second relationship, the storage–discharge relation, is also required between outflow rate and storage in the system. Applications of hydrologic routing techniques to problems of flood prediction, flood control measures, reservoir design and operation, watershed simulation, and urban design are numerous. Examples of techniques for hydrologic river routing and hydrologic reservoir routing can be Muskingum and storage indication methods, respectively. For more details, refer to Chapter 6.

13.6 URBAN FLOODS

Through the development of new urban areas, infiltration reductions and water retention characteristics of the natural land should be considered. The increasing quantity as well as the short duration of drainage produces high flood peaks that exceed the conveyed secure capacities of urban streams. The total economic and social damage in urban areas tends to make significant impacts on the national economies as flood frequencies increase. Recent events even in North America have been devastating in urban areas such as New Orleans.

With uncontrolled urbanization in the floodplains, a sequence of small flood events could be managed, but with higher flood levels, damage increases and the municipalities' administrations have to invest in population relief. The costs of application of structural solutions for flood mitigation are higher but they are commonly used when damage is greater than development costs or because of intangible social aspects. Nonstructural measures have lower costs, but with less chance to be implemented because they are not politically attractive in developing regions (Tucci 1991).

13.6.1 Urban Flood Control Principles

Certain principles of urban drainage and flood control are proposed by Tucci (1991):

- Promoting an urban drainage master plan
- Involvement of the whole basin in evaluating flood control
- Any city developments should be within urban drainage control plans
- Priority is given to source control and keeping the flood control measures away from downstream reaches
- Application of nonstructural measures for flood control such as flood warning, flood zoning, and flood insurance
- Public participation in urban flood management
- Consideration of full recovery investments

In developing countries, a set principle for urban drainage practices has not been established due to fast and unpredictable developments (Dunne 1986). Furthermore, the local regulations are neglected in urbanization of pre-urban areas such as unregulated developments and invasion of public areas.

In many developing urban areas, the above principles are not incorporated because of the following:

- Insufficient funds
- Lack of appropriate waste collection and disposal system resulting in decrease of water quality and the capacity of the urban drainage network due to filling
- Absence of a preventive program for risk area occupation
- Lack of adequate knowledge on how to deal with floods
- Lack of institutional organization at a municipal level for urban drainage management

One of the most common problems facing a practicing civil engineer is the estimation of the hydrograph of the rise and fall of a river at any given point on the river during the course of a flood event. The problem is solved by the techniques of flood routing, which is the process of following the behavior of a flood hydrograph upstream or downstream from one point to another point on the river. It is more usual (and more natural) to work downstream from an upstream point where a flood hydrograph is specified; the reverse procedure against the flow is more complex and is less often required.

13.7 UNDERSTANDING FLOOD HAZARDS

Flooding is the result of a combination of meteorological and hydrological conditions, some of which are indicated in Table 13.6. These conditions are influenced by human factors. These influences are very different but they commonly increase flood hazards by accentuating flood peaks. Thus, flood hazards are considered to be the consequence of natural and man-made factors.

13.7.1 Climate Change and Flooding

Floods have always been a source of major concerns to human societies in different regions. Although there has been great improvement in understanding floods and there are technological means to deal with them, people still suffer from the consequences of severe floods. Floods cause damage to different infrastructures such as settlements, roads, and railways and destroy human heritage. Climate change has a potential to increase the frequency of extreme events as well as flooding in many regions of the world.

TABLE 13.6
Factors Contributing to Flooding

Meteorological Factors	Hydrological Factors	Human Factors
• Rainfall • Cyclonic storms • Small-scale storms • Temperature • Snowfall and snowmelt	• Soil moisture level • Groundwater level prior to storm • Natural surface infiltration rate • Presence of impervious cover • Channel cross-sectional shape and roughness • Presence or absence of over bank flow, channel network • Synchronization of runoffs from various part of watershed • High tide impeding drainage	• Land-use changes (e.g., surface sealing due to urbanization, deforestation) increase runoff and maybe sedimentation • Occupation of the floodplain obstructing flows • Inefficiency or non-maintenance of infrastructure • Too efficient drainage of upstream increases flood peaks • Climate change affects magnitude and frequency of precipitations and floods • Urban microclimate may enforce precipitation events

Source: APFM, Urban flood risk management, *Flood Management Tools Series*, 2008. With permission.

Global warming may result in intensifying many subsystems of the global water cycle. This can increase the flood magnitude as well as flood frequency, making weather less predictable and increasing precipitation uncertainty. Some other factors such as urbanization may increase thunderstorm activity because of heat islands and create local air circulation. Dust particles that circulate act as nuclei for condensation of the moisture in clouds, forming rain droplets. These droplets can eventually develop into large raindrops in a major thunderstorm.

The Intergovernmental Panel on Climate Change has carried out several studies on the potential impacts of climate change on flooding. These studies show 15% potential increase in flood peaks in temperate zones due to increased storm activity and precipitation depth. Currently, it is not possible to predict potential increases in flood peaks due to climate change for specific basins with the level of accuracy needed for design and planning purposes, but it seems that the freeboard on levees and other flood control structures can accommodate the potential changes in extremes due to climate change, if some changes are made in operating procedures of control structures.

13.7.2 Sea Level Rise and Storm Surge

Sea level rise, as a result of climate change impacts, is an added factor that could intensify the inverse flood impacts. Sea level rise increases the risk of coastal flooding, specifically in the case of storm surges. The sea level projections by the 2080s show that millions of people are in areas with flooding potential due to sea level rise. The risk is higher in densely populated low-lying areas with low adaptive capacity.

Coastal communities should consider sea level rise, tsunamis, and ocean storm surge in preparing and dealing with flooding events. As an example, sea level rise results in decreased river slopes at the upstream of river entries to the ocean. This decreases the secure channel capacity of passing flood flows and increases the elevation of floods in coastal cities. Due to the slow rate of sea level rise, the long-term protective works or floodplain management exercises are planned to incorporate the predicted rise. Some studies have indicated that there is potential for increased frequency of storm surges, which result from high winds and increased barometric pressure. Tsunamis can also be devastating natural disasters and must be considered in a manner similar to flooding. Forecasting and emergency responses to these events must be based on the same principles of acceptable risk and advance planning.

13.8 EVACUATION ZONES

To deal with floods and prevent loss of human life, evacuation zones are defined in the coastal regions. Evacuation zones in different coastal regions are determined based on (1) vulnerability of respondents, (2) types of communities, (3) demographic characteristics of the populations, (4) sample size, (5) type of housing, and (6) time between the evacuation and the flood occurrence (Nelson et al. 1989).

The purpose of a regional evacuation study is to provide emergency management officials with realistic data by quantifying the major factors in hurricane evacuation decision making. These data are provided as a framework of information that counties can use to update and revise their hurricane evacuation plans and operational procedures to improve their response to future hurricane threats. It should be noted that hurricane evacuation zones are different from flood insurance risk zones, which are designated by FEMA and published in the form of Flood Insurance Rate Maps.

With the evacuation maps, each zone will be evacuated depending on the hurricane's track and projected storm surge. For example, in New York City (NYC), hurricane contingency plans are based on three evacuation zones (Figure 13.11). These zones represent varying threat levels of coastal flooding resulting from storm surge. Manhattan and its surrounding areas have been sliced up into Zones A, B, and C depending on the strength of hurricanes. Residents in Zone A were asked

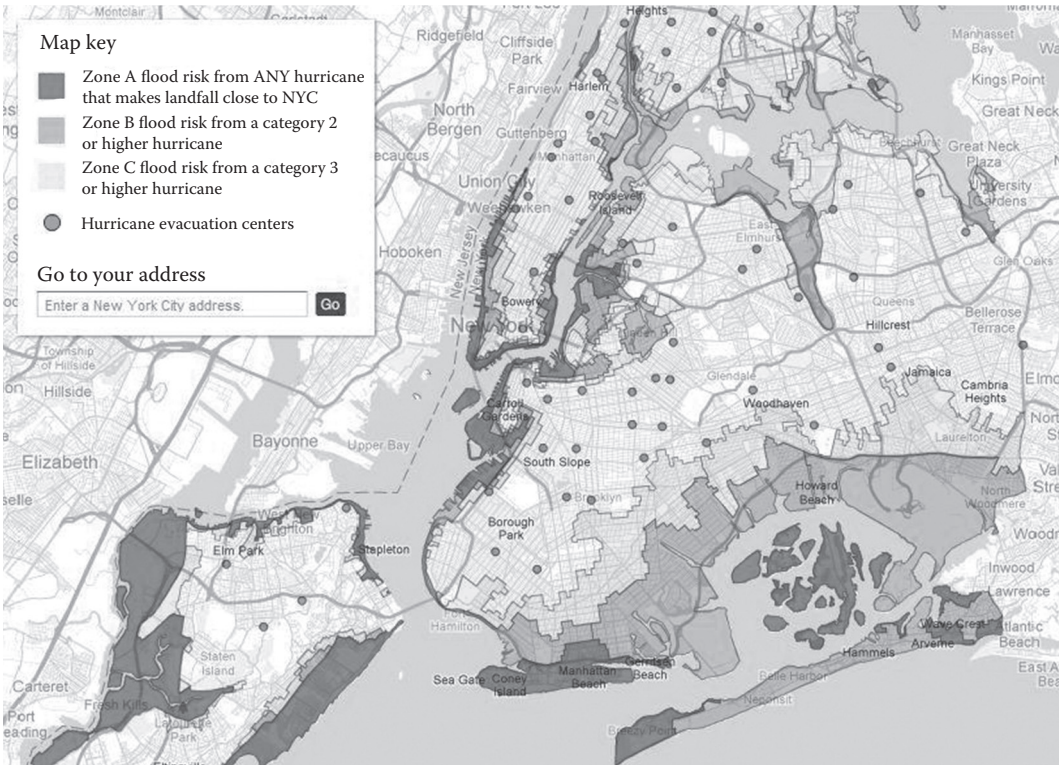

FIGURE 13.11 New York City evacuation zone, August 28, 2011 (http://www.nytimes.com/interactive/2011/08/26/nyregion/new-york-city-hurricane-evacuation-zones.html).

to evacuate a day before hurricane Irene hit NYC. They were facing the highest risk of flooding from a hurricane category that became a storm surge when it reached NYC. Zone A includes all low-lying coastal areas and other areas that could experience storm surge from a hurricane making landfall close to NYC. Residents in Zone B may experience storm surge flooding from a moderate (category 2 and higher) hurricane. Residents in Zone C may experience storm surge flooding from a major (category 3 and 4) hurricane making landfall just south of NYC. A major hurricane is unlikely in NYC, but not impossible. Zone A in this region is determined based on 1% per year probability of flooding plus 26% probability (risk) of failure in 30 years. This is equivalent to another 1% per year due to insurance and home considerations.

Residents in the Zone A region are at the highest risk of flooding from a storm surge. Almost any hurricane or near-hurricane-type event making landfall in NYC could cause these areas to flood, requiring evacuation.

In order to reduce flood impacts, current flood risk management strategies and floodplains and evacuation zones, which are often outdated by a couple of decades, need a major overhaul and should be reassessed to meet the public's expectation of accuracy, responsiveness, and safety and security. The concept of resilience is used in various disciplines and has become multi-interpretable. Resilience theory offers insights into the behavior of complex systems and the importance of system criteria such as system memory and self-organization. Resilience is a measure of how our municipalities and emergency response unit are ready to resume a close-to-normal operation in a disaster area.

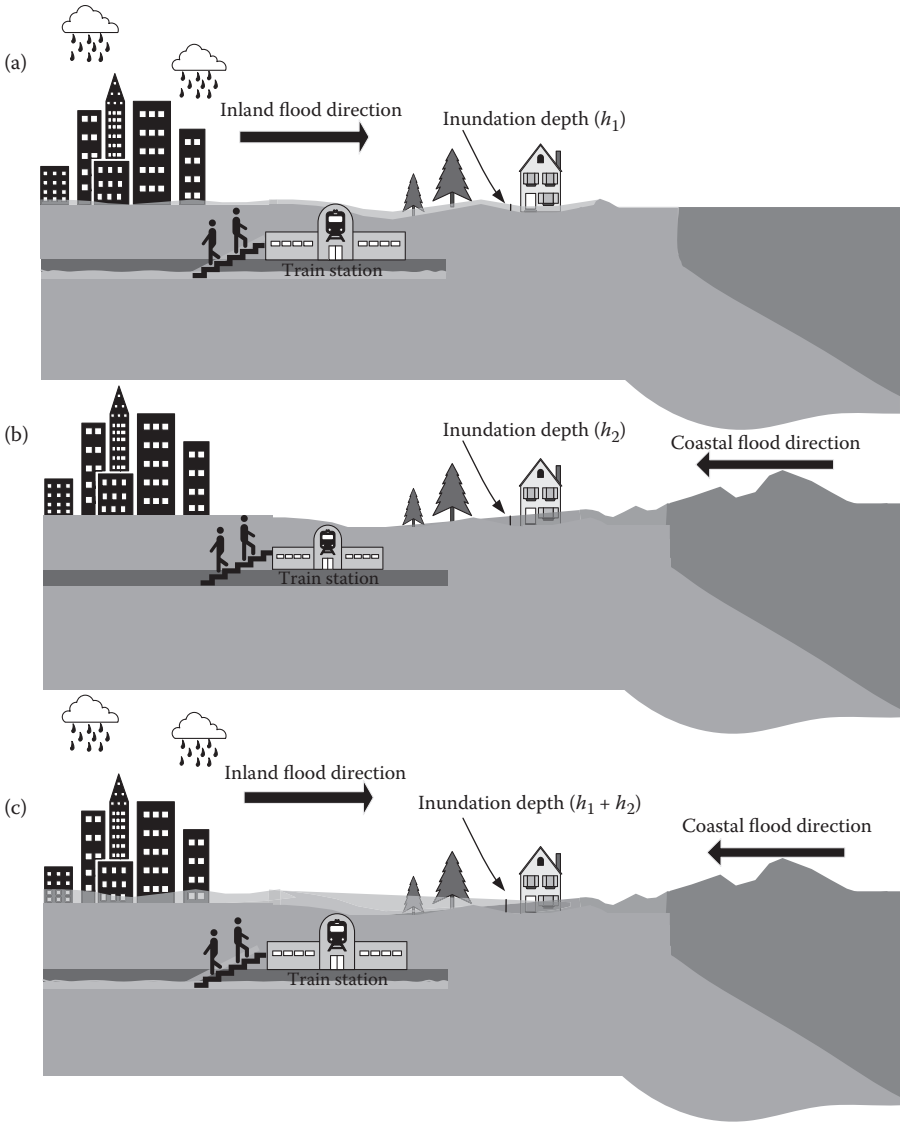

FIGURE 13.12 (a) Inland flood; (b) coastal flood; (c) the integration of inland and coastal floods' impacts on a region.

The schematic of overlay of inland and coastal flood impacts is given in Figure 13.12. Based on this figure, the overlay of inland and coastal floods resembles the actual most severe flood zones. The results of these events should be analyzed considering the conjunctive impacts of these floods in addition to each event individually. A combined probability distribution should be considered to analyze the impact of simultaneous inland and coastal floods on an urban area.

13.9 FLOOD DAMAGE

Flood vulnerability (the severity of the damage) depends on the flood type and characteristics such as flow depth, velocity, quality, and duration, as well as sediment load. In rural and undeveloped areas, flood damage is mostly loss of agricultural production, but the damage in the urban region is more complex. Flood damage can be categorized as follows:

Direct losses: These losses are the result of direct contact of floodwater with buildings, infrastructure, and properties.

Indirect losses: These losses are event consequences but not direct impacts. Examples of indirect losses are transport disruption, business losses that cannot be made up, and losses of family income.

Both direct and indirect losses include two subcategories: tangible and intangible losses.

Tangible losses: These refer to loss of things that have a monetary (replacement) value such as buildings, livestock, and infrastructure.

Intangible losses: These refer to loss of things that cannot be bought and sold. Examples of intangible losses are lives and injuries, heritage items, and memorabilia.

Various techniques have been used to calculate direct damage. Grigg and Helweg (1975) used three categories of techniques: aggregate equations, historical damage curves, and empirical depth damage curves. One of the more familiar aggregate equations is that suggested by James (1972):

$$C_D = K_D U M_S h A, \tag{13.28}$$

where C_D is the flood damage cost for a particular flood event, K_D is the flood damage per foot of flood depth per dollars of market value of the structure, U is the fraction of floodplain in urban development, M_S is the market value of the structure inundated in dollars per developed area, h is the average flood depth over the inundated area in feet, and A is the area flooded in acres. Eckstein (1958) presented the historical damage curve method in which the historical damage of floods is plotted against the flood stage.

13.9.1 Stage–Damage Curve

The stage–damage (depth–damage) curve is a relationship between extents of damage corresponding to the floodwater level (Figure 13.13a). It is a graphical representation of the expected losses from a specified flooding depth. These curves are typically used for housing and other structures. The stage or depth is the depth of water inside a building and the damage refers to the expected damage from that depth of water (Emergency Management Australia 2007).

The use of empirical depth–damage curves requires a property survey of the floodplain and either an individual or aggregated estimate of depth (stage) versus damage curves for structures, roads, crops, utilities, etc. that are in the floodplain. This stage–damage is then related to the relationship for the stage discharge (Figure 13.13b) to derive the damage–discharge relationship (Figure 13.13c), which is then used along with the discharge–frequency relationship to derive the damage–frequency curve, as shown in Figure 13.13e.

There are two ways for developing stage–damage curves. The first way involves using data on building contents and structure repair costs to generate synthetic or artificial estimates of damage curves. In the second way, the information on damage caused by previous floods and corresponding depths is used.

Vulnerability can be represented through vulnerability functions illustrating graphically how a selected consequence variable depends on a selected threat parameter. It can be necessary to use many such functions to represent a particular vulnerability comprehensively. This level of representation is similar to damage functions used in many vulnerability assessments. For river flood management, a classic example of vulnerability would relate a threat (flood height above the floodplain) to its consequence (damage) (Figure 13.14).

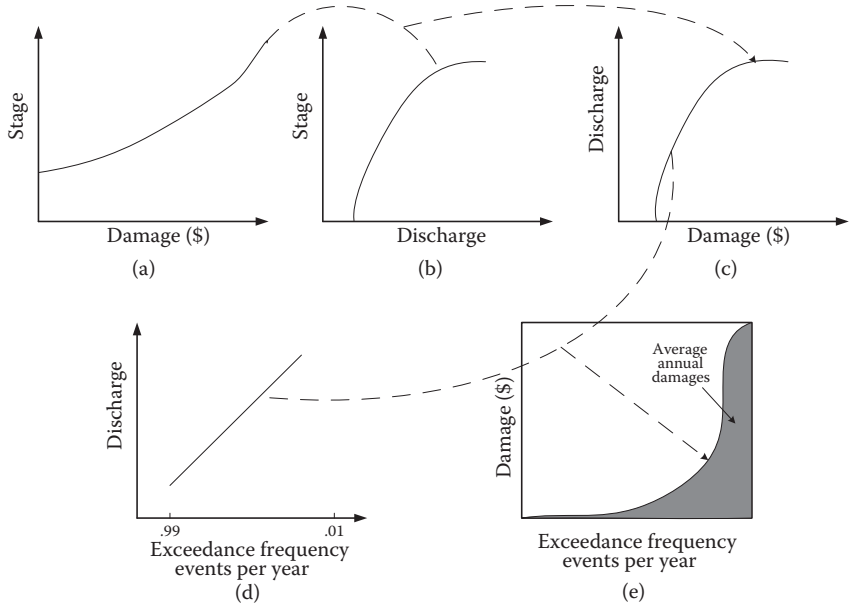

FIGURE 13.13 Development of damage–probability curves of floods in a region (a) damage–stage relationship; (b) discharge–stage relationship; (c) damage–discharge relationship; (d) exceedance frequency–discharge relationship, and (e) exceedance frequency–damage relationship (dashed line shows the process of damage–probability curve development) (Mays 2001).

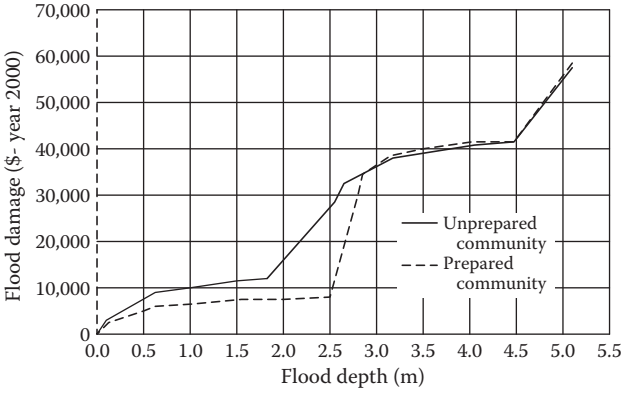

FIGURE 13.14 Sample damage curve for residential properties. The damage is expressed as a function of water depth.

13.9.2 Expected Damage

The annual expected damage cost $E(D)$ is the area under the damage–frequency curve as shown in Figure 13.13e, which can be expressed as

$$E(D) = \int_{q_c}^{\infty} D(q_d) f(q_d)\, dq_d = \int_{q_c}^{\infty} D(q_d)\, dF(q_d), \tag{13.29}$$

where q_d is the threshold discharge beyond which damage would occur, $D(q_d)$ is the flood damage for various discharges q_d, which is the damage–discharge relationship, and $f(q_d)$ and $F(q_d)$ are the probability density function (PDF) and the cumulative distribution function (CDF), respectively, of the discharge q_d. In practical applications, the evaluation of $E(D)$ by Equation 13.29 is carried out using numerical integration because of the complexity of damage functions and probability distribution functions. Therefore, the shaded area in Figure 13.13e can be approximated, numerically, by the trapezoidal rule, as an example,

$$E(D) = \sum_{j=1}^{n} \int_{q_c}^{\infty} \frac{[D(q_j) + D(q_{j+1})]}{2} [D(F_{j+1} - F(q_j))] \text{ for } q_c = q_1 \le q_2 \le \ldots \le q_n < \infty, \quad (13.30)$$

in which q_j is the discredited discharge in interval (q_c,∞).

Example 13.4

Use the damage–frequency relationships in Table 13.7 for flood control alternatives to rank their merits on the basis of expected flood damage reduction.

Solution:

The economic merit of each flood control alternative can be measured by the annual expected savings in flood damage of each alternative, which can be calculated as the difference between the annual expected damage at the existing condition (without flood control measures) and the annual expected damage with a given flood control measure under consideration. Using Tables 13.8 and 13.9, the damage reduction associated with each flood control measure at different return periods is determined.

From the data in Table 13.8, the average damage reduction for each flood control alternative and incremental probability can be developed as shown in Table 13.9. The best alternative with the highest benefit of annual expected flood reduction is to build a detention basin upstream.

TABLE 13.7
Damage–Frequency Relationships in Example 13.4

Exceedance Probability (%)	Damage^0 ($10^6)	Damage^1 ($10^6)	Damage^2 ($10^6)	Damage^3 ($10^6)	Damage^4 ($10^6)
20	0	0	0	0	0
10	6	0	0	0	0
7	10	0	0	0	0
5	13	13	2	4	3
2	22	22	10	12	10
1	30	30	20	18	12
0.5	40	40	30	27	21
0.2	50	50	43	40	35
0.1	54	54	47	43	45
0.05	57	57	55	50	56

Note: 0—Existing condition, 1—Dike system, 2—Upstream diversion, 3—Channel modification, 4—Detention basin.

TABLE 13.8
Damage–Frequency Relationships in Example 13.4

Exceedance Probability (%)	Damage Reduction ($10^6)			
	1	2	3	4
20	0	0	0	0
10	6	6	6	6
7	10	10	10	10
5	0	9	7	10
2	0	11	9	12
1	0	10	12	18
0.5	0	10	13	19
0.2	0	7	10	15
0.1	0	5	9	9
0.05	0	2	7	1

Note: 1—Dike system, 2—Upstream diversion, 3—Channelization, 4—Detention basin.

TABLE 13.9
Damage–Frequency Relationships in Example 13.4

Increm. Prob. (ΔF)	Damage Reduction ($10^6)			
	1	2	3	4
0.1	3	3	3	3
0.03	8	8	8	8
0.02	5	9.5	8.5	10
0.03	0	10	8	11
0.01	0	10.5	10.5	15
0.005	0	10	12.5	18.5
0.003	0	8.5	11.5	17
0.001	0	6	9.5	12
0.0005	0	3.5	8	5
$\Sigma(\Delta D \times \Delta F)$	0.64	1.218	1.251	1.378

Note: 1—Dike system, 2—Upstream diversion, 3—Channelization, 4—Detention basin.

13.10 FLOOD RISK MANAGEMENT

Flood risk management for a system in a narrow sense is the process of managing a flood risk situation. In a wider sense, it includes the planning of a system that will reduce the flood risk.

These two aspects of flood risk management will be considered separately, starting with the management of a system that consists of the processes indicated in Figure 13.15. Risk management for the operation of a flood protection system is the sum of actions for a rational approach to flood disaster mitigation. Its purpose is the control of flood disasters, in the sense of being prepared for a flood, and to minimize its impact.

It includes the process of risk analysis, which provides the basis for long-term management decisions for the existing flood protection system. Continuous improvement of the system requires a reassessment of the existing risks and an evaluation of the hazards depending on the newest

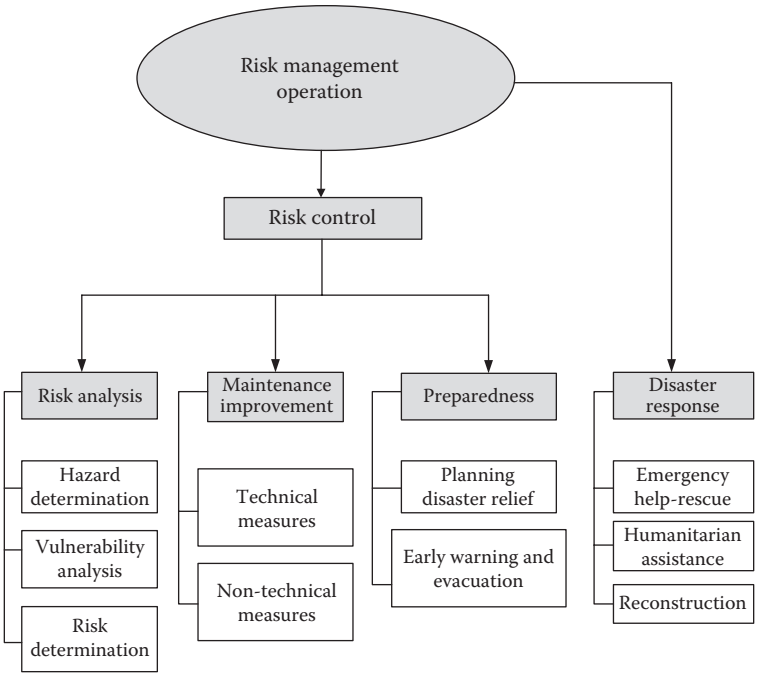

FIGURE 13.15 Stages of operational risk management. (Adapted from Eikenberg, C., Journalistenhandbuch zum Katastrophenman-agement, 5th ed., German IDNDR-Committee, Bonn, 1998.)

information available: on new data, on new theoretical developments, or on new boundary conditions, for example, due to change of land use.

The hazards are to be combined with the vulnerability into the risk. The vulnerability of the persons or objects (the elements at risk) in an area, which is inundated if a flood of a certain magnitude occurs, is weighted with the frequency of occurrence of that flood. A good risk analysis process yields hazard or risk maps, which today are drawn by means of Geographical Information Systems based on extensive surveys of vulnerability combined with topographic maps. Such maps serve to identify weak points of the flood defense system or indicate a need for action, which may lead to a new project. Other weaknesses of the system become evident during extreme floods. For example, the Oder flood of 1997 has indicated that weak points contributing to flooding of a city in a floodplain not only are failures of dikes but also seepage through the dikes and penetration of floodwaters through the drainage system, i.e., through the sewerage system or water courses inside the city (Kowalczak 1999).

Risk analysis forms the basis for decisions on maintaining and improving the system, which is the second part of the operation of an existing system. It is a truism that a system requires continuous maintenance to be always functioning as planned and new concepts of protection may require local improvements of the existing system.

The third part of the management process is the preparedness stage, whose purpose is to provide the necessary decision support system for the case that the existing flood protection system has failed. It is evident that no technical solution to flooding is absolutely safe. Even if the system always does what it is supposed to do, it is hardly ever possible to offer protection against any conceivable flood. There is always a residual risk, due to failure of technical systems, or due to the rare flood that exceeds the design flood. The Oder river flood of 1997 (Bronstert et al. 1999; Grunewald 1998) comes to mind. It is the purpose of preparedness to reduce the residual risk through early warning systems and measures that can be taken to mitigate the effect of a flood disaster.

An important step in improving an existing flood protection system is the provision of better warning systems. Obviously, the basis for a warning system has to be an effective forecasting

system, which permits the early identification and quantification of an imminent flood to which a population is exposed. If this is not accurately forecasted or at least estimated early enough, a warning system for effective mitigating activities cannot be constructed. Therefore, it is an important aspect that systems managers remain continuously alerted to new developments in flood forecasting technology and to be prepared to use this technology to the fullest extent.

The final part of operational risk management is disaster relief, i.e., the set of actions to be taken when disaster has struck. It is the process of organizing humanitarian aid to the victims, and later reconstruction of damaged buildings and lifelines.

13.10.1 Resiliency and Flood Risk Management

Resilience, in its most basic sense, means the ability to deal with change and continue to operate. The defining characteristic of flood-resilient communities is their ability to reduce, prevent, and cope with the flood risk. Resilient communities have improved their capacity in each phase of the flood management cycle. They are knowledgeable and aware of the risk, well prepared, respond better when a flood occurs, and recover more quickly from disasters.

Over the past decades, there has been a shift away from structural and large-scale flood defense towards integrated flood risk management. The modern flood risk management approach acknowledges that floods cannot be stopped from occurring and places emphasis on how to reduce hardship and vulnerability of risk-prone communities (e.g., Bharwani et al. 2008; Krywkow et al. 2008; Vis et al. 2003).

Resilience strategies for flood risk management focus on minimizing flood impacts and enhancing recovery in contrast to resistance strategies that aim at preventing floods entirely. Since resilience strategies are expected to result in improved flood risk management, they deserve careful evaluation. For the evaluation and comparison of strategies for flood risk management, it is necessary to be able to quantify the resilience of the resulting flood risk management systems. Therefore, indicators for quantifying the resilience of flood risk management should be developed and evaluated. To evaluate the behavior of these indicators, they can be applied to a case study such as NYC or hypothetical cases that resemble the challenges we are facing in the eastern coastal area of the United States.

Resilience as a criterion for the operation and design of water supply systems in water management has been quantified by Karamouz et al. (2003) and others. There have been some other studies on adopting resilience to measure the performance of water distribution systems (Zongxue et al. 1998), to characterize reservoir operation rules (e.g., Burn et al. 1991; Moy et al. 1986), or to quantify sustainability of water resource systems (ASCE and UNESCO 1998). In these applications, resilience is described as how quickly a system recovers from failure and is a measure of the duration of an unsatisfactory condition. A flood risk management system is a complex system and assessing its recovery time for the future is difficult. Because responses and recoveries are not easily measured, indicators for resilience have to be found.

13.11 FLOODPLAIN MANAGEMENT

Floodplain is the area of periodic flooding along a river. The floodplains are flat lands beside the river that are formed due to the actions of the river. By exceeding the river discharge from the capacity of the channel, water floods the surrounding low-lying lands. By analysis of the floodplains and their changes over the time, the size of floods that occurred can be estimated.

The sediments resulting from the riverbanks' erosion are redeposited downstream or added to the floodplain during floods, which is called overbank deposition. During the river overflow, some alluvium is deposited on the banks forming levees (raised riverbanks). This water slowly seeps onto the floodplain and deposits a new layer of rich fertile alluvium. The underlined material of floodplains is a mixture of thick layers of sand and thin layers of mud.

All of the flood control plans including dams, dredging, and channel modifications may fail and put at risk the downstream towns and villages, built on the floodplain. Therefore, it is more logical to allocate floodplains to practices that are more compatible with flooding, such as agriculture or parks.

The floodplains in their natural form can also provide some benefits, including the following:

- Reducing the number and intensity of floods: In severe storms, water overflows the riverbank and spreads over the floodplain. This decreases the flow velocity and prevents severe erosion and flooding downstream.
- Reducing nonpoint water pollution sources: The vegetated floodplains filter contaminants out of the water flowing into the river. Furthermore, these floodplains provide shade for the adjacent rivers and streams, increasing dissolved oxygen levels.
- Filtering storm water: During increased water flow, some of the water is absorbed by the floodplain, delaying/preventing the river overflow. The absorbed water is returned to the stream in dry seasons.
- Providing habitat for plants and animals: The floodplains provide habitat for insects, birds, reptiles, amphibians, and mammals.
- Aesthetic beauty and outdoor recreation benefits: Some floodplains have forests and wetlands on or adjacent to them. Exceptional productivity of floodplains especially in arid areas is very important to the local economy.

Floodplain management is the operation of a community program of corrective and preventative measures for reducing flood damage. These measures take a variety of forms and generally include requirements for zoning, subdivision or building, and special-purpose floodplain ordinances.

There are countless scenarios for design application in modern floodplain management. Typically, the main objective of such applications is flood damage reduction. In a simple sense, this involves the reduction of flood levels for a given storm event, such that properties and structures are not negatively affected by high floodwaters. In many cases, the reduction of floodwaters involves the protection of human life as well. In other applications of floodplain management, designs are often employed to provide prevention of erosion at bridge structures and the protection of stream banks and other such physical features.

13.11.1 Structural Measures in Flood Management

The classic methods used in flood management are storage of floodwaters and increase in discharge capacity of the river system. Storage of floodwaters can be achieved either by storing (part of) the flood wave in upstream reservoirs or by storing floodwaters in riverine areas set aside for that purpose in the lower reaches of the river. Also, for the increase in discharge capacity of the river system, several methods are used, such as (i) deepening and widening of the existing river channel(s), (ii) introduction of additional floodways parallel to the river or conveying part of the flood to another river or to an another outlet into the sea, and, finally, (iii) flood embankments along the river.

All these methods have been used in the past individually or in combination, but many of today's main considerations are ignored when designing flood control measures. Such considerations are environment, ecology, nonstructural measures, risks remaining after implementation of the agreed measures, etc.

Nevertheless, it is worthwhile to describe the said classic methods in some detail as they are still at the basis of any form of flood management. The five classic methods used, as mentioned above, are

- Storage in reservoirs
- Storage in parts of the floodplain or other flat lands in the lower river reaches
- Improvement of river channel(s)
- Creation of additional floodways (so-called bypasses)
- Flood embankments

Generally speaking, it may be stated that reservoirs, channel improvements, and floodways have a regional impact on flooding while embankments are only effective locally. Also, the channel improvements and embankments sometimes result in more serious and frequent flooding elsewhere.

13.11.2 The Role of Nonstructural Measures

Nonstructural approaches to flood management comprise those activities that are planned to eliminate or mitigate adverse effects of flooding without involving the construction of flow-modifying structures. Structural approaches to flood management—dams, levees, dikes, diversions, floodways, etc. that provide some control of floodwater by storage, containment, or flow modification or diversion—may or may not be used conjunctively with nonstructural approaches but are not a prerequisite to the use of nonstructural measures. However, nonstructural measures should always be considered conjunctively in the planning and use of structural measures because of the potential for synergistic enhancement of their effectiveness. Under some river basin conditions, the introduction of nonstructural methods to limit flood damage may alone be more cost-effective than alternatives involving structural methods.

Nonstructural approaches to flood management fall naturally into two categories:

- Those anticipatory measures that can be assessed, defined, and implemented in the floodplains to reduce the risk to property from identifiable potential floods
- Those planned emergency response measures that are applied when a damaging flood is forecast, imminent, or underway, to help mitigate its damaging effects

Accordingly, a distinction is made between planning measures and response measures:

- Planning measures:
  Flood forecasting
  Control of floodplain development
  Flood insurance
  Flood proofing
  Catchment management
- Response measures:
  Flood emergency response planning
  Flood fighting
  Flood warning
  Evacuation
  Emergency assistance and relief

13.11.3 BMPs and Flood Control

Flooding is a natural phenomenon that cannot be prevented; therefore, flood control practices should focus on mitigation of flood damage instead of flood prevention. The government should help people through allocation of needed resources, to adapt their lifestyle to their natural environment. Some of these indigenous solutions are changing the housing structures and crop patterns for reducing flood damage. For a sustainable economic development and reduction of environmental degradation, good governance and appropriate environmental laws, acts, and ordinances are necessary. Furthermore, application of real-time flood warning systems can greatly reduce flood damage.

A better understanding of the processes that result in increasing flood damage can also help in more efficient mitigation of the adverse effects of floods on human lives, environment, and economy. For flood mitigation, both the government and the people should shift their paradigms and adopt BMPs in agriculture, forestry, land-use planning, water resources management, and urbanization. The flood BMPs will result in less runoff, more carrying capacity of drainage system, and

TABLE 13.10
List of BMPs and Their Effects on Flood Mitigation

BMPs	Expected Effects on Mitigation of Flooding
Dredging rivers and streams	Increase carrying capacity of drainage
Re-excavation of abandoned channels, ponds, and lakes	Increase carrying capacity of drainage, reduce runoff
Dispersal of dredged/excavated sediments on lands	Increase elevations of earthen roads and village platforms
Conservation tillage	Reduce soil erosion and runoff
Establishment of vegetated buffer zone along rivers and streams	Reduce soil erosion, runoff, and bank erosion
Silt fence around construction sites	Reduce soil erosion and runoff
Sediment and runoff detention ponds in construction sites	Reduce soil erosion and runoff
Removal of coastal polders	Increase land elevation by tidal inundation
Planned urbanization and compact township	Reduce impervious surface and runoff
Efficient storm sewer systems in cities	Increasing carrying capacity and reduce waterlogging in cities
Watershed-scale land-use planning	Reduce soil erosion, runoff impervious surface, sustainable economic development
Reforestation programs	Reduce soil erosion and runoff
Good governance, self-reliance, and implementation of environmental acts	Implementation of BMPs to mitigate flooding problems, sustainability in economy and environment
Integrated regional water resources development plan for basins	Flood/drought control, optimal uses of natural resources in the region, sustainable environment and development

increased land elevations with respect to sea level or riverbeds. Table 13.10 summarizes the BMPs and the expected effects on mitigation of flooding problems.

13.11.4 Watershed Flood Early Warning System

The need for flood early warning systems is identified as the way forward in pre- and post-flooding incidents for the major watersheds. A flood warning system reduces the damages downstream of a reservoir by continuous and active monitoring, attending to the readiness of reservoir conditions, and flood control capacity building in the reservoir.

Flood warning algorithms are the simplest and easiest flood warning systems handled by a manual operation. These systems are outfitted with simple gauges in the critical points of the system. The data are reported to the system manager. The system manager uses real-time hydrometeorological data to estimate flood events through predetermined tables and algorithms. The predictions can be included in determining the return period of the flood, the peak discharge of the flood and the time the flood reaches the reservoir as well as the time of concentration of each sub-basin. Three groups of instruments are needed for developing a flood warning system:

- Measuring instruments: These instruments are set up in the meteorologic and hydrologic stations and collect hydrometeorological data automatically.
- Hardware instruments: This group of instruments includes computers, data transfer tools, and receiver and amplifier centers.
- Software instruments: Databanks, data processors, flood prediction models (including rainfall–runoff and flood routing models), visualization models, and user interfaces are included in this group.

In this chapter, as an example, a general framework for the design of a flood warning system for the Kajoo watershed located in the southeastern part of Iran is presented (Figure 13.16). A main

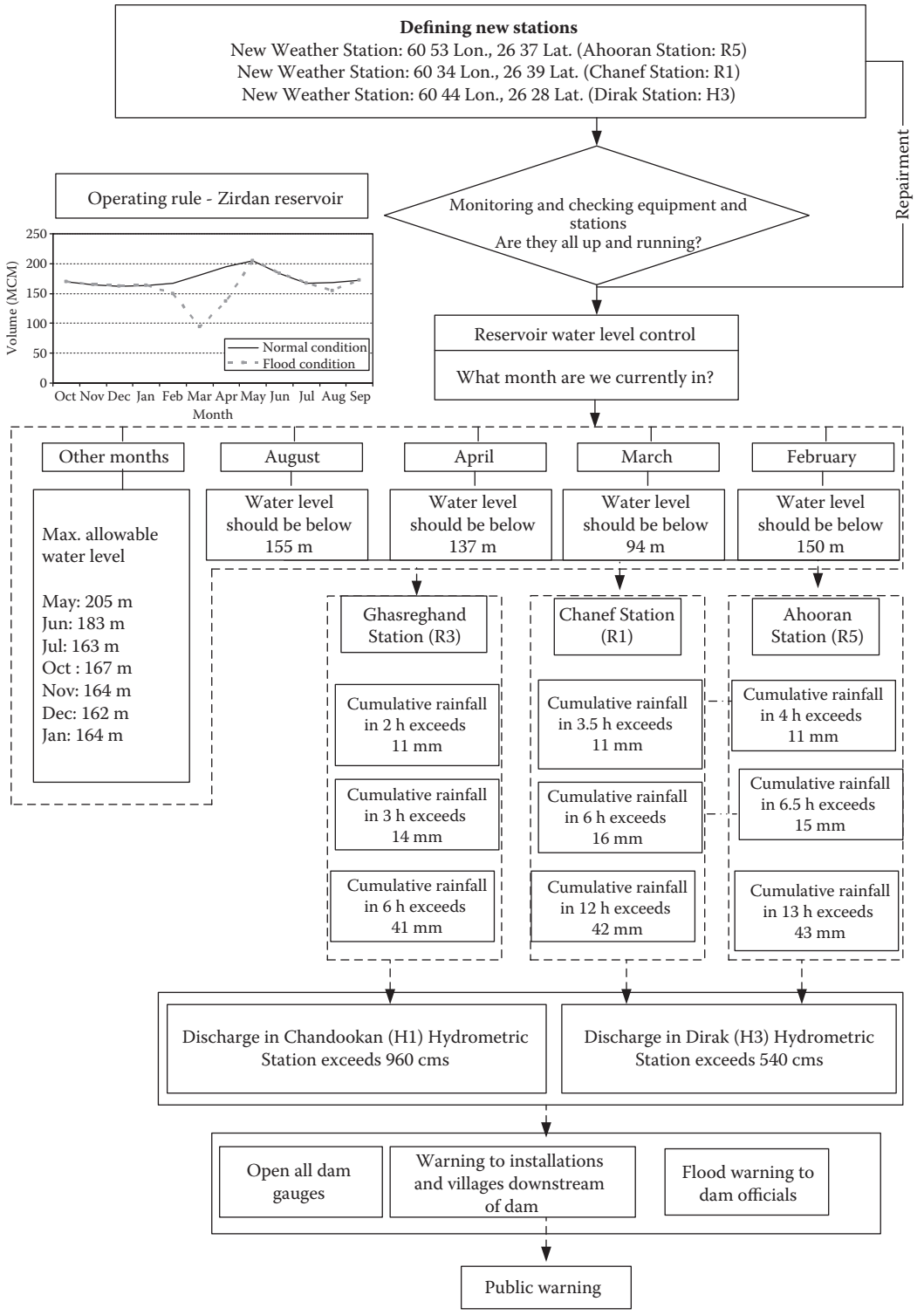

FIGURE 13.16 Flood warning system algorithm.

component of this flood warning system is the assessment of the observed cumulative precipitation in the upstream climatic stations as well as the observed flood hydrograph in the upstream hydrometric stations. To forecast floods, control points have to be determined and flood characteristics can be estimated once the precipitation is observed using rainfall–runoff models such as HEC-HMS. This flood warning algorithm is developed based on the data from weather and hydrometric stations upstream of the watershed. The components of this algorithm are rainfall and runoff thresholds, corresponding time of thresholds in existing and proposed stations, and the state of reservoir management, including the flood control capacity and the river carrying capacity downstream of the reservoir. Floodplains can be determined using the HEC-RAS model and different warning levels can be announced depending on the expected flow progression in the floodplains.

This type of system could provide early warning to other reservoir–river systems and could be utilized if the information about upstream weather and hydrometric stations could be gathered in a timely fashion. This information will guide the decision makers and/or operators to lower the water level in the reservoir and/or undertake other flood control alternatives. It will also give an early warning to farmers and the public.

13.11.5 Flood Insurance

Flood insurance is one of the approaches to reduce vulnerability in flood risk assessment. Disaster vulnerability and poverty are mutually reinforcing. Low income, poor housing and public services, and lack of social security and insurance coverage make poor people behave in a way that puts them at greater risk. Since natural disasters greatly affect poor people, specific policies and strategies are required for tackling the link between poverty and disaster vulnerability.

An effective way for lessening damages and increasing resiliency is risk sharing and transfer at national, community, and household levels (UN/ISDR 2002). An example of this approach is insurance. Insurance can improve the situation of individuals by compensation and spreads the risk of disaster across society.

In the 1960s, nonstructural measures, such as warning systems based on real-time flood forecasting techniques, floodplain zoning to restrict occupancy of the plain to certain uses, local flood proofing, and flood insurance programs, started to receive more attention in flood risk management. Therefore, flood insurance has often been advocated as a long-term nonstructural measure for building resilience among flood victims. The unsatisfactory status of flood insurance in developing countries, however, shows that financial support mechanisms (subsidies, funds, and loans for spreading the financial burden in terms of equity and fairness) should be combined in flood management to incorporate equity with economic effectiveness.

Flood insurance is an effective way for reducing economic vulnerability especially in industrialized societies. Insurance is a classic form of risk sharing since it distributes financial risk approximately evenly among all policyholders. However, for the poor people, who are more vulnerable to floods, flood insurance is often economically unfeasible. In such cases, cooperation between the government and insurance companies is necessary in order to encourage the latter to provide affordable flood insurance policies for low-income groups. Risk-adequate insurance premiums are distributed spatially as a function of the size of the risk community to make premiums more affordable by enlarging the number of policyholders (APFM 2008).

In spite of the various efforts for mitigating flood damage, floods damage properties and interrupt economic activities. Some of the tangible losses are absorbed by the retained risks (a component of general risk). In a systematic risk management process, for sharing the cost of recovery, some of the tangible risk is transferred through insurance as the last step. Insurance has different benefits: it protects capital, enhances solvency, and allows recovery. A well-designed insurance scheme could also encourage risk reduction behavior. For small-scale floods, which are usually predictable, risk reduction methods are more advisable. High-risk floods (low-probability and high-consequence events) easily destroy the insurance market. Therefore, insurance instruments are appropriate for middle levels of risk.

13.12 CASE STUDIES

So far in this chapter, different issues related to floodplain management, the use of BMPs in flood management, and climate change impact on flooding have been discussed. In the next subsections, some case studies that will show the applications that can be used in practice will be discussed.

13.12.1 Case Study 1: Probabilistic Optimization Model for Floodplain Management

In Integrated Flood Management in the watershed, the river is a dynamic system in time and space. The upstream flood control options have a significant effect on the flood control options and flood flow characters downstream of the river. Floodplain and land use should be managed considering hydraulic and economic issues of floodplains within the context of flood risk management. Karamouz et al. (2008) presented a probabilistic optimization model for determining structural flood control options and crop pattern along the Kajoo River.

The Kajoo watershed is located in the southeastern part of Iran and the Kajoo River is the main river of this watershed, which is 254 km long and runs from the north to the south of the watershed and which reaches to Gouatr Bay in the Oman Sea. Because of the limited carrying capacity of the Kajoo River, yearly floods cause lots of damage in the agricultural fields. The cross sections downstream of the river are too tight and the carrying capacity of the river is too low in these sections. Therefore, the downstream floodplain is too wide and structural flood control options are needed.

In this study, the optimal combination of flood control options is determined using the Genetic Algorithm, which minimizes flood damage with different return periods (25, 50, 100, and 200 years) and costs of flood control alternatives. In order to consider the effects of flood control options on the hydraulic characteristics of flood, two hydrological routing models for the reservoir and the river are coupled with the optimization model. In the optimization model, different types of discharge–elevation and elevation–damage curves are obtained for each configuration of flood control options along the river based on hydraulic routing of floods. The parameters of a hydrologic river routing model are calibrated based on the result of the hydraulic routing model.

Figure 13.17 presents the flow chart and different steps of the proposed methodology for probabilistic floodplain management of the present case study. As shown in Figure 13.17, the proposed methodology consists of two separate parts: an optimization–simulation model and a river hydraulic simulation model. Considering this figure for the calibration of hydrological routing parameters in different reaches, a hydraulic simulation model (HEC-RAS) was developed simultaneously. One of the important tasks of the hydraulic routing model was to develop the discharge–elevation–damage curves in each reach along the river. The probability of flood occurrence is incorporated to discharge values for different return periods. The damage data are scarce in the study area, and using them requires a careful economic analysis of different consequences of flood occurrences including damage to agricultural products and residential properties. The damage under different flood return periods were estimated based on flood routing, floodplain zoning, and the cost of floodplain per square meter.

The storage routing method is used for reservoir flood routing for floods with different return periods. Using the hydrological routing model, the outflow hydrograph of the reservoir for each level of the spillway is obtained for floods with different return periods.

In this case, the Muskingum method is used for hydrological flood routing in the river. This is a simple and well-cited method that works just as well as the sophisticated methods that are more data intensive and are more difficult to calibrate with the limited data available in the case study mentioned here. To estimate the hydrological routing parameters (k and x) and to calculate the discharge–elevation and the damage–elevation curves in each reach of the river, unsteady- and steady-state hydraulic simulation of the river are used. By using these curves, the routing model can estimate the damage in each reach of the river. By calculating the flood damage and the construction costs of flood control options in each reach, the objective function can be assessed.

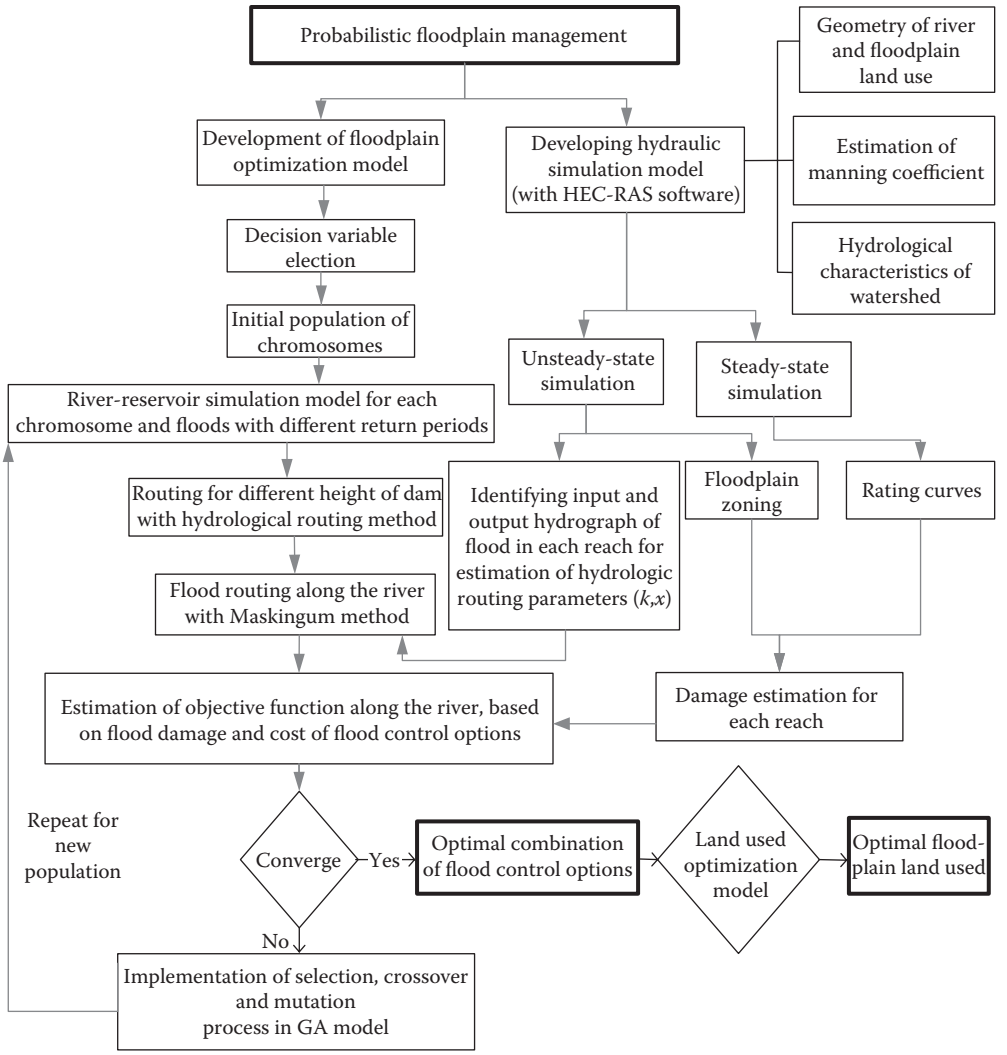

FIGURE 13.17 Flow chart of the proposed methodology of case study 1 for probabilistic optimization model of floodplain management (Karamouz et al. 2008).

The results of the optimization model recommend the construction of a levee downstream of 6 out of 14 reaches in the watershed. There are too many villages and sizable agricultural activities in the study area. Based on the results of the optimization model, the optimal combination and height of different flood control options are obtained. In order to manage future development in the study area, the model provides a better combination of land use among the given alternatives. The results of this case study demonstrate the integration of various flood damage reduction schemes by implementing different flood control and crop pattern options along the river. The results show the significant value of the proposed model in floodplain management.

13.12.2 Case Study 2: Improvement of Urban Drainage System Performance under Climate Change Impact

In recent years, climate change and its consequences have affected flood characteristics especially in urban areas. In this way, incorporating the climate change effects in urban flooding studies can

help achieve more reliable results that will be applied in real-time planning of urban areas through selection of BMPs. Karamouz et al. (2011a) proposed an algorithm for selecting the BMPs in order to improve system performance and reliability in dealing with urban flash floods, considering the anthropogenic changes as well as climate change effects. The suggested algorithm is applied in the Tehran metropolitan area, as a case study.

In recent years, Tehran, the capital of Iran, has undergone rapid development without considering the diverse impacts this may have on the environment especially the water cycle. This has resulted in a wide range of challenges and obstacles in water- and sanitation-related infrastructures in the area. Lack of a systematic approach to runoff management in Tehran has led to the frequent overflow of channels and some health hazard problems in rainy seasons. This case is a mountainous area with high population density. Therefore, urban floods can cause considerable damage and the evaluation and simulation of the effects of flood in this area are very important.

The drainage system of the study area is composed of natural and man-made channels. These channels carry large amounts of sediments especially during floods, which drastically decrease their safe carrying capacity. These channels are used as a combined facility for surface water and wastewater drainage and snowmelt discharge.

In recent years, some river training projects have been performed on these channels, which have changed the characteristics of the surface water collection system. For evaluation of the effects of these projects on the runoff collection system of Tehran, three scenarios have been considered:

Scenario 1: In this scenario, the surface water collection system of about 10 years ago is simulated.

Scenario 2: In this scenario, the present surface water collection system of Tehran is modeled. The effectiveness of development projects utilized in recent years for improving the performance of the drainage system is evaluated in this scenario.

Scenario 3: Future plans for the improvement and development of the drainage system of the case study have been modeled in this scenario. Here, a channel and two detention ponds are added to improve the performance of the drainage system.

The possible changes in rainfall pattern of the study area under climate change impact are simulated. The effectiveness of present and future planned projects for the improvement of drainage system performance in transmitting urban floods is evaluated under different scenarios. Also, the effect of solid wastes and sediments carried with surface runoff on system performance is considered. In suggestion of BMPs, feasibility and effectiveness are related to the cost and benefit.

In this case, an algorithm is developed for evaluating the performance of the urban drainage system considering development projects and climate change effects. Three scenarios—past, present, and future—for the drainage system have been considered. The proposed algorithm for evaluating climate change impact on the urban water drainage system is illustrated in Figure 13.18.

The downscaling model used in this case is SDSM. In this study, StormNET developed by Boss International (2005) is used as a rainfall–runoff model. Information on channel and pipe links, snow packs, sub-basins, detention ponds, and flow diversions is needed to develop this model. In order to choose the critical daily rainfall of each season that may result in a flood, the maximum value of each season's rainfall is selected among the rainfall data of each year as the most critical rainfall of that season of that year.

To provide a realistic configuration of the performance of the urban drainage system, simultaneous simulation of rainfall and sediment load during flood is needed. For this purpose, the Copula theory has been used in this study to calculate the joint return period of rainfall and sediment. Investigation of the sediment data shows that the sediment load in the spring and winter is much more than that in the fall and summer, and sediment load is at a minimum level in the summer. According to the available reports on recent floods, the volume of channels that have blockage problems has decreased based on the sediment data in each season. Then, the model is analyzed for different sediment loads in different

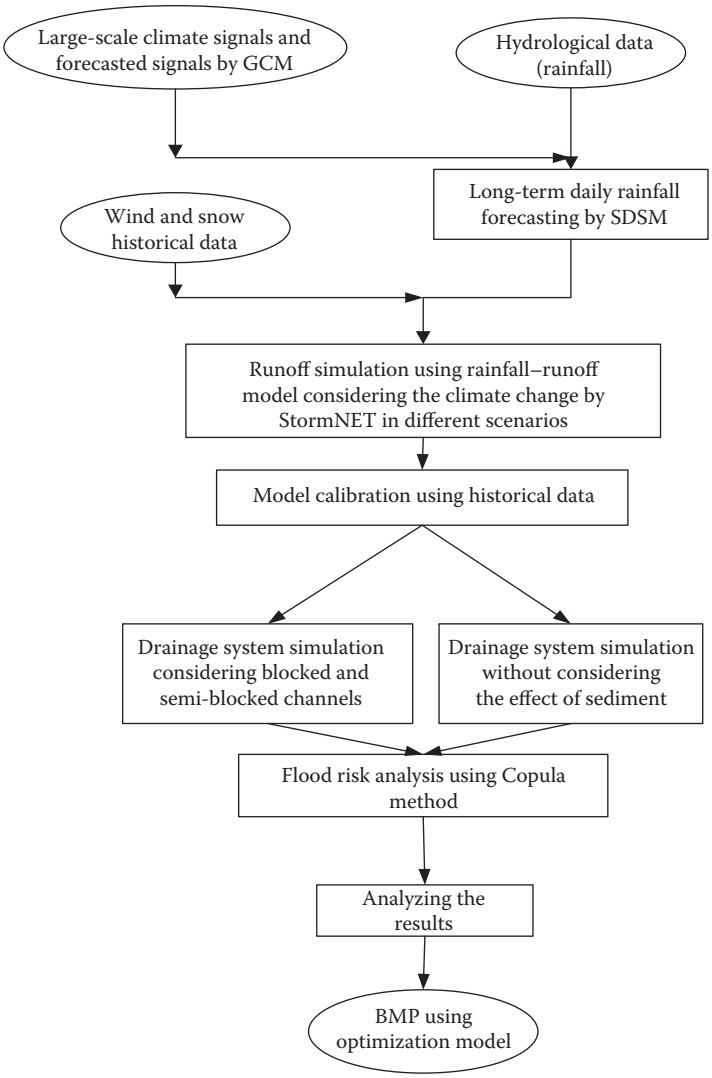

FIGURE 13.18 Proposed algorithm of case study 2 for the improvement of drainage system performance in urban areas.

seasons. In these models, the 20-, 50-, 100-, and 200-year return period rainfalls are considered. The results of a 20-year return period rainfall are shown in Figure 13.19.

The volume of surface flood of the entire study area in scenario 3 is a little less than that in scenario 2 (an average of 5%) due to little improvement of the drainage system performance in scenario 3 in dealing with high sediment loads. However, because of the decrease in perviousness in scenario 2, the surface flood volume of the entire study area has been increased by about 40% in comparison with the first scenario. Factors such as urbanization, which has destroyed green space and replaced it with impervious structures, and construction regardless of the channels' right of way result in high flood volumes in scenario 3.

The joint return period of rainfall and sediment is considered in this study for flood risk evaluation. The results show that the frequency of flood events will considerably decrease in the future owing to climate change effects and modification of drainage systems.

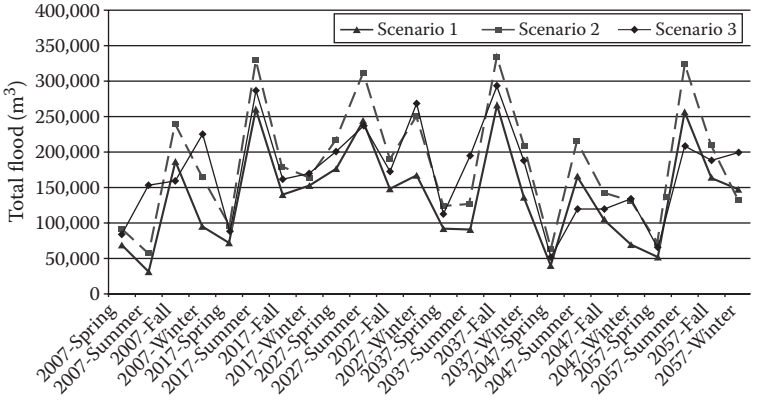

FIGURE 13.19 Surface flood of total basin in different seasons (considering sediment).

The study area has a short concentration time because of steep slopes especially upstream. In this kind of situation, enhancing the density of grasslands can help lag the peak time of urban floods. Since the upstream sub-basins of the study area are nonresidential, enhancing the green space, which results in an increase of soil penetration and a decrease of soil erosion, is considered as a BMP. Also, due to steep slopes of upstream mountainous sub-basins, detention ponds are proposed to decrease flood hazards by increasing the lag time of the flood peak as well as decreasing the sediment load. The land-use pattern of the study areas should be cautiously considered when increasing the capacity of the existing channels. Since developing a closed channel system is more reasonable and economical in an urban area, it is also considered as another BMP. The risk of flooding is drastically increased downstream of junctions that receive large channels. In these cases, some part of channel flows can be diverted to adjacent channels with less flooding risks and damages or extra capacity for safe stormwater transfer. Therefore, the development of appropriate diversion systems is considered as another BMP in developing flood management schemes in the study area.

The BMPs' performance is evaluated through their employment in scenario 3 of the watershed drainage system considering the climate change effects on rainfall and sediment. An optimization process is followed to determine the optimal BMPs and their location in the drainage system. Since the considered case study here has limited choices for application of BMPs, the optimal composition of BMPs is determined by evaluating all possible situations with regard to the objective function and constraints of the proposed optimization model. In this optimum BMP, the total cost of flooding in the study area has decreased about 75% in comparison with the condition that no BMP is developed.

Using the optimal combination of BMPs in the study area has resulted in a significant decrease in flood volume and flooded area, especially at downstream sub-basins. The results show that in the future, because of climate change effects, the intensity of extreme events will decrease. The results of the study show that the probability of accruing flash floods with high intensity in short time periods is increasing also the best way to decrease the risk of floods in urban areas is to pay more attention to waterways and maintain their capacity.

13.12.3 Case Study 3: Evaluation of Floodplain Variability Considering Climate Change Impacts

Considering uncertainties in floodplain determination is an important issue in site selection of regional infrastructures. Also, changes in hydrological condition due to climate change and river morphological characteristics are other important issues impacting the floodplain extent. Karamouz et al. (2011b) proposed a methodology for considering hydraulic uncertainties in floodplain analysis

in the Kajoo River located at the southeastern part of Iran. In the study area, the irrigation fields located in the floodplains are subjected to flood hazard every year. Determination of floodplain uncertainty can be used for flood damage reduction through characterizing the activities needed for overcoming flood hazards. Because of the potential for cultivation of the riverbanks, a good portion of floodplains are used for agriculture by local farmers. The general arid nature of this region forces the local population to live and farm near the river downstream of the reservoir to take advantage of the slightest water/soil moisture. Therefore, flood management aimed at decreasing damages and increasing available water resources by controlling and storing floodwaters is a matter of regional importance. Kajoo is a seasonal river with frequent flash floods that affect the river's morphology and change the carrying capacity of the river and the floodplain extent.

River morphology is an important characteristic of river flood and is affected by sedimentation and erosion in the river's path. The depth and the width of a river's cross section highly change (expand or decrease) due to sedimentation and erosion resulting in floodplain extension. To incorporate the uncertainties in determining inundated region boundaries, the mean first-order second-moment (MFOSM) analysis is employed.

Climate change is another factor indirectly affecting the characteristics of the floodplain. Climate change alters the magnitude, extent, and depth of inundation, resulting in intensified flood problems. Therefore, it is necessary to simulate the future rainfall pattern of the study area under climate change. Then, the floodplain extent is determined through a hydraulic routing model. To evaluate flood inundation probability, the Copula function was used to estimate the joint probability of the changes of the inundation area due to changes in river morphology and the rainfall changes due to climate change impacts.

The proposed methodology consists of three parts, and the algorithm and different steps of this study are shown in Figure 13.20. Part A deals with rainfall and flood projection utilizing General Circulation Model (GCM) outputs, part B is about evaluation of uncertainties based on floodplain simulation, and part C discusses assessment of the impacts of the river's morphological changes on the floodplains.

In part A, rainfall is simulated for future conditions using the effective climatic predictors based on the GCM output data through the statistical downscaling method. In this process, 100 ensembles of downscaled daily rainfall have been generated. In the next step, a rainfall–runoff model is used to simulate the floods by way of the Soil Conservation Service (SCS) method. Also, the simulated flood hydrograph is chosen based on its similarity to the observed trend, which is used to calibrate the model. In part B of Figure 13.20, the simulated floods based on generated rainfall are routed through the river's cross sections for the assessment of floodplain uncertainties. The HEC-RAS model, a hydraulic routing model, is applied to simulate the river and floodplain zoning in an unsteady state and then the floodplain boundaries are determined. In part C, HEC-RAS in steady-state flow condition is simulated based on flood discharge with different return periods and the floodplain extent is determined. Then, the impacts of river morphology changes on the floodplain extent are assessed. In addition, a probability distribution of flood hydrograph peak is fitted to determine the probable flood, and consequently, the floodplain variations are estimated. Next, based on the results of the inundation area and the rainfall, the joint probability of these two factors is evaluated.

In this study, the HEC-RAS model is used to simulate the floodplain zoning downstream of the reservoir. The results can be used to determine the floodplain uncertainties due to river morphology changes and climate change impacts. This model simulates the one-dimensional flow in both steady and unsteady states and for subcritical, supercritical, and mixed flow regime. It should be mentioned that the unsteady state is more accurate in flood routing. HEC-RAS computes the surface water profile by a standard step-by-step method solving the energy equation for different river cross sections. Also, in the unsteady-state condition, the model uses the numerical finite difference method to solve Saint Venant equations for developing the discharge–elevation curve. In this work, the river's geometric form is considered as the model input to simulate each river section bank. The meanders

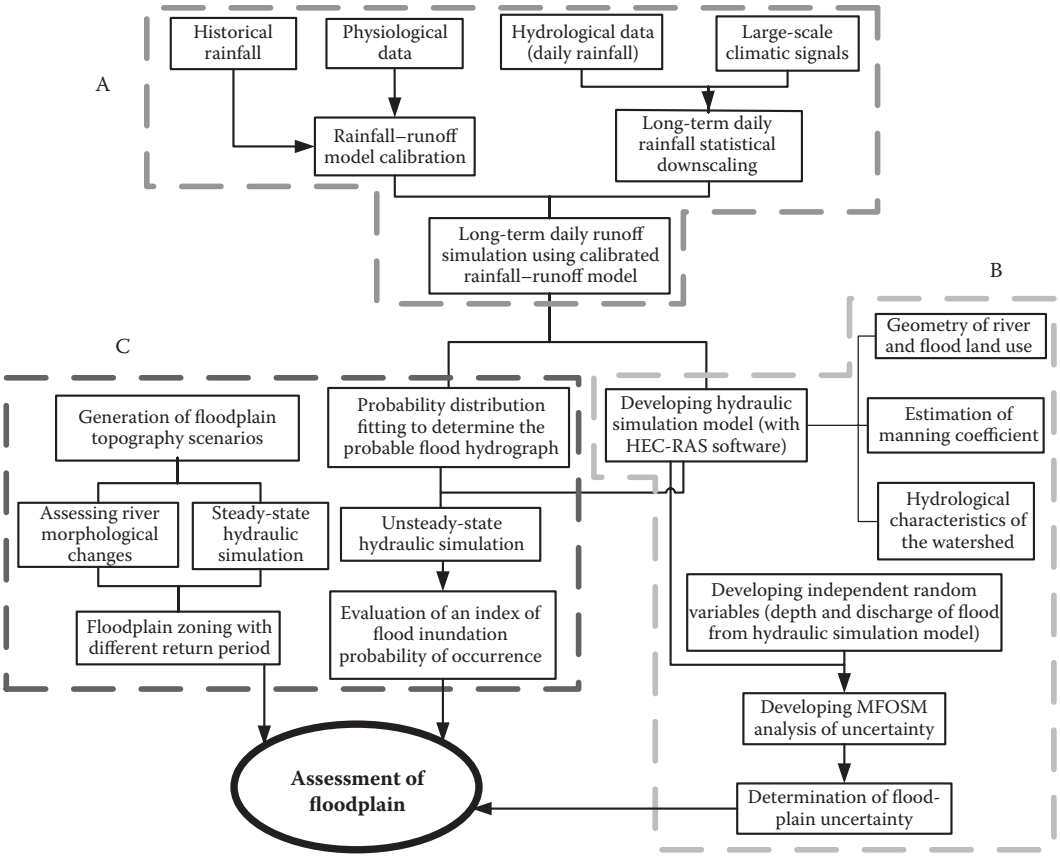

FIGURE 13.20 Flow chart of the proposed methodology of case study 3 for the evaluation of floodplain variability considering climate change impact.

are simulated based on the distances between the main channel, right channel, and left channel in the model. Three values of Manning's coefficient are needed to be determined for the main channel, the left channel, and the right channel.

In order to evaluate morphological changes, first, the floodplain for a 25-year return period flood is simulated by HEC-RAS in years 2002 and 2007. Their differences in some cross sections are noticeable. As illustrated in Figure 13.21(b), the floodplain of surveyed cross sections in 2007 increases about 8600 m in comparison with Figure 13.21(a). The floodplain tendency of changes is shifted toward the right bank of the river.

Determining the inundation zone could give early warning to some residents' activities near the river, thus leading to a decrease in damage due to flooding. In this study, the Copula function is utilized to estimate the joint probability of the changes of the inundation area due to changes in river morphology and the rainfall changes due to climate change impacts. The use of the Copula function in the probability and statistics field has been growing during the last decade. The original definition of the Copula function is given by Sklar (1959). It is concluded that river morphological changes in the study area (and not rainfall variations) are the main reason for floodplain variations.

The results of this study show that the uncertainties of floodplain extent are affected by climate change and river morphology leading to noticeable changes in flood magnitude and frequency. Investigating the impacts of these factors and estimating the corresponding river discharges from rainfall values will help in the present (and future) study of river dynamics and also contribute towards devising effective mitigation and management strategies.

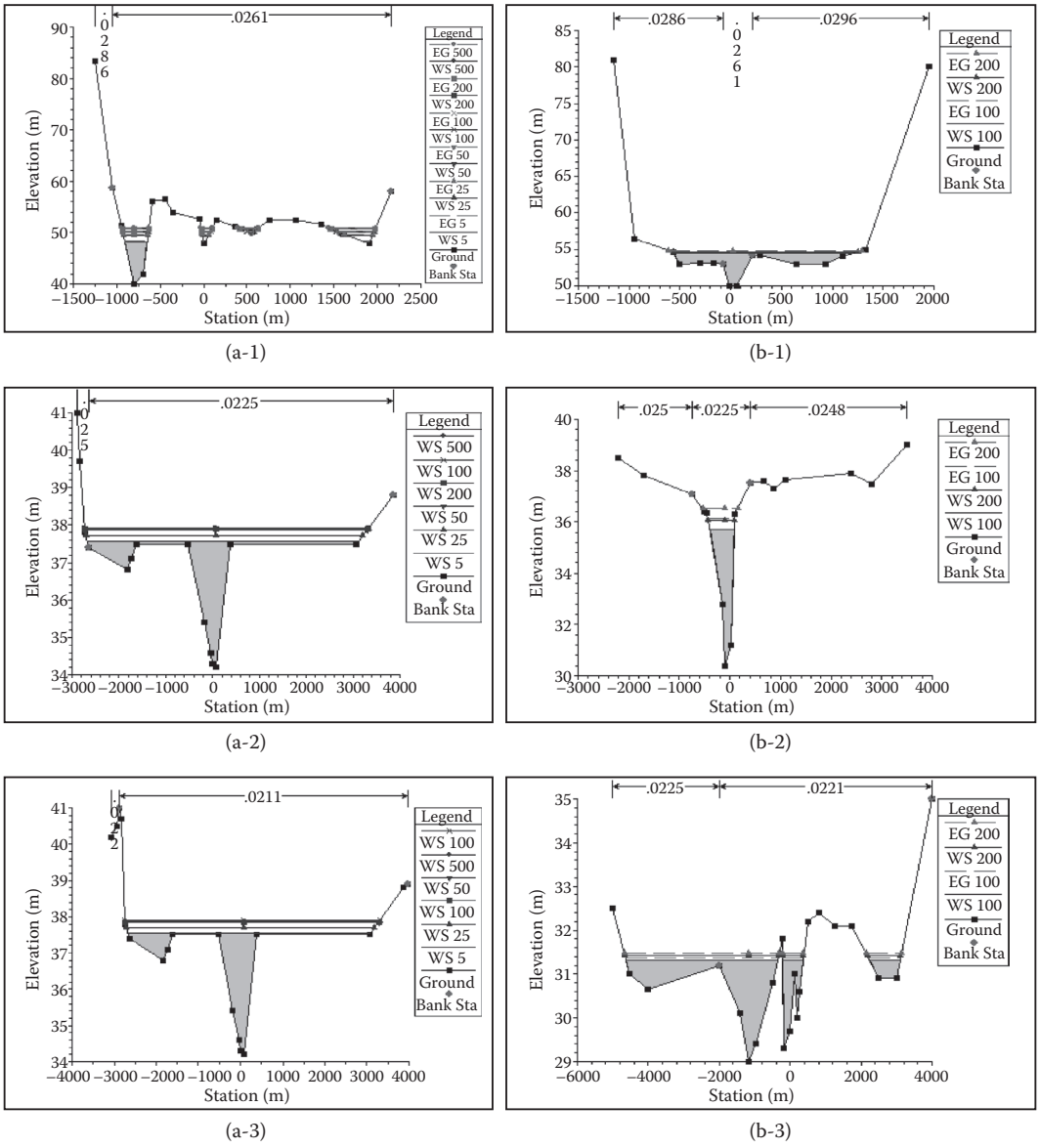

FIGURE 13.21 Floodplains based on surveyed cross sections in (a) 2002 and (b) 2007 for three river sections along the studied river.

Applying the proposed method and strengthening the warnings and forecast systems in the region not only could minimize the risk of flooding but also could be key factors in reducing social and economic impacts due to floods.

13.12.4 Case Study 4: Optimal Flood Management Options with Probabilistic Optimization

Flooding causes significant damage to local populations and infrastructure near the river, and knowing the risk of flood occurrences can increase the accuracy of estimation of expected flood damage. Therefore, an integrated approach for floodplain management could significantly reduce

the damage. Karamouz et al. (2009) presented a risk-based optimization model for determining flood management options. The proposed methodology is applied to the Sefidrud River, which is located in the largest watershed in the central and northern part of Iran.

The proposed model minimizes the flood damage and costs based on optimal flood management options such as structural, nonstructural, emergency, and permanent actions in a probabilistic framework considering risk in decision making. In the optimization model, different discharge–elevation–damage–probability curves are used as the inputs, which are developed based on routing of floods with different return periods. In this study, the HEC-RAS model is used for hydraulic routing of floods with different return periods along the river considering different types of flood management options. The estimated flood damage is the basis for comparing different options and determining appropriate actions.

Figure 13.22 shows the proposed model flow chart. As shown in this figure, in step 1, flow data needed for the simulation model are collected. These data consist of river cross sections, land use, hydrological characteristics of the river, and topography of the river basin. In step 2, the collected data must be analyzed and processed. This processing includes fitting a statistical distribution to annual maximum flood peaks. The probabilities of different flood events are used to obtain flood discharge with different return periods. These probabilities are obtained through the PDF of flood peaks and are used in the HEC-RAS model. HEC-RAS simulates the flood routing in the main channel and determines the extent of floodplains. This routing of floods is done in step 3 for different reaches of the river. According to the result of the simulation model, damage can be estimated by the elevation of water in the floodplain. The results of the simulation model are coupled in four curves representing discharge–depth–damage–probability distribution. These curves provide the needed input data for the optimization model in step 4. These curves are discharge–elevation, discharge–probability, elevation–damage, and damage–probability, which are obtained in step 3. Selecting the better options for flood control in the river and the floodplain is the most important task in step 4. These options are the decision variables in the optimization model. In step 5, the value of damages is estimated based on the level of water in the floodplains considering the simulation results of step 3 and the decision variables of step 4. Also, the construction cost of flood control options is estimated to calculate the total cost of different alternatives along the river that are estimated in this step. The estimated damage and costs are entered into the optimization model in the final step (step 6) to select better alternatives. In the end, an economic analysis on the results of the optimization model is performed to help decision makers.

As mentioned before, the HEC-RAS software is used for hydraulic simulation of the river and routing floods along the river. The discharge–elevation curve (rating curve) is an output of this model that shows the stage of water in the floodplain. These curves are estimated for all cross sections along the river. All cross sections must be classified into groups with respect to the number of reaches in the river. A total discharge–elevation curve is needed for each reach of the river, and therefore, the weighted average is used to determine the hydraulic depth or flooding area in each reach.

The record of past floods and their peaks is processed, and a flow duration curve (FDC) is developed for different return periods using a Weibull distribution. The discharge–probability curve is generated by the FDC.

There are two types of damage associated with an increase of the water level in the floodplain (financial damage and loss of life). The values of these are different for different types of land use and they are estimated according to the flooding area. They are estimated separately for all reaches along the river (Table 13.11). Hence, the damage–elevation curves are obtained for each reach of the river on the basis of the flooding area and the water level for different land uses.

The results of this case demonstrate the integration of various options in flood damage reduction and show the high potential of this approach in floodplain planning and management. The results also show the significant value of using the probabilistic approach in flood management and its applications in decision making.

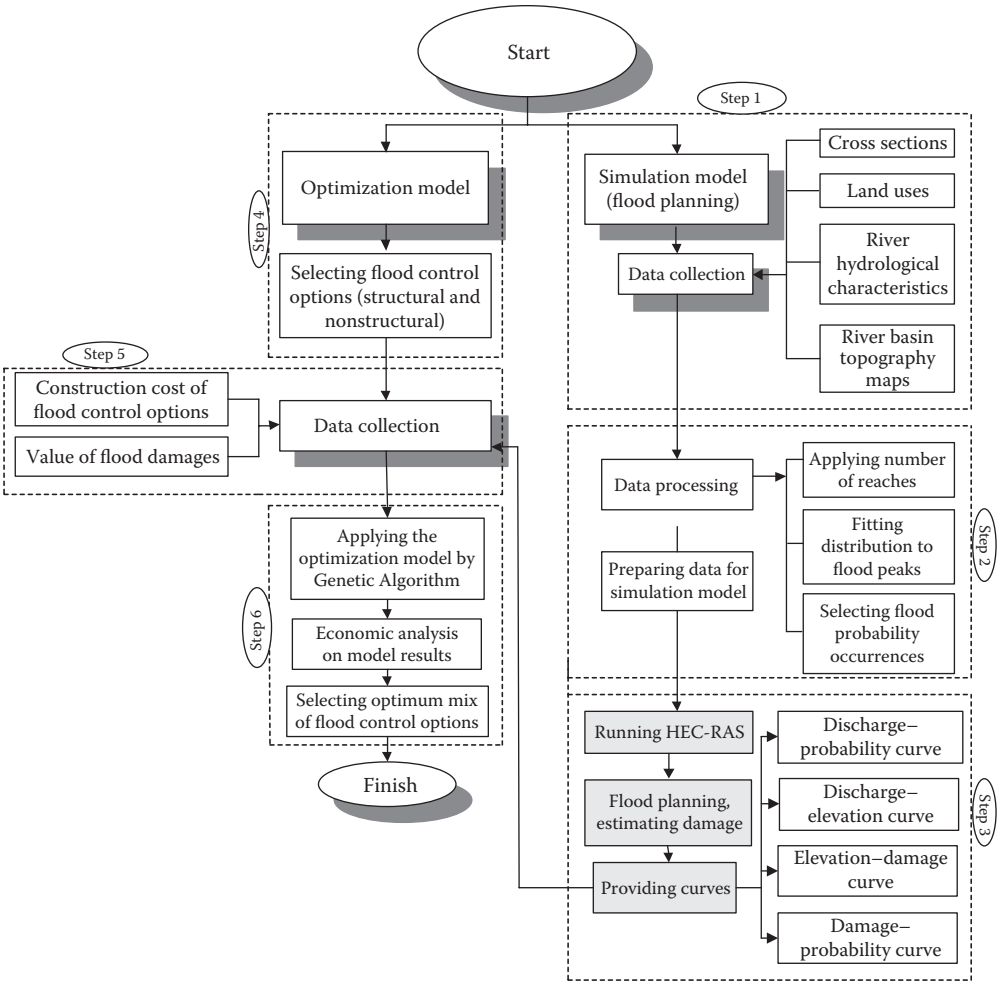

FIGURE 13.22 Flow chart of the proposed algorithm of case study 4 for optimal management options with probabilistic optimization.

The innovative aspect of this study is the application of HEC-RAS modeling with the Genetic Algorithm optimization model utilizing discharge–elevation–damage–probability curves. According to the results, by investing about $2.4 million for the construction of flood control and warning measures along the river, the expected value of damage is reduced to $118 million. This considerable gain shows the significant value of utilizing the proposed approach.

TABLE 13.11
Percentage of Financial Damage for Different Land Uses

Water Elevation (m)	Industrial Damage (%)	Agricultural Damage (%)	Residential Damage (%)
0–0.5	28	0	14
0.5–1.0	50	50	25.9
1.0–1.5	75	75	34.2
1.5–2.0	80	87	35.5
>2	100	100	100

13.12.5 Case Study 5: Evaluation of Climate Change Impact on Regional Flood Characteristics

Occasional tropical or monsoon rains could produce floods that are sometimes beneficial especially in arid and semiarid regions where water is scarce. By simulating the hydrograph of probable floods in each year, action plans could be implemented to reduce damage and also better plan for utilizing the potential of flood as a water resource. By simulating future rainfall and estimating the resulting runoff, whether a severe flood would occur or not could be determined. The simulated flood hydrograph is affected by uncertainties in future rainfall simulation and runoff modeling that should be considered when flood prevention plans are developed. Karamouz et al. (2007) developed a long-lead flood simulation model, considering the uncertainties in the simulation process. The proposed model for long-lead flood simulation has been applied to the Kajoo basin located in the southeastern part of Iran.

This area is the Zirdan dam sub-basin of the Kajoo River basin (with an area of 3659 km^2) in the South Baloochestan region. Because of the limited flood carrying capacity of the Kajoo River, yearly floods cause damage to agricultural land and rural areas.

In this study, the SDSM is used to generate hourly and daily rainfall data, needed for flood simulation, based on GCM outputs. The extreme simulated rainfalls in each year are considered as a probable flood, and a rainfall–runoff model developed using the HEC-HMS software environment and the SCS method is used for simulation of the corresponding hydrograph. The available rainfall data of the 1991 flood are converted to the hourly hyetograph that is needed for rainfall–runoff model calibration. This has been done using the central pattern of the SCS hyetograph. This pattern has a monotonic and steady intensity during rains, which is the same as the observed rainfall pattern in the study area.

The uncertainties in hydrograph development are considered through variation of curve number (CN) and time of concentration (T_c). An average CN of 85 for moderate humidity antecedent moisture condition (AMC-II) has been estimated for the basin. In this study, uncertainties of long-lead flood simulation in each year are analyzed using two approaches: first, uncertainty analysis of the results of rainfall simulations that are used for future flood simulation, and the second, evaluation of uncertainty in simulated floods by a rainfall–runoff model.

The effect of climate change on flooding probability is evaluated by comparing the CDF of the simulated floods with historical floods. To consider the effects of future climate change on the probability of exceedance of flood events, the CDFs of simulated rainfall and flood values in 1976–1999, 2000–2020, and 2020–2040 are developed (Figure 13.23).

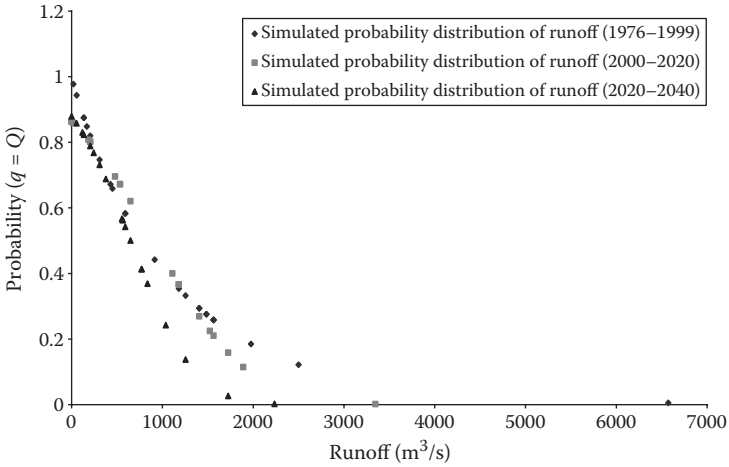

FIGURE 13.23 Flood (maximum runoff) distribution for 1976–1999, 2000–2020, and 2020–2040. (From Karamouz, et al., *Iranian Journal of Science and Technology* [forthcoming], 2012. With permission.)

Figure 13.23 shows the corresponding probability of exceedances of historical rainfalls and floods in the CDF of different periods, which are compared to evaluate the effect of climate change on hydrological events. The derived simulated rainfall CDF shows that for the low-end rainfall values, the probability of exceedances is increasing, but for higher rainfall values, the probability of exceedances is decreasing. This is also true for flood events. It can be concluded that the severity of the rainfall and flood events in the study region is decreasing due to climate change effects. Finally, the results of this study show the significant value of developing tools for contributing uncertainties in long-lead flood simulation.

PROBLEMS

1. Estimate the 25-year and the 100-year peak discharges using the data in Table 13.12. The map skew for this location is –0.015.
2. Using the data in Table 13.13, compute the 25-year and the 100-year peak discharges. The map skew for this location is 4.4.
3. Use the data of Table 13.14 to estimate the 10-year and 200-year peak discharge using the log-Pearson Type III distribution.
4. In Problem 5, what is the 100-year flood using the normal distribution?

TABLE 13.12
Annual Peak Discharge in Problem 1

Year	Annual Peak Discharge (m^3/s)	Ranked Annual Peak Discharge (m^3/s)	Weibull Plotting Position	y	y^2	y^3
1962	2930	2190	0.521	3.34044	11.15854	37.27443
1963	574	1960	0.542	3.29226	10.83898	35.68473
1964	159	1800	0.563	3.25527	10.59678	34.49539
1965	1400	1750	0.583	3.24304	10.51731	34.10805
1966	1800	1510	0.604	3.17898	10.10591	32.1265
1967	2990	1420	0.625	3.15229	9.93693	31.32409
1968	4470	1400	0.646	3.14613	9.89813	31.14082
1969	2280	1630	0.667	3.13354	9.81907	30.76846
1970	734	1240	0.688	3.09342	9.56925	29.6017
1971	4710	1080	0.708	3.03342	9.20164	27.91243
1972	1360	1050	0.729	3.02119	9.12759	27.57618
1973	265	734	0.75	2.8657	8.21224	23.53381
1974	592	592	0.771	2.77232	7.68576	21.30738
1975	1050	574	0.792	2.75891	7.61158	20.99968
1976	1960	560	0.813	2.74819	7.55255	20.75584
1977	4660	465	0.833	2.66745	7.11529	18.97968
1978	297	427	0.854	2.63043	6.91916	18.20037
1979	400	400	0.875	2.60206	6.77072	17.61781
1980	560	297	0.896	2.47276	6.11454	15.11979
1981	38	265	0.917	2.42325	5.87214	14.22966
1982	1420	159	0.938	2.2014	4.84616	10.66834
1983	427	119	0.958	2.07555	4.30791	8.941278
1984	119	38	0.979	1.57978	2.4957	3.942665

TABLE 13.13
Annual Peak Discharge in Problem 2

Year	Annual Peak Discharge (m^3/s)
1962	1.53
1963	2.18
1964	7.89
1965	4.54
1966	3.72
1967	1.45
1968	4.76
1969	2.1
1970	42.15
1971	5.01
1972	1.11
1973	0.39
1974	1.51
1975	1.49
1976	2.53
1977	2.95
1978	2.95
1979	6.22
1980	1.77
1981	1.55
1982	1.3
1983	1.59
1984	5.83

5. Use the damage–frequency relationships in Table 13.15 for flood control alternatives to rank their merits on the basis of expected flood damage reduction.
6. Determine the optimal design return period from a flood control project with damage and capital costs as given in Table 13.16.
7. The frequency-discharge-storage-damage data for existing conditions at a particular area along a river is given in Table 13.17. The storage-discharge data make up the rating curve,

TABLE 13.14
Annual Peak Discharge in Problem 5

Year	Annual Peak Discharge (m^3/s)
1990	10.2
1991	11
1992	3.5
1993	6.7
1994	4.2
1995	5.3
1996	1.8
1997	9.2
1998	4.5
1999	7.2
2000	1.1

TABLE 13.15
Damage–Frequency Relationships in Problem 7

Exceedance Probability (%)	Damage^0 ($10^6)	Damage^1 ($10^6)	Damage^2 ($10^6)	Damage^3 ($10^6)	Damage^4 ($10^6)
20	0	0	0	0	0
10	6	0	0	0	0
7	10	0	0	0	0
5	13	13	2	4	3
2	22	22	10	12	10
1	30	30	20	18	12
0.5	40	40	30	27	21
0.2	50	50	43	40	35
0.1	54	54	47	43	45
0.05	57	57	55	50	56

the discharge-frequency data compose the frequency curve, and the storage-damage data make up the storage-damage curve. Plot these three relationships.

8. If a dike system with a capacity of 15 m^3/s were used as one alternative for the situation in Problem 7, develop the damage frequency curve for this alternative.
9. If an upstream permanent diversion that will protect up to a natural flow of 15 m^3/s is used for the situation in Problem 7, develop the damage frequency curve for this alternative.
10. If channel modification is used for the situation in Problem 7 to increase the conveyance capacity of the river up to 15 m^3/s, develop the damage frequency curve for this alternative.
11. Considering Problems 7 and 8, determine the return period for the dike system that maximizes annual expected benefit.

TABLE 13.16
Return Period, Damage Cost, and Capital Cost in Problem 6

T (Return Period)	1	2	5	10	15	20	25	50	100	200
Damage cost ($ ×10^3)	0	40	120	280	354	426	500	600	800	1000
Capital cost ($/year ×$10^3$)	0	6	28	46	50	54	58	80	120	160

TABLE 13.17
Frequency–Discharge–Storage–Damage Data in Problem 7

Exceedance Probability	*Q* (m^3/s)	Stage (m)	Damage ($10^6)
20	339.84	103.7	0
10	396.48	120.9	6
7	424.8	129.6	10
5	452.8	138.1	13
2	509.4	155.4	22
1	566.4	172.8	30
0.5	623.04	190.0	40
0.2	708	215.9	50
0.1	736.32	224.6	54
0.05	792.96	241.9	57

12. Considering Problems 7 and 9, determine the return period for the diversion capacity with maximum expected annual benefit.
13. Considering Problems 7 and 10, determine the return period associated with the flow capacity that maximizes the expected annual benefit in the channel modification.

REFERENCES

APFM. (2008). "Urban flood risk management," *Flood Management Tools Series*.

ASCE and UNESCO. (1998). *Sustainability Criteria for Water Resource Systems*, ASCE, Reston, VA.

Benson, M.A. (1968). "Uniform flood frequency estimating methods for federal agencies," *Water Resources Research*, 4, 891–908.

Bharwani, S., Magnuszewski, P., Sendzimir, J., Stein, C. and Downing, T.E. (2008). Vulnerability, Adaptation and Resilience. Progress toward Incorporating VAR Concepts into Adaptive Water Resource Management, Report of the NeWater Project—New Approaches to Adaptive Water Management under Uncertainty.

Boss International (2005). StormNet and Wastewater Model User's Manual. Available at http://www.bossinti.com

Bronstert, A., Ghazi, A., Hljadny, J., Kundzevicz, Z.W. and Menzel, L. (1999). Proceedings of the European Expert Meeting on the Oder Flood, May 18, Potsdam, Germany, European Commission.

Burn, D.H., Venema, H.D. and Simonovic, S.P. (1991). "Risk based performance criteria for real time reservoir operation," *Canadian Journal of Civil Engineering*, 18 (1), 36–42.

Dunne, T. (1986). Urban Hydrology in the Tropics: Problems, Solutions, Data Collection and Analysis. In *Urban Climatology and Its Application with Special Regards to Tropical Areas*. Proceedings of the Mexico Tech Conf. Nov. 1984 World Climate Programme. WMO.

Eckstein, O. (1958). *Water Resources Development, the Economics of Project Evaluation*, Harvard University Press, Cambridge, MA.

Eikenberg, C. (1998). Journalistenhandbuch zum Katastrophenman-agement, 5th ed., German IDNR-Committee, Bonn.

Emergency Management Australia (2007). *Disaster Loss Assessment Guidelines*, Australian Emergency Manuals Series, Part III, Volume 3, Guide 11. Available at http://www.ema.gov.au/.

FEMA (2008). Flood Damage-Resistant Materials Requirements for Buildings Located in Special Flood Hazard Areas in Accordance with the National Flood Insurance Program. NFIP Technical Bulletin 2. Washington, DC, August.

Grigg, N.S. and Helweg, O.J. (1975). "State of the art of estimating damage in urban areas," *Water Resources Bulletin*, 11 (2), 379–390.

Gringorten, I.I. (1963). "A plotting rule for extreme probability paper," *J. Geophys. Res.*, 68, 813–814.

Grunewald, U. (1998). The Causes, Progression, and Consequences of the River Oder Floods in Summer 1997, Including Remarks on the Existence of Risk Potential, German IDNDR Committee for Natural Disaster Reduction, German IDNDR Series No. 10e, Bonn.

James, L.D. (1972). "Role of economics in planning floodplain land use," *Journal of the Hydraulics Division, ASCE*, 98 (HY6), 981–992.

Karamouz, M., Szidarovszky, F. and Zahraie, B. (2003). *Water Resources Systems Analysis*, Lewis Publishers, CRC Press, Boca Raton, FL.

Karamouz, M., Nazif, S., Fallahi, M. and Imen, S. (2007). Assessment of uncertainty in flood forecasting using downscaled rainfall data, Proceedings of ASCE Environmental and Water Resources Institute Conference, Tampa, Florida, USA.

Karamouz, M., Abesi, O., Moridi, A. and Ahmadi, A. (2008). "Probabilistic optimization model for floodplain management," *Springer Journal of Water Resource Management*, 23 (9), 1743–1761.

Karamouz, M., Imani, M., Ahmadi, A. and Moridi, A. (2009). "Optimal flood management options with probabilistic optimization: A case study," *Journal of Science and Technology*, 33 (B1), 109–121.

Karamouz, M., Hosseinpour, A. and Nazif, S. (2011a). "Improvement of urban drainage system performance under climate change impact: A case study," *ASCE Journal of Hydrologic Engineering*, 15 (5), 395–412.

Karamouz, M., Noori, N. and Moridi, A. (2011b). "Evaluation of floodplain variability considering climate change impacts," *Journal of Hydrological Processes*, 25 (1), 90–103.

Karamouz, M., Fallahi, M. and Nazif, S. (2012). "Evaluation of climate change impact on regional flood characteristics," *Iranian Journal of Science and Technology* (Forthcoming).

Kowalczak, P. (1999). *Flood 1997—Infrastructure and Urban Context*, Bronstert, A., ed. Proceedings of the European Expert Meeting on the Oder Flood, May 18, Potsdam, Germany, European Commission, pp. 99–104.

Krywkow, J., Filatova, T. and van der Veen, A. (2008). "Flood risk perceptions in the Dutch province of Zeeland: Does the public still support current policies?" *Flood Risk Management: Research and Practice*, CRC Press/Balkema Proceedings and Monographs in Engineering, Water and Earth Science. Taylor & Francis Group, 1513–1521.

Mays, L.W. (2001). Water Resources management, John Wiley and Sons Inc., New York.

Moy, W., Cohon, J.L. and Revelle, C.S. (1986). "A programming model for analysis of the reliability, resilience and vulnerability of a water supply reservoir," *Water Resources Research*, 22 (4), 489–498.

Nelson, C.E., Crumely, C., Fritzsche, B. and Adcock, B. (1989). Lower southeast Florida hurricane evacuation study. Report prepared for the US Army Corps of Engineers, Jacksonville, FL.

Sklar, A. (1959). "Fonctions de répartition à n dimensions et leus marges," *Publications de l'Institut de Statistique de L'Université de Paris*, 8, 229–231.

Stormpulse. (2012). http://www.stormpulse.com/hurricane-irene-2011.

Tucci, C.E.M. (1991). Flood control and urban drainage management. Available at http://www.cig.ensmp .fr/~iahs/maastricht/s1/TUCCI.htm.

Tung, Y.-K. and Mays, L.W. (1981). "Generalized skew coefficients for flood frequency analysis," *Journal of the American Water Resources Association*, 17 (2), 262–269.

UN/ISDR. (2002). Living with Risk: A Global Review of Disaster Reduction Initiatives. Preliminary version prepared as an interagency effort co-ordinated by the ISDR Secretariat, Geneva, Switzerland.

US Water Resources Council. (1981). *Estimating Peak Flow Frequencies for Natural Ungauged Watersheds—A Proposed Nationwide Test*, Hydrology Subcommittee, US Water Resources Council.

Vis, M., Klijn, F., De Bruijn, K.M. and Van Buuren, M. (2003). "Resilience strategies for flood management in the Netherlands," *International Journal of River Basin Management*, 1 (1), 33–40.

Wallis, J.R., Matalas, N.C. and Slack, J.R. (1974). "Just a moment," *Water Resources Research*, 10 (2), 211–219.

World Bank (2007). *An East Asian Renaissance*, Gill I. and Kharas H., eds, The International Bank for Reconstruction and Development/The World Bank, Washington.

NOAA. (2012). http://www.tsunami.noaa.gov.

Zongxue, X., Jinno, K., Kawamura, A., Takesaki, S. and Ito, K. (1998). "Performance risk analysis for Fukuoka water supply system," *Water Resources Management*, 12 (1), 13–30.

Hydrology and Hydroclimatology

Principles and Applications

A comprehensive compilation of scientific and engineering topics, **Hydrology and Hydroclimatology: Principles and Applications** combines coverage of many new challenges and emerging issues missing from many other textbooks in this field. The authors take a systems approach to understanding and applying the principles of hydrology and hydroclimatology, considering interactions among different components of water cycle.

The book provides a fresh look at the fundamentals and new challenges in hydrologic and hydroclimatic systems and climate change. The authors underscore the importance of the underlying concepts due to the emergence of non-traditional data sets and new investigation techniques applied to an expanding array of water-related problems.

Highlights include:

- System's view of hydroclimatology and hydrology
- Basic principles of hydrologic cycles and their interactions with hydroclimatic system
- Watersheds at the holistic scale in hydrologic studies
- Deterministic and stochastic investigations in hydrology
- Emerging issues in large and non-traditional data sets and regionalizing data
- Climate change assessment and evaluation of its impacts on hydrologic cycle
- Simulation and modeling tools and techniques in hydrology
- Quantifying risks and uncertainty including hazard, vulnerability, and resiliency
- Dealing with extreme hydrologic events: floods and droughts

Examining topics through the lens of current engineering issues, the book provides clear understanding of the hydrologic systems and their interactions, time series analysis, long lead forecasting and simulation, drought and flood management as well as risk and uncertainty in hydrologic design. The combined coverage of surface and groundwater hydrology, as well as deterministic and stochastic aspects of water science and engineering, provides practical tools and techniques for handling pressing water issues that have been amplified in urban areas.

CRC Press
Taylor & Francis Group
an **informa** business
www.taylorandfrancisgroup.com

6000 Broken Sound Parkway, NW
Suite 300, Boca Raton, FL 33487
711 Third Avenue
New York, NY 10017
2 Park Square, Milton Park
Abingdon, Oxon OX14 4RN, UK

K14878
ISBN: 978-1-4665-1219-1
90000
9 781466 512191
www.crcpress.com